IAVCEI

Field excursions to volcanic terranes in the western United States, Volume II: Cascades and Intermountain West

Edited by Charles E. Chapin and Jiri Zidek

MEMOIR 47 New Mexico Bureau of Mines & Mineral Resources 1989

A DIVISION OF
NEW MEXICO INSTITUTE OF MINING & TECHNOLOGY

INTERNATIONAL ASSOCIATION OF VOLCANOLOGY AND CHEMISTRY OF THE EARTH'S INTERIOR (IAVCEI)
1989 GENERAL ASSEMBLY

Sponsors

U.S. Geological Survey
Institute for the Study of Earth and Man, Southern Methodist University
Los Alamos National Laboratory
New Mexico Bureau of Mines and Mineral Resources
University of New Mexico
Institute for Geophysics and Planetary Physics, University of California
National Science Foundation
American Geophysical Union
U.S. Department of Energy
Sandia National Laboratories

Organizing Committee

Chairman: MICHAEL DUNGAN, *Dallas*
Secretary: SCOTT BALDRIDGE, *Los Alamos*
Program: PETER LIPMAN, *Denver*
Field Trips: WOLFGANG ELSTON, *Albuquerque*
Publications: CHARLES CHAPIN, *Socorro*
Local Arrangements: GRANT HEIKEN, *Los Alamos*
KENNETH WOHLETZ, *Los Alamos*
IAVCEI Secretary General: HANS-ULRICH SCHMINCKE, *Bochum*

FRONT COVER—Looking from the top of Harrys Ridge into the crater of Mount St. Helens on 19 May 1982, two years and one day after the crater was formed and five days after the start of a brief dome-building event. Plume rises from the growing dacite dome, at that time about 630 m wide and 200 m high. Photo Lyn Topinka, USGS.

BACK COVER—Digitally enhanced Landsat Thematic Mapper image of the Mount Shasta region, northern California and southern Oregon.

This image depicts the Cascade Range within about 120 km of its southern terminus; the mountainous region in the western part of the image is part of the Klamath Mountains province, mainly comprising accreted Paleozoic and Mesozoic oceanic and island-arc terranes. Along the prominent valleys just east of the Klamath Mountains, marine to lowland sedimentary rocks of Upper Cretaceous to Eocene age dip unconformably eastward off the Klamath basement. East of those valleys, the western flank of the Cascade Range exposes older Miocene volcanic rocks beneath the uppermost Miocene to Quaternary volcanoes of the present Cascades axis. The long-lived and still active composite volcano Mount Shasta, the prominent snow-covered peak in the southern part of the image, is the largest stratovolcano of the range, rising to 4316 m above sea level. It is flanked on all sides but the east by shallow topographic depressions in which volcanic debris flows have accumulated. The large open valley extending 50 km to the northwest from Mount Shasta is floored by a gigantic volcanic sector avalanche of about 300 ka. The main axis of the Southern Cascades spans the image along a gently curving north-northwest to north–south line just east of Mount Shasta. The prominent snow-covered peak near the north end is Mount McLoughlin, a stratocone of mainly late Pleistocene age. Most of the rest of the main axis comprises individual shield volcanoes, mainly of femic-andesite compositions and short eruptive lifespans; some of the younger shields preserve prominent agglutinate cones at their summits. East of the Cascades, in the northeastern and east-central parts of the image, is the Klamath Lakes–Tule Lake Basin, part of the Basin and Range province, the fault-block structures of which can be discerned. The Klamath River drains the northern part of this area across the Cascades axis through prominent canyons that cross the image diagonally. Young volcanic vents trend east-northeast across the main Cascades axis just east of Mount Shasta, connecting it with the Medicine Lake Highland, a Pleistocene and Holocene shield volcano with a notable caldera—the most voluminous volcanic edifice of the Cascades region. Prominent on the flanks of the Medicine Lake Highland are several late Holocene basaltic lava-flow complexes, the largest of which, the Giant Crater flow, extends south-southeast nearly 50 km from the Highland, to the edge of the image. Also prominent near the rim of the caldera are rhyolite to dacite lava flows of about 1 ka. The volcanic axis of the Cascades is interrupted by an eastward salient of the Klamath Mountains near the south edge of the image, but similar volcanoes resume just a little farther south and continue to the Lassen Peak region at the south end of the Cascades volcanic arc.

Caption by R. L. Christiansen, U.S. Geological Survey. See Excursion 12B for details of this area. Image (GEOPIC) provided by Earth Satellite Corporation, 7222 47th Street, Chevy Chase, Maryland 20815.

Memoir 47

New Mexico Bureau of Mines & Mineral Resources

A DIVISION OF
NEW MEXICO INSTITUTE OF MINING & TECHNOLOGY

Field excursions to volcanic terranes in the western United States, Volume II: Cascades and Intermountain West

Edited by Charles E. Chapin and Jiri Zidek
New Mexico Bureau of Mines & Mineral Resources, Socorro, New Mexico 87801

Published for
IAVCEI GENERAL ASSEMBLY
Santa Fe, New Mexico, USA
June 25–July 1, 1989

SOCORRO 1989

Original Printing

Published by Authority of State of New Mexico, NMSA 1953 Sec. 63–1–4
Printed by University of New Mexico Printing Services, May 1989

Available from New Mexico Bureau of Mines & Mineral Resources, Socorro, NM 87801

Preface

This is Volume II of a two-volume set of field guides to volcanic terranes in the western United States published in conjunction with the General Assembly of the International Association of Volcanology and Chemistry of the Earth's Interior (IAVCEI), Santa Fe, New Mexico, June 1989. Volume I (Memoir 46) contains nine field guides to volcanic terranes in the Southern Rocky Mountain region. Volume II (Memoir 47) contains seven field guides to volcanic terranes in the Cascades and Intermountain West. Both volumes contain a combination of scientific papers and road logs designed to familiarize the reader with the geology of a particular volcanic field and then lead him through it. The technical papers contain much new data and should serve as useful references for many years.

The individual field guides were compiled from contributions of three to eleven authors each; a total of 105 authors contributed to the 16 field guides. Because of the large number of authors, their geographic separation, and the short time from submittal to publication, it was not possible to completely standardize the format. However, a detailed table of contents is available in the front of each volume. A list of references is provided at the end of each field guide. Abstracts of papers presented at the sessions in Santa Fe have been published as Bulletin 131 (340 pp.). The two volumes of field guides and the abstract volume can be obtained from Publications Office, New Mexico Bureau of Mines & Mineral Resources, Socorro, New Mexico 87801.

On behalf of IAVCEI and the Organizing Committee for the Santa Fe General Assembly, the editors take this opportunity to thank the authors for their contributions and the University of New Mexico Printing Services for a job well done.

Charles Chapin
Jiri Zidek

E
A
Z

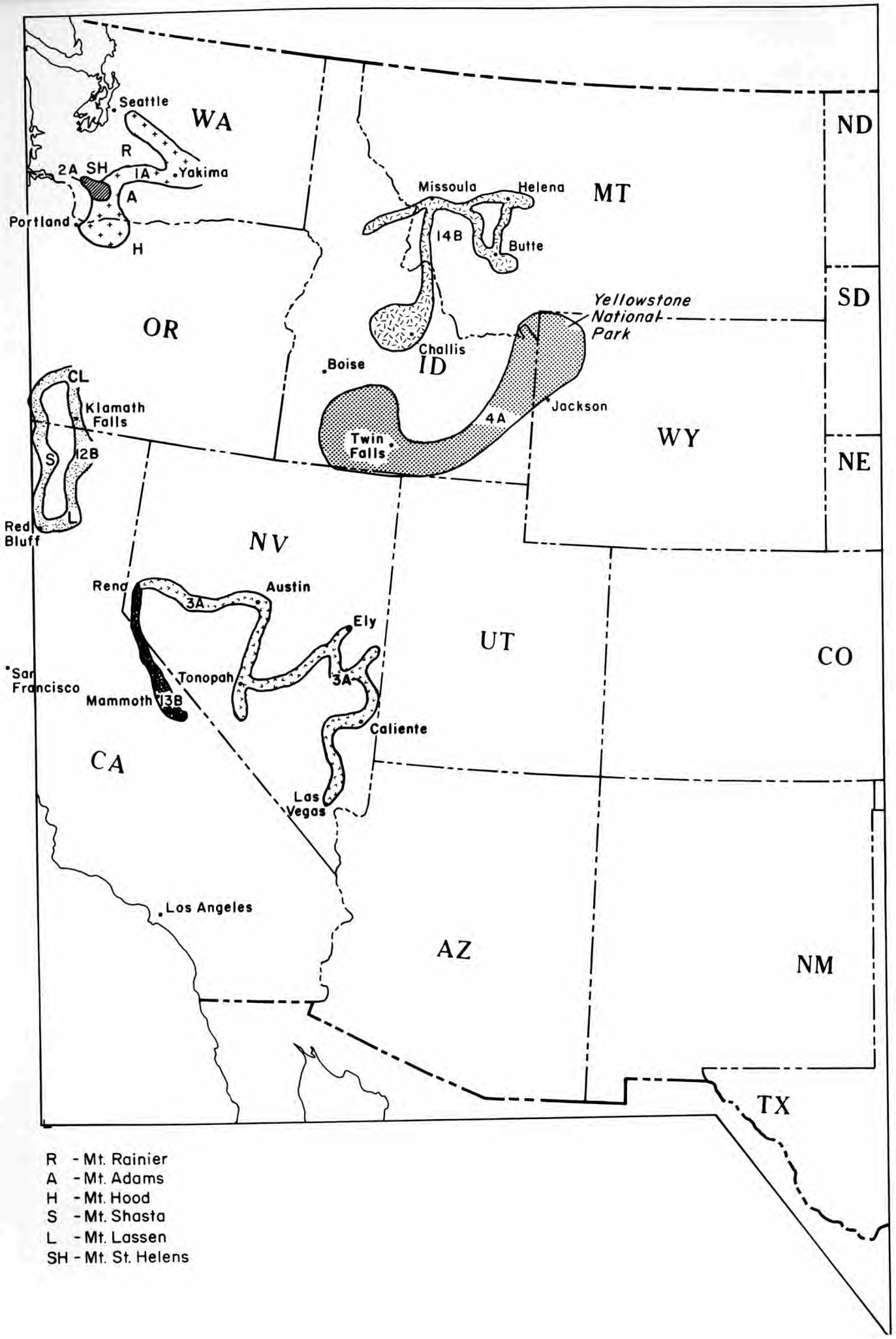

R - Mt. Rainier
A - Mt. Adams
H - Mt. Hood
S - Mt. Shasta
L - Mt. Lassen
SH - Mt. St. Helens

Contents

EXCURSION 1 A:
Cenozoic volcanism in the Cascade Range and Columbia Plateau, southern Washington and northernmost Oregon

Donald A. Swanson[1], Kenneth A. Cameron[1], Russell C. Evarts[2], Patrick T. Pringle[1], and Joseph A. Vance[3]

[1]U.S. Geological Survey, Cascades Volcano Observatory, Vancouver, Washington 98661; [2]U.S. Geological Survey, Menlo Park, California 9402S; [3]Department of Geological Sciences, University of Washington, Seattle, Washington 98195

Introduction

This text is for a six-day excursion between Issaquah, Washington (just east of Seattle), and Portland, Oregon, that emphasizes Tertiary and Quaternary volcanic geology of the western Columbia Plateau and the Cascade Range of southern Washington and northern Oregon (Figs. 1, 2). It summarizes the geology of selected areas along the route and provides a brief introduction to the general volcanic history of the Columbia River Basalt Group and the southern Washington Cascades. An extensive but not exhaustive list of references is included. The road logs are designed to be self-guiding; as such, they are more complete than necessary for guided bus excursions.

Tectonic and geophysical setting of the Cascade Range in southern Washington

The Cascade Range has been an active arc for about 36 Ma as a result of plate convergence (Atwater, 1970). Volcanic rocks between 55 and 42 Ma occur in the Cascades (Vance et al., 1987) but are probably related to a rather diffuse volcanic episode that created the Challis arc extending southeastward from northern Washington to northwest Wyoming (Armstrong, 1978; Vance, 1979). Convergence between the North American and Juan de Fuca plates continues at about 4 cm/yr in the direction of N50°E, a slowing of 2-3 cm/yr since 7 Ma (Riddihough, 1984). According to most interpretations, volcanism in the Cascades has been discontinuous in time and space (McBirney, 1978; Luedke and Smith, 1982; Guffanti and Weaver, 1988), with the most recent episode of activity beginning about 5 Ma and resulting in more than 3000 vents (Guffanti and Weaver, 1988). In Oregon, the young terrane is commonly called the High Cascades and the old terrane the Western Cascades, terms that reflect present physiography and geography. The terms are not useful in Washington, where young vents are scattered across the dominantly middle Miocene and older terrane.

Oligocene and Miocene rocks in the southern Washington Cascades and adjacent western Washington and Oregon are tectonically rotated in a clockwise sense according to paleomagnetic data (Simpson and Cox, 1977; Beck and Burr, 1979; Bates et al., 1981; Wells and Coe, 1985). The amount of rotation in general increases with increasing age. Rocks probably about 30-35 Ma in the southern Washington Cascades are rotated about 34° (Bates et al. , 1981), whereas the 12 Ma Pomona Member of the Saddle Mountains Basalt is rotated only 8-10° at the western end of the Columbia Gorge (Wells and England, in press; Wells et al., in press). Middle Eocene rocks in the Oregon Coast Range are rotated from 20° to as much as 65° (Wells and Coe, 1985), and Eocene rocks in central Oregon (Clarno Formation), more than 300 km inboard of the continental margin, an average of 16° (Grommé et al., 1986). In some models, the rotation pattern implies that the Paleogene trend of the Cascades was northwestward rather than northward as at present (Magill et al., 1981). In other models, the rotation is confined to domains tens of meters to as much as 30 km across and is related to shear along dextral northwest-trending faults or Riedel shears rather than to wholesale regional block rotation of microplates (Beck, 1980; Wells and Coe, 1985). The continuum model of Wells and England (in press) suggests that the average rate of rotational shear is about 1.3° per million years near the southwest margin of the southern Washington Cascades. The origin of the rotations remains unresolved, but appropriate strike—slip faults in the region make the dextral-shear model attractive. No evidence for significant rotation younger than 12 Ma has been recognized, owing in large measure to the paucity of upper Miocene rocks in southern Washington and northern Oregon.

In Washington and Oregon, a striking contrast has existed for the past 5 Ma in the style of volcanism in the Cascades relative to geography (Weaver and Malone, 1987; Guffanti and Weaver, 1988). North of Mount Rainier, young volcanism is concentrated in only a few isolated andesitic and dacitic composite cones (notably Glacier Peak, Mount Baker, and the volcanoes of the Garibaldi belt in British Columbia), whereas south of Mount Hood moderate-sized andesitic and dacitic composite cones are relatively unimportant features of a landscape dominated by small andesite and basalt vents (Guffanti and Weaver, 1988). The area between Mounts Rainier and Hood is transitional; large andesite and dacite composite cones (Rainier, Adams, St. Helens, Hood, and the extinct Goat Rocks volcano) occur together with fields and scattered vents of olivine basalt (Indian Heaven, Simcoe Mountains, and the King Mountain fissure zone south of Mount Adams).

Weaver and Malone (1987) point out that the southern Washington Cascades are also transitional geophysically (Fig. 3). An east—west saddle in an otherwise west-to-east Bouguer gravity gradient occurs along the Columbia River between Oregon and Washington (Thiruvathukal et al. , 1970; Couch and Baker, 1979). North of Mount Adams a broad gravity low follows the Cascade crest, whereas south of Mount Hood the Cascade gravity low merges eastward into a low related to extension of southeast Oregon (Weaver and Malone, 1987).

Magnetotelluric profiles south of Mount Hood reveal a flat-lying, relatively simple conductivity structure (Stanley,

1984), whereas profiles in the southern Washington Cascades show a high-conductivity anomaly that dips eastward and may reflect accreted marine sedimentary rocks in a compressed forearc basin (Stanley et al., 1987) (Fig. 3; see following section).

Heat flow in the southern Washington Cascades is between 70 and 90 mWm^{-2} (Blackwell and Steele, 1983), whereas that south of Mount Hood averages about 100 mWm^{-2} (Blackwell et al. , 1982) and that north of Mount Rainier a relatively low 40-60 mWm^{-2}. A rapid transition occurs from low heat flow west of the Cascades to high heat flow in the Cascade Range in both Oregon and southern Washington (Blackwell and Steele, 1983).

The southern Washington Cascades are seismically active (Fig. 3). Most earthquakes occur along the 100 km long, north-northwest-trending St. Helens seismic zone (Weaver and Smith, 1983), where most focal mechanisms show dextral slip parallel to the trend of the zone and consistent with the direction of plate convergence (Grant et al. , 1984; Weaver et al. , 1987). Other crustal earthquakes are concentrated just west of Mount Rainier and in a broad area near Portland (Weaver and Malone, 1987). Few earthquakes occur north of Mount Rainier or south of Mount Hood (Weaver and Michaelson, 1985).

From tomography, Rasmussen and Humphreys (1988) interpret the subducted Juan de Fuca plate as a quasi-planar feature dipping about 65° to about 300 km under the southern Washington Cascades. The plate is poorly defined seismically, however, owing to a lack of earthquakes within it (Weaver and Baker, 1988). Guffanti and Weaver (1988)

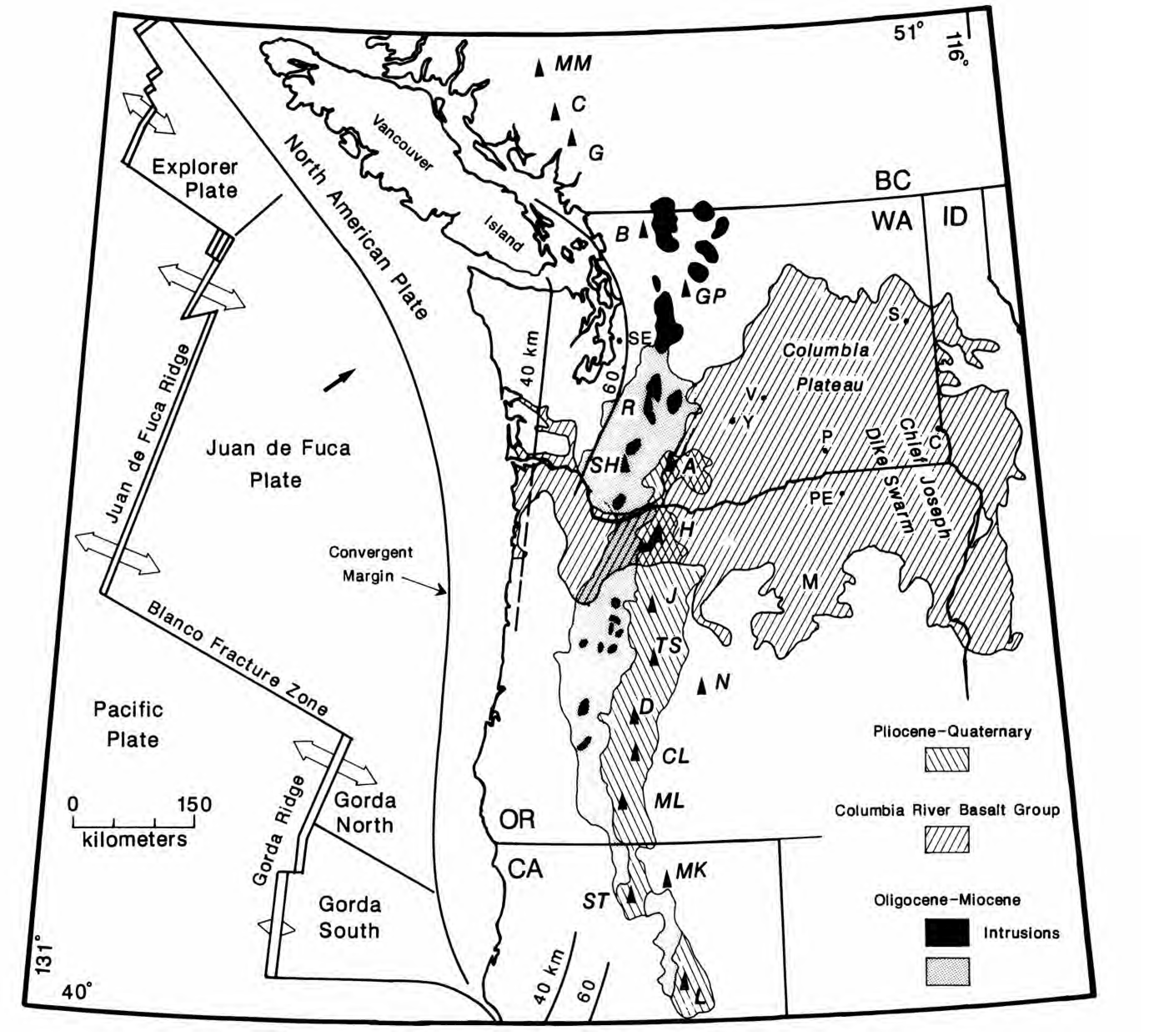

FIGURE 1—Features of Juan de Fuca–North American subduction system (Riddihough, 1984) relative to Cascade Range and Columbia Plateau. Open arrows, ridge-spreading directions; solid arrow, convergence direction. The 40 and 60 km contours show depth of seismicity in upper part of downgoing slab (Weaver and Baker, 1988). Generalized subdivision of Cascade Range from Hammond (1979). Distribution of Columbia River Basalt Group from Tolan et al. (in press). Solid triangles, major Quaternary volcanoes: MM, Meager Mountain; C, Mount Cayley; G, Mount Garibaldi; B, Mount Baker; GP, Glacier Peak; R, Mount Rainier; SH, Mount St. Helens; A, Mount Adams; H, Mount Hood; J, Mount Jefferson; TS, Three Sisters; N, Newberry; D, Diamond Peak; CL, Crater Lake (Mount Mazama); ML, Mount McLoughlin; MK, Medicine Lake; ST, Mount Shasta; L, Lassen Peak. M, Monument dike swarm; SE, Seattle; V, Vantage; Y, Yakima; P, Pasco; PE, Pendleton; S, Spokane; C, Clarkston.

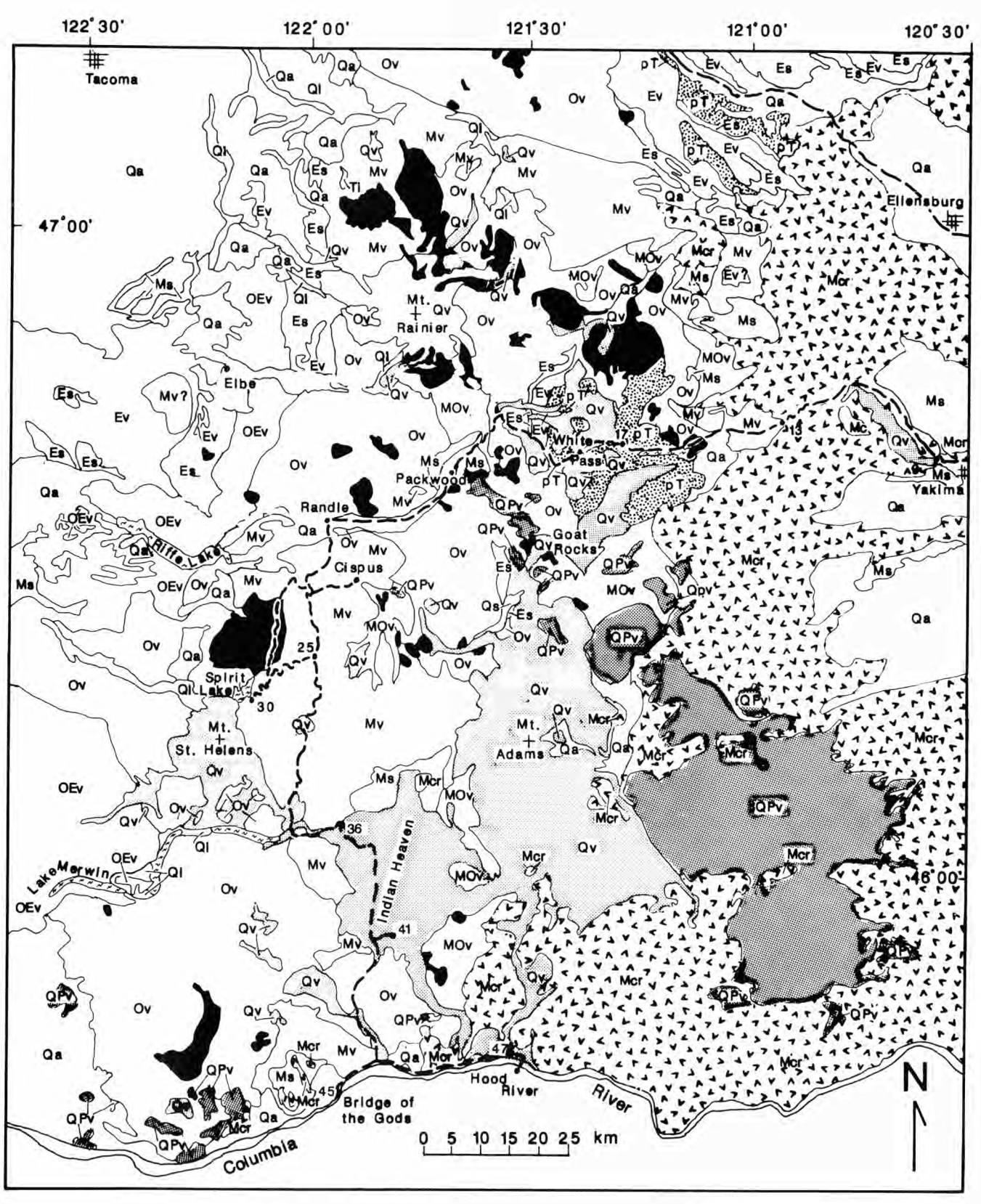

FIGURE 2—Geologic map (faults not shown) for southern Washington Cascades and adjacent Columbia Plateau, simplified from Walsh et al. (1987). Units in order of increasing age: Qa, basin-fill, alluvium, drift, and landslide deposits; Ql, lahars, including 1980 debris avalanche at Mount St. Helens; Qv, Quaternary volcanic rocks; QPv, Quaternary and Pliocene volcanic rocks; Ms, Miocene sedimentary rocks, mostly younger than bulk of Yakima Basalt Subgroup; Mcr, Yakima Basalt Subgroup; Mv, lower and middle Miocene volcanic rocks; MOv, Miocene and Oligocene volcanic rocks; Ov, Oligocene volcanic rocks; OEv, Oligocene and Eocene volcanic rocks; Ev, Eocene volcanic rocks; Es, Eocene sedimentary rocks; pT, pre-Tertiary rocks; solid, intrusions, mostly of early and middle Miocene age. Dashed line, route of field trip with selected stops numbered.

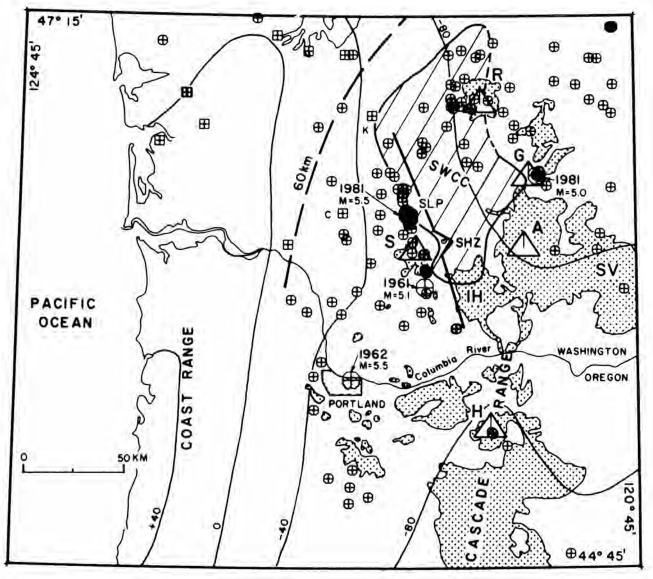

FIGURE 3—Map from Weaver and Malone (1987) showing selected geophysical and geologic elements of southern Washington and northern Oregon Cascades. Stippled, late Cenozoic volcanic rocks (Luedke and Smith, 1982). Large letters, volcanic centers: R, Rainier; G, Goat Rocks; A, Adams; S, St. Helens; IH, Indian Heaven; SV, Simcoe volcanics; H, Hood. Ruled area, southern Washington Cascades conductor (SWCC) (Stanley et al., 1987). Earthquakes: circles with cross, depth <30 km; squares with cross, depth >30 km; date and magnitude given for magnitudes >5; small symbols for magnitudes between 2.5 and 4.9. Bold solid line (SHZ), St. Helens seismic zone. Bold dashed line, location of Juan de Fuca plate at 60 km depth. Light lines, Bouguer gravity contours in milligals, filtered to pass wavelengths >100 km at reduction density of 2.43 g/cm^3. SLP, Spirit Lake pluton.

show that the present volcanic front of the Washington Cascades, defined by the westernmost young vents, parallels the curved trend of the subducting plate reflected by the 60 km depth contour. The front trends northwest in northern Washington—where Glacier Peak, Mount Baker, and the volcanoes of southern British Columbia occur along a virtually straight line—and northeast in southern Washington. A 90 km gap free of young volcanoes between Mount Rainier and Glacier Peak is landward of that part of the sub-ducting plate with the least average dip to a depth of 60 km (Guffanti and Weaver, 1988). South of Portland, the volcanic front is offset 50 km eastward and extends southward into California, probably still parallel to the trend of the convergent margin (Guffanti and Weaver, 1988).

The southern Washington Cascades conductor

A recent magnetotelluric survey of the southern Washington Cascades, combined with geomagnetic variation data (Law et al. , 1980), defines a broad, high-conductivity anomaly with a resistivity of 1-4 ohm m and a thickness possibly more than 15 km, whose top is 2-8 km below less conductive volcanic and sedimentary rocks at the surface (Stanley et al. , 1987). This anomaly, the "southern Washington Cascades conductor " (SWCC) of Stanley et al. , is roughly within the area bounded by Mounts Rainier, St. Helens, and Adams but extends somewhat farther north than Mount Rainier (Fig. 3). Three aeromagnetic lows approximately enclose the SWCC. One of the lows coincides with the western margin of the SWCC and with the St. Helens seismic zone (Weaver and Smith, 1983), in which clusters of 5-15 km deep earthquakes occur in an apparent dextral shear zone. Another aeromagnetic low occurs within the SWCC west and south of Mount Rainier and correlates with a zone of folds mapped by Hammond (1980) and Fiske al. (1963); the north end of the low coincides with an elongate belt of seismicity just west of Mount Rainier. The third low coincides with the southern end of the SWCC but extends farther south into Oregon.

Stanley et al. (1987) interpret the SWCC as caused by " marine sedimentary rocks of early Jurassic to Eocene age, containing hypersaline fluids and possibly dominated by shale facies" that form-an accreted seamount complex in a compressed forearc basin. Mount Rainier lies on the eastern edge of the SWCC (Stanley et al., 1987), and Mount St. Helens is on the western edge as well as on the St. Helens seismic zone (Fig. 3). Fundamental tectonic controls on the locations of these volcanoes may reflect the accretionary history of the region.

Traverse across the Cascades on Interstate 90

The rocks along and south of this route are largely Cenozoic, but Mesozoic basement is locally exposed in inliers and fault blocks. The route follows a transition from dominantly Tertiary volcanic rocks south of 1-90 to the largely pre-Tertiary North Cascades. Four major groupings of rocks are present:

Mesozoic: Jurassic ophiolite and island-arc rocks and their associated Jurassic and Cretaceous sedimentary cover; Early Cretaceous high P–T metamorphic rocks, largely blueschist, greenschist, and phyllite; and Cretaceous plutonic rocks.

Eocene strata: Thick sections of nonmarine arkose and interbedded volcanic rocks.

Rocks of the Cascade magmatic arc: Lava flows and volcaniclastic rocks of the Oligocene Ohanapecosh Formation and the overlying upper Oligocene and lower Miocene Fifes Peak Formation, and the shallow granitoid plutonic rocks of the Miocene Snoqualmie batholith.

Columbia River Basalt Group: Miocene flood basalt erupted from vents far east of the Cascade Range.

Smith (1904) and Smith and Calkins (1906) worked out much the basic geology of this area. Porter (1976) described the Quaternary deposits along 1-90.

1-90 crosses the southern end of the Straight Creek fault, a major Tertiary structure. This fault, more than 500 km long, extends southward down the Fraser River in British Columbia into the Washington Cascades to 1-90, where it splits into a series of southeast-trending splays that disappear beneath the Columbia River Basalt Group. About 90-110 km of dextral strike–slip occurred on the fault (Vance, 1985; Kleinspehn, 1985). Marked lithologic differences distinguish the Mesozoic and Eocene units on either side of the Straight Creek fault.

Mesozoic rocks

A wide variety of units, mostly of Jurassic or Cretaceous age, represent several exotic terranes that accreted to western North America certainly before the Eocene and probably before the end of the Mesozoic. The Mesozoic section west of the Straight Creek fault consists of graywacke and argillite with local chert and limestone. These sedimentary rocks are associated with greenstone, gabbro, and minor tonalite; all rocks are highly folded, faulted, and sheared. Contacts between units are commonly tectonic. Frizzell et al. (1987) mapped the suite as two tectonic-melange belts distinguished by differences in relative abundance of sedimentary

and igneous rocks. The western melange belt, consisting largely of Jurassic marine turbidites, is widely exposed along the western front of the Cascades north of North Bend. The eastern melange belt, distinguished by more abundant greenstone, chert, and limestone, occurs in scattered outcrops north of Snoqualmie Pass. U—Pb ages for tonalite and gabbro in the melanges are Jurassic, and fossils from the chert and clastic sedimentary rocks have mostly Late Jurassic and Early Cretaceous ages. The lithology and age of the melanges led Frizzell et al. (1987) to conclude that the igneous rocks are an oceanic suite (root of an island arc?) that were intruded into the sedimentary rocks prior to the deformation that formed the melange.

Several Mesozoic units lie just east of the Straight Creek fault and between its southeasterly splays. The most widespread is the high P—T Easton Metamorphic Suite consisting of blueschist, greenschist, and phyllite. Farther north, lithologically equivalent rocks of the Shuksan Metamorphic Suite (Misch, 1966) occur extensively west of the Straight Creek fault and have been offset about 90 km from the Easton by dextral slip (Vance, 1985). Most workers have interpreted the Easton and related rocks as metamorphosed oceanic basalt of MORB affinity and its sedimentary cover (Brown, 1986; Dungan et al., 1983). Radiometric dating suggests a Late Jurassic age for the Easton protolith and an Early Cretaceous age for its metamorphism (Brown et al., 1982). Other Mesozoic units between the Straight Creek splays include medium-grade pelitic schist (Stout, 1964) and gneissic tonalite of Jurassic age (Frizzell et al. , 1984).

Two other Mesozoic units are visible from 1-90 in the Stuart Range 30 km north of Cle Elum. The older, the Upper Jurassic and Lower Cretaceous Ingalls Tectonic Complex, consists of a faulted sequence of ultramafic rocks, gabbro, diabase, pillow basalt, and associated sedimentary rocks generally interpreted as an ophiolite (Southwick, 1974; Tabor et al. , 1982b, 1987; Miller, 1985a). The younger unit (95-88 Ma) consists of tonalite, diorite, and granodiorite of the Upper Cretaceous Mount Stuart batholith, which intrudes the Ingalls.

Eocene sedimentary and volcanic rocks

Eocene strata dominate the bedrock along 1-90 between Issaquah and Cle Elum. They include volcanic and fluvial arkosic rocks, in places interbedded. The sedimentary units are quartzose to arkosic micaceous sandstone, shale, and conglomerate derived from a plutonic and metamorphic terrane farther east or northeast. They are locally marine but mostly fluvial and deltaic. Major coal production came from the Puget Group and the Roslyn Formation. The Eocene units are thick (2-4 km) and were deposited in rapidly subsiding, fault-bounded extensional basins (Tabor et al. , 1984; Johnson, 1985). Many of the Eocene volcanic assemblages are bimodal, composed of basalt (or andesite) and high-silica rhyolite. Radiometric ages of the volcanic rocks are 51-42 Ma, mostly middle Eocene (Tabor et al. , 1984; Turner et al. , 1983; Frizzell et al. , 1984). Invertebrate faunas in the rare marine sedimentary units are middle to late Eocene. The volcanic rocks do not belong to the Cascade arc but instead to the older and much broader Challis arc (Armstrong, 1978), which encompasses large areas of Eocene volcanic and shallow plutonic rocks in the Pacific Northwest. Ewing (1980) and Heller et al. (1987) discussed the regional tectonics and paleogeography during the Eocene.

Fig. 4 is a simplified correlation chart for some of the

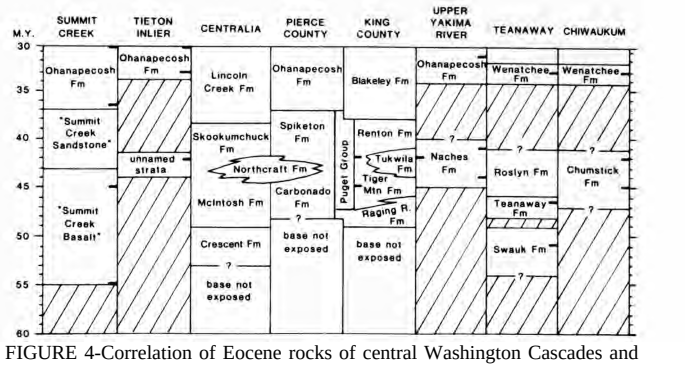

FIGURE 4-Correlation of Eocene rocks of central Washington Cascades and vicinity. Diagram and sources of data from Vance et al. (1987).

Eocene units along the field-trip route. These units pose several stratigraphic and tectonic problems. Obvious contrasts exist between Eocene rocks east and west of the Straight Creek fault. The extent to which the fault merely separated adjacent basins with different histories or juxtaposed the basinal sequences by major dextral movement is unresolved. Stratigraphic relations are not fully understood for the Eocene units separated by the southeastern splays of the Straight Creek fault.

Some Eocene volcanic units exhibit clear structural control. For example, eruption of basalt in the Teanaway Formation was localized in the southeastern bend of the Straight Creek fault. However, no structural control has been identified for other thick volcanic units, such as the Tukwila Formation interbedded in the Puget Group between North Bend and Seattle.

The Puget Group is widely exposed in the eastern Puget Sound basin and in the western Cascade foothills, where it is at least 2.7 km thick (Buckovic, 1979). East of Seattle the Puget Group is underlain by the Raging River Formation and is subdivided into three formations (Vine, 1962, 1969). From the base upward the four units are: (1) Raging River Formation, fossiliferous and tuffaceous marine sedimentary rocks of middle Eocene age; (2) Tiger Mountain Formation, nonmarine arkosic sedimentary rocks; (3) Tukwila Formation, largely coarse andesitic pyroclastic and volcaniclastic rocks with arkosic interbeds; (4) Renton Formation, non-marine arkose.

Abrupt facies changes characterize the Puget Group. The volcanic rocks of Mount Persis (Tabor et al. , 1982a), probably correlative with the Tukwila Formation, make up the entire Eocene section in the western Cascade foothills of southern Snohomish County but are absent in the thick Puget section of southern King County.

Interbedded volcanic and arkosic sandstones of the Naches Formation occur along 1-90 between Snoqualmie Pass and Easton west of the Straight Creek fault. The Naches is as thick as 3 km and is mostly coeval with, and lithologically similar to, the Puget Group. Silicic lava flows and ash-flow tuffs are abundant in the Naches; one prominent silicic welded tuff, the Mount Catherine Rhyolite Member (Foster, 1960; Hammond, 1977; Tabor et al. , 1984), has been mapped separately.

The Puget Group over most of its extent is deformed into tight plunging folds. The Oligocene marine Blakeley formation (informal), which conformably overlies the Puget Group, is likewise folded, but farther north the volcanic rocks of Mount Persis, coeval with the Blakeley, are not.

The Naches Formation is modestly to strongly deformed, particularly near the Straight Creek fault, where tight overturned folds occur. The Naches was folded in at least two episodes. The first predates the Oligocene Ohanapecosh Formation, which overlies the Naches with marked angular unconformity near the Straight Creek fault. This unconformity is absent above the Puget farther west. The second, weaker episode of folding warped both the Ohanapecosh and Naches.

The Eocene stratigraphic sequence near the bend of the Straight Creek fault (Fig. 5) was described and named by Smith (1904) and Smith and Calkins (1906) and further studied by Foster (1960), Stout (1964), and Tabor et al. (1982b, 1984). Field-trip guides (Hammond, 1977; Gresens et al. , 1977) provide additional data on the Eocene units. The Eocene section in this area is quite different from that west of the Straight Creek fault. The oldest unit, the Swauk Formation, is a thick nonmarine arkosic unit that unconformably overlies the Ingalls Tectonic Complex. Silicic volcanic rocks (Silver Pass Volcanic Member) interbedded in the Swauk Formation are dated at about 50 Ma. Consequently, the Swauk is older than the Eocene rocks west of the Straight Creek. The Swauk was moderately folded about 48 Ma. Basalt flows of the Teanaway Formation (about 47 Ma) and the overlying sandstone of the Roslyn Formation were deposited unconformably on the eroded Swauk. The Swauk—Teanaway unconformity is the earliest clear evidence of movement on the Straight Creek fault. A swarm of north-northeast-trending feeder dikes for the Teanaway reflects continued dextral shear on the Straight Creek fault

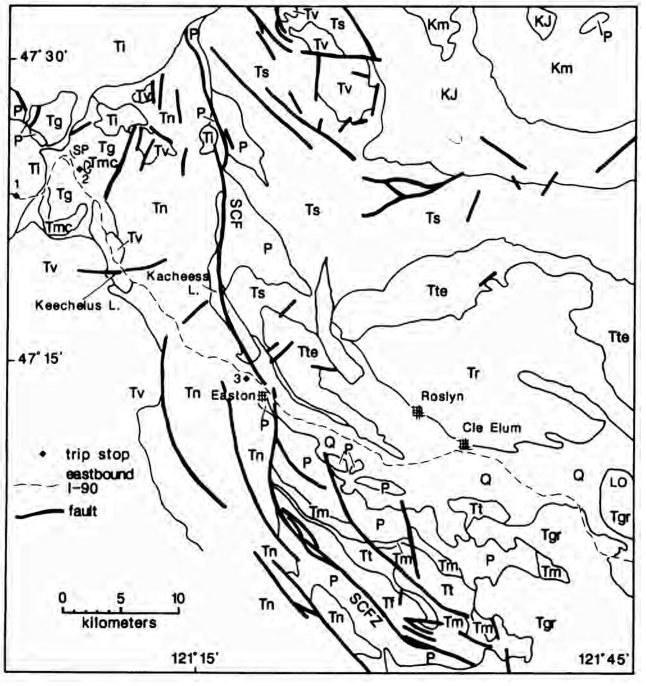

FIGURE 5—Generalized geologic map of central Cascades in Washington, simplified from Tabor et al. (1984). SP, Snoqualmie Pass; LO, Lookout Mountain; SCF, Straight Creek fault. Geologic units, in order of increasing age; Q, Quaternary deposits; Tgr, Grande Ronde Basalt; Ti, Snoqualmie batholith; Tv, Miocene and Oligocene volcanic rocks; Tn, Naches Formation, undivided; Tmc, Mount Cathrine Rhyolite Member of Naches Formation; Tg, Guye Sedimentary Member of Naches Formation; Tr, Roslyn Formation; Tf, basalt of Frost Mountain; Tte, Teanaway Formation; Tt, Taneum Formation; Tm, Manastash Formation; Ts, Swauk Formation; P, pre-Tertiary rocks, undivided. Stops 1-3 labeled.

during Teanaway time. The Teanaway and Roslyn were then deformed into a broad synclinal fold, probably in response to late movement on the Straight Creek fault.

Cascade arc

The Cascade magmatic arc in Washington is defined by a narrow north—south belt of Oligocene and Miocene shallow plutons and coeval volcanic rocks. This belt coincides closely with the zone of large Quaternary stratovolcanoes that dominate the present landscape. In Washington, the Cascade arc is superposed on the older, unrelated Eocene rocks of the much broader and more diffuse Challis magmatic field (Vance, 1982). Inception of the Cascade arc occurred about 36 Ma and is marked by the outbreak of volcanism (Ohanapecosh Formation) and emplacement of the earliest Cascade plutons in the Index and Chilliwack batholiths (Vance et al. , 1986).

Rocks of the Cascade arc are widely exposed south of I90. The two major units are the Ohanapecosh Formation and the uppermost Oligocene and lower Miocene Fifes Peak Formation (Fiske et al. , 1963; Vance et al. , 1987). The Ohanapecosh includes thick sequences of well-bedded volcaniclastic rocks of intermediate composition and debatable depositional environment (Fiske, 1963; Vance et al. , 1987), as well as andesitic and local silicic lava flows and silicic ash-flow tuffs. Hammond (1977) described thick, near-vent rhyodacitic ash-flow tuff along the shore of Lake Keechelus that correlates with the Ohanaceposh on the basis of field relations and radiometric ages (Tabor et al., 1984). The volcaniclastic rocks of Wildcat Creek (Swanson, 1978) in the Tieton River area on the east flank of the Cascades are a distal facies of the Ohanapecosh (Vance et al. , 1987). Oligocene forearc-basin deposits west of the Cascades (Blakeley formation of the Puget Sound basin and Lincoln Creek Formation of southwest Washington) consist largely of volcaniclastic debris reworked from the Ohanapecosh.

The Ohanapecosh Formation is overlain, commonly unconformably, by the Fifes Peak Formation, which consists mostly of andesitic to basaltic lava flows, pyroclastic rocks, and lahars, as well as several thick silicic ash-flow tuffs. Vents for the Fifes Peak are known in the Fifes Peaks themselves (Carkin, 1985) and in the Tieton River area (Swanson, 1978). Fiske et al. (1963) defined the Stevens Ridge Formation to include silicic ash-flow tuffs between the Ohanapecosh and Fifes Peak Formations in Mount Rainier National Park. Recent work shows that such tuffs are common throughout the section and are not useful for regional stratigraphic subdivision. Therefore, Vance et al. (1987) referred the Stevens Ridge to member status within the Fifes Peak Formation.

Volcanic rocks in the range 18-5 Ma are sparsely represented in the Cascade arc in Washington. However, scattered plutons in this interval are present, and recent sedimentological studies and radiometric dating (Smith et al. , 1988) confirm that the dacitic volcaniclastic detritus in the Ellensburg Formation, which overlies and interleaves with the Columbia River Basalt Group, is the distal volcanic debris from eruptions of this time.

The Snoqualmie batholith, a typical shallow plutonic complex of the Cascade arc, is exposed in many places along 1-90 for about 15 km west of Snoqualmie Pass. This composite intrusive body ranges from gabbro to granite, but is dominantly hornblende—biotite tonalite and granodiorite (Erikson, 1969; Tabor et al., 1982a; Frizzell et al. , 1984).

Radiometric dating indicates that the batholith consists of two major phases, each with a wide compositional range. A northeastern phase is about 25 Ma and correlates with the Grotto batholith and related smaller plutons farther north. This phase intruded and postdates movement on the Straight Creek fault. The southern part of the batholith, including the exposures along 1-90, is in the range 20-17 Ma.

Summary of the geology of the Mount St. Helens area

Mount St. Helens rests on the deeply dissected remains of the mid-Tertiary Cascade magmatic arc, represented by a diverse assemblage of variably altered subaerial volcanic and plutonic rocks (Fig. 6). Near the volcano, 5-7 km of Tertiary rocks are exposed in the east-dipping limb of a broad, south-trending and plunging anticline. Exceptional exposures occur near Spirit Lake, where vegetation and surficial deposits were removed by the May 1980 eruption and subsequent erosion.

Many age determinations show that volcanic and plutonic activity that constructed the Tertiary arc in southern Washington occurred largely between 36 and approximately 17 Ma (Frizzell et al. , 1984; Phillips et al. , 1986; Evarts et al. , 1987; Vance et al. , 1987). Volcanism was more or less continuous during this period. Although unconformities are common in the section in southern Washington (Fiske et al. , 1963; Evarts et al. , 1987; Vance et al. , 1987), none has regional extent. K—Ar and ^{40}Ar-^{39}Ar ages from just north of Mount St. Helens indicate a deposition rate of about 360 m/m.y. , similar to those compiled by Smith (in press, a) for other well-mapped and dated mid-Tertiary sequences in the Washington Cascades. Radiometric ages suggest that the rate of volcanism in southern Washington declined between 20 and 17 Ma, and that a subsequent further downturn coincided with eruption of the Grande Ronde Basalt on the Columbia Plateau. Beds of Cascade-derived tephra between flows of Grande Ronde Basalt indicate that explosive volcanism did not stop entirely, but reliable age determinations from the Cascades in the 17-5-Ma range are rare (Smith et al., 1988; Smith, in press, a).

The rate of volcanism in southern Washington increased in the early Pliocene, after regional folding, uplift, and extensive erosion. The volcanism continues but is localized and sporadic relative to that of the mid-Tertiary. Products of this period include basalt fields such as Indian Heaven as well as the prominent composite cones of Mounts Rainier, Adams, and St. Helens.

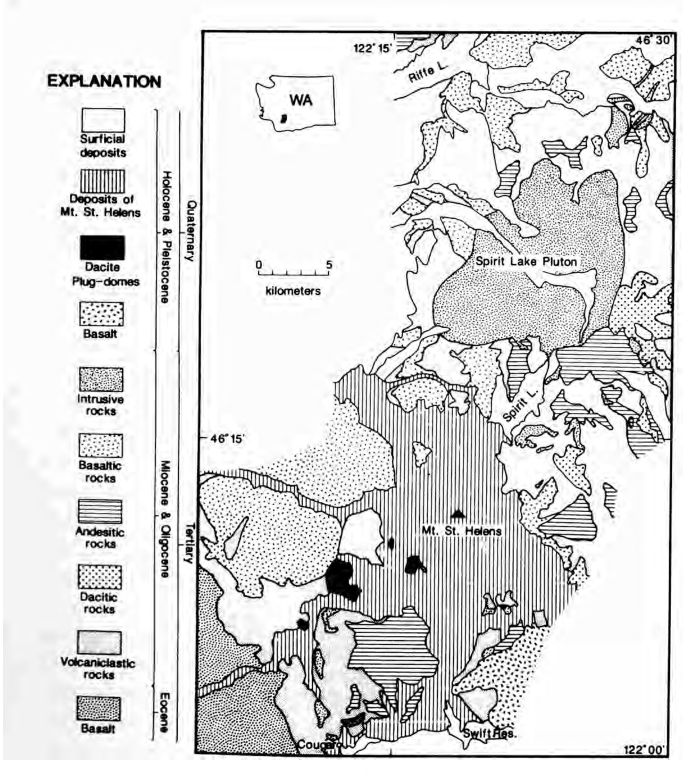

FIGURE 6—Simplified geologic map of the area near Mount St. Helens.

Mid-Tertiary volcanic rocks

The Tertiary section near Mount St. Helens contains rocks typical of near-vent depositional environments, characterized by abundant lava flows and domes, coarsely pumiceous pyroclastic rocks, coarse lithic tuff breccia and lapilli tuff, fine- to medium-grained intrusive rocks, and widespread, locally intense, hydrothermal alteration. Most of the units are discontinuous and lenticular. Well-bedded, finer-grained volcaniclastic rocks of more distal character, such as those in the Ohanapecosh Formation near Mount Rainier (Fiske et al., 1963), are common only near Cougar south of Mount St. Helens (Fig. 6).

The eruptive products range from olivine-phyric basalt to pyroxene rhyodacite. The distribution of these chemically diverse rocks is complex but not random. The upper Eocene and lower Oligocene section west of Mount St. Helens is almost entirely basalt and basaltic andesite, whereas lower Miocene rocks farther east are mostly pyroxene andesite and dacite. The relative volume of pyroclastic rocks increases upsection. Vent areas of several kinds have been recognized, including a swarm of mafic dikes west of Spirit Lake, a silicic dome field on the east flank of Strawberry Mountain north of Bear Meadow, and an inferred caldera along Quartz Creek.

Most rocks are phyric, but sparsely phyric to aphyric andesite and dacite are common. Phenocrysts in basalt are plagioclase, olivine, and in some samples augite; andesite and dacite typically contain plagioclase, augite, and hypersthene. Rhyodacite and silicic tuff rarely contain quartz phenocrysts. Notably absent from the Tertiary volcanic rocks are hornblende and biotite, although hornblende occurs rarely in a few subvolcanic intrusions.

Chemical analyses of the least altered samples have subalkaline tholeiitic to calc-alkaline compositions typical of volcanic arcs (Ewart, 1982). The ratio of calc-alkaline to tholeiitic rocks increased with time. The most notable chemical feature is relatively low K_20 (Fig. 7); in this respect the rocks resemble those of evolved ensimatic arcs such as the Aleutians more than those of the Quaternary Cascades (Evarts et al. , 1987).

Plutonic rocks

Intrusive rocks are widespread near Mount St. Helens and elsewhere in southern Washington (Hammond, 1980). They range from shallow subvolcanic dikes and plugs to medium-to coarse-grained epizonal granitic bodies typified by the Spirit Lake pluton (Evarts et al. , 1987). Compositions of the intrusive and volcanic rocks span the same range, from olivine gabbro to granite, and many probably fill synvolcanic conduits. Most of the smaller bodies have not been dated. A composite sill complex along Windy Ridge east of Spirit Lake has a K—Ar age (plagioclase) of about 24 Ma

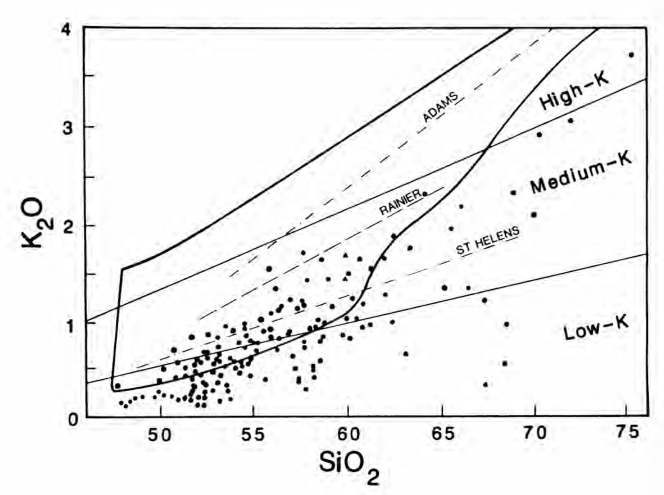

FIGURE 7—K_2O - SiO_2 variation for Tertiary volcanic rocks near Mount St. Helens. Heavy line encircles field of Quaternary volcanic rocks in southern Washington Cascades (Hammond and Korosec, 1983). Generalized trends for Quaternary rocks at Mounts St. Helens, Rainier, and Adams from Greeley and Hyde (1972), Condie and Swensen (1973), Hoblitt et al. (1980), and Hildreth and Fierstein (1985). Modified from Evarts et al. (1987).

(roughly 2 Ma younger than its host rocks), and several KAr and fission-track ages on the Spirit Lake pluton are about 21 Ma. Most of the intrusive bodies are probably only slightly younger than their volcanic country rock, late Oligocene to early Miocene. Intrusions elsewhere in the Cascades generally have similar ages (Tabor and Crowder, 1969; Engels et al., 1976; Mattinson, 1977; Power et al. , 1981; Tabor et al. , 1982a; Frizzell et al., 1984; Vance et al., 1987).

The Spirit Lake pluton consists of three major phases, each containing many smaller units. The earliest phase corn-prises phyric quartz diorite and granodiorite that occur as relatively fine-grained dikes with hornfels screens in the northwest part of the pluton and as isolated bodies in the main phase. Most of these rocks display intense deuteric alteration and are intruded by rocks resembling those of the main phase. The pluton consists mostly of the main and granite phases, which are coarser and more massive than the quartz diorite. The pluton has a configuration of a flat-roofed cylinder tilted eastward with its country rock. Its contact sharply truncates wall rock and is generally simple, but complex to gradational contacts are common internally. Stratigraphic evidence suggests an emplacement less than 3 km deep.

Chemical and petrographic attributes of the Spirit Lake pluton are those of I-type granitic rocks found in most arc environments (Brown et al. , 1982). Plagioclase, augite, and hypersthene generally form euhedral to subhedral crystals in a matrix of coarse anhedral to micrographic quartz and K-feldspar. Minor late hornblende and biotite occur sparingly, mainly in the deeper western half of the pluton. SiO_2 contents vary from 56 to 75%.

Metamorphism and hydrothermal alteration

The Tertiary rocks were affected by very low-grade, zeolite-facies burial metamorphism. Some massive flows and densely welded ash-flow tuffs still contain glass (albeit hydrated), but generally the glass was replaced by iron-rich smectitic clay minerals that provide the green colors characteristic of the Tertiary units. More intense recrystallization took place around plutonic bodies. The Spirit Lake pluton produced a well-developed contact-metamorphic aureole consisting of an inner zone of fine-grained black amphibole hornfels and an outer zone of green albite—epidote hornfels. Broad zones of epidote-bearing hornfels commonly surround even small phaneritic intrusive bodies, which may therefore be cupolas extending from a much larger pluton at shallow depth.

Intense metasomatic alteration of several types has been recognized in the area (Evarts et al., 1987). Widespread but localized low-temperature alteration to carbonate and clay is particularly common near abundant dikes and along minor faults, such as on Johnston Ridge. Higher-temperature argillic to advanced argillic assemblages occur in three areas near the north end of the Spirit Lake pluton. A few kilometers farther south is the Earl porphyry copper—molybdenum deposit, the largest of many such occurrences in the Washington Cascades. The Earl is within the Spirit Lake pluton, yet multiple age determinations indicate that it is about 4 m.y. younger than, and thus not genetically related to, the pluton.

Quaternary volcanism exclusive of Mount St. Helens

Quaternary rocks near Mount St. Helens are restricted to isolated monogenetic vents south and southwest of the volcano. Basalt and basaltic andesite are dominant, but a few silicic domes and plugs follow an east-northeast trend southwest of Mount St. Helens (Evarts et al., 1987).

In contrast to the Tertiary rocks, many of the younger intermediate to silicic rocks contain phenocrysts of hornblende and biotite. They are typically more phyric (especially the dacite) and richer in K_2O at equivalent silica contents than the Tertiary rocks (Evarts et al. , 1987).

Structural elements

Broad, open folds with north- to northwest-trending axes dominate the structure of the southern Washington Cascades (Hammond, 1980; Walsh et al. , 1987). The age of folding is poorly constrained, but much probably occurred in the middle to late Miocene, for all mid-Tertiary rocks are affected whereas Pliocene rocks apparently are not. A few low-angle unconformities within the mid-Tertiary section suggest that minor folding took place as the rocks were accumulating (Evarts et al., 1987; Vance et al., 1987), although such unconformities are easily confused with those caused by primary dips at volcanoes.

Few faults of regional significance have been documented in the southern Washington Cascades (Walsh et al., 1987). Rapid facies changes within the volcanic pile make faults hard to find. However, even mapped faults in the well-exposed area north of Mount St. Helens are clearly minor features that may reflect local stress near volcanoes rather than regional tectonic stress. Many of these faults are associated with hydrothermal alteration or are occupied or cut by Tertiary dikes. The only demonstrably young faulting was related to emplacement of the Goat Mountain dacite plug west of Mount St. Helens. No surface offset along the north-northwest-trending St. Helens seismic zone (Weaver and Smith, 1983) is apparent; this zone connects several clusters of shallow earthquakes, including those beneath Mount St. Helens, whose preferred focal mechanisms suggest dextral displacement parallel to the trace of the zone.

Minor but pervasive north- and northwest-trending dextral-shear zones, as well as northeast-trending sinistral-shear

zones, occur in the area east of Mount St. Helens. Subhorizontal slickensides on stepped fault surfaces allow the sense of displacement to be determined, but offsets are less than a few centimeters. These shear zones are part of a regional system of similar structures, chiefly dextral, recognized on the western Columbia Plateau in Washington and northern Oregon; in places they are simply shear zones with little displacement and in other places faults with offsets of hundreds of meters or more (Bentley and Anderson, 1980; Anderson et al., 1987).

Evarts et al. (1987) and Weaver et al. (1987) discuss linear trends of geologic features that may reflect deep crustal structures in the Mount St. Helens area (see also Stop 34). Mount St. Helens, Mount Rainier, and Glacier Peak define a north-northeast-trending segment of the modern arc. This trend coincides with that of the major epizonal Miocene intrusions of the region, such as the Silver Star (east of Vancouver (Felts, 1939)), Snoqualmie, Tatoosh, and Spirit Lake bodies, which define the core of the Tertiary arc. Thus the position of the volcanic front in southern Washington has been more or less fixed for 25 Ma. The position of Mount St. Helens may be determined by the intersection of this broad trend with younger crustal flaws manifested in a line of Quaternary silicic vents and the St. Helens seismic zone.

Geophysics

Williams et al. (1987) inferred a large, shallow "intrusive complex" under Mount St. Helens on the basis of gravity data. The inferred complex is interpreted to be 5-6 km thick and to intrude the putative compressed forearc marine basin in the southern Washington Cascades conductor (Stanley et al., 1987). Conceivably, this complex could be the source of gabbroic inclusions (Heliker, 1984) in the dacite of Mount St. Helens, although its size (10 by 20 km to as large as 18 by 22 km) is much larger than the inferred current magma reservoir.

Finn and Williams (1987) found a residual magnetic high over Mount St. Helens after correcting pre- and post-1980 aeromagnetic data for terrane effects. The high is about 200 m deep and is within the edifice of the volcano. They suggest that the high, which is not reflected by the gravity data, results from terrain that predates Mount St. Helens, such as a buried andesitic or basaltic cone or a valley filled with lava flows. These two possibilities cannot be distinguished, although the presence of an eroded and buried cone, perhaps fed by the inferred intrusive complex, is appealing. Such a cone would probably be older than 50 ka, the approximate age of the oldest dacite from Mount St. Helens.

Mount St. Helens

Mount St. Helens is young. Its oldest known deposits were erupted about 50-40 ka, and the cone that partly collapsed in 1980 is only 2200 years old. Since its birth it has produced more than 60 tephra layers (Mullineaux, 1986), several tens of volcanically induced debris flows (at least six of which entered the Columbia River 100 km downstream (Scott, 1988)), and the equivalent of 60 km^3 of dacitic lava (Smith, 1987). It has been the most active volcano in the Cascades during the Holocene, and for that reason its eruption in 1980 came as no surprise. The volcano has been studied intensively, and its eruptive history is known with greater clarity than that of any other Cascade volcano.

Eruptive history

Crandell (1987) divides the eruptive history of the volcano into "four extended stages of intermittent activity, each lasting two thousand years or longer. The volcano is now in such a stage that began about 4000 radiocarbon years ago" (Table 1). The stages are separated by dormant intervals of thousands of years. Each stage contains eruptive periods with durations of decades to centuries; those periods for the current stage are named, but those for past stages are not. Many ^{14}C and dendrochronologic ages (Crandell et al. , 1981; Mullineaux, 1986; Yamaguchi, 1983, 1985) provide a well-constrained context within which to interpret the volcanic history.

Mullineaux (1986) recognized at least one tephra set, containing several layers of tephra, in each eruptive stage and period except the Sugar Bowl and Goat Rocks periods, each of which has a single layer. The tephra sets and even single tephra layers form distinctive markers, recognizable by the assemblage and relative proportions of ferromagnesian phenocrysts (hypersthene, hornblende, biotite, cummingtonite, olivine, and augite). The tephra sets and some of the layers can be correctly identified in the field with a mortar, pestal, and binocular microscope using methods developed by D. R. Mullineaux.

The tephras are the most useful means of placing deposits of Mount St. Helens in proper stratigraphic context. They are also used to date events far from the volcano. For example, set S, about 13 ka, is interbedded with deposits of the Missoula floods on the Columbia Plateau and provides one of the best dates for the floods (Mullineaux et al., 1978; Waitt, 1985). Tephra layer Cs, about 37 ka, spread far southward into the Lake Lahontan basin of Nevada, where it is probably equivalent to the Marble Bluff Bed (Davis,

TABLE 1—Eruptive history of Mount St. Helens. Simplified from Crandell (1987). [1]Stages are capitalized; periods are in Spirit Lake eruptive stage. [2] Approximate ^{14}C age in years before 1950. [3]t., tephra; p.f., pyroclastic flow; lahars formed in each stage. [4]Years before 1980, from tree-ring ages and historical records. [5]Years before 1980, from tree-ring and ^{14}C ages. [6]One tephra layer only. [7]Probably includes dormant intervals of at least a few centuries.

Eruptive stage or period[1]	Age[2]	Tephra set	Nature of volcanism[3]
Present	1980–	1980	Phreatic explosions, cryptodome, landslide, blast; dacite t. , p.f., and dome
Goat Rocks	180-123[4]	T[6]	Dacite t. and dome; andesite flow
Kalama	500-350[5]	X W	Dacite t. , p.f., and dome; andesite t.
Sugar Bowl	1150	D[6]	Dacite dome, blast, t., and p.f.
Castle Creek	2200-1700	B	Andesite, dacite, and basalt, t.; andesite and basalt flows; andesite and dacite p.f.
Pine Creek	3000-2500	P	Dacite t., dome, p.f.
Smith Creek	4000-3300[7]	Y	Dacite t., dome, p.f.
SWIFT CREEK	13-10 ka[7]	J S	Dacite t., dome, p.f.
COUGAR	21-18? ka[7]	K M	Dacite t., dome, p.f. and lava flows
APE CANYON	<50-36? ka	C	Dacite t. and p.f.

1978; Mullineaux, 1986). Layer Yn, about 4 ka, occurs near Entwhistle, Alberta, 900 km north-northeast of Mount St. Helens (Westgate et al., 1970; Mullineaux, 1986). Layer Ye occurs in northeast Oregon, 300 km from the volcano (Borchardt et al., 1973). Layers Wn (1480 A.D.) and We (1482 A.D.) (Yamaguchi, 1983, 1985) have been identified 400 km northeast and east of the volcano, respectively (Smith et al., 1977). Layer T (1800 A.D.) occurs in northwestern Montana, 375 km away (Okazaki et al., 1972).

Pyroclastic flows and lahars formed in each eruptive stage and period (Mullineaux and Crandell, 1981; Crandell, 1987). Many pyroclastic flows carry lithic fragments probably derived from coeval domes. Lava flows are known with certainty from only the Cougar stage and the Castle Creek and Kalama periods, although the "floating island" lava flow (Lawrence, 1941; Hoblitt et al., 1980) probably erupted in the 19th century (Crandell, 1987).

All chemical analyses reported by Smith and Leeman (1987; see also Smith, 1984) and Crandell (1987) from pre-Castle Creek tephras are silicic andesite or dacite (Fig. 8), mostly with water-free SiO_2 contents of 61-68%, but rarely as low as 57%.

The lack of mafic tephra suggests that no basaltic andesite or basalt was erupted before Castle Creek time. Proximal exposures are needed to test this suggestion, however, because mafic lava flows can be erupted with little tephra. Large dacite or silicic andesite domes of Pine Creek age, but no mafic flows, occur in the lower half of the present crater wall, so it is unlikely that mafic flows were produced during Pine Creek time. Three dacite or silicic andesite domes of possible Smith Creek age or older are exposed in the northern part of the crater; their age assignment is based on the presence of cummingtonite, which is absent in younger deposits. However, domes and tephras of a given period need not have the same phenocryst assemblage. Aside from these questionably older domes, no pre-Pine Creek deposits occur in the crater. Near-vent mafic flows, perhaps in a small cone (Finn and Williams, 1987), conceivably could be hidden by the Pine Creek domes. No direct evidence exists for such flows, but gabbro inclusions resembling those in the present dome (Heliker, 1983, 1984) occur in Cougar and Pine Creek deposits (J. S. Pallister, written comm. 1988) and suggest that mafic magma was in the reservoir system during much of Mount St. Helens' history, possibly even before 50 ka (Williams et al., 1987). Nonetheless, the volcano has surely been dominated by silicic domes throughout most of its history.

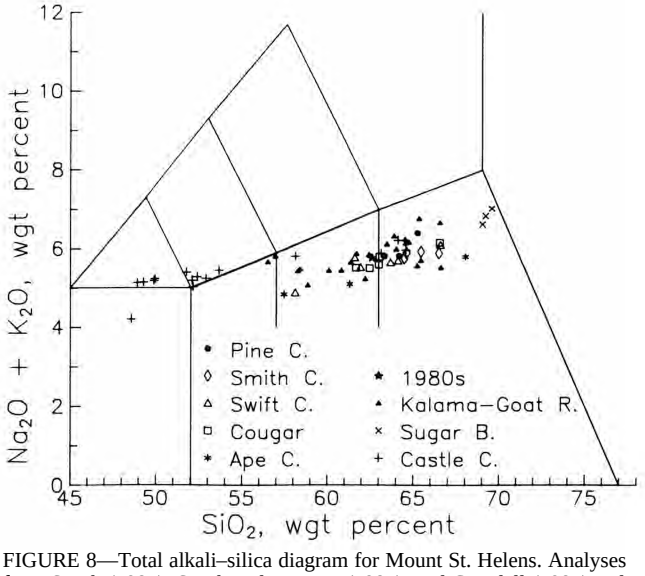

FIGURE 8—Total alkali–silica diagram for Mount St. Helens. Analyses from Smith (1984), Smith and Leeman (1987), and Crandell (1987), calculated water-free to 100%. Symbols indicate age (see text). See Fig. 15 for field names.

A major compositional change occurred at the onset of Castle Creek time about 2200 years B.P. The period began, was dominated by, and ended with basalt, basaltic andesite, and lesser andesite, although dacite tephras, pyroclastic flows, and possibly a dome also formed (Fig. 8) (Mullineaux and Crandell, 1981; Smith and Leeman, 1987; Crandell, 1987). Numerous mafic lava flows, mostly borderline trachybasalt and trachybasaltic andesite (Le Bas et al., 1986) (Fig. 8) although more often called olivine basalt and two-pyroxene basaltic andesite, were erupted from all sides of the volcano, especially the southwest and north. The Cave Basalt (the one basalt plotted in Fig. 8) issued from an unknown vent probably near the southwest base of the cone about 1700 ^{14}C years B P. ; it contains 3.4 km long Ape Cave, the longest known uncollapsed segment of a lava tube, as part of its 8.3 km long tube system (Greeley and Hyde, 1972).

Sugar Bowl dome on the north flank of the cone east of the Breach formed about 1200 ^{14}C years B.P. Two lateral blasts, the largest of which threw lithic debris 10 km north- east of the vent, probably accompanied dome growth (Crandell and Hoblitt, 1986). East dome, at the east base of the volcano, chemically resembles Sugar Bowl; it is undated, but bracketing ages allow it to be of Sugar Bowl age. The rhyodacitic compositions of both domes (Fig. 8) are the most silicic (69-70%) yet found at Mount St. Helens (Smith and Leeman, 1987).

The Kalama eruptive period began in winter or early spring of 1479-1480, as deduced from dendrochronologic dating of the dacitic Wn tephra (Yamaguchi, 1983, 1985), the most voluminous tephra from Mount St. Helens since the Y tephras about 4000 years B.P. Another widespread tephra fall, We, occurred in winter or early spring of 1481-1482. Episodic activity thereafter produced voluminous silicic andesite lava flows. The symmetric pre-1980 cone, known as North America's Fuji, was built by these and the older Castle Creek flows. A dacite dome formed at the summit during Kalama time, and lahars and pyroclastic flows were frequently produced.

The Goat Rocks eruptive period began in 1800 A.D. with the dacitic tephra layer T and ended in 1857 (Crandell, 1987). The "floating island" silicic andesite flow was erupted before 1838, and an explosion sent lithic ash 100 km downwind in 1842. The Goat Rocks dome was extruded on the northwest flank of the volcano 600-700 m below the summit within several years after the 1842 explosion, possibly during or before 1847, when Paul Kane, a Canadian artist, painted a famous canvas of its growth. A large fan of debris spread downslope from the Goat Rocks dome; prismatic jointing is common in blocks of the fan, and paleomagnetic measurements indicate that some of the blocks were deposited above the Curie point and others below (R. P. Hoblitt *in* Crandell, 1987). Contemporary accounts indicate activity several times during the 1840's and 1850's, but are nonspecific and even contradictory. The last significant activity before 1980 was "dense smoke and fire" in 1857, although minor, unconfirmed eruptions were reported in 1898, 1903, and 1921 (Majors, 1980).

Volcanic activity, 1980-1988

This activity has been thoroughly documented and is familiar to most volcanologists. See especially the papers in Lipman and Mullineaux (1981), a series of nine papers in Science (v. 221, no. 4618, 1983), and Swanson et al. (1987) for general summaries. Only a brief synopsis is given here; other specifics are mentioned in the road log.

Seismicity began several days before March 20, 1980, when an earthquake (M = 4.2) centered under the volcano commanded wide attention. The first of a series of small phreatic explosions occurred on March 27, accompanying the opening of a crater within a horseshoe-shaped graben concave northward at the summit of the cone. Strong seismicity continued, at times with bursts of volcanic tremor (Endo et al. , 1981; Qamar et al., 1983); deep tremor was felt statewide in early April but died away without returning. By mid-April a bulge was obvious on the north flank of the volcano; geodetic measurements began shortly thereafter and documented horizontal growth of the bulge at a steady maximum rate of >1.5 m/day (Lipman et al. , 1981a). The bulge was surface evidence of a cryptodome intruding the volcano. Seismicity continued into May, with fewer but larger earthquakes, and phreatic activity was intermittent. No magmatic gas was detected, although new fumaroles appeared in the crater and at the head of the bulge.

At 0832 on May 18, a complex earthquake (M = 5.1) shook the volcano, probably causing (but possibly caused by) a huge, 2.7 km^3 landslide that in three different blocks successively removed the bulge and upper 400 m of the volcano (Voight et al. , 1981, 1983), leaving a 600 m deep crater 2 km wide rim-to-rim. The landslide quickly developed into a debris avalanche that sped at 110-240 km/hr for 24 km down the North Fork Toutle River; arms of the avalanche entered Spirit Lake, 8 km from the summit, and overtopped 300-380 m high Johnston Ridge north of the Toutle. The avalanche buried the Toutle Valley to a depth of nearly 50 m. Its hummocky deposit is distinctive; similar morphology at other volcanoes has been reinterpreted in light of its observed origin (Siebert et al., 1987).

The landslide removed confining pressure on the cryptodome and its surrounding hydrothermal system. Juvenile gas was rapidly released from the cryptodome and superheated ground water flashed to steam, causing a blast that exploded laterally from the collapsing north flank. The blast, called a "stone wind" by local journalists, knocked down most trees (the equivalent of about 150,000 houses) in a 600 km^2 area. Its maximum velocity may have been supersonic (Kieffer, 1981b). The degree to which juvenile gas or flashed ground water drove the blast is debated (Eichelberger and Hayes, 1982; Kieffer, 1981a, b; see also Brugman, 1988), as is the question of whether the blast was, in volcanologic terms, a low-aspect-ratio ignimbrite (Walker and McBroome, 1983) or a surge (Hoblitt and Miller, 1984; Waitt, 1984b).

Soon after the blast, a lahar rushed down the South Fork Toutle River and several streams draining the south and east flanks of the volcano. Whether water for these lahars came from snowmelt or from ground water ejected by the eruption is hotly argued. The largest lahar, down the North Fork Toutle, did not start until early afternoon; it was fed as the debris avalanche dewatered (Janda et al 1981). In addition to causing havoc along the rivers themselves, the lahars fed so much debris into the Columbia River that 31 ships were stranded in upstream ports until the 4 m deep channel was dredged to its pre-eruption depth of 12 m—the first in a series of similar dredgings to maintain Portland as a seaport.

Juvenile dacite pumice and ash mixed with lithic debris began erupting soon after the blast (Criswell, 1987), perhaps from the shallow root of the cryptodome. The flux increased about noon, apparently with arrival of pumice from a 7-10 km deep reservoir (Rutherford et al., 1985; Carey and Sigurdsson, 1985; Scandone and Malone, 1985). Experimental work suggests that just before eruption this reservoir was at a pressure of 220 ± 30 MPO, P_{water}, was 0.5-0.7 P_{total}, and the temperature was 930° ± 10°C (Rutherford et al., 1985). Pyroclastic flows fed by the eruption column covered the debris avalanche in the upper North Fork Toutle basin, forming the pumice plain. Hydroexplosions created phreatic pits on the pumice plain, possibly as the pyroclastic flows covered the dewatering debris avalanche (Moyer and Swanson, 1987).

Plinian to subplinian explosions took place on May 25, June 12, July 22, August 7, and October 16-18, 1980. Products of the explosions decreased in SiO_2 content with time from 65 to 63% or less, possibly because they tapped a magma body zoned chemically (Lipman et al., 198 lb), mineralogically (Kuntz et al. , 1981), and in gas content (Melson, 1983; Scandone and Malone, 1985).

Small domes grew in June and August but were destroyed by the next explosion. The current dome began growing after the last major explosion on October 18. As of November 1988, 17 episodes of dome growth have taken place, each lasting several days to one year (1983-1984), with the latest in October 1986. The dome stands 267 m above its vent and 350 m above its north base, is 860 x 1060 m across, and contains 74 x 10^6 m^3. The dome is highly phyric—with 30-35% plagioclase, 5% hypersthene, 1-2% hornblende, 1-2% Fe–Ti oxides, and <0.5% clinopyroxene (Cashman, 1988)—about 50% crystalline, and contains about 63% SiO_2. Its episodes of growth were preceded by geodetic and seismic precursors that enabled their prediction (Swanson et al., 1983, 1985; Chadwick et al., 1988). The geometry and volumetric rate of growth of the dome followed consistent patterns with time (Swanson and Holcomb, in press). Several hundred small explosions occurred from the dome between 1980 and 1986, and a few large rockfalls spawned minor lithic pyroclastic flows and surges, none of which had sufficient volume to leave the crater (Mellors et al., 1988). Several small lahars formed when snow melted during explosions and rockfalls (Waitt et al., 1983; Waitt and MacLeod, 1987).

Petrologic interpretation

Smith and Leeman (1987) found that the St. Helens dacite has similar or even lower contents of many incompatible elements than do basalt and andesite from the volcano, but is relatively enriched in Ba, Rb, K, Cs, and Sr. The unusual depleted nature of the dacite, and low bulk distribution coefficients for numerous trace elements, preclude an origin by fractionation of the basalt or andesite. Smith and Leeman (1987) favor an interpretation involving melting of metabasaltic crustal rocks enriched in Ba, Rb, Cs, and Sr owing to interbedded sedimentary rocks or metasomatic enrichment of the source region. They consider mantle-derived basaltic magma to be the heat source for crustal melting.

White Pass—Goat Rocks Neogene volcanism

The White Pass—Goat Rocks area has been the site of volcanism since 4 Ma, producing at least 25 volcanoes and more than 175 km^3 of material (Clayton, 1983). Geoffrey Clayton has been working on these rocks for many years, and the following is excerpted from his M.S. thesis (Clayton, 1983) and a USGS open-file report on the Goat Rocks Wilderness (Swanson and Clayton, 1983).

Pliocene volcanism (4-2.8 Ma) resulted in domes, tuff, and shallow intrusions of hornblende dacite north of White Pass. South of the pass, high-silica rhyolite tuff, many layers of which are welded, forms a 650 m thick section on the east flank of the present Goat Rocks area. Flow-layered rhyolite and autobreccia probably belong to one or more domes and have a zircon fission-track age of 3.2 Ma. Smith (in press, b) mapped part of a caldera margin enclosing the rhyolitic deposits.

Silicic volcanism ended about 3 Ma, and undated olivine basalt was locally erupted onto the rhyolitic rocks. Soon thereafter, lava flows of high-K_2O andesite, dominantly pyroxene-phyric but including some flows with abundant hornblende, began to form the large composite Goat Rocks volcano. Eruptions probably took place between about 2.5 Ma and 0.6 Ma, as judged from zircon fission-track ages and magnetic polarity. Some large-volume lava flows entered paleovalleys and advanced many kilometers from their source. The most notable of these flows is 2 km^3 Tieton Andesite, which moved about 80 km eastward down the valleys of the ancestral Tieton and Naches Rivers. Thick sections of lava flows with radial dips of 10-20° surround the hydrothermally altered core of the volcano; dikes cut the flows and define several sectors of a radial swarm. The Cispus Pass pluton occupies the southern part of the altered core and may be as young as 1 Ma (based on one fission-track age).

After a period of erosion, hornblende andesite erupted from vents near the core of Goat Rocks volcano. The highest point in the Goat Rocks area, Gilbert Peak (2476 m), is capped with hornblende andesite. Old Snowy Mountain along the Cascade crest erupted lava flows of hornblende andesite that poured westward into the glaciated valley of the Cispus River. The hornblende andesite is glaciated and at least as old as late Pleistocene. Whether it represents rejuvenation of the Goat Rocks volcano or independent volcanism is not clear.

More than 200 olivine basalt and basaltic andesite lava flows formed the 700 m high Hogback Mountain shield volcano just south of White Pass during the late Pliocene and early Pleistocene. The flows intertongue with those from Goat Rocks. A magnetic reversal in the upper part of the shield may mark the base of the Olduvai event (1.7-1.9 Ma; Mankinen and Dalrymple, 1979).

As volcanism at Goat Rocks and Hogback Mountain waned in the early Pleistocene, activity shifted to the Tumac Plateau north of White Pass. Most of the plateau is composed of hornblende andesite and olivine-bearing basaltic andesite. At least five volcanoes on the plateau are of late Pleistocene age. The youngest, Tumac Mountain, is a basaltic shield that last erupted 20-30 ka as estimated from tephra studies (Clayton, 1983).

Many Pliocene and Quaternary lava flows of olivine basalt erupted in a zone extending 25 km south from the Goat Rocks to the base of Mount Adams (Hildreth and Fierstein, 1985). One vent, the subglacial Walupt Lake volcano, may date from the Evans Creek maximum ca 18-15 ka (Hammond, 1980; Swanson and Clayton, 1983).

Indian Heaven volcanic field

The Indian Heaven volcanic field, midway between Mount St. Helens and Mount Adams, is a Quaternary center, chiefly of basalt. Paul Hammond has worked here for many years but has published few detailed results (Hammond et al. , 1976; Hammond and Korosec, 1983; Hammond, 1984, 1987). He graciously allowed some of his work to be summarized, mainly from an informal field guide he wrote in 1985.

About 60 eruptive centers lie on the 30 km long, N10°E-trending, Indian Heaven fissure zone (Hammond, 1984; Hammond et al. , 1976). The 600 km^2 field has a volume of about 100 km^3 and forms the western part of a 2000 km^2 Quaternary basalt field in the southern Washington Cascades, including the King Mountain fissure zone along which Mount Adams was built (Hammond et al. , 1976; Hildreth et al., 1983).

All lava flows at Indian Heaven have normal magnetic polarity (Hammond et al. , 1976) and so are assumed to be younger than about 0.73 Ma, consistent with their morphology and geomorphic relations. Two K—Ar ages (Hammond and Korosec, 1983; Hammond, 1987) suggesting ages between 3 and 4 Ma are probably too old (Korosec, 1987a, b); they are based on trace contents of radiogenic argon, and no evidence exists for a long hiatus or marked erosion to explain the lack of reversely magnetized flows in the section. The youngest eruption produced Big Lava Bed about 8200 ^{14}C years B.P.

The field is dominated by small shield volcanoes surmounted by cinder and spatter cones. Subglacial vents occur on the northwest flank of the field (Hammond, 1987). The overall shape of the field is that of a north—south elongate shield, with basal diameters of 30 km and 10-15 km, whose center rises about 1 km above its base. Hammond (1984) noted that most of the flows erupted from the center of the field. Hence Indian Heaven can be interpreted as a large, complex shield volcano, fed by a central reservoir, that supports numerous flank vents. Pahoehoe and a'a typify the basalt flows; some of the andesite is block lava. Tephra production was minimal, although the basaltic tephra accompanying extrusion of the Big Lava Bed flow has a volume of about 10^5 m^3. Big Lava Bed is known for its tubes and for the remarkable microtopography on its surface, which mostly results from inflation of the flow when its feeder tubes clogged.

The field is dominantly basaltic (Fig. 9) (Smith, 1984; Hammond, 1984), but basaltic andesite and andesite also occur. Mann Butte, a rhyolite dome or plug east of the field, was once considered to be Pleistocene (Hammond et al. , 1976) but is now interpreted as Tertiary (P. E. Hammond, oral comm. 1986). About half of the basaltic andesite and andesite was erupted on the flank of the field, possibly from fractionated stranded magma bodies, and the rest in the central part of the field (Hammond, 1984). Both low-K, olivine-normative tholeiitic basalt and high-Al, hypersthene-normative calc-alkaline basalt occur (Smith, 1984; Hammond, 1984), as well as transitional types. In this regard the basalt at Indian Heaven is representative of basalt elsewhere in the southern Washington Quaternary field (Smith, 1984).

The field occupies a 100 mgal gravity low (Hammond et al. , 1976; Williams et al. , 1988) that may reflect light Ter-

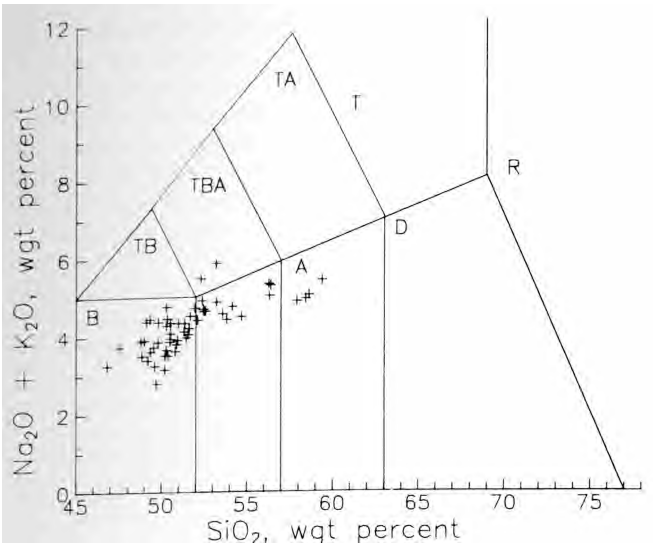

FIGURE 9—Total alkali—silica diagram for Indian Heaven. Unpublished analyses courtesy of P. E. Hammond; published analyses from Smith (1984). Field names as in Fig. 15; R, rhyolite; T, trachyte.

tiary rocks below the field, a hydrothermally altered or fractured zone, or a shallow magma reservoir as yet undetected by other means.

The elongate field follows the direction of regional extension and faulting as well as overall volcanism in the Cascades. A few north-trending normal faults are mapped just northeast and southwest of the field (Walsh et al. , 1987), chiefly on the basis of relations within the Tertiary section. Little is known of their ages.

Mount Hood

Mount Hood, 3428 m high, is the fourth highest peak in the Cascades and the highest in Oregon. It was named after a British admiral and first described in 1792 by William Broughton, member of an expedition under command of Captain George Vancouver (Broughton, 1929). The first geologic reconnaissance primarily described the existing glaciers (Hague, 1871). A complete geologic study of Mount Hood is still wanting; no detailed geologic map exists, and few ages have been obtained on lava flows that form most of the cone.

Early history

The Mount Hood area has hosted volcanic activity since at least the middle Miocene. More than 400 m of locally derived intermediate and silicic volcaniclastic rocks (1411-Ma Rhododendron Formation) interfinger with and overlie the Wanapum Basalt (Wise, 1968, 1969; Priest et al. , 1982; Keith et al., 1982, 1985). The Rhododendron underlies flows of the 10.5-Ma Last Chance andesite of Priest et al. (1982). These units are cut by the Laurel Hill and Still Creek quartz diorite plutons and related offshoots, with K—Ar ages of about 9.3-8. 5 Ma (Bikerman, 1970; Priest et al. , 1982; Keith et al. , 1985). In the Pliocene, local vents erupted thick flows of andesite and minor basalt that cap many of the ridges surrounding Mount Hood (Zigzag Mountain, Tom Dick and Harry Mountain) (Wise, 1969).

The late Pliocene Sandy Glacier volcano (Fig. 10) produced basalt, basaltic andesite, and minor andesite near the site of Mount Hood (Wise, 1968, 1969). More than 900 m of this composite cone are exposed on the west flank of Mount Hood under Sandy and Reid Glaciers and contain

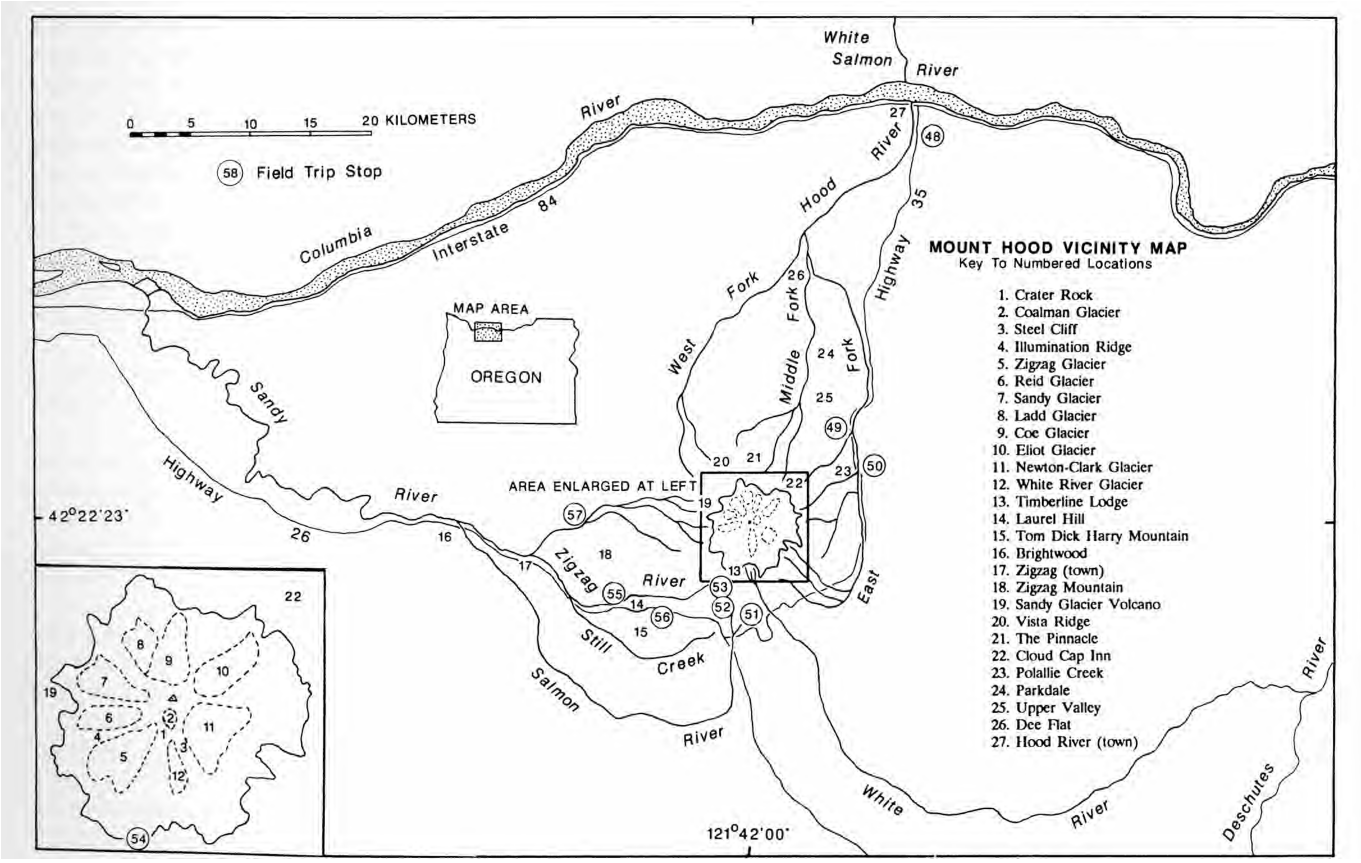

FIGURE 10—Map of Mount Hood area, showing localities mentioned in text and locations of stops.

the most mafic rocks known on Mount Hood (Figs. 11, 12). The youngest exposed flows of the Sandy Glacier volcano have a K–Ar whole-rock age of about 1.3 Ma (Keith et al. , 1985). Reversely magnetized andesite flows of approximately the same age (Keith et al. , 1985) occur in the inverted topography of Vista Ridge and apparently came from a vent now buried under the northern flanks of the mountain. Aeromagnetic data indicate a reversely magnetized body, perhaps the source of the flows, beneath the northern flank (Flanagan and Williams, 1982; Williams and Keith, 1982).

Construction of the cone

The age of the main edifice of Mount Hood is poorly known. All lava flows tested have normal magnetic polarity, so the cone is probably less than 0.73 Ma. Whole-rock K-Ar ages for two andesite flows and one dike of the main cone range from 0.6 to 0.3 Ma (Keith et al., 1985); the dated flows are from stratigraphically low parts of the section in the upper Zigzag River canyon.

The volcano comprises approximately 70% andesite flows and 30% clastic material (mostly concentrated high on the cone) (Wise, 1969). Flows near the summit dip away from a source higher than, and north of, the present summit. Most of the flows are less than 3 m thick, but notable exceptions occur in Steele Cliff and Illumination Ridge, where lava apparently ponded to depths of over 100 m. Eruptions were relatively non-explosive, and significant tephra deposits were limited to the flanks and a small area east of the mountain, where they rarely have a total thickness in excess of 1 m.

Most of the cone-building flows are medium-K silicic andesites (Fig. 12); a few others are mafic dacite. The cone-building flows include no basaltic andesite or basalt, in contrast to the older Sandy Glacier volcano. The cone-building flows are phyric, chiefly two-pyroxene andesite with lesser olivine andesite; hornblende is a disequilibrium phase in about half the flows. Neither Wise (1969) nor White (1980) recognized an overall chemical trend with time in major- or trace-element compositions.

After construction of most of the cone, flank eruptions produced relatively small flows from satellite vents on Vista Ridge and The Pinnacle. A flow from The Pinnacle has a

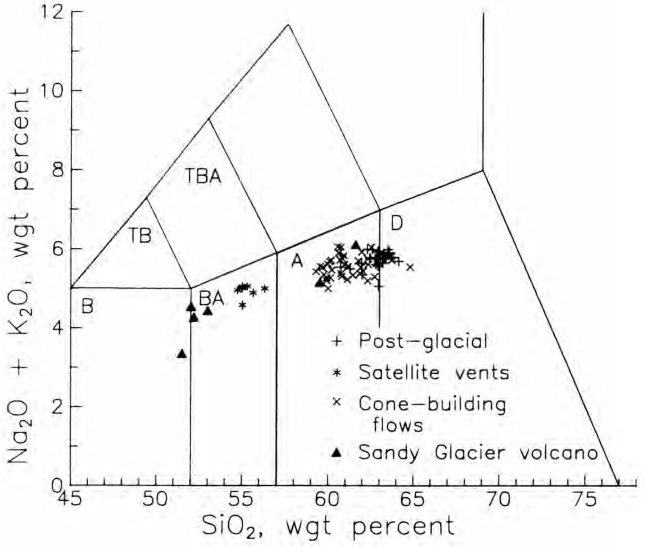

FIGURE 11—Total alkali–silica diagram for Mount Hood. Representative analyses from Wise (1969) and White (1980), recalculated water-free to 100%. Field names as in Fig. 15.

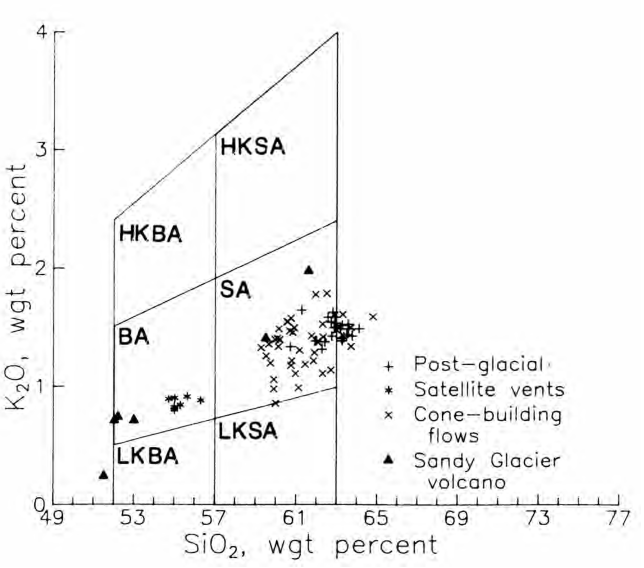

FIGURE 12—Andesite classification for Mount Hood, from Gill (1981) except that basalt–andesite division is 52, not 53%. Data sources as in Fig. 11. HKBA, high-K basaltic andesite; BA, basaltic andesite; LKBA, low-K basaltic andesite; HKSA, high-K silicic andesite; SA, silicic andesite; LKSA, low-K silicic andesite.

K–Ar whole-rock age of 0.15 ± 0.02 Ma (Keith et al., 1985). Wise (1969) interpreted flows erupted near Cloud Cap Inn to be young, but one sample yielded whole-rock K–Ar ages of 0.49 to 0.65 Ma, similar to, or even older than, the age of the main cone (Keith et al. , 1985). The satellite flows including Cloud Cap are chemically more mafic than the andesite forming the main cone (Wise, 1969; White, 1980), comprising medium-K mafic andesites or basaltic andesites (Figs. 11, 12).

Between about 0.05 and 0.1 Ma (based on profiles of soil development), a sector collapse on the north or northeast side of the volcano formed a debris avalanche that traveled the length of Hood River, crossed the Columbia River, and moved 5 km up the White Salmon River—a distance of at least 40 km (Vallance, 1986). The avalanche deposits locally are more than 40 m thick; much of Hood River town is built on them. No source for the avalanche is evident, and no avalanche deposits crop out within 10 km of the volcano, because of a thick blanket of glacial outwash. This leaves as a mystery the exact point of origin of what is probably the largest single event to occur on Mount Hood.

The 5 km long Parkdale flow erupted in Upper Hood River Valley about 6 ka. It chemically resembles the basaltic andesite from The Pinnacles (Wise, 1969).

The latest addition to the cone was a composite hornblende dacite dome, Crater Rock, just south of the summit. Wise (1969) considered the dome as coeval with the main stage of cone building, but Crandell (1980) and Cameron and Pringle (1986) interpreted it to have formed 200-300 years ago.

The summit of Mount Hood is about 1 km south of the apex of a gravity high of at least 8 mGals. Williams and Keith (1982) interpreted the high to reflect a dense intrusive body that fed Mount Hood and its forerunners.

Glaciation

Twelve glaciers and named snowfields cover approximately 80% of the cone above the 2100 m level and contain about 0.35 km^3 of ice (Driedger and Kennard, 1986). Most

of the glaciers have remained roughly constant in size over the last few decades, after retreating from a neo-glacial maximum early in the 18th century (Lawrence, 1948).

Modem glacier termini are at about 2100 m, but in the last major alpine glaciation (Fraser, about 29-10 ka) glaciers reached the 700-800 m level. During this time, ice spread 15 km from the summit area (Crandell, 1980).

Lacustrine siltstone from near-terminus periglacial lakes plaster valley walls just upstream from the mouth of Polallie Creek on the east side of the mountain. Highway 35 crosses White River near the maximum extent of Fraser ice, and the left-lateral moraine is prominent just upstream from the bridge. The full extent of the Fraser-age glaciers has not been accurately mapped.

Glacier retreat released large volumes of outwash, some of which filled the ancestral Hood River Valley near Parkdale, forming the flat surfaces of Upper Hood River Valley and Dee Flat. Outwash also formed a debris fan in the upper East Fork Hood River.

Evidence of older glaciation is seen in roadcuts on the southeast side of the volcano and in rolling morainal landscape near Brightwood west of the volcano. The deposits are not dated but may be coeval with the Hayden Creek Drift near Mount Rainier (Crandell, 1980), probably about 0.14 Ma (Colman and Pierce, 1981).

Postglacial eruptive history

Mount Hood has had at least four eruptive periods in and after late Fraser time, in order of decreasing age: (1) Polallie (15-12 ka; Crandell, 1980), (2) Timberline (1400-1800 yrs B. P.; Crandell, 1980; Cameron and Pringle, 1986), (3) Zigzag (400-600 yrs B.P.; Cameron and Pringle, 1986), and (4) Old Maid (170-220 yrs B.P.; Cameron and Pringle, 1987). Work in progress will determine the details of these episodes in order to assess hazards of a future eruption.

The Polallie eruptive period occurred during the final stage of the Fraser Glaciation (Crandell, 1980). Lahars, thin tephras, and pyroclastic flows intertongue with late Fraser-age outwash in Upper Hood River Valley. Elsewhere, Polallie deposits mantle ridge crests and valley walls but not valley floors. Probably glacial ice still occupied valley floors at the time of the eruptions. No radiometric ages have been obtained for the Polallie.

The Timberline eruptive period broke the apparent 10 ka long post-Polallie quiescence. The vent shifted from its summit location during Polallie time to the high southwest flank. Erupted material except airfall tephra was consequently confined to the Sandy, Salmon, and Zigzag River drainages, where it formed the broad, gently sloping debris fan that dominates the southwest flank of the volcano. Pyroclastic flows dated at 1440 ± 155 yrs B.P. (Cameron and Pringle, 1986) moved at least 8 km down the Zigzag River, and lahars reached the mouth of the Sandy River more than 80 km from the volcano. Small debris fans formed in the canyons of the upper Salmon and Sandy Rivers. An upper age for the Timberline of 1830 ± 50 yrs B.P. was obtained from a pyroclastic-flow deposit near Zigzag (K. A. Cameron and P. T. Pringle, unpubl. data).

The Zigzag eruptive period was apparently minor, feeding several lahars and related floods into the Zigzag River and one pyroclastic flow into the Sandy River. The pyroclastic flow has an age of 455 ± 135 yrs B.P. , and trees buried by the first lahars are 550 ± 130 yrs old (Cameron and Pringle, 1986).

The Old Maid eruptive period apparently began with emplacement of the Crater Rock hornblende dacite dome high on the north flank of the cone. Reconnaissance work shows that the dome comprises three lobes of markedly differing internal structure (Cameron and Pringle, 1986) but does not clarify how each lobe relates to the others. Numerous lahars probably fed by avalanches from the dome and accompanying snowmelt entered the Sandy, Zigzag, Salmon, and White Rivers; a pyroclastic flow traveled from the Crater Rock area at least 9 km along the White River. One lahar extends 65 km along the White River, and the sandy run-out deposit from another is identifiable 80 km from the mountain. At least 60 m of lahar and fluvial deposits partly fill the upper White River canyon near Timberline Lodge. A terrace composed of a lahar overlain by reworked eruptive debris is more than 13 m thick on the lower Sandy River, 60 km from the mountain. Dendrochronologic dating of some of these events (Cameron and Pringle, 1987) indicates that the Sandy River lahar occurred in the mid-1790's, the pyroclastic flow in the upper White River about 1800, and the lahar that traveled 80 km down the White River between 1800 and 1810.

The post-glacial products are dominantly mafic dacite and silicic, medium-K andesite (Wise, 1969; White, 1980; Crandell, 1980), generally more silicic than the cone-building flows. White (1980: 5) claims that, within the post-glacial sequence, "a general trend can be seen in which rocks from the younger units are slightly richer in SiO_2 and poorer in MgO, CaO, and Fe_2O_3."

Historical activity

No major eruptive events have occurred at Mount Hood since systematic records began in the 1820's. Reports of steam and tephra emissions accompanied by red glows or " flames" from the area of the post-glacial vent are known from 1859, 1865 (twice), and 1903 A.D. No tephra deposits have been correlated with these events, though the summit area is capped by stratified tephra and scattered pumice blocks and breadcrust bombs.

Present thermal activity is in fumarole fields near Crater Rock, which stands at the apex of a semicircular zone of fumaroles and hydrothermally altered, heated ground. In summer 1987, maximum ground temperatures were near 85°C and maximum fumarole temperatures were about 92°C (Cameron, 1988), slightly above the boiling point of water at 3100 m. Many of the fumaroles are actively precipitating crystalline sulfur. Comparison of modem and historical photographs shows that the amount of perpetually snow-free ground surrounding the fumarole fields has been increasing since last century. Until the 1980 eruption of Mount St. Helens, the only volcanically related human fatality in the Cascades occurred in the thermal area at Mount Hood in 1934, when a climber exploring ice caves in Coalman Glacier suffocated in the oxygen-poor gas.

Jökulhlaups (glacial-outburst floods) have been recorded from the Zigzag, Ladd, Coe, and White River Glaciers. In 1922, a dark debris flow issued from a crevasse high on Zigzag Glacier and moved 650 m over the ice before entering another fissure; this event initiated a scare that Mount Hood was erupting (Conway, 1921). The Ladd Glacier jökulhlaup in 1961 destroyed sections of the only road around the west side of the mountain and partly undermined a tower of a major powerline (Birch, 1961). The Coe Glacier outburst occurred around 1963, causing a section of trail to be

abandoned and the "round-the-mountain" trail to be rerouted farther from the glacier. Jökulhlaups from White River Glacier were reported in 1926, 1931, 1946, 1949, 1959, and 1968; the Highway 35 bridge over the White River was destroyed during each episode. The more frequent outbursts from White River Glacier may be due in part to an increase in size of the fumarole field at the head of the glacier at Crater Rock (Cameron, 1988).

A rainfall-induced debris flow on Polallie Creek on Christmas 1980 killed one and destroyed an 8 km section of Highway 35. The flow started as a moderate slope failure of only 3800 m^3, but rapidly bulked up and deposited over 76,000 m^3 of debris at the mouth of Polallie Creek (Gallino and Pierson, 1984). The debris dammed the East Fork Hood River, creating a temporary lake; the dam breached, and flooding destroyed the highway.

Felt earthquakes occur on Mount Hood every two years on average. Seismic monitoring, in effect since 1977 (Weaver et al., 1982), indicates a generalized concentration of earthquakes just south of the summit area and 2-7 km below sea level. A seismic swarm in July 1980, during which nearly 60 earthquakes (mostly 5-6 km deep, with a maximum bodywave magnitude of 2.8) were recorded in a 5 day period (Rite and Iyer, 1981), prompted development of an emergency response plan to coordinate local authorities in the event of future eruption.

Geodetic surveillance of the volcano was initiated in 1980, and 30 EDM lines and several tilt stations were resurveyed in 1983 and 1984 (Chadwick et al., 1985; Cascades Volcano Observatory, unpubl. data). Observed changes are within the range of expected error.

Columbia River Basalt Group

The Columbia River Basalt Group is the youngest and most studied flood basalt. The province underlain by the basalt is loosely termed the Columbia Plateau. Such a designation for the entire province is a misnomer, however, because the basalt has been sharply folded and broadly warped, so that its top varies in elevation from slightly below sea level in the Pasco Basin to more than 2.5 km above sea level in the Wallowa Mountains of northeast Oregon. On this trip we will see only a small part of the western section of the plateau, as well as part of the route taken by some flows as they followed the ancestral Columbia River across the Cascades.

Stratigraphy and age

The group is formally divided into five formations (Fig. 13) , which in turn are broken into formal and informal members (Swanson et al., 1979a; Camp, 1981; Beeson et al., 1985; Reidel et al., in press; Bailey, in press). On this trip we will visit flows in the Grande Ronde and Wanapum Basalts only.

The group has a volume of about 174,000 km^3 and covers about 164,000 km^2 (Tolan et al., in press). These figures have been revised downward from previous estimates. It was erupted between 17.5 and 6 Ma, as measured by KAr and ^{40}Ar-^{39}Ar ages (Long and Duncan, 1983; McKee et al., 1977, 1981; Swanson et al., 1979a). Early eruptions (17.5-17 Ma) fed the Imnaha Basalt, which is confined to the southeast part of the province (Hooper et al., 1984). More than 85% of the group was formed during a 1.5 m.y. period between about 17 and 15.5 Ma (Fig. 14), resulting

series	group	sub-group	formation	member	mag polarity
Miocene	Columbia River Basalt Group	Yakima Basalt Subgroup	Saddle Mountains Basalt	Lower Monumental Member	N
				Ice Harbor Member	N,R
				Buford Member	R
				Elephant Mountain Member	R,T
				Pomona Member	R
				Esquatzel Member	N
				Weissenfels Ridge Member	N
				Asotin Member	N
				Wilbur Creek Member	N
				Umatilla Member	N
			Wanapum Basalt	Priest Rapids Member	R3
				Roza Member	T,R
				Frenchman Springs Member	N2
				Eckler Mountain Member	N2
			Grande Ronde Basalt		N2
					R2
			Picture Gorge Basalt		N1
					R1
			Imnaha Basalt		R1
					T
					N0
					R0

FIGURE 13—Stratigraphic subdivision of Columbia River Basalt Group. N, normal magnetic polarity; R, reversed polarity; T, transitional polarity. Subscripts denote magnetostratigraphic units.

in the Grande Ronde Basalt (Mangan et al., 1986; Reidel et al., in press) and the greatly subordinate and geographically limited Picture Gorge Basalt (Waters, 1961; Bailey, 1986). Later eruptions formed the Wanapum Basalt (about 15.5-14.5 Ma) and the Saddle Mountains Basalt (about 146 Ma) (Swanson et al., 1979a; Camp, 1981; Beeson et al., 1985). Relatively little erosion took place between flows, owing to the rapid rate of accumulation, except during Saddle Mountains time. However, a regionally extensive saprolite (fossil soil) or a sedimentary interbed separates the Grande Ronde and Wanapum in most places; flows just below and above the contact typically are normally magnetized, so that the time represented by the break is probably less than a few hundred thousand years, most likely less

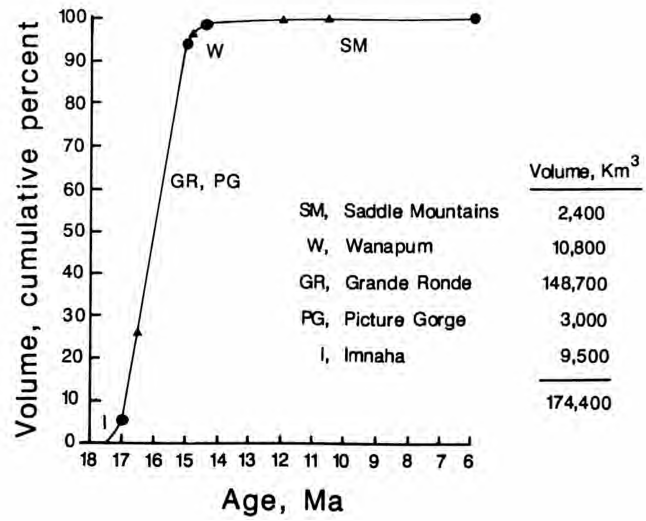

FIGURE 14—Cumulative volume erupted vs. age for units of Columbia River Basalt Group. Dots separate formations; solid triangles are selected radiometric dates. Data from Tolan et al. (in press).

than 100,000 yrs. In Saddle Mountains time, however, interflow erosion was significant, and most contacts are erosional unconformities.

Chemical composition

All major flows within the Yakima Basalt Subgroup (focus of this trip) are tholeiitic, with MgO contents from 2.75 to 8.25% (Table 2; Fig. 15). Specific chemical compositions characterize each formation (Wright et al., in press). Flows of the Grande Ronde Basalt are aphyric and have low MgO (3-6%), high SiO_2 (52-58%), relatively low TiO_2 (1.52.5%) and FeO (9-13%), and a relatively low initial $^{87}Sr/^{86}Sr$ isotopic ratio (0.703-0.705). Most flows of the Wanapum Basalt have lower SiO_2 (49-52%) for the same range of MgO, much higher contents of TiO_2 (>3%) and FeO (1315%), and slightly higher initial $^{87}Sr/^{86}Sr$ (0.704-0.7055). Both formations contain similar trace-element contents despite the contrasts in major-oxide composition. Chondritenormalized rare-earth patterns for both formations are enriched in light rare earths, slightly concave upward with small or no negative europium anomalies, and parallel or slightly convergent toward the heavy rare earths at differing degrees of absolute rare-earth content. Flows of the Saddle Mountains Basalt span a wide range of major-oxide compositions, some of which resemble those of older units. With few exceptions, incompatible trace elements are enriched and compatible elements (particularly Sr and Sc) depleted relative to older units, and $^{87}Sr/^{86}Sr$ ratios are higher (>0.707). Chondrite-normalized rare-earth patterns for many units are steeper and show a more pronounced negative europium anomaly than are those of the older formations. The Umatilla is the only member in the Saddle Mountains with a large positive europium anomaly.

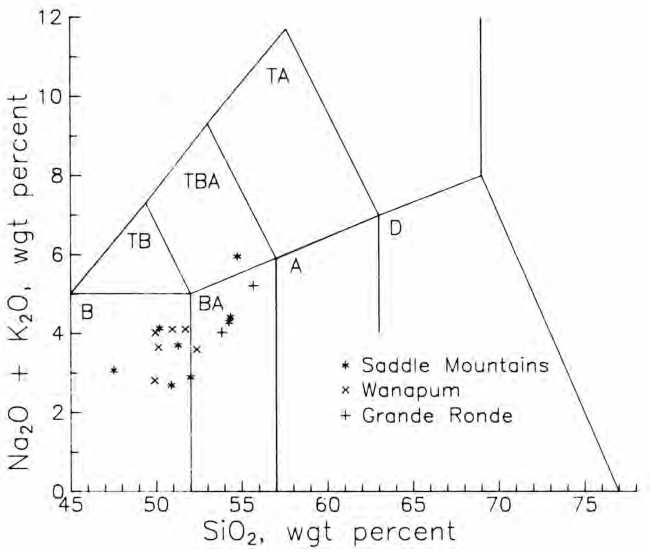

FIGURE 15-Total alkali-silica diagram for Yakima Basalt Subgroup. Selected analyses from Wright et al. (in press). Rock types and fields from Le Bas et al. (1986). B, basalt; BA, basaltic andesite; A, andesite; D, dacite; TB, trachybasalt; TBA, trachybasaltic andesite; TA, trachyandesite.

Vent systems

Linear vent systems are located only in the eastern half of the province, except for feeders for the Picture Gorge near the southern limit of the province (Fig. 1) (Waters, 1961; Swanson et al., 1975, 1979a; Tolan et al., in press). Some of the vent systems are longer than 150 km, and all trend within a few degrees of due north, commonly slightly north-northwest. The systems are correlated with specific

TABLE 2-Representative major-oxide and trace-element analyses of Grande Ronde, Wanapum, and Saddle Mountains Basalts (Wright et al., in press).

	1	2	3	4	5	6	7	8	9	10	11	12	13	14	15	16
SiO_2	53.84	55.69	49.90	52.37	51.70	50.94	49.95	50.12	54.76	54.34	50.87	54.26	52.00	51.27	47.51	50.20
$A1_2O_3$	14.37	13.78	16.82	15.47	13.48	14.27	13.44	14.17	14.24	14.49	16.05	13.85	15.04	13.28	13.79	14.17
"FeO"	11.37	11.85	10.16	10.78	14.35	13.50	14.78	13.93	12.29	11.18	9.54	12.65	10.45	14.79	15.03	14.21
MgO	5.25	3.51	8.21	5.91	4.44	4.57	4.50	5.16	2.75	4.51	8.25	3.98	7.19	4.18	6.05	4.89
CaO	8.97	7.11	10.83	9.90	8.08	8.56	8.67	8.82	6.21	8.42	10.79	7.40	10.39	8.35	9.75	8.63
Na_2O	2.92	3.20	2.43	2.91	2.74	2.85	2.80	2.59	3.39	2.65	2.29	2.58	2.23	2.44	2.28	2.69
K_2O	1.10	2.01	0.37	0.68	1.36	1.25	1.21	1.05	2.56	1.76	0.39	1.71	0.65	1.25	0.78	1.44
TiO_2	1.75	2.23	0.97	1.46	3.02	3.12	3.60	3.23	2.79	1.90	1.48	2.92	1.62	3.61	3.70	2.93
P_2O_5	0.23	0.43	0.17	0.36	0.61	0.68	0.84	0.73	0.82	0.51	0.19	0.44	0.24	0.60	0.87	0.64
MnO	0.19	0.20	0.14	0.l5	0.22	0.25	0.20	0.19	0.19	0.23	0.14	0.22	0.18	0.23	0.24	0.20
Ba	472	730	175	348	549	556	600	539	3313	876	303	592	243	485	611	541
Ce	38.0	54.2	16.3	32.3	51.0	54.2	62.7	57.4	88.2	80.5	31.5	73.8	35.3	68.7	85.6	67.8
Cr	54.9	12.5	151.4	159.7	39.5	44.3	13.6	82.0	3.6	36.6	283.7	18.9	109.0	18.5	148.8	24.0
La	19.5	27.6	7.6	15.2	25.4	27.0	31.1	28.0	46.7	43.7	15.7	38.2	17.0	33.7	42.9	35.3
Nb	11.5	13.0	6.0	8.7	13.0	17.0	17.0	15.8	21.3	16.7	13.0	21.8	13.0	24.5	23.7	25.7
Ni	15.5	-	117.0	42.7	39.3	33.6	27.0	35.0	2.7	47.0	203.3	16.0	51.3	30.7	42.0	28.5
Rb	30.5	45.4	-	15.8	35.4	31.4	34.6	26.6	47.0	38.2	10.0	47.3	10.0	27.6	19.8	18.0
Sm	5.6	7.3	2.7	4.2	6.1	6.9	7.6	7.9	9.8	7.8	4.3	8.4	4.7	9.4	10.7	7.1
Sr	335	359	353	397	317	313	286	302	276	277	252	257	227	213	227	350
Th	3.4	6.38	0.37	1.16	3.88	3.98	4.04	3.56	7.25	6.65	2.05	8.67	2.55	5.91	2.19	4.98
Yb	3.25	3.13	2.10	3.08	3.52	3.89	4.62	3.92	4.52	4.23	2.37	3.65	2.73	4.58	5.64	3.13
Zr	135	178	96	136	196	223	238	223	520	282	-	240	-	316	293	350

Grande Ronde Basalt:
1, High MgO
2, Low MgO

Wanapum Basalt:
3, Eckler Mountain Member, Robinette Mountain flow
4, Eckler Mountain Member, Dodge flow
5, Frenchman Springs Member
6, Roza Member
7, Priest Rapids Member, Rosalia type
8, Priest Rapids Member, Lolo type

Saddle Mountains Basalt:
9, Umatilla Member
10, Wilbur Creek Member
11, Asotin Member
12, Esquatzel Member
13, Pomona Member
14, Elephant Mountain Member
15, Ice Harbor Member, Basin City flow
16, Lower Monumental Member

stratigraphic units chiefly by the presence of dikes of appropriate chemical composition, petrography, magnetic polarity, and stratigraphic position. Hundreds of dikes have been identified, although many probably represent en-echelon segments of one vent system (Waters, 1961; Taubeneck, 1970). Most dikes are known from the tri-state area of Washington, Oregon and Idaho, where they form the Chief Joseph dike swarm (Taubeneck, 1970). Distribution patterns for some flows of the Grande Ronde Basalt suggest that their feeder dikes are hidden beneath younger flows north of the Chief Joseph swarm (Reidel et al. , in press). The dikes typically are a few meters wide, but some are wider than 20 m. Composite dikes, consisting of basalt of two or more different compositions and hence ages, have not been found, but multiple dikes, with internal jointing patterns suggestive of two or more pulses during the same intrusive event, are common. Remnants of spatter cones and other near-vent features, similar to those of modem Kilauea, occur locally (Swanson et al., 1975). The degree of vesicularity and breakage of pyroclasts in these deposits resembles that of modem basaltic tephra, so it is unlikely that the magma was unusually rich in gas.

Volumes and eruption rates

Flood-basalt provinces by definition contain flows of huge volume, on the order of 5-10 km^3 or more; this is the major distinction between flood-basalt and plains-basalt provinces (Greeley, 1977), such as the Snake River Plain and Iceland, in which flows are generally much less than 1 km^3. Recent work by Tolan et al. (1987, in press) suggests that about 300 *great* flows were erupted on the Columbia Plateau, with an average volume per flow of about 580 km^3. Numerous low-volume flows are probably present near vents, but the great flows form most of the province. Flows with volumes more than 100 km^3 occur in all of the formations, but most such flows were erupted during Grande Ronde time, when at least 110 major flows with volumes of 90 km^3 to more than 5000 km^3 were produced (Reidel et al. , in press; Tolan et al., 1987, in press). Such a huge eruption, if from a shallow crustal source, would probably have resulted in recognizable subsidence along the trace of its fissure system. No such evidence has been found, so the inference on geologic grounds alone is that the eruptions tapped a deep reservoir. Viewed regionally, the overall saucer-like subsidence of the province might reflect withdrawal of magma, but its amplitude and diameter would demand a deep source. Petrologic evidence (Helz, 1978; Hooper, 1984; Wright et al. , in press) supports a deep storage reservoir, perhaps at the base of the lithosphere.

Model calculations (Shaw and Swanson, 1970), based on evidence that little cooling occurred during flowage of hundreds of kilometers, suggest that eruption and emplacement spanned only a few days for these huge outpourings. The flows evidently moved 5-15 km/hr or faster (Shaw and Swanson, 1970) and advanced as sheet floods; no lava tubes have been found. The evidence for little cooling during transport is that flows quenched to glass when they entered water after traveling several hundred kilometers; the crystal content of the glass is no higher than that of chilled margins of feeder dikes. The effective viscosity of the lava was *not* unusually low; in fact, calculations of the viscosity based on the chemical composition for a range of reasonable water contents indicate that the lava was somewhat more viscous than modem Kilauea lava. According to Shaw and Swanson (1970), the high rate of eruption (about 1 km^3/day/linear kilometer of fissure or higher, 3-4 orders of magnitude faster than rates of Hawaiian and Iceland eruptions; Swanson et al. , 1975) combined with the huge volume of available magma enabled the flows to travel so far, a relation that Walker (1973) found on empirical grounds (Fig. 16). Regional mapping (Swanson et al. , 1979b, 1980, 1981) indicates that the flows ponded against opposed slopes, including locally recognizable natural levees, and formed lowaspect-ratio (0. 0002-0.0001) lava lakes generally 30-40 m thick and 200-400 km in diameter. The lakes cooled to ambient temperatures within a few years to a few tens of years (Long and Wood, 1986).

Average magma supply rate

About 5.5% of the group was erupted during the first 0.5 m.y. of volcanism to form the Imnaha Basalt (Tolan et al., in press). Activity peaked during the 1.5 m.y. Grande Ronde time, when 87% of the group was erupted, 85% as the Grande Ronde Basalt and 2% as the Picture Gorge Basalt and other coeval units. Activity waned thereafter, accounting for 6% of the group during Wanapum time, which lasted about 1 m.y. , and the remaining 1.5% during prolonged Saddle Mountains time from about 14 to 6 Ma.

During peak activity the average interval between major eruptions was about 13,500 yrs, the average volume per major flow was about 1350 km^3, and the average magma supply rate to the surface was 0.1 km^3/yr. This average supply rate is identical to that calculated for historical time at Kilauea (Swanson, 1972; Dzurisin et al., 1984). On this basis, a larger heat source for Grande Ronde Basalt than for modem Kilauea is unnecessary. An important distinction between the two provinces is that magma "leaks" from Kilauea almost continuously, whereas magma for the Columbia River Basalt Group, if produced at the Kilauea rate, must have been stored for thousands of years before ascent to the surface in order to account for the huge volumes of single flows. (Baksi, 1988, believes the maximum rate of supply, in R2 and N2 time, was two to three times that at Kilauea; this interpretation is based on his revision of the geomagnetic time scale and seems overdependent on the model he assumes.)

The difference in eruption style between Kilauea and the Columbia River Basalt Group could relate to the presence of a 40 km thick continental crust (Catchings and Mooney,

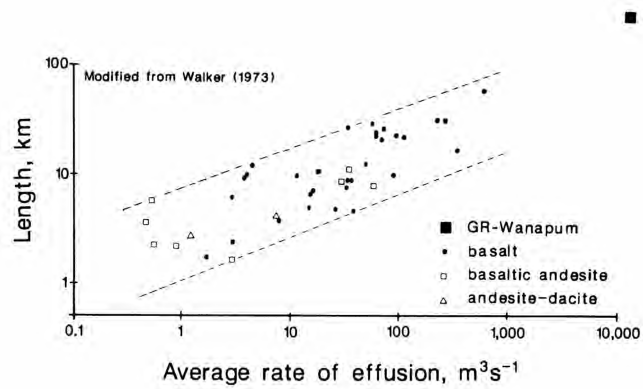

FIGURE 16—Relation of length and rate of effusion for representative lava flows of Grande Ronde and Wanapum Basalts and for historical flows throughout world. Modified from Walker (1973). Rates were observed except for Grande Ronde and Wanapum, which were calculated using model of Shaw and Swanson (1970).

1988; Michaelson and Weaver, 1986) above the melting zone for the Grande Ronde and an oceanic crust over the melting zone for Kilauea. The continental crust may have provided a density trap preventing magma from rising until the trap was ruptured tectonically. Petrologic evidence suggests that the basalt was derived from a complex, multi-source mantle with little crystal fractionation or crustal contamination during rise to the surface (Hooper, 1982, 1984; Wright et al., in press; Carlson, 1984; Carlson and Hart, 1988; Hart and Carlson, 1987). This interpretation implies that the rise was rapid, consistent with the idea that fracturing was responsible for tapping magma at the crust—mantle interface.

Coeval deformation

The basalt was erupted into a subsiding basin centered north of Pasco, Washington, in which sediment was accumulating (Reidel, 1984; Reidel et al., in press). How much of the subsidence owes itself to isostatic response caused by magma withdrawal, to weighting of the crust, and to tectonism is unclear (Catchings and Mooney, 1988). Recent seismic-refraction data, in concert with other geophysical data, suggest that rifting beneath the central part of the province occurred in the Eocene and possibly later (Catchings and Mooney, 1988). If part of the Miocene subsidence was caused by magma withdrawal, significant lateral transport of magma from beneath the center of the province to its eastern flank, the locus of venting, is required.

Tectonic deformation was clearly taking place as the basalt accumulated, because single flows change thickness in anticlines and synclines (Reidel, 1984; Reidel et al., in press). The fold pattern is complex, and no fully satisfactory model for its development exists (Laubscher, 1981; Davis, 1981; Barrash et al. , 1983; Hart and Carlson, 1987). Most folds trend within 20° of east, but some of the largest structures, such as the Pasco Basin and the Naneum Ridge anticline—Hog Ranch uplift, trend nearly north, as does the Cascade Range, whose uplift raised the basalt as much as 2 km. Most of the folds are confined to the western half of the province, but the longest structure, the Blue Mountains uplift, bounds the Columbia Plateau along most of its southern margin.

Ongoing folding, coupled with Cascade uplift and broad subsidence centered on the Pasco Basin, markedly influenced drainage patterns, particularly during Saddle Mountains time when quiet periods were longer and canyons had time to form (Swanson and Wright, 1979; Fecht et al., 1987; Waitt and Swanson, 1987). This topography in turn controlled the distribution of many flows of the Saddle Mountains Basalt. The most notable example is the Pomona Member, which was erupted east of Lewiston, Idaho, flowed down the ancestral Clearwater and lower Snake Rivers, spread across the sagging central plateau, and left the plateau via structurally controlled channels that led through the Cascade Range and finally to the Pacific Ocean, more than 600 km from its vent (Swanson et al., 1979a; Anderson, 1980; Camp, 1981; Tolan and Beeson, 1984c; Anderson and Vogt, 1987; Wells and Simpson, 1987).

Invasive flows and sedimentary interbeds

Sediment deposited between eruptions was commonly invaded by the next basalt flow that entered the area (Schmincke, 1967c; Byerly and Swanson, 1978, 1987; Swanson et al. , 1979a; Niem and Niem, 1985; Wells and Niem, 1987), producing pépérites and sill-like bodies called *invasive flows* that closely resemble classic intrusions. The only way to distinguish invasive flows from intrusions in such a setting is to know the stratigraphy and map the relations between subaerial and invasive components of the flow.

The sediment between the basalt flows has four general sources: erosion of highlands along the margin of the province, erosion of basalt within the province, deposition of diatomite in lakes within the province, and explosive volcanism in the adjacent Cascade Range.

Evidence for coeval Cascade volcanism is clear. Primary pyroclasts, generally mixed with epiclastic detritus but forming pure tuff in places, occur in interbeds in the section of basalt (Schmincke, 1964, 1967d; Swanson, 1967, Priest et al., 1982). However, no lava flows from the Cascades have been shown to be interbedded with the Grande Ronde or Wanapum Basalt; drilling in these formations just west of Mount Hood, Oregon, encountered andesite once thought to be flows (Priest et al., 1982) but now interpreted by some as intrusions (D. R. Sherrod and T. L. Tolan, oral comm. 1988). Apparently, active vents in the Cascades were beyond the limit of the basalt flows, so that only tephra and laharic debris reached them. Cascade-derived debris in interbeds of Grande Ronde and Wanapum age is so sparse relative to that in beds of Saddle Mountains age and younger (Schmincke, 1964, 1967d, Smith, 1988; Smith et al., 1988) that some workers (e.g., Smith, in press, a; Sherrod and Smith, in press) suggest a downturn in Cascade activity followed by an upsurge during Saddle Mountains time. This idea is reasonable, although the short span of Grande Ronde and Wanapum time would by itself have resulted in minimal interbedding, all else being equal.

Speculations on origin

Rampino and Stothers (1988) and Alt et al. (1988) recently suggested that flood-basalt provinces are generated by boloid impacts. The Columbia River Basalt Group was probably not so generated. Geophysical work and deep drilling show no evidence of such an impact; in fact, the rift-like topography indicated by seismic refraction (Catchings and Mooney, 1988) beneath the center of the plateau would be nearly impossible to duplicate by impact. Moreover, calc-alkaline volcanism in the Cascades continued during flood-basalt volcanism but did not upsurge when basaltic eruptions began. One might expect that activity in the nearby Cascades would have followed suit if impact had triggered the basalt. Apparently the flood-basalt volcanism was independent of calc-alkaline volcanism, and neither was caused by impact.

Morgan (1981, 1988) suggested that new hot spots (mantle plumes) give rise to flood basalts, and Duncan (1982) argued that the Columbia River Basalt Group is the product of the Yellowstone hot spot. At least two major problems exist with this idea. First, no fossil hot-spot track is preserved in the province, despite 11 m.y. of volcanism (176 Ma). Instead, feeder dikes are distributed randomly across the eastern half of the province; for example, the 8.5 Ma feeders for the Ice Harbor Member are on the east flank of the Pasco Basin (Swanson et al., 1979a), the 12 Ma feeder for the Pomona Member is more than 210 km *east* of there (in the opposite direction from that expected of a hot-spot trace) (Camp, 1981), and the other dikes lie in between. Second, the feeder system is only the northernmost part of a complex zone of basaltic dikes extending onto the Co-

lumbia Plateau from the Basin and Range province of Nevada (Fig. 17) (Zoback and Thompson, 1978; Christiansen and McKee, 1978). This zone is not only a locus of basaltic magmatism but also a "plane of symmetry" separating traces of silicic volcanism migrating west-northwest across eastern Oregon and east-northeast across Idaho (Armstrong et al. , 1975; MacLeod et al . , 1975; Eaton et al. , 1978). The basaltic activity along the zone began about 17 Ma, and the initiation of the migrating silicic volcanism about 13-14 Ma. The Yellowstone hot spot cannot easily explain these observations.

Lachenbruch and Sass (1977) and Christiansen and McKee (1978) pointed out that the high heat flow of the Basin and Range province requires the presence of a huge volume of Neogene basaltic magma, possibly equivalent to that produced on the Columbia Plateau, in the form of cooling intrusions in, or underplated (Furlong and Fountain, 1986) on, the base of the crust. In this context, Christiansen and McKee (1978) and R. L. Christiansen (numerous oral comms.) suggested that stress relief at the base of the lithosphere, in response to crustal extension resulting from plate interactions, generated the voluminous basaltic magma. In this hypothesis, extension was greatest in the Basin and Range, so that magma could be stored in crustal reservoirs that developed in response to the extension, and least on the Columbia Plateau, so that crustal reservoirs were not formed and most of the basaltic magma that intruded the crust continued through it to the surface and fed the flood-basalt eruptions. This idea does not explain the bilaterally symmetrical nature of migrating silicic volcanism (no published hypothesis does, although the traction concept of Eaton et al. , 1978, is stimulating), but does link the middle Miocene basaltic magmatism throughout the zone to plate interaction and as such is more appealing than either the hot spot or boloid-impact models.

Wright et al. (in press), building on work of Carlson (1984), conclude that the source for the basalt is a mixed oceanic—continental mantle that includes depleted oceanic mantle, subducted oceanic crust, original continental mantle, and old continental crust. They postulate that large bodies of magma generated from this material were underplated as sill-like bodies at the base of the continental crust and then tapped during deep continental extension or rifting. All of the magmas are inferred to have equilibrated with clinopyroxene during either melting or storage, but little evidence exists for fractionation of olivine, augite, and plagioclase as the petrogenetic models of Cox (1980) and Hooper (1984) demand. Wright et al. (in press) interpret the Grande Ronde as derived from relatively young oceanic mantle contaminated with subducted oceanic sediment, possibly with minor interaction with lower crustal rocks prior to or during ascent. They interpret the Wanapum to have much the same origin, except from a part of the oceanic mantle that had undergone Fe—Ti—P metasomatism. They interpret the Saddle Mountains to have a source related in some way to those for the Grande Ronde and Wanapum, owing to the similarity in major-element chemistry. However, the different trace-element abundances and ratios require additional complexity such as a second metasomatic event or melting of 2.5 Ga continental mantle with relatively high incompatible-element contents.

Field guides

These guides are planned for use with a large bus, but we designed optional stops and routes for use by vans and automobiles. We list too many stops (Fig. 18) for a bus load each day, but vans and passenger vehicles should have little trouble in visiting all of them.

Each day has a specific emphasis. The first stresses the Columbia River Basalt Group but also introduces the middle Tertiary geology of the Cascades. This day involves considerable driving on high-speed roads and ends in Yakima. The second day crosses a section of Oligocene to Quaternary

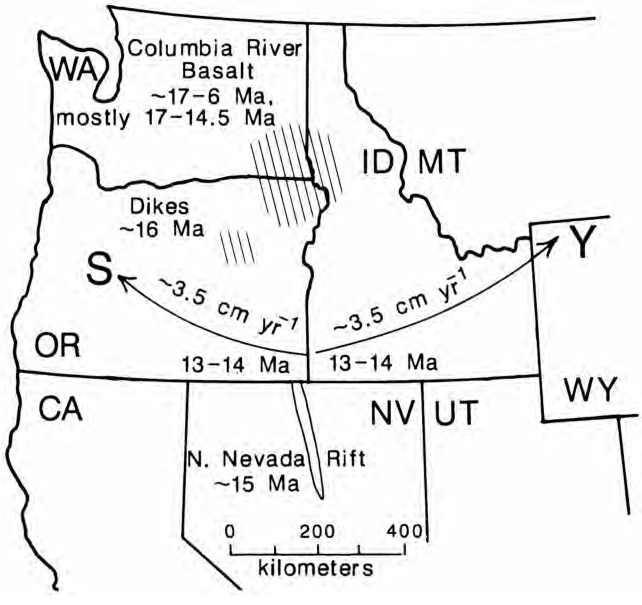

FIGURE 17—Map showing spatial and temporal relations of dikes of Columbia River Basalt Group, Northern Nevada rift, and direction, onset time, and rates of migrating silicic volcanism toward South Sister, Oregon (S) and Yellowstone (Y). See text for discussion.

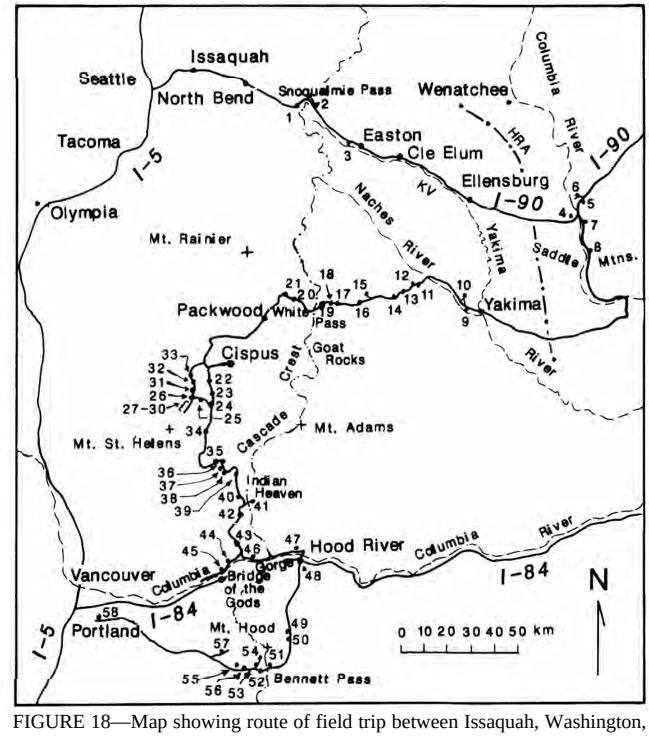

FIGURE 18—Map showing route of field trip between Issaquah, Washington, and Portland, Oregon. Numbers are stops. KV, Kittitas Valley; HRA, Hog Ranch axis.

volcanic rocks on the east flank of the Cascade Range west of Yakima, ending in Packwood. The third day will involve a trip to the Mount St. Helens area, stressing the Tertiary geology as well as the May 18, 1980, eruption. The fourth day will be devoted to hiking trips around Mount St. Helens, including an arduous trip into the crater and a less strenuous excursion onto the Pumice Plain. No guide has been written for this trip, because the area is not open to the public and we do not want to encourage self-guided tours. However, we will supply handouts. The fifth day involves a long drive on back-country roads to see Quaternary basalt of the Indian Heaven area, including subglacial deposits, and some of the geology of the Columbia Gorge, ending in Hood River, Oregon. The sixth day emphasizes the Quaternary volcanic geology of Mount Hood and ends in Portland.

Cumulative mileage is listed for each day of the trip, and interval mileages are given in boldface at the end of each entry. Numerous mileage check points are available.

Day 1, Issaquah to Yakima via Vantage

Drive east on 1-90 from Seattle to Issaquah.

Mileage

0.0 Exit 17 to Issaquah; continue on I-90. **0.7**

0.7 Climb onto kame terrace formed about 12 ka by the Puget Lobe during the Vashon stage of the Fraser glaciation. Large gravel pit visible to left just before start of log is in this terrace. **1.0**

1.7 Hills are underlain by the Puget Group. **1.4**

3.1 High Point offramp. Tukwila Formation, andesitic mudflow breccias of middle Eocene age, in roadcuts to left. The Tukwila is probably correlative with the Naches Formation, about 44–40 Ma (Tabor et al., 1984). **1.5**

4.6 Tukwila Formation in roadcut to left. **4.9**

9.5 Exposures of steeply dipping arkose and volcaniclastic rocks of the Eocene Puget Group. The Puget Group is moderately folded in most places. It crops out discontinuously from here to North Bend. **2.1**

11.6 Craggy peak to left is Mount Si, underlain by Jurassic gabbroic and diabasic greenstone, possibly a dismembered ophiolite and its sedimentary cover in the western melange belt of Frizzell et al. (1984). The belt contains mostly Jurassic and Lower Cretaceous rocks and bounds the west flank of the Cascades north of here. **5.0**

16.6 Rugged ridge crest at 11:00 is underlain by the Snoqualmie batholith. **1.0**

17.6 Low ridge ahead is a kame terrace formed by the Puget Lobe about 12 ka. Such features were built as deltas formed in lakes when the Puget Lobe blocked drainage from the Cascades. **2.0**

19.6 Range front of the Cascades, here mostly underlain by the volcanic rocks of Huckleberry Mountain (Frizzell et al., 1984), correlative with the Ohanapecosh Formation seen later in the trip. **3.5**

23.1 Gabbro related to Snoqualmie batholith in roadcut on left. From here road stays in the batholith for 9–10 mi and enters the area of Fig. 5 near Stop 1. **8.7**

31.8 **STOP 1. Snoqualmie batholith.** Pull off on shoulder of freeway. If this is deemed too dangerous, vehicle can continue for 0.4 mi to a small road where parking is available, and geologists can walk back to stop. In roadcut view granodiorite of the Snoqualmie batholith, cut by aplite veins and containing mafic enclaves. The Snoqualmie is a large composite intrusive body and one of a series of shallow mid-Tertiary plutons in a narrow north–south belt in the Cascades. Radiometric ages are consistently between 20 Ma and 17 Ma (Frizzell et al., 1984), mostly about 19 Ma, in this area, which is the main outcrop area of the batholith. The eastern part of the batholith, where individual plutons such as the Grotto have been delineated, is older, about 25 Ma. The batholith consists mainly of hornblende–biotite granodiorite and tonalite but includes gabbro, diorite, monzonite, and granite.

Sandstone float from the Naches Formation occurs along the road. **1.0**

32.8 Bare Snoqualmie Mountain in distance, 1890 m elevation. Contact with hornfelsed basalt of the Naches Formation in roadcut nearby. **2.1**

34.9 Roadcuts in argillite and sandstone of the Guye Sedimentary Member of the Naches Formation (Tabor et al., 1984), metamorphosed by the batholith. **0.6**

35.5 Summit of Snoqualmie Pass, 921 m, the lowest pass across the Washington Cascades owing to the presence of nonresistant argillite in the Guye. **2.1**

37.6 Leave freeway at Hyak–Rocky Run exit. **0.2**

37.8 Turn left at stop sign and go under freeway. **0.3**

38.1 Turn right on pavement toward Rocky Run. **0.4**

38.5 **STOP 2. Mount Catherine Rhyolite Member of Naches Formation** (Tabor et al., 1984), a welded ash-flow tuff. Bus can stop on road, which has little traffic. Two fission-track ages of about 35 Ma for the Mount Catherine have probably been reset by Snoqualmie batholith from true ages of about 44–40 Ma (Tabor et al., 1984). Note steeply dipping (about 65° SE), vague foliation in the welded tuff. **0.2**

38.7 Bus turnaround. High country to left up Gold Creek is underlain chiefly by basalt and feldspathic sandstone of the Naches Formation. **1.2**

Return to freeway and turn east toward Spokane.

39.9 Lake Keechelus on right is a natural lake further dammed for irrigation use. Roadcuts expose sandstone of the Naches Formation to mileage 42.6. **2.7**

42.6 Start of series of roadcuts in massive dacitic ash-flow tuff of Lake Keechelus (Frizzell et al., 1984). Zircon fission-track ages are 32–30 Ma, equivalent to age of Ohanapecosh Formation farther south, where similar tuff is interbedded with Ohanapecosh. The tuff is quartz-phyric and contains numerous large pumice lapilli and lithic inclusions. It is columnar jointed in places, and commonly thoroughly welded and lithophysal. The tuff has a relatively gentle dip and rests on the eroded surface of the steeply dipping Naches Formation. It forms both north and south shores of Lake Keechelus. **1.8**

44.4 Last roadcut in the tuff of Lake Keechelus. **1.5**

45.9 Roadcuts in an ash-flow tuff in Naches Formation dipping about 45°. The freeway stays in Naches Formation until it crosses Straight Creek fault. The Naches consists chiefly of interbedded sandstone

and a variety of volcanic rocks, chiefly basalt, basaltic andesite, and rhyolite, forming a more or less bimodal suite. It is about 4 km thick, comparable to the Puget Group farther west, and was apparently deposited in a subsiding extensional basin. The Naches is highly deformed; near-vertical dips are common in this area. It comprises most of the Cabin Creek block of Tabor et al. (1984) and Frizzell et al. (1984), a structural block west of Straight Creek fault. The freeway follows southeast strike of the formation. **8.8**

54.7 Basalt flows of the 48–47 Ma Teanaway Formation (Tabor et al., 1984) occur at 10:00 on a ridge in Teanaway River structural block east of Straight Creek fault (Frizzell et al., 1984). **0.5**

55.2 Leave I-90 at Exit 70. At stop sign follow road toward Easton. **0.4**

55.6 **STOP 3. Straight Creek fault.** Look up Lake Kachess valley, which is trace of Straight Creek fault (Fig. 5), to see Teanaway Formation overlying steeply dipping Silver Pass Volcanic Member of Swauk Formation (Tabor et al., 1984) in Teanaway River block. The Silver Pass Member, chiefly andesitic to dacitic flows and pyroclastic rocks, is about 1.8 km thick and is interbedded with fluvial subquartzose sandstone of Swauk Formation. The Silver Pass is 52–50 Ma on basis of zircon fission-track ages (Vance and Naeser, 1977; Tabor et al., 1984). The Straight Creek fault is a major structure with possible right-lateral displacement extending from central Washington into Canada (Misch, 1977; Davis et al., 1978). The northern segment of the fault in Washington separates low-grade metamorphosed rocks on the west from plutonic and high-grade metamorphic rocks of the North Cascades on the east. The southern segment separates lower Eocene sedimentary and volcanic rocks on the east (Teanaway River block) from upper Eocene to Oligocene(?) rocks on the west (Cabin Creek block) (Tabor et al., 1984). Movement of southern part of the fault began at or before 48–47 Ma, as reflected by angular unconformity separating Silver Pass Member from overlying Teanaway Formation. Movement continued until at least 42 Ma, because Naches Formation is cut by fault splays. The 25 Ma eastern part of Snoqualmie batholith is not offset by the fault (Vance and Miller, 1981). **0.4**

Bus can continue along road, turn around, and come back to the site. Return to freeway.

56.0 Re-enter eastbound freeway. Just to south the Straight Creek fault bends southeast and splits into splays covered by the 17–15 Ma Grande Ronde Basalt. **5.4**

61.4 Teanaway Formation underlies ridge to left. Light-gray exposures on ridge behind Cle Elum are sandstones of Roslyn Formation. **7.3**

68.7 At 12:00 is Lookout Mountain (Fig. 5), underlain by N_2 and R_2 flows of Grande Ronde Basalt near western limit of area underlain by Columbia River Basalt Group. The basalt dips about 5° SE and defines the plunging trough of Kittitas Valley syncline. Grande Ronde Basalt also forms most of Cle Elum Ridge south of the valley, where it rests on Teanaway Formation (Tabor et al., 1982b). **9.1**

As we drive, observe Stuart Range northwest of here. The brown rocks are ophiolite of Upper Jurassic and Lower Cretaceous Ingalls Tectonic Complex (Miller, 1985a; Tabor et al., 1987). The gray peaks are tonalite of Upper Cretaceous Mount Stuart batholith.

77.8 Elk Heights pass. From here the route is within Kittitas Valley syncline, developed principally in Grande Ronde Basalt. The basalt is overlain in most places by Pliocene Thorp Gravel capped by modern stream alluvium and glacial drift. **5.4**

83.2 White bluffs to north are in volcaniclastic rocks of Ellensburg Formation interbedded with flows of Grande Ronde Basalt. The Ellensburg here is pumiceous diamict and sandstone that indicates contemporaneous dacitic volcanic activity in the Cascades as the Grande Ronde Basalt was being erupted. **1.8**

85.0 Dark exposures north of road are type locality of Thorp Gravel, deposited by ancestral Yakima River and its tributaries. The gravel contains two facies: mainstream alluvium dominated by durable silicic volcanic rocks derived from Naches and Ohanapecosh Formations, and sidestream alluvium eroded from Grande Ronde Basalt in the limbs of the syncline (Waitt, 1979; Tabor et al., 1982b). Waitt (1979) recognized three east-trending faults cutting the Thorp, which is about 4 Ma on the basis of fission-track ages on interbedded tuff and is youngest deformed unit in the area. **2.3**

87.3 To south is Manastash Ridge, a complex thrusted anticline. Manastash is one of the most northern uplifts in Yakima fold belt (Bentley, 1977). **7.4**

94.7 Continue past Exit 109 to Canyon Road, which follows Yakima River Canyon across several well-exposed, east-southeast-trending anticlines and synclines. The river follows structural sags in the anticlines and thus is considered consequent (Waitt and Swanson, 1987). Continued folding caused the river to incise anticlines within the broad N–S sag between the Hog Ranch and Cascade uplifts (Schmincke, 1964; Waitt and Swanson, 1987). **0.8**

95.5 Continue past junction with I-82. Cuts along I-82 show deformed Wanapum Basalt and interbedded Ellensburg Formation (Bentley, 1977), but are hard to see owing to restrictions against walking along freeway. **2.6**

98.1 Kittitas Valley gradually ends to east, where a low south-trending ridge system, the Hog Ranch uplift (Mackin, 1961), cuts off southeast-trending Kittitas Valley syncline. The uplift, largely defined by culminations of transverse anticlines, is a southward extension of Naneum Ridge anticline (Tabor et al., 1982b). Major east-trending folds cross the uplift. **7.4**

105.5 Cuts in coulee left of freeway show pillowed flow in Frenchman Springs Member, which in this area is separated from Grande Ronde Basalt by tuffaceous sandstone in Vantage Member of Ellensburg Formation. Exposures of Frenchman Springs (in places pillowed), Vantage, and upper flow of the Grande Ronde occur for many miles as highway crosses Hog Ranch uplift. **5.4**

110.9 Ryegrass Crest, 773 m elevation. From here high-

way descends from Hog Ranch uplift to Columbia River. White tuffaceous sandstone of Vantage crops out in places between Frenchman Springs Member and underlying Grande Ronde Basalt. **10.3**

121.2 Exit 136. Leave I-90 toward Vantage. **0.3**

121.5 Stop, turn left, and drive through Vantage. **0.7**

122.2 Turn right to Ginkgo Museum. **0.5**

122.7 **STOP 4. Ginkgo Museum; basalt stratigraphy.** The museum displays petrified wood from the Vantage Member. The trees and logs were engulfed by, and mixed with, pillows and hyaloclastic debris when the basal flow of the Frenchman Springs Member crossed a swamp. The wood, chiefly cypress and ginkgo, indicates a warm, humid to wet setting, quite different from today's aridity.

Across the Columbia River, I-90 follows a prominent bench eroded along Vantage Member. The bench rises northward toward crest of Frenchman Hills anticline. Flows in Grande Ronde Basalt below Vantage Member have been given informal names. The two best known are the Museum member, the thin upper flow just below the east bridge abutment and the museum, and the underlying Rocky Coulee member, a thick, complex flow that forms most of the cliff near east end of bridge. Flows of Wanapum Basalt above Vantage Member likewise have only informal names but belong to formal members (Fig. 13). The lowest, named the Ginkgo flow by Mackin (1961), is mostly covered by talus above east end of bridge; it is the flow beneath which the petrified forest occurs. The overlying flow, the Sand Hollow, has a "double-barreled" jointing aspect (Mackin, 1961) that suggests a compound cooling unit. The highest flow is the Sentinel Gap, here consisting of foreset-bedded pillows and hyaloclastite near the flow terminus. All three flows belong to Frenchman Springs Member. On skyline is Roza Member, and still farther back from river is Priest Rapids Member. These three members can be traced across much of the Columbia Plateau and form key marker units whose distributions, vent areas, and chemical compositions are among the best known of the province. **2.4**

Return to eastbound I-90.

125.1 Straight ahead note foreset-bedded pillows in Sentinel Gap flow on top of cliff. North dip of foresets indicates direction of flow. **1.8**

126.9 West of river, note the museum and the bench formed on top of Grande Ronde by stripping of the Vantage. **4.5**

131.4 Exit 143. Turn right on Champs deBrionne Winery road. **0.3**

131.7 **STOP 5. Roza Member pépérite; Priest Rapids Member.** Just before intersection with the winery road. Plagioclase-phyric Roza Member invades diatomite to form a pépérite, which is overlain by silicic tuff capped by very sparsely plagioclase-phyric Priest Rapids Member (Fig. 19). Note the stringers and dikelets of Roza mixed with diatomite, and the sharp contact between the pépérite and the younger tuff. Observe the sparsely phyric Priest Rapids and contrast it with the highly plagioclase-phyric Roza. Note that the vesicular top of the Roza is relatively less phyric than the rest of the flow. **0.1**

FIGURE 19—Person points to Roza Member of Wanapum Basalt invading and mixed with diatomite to form pépérite at Stop 5. Priest Rapids Member of Wanapum (top of photo) overlies thin silicic tuff (massive unit above lithic-rich pépérite near upper right edge of photo) deposited on pépérite.

131.8 Turn left on Champs deBrionne Winery road. **0.7**

132.5 Turn left at stop sign. **0.2**

132.7 Roza Member in roadcut. **0.4**

133.1 Bench on top of Frenchman Springs Member. Farther along, roadcuts show the vesicular top on this flow, the Sand Hollow. **0.6**

133.7 **STOP 6. Spiracle at base of Roza Member; jointing in basalts.** Spiracles presumably form as steam blasts through a flow from a wet substrate. A natural "Stonehenge" of platy columns has been eroded from Roza Member just beyond stop. Platy jointing is common in relatively coarse flows; the joints do not cross column boundaries and probably form during cooling. Frenchman Coulee below is a flood-carved coulee eroded as waters poured from Quincy basin to northeast and descended to the Columbia. The coulee is dry except for excess irrigation water. White mounds on Roza Member north of coulee are spoil from diatomite mines in Squaw Creek Member of Ellensburg Formation, the deposit invaded by the Roza. Note the varied jointing patterns of flows in the coulee wall, which illustrate the problems in using jointing habits for flow correlation. **0.1**

133.8 Good bus turnaround. Return to I-90. **1.9**

135.7 Turn right onto I-90. **1.2**

136.9 At 12:00 is good view of high sharp peak in distance, Whiskey Dick Mountain. Shell Oil drilled an exploration hole near Whiskey Dick, as well as in several other areas in the western plateau, during the 1980's. The Whiskey Dick hole penetrated about 1.5 km of basalt, and a hole in the Saddle Mountains south of here went through more than 3.5 km of basalt, about 3.2 km of which was Grande Ronde only. No oil was found in the target beneath the basalt, presumably Eocene sandstone. Few data are publicly available for these holes. Drilling was continuing in summer 1988. **3.8**

140.7 Roadcut in Museum flow and underlying hackly jointed Rocky Coulee flow of Grande Ronde Basalt. **0.7**

141.4 Take Highway 26 at Exit 137. **0.7**

142.1 Good exposure in cliff at 9:00 of "double-barreled" Sand Hollow flow. **0.7**

142.8 Keep left at junction with Highway 243. **0.2**

143.0 **STOP 7. Pillows and palagonite in Ginkgo flow of Frenchman Springs Member.** Mouth of Sand Hollow; walk 100 m to next roadcut. Note the dipping foresets in a lava delta that indicates local movement toward the west or northwest. **2.2**

145.2 Bus turnaround at road junction. **2.4**

147.6 Return to Highway 243 and turn left. **0.3**

147.9 Start up grade across Frenchman Springs and overlying Roza Members. Type locality for the Wanapum Basalt, named from nearby Wanapum Dam. **4.3**

152.2 At 12:00 is Sentinel Gap, eroded across Saddle Mountains anticline (Reidel, 1984). **2.7**

154.9 White layer high on west wall of Sentinel Gap is sandstone of Vantage Member. **2.9**

157.8 **STOP 8** at turnout along right side of highway in Sentinel Gap. The Sentinel Bluff section of basalt here has been closely studied by geologists formerly of Rockwell Hanford Operations, in particular Steve Reidel (Reidel, 1984) and Phil Long (Long and Wood, 1986; McMillan et al., 1987), during investigation for a potential nuclear-waste repository within the basalt on the Hanford Reservation. The four oldest exposed flows are in Grande Ronde Basalt, have a relatively low-MgO composition (Myers and Price, 1979), and are assigned to Schwana unit. The oldest Schwana flow, not exposed here but cropping out just to north, has reversed magnetic polarity. The youngest Schwana flow, the Umtanum, is approximately 60 m thick, divided equally between a lower colonnade and an upper entablature. The Umtanum was the main candidate flow for the nuclear-waste repository at Hanford. Overlying the low-MgO flows are eight relatively high-MgO flows in Sentinel Bluffs unit of Grande Ronde (Myers and Price, 1979), the uppermost of which is the Museum flow. A prominent bench, eroded back along Vantage Member of Ellensburg Formation, separates the Sentinel Bluffs unit from the overlying Frenchman Springs Member of the Wanapum Basalt. Work based on jointing in this section and elsewhere led Long and Wood (1986) and DeGraff and Aydin (1987) to conclude that entablatures are produced by rapid cooling as water percolates downward into opening joints.

A prominent tongue of basalt southwest of the gap (the Huntzinger flow of Mackin, 1961) belongs to the Asotin Member of the Saddle Mountains Basalt; it partly fills a paleovalley eroded into the Priest Rapids Member of the Wanapum Basalt along course of ancestral Columbia River about 13 Ma.

The Saddle Mountains anticline is asymmetric with a faulted north limb. The fold axis on east side of river is 2.5 km south of that on west side, perhaps because of a tear fault (Reidel, 1984). The Saddle Mountains fault is a reverse fault best exposed across river on north limb of fold. Some flows thin and even pinch out against the uplift, as does Vantage Member (Reidel, 1984). Apparently the fold was growing during deposition of basalt and interbeds.

Ash erupted about 7 ka from Mount Mazama (Crater Lake, Oregon) 475 km to south occurs in colluvium. Evidence of the Missoula floods is obvious. **1.2**

159.0 High on ridge at 8:00 is an abandoned quarry exposing two layers of vitric rhyolite tuff between Wanapum and Saddle Mountains Basalts. The lower tuff, as thick as 15 m, contains prominent layers rich in accretionary lapilli (Schmincke, 1967a, 1967c). The Pomona Member of Saddle Mountains Basalt invades the tuff just above lapilli layers. This duo—Pomona lying above accretionary lapilli in a vitric tuff (commonly welded) (Schmincke, 1967c)—occurs in many places on the Columbia Plateau as far east as Clarkston, Washington. The ash and far-flung accretionary lapilli testify to a powerful explosion in the Cascades just before eruption of Pomona Member in northern Idaho about 12 Ma. **5.2**

164.2 Ahead is Umtanum Ridge, one of the larger and most studied anticlines on the Plateau (Price, 1982). **5.5**

169.7 At 12:00 is view of rollover in Umtanum Ridge anticline. The north limb is locally overturned. The fold is cut by thrust faults (Price, 1982). **1.1**

170.8 Steeply overturned flow at 3:00. **1.7**

172.5 Road travels along 82 km Hanford Reach, the only free-flowing stretch of Columbia River from Canadian border to Bonneville Dam near Portland. **3.2**

175.7 Stay right at junction to Vernita Bridge. **2.5**

178.2 Pomona Member overlies Umatilla Member of Saddle Mountains Basalt on hillslope along grade up from Vernita Bridge. Ridges in distance, Gable Mountain and Gable Butte, are local culminations of largely buried Umtanum Ridge anticline. **3.8**

182.0 Turn right on Highway 24 toward Yakima. Road goes up Cold Creek syncline, whose lower, broader part was the favored site of a planned storage repository for high-level nuclear waste. The site was abandoned in 1988 in favor of one in Nevada, owing to a complex decision involving hydrologic questions and politics. **4.9**

186.9 Ridge at 10:00 is Rattlesnake Hills. Near its crest, the first deep hole was drilled on the Columbia Plateau in 1957–58, a wildcat owned by Standard of California. The hole bottomed at 3248.6 m in Grande Ronde Basalt, as interpreted from the chemical compositions of the cuttings (Reidel et al., 1982). Drilling by Shell in 1980's confirmed the great thickness of the basalt, particularly the Grande Ronde.

Scattered outcrops for next several miles expose Pomona and Elephant Mountain Members of Saddle Mountains Basalt. **2.3**

189.2 Keep right at junction with road to Sunnyside, and follow axis of Black Rock syncline. **2.5**

191.7 Ridge to left is continuation of Rattlesnake Hills, which extends from 50 km west of Yakima to 23 km southeast of Pasco, a total length of about 175 km—the longest anticlinal structure on the Columbia Plateau. **14.5**

206.2 Rounded hill at 11:00 is Elephant Mountain, local high point on Rattlesnake Ridge anticline and type locality of Elephant Mountain Member of Saddle Mountains Basalt (Waters, 1955; Schmincke, 1967a). The Elephant Mountain erupted in northeast Oregon

about 10.5 Ma and flowed via a canyon system to the western plateau (Swanson et al., 1979a). **9.1**

215.3 At 9:00 is Union Gap, a water gap exposing Wanapum and Saddle Mountains Basalt cut by Yakima River through Rattlesnake Hills anticline. **3.8**

219.1 Turn north on I-82. **3.1**

222.2 Exit 31 to North First Street in Yakima.

Day 2, Yakima to Packwood

Mileage

0.0 Entrance to freeway bypass at north end of North First Street in Yakima. **0.1**

0.1 Selah Gap cut through Yakima Ridge anticline exposes flows of Frenchman Springs and Priest Rapids Members. **2.7**

2.8 At 11:00 is bluff of Tieton Andesite. **0.7**

3.5 Turn left on Ackley Road. **0.1**

3.6 **STOP 9. Tieton Andesite.** At stop sign turn left and park. Walk 100 m west and climb stairs to view the reversely magnetized, 1.0 Ma Tieton Andesite. This is an archaeological site (Indian paintings); **do not sample here;** a sampling opportunity may be possible at Stop 11. This is the most voluminous of several flows erupted from the Goat Rocks volcano, a Pliocene and Pleistocene andesitic cone on the crest of the Cascades 80 km west of here. The flow poured down the ancestral canyon of Tieton River until debouching into the lower-gradient Naches Valley, where it spread out, developed pressure ridges and tumuli, and terminated at this site (Warren, 1941; Becraft, 1950; Swanson, 1964, 1978; Clayton, 1983). The flow has about 60% SiO_2, 2.8% K_2O, and is a high-potassium andesite. It contains 30–35% phenocrysts of plagioclase (greatly dominant), clinopyroxene, hypersthene, and magnetite. These characteristics suggest rather low fluidity, yet it is the longest known andesite flow, longer than any in Walker's (1973) compilation. Apparently the flow advanced so far because of its large volume (conservatively estimated as 2 km^3), possibly high eruption rate, and confined course in the canyon. Note the complicated columnar joints, which probably record cooling against a vertical channel wall eroded into volcaniclastic rocks of the Ellensburg Formation (since removed). Note the glassy texture, typical of its entire length. **0.1**

3.7 Return to highway and turn left. **0.8**

4.5 Turn right on Old Naches Highway and stay left at Y-junction immediately after turn. **0.8**

5.3 Turn right on Mapleway Road. Bluffs ahead and to left are considered by many workers as the "type" locality of Ellensburg Formation, although Ellensburg itself is more than 30 km farther north. **0.6**

5.9 Roadcut exposes tuffaceous sandstone and dacite-rich conglomerate representative of the volcaniclastic upper part of the Ellensburg Formation in this area. The dacite was produced by explosive activity in the Cascades mostly between 12 and 8 Ma (Smith et al., 1988). Specific sources have not been identified, but a dacite porphyry intrusion near Bumping Lake 60 km west-northwest of here has a K–Ar age of 8.8 ± 0.2 Ma and could be an Ellensburg feeder (Smith et al., 1988). The Ellensburg here is overlain by dacite-poor conglomerate that contains reworked tephra with a K–Ar age of 7.4 ± 0.4 Ma (Smith, 1988). Smith (1988) interprets the dacite-poor conglomerate, forming part of his Pleasant Hill conglomerate unit, as partly filling a paleovalley eroded into the volcaniclastic Ellensburg Formation. **0.3**

6.2 **STOP 10.** Examine pumiceous debris flow with fine-grained base in Pleasant Hill conglomerate (Fig. 20). The origin of the fine-grained base, a photo of which appears in Schmincke (1967b), is debatable. The debris flow contains scattered prismatically jointed blocks of dacite, rests on dacite-poor conglomerate, and underlies dacite-rich conglomerate. Apparently the debris flow formed during a period of renewed dacitic volcanism in the ancestral Naches River basin (Smith et al., 1988). Walk to bottom of grade from here to examine deposits described at mileage 5.9. Bus continues up hill. **0.3**

6.5 Bus turns around at top of hill, returns to bottom of hill, and waits for group. **1.1**

7.6 Stop at Old Naches Highway and continue straight on Mapleway Road. **1.1**

8.7 Turn left on McCormick Road and then right on Highway 12. **0.2**

8.9 At 9:00 is bluff of Tieton Andesite. The present flow margin probably approximates its original margin, a conclusion consistent with its overall jointing characteristics. If so, the Naches Valley has widened about 2 km to its present position in the last 1 m.y., presumbly when high discharge during glacial periods eroded the relatively nonresistant deposits of the Ellensburg. Wells drilled on the bluff tap water from river gravel below the Tieton Andesite, good evidence that the flow advanced down the main channel of the ancestral Naches. Presumably the Naches then re-established itself along the margin of the flow and commenced widening its valley asymmetrically northward. **2.5**

11.4 At 3:00 Pomona Member of Saddle Mountains Basalt rests on white tuffaceous rocks of Ellensburg Formation. **0.8**

FIGURE 20—Fine-grained base of pumiceous debris flow containing rare " hot" dacite blocks. Stop 10.

12.2 Roadcut in Frenchman Springs Member of Wanapum Basalt just before substation. This is the farthest west the Frenchman Springs and Pomona can be traced in this area. **0.7**

12.9 Bluffs to north show Ellensburg stratigraphically higher than Pomona Member. **0.9**

13.8 Ahead is Cleman Mountain, one of the highest anticlines on Columbia Plateau. It stood high enough to trap most coarse Ellensburg detritus in the Nile basin just west of the mountain, keeping it from reaching the Naches Valley (R. S. Fiske, oral comm. 1962; Smith, 1988). The anticline continued to grow after Ellensburg deposition to its present elevation. **2.5**

16.3 Good views of Tieton Andesite left of road. Note hummocky nature of its surface, caused by large pressure ridges. Cleman Mountain looms at 1:00. The south limb of the anticline is locally overturned. The structure of the anticline is poorly known, owing to absence of marker flows younger than Grande Ronde and to complexity of the structure itself. **3.5**

19.8 Turn left toward White Pass on Highway 12. **0.2**

20.0 Cross Naches River just upstream from mouth of Tieton River. View to left of Tieton Andesite, which flowed down the Tieton River canyon. Note angular discordance with underlying northeast-dipping Grande Ronde Basalt. Remnants of Tieton Andesite hang on walls of canyon, carved in Grande Ronde Basalt and Fifes Peak Formation, for next 30 km into Tieton basin. Tieton Andesite can generally be recognized in the canyon by its unconformable contact and notable columnar jointing, commonly with an entablature above long subvertical columns. **1.9**

21.9 Entrance to Oak Creek Wildlife Recreation Area. Exposures at 2:00 show Tieton Andesite only a few meters above river level. Apparently base level did not change much during the last Ma, so that no downcutting took place except through the lava flow. **0.7**

22.6 **STOP 11. Base of Tieton Andesite.** Dangerous curve. Pull bus to left of road if traffic is light. Tieton Andesite rests on imbricated boulder gravel of ancestral Tieton River (Fig. 21). East of river, erosional unconformity between Grande Ronde Basalt and Tieton Andesite is well exposed. **1.3**

23.9 **STOP 12. Sedimentary interbeds between Grande Ronde flows.** Micaceous sandstone and siltstone between two N_2 flows of Grande Ronde Basalt (Fig. 22; locality 2 in table 10 of Swanson, 1967). The lower flow is invasive into wood-bearing subarkose, probably unconsolidated at time of invasion; note dense glassy top on the flow and disruption and tilting of sediment. Mica-bearing sediment and accompanying metamorphic and plutonic heavy-mineral suite (Swanson, 1967) indicate a northern provenance and therefore imply a south-flowing river during Grande Ronde time, which is interpreted from regional evidence to be ancestral Columbia or a major tributary. During Grande Ronde time, no ancestral Columbia is known from within the Columbia Plateau itself. A reasonable interpretation is that the river had been diverted to margin of the province by basalt flows (Fecht et al., 1987; Waitt and Swanson, 1987). Mixed with the metamorphic and plutonic suite is a pyroclastic suite, including euhedral oxyhornblende, glass shards, and glass-rimmed plagioclase and mafic minerals. This suite provides clear evidence of explosive activity from Cascade volcanoes during Grande Ronde N_2 time, 17–16 Ma. Pyroclastic debris in older interbeds shows that Cascade activity also occurred in N_1 and R_2 time. **0.8**

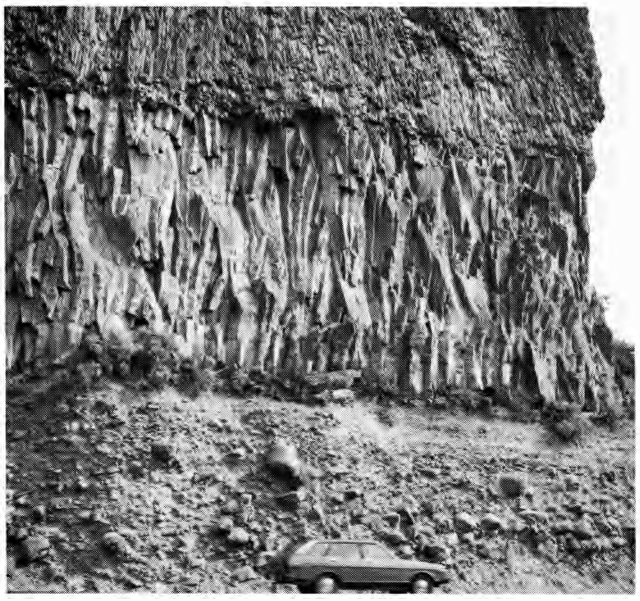

FIGURE 21—Base of columnar Tieton Andesite resting on gravel of ancestral Tieton River, Stop 11.

24.7 Steep contact between Tieton Andesite and Grande Ronde Basalt at 11:30. **1.5**

26.2 Roadcut shows flow of Grande Ronde Basalt that invaded unconsolidated micaceous sand (locality 1, table 10 of Swanson, 1967). **1.7**

27.9 Windy Point measured section of Grande Ronde Basalt ahead. Lower three flows are in magnetostratigraphic unit R_2, and the upper nine in N_2 (Swanson, 1978). **0.6**

28.5 Polished fault plane cutting pillows of Grande Ronde. The fault cannot be traced from the cut. **0.3**

28.8 Pillowed Grande Ronde Basalt west of bridge. **0.2**

FIGURE 22—Micaceous sandstone and siltstone between flows of Grande Ronde Basalt at Stop 12. Lower flow invades sandstone. Hammer at contact.

29.0 **STOP 13. Tieton volcano.** Local margin of Grande Ronde Basalt, where it lapped onto eroded remnant of Tieton volcano (Swanson, 1966, 1978), a large stratocone in the Fifes Peak Formation (Fig. 23). The contact is obscured by landsliding. Note the foreset-bedded lava delta in one of the lower R_2 flows of Grande Ronde that indicates westward advance of the basalt.

The base of Tieton volcano consists of gently dipping two-pyroxene basaltic andesite flows that lap against the deformed flanks of an older cone and form a shield about 200 m thick (Fig. 24). More than 1500 m of bedded tuff, lithic-lapilli tuff, and breccia overlie the shield (Fig. 25); the steep radial dips of fragmental rocks define a volcaniclastic cone. The reconstructed volcano had a basal diameter of at least 1.5 km and probably towered 2400–3000 m above its base before erosion and partial inundation by Grande Ronde Basalt.

On Bethel Ridge, 6–10 km west of the center of the volcano, at least 300 m of gently dipping debris-flow deposits (mainly lahars), lava flows, and low-silica rhyolitic pyroclastic flows can be traced nearly continuously into the cone. Some breccias thin and pinch out to the west, and one andesite flow ends with westward-inclined foreset lenses of breccia and lava at its snout. The Bethel Ridge rocks probably formed part of a lowland apron at the foot of Tieton volcano.

The volcano erupted block-lava flows, coarse- to fine-grained bedded tuff, and chaotic breccia of multiple origins. Intruding them are more than 200 dikes that form the southern half of a radial swarm centered on the volcano. Single dikes are 1.5–6 m wide and dip 70–90°. They decrease in abundance upward in the volcano and were injected subvertically, not laterally, as indicated by lineations on the dike margins. The dikes and lava flows are medium-K mafic and slightly silicic andesite (or basaltic andesite and lesser andesite).

A lava flow in the apron of Tieton volcano yielded a fission-track age of 23.3 ± 2.0 Ma (Vance et al., 1987, sample JV 140). Other isotopic ages for the Fifes Peak Formation range from 20.0 ± 2.0 to 27.3 ± 2.9 Ma (Vance et al., 1987). Centers similar to those in the Tieton River area occur at the "type" locality in the Fifes Peaks themselves, 40 km northwest of Tieton volcano.

Tieton volcano cannot be seen well from the highway, because the canyon is so narrow, but it is splendidly displayed from a high ridge road, inaccessible to buses, that turns off at mileage 28.3. Many of the radial dikes are visible from the highway, however. Keep track of their trends as we drive through the canyon to convince yourself that they radiate from a common center. **0.2**

Holocene	Alluvium and colluvium
Pleistocene	Intracanyon flows of hypersthene-augite Tieton Andesite (1 Ma) and olivine basalt erupted from vents near Goat Rocks and the White Pass area. Overlain and underlain by till.
Pleistocene and Pliocene	Small plugs of olivine basalt and andesite.
	UPLIFT
Pliocene(?)	Gravel on top of Grande Ronde Basalt
	EROSIONAL AND ANGULAR UNCONFORMITY
Middle Miocene	Grande Ronde Basalt (approx. 17-15 Ma). As much as 520 m of gently eastward-tilted flows. Local discontinuous interbeds of clastic sediment, tuff, and palagonite.
	EROSIONAL AND POSSIBLE ANGULAR UNCONFORMITY
Early Miocene	Fifes Peak Formation (approx. 23 Ma in this area). More than 1 km-thick section of andesite and basaltic andesite lava flows and breccia, and dacite-rhyolite pyroclastic flows, erupted from at least two large composite cones. Prominent radial dike swarm. Cut by andesitic and microdioritic intrusions in western part of area.
	ANGULAR UNCONFORMITY
Oligocene	Volcaniclastic rocks of Wildcat Creek, probable correlatives with Ohanapecosh Formation (about 32-33 Ma in this area). More than 300 m of volcaniclastic rocks, many of which are graded, have continuous bedding across outcrops, generally lack current structures, and have poorly developed sole marks. Vertebrate fossils. Zeolitized. Probably deposited either by subqueous turbidity currents or subaerial debris flows.
	EROSIONAL AND POSSIBLE ANGULAR UNCONFORMITY
Eocene	Welded tuff of Spencer Creek (about 42 Ma) and associated epiclastic sandstone and conglomerate.
	ANGULAR UNCONFORMITY
Cretaceous and Jurassic	Russell Ranch Formation, graywacke and argillite with lesser pillow basalt (greenstone) and chert. Also includes Indian Creek unit, mainly sheared orthogneiss of tonalitic composition but varying from gabbro to trondhjemite. Together comprise the "Tieton inlier" of pre-Tertiary rocks.

FIGURE 23—Stratigraphy of Tieton River area, simplified from Swanson (1967). Ages for rocks older than Grande Ronde Basalt from Vance et al. (1987). Data for Indian Creek unit from Miller (1985).

30.2 Dike in roadcut, with strike of about 295°. Wallrock is andesite flow and breccia of Tieton volcano. **0.8**

30.0 Slope above road shows rocks of older Fifes Peak volcano cut by radial dikes of Tieton volcano. **0.6**

30.6 **STOP 14. Dike swarm.** Bus stops here. Group walks 100 m ahead to examine roadcut exposing at least 11 basaltic andesite dikes belonging to the radial dike swarm cutting rocks of the older volcano. **1.2**

31.8 Prominent knob to left is Sentinel Rock, capped by Tieton Andesite. **2.2**

34.0 Radial dikes at 3:00. Remnant of Tieton Andesite high on ridge. **1.7**

35.7 Breccia and platy basaltic andesite of older Fifes Peak volcano. The units resemble those of Tieton volcano but can be distinguished by map relations. **0.5**

36.2 Enter Tieton basin, chiefly underlain by landslide debris. **0.8**

37.0 Goose Egg Mountain microdiorite ahead. **0.9**

37.9 Start series of roadcuts in bedded volcaniclastic rocks of Wildcat Creek, possibly stratigraphic correlatives of the Ohanapecosh Formation. A fission-track age of 32.2 ± 3.3 Ma was obtained on a pumiceous ash-flow tuff near the west end of these cuts (Vance et al., 1987, sample JV 139). **0.8**

38.7 Straight ahead is Westfall Rocks, a microdiorite twin of Goose Egg Mountain. **0.3**

39.0 Turn right on Wildcat Road 1306. **0.6**

FIGURE 24—Nearly horizontal andesite flows in basal shield of Tieton volcano, overlain by volcaniclastic cone. Base of shield (dashed line) overlies tilted flows and breccia of older volcano. Between Stops 13 and 14 on north side of canyon.

39.6 Cattleguard. **0.2**

39.8 **STOP 15. Volcaniclastic rocks of Wildcat Creek.** Climb steep slope to examine deposits typical of the upper part of Wildcat Creek unit (Fig. 26), which consists dominantly of laterally extensive, graded beds 1–6 m thick separated by thinly bedded tuff. The lower several centimeters of each thick bed is typically framework-supported, zeolite-cemented lapillistone, which locally has sole marks on its base (Fig. 27). The lapillistone grades abruptly upward into poorly sorted lapilli tuff, which grades gradually upward into well-sorted tuff. The thin beds are commonly graded, and some beds are crudely laminated; small-scale crossbedding and channeling occur in some thin beds.

Clasts are freshly erupted crystals (commonly exhibiting bubble-wall texture), dense lithic fragments (chiefly andesite and dacite), pumice (mostly of the long-tube type), and ash. Accretionary lapilli, both broken and whole, occur in the lapilli tuff and tuff, and fragmentary vertebrate fossils have been found (Grant, 1941; Swanson, 1964; Lander, 1977). All glass is entirely altered to, in order of formation, opal or chalcedony, clay and celadonite, heulandite, mordenite, and calcite.

At base of the outcrop is a poorly exposed pumice-lapilli tuff probably deposited by a pyroclastic flow; this unit is better exposed in roadcuts along Highway 12 and is the one dated by Vance et al. (1987). Farther down section, obvious fluvial deposits occur; current directions indicate southeast-directed transport.

The origin of these beds is debatable. Swanson (1964, 1978) interpreted the thick graded units as products of subaqueous turbidity currents carrying a mixture of freshly erupted and older detritus. Recent work on lahars and hyperconcentrated streamflows (Scott, 1988; Pierson and Scott, 1985; Pierson, 1985; Smith, 1986) raises the possibility of such subaerial origins for these rocks. The volcaniclastic rocks of Wildcat Creek are interpreted as a distal facies of the Ohanapecosh Formation in Mount Rainier National Park, where lava flows and coarser, thicker graded beds occur (Vance et al., 1987). **0.4**

FIGURE 25—Bedded volcaniclastic rocks forming cone of Tieton volcano on north side of canyon between Stops 13 and 14. Note concave-upward attitude.

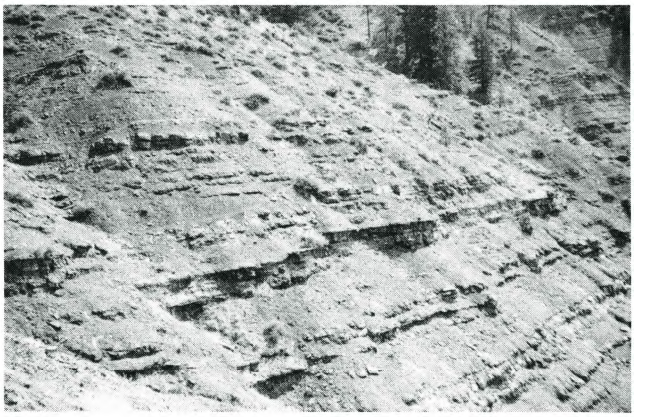

FIGURE 26—Volcaniclastic rocks of Wildcat Creek at Stop 15.

FIGURE 27—Lapillistone base of graded lapilli tuff at Stop 15. Note possible load casts at base of bed.

40.2 Bus turnaround. Return to Highway 12. **1.1**

41.3 Junction with Highway 12. Turn right. **0.2**

41.5 Cross Wildcat Creek. At 5:00 is remnant of a Pleistocene olivine basalt flow that elsewhere fills a channel eroded into Tieton Andesite. **0.3**

41.8 Westfall Rocks microdiorite unit. **1.1**

42.9 **STOP 16. Westfall Rocks microdiorite; uplift of Grande Ronde Basalt.** Margin of Westfall Rocks microdiorite unit with dark hornfelsed Wildcat Creek lapilli tuff hanging on margin (Fig. 28). This intrusion, as well as Goose Egg Mountain and two other dikelike bodies of similar lithology, Kloochman Rock and Chimney Peaks, are of mid-Tertiary age but have not been dated. Whether they are feeders for andesite in the Fifes Peak Formation is problematic. The Westfall Rocks and Goose Egg intrusions are probably connected at depth but have joint patterns that suggest they are separate bodies at the present level of exposure. Both bodies were intruded along the contact between the volcaniclastic rocks of Wildcat Creek and pre-Tertiary rocks of the Rimrock Lake inlier (Miller, 1985b) that underlie Rimrock Lake. The nature of this contact is not clear, but Miller (1985b) believes that contacts of the Rimrock Lake inlier and the Cenozoic rocks "are generally pronounced angular unconformities that only locally show minor modification by faulting."

FIGURE 28—Hornfelsed lapilli tuff along margin of Westfall Rocks microdiorite unit at Stop 16.

Cliffs on the southern skyline expose the Divide Ridge section of Grande Ronde Basalt, about 500 m of basalt and interbedded micaceous sandstone (Swanson, 1967). Twelve to 15 flows are present; the lower three or four are in the N_1 magnetostratigraphic unit, the middle six or seven in the R_2 unit, and the upper three or four in the N_2 unit. At least three sill-like invasive flows occur in the section.

The Grande Ronde dips gently eastward on the flank of the Cascade uplift. The uppermost flow, which correlates with the upper part of the Sentinel Bluffs sequence at Sentinel Gap (Mangan et al., 1986), is at a maximum elevation of about 2100 m at the west end of the ridge (Swanson, 1967, 1978). A similar stratigraphic position below the museum at Vantage is at an elevation of less than 150 m and in the Pasco Basin is as low as 600 m below sea level (Myers and Price, 1979). Structural relief of more than 2700 m is thus indicated. East of Pasco Basin, a general elevation for the top of the Grande Ronde is about 730 m near the northern and northeastern periphery of the province, where the basalt has not been markedly deformed (Swanson et al., 1979c). If this reflects a "stable" datum, then the Divide Ridge area has been uplifted about 1370 m absolutely.

Whether the uplift is truly absolute is uncertain, but the calculation emphasizes the general observation that the Cascade Range at this latitude has been significantly uplifted in the last 15 m.y. About 75% of this uplift is confined to the western 16 km of the present Columbia Plateau, for the top of the Grande Ronde is lower than 580 m near Tampico, about 19 km southeast of here, whereas it is higher than 2100 m only 16 km farther west (Swanson, 1967). West of Divide Ridge the basalt projects into a younger volcanic center (Goat Rocks volcano) built on an uplifted platform of lower Tertiary rocks (Swanson and Clayton, 1983), and the basalt does not occur farther west at this latitude on the western flank of the Cascades.

The gently sloping, flat-topped ridge south of Rimrock Lake is Pinegrass Ridge, underlain by Tieton Andesite and several other Pleistocene lava flows. This marks the pathway by which the long flow of Tieton Andesite moved from Goat Rocks volcano into Tieton basin. **0.6**

43.5 Sheared trondhjemitic phase of the Jurassic Indian Creek unit (Miller, 1985b; Swanson, 1964). **0.1**

43.6 Fault contact of trondhjemite with the "eastern greenstone belt" (Miller, 1985b) of the Russell Ranch Formation. **1.2**

44.8 Roadcuts in Russell Ranch Formation of Jurassic and Cretaceous age (Miller, 1985b) to Indian Creek. This assemblage (dominantly graywacke and argillite, with lesser pillow basalt, radiolarian chert, green tuffs, and red shale) dominates the pre-Tertiary Rimrock Lake inlier, which is the southernmost occurrence of pre-Tertiary rocks in the Washington Cascades. Miller (1985b) believes that "the various rock types originally formed at a considerable distance from each other" and were juxtaposed by faulting and major lateral transport. **4.0**

48.8 Cut along highway at junction is olivine basalt of

Tumac Mountain, a late Pleistocene cone on the Cascade crest 10 km to the northwest (Clayton, 1983). **2.0**

50.8 **STOP 17. Sheared Indian Creek unit,** a weakly foliated orthogneiss that Hopson and Mattinson (1973) suggested was part of a dismembered ophiolite. **0.1**

50.9 Upper Pleistocene hornblende andesite in roadcut. Cuts for next 3 km expose this andesite. **0.6**

51.5 **STOP 18. Hornblende andesite flow.** Park along road just **before** "No Parking" sign. Platy upper Pleistocene hornblende andesite flow erupted from Tumac Plateau north of road. Its vent is not known, but similar flows issued from vents now filled by small domes (Clayton, 1983). Chemical analyses from farther west in the roadcuts indicate silicic andesite (about 62.8% SiO_2) (Clayton, 1983). **1.5**

53.0 Spiral Butte at 12:00 is a hornblende dacite (64–66% SiO_2) dome that merges outward into a 4–5 km long flow (Clayton, 1983). Clayton (1983) suggests that Spiral Butte is the youngest hornblende andesite or dacite vent in the area and is no more than 45 ka, judged from sedimentation rates on the butte below Mount St. Helens tephra layer C (about 36 ka). **0.8**

53.8 **STOP 19. Clear Creek Falls Overlook.** Restrooms. The hornblende silicic andesite of Deer Lake Mountain (Clayton, 1983) forms the falls. It was erupted from a vent about 5 km farther west (now occupied by a 250 m high dome) and advanced into the glaciated North Fork Clear Creek valley. The flow is more than 100 m thick, overlies a basalt dated at 0.65 ± 0.08 Ma, and is normally magnetized (Clayton, 1983). **0.2**

54.0 Outlet for Dog Lake with Spiral Butte towering above. Growth of Spiral Butte dome impounded Dog Lake, according to Clayton (1983). **0.9**

54.9 Roadcuts in Deer Lake Mountain flow. **1.3**

56.2 Summit of White Pass (1362 m), with Deer Lake Mountain flow to north dipping from its dome-like vent. The pass is eroded into relatively nonresistant graywacke and argillite of the Russell Ranch Formation. Chair lift crosses gentle slopes of Russell Ranch capped by more resistant olivine basalt and basaltic andesite erupted in the late Pliocene or early Pleistocene from Hogback Mountain 5 km south of White Pass. **1.1**

57.3 Russell Ranch Formation in roadcuts here and following. **1.2**

58.5 Ridge ahead of Ohanapecosh Formation, in places overlain by quartz-phyric ash-flow tuff of the Stevens Ridge Formation (Swanson and Clayton, 1983). **1.6**

60.1 Roadcuts still in Russell Ranch Formation. **0.9**

61.0 Bench to left across canyon is on top of Clear Fork andesite flow (see Stop 20) (Ellingson, 1972; Clayton, 1983; Swanson and Clayton, 1983). **0.4**

61.4 Cortright Creek (Hammond, 1980) fault zone between Russell Ranch and Ohanapecosh Formations. Miller (1985b) found that the "straightness of the map pattern for much of this contact is compatible with a steep fault" but saw "little evidence to indicate that there has been anything more than minor movement along this contact." Extensive landslides obscure the contact south of here (Swanson and Clayton, 1983). **0.3**

61.7 Cuts in Ohanapecosh Formation, riddled by fine-grained plagioclase-phyric andesitic sills. The sills resemble those in nearby Mount Rainier National Park that Fiske et al. (1963) and Mattinson (1977) ascribe to an early hypabyssal stage of the Tatoosh pluton, a Miocene granodiorite and quartz-monzonite body. **2.0**

63.7 First cuts in the Pliocene or Pleistocene olivine basalt of Hogback Mountain. **1.3**

65.0 Prominent columnar-jointed sill cutting Ohanapecosh Formation in roadcut, near base of measured section of the Ohanapecosh (Fiske et al., 1963). Lower part of formation is exposed farther north, where it intertongues with arkosic sandstone (Vance et al., 1987). **1.2**

66.2 Turn left into Palisades viewpoint. **0.1**

66.3 **STOP 20. Columnar-jointed andesite flow.** Restrooms. The remarkably columnar hornblende andesite of Clear Fork (Fig. 29) (Ellingson, 1972; Hammond, 1980; Clayton, 1983) has 59–62% SiO_2 (Clayton, 1983), slightly lower than other hornblende andesites in the White Pass area. The flow was erupted near Coyote Lake, 9 km to the southeast (Swanson and Clayton, 1983), and moved down the canyon in the late Pleistocene. It partly fills a glaciated canyon but is overlain by Evans Creek Drift (ca 18–15 ka) of the Fraser glaciation. Hammond (1980) suggested, because of the abrupt termination and vertical columns indicative of ponding, that the flow was blocked by the Cowlitz Glacier during the Hayden Creek stade (ca 0.14 Ma) of the Salmon Springs glaciation. **0.1**

66.4 Leave viewpoint and turn left on highway. **0.5**

66.9 Ohanapecosh Formation along road. **1.9**

68.8 Junction of Highways 12 and 123. Turn right and then immediately left into parking area. **0.1**

68.9 **STOP 21. Ohanapecosh Formation.** Restrooms. Roadcut in Ohanapecosh Formation shows wood-bearing, well-bedded volcanic siltstone, lapillistone, and lithic-lapilli tuff above an ash-flow tuff. Thin sill cuts the ash-flow tuff. **0.1**

69.0 Return to Highway 12 heading west. **1.6**

70.6 Roadcut in bedded volcaniclastic rocks of the Ohanapecosh Formation. **0.2**

FIGURE 29-Columnar-jointed hornblende andesite of Clear Fork at Stop 20. Trees on flow about 25 m high.

70.8 Quartz-phyric ash-flow tuff overlying bedded volcaniclastic rocks. This tuff, formerly considered the basal unit of the Stevens Ridge Formation, has been fission-track dated as 36.4 ± 3.6 Ma (Vance et al., 1987, sample JV 126). This age is consistent with assignment to the lower part of the Ohanapecosh (Vance et al., 1987). Several roadcuts from here to Packwood expose ash-flow tuff and volcaniclastic rocks of the Ohanapecosh. **5.1**

75.9 Quarry to right has volcanic siltstone under sill. **0.3**

76.2 Forest Service station on left in Packwood, opposite junction with Forest Road 52.

Day 3, Packwood to Cispus Center via Windy Ridge

Mileage

0.0 Leave Forest Service station in Packwood. **1.0**

1.0 Hills to left and ahead have not yet been mapped in detail. Reconnaissance suggests a middle Tertiary terrane intruded by dikes and sills. **7.4**

8.4 Cowlitz River, which heads at Cowlitz Glacier on Mount Rainier. The river flows on a terraced flood plain developed on Evans Creek Drift (about 18–15 ka) of the Fraser glaciation (Crandell and Miller, 1974). **7.8**

16.2 Turn left at light in Randle onto Cispus Road. **0.9**

17.1 Keep right on Road 25 at junction. **0.4**

17.5 At 2:00 is basalt and basaltic-andesite center of Huffaker Mountain, about 23.5 Ma (Evarts et al., 1987), with east dip of 20° toward synclinal trough. **7.3**

24.8 Turn left on Road 25 at junction just after bridge across Cispus River. **0.2**

25.0 Bedded volcaniclastic rocks, chiefly sandstone. **0.9**

25.9 Continue on Road 25 at junction. Landslide. **4.3**

30.2 Active landslide disrupts road. Volcaniclastic rocks dip east parallel to the slope, facilitating sliding. **0.1**

30.3 Lithic-lapilli tuff in cuts near Benham Creek, about 23 Ma as judged by field relations between here and junction of Roads 25 and 99. **0.2**

30.5 **STOP 22. Warped volcanic sandstone and siltstone,** probably deformed during landsliding or soft-sediment deformation. Similar small outcrops of disturbed fine-grained volcaniclastic rocks occur throughout the area, with no consistency of attitudes. **0.9**

31.4 Lapilli tuff and sandstone at Fourmile Creek. **2.1**

33.5 **STOP 23. Basaltic andesite** with phenocrysts of plagioclase and two pyroxenes, representative of the middle Tertiary section in this area. Not hornfelsed, as are other flows seen later today. **2.1**

35.6 Basaltic andesite in roadcut. This flow caps the dominantly volcaniclastic section since last stop. **0.4**

36.0 Turn right on Road 99 toward Windy Ridge. **0.1**

36.1 **STOP 24. Vitrophyre at base of dacitic ash-flow tuff.** Contact with underlying fine-grained tuffaceous siltstone exposed. Columnar, with columns indicating east dip. Vitrophyre grades up into lithic-lapilli tuff. Dated as 23.3 ± 1.8 Ma by Ar–Ar on plagioclase separate (R. C. Evarts and J. G. Smith, unpubl. data 1987). **0.9**

37.0 Road traverses through ash-flow tuff, with andesite flows visible on hillslope to north (right). **2.4**

39.4 Thin andesite in a mainly tuffaceous section. **0.7**

40.1 Altered, fine-grained, phyric granodiorite in roadcut. Sill-like body underlies hill south of Bear Meadow. **0.4**

40.5 **STOP 25. Bear Meadow parking area.** Restrooms. This is the site from which the two most famous series of photographs of the May 18, 1980, landslide and blast from Mount St. Helens were taken by Gary Rosenquist and Keith Ronholm. The following description, abstracted from Rosenbaum and Waitt (1981), is from accounts of eyewitnesses at Bear Meadow:

> One observer watching with binoculars saw the north side of the volcano get "fuzzy, like there was dust being thrown down the side." Several seconds later the north face began to slide. The "bulge was moving . . . the whole north side was sliding down." The first cloud appeared to form at the base of a "cirque-like" wall from which the bulge had moved. In about 20 sec the landslide was out of view behind a ridge. At this time, two distinct clouds seemed to issue from separate vents. An extremely dark cloud grew vertically from the summit. A lighter cloud (the blast cloud), which seemed to come from the area vacated by the landslide, expanded uniformly except for a large "arm" that shot out to the north in the direction of the avalanche. As the blast cloud grew, what appeared to be a shock wave similar to that associated with a nuclear explosion moved ahead of it. About 1½ min after the blast, a noise resembling a thunder clap was heard at Bear Meadow, accompanying a sudden pressure change. This noise was followed by continuous rumbling "like a freight train." The blast cloud moved toward Bear Meadow, reaching the ridge nearest the mountain 25–30 sec after the start of the landslide. When the cloud hit the ridge, it rose and "boiled" upward. Just before the top of the mountain became obscured, observers saw the south side of the summit crumble into the hole formed by the landslide. Seven or eight minutes after the eruption's start, rocks began falling on one of the witnesses 3–5 km northeast of Bear Meadow. He collected two "golfball-sized" rocks (determined later to be cryptodome dacite) from the fall, which continued for roughly 30 sec. As he drove, this material was replaced by "mud drops" that flattened on impact. The largest observed flattened mud drop was 19 mm across. Gradually mudfall abated, but fine ash fell more heavily until the witness could no longer see to drive. Ashfall then abated slowly.

Note that the blast stopped little more than 3 km from Bear Meadow. An anecdote illustrates the serendipity of the remarkable Rosenquist photographs. His camera was mounted on a tripod and centered on the volcano. When the eruption began, Rosenquist was looking away from the volcano. As he quickly turned, he hit the tripod, rotating the camera slightly clockwise so that the mountain was no longer centered but instead was far to the left side of the image. This accident improved coverage of the north flank of the volcano, thereby enabling the sequence of events to be captured in the series of photographs that was later made into a kind of time-lapse video.

Examine the altered, flow-layered dacite, typical of the Strawberry Mountain dacite dome and flow field, in roadcuts 100 m beyond Bear Meadow. North of here, the dacite generally dips eastward and interfingers with the section of ash-flow tuff that we traversed beginning at Stop 24. Thus the dome and flow field may be the source area for the tuffs. **0.2**

40.7 Volcaniclastic rocks beneath the dacite flow. **0.1**

40.8 Flow-layered dacite; breccia just beyond. **0.3**

41.1 Andesite flow in roadcut. **0.6**

41.7 Epidote-bearing andesite in the outer part of the hornfels zone around the Spirit Lake pluton. From this point, the road roughly parallels the margin of the pluton, and most of the rocks are recrystallized to assemblages of the albite–epidote hornfels facies. **0.3**

42.0 Margin of 1980 devastated zone just above to right. Standing dead trees typify the outer few hundred meters of the devastated area. The *standing dead* were killed by the heat of the blast cloud, which had lost so much lithic debris at its margins that it became lighter than air and lifted off the ground. **0.5**

42.5 Enter the devastated area. Still in andesite. **1.4**

43.9 Lithic-lapilli tuff interbedded in the dominantly andesitic section. **1.0**

44.9 **STOP 26. Mount St. Helens tephra.** Junction with Road 26. Park just beyond junction and walk back to roadcut exposing Mount St. Helens tephra deposits: 1980 pumice and blast, layer T (early 1800) (Yamaguchi, 1983), set X (16th century?), layers Wn and We (early 1480 A.D. and early 1482 A.D., respectively) (Yamaguchi, 1985), and sets B (2.2–1.6 ka), P (2.5 ka), Y (3.5–3.0 ka), and J (11 ka) (Mullineaux, 1986). All the tephras are dacitic except for T (andesitic) and part of B (basaltic and andesitic). Yamaguchi's tree-ring ages recognize that the 1800, 1480, and 1482 eruptions could have occurred in the last three to four months of the preceding year—remarkable precision for geologic events of prehistoric vintage! **0.1**

Continue straight on Road 99.

45.0 Miner's car, destroyed in blast and preserved here as a much-vandalized relic. Interbedded andesite flows and volcaniclastic rocks on skyline to west are in albite–epidote hornfelsed zone. **0.1**

45.1 Trailhead to Meta Lake, which was covered by ice on May 18, 1980, and so retained abundant aquatic life, including trout. Young evergreens around the lake survived the blast because of snow cover. **0.5**

45.6 Nice example of blowdown on hill to right. **0.5**

46.1 Pyroxene-diorite dikes, nearly parallel to road, cut hornfelsed volcaniclastic rocks in roadcut. Minor intrusions ranging from pyroxene diorite to monzogranite are common in the Tertiary rocks of the area. Few have been dated directly, but most are believed to be of early Miocene age (25–17 Ma). **0.3**

46.4 **STOP 27. Cascade Peaks Viewpoint** and Crater House Restaurant and Gift House. Restrooms. Views of Mounts St. Helens, Adams, and Hood (in Oregon). Roadcut opposite restaurant exposes Mount St. Helens tephra deposits, including layer D (1200 B.P.), a thin dacitic blast deposit formed during emplacement of the Sugar Bowl dome (Crandell and Hoblitt, 1986), between sets W and B. The tephra overlies hornfelsed pumice-lapilli tuff, probably ash-flow tuff. **0.3**

46.7 Dacite plug visible in hill west of road. **0.6**

47.3 Up creek to right is relatively fresh hornblende andesite dike cutting hornfelsed dacite breccia. Hornblende dated as 19.9 ± 0.7 Ma (Evarts et al., 1987). **0.1**

47.4 Diorite in roadcut. **0.5**

47.9 **STOP 28. Blast deposit, Spirit Lake views, tree blowdown.** Trail to Independence Pass. Hike 200 m to small bench on crest of low hill. The blast deposit is easily recognized by its gray color, poor sorting, and content of shredded wood. Note the tack driven in the sawn end of log at switchback; it marks a period of stressed growth (narrow tree rings) in 1801–1805 A.D. caused by fall of the dacitic T tephra in 1800. From the bench are good views of Spirit Lake, tree blowdown, and the northwest corner of the dacite dome in the crater. Standing tree trunks on and behind ridge to north indicate that the blast lofted but snapped off their crowns. Note zone of tree removal on Harry's Ridge west of the lake; trees were removed as the debris avalanche scoured the lower part of the ridge. Below is Harmony Falls basin, through which a trail leads to the shore of Spirit Lake, whose high level drowns most of the falls. Hill between here and Mount St. Helens is underlain by an andesite flow (cliffs along Harmony Falls trail) capped by the dacite dome seen at Stop 29.

The Tertiary rocks visible across the lake are east-dipping andesite flows and volcaniclastic rocks similar to those already seen. North of the lake, the rocks are progressively more thoroughly recrystallized as the southern contact of the Spirit Lake pluton is approached. The ridge on the skyline is made of hard flinty hornblende hornfels adjacent to the contact, which is just north of the ridgeline. **0.1**

48.0 Coarse lithic-lapilli tuff, containing clasts of dacite seen at next stop, cut by a northwest-trending (335°) shear with horizontal slickensides and steps indicating dextral slip. The southern Washington Cascades and adjacent Columbia Plateau are host to hundreds of such northwest-trending dextral shears, in most places with little demonstrated displacement. **0.6**

48.6 On inside of curve, brecciated andesite flow fills a vertically walled channel eroded into wood-bearing lithic-pumice-lapilli tuff cut by zeolite veins. **0.6**

49.2 Trail to Harmony Falls. Enjoyable walk to shore of Spirit Lake, with well-exposed volcaniclastic rocks near water's edge. Harmony basin was site of floods fed by water displaced from Spirit Lake by the debris avalanche (Waitt, 1984a; Doukas and Swanson, 1987). **0.3**

49.5 **STOP 29.** Cedar Creek Viewpoint. Excellent view of Spirit Lake. Walk back along road 150 m to quarry in dacite flow. The dacite, probably a dome or small intrusion, is very fine-grained, essentially aphyric, and has numerous limonitic stains along flow layers that probably represent oxidized pyrite. **0.9**

50.4 Donnybrook Viewpoint. Complex of granodiorite sills at 2:00. Good exposure of Mount St. Helens tephra deposits in roadcut opposite viewpoint. **0.5**

50.9 Smith Creek Viewpoint. Good views into the Smith Creek drainage, devastated by the blast and later lahars (Brantley and Waitt, 1988), and, farther east, the shield-like Indian Heaven Wilderness, made of Quaternary olivine basalt. The huge andesitic cone of Mount Adams, the second most voluminous Cascade volcano after Mount Shasta, dominates the

eastern skyline. Tertiary rocks underlying Mount St. Helens below Plains of Abraham include many small intrusions, like those seen along this road, cutting andesite flows and volcaniclastic rocks. Much of the host rock is hornfelsed even between the small intrusions, perhaps because a master intrusion is at shallow depth. **0.1**

51.0 Roadcuts in multiphase granodiorite intrusive complex of Windy Ridge. Some phases contain hornblende, a sample of which was K–Ar dated at 24.3 ± 1.3 Ma (Evarts et al., 1987). **0.9**

51.9 **STOP 30. Windy Ridge Viewpoint.** Restrooms. Ascend steps for best views of Spirit Lake, Harry's Ridge, hummocky debris avalanche that dams Spirit Lake, the Pumice Plain, and lahar fan directly north of crater. The Pumice Plain was at one time entirely covered by 1980 pyroclastic flows, but lahars generated by eruption-induced snow melt in the crater have swept away or covered most of the flows due north of the crater. Part of the Pumice Plain west of the lahar fan still has an intact primary surface, although deeply gullied.

The debris avalanche dammed and partly filled Spirit Lake, displacing water so that the surface of the new lake was about 61.5 m higher than before (1036.3 m vs. 974.8 m). Harry Truman, who stubbornly refused to vacate his lodge on the shore of Spirit Lake, was buried beneath about 45 m of debris and 25 m of water in the southwest corner of the lake. The avalanche formed an unstable debris dam that threatened to fail catastrophically when lake level rose to the approximate height of the low point on the dam. The Army Corps of Engineers began pumping the lake in November 1982 to stabilize water level at an acceptable elevation (1055.2 m). This costly venture was ended in April 1985 when a 2.6 km, 14 million dollar tunnel was opened through Harry's Ridge and began to serve as a gravity-fed controlled outlet for the lake (Sager and Chambers, 1986). The tunnel is 3.4 m in diameter, has a grade of 1%, and was constructed with a tunnel-boring machine advancing at an average rate of 20 m/day for 5.5 months. The portal to the tunnel, which crosses the St. Helens seismic zone with a capability of a M = 7 earthquake (Weaver and Smith, 1983), is visible about halfway along the western shore in basaltic andesite and breccia. Opening the tunnel caused lake level to drop about 6.7 m to the elevation of the portal, resulting in the prominent shoreline with stranded logs. Water from the tunnel eventually enters the Toutle River after flowing through South Coldwater Creek and Coldwater Lake.

The northwest corner of the 1980–86 dacite dome can be seen from the top of the hill (Swanson et al., 1987; Swanson and Holcomb, in press). At the time of writing (November 1988), the dome had last grown in October 1986 and was about 267 m high, 1060 m long, 860 m wide, and had a volume of 74.1×10^6 m^3. Its volumetric rate of growth and geometry were notably regular (Swanson and Holcomb, in press), and each period of growth was easily predicted on the basis of precursory ground deformation and seismicity (Swanson et al., 1983, 1985).

A small shed on top of Harry's Ridge houses surveying and radio equipment used by volcanologists of the U.S. Geological Survey's Cascades Volcano Observatory (CVO) to monitor volcanic activity. Most monitoring is now conducted within the crater and on the dome. CVO notifies the U.S. Forest Service and other governmental agencies when monitoring indicates significant changes in activity. All decisions regarding access and land use in Mount St. Helens National Volcanic Monument are made by the Forest Service. **7.2**

59.1 Return to Road 26 and turn left (north). **0.6**

59.7 The family of three who owned the car on display was killed in a small cabin near the portal to their prospect high on the hillside at 9:00. They had reopened an adit originally excavated during a period of mining in the southern Washington Cascades around the turn of the century. The adit was driven along a polymetallic sulfide (pyrite, chalcopyrite, sphalerite) vein, one of a set of northwest-trending veins peripheral to the Earl porphyry copper deposit. The only known production from the St. Helens district was a few hundred kilograms of copper from the Sweden mine, now under 30 m of water at the northeast end of Spirit Lake. All the copper reportedly found its way into a statue of Sacajewea, the guide for the Lewis and Clark expedition, that stands in a park in Portland (Moen, 1977). **0.3**

60.0 Trailhead to Norway Pass, which affords excellent views of Spirit Lake and the crater. From Norway Pass, trails connect to Independence Pass and continue into the high country north of Spirit Lake. **0.4**

60.4 Cross from hornfelsed wallrock into Spirit Lake pluton. No place to stop. The pluton underlies the Green River basin and tree-covered hillside ahead, beneath which most of the 17 Ma Earl porphyry-copper deposit resides. This large-tonnage, low-grade deposit would probably have been open-pit mined if it were in Arizona, but mining was not done here, because of: (1) the eruption in 1980 and presumed hazards thereafter, (2) the steep decline in copper prices in the early 1980's, and (3) environmental concerns about acid waste. Molybdenum would have been a byproduct of the copper mining. **1.5**

61.9 Looking west down Green River at 9:00, all exposures are of the Spirit Lake pluton. **0.7**

62.6 Note margin of tree-blowdown area. Much of this area had been logged before 1980, as seen by the sawn stumps, but the standing dead that fringe some clearcuts provide evidence of the waning blast. **0.2**

62.8 Turn left on Road 2612 beyond Ryan Lake. **0.1**

62.9 **STOP 31. Spirit Lake pluton.** Granodiorite porphyry, representative of the main phase of Spirit Lake pluton, occurs in a nearby roadcut. The pluton consists of three phases, each displaying substantial internal compositional and textural variation (Evarts et al., 1987). The main phase, constituting most of the intrusion, ranges from diorite to granodiorite and is well dated at 21 Ma. The porphyritic texture exhibited here is typical of the main phase in eastern half of the pluton. To the west, coarser-grained, more equigranular textures predominate. This pat-

tern suggests that the pluton and its host rocks have been tilted eastward and eroded more deeply in the west.

Ryan Lake was once nestled in old-growth forest out of sight (and mind) of Mount St. Helens. The campground was in use on May 18, 1980. Imagine the terrifying sensation when the blast cloud appeared over the hill with little if any warning. A body buried by ash alongside the outhouse was found a month after the explosion, and others were killed in the Green River basin. One miner managed to walk from his work site farther west to his pickup parked here, to drink a bottle or two of beer to try to clear his throat of the choking ash, and then to walk (downed trees kept him from driving) several kilometers down Road 26 before collapsing. An autopsy showed his lungs coated with ash.

Bus can go 0.3 mi farther to Goat Mountain trailhead to turn around and return to stop. **0.1**

63.0 Return to Road 26 and continue north. **0.7**

63.7 Note standing and fallen dead trees on east side of Quartz Creek basin. The prominent scars on the hillside record pumiceous debris flows of the last several winters. Such flows were a problem before 1980 that has been exacerbated by the May 18 deforestation. **2.1**

65.8 Cross contact from main phase, seen at Ryan Lake, into granite phase of Spirit Lake pluton. The contact is difficult to pin down in this area owing to an overprint of intense deuteric alteration, but it appears gradational. Elsewhere, sharp contacts locally marked by intrusion breccia indicate that the granite phase is younger. **0.3**

66.1 **STOP 32. Granite phase of the Spirit Lake pluton** in roadcut. Rocks of the granite phase are distinctly lighter in color, finer-grained, and more felsic than those of the main phase. Outcrops of the granite phase are concentrated along the eastern margin (top) of the exposed part of the pluton. **0.3**

66.4 At 9:00, note standing dead trees along road. **0.3**

66.7 Leave devastated area. Green trees again! **0.5**

67.2 Roadcut in main phase of pluton. **0.6**

67.8 Back in granite phase of pluton. **0.8**

68.6 Series of roadcuts in granite phase of pluton. **1.1**

69.7 **STOP 33. Wallrock of Spirit Lake pluton.** Screens of hornfelsed host rock, originally lithic and pumice-lapilli tuff, cut by several aplite dikes and at least one granite dike. Contact with Spirit Lake pluton is obscured by forest just up road from here. The wallrock outside of the hornfelsed zone is coarse breccia and dacite flows, whose attitudes suggest the site of a Miocene caldera (Evarts et al., 1987). **0.4**

70.1 Hornfelsed dacite, in places with relict flow layering, and dacite breccia. **0.6**

70.7 Clastic dacite and andesite, possibly caldera fill, cut by two andesite dikes. Entire assemblage is recrystallized to albite–epidote hornfels. Similar rocks occur in discontinuous roadcuts for next 3 mi. **0.4**

71.1 At 9:00, dacite flow in quarry dips east. **1.7**

72.8 Bedded volcaniclastic rocks, chiefly sandstone and siltstone, with Cispus River to right. Some of the sandstone is normally graded. **0.3**

73.1 Turn right at junction with Road 25. **0.2**

73.3 Same unit as at mileage 72.8. **0.9**

74.2 Turn left onto Road 76 to Cispus Center. **0.1**

74.3 Bridge across Iron Creek. Bedded sandstone in stream-cut. **2.8**

77.1 Columnar ash-flow tuff over tuffaceous sandstone, siltstone, and lithic-lapilli tuff. **2.6**

79.7 Keep right at intersection. At 2:00 is Tower Rock monolith, an intrusion whose face was greatly steepened by glaciation in Cispus valley. **1.5**

81.2 Turn left into Cispus Center.

Day 4, Hiking trips around Mount St. Helens

No guide has been written for this day because the area is not open to public and we do not want to encourage self-guided tours. Participants will be provided with handouts.

Day 5, Cispus Center to Hood River via Indian Heaven

Retrace route back to Road 25 and then to junction with Road 99, where log starts.

Mileage

0.0 Continue south on Road 25. **0.6**

0.6 Andesite flow in roadcut. **2.2**

2.8 Pumice-lithic-lapilli tuff, probably ash-flow tuff. **2.1**

4.9 Basaltic andesite flow cut by narrow, petrographically similar dike trending 280°. This trend typifies that of a major dike swarm in this area. **0.8**

5.7 Basaltic andesite, with complex platy jointing. **0.4**

6.1 Lithic-pumice-lapilli tuff, probably an ash flow, that slides easily because of clay alteration. Underlies andesite flow seen in previous roadcut. **0.7**

6.8 At 2:00 is stack of thin near-vent basaltic andesite flows, slightly older than the flows in the roadcuts. **0.1**

6.9 Start of cuts in mafic intrusion. Probably subvolcanic, but overall shape is unknown. **1.9**

8.8 Continue straight on Road 25 at junction. *Note: Major road work was underway when the trip was logged from here to Road 2573. Exposures and mileages may differ significantly from those given below.* **0.2**

9.0 Clearwater Overlook. Cut in finely hornblende-phyric fragmental dacite flow or ash-flow tuff. **0.4**

9.4 This unit cut by 5 m thick columnar sill of plagioclase-phyric andesite. Similar exposures occur for next 0.4 mi. **0.8**

10.2 Andesite flow(?) in roadcut. **0.2**

10.4 **STOP 34. Basalt of Paradise Falls; Tumtum–Badger Ridge vent line.** Start of 0.6 mi of roadcuts in Quaternary olivine basalt of Paradise Falls (Korosec, 1987a), which erupted on the ridge crest just east of the road and poured into the valley of Clearwater Creek. It contains large phenocrysts of olivine (rimmed by iddingsite in oxidized samples) but none of plagioclase.

The vent for this flow lies midway along a N35°E line of Quaternary vents extending for about 50 km from Tumtum Mountain south of the Lewis River to Badger Ridge south of Cispus Center (Fig. 30). Six vents lie along the Tumtum–Badger Ridge line,

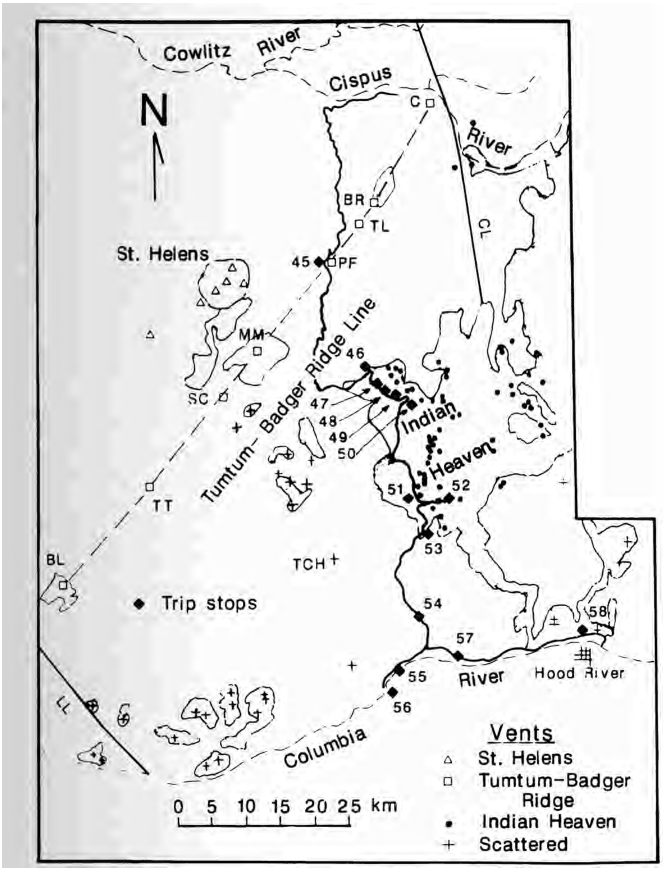

FIGURE 30—Map showing Pliocene and Quaternary vents (keyed to location) and major flow fields (shaded) near field-trip route between Cispus Center and Hood River. Tumtum–Badger Ridge line connects isolated vents. BL, Battle Ground Lake; TT, Tumtum Mountain; SC, vent south of Swift Creek Dam; MM, Marble Mountain; PF, basalt of Paradise Falls; TL, The Loaf; BR, Badger Ridge; C, basalt east of Cispus Center; TCH, Trout Creek Hill; LL, Lacamas Lake lineament; CL, Cispus–Lewis fault zone. See text for discussion.

and only a few other Quaternary vents occur near it, except for a cluster around Mount St. Helens. The line can be extended with only slight bends to include a vent east of Cispus Center and the Battle Ground Lake maar (Mundorff, 1964) and adjacent vent (Walsh et al., 1987), a total length of about 87 km (Fig. 30). K–Ar whole-rock ages are available for the basalt of Paradise Falls (0.04 ± 0.03 Ma (Hammond and Korosec, 1983)), a flow on Marble Mountain (0.16 ± 0.01 Ma (Hammond and Korosec, 1983)), and the olivine basaltic andesite of Badger Ridge (0.65 ± 0.02 Ma; J. G. Smith, written comm. 1986). Mundorff and Eggers (1988) interpreted Tumtum Mountain as slightly younger than the Amboy Drift, a likely correlative (Walsh et al., 1987) to the ca 0.14 Ma Hayden Creek Drift. Battle Ground Lake maar is older than 20,200 ± 400 ^{14}C years, the age of the oldest dated sediment in the lake (Barnosky, 1985). The undated vents have normal magnetic polarity (except for that east of Cispus Center) and so are younger than about 0.73 Ma. Seven vents produced olivine basalt or basaltic andesite, but Tumtum Mountain erupted hornblende dacite (68% SiO_2) (Mundorff and Eggers, 1988). Marble Mountain, the largest Quaternary vent area in southern Washington west of Indian Heaven (except for Mount St. Helens), grew where the line crosses the St. Helens seismic zone (Weaver and Smith, 1983).

Whether the Tumtum–Badger Ridge line reflects tectonic control is unclear. Relatively few Tertiary dikes in the area parallel the line, which is slightly oblique to the plate-convergence direction of N50°E (Riddihough, 1984), although minor sinistral shears have northeast trends. The line does not extend northeast of the Cispus–Lewis fault zone mapped by Hammond (1980) or southwest of the Lacamas Lake fault and associated lineament (Walsh et al., 1987). The line is not directly reflected by the southern Washington Cascades conductor (SWCC) or other anomalies (Stanley et al., 1987), although its projected trend merges into and parallels that of conductance contours in the south part of the SWCC. **1.2**

11.6 Highly plagioclase-phyric, oxidized, Tertiary andesite. Similar cuts occur sporadically for next 5 mi. **5.4**

17.0 Pumice-lapilli tuff, probably an ash flow. **2.3**

19.3 Section of Mount St. Helens tephra deposits in roadcut above oxidized Tertiary ash-flow tuff. **0.7**

20.0 Small roadcut of ash-flow tuff, with andesite flow just beyond. **0.4**

20.4 Alder-covered surface of lahar of May 18, 1980, which was generated on the southeast flank of Mount St. Helens by rapid melting of eroded snow incorporated into the blast surge and possibly enhanced by water ejected from the volcano (Pierson, 1985). Mudlines 4–6 m above this surface (still evident on some trees in 1988) indicate maximum thickness of flowing lahar. The lahar reached a peak velocity of 30–40 m/sec near the base of the volcano but had slowed to an approximately constant 3–6 m/sec by the time it reached here (Pierson, 1985). The lahar was generated soon after the start of eruption at 0832 and reached the site of the bridge (destroyed by the lahar) at about 0856. A smaller, pumiceous lahar, generated by a pyroclastic flow on the volcano's southeastern slope between 1530 and 1610, probably reached the site of the bridge at about 1625 (Pierson, 1985). **0.3**

20.7 Bridge across Muddy River. From here to Pine Creek the road crosses pyroclastic-flow and laharic deposits older than 2200 yrs B.P. (Phillips, 1987). **3.6**

24.3 Pine Creek. Another branch of the first May 18 lahar roared down Pine Creek at a peak discharge of about 29,000 m^3/sec (Pierson, 1985). Here erosion on one side of the channel was balanced by deposition on the other (Pierson, 1985). The Muddy River and Pine Creek lahars destroyed 16 bridges, buried several kilometers of road, and raised the level of Swift Reservoir 0.8 m by depositing 13.4 million m^3 of slurry (Cassidy et al., 1980, quoted *in* Schuster, 1981, and Pierson, 1985). **0.8**

25.1 Turn left at junction with Road 90. **0.4**

25.5 Cross Lewis River at east end of Swift Reservoir. Most logs along river were carried by lahars on May 18, 1980. Eagles Cliff to left is columnar welded ash-flow tuff, probably of early Miocene age (Phillips, 1987), overlain by Quaternary(?) basalt of

Thomas Lake (Hammond, 1987; Korosec, 1987a; Walsh et al., 1987). **0.6**

26.1 Roadcuts on left are in lahar deposit that predates the Castle Creek eruptive period (Phillips, 1987). **0.3**

26.4 Start of a long roadcut in highly plagioclase-phyric, densely welded ash-flow tuff of Eagles Cliff. The tuff underlies ridge left of road for next 2 km. **1.6**

28.0 Roadcuts of bedded lapillistone, tuff, and wood-bearing mudstone. Andesite dike 3 m wide cuts section. Similar roadcuts occur for next 600 m. **2.2**

30.2 Landslide blocks of the basalt of Thomas Lake (Korosec, 1987a). **0.4**

30.6 Stay on Road 90 at junction with Road 51. **0.9**

31.5 Lithic-pumice-lapilli tuff at Rush Creek. Cliff of basalt of Thomas Lake high ahead. **0.8**

32.3 Roadcuts of augite–plagioclase–olivine-phyric, vesicular Quaternary(?) basalt of Thomas Lake. A whole-rock K–Ar age of 3.8 ± 0.5 Ma was obtained for this flow from next series of cuts (Hammond and Korosec, 1983); however, this age is analytically questionable (only 2.7% radiogenic Ar), and the normally magnetized basalt is mapped as Quaternary on the basis of field relations and general appearance (Korosec, 1987a). Nonetheless, the basalt is one of the oldest units of the Indian Heaven volcanic field (Korosec, 1987a; Hammond, 1987). It was erupted just south of East Crater (15 km southeast of here) and flowed northwest into the ancestral Lewis River. The unit has a volume of about 4 km^3 (Korosec, 1987a) and is locally as thick as 150 m in the ancestral Lewis River valley (Hammond, 1987). **0.2**

32.5 Basalt of Thomas Lake in discontinuous roadcuts for next mile. **1.0**

33.5 **STOP 35. Basalt of Thomas Lake.** Possible bus parking at last chance to observe basalt of Thomas Lake. **0.4**

33.9 Turn right on obscure gravel road (3211) in middle of straight segment of Road 90. **2.2**

36.1 Intraglacial basalt of Burnt Peak in roadcut (Stop 14 of Hammond, 1987). Radially jointed olivine basalt is partly enclosed in pillow lava. **0.5**

36.6 Pillowed basalt of Burnt Peak, with minor palagonitized hyaloclastite. **0.4**

37.0 **STOP 36. Pillows and pépérite of basalt of Burnt Peak.** Stop 13 of Hammond (1987). Pillows in the basalt of Burnt Peak dominate the outcrop. They invade thinly bedded lacustrine and fluvial or turbidite "black sand" hyaloclastite (Fig. 31). The sediments terminate against a nearly vertical invasive or intrusive contact toward the left side of the cut. The interstices between the pillows are filled by bedded sediment, which is locally distorted, has truncated bedding, and is mixed with glassy basalt in a pépérite. A lower layer of pillows has similar interstitial fillings and clearly invades white laminated lacustrine(?) siltstone. The siltstone is overlain by bedded sand that may have been deposited on top of the basalt (relations not definitive). The bedded sand contains a few large blocks of glassy basalt that lack pillow forms and may have broken off a pillow complex. Overlying the pillow basalt and sediment is lithic-rich hyaloclastite in erosional contact with the bedded sand. The hyaloclastite is crudely layered and has west-dipping foreset bedding. A small fault offsets the diamict–basalt contact near the left end of the cut. **0.2**

FIGURE 31—Subglacial pillowed basalt invading lacustrine silt (light unit in floor of depression) overlain by sand at Stop 36. Crudely layered hyaloclastite overlies the sand. Height of exposure about 10 m.

37.2 Narrow basalt dike intrudes pillows and hyaloclastite. Similar exposures continue for 200 m. **0.3**

37.5 Broken pillow breccia and hyaloclastite. **0.3**

37.8 **STOP 37. Hyaloclastite.** Stop 12 in Hammond (1987). Well-bedded, reworked hyaloclastite, white because of opal cement, grades laterally into primary hyaloclastite cored by jointed and quenched basalt. Exposure extends about 100 m in roadcut. Bus parks at start of cut. **0.2**

38.0 Top of plateau in Crazy Hills, so named by early surveyors who were puzzled by the morphology, which is dominated by erosionally modified moberg hills (hills consisting of palagonitized hyaloclastite and pillows) (Kjartansson, 1959). The Crazy Hills moberg field covers about 21 km^2, has a volume of about 1.7 km^3, and contains hills and ridges 122–366 m high (Hammond, 1987). According to Hammond, the hills are composed chiefly of palagonitized hyaloclastite in massive, thick to thin beds containing clasts of silt to boulder size. The basal parts of the hills are thought to consist of pillow lava, and the entire complex is interpreted to overlie subglacial and intraglacial lava flows and pillow lavas. The higher hills are held up by dikes, sills, and lava flows. View straight ahead of Lone Butte (Hammond, 1987), a tuya (volcano that erupts initially beneath a glacier, melts through the ice, and develops an upper, subaerial, commonly flat top (Jones, 1969)).

Lone Butte and the Crazy Hills apparently formed during the Hayden Creek stade of the Salmon Springs glaciation, probably about 0.14 Ma (Hammond, 1987; Crandell and Miller, 1974; Coleman and Pierce, 1981). The glacier filled the Lewis River valley, spilled onto the site of the Crazy Hills, and merged with a local glacier from the northern end of Indian Heaven. The hills and tuya have been modified by the later Evans Creek glaciation, which climaxed about 18–15 ka. **0.1**

38.1 Hyaloclastite in cut on curve. After rounding curve, Burnt Peak is straight ahead. **0.4**

38.5 Keep right on Road 3211 at junction. **0.4**

38.9 Broken pillow hyaloclastite. **0.2**

39.1 Crudely bedded palagonitized hyaloclastite, possibly reworked. Stop 5 in Hammond (1987). **1.1**

40.2 **STOP 38. Hyaloclastite and pillowed basalt of Burnt Peak.** Stop 4 in Hammond (1987). Small quarry shows pillowed basalt of Burnt Peak invasive into crudely bedded hyaloclastite. Pépérite halos surround sediment clasts between pillows. At west end of exposure, steeply dipping dikes of hyaloclastite cut bedded hyaloclastite, as if squeezed up from below by weight of pillow complex. In middle of cut above the pillow zone is a possible pipe of explosion breccia containing abundant angular lithic clasts of basalt with differing degrees of vesicularity. The pipe is cut off by the pillows. The explosion pipe dies out upward, but traces of it continue to top of second cut (not visible from road). Other narrow sediment dikes cut the hyaloclastite in the second cut; walk above the exposure to see this. Small faults cut tilted hyaloclastite at east end of cut. **0.2**

40.4 Turn right at junction with Road 32. **0.2**

40.6 Turn left at junction with Road 30. **0.1**

40.7 View ahead of 430 m high, 0.3 km^3 Lone Butte tuya (Hammond, 1987). According to Hammond, the lower 230 m of the tuya is palagonitized hyaloclastite, overlain by 40 m of hyaloclastic surge deposits at the eastern end of the tuya and 40 m of foreset-bedded pillow breccia at the western end (exposed in the quarry visible from here). These subaqueous deposits are capped by a 145 m thick remnant of a subaerial scoria cone, whose western flank is overlain by 65 m of subaerial basalt flows. Four dikes cut the hyaloclastite. At least three hours of hiking are needed to see these relations. **1.2**

41.9 At 10:00 is subaerial cap on Lone Butte. **0.4**

42.3 Turn right on Road 65. **1.3**

43.6 **STOP 39. Basalt of Outlaw Creek.** Bus can stop just before bridge over Rush Creek. Basalt of Outlaw Creek, a fine-grained, olivine-phyric diktytaxitic basalt with about 51.6% SiO_2 and 0.96% K_2O (P. E. Hammond, unpubl. data), crops out along the creek. This flow is stratigraphically the oldest in the Indian Heaven field. **4.3**

47.9 Roadcut in basalt of Indian Heaven, diktytaxitic and highly plagioclase- and olivine-phyric (Hammond, 1987). Flow was erupted from west vent of 120 m high East Crater in the Indian Heaven Wilderness between 29 ka and Evans Creek time (Hammond, 1987). The basalt has about 50.2% SiO_2 and 0.45% K_2O (P. E. Hammond, unpubl. data 1985). **0.5**

48.4 Roadcut in basalt of Indian Heaven. **3.7**

52.1 Continue straight at junction, crossing drift-covered andesite of Black Creek (Korosec, 1987b). **1.2**

53.3 At 9:00 is The Wart, a 145 m high cinder cone that erupted a small basaltic andesite flow just prior to Evans Creek time. Also visible is top of 1514 m high Red Mountain (with lookout tower), a vent complex that erupted andesite, basaltic andesite, and olivine basalt several times, most recently between the Hayden Creek and Evans Creek stades (P. E. Hammond, written comm. 1983; Wise, 1970). **0.5**

53.8 **STOP 40. Roadcut in basaltic andesite of The Wart** (P. E. Hammond, written comm. 1983), included with andesite of Black Creek by Korosec (1987b). Fine-grained and finely plagioclase–olivine-phyric. Contains about 53.8% SiO_2 and 0.8% K_2O (P. E. Hammond, unpubl. data 1985). **0.2**

54.0 Turn left toward Trout Lake on Road 60 and stay on this road to Stop 41. **0.9**

54.9 Small roadcut in basalt of Sheep Lakes, erupted from east base of Red Mountain just before eruption at The Wart (P. E. Hammond, written comm. 1983). **0.4**

55.3 Basalt of Big Lava Bed visible right of road. **1.0**

56.3 Cross west margin of Big Lava Bed tephra. **0.4**

56.7 **STOP 41.** Glaciated cinder cone covered by 3 m of Big Lava Bed tephra deposit along edge of Big Lava Bed flow. The cinder cone is oxidized, weathered, and clay-rich. It is locally overlain by 5 m of Evans Creek Drift (P. E. Hammond, written comm. 1983).

The Big Lava Bed tephra deposit was erupted from a 295 m high cone about 3.5 km east of here. This cone is the source of the tube-fed basalt flow that forms Big Lava Bed itself. The tephra blanket is oval, extends northeastward toward Trout Lake, covers about 200 km^2, and contains about 10^5 m^3 (P. E. Hammond, written comm. 1985). The Big Lava Bed flow moved west from the cone before turning south, eventually reaching the Little White Salmon River nearly 17 km from its source (Korosec, 1987b). It consists of many thin flow units fed by lava tubes. Pressure ridges and plateaus testify to inflation of the flow when lava poured into blocked tubes. A platform at the west base of the source cone was apparently uplifted about 60 m during the eruption (P. E. Hammond, written comm. 1985). The Big Lava Bed flow contains about 0.9 km^3, covers 59 km^2 (Korosec, 1987b), and its ^{14}C age is 8200 ± 100 yrs B.P. (Hammond and Korosec, 1983). **2.6**

Return to Road 65.

59.3 Turn left on Road 65. Andesite of Black Creek underlies Evans Creek Drift. A K–Ar whole-rock age of 3.3 ± 0.25 Ma was obtained on the andesite about 1 km south of here (Hammond and Korosec, 1983); Korosec (1987b) considers this too old, partly because no reversely magnetized flows overlie the andesite (or occur anywhere in the Indian Heaven area). **2.9**

62.2 Road winds into canyon of Panther Creek, which is eroded into middle Tertiary volcaniclastic rocks unconformably capped by the andesite of Black Creek (Wise, 1970; Korosec, 1987b). **0.4**

62.6 Roadcuts in bedded volcaniclastic rocks. Korosec (1987b) considers these and other Tertiary rocks along Panther Creek to be of late Oligocene age. Wise (1970) tentatively correlated them with the Ohanapecosh Formation on the basis of lithology and reconnaissance tracing of the Ohanapecosh southward from Mount Rainier by R. S. Fiske and A. C. Waters in the early 1960's. A firm basis for this correlation is lacking. **0.2**

62.8 **STOP 42. Andesite of Black Creek.** Quarry in columnar intracanyon flow of olivine-phyric andesite of Black Creek. This flow came down the

valley of ancestral Panther Creek from an unknown vent near Red Mountain. A similar remnant occurs in 0.9 mi. **1.3**

64.1 Start of series of cuts in middle Tertiary rocks. **6.1**

70.2 Turn right at junction with Old State Highway. **0.1**

70.3 Turn left at T-intersection. For next 8 km the road follows the Wind River valley on the surface of a basalt flow erupted from Trout Creek Hill 12 km northwest of here (Wise, 1970; Korosec, 1987b). **1.0**

71.3 Skyline hill with tall antenna at 12:00 is Mount Defiance, Oregon, a middle or late Pleistocene shield volcano of basaltic andesite and andesite on the rim of the Columbia Gorge (D. R. Sherrod, written comm. 1988; Hammond, 1980). **0.7**

72.0 Small hill of Tertiary lapilli tuff surrounded by basalt of Trout Creek Hill. **0.2**

72.2 **STOP 43. Basalt of Trout Creek Hill.** Bus parking just before roadcut. Coarsely olivine-phyric (clots to 5 mm or more) diktytaxitic basalt. Several flows were erupted from Trout Creek Hill about 0.34 ± 0.075 Ma (whole-rock K–Ar age) (Hammond and Korosec, 1983; Korosec, 1987b). The cumulative thickness of flows in the Wind River valley is at least 70 m, measured below the bridge 500 m southeast of here (Wise, 1970; Korosec, 1987b). The flows moved down valley to the Columbia River and built a hyaloclastite dam across the Columbia (Waters, 1973). The Wind River formed a delta 45 m thick into the temporary lake (Waters, 1973) before the Columbia breached the dam and drained the lake. **0.3**

72.5 Bridge across Wind River, where the river crosses the 70 m thick basalt fill just upstream from the mouth of Panther Creek. Before basalt flooded the ancestral drainage, Panther Creek and Wind River must have joined near the spot where we first met the Wind River Road. The flows diverted Panther Creek along the northeast margin of the valley fill and Wind River along the southwest margin. Enter Carson. **0.4**

72.9 Roadcut in basalt of Trout Creek Hill. **1.7**

74.6 Conical hill between 9:00 and 10:00 is Wind Mountain, a quartz diorite intrusion (see Stop 46). **0.7**

75.3 Roadcut in columnar andesite flow in the lower Miocene volcanic rocks of Stevenson Ridge (Korosec, 1987b). Roadcuts from here to the outskirts of Stevenson are in this unit, which Korosec (1987b) estimated from K–Ar ages and geology to be 24–21 Ma. **0.8**

76.1 Turn right on Highway 14 and drive west along the Columbia River, ponded behind Bonneville Dam. **0.4**

76.5 Start of a prominent series of roadcuts in andesite flows and minor volcaniclastic rocks of Stevenson Ridge. **2.4**

78.9 Enter Stevenson, built on volcaniclastic rocks of the 22–17 Ma Eagle Creek Formation (Korosec, 1987b). **0.3**

79.2 Turn left on Russell Avenue at flashing caution light in front of Court House. **0.1**

79.3 **STOP 44. Age of Cascade uplift.** Cross railroad tracks, turn right, and park opposite Waterfront Park. Walk to viewing area. (Stop 18 in Tolan and Beeson, 1984b). A thick red hyaloclastite of Pliocene or Pleistocene high-alumina basalt is exposed 500–600 m above the river. The hyaloclastite must have formed in water, yet the deposit is too low in elevation to have formed subglacially. Tolan and Beeson (1984b) reasoned that the most likely source of water was from the Columbia River. Tolan and Beeson (1984b: 112) "think that the complex probably formed near present river level when the river was invaded by high-alumina basalt lava flows and was later elevated by Cascade upwarping while the river incised the Columbia River Gorge." They felt that the incision would have occurred in the last 2 m.y., the approximate age of the youngest alluvial deposits of the ancestral Columbia (the Troutdale Formation) that were incised during uplift (Tolan and Beeson, 1984a, c; Lowry and Baldwin, 1952; Trimble, 1963). Their concluson is rather controversial, but the main point is that Cascade uplift in this area is of late Neogene age, whatever the exact age might be.

Back bus up and return across tracks. **0.3**

79.6 Turn left on First Street, right at stop sign, and left on Highway 14. **0.1**

79.7 View ahead of part of the Columbia Gorge. On north side, dark, nearly shear cliffs of Grande Ronde Basalt overlie light-colored bedded volcaniclastic rocks of the Eagle Creek Formation that dip south, are rich in clay, and slide easily. The area south of the cliffs is the giant Bonneville landslide complex, parts of which are still active and on which the northern end of Bonneville Dam, the first dam constructed across the Columbia, is based. On the Oregon side of the gorge, the cliffs are mainly Grande Ronde Basalt capped in places by Pliocene and Pleistocene basalt and andesite flows. Locally, the Priest Rapids and Pomona Members partly fill channels carved in the Grande Ronde (Tolan and Beeson, 1984c). From here to Bridge of the Gods, Highway 14 crosses three of the four units that form the Bonneville landslide complex: the Red Bluff, Mosley Lakes, and Bonneville slides (Wise, 1961; Minor, 1984). **2.4**

82.1 **STOP 45. Bridge of the Gods.** Turn left at Historical Marker sign and stop in parking lot. View of Bridge of the Gods at the site of the original "Bridge of the Gods" of Native American legend, which formed in about 1100 A.D. (Minor, 1984) when the Bonneville landslide temporarily dammed the Columbia. The legend tells of crossing the river on dry land. The river was about 1.5 km wide and relatively straight before the slide displaced it at least 1 km southward. The resulting dam impounded a lake whose surface elevation reached 60–90 m above sea level and whose water drowned forests for 60 km upstream. After a few weeks the dam broke and generated a major flood (Minor, 1984). The breaching resulted in the narrowest constriction in the Columbia Gorge and produced four main rapids with a total fall of 11 m (Hodge, 1938). Native Americans established villages and seasonal camps, now important archaeologic sites, along the

rapids for fishing and trade control. **5.8**

Return to the junction of Highway 14 and road to Carson.

87.9 Continue east at junction with road to Carson. **0.5**

88.4 Start of a series of cuts in flow and talus of basalt of Trout Creek Hill. **2.1**

90.5 Wind Mountain intrusion at 11:00. **1.3**

91.8 **STOP 46. Wind Mountain intrusion,** a fine-grained, plagioclase-phyric quartz diorite, in places with hypersthene and hornblende phenocrysts. The intrusion contains inclusions of Grande Ronde Basalt, and basalt on the west side of Dog Mountain, 3 km farther east, was hornfelsed by the intrusion. A similar quartz diorite occurs south of the river at Shellrock Mountain. These shallow bodies, and several others in the area, presumably were related to volcanic activity. K–Ar whole-rock ages of 4.9 ± 0.1 Ma (Korosec, 1987b) and 6.6 ± 0.7 Ma (T. L. Tolan *in* Korosec, 1987b) have been obtained for the Wind Mountain intrusion, and one age of 5.7 ± 0.6 Ma (T. L. Tolan *in* Korosec, 1987b) exists for Shellrock Mountain. No clasts of these quartz diorite bodies have been identified in the coeval Troutdale Formation (Tolan and Beeson, 1984b). If the intrusions fed volcanoes, where is the eruptive debris? **2.0**

93.8 Start of a long series of roadcuts in tectonically fractured and faulted flows of Grande Ronde Basalt in the Dog Mountain section, the thickest (more than 1.3 km) unrepeated section of Grande Ronde Basalt (almost entirely the R_2 magnetostratigraphic unit) exposed west of the Columbia Plateau. **2.1**

95.9 At 12:00 is narrow dike-like fault breccia 10–20 m above road. **1.4**

97.3 Bridge across the Little White Salmon River. Thin flows of Quaternary olivine basalt from Underwood shield volcano, about 7 km northeast of here, cap tilted flows of Grande Ronde Basalt at 10:00. Start series of five tunnels through tilted Grande Ronde. **2.2**

99.5 Good exposure of olivine basalt flows of Underwood volcano at 12:00. One of these flows has a K–Ar age of 0.85 ± 0.02 Ma (Korosec, 1987b), although at least some flows from the volcano are normally magnetized, not reversely as would be expected for this age. From here to sawmill at Hood these flows cap Grande Ronde and are pillowed where they poured into the ancestral Columbia. **4.0**

103.5 Quartzite-bearing gravel and sand of the ancestral Columbia River. The deposit is younger than the 12 Ma Pomona Member of the Saddle Mountains Basalt and correlates with part of the Troutdale Formation farther west and the Snipes Mountain conglomerate on the Columbia Plateau (Tolan and Beeson, 1984b). **0.3**

103.8 Turn left on Cook Underwood Road at mouth of White Salmon River. **0.6**

104.4 **STOP 47. Debris-avalanche deposit.** Examine deposit of a huge debris avalanche probably formed by collapse of the north or northeast flank of an ancestral Mount Hood 0.05–0.1 Ma. The avalanche traveled down Hood River, crossed the Columbia, and back-filled 5 km up the White Salmon River, a distance of 40 km (Vallance, 1986). Here the deposit overlies fluvial gravel of the ancestral White Salmon River and underlies sand and gravel of the upper Pleistocene Missoula floods. The base of the avalanche deposit is 30 m above present lake level and 30 m thick. The deposit is about 80 m thick across the Columbia in Hood River, where its top is at about 105 m elevation and its base only slightly above river level (22 m). **0.8**

105.2 Turn left at fire-station sign. **0.1**

105.3 Turn around at Underwood Community Center and return to Highway 14. **1.5**

106.8 Turn left on Highway 14. **0.2**

107.0 Stratified hyaloclastite and pillowed olivine basalt erupted from White Salmon volcano about 2 km farther east. Its age is unknown, but Korosec (1987b) suggested that it is coeval with the basalt of Underwood Mountain. The basal flows have normal magnetic polarity and are probably younger than 0.73 Ma. Similar exposures continue to White Salmon. **1.6**

108.6 Turn right across Hood River Toll Bridge. **1.1**

109.7 Intersection south of toll booth.

Day 6, Hood River to Portland via Mount Hood

Mileage

0.0 First 4-way stop south of toll bridge in Hood River. Follow Highway 35 south over railroad tracks. **0.4**

0.4 Stop and continue south on Highway 35, which climbs up Hood River Valley. Roadcuts in Frenchman Springs Member of Wanapum Basalt (Swanson et al., 1981; Korosec, 1987b). **1.4**

1.8 Roadcut in Pliocene or Pleistocene olivine basalt underlying much of Hood River Valley (Korosec, 1987b). **0.3**

2.1 Roadside quarry in this olivine basalt. **0.1**

2.2 Start of cuts in debris flow from Mount Hood (see Stop 47). **0.2**

2.4 Turn left at junction to Panorama Point. **0.5**

2.9 Turn left at T-intersection. **0.6**

3.5 Turn left into Panorama Park. **0.2**

3.7 **STOP 48. Panorama Point.** From right to left: Underwood Mountain volcano on west side of White Salmon River; Columbia Gorge, with Hood River Valley in foreground capped near shopping center by deposits of Missoula floods; Pleistocene Mount Defiance volcano across terraced Hood River Valley; main part of Hood River Valley; Middle Mountain separating Upper Valley from the main valley; Mount Hood; and Hood River fault zone bounding the east side of the valley. Several cones of olivine basalt occur in Hood River Valley south of here. The orchards are developed on Parkdale soils (Harris, 1973), probably ash-cloud deposits (perhaps flushed by rain as suggested by the presence of accretionary lapilli) associated with pyroclastic flows erupted from Mount Hood during late Polallie time about 12 ka (Crandell and Rubin, 1977; Crandell, 1980). **0.7**

Retrace route toward Highway 35.

4.4 Turn right on Whiskey Creek Road and then left on Highway 35. **0.7**

5.1 Cuts in olivine basalt. **4.2**

9.3 Parkdale soils on basalt opposite Odell Road. **0.6**

9.9 Road gradually climbs to saddle east of Middle Mountain, underlain by faulted N_2 flows of the Grande Ronde Basalt and Frenchman Springs Member (Swanson et al., 1981; Korosec, 1987b). Pliocene or Pleistocene olivine basalt occurs in and east of saddle. **0.6**

10.5 Hills ahead are eroded vents for the Pliocene or Pleistocene olivine basalt. **1.8**

12.3 At 10:00 is ridge in R_2 and N_2 flows of Grande Ronde Basalt and Frenchman Springs Member of Wanapum Basalt in Hood River fault zone (Swanson et al., 1981). **6.4**

18.7 Roadcut in Frenchman Springs Member cut by fault of Hood River fault zone (Swanson et al., 1981). **1.6**

20.3 Cuts in faulted N_2 Grande Ronde and Frenchman Springs in Hood River fault zone. **0.2**

20.5 Overbank deposits from Christmas 1980 flood down Polallie Creek and East Fork Hood River (Gallino and Pierson, 1984). **1.1**

21.6 **STOP 49. Andesite of Cloud Cap.** Be alert for rockfalls! Cliff face exposes intracanyon flows of normally magnetized plagioclase–olivine andesite of Cloud Cap (Keith et al., 1982; Wise, 1969), erupted from a vent at Cloud Cap on the northeast flank of Mount Hood about 10 km southwest of here. At least five flows totaling about 150 m thick were produced from this vent (Wise, 1969). The eruptions supposedly occurred after the main cone-building stage of Mount Hood but preceded the Fraser glaciation about 29 ka (Wise, 1969; Crandell, 1980). However, three K–Ar whole-rock ages from one sample near Cloud Cap vent are about 0.49, 0.63, and 0.65 Ma (Keith et al., 1985), coeval or even older than the main cone. Wise (1969) believed that the flows are not genetically related to those forming the cone of Mount Hood. Glaciofluvial deposits and Polallie-age lahars abut and overlie the andesite at this locality. **1.0**

22.6 To left on ridge are exposures of white pumiceous ash-flow tuff interleaved with hornblende dacite flows partly filling old valley (Wise, 1969). Both tuff and flows were erupted from dacite domes at Mill Creek Buttes; the domes have a K–Ar (hornblende) age of 6.2 ± 1.3 Ma (Fiebelkorn et al., 1983). Rugged point at 12:00 is olivine andesite of Cloud Cap. **0.6**

23.2 Cut in upper Miocene pyroxene andesite (Wise, 1969; Keith et al., 1982). Keith et al. (1985) obtained a K–Ar whole-rock age of 8.18 ± 0.06 Ma near here. **0.4**

23.6 Fault zone in upper Miocene andesite flow. **0.9**

24.5 Deposits of Christmas 1980 Polallie Creek flood along river, in places reworked by man. **0.4**

24.9 Good exposures east of river of upper Miocene andesite, K–Ar dated as 7.0 ± 0.8 Ma (Wise, 1969). The andesite is overlain by Quaternary olivine basalt and basaltic andesite (Wise, 1969). **0.3**

25.2 **STOP 50. Debris-flow deposits.** Mouth of Polallie Creek. Observe deposits and effects of the Christmas 1980 debris flow, whose volume is more than 20 times that of the initial slumped material and illustrates the process of sediment-bulking during transport (Gallino and Pierson, 1984). The debris flow, generated by intense rainfall, rushed down Polallie Creek, which cut into volcaniclastic deposits of Polallie age that contributed to the bulking. The debris flow dammed the river for 12–18 minutes; once the dam breached, a flood surged downstream, destroying 13 km of road and causing $13 million damage. **0.2**

25.4 Upper Miocene andesite in roadcuts. **1.2**

26.6 Roadcut exposing interbedded lake and lahar deposits of Polallie age (Crandell, 1980). Several cuts farther along show similar deposits. Polallie deposits, mainly pyroclastic flows near the volcano and lahars farther away, formed on all sides of the volcano. Here on the northeast side, the deposits form a broad triangular apron converging on Cooper Spur, 825 m below the present summit (Crandell, 1980). The deposits flank both sides of Polallie Creek and form a fill (mostly eroded) in the valley of East Fork Hood River downstream from the mouth of the creek (Crandell, 1980). These deposits created temporary dams and lakes upstream from Polallie Creek, and the thinly bedded fine sand and silt deposits in the roadcuts record these lakes (Crandell, 1980). **0.3**

26.9 Good exposure of interbedded lake and lahar deposits in cut opposite Sherwood Campground. **1.7**

28.6 Smooth topography is caused by huge fan of Fraser-age outwash that fills valley and extends down from Newton Clark Glacier. **5.7**

34.3 Roadcut in Quaternary andesite flow of the cone-building stage (Wise, 1969) (called Main Stage by White, 1980) of Mount Hood, with outwash beyond. **0.9**

35.2 Bennett Pass. Roadcuts expose three tills, the youngest of which is of Fraser age (Crandell, 1980). The ages of the older tills are not known. **0.3**

35.5 Next few cuts are in Miocene andesite flows. **1.3**

36.8 Cone-building andesite flow of Mount Hood. **0.4**

37.2 Cross White River. Terrace upstream is of Old Maid age (Crandell, 1980), about 1760–1810 A.D. (Cameron and Pringle, 1987). Outburst floods from White River Glacier destroyed bridges here five times in this century, most recently in 1959 and 1968. **0.1**

37.3 Turn right into parking area and then right on gravel road. **0.5**

37.8 Turn right onto top of levee. If road is bad, continue straight and park wherever possible. **0.2**

38.0 **STOP 51. Pyroclastic flow.** Walk to stream cuts exposing dacitic lithic pyroclastic flow (as thick as 10 m) of Old Maid age capped locally by at least two thin lahars (Crandell, 1980; Cameron and Pringle, 1987). The pyroclastic flow contains thoroughly charred wood and radially jointed blocks that magnetic measurements indicate were above the Curie point when deposited (Crandell, 1980). A ^{14}C age of 260 ± 150 yrs was obtained on the charred wood (Crandell, 1980). The pyroclastic flow

traveled down the easternmost drainage of the White River, probably from near Crater Rock, and entered the main drainage at a high angle, running about 75 m up the west valley wall; Cameron and Pringle (1987) calculated a minimum velocity of 135 km/hr from this relation. A Fraser-age lateral moraine stands above the left bank of the river. **1.1**

Return to Highway 35 and turn right.

39.1 Next several roadcuts are in Miocene andesite. **2.5**

41.6 Roadcut in Miocene platy andesite. **0.9**

42.5 Keep right toward Government Camp, merging onto Highway 26. Cross Salmon River drainage. **1.3**

43.8 Cuts in platy andesite of cone-building stage. **0.2**

44.0 **STOP 52. Andesite flow.** Quarry on right in platy, plagioclase–hypersthene andesite flow from cone-building stage of Mount Hood. Hypersthene is visible as light-brown phenocrysts. Flow contains abundant rounded inclusions of fresh holycrystalline microdiorite. More than 90% of the cone consists of preglacial (older than 29 ka) lava flows, breccia, and pyroclastic rocks, most of which are andesitic and about 70% of which are lava flows (Wise, 1969; White, 1980). No rocks with reversed magnetic polarity have been found, so the cone is assumed to postdate 0.73 Ma (White, 1980; Mankinen and Dalrymple, 1979). Keith et al. (1985) present K–Ar whole-rock ages ranging from 0.57 to 0.35 Ma for two cone-building lava flows in Zigzag Canyon. **1.0**

45.0 Turn right toward Timberline Lodge. For the next 2.6 mi the road passes through small cuts of Fraser-age till and cone-building andesite. **2.6**

47.6 Andesite flow overlying andesitic breccia. **1.5**

49.1 **STOP 53. Ash and diamict.** Cut in interlayered fine pink ash and coarse, grayish-pink diamict. A few clasts are radially jointed. Possibly the diamict was a lahar generated by collapse of a hot dome onto snow. The age is unknown but probably Polallie. **0.5**

49.6 Roadcut exposes diamict with scattered hot blocks capped by ash or wind-blown sand. Diamict overlies a cone-building andesite flow. **0.6**

50.2 Andesite flow capped by thin tephra layers. **0.3**

50.5 **STOP 54. Timberline Lodge.** Turn left into **bus** parking lot just before Lodge. Restrooms in building nearest the lot. Walk back down road 100 m to overflow parking lot and then up dirt road and cross country to Timberline (Skyline) Trail contouring on hill slope. Follow trail east across small creek (headwaters of Salmon River). Stop on crest of next ridge at Ghost Forest Overlook. From here one can look down White River and see a buried forest engulfed by fluvial and cold-lahar deposits of Old Maid age that form a flat-topped terrace. A ^{14}C age of 250 ± 150 yrs B.P. dates one of the buried stumps (Crandell, 1980). The Old Maid deposits formed a fill whose surface is about 100 m above the White River. Upstream is White River Glacier, source of the outburst floods that periodically destroy the bridge on Highway 35. The main thermal area of the volcano (in Devil's Kitchen) can be seen between the head of White River Glacier and the summit ridge; temperatures as high as 92°C, which is above boiling at 3171 m, have been measured (Nehring et al., 1981; Cameron, 1988). Crater Rock, remnant of a three-lobed hornblende dacite dome (Cameron and Pringle, 1986), can be seen left (west) of Devil's Kitchen. Crater Rock was probably emplaced at least in part in Old Maid time (Crandell, 1980; Cameron and Pringle, 1986), although Wise (1968, 1969) ascribed it to what today is called the Timberline eruptive period. Trim lines from the neoglacial maximum (about 1740 A.D.) can be seen below Steel Cliff, to right of White River Glacier.

Many trees near Timberline Lodge, including those at this locality (the Ghost Forest), were killed around 1795–1810, probably near 1800 A.D. (Lawrence, 1948). The trees were killed neither by beetles (no galleries exist below the remaining bark) nor by forest fire (no charring can be found on the dead trees). The ghost forest occurs only within about 500 m of the west side of White River canyon and within 2 km of the east side (Cameron and Pringle, 1987). The trees were probably killed by a hot ash cloud that rose from the dacitic lithic pyroclastic flow observed at Stop 51 (Cameron and Pringle, 1987).

Walk to south end of lower paved parking area near bus parking lot. Several layers of Timberline tephra in a 35 cm thick section overlie the weathered top of a Polallie-age lahar and underlie young soil and possibly an Old Maid-age tephra. The Timberline-age tephra here comprise two or three light-colored ash layers sandwiched in dark andesitic or muddy ash. Note the surrounding ghost forest, near its western limit. **5.2**

Return to Highway 26.

55.7 Junction with Highway 26. Turn right. **2.3**

58.0 Polallie-age lahars in roadcuts (Crandell, 1980). **0.2**

58.2 Roadcut in quartz diorite of Laurel Hill. **0.4**

58.6 Fractured margin of Laurel Hill pluton. **0.3**

58.9 At 3:00 across Little Zigzag Canyon is cliff of Mount Hood andesite flows. **0.1**

59.0 Roadcut in Laurel Hill pluton. Many cuts in next mile expose this pluton. **1.2**

60.2 Two dikes cut the Laurel Hill pluton. We will stop here later in the day. Roadcuts expose the Laurel Hill pluton for next 1 mi. **1.2**

61.4 Turn right from Highway 26 onto road toward Mount Hood Kiwanis Camp. **1.9**

63.3 **STOP 55. Pyroclastic flows.** Bus can turn around 0.2 mi farther. Small quarry in three lithic pyroclastic flows of Timberline age. Wood is entirely charred in uppermost thick gray deposit and partly charred in the underlying two flows. Prismatically jointed blocks are scarce. Below the thickest gray flow is a poorly exposed thin unit with noncharred wood that may record high-energy, surgelike emplacement. Radiocarbon ages on wood in the deposits indicate that the thick gray flow is 1440 ± 155 yrs B.P. (Cameron and Pringle, 1986) and the second unit below it is 1830 ± 50 yrs B.P. (K. A. Cameron and P. T. Pringle, unpubl. data). Tan unit on top of gray pyroclastic flow is cold lahar that is also likely of Timberline age, for no recognizable

weathering zone separates it from the pyroclastic flows. **0.2**

63.5 Bus turnaround. Return to quarry. **2.0**

65.5 Highway 26. Turn left and retrace route to Laurel Hill pluton. **1.2**

66.7 **STOP 56. Laurel Hill pluton.** Stop on outside of curve. The Laurel Hill pluton is plagioclase–hornblende-phyric quartz diorite with lesser quartz monzonite and patches of granophyre (Wise, 1969). Its groundmass is pervasively propylitized. Similar bodies crop out 4 km to the south along Still Creek and 2 km to the west along Zigzag River. Drilling on the south side of Zigzag Mountain and in the Old Maid Flat area, 4 km and 10 km respectively northwest of here, penetrated similar quartz diorite. These bodies are likely connected at depth (Wise, 1969). The quartz diorite intrudes the Grande Ronde and Wanapum Basalts, the Rhododendron Formation (about 14–11 Ma; D. R. Sherrod, written comm. 1988), and the Last Chance andesite (K–Ar whole-rock ages of 10.7 ± 0.5 and 10.5 ± 0.5 Ma) (Priest et al., 1982). For the Laurel Hill pluton, Bikerman (1970) obtained K–Ar hornblende ages of 8.4 ± 0.6 and 8.0 ± 0.6 Ma, and Keith et al. (1985) determined K–Ar whole-rock ages of 8.6 ± 0.14 and 8.75 ± 0.18 Ma on a single sample. Priest et al. (1982) reported a K–Ar hornblende age of 9.3 ± 0.9 for biotite-bearing hornblende microquartz diorite in a drill hole near Old Maid Flat. Wise (1969) noted that a K–Ar age of 11.6 ± 1.2 Ma for the Laurel Hill was too old, for the pluton intrudes definitely younger rocks. The Laurel Hill pluton, just as the Tatoosh pluton at Mount Rainier, cooled during a field reversal (from reverse to normal) (Dunn et al., 1971). Walk up road 200 m to see two slightly vesicular andesite dikes cutting the quartz diorite. Bikerman (1970) apparently dated one of these dikes as about 5 Ma (K–Ar whole-rock). **0.5**

67.2 Tom Dick and Harry Mountain at 3:00, composed of upper Miocene and Pliocene andesite. **2.7**

69.9 Turn right into parking area, turn around, and continue west. **5.7**

75.6 Road is on lahar surface of post-Fraser age. Valley walls in Rhododendron Formation. **4.4**

80.0 Forest Service Station in Zigazg. Continue west on Highway 26 toward Portland or turn right on East Lolo Pass Road for optional side trip. **2.5**

Optional side trip to Old Maid Flat

Mileage

(0.0) Junction of Highway 26 and East Lolo Pass Road. Leave Highway 26. **4.3**

(4.3) Stay left at junction with Road 1825 to Old Maid Flat. **0.2**

(4.5) **STOP 57. Andesite flow and view of west flank of Mount Hood.** Dirt road on left to abandoned quarry. Bus can turn around easily and park. Walk up road 350 m to roadcut in andesite flow of Rhododendron Formation (Keith et al., 1982). A dirt road leads uphill and under the power lines from the downhill end of the roadcut. Valley of the Sandy River and the west flank of Mount Hood can be seen from under the power lines. The flat valley floor (Old Maid Flat) is formed from clastic debris from all four of the syn- and post-glacial eruptive periods. The two large glaciers on the mountain are the Sandy (left) and Reid, separated by Yocum Ridge. Right of Reid Glacier is Illumination Ridge, formed by a very thick cone-building andesite flow. Far right shoulder of volcano is smooth profile of debris fan mostly constructed during Timberline time, 1400–1800 yrs B.P. **0.2**

(4.7) Retrace route to Road 1825 and turn left. **0.5**

(5.2) Keep right on Muddy Fork Road 1825 at junction. Snags visible about 0.25 mi upstream in the Sandy River record a forest buried by Old Maid-age lahars. **1.3**

(6.5) Continue on narrow paved road across Old Maid Flat. Some parts of the flat are primary lahar surfaces; others are reworked and channeled. The droughty vegetation generally reflects poor soil development on the young lahars. Trees cannot root deeply on the lahar deposit, so windfalls are common. **1.5**

(8.0) **STOP 58. Old Maid lahars and other Mount Hood eruptive products.** At Lost Creek turnoff, continue straight toward Ramona Falls trailhead (Old Portage trail on some maps). Just south of parking area, an Old Maid lahar deposit exposed in an 8 m high terrace sequence abutting the valley wall contains snags of western red cedar and tree molds that are probably relics of rotted western hemlocks. Large Douglas firs growing on lower terrace postdate the Old Maid-age lahar.

Walk to trailhead at north side of parking lot, cross bridge, and hike about 400 m up Ramona Falls loop trail in a counterclockwise direction to see an assemblage of deposits from the last three eruptive periods of Mount Hood. Exposed in south-facing bank are a 1.5 m thick, terrace-capping lahar of Old Maid age (emplaced in the 1790's according to provisional tree-ring ages), a thin (10 cm) pink Zigzag-age tephra layer (560 ± 150 yrs B.P. (Cameron and Pringle, 1986)), and a pink, probably Timberline (1400–1800 yrs B.P.) lahar.

Those who complete the Ramona Falls loop will find that the trail ascends a series of nested, lahar-capped terraces of respectively older material. The thick, pink Timberline-age debris fan forming the south bank of Sandy River is visible along trail. Ramona Falls is in a columnar basalt of late Pliocene age. Relics of ancestral riparian forest buried by Old Maid-age lahars occur about 500 m southeast of Muddy Fork bridge, where large snags are visible to north. Walk toward snags to find tree molds, some of which are 7 m deep. The snags and tree molds probably define a pre-Old Maid-age channel of the Muddy Fork. **8.0**

(16.0) **End of optional trip.** Return to Highway 26 and turn right to rejoin regular trip.

82.5 Signal light in Welches, built on a Timberline lahar surface. **44.5**

To reach I-84, continue on Highway 26 to Gresham. Then:

127.0 Continue straight on Burnside rather than turning left on Highway 26 toward Portland. **0.7**

127.7 Turn right at signal on SE 242nd. Drive toward I-84 and follow signs; stay on same road all the way. **2.8**

130.5 Wood Village–Gresham Interchange at I-84.

Optional trip to Mount Tabor and Boring Lava

Mileage

(0.0) At mileage 127.7, continue straight on Burnside. **0.3**

(0.3) At signal light, turn left onto Division. Follow Division to mile 8.9. **2.1**

(2.4) At 9:00 is a cone-shaped hill of Pliocene and early Pleistocene Walters Hill Formation (conglomerate, sandstone, and mudflows) (Trimble, 1963). **4.0**

(6.4) At 9:00 is Kelly Butte, a cinder cone of the Boring Lava (Treasher, 1942; Trimble, 1963; Allen, 1975; Tolan and Beeson, 1984), which contains Pliocene and Pleistocene olivine-basalt and basaltic-andesite flows with vents throughout the Portland metropolitan area. **0.7**

(7.1) Pass beneath I-205. **0.8**

(7.9) Mount Tabor, another Boring cone, to right. **1.0**

(8.9) Turn right on SE 60th Avenue. **0.5**

(9.4) Turn right on SE Salmon for Mount Tabor. **0.3**

(9.7) Sharp turn to left. Parking lot here affords view of city center and the Portland Hills, which are a faulted anticline of Grande Ronde and Wanapum (Frenchman Springs) Basalts overlain in places by Boring Lava. **0.3**

(10.0) **STOP 59. Mount Tabor basalt cone.** Turn into parking lot. A partial cross section of the Mount Tabor cone of olivine basalt is exposed beside the basketball court and outdoor theater. Some of the cinder beds contain very large ejecta (more than 1 m in long dimension), whereas other beds, especially high in the section, are relatively fine-grained and well sorted. The general dip is northwestward, away from the breached crater that the road traverses. Several fault surfaces suggest slumping of the flank of the cone during its formation. Gravel in some of the younger beds in the middle of the exposure was probably derived from the underlying Troutdale Formation (Trimble, 1963), and the younger beds at the north end of the exposure are partly palagonitized. This evidence suggests interaction with water.

Allen (1975) located more than 30 Boring vents within 21 km of here and more than 90 vents (about 50 of which he classified as "certain") within 32 km of Troutdale (5 km northeast of Gresham). The Boring Lava in this area is between 1.3 Ma (Rocky Butte, 3 km northest of here) and 2.1 Ma (in bluffs near Oregon City, 18 km south of here), judging from unpublished K–Ar ages (D. R. Sherrod, oral comm. 1988) and a K–Ar age of 1.56 ± 0.2 Ma on a flow at Bear Prairie 29 km east-northeast of here (Tolan and Beeson, 1984).

The setting of the basalt field is puzzling and not understood. The vents lie well west of the crest of the Cascades, and those such as Kelly Butte, Mount Tabor, and the vents in the Portland Hills are in and even west of the Portland basin.

Acknowledgments

We thank Dave Sherrod and Jim Moore for providing incisive reviews; Paul Hammond for graciously contributing unpublished information about Indian Heaven, and Jim Vallance for doing likewise for Stop 58; Gordon Keating and Lyn Topinka for preparing many of the illustrations; Craig Weaver for allowing use of Fig. 3; and Barbara White for helping to log several legs of the trip. Prime responsibility for preparation of the road logs is as follows: Vance for Issaquah to Cle Elum and related text; Evarts for Tertiary geology near Mount St. Helens; Cameron and Pringle for Mount Hood; and Swanson for the remainder.

References

Allen, J. E., 1975, Volcanoes of the Portland area, Oregon: Ore Bin, 37: 145–157.

Alt, D., Sears, J. W., and Hyndman, D. W., 1988, Terrestrial maria: the origins of large basalt plateaus, hotspot tracks and spreading ridges: Journal of Geology, 96: 647–662.

Anderson, J. L., 1980, Pomona Member of the Columbia River Basalt Group: an intracanyon flow in the Columbia River Gorge, Oregon: Oregon Geology, 42: 195–199.

Anderson, J. L., and Vogt, B. F., 1987, Intracanyon flows of the Columbia River Basalt Group in the southwest part of the Columbia Plateau and adjacent Cascade Range, Oregon and Washington: Washington Division of Geology and Earth Resources, Bulletin, 77: 249–267.

Anderson, J. L., Beeson, M. H., and Tolan, T. L., 1987, Tectonic evolution of the southwest Columbia Plateau (abs.): Geological Society of America, Abstracts with Programs, 19: 354–355.

Armstrong, R. L., 1978, Cenozoic igneous history of the U.S. Cordillera from lat 42° to 49° N: Geological Society of America, Memoir 152: 265–282.

Armstrong, R. L., Leeman, W. P., and Malde, H. E., 1975, K–Ar dating, Quaternary and Neogene volcanic rocks of the Snake River Plain, Idaho: American Journal of Science, 275: 225–251.

Atwater, T., 1970, Implications of plate tectonics for the Cenozoic tectonic evolution of western North America: Geological Society of America, Bulletin, 81: 3513–3536.

Bailey, M. M., 1986, The stratigraphy and petrochemistry of the Picture Gorge Basalt, north-central Oregon: Unpublished M.S. thesis, Washington State University, Pullman, 156 pp.

Bailey, M. M. (in press), Revisions to stratigraphic nomenclature of the Picture Gorge Basalt Subgroup, Columbia River Basalt Group; *in* Reidel, S. P., Hooper, P. R., and Anderson, J. L. (eds.), Volcanism and Tec-

tonism on the Columbia Plateau: Geological Society of America, Special Paper.
Baksi, A. J., 1988, Estimation of lava extrusion and magma production rates for two flood basalt provinces: Journal of Geophysical Research, 93: 11,809–11,815.
Barnosky, C. W., 1985, Late Quaternary vegetation near Battle Ground Lake, southern Puget Trough, Washington: Geological Society of America, Bulletin, 96: 263–271.
Barrash, W., Bond, J., and Venkatakrishnan, R., 1983, Structural evolution of the Columbia Plateau in Washington and Oregon: American Journal of Science, 283: 897–935.
Bates, R. G., Beck, M. E., Jr., and Burmester, R. F., 1981, Tectonic rotations in the Cascade Range of southern Washington: Geology, 9: 184–189.
Beck, M. E., Jr., 1980, Paleomagnetic record of plate-margin tectonic processes along the western edge of North America: Journal of Geophysical Research, 85: 7115–7131.
Beck, M. E., Jr., and Burr, C. D., 1979, Paleomagnetism and tectonic significance of the Goble Volcanic Series, southwestern Washington: Geology, 7: 175–179.
Becraft, G. E., 1950, Definition of the Tieton andesite on lithology and structure: Unpublished M.S. thesis, Washington State University, Pullman, 26 pp.
Beeson, M. H., Fecht, K. R., Reidel, S. P., and Tolan, T. L., 1985, Regional correlations within the Frenchman Springs Member of the Columbia River Basalt Group: new insights into the middle Miocene tectonics of northwestern Oregon: Oregon Geology, 47: 87–96.
Bentley, R. D., 1977, Stratigraphy of the Yakima basalts and structural evolution of the Yakima Ridges in the western Columbia Plateau; *in* Brown, E. H., and Ellis, R. C. (eds.), Geological excursions in the Pacific Northwest: Department of Geology, Western Washington University, Bellingham, pp. 339–389.
Bentley, R. D., and Anderson, J. L., 1980, Wrench tectonics in the Yakima ridges of the Columbia Plateau, Washington and Oregon (abs.): Geological Society of America, Abstracts with Programs, 12: 267.
Bikerman, M., 1970, K–Ar ages of Laurel Hill pluton and dike, Oregon: Ore Bin, 32: 211–215.
Birch, D. C., 1961, Big Eddy–McLoughlin Line Tower 36/2 Ladd Creek washout: Bonneville Power Administration in-house memorandum, 9 pp.
Blackwell, D. D., and Steele, J. L., 1983, A summary of heat flow studies in the Cascade Range: Geothermal Resources Council, Transactions, 7: 233–236.
Blackwell, D. D., Bowen, R. G., Hull, D. A., Riccio, J., and Steele, J. L., 1982, Heat flow, arc volcanism, and subduction in northern Oregon: Journal of Geophysical Research, 87: 8735–8754.
Borchardt, G. A., Norgren, J. A., and Harward, M. E., 1973, Correlation of ash layers in peat bogs of eastern Oregon: Geological Society of America, Bulletin, 84: 3101–3108.
Brantley, S. R., and Waitt, R. B., 1988, Interrelations among pyroclastic surge, pyroclastic flow, and lahars in Smith Creek valley during first minutes of 18 May 1980 eruption of Mount St. Helens, USA: Bulletin of Volcanology, 50: 304–326.
Broughton, W. R., 1929, The exploration of the Columbia River; *in* An extract from the journal of Captain George Vancouver: Longview Daily News Press, Longview, Wash., 39 pp.
Brown, E. H., 1986, Geology of the Shuksan Suite, North Cascades, Washington: Geological Society of America, Memoir, 164: 143–154.
Brown, E. H., Wilson, D. L., Armstrong, R. L., and Harakal, J. E., 1982, Petrologic, structural, and age relations of serpentinite, amphibolite, and blueschist in the Shuksan Suite of the Iron Mountain–Gee Point area, North Cascades, Washington: Geological Society of America, Bulletin, 93: 1087–1098.
Brown, G. C., 1982, Calc-alkaline intrusive rocks: Their diversity, evolution, and relation to volcanic arcs; *in* Thorpe, R. S. (ed.), Andesites: Orogenic Andesites and Related Rocks: John Wiley, New York, pp. 437–461.
Brugman, M. M., 1988, Groundwater discharge within a glaciated stratovolcano: what happens to missing surface runoff? (abs.): Geological Society of America, Abstracts with Programs, 20: 115.
Buckovic, W. A., 1979, The Eocene deltaic system of west-central Washington; *in* Cenozoic paleogeography of the western United States: Society of Economic Paleontologists and Mineralogists, Pacific Coast Section, Los Angeles, pp. 147–163.
Byerly, G. R., and Swanson, D. A., 1978, Invasive Columbia River basalt flows along the northwestern margin of the Columbia Plateau, north-central Washington (abs.): Geological Society of America, Abstracts with Programs, 10: 98.
Byerly, G. R., and Swanson, D. A., 1987, The transition from subaerial to invasive lava flows, Grande Ronde Basalt, northwestern Columbia Plateau (abs.): Geological Society of America, Abstracts with Programs, 19: 363.
Cameron, K. A., 1988, Fumarole fields and thermal features at Mount Hood, Oregon: Northwest Science, 62: 82.
Cameron, K. A., and Pringle, P., 1986, Post-glacial lahars of the Sandy River basin, Mount Hood, Oregon: Northwest Science: 60: 225–237.
Cameron, K. A., and Pringle, P., 1987, A detailed chronology of the most recent major eruptive period at Mount Hood, Oregon: Geological Society of America, Bulletin, 99: 845–851.
Camp, V. E., 1981, Geologic studies of the Columbia Plateau: Part II. Upper Miocene basalt distribution, reflecting source locations, tectonism, and drainage history in the Clearwater embayment, Idaho: Geological Society of America, Bulletin, 92: 669–678.
Carey, S., and Sigurdsson, H., 1985, The May 18, 1980 eruption of Mount St. Helens 2. Modeling of dynamics of the Plinian phase: Journal of Geophysical Research, 90: 2948–2958.
Carkin, B. A., 1985, Geology and petrology of the Fifes Peak Formation in the Cliffdell area, central Cascades, Washington (abs.): Geological Society of America, Abstracts with Programs, 17: 347.
Carlson, R. W., 1984, Isotopic constraints on Columbia River flood basalt genesis and the nature of the subcontinental mantle: Geochimica et Cosmochimica Acta, 48: 2357–2372.
Carlson, R. W., and Hart, W. K., 1988, Flood basalt volcanism in the northwestern United States; *in* Macdougall, J. D. (ed.), Continental Flood Basalts: Kluwer Academic Publishers, Dordrecht, pp. 35–61.
Cashman, K. V., 1988, Crystallization of Mount St. Helens 1980–1986 dacite: a quantitative textural approach: Bulletin of Volcanology, 50: 194–209.
Cassidy, J. J., Coombs, H. A., and Shannon, W. L., 1980, Study of effects of potential volcanic activity on Lewis River projects: Unpublished report to the Pacific Power and Light Co., Portland, Oregon, 91 pp.
Catchings, R. D., and Mooney, W. D., 1988, Crustal structure of the Columbia Plateau: evidence for continental rifting: Journal of Geophysical Research, 93: 459–474.
Chadwick, W. W., Archuleta, R. J., and Swanson, D. A., 1988, The mechanics of ground deformation precursory to dome-building extrusions at Mount St. Helens 1981–1982: Journal of Geophysical Research, 93: 4351–4366.
Chadwick, W. W., Iwatsubo, E. Y., Swanson, D. A., and Ewert, J. W., 1985, Measurements of slope distances and vertical angles at Mount Baker and Mount Rainier, Washington, Mount Hood and Crater Lake, Oregon, and Mount Shasta and Lassen Peak, California, 1980–1984: U.S. Geological Survey, Open-File Report 85-205: 96 pp.
Christiansen, R. L., and McKee, E. H., 1978, Late Cenozoic volcanic and tectonic evolution of the Great Basin and Columbia Intermontane regions: Geological Society of America, Memoir 152: 283–311.
Clayton, G. A., 1983, Geology of the White Pass area, south-central Cascade Range, Washington: Unpublished M.S. thesis, University of Washington, Seattle, 212 pp.
Coleman, S. M., and Pierce, K. L., 1981, Weathering rinds on andesitic and basaltic stones as a Quaternary age indicator, western United States: U.S. Geological Survey, Professional Paper 1210: 56 pp.
Condie, K. C., and Swensen, D. H., 1973, Compositional variation in three Cascade stratovolcanoes: Jefferson, Rainier, and Shasta: Bulletin Volcanologique, 37: 205–230.
Conway, T. R., 1921, Mount Hood in eruption: Mazama, 6: 40–43.
Couch, R. W., and Baker, B., 1979, Geophysical investigations of the Cascade Range in central Oregon: Final report, grant 14-08-001-G-393, U.S. Geological Survey, Reston, Virginia, 95 pp.
Cox, K., 1980, A model for flood basalt volcanism: Journal of Petrology, 21: 629–650.
Crandell, D. R., 1980, Recent eruptive history of Mount Hood, Oregon, and potential hazards from future eruptions: U.S. Geological Survey, Bulletin 1492: 81 pp.
Crandell, D. R., 1987, Deposits of pre-1980 pyroclastic flows and lahars from Mount St. Helens volcano, Washington: U.S. Geological Survey, Professional Paper 1444: 95 pp.
Crandell, D. R., and Hoblitt, R. P., 1986, Lateral blasts at Mount St. Helens and hazard zonation: Bulletin of Volcanology, 48: 27–37.
Crandell, D. R., and Miller, R. D., 1974, Quaternary stratigraphy and extent of glaciation in the Mount Rainier region, Washington: U.S. Geological Survey, Professional Paper 847: 59 pp.
Crandell, D. R., and Mullineaux, D. R., 1978, Potential hazards from future eruptions of Mount St. Helens, Washington: U.S. Geological Survey, Bulletin 1383-C: 26 pp.
Crandell, D. R., and Rubin, M., 1977, Late-glacial and postglacial erup-

tions at Mt. Hood, Oregon (abs.): Geological Society of America, Abstracts with Programs, 9: 406.

Crandell, D. R., Mullineaux, D. R., Rubin, M., Spiker, E., and Kelley, M. L., 1981, Radiocarbon dates from volcanic deposits at Mt. St. Helens, Washington: U.S. Geological Survey, Open-File Report 81-844, 15 pp.

Criswell, C. W., 1987, Chronology and pyroclastic stratigraphy of the May 18, 1980, eruption of Mount St. Helens, Washington: Journal of Geophysical Research, 92: 10,237–10,266.

Davis, G. A., 1981, Late Cenozoic tectonics of the Pacific Northwest with special reference to the Columbia Plateau: Final Safety Analysis Report WNP-2, Amendment 18, appendix, Washington Public Power Supply System, Richland, 69 pp.

Davis, G. D., Monger, J. W. H., and Burchfiel, B. C., 1978, Mesozoic construction of the Cordilleran "Collage," central British Columbia to central California; *in* Mesozoic paleogeography of the western United States: Society of Economic Paleontologists and Mineralogists, Pacific Coast Paleography Symposium 2, Los Angeles, pp. 33–70.

Davis, J. O., 1978, Quaternary tephrochronology of the Lake Lahontan area, Nevada and California: Nevada Archeological Survey, Research Paper 7: 29 pp.

DeGraff, J. M., and Aydin, A., 1987, Surface morphology of columnar joints and its significance to mechanics and direction of joint growth: Geological Society of America, Bulletin, 99: 605–617.

Doukas, M. P., and Swanson, D. A., 1987, Mount St. Helens, Washington, with emphasis on 1980–85 eruptive activity as viewed from Windy Ridge: Geological Society of America, Centennial Field Guide—Cordilleran Section, pp. 333–338.

Driedger, C. L., and Kennard, P. M., 1986, Ice volumes on Cascade volcanoes: Mount Rainier, Mount Hood, Three Sisters, and Mount Shasta: U.S. Geological Survey, Professional Paper 1365: 28 pp.

Duncan, R. A., 1982, A captured island chain in the Coast Range of Oregon and Washington: Journal of Geophysical Research, 87: 10,827–10,837.

Dungan, M. A., Vance, J. A., and Blanchard, D. P., 1983, Geochemistry of the Shuksan greenschists and blueschists, North Cascades, Washington: variably fractionated and altered meta-basalts of oceanic affinity: Contributions to Mineralogy and Petrology, 82: 131–146.

Dunn, J. R., Fuller, M., Ito, H., and Schmidt, V. A., 1971, Paleomagnetic study of a reversal of the Earth's magnetic field: Science, 172: 840–845.

Dzurisin, D., Koyanagi, R. Y., and English, T. T., 1984, Magma supply and storage at Kilauea Volcano, Hawaii, 1956–1983: Journal of Volcanology and Geothermal Research, 21: 177–206.

Eaton, G. P., Wahl, R. R., Prostka, H. J., Mabey, D. R., and Kleinkopf, M. D., 1978, Regional gravity and tectonic patterns: their relation to late Cenozoic epierogeny and lateral spreading in the western Cordillera: Geological Society of America, Memoir 152: 51–91.

Eichelberger, J. C., and Hayes, D. B., 1982, Magmatic model for the Mount St. Helens blast of May 18, 1980: Journal of Geophysical Research, 87: 7727–7738.

Ellingson, J. A., 1972, The rocks and structure of the White Pass area, Washington: Northwest Science, 46: 9–24.

Endo, E. T., Malone, S. D., Noson, L. L., and Weaver, C. S., 1981, Locations, magnitudes and statistics of the March 20–May 18 earthquake sequence: U.S. Geological Survey, Professional Paper 1250: 93–107.

Engels, J. C., Tabor, R. W., Miller, F. K., and Obradovich, J. D., 1976, Summary of K–Ar, Rb–Sr, U–Pb, Pb-alpha, and fission-track ages of rocks from Washington state prior to 1975 (exclusive of Columbia Plateau basalts), scale 1:1,000,000: U.S. Geological Survey, Miscellaneous Field Studies Map MF-710.

Erikson, E. H., Jr., 1969, Petrology of the composite Snoqualmie batholith, central Cascade Mountains, Washington: Geological Society of America, Bulletin, 80: 2213–2236.

Evarts, R. C., and Ashley, R. P., 1984, Preliminary geologic map of the Spirit Lake quadrangle, Washington, scale 1:48,000: U.S. Geological Survey, Open-File Map 84-480.

Evarts, R. C., Ashley, R. P., and Smith, J. G., 1987, Geology of the Mount St. Helens area: record of discontinuous volcanic and plutonic activity in the Cascade arc of southern Washington: Journal of Geophysical Research, 92: 10,155–10,169.

Ewart, A., 1982, The mineralogy and petrology of Tertiary–Recent orogenic volcanic rocks: With special emphasis to the andesite–basaltic andesite range; *in* Thorpe, R. S. (ed.), Andesites: Orogenic Andesites and Related Rocks: John Wiley, New York, pp. 25–95.

Ewing, T. E., 1980, Paleogene tectonic evolution of the Pacific Northwest: Journal of Geology, 88: 619–638.

Fecht, K. R., Reidel, S. P., and Tallman, A. M., 1987, Paleodrainage of the Columbia River system on the Columbia Plateau of Washington state—a summary: Washington Division of Geology and Earth Resources, Bulletin, 77: 219–248.

Felts, W. M., 1939, A granodiorite stock in the Cascade Mountains of southwestern Washington: Ohio Journal of Science, 39: 297–316.

Fiebelkorn, R. B., Walker, G. W., MacLeod, N. S., McKee, E. H., and Smith, J. G., 1983, Index to K–Ar determinations for the state of Oregon: Isochron/West, 37: 3–60.

Finn, C., and Williams, D. L., 1987, An aeromagnetic study of Mount St. Helens: Journal of Geophysical Research, 92: 10,194–10,206.

Fiske, R. S., 1963, Subaqueous pyroclastic flows in the Ohanapecosh Formation, Washington: Geological Society of America, Bulletin, 74: 391–406.

Fiske, R. S., Hopson, C. A., and Waters, A. C., 1963, Geology of Mount Rainier National Park, Washington: U.S. Geological Survey, Professional Paper 444: 93 pp.

Flanagan, G., and Williams, D. L., 1982, A magnetic investigation of Mount Hood, Oregon: Journal of Geophysical Research, 87: 2804–2814.

Foster, R. J., 1960, Tertiary geology of a portion of the central Cascade Mountains, Washington: Geological Society of America, Bulletin, 71: 99–125.

Frizzell, V. A., Jr., Tabor, R. W., Zartman, R. E., and Blome, C. D., 1987, Late Mesozoic or early Tertiary melanges in the western Cascades of Washington: Washington Division of Geology and Earth Resources, Bulletin, 77: 129–148.

Frizzell, V. A., Jr., Tabor, R. W., Booth, D. B., Ort, K. M., and Waitt, R. B., Jr., 1984, Preliminary geologic map of the Snoqualmie Pass 1:100,000 quadrangle, Washington: U.S. Geological Survey, Open-File Report 84-693: 42 pp.

Furlong, K. P., and Fountain, D. M., 1986, Continental crustal underplating: thermal considerations and seismic–petrologic consequences: Journal of Geophysical Research, 91: 8285–8294.

Gallino, G. L., and Pierson, T., 1984, The 1980 Polallie Creek debris flow and subsequent dam-break flood, East Fork Hood River basin, Oregon: U.S. Geological Survey, Open-File Report 84-578: 37 pp.

Gill, J., 1981, Orogenic andesites and plate tectonics: Springer Verlag, New York, 390 pp.

Grant, R. Y., 1941, A John Day vertebrate fossil discovered in the Keechelus Series of Washington: American Journal of Science, 239: 590–593.

Grant, W. C., Weaver, C. S., and Zollweg, J. E., 1984, The 14 February Elk Lake, Washington, earthquake sequence: Seismological Society of America, Bulletin, 74: 1289–1309.

Greeley, R., 1977, Basaltic "plains" volcanism; *in* Greeley, R., and King, J. S. (eds.), Volcanism of the eastern Snake River Plain, Idaho: NASA CR-154621, pp. 23–44.

Greeley, R., and Hyde, J. H., 1972, Lava tubes of the Cave Basalt, Mount St. Helens, Washington: Geological Society of America, Bulletin, 83: 2397–2418.

Gresens, R. L., Whetten, J. T., Tabor, R. W., and Frizzell, V. A., 1977, Part III: Tertiary stratigraphy of the central Cascade Mountains, Washington state; *in* Brown, E. H., and Ellis, R. C. (eds.), Geological excursions in the Pacific Northwest: Geological Society of America, Field Guide, Seattle, pp. 84–126.

Grommé, S. C., Beck, M. E., Jr., Wells, R. E., and Engebretson, D. C., 1986, Paleomagnetism of the Tertiary Clarno Formation of central Oregon and its significance for the tectonic history of the Pacific Northwest: Journal of Geophysical Research, 91: 14,089–14,103.

Guffanti, M., and Weaver, C. S., 1988, Distribution of late Cenozoic volcanic vents in the Cascade Range: Volcanic arc segmentation and regional tectonic considerations: Journal of Geophysical Research, 93: 6513–6529.

Hague, A., 1871, Glaciers of Mount Hood: American Journal of Science (3), 1: 165–167.

Hammond, P. E., 1977, Part IV: Stratigraphy, structure, and plutonism along the upper Yakima and South Fork Snoqualmie River valleys, central Cascade Range, Washington; *in* Brown, E. H., and Ellis, R. C. (eds.), Geological Excursions in the Pacific Northwest: Geological Society of America, Field Guide, Seattle, pp. 292–308.

Hammond, P. E., 1979, A tectonic model for evolution of the Cascade Range; *in* Cenozoic paleogeography of the western United States: Society of Economic Paleontologists and Mineralogists, Pacific Coast Paleogeography Symposium 3, Los Angeles, pp. 219–237.

Hammond, P. E., 1980, Reconnaissance geologic map and cross sections of southern Washington Cascade Range: Publications of Department of Earth Science, Portland State University, Portland, Oregon.

Hammond, P. E., 1984, Indian Heaven, S. Washington Cascade Range: A basaltic volcanic field supplied by a central magma system? (abs.): Geological Society of America, Abstracts with Programs, 16: 528.

Hammond, P. E., 1987, Lone Butte and Crazy Hills: Subglacial volcanic complexes, Cascade Range, Washington: Geological Society of America, Centennial Field Guide—Cordilleran Section, pp. 339–344.

Hammond, P. E., and Korosec, M. A., 1983, Geochemical analyses, age dates, and flow-volume estimates for Quaternary volcanic rocks, southern Cascade Mountains, Washington: Washington Division of Geology and Earth Resources, Open-File Report 83-13: 36 pp.

Hammond, P. E., Petersen, S. A., Hopkins, K. D., Aiken, D., Harle, D. S., Daneš, Z. F., Konicek, D. L., and Stricklin, C. R., 1976, Geology and gravimetry of the Quaternary basaltic volcanic field, southern Cascade Range, Washington; *in* Proceedings of Second United Nations Symposium on Development and Use of Geothermal Resources, 1: San Francisco, pp. 397–405.

Harris, B. L., 1973, Genesis, mineralogy, and properties of Parkdale soils, Oregon: Unpublished Ph.D. dissertation, Oregon State University, Corvallis, 174 pp.

Hart, W. K., and Carlson, R. W., 1987, Tectonic controls on magma genesis and evolution in the northwestern United States: Journal of Volcanology and Geothermal Research, 32: 119–136.

Heliker, C. C., 1983, Inclusions in the 1980–1983 dacite of Mount St. Helens: American Geophysical Union (EOS), Transactions, 64: 894.

Heliker, C. C., 1984, Inclusions in the 1980–83 dacite of Mount St. Helens, Washington: Unpublished M.S. thesis, Western Washington University, Billingham, 185 pp.

Heller, P. L., Tabor, R. W., and Suczek, C. A., 1987, Paleogeographic evolution of the United States Pacific Northwest during Paleogene time: Canadian Journal of Earth Sciences, 24: 1652–1667.

Helz, R. T., 1978, The petrogenesis of the Ice Harbor Member, Columbia Plateau, Washington—a chemical and experimental study: Unpublished Ph.D. dissertation, Pennsylvania State University, University Park, 284 pp.

Hildreth, E. W., and Fierstein, J., 1985, Mount Adams: Eruptive history of an andesite–dacite volcano at the focus of a fundamentally basaltic volcanic field: U.S. Geological Survey, Open-File Report 85-521: 44–50.

Hildreth, W., Fierstein, J., and Miller, M. S., 1983, Mineral and geothermal resource potential of the Mount Adams Wilderness and contiguous roadless areas, Skamania and Yakima Counties, Washington: U.S. Geological Survey, Open-File Report 83-474: 50 pp.

Hoblitt, R. P., and Miller, D. C., 1984, Comment: Geology, 12: 692–693.

Hoblitt, R. P., Crandell, D. R., and Mullineaux, D. R., 1980, Mount St. Helens eruptive behavior during the past 1,500 yr: Geology, 8: 555–559.

Hodge, E. T., 1938, Geology of the Lower Columbia River: Geological Society of America, Bulletin, 49: 831–930.

Hooper, P. R., 1982, The Columbia River basalts: Science, 215: 1463–1468.

Hooper, P. R., 1984, Physical and chemical constraints on the evolution of the Columbia River basalt: Geology, 12: 495–499.

Hooper, P. R., Kleck, W. D., Knowles, C. R., Reidel, S. P., and Thiessen, R. L., 1984, The Imnaha Basalt, Columbia River Basalt Group: Journal of Petrology, 25: 473–500.

Hopson, C. A., and Mattinson, J. M., 1973, Ordovician and Late Jurassic ophiolitic assemblages in the Pacific Northwest (abs.): Geological Society of America, Abstracts with Programs, 5: 57.

Janda, R. J., Scott, K. M., Nolan, K. M., and Martinson, H. A., 1981, Lahar movement, effects, and deposits: U.S. Geological Survey, Professional Paper 1250: 461–478.

Johnson, S. Y., 1985, Eocene strike–slip faulting and nonmarine basin formation in Washington: Society of Economic Paleontologists and Mineralogists, Special Publication 37: 283–302.

Jones, J. G., 1969, Intraglacial volcanoes of the Laugarvatn region, southwest Iceland—I: Geological Society of London, Quarterly Journal, 124: 197–211.

Keith, T. E., Beeson, M. H., and Bargar, K. E., 1982, Geologic map of the Mount Hood Wilderness, Clackamas and Hood River Counties, Oregon: U.S. Geological Survey, Miscellaneous Field Studies Map MF-1379A.

Keith, T. E., Donnelly-Nolan, J. M., Markman, J. L., and Beeson, M. H., 1985, K–Ar ages of rocks in the Mount Hood area, Oregon: Isochron/West, 42: 12–16.

Kieffer, S. W., 1981a, Blast dynamics at Mount St. Helens on 18 May 1980: Nature, 291: 568–570.

Kieffer, S. W., 1981b, Fluid dynamics of the May 18 blast at Mount St. Helens: U.S. Geological Survey, Professional Paper 1250: 379–400.

Kjartansson, G., 1959, The Moberg Formation; *in* Thorarinsson, S., Einarsson, T., and Kjartansson, G. (eds.), On the geology and geomorphology of Iceland: Geografisk Annaler, 41: 135–169.

Kleinspehn, K. L., 1985, Cretaceous sedimentation and tectonics, Tyaughton–Methow Basin, southwestern British Columbia: Canadian Journal of Earth Sciences, 22: 154–174.

Korosec, M. A., 1987a, Geologic map of the Mount Adams quadrangle, Washington: Washington Division of Geology and Earth Resources, Open-File Report 87-5: 33 pp.

Korosec, M. A., 1987b, Geologic map of the Hood River quadrangle, Washington and Oregon: Washington Division of Geology and Earth Resources, Open-File Report 87-6: 41 pp.

Kuntz, M. A., Rowley, P. D., MacLeod, N. S., Reynolds, R. L., McBroome, L. A., Kaplan, A. M., and Lidke, D. J., 1981, Petrography and particle-size distribution of pyroclastic-flow, ash-cloud, and surge deposits: U.S. Geological Survey, Professional Paper 1250: 525–539.

Lachenbruch, A. H., and Sass, J. H., 1977, Heat flow in the United States and the thermal regime of the crust: American Geophysical Union, Geophysical Monograph 20: 626–675.

Lander, E. B., 1977, A review of the Oreodonta (Mammalia, Artiodactyla): Unpublished Ph.D. dissertation, University of California, Berkeley, 474 pp.

Laubscher, H. P., 1981, Models of the development of Yakima deformation: Final Safety Analysis Report WNP-2, Amendment 18, appendix, Washington Public Power Supply System, Richland, 69 pp.

Law, L. K., Auld, D. R., and Booker, J. R., 1980, A geomagnetic variation anomaly coincident with the Cascade volcanic belt: Journal of Geophysical Research, 85: 5297–5302.

Lawrence, D. B., 1941, The "floating island" lava flow of Mount St. Helens: Mazama, 36: 41–44.

Lawrence, D. B., 1948, Mount Hood's latest eruption and glacier advances: Mazama, 30: 22–29.

Le Bas, M. J., Le Maitre, R. W., Streckeisen, A., and Zenettin, B., 1986, A chemical classification of volcanic rocks based on the total alkali–silica diagram: Journal of Petrology, 27: 745–750.

Lipman, P. W., and Mullineaux, D. R. (eds.), 1981, The 1980 eruptions of Mount St. Helens, Washington: U.S. Geological Survey, Professional Paper 1250: 844 pp.

Lipman, P. W., Moore, J. G., and Swanson, D. A., 1981a, Bulging of the north flank before the May 18 eruption—geodetic data: U.S. Geological Survey, Professional Paper 1250: 143–155.

Lipman, P. W., Norton, D. R., Taggart, J. E., Brandt, E. L., and Engleman, E. E., 1981b, Compositional variations in 1980 magmatic deposits: U.S. Geological Survey, Professional Paper 1250: 631–640.

Long, P. E., and Duncan, R. A., 1983, ^{40}Ar–^{39}Ar ages of Columbia River basalt from deep boreholes in south-central Washington: American Geophysical Union (EOS), Transactions, 64: 90.

Long, P. E., and Wood, B. J., 1986, Structures, textures and cooling histories of Columbia River basalt flows: Geological Society of America, Bulletin, 97: 1144–1155.

Lowry, W. D., and Baldwin, E. M., 1952, Late Cenozoic geology of the lower Columbia River Valley, Oregon and Washington: Geological Society of America, Bulletin, 63: 1–24.

Luedke, R. G., and Smith, R. L., 1982, Map showing distribution, composition, and age of late Cenozoic volcanic centers in Oregon and Washington: U.S. Geological Survey, Miscellaneous Investigations Map I-1091D.

Mackin, J. H., 1961, A stratigraphic section in the Yakima Basalt and the Ellensburg Formation in south-central Washington: Washington Division of Mines and Geology, Report of Investigations 19: 45 pp.

MacLeod, N. S., Walker, G. W., and McKee, E. H., 1975, Geothermal significance of eastward increase in age of upper Cenozoic rhyolitic domes in southeastern Oregon; *in* Proceedings of United Nations 2nd Symposium on Development and Use of Geothermal Resources, 1: 465–474.

Magill, J., Cox, A., and Duncan, R., 1981, Tillamook volcanic series: further evidence for tectonic rotation of the Oregon Coast Range: Journal of Geophysical Research, 86: 2953–2970.

Majors, H. M., 1980, Three newly discovered accounts of activity on Mount St. Helens, 1898, 1903 and 1921: Northwest Discovery, 1: 36–41.

Mangan, M. T., Wright, T. L., Swanson, D. A., and Byerly, G. R., 1986, Regional correlation of Grande Ronde Basalt flows, Columbia River Basalt Group, Washington, Oregon, and Idaho: Geological Society of America, Bulletin, 97: 1300–1318.

Mankinen, E. A., and Dalrymple, G. B., 1979, Revised geomagnetic polarity time scale for the interval 0–5 m.y. B.P.: Journal of Geophysical Research, 84: 615–626.

Mattinson, J. M., 1977, Emplacement history of the Tatoosh volcanic–plutonic complex, Washington: Ages of zircons: Geological Society of America, Bulletin, 88: 1509–1514.

McBirney, A. R., 1978, Volcanic evolution of the Cascade Range: Annual Reviews of Earth and Planetary Science, 6: 437–456.

McKee, E. H., Hooper, P. R., and Kleck, W. D., 1981, Age of the Imnaha Basalt—oldest flows of the Columbia River Basalt Group, northwest United States: Isochron/West, 31:31–33.

McKee, E. H., Swanson, D. A., and Wright, T. L., 1977, Duration and volume of Columbia River basalt volcanism, Washington, Oregon, and Idaho (abs.): Geological Society of America, Abstracts with Programs, 9: 463–464.

McMillan, K., Cross, R. W., and Long, P. E., 1987, Two-stage vesiculation in the Cohassett flow of the Grande Ronde Basalt, south-central Washington: Geology, 15: 809.

Mellors, R. A., Waitt, R. B., and Swanson, D. A., 1988, Generation of pyroclastic flows and surges by hot-rock avalanches from the dome of Mount St. Helens volcano, USA: Bulletin of Volcanology, 50: 14–25.

Melson, W. G., 1983, Monitoring the 1980–82 eruptions of Mt. St. Helens: compositions and abundances of glass: Science, 221: 1387–1391.

Michaelson, C. A., and Weaver, C. S., 1986, Upper mantle structure from teleseismic P-wave arrivals in Washington and northern Oregon: Journal of Geophysical Research, 91: 209–250.

Miller, R. B., 1985a, The Ingalls ophiolitic complex, north-central Cascade Mountains, Washington: Geological Society of America, Bulletin, 96: 27–42.

Miller, R. B., 1985b, The pre-Tertiary Rimrock Lake inlier, southern Cascades, Washington: Washington Division of Geology and Earth Resources, Open-File Report 85-2: 16 pp.

Minor, R., 1984, Dating the Bonneville landslide in the Columbia River Gorge: Heritage Research Associates (Eugene, Oregon), Report 31: 19 pp.

Misch, P., 1966, Tectonic evolution of the northern Cascades of Washington state: A west-Cordilleran case history: Canadian Institute of Mining and Metallurgy, Special Volume 8: 101–148.

Misch, P., 1977, Dextral displacements at some major strike faults in the North Cascades (abs.): Geological Association of Canada, Program with Abstracts, 37 (no page number).

Moen, W. S., 1977, St. Helens and Washougal mining districts of the southern Cascades of Washington: Washington Division of Geology and Earth Resources, Information Circular 60: 71 pp.

Morgan, W. J., 1981, Hotspot tracks and the opening of the Atlantic and Indian oceans; *in* The sea, v. 7: John Wiley, New York, pp. 443–487.

Morgan, W. J., 1988, Flood basalts and mass extinctions; *in* Global catastrophes in Earth history: an interdisciplinary conference on impacts, volcanism, and mass mortality: Lunar and Planetary Institute, Contribution 673: 126.

Moyer, T. C., and Swanson, D. A., 1987, Secondary hydroeruptions in pyroclastic-flow deposits: examples from Mount St. Helens: Journal of Volcanology and Geothermal Research, 32: 299–319.

Mullineaux, D. R., 1986, Summary of pre-1980 tephra-fall deposits erupted from Mount St. Helens, Washington state, USA: Bulletin of Volcanology, 48: 17–26.

Mullineaux, D. R., and Crandell, D. R., 1981, The eruptive history of Mount St. Helens: U.S. Geological Survey, Professional Paper 1250: 3–15.

Mullineaux, D. R., Wilcox, R. E., Ebaugh, W. R., Fryxell, R., and Rubin, M., 1978, Age of the last major scabland flood of the Columbia Plateau in eastern Washington: Quaternary Research, 10: 171–180.

Mundorff, M. J., 1964, Geology and ground-water conditions of Clark County, Wash., with a description of a major alluvial aquifer along the Columbia River: U.S. Geological Survey, Water Supply Paper 1600: 268 pp.

Mundorff, M. J., and Eggers, A. A., 1988, Tumtum Mountain, a late Pleistocene volcanic dome in southwestern Washington: Northwest Science, 62: 10–15.

Myers, C. W., and Price, S. M. (eds.), 1979, Geologic studies of the Columbia Plateau: Rockwell Hanford Operations (Richland, Washington), RHO-BWI-ST-4, III-23-III-32.

Nehring, N. L., Wollenberg, H. A., and Johnston, D. A., 1981, Gas analyses of fumaroles from Mt. Hood, Oregon: U.S. Geological Survey, Open-File Report 81-236: 9 pp.

Niem, A. R., and Niem, W. A., 1985, Oil and gas investigation of the Astoria Basin, Clatsop and northernmost Tillamook Counties, northwest Oregon: Oregon Department of Geology and Mineral Industries, Oil and Gas Investigations Report OGI-14.

Okazaki, R., Smith, H. W., Gilkeson, R. A., and Franklin, J., 1972, Correlation of West Blacktail Ash with pyroclastic layer T from the 1800 A.D. eruption of Mt. St. Helens: Northwest Science, 46: 77–89.

Phillips, W. M., 1987, Geologic map of the Mount St. Helens quadrangle, Washington and Oregon: Washington Division of Geology and Earth Resources, Open-File Report 87-4: 59 pp.

Phillips, W. M., Korosec, M. A., Schasse, H. W., Anderson, J. L., and Hagen, R. A., 1986, K–Ar ages of volcanic rocks in southwest Washington: Isochron/West, 47: 18–24.

Pierson, T. C., 1985, Initiation and flow behavior of the 1980 Pine Creek and Muddy River lahars, Mount St. Helens, Washington: Geological Society of America, Bulletin, 96: 1056–1069.

Pierson, T. C., and Scott, K. M., 1985, Downstream dilution of a lahar: transition from debris flow to hyperconcentrated streamflow: Water Resources Research, 21: 1511–1524.

Porter, S. C., 1976, Pleistocene glaciation in the southern part of the North Cascade Range, Washington: Geological Society of America, Bulletin, 87: 61–75.

Power, S. G., Field, C. W., Armstrong, R. L., and Harakal, J. E., 1981, K–Ar ages of plutonism and mineralization, western Cascades, Oregon and southern Washington: Isochron/West, 31: 27–29.

Price, E. H., 1982, Structural geometry, strain distribution, and mechanical evolution of eastern Umtanum Ridge, and a comparison with other selected localities within Yakima fold structures, south-central Washington: Rockwell Hanford Operations (Richland, Washington), RHO-BWI-SA-138: 109 pp.

Priest, G. R., Beeson, M. H., Gannett, M. W., and Berri, D. A., 1982, Geology, geochemistry, and geothermal resources of the Old Maid Flat area, Oregon: Oregon Department of Geology and Mineral Industries, Special Paper 14: 16–30.

Qamar, A., St. Lawrence, W., Moore, J. N., and Kendrick, G., 1983, Seismic signals preceding the explosive eruption of Mount St. Helens, Washington on 18 May 1980: Seismological Society of America, Bulletin, 73: 1797–1813.

Rampino, M. R., and Stothers, R. B., 1988, Flood basalt volcanism during the past 250 million years: Science, 241: 663–668.

Rasmussen, J., and Humphreys, E., 1988, Tomographic image of the Juan de Fuca plate beneath Washington and western Oregon using teleseismic P-wave travel times: Geophysical Research Letters, 15: 1417–1420.

Reidel, S. P., 1984, The Saddle Mountains—the evolution of an anticline in the Yakima fold belt: American Journal of Science, 284: 942–978.

Reidel, S. P., Long, P. E., Myers, S. W., and Mase, J., 1982, New evidence for greater than 3.2 km of Columbia River basalt beneath the central Columbia Plateau: American Geophysical Union (EOS), Transactions, 64: 173.

Reidel, S. P., Tolan, T. L., Hooper, P. R., Beeson, M. H., Fecht, K. R., and Anderson, J. L. (in press), The Grande Ronde Basalt, Columbia River Basalt Group: Stratigraphic descriptions and correlations in Washington, Oregon, and Idaho; *in* Reidel, S. P., Hooper, P. R., and Anderson, J. L. (eds.), Volcanism and Tectonism on the Columbia Plateau: Geological Society of America, Special Paper.

Riddihough, R., 1984, Recent movements of the Juan de Fuca plate system: Journal of Geophysical Research, 89: 6980–6994.

Rite, A., and Iyer, H. M., 1981, July 1980 Mt. Hood earthquake swarm: U.S. Geological Survey, Open-File Report 81-48: 21 pp.

Rosenbaum, J. G., and Waitt, R. B., Jr., 1981, Summary of eyewitness accounts of the May 18 eruption: U.S. Geological Survey, Professional Paper 1250: 53–67.

Rutherford, M. J., Sigurdsson, H., Carey, S., and Davis, A., 1985, The May 18, 1980, eruption of Mount St. Helens 1. Melt composition and experimental phase equilibria: Journal of Geophysical Research, 90: 2929–2947.

Sager, J. W., and Chambers, D. R., 1986, Design and construction of the Spirit Lake outlet tunnel, Mount St. Helens, Washington: American Society of Civil Engineers, Geotechnical Special Publication 3: 42–58.

Scandone, R., and Malone, S. D., 1985, Magma supply, magma discharge and readjustments of the feeding system of Mount St. Helens during 1980: Journal of Volcanology and Geothermal Research, 23: 239–262.

Schmincke, H.-U., 1964, Petrology, paleocurrents, and stratigraphy of the Ellensburg Formation and interbedded Yakima Basalt flows, south-central Washington: Unpublished Ph.D. dissertation, Johns Hopkins University, Baltimore, 425 pp.

Schmincke, H.-U., 1967a, Stratigraphy and petrography of four upper Yakima basalt flows in south-central Washington: Geological Society of America, Bulletin, 78: 1385–1422.

Schmincke, H.-U., 1967b, Graded lahars in the type sections of the Ellensburg Formation, south-central Washington: Journal of Sedimentary Petrology, 78: 438–448.

Schmincke, H.-U., 1967c, Fused tuff and pépérites in south-central Washington: Geological Society of America, Bulletin, 78: 319–330.

Schmincke, H.-U., 1967d, Flow directions in Columbia River basalt flows and paleocurrents of interbedded sedimentary rocks, south-central Washington: Geologische Rundschau, 56: 992–1020.

Schuster, R. L., 1981, Effect of the eruptions on civil works and operations in the Pacific Northwest: U.S. Geological Survey, Professional Paper 1250: 701–718.

Scott, K. M., 1988, Lahars and lahar-runout flows in the Toutle-Cowlitz River system, Mount St. Helens, Washington, U.S. Geological Survey, Professional Paper 1447A: 74 pp.

Shaw, H. R., and Swanson, D. A., 1970, Eruption and flow rates of flood basalts; *in* Proceedings of Second Columbia River Basalt Symposium: Eastern Washington State College Press, Cheney, pp. 271–299.

Sherrod, D. R., and Smith, J. G. (in press), Preliminary map of upper Eocene to Holocene volcanic and related rocks of the Cascade Range, Oregon, scale 1:500,000: U.S. Geological Survey, Open-File Report.

Siebert, L., Glicken, H., and Ui, T., 1987, Volcanic hazards from Bezymianny- and Bandai-type eruptions: Bulletin of Volcanology, 49: 435–459.

Simpson, R. W., and Cox, A., 1977, Paleomagnetic evidence for tectonic rotation of the Oregon Coast Range: Geology, 5: 585–589.

Smith, D. R., 1984, The petrology and geochemistry of High Cascade volcanics in southern Washington: Mount St. Helens volcano and the Indian Heaven basalt field: Unpublished Ph.D. dissertation, Rice University, Houston, Texas, 409 pp.

Smith, D. R., and Leeman, W. P., 1987, Petrogenesis of Mount St. Helens dacitic magmas: Journal of Geophysical Research, 92: 10,313–10,334.

Smith, G. A., 1986, Coarse-grained nonmarine volcaniclastic sediment: Terminology and depositional process: Geological Society of America, Bulletin, 97: 1–10.

Smith, G. A., 1988, Neogene synvolcanic and syntectonic sedimentation in central Washington: Geological Society of America, Bulletin, 99: 1479–1492.

Smith, G. A., Campbell, N. P., Deacon, M. W., and Shafiqullah, M., 1988, Eruptive style and location of volcanic centers in the Miocene Washington Cascade Range: Reconstruction from the sedimentary record: Geology, 16: 337–340.

Smith, G. O., 1904, Description of the Mount Stuart quadrangle, Washington: U.S. Geological Survey, Geologic Atlas Mount Stuart, Folio 106: 10 pp.

Smith, G. O., and Calkins, F. C., 1906, Description of the Snoqualmie quadrangle, Washington: U.S. Geological Survey, Geologic Atlas Snoqualmie, Folio 139: 14 pp.

Smith, H. W., Okazaki, R., and Knowles, C. E., 1977, Electron microprobe analysis of glass shards from tephra assigned to set W, Mt. St. Helens, Washington: Quaternary Research, 7: 207–217.

Smith, J. G., 1987, New compilation geologic map of the Cascade Range in Washington: Geothermal Resources Council, Transactions, 11: 309–314.

Smith, J. G. (in press, a), Geologic map showing upper Eocene to Holocene volcanic and related rocks in the Cascade Range of Washington: U.S. Geological Survey, Miscellaneous Investigations Map.

Smith, J. G. (in press, b), Geologic map of the Yakima 2-degree sheet: U.S. Geological Survey, Miscellaneous Investigations Map.

Southwick, D. L., 1974, Geology of the alpine-type ultramafic complex near Mount Stuart, Washington: Geological Society of America, Bulletin, 85: 391–402.

Stanley, W. D., 1984, Tectonic study of the Cascade Range and Columbia Plateau in Washington State based upon magnetotelluric soundings: Journal of Geophysical Research, 89: 4447–4460.

Stanley, W. D., Finn, C., and Plesha, J. L., 1987, Tectonics and conductivity structures in the southern Washington Cascades: Journal of Geophysical Research, 92: 10,179–10,193.

Stout, M. L., 1964, Geology of a part of the south-central Cascade Mountains, Washington: Geological Society of America, Bulletin, 75: 317–334.

Swanson, D. A., 1964, The middle and late Cenozoic volcanic rocks of the Tieton River area, south-central Washington: Unpublished Ph.D. dissertation, Johns Hopkins University, Baltimore, Maryland, 330 pp.

Swanson, D. A., 1966, Tieton volcano, a Miocene eruptive center in the southern Cascade Mountains, Washington: Geological Society of America, Bulletin, 77: 1293–1314.

Swanson, D. A., 1967, Yakima Basalt of the Tieton River area, south-central Washington: Geological Society of America, Bulletin, 78: 1077–1100.

Swanson, D. A., 1972, Magma supply rate at Kilauea Volcano, 1952–1971: Science, 175: 169–170.

Swanson, D. A., 1978, Geologic map of the Tieton River area, Yakima County, south-central Washington, scale 1:48,000: U.S. Geological Survey, Miscellaneous Field Studies Map MF-968.

Swanson, D. A., and Clayton, G. A., 1983, Generalized geologic map of the Goat Rocks Wilderness and roadless areas (6036, Parts A, C, and D), Lewis and Yakima Counties, Washington: U.S. Geological Survey, Open-File Report 83-357: 10 pp.

Swanson, D. A., and Holcomb, R. T. (in press), Regularities in growth of the Mount St. Helens dacite dome, 1980–86; *in* The mechanics of lava flow emplacement and dome growth: IAVCEI Proceedings in Volcanology, v. 2, Springer Verlag, Heidelberg.

Swanson, D. A., and Wright, T. L., 1979, Paleogeography of southeast Washington during the middle and late Miocene based on the distribution of intracanyon basalt flows; *in* Cenozoic paleogeography of the western United States: Society of Economic Paleontologists and Mineralogists, Pacific Coast Paleogeography Symposium 3, Los Angeles, p. 31.

Swanson, D. A., Wright, T. L., and Helz, R. T., 1975, Linear vent systems and estimated rates of magma production and eruption for the Yakima Basalt on the Columbia Plateau: American Journal of Science, 275: 877–905.

Swanson, D. A., Wright, T. L., Hooper, P. R., and Bentley, R. D., 1979a, Revisions in stratigraphic nomenclature of the Columbia River Basalt Group: U.S. Geological Survey, Bulletin 1457-G: 59 pp.

Swanson, D. A., Anderson, J. L., Bentley, R. D., Byerly, G. R., Camp, V. E., Gardner, J. N., and Wright, T. L., 1979b, Reconnaissance geologic map of the Columbia River Basalt Group in eastern Washington and northern Idaho: U.S. Geological Survey, Open-File Report 79-1363: 26 pp.

Swanson, D. A., Brown, J. C., Anderson, J. L., Bentley, R. D., Byerly, G. R., Gardner, J. N., and Wright, T. L., 1979c, Structure contour maps on the top of the Grande Ronde and Wanapum Basalts, eastern Washington and northern Idaho: U.S. Geological Survey, Open-File Report 79-1364.

Swanson, D. A., Wright, T. L., Camp, V. E., Gardner, J. N., Helz, R. T., Price, S. M., Reidel, S. P., and Ross, M. E., 1980, Reconnaissance geologic map of the Columbia River Basalt Group, Pullman and Walla Walla quadrangles, southeast Washington and adjacent Idaho: U.S. Geological Survey, Miscellaneous Investigations Map I-1139.

Swanson, D. A., Anderson, J. L., Camp, V. E., Hooper, P. R., Taubeneck, W. H., and Wright, T. L., 1981, Reconnaissance geologic map of the Columbia River Basalt Group, northern Oregon and western Idaho: U.S. Geological Survey, Open-File Report 81-797: 32 pp.

Swanson, D. A., Casadevall, T. J., Dzurisin, D., Malone, S. D., Newhall, C. G., and Weaver, C. S., 1983, Predicting eruptions at Mount St. Helens, June 1980 through December 1982: Science, 221: 1369–1376.

Swanson, D. A., Casadevall, T. J., Dzurisin, D., Holcomb, R. T., Newhall, C. G., Malone, S. D., and Weaver, C. S., 1985, Forecasts and predictions of eruptive activity at Mount St. Helens, 1975–1984: Journal of Geodynamics, 3: 397–423.

Swanson, D. A., Dzurisin, D., Holcomb, R. T., Iwatsubo, E. Y., Chadwick, W. W., Jr., Casadevall, T. J., Ewert, J. W., and Heliker, C. C., 1987, Growth of the lava dome at Mount St. Helens, Washington (USA), 1981–83: Geological Society of America, Special Paper 212: 1–16.

Tabor, R. W., and Crowder, D. F., 1969, Of batholiths and volcanoes: Intrusion and eruption of Late Cenozoic magmas in the Glacier Peak area, north Cascades, Washington: U.S. Geological Survey, Professional Paper 604: 67 pp.

Tabor, R. W., Frizzell, V. A., Jr., Vance, J. A., Naeser, C. W., 1984, Ages and stratigraphy of lower and middle Tertiary sedimentary and volcanic rocks of the central Cascades, Washington: Application to the tectonic history of the Straight Creek fault: Geological Society of America, Bulletin, 95: 26–44.

Tabor, R. W., Zartman, R. E., and Frizzell, V. A., Jr., 1987, Possible tectonostratigraphic terranes in the North Cascades crystalline core, Washington: Washington Division of Geology and Earth Resources, Bulletin 77: 107–127.

Tabor, R. W., Frizzell, V. A., Jr., Booth, D. B., Whetten, J. T., Waitt, R. B., Jr., and Zartman, R. E., 1982a, Preliminary geologic map of the Skykomish River 1:100,000 quadrangle, Washington: U.S. Geological Survey, Open-File Map, 82-747.

Tabor, R. W., Waitt, R. B., Jr., Frizzell, V. A., Jr., Swanson, D. A., Byerly, G. R., and Bentley, R. D., 1982b, Geologic map of the Wenatchee 1:100,000 quadrangle, central Washington: U.S. Geological Survey, Miscellaneous Investigations Map, I-1311: 26 pp.

Taubeneck, W. H., 1970, Dikes of Columbia River basalt in northeastern Oregon, western Idaho, and southeastern Washington; *in* Proceedings of Second Columbia River Basalt Symposium: Eastern Washington State College Press, Cheney, pp. 73–96.

Taylor, E. M., 1987, Field geology of the northwest quarter of the Broken Top 15′ quadrangle, Deschutes County, Oregon: Oregon Department of Geology and Mineral Industries, Special Paper 21: 20 pp.

Thiruvathukal, J. V., Berg, J. W., and Heinrichs, D. F., 1970, Regional gravity of Oregon: Seismological Society of America, Bulletin, 81: 725–738.

Tolan, T. L., and Beeson, M. H., 1984a, Exploring the Neogene history of the Columbia River: Discussion and geologic field trip guide to the Columbia River Gorge. Part I. Discussion: Oregon Geology, 46: 87–97.

Tolan, T. L., and Beeson, M. H., 1984b, Exploring the Neogene history of the Columbia River: Discussion and geologic field trip guide to the Columbia River Gorge. Part II. Road log and comments: Oregon Geology, 46: 103–112.

Tolan, T. L., and Beeson, M. H., 1984c, Intracanyon flows of the Columbia River Basalt Group in the lower Columbia River Gorge and their relationship to the Troutdale Formation: Geological Society of America, Bulletin, 95: 463–477.

Tolan, T. L., Reidel, S. P., Beeson, M. H., Anderson, J. L., Fecht, K. R., and Swanson, D. A., 1987, Revisions to the areal extent and volume of the Columbia River Basalt Group (CRBG) (abs.): Geological Society of America, Abstracts with Programs, 19: 458.

Tolan, T. L., Reidel, S. P., Beeson, M. H., Anderson, J. L., Fecht, K. R., and Swanson, D. A. (in press), Revisions to the estimates of the areal extent and volume of the Columbia River Basalt Group; *in* Reidel, S. P., Hooper, P. R., and Anderson, J. L. (eds.), Volcanism and tectonism on the Columbia Plateau: Geological Society of America, Special Paper.

Treasher, R. C., 1942, Geologic history of the Portland area: Oregon Department of Geology and Mineral Industries, Short Paper 7: 17 pp.

Trimble, D. E., 1963, Geology of Portland, Oregon and adjacent areas: U.S. Geological Survey, Bulletin, 1119: 119 pp.

Turner, D. L., Frizzell, V. A., Jr., Triplehorn, D. M., and Naeser, C. W., 1983, Radiometric dating of ash partings in coals of the Eocene Puget Group, Washington: Implications for paleobotanical stages: Geology, 11: 527–531.

Vallance, J. W., 1986, Late Quaternary volcanic stratigraphy of the southwestern flank of Mount Adams volcano, Washington: Unpublished M.S. thesis, University of Colorado, Boulder.

Vance, J. A., 1979, Early and middle Cenozoic arc magmatism and tectonics in Washington state (abs.): Geological Society of America, Abstracts with Programs, 11: 132.

Vance, J. A., 1982, Cenozoic stratigraphy and tectonics of the Washington Cascades (abs.): Geological Society of America, Abstracts with Programs, 14: 241.

Vance, J. A., 1985, Early Tertiary faulting in the North Cascades (abs.): Geological Society of America, Abstracts with Programs, 17: 415.

Vance, J. A., and Miller, R. B., 1981, The movement history of the Straight Creek fault in Washington State (abs.): Geological Association of Canada, Cordilleran Section, Program with Abstracts, pp. 39–41.

Vance, J. A., and Naeser, C. W., 1977, Fission track geochronology of the Tertiary volcanic rocks of the central Cascade Mountains, Washington (abs.): Geological Society of America, Abstracts with Programs, 9: 520.

Vance, J. A., Walker, N. W., and Mattinson, J. M., 1986, U/Pb ages of early Cascade plutons in Washington state (abs.): Geological Society of America, Abstracts with Programs, 18: 194.

Vance, J. A., Clayton, G. A., Mattinson, J. M., and Naeser, C. W., 1987, Early and middle Cenozoic stratigraphy of the Mount Rainier–Tieton River area, southern Washington Cascades: Washington Division of Geology and Earth Resources, Bulletin, 77: 269–290.

Vine, J. D., 1962, Preliminary geologic map of the Hobart and Maple Valley quadrangles, King County, Washington, scale 1:24,000: Washington Division of Mines and Geology, Map GM-1.

Vine, J. D., 1969, Geology and coal resources of the Cumberland, Hobart, and Maple Valley quadrangles, King County, Washington: U.S. Geological Survey, Professional Paper 624: 67 pp.

Voight, B., Glicken, H., Janda, R. J., and Douglass, P. M., 1981, Catastrophic rockslide avalanche of May 18: U.S. Geological Survey, Professional Paper 1250: 347–377.

Voight, B., Janda, R. J., Glicken, H., and Douglass, P. M., 1983, Nature and mechanics of the Mount St Helens rockslide–avalanche of 18 May 1980: Geotechnique, 33: 243–273.

Waitt, R. B., 1979, Late-Cenozoic deposits, landforms, stratigraphy, and tectonism of Kittitas Valley, Washington: U.S. Geological Survey, Professional Paper 1127: 18 pp.

Waitt, R. B., 1984a, Deposits and effects of devastating lithic pyroclastic density current from Mount St. Helens on 18 May 1980—field guide for northeast radial: U.S. Geological Survey, Open-File Report 84-839: 10 pp.

Waitt, R. B., 1984b, Comment: Geology, 12: 693.

Waitt, R. B., 1985, Case for periodic, colossal jökulhlaups from Pleistocene glacial Lake Missoula: Geological Society of America, Bulletin, 96: 1271–1286.

Waitt, R. B., and MacLeod, N. S., 1987, Minor explosive eruptions at Mount St. Helens dramatically interacting with winter snowpack in March–April 1982: Washington Division of Geology and Earth Resources, Bulletin, 77: 355–379.

Waitt, R. B., and Swanson, D. A., 1987, Geomorphic evolution of the Columbia Plain and River: Geological Society of America, Centennial Special Volume 2: 403–423.

Waitt, R. B., Pierson, T. C., MacLeod, N. S., Janda, R. J., Voight, B., and Holcomb, R. T., 1983, Eruption-triggered avalanche, flood, and lahar at Mount St. Helens—effects of winter snowpack: Science, 221: 1394–1397.

Walker, G. P. L., 1973, Lengths of lava flows: Royal Society of London, Philosophical Transactions (A), 107–118.

Walker, G. P. L., and McBroome, L. A., 1983, Mount St. Helens 1980 and Mount Pelée 1902—flow or surge?: Geology, 11: 571–574.

Walsh, T. J., Korosec, M. A., Phillips, W. M., Logan, R. L., and Schasse, H. W., 1987, Geologic map of Washington—southwest quadrant, scale 1:250,000: Washington Division of Geology and Earth Resources, Geologic Map GM-34: 28 pp.

Warren, W. C., 1941, Relation of the Yakima basalt to the Keechelus andesitic series: Journal of Geology, 49: 795–814.

Waters, A. C., 1955, Geomorphology of south-central Washington, illustrated by the Yakima East quadrangle: Geological Society of America, Bulletin, 66: 663–684.

Waters, A. C., 1961, Stratigraphic and lithologic variations in the Columbia River basalt: American Journal of Science, 259: 583–611.

Waters, A. C., 1973, The Columbia River Gorge, basalt stratigraphy, ancient lava dams, and landslide dams: Oregon Department of Geology and Mineral Industries, Bulletin 77: 133–162.

Weaver, C. S., and Baker, G. E., 1988, Geometry of the Juan de Fuca plate beneath Washington—evidence from seismicity and the 1949 south Puget Sound earthquake: Seismological Society of America, Bulletin, 78: 264–275.

Weaver, C. S., and Malone, S. D., 1987, Overview of the tectonic setting and recent studies of eruptions of Mount St. Helens, Washington: Journal of Geophysical Research, 92: 10,149–10,154.

Weaver, C. S., and Michaelson, C. A., 1985, Seismicity and volcanism in the Pacific Northwest: evidence for the segmentation of the Juan de Fuca plate: Geophysical Research Letters, 12: 215–218.

Weaver, C. S., and Smith, S. W., 1983, Regional tectonic and earthquake hazard implications of a crustal fault zone in southwestern Washington: Journal of Geophysical Research, 88: 10,371–10,383.

Weaver, C. S., Green, S. M., and Iyer, H. M., 1982, Seismicity of Mount Hood and structure as determined from teleseismic P-wave delay studies: Journal of Geophysical Research, 87: 2782–2792.

Weaver, C. S., Grant, W. C., and Shemata, J. E., 1987, Local crustal extension at Mount St. Helens, Washington: Journal of Geophysical Research, 92: 10,170–10,178.

Wells, R. E., and Coe, R. S., 1985, Paleomagnetism and geology of Eocene volcanic rocks of southwest Washington, implications for mechanisms of volcanic rotation: Journal of Geophysical Research, 90: 1925–1947.

Wells, R. E., and England, P. C. (in press), Continuum model of rotations recorded in Miocene flows of the Columbia River Basalt Group, Oregon and Washington: American Geophysical Union (EOS), Transactions.

Wells, R. E., and Niem, A. R., 1987, Geology of the Columbia River Basalt Group in the Astoria Basin, Oregon and Washington: evidence for invasive flows (abs.): Geological Society of America, Abstracts with Programs, 19: 462–463.

Wells, R. E., and Simpson, R. W., 1987, More paleomagnetic results from the Miocene Columbia River Basalt Group, Oregon and Washington (abs.): Stratigraphic and tectonic implications: Geological Society of America, Abstracts with Programs, 19: 463.

Wells, R. E., Simpson, R. W., Bentley, R. D., Beeson, M. H., Mangan, M. T., and Wright, T. L. (in press), Correlation of Miocene flows of the Columbia River Basalt Group from the central Columbia Plateau to the coast of Oregon and Washington; *in* Reidel S. P., Hooper, P. R., and Anderson, J. L. (eds.), Volcanism and tectonism on the Columbia Plateau: Geological Society of America, Special Paper.

Westgate, J. A., Smith, D. G. W., and Nichols, H., 1970, Late Quaternary pyroclastic layers in the Edmonton aea, Alberta; *in* Pedology and Qua-

ternary research: University of Alberta Printing, Edmonton, Alberta, pp. 179–186.

White, C., 1980, Geology and geochemistry of Mt. Hood volcano: Oregon Department of Geology and Mineral Industries, Special Paper 8: 26 pp.

Williams, D. L., and Keith, T. E. C., 1982, Aeromagnetic and Bouguer gravity maps of Mount Hood Wilderness, Clackamas and Hood River Counties, Oregon: U.S. Geological Survey, Miscellaneous Field Studies Map MF-1379D.

Williams, D. L., Abrams, G., Finn, C., Dzurisin, D., Johnson, D. J., and Denlinger, R., 1987, Evidence from gravity data for an intrusive complex beneath Mount St. Helens: Journal of Geophysical Research, 92: 10,207–10,222.

Williams, D. L., Finn, C., Couch, R. W., Danes, Z. F., Pitts, G. S., Phillips, W. M., and Riddihough, R. P., 1988, Residual Bouguer gravity anomaly map of the Cascade Range, California, Oregon, Washington, and British Columbia: U.S. Geological Survey, Geophysical Investigations Map GP-973.

Wise, W. S., 1961, The geology and mineralogy of the Wind River area, Washington, and the stability relations of celadonite: Unpublished Ph.D. dissertation, Johns Hopkins University, Baltimore, Maryland.

Wise, W. S., 1968, Geology of the Mount Hood volcano: Oregon Department of Geology and Mineral Industries, Bulletin, 62: 81–98.

Wise, W. S., 1969, Geology and petrology of the Mount Hood area: a study of High Cascade volcanism: Geological Society of America, Bulletin, 80: 969–1006.

Wise, W. S., 1970, Cenozoic volcanism in the Cascade Mountains of southern Washington: Washington Department of Natural Resources, Bulletin, 60: 45 pp.

Wright, T. L., Mangan, M., and Swanson, D. A. (in press), Chemical data for flows and feeder dikes of the Yakima Basalt Subgroup, Columbia River Basalt Group: Constraints on a petrogenetic model: U.S. Geological Survey, Bulletin 1821.

Yamaguchi, D. K., 1983, New tree-ring dates for recent eruptions of Mount St. Helens: Quaternary Research, 20: 246–250.

Yamaguchi, D. K., 1985, Tree-ring evidence for a two-year interval between recent prehistoric explosive eruptions of Mt. St. Helens: Geology, 13: 554–557.

Zoback, M. L., and Thompson, G. A., 1978, Basin and Range rifting in northern Nevada, clues from a mid-Miocene rift and its subsequent offsets: Geology, 6: 111–116.

EXCURSION 2A:
Recent volcaniclastic deposits and processes at Mount St. Helens volcano, Washington

Richard B. Waitt[1], Richard P. Hoblitt[1], C. William Criswell[2], Kevin M. Scott[1], Harry Glicken[3], and Steven R. Brantley[1]

[1]*U.S. Geological Survey, Cascades Volcano Observatory, 5400 MacArthur Blvd., Vancouver, Washington 98661;* [2]*Geology Department, University of New Mexico, Albuquerque, New Mexico 87131;* [3]*Department of Geological Sciences, University of California, Santa Barbara, California 93106*

General information

Richard P. Hoblitt and Richard B. Waitt

Mount St. Helens is a young composite volcano situated in southwestern Washington State, U.S.A. Participants of IAVCEI field excursion 2A will investigate deposits that range from prehistoric to modern. Most attention will be given to deposits of the 18 May 1980 eruption. In the course of six days, most flanks of the volcano will be visited (Fig. 1).

Pre-1980 activity

Mount St. Helens is 40-50 thousand years old. Reconstructed from stratigraphic and chronologic studies (Mullineaux and Crandell, 1981; Mullineaux, 1986; Crandell, 1987), eruptive stages alternate with extended repose intervals, both lasting thousands of years. The stages are divided into eruptive periods that last for decades to centuries, separated by dormant periods also of decades to centuries (Table 1). Through most of its history, Mount St. Helens has erupted dacitic lavas as tephra, domes, and pyroclastic flows. This pattern changed about 2200 years ago when andesite and basalt also began to appear. The current Spirit Lake stage began about 4000 years ago.

18 May 1980 eruption and precursors

Before 1980, Mount St. Helens was somewhat less known than other Cascade volcanoes such as Mount Rainier, Mount Hood, and Mount Shasta. That situation changed on 20 March 1980 when seismic activity began to increase above background level. Seismic activity increased sharply on 25 March and continued at a high level until 27 March when the first in a series of small eruptions occurred. Thereafter until 18 May, the number of seismic events per day slowly decreased though the mean magnitudes slowly increased. Numerous eruptions occurred on 28 March. The number, duration, and vigor of the eruptions then slowly decreased until 22 April, when they temporarily stopped. A second interval of minor eruptive activity occurred between 7 and 14 May. No juvenile material was detected in any of these small precursory eruptions. The seismic and eruptive activity was accompanied by dramatic deformation of the summit and north flank of the mountain (Moore and Albee, 1981). Deformation became apparent as early as on 27 March, the day of the first eruption, when observers noted east-trending fractures across the summit. Fracturing and bulging of the north flank of the mountain grew progressively more conspicuous through the period of precursory activity (Lipman et al., 1981a).

At 08:32 PDT on 18 May 1980, a magnitude 5.2 earthquake triggered* a collapse on Mount St. Helens's north flank, the part of the volcano that had become so dramatically deformed. [*Some suggest that the earthquake was caused by the initial movement of the landslide and not vice versa (Kanamori et al., 1984).] Photographs reveal that the initial landslide consisted of two slideblocks. The landslide removed about 1 km of overburden from a "cryptodome" that had been intruding the volcano in the preceding two months—the inferred cause of the seismicity, north-flank bulging and surface fracturing, and phreatic eruptions before 18 May. The sudden depressurization of the cryptodome and its surrounding hydrothermal system caused the rapid expansion of the cryptodome and hydrothermal fluids. This series of explosions began about 30 seconds after the triggering earthquake and issued from the steep north-dipping scarp formed by the descending first slideblock (Voight, 1981). The explosions projected a hot gas–rock mixture upward and northward; it swept northward as a ground-hugging pyroclastic density current. The front of the current swept over the volcano's flanks at more than 600 km/hr. A second magnitude 5 + earthquake occurred about two minutes after the first (Endo et al., 1981; Kanamori et al., 1984). The effect of this event on the edifice is uncertain, because by that time the explosions and developing density current obscured the volcano's north flank. Photographs taken at about that time from the south show an odd ring of white clouds, which suggests that the second large earthquake may have been associated with a second edifice collapse (perhaps slideblock III?, perhaps also with an attending second series of explosions?) that trailed the first two slideblocks. Within about five minutes of the first earthquake, the density current extended 16-28 km from its source and devastated 600 km^2 of high-relief terrain to the north, east, and west. As the current moved outward, it slowed and deposited sediment until its net density became less than that of the ambient air. It then rose buoyantly, although it still had a lateral velocity of several tens of km/hr. The outward motion ceased and a great mushroom-shaped cloud rose buoyantly from the devastated area (Sparks et al., 1986). By 09:00 this cloud reached a height of 30 km.

At about 08:42, a second density current evidently began

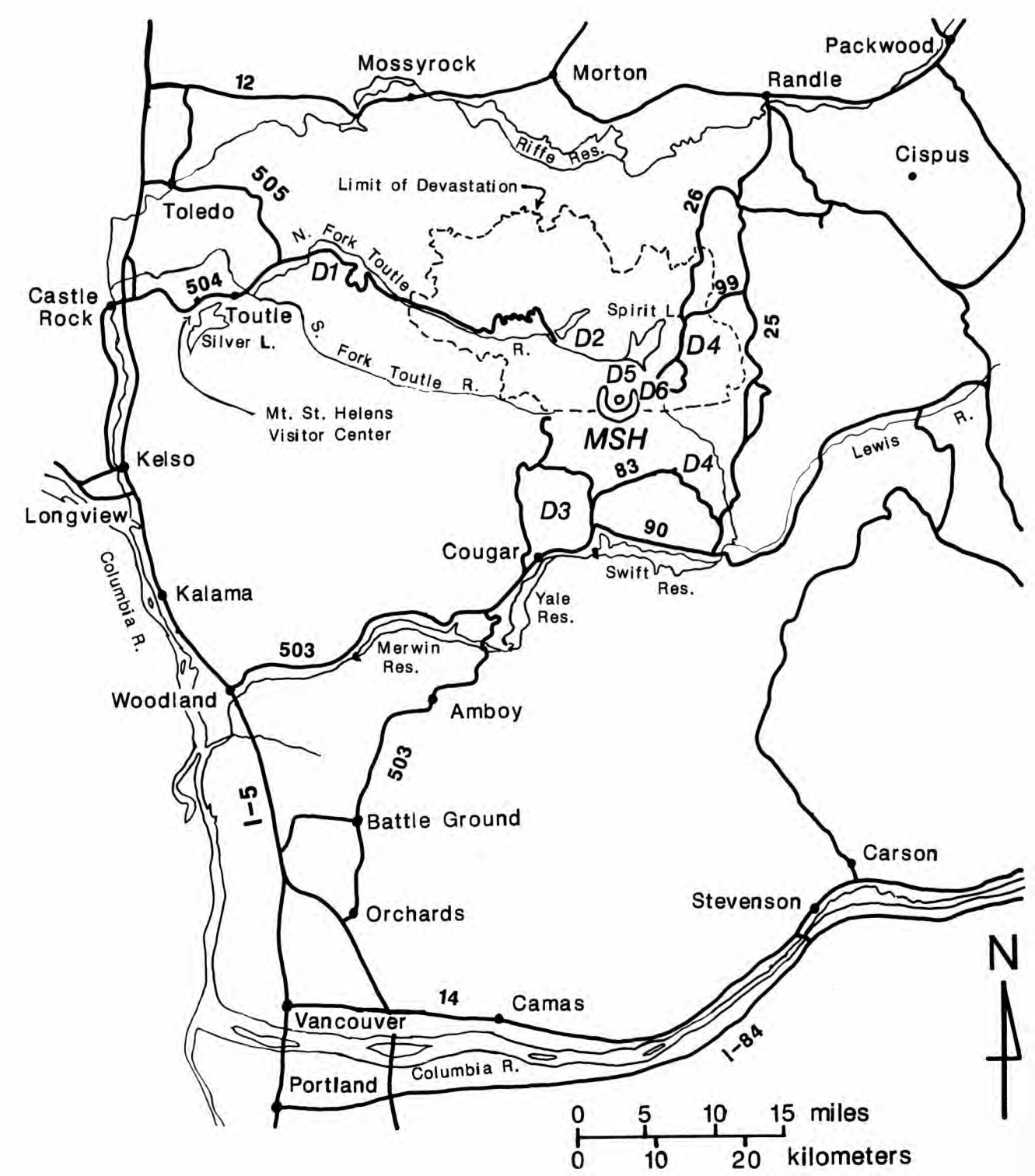

FIGURE 1—Index map showing road access to Mount St. Helens and general location of the six days of field trips; e.g., D4 = area of trip for Day 4.

to move down the North Fork Toutle valley. Distant eyewitnesses northwest of the volcano reported that it reached its maximum extent (20-25 km?) at about 09:20. Unlike the larger initial event, the second density current was confined to the one valley and seemed to stagnate near the ground rather than to rise convectively.

Meanwhile, the three or more slideblocks evolved into an enormous composite debris avalanche that flowed as much as 28 km westward down the North Fork Toutle valley. The first slideblock was set in motion before the initial explosions. Saturation of the seismic records indicates that the composite debris avalanche probably took about 10 to 12 minutes to reach its maximum extent, several minutes after the density current had reached its maximum extent. The avalanche produced a hummocky deposit as thick as 200 m and with a relief of as much as 100 m (Voight et al., 1981).

While the density current was underway, high-velocity

TABLE 1—Summary of eruptive history of Mount St. Helens (from Crandell, 1987, table 3). [1]Years before 1980, based on tree-ring dates and historic records. [2]Years before 1980, based on tree-ring dates and ^{14}C dates.

Eruptive stage, period, and dormant intervals	Approximate ^{14}C age in years before A.D. 1950	Tephra unit	Nature of volcanism
Spirit Lake eruptive stage			
Eruption that began in 1980		1980	Laterally directed blast from cryptodome followed by eruption of dacite tephra and pyroclastic flows and development of dome in new crater.
Dormant interval ~123 yrs			
Goat Rocks eruptive period	[1]180-123	T	Eruption of dacite tephra, andesite lava flow, dacite dome.
Dormant interval ~200 yrs			
Kalama eruptive period	[2]2500-350	X W	Eruptions of dacite and andesite tephra, dacite dome(s), pyroclastic flows, and andesite lava flows.
Dormant interval ~650 yrs			
Sugar Bowl eruptive period	1150	unnamed	Eruption of dacite dome, laterally directed blast, pyroclastic flow(s), tephra falls.
Dormant interval ~600 yrs			
Castle Creek eruptive period	2200-1700	B	Eruptions of andesite, dacite, and basalt tephra, andesite and basalt lava flow, andesite and dacite pyroclastic flows.
Dormant interval ~300 yrs			
Pine Creek eruptive period	3000-2500	P	Eruption of dacite tephra, dacite domes, pyroclastic flows.
Dormant interval ~300 yrs			
Smith Creek eruptive period	4000-3300	Y	Eruptions of dacite tephra, dacite domes, pyroclastic flows; probably included dormant intervals as long as several centuries.
Dormant interval ~5000 yrs?			
Swift Creek eruptive stage	13,000-10,000	J S	Eruptions of dacite tephra, dacite domes, lithic and pumiceous pyroclastic flows; probably included dormant intervals of at least a few centuries.
Dormant interval ~5000 yrs?			
Cougar eruptive stage	21,000?-18,000?	K M	Eruptions of pumiceous tephra, one or more dacite domes and lava flows, lithic and pumiceous pyroclastic flows; probably included dormant intervals of at least several centuries.
Dormant interval ~15,000 yrs			
Ape Canyon eruptive stage	<50,000-36,000?	C	Eruption of tephra and pumiceous pyroclastic flows.

floods (lahars) were generated on all flanks of the volcano except the collapsing north flank. The largest of the early lahars moved down the South Fork Toutle, Smith Creek, Muddy River, and Pine Creek drainages (Pierson, 1985; Brantley and Waitt, 1988; Scott, 1988a; Waitt, in press). However, the most voluminous lahar began hours later and did not reach its peak until about 13:30, some five hours after the paroxysmal eruption. This lahar originated in the upper North Toutle valley from water-saturated parts of the debris-avalanche deposit. It caused widespread destruction along the 120 km of river channel between its source and the Columbia River (Janda et al. , 1981).

Just after the edifice collapse and explosions, only a weak, drifting subvertical ash plume issued from the crater. The vigor of this plume increased slowly (Criswell, 1987). By 09: 00 it developed into a weak vertical Plinian eruption, and by 10:10 into a strong one. Winds carried tephra to the east. At about 12:15 the shape of the eruption column changed as ejecta began to feed voluminous pumiceous pyroclastic flows as well as a vigorous vertical eruption column, though the column soon became much weaker while the flows continued. The pyroclastic flows poured through the breached crater into the upper North Toutle valley. Flows were produced at varying size and frequency until about 16:30, when they ceased and vigor of the vertical eruption increased (Rowely et al., 1981; Criswell, 1987). After reaching a maximum height at about 17:15, the column height decreased rapidly. By 18:15 only a weak eastward-drifting ash plume issued from the crater; the eruption was essentially over.

Activity after 18 May 1980

Smaller explosive eruptions produced pumiceous pyroclastic flows on 25 May, 12 June, 22 July, 7 August, and 16-18 October. The explosive activity on 12 June was followed by the emplacement of a dome, which was partly destroyed by the eruptions of 22 July. A second dome was extruded after the explosive activity on 7 August; this was in turn destroyed in the October eruptions but was soon replaced by a third dome. Fifteen subsequent effusive eruptions have built the dome into a hemispherical mass about 270 m high and 1 km in diameter. As of April 1989, the latest such dome-building eruption occurred on 21 October 1986.

Terminology

The paroxysmal explosions of 18 May 1980 have attracted much attention from the scientific community. Different schools of thought have formed regarding their nature and genesis; the diversity of opinion has spawned a parallel diversity in terminology. At least 15 terms have been applied to the composite phenomenon, a new one introduced in nearly each new publication on the subject. Most workers would agree that the phenomenon responsible for the wide-

spread devastation was a type *of pyroclastic density current.* While this term denotes pyroclastic flow and (or) pyroclastic surge nonspecifically, it is rather cumbersome to use repeatedly in the text. We will use *surge* as a terse synonym for the density current, and *surge deposit* for the deposit it produced.

A *pyroclastic surge* (Wohletz and Sheridan, 1979) travels as a fast-moving, turbulent, generally ground-hugging pyroclastic density current (Middleton and Hampton, 1976; Fisher, 1983). In a pyroclastic surge (herein sometimes abbreviated as *surge)* the volume proportion of particles to gas is thought to be relatively low (Sparks et al., 1973; Walker and McBroome, 1983).

A *pyroclastic flow* is a relatively nonturbulent, highly fluidized, hot pyroclastic density current in which the volume proportion of particles to gas is high (Sparks et al., 1973; Walker and McBroome, 1983).

A *lahar* is a mass flowage of water-saturated rock debris originating from the flank of a volcano (Crandell, 1971, 1987).

A *debris avalanche* is a rapid flow of rock debris (Varnes, 1978) that may contain some water, although water is not necessary for the transport of the material. Large volcanic debris avalanches, common around stratovolcanoes, commonly produce lahars (Siebert et al., 1987).

We use the standard Wentworth particle-size terminology for sediments (Folk, 1966), which is increasingly used for volcanic materials (see Fisher and Schmincke, 1984, table 5-7) . These terms describe only grain size and imply nothing whatever about grain shape, sorting, fragmentation mechanism, or depositional process.

Bibliography

The reference list is limited to papers cited in the text. A fairly comprehensive listing of hundreds of works on Mount St. Helens published between 1882 and 1986 is given by Manson et al. (1987).

Day 1: Modern and ancient volcaniclastic sedimentation in Toutle River valley, Mount St. Helens

Kevin M. Scott

Introduction

Observations of a 1982 lahar from Mount St. Helens during and just after its emplacement in the North Fork Toutle valley (Fig. 2), as well as of deposits of ancient lahars such as those we view today, show that a single flow wave can vary substantially during flow and leave deposits with rather different characteristics. The most common form upvalley is a *debris flow* having yield strength probably exceeding 400 dynes/cm^2, whose deposit is a very poorly sorted sandy gravel or gravely sand commonly inversely

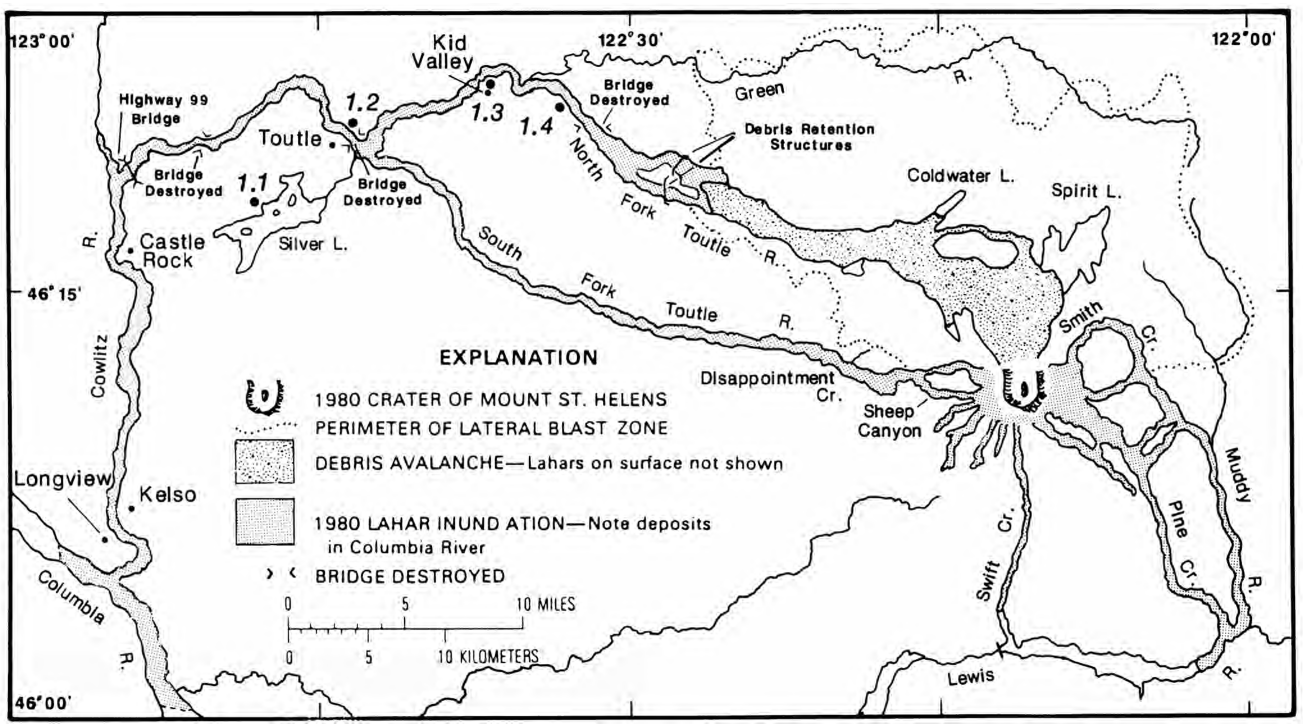

FIGURE 2—Map showing locations and geography of North Fork Toutle valley, route of trip for Day 1. Patterns show generalized distributions of main distal deposits resulting from 18 May 1980 eruption.

graded at its base and normally graded at its top (*lahar facies*). The inferred sediment concentration during flow is 80-90% sediment by weight (Pierson and Scott, 1985). Downstream, the debris flow may incorporate water by overriding streamflow to transform into a *hyperconcentrated flow* having some strength with an initial sediment concentration of 60-70% by weight (the hyperconcentrated range is defined as 40-80% by weight) and leaving a moderately to poorly sorted deposit of sand or gravelly sand that is commonly structureless but may be distinctly but weakly stratified (*lahar-runout facies*) . Still farther downstream the flow may, by further incorporation of water, transform into *normal streamflow* with little or no yield strength and sediment concentration less than 40% sediment by weight. The deposits are moderately well- to well-sorted sand or gravel and are conspicuously cross-stratified or plane-stratified (*streamflow facies*) (Fig. 3). In vertical section, two or all three facies may be stacked (Fig. 4).

Our focus will be on the record of volcanically induced sedimentation downstream from Mount St. Helens in the North Fork Toutle valley (Fig. 2) (Scott, 1988a). The record of flows extending many tens of kilometers from the volcano may be more complete than that on or near the edifice. For example, some of the largest lahars (volcanic debris flows) resulting from prehistoric lake breakouts through volcanically emplaced blockages did not transform from water surges to debris flows until as much as 20 km away from Mount St. Helens.

The debris flows represent the middle segment of a flow wave both beginning and ending as normal streamflow. The transformations from an initial water surge to hyperconcentrated flow and then to debris flow occur near or on the volcano, however, and the deposits recording these transformations are commonly eroded or may be covered by other volcanic deposits. Water surges erode sediment rapidly on steep slopes of the edifice to form a wave of hyperconcentrated flow, and sediment incorporation remains rapid as debris flow is formed. The debris-flow segment of the wave may continue to enlarge by the same process. The downstream transformations, in reverse order from that described above, commonly occur over tens of kilometers, yielding deposits much more extensive and likely to be preserved in the stratigraphic record. The characteristic facies associated with the downstream sequence of transformations are illustrated in Fig. 3. Note the presence of a transition facies in the channel interval where the debris flow transformed to hyperconcentrated flow. Hyperconcentrated-flow deposits most typically are thick, nearly structureless units of medium to coarse sand (0-2Φ) . They may be characterized by well-developed inverse grading, especially in, and downstream from, the transition facies.

The downstream record of flow deposits can also reveal volcanic events that are not evident from the study of deposits on the volcano. An example is the series of four large lahars in the Toutle River system that occurred in a short period of time near the end of the Pine Creek eruptive period, about 2500 radiocarbon years ago (Scott, 1988b). The two largest flows in the series are the largest in the history of the river system. The evidence for the origin of this series of flows as lake-breakout flood surges will be reviewed throughout the trip. A possible analog is the 1980 debris avalanche and the consequent formation of several large lakes by tributary blockage. Without intervention, a series of large flood surges would have been released by blockage failure or overtopping within several years after 1980.

Field guide

STOP 1-1. Mount St. Helens Visitor Center (U.S. Forest Service). Examine exhibits (center hours: 09:00–18:00). The visitor center is built on the shore of Silver Lake, a 15 km^2 lahar-impounded lake. The lake covers a large tributary valley of the main Toutle River and overlies a thick fill of lahars from Mount St. Helens. Present outflow is through Outlet Creek, adjacent to Stop 1-2. Most of the fill consists of deposits of the four large lahars mentioned above. These flows occurred in a rapid succession about 2500 radiocarbon years ago. The lake, in its present configuration, formed at that time. The basic origin of the lake was recognized by Mullineaux and Crandell (1962); the sedimentology, dynamics, and origin of the flows, and their unique boundary features, are described by Scott (1988a, b). The flow deposits will be seen at Stops 1-2 and 1-3.

Silver Lake has a maximum depth of only 3 m, determined by hydrographic survey. Shallow depth is a charac-

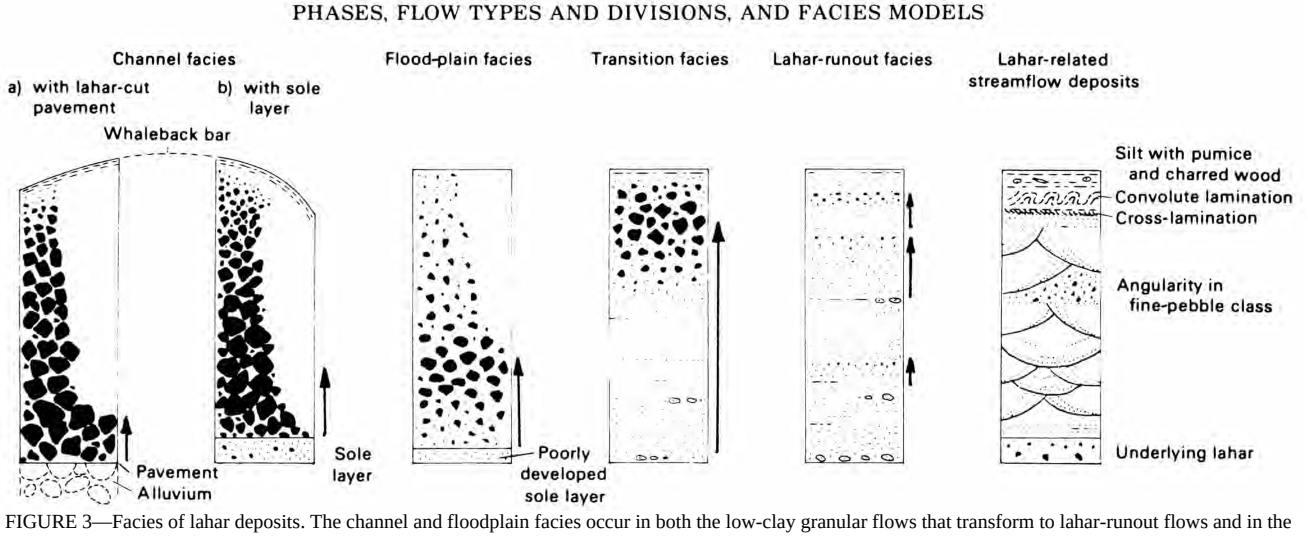

FIGURE 3—Facies of lahar deposits. The channel and floodplain facies occur in both the low-clay granular flows that transform to lahar-runout flows and in the high-clay flows that do not readily transform. The transitional and lahar-runout facies occur mainly in the granular flows. Arrows signify inversely graded bases of flows.

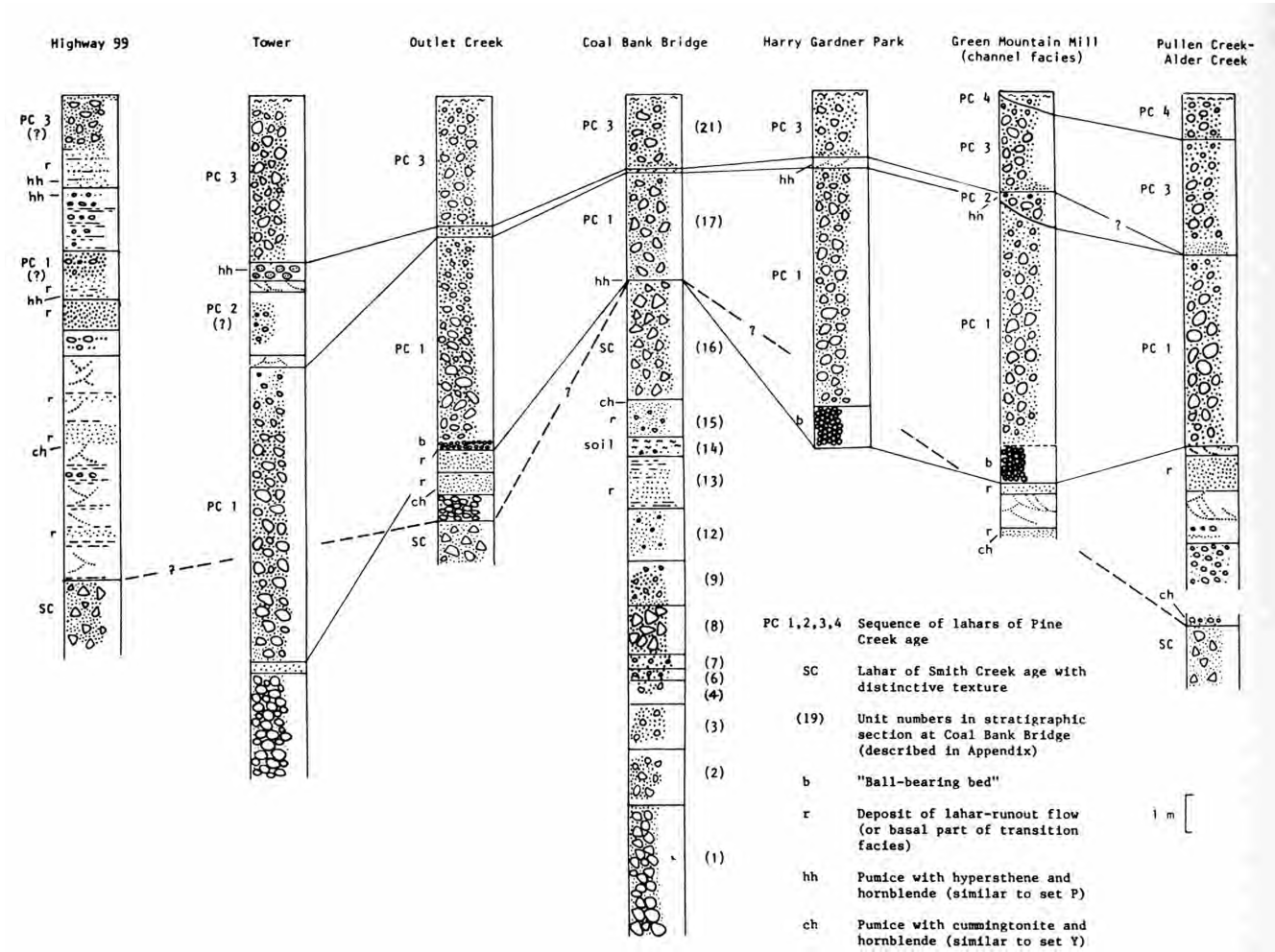

FIGURE 4—Columnar sections of lahars and associated deposits at selected locations in the Toutle River system. The Coal Bank Bridge section contains the most complete sections of flow deposits of Swift Creek age.

teristic of lahar-impounded lakes, reflecting the fluidity of the lahars and their ability to fill backwater areas.

STOP 1-2. Coal Bank Bridge. One of the most complete sequences of sediment gravity flows in the river system occurs just upstream on the west bank. Unfortunately, exposures have deteriorated in recent years, and unit 8 (Fig. 4) is presently the oldest unit exposed. The original section was described from the cliff face (now failed) and from excavations for the new bridge piers. A spectacular photo of this bridge being destroyed by a 1980 lahar appears in National Geographic Magazine (January 1981).

By interpreting the flow deposits as "frozen" flood peaks, a nearly complete flow history for the watershed can be assembled from many similar downstream sequences, and a "flood-frequency" analysis can be prepared. The Cascades Volcano Observatory (CVO) staff has now deciphered the flow history at several Cascade Range volcanoes as well as that for the other major drainage of Mount St. Helens, the Lewis River, on the south side of the volcano.

The section contains deposits of the following (informal) eruptive stages and periods, as defined by Mullineaux and Crandell (1981) and Crandell (1987) (Table 1):

Ape Canyon eruptive stage (50,000–36,000? yrs B.P.): Pumice-rich deposits of the oldest eruptive stage filled the valley of the Toutle River to a level 10–30 m above the highest subsequent lahar-emplaced terrace deposits. The fill was gradual, however, and consisted of alluvium, lahars, and the deposits of hyperconcentrated lahar-runout flows. These deposits underlie valley-side slope on the west bank and are overlain by deposits of the downstream section.

Swift Creek eruptive stage (13,000–10,000 yrs B.P.): Units 1–14 (Fig. 4) include 9 or 10 lahars of this stage. Note the basal inverse grading in most units (Fig. 3, column 3). Unit 12 is a good example of a hyperconcentrated-flow deposit. Note the contrast between the massive structure of that unit and the well-defined stratification in the overlying unit 13, the product of "normal streamflow," having sediment concentrations below the hyperconcentrated range.

Smith Creek eruptive period (4000–3000 yrs B.P.): Units 15 and 16 record volcanic activity during this time. Unit 15 is transitional between a lahar and a lahar-runout flow.

Pine Creek eruptive period (3000–2500 yrs B.P.): Units 17 and 21 record the two largest flows in the history of the river system (PC 1 and PC 3 in Fig. 4). Both deposits are abnormally thin here, but are normally developed in exposures a short distance up Outlet Creek, which joins the Toutle River just downstream from the bridge. These two flows dammed Outlet Creek, creating Silver Lake.

The frequency of overbank lahars and lahar-runout flows during eruptive periods of the last 4500 yrs is about 1 per 100 yrs at this distance from the volcano. Multiple lahars apparently occurred in relatively short time intervals within

eruptive periods. Note the eroded and rapidly vegetated surfaces of the floodplain facies of the 1980 lahars, and the planar, originally unvegetated surfaces forming many of the contacts in the older units of the floodplain facies.

STOP 1-3. Kid Valley. In the roadcut leading uphill to the southeast, on the downstream side of the bridge, deposits of the largest lahar in the history of both the river system and the volcano (Fig. 5, PC 1) can be seen as a coating on the valley-side slope. Peak stage is well defined at a hydraulically consistent level by the highest clasts of Mount St. Helens lithologies. High "water" marks approach 30 m above the present river surface. Note the relative sizes of the flow cross sections of this lahar and the flow which occurred in 1980 (Fig. 5). The mudcoats left by the 1980 lahar may still be visible on the bridge piers.

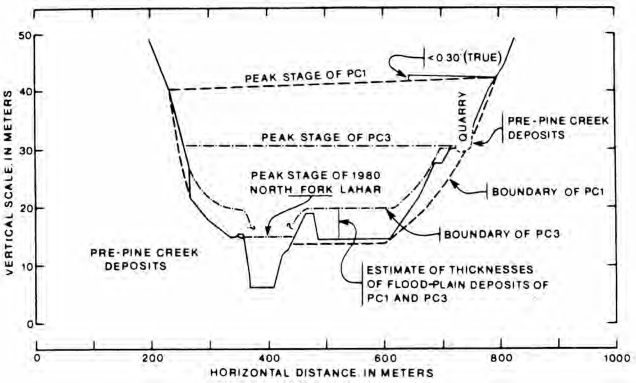

FIGURE 5-Cross section of peak-flow lahars of PC-1, PC-3, and 1980 (at Kid Valley, Stop 1-3). The unique boundary features by which individual flows are correlated are described in Scott (1988a).

STOP 1-4. Sediment-Retention Structure. At this site, the Corps of Engineers is constructing a permanent sediment dam to reduce the more costly operation of long-term downstream dredging. The structure will be 55 m high. Pre-1980 lahars have inundated the basalt bench upon which Highway 504 is built, but this occurred early in the history of the volcano (Ape Canyon eruptive stage), when pumiceous alluvium partially filled most of the surrounding valleys.

Day 2: 18 May 1980 debris avalanche and pyroclastic surge ("blast") near Elk Rock and Coldwater Lake, North Fork Toutle valley

Richard P. Hoblitt and Harry Glicken

Introduction

The events of 18 May 1980 began at 08:32 PDT with a magnitude 5.2 earthquake (Christiansen and Peterson, 1981; Endo et al., 1981), which triggered a collapse of the north side of Mount St. Helens. The resulting great rockslides and debris avalanche (Voight et al., 1981; Glicken, 1986, in press) became the world's largest historic mass movement. The initial rockslide relieved pressure on an intruding cryptodome and surrounding hydrothermal system, which resulted in a series of explosions that quickly developed into a pyroclastic surge (also known as the "blast"). Today we visit the Elk Rock and Coldwater Lake areas (Fig. 6) to examine deposits of the 18 May 1980 pyroclastic surge and debris avalanche.

Rockslides and debris avalanche

The rockslide consisted of three slideblocks (Fig. 7), the first two of which are apparent on eyewitness photographs. The first (slideblock I) remained relatively intact as it slid to the north. The initial explosions began on a steep north-dipping face of slideblock II that developed behind the descending slideblock I. Slideblock I deposited material on, and adjacent to, Johnston Ridge and in Spirit Lake. Part of slideblock I flowed downvalley to the west where it formed the margins of the debris-avalanche deposit. Most of slideblock II and all of slideblock III were steered westward by Johnston Ridge and became a flowing debris avalanche. Slideblock III was not observed directly and may have consisted of a number of smaller slideblocks.

The 2.5 km^3 debris-avalanche deposit (Fig. 8) comprises: (1) a block facies—pieces of the pre-1980 mountain transported relatively intact; each piece is called a debris-avalanche block, or debris block for brevity, and (2) a mixed facies—a mixture of old Mount St. Helens rocks, cryptodome dacite, and diverse material picked up during flow; it is sometimes called "matrix facies." The eastern or up-valley part of the deposit was emplaced by a flow of discrete debris blocks derived from all three slideblocks. It is divided into five map units correlated with rock types on Mount St. Helens. The western part of the debris-avalanche deposit (more than 17 km from the source) consists of mixed facies with subordinate debris blocks. It was derived from an explosively motivated flow that was generated mainly from slideblock III and swept over the flow of debris blocks. Some of the mixed facies was also derived from disaggregation and mixing of debris blocks in the flow of debris blocks.

The entire deposit is characterized by hummocks interspersed with irregular to circular depressions. This surface has as much as 75 m of relief. Hummocks of the block-dominated flow are generally larger than hummocks of the explosively motivated flow (Fig. 9). The hummocks partly reflect the extreme inhomogeneity in the moving debris avalanche.

The density of the old cone (2.2-2.4 g/cm^3) was about 20% greater than the measured density (1.8 ± .4 g/cm^3) of the debris-avalanche deposit (Glicken, 1986: 189-197). The average density of the deposit does not decrease with dis-

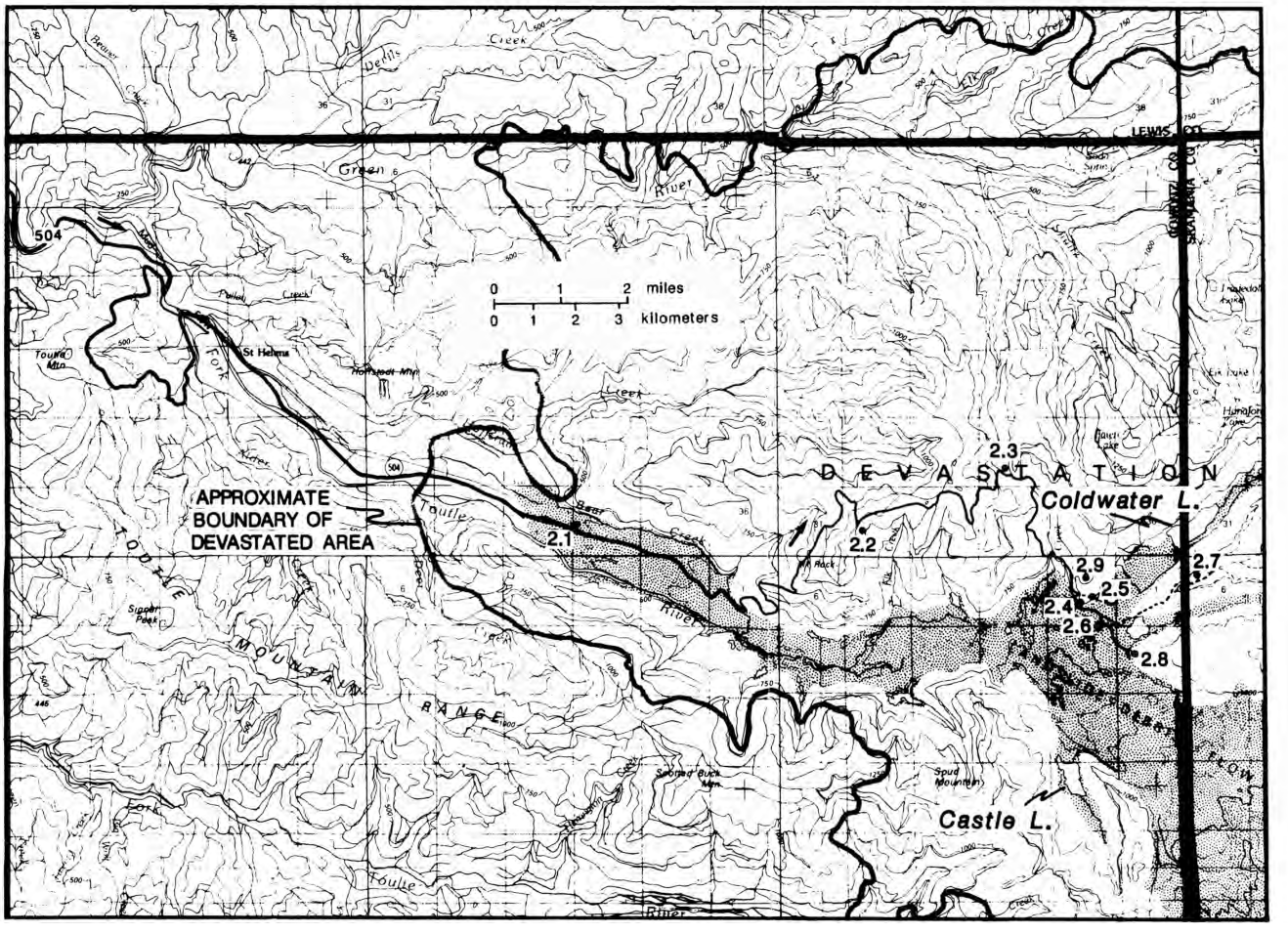

FIGURE 6-Index map of upper North Fork Toutle valley showing distribution of deposit of 18 May 1980 debris avalanche from Mount St. Helens and indicating route and stops for Day 2.

tance, which indicates that debris-avalanche blocks were dilated at the mountain rather than during transport (Fig. 10). Grain-size data indicate that the size of clasts (rocks that can be sieved without breaking) also does not decrease with distance, which suggests that dilation resulted mainly from shattering at the mountain.

The flow of debris blocks in the debris avalanche can be considered as a grain flow, where particles, either debris blocks or the clasts within the blocks, collide and create dispersive stresses normal to the general movement of material. Water as liquid or vapor within the debris avalanche lowered the internal friction of the avalanche. Preservation of original volcanic stratigraphy and structures within many exposures of the debris-avalanche deposit indicates that particles commonly remained in contact with one another. Although such features suggest laminar movement, the abundant evidence of disaggregation of debris blocks, mixing of their constituent clasts, and convoluted textures at some exposures suggest that the debris avalanche also had some characteristics of turbulent flow.

The high mobility of the debris avalanche, expressed in low ratio of fall height to travel distance, probably resulted mainly from the explosions that accompanied the mass movement. The explosions facilitated mixing of material. In addition, water vapor and volcanic gas released in the explosions lowered interparticle friction.

The debris avalanche deranged the North Fork Toutle River drainage. Spirit Lake was inundated with about 0.4 km3 of debris-avalanche deposit and its outlet was blocked (Glicken et al. , in press; Glicken and Voight, in press). The debris avalanche dammed Coldwater and South Fork Castle Creeks to form Coldwater and Castle Lakes. Because of the possibility of catastrophic flooding from eventual overtopping and consequent dam failure (Youd et al. , 1981; U.S. Army Corps of Engineers, 1984; Meyer et al. , 1986), the army engineers constructed artificial spillways to reduce the hazard posed by the three lakes (Fig. 6).

Pyroclastic surge

The explosion resulting from the rapid depressurization of the cryptodome produced a pyroclastic density current (here called *surge)* that devastated about 550 km^2 of terrain near Mount St. Helens (Fig. 1). Early studies assumed that the explosion consisted of one extended impulse, but several independent data sets—seismic, photographic, eyewitness accounts, satellite sensors—suggest that explosions occurred in at least three major impulses. As is clear from photographs, the first series of explosions issued from slide-block II**.** This impulse overtook the front of the debris avalanche on the north flank of the volcano. A second impulse, inferentially associated with slideblock III, began about two minutes after the beginning of the first impulse. A third impulse started about eight minutes later. The relative contributions of these impulses to the stratigraphy of the pyroclastic-surge deposit are still under investigation.

The deposit and other effects of the explosions and pyro-

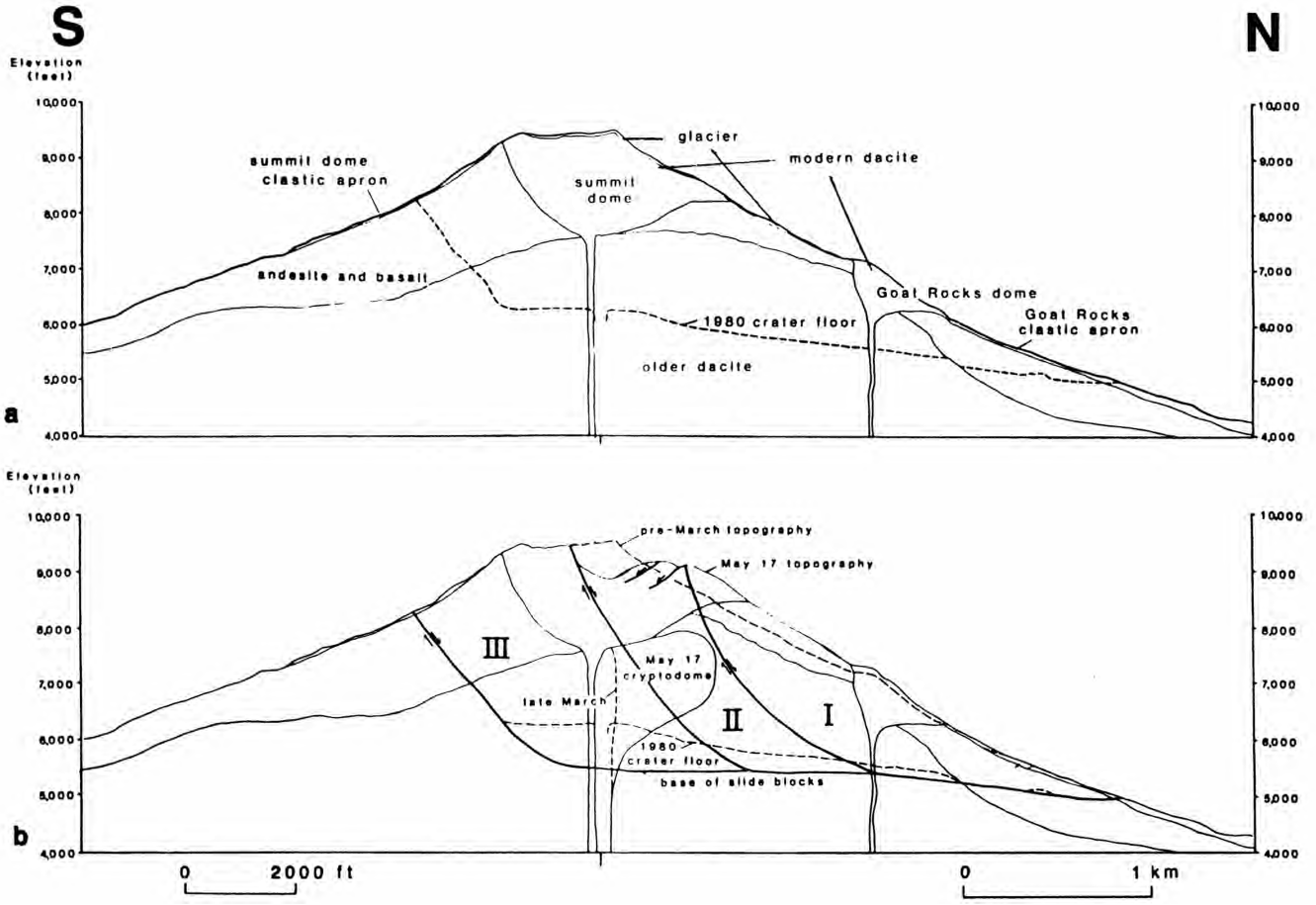

FIGURE 7-Cross section of Mount St. Helens (north is to right). **a,** Before March 1980; **b,** just before eruption of 18 May 1980, showing slideblocks seen on eyewitness photographs and inferred from post-eruption topography. From Glicken (1986, fig. 2).

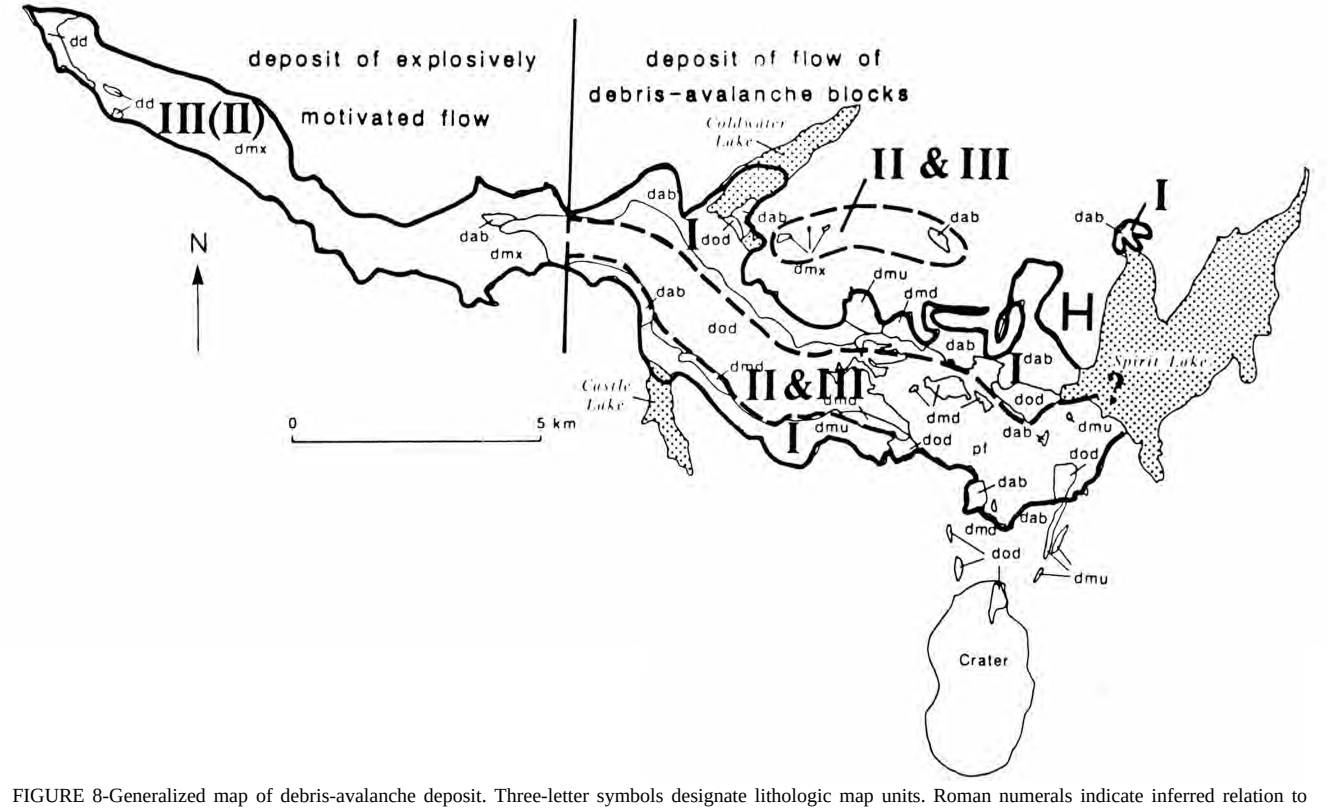

FIGURE 8-Generalized map of debris-avalanche deposit. Three-letter symbols designate lithologic map units. Roman numerals indicate inferred relation to slideblocks from Mount St. Helens (compare to Fig. 7). From Glicken (1986, fig. 60). J, Johnston Ridge; H, Harrys Ridge. Patterned areas, lakes created or elevated by damming of debris-avalanche deposit. Symbols: dd, distal unit, dab, andesite-and-basalt unit; dmd, modern-dacite unit; dmu, modern undifferentiated unit; dod, older-dacite unit; dmx, mixed-block facies and matrix-facies unit; pf, pumiceous pyroclastic-flow deposits.

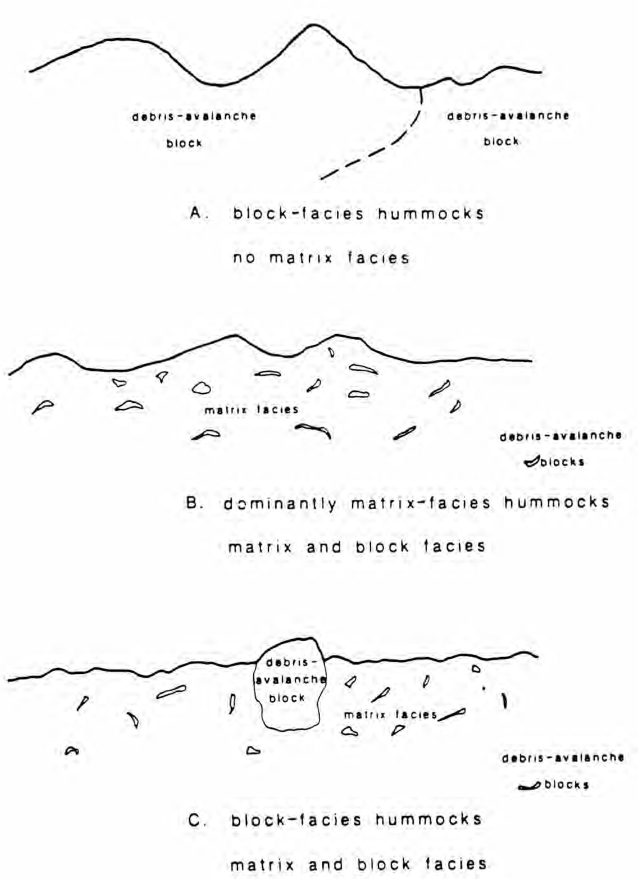

FIGURE 9—Sketch showing types of hummocks in debris-avalanche deposit. Matrix facies of this figure is called *mixed facies* in text. From Glicken (1986, fig. 12).

clastic surge of 18 May have been described in several published studies (Hoblitt et al., 1981; Moore and Sisson, 1981; Waitt, 1981; Fisher et al., 1987; Criswell, 1987; Brantley and Waitt, 1988). The deposit thins with distance from the source, from as much as a few meters near Mount St. Helens to as little as a few millimeters near its margin. The average grain size also decreases with distance from the source. The deposit is thicker in topographic lows and in the lee of obstacles than it is on topographic highs and on the stoss side of obstacles. The stratigraphy is variable and

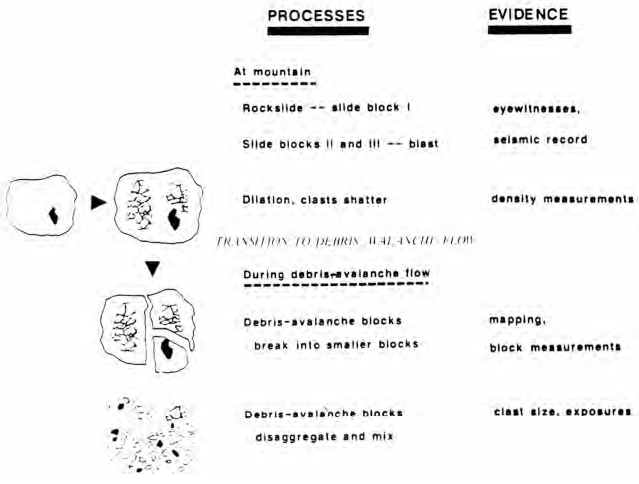

FIGURE 10—Sketch relating evidence from debris-avalanche deposit to inferred processes. From Glicken (1986, fig. 61).

complex, and many exposures differ in detail from the idealized composite sections described in the literature. Nevertheless, some generalities are still valid. The basal part of the deposit generally consists of coarse, grain-supported debris. Commonly this coarse basal material is mixed with wood fragments and conifer needles and contains a relatively high proportion of cryptodome dacite. In distal areas, the coarse basal unit is overlain by stratified sand and silt. In proximal areas, massive matrix-supported material may be sandwiched between the coarse basal unit and the overlying stratified unit. The uppermost part of the deposit is capped by a layer of silt-sized material that commonly contains accretionary lapilli. At any given site, any or several of these strata may be absent. Parts of the debris-avalanche deposit containing cryptodome dacite are difficult to distinguish from the surge deposit.

Field guide

Parts of the maze of private roads in the upper North Fork Toutle valley frequently become washed out or closed by construction, and other routes then become the main track. Changes occur even as we write, and so some of the described roads will probably no longer be in service at the time of the field trip. The field-trip leaders will indicate any such changes just before the trip begins.

Mileage

0.0 Intersection of WA-504 at I-5, Castle Rock, Washington. **5.4**

5.4 Mount St. Helens National Volcanic Monument Visitor Center at Silver Lake. **3.2**

8.6 Silver Lake, Washington. This lake formed when Mount St. Helens lahars of Pine Creek age dammed a tributary valley of the Toutle River (guide for Day 1). **1.8**

10.4 Toutle, Washington. The road splits at "Country Store"; bear left. **0.9**

11.3 Coal Bank Bridge crosses the Toutle River just downstream from the confluence of its North and South Forks. A short distance beyond the bridge, the road proceeds along the north side of the North Fork. Parts of this road in this area were destroyed on 18 May 1980. **3.7**

15.0 Highway 505 to left; stay on 504. **2.8**

17.8 Kid Valley Bridge crosses to the south side of the North Fork Toutle River. This is the only bridge across the Toutle River that survived the 1980 lahars. **1.1**

18.9 Kid Valley, Washington: last chance for eastbound travelers to buy food and gasoline. **3.5**

22.4 Field office for construction of Sediment Retention Structure. Leave paved road, and detour to right at the "To SR 504, Green River, Hoffstadt Bluff" sign. There will be more of these signs; follow them. When in doubt, choose the more heavily traveled road. **1.0**

23.4 Overlook of Sediment Retention Structure. **2.3**

25.7 Intersection. At this point you leave Weyerhauser road 2418 and go to left on Weyerhauser road 2400. **2.2**

27.9 Cross single-lane bridge. **1.8**

29.7 Return to pavement. **0.3**

30.0 Bridge across North Toutle River. **0.1**

30.1 Road to left with "Pullen Cr. Bridge" sign; stay on paved road. **0.9–1.9**

32–33 Against north side of valley is site of Weyerhauser's Camp Baker, a log-sorting facility from which hundreds of big logs, trucks, railroad cars, etc. were incorporated in the great lahar of afternoon 18 May 1980. **0.5–1.5**

33.5 Pavement ends, continue straight ahead on unpaved road. **0.5**

34.0 Road to left across the crest of a dam (N-1 debris retention structure); continue straight ahead. The dam was built in fall 1980 and was breached during floods in following winters; it was filled by lahars on 19 March 1982. **0.4**

34.4 Road crosses bridge. This is the site of distal end of the debris-avalanche deposit, leveled during construction of the N-1 dam. **1.3**

35.7 Enter hummock field of 18 May 1980 debris avalanche from Mount St. Helens. **0.1**

35.8 Crossroads; go right onto 3500 road. **0.4**

36.2 **STOP 2-1. Facies of debris-avalanche deposit.** On left side of the road is a small shovel-dug exposure in the debris-avalanche deposit (Glicken, 1986, in press, locality DXS-1). To view the exposure well, one should clean it with a trowel and, if it is dry, spray it with water. This material lies within map unit *dmx* (Fig. 8) that contains both debris blocks (relatively intact pieces of the old mountain) and mixed facies of the debris-avalanche deposit. The debris blocks are highly deformed rubble. The mixed facies is olive in color and contains juvenile "blast" dacite, which suggests that the material was explosively motivated and had an origin in slideblock III (Fig. 7). Slideblock III, not visible in the eyewitness photographs, is interpreted to have formed from several individual failures. The debris blocks contained within these mass movements were then carried out in a flow of mixed facies containing juvenile dacite. **1.6**

37.8 Road crosses bridge. **1.2**

39.0 Begin to climb north side of valley on road 3300. **1.3**

40.3 Intersection of roads 3300 and 3320; go left on 3300. **0.5**

40.8 Intersection of roads 3300 and 3330; go right/straight on 3330. **0.4**

41.2 Intersection with 3332 to the left; continue straight ahead on 3330 (becomes road 3340 after about 0.3 mi). **0.7**

41.9 Unmarked road (3341) to left; go right/straight. **0.3**

42.2 Road 3342 to right; go left/straight. **0.5**

42.7 Intersection with 3344; go right on 3340. **0.1**

42.8 Intersection with 3345; continue on 3340 to left. **0.8**

43.6 Intersection with 3340 to left and 3346 to right; go to right on 3346. **0.6**

44.2 **STOP 2-2. Top of Elk Rock: Panoramic view of debris-avalanche deposit.** The western part of the debris-avalanche deposit, inferred to have been explosively motivated, consists of mixed facies containing juvenile dacite and debris blocks. The eastern part of the deposit consists almost entirely of debris blocks (Fig. 8).

Farther east, wavy-surfaced blast deposits mantle the debris-avalanche deposit. Flat-surfaced, light-colored lahars that formed from dewatering of the debris-avalanche deposit in the late morning and afternoon of 18 May extend downstream from Coldwater Lake, progressively covering more of the surface of the debris-avalanche deposit with increasing distance westward.

Intersection of roads 3346 and 3540; go left on 3540. **0.8**

45.6 Crossroads; go east on 3540. **0.8**

46.4 Intersection with road to right; keep to left. **0.5**

47.9 **STOP 2-3. Example of surge deposit.** A good exposure of the surge deposit lies along the north side of the road on interfluve between Maratta Creek and west fork of Schultz Creek. The surge section, 45–70 cm thick, rests on a surface probably disturbed by pre-1980 road-building. The lowest unit in the section (0–25 cm thick) tends to be richer in organic material, coarser (clasts as coarse as 8 cm in diameter), more friable, and grayer than the yellowish overlying units. The lowest unit is overlain by 30–35 cm of lapilli as large as 3 cm, supported in a cohesive ash matrix. This pyroclastic-flowlike unit has a discontinuous stratified zone 0–3 cm thick at its base. The flowlike unit is overlain by 2–10 cm of stratified, sand-sized ash. The uppermost blast unit consists of 4–5 cm of fine ash that includes accretionary lapilli. This unit is being eroded away in exposed locations but is preserved here by overlying colluvium.

How many depositional impulses produced this section? Component analysis of the 8–16 mm fraction indicates that the friable lower unit contains more juvenile dacite (54% vs. 43%) and less hydrothermally altered lithic clasts (8% vs. 20%) than the cohesive upper unit. The same relations, consistent wherever the two units are found, suggest that the two units are products of two depositional impulses. **0.1**

48.0 Road to left with sign that reads "To Morton"; go straight/right on 3540. **0.1**

48.1 Road 3544 to left, go straight/right on 3540. **0.2**

48.3 Road to right; go straight/left on 3540. **2.2**

50.5 Crossroads at margin of debris-avalanche deposit; go downhill to right. **0.1**

50.6 **STOP 2-4. Relations between the surge and debris-avalanche deposits.** The walls of the Coldwater Lake spillway and nearby roadcuts expose the lower contact of the debris-avalanche deposit, which is locally underlain by material deposited by the pyroclastic surge. The surge deposit may be seen beneath the avalanche debris on the east side of the road about 70 m northwest of the bridge (Fig. 6). The avalanche deposit, only about 1 m thick here, consists of unsorted clasts of pre-1980 Mount St. Helens rock types. The surge deposit is 10–20 cm thick and is sandwiched between the avalanche deposit and an underlying organic mat covering the pre-blast surface. The surge deposit may be distinguished from the avalanche deposit by its greater friability and organic content. The lowermost few millimeters to few centimeters of the surge deposit consist of friable, gray, sand-sized ash mixed with

organic material, particularly conifer needles. This is overlain by as much as 10 cm of a brown, cohesive mixture of organics and surge fragmentia. As much as 10 cm of friable gray ash and lapilli rests in turn on the cohesive brown material. Lenses of this material are locally incorporated in the base of the avalanche deposit. Cryptodome dacite is abundant throughout the surge deposit, but it is absent in the overlying avalanche debris.

The surge clearly reached this site before the debris avalanche. The avalanche debris at the spillway is part of slideblock I, derived from the outer part of Mount St. Helens. Slideblock I had a velocity of about 70 m/sec near St. Helens (Voight et al., 1983) and emplaced debris as far as 16 km from its source (Glicken, 1986, in press). The avalanche must have arrived at the Coldwater site four to five minutes after the avalanche began—about when the surge reached its maximum extent (Sparks et al., 1986). Data from infrared sensors aboard satellites indicate that the first surge impulse arrived at the Coldwater area about 2.8 minutes after the triggering earthquake (Moore and Rice, 1984). The arrival time of the second surge impulse is uncertain, but is probably less than two minutes after the arrival of the first impulse. Thus, it is uncertain whether the second impulse arrived at the Coldwater site before the debris avalanche.

Return to the crossroads at mile 50.5. **0.1**

50.7 **STOP 2-5. Relations of the surge and debris-avalanche deposits.** Part of the surge deposit overlies the debris avalanche near Coldwater spillway. Such outcrops are discontinuous and best examined north of the spillway, where the margin of the avalanche deposit forms a low ridge. Walk east from the crossroads along the low ridge of avalanche debris. The avalanche deposit is mantled with from zero to several decimeters of surge material. This surge material is olive gray when moist and tends to be finer-grained than the blast materials beneath the avalanche deposit. The base of the post-avalanche blast deposit consists of a fines-rich cohesive basal zone that locally contains rounded voids and incorporates lenses of avalanche debris. This zone is locally overlain by a somewhat coarser, moderately friable zone suggestive of a ground layer. This grades upward into massive to stratified ash. This in turn grades upward into the uppermost unit, composed mainly of fine ash and accretionary lapilli.

The presence of the surge deposit above the avalanche deposit indicates that the surge was still depositing material at this site more than four to five minutes after the triggering earthquake. If the surge front arrived 2.8 minutes after the triggering earthquake, a single extended depositional impulse would have to have lasted about one to two minutes to produce the observed stratigraphy. A second or third depositional impulse could also account for the stratigraphy. Studies of the time–altitude behavior of clouds generated by the surge (Sparks et al., 1986) indicate a third pulse began about 10 minutes after the triggering earthquake. Criswell (1987) argues that this pulse was a post-surge, pre-Plinian event, and suggests that it was responsible for the emplacement of a pyroclastic flow that rests atop the debris avalanche in the North Toutle valley. The deposit overlying the debris-avalanche deposit at this site thus may be the product of the third eruptive pulse. **0.2**

50.9 Coldwater spillway. **0.4**

51.3 **STOP 2-6 (optional). Effects of the surge on a bulldozer.** Park near the intersection with the unmaintained road to the left; walk east on the unmaintained road. Cross South Coldwater Creek and follow old logging roads about 2 km up Coldwater Ridge, gaining about 1000 ft in altitude. A bulldozer that survived the surge sits at an altitude of about 3540 ft on the north side of the ridge, between the Coldwater and South Coldwater valleys. This artifact is one of the few remaining examples of a large quantity of commercial logging equipment and privately owned vehicles that were damaged or destroyed by the surge. Other artifacts lie just west of the bulldozer. The bulldozer seems to be roughly in its pre-surge position, although it may have been rotated somewhat to the north. The paint was stripped from surfaces that face St. Helens, and the stoss side of the heavy screen that protected the operator compartment was torn from its anchors. The screen on the lee side became a crude sediment trap and is clogged with wood and rock fragments as large as 10 cm.

Return to maintained road and walk another 0.2 mi. **0.2**

51.5 **STOP 2-7. Walk across debris-avalanche deposit.** Our walk through the debris-avalanche deposit (Fig. 11) begins at "Teacup hummock" in front of the small lake.

Walk Stop A. The "Teacup hummock" shows a contact of white hornblende–hypersthene dacite of the "older dacite unit" (Fig. 7) overlain by the "andesite and basalt" unit. This contact is identical to that seen within the crater of Mount St. Helens. The hummock thus represents a single debris block. Most commonly the contact is right-side-up, suggesting that the material moved by sliding and turning about a vertical axis, but it did not tumble end-over-end. Although the contact from the old mountain is preserved, the rocks themselves are thoroughly shattered. Shattered phenocrysts are commonly visible in the light-colored older dacite.

Walk Stop B. Good exposure of andesite hummock topped by blast deposit. The andesite has a typical shattered-block texture.

Walk Stop C. This highest hummock in the area gives a good view into Mount St. Helens crater. Older dacite (older than about 2500 years; pre-Castle Creek age) is overlain by andesite and basalt lava flows (Fig. 7). The modern dacite domes (Goat Rocks and Summit domes) were removed by the debris avalanche (geology from C. A. Hopson, unpublished mapping; summarized in Glicken, 1986, in press).

In the debris-avalanche deposit, colors and mineralogy roughly indicate the rock types. The older dacite is a white, gray, or pink hornblende–hypersthene dacite with mafic and plagioclase phenocrysts more than 2 mm long, giving a salt-and-

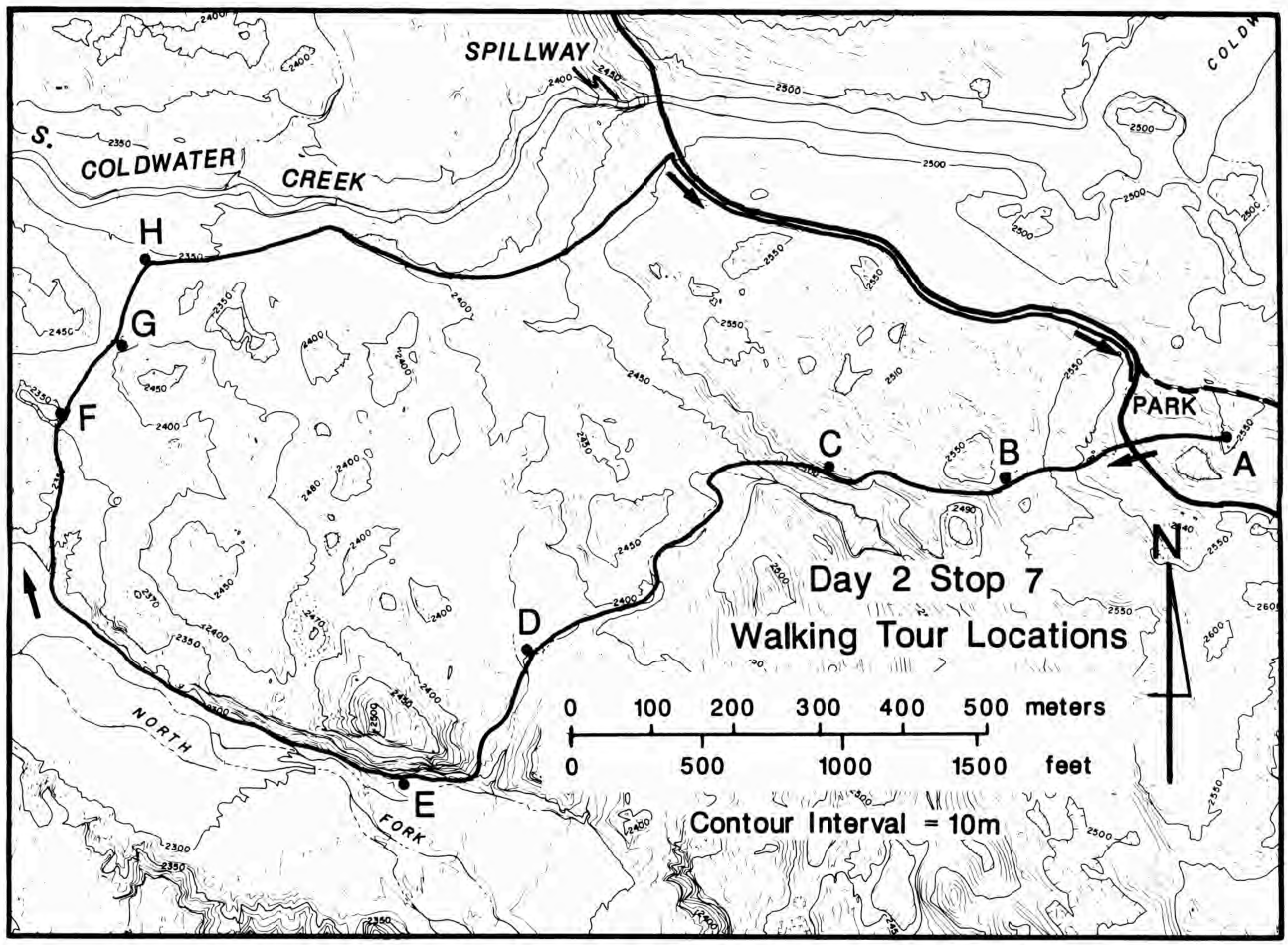

FIGURE 11—Map showing walking tour of debris-avalanche deposit (Stop 2-7).

pepper appearance. Andesite (with subordinate basalt) is generally black, red when altered, and is aphyric or contains plagioclase and pyroxene phenocrysts. Basalt is vesicular and olivine-phyric. Modern dacite is a grayish-pink hornblende–hypersthene dacite with abundant inclusions, and generally contains small phenocrysts (less than 2 mm).

In the debris avalanche, the rock types have been mapped at 1:2400 scale (Glicken, 1986, in press). The generalized pattern of the rock types is shown in Fig. 8 which shows the resting places of the slideblocks in Fig. 7. The basic pattern of rock types can be viewed from this site: black andesite and basalt on the margins of the debris-avalanche deposit surround older dacite in the center of the deposit. Shattered lava flows or dikes are preserved in the debris-avalanche deposit.

A comparison of the pattern of rock types with the cross section of the old mountain allows an interpretation of the places of deposition of the slideblocks (Fig. 8). For details of this interpretation, see Glicken (1986, in press).

Deposits overlying the debris avalanche are visible. The surge deposit is olive gray and mantles the hummocks of the debris avalanche up to the mountain. The lahar deposits, flat-surfaced and light-colored, lie between hummocks in the middle of the deposit.

Walk Stop D. Several terraces indicate different levels of 18 May 1980 lahars. The lahars formed from dewatering of the debris-avalanche deposit.

Walk Stop E. This lahar deposit formed when an explosion from the west side of the dome on 14 May 1984 threw dome material against the western crater wall, dislodging a dirty-snow avalanche. The avalanche turned into a lahar downstream from the crater, and material was picked up from the north flank of the volcano and the pumice plain. Well-sorted sand and gravel at the base of the lahar record sediment-laden hyperconcentrated stream flow that outran the debris-flow front.

From here we walk down a gully of the North Fork Toutle River canyon, which formed entirely since the 1980 eruption.

Walk Stop F. This is a good example of "fill-spill" in 18 May 1980 lahars. Here a lahar flowed into a depression, filled it, and then ran into the next depression to the northwest.

Walk Stop G. A depression in the surge deposit on top of the debris avalanche probably resulted from collapse into void space within the debris-avalanche deposit. The void space may have resulted from melting of shattered ice fragments, but more likely resulted from the irregular emplacement of the debris-avalanche deposit. Many ice fragments on the surface of the deposit did not melt until weeks

after 18 May, but voids were observed just after emplacement.

Walk Stop H. This channel was eroded by water released from the channel cut to provide a temporary outlet for Coldwater Lake in 1983. From here we have a view of igneous dikes of Mount St. Helens preserved (but shattered) in the debris-avalanche hummocks. It is also apparent that the deposit is composed entirely of debris blocks (no mixed facies between hummocks).

From here, return to vehicles. There are many views of the deposit along the way.

Walk or drive eastward along road. **0.5**

52.0 **STOP 2-8. Relations of leveled trees and debris-avalanche deposit at west end of Johnston Ridge.** Trees blown down by the surge on the west end of Johnston Ridge have their ends buried by the margin of the debris-avalanche deposit. This relation indicates that the surge reached this site before the avalanche. Otherwise some trees would lie on top of the avalanche. The contact between the trees and the avalanche deposit is now covered by reworked material.

Return to crossroads at mile 50.5; take the steepest road up hill (road 3500, unmarked). **0.7**

52.7 **STOP 2-9. Influence of topography on effects of the surge on trees.** Intersection of 3536 (to the left) and 3500. Park near the intersection and walk west a short distance into the standing trees killed by the surge. Because of its high velocity of 100–200 m/sec, the density current (surge) detached from the ground surface at breaks in slope, such as ridge crests. In places, resultant eddies knocked trees down in a direction opposite to the direction of general flow. Here many dead trees are still standing, but their tops have been torn away. Abrasion increases upward and also from the lee to the stoss sides of the snags. The tops of the snags define a surface that probably approximates the flow separation surface (Fig. 12).

Return to Kelso by vehicles.

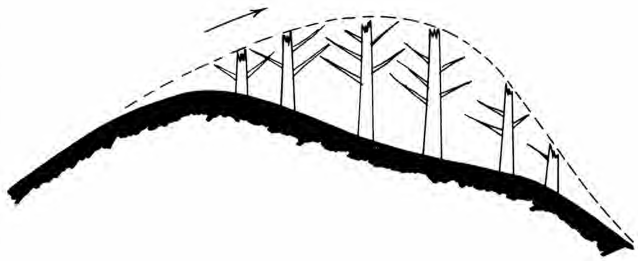

FIGURE 12—Sketch showing relation of sheared-off trees to topography at Stop 2-9. Arrow points in general flow direction of surge and dashed line marks its inferred base.

Day 3: The Kalama eruptive period, southwest and south flanks

Richard P. Hoblitt

Introduction

Today we examine Kalama-age deposits on the southwest and south flanks of Mount St. Helens (Fig. 13). The Kalama is Mount St. Helens's most thoroughly studied prehistoric eruptive period. The Kalama period may be divided by the chemistry of its eruptive products into early dacite, andesite, and late dacite (Fig. 14).

Early dacite

After an apparent repose interval of about 600-700 years (Hoblitt et al., 1980; Mullineaux and Crandell, 1981; Crandell, 1987), activity commenced in A.D. 1480 (Yamaguchi, 1983) with the eruption of layer Wn tephra (Table 1, Fig. 14) (Mullineaux, 1986). Subsequently a series of smaller-volume tephras (layers Wa, Wb, We, Wd) were erupted over a period that lasted between two and perhaps 25 years (Fig. 14). Prevailing winds dispersed these early dacitic set-W tephras mainly to the northeast and east. "Early dacite" flowage deposits were emplaced mainly to the southwest in the Kalama River valley. Because there is little overlap between the areas of the tephras and the flowage deposits, chronologic relations between the two are not certain, but the tephras probably preceded the flowage deposits. Most of the flowage deposits consist largely of dense, poorly vesiculated dacite that is thought to have originated from collapse of an ancestral summit dome, the only evidence of which is the flows themselves. These flows are intercalated with less voluminous pumiceous flows probably produced by explosive eruptions. Some of the flowage deposits are clearly the products of pyroclastic flows or surges, and others were emplaced as lahars. The mode of origin of many flows is not evident from field criteria, but paleomagnetic determination of minimum emplacement temperatures helps to resolve the ambiguity. The bulk chemistry of the early dacites changed systematically with time. The SiO_2 content declined from about 67% for the first tephras to about 65% for the uppermost early dacites (Fig. 14).

Andesite

Between two and 25 years after the beginning of the Kalama activity, the dacitic eruptions gave way to eruptions of andesitic tephras with a bulk SiO_2 content of about 58% (Fig. 14). The andesitic tephras of set X consist of many beds that are most abundant to the northeast and east, the prevailing wind direction, but are also present on all other flanks of the volcano. This pattern suggests that the andesitic tephras were erupted over perhaps months to years. The tephras were succeeded by the extrusion of numerous blocky andesite (SiO_2 content 57-58%) lava flows on all flanks of the volcano, particularly to the southeast and east. These lavas are locally overlain by pyroclastic flows of identical chemistry and mineralogy, examples of which crop out in

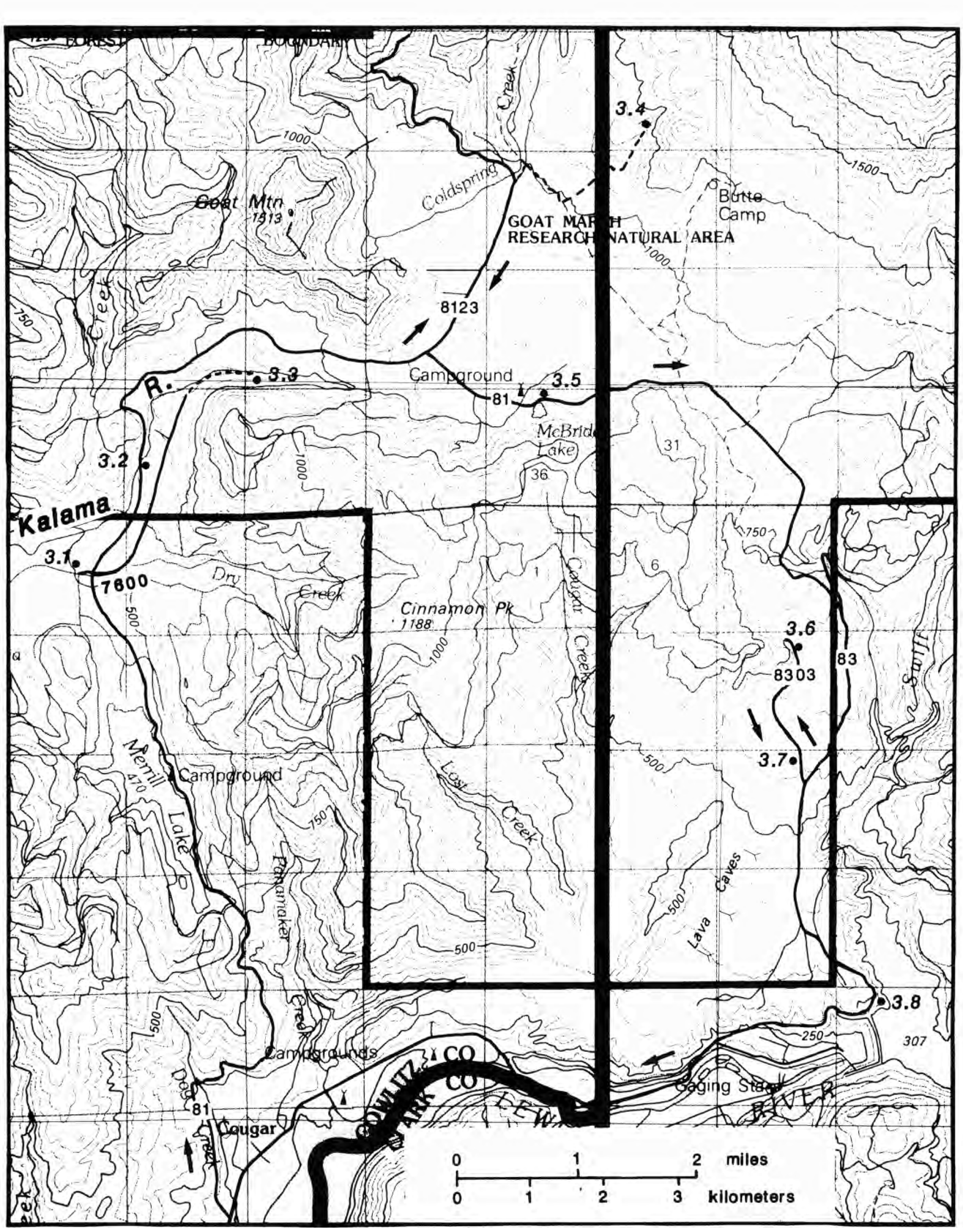

FIGURE 13—Index map for Day 3.

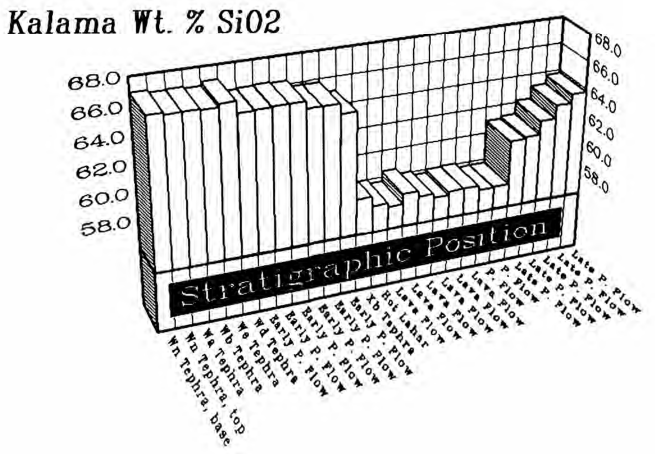

FIGURE 14—Plot of SiO_2 content of Kalama-age materials. Upsection is to the right; the time of eruption increases irregularly to the right; P. flow = pyroclastic flow.

the Kalama River valley; tree-ring ages indicate the deposits were emplaced within about 90 years of the start of the Kalama eruptive period (D. K. Yamaguchi, unpubl. data).

Late dacite

The eruptive style and magma chemistry changed again sometime between about 25 and 167 years after the Kalama eruptive period began. A new dacitic summit dome (SiO_2 about 61%) (Fig. 14) began to shed nonvesicular debris down the volcano flanks, at first mainly to the west and northwest. In A.D. 1647 (Yamaguchi, 1986), one or more explosions at the dome sent pyroclastic flows of vesicular dacite debris to the west-northwest into the Castle Creek valley (Fig. 6) and west into the South Fork Toutle River. The vesicular dacite is as much or more silicic (61-62% SiO_2) than the preceding nonvesicular summit-dome debris. Subsequent summit-dome debris was nonvesicular; the vesicular summit-dome dacites constitute the only marker beds within the otherwise monotonous nonvesicular summit-dome dacites. After the eruption of the vesicular dacite, the dome continued to shed nonvesicular dacite for nearly 150 years. It is not known how the rate of this extrusion varied through time, it probably waxed and waned, but hot debris was still being emplaced on the east flank of the volcano late in the 18th century. Growth of the summit dome ceased at, or shortly before, the eruption of the T tephra in A.D. 1800, which has been defined as the beginning of the Goat Rocks eruptive period. The Kalama summit dome was destroyed on 18 May 1980. The last nonvesicular summit-dome debris of the Kalama eruptive period has a silica content of 63— 64% . The only tephra associated with the growth of the summit dome is layer Z tephra (Mullineaux, 1986). This association is evidenced by the tephra's stratigraphic position (sandwiched between late-dacite pyroclastic deposits), by its wide azimuthal distribution (which suggests an extended period of eruption like that of the dome-derived flowage deposits), and by the local presence of scattered lapilli of vesicular summit-dome dacite.

The silica contents from 27 sequential stratigraphic units within the Kalama eruptive period are shown in Fig. 14. The abrupt change from early dacites to andesites apparently is due to mixing of dacitic and basaltic magma endmembers (Pallister and Hoblitt, 1985).

Field guide

Mileage

0.0 Intersection of WA-503 and U.S. Forest Service (USFS) road 81, about 0.5 mi southwest of Cougar, Washington. Go north on road 81 (Fig. 13). **3.7**

3.7 Unpaved roads to right and left, stay on road 81 (paved). **1.3**

5.0 Merrill Lake on left side of road. The lake formed when lava flows moving down the Kalama River valley dammed a tributary valley. The lava is thought to be contemporaneous with the Cave Basalt (Greeley and Hyde, 1972), a flow south of Mount St. Helens that was emplaced about 1600 yrs ago (Crandell, 1987; Hyde, 1970). Drill holes indicate the lava is about 20 m thick near the north end of Merrill Lake. Although the lava flow is nearly 13 km long, it is well exposed only on the steep flanks of the volcano and along its terminal 5 km. The rest is covered by younger deposits, mainly of Kalama age. Merrill Lake has no surface outlet; drainage probably occurs through fractures in the basalt and the fragmental deposits that underlie it. Exposures of Cave Basalt may be seen along road 81 as you pass Merrill Lake. **2.1**

7.1 Intersection of road 7600 (unpaved) with road 81; go left (west) on road 7600. **0.1**

7.2 **STOP 3-1. Alluvium from early Kalama pyroclastic-flow deposits.** Aggregate quarry to the right. The quarry exposes alluvium derived from early Kalama pyroclastic flows whose terminus is 1.5 km to the north. The alluvium was formed as the Kalama River rapidly incised the new pyroclastic-flow deposits. Return to intersection of roads 81 and 7600. **0.1**

7.3 Intersection of roads 7600 and 81; go left (north) onto road 81. **0.5**

7.8 Break in slope marks the terminus of the early Kalama pyroclastic-flow deposits. **0.9**

8.7 **STOP 3-2. Early Kalama flowage deposits.** Aggregate quarry on east side of Kalama River near where road 81 crosses the river. Two of the longest early Kalama pyroclastic flows are exposed in the north face of this quarry. This site is 13.5 km from the pre-1980 summit and 0.6 km from the terminus of the pyroclastic-flow deposits. The lower unit consists of angular to subangular clasts in a friable matrix of gray ash. Most clasts are composed of poorly vesiculated hypersthene–hornblende dacite, but about 20% are basalt and hypersthene–hornblende pumice. Excavations revealed that this unit is more than 13 m thick. Paleomagnetic emplacement temperatures were obtained from clasts from the lower unit (Hoblitt, 1978; Hoblitt and Kellogg, 1979). Half of the studied clasts were emplaced above their maximum blocking temperatures, which ranged from about 400 to 450 °C. The other half were emplaced below 450 but above 300 °C. These data do not exclude a laharic origin but suggest that the lower unit was emplaced as a pyroclastic flow.

The upper unit consists of lapilli and blocks of pumice and lithic debris in a matrix of moderately cohesive ash. The pumice is pale yellow, rounded, and inversely graded; the lithic debris is dominantly early Kalama dacite but also includes some pre-

Kalama accidental clasts. The deposit is gray at the base and grades upward to grayish pink. On the basis of its pinkish top, this unit is interpreted as a pyroclastic-flow deposit. This unit is capped with a few decimeters of alluvium on the east side of the pit.

Return to intersection of roads 81 and 7600. **1.4**

10.1 Intersection of roads 81 and 7600; go left (east) onto 7600. **0.2**

10.3 Intersection of 7600 and 7601; go left on 7601. **0.2**

10.5 Intersection of roads 7601A and 7601; stay on 7601 to the left. **0.3**

10.8 Intersection of roads 7602 and 7601; go straight ahead (left) on 7602. **0.7**

11.5 Intersection with an unmarked road to the left; continue straight/right on 7602. **0.4**

11.9 Another intersection with an unmarked road to the left; go straight/right. **0.2**

12.1 **STOP 3-3 (optional). Carbonized logs near base of early Kalama section.** Road ends here. Walk down the steep valley side to the Kalama River, then go upstream about 1.25 km. Carbonized tree stumps are present in growth position on south side of river. In the same area a carbonized log jam lies within a pyroclastic-flow deposit of early Kalama age. The abundance of carbonized vegetation and the presence of stumps in growth position indicate that the unit containing the logjam probably was the first early Kalama flow to affect this part of the ancestral Kalama valley. A dendrochronologic study is underway to determine the year in which the trees were killed.

Return to the intersection of roads 81 and 7600. **2.0**

14.1 Intersection of roads 7600 and 81; turn right (north) onto road 81 (paved). **1.7**

15.8 Intersection with an unmarked, unpaved road straight ahead; continue right on road 81 (paved). **2.4**

18.2 Pavement ends at intersection with a road to the right; go straight ahead/left. **0.7**

18.9 Intersection of road 81 to the right and road 8123; go straight ahead on 8123. **0.6**

19.5 Goat Marsh trailhead to the left. **1.1**

20.6 **STOP 3-4. Kalama stratigraphy in Butte Canyon.** Intersection of road 8123 and an unmaintained road to the right. Park near the road intersection, walk northeast on unmaintained road for 0.25 km to the obstruction. At this point, leave the road and follow the trail to the right (southeast) for about 0.5 km through the coniferous forest. The trail traverses Kalama-age andesitic pyroclastic flows that are littered with large scoriaceous bombs. Leave the trail at the point where it crosses a low area with deciduous bushes and go about 0.5 km to the northeast, keeping just left of the bushes.

You are now near the terminus of a Kalama-age andesite lava flow that lies on a sequence of early Kalama pyroclastic flows and lahars. The lava flow followed a channel eroded into the dacitic flowage deposits; the sides of this paleochannel are exposed along both sides of the terminus of the lava flow. The andesitic pyroclastic flow overlies both the lava flow and the dacitic lahars and pyroclastic flows.

At the flow terminus, go southeast for about 0.25 km to the gully that drains the north sides of Butte Camp dome. The vegetation near the gully was destroyed on 18 May 1980 by lahars, which were mantled by tephras on 25 May and 12 June 1980. The surface of the new lahars was colonized by conifer seedlings within one year. Enter the gully and climb for about 0.1 km to the first of a series of Kalama-age outcrops.

This outcrop includes an early Kalama surge(?) dune that lacks internal structures and is rich in pumice. The contact between the scoriaceous andesite pyroclastic flow and the early Kalama dacites is near the top of the section.

Proceed up the gully for another 0.5 km, to the mouth of the narrow canyon between Butte Camp dome and the Kalama-age lava flow. Except for the early dacitic tephras, much of the history of the Kalama eruptive period is recorded by deposits in and near this canyon.

Early Kalama dacitic flowage deposits are exposed beneath Kalama andesite flows on the northwest side of the canyon's mouth (see measured section at end of Day 3). **Please be careful when approaching this unstable outcrop—it is prudent to use hard hat.** The early Kalama deposits are underlain by Smith Creek-age deposits (about 4000 to 3300 yrs B.P.). Paleomagnetic analysis of each early Kalama dacitic unit in the section reveals both lahars and pyroclastic flows. The distinction is difficult or impossible to make on the basis of visual criteria alone.

Climb the trail on the left side of the outcrop to the top of the bench adjacent to the lava flow. Follow this surface toward Mount St. Helens as far as possible to the northeast.

The early dacite–andesite contact is near this point. The early dacites are overlain by the andesitic tephra of set X, which in turn are overlain by rubble from the andesitic lava flows. Lahar deposits of summit-dome debris (late Kalama dacites) locally overlie the lavas and associated rubble. Looking up canyon from this point, one sees an orangish-brown outcrop. This exposes the same scoriaceous andesite pyroclastic flows that were traversed along the entrance trail. The scoriaceous pyroclastic flows ponded in a low area between the Kalama lava flow and Butte Camp dome, before the canyon formed. The scoriaceous flows also overlie the lava flows. The ponded scoriaceous flows were dissected shortly after emplacement as the canyon began to form between the dome and the lava flow. The incipient canyon cut into the pyroclastic flow was then partly filled with lahars composed mainly of late Kalama dacites. This fill, visible as the light-colored outcrop to the left of the orangish-brown outcrop, was in turn dissected as canyon cutting continued.

The erosion rate in this canyon increased markedly on 18 May 1980, apparently as a consequence of devegetation of the canyon walls by the lahars. The canyon is now several meters deeper than it was before the 1980 eruption, and exposures are much better. This is also true in many other drainages around Mount St. Helens. Just after an eruption

is an opportune time for studying old as well as new deposits.

Return to vehicles; backtrack on road 8123. **1.7**

22.3 Intersection of roads 8123 and 81; go left on road 81. The roadcut just southeast of the intersection exposes an early Kalama pyroclastic-flow deposit reddened by high-temperature oxidation. **0.9**

23.2 **STOP 3-5. Relation of early Kalama flowage deposits to early Kalama tephras.** McBride Lake is to the south of the road; the roadcut across from the lake is capped by a friable, gray early Kalama pyroclastic flow that contains charcoal. The flow overlies scattered lapilli of early Kalama hypersthene–hornblende pumice that is part of layer We tephra (Table 1, Fig. 14), erupted in A.D. 1482. This outcrop provides the best available evidence relating the early Kalama tephras and flowage deposits. It establishes that part of the early Kalama tephras predates part of the early Kalama flowage deposits.

Continue east on road 81. **1.2**

24.4 Redrock Pass, so named because the roadcut to left exposes oxidized rubble from a Castle Creek-age (2200 to 1600 yrs B.P.) andesite lava flow. This is the trailhead to Butte Camp and the southwest flank of Mount St. Helens. **1.2**

25.6 Intersection of road 81 and road 830 to left (Ptarmigan Trail); go straight ahead on road 81. **1.7**

27.3 Intersection of road 81 and USFS road 83; go right on road 83. **1.4**

28.7 Intersection of roads 83 and 8303; go right on road 8303. **1.1**

29.8 **STOP 3-6. Ape Cave.** Intersection of roads 8303 and 060; go right on 060 into the parking lot. The path leads to the entrance of Ape Cave. Ape Cave is the longest known uncollapsed lava-tube segment (3400 m) in the world (Greeley and Hyde, 1972). This beautifully formed lava tube is within the Cave Basalt, which contains numerous other lava tubes. This most extensive part of the Cave Basalt flowed southward from Mount St. Helens down a stream channel cut into dacitic pyroclastic-flow and lahar deposits of Swift Creek age (13,000–<10,000; Crandell, 1987). The 1600 yrs old lava flow reached the Lewis River about 15.5 km from the flank of the volcano.

The cave is cool and damp, so dress warmly. You must provide your own illumination; a flashlight is adequate, a propane lantern superior; a backup light is recommended. Descend the stairway to the cave floor. The part of the cave downhill (south) from the entrance, having few obstructions (rubble from roof collapses), is best for short visits such as ours. Numerous large rubble piles must be surmounted in the uphill part of the cave. Explore the downhill part of the cave for as long as time and interest permit.

Return to vehicles; leave the parking lot to the left onto 8303. **0.9**

30.7 **STOP 3-7. Lava Cast picnic area.** Turn right into the parking lot. Trails lead to numerous tree molds in the Cave Basalt. **0.2**

30.9 Intersection of roads 8303 and 83; go right on road 83. **1.8**

32.7 Intersection of roads 83 and 90; go right on road 90. **0.8**

33.5 **STOP 3-8. Swift dam overlook.** This overlook is on remnants of a Cougar-age fan (about 20,000 to 19,000–18,000 yrs B.P.; Crandell, 1987) that once crossed and blocked the Lewis River valley (Hyde, 1975). Other remnants of this surface can be seen to the east, just beyond the mouth of Swift Creek, and to the southwest on the south side of the Lewis River about 70 m lower than the overlook. The fan is composed of tephras, lahar and pyroclastic-flow deposits, and a probable debris-avalanche deposit (Mullineaux and Crandell, 1981; Newhall, 1982).

Proceed west on road 90 through Cougar, Washington. Continue west on WA-503 to Woodland, Washington. Return to Kelso via I-5.

Appendix: Kalama stratigraphy in Butte Canyon near Stop 3-4

Unit	Thickness	Description
Late dacite		
21.	0~4 m	Lahar deposit: Granules to boulders supported in a matrix of cohesive, light pinkish-brown, silty fine sand; clasts consist of lithic, angular to subangular, gray and pink dacite of the Kalama summit dome; pinches out against lateral flow rubble of unit 20.
Andesite		
20.	>10 m	Marginal rubble of andesite lava flows: Large, angular blocks of andesite, grain-supported.
19.	0–30 cm	Set-X tephra: Dust and ash, bedded, brown, yellowish brown and black; beds are faulted and contorted in response to loading by overlying flow rubble of andesite flow.
Early dacite		
18C.	~1.4 m	Pyroclastic-surge deposit(?): Dust and ash (lower 0.5 m), planar and crossbedded, gray and pinkish gray; grades upward into 0.7 m of lapilli and small blocks supported in a matrix of massive grayish-brown ash; grades upward into 0.2 m of planar and crossbedded, grayish-brown to pinkish-brown dust and ash.
18B.	~5–40 cm	Pyroclastic-surge deposit (?): Lapilli of early Kalama dacite supported in a matrix of friable gray ash; massive; gradational contact with unit 18A.
18A.	~5–30 cm	Pyroclastic-flow or surge (?): Coarse ash, lapilli, and small blocks; massive, grain-supported, friable, consisting dominantly of lithic, gray early Kalama dacite, subordinate pink early Kalama dacite, white pumice, and dark-colored pre-Kalama accidental clasts; gradational contact with unit 18B.
17.	0–35 cm	Pyroclastic-surge deposit: Dust and ash, pumiceous, planar and crossbedded, gray, pinkish-gray and tan.
16.	1–2 m	Pyroclastic-flow deposit: Lapilli to large blocks of dominantly gray, angular to subrounded, lithic to subpumiceous early Kalama dacite, subordinate pink early Kalama dacite, white pumice, and dark-colored pre-Kalama accidental clasts supported in a matrix of pinkish-brown cohesive ash; zone of friable coarse ash along lower contact; many angular clasts are prismatically jointed.
15.	2.5–3 m	Pyroclastic-flow deposit: Lapilli to large blocks, grain-supported, subangular to subrounded, dominantly lithic to subpumiceous early Kalama dacite, subordinate pink early Kalama dacite, and dark pre-Kalama accidental clasts; matrix of cohesive, grayish-brown ash; abundant gas-escape structures present.
14.	10–50 cm	Pyroclastic-flow deposit (?): Lapilli and scattered small blocks of dominantly gray and pink, subangular, lithic

		to subpumiceous early Kalama dacite and subordinate white pumice, and dark pre-Kalama accidental clasts supported in a matrix of cohesive brownish-gray ash; contact with overlying unit only marked by texture change; may be a fine-grained facies of overlying unit.
13.	~2.4 m	Lahar deposit: Cobble, grain-supported, subangular to subrounded, dominantly gray, subpumiceous early Kalama dacite, subordinate pink dacite, and dark pre-Kalama accidental lithologies; interstices filled with lapilli of cobble lithologies in a matrix of cohesive pinkish-gray ash; scattered boulders along upper contact.
12.	~2.5 m	Pyroclastic-flow deposit: Lapilli, blocks, and large blocks of dominantly gray, subpumiceous early Kalama dacite, normally graded, grain-supported along basal contact, grading upward to matrix-supported (matrix consists of friable gray ash); subordinate proportion of pre-Kalama accidental clasts and gray and pink early Kalama lithic clasts.
11.	0.8–1 m	Lahar deposit: Granules, gravels, and cobbles of white pumice and light-gray, subpumiceous early Kalama dacite, concentrated along lower contact, supported in a matrix of gray, cohesive, fine to coarse sand; grades upward into a zone dominated by granules, gravels, and cobbles of pink and gray lithic and subpumiceous early Kalama dacite and dark-colored pre-Kalama accidental clasts, supported in a matrix similar to that of the pumice-rich zone; upper part of unit locally appears to have been cut and filled by small lahars.
10.	1–10 cm	Pyroclastic-surge deposit (?): Ash, planar-bedded, gray to pinkish gray.
9.	0–70 cm	Pyroclastic-flow deposit: Lapilli to blocks of dominantly subpumiceous gray early Kalama dacite supported in a matrix of cohesive, pinkish-gray ash; dacite clasts are subangular, small proportion of pre-Kalama accidental clasts present.
8.	0–15 cm	Pyroclastic-surge deposit (?): Dust and ash, planar and crossbedded, gray and pinkish gray, no oxidation; may be genetically related to unit 9.
		——————Base of Kalama-age deposits——————
7.	~35 cm	Tephra deposits (?): Multiple beds of ash and dust; various shades of pink, gray and brown, faint yellow oxidation.
6.	1 m	Pyroclastic-flow deposit and fluvially reworked equivalent: Lapilli and blocks of light-yellow cummingtonite–hornblende pumice and gray subpumiceous dacite supported in a matrix of pumiceous ash; massive, moderately cohesive; abundant carbonized and incipiently carbonized limbs and wood fragments; upper part fluvially reworked, maximum thickness of undisturbed pyroclastic-flow deposit is 40 cm; faint yellow oxidation throughout.
5.	10–20 cm	Set-Y tephra: Multiple beds of ash and (or) small lapilli; lapilli are dominantly light-yellow cummingtonite–hornblende pumice, subordinate proportion of lithic lapilli; tephra beds are variably eroded and distorted by overlying unit.
4.	1–80 mm	Organic-rich alluvium: Organic matter, 1–4 mm, brown, uncharred; locally interbedded with as much as 8 cm of gray silt.
3.	0–5 cm	Alluvium (?): Silty sand, brown; contains abundant small fragments of charcoal.
2.	0–7 cm	Tephra deposit (?): Ash and small lapilli of pumice and lithic clasts; ash is pinkish gray, lapilli are light gray; lapilli angular to subangular; discontinuous.
1.	>1 m	Dome rubble: Large blocks of Butte Camp dome dacite, grain-supported; interstices filled with silty sand (ash ?); soil developed on top, charcoal fragments and bright-orange discontinuous lenses of Mazama ash present in soil.

Day 4: Prehistoric tephra falls on southeast and northeast flanks, devastating 18 May 1980 pyroclastic surge along northeast radial

Richard B. Waitt and Richard P. Hoblitt

Introduction

From the motel at Kelso, today's trip proceeds via the south and southeast flanks of Mount St. Helens to the devastated area northeast of the volcano. The day ends at Cispus Center about 30 mi northeast of the volcano, our accommodations for three nights. Viewing exposures entails hikes of less than 1 mi (1.5 km).

Leg I: Prehistoric lava flows and tephra-fall deposits

From Swift Overlook on USFS road 90, proceed northeast about 9.5 mi (15 km) via roads 90 and 83 across south flank of Mount St. Helens to parking area within the vegetation-free bouldery path of a great lahar on the composite fan of Pine Creek and Muddy River on the southeast flank of Mount St. Helens (Fig. 15). Walk on trail to east and cross Muddy River to a prominent outcrop of layered tephra. The lahar passed down this part of the Pine–Muddy fan about 15 minutes after the start of the 18 May 1980 eruption. It stripped off regolith to expose a fairly complete stratigraphic section of tephra-fall deposits (review Table 1).

STOP 4-1. Ancient tephra-fall sequence. The deposits include the conspicuous thick pumice tephra set S (about 13,000 yrs B.P.), highly oxidized set J (about 11,000 yrs B.P.), layer Ye (3300 yrs B.P.), and layer We (A.D. 1480). The section also contains several intercalated lahar and surge deposits and is capped by tephra set X (about A.D. 1680?) and the 1980 lahar (Fig. 16). Set S, at the bottom of the section, may be buried by recent debris deposited by the aggrading Muddy River.

A more detailed section of tephra set S, which comprises at least three major pumiceous tephra-fall layers, can be seen at nearby exposures to the northeast.

Hike 0.2–0.5 mi to southeast and east along the course of Muddy River. If water is too high in canyon area, use south valley side (trail will be under construction by late summer 1989).

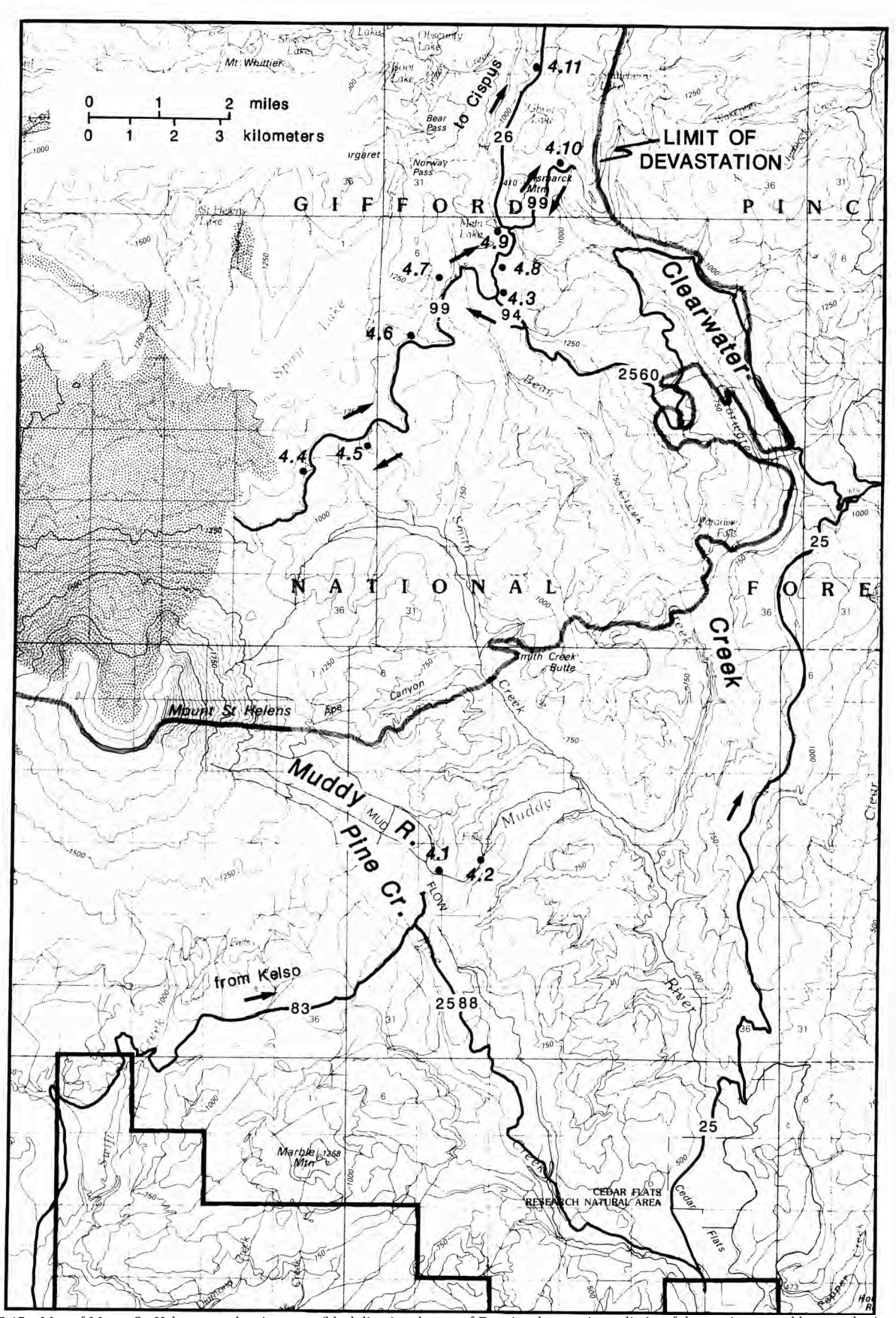

FIGURE 15—Map of Mount St. Helens area showing route (black lines) and stops of Day 4 and approximate limits of devastation caused by pyroclastic surge on 18 May 1980 (gray stipple line). Stippled area at left is approximate extent of debris avalanche.

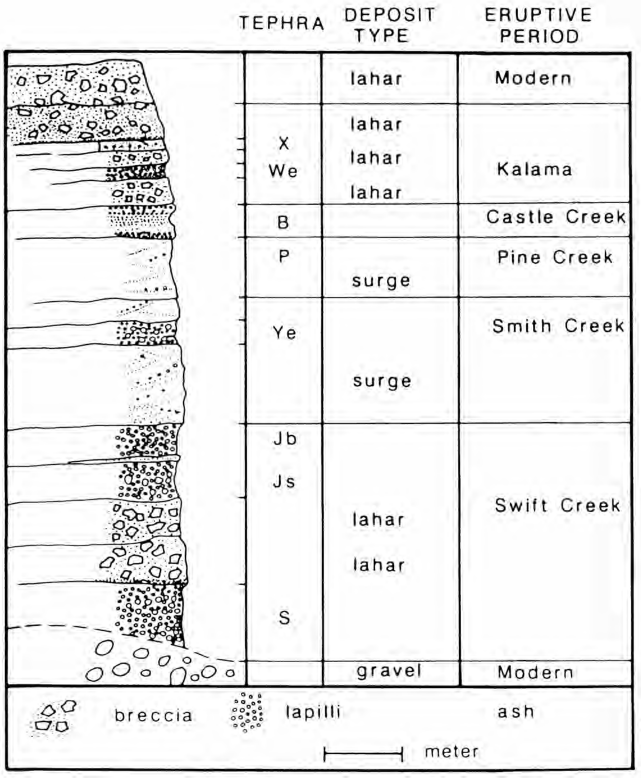

FIGURE 16—Stratigraphic section seen at Stop 4-1. Deposits from lahars and surges (ash clouds) alternate with ash fall. In nearby valleys, pyroclastic-flow deposits are also represented. A lava flow of Castle Creek age lies buried beneath the active stream channel. From Doukas (in press), adapted from Mullineaux (1986) and Crandell (1987).

STOP 4-2. Intracanyon lava flow. Inspect intracanyon andesite lava flow of Castle Creek eruptive period (about 1800 yrs B.P.). In the lava flow, here about 16 m thick, two styles of jointing are evident: a lower set of well-formed columns (colonade) about 8 m thick evidently formed by cooling upward from base of flow; and an upper set of small, irregular, ill-formed columns (entablature) about 8 m thick formed by downward cooling from top of flow and probably was influenced by percolation of surface water down the developing joints.

Proceed as far as head of steep part of canyon, where Muddy River forms waterfalls over the lava flow. The contact of the unweathered lava flow overlying oxidized lower Oligocene rocks (abut 29 Ma) is photogenic.

Return to vehicles. From the intersection of roads 83 and 2588, proceed southeast down road 2588 for about 7 mi (11 km) to USFS road 25. Take road 25 northward. After about 2 mi road crosses Muddy River, where the path of lahar on 18 May 1980 is being rapidly revegetated. Continue for another 9 mi to road 2560.

Road 2560 passes westward sinuously for 13 mi through area devastated by the great 18 May 1980 surge along Clearwater Creek valley and a high ridge to the west. Stop at concession area at intersection of USFS roads 2565 and 99.

Leg II: Prehistoric tephra-fall deposits and 18 May 1980 pyroclastic-surge deposit

Road 99 provides easy access to the northeast radial through the devastated area to within a few kilometers from the volcano. Proceeding generally from proximal to distal areas, we shall examine several exposures along and near the road. The longest two hikes are each only about 0.5 mi with altitude gain of less than 100 m.

STOP 4-3. Ancient tephra-fall deposits. Outcrop along road 99 about 50–100 m north of concession area shows stratigraphy of coarse pumiceous tephra layers (review Table 1 and Fig. 16). Conspicuous are set J (about 11,000 yrs B.P.) at the base, sets Y (3300 yrs B.P.) and W (A.D. 1470) in the middle, and set T (A.D. 1800), each 0.5–1 m thick. The 1980 deposit is at top of section.

Return to vehicles and drive road 99 southwestward toward Mount St. Helens. This leg of field trip is along a radial direction northeast of the mountain and shows deposits and other evidence of the nature of the 18 May 1980 pyroclastic density current (surge or blast) between the proximal and distal areas. Paved road ends at large parking lot at Windy Ridge overlook. Informal stop here before we proceed via road past locked gate to crest of ridge south of parking lot. Pass through locked gate toward Restricted Area [permission required from Mount St. Helens National Volcanic Monument headquarters (USFS) at Chelatchie Prairie]. Park about 0.5 km beyond gate, in excavated area on right. Hike north along ridge crest to summit. Alternatively, leave on foot from Windy Ridge parking lot and hike south to summit. This way you need not pass through the gate and may avoid need for permission (Stop 4-4 lies along boundary of Restricted Area, not within it).

STOP 4-4A. Proximal deposit of pyroclastic surge. Stop is a summit just south of Windy Ridge parking lot. Overview of the north flank of Mount St. Helens showing major products and effects of the 18 May 1980 eruption: great landslides, pyroclastic surge, pumiceous pyroclastic flows, and ash clouds. On the "Pumice Plain," 18 May deposits are overlain by June–October 1980 pumiceous pyroclastic flows (Rowley et al., 1981; Criswell, 1987) and by snow-avalanche and lahar deposits of March 1982 and later (Waitt et al., 1983). The hummocky deposit at the head of the west arm of Spirit Lake is 18 May landslide that traveled through the lake.

A prepared trench near summit shows 18 May 1980 deposit of the pyroclastic surge (unit A) containing more than 50% of juvenile dacite from the March–May 1980 cryptodome. Fragments of the cryptodome dacite are bimodally distributed with respect to density: low-density fragments are gray and microvesicular, high-density fragments grayish black and essentially nonvesicular (R. P. Hoblitt, unpubl. data). About 1 m thick, the deposit is normally graded from pebble gravel at the base to silt at top. Using the simple field terminology of 1980 (Waitt, 1981; Waitt and Dzurisin, 1981), layer A1 (gravel) is about 85 cm thick, layer A2 (sand) 14 cm thick, and layer A3 (silt) 1 cm thick. The lower half of unit A1 is rich in logs and wood litter stripped from trees, and it contains gray dacite and denser lithic clasts as large as 20 cm in diameter. The lower half of A2 is massive, granular sand and can be regarded as the fine graded top of massive layer A1 (the two composing a single graded bed). The upper half of A2 is laminated sand that resembles classic "surge" deposits. Layer A3, mainly tephra fall from the great mushroom cloud, began accumulating 20 minutes after beginning of the eruption. Layer A3 is overlain by 18 May 1980 pumice-fall deposit (unit B) and co-ignimbrite ash (unit C), which is capped by pumice from 22 July 1980 (Waitt et al., 1981).

The published literature on the devastating event includes divergent interpretations:

A. Field investigators in 1980 inferred that the devastating event emanated from Mount St. Helens and began with the initial explosions (for example, Hoblitt et al., 1981; Moore and Sisson, 1981; Waitt, 1981). However, Moore and Rice (1984) inferred that the main devastating explosion occurred several kilometers north of the mountain about two minutes after the initial explosions. **Comments:** The idea of a second explosion away from the main vent is based on interpretation of satellite data. Ground-based data indicate that the current flowed from the cone of Mount St. Helens.

1. Mature trees on ridges south and north of Stop 4-4 were toppled northeastward, which is appropriate for a flow from Mount St. Helens but athwart the direction of a flow issuing from near Spirit Lake.
2. The south sides of downed logs are much more abraded than the north sides; the sustained, waning phase of the current was aligned with Mount St. Helens.
3. The preferred accumulation of surge deposit against the *south* side of the downed logs also indicates the flow was from Mount St. Helens.
4. Minor pumice near the base of layer A3 near Spirit Lake cannot constitute stratigraphic evidence for the hypothesized second explosion near Spirit Lake, because the pumice extends southeastward directly east of Mount St. Helens. Thus it originated from the central vent and drifted downwind, not from a northern source.

B. Investigators in 1980 inferred that the devastating current was mainly a relatively low-concentration surge, but Walker and McBroome (1983) instead concluded that it was mainly a high-concentration flow. This issue is discussed by Hoblitt and Miller (1984), Waitt (1984), and Walker and Morgan (1984). **Comments:** The deposits and timber here and at other proximal sites suggest that the devastating density current was fundamentally a relatively low-concentration pyroclastic surge, not a high-concentration pyroclastic flow. Many questions can be asked of the field characteristics, among them:

1. Much of the coarse basal half of the deposit is clast-supported and thus poor in fines. Did the erupted mixture contain much fine material, and were the fines largely winnowed out by turbulent, low-concentration surge?
2. Many or most tree trunks lie where they fell. Could a high-concentration flow of dense lithic clasts fail to transport most of these lower-density logs?
3. The upper surfaces of downed logs that project above the deposit are far more abraded than the undersides. Should not a high-concentration flow have done more to the undersides of downed logs?

Walk back north along ridge to road.

STOP 4-4B. Multiple-layered base of proximal surge deposit. A small prepared pit shows multiple-layer stratigraphy near base of unit A, evidence of two depositional impulses at the base of the proximal surge deposit. The upper part of this 1 m thick section is very friable. The surge deposit is underlain by soil developed on pumiceous tephra. Of the 18 May 1980 surge deposit, the lowest unit is a lens as much as 20 cm thick, mostly of angular, fines-poor, grain-supported cryptodome dacite. This lens possibly is the product of the first impulse (see Introduction for Day 2). The lens is overlain by a more cohesive layer rich in soil, old pumice clasts, and organic material. This layer is typically about 10 cm thick. The 70 cm of material above the soil-rich layer contain a lower proportion of cryptodome dacite and a higher proportion of hydrothermally altered lithic clasts than the material below the soil-rich layer. It thus appears that the material above the soil-rich layer is the product of a second major impulse of the surge.

Return to Windy Ridge parking lot again. Proceed northeastward along road 99 for about 0.5 mi to Smith Creek Overlook (sign).

STOP 4-5. Smith Creek Overlook. From the parking area, walk southeastward along ridge crest to former road, where pyroclastic-surge deposit is exposed in gullies. Standing trunks of large trees on the lee (east) side of the ridge show that the front of the surge lofted off the ridge crest; many standing trunks are debarked, but many retain bark even at their bases. Most small-diameter trees remained upright in the current. These relations seem inconsistent with the idea that the density current was mainly a dense, high-concentration flow, but are consistent with the idea of relatively light, low-concentration surge.

The normally graded deposit on the former roadbed is thinner and the base finer than at the more proximal Stop 4-4. The deposit is decimeters thick on the near-level roadbed, but it pinches out abruptly on steep faces both upslope and downslope. The sequence is capped by layer A3, which shows that the lateral variations were caused by emplacement and not by more recent erosion. Slopes steeper than about 25° did not retain deposits of the surge, though some tephra-fall deposits (A3, B, C) accumulated there later. The still-fluid density-current material must have drained off such steep slopes as secondary flows.

STOP 4-6. Harmony Basin viewpoint. Harmony basin shows effects of the pyroclastic surge and of a catastrophic wave of lake water displaced by the landslide (Waitt, unpubl. report). The inferred sequence is:

1. Pyroclastic surge sweeps northeastward, leveling forest and depositing layer A1. Patterns of downed timber indicate that topography channeled the ground-hugging current. Most of the area was swept by a northeast-moving arm of the surge that was channeled along Spirit Lake basin, but the head of Harmony basin was swept by current moving northward up the Smith Creek tributary and over the divide into the head of Harmony basin. This north-running surge turned west into the southeast part of basin in the lee of a sharp ridge crest.
2. Landslide entering south end of Spirit Lake at about 250 km/hr creates catastrophic wave; part of wave surges up Harmony basin, washing away trees and layer A1 up to a level marked by a sharp trimline on north valley side.
3. Losing momentum, this water descends to the basin floor and flows back to Spirit Lake, depositing rafts of randomly oriented logs on basin floor but carrying most logs into the lake, where they remain.
4. Gradually waning pyroclastic surge continues, depositing layer A2.
5. Layer A3 and later tephras accumulate.

The presence and only moderate battering of downed and standing trees in this area suggest that the pyroclastic density current was a low-concentration surge.

Continue on road 99 for about 1 mi to parking area for trailhead to Independence Pass.

STOP 4-7. Independence Pass trail. Hike along the trail to the ridge crest (0.3 km); please do not dig holes in this area frequented by tourists. The density-current deposit is only about 20 cm thick along the trail. The hike through downed trees is an opportunity to explore diverse effects of the density current on large and small trees. Most of these suggest that the flow had low concentration. For instance, few trees or none were transported or re-oriented after they fell. Some small trees, evidently snow-covered during the 18 May eruption, retained their bark and thus life. Standing trunks on and behind summit to north indicate that the sedimentary flow lofted.

Return to vehicles. Proceed on road 99 for about 1.5 mi to obscure gravel road descending sharply to the right. Park on the gravel road or another nearby safe spot.

STOP 4-8. Clearwater Creek headwaters. Descend along the gravel road, across tributary valley, and hike to the ridge crest 0.3 km to the south. The pyroclastic-surge deposit is as thick as 50 cm in tributaries on the valley floor and is normally graded from sandy, small-pebble gravel (A1) to medium sand (lower A2). It is overlain by bedded fine sand (upper A2) and sandy-silt tephra (A3). Where the bed thins to as little as 10 cm, its base is granular sand. Rare blocks as large as 25 cm were transported (in saltation?) and deposited by the surge.

On the ridge crest south of the valley, a prepared trench exposes the 8 to 25 cm thick deposit whose base is granule gravel. Thus along the northeast radial (Stops 4-4 to 4-5 to 4-8), the deposit grades outward to generally thinner and finer material. Overlying density-current layer A2 is the tephra sequence: A3 (great mushroom cloud), B (main-vent pumice), C (distal ash from pumiceous ash flows and ash clouds), D (late main vent), and 22 July pumice. The ridge provides an overview of the intermediate to distal part of devastated area, including downed and standing trees, as well as the fringing zone of scorched standing trees with intact limbs. Was the devastating current a flow or surge, neither, or both?

Return to vehicles and proceed on road 99 northeast to a large parking area at Meta Lake (sign).

STOP 4-9. Surge-wrecked automobile and Meta Lake. The surge moved the automobile only a few meters northeastward off the road, battering it mostly with flying wood fragments. Subsequently a sustained, trailing, hotter part of the current burned off the paint and plastic parts. Nearby, the owners of the vehicle briefly outlived the current, but died from suffocation due to inhaled ash (Eisele et al., 1981).

A hike along the prepared trail to Meta Lake gives good views of downed big trees, small trees that survived (by virtue of lying buried in snowpack on 18 May 1980), the lake in which big trout survived, and the rapid return of life to the devastated area on slopes where deposits are only centimeters thick.

Continue along road 99 to edge of standing trees.

STOP 4-10. Scorch zone (stop at any convenient place in area). The outer edge of downed trees merged in 1980 into a zone tens to hundreds of meters wide in which the trees were scorched but not downed. The brown needles fell off by 1981 and since then so have many of the smallest branches. By the time it reached this area, the ground-hugging surge lost enough lateral momentum and deposited enough material to rise because of increased buoyancy. The trees were thus left standing but were killed by the heat.

In this area the surge deposit is merely 1–1.5 cm thick and consists only of sand (A2) capped by ash-fall layer A3. On the north and northwest radials, the thickness and grain-size decrease more gradually than between Stops 4-7 and 4-9 on this northeast radial.

Return to Stop 4-9 and take road 26 northward toward Randle. Along the way there are spectacular overviews of the leveled forest and opportunities for closer examination of the downed trees.

STOP 4-11. Photographic stop and overview of downed trees.

Return to Cispus center, about 20 mi north and east, via roads 26, 25, and 76.

Day 5, Trip B: Pumiceous pyroclastic deposits of Pumice Plain

C. William Criswell

Introduction

The Pumice Plain covers an area of about 9 km^2 on the north flank of Mount St. Helens. The Pumice Plain contains a composite sequence of unwelded pumiceous pyroclastic-flow deposits emplaced during six explosive eruptions in 1980: 18 May, 25 May, 12 June, 22 July, 7 August, and 16-18 October (Christiansen and Peterson, 1981; Rowley et al. , 1981). The 18 May eruption produced the most voluminous deposits (0. 12 km^3), which are the focus of today's tour. The later eruptions produced deposits of much smaller volume that are confined to the center of the Pumice Plain. Most of these smaller deposits were buried by volcaniclastic debris from a snow avalanche and lahar that occurred on 19 March 1982 (Waitt et al. , 1983), and by more recent deposits.

Today's field guide describes a walking tour of the 18 May 1980 deposits of the western Pumice Plain (Fig. 17). Stratigraphy, depositional facies, and pristine surface features of deposits along tributaries of the North Fork Toutle River will be examined. The approximately 7 mi round trip

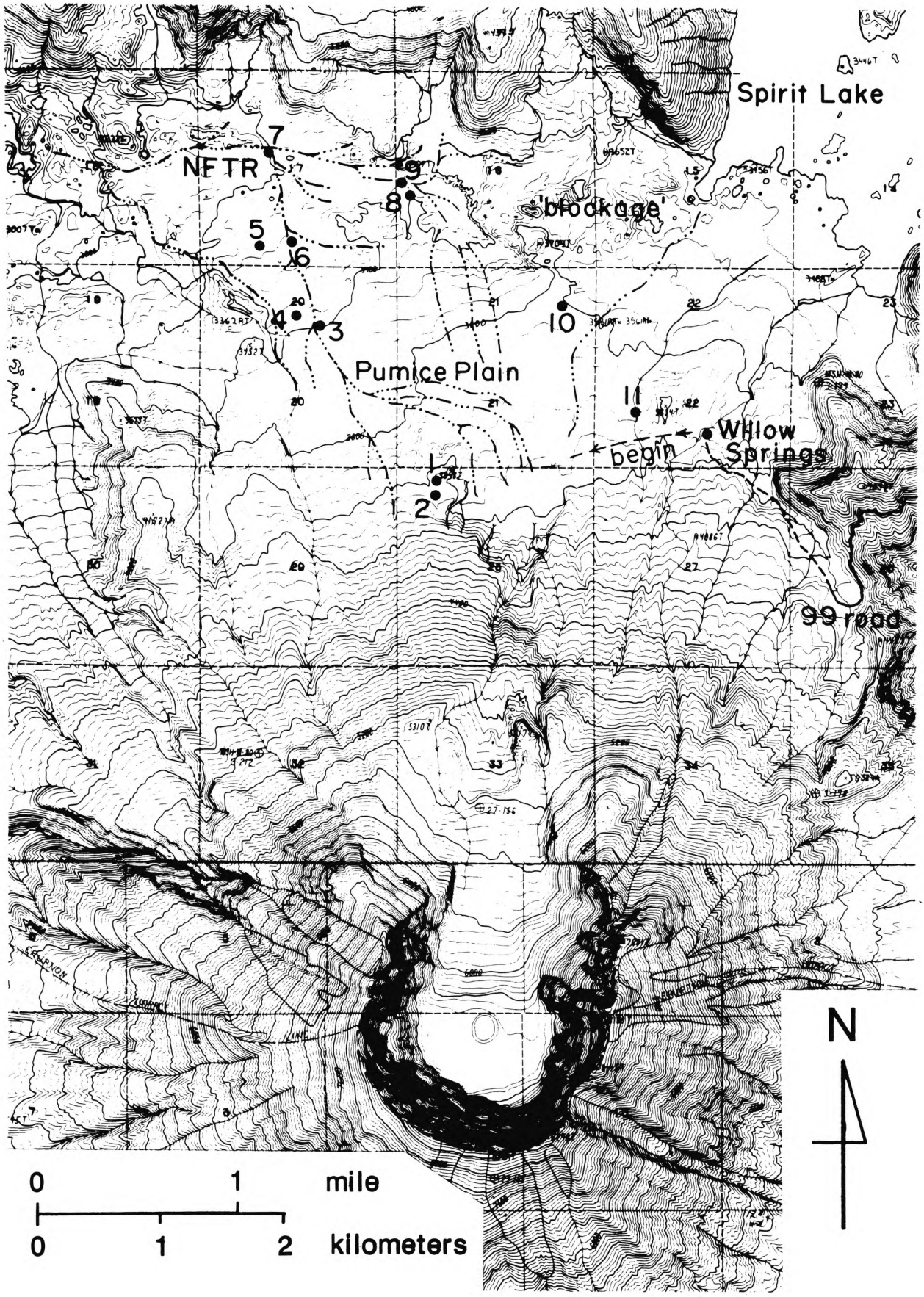

FIGURE 17—Topographic map of Mount St. Helens and upper North Fork Toutle Valley showing stops of walking tour of Pumice Plain. Some drainage trends shown (including the North Fork Toutle River, NFTR), although map was compiled in 1980. Contour interval 40 ft (12.2 m).

begins at Willow Springs in the upper Toutle Valley about 1 mi south of Spirit Lake (cumulative altitude gain and loss of a few hundred meters). The tour proceeds southwest to the north flank of Mount St. Helens, north through western parts of the Pumice Plain, and loops back east via the Pumice Pond area to Willow Springs.

Willow Springs is a natural landmark and starting point for walking trips in the upper Toutle Valley. The willow trees are growing from surviving rhizomes. It is necessary to park above the springs; follow the road down to the springs to begin this field guide.

Proceed from Willow Springs west-southwest along the base of Mount St. Helens to Stop 1 below Goat Rocks fan just east of a perennial stream. Stay close to the base of Mount St. Helens to avoid large gullies to the north carved by several small ephemeral streams that must be crossed.

Field guide

STOP 5B-1. Overview. Deposits of the 18 May Pumice Plain consist of a series of pumice and ash-flow sheets emplaced during the afternoon eruptions that began about 12:15 PDT (local time), climaxed from 15:00 to 17:00, and terminated about 18:30. The entire suite of 18 May deposits becomes more pumice-rich and more compositionally diverse upsection, which suggests that a zoned magma chamber was tapped that became progressively depleted in volatiles.

The pumice flows were largely topography-controlled sediment gravity flows, as the deposits are thin in upper valley areas and thicker downvalley. The 18 May pyroclastic-flow deposits of the Pumice Plain are informally subdivided into lower, middle, and upper stratigraphic sequences, each comprising many flow units, that are correlated with observed eruption events and tephra deposits (Fig. 18). The lower sequence, erupted during the early afternoon, is generally poorly exposed but appears thickest in the central areas, is thinner downvalley, and is absent in upper valley areas. The voluminous middle sequence, associated with the climactic eruptions, consists of several thick extensive sheets that form the Pumice Plain and small outliers on other flanks and valleys. The upper sequence, erupted during the waning phases of the early evening, consists of a few small tongues that spread over the central and western parts of the middle sequence. The lower and middle sequences rest on deposits of the debris avalanche (unit *da* of Fig. 18) and a basal sequence. The basal sequence is a complex of lithic pyroclastic deposits that contain poorly vesicular juvenile clasts erupted during the first minutes and that swept outward through the devastated area (Hoblitt et al., 1981; Waitt, 1981). Although the basal sequence in the Toutle Valley generally correlates with the blast deposits, no specific correlations have been made between individual flow units because there are several flow units present in the valley as well as in the devastated area.

Deposits of the Pumice Plain can also be subdivided into proximal, medial, and distal facies that exhibit a general fining with distance from vent. The proximal deposits mantle the north flank of the volcano; the medial deposits form the southern parts of the Pumice Plain; the distal deposits are typically banked against Johnston Ridge to the north.

Proximal deposits (within 3 km of vent) mantle the north flank; their character depends on the local topography and surface roughness. Although we will not visit the area, the irregular surface of the northeast flank contains the proximal fines-poor bedded deposits described by Rowley et al. (1985).

STOP 5B-2. Proximal lithic breccia. The northwest flank in this area is relatively smooth because the Goat Rocks talus fan (ca. 1857) covers older lava flows. This was the area of axial flow of most pyroclastic flows on 18 May; lower parts of the Goat Rocks fan are mantled by the 18 May deposits. The afternoon pumice flows locally carved deep channels into the debris-avalanche and basal-sequence deposits erupted only hours earlier. These channels were deepened in later years into the large erosional gullies of today.

Pumiceous deposits in this area consist of matrix-poor lithic breccia that grades laterally and irregularly into thin, matrix-rich selvages of the southern Pumice Plain. These breccias form a discontinuous mantle of longitudinal ridges and sheets with upper surfaces sloping northward steeper than 5° and lower contacts as steep as 25°. Some ridges formed on the lee sides of large obstructing boulders. The sheet deposits may have formed by accumulation of anastomosing ridges or may represent deposition from much broader flows. Some boulders appear to be part of the pumiceous breccia, others part of the underlying basal-sequence breccias. Cuspate scarps dipping 30° typically truncate the proximal deposits on the downslope side and appear to have formed by upslope propagation of a toe-slope failure. The proximal deposits are overall much richer in coarse ash and lack the finer ash fractions (Fig. 19) typical of the ponded deposits of the Pumice Plain. The clast-support and fines-poor character of the breccias is interpreted to have resulted from enhanced fluidization (increased air engulfment) and turbulent flow down the slope.

Proceed downslope ~100 m into the large gully that dissects the thickly ponded deposits of the Pumice Plain.

STOP 5B-3. Middle (medial facies) and upper sequences. This area is just west of the main axis of flow of the lower sequence. It experienced considerable deposition during the climactic phases (middle sequence) and continued to be the route of small flows thereafter (upper sequence and 12 June flows). The gully initially formed along the west edge of a large fan-shaped flow unit that forms much of the exposure of the western Pumice Plain. The deposits exposed along this stretch of the gully are typically rich in crystals and poor in the fine vitric-ash fractions (Fig. 19). This characteristic is attributed to the preferential loss of fines during transport down the flank and subsequent deposition on the gentler valley slopes. Characterized by scattered lithic boulders and abundant degassing pipes, these flows compose the medial facies of the Pumice Plain. The prominent planar base of a concentration of lithic fragments marks the base of the upper sequence. The gully cuts slightly oblique to flow direction, so the channelled tongue of the upper sequence appears unusually wide. It is flanked by thin ($\leq$2 m) channel-overflow deposits. In many nearby exposures the base of the upper sequence is marked by ground-surge deposits and buried phreatic crater-rim deposits.

Proceed up the spur gully along the western bank and climb up to the surface of the pumice flows.

STOP 5B-4. Primary surface of the Pumice Plain. The deposits of the Pumice Plain are nearly pristine in this area because the large gully protected them from post-1980 avalanches and floods (Waitt et al., 1983). Walk northward along the axis of a tongue of the upper sequence and observe the morphology of it and the underlying middle sequence.

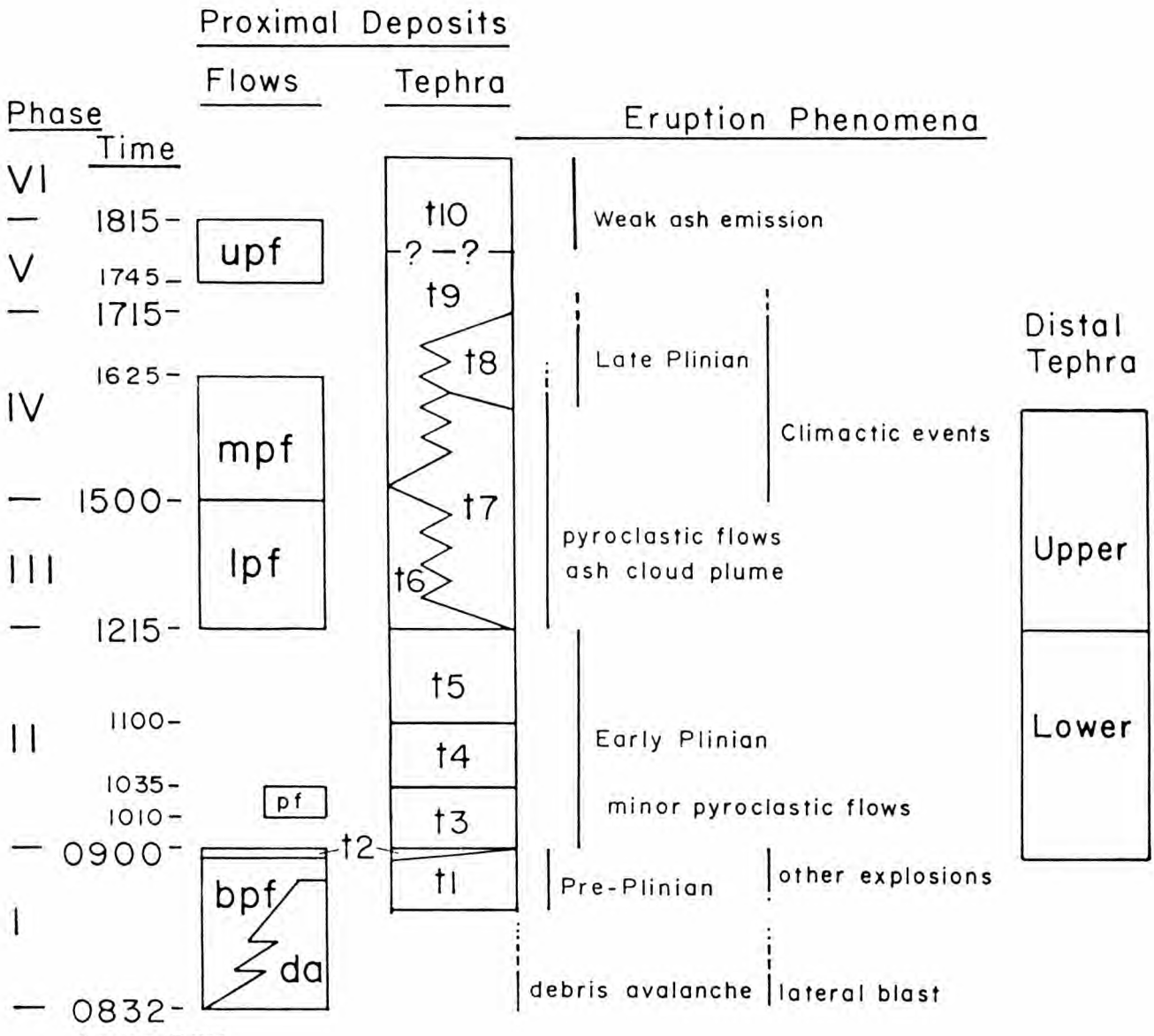

Eruption Phases		Pyroclastic-Flow Deposits		Proximal Tephra Deposits		
VI	Posteruption			t_{10}	capping fine ash	
V	Late Ash Flow	upf	Upper Sequence	t_9	upper fine ash	Afternoon Sequence
IV	Climactic	mpf	Middle Sequence	t_8	upper pumice lapilli	
III	Early Ash Flow	lpf	Lower Sequence	t_7	middle pumice ash	
				t_6	lower fine ash	
II	Early Plinian	pf	undivided	t_5	middle pumice lapilli	
				t_4	lower lithic ash	Morning Sequence
				t_3	lower pumice lapilli	
I	Paroxysmal	bpf	Basal Sequence	t_2	pisolitic ash	
				t_1	basal pumice lapilli	

FIGURE 18—General stratigraphic and chronologic correlations of pyroclastic-flow and tephra-fall deposits of the 18 May 1980 eruption of Mount St. Helens. From Criswell (1987).

This tongue was seen in cross section at Stop 5B-3. On the surface above Stop 5B-3, deposits of lithic breccia form rounded, ellipsoidal mounds. Farther east these mounds dominate the southernmost surface of the middle sequence. In 1980 other workers mistook the mounds for debris-avalanche deposits and thus interpreted the pumice flows to be very thin through this area.

Just north are two small phreatic craters that were infilled by the 19 March 1982 flood deposit, but parts of the stratified rim deposits remain exposed. These phreatic-explosion deposits have a thickness maximum trending east-northeast, thin away from the source, and form a coarse debris blanket of scattered lithic fragments and ash around the two craters. The northern crater is being consumed by the failure of the gully wall. **Please stay away from the unstable edge.** The shape of the southern crater suggests multiple explosions; it was observed filled with water on 19 May.

Continue northward. Just to the west is a scarp that dips gently eastward. This scarp is the remnant of the side of a set of nested, longitudinal channels cut into the middle se-

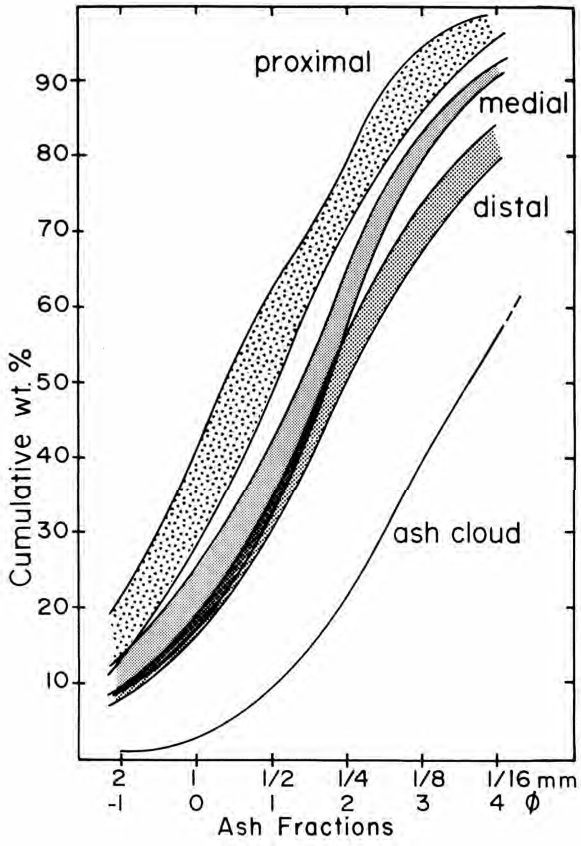

FIGURE 19-Cumulative grain-size analyses of matrix ash fractions from proximal, medial, and distal facies of the 18 May pumiceous pyroclastic-flow deposits of the Pumice Plain (C. W. Criswell, unpubl. data). A typical analysis of ash-cloud deposit is also shown.

quence deposits by the upper sequence on 18 May. When reconstructed in three dimensions, the scarps project downward to the lithic-concentration zone of Stop 5B-3.

STOP 5B-5. Terminal margin of flow units. The 18 May upper-sequence pumice flows consist of sheetlike lenticular deposits that have lacy, anastomosing pumice lobes lacking marginal levees. The surface of the underlying middle sequence, in contrast, is marked by curving longitudinal ridges centimeters to decimeters high that typify the central parts of these sheetlike deposits. These small ridges appear not to be rooted in the deposit and, therefore, they are interpreted as products of dilute clouds during the last stages of flow emplacement.

Pumice clasts in the lacy margin lobes of the upper sequence consist of two chemical types (Table 2): a volumetrically dominant mafic dacite (64% SiO_2) and a denser, more crystal-rich silicic andesite (62% SiO_2). The silicic andesite, generally distinguished by density and the presence of augite, is found as individual clasts and intermingled bands.

The mafic dacite dominated the eruption and appears to constitute the entire juvenile component of the initial explosions and the morning plinian column. The silicic andesite began to erupt late in the morning, just before the beginning of the ash flows, as it comprises only a few percent of the airfall tephra along its dispersal axis. Within the pumice flows, the proportion of silicic andesite varies (20–50% of juvenile clasts) and appears to increase upsection. These relations suggest that the change in eruption

TABLE 2-Representative chemical analysis of 18 May 1980 pumice. Recalculated from Criswell (1987); normalized to 100% on water-free basis.

	Mafic dacite	Silicic andesite	Mafic scoria
Density (g/cm^3)	0.83	1.29	1.09
SiO_2	63.94	62.22	60.96
$A1_2O_3$	17.78	18.02	18.22
Fe_2O_3	1.55	1.83	2.09
FeO	2.76	3.16	3.40
MgO	1.91	2.31	2.70
CaO	4.86	5.37	5.92
Na_2O	5.08	4.96	4.68
K_2O	1.38	1.26	1.13
TiO_2	0.61	0.71	0.75
P_2O_5	10.13	0.15	0.15
Total	100.00	100.00	100.00

style from plinian ejection of tephra to pyroclastic flows was due to chemical changes of the magma.

Return eastward and re-enter the large gully.

STOP 5B-6. Basal and lower sequences. This central area of the gully reveals the stratigraphy of the hummocky debris-avalanche deposits, flat-surfaced basal sequence, and lower parts of the pumiceous deposits. The debris-avalanche deposit has a coarse-textured, shattered-block appearance. Individual blocks are generally lithologically homogeneous, but the lithology varies from block to block. Thus the blocks are shattered but not mixed (Voight et al., 1981; Glicken, 1986).

Resting on the debris-avalanche deposits are poorly sorted deposits of the basal sequence. These contain variable proportions (10–50%) of poorly vesicular juvenile clasts. In this part of the valley, deposits of the basal sequence generally consist of an ungraded, very coarse lower unit overlain by one or two finer-grained, massive units capped by the pisolitic ash t2 (commonly called layer A3). The coarse layer is present in the deep exposures along the North Fork Toutle River and as far west as Coldwater Lake. The finer-grained layers are present in exposures along the south side of the valley where they form a depositional fan as far as 10 km downvalley. Along the north side of the valley, the fine layers form discontinuous exposures in topographic lows of the hummocky debris-avalanche deposits.

The pumiceous deposits are relatively thin in this stretch of the gully, but thicken toward the North Fork Toutle River where they appear to fill a local depression. Outcrops of the lower sequence consist of a variably thick sequence of thin pumice flows erupted during the early afternoon. The early pyroclastic flows appear to have flowed directly out of the crater breach and spread into the low areas of the central Pumice Plain to form an aggrading fan over the basal sequence. Some of the flows ponded against Johnston Ridge near the nested explosion crater (Stops 5B-8 and 5B-9). A few flows apparently drained away downvalley to form relatively thin (<2 m) deposits in this area.

The basal and lower sequences in this area are overlain by clast- to matrix-supported lithic-breccia layers 1–2 m thick that define the base of the middle sequence. These breccias are traceable throughout the exposures of the Pumice Plain and will be examined at Stops 5B-7, 5B-9, and 5B-11.

Proceed northward along the stream to the confluence of the North Fork Toutle River.

STOP 5B-7. Basal sequence and distal facies of middle sequence. Deposits of the middle sequence, almost 40 m thick in this area, resulted from the voluminous pyroclastic flows of the climactic phase of the 18 May eruption. These flows overtopped local topographic highs that had confined flows of the lower sequence. These deposits are typically rich in lithic debris and large pumice clasts, the pumice lying in swarms within flows and as surface accumulations. Lithic clasts typically range from granule to pebble size; the larger clasts are concentrated in linear zones. The matrix sand (ash) here contains a higher proportion (to 21%) of fine vitric ash than is found in deposits to the south (Fig. 19). The enrichment of fine ash in the distal facies is inferred to reflect depletion of coarser fragments because of (1) decreasing emplacement energy due to increasing deflation and compaction of the flows, and (2) reduced fluidization (reduced air engulfment and gas exsolution) and saltation, which result in retention of fines.

The middle sequence in this area rests on thick deposits of debris avalanche ($\geq$100 m) and the basal sequence ($\geq$15 m). On the north side of the North Fork Toutle River, the basal sequence is cut by graded lapilli and blocks in vertical pipe structures 1 m wide and several meters high. Although these resemble degassing pipes, I interpret them as dewatering structures. On a topographic high just north of the confluence is the remnant of a scarp structure that I interpret as either a phreatic crater rim or (more likely) the rim of a large collapse structure with small superimposed phreatic craters. Collapse was due to water withdrawal and compaction of the debris-avalanche deposit. Inspection of aerial photographs taken in 1980 indicates that a group of mudflow deposits originates in this area but may not have integrated with the large North Fork Toutle mudflow that originated downstream (Janda et al., 1981; Criswell, unpubl. data).

Proceed south into the large tributary gully and enter the spur gully to the east, which leads to the surface of the pumice flows along the south side of the river. Proceed eastward along the surface to the western rim of the nested explosion crater (the big phreatic-explosion pit of Rowley et al., 1981). **Stay away from the unstable edges.**

No formal stop is planned along this traverse, but the path crosses some of the most spectacular swarms of surface pumice blocks preserved in the Pumice Plain. The largest pumice clasts were found in this area (>2 m), but they were eroded away during channel entrenchment (ca. 1983).

STOP 5B-8. View of nested explosion crater. This area, now deeply dissected by posteruption streams, was the site of intense secondary explosions during and just after 18 May 1980. The explosions probably were caused by emplacement of thick pumiceous pyroclastic flows into water that was ponded in the irregular topography of the debris-avalanche deposits. A remnant of the stratified ejecta blanket from the buried explosion craters is located about 200 m to the east at the same altitude as this rim. These deposits are similar to those surrounding other explosion craters on the Pumice Plain. After the nested explosion craters were partly filled by the 12 June 1980 pyroclastic flows, the area become known as the Pumice Pond. The Pumice Pond was breached by eruption-melted floodwater of 19 March 1982; intense dissection began with the pumping of Spirit Lake in late 1982 and early 1983. Spirit Lake lies just beyond the debris-avalanche deposits to the east, and the pump outlet was located just out of sight in a group of hummocks known as "the blockage" (Glicken and Voight, in press). During the 19 March 1982 flood and initiation of the Spirit Lake pumping, the water cut rapidly through still-hot and unconsolidated pumice deposits to cause further explosions. The North Fork Toutle River channel was cut mainly by the pump effluent and has changed little since the pumping stopped in 1985. The bottom of the channel is underlain by coarse pyroclastic deposits of the basal sequence that are resistant to erosion.

Proceed southeast to the spur gully cutting down to the alluvial plain forming the floor of the Pumice Pond crater. If time permits, drop down into the gully leading north to the river channel to Stop 5B-9. Otherwise proceed eastward across the alluvial plain and climb up onto the pumice flows on the far east side for Stop 5B-10. **Be careful, some of the gullies leading south contain quicksand.**

STOP 5B-9 (optional). Pumice Pond stratigraphy. This area exposes some of the most spectacular and instructive deposits in the valley, but locally also has **pockets of quicksand.** Walking down the spur to the confluence with the river, one traverses deposits of the thick (20 m) middle sequence with lithic-breccia zones near the base. The middle sequence overlies the lower sequence (12 m), which consists of many thin flow units. These are the thickest known exposures of the lower-sequence deposits. The adjoining east-trending gully exposes the interior fill of the Pumice Pond, including the gray 12 June 1980 ash flows and the 19 March 1982 flood deposits.

Farther down toward the river, the pumiceous lower sequence rests on deposits of the basal sequence. The contact was locally reworked by water on 18 May before the thick pumice flows were emplaced. The erosion-resistant deposit that contains the river channel is a juvenile-rich, slightly indurated facies of the basal sequence. I think that it had condensed water (as opposed to steam) involved with its emplacement, either from initial water (snowmelt) or incorporation of standing water from this area. It appears to grade laterally into the coarse unit seen at Stops 5B-6 and 5B-7, and is overlain by a finer-grained, massive flow unit that is capped by the pisolitic-ash marker bed (layer A3 of Waitt and Dzurisin, 1981).

Proceed back up the gully to the alluvial plain, walk to the far eastern side, and climb up onto the pumice flows. **Be careful, some of the gullies leading south contain quicksand.**

STOP 5B-10. 12 June and 22 July 1980 pyroclastic-flow deposits. This area contains the only remnants of the 12 June and 22 July deposits other than local gully-wall exposures. The gray 12 June deposits are relatively fine-grained, with scattered boulders and surface morphology of cuspate scarps. The scarps appear to have formed shortly after the flows came to rest by secondary flowage induced by gravitational failure at topographic irregularities. The slightly orange 22 July deposits exhibit a striking tongue and levee morphology that reflects the block-rich and gas-poor nature of the pyroclastic flows (Kuntz et al., 1981; Rowley et al., 1981). The 22 July deposits also contain numerous scoriaceous clasts (Lipman et al., 1981b) of slightly more mafic composition (61% SiO_2) (Table 1, column 3) than the common silicic andesite (62% SiO_2). Small amounts ($\geq$1%) of these scoriaceous clasts also occur in the middle sequence of 18 May (Criswell, 1987).

Proceed southeast across the alluvial channel to the large debris-avalanche hill west of Willow Springs. This alluvial channel drains into Spirit Lake and follows a course used by pyroclastic flows of 18 May, 12 June, 22 July 1980, and the 19 March 1982 floodflow.

STOP 5B-11 (optional). Pumiceous and lithic-breccia deposits. This area exposes some of the most spectacular pumiceous and lithic breccias of the 18 May Pumice Plain. Deposits of the middle sequence here are typically clast-supported, ungraded to crudely normally graded, ≥ 5 m thick, and consist of at least two flow units. The breccia grades upward to typically crystalline pyroclastic-flow deposits that are ≤ 1 m thick. The pumice flows that deposited the breccias are interpreted to have been voluminous and to lie farther north, just south of and in Spirit Lake. Inspection of 1980 aerial photos indicates that these breccias rest in channels cut into underlying deposits (exposed just east of the breccias). Tongues of the upper sequence were emplaced on top of, and just west of, the breccias in the channels that drain to Spirit Lake. The upper sequence in this area had distribution patterns similar to the small flows of 12 June and 22 July.

Proceed southeast across the southern part of the adjacent debris-avalanche hill to Willow Springs and then to the parking area. The trip back to the parking area traverses thin deposits of breccia and basal-sequence breccias that mantle the hummocky debris-avalanche deposits.

Day 5, Trip C-1: Harmony Falls basin—Relations between great pyroclastic surge and landslide-impelled tsunami of Spirit Lake water

Richard B. Waitt

Introduction

This trip is a walking tour of about 3 mi from road 99 to Spirit Lake and back, mostly by trail. Total altitude gain and loss is 888 ft (240 m). On this trip we will examine deposits and erosional effects of the pyroclastic surge and a great displacement of Spirit Lake water (a tsunami) in Harmony Falls basin (Fig. 20).

On 18 May 1980, the new deposits in Spirit Lake and the new dam of landslide debris on the west caused the lake surface to rise suddenly from 975 m to 1038 m. By late 1982, inflow had further raised the lake level to 1056 m. In 1984 lake level was lowered to 1049 m by an engineered tunnel spillway.

The 500 m height of the debris-avalanche runup over Johnston Ridge suggests that the east margin of the avalanche entered Spirit Lake at 200-300 km/hr. Various unusual erosional and depositional features around the lake margin show that the landslide catastrophically displaced the lake water, generating a local tsunami.

West arm of Spirit Lake

A large patch of the hummocky debris avalanche in lower Bear Creek valley at the head of the west arm of Spirit Lake traveled north-northeastward through the lake. The lake water, catastrophically forced to the head of the valley by the debris avalanche, flooded back to the lake basin across the new hummocky avalanche deposit and deposited logs and boulders that it jammed against the north side of the hummocks.

The valley sides are almost devoid of shattered stumps, downed timber, and sediment below a sharp line on both arms of Spirit Lake that slopes from altitude 1250 m north of the lake head down to 1100 m at the south end of the lake (Fig. 20). On the spur between the two arms of the lake, the coarse layer A 1 is as thick as 50 cm above altitude 1200 m, but is nearly absent below (stratigraphic labels of Waitt, 1981). Apparently not overridden by the debris avalanche, the spur was swept clean by a wave of water displaced when the avalanche entered the lake. Long flutes across the ridge record the wavepath northeastward to the east arm of the lake. The absence of layer A 1 below altitude 1200 m (the fine layer A2 forms the base of the surge deposit on the fluted part of the spur) indicates that the front of the pyroclastic surge preceded the catastrophic water wave. The tsunami must have occurred near the end of A 1 accumulation.

East arm of Spirit Lake and Harmony Falls basin

The pronounced trimline of the catastrophic wave along the east arm of the lake rises from altitude 1050 m on the south to 1250 m on the north (Fig. 20). Like oceanic tsunami, the wave height increased where the water was projected into shoals and a narrowing valley at the north end of the lake; the wave thus swept destructively inland far above new lake level.

A sharp trimline lies at altitude 1200 m along the north side of Harmony Falls basin. Above the line lies abundant timber felled northeastward by the pyroclastic surge; below the line the timber and deposits were scraped off by the tsunami surging eastward up the basin. Toward the valley head the trimline descends steeply, delineating the limits of the water as it lost lateral momentum and plunged to the valley floor. The floor of the north part of the basin is discontinuously overlain by large logs and other timber rinsed from the slopes and collected into rafts, but most of the timber floated with the water back into Spirit Lake.

On a flat, nearly timber-free spur at the northwest edge of Harmony Falls basin, the upper part of the pumice set W (A. D. 1480) and set T (A.D. 1800) (Mullineaux, 1986;

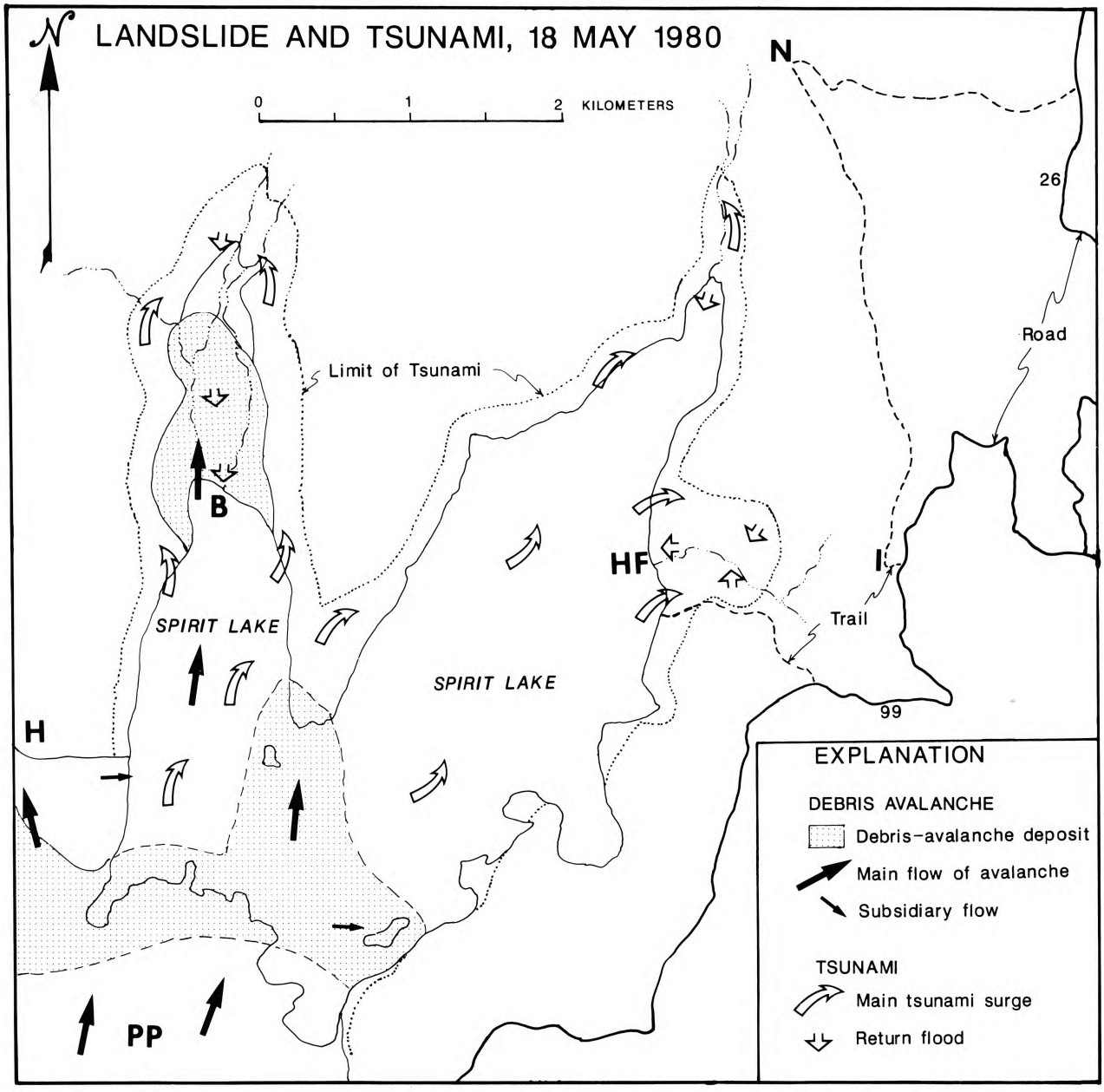

FIGURE 20—Map of Spirit Lake basin showing distribution of 18 May 1980 debris-avalanche deposits, limits of Spirit Lake water displaced as a local tsunami, and trail access to Harmony Falls basin and Norway Pass area. B, Bear Creek valley and Bear Cove; H, Harrys Ridge; HF, Harmony Falls; I, Independence Pass; N, Norway Pass; PP, Pumice Plain.

Yamaguchi, 1983) (review Table 1 and Fig. 16) was discontinuously eroded. Also removed were stumps and tree trunks of the old-growth forest that the pyroclastic surge leveled moments earlier. On this washed surface, layer A 1 lies as thick as 18 cm but is discontinuous. Layer A2 continuously mantles the scour depressions with variable thickness. Layer A3 and unit C mantle layer A2 with little variation in thickness. The catastrophic wave evidently arrived when layer A 1 was nearly deposited; the wave drained away swiftly because the last of A 1 accumulated in new scour depressions. The area then remained stable during deposition of layer A2 by the waning surge and during the ensuing falls of A3 and C materials.

The south side of Harmony Falls basin also shows a sharp trimline that registers the upper limit of the catastrophic wave. In 1980, many shattered stumps on the floor of the south part of the basin were encircled by horseshoe-shaped scour depressions that opened north, a record of sheetflood that swept northward toward the valley axis. Part of layer A2 and all of layer A3 pass from uneroded parts of the surface into the bottoms of the scour depressions. Scarps cut by water 20 cm into layer A1 also are overlain successively by layer A2, layer A3, and unit C. The absence of part of layer A2 indicates that the displaced water returning to Spirit Lake must have crossed these surfaces toward the valley axis while layer A2 was accumulating.

Near the valley axis are shallow channels by which water drained from the sides of the basin toward the axial mainstream, which was incising into new pyroclastic-surge and waterlaid deposits. These channels truncate layer A3 and surge layers A2 and A 1, but are lined by the entire unit C. After the main sheetflood subsided, a waning flow of water

from the sides of the basin must have continued until after layer A3 accumulated (by 10:00), but ceased before unit C began to accumulate (after 12:30). Like the channels, scarps formed by slumping of surge material into the newly incised mainstream channel truncate, and are not overlain by, layer A3, but are overlain by all of unit C. Such relations indicate that the main channel eroded 1-1.5 m deep to promote bank slumping some time after layer A3 accumulated (by 10:00), but before the base of unit C accumulated (about 12:30). Thus all water-worked surfaces except the mainstream channel ran dry before unit C began to accumulate after midday.

1980 islands in south part of Spirit Lake

Inconsistent stratigraphy of the upper part of layer A2 among low-altitude sites suggests complications to the single-wave idea: (1) The main tsunami may have sloshed around, eroding some low-altitude deposits. (2) Besides the large mass of north-transported debris-avalanche material (such as at the head of Bear Cove) that caused the tsunami, a debris-avalanche tongue also descended the south nose of Harrys Ridge eastward, directly downslope to the lake. A second avalanche tongue entering the lake may have caused a second but lesser displacement of the lake water.

Day 5, Trip C-2: Norway Pass Trail

Richard B. Waitt

This part of trip is a round-trip hike of about 5 mi by trail with an altitude gain and loss of less than 200 m.

From road 99 at trailhead to Independence Pass, hike trail to ridge crest (Independence Pass) and then continue along trail northward for about 2.5 mi to Norway Pass (Fig. 20). The trail provides detailed views of trees downed by the great surge, small trees that survived because of having been partly or wholly buried by snowpack on 18 May 1980, and numerous other features associated with emplacement of the surge. Trimlines and other effects of the great local tsunami caused by debris avalanche entering the lake on 18 May 1980 are also visible.

Return on same trail to vehicles. Return by road to Cispus Center.

Day 6: Pyroclastic surge, pyroclastic flows, and lahars in Smith Creek valley during first minutes of 18 May 1980 eruption

Richard B. Waitt and Steven R. Brantley

Introduction

Today's trip examines deposits in and near Smith Creek valley just off the east flank of Mount St. Helens. After three roadside stops , the focus of the trip is a hike of about 8 mi on the floor of Smith Creek valley with cumulative altitude gain and loss of perhaps 300 m. The northeast flank of Mount St. Helens and Smith Creek valley contain strati-graphically complex deposits produced by the devastating pyroclastic surge and resultant lahars. Tributaries that head on the volcano descend steeply 1800 m to the gentle floor of Smith Creek valley (Fig. 21). Of these tributaries, Windy and Cataract canyons lie within the area swept by the surge, but Ape Canyon lies mostly south of the devastated area.

Deposits and effects of pyroclastic surge

On ridgetops that overlook upper Smith Creek valley, the pyroclastic-surge deposit of 18 May 1980 consists of a gravelly lower layer (A 1 of Waitt, 1981), which generally grades up into a sandy upper layer (A2). The combined A 1—A2 surge deposit thins from decimeters near the vent to only millimeters near the outer margins of the devastated area; it also becomes finer and thinner southward through the Smith Creek area toward the lateral margin. The deposit is thickest in topographic lows and thinnest on steep slopes. The most abundant rock type in the deposit is a gray microvesicular juvenile dacite that intruded into Mount St. Helens between March and May 1980. The whole deposit is capped by 1-2 cm of silt (layer A3) containing accretionary lapilli, material that mainly fell from a huge mushroom-shaped cloud 20-100 minutes after the eruption began (Rosenbaum and Waitt, 1981; Waitt, 1981).

The directions in which trees were felled show the varying azimuths of motion of the lobate front of the surge as it swept outward from Mount St. Helens. In many places, steep and high-relief topography channeled the flow. Where the surge crossed sharp ridge crests, its base lofted to create a backflow in the lee of the ridge, and in such places downed trees point toward the volcano. On trees that were felled

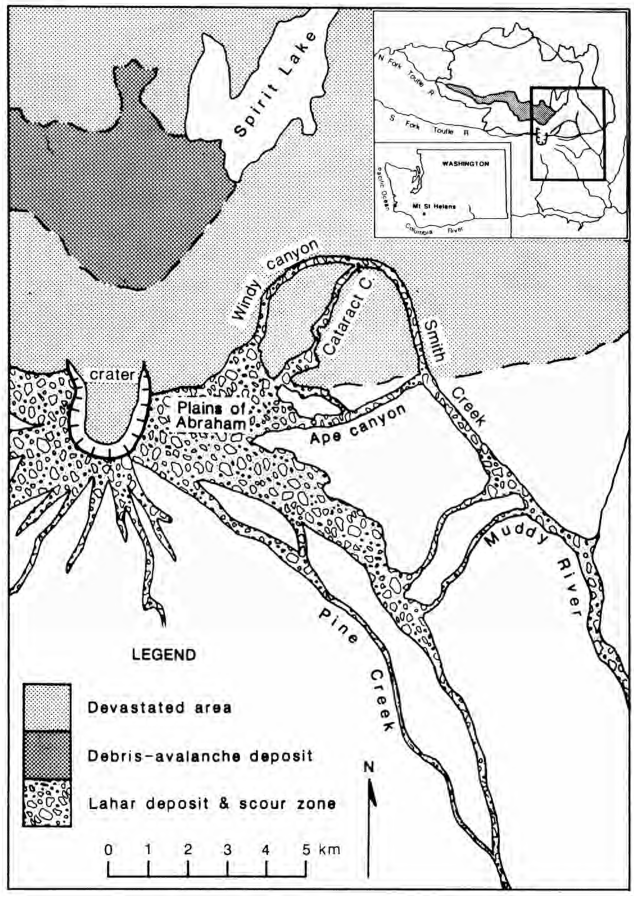

FIGURE 21—Map of Mount St. Helens, Smith Creek valley, and area affected by the devastating pyroclastic surge of 18 May 1980.

pointing away from the volcano, the former undersides of limbs are somewhat abraded or scorched, which shows that the surge was sustained and hot perhaps for a minute or more after the trees fell.

Lahars in Smith Creek tributaries

Plains of Abraham

Within minutes of the first explosions of 18 May 1980, lahars descended the east-northeast flank of the volcano, swept across the Plains of Abraham and up a transverse ridge, and overflowed into the Smith Creek tributaries. Maximum runup as high as 60 m on the ridge yields a calculated velocity of 34 m/sec (123 km/hr). The Plains are floored with a cohesive and clast-supported, gravel-rich lahar deposit.

Cataract and Windy canyons

Spilling from the Plains of Abraham, the lahars eroded most of the soil, pre-1980 tephra, and trees from the bottoms of Cataract and Windy canyons. The limit of the peak lahar in upper Cataract canyon is marked by sharp tramlines and log jams. The discontinuous deposit consists of cohesive, brown sandy gravel carrying lithic fragments as large as 2 m. Absence of an overlying pyroclastic-surge deposit shows that the lahar lagged behind even the trailing phase of the surge. Beyond the lahar trimline in Cataract canyon, the trees downed by the surge and the surge deposit both remain undisturbed.

In lower Cataract and Windy canyons, the upper limit of brown muddy diamict delineates the limit of the peak lahar. The base of the lahar is in places convoluted with the underlying pyroclastic deposit. The undisturbed pyroclastic-surge deposit lies only above the lahar limit. In contrast to the loose gray surge deposit, the lahar deposit (1) consists of a cohesive, brown, muddy sand matrix derived from eroded pre-1980 soil and tephra, (2) supports large lithic boulders and blocks of fragile surge material, and (3) contains abundant round vesicles.

Smith Creek valley fill

The ponded 18 May 1980 deposits on the floor of Smith Creek valley are divided by texture and structure into three major units. In stratigraphic order they are: (1) valley-bottom facies of pyroclastic-surge deposit divided into two subunits; (2) a coarse, hummocky diamict, a mixture of lahar and surge deposits; and (3) surge material redeposited as secondary pyroclastic flows. The pisolitic gray sandy silt (layer A3) and the pumiceous tephra-fall sequence from the main vent overlie the whole suite of deposits (Figs. 22-24).

Pyroclastic deposits

The pyroclastic-surge and attendant phenomena deposited four identifiable beds in Smith Creek valley. Two beds (basal and middle) underlie the prominent hummocky diamict, and two beds (upper and A3) overlie it.

Basal bed

The lowest pyroclastic bed, 10-50 cm thick, consists of friable granular sand that lacks grains finer than 4 Φ. More than half of the clasts are of juvenile dacite, the matrix is gray, and the bed contains abundant wood fragments and needles, many of them charred.

Middle bed

The middle bed, as thick as 2.5 m, lies along the valley walls. Its base is marked by planar laminae of fine sand, suggesting turbulent flow. Lithic fragments are reversely graded at the base, but normal grading through most of the flow mimics pyroclastic-flow layers 2a and 2b of Sparks et al. (1973). In places, several such layers are stacked. The middle bed contains small wood fragments, many of them charred, and is interrupted by vertical fines-depleted, gas-escape pipes. It is either overlain by the coarse, hummocky diamict or grades up into the upper pyroclastic bed.

Upper bed

The upper pyroclastic bed, the most voluminous of the valley-bottom pyroclastic deposits, is massive pebbly sand, as thick as 4.5 m, and consisting mainly of juvenile dacite clasts, lithic clasts, and disaggregated pre-1980 pumice.. Locally the base is reversely graded and the upper 5-20 cm grades up to poorly sorted fine sand. Vertical fines-depleted gravel pipes (gas-escape structures) are as much as 5 cm wide and 3 m long. The bed contains abundant charred wood fragments, large wood debris is concentrated toward the top of the bed, and log jams occur where it abuts and overlies the hummocky diamict. The deposit was hot and dry after the eruption (Hoblitt et al. , 1981). The upper pyroclastic bed overlies the hummocky diamict; it is thick and flat-surfaced in topographic lows and thins to nearly nil over hummocks and against valley sides. This bed in places in-

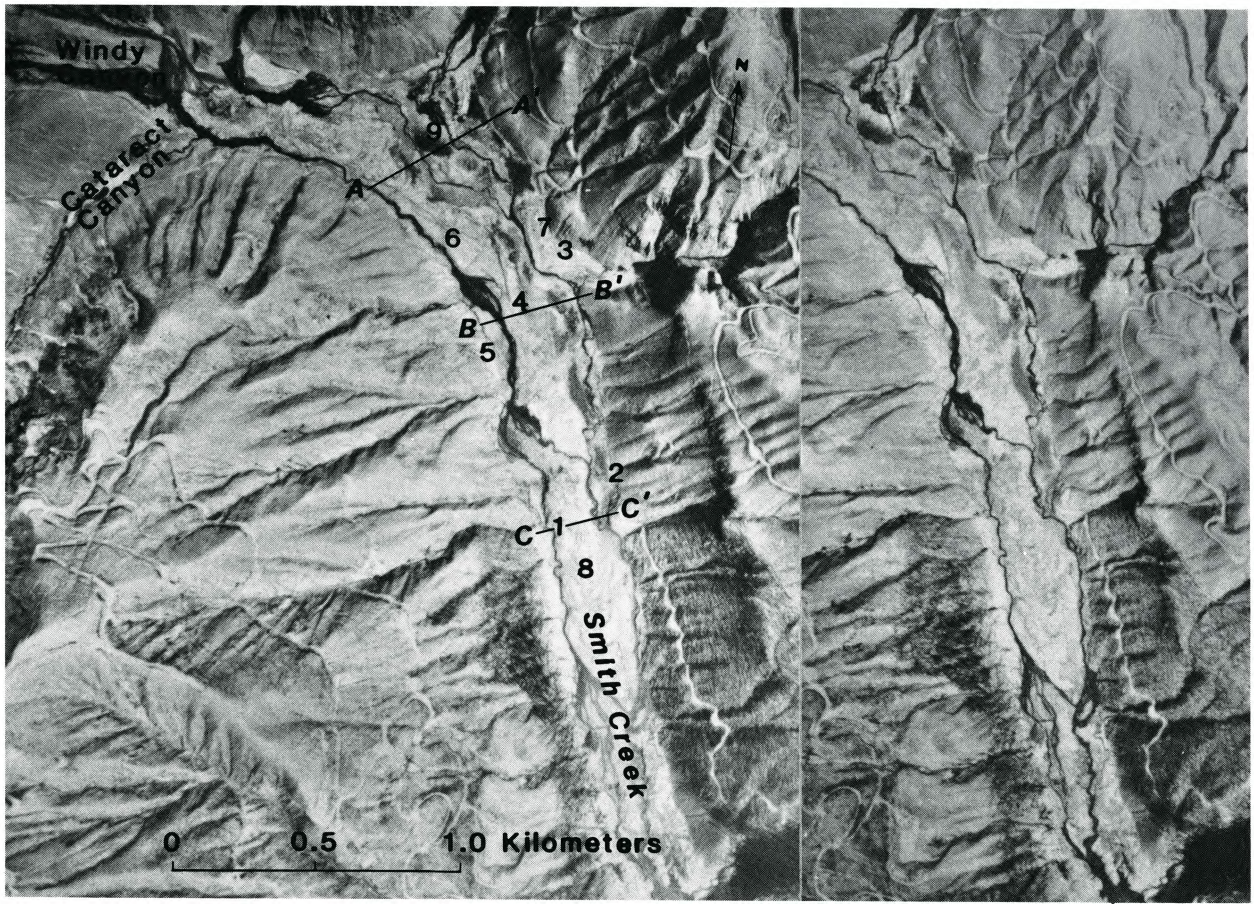

FIGURE 22—Stereographic aerial photographs of Smith Creek valley taken on 7 July 1980. Localities marked by numbers, ends of cross sections (see Fig. 24) marked by letters.

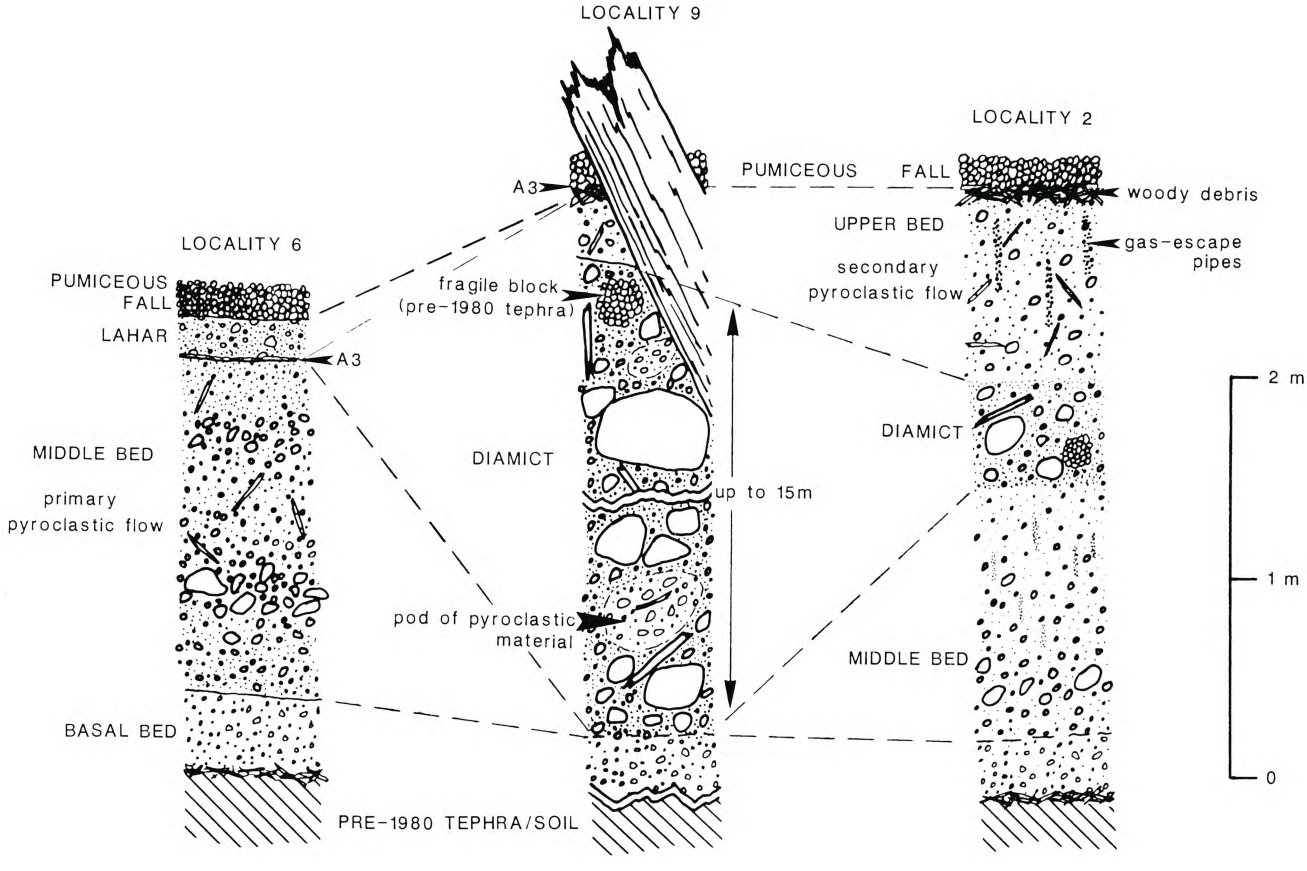

FIGURE 23—Schematic diagram of valley-fill facies in Smith Creek. Localities are shown in Fig. 22.

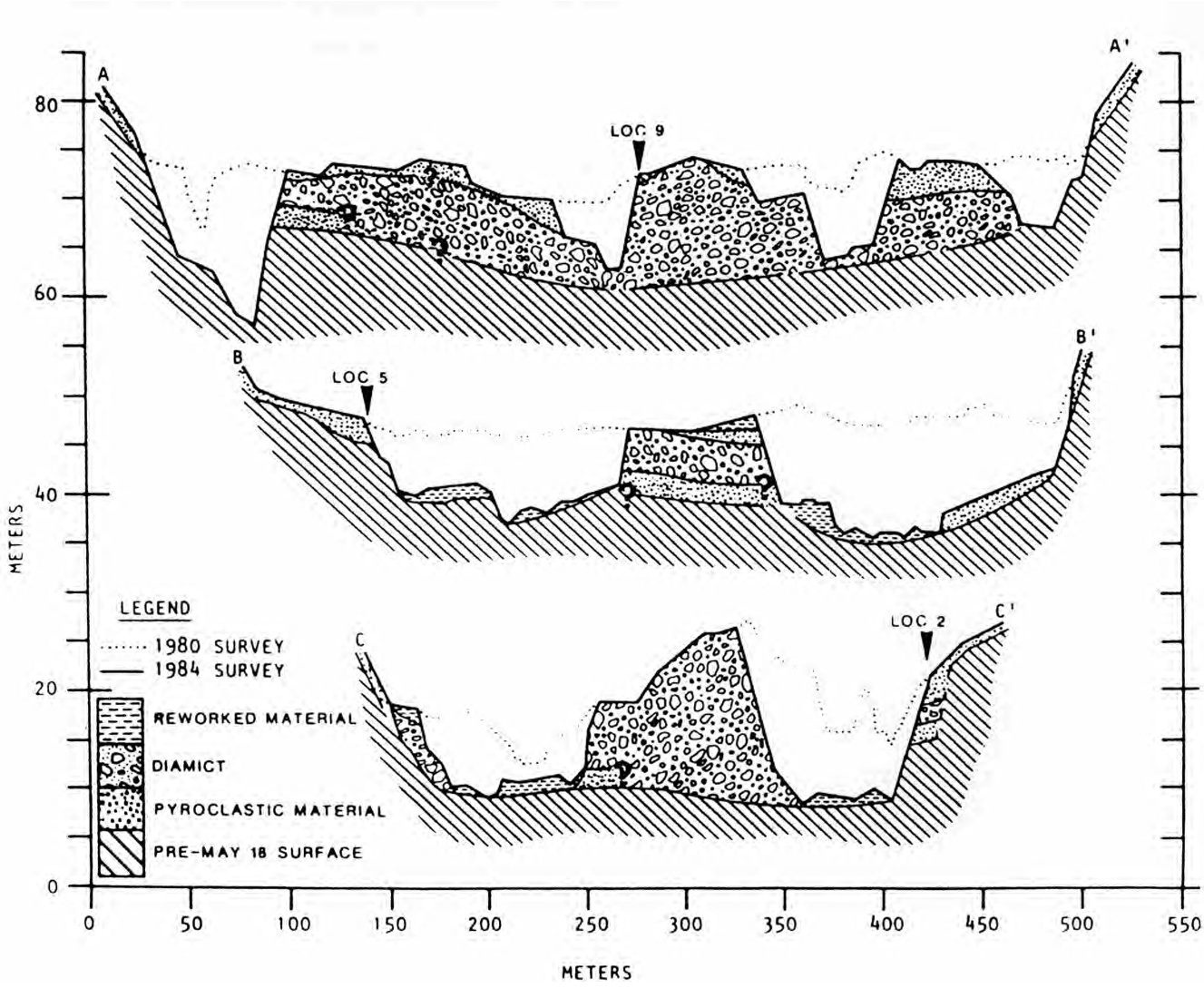

FIGURE 24-Geologic cross sections of valley-fill facies across Smith Creek valley. No altitudinal relation is implied by vertical scale. Cross sections and localities are marked in Fig. 22.

terdigitates with the brown diamict, evidence that parts of the two accumulated together.

Ash-fall bed (A3)

The capping pyroclastic layer A3 is sandy silt thinner than 2 cm that contains accretionary lapilli and sparse granular pumice; it overlies in sharp contact the suite of flow deposits. Eyewitnesses 7 km east of Smith Creek valley testify that this layer began to accumulate 20-30 minutes after the onset of the eruption as wet mud falling from a great cloud expanding overhead. This thin but widespread layer is a marker bed for correlating May 1980 deposits within and beyond Smith Creek valley. Layer A3 is overlain by the pumiceous 18 May tephra-fall unit B.

Lahar deposits

The dominant unit in Smith Creek valley is a massive, poorly sorted diamict as thick as 15 m. Much of the unit has a cohesive, brown, muddy-sand matrix. It contains lithic clasts as large as 2.5 m, juvenile-dacite fragments as large as 50 cm, and fragile blocks of bedded pre-1980 pumice. Twigs to tree trunks 30 m long are scattered through the unit, the logs forming 10% of the deposit. The tough, brown matrix of the deposit, large lithic and tree fragments, and sparse charring of the wood indicate that the diamict was emplaced wet and relatively cool, not as a facies of surge deposit.

Yet within the diamict are irregular pods as large as 4 m of loose granular sand to pebble gravel, richer in juvenile dacite and better sorted than the diamict—material similar to the lower and middle pyroclastic beds. Lithic clasts in the pods are smaller than 40 cm, and juvenile dacite clasts are smaller than 20 cm. The pods are generally fines-poor, clast-supported, and friable; wood fragments are charred. Contacts between the pods and the surrounding diamict range from sharp to gradational.

The composite unit (brown diamict enclosing friable pods) has an irregular hummocky surface with relief as much as 5 m, steep margins and lateral flow levees as high as 8 m, and arcuate, convex-downstream ridges and depressions. The hummocky diamict overlies the lower and middle pyroclastic beds and is overlain by the upper pyroclastic bed.

Grain-size characteristics

Sieved samples of valley-fill deposits (units ***Di*** and ***Up*** of Fig. 25), supplemented by field counting of larger clasts (Brantley and Waitt, 1988), give weakly bimodal grain-size distributions. The coarse and fine peaks of the diamict reflect

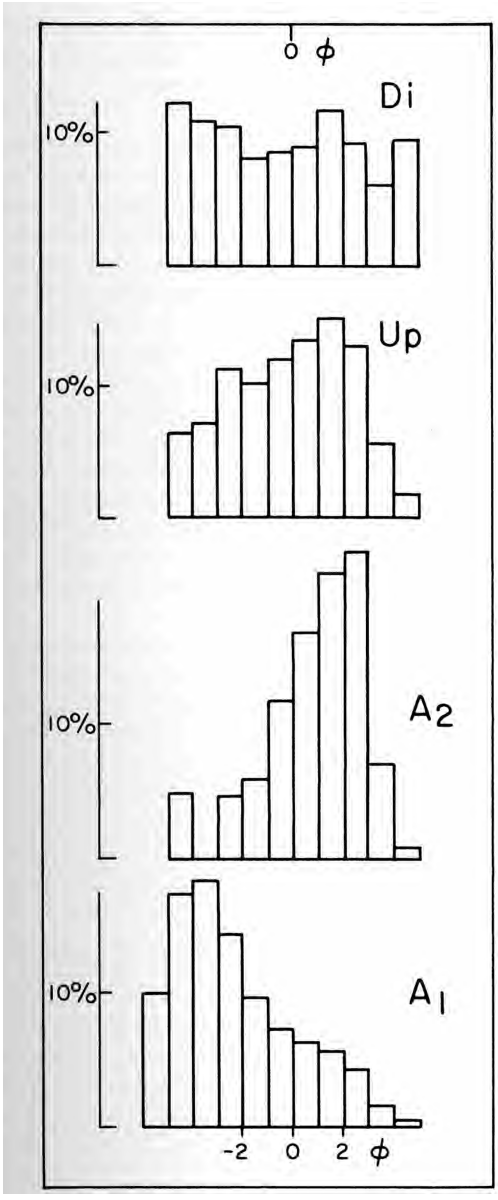

FIGURE 25—Examples of grain-size histograms of Smith Creek deposits. Abscissa is labeled in phi (Φ) grain-size units, ordinate in percent of whole sample. A 1 and A2, layers of ridge-top facies of pyroclastic surge; Up, upper pyroclastic bed of Smith Creek valley-floor deposits; Di, laharic facies of valley-floor diamict.

pre-1980 accidental debris and soil incorporated by lahar. The ridgetop pyroclastic facies consists of a normally graded sequence comprising a coarse population between – 2 and – 4 Φ (layer A 1) and a fine population between 2 and 4 Φ (layer A2). A plot of graphically derived Mz(Φ) vs. weight percent of particles smaller than 4 Φ distinguishes the diamict from the pyroclastic units and shows less fines in the basal bed and layer A 1 than in other pyroclastic and lahar deposits (Brantley and Waitt, 1988, fig. 15A). Mean size plotted against sorting shows that the hummocky diamict is much less sorted than the basal pyroclastic bed (Brantley and Waitt, 1988, fig. 15B). The fact that the upper pyroclastic bed plots between the fields of the lower (A 1) and upper (A2) layers of the ridgetop facies suggests that the upper pyroclastic bed was largely derived from the ridgetop facies.

Genesis and timing of flows

Pyroclastic surge and related flows

The first models of the pyroclastic surge at Mount St. Helens depict a high-velocity turbulent head rich in coarse material and a trailing phase rich in fine material—particle concentration and size decreasing both upward and backward from the surge front (Waitt, 1981; Hoblitt et al. , 1981; Moore and Sisson, 1981). Perhaps heated, expanding air entrained in the turbulent head of the surge winnowed fine material to enrich the trailing part of the flow with fines and to deplete them from the turbulent head that formed the mostly fines-poor basal layer.

Stratigraphy in Smith Creek valley indicates that the surge segregated further. The basal pyroclastic bed in the valley is thought to be equivalent to the ridgetop facies. The middle pyroclastic bed in the valley is thought to be material that quickly settled from the surge on steep slopes and formed dense pyroclastic flows that were channeled to Smith Creek valley.

The upper pyroclastic bed in Smith Creek valley is thought to be a deposit of secondary pyroclastic flows derived from material that the overland surge initially emplaced on steep slopes. Most of the upper pyroclastic bed overlies the hummocky diamict, which formed after the surge and its pyroclastic flows. Most of the upper pyroclastic bed accumulated several minutes after the surge had passed beyond the valley.

The stratigraphic sequence shows that the lahars reached the Smith Creek tributaries only after the tail of the surge passed through the area. The head of the surge crossed Smith Creek valley some two minutes after the earthquake; its body may have persisted a minute longer. Calculated velocities of the lahars suggest that the hummocky diamict probably arrived in lower Smith Creek six to eight minutes after the earthquake. Thus, the upper bed must have been emplaced at least as late as four to five minutes after the pyroclastic surge passed beyond Smith Creek valley—clearly a secondary flow.

Lahars

A lahar may originate at the volcano as a watery flow but becomes a debris flow by engulfing sediment while moving down a valley (Waitt et al. , 1983; Pierson and Scott, 1985; Scott, 1988a). The hummocky diamict in Smith Creek valley is the deposit of a debris flow formed when lahars encountered and mixed with a loose, hot, dry pyroclastic deposit 1-4 m deep. The pyroclastic debris was only partially digested by the lahars as the two poorly mixed materials moved en-masse downstream; this is indicated by the heterogeneous texture of the diamict. High shear stress at the base of the flow allows the basal part to move in laminar flow and carry a plug above it, whose much slower deformation can preserve even unconsolidated blocks.

The lahars that swept off the volcano flanks clearly were related to the pyroclastic surge, but the prime source of water is debated. Scott (1988a) and Pierson (1985) argue that large lahars on the west and southeast flanks of Mount St. Helens resulted when erupted heavy components gravitationally segregated out of a hypothetically wet pyroclastic surge. Yet if the ejected debris had been wet, surge deposits on interfluves and in valleys should have some characteristics typical of " wet" pyroclastic deposits—such as retained fine material, abundant accretionary lapilli, thin

bedding, and plastering on upright objects. Such features are absent from the Mount St. Helens surge deposit.

The lack of layer A2 atop all lahar deposits (Fig. 26) shows that lahars on both the east and west flanks followed the tail of the surge. This stratigraphy and the lack of wet characteristics of surge deposit show that the lahars in Smith Creek tributaries formed separately from the surge. The water must have resulted from melting snow at the base of the hot, turbulent surge rather than from segregation of water erupted with the initial explosions or by turbulently admixed snow (Waitt, in press).

Field guide

From Cispus Center, drive west to USFS road 25 and then south on road 25 to road 99 (big sign). Turn west on road 99 toward Mount St. Helens National Volcanic Monument and Windy Ridge (Fig. 27).

STOP 6-1. Bear Meadows (restrooms). Site of magnificent 18 May eruption photographs by Keith Ronholm and Gary Rosenquist. West of Bear Meadows we enter devastated area. The outer ridge is marked by a fringe of standing scorched trees that retain limbs and branches. In 1980 they retained even the scorched needles. Drive several kilometers southwestward through the downed-timber zone toward the proximal area.

STOP 6-2. Donnybrook Overlook of Spirit Lake. We pause here because lighting on Harrys Ridge is better than on afternoon of Day 4. Inferred from geomorphic and stratigraphic relations, the general sequence of catastrophes at Spirit Lake on morning of 18 May 1980 is:

1. Front of the pyroclastic surge sweeps northeast at roughly 400 km/hr, leveling mature coniferous forest and depositing gravel layer A1.
2. Toe of first landslide enters lake at about 250 km/hr and plows northward along west arm of lake.
3. The landslide suddenly displaces lake water, causing a catastrophic wave that sweeps northward up both arms of lake (trimline rises up both arms) and across middle spur from west to east arm of the lake.
4. The water, having sloshed up both arms of the lake and side valleys, rushes back into the lake, now dammed 60 m higher by landslide mass on the west.
5. Arm of great landslide mass to the west descends Harrys Ridge directly downslope (eastward) into lake basin, perhaps causing a second, but much smaller, displacement of the now-higher lake water.
6. Meanwhile the sustained surge wanes gradually, all the while depositing sandy layer A2.
7. All this excitement lasts perhaps two minutes; ensuring tephra falls occurred between mid-morning and late afternoon.

STOP 6-3. Overview of upper Smith Creek valley and tributaries. The main-valley fill comprises several deposits: (1) ponded primary pyroclastic-surge material, (2) debris flow emplaced as plugflow that incorporated much surge material, (3) secondary lithic pyroclastic flows derived from valley sides and tributaries. The paths taken by meltwater from the east flank of the volcano can be traced by trimlines and levees down tributaries into Smith Creek valley. The floods or lahars and the consequent plugflows on the valley floor must have all together taken several minutes to descend from Plains of Abraham to the valley floor. Therefore, pyroclastic-flow material overlying the debris-flow deposits in the main valley is truly secondary, emplaced at least five minutes after the surge swept overland across the valley. All the pyroclastic and laharic deposits are capped by layer A3, which shows that the entire sequence accumulated and stabilized in less than 30 minutes.

Return along road 99 eastward to concession area. Turn right on road 94 and proceed generally southward for about 9 mi along ridge east of Smith Creek, and then down to Smith Creek valley opposite mouth of Ape Canyon.

It takes several hours to hike up Smith Creek, to visit about eight sites that together summarize the character and stratigraphy of the deposits ponded on the valley floor, and to return. The sequence of inferred processes is integrated in a narrative digest (above) of the report by Brantley and Waitt (1988). The below descriptions of stops are limited to a list of features important to see.

STOP 6-4. Confluence of Ape Canyon and Smith Creek. This area experienced at least three lahars on 18 May 1980. A log jam on the north side of the mouth of Ape Canyon marks the approximate upper limit of the peak lahar that shot down Ape Canyon only a few minutes after the eruption began. If exposures are available, we may see part or all of a three-layer lahar stratigraphy revealing the sequence of floods here:

1. Basal diamict poor in gray dacite, the deposit of the lahar that shot down Ape Canyon.
2. Thick diamict containing much gray dacite, the deposit of a complex lahar that arrived later, having followed a less direct path down Smith Creek valley.
3. Thin, pumice-rich diamict, the deposit of small lahars that swept down Ape Canyon in the afternoon during the height of the magmatic pumiceous eruptions.

The water for each lahar is inferred to be snowmelt caused

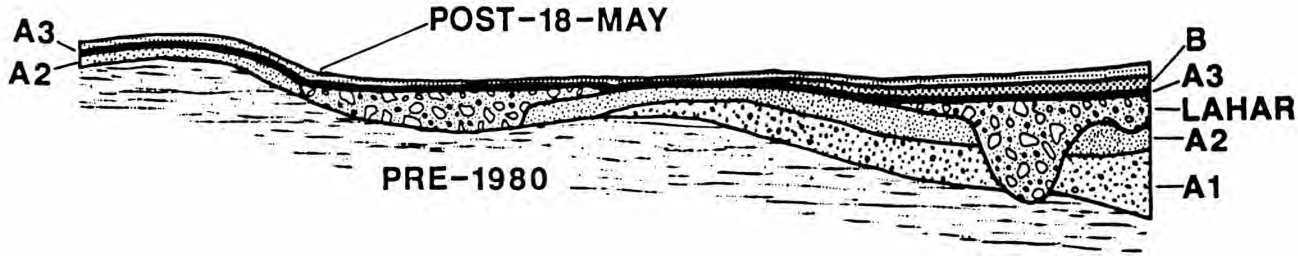

FIGURE 26—Schematic stratigraphy of deposits in headwaters of Smith Creek. Surge unit A 1 and associated pyroclastic-flow deposits lie close to volcano in northeast sector (Waitt, 1981, figs. 259, 262). Ash-fall unit B lies only in northeast-through-east sector (Waitt and Dzurisin, 1981, fig. 358). The post-18 May ash-fall deposit in Smith Creek area is mostly from eruption of 22 July 1980 (Waitt et al., 1981, figs. 366, 371).

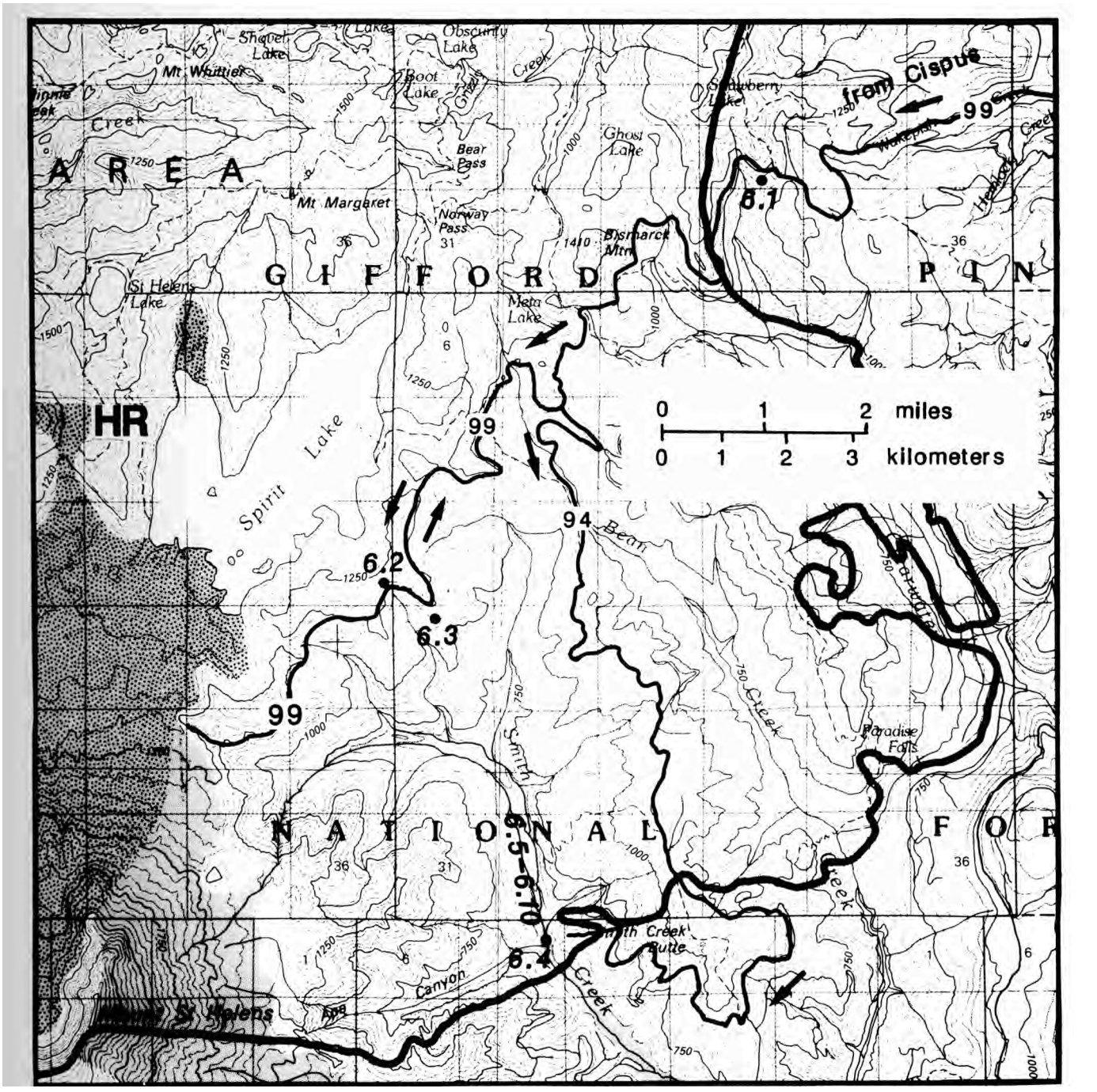

FIGURE 27—Topographic map showing route and stops for Day 6 (in black). Also shown are approximate limit of debris-avalanche deposit (coarse stipple), devastated area (gray line), and laharic floods (light stipple). HR, Harrys Ridge.

by pyroclasts turbulently mixing with surface snow on the upper flanks of the volcano. The first two lahars occurred as a result of the pyroclastic surge (blast) just after 08:32.

STOP 6-5. Wavelike surface of lower end of hummocky diamict and internal character of the deposit.

STOP 6-6A. Hummocky diamict. In center of valley, hummocky diamict at least 8 m thick contains large lithic blocks, numerous huge logs, and fragile blocks of pre-1980 tephra (Brantley and Waitt, 1988, fig. 12).

STOP 6-6B. Stratigraphic section. Along the east side of valley near the margin of the diamict, stratigraphic section over pre-1980 material shows lower and middle pyroclastic beds overlain by the diamict containing wood debris and fragile blocks (Brantley and Waitt, 1988, fig. 10).

STOP 6-6C. Stratigraphic section just up valley from Stop 2B shows diamict overlying pre-1980 surface and overlain by upper pyroclastic bed.

STOP 6-7. Upper pyroclastic bed. Near east side of valley, upper pyroclastic bed overlies hummocky diamict and partly buries its flow levees (Brantley and Waitt, 1988, loc. 3).

STOP 6-8. Internal character of hummocky diamict in center of valley. Muddy, brown, tough-matrix laharic ma-

terial containing large lithic clasts and logs encloses poorly digested pods of incorporated loose pyroclastic material rich in the gray dacite (Brantley and Waitt, 1988, loc. 4).

STOP 6-9. Stratigraphic section. Near west side of valley just outside margin of hummocky diamict, 2.5 m stratigraphic section shows pyroclastic sequence invaded by lahars. Overlying pre-1980 material and soil are the basal and middle pyroclastic beds, capped by the ash falls: lithic layer A3 from mushroom cloud and pumiceous unit B from main vent (Brantley and Waitt, 1988, fig. 9).

STOP 6-10. Stratigraphic section. Cohesive brown-matrix diamict interfingers with several looser layers of middle and (or) upper pyroclastic bed. Sequence shows that pyroclastic flows came off valley sides over a period of time, while diamict was being emplaced.

References

Brantley, S. R., and Waitt, R. B., 1988, Interrelations among pyroclastic surge, pyroclastic flow, and lahars in Smith Creek valley during first minutes of 18 May 1980 eruption of Mount St. Helens, USA: Bulletin of Volcanology, 50: 304–326.

Christiansen, R. L., and Peterson, D. W., 1981, Chronology of the 1980 eruptive activity; *in* Lipman, P. W., and Mullineaux, D. R. (eds.), The 1980 eruptions of Mount St. Helens, Washington: U.S. Geological Survey, Professional Paper 1250: 17–30.

Crandell, D. R., 1971, Postglacial lahars from Mount Rainier volcano, Washington: U.S. Geological Survey, Professional Paper 677: 73 pp.

Crandell, D. R., 1987, Deposits of pre-1980 pyroclastic flows and lahars from Mount St. Helens volcano, Washington: U.S. Geological Survey, Professional Paper 1444: 91 pp.

Criswell, C. W., 1987, Chronology and pyroclastic stratigraphy of the May 18, 1980, eruption of Mount St. Helens, Washington: Journal of Geophysical Research, 92: 10237–10266.

Doukas, M. P. (in press), Road guide to volcanic deposits of Mount St. Helens and vicinity, Washington: U.S. Geological Survey, Bulletin.

Eisele, J. W. et al., 1981, Deaths during 18 May 1980 eruption of Mount St. Helens: New England Journal of Medicine, 305: 931–936.

Endo, E. T., Malone, S. D., Noson, L. L., and Weaver, C. S., 1981, Locations, magnitudes, and statistics of the March 20–May 18 earthquake sequence; *in* Lipman, P. W., and Mullineaux, D. R. (eds.), The 1980 eruptions of Mount St. Helens, Washington: U.S. Geological Survey, Professional Paper 1250: 93–107.

Fisher, R. V., 1983, Flow transformations in sediment gravity flows: Geology, 11: 273–274.

Fisher, R. V., and Schmincke, H.-U., 1984, Pyroclastic rocks. Springer-Verlag, New York, 472 pp.

Fisher, R. V., Glicken, H., and Hoblitt, R. P., 1987, May 18, 1980, Mount St. Helens deposits in South Coldwater Creek, Washington: Journal of Geophysical Research, 92: 10267–10283.

Folk, R. L., 1966, A review of grain-size parameters: Sedimentology, 6: 73–93.

Glicken, H., 1986, Rockslide–debris avalanche of May 18, 1980, Mount St. Helens Volcano, Washington: Unpublished Ph.D. dissertation, University of California at Santa Barbara, 303 pp.

Glicken, H. (in press), Rockslide–debris avalanche of May 18, 1980, Mount St. Helens volcano, Washington: U.S. Geological Survey, Professional Paper 1488: 304 pp.

Glicken, H., and Voight, B. (in press), Geology of the North Fork Toutle River blockages; *in* Schuster, R. L., and Meyer, W. (eds.), Major lakes impounded by the May 18, 1980, eruption of Mount St. Helens, and the stability of their blockages: U.S. Geological Survey, Professional Paper 133.

Glicken, H., Meyer, W., and Sabol, M. A. (in press), Geology and groundwater hydrology of Spirit lake blockage, with implications for lake retention: U.S. Geological Survey, Bulletin 1789: 53 pp.

Greeley, R., and Hyde, J. H., 1972, Lava tubes of the Cave basalt, Mount St. Helens, Washington: Geological Society of America, Bulletin, 83: 2397–2418.

Hoblitt, R. P., 1978, Emplacement mechanisms of unsorted and unstratified deposits of volcanic rock debris as determined from paleomagnetically derived emplacement-temperature information: Unpublished Ph.D. dissertation, University of Colorado, Boulder, 206 pp.

Hoblitt, R. P., and Kellogg, K. S., 1979, Emplacement temperatures of unsorted and unstratified deposits of volcanic rock debris as determined by paleomagnetic techniques: Geological Society of America, Bulletin, 90: 633–642.

Hoblitt, R. P., and Miller, C. D., 1984, Comment on "Mount St. Helens 1980 and Mount Pelee 1902—flow or surge?": Geology, 12: 692–693.

Hoblitt, R. P., Crandell, D. R., and Mullineaux, D. R., 1980, Mount St. Helens eruptive behavior during the past 1,500 yr.: Geology, 8: 555–559.

Hoblitt, R. P., Miller, D. C., and Vallance, J. W., 1981, Origin and stratigraphy of the deposit produced by the May 18 directed blast; *in* Lipman, P. W., and Mullineaux, D. R. (eds.), The 1980 eruptions of Mount St. Helens, Washington: U.S. Geological Survey, Professional Paper 1250: 401–419.

Hyde, J. H., 1970, Geologic setting of Merrill Lake and evaluation of volcanic hazards in the Kalama River Valley near Mount St. Helens, Washington: U.S. Geological Survey, Open-File Report, 17 pp.

Hyde, J. H., 1975, Upper Pleistocene pyroclastic-flow deposits and lahars south of Mount St. Helens volcano, Washington: U.S. Geological Survey, Bulletin 1383-B: 20 pp.

Janda, R. J., Scott, K. M., Nolan, K. M., and Martinson, H. A., 1981, Lahar movement, effects and deposits; *in* Lipman, P. W., and Mullineaux, D. R. (eds.), The 1980 eruptions of Mount St. Helens, Washington: U.S. Geological Survey, Professional Paper 1250: 461–478.

Kanamori, H., Given, J. W., and Lay, T., 1984, Analysis of seismic body waves excited by the Mount St. Helens Eruption of May 18, 1980: Journal of Geophysical Research, 89: 1856–1866.

Kuntz, M. A., Rowley, P. D., MacLeod, N. S., Reynolds, R. L., McBroome, L. A., Kaplan, A. M., and Dike, D. J., 1981, Petrography and particle-size distribution of pyroclastic-flow, ash-cloud and surge deposits; *in* Lipman, P. W., and Mullineaux, D. R. (eds.), The 1980 eruptions of Mount St. Helens, Washington: U.S. Geological Survey, Professional Paper 1250: 525–540.

Lipman, P. W., Moore, J. G., and Swanson, D. A., 1981a, Bulging of the north flank before the May 18 eruption—geodetic data; *in* Lipman, P. W., and Mullineaux, D. R. (eds.), The 1980 eruptions of Mount St. Helens: Washington, U.S. Geological Survey, Professional Paper 1250: 143–155.

Lipman, P. W., Norton, D. R., Taggart, J. E., Brandt, E. L., and Engleman, E. E., 1981b, Compositional variations in 1980 magmatic deposits; *in* Lipman, P. W., and Mullineaux, D. R. (eds.), The 1980 eruptions of Mount St. Helens, Washington: U.S. Geological Survey, Professional Paper 1250: 631–640.

Manson, C. J., Messick, C. H., and Sinnott, G. M., 1987, Mount St. Helens—a bibliography of geoscience literature, 1882–1986: U.S. Geological Survey, Open-File Report 87-292: 205 pp.

Meyer, W., Sabol, M. A., and Schuster, R. L., 1986, Landslide dammed lakes at Mount St. Helens, Washington; *in* Schuster, R. L. (ed.), Landslide dams—processes, risk, and mitigation: American Society of Civil Engineers, Geotechnical Special Publication 3: 21–41.

Middleton, G. V., and Hampton, M. A., 1976, Subaqueous sediment

transport and deposition by sediment gravity flows; *in* Stanley, D. J., and Swift, D. P. (eds.), Marine sediment transport and environmental management: Wiley & Sons, New York, 197–218.

Moore, J. G., and Albee, W. C., 1981, Topographic and structural changes, March–July 1980—photogrammetric data; *in* Lipman, P. W., and Mullineaux, D. R. (eds.), The 1980 eruptions of Mount St. Helens, Washington: U.S. Geological Survey, Professional Paper 1250: 123–134.

Moore, J. G., and Rice, C. J., 1984, Chronology and character of the May 18, 1980 explosive eruptions of Mount St. Helens; *in* Explosive volcanism—inception, evolution, and hazards: National Academy Press, Washington, D.C., p. 133–142.

Moore, J. G., and Sisson, T. W., 1981, Deposits and effects of the May 18 pyroclastic surge; *in* Lipman, P. W., and Mullineaux, D. R. (eds.), The 1980 eruptions of Mount St. Helens, Washington: U.S. Geological Survey, Professional Paper 1250: 421–438.

Mullineaux, D. R., 1986, Summary of pre-1980 tephra-fall deposits erupted from Mount St. Helens, Washington State, USA: Bulletin of Volcanology, 48: 17–26.

Mullineaux, D. R., and Crandell, D. R., 1962, Recent lahars from Mount St. Helens, Washington: Geological Society of America, Bulletin, 73: 855–870.

Mullineaux, D. R., and Crandell, D. R., 1981, The eruptive history of Mount St. Helens; *in* Lipman, P. W., and Mullineaux, D. R. (eds.), The 1980 eruptions of Mount St. Helens, Washington: U.S. Geological Survey, Professional Paper 1250: 3–15.

Newhall, C. G., 1982, A prehistoric debris avalanche from Mount St. Helens (abs): American Geophysical Union, Transactions, 63: 1141.

Pallister, J. S., and Hoblitt, R. P., 1985, Magma mixing at Mount St. Helens (abs): American Geophysical Union Transactions, 66: 1111.

Pierson, T. C., 1985, Initiation and flow behavior of the 1980 Pine Creek and Muddy River lahars, Mount St. Helens, Washington: Geological Society of America, Bulletin, 96: 1056–1069.

Pierson, T. C., and Scott, K. M., 1985, Downstream dilution of a lahar—transition from debris flow to hyperconcentrated streamflow: Water Resource Research, 21: 1511–1524.

Rosembaum, J. G., and Waitt, R. B., 1981, Summary of eyewitness accounts of 18 May eruption; *in* Lipman, P. W., and Mullineaux, D. R. (eds.), The 1980 eruptions of Mount St. Helens, Washington: U.S. Geological Survey, Professional Paper 1250: 53–67.

Rowley, P. D., Kuntz, M. A., and MacLeod, N. S., 1981, Pyroclastic-flow deposits; *in* Lipman, P. W., and Mullineaux, D. R. (eds.), The 1980 eruptions of Mount St. Helens, Washington: U.S. Geological Survey, Professional Paper 1250: 489–512.

Rowley, P. D., MacLeod, N. S., Kuntz, M. A., and Kaplan, A. M., 1985, Proximal bedded deposits related to pyroclastic flows of May 18, 1980, Mount St. Helens, Washington: Geological Society of America, Bulletin, 96: 1373–1383.

Scott, K. M., 1988a, Origins, behavior, and sedimentology of lahars and lahar-runout flows in the Toutle–Cowlitz River system, Mount St. Helens, Washington: U.S. Geological Survey, Professional Paper 1447-A: 74 pp.

Scott, K. M., 1988b, Origin, behavior, and sedimentology of prehistoric lahars at Mount St. Helens, Washington; *in* Clifton, H. E. (ed.), Sedimentologic consequences of convulsive geologic events: Geological Society of America, Special Paper 229: 23–36.

Siebert, L., Glicken, H., and Ui, T., 1987, Volcanic hazards of Bezymianny- and Bandai-type eruptions: Bulletin of Volcanology, 49: 435–459.

Sparks, R. S. J., Self, S., and Walker, G. P. L., 1973, Products of ignimbrite eruptions: Geology, 1: 257–274.

Sparks, R. S. J., Moore, J. G., and Rice, C. J., 1986, The initial giant umbrella cloud of the May 18th, 1980, explosive eruption of Mount St. Helens: Journal of Volcanology and Geothermal Research, 28: 257–274.

U.S. Army Corps of Engineers, 1984, Alternative strategies for a permanent outlet for Spirit Lake near Mount St. Helens, Washington; final environmental impact statement: U.S. Army Corps of Engineers, Portland, Oregon.

Varnes, D. J., 1978, Slope movement types and processes; *in* Schuster, R. L., and Krizek, R. J. (eds.), Landslides—analysis and control: Transportation Research Board, Special Report 176: 11–35.

Voight, B., 1981, Time scale for the first moments of the May 18 eruption; *in* Lipman, P. W., and Mullineaux, D. R. (eds.), The 1980 eruptions of Mount St. Helens, Washington: U.S. Geological Society, Professional Paper 1250: 69–86.

Voight, B., Glicken, H., Janda, R. J., and Douglass, P. M., 1981, Catastrophic rockslide avalanche of May 18; *in* Lipman, P. W., and Mullineaux, D. R. (eds.), The 1980 eruptions of Mount St. Helens, Washington: U.S. Geological Survey, Professional Paper 1250: 347–377.

Voight, B., Janda, R. J., Glicken, H., and Douglass, P. M., 1983, Nature and mechanics of the Mount St. Helens rockslide–avalanche of 18 May 1980: Geotechnique, 33: 243–273.

Waitt, R. B., 1981, Devastating pyroclastic density flow and attendant air fall of May 18—stratigraphy and sedimentology of deposits; *in* Lipman, P. W., and Mullineaux, D. R. (eds.), The 1980 eruptions of Mount St. Helens, Washington: U.S. Geological Survey, Professional Paper 1250: 439–458.

Waitt, R. B., 1984, Comment of "Mount St. Helens 1980 and Mount Pelee 1902—flow or surge?": Geology, 12: 693.

Waitt, R. B. (in press), Swift snowmelt and floods (lahars) caused by great pyroclastic surge at Mount St. Helens volcano, Washington, 18 May 1980: Bulletin of Volcanology, 51.

Waitt, R. B. (unpubl. report), Timed stratigraphic relations between air-fall and flow deposits of the 18 May 1980 eruption: Intended for U.S. Geological Survey, Paper 1251.

Waitt, R. B., and Dzurisin, D., 1981, Proximal air-fall deposits from May 18 eruption—stratigraphy and field sedimentology; *in* Lipman, P. W., and Mullineaux, D. R. (eds.), The 1980 eruptions of Mount St. Helens, Washington: U.S. Geological Survey, Professional Paper 1250: 601–616.

Waitt, R. B., Hansen, V. L., Sarna-Wojcicki, A. M., and Wood, S. M., 1981, Proximal air-fall deposits of eruptions between May 24 and August 7, 1980—stratigraphy and field sedimentology; *in* Lipman, P. W., and Mullineaux, D. R. (eds.), The 1980 eruptions of Mount St. Helens, Washington: U.S. Geological Survey, Professional Paper 1250: 617–628.

Waitt, R. B., Pierson, T. C., MacLeod, N. S., Janda, R. J., Voight, B., and Holcomb, R. T., 1983, Eruption-triggered avalanche, flood and lahar at Mount St. Helens—effects of winter snowpack: Science, 221: 1394–1397.

Walker, G. P. L., and McBroome, L. A., 1983, Mount St. Helens 1980 and Mount Pelee 1902—flow or surge?: Geology, 11: 571–574.

Walker, G. P. L., and Morgan, L. A., 1984, Reply to "Mount St. Helens 1980 and Mount Pelee 1902—flow or surge?": Geology, 12: 693–695.

Wohletz, K. H., and Sheridan, M. F., 1979, A model of pyroclastic surge: Geological Society of America, Special Paper 180: 177–193.

Yamaguchi, D. K., 1983, New tree-ring dates for recent eruptions of Mount St. Helens: Quaternary Research, 20: 246–250.

Yamaguchi, D. K., 1986, Interpretation of cross correlation between tree-ring series: Tree-Ring Bulletin, 46: 47–54.

Youd, T. L., Wilson, R. C., and Schuster, R. L., 1981, Stability of blockage in North Fork Toutle River; *in* Lipman, P. W., and Mullineaux, D. R. (eds.), The 1980 eruptions of Mount St. Helens, Washington: U.S. Geological Survey, Professional Paper 1250: 821–828.

EXCURSION 3A:

Eocene through Miocene volcanism in the Great Basin of the western United States

Myron G. Best[1], Eric H. Christiansen[1], Alan L. Deino[2], C. Sherman Grommé[3], Edwin H. McKee[3], and Donald C. Noble[4]

[1]Brigham Young University, Provo, Utah 84602; [2]Berkeley Geochronology Center, Berkeley, California 94709; [3]U.S. Geological Survey, Menlo Park, California 94025; [4]University of Nevada, Reno, Nevada 89557

Introduction

Cenozoic magmatic rocks in the western United States define a complex space—time—composition pattern that for many years has posed numerous interpretive challenges. One of the more intriguing tectonomagmatic provinces is the northwestern segment of the Basin and Range province in Nevada, western Utah, and minor adjacent parts of Oregon, Idaho, and California. This segment, characterized for the most part by internal drainage, is called the Great Basin (Fig. 1). This paper summarizes characteristics of volcanic rocks in the Great Basin, primarily ash-flow tuff and subordinate lava, which were deposited from Eocene through Miocene time. Although widespread younger volcanic deposits exist, their volume is much less and they are not considered here. Only a few general and preliminary interpretations of our observations are presented.

The support of the National Science Foundation through Grant EAR-8604195 to M. G. Best is gratefully acknowledged.

Contributions of several geologists have provided the basis for study of volcanic rocks in the Great Basin. Howell Williams in the 1950's (unpublished reconnaissance) first realized that many of the volcanic rocks are ash-flow deposits. J. Hoover Mackin (1960) recognized the extensive nature of the ash-flow sheets, gave stratigraphic names to some, and emphasized their usefulness as "instantaneous" time horizons to better understand basin and range structure. Paul L. Williams (1960) and Earl F. Cook (1965), students of Mackin, used petrographic properties, especially phenocryst proportions, as well as stratigraphic position, to correlate extensive ash-flow sheets in the eastern Great Basin. Cook named units, recognized the southward transgression in time of their sources, and realized that the volcanism occurred over a brief interval of geologic time. He grappled with the significance of the basal Cenozoic unconformity, and concluded that basin and range topography originated after deposition of the tuffs.

Geologists of the U.S. Geological Survey, beginning with the Nevada Test Site project in the early and middle 1960's, mapped individual ash-flow sheets over thousands of square kilometers in the south-central and western Great Basin and identified many of their sources. These investigations demonstrated the feasibility of systematic geologic mapping of ash-flow terranes and the utilization of such data for recognizing volcanic centers and working out the history of volcanic fields.

The magmatic and tectonic development of the Great Basin during Cenozoic time was the focus of a number of papers in the late 1960's and early 1970's based on the body of chemical, petrologic, and radiometric-age data then available. This information was used by Armstrong et al. (1969) and McKee et al. (1970) to define patterns in age and rock distribution. Models of tectonic evolution were developed by McKee (1971), Christiansen and Lipman (1972), Lipman et al. (1972), and Noble (1972). A landmark paper by Atwater (1970) showed that early Tertiary plate convergence along the southwestern margin of North America has been supplanted since sometime in the Oligocene by transform motion on the San Andreas system; this transform motion began just south of the U.S.—Mexico border and has now migrated to just north of San Francisco (Fig. 2). Numerous later publications have refined, summarized, and/or reviewed the information in these early papers, but have not fundamentally changed the original concepts.

Despite these past efforts, research on volcanic deposits in the Great Basin is still in its infancy, in comparison to volcanic fields such as the San Juan field of Colorado. This is in part because of the vast area and enormous volume of volcanic rock in the Great Basin (Table 1). Although the entire region is covered by county, state, or other geologic maps at a scale of 1:250,000, generalization of rock units hampers their usefulness for structural, stratigraphic, and petrologic interpretations, such as delineation of source calderas and associated outflow-tuff sheets. Less than half of

TABLE 1—Comparison of major Tertiary volcanic fields in western North America that contain significant volumes of ash-flow deposits (Lipman, 1975; Steven and Lipman, 1976; Steven et al., 1984; Ratté et al., 1984; Stewart and Carlson, 1976; Swanson and McDowell, 1984). See Fig. 2.

		Intermediate lava		Silicic tuff		
Volcanic field	Area (10^3 km^3)	Inception of major activity (Ma)	Approximate volume (10^3 km^3)	Period of major activity (Ma)	Approximate volume (10^3 km^3)	Number of calderas
Great Basin	360*	40	?5?	33-20	50?	50 ±
Marysvale	10	30	7	27-23	<1	4
San Juan	25	35	50	29-27	10	15
Mogollon–Datil	25	40	?	29-27	10	10?
Sierra Madre Occidental	300	42	?	Oligocene	?300?	?350?

the region is covered by larger-scale maps (1:62,500 or greater) that show individual formations. Relatively few detailed petrologic investigations of individual ash-flow sheets and their magma systems have been published.

Regional geologic setting

Building on earlier publications, Lipman (1980), Stewart (1983), Elston (1984), Chadwick (1985), and Wernicke et al. (1987) addressed the late Mesozoic and Cenozoic tectonomagmatic evolution of the western United States. Fundamental elements of this evolution include Cretaceous (and locally latest Jurassic) to early Eocene east—west crustal shortening and granitic plutonism. This was followed by east—west crustal extension and widespread, locally voluminous high-K subalkaline volcanism that shifted in many places to bimodal basalt—rhyolite activity since about middle Miocene time.

In the region that now forms the Great Basin and surrounding areas, volcanism began in the north in the Eocene about 43 Ma (Armstrong et al. , 1969) and swept southward along an arcuate, roughly east—west front into southern Nevada (McKee, 1971; McKee and Silberman, 1975; Noble et al. , 1976) by Miocene time (Fig. 2). Accompanying this transgressive volcanism was a southward-moving wave of east—west to northwest—southeast crustal extension, which, though imperfectly defined, is expressed in detachment-fault terranes and metamorphic core complexes. Locally, hundreds of percent extension have been documented (e.g., Wernicke et al. , 1987; Gans et al. , submitted; Taylor et al. , 1987; Wust, 1986). South of the region of southward migrating volcanism is an east—west amagmatic corridor where there has been sparse Phanerozoic magmatism. This corridor effectively separates the Great Basin from the southern Basin and Range province where *northward-sweeping* volcanism

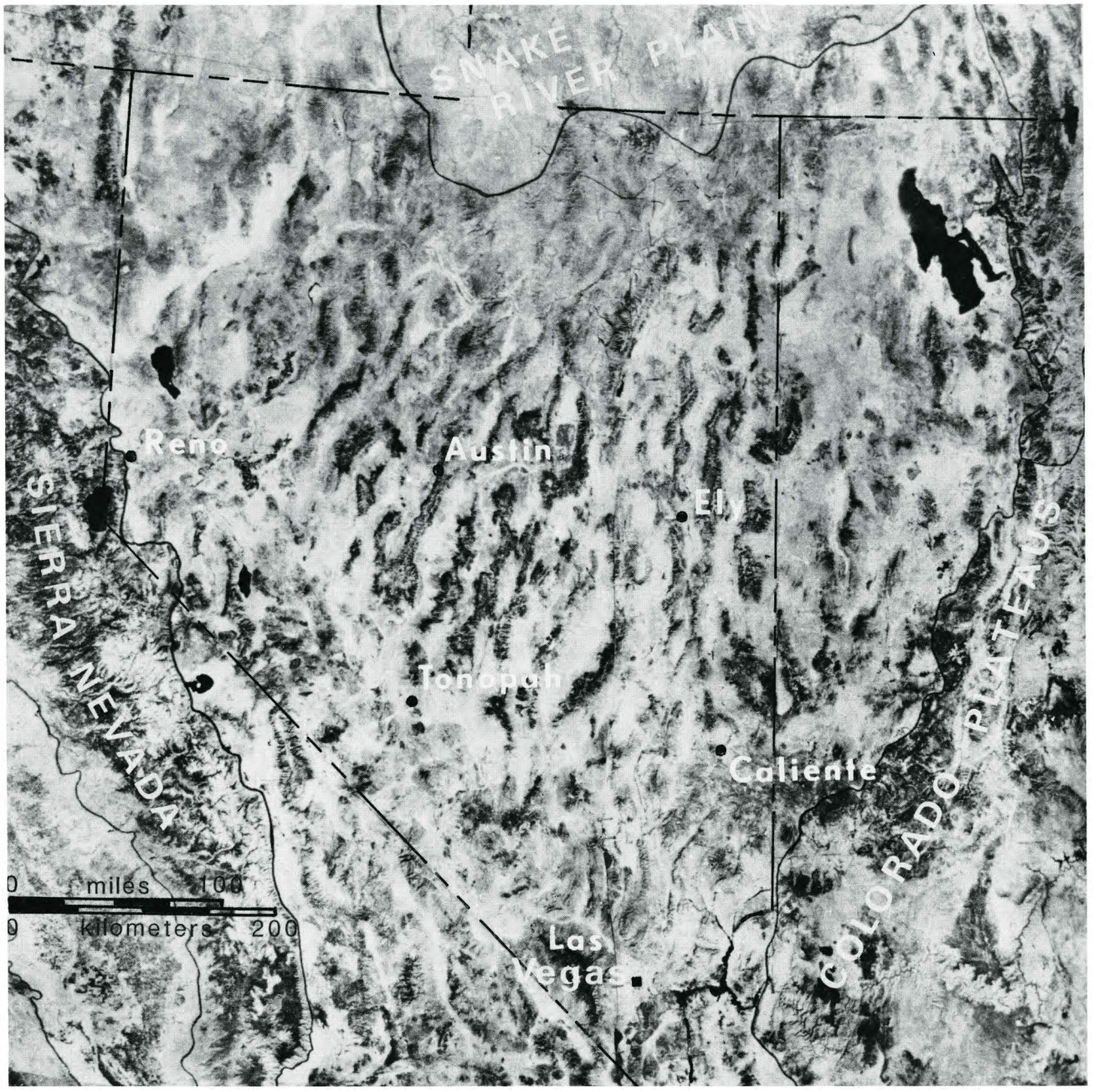

FIGURE 1—Composite satellite image of the Great Basin that approximately covers the northwestern part of the Basin and Range province, bounded on the west by the Sierra Nevada and on the east by the Colorado Plateaus. The state of Nevada is shown by dashed line.

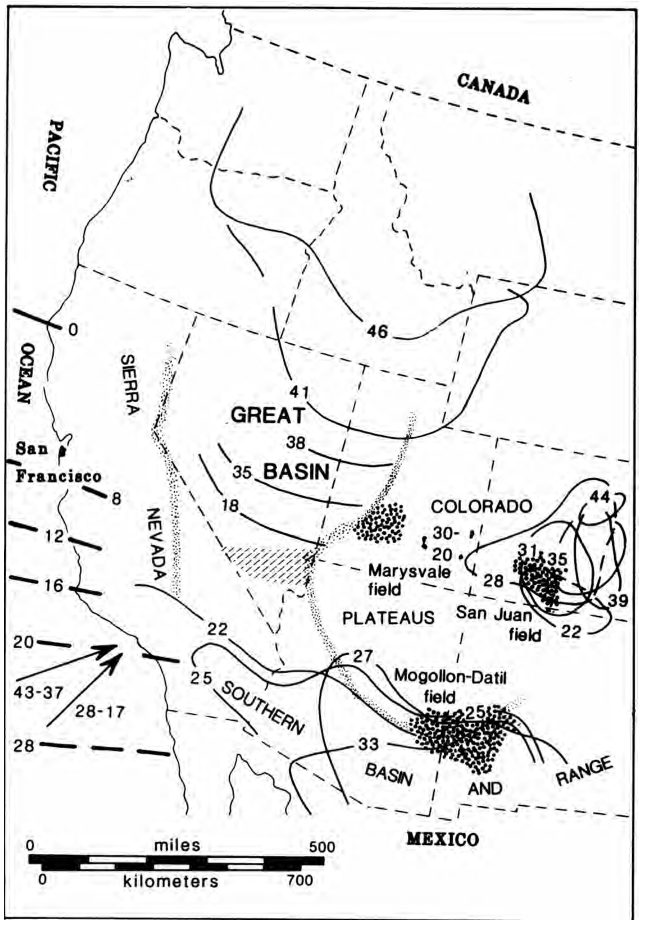

FIGURE 2—Pattern of Eocene–Miocene volcanism in the Great Basin, flanking Sierra Nevada and Colorado Plateaus (delineated by fine stippling), and southern Basin and Range province. Solid lines are isochrons (in Ma) showing transgressive sweep of volcanism (isochrons labeled 38, 35, and 18 in Great Basin are from this study and indicate most southerly progress of activity at the given time; other isochrons from Cross and Pilger, 1978; cf. Noble, 1972; Armstrong, 1975; Stewart and Carlson, 1976; Burke and McKee, 1979; Nilsen and McKee, 1979; Lipman, 1980). A more regular southward time transgression in Colorado than shown here is indicated by Lipman (1987). After 17 Ma, volcanism flourished in the northern, western, and southern Great Basin, but to a lesser degree in the eastern part (see Fig. 4). Coarse stippling shows locations of major volcanic fields outside the Great Basin. Laccoliths of felsic rocks of transitional to alkaline compositions (solid black) in the Colorado Plateaus have recently been shown to range in age from 30 to 20 Ma (Sullivan, 1987). Arrows off southern California coast indicate direction of motion of converging oceanic plate relative to North American plate at 43-37 and 28-17 Ma, and heavy dashed lines are approximate locations of Mendocino Fracture Zone at indicated times in Ma (Engebretson et al., 1985). Amagmatic corridor shown by diagonal ruling is from the Geologic Map of the United States.

and crustal extension occurred during the same period of time (Fig. 2) as the south-sweeping activity in the Great Basin (Glazner and Bartley, 1984).

Magmatism in the Great Basin and surrounding areas during Tertiary time at the present level of erosion is expressed dominantly in volcanic deposits; only small exposures of granitic rock occur. Until the early Miocene, about 25 Ma, volcanism produced dominantly andesitic to dacitic lava and breccia flows and dacite to rhyolite ash-flow tuffs (McKee et al. , 1970; McKee and Silberman, 1975). During the next eight million years eruption rates decreased, dacitic ash-flow eruptions waned, and a broader compositional spectrum appears in the volcanic record. Basaltic volcanism began after the middle Miocene, about 17 Ma, and has been a significant aspect of Great Basin activity since about 12 Ma, particularly along the eastern and western margins of the region but also locally in the center (Best and Hamblin, 1978; McKee and Noble, 1986). Many silicic tuffs and lavas younger than about 17 Ma are peralkaline or topaz-bearing (Noble and Parker, 1975; Christiansen et al. , 1986). After the middle Miocene, the general east—west orientation of magmatic zones changed to north—south (Best et al. , 1980; Stewart, 1983), probably reflecting a fundamental change in the state of stress in the lithosphere (Best, 1988a).

Since the middle Miocene, crustal extension affected a larger area (Anderson and Ekren, 1968; Armstrong et al. , 1969; Scholz et al., 1971; Proffett, 1977; McKee and Noble, 1986; Wernicke et al. , 1987), forming what has conventionally been called the Basin and Range province of western North America. The existence of early Miocene ash-flow sheets derived from sources within the Great Basin in the flanking, generally topographically higher Colorado Plateaus and Sierra Nevada (Figs. 1, 2) proves uplift and tectonic differentiation of these two provinces did not begin until some time later (Rowley et al. , 1978; Deino, 1985). Thus, considerations of at least pre-Miocene volcanism of the Great Basin should include deposits in the Marysvale field on the western Colorado Plateaus. There is, however, no documented pre-Miocene volcanism in the Sierra Nevada.

In the Great Basin, middle Tertiary volcanic rocks were almost everywhere deposited on a clean erosion surface of subdued relief carved into Paleozoic and Mesozoic rocks (McKee, 1988). Only locally are pre-volcanic fluvial and lacustrine deposits found above this profound unconformity (McKee et al. , 1970; McKee and Silberman, 1975; Nilsen and McKee, 1979). The most widespared of these is the Paleocene—Eocene Sheep Pass Formation, a clastic unit that crops out over an area of only 4100 km^2 in east-central Nevada, but is locally as thick as 1 km. Not only are Tertiary sedimentary rocks highly localized beneath the volcanic deposits, but they are virtually nonexistent within the volcanic sequence before about 20 Ma (McKee et al. , 1970; McKee and Noble, 1974). Water-laid tuffaceous rocks occur locally, but in many ranges the entire volcanic section consists only of ash-flow sheets and minimal amounts (probably on the order of a few percent) of associated air-fall and surge deposits.

Lava flows

Cenozoic lavas are widely scattered throughout the Great Basin (Figs. 3, 4), but for the most part appear to have been erupted in relatively small volumes, on the order of about 10% of the total volume of Cenozoic volcanic rock. Typically, lavas occur as isolated domes and flows within a sequence of ash-flow deposits (see, for example, Ekren et al. , 1971, 1977; Quinlivan et al., 1974; Willis et al., 1987). In contrast to the more or less contemporaneous San Juan volcanic field in Colorado, for example, large constructional volcanoes and associated volcanic debris flows (lahars) are absent in most Great Basin eruptive centers (Table 1). Debris flows are widespread, however, on the eastern (Steven et al. , 1984) and western (Slemmons, 1966) margins of the Great Basin.

Lavas range widely in composition from rhyolite to basalt (Fig. 5). Most are calc-alkaline, but some show tholeiitic affinities on Fe—Mg diagrams; virtually all are more potassic (K_2O>Na_2O) than common "orogenic" volcanic rocks

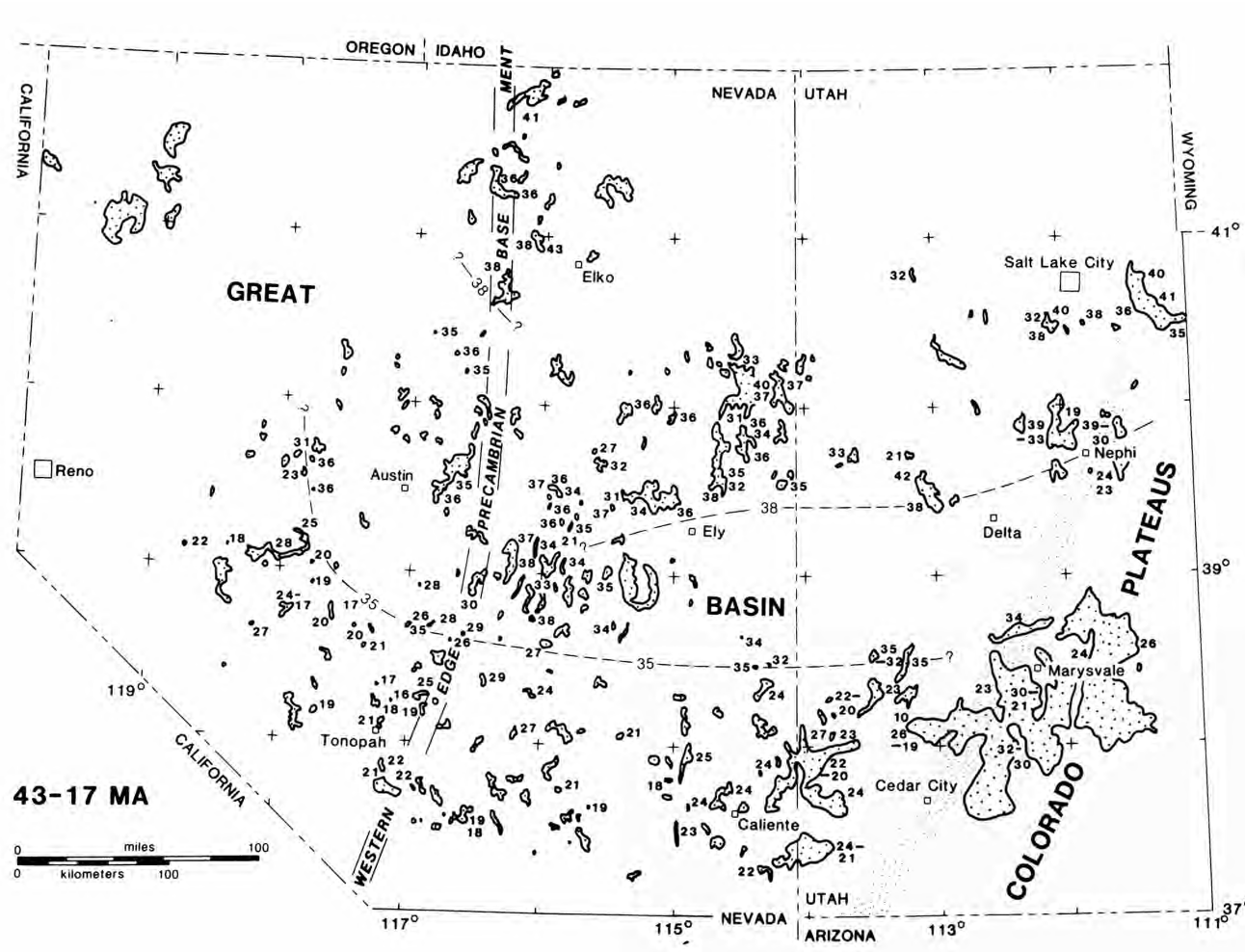

FIGURE 3—Pre-17 Ma Tertiary lava flows in the Great Basin and adjoining Colorado Plateaus (after Hintze, 1975; Stewart and Carlson, 1976). Ages in Ma from many published sources and unpublished data of E. H. McKee and B. J. Kowallis. Southern and western limits of 38 and 35 Ma lava flows shown by dashed lines. Western edge of Precambrian basement is based upon Nd-isotopic data (Farmer and DePaolo, 1983). See also Figs. 2, 4, 8.

worldwide (cf. Gill, 1981; Ewart, 1982). Pb-, Sr-, Nd-, and O-isotope ratios show the presence of both crustal and mantle components (Zartman, 1974; C. E. Hedge and D. C. Noble, unpubl. data 1969-1973; Grunder et al. , 1987; Gans et al. , submitted). Additional petrochemical features are time-dependent and will be discussed in the time—composition section.

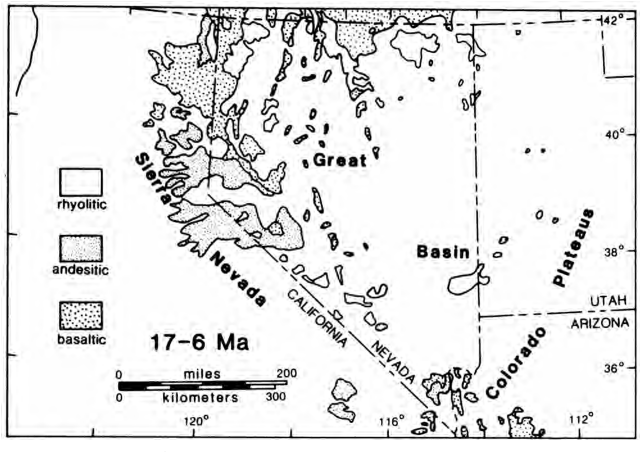

FIGURE 4—Lava flows 17-6 Ma in the Great Basin (Stewart and Carlson, 1976). See also Fig. 3.

Ash-flow deposits

Tertiary volcanic rocks in the Great Basin are dominantly silicic ash-flow tuff. Several tens of thousands of cubic kilometers of pyroclastic material represented in more than one hundred ash-flow sheets were erupted chiefly during the late Oligocene and early Miocene 33-20 Ma from more than 50 caldera centers. In single mountain ranges in southeastern Nevada, sequences of 6-10 cooling units are commonly exposed, and locally as many as 16; thicknesses range to about 2 km. In central and western Nevada, ash-flow sequences typically consist of fewer units, but as much as 4 km of tuff is found within calderas.

All of the zonal variations in ash-flow deposits described by Smith (1960) have been recognized in Great Basin sheets. Zones of hydrated glass ranging from non-welded to densely welded (vitrophyre) are common near the base of cooling units. In the devitrified zone, elimination of glass is generally complete, although in a few cases collapsed pumice remains glassy in a matrix of devitrified welded shards. Lithophysae are uncommon, even in densely welded crystal-poor rhyolitic tuff; exceptions include the upper cooling unit of the lower Miocene Bates Mountain Tuff and the possibly equivalent Nine Hill Tuff. Many deposits of densely welded, devitrified, crystal-poor rhyolite tuff have closely spaced fractures that result in disaggregation into popcorn-size gnus.

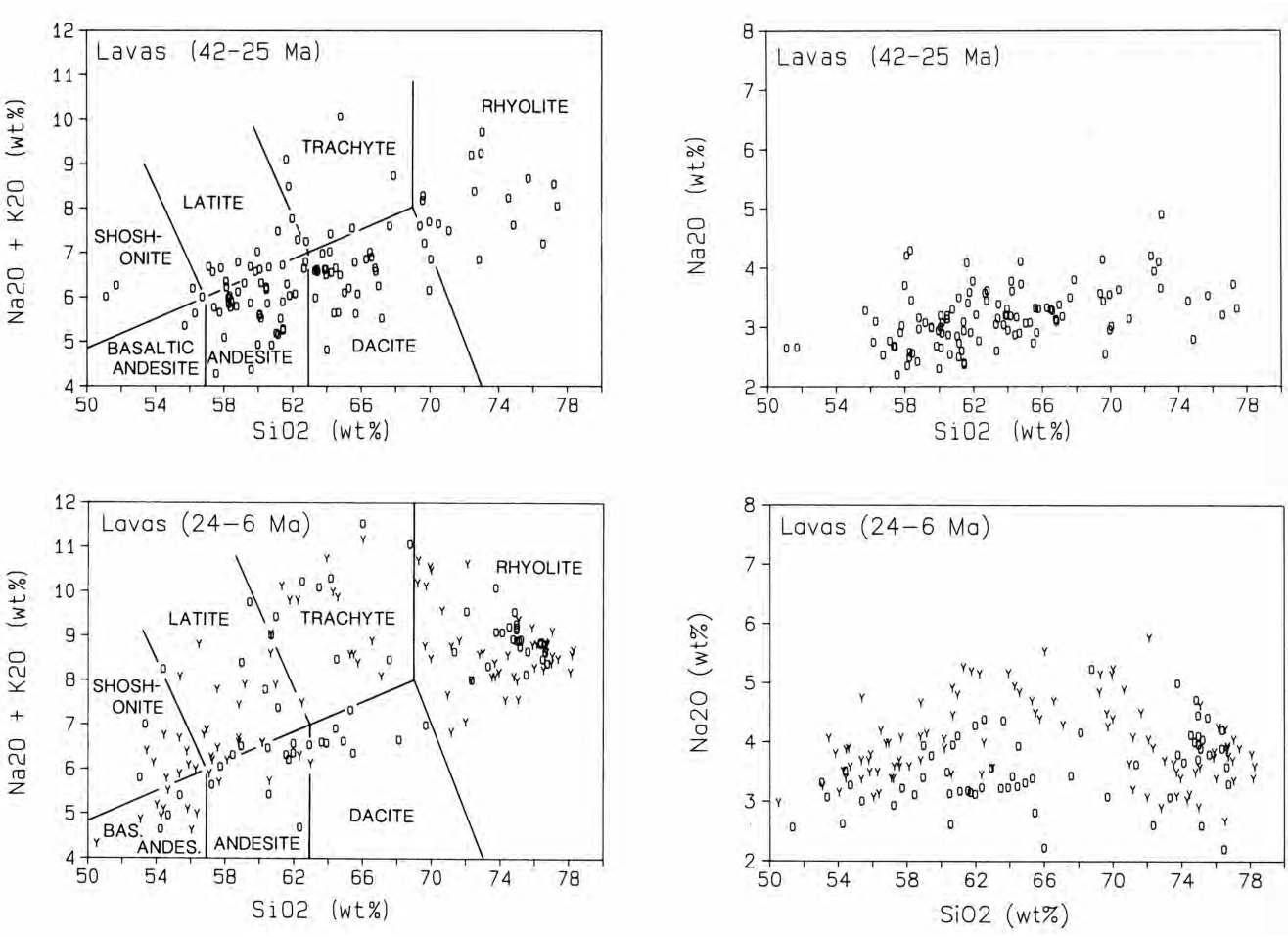

FIGURE 5—Variation diagrams and IUGS classification (Le Bas et al. , 1986) of late Eocene through Oligocene (42-25 Ma) and Miocene (24-6 Ma) lavas in the Great Basin. O, older 24-18 Ma lavas; Y, younger 17-6 Ma lavas. Data from our unpublished analyses and from many published sources which mostly provide only limited age data.

In some places, ash-flow sheets have experienced rheomorphic flow after deposition on sloping surfaces.

Dimensional aspects

For convenience, in the following discussion ash-flow sheets are arbitrarily classified in terms of volume (km^3): small <10, medium 10-100, large 100-1000, very large >1000. Although small and medium sheets occur in the Great Basin, regional studies of many sequences of ash-flow tuff demonstrate that most are large to very large.

Regionally extensive ash-flow sheets are commonly exposed in two or more ranges east to west, and some span half of the Great Basin and have a present areal extent of more than 40,000 km^2. East—west crustal extension of 50(?)% (Best, 1988b) since deposition of most sheets has of course extended their areal distribution; this is reflected in the fact that most known markedly nonequant distributions surrounding sources are elongate in the east—west direction. However, some ash-flow sequences (e.g., the Quichapa Group of southeastern Nevada and southwestern Utah) derived from a nearly common source area comprise alternating sheets of equant and east—west elongate distributions, suggesting that eruption dynamics and paleotopography, dictated by faulting and erosion concurrent with volcanism, must have played a role in the distribution of the ash flows (Best, 1988b). Widespread, relatively thin rhyolite ash-flow sheets (e.g., Bates Mountain, Shingle Pass, Bauers) indicate that the relief at the time of their eruption in the early Miocene was much less than today.

Single cooling units near their sources can be as much as 200-300 m thick, but are thicker in paleovalleys and are commonly an order of magnitude thicker in calderas predating, or produced by, eruption of the unit. Other factors, in addition to the relief of the pre-eruption surface and distance from the source, govern the thickness of a sheet. Sheets of crystal-rich tuff (>25% phenocrysts) in the Great Basin can be as extensive as crystal-poor sheets, yet for a particular areal extent they tend on the average to be thicker; the largest-volume deposits are crystal-rich. Abundant suspended crystals in the ejecta may reduce the mobility of ash flows, possibly in part because of proportionately fewer glass particles exsolving gas to maintain their mobility as they sweep across the land. Thicker sheets may also have been built up by many rapidly erupted ash flows to form a single cooling unit. Also, the relative thickness of crystal-rich ash-flow deposits may be due to the fact that they compact less than crystal-poor deposits.

Composition

Most Great Basin ash-flow tuffs are rhyolite, but range to dacite and trachyte and rare andesite and latite (Fig. 6). Most are calc-alkaline, but some, particularly middle Miocene and younger tuffs, have especially high FeO/(FeO + MgO) ratios (0.85 to 0.99 +), and some of these are per-

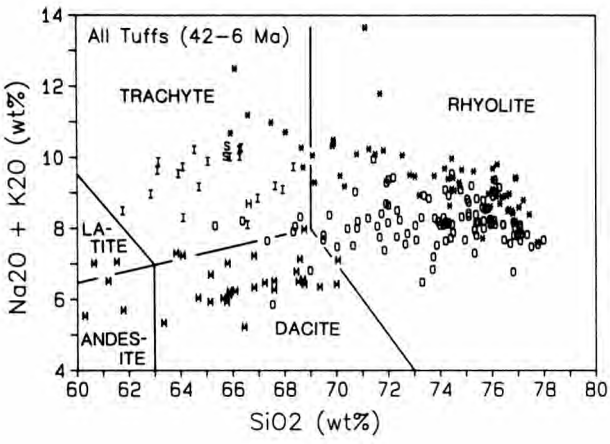

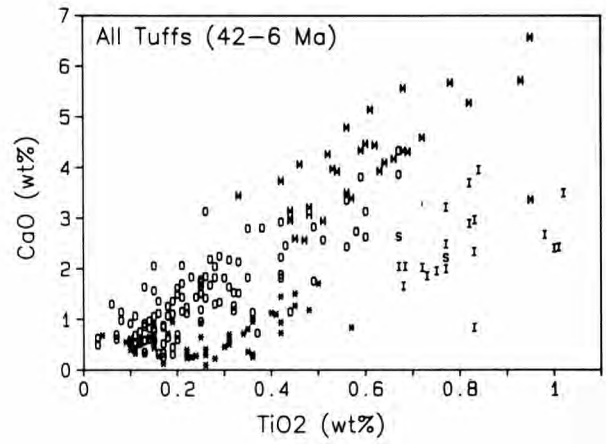

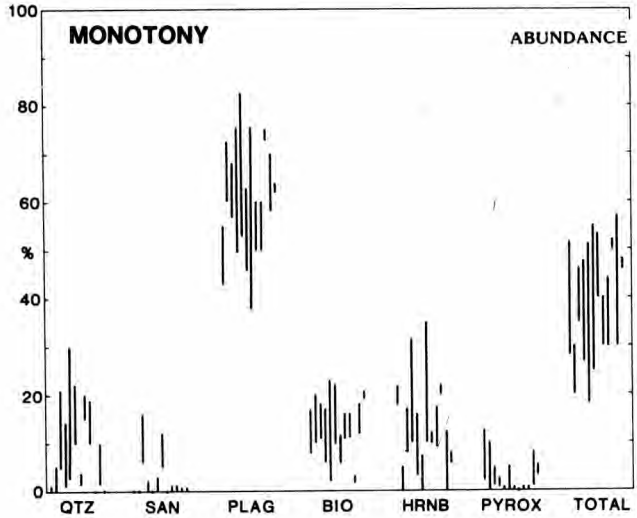

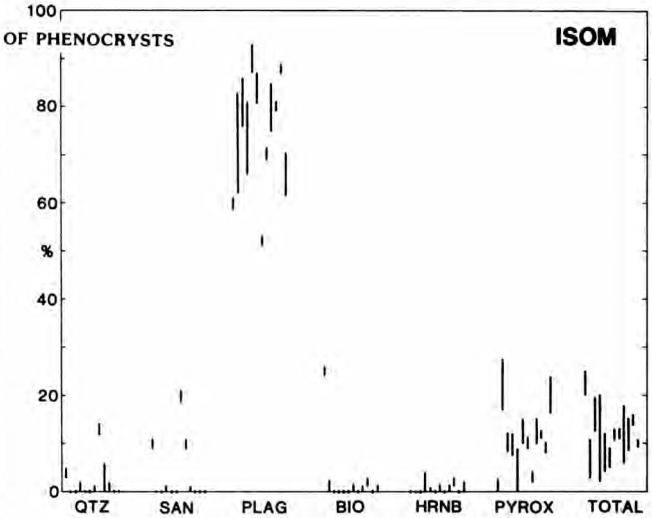

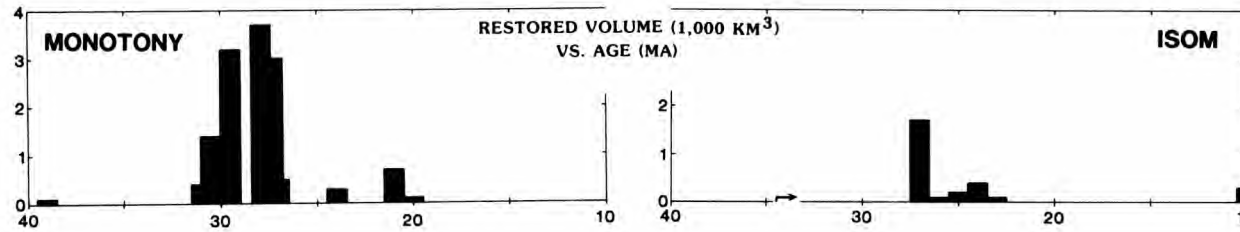

MONOTONY COMPOSITIONAL TYPE

1. MT. LAIRD TUFF (39± MA)
2. TUFF OF HOODOO CANYON (31±)
3. COTTONWOOD WASH TUFF (30.6)
4. WAH WAH SPRINGS FORMATION (29.5)
5. LUND FORMATION (27.9)
6. MONOTONY TUFF (27.3)
7. THREE CREEKS TUFF MEMBER OF BULLION CANYON VOLCANICS (27±)
8. UPPER TUFF OF BUCKSKIN POINT (24±)
9. UPPER TUFF OF BUCKWHEAT RIM (24±)
10. DELANO PEAK TUFF MEMBER OF BULLION CANYON VOLCANICS (24±)
11. HARMONY HILLS TUFF (21±)
12. RENCHER FORMATION (20±)

ISOM COMPOSITIONAL TYPE

1. WELDED TUFF MEMBER OF LATITE RIDGE LATITE (<34 MA)
2. PETROGLYPH CLIFF IGNIMBRITE OF COOK (1965) (27±)
3. TUFF OF ALBINUS CANYON (27±)
4. ISOM FORMATION (27±)
5. LOWER TUFFS OF PAHROC SPRING (25±)
6. TUFFS OF HAMLIGHT CANYON (25±)
7. ANTIMONY TUFF MEMBER OF MT. DUTTON FORMATION (24±)
8. TUFF OF GEORGES CANYON RIM (24±)
9. TUFF OF BLACK BEAUTY MESA (24±)
10. LOWER TUFF OF BUCKSKIN POINT (24±)
11. UPPER TUFF OF PAHROC SPRING (23±)
12. EUREKA VALLEY TUFF (10±)

FIGURE 6—Top pair of diagrams are alkalies–silica diagram with IUGS classification (Le Bas et al. , 1986) and CaO–TiO_2 diagram of all ash-flow tuffs for which chemical analyses are available in the Great Basin and western Colorado Plateaus; most analyses are from numerous publications, but included are some unpublished XRF analyses done at Brigham Young University. Some deposits or stratigraphic units are represented by more than one analysis. M, Monotony compositional type; I, Isom compositional type; S, Osiris Tuff (about 23 Ma) in the Marysvale volcanic field, which contains about 22% phenocrysts of plagioclase, lesser sanidine, and minor biotite, pyroxene, and magnetite, and is therefore not mineralogically strictly an Isom type; H, tuff of Hoodoo Canyon (about 31 Ma) is mineralogically a Monotony type except for slightly more sanidine and K_20 than average, so it plots in the Isom-type field on the alkalies–silica diagram; *, tuffs 17-6 Ma; O, other tuffs. Middle pairs of diagrams show range of phenocryst proportions and restored volume versus age of the stratigraphic units listed at bottom of figure represented in the Monotony (left) and Isom (right) compositional types. List of stratigraphic units 1-12 corresponds to vertical lines from left to right, showing range in phenocryst proportions.

alkaline. Although analyses of hydrated glass from tuffs commonly have elevated K_2O/Na_2O ratios, primarily devitrified Great Basin tuffs also typically have ratios greater than one and, hence, source magmas are considered to be inherently potassic.

Quartz and two feldspars are the most common phenocrysts; mafic phases typically include biotite, hornblende, magnetite, and less common ilmenite, augite, hypersthene, fayalite, and, in peralkaline tuffs, aenigmatite and sodic amphibole, and pyroxene. Most tuffs contain trace amounts of apatite and zircon. Titanite (sphene) occurs in only about 10% of the tuffs and a trace of allanite and/or chevkinite has been found in several rhyolite tuffs.

Phenocryst concentrations in Great Basin tuffs range from zero (e.g. , aphyric lower part of middle Miocene Grouse Canyon Member of Belted Range Tuff) to 40 and rarely to 50% (e.g. , Harmony Hills Tuff). The maximum concentration of crystals may reflect a viscosity barrier precluding eruption of more crystal-rich magma (Smith, 1979; also cf. Marsh, 1981). Some of the ash-flow sheets with >40% phenocrysts are low-silica dacite or andesite composition, which suggests that the lower viscosity of a less siliceous melt might compensate for the greater concentration of crystals. However, winnowing of lighter, finer glass particles from the ash flow during eruption and emplacement influences the phenocryst/glass ratio in the tuff (e.g. , Noble et al. , 1974); some extensive beds of air-fall tuff of Oligocene age found in the mid-continent might represent co-ignimbrite deposits of Great Basin eruptions (G. A. Izett, oral comm. 1987).

Although rhyolite tuffs range widely in phenocryst content, nearly all dacite and andesite tuffs are crystal-rich. Some ash-flow sheets are strikingly zoned from crystal-poor rhyolitic lower parts to more crystal-rich dacitic upper parts (e. g. , Nine Hill, Kalamazoo, and Civet Cat Canyon Member of the Stonewall Flat Tuff). In contrast, very large-volume, crystal-rich dacite ash-flow sheets (i.e. , the "monotonous intermediates" of Hildreth, 1981), such as the Cottonwood Wash, Wah Wah Springs, and Lund, each have the same types of phenocrysts throughout and in much the same proportions. Pumice clasts throughout the Wah Wah Springs also differ little in bulk chemical composition (Best et al. , 1989).

Some ash-flow deposits appear to be free of accidental rock inclusions, even those within their caldera (e.g. , tuff of Williams Ridge and Morey Peak); however, others are choked with noncognate lithic fragments, particularly near their vents and within source calderas, where the intracaldera rocks can locally consist of breccia or megabreccia in which tuff is a subordinate matrix (see next section). Fragments of cogenetic magmatic material larger than ash size are almost universally present; most of these are pumice lapilli. However, football-size pumice blocks have sometimes been transported as much as a few tens of kilometers from the source. Compositionally similar but non-vesicular cognate clasts are present in a number of ash-flow sheets (e.g. , Noble et al. , 1974). Finally, it must be noted that mixed pumice blocks with strikingly variable compositions have been documented in some deposits (Vogel et al., 1987, 1989).

Correlation

The most reliable method of determining the distribution of ash-flow sheets is by geologic mapping. However, the Great Basin presents two obstacles. First, mountain ranges are cut by post- and some syn-volcanic faults that in many places are so complex that both stratigraphy and structure are uncertain; hence, structural and stratigraphic studies must be made concurrently through careful geologic mapping. Second, ash-flow sheets are typically preserved only discontinuously in isolated exposures, necessitating application of reliable correlation techniques. Such correlation becomes critically important in the case of very large sheets that have wide areal extent and where large distances intervene between exposures.

Practical and successful methods of correlation have been developed over the past few decades by many geologists working in the Great Basin. We and our coworkers have found that in most cases stratigraphic sequence combined with modal phenocryst composition (e.g. , Williams, 1960; Byers et al. , 1968) serve as primary correlation criteria. Secondary criteria such as size and microscopic characteristics of phenocrysts, abundance and nature of lithic and pumice clasts, character of welding and devitrification and vapor-phase crystallization, and magnetic polarity are useful in certain cases. Even thickness of a unit can help correlation if a pattern has emerged by study of nearby areas. A common pitfall in field correlation is the use of superficial criteria such as color or welding characteristics in lieu of the primary tools of mineralogy and stratigraphic succession. Some very large, crystal-rich ash-flow sheets in the Great Basin, as noted above, have quite uniform modal compositions; phenocryst size may vary vertically, but marked variation in types and proportions of phenocrysts is uncommon, allowing one to make reliable correlations on the basis of phenocrysts.

For especially difficult correlation problems that cannot be solved in the field, or where correlation needs careful documentation, radiometric age, minor- and trace-element composition, and quantitative thermoremanent-magnetization data are especially useful. Confidence is greatest where a variety of field, petrographic, and laboratory methods is applied (e.g. , Noble et al. , 1984).

In some cases, radiometric ages of ash-flow tuffs can be used for correlation. Techniques that prove useful for Cenozoic tuffs are conventional K—Ar and especially more precise $^{40}Ar/^{39}Ar$ methods. Potassium-bearing phenocrysts such as biotite, sanidine, oligoclase (with 1% or more K), and hornblende are common in Great Basin tuffs. In many rocks, two different phenocryst species from the same specimen can be dated, giving more confidence in the determined age. Less precise fission-track ages have limited application (Naeser and McKee, 1970).

In the Great Basin, many hundreds of conventional K-Ar age determinations have been made on Cenozoic tuffs and lavas. Probably every major unit has been dated at least once, and some as many as 20 times. Because of the great number of ages, it is possible to evaluate the reproducibility of the various analyses and, more importantly, to establish the actual age of a volcanic unit (the accuracy of the radiometric age). In a study that addresses this problem, McKee and Silberman (1970) showed that an estimate of about 3% may be used as the uncertainty of a particular age that is based upon a single K—Ar determination. Thus, age determinations from widely separated localities that differ by no more than 3% should be considered the same and to constitute permissive evidence for correlation of the unit.

Application of the $^{40}Ar/^{39}Ar$ technique to middle Tertiary

ash-flow sheets promises to improve precision to better than 1% (Lanphere, 1988). This improvement over the conventional K—Ar method is largely due to the measurement of the potassium content of the sample, in the form of ^{39}Ar converted from ^{39}K in a nuclear reactor, during the same experiment in which radiogenic ^{40}Ar is measured. Moreover, this self-contained aspect of the $^{40}Ar/^{39}Ar$ method in conjunction with laser fusion allows age determinations of individual grains, or even parts of a single grain, with still better analytical precision (Dalrymple and Duffield, 1988). Thus, contaminant or altered grains can be discerned and eliminated from the computation of the mean age of the sample. In a preliminary study (Deino and Best, 1988) of a rhyolite ash-flow sheet in south-central Nevada, six sanidine grains from each of four widely separated samples were analyzed; the total age spread for the mean ages of the samples is only 40,000 years and the standard error of the weighted mean of 22.65 Ma is 9000 years. These advancements in dating technique provide a powerful tool to aid in correlation of ash-flow sheets and to investigate the chronologic evolution of middle Tertiary volcanic centers.

Criteria for the chemical correlation of ash-flow sheets are summarized in Hildreth and Mahood (1985). Bulk samples can differ significantly in composition over the extent of a sheet (and from the original magma) due to contamination by xenocrysts and xenoliths, mechanical sorting and mixing, preferential elutriation of vitric ash during outflow, and secondary hydration and devitrification processes. Analysis of pumice blocks, representing more or less unmodified samples of magma, largely circumvents these problems. Even so, major complexities remain due to the practical difficulty in extracting clean, unaltered pumice from a wide variety of tuffs. Additional problems arise in some cases because of marked disequilibrium between phenocrysts from individual pumice fragments and compositionally variable cognate clasts that reflect compositional gradients within the pre-eruption magma chamber. Plots of less mobile major and minor elements (Ti, P, Mn) and trace elements (Y, Zr, Nb, REE) often yield trends rather than clusters of points, although such trends may not overlap and therefore be useful in distinguishing between two or more ash-flow deposits (e.g., Noble et al., 1984). Glass and phenocryst compositions, especially feldspars and pyroxenes, can also be diagnostic, but may also vary due to compositional gradients in the magma chamber.

Deino (1985) used bulk-rock compositions of the densely welded Nine Hill Tuff of western Nevada and eastern California to establish a close chemical similarity with the Bates Mountain Tuff (Unit D) of central and eastern Nevada (Fig. R5 in road log). A close chemical affinity in Zr—Nb content, distinct from other tuffs in the region, was also noted between the crystal-rich, moderately welded tuff of Chimney Spring of western Nevada and the lithologically similar New Pass Tuff of central Nevada.

Paleomagnetism was used to distinguish between and/or correlate ash-flow sheets by Noble et al. (1968) and Cox (1971), and was extensively employed by Grommé et al. (1972) in the eastern Great Basin. The method depends upon the fact that during cooling an ash-flow deposit acquires a stable thermoremanent magnetization parallel to the geomagnetic field. In nearly all instances, plastic deformation in the sheet ceased at a higher temperature than the onset of magnetization acquisition (630° C or less), but exceptions to this rule are the Swett Tuff in Condor Canyon (Gose, 1970) and the Topopah Spring Member of the Paintbrush Tuff in the Nevada Test Site (Rosenbaum, 1986). The geomagnetic field exhibits two sorts of time variations that are important in this context. First is secular variation of the direction, with a characteristic time of one to a few centuries and an amplitude of 10-20° of arc. Second is complete reversals of polarity, with a characteristic frequency of a few thousand centuries. Reversals occur seemingly at random intervals, and secular variation is also a quasi-random, but continuous, phenomenon.

During an interval of constant polarity, a spot-sampling through time of the field direction at a site will have a probability distribution centered on the direction that would be produced by a geocentric axial dipole, and the radial density function will have a shape analogous to a two-dimensional Gaussian distribution. Clearly, if two ash-flow sheets have paleomagnetic directions that are opposite in polarity, or are significantly different from each other, they cannot have erupted at the same time. The converse hypothesis, that if two sheets have the same paleomagnetic direction they are contemporaneous, can only be assigned a probability of truth depending on how different their common direction is from the most likely field direction, that of the geocentric axial dipole (Cox, 1971).

In practice, application of paleomagnetism can be hampered by inaccuracy of the geometric correction for post-eruptive tectonic tilting far more than by plastic deformation during initial cooling. Commonly, the bedding attitude is measured in the eutaxitic structure of the tuff because the top or bottom of the sheet frequently is not exposed. The eutaxitic structure tends to be parallel to the pre-eruption ground surface rather than exactly horizontal, and if there was much topographic relief, the structural corrections will be wrong. The success of the application of this method by Grommé et al. (1972) depended on the fact that the middle Tertiary tuffs of the eastern Great Basin were mostly erupted onto a nearly flat ground, and that none of their sampling sites were within or near calderas.

Calderas

Most geologists consider it axiomatic that catastrophic explosive eruption of a large to very large volume of pyroclastic material sufficiently reduces support of the roof of the magma chamber to cause its collapse. The resulting caldera is commonly, but not in all cases, more or less centrally located within the areal distribution of its associated extracaldera deposit of ash-flow tuff, or outflow sheet.

Recognition

Recognition of Oligocene and Miocene calderas in the Great Basin presents special challenges because of burial by post-caldera volcanic and sedimentary rocks, and especially because of subsequent dismemberment by faulting and erosion. Although parts of 16-15 Ma calderas in the McDermitt volcanic field on the Oregon—Nevada state line have topographic expression (Rytuba and McKee, 1984), generally only the youngest in the Great Basin have complete circular definition. For example, in the cluster of several calderas in the Nevada Test Site in the southern Great Basin (Fig. 7), only the Timber Mountain (11.3 Ma) and Black Mountain (7.7 Ma) calderas are topographically well defined (Christiansen, 1979).

Post-caldera basin and range faulting has been both a curse and blessing in the search for sources of ash-flow

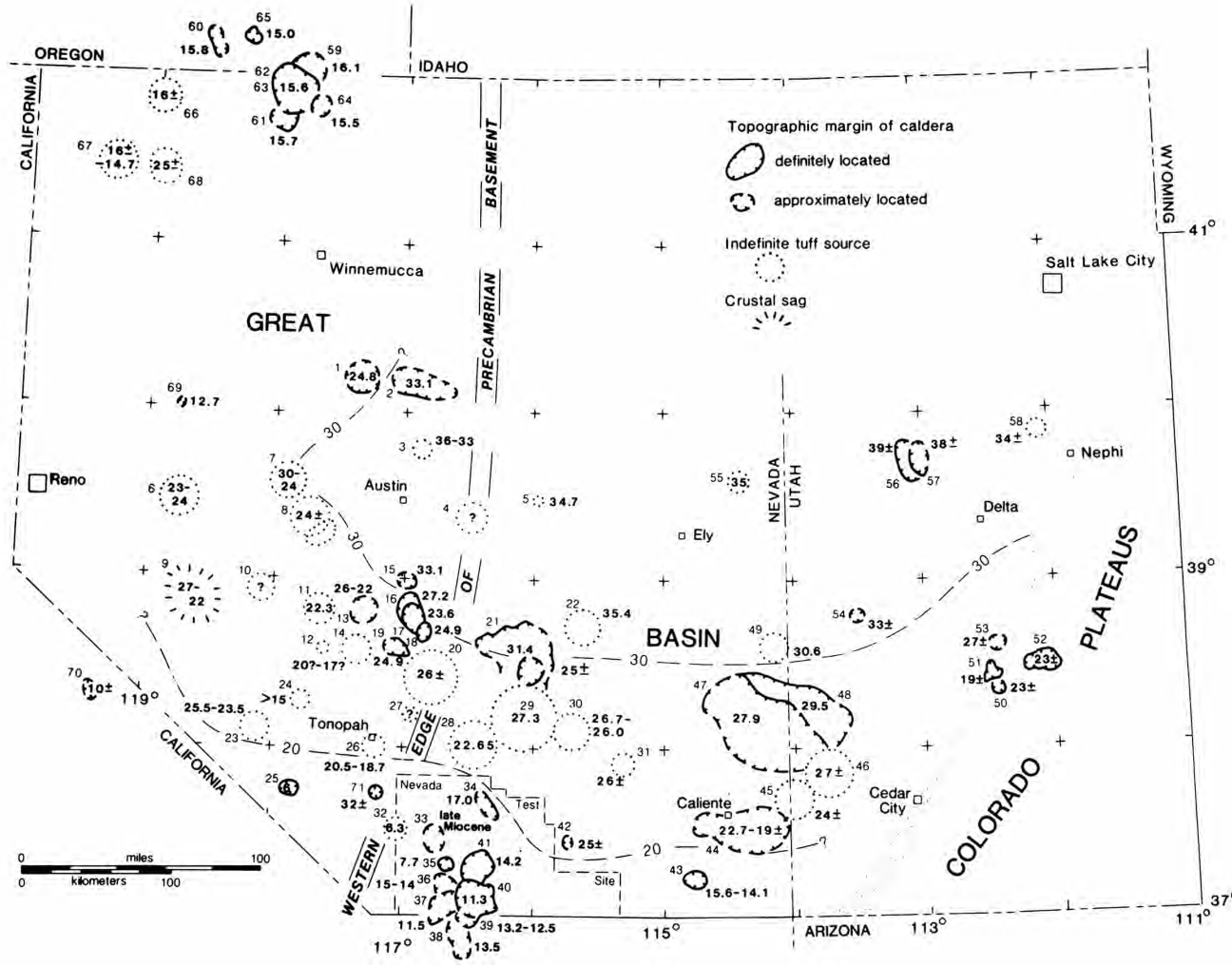

FIGURE 7—Sources of large and very large ash-flow tuff deposits in the Great Basin and western Colorado Plateaus. Bolder number is age in Ma. Lighter number is from Table 2, which also lists names of calderas and associated outflow deposits. Western edge of Precambrian basement from Ndisotopic data of Farmer and DePaolo (1983). Dashed lines show southern and western limit of caldera-forming eruptions at 30 and 20 Ma.

sheets. Wide alluvial valleys conceal parts of calderas and appear to wholly mask others; on the other hand, the internal structure and stratigraphy of segments of some calderas are well exposed in tilted and uplifted fault-block ranges (e.g., Toquima Range and Northumberland caldera; Needle Range and Indian Peak caldera). Some of the calderas shown in Fig. 7 are conjectural because only incomplete data such as the distribution of an outflow sheet or the recognition of a thick intracaldera deposit are available. Topographic margins are poorly known even for some of the better located calderas because of younger cover. Many ash-flow sheets have no known source, or at best only a conjectured one, and several identified calderas have no recognized outflow sheets (Table 2) .

TABLE 2—Known or conjectured calderas and sources shown in Fig. 7. Tuff related to caldera collapse is indicated. SRSC in reference column refers to Sargent and Roggensack (1984) and Stewart and Carlson (1976).

No.	Caldera Lat.N, Long.W	Tuff	Age(Ma)	Comment	Reference
1	Fish Creek Mtns. 40.2°,117.3°	Fish Creek Mtns.	24.8	Virtually all intracaldera	McKee (1970); Stewart and McKee (1977)
2	Unnamed 40.2°,116.9°	Caetano	33.1	Little outflow preserved	Stewart and McKee (1977)
3	Unnamed 39.7°,116.9°	Hall Creek	36-33		SRSC
4	Unnamed 3.94°,116.5°				SRSC
5	Unnamed 39.5°,116.0°	Pancake Summit	33.7		M. G. Best and A. L. Deino (unpubl. data)
6	Unnamed 39.5°,118.8°	Nine Hill and possibly D unit of Bates Mtn.	23-24	Caldera location based on compositional, chronologic, paleomagnetic similarity of these two tuffs	Deino (1985); Stewart and McKee (1977)

Table 2, continued

No.	Caldera Lat.N, Long.W	Tuff	Age(Ma)	Comment	Reference
7	Unnamed 39.6°,117.9°		30-24		SRSC
8	Unnamed 39.3°,117.7°		24 ±	Caldera filled with 1000 m of crystal-rich rhyolite of Desatoya Mtn.	McKee and Conrad (1987)
9	Unnamed 38.8°,118.6°	Hu-pwi Rhyodacite, Blue Sphinx, Singatse, Mickey Pass	23-22 25-23 27-24 27-24	No evidence for a fault- bounded caldera; instead a broad crustal sag is postulated to have developed as roughly 3000 km^3 of magma was erupted, possibly from deep magma bodies; tuffs cover an area of roughly 8000 km^2	Ekren et al. (1980)
10	Unnamed 38.9°,118.1°				SRSC
11	Unnamed 38.7°,117.5°	Toiyabe Quartz Latite	22.3	Position highly uncertain	McKee and John (unpubl. data)
12	Unnamed 38.6°,117.6°				SRSC
13	Darrough 38.8°,117.3°	Darrough Felsite	26-22	Could be older	Speed and McKee (1975)
14	Peavine	Peavine Canyon	20?-17?		SRSC
15	Northumberland 39.0°,117.0°	Northumberland	33.1	Landslide blocks as large as 1. 5 km of Paleozoic rocks in caldera	McKee (1974)
16	Moores Creek 38.8°,116.9°	Moores Creek	27.2	No outflow tuff recognized	Boden (1986)
17	Mt. Jefferson 38.8°,116.9°	Mt. Jefferson	26.4	Limited extent of outflow tuff (Round Mtn. Mbr.)	Boden (1986)
18	Trail Canyon 38.7°,116.8°	Trail Canyon	23.6	No outflow tuff exposed	Boden (1986)
19	Manhattan 38.6°,117.1°	Round Rock	24.9		Shawe et al. (1986)
20	Big Ten Peak 38.5°,116.8°	Rye Patch of Bonham and Garside (1979) equivalent(?) to Big Ten Peak of McKee and John (unpubl. data)	26 ±	Caldera has landslide blocks of Paleozoic rocks as large as 1.6 km across	Bonham and Garside (1979)
21	Williams Ridge 38.6°,116.1°	Windous Butte Fm. is outflow sheet tuff of Williams Ridge and Morey Peak is intracaldera deposit	31.37 31.33	Hot Creek Valley caldera (not shows) nested within northwest segment of Williams Ridge caldera, collapsed during eruption of tuff of Hot Creek Canyon shortly after eruption of tuff of Williams Ridge and Morey Peak. Enclosed Lunar Lake caldera collapsed about 25 Ma as tuff of Lunar Cuesta was erupted	Ekren et al. (1974); John (1987); M. G. Best and A. L. Deino (unpubl. data)
22	Unnamed 38.5°,115.8°	Stone Cabin	35.4		M. G. Best, G. L. Dixon, A. L. Deino (unpubl. data)
23	Unnamed 38.1°,118.1°	Candelaria Hills sequence	25.5-23.5		Robinson and Stewart (1984)
24	Monte Cristo 38.2°,117.8°	Castle Peak	>15		SRSC
25	Silver Peak 37.7°,1 17.8°		6		Robinson (1972)
26	Fraction 38.0°,117.2°	Fraction	20.5-18.7	Caldera name from Sargent and Roggensack (1984)	Bonham and Garside (1979)
27	Unnamed 38.2°,116.9°				SRSC
28	Kawich 38.0°,116.5°	Probably Pahranagat Lakes Tuff of Williams (1967) and tuff of White Blotch Spring of Ekren et al. (1971)	22.65		Deino and Best (1988)
29	Unnamed 38.3°,116.0°	Monotony	27.3		Ekren et al. (1974); M. G. Best and A. L. Deino (unpubl. data)

Table 2, continued

No.	Caldera Lat.N, Long.W	Tuff	Age(Ma)	Comment	Reference
30	Quinn Canyon Range 38.1°,115.7°	Probably Shingle Pass	26.7-26.0	Thick section of Shingle Pass Tuff and center of areal distribution of this large sheet	SRSC; M. G. Best and A. L. Deino (unpubl. data)
31	Unnamed 37.9°,115.3°	Hancock Summit	26 ±		M. G. Best (unpubl. data)
32	Stonewall Mt. 37.5°,117.0°	Stonewall Flat	6.3	Two nested calderas	Noble et al. (1984); Weiss and Noble (1989)
33	Mount Helen 37.4°,116.7°	Tolicha Peak	late Miocene (<14)		Ekren et al. (1971)
34	Cathedral Ridge 37.6°,116.3°		17.0	Caldera filled with 2200 m of tuff called Fraction Tuff by Ekren et al. (1971), but shown by Bonham and Garside (1979) to be younger and of different composition from Fraction at type locality near Tonopah	Ekren et al. (1971)
35	Black Mtn. 37.3°,116.7°	Thirsty Canyon	7.7	Two nested calderas	Noble and Christiansen (1974); Noble et al. (1984); Weiss et al. (1989)
36	Unnamed 37.2°,116.8°	Tuff of Sleeping Butte	15-14		D. C. Noble (unpubl. data)
37	Oasis Valley 37.1°,116.7°	Rainier Mesa Mbr. of Timber Mtn. Tuff	11.5		Byers et al. (1976); Christiansen et al. (1977)
38	Crater Flat—Prospector Pass 36.8°,116.5°	Crater Flat	14.4-13.8	Bullfrog Mbr. has volume of 1000 km^3	Carr et al: (1986)
39	Claim Canyon 37.0°,116.5°	Paintbrush	13.5-12.8	Tiva Canyon and Topopah Spring Mbrs. have volume of 1300 km^3	Byers et al. (1976); Christiansen et al. (1977)
40	Timber Mtn. 37.1°,116.4°	Ammonia Tanks Mbr. of Timber Mtn. Tuff	11.3		Byers et al. (1976); Christiansen et al. (1977)
41	Silent Canyon 37.3°,116.4°	Belted Range	14.2	Grouse Canyon Mbr. is most voluminous	Noble et al. (1968); Orkild et al. (1968)
42	Bald Mtn.	Bald Mtn.	25 ±	Tuff known in only one locale (80 km north) outside of caldera	Ekren et al. (1977)
43	Kane Springs Wash 37.2°,114.8°	Kane Wash	15.6-14.1		Noble (1968, unpubl. data); Novak (1984)
44	Caliente cauldron complex 37.5°, 114.4°	Bauers, Harmony Hills, Hiko, Racer	22.7-19 ±	Nest of calderas	Williams (1967); Noble and McKee (1972); Ekren et al. (1977); P. D. Rowley and R. E. Anderson (unpubl. data)
45	Unnamed 37.7°,114.0°	Leach Canyon	24 ±		Williams (1967); M. G. Best (unpubl. data)
46	Unnamed 37.8°,113.7°	Isom	27 ±		Best et al. (1989)
47	White Rock 38.2°,114.3°	Lund	27.9	Part of the Indian Peak caldera comple	Best et al. (1989)
48	Indian Peak 38.2°,114.0°	Wah Wah Springs	29.5	Part of the Indian Peak caldera comple	Best et al. (1989)
49	Unnamed 38.6°,114.2°	Cottonwood Wash	30.6	Part of the Indian Peak caldera comple	Best et al. (1989)
50	Big John 38.3°,112.5°	Delano Peak	23 ±		Steven et al. (1984)
51	Mt. Belknap 38.4°,112.5°	Joe Lott	19 ±		Steven et al. (1984)
52	Monroe Peak 38.5°,112.1°	Osiris	23 ±		Steven et al. (1984)
53	Three Creeks 38.6°,112.5°	Three Creeks	27 ±		Steven et al. (1984)
54	Unnamed 38.8°,113.5°	Tunnel Spring	33 ±		Bushman (1973)
55	Unnamed 39.6°,114.4°	Kalamazoo	35+		Gans et al. (submitted)

table 2. continued

No.	Caldera Lat.N, Long.W	Tuff	Age(Ma)	Comment	Reference
56	Thomas 39.7°,113.1°	Mt. Laird	39 ±		Lindsey (1982)
57	Dugway Valley 33.7°,113.0°	Joy	38 ±		Lindsey (1982)
58	Unnamed 39.8°,112.1°	Fernow	34 ±		J. Hannah (unpubl. data)
59	Washburn 42.0°,117.8°	Oregon Canyon	16.1	Mostly buried	Rytuba and McKee (1984)
60	Pueblo 42.2°,118.6°	Trout Creek Mtns.	15.8		Rytuba and McKee (1984)
61	Calavera 41.8°,118.1°	Double H	15.7	Calderas 61, 62, and 63 comprise the McDermitt caldera complex	Rytuba and McKee (1984)
62	Jordan Meadow 41.9°,118.0°	Long Ridge mbrs. 2 and 3	15.6	Calderas 61, 62, and 63 comprise the McDermitt caldera complex	Rytuba and McKee (1984)
63	Long Ridge 41.9°,118.0°	Long Ridge mbr. 3	15.6	Calderas 61, 62, and 63 comprise the McDermitt caldera complex	Rytuba and McKee (1984)
64	Hoppin Peaks 41.85°,117.7°	Hoppin Peaks	15.5		Rytuba and McKee (1984)
65	Whitehorse 42.25°,118.3°	Whitehorse Creek	15.0		Rytuba and McKee (1984)
66	Virgin Valley 41.8°,119.0°	Idaho Canyon	16 ±	Calderas 66 and 67 based on geological and geophysical data	Noble et al. (1970)
67	Highrock 41.5°,119.4°	Soldier Meadow; Summit Lake	14.7 16 ±	Calderas 66 and 67 based on geological and geophysical data	Noble (1988); Noble et al. (1970); Turrin et al. (1988)
68	Unnamed 41.4°,118.9°	Ashdown	25 ±	Source inferred from tuff distribution and facies	Noble et al. (1970); McKe et al. (1972)
69	Ragged Top 40.0°,118.8°		12.7		Heggeness (1982)
70	Little Walker 38.2°,119.4°	Eureka Valley	10 ±		Noble et al. (1974, 1976)
71	Goldfield 37.7°,117.2°		32 ±		Ashley (1974)

Internal character

The internal nature of calderas formed by extrusion of ash flows has been reviewed by Lipman (1984); only a few pertinent comments regarding characteristics of Great Basin calderas are made here. Even the smallest part of a dismembered caldera is marked by a thick prism of coeval intracaldera tuff whose thickness is generally about an order of magnitude greater than that of the associated outflow sheet, but is of comparable volume. The intracaldera tuff forms either a simple or compound cooling unit and typically encloses lenses of coarse collapse breccia shed off the unstable wall of the deepening caldera during eruption. Because a significant proportion of the ejecta from the magma chamber forms extracaldera deposits, the collapse volume exceeds the volume of the intracaldera deposits. Younger post-caldera deposits, including volcaniclastic and epiclastic sediments, ash flows and locally vented lava flows, domes, and even composite volcanoes, may completely fill the caldera depression (e.g., Novak, 1984).

Deep drilling has disclosed presumably unrepeated sections of intracaldera tuff as thick as 1830 m (6000 ft) in the Williams Ridge caldera (road-log Fig. R21; Ekren et al. , 1973); a similar thickness has been found in the Mount Jefferson caldera (Boden, 1986), in the resurgent dome of the Timber Mountain caldera (Fig. 7; Byers et al. , 1976), as well as in individual calderas of the Indian Peak caldera complex (road-log Figs. R29, R32—R38). Thick, generally densely welded intracaldera piles that are commonly subjected to propylitic alteration tend to resist erosion relative to the caldera wall rocks and hence lead to the development of inverted topography that is a clue to the existence of the caldera. Intracaldera tuff may differ in composition from that of the associated outflow sheet; this difference may be significant if a strongly zoned magma body was tapped. Lithic fragments are commonly more abundant near the vents and such lithic-rich tuff can grade into lag-fall or collapse breccia as the proportion of foreign clasts increases.

Lenses of landslide breccia within the intracaldera tuff thin away from the caldera wall from which they were derived, but can extend many kilometers into the center of the depression. Megabreccia (Lipman, 1976, 1984) and "rafts" of internally shattered but nonetheless stratigraphically coherent rock as much as 1.5 km across and hundreds of meters thick occur within a few kilometers of caldera walls (McKee, 1974; road-log Figs. R12, R24, R25, R37, and R38). Lipman (1976) suggested that in-sliding masses

of rock caved off unstable caldera walls may travel far on a cushion of pyroclastic material and volcanic gas. Caving of the unstable caldera escarpment enlarges the perimeter of a caldera so that topographic diameters can be several kilometers greater than the ring-fault system (e.g., the Indian Peak caldera in road-log Fig. R32).

Comagmatic intrusions are present in many intracaldera sequences in the Great Basin but, at least at the present level of erosion, are generally not large. Intracaldera epiclastic deposits are likewise common but not extensive, possibly because of rapid accumulation of younger volcanic material within the caldera from local as well as distant sources.

Some calderas in the Great Basin (e.g., Timber Mountain and Indian Peak) show evidence of resurgent uplift following caldera collapse. Tuff sheets resting on the intracaldera sequence thicken and thin across short distances, suggesting an uneven depositional surface related to uplift. Dips of intracaldera sequences manifest doming.

In the classic Valles caldera cycle (Smith and Bailey, 1968), regional tumescence allowing for ring fracturing is a postulated first-stage event. But few definitive examples have been documented in calderas worldwide. In the Great Basin, very large outflow sheets such as the Windous Butte and Wah Wah Springs Formations causing collapse of the Williams Ridge and Indian Peak calderas, respectively, are 500-600 m thick just beyond their northern topographic walls, providing little indication of a domed land surface centered on the future caldera. Late-stage extrusion of lava domes from the ring fracture recognized in the Valles caldera cycle is not manifest in some well-mapped very large Great Basin calderas (e.g. , Williams Ridge and Indian Peak).

Space—time—composition relations

Space—time patterns

The southward sweep of chiefly calc-alkaline volcanism from Washington, Oregon, Idaho, and Montana in the Paleocene through the Great Basin in the late Eocene to Miocene (Fig. 2) is a fundamental pattern recognized for the past two decades (Armstrong, 1975, 1979; Armstrong et al., 1979; McKee, 1971; McKee and Silberman, 1975; Nilsen and McKee, 1979). Noble (1972) and Cross and Pilger (1978) show a retardation in the sweep along the west and east margins of the Great Basin as well as a decelerating southward rate of transgression.

These patterns can be examined in the light of additional data and particularly by discriminating between ages of lava flows and sources of large and very large tuffs as done by Armstrong et al. (1969). Blurring of the pattern caused by plotting the ages of tuff from distant sources is thus minimized. Lavas were extruded from about 43 to 33 Ma over much of the northern Great Basin, creating a well-defined peak in Great Basin volcanic activity (Fig. 8). South of 38.5°N latitude and after 35 Ma the volcanic transgression appears to have decelerated to the point of near stagnation; lavas as young as early Miocene are widely interspersed with Oligocene lavas in such a way as to preclude delineation of isochrons. A fairly well-defined east-northeast-trending zone of lava flows and minor east-striking vertical dikes lies just to the south of the 35 Ma isochron in the eastern half of the Great Basin (Best, 1988a); many of these lower Miocene rocks are two-pyroxene shoshonite and latite

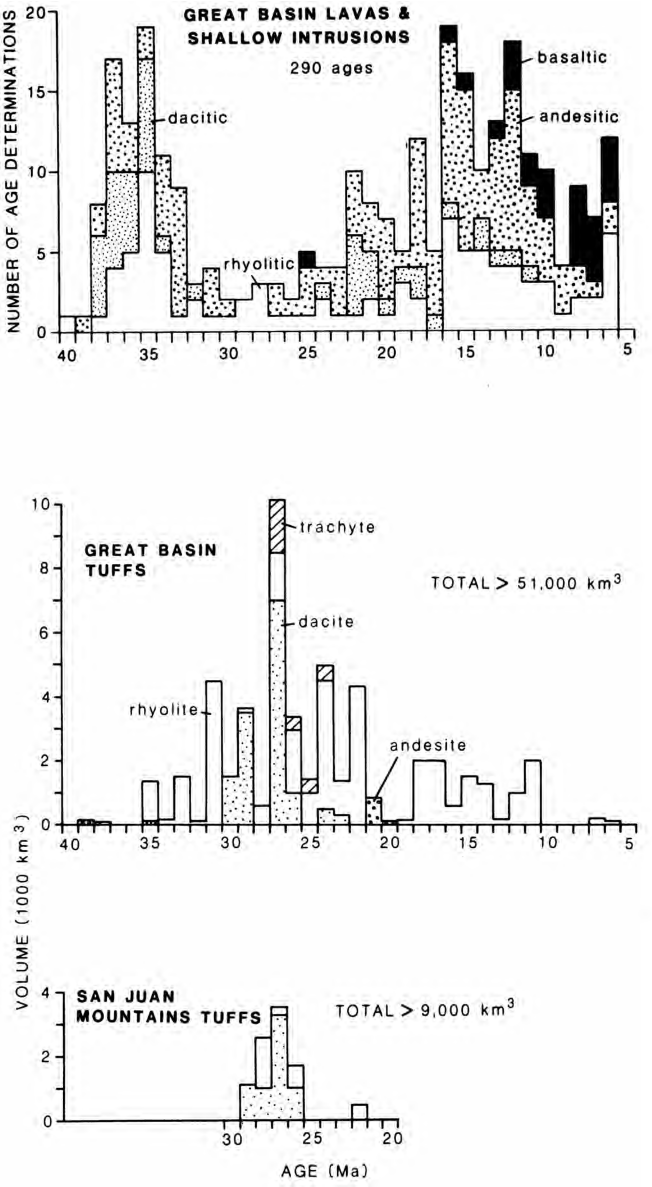

FIGURE 8—Age spectra of lavas (including minor shallow intrusions) and ash-flow tuffs shown in previous figures and ash-flow tuffs in the San Juan Mountains field (Steven and Lipman, 1976). Only a few of the dated lavas have published chemical analyses, and rock-type designations thus are approximate. Andesitic rocks include trachyandesite and latite, dacitic rocks include quartz latite. A large proportion of 17-12 Ma lavas are of andesite in the westernmost Great Basin (Fig. 4). Note the antithetic relation between peaks in eruption of tuffs and lavas in the Great Basin and the similarity in time of peak ash-flow activity in the Great Basin and San Juan Mountains. Striking gaps in histograms, e.g. at 28 Ma in Great Basin tuffs, are probably artifacts of inaccurate ages.

(Fig. 5). Thick sequences of andesitic lava and debris flows accumulated in the western Great Basin after 25 Ma, particularly between 17 and 12 Ma (note peak activity in Fig. 8), when volcanism extended into the Sierra Nevada and continued until the end of the Miocene; volcanism appears to have progressed westward (Morton et al., 1977) to eventually become a part of the north—south Cascade arc. Volcanism in the northern Great Basin after 17 Ma (Figs. 4, 8) was largely related to bimodal activity in the Snake River Plain just to the north. Transgressive ash-flow volcanism (Fig. 7) lagged behind extrusion of lavas. Well-dated and

located sources of tuff which range in age from 39 to 14 Ma define a corridor of consistent southward migration along the Nevada–Utah state line. The chronologic pattern is cluttered west of the line, marking the western edge of Precambrian basement.

A minor, easterly trending zone of early Miocene volcanism superposed on the Oligocene is apparent near the 38 Ma isochron in Fig. 3. It extends into the Colorado Plateaus east of Nephi as 32-18 Ma mafic, alkalic dikes and plugs (Witkind and Marvin, 1988; Tingey, 1986).

The zone of nonmigrating volcanic activity less than 35 Ma in the southern Great Basin can be projected eastward into the Colorado Plateaus, where magmatism is expressed in laccolithic complexes (Sullivan, 1987), and farther east into the San Juan field (Fig. 2). This zone is a major element of magmatic activity in the western United States and was contemporaneous with peak ash-flow activity in the Mogollon–Datil and Sierra Madre fields (Table 1).

Although the antithetic relation between peak intensity of lava and pyroclastic eruptive activity shown in Fig. 8 could be influenced by incomplete information, we believe it is real. The map of Stewart and Carlson (1976) for Great Basin deposits 34-17 Ma shows an overwhelming dominance of ash flows over lavas. Examination of many published larger-scale maps together with our own unpublished observations and mapping indicate that lavas extruded during this time formed only local flows and domes, as opposed to the major composite edifices that typify the nearby and nearly contemporaneous Marysvale and San Juan fields (Fig. 2, Table 1). It is unlikely that major edifices were largely engulfed by collapse of extensive calderas and now lie buried beneath thick intracaldera tuff deposits, because lahars that might represent flank deposits are conspicuously sparse or, in many places, totally absent beneath outflow sheets next to caldera margins.

Time–composition patterns

Rhyolite magmas were erupted throughout the entire span of activity in the Great Basin; rhyolite ash flows form the greatest volume of the volcanic deposits. Apart from this preponderance, geologists have recognized for at least two decades that some compositionally similar volcanic rocks were deposited during a particular time interval (Anderson and Ekren, 1968; Armstrong et al. , 1969; McKee et al. , 1970; Noble, 1972; McKee, 1976; Ekren and Byers, 1976; Best et al. , 1980). Two time-dependent *compositional types* of ash-flow tuff are particularly striking (Fig. 6). The Isom type, named after a widespread formation of this type of tuff, was emplaced chiefly 27-23 Ma. It consists of calc-alkaline trachyte containing less than 20% phenocrysts, most of which are plagioclase; clinopyroxene, orthopyroxene, and magnetite are commonly present and trace amounts of sanidine, quartz, amphibole, and biotite are found in some. Clasts of pyroxene andesite are common. Isom-type tuffs have unusually high concentrations of TiO_2, K_2O, and Zr compared to rocks of similar SiO_2 and CaO content. They generally occur as relatively thin (10-20 m thick), densely welded sheets of medium to large volume; the Isom Formation is comprised of as many as four cooling units with an aggregate volume of about 1300 km^3. Of the recognized deposits in this compositional type, all but three were erupted from vents located from south-central Utah to central Nevada in a brief time interval about 27-23 Ma. Two sheets of the Eureka Valley Tuff (Noble et al., **1974,** 1976) were erupted about 10 Ma from the Little Walker center in California and one sheet from a vent just northwest of Nephi, Utah, sometime after 34 Ma.

The Monotony compositional type, named for the Monotony Tuff of southeastern Nevada, includes fewer deposits that are generally of larger volume and variably welded; they were erupted from vent areas mostly near the Isom-type sources. With one exception, they range from 31 to 20 Ma. Over 10^4 km^3—on the order of one-fifth of the total ash-flow volume in the Great Basin—was erupted from just four sources 31-27 Ma, immediately preceding the peak Isom-type eruptions. The Monotony type (compare the "monotonous intermediates" of Hildreth, 1981) are crystal-rich ash-flow deposits, generally dacite containing 25-50% phenocrysts, mostly plagioclase; quartz, biotite, hornblende, and pyroxene occur in variable but lesser amounts, whereas sanidine is sparse or absent.

As more data on Great Basin tuffs are gathered and scrutinized, additional compositional types may emerge, but their definition is likely to be more subtle than that of the Isom and Monotony.

The significance of the compositional types is two-fold. First, stratigraphic units within a type are commonly so similar that correlation problems abound, hence the extended discussion above. Second, the eruption of significant volumes of similar magma, in terms of bulk chemical as well as phenocryst composition, from many widely separated vents over a restricted interval of time poses intriguing interpretive problems. Although some early explanations invoked tapping of a widespread single magma chamber, the present-day 400 km east–west dimension of the known and probable source areas of the Isom and Monotony types makes such an interpretation unlikely. Rather, we postulate that magmas forming deposits of each compositional type had similar origins and crystallization histories. Discussion of the details of these convergent magmatic factors is beyond the scope of this overview paper, but such factors must include: rate of input of mantle-derived mafic magma into the crust; the thermal, density, and rheologic properties of the crust; and relative importance of fractional crystallization, mixing, and assimilation–anatexis of silicic wallrock, among others.

In contrast to ash-flow deposits, Oligocene Great Basin lavas are less variable through time and form a more uniform population on any variation diagram. Miocene lavas younger than 24 Ma (Fig. 5), however, are different in three respects: (1) Over the entire range of SiO_2 they tend to be more sodic (Fig. 5). (2) Nonetheless, K_2O is still greater than Na_2O for most lavas (and, incidentally, also for most tuffs), so that they are trachyte, shoshonite, and latite in the IUGS classification (Le Bas et al., 1986). (3) Rhyolite and mafic lavas (with <57 weight % silica) are more common, but nonetheless impart only a subtle bimodal character in silica to the group.

Following a lull in volcanism from about 18 to 13 Ma, subsequent activity in the eastern Great Basin was of only small volume and consisted of episodic eruption of bimodal associations of rhyolite and basalt (Best et al., 1980, 1987). In contrast, in the western Great Basin volcanism was continuous through the Miocene and yielded substantial volumes of a spectrum of lavas and tuffs. Miocene rhyolite includes topaz-bearing lava in the eastern Great Basin, commonly not related to calderas, and peralkaline extrusions

associated with caldera complexes around the remaining perimeter of the Great Basin.

Summary

1. From the Eocene through the Miocene, the area of the present Great Basin was fundamentally an ash-flow province. In contrast, in the partly contemporaneous San Juan and Marysvale fields to the east (Fig. 2), large coalesced composite volcanoes developed and proportions of tuff to lava and debris-flow deposits emplaced before, during, and after ash-flow activity are reversed to that in the Great Basin (Table 1). From about 31 to 26 Ma the dominance of tuff over lava in the Great Basin was considerable.

2. Lavas and tuffs in the Great Basin erupted during subduction along the North American plate margin are unusually potassic for such a setting (Figs. 5, 6). Although remaining potassic, they became more sodic during the Miocene as subduction was replaced by transform plate motion.

3. Tertiary volcanism swept southward through the Great Basin, decelerating and finally stagnating after 35-30 Ma south of about 38.5°N latitude (Figs. 3, 7). In the western Great Basin, west of the edge of the Precambrian basement, east—west isochrons marking the sweep bend northward, indicating an apparent west to southwest migration of activity. After 17 Ma, volcanism flourished in the western and northern Great Basin (Fig. 4).

4. The region of stagnation coincides with that of the most voluminous ash-flow activity in the Great Basin. Contemporaneous magmatic activity approximately 35-20 Ma extended to the east into the Colordo Plateaus and San Juan Mountains and defined a major arcuate magmatic zone extending from Reno, Nevada, to the San Juan Mountains in Colorado.

5. Peak ash-flow activity in the Great Basin occurred during a lull in extrusion of lava about 32-23 Ma (Fig. 8).

6. Rhyolite ash flows were erupted throughout the entire span of such activity in the Great Basin. However, an enormous volume of crystal-rich dacite ash flows was extruded chiefly from only five sources about 31-27 Ma; this episode was succeeded from about 27 to 23 Ma by more numerous but smaller eruptions of calc-alkaline plagioclase—pyroxene trachyte ash flows.

7. Lavas erupted chiefly during the Oligocene in an early peak of activity (Figs. 5, 8) are high-K calc-alkaline compositions and include mostly andesite, dacite, and minor rhyolite. Miocene lavas tend to have higher sodium concentrations and include more rhyolitic and basaltic compositions; some Miocene rhyolite lavas in the eastern Great Basin are topaz-bearing and some ash-flow tuffs are peralkaline and associated with calderas around the remaining perimeter of the region.

Field guide

This field guide is a west to east to south transect through the Great Basin, focusing on Oligocene and Miocene ash-flow tuffs and their source calderas. The area to be covered is large and the sheets of tuff numerous (Fig. R1). Emphasis will be placed on the stratigraphic, petrographic, and compositional aspects of the deposits, means of correlating them over hundreds of kilometers, their compositioanl variations in space and time, and the character and evolution of related source calderas. Numerous interpretive problems persist in these tuff—caldera complexes, only a few of which have been studied in much detail.

Numerous cited ages in this field guide have different uncertainties. Ages no better than plus or minus one Ma are indicated as, for example, "about 24 Ma" or "24 ± Ma." Averages of two or more K—Ar analyses with uncertainties somewhat less than one Ma are cited to nearest tenth of a Ma. Some recent single crystal $^{40}Ar/^{39}Ar$ determinations by Deino with uncertainties of about 0.1% are cited to nearest hundredth of a Ma. Some single K—Ar analyses are shown as, for example, 8.3 ± 0.7 Ma.

Day 1

In stops today we will view regionally extensive rhyolite ash-flow deposits of late Oligocene—early Miocene age in the northwestern Great Basin. Problems in their correlation and dispersal over large distances from the source will be considered.

Mileage

0.0 Drive east out of Reno using Keystone ramp as starting mileage onto I-80. **4.1**

4.1 Take exit 18, go north on Pyramid Way, follow NV-445 northeast along Spanish Springs Valley which is flanked by an unnamed range on northwest and on southeast by the western block of Pah Rah Range. Rocks exposed up to about mile 12 consist mostly of late Tertiary andesite and basalt after which 30–20 Ma silicic tuffs blanket the northern end of Pah Rah Range. **19.8**

23.9 Turn right (east) at Palomino Valley Wild Horse and Burro Placement Center, entering southern part of Warm Springs Valley which here forms a re-entrant in Pah Rah Range. **1.6**

25.5 **STOP 1-1 (Deino). Extensive Oligocene to lower Miocene ash-flow sheets of western Nevada.** Stop along right side of road. Exposed in near slope to the west are three ash-flow tuffs representing important emplacement events in western Nevada about 29–22 Ma (Fig. R2). The lowest unit, the tuff of Coyote Spring (Garside et al., 1981; Deino, 1985), is the only widespread, plagioclase–biotite dacitic deposit north of Carson City (Fig. R3) in the western Nevada middle Tertiary ash-flow field. It is relatively small (area about 3100 km^2; volume >120 km^3) compared to roughly contemporaneous and compositionally similar crystal-rich dacite sheets in the central and eastern Great Basin (Fig. R1) and the Petrified Spring Tuff in the Gillis and Gabbs Valley Ranges 140 km to the southeast (Ekren et al., 1980).

The overlying Nine Hill Tuff erupted about 24 Ma is generally zoned from a crystal-poor, high-silica rhyolite at the base to crystal-vitric, low-silica rhyolite–rhyodacite, although here only the rhyodacite is represented. This deposit has the largest areal distribution of any ash-flow sheet in western Nevada and extends southwestward 220 km into the foothills of the Sierra Nevada (Fig. R3); with a maximum thickness of about 250 m it has an estimated volume of >600 km^3. The rhyolitic part may correlate with the D unit of the Bates Mountain Tuff (see next stop). The upper rhyodacitic lithology is

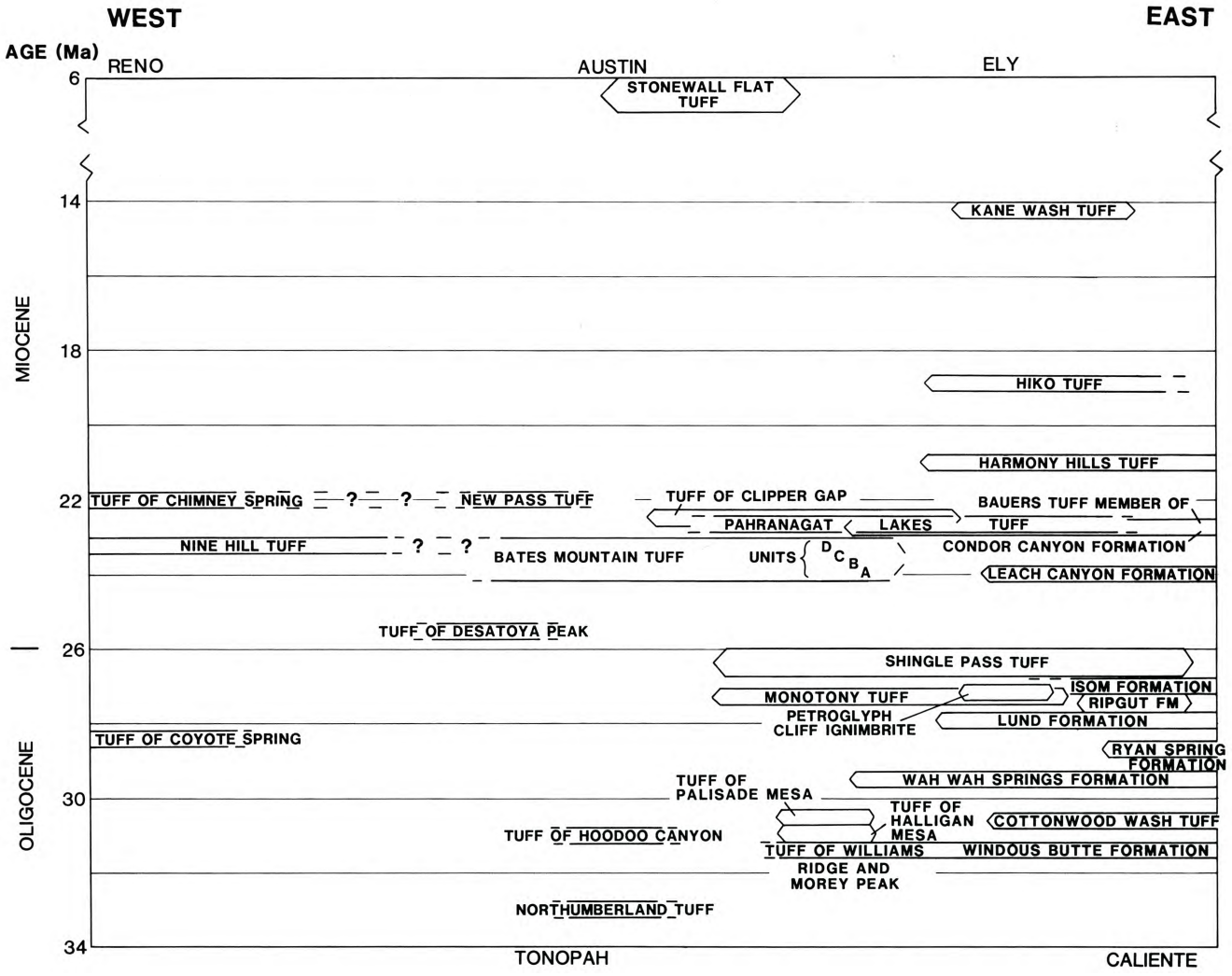

FIGURE R1—Stratigraphic units seen on field trip arranged by age and approximate west to east location and extent (queried where uncertain). Recent single-crystal $^{40}Ar/^{39}Ar$ analyses by Deino (unpubl.) suggest the tuff of Chimney Spring and Nine Hill Tuff were erupted at 25 Ma.

restricted to the central and northern portion of the known distribution of the Nine Hill Tuff (Fig. R3). Both parts commonly show rheomorphic textures in western Nevada.

The uppermost ash-flow deposit at this stop is the crystal-rich rhyolitic tuff of Chimney Spring erupted about 23 Ma, which here ranges upward from unwelded white tuff to welded red tuff. It is widespread in western Nevada north of Carson City and is characterized by abundant chatoyant sanidine and bipyramidal, smoky quartz. This unit possibly correlates with New Pass Tuff of central Nevada (McKee and Stewart, 1971) about 200 km to east

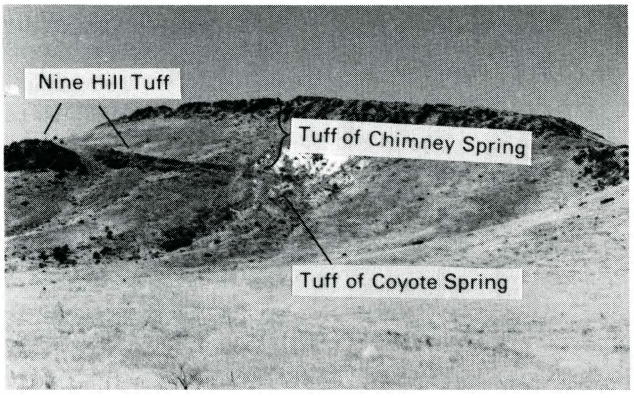

FIGURE R2—Sequence of three tuffs at Stop 1-1. Best exposures are in area of pinchout of Nine Hill Tuff near white tuff of Chimney Spring.

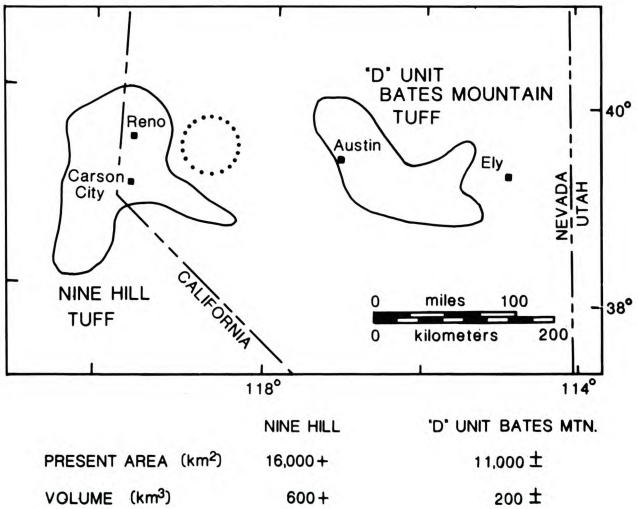

FIGURE R3—Dimensions and extent of Nine Hill Tuff and its possible correlative, the "D" unit of Bates Mountain Tuff. Possible source in the Carson Sink area is dotted circle.

(Stop 1-5). The combined areal extent of the two sheets is >16,000 km^2 and the volume >1000 km^3.

Continue in same direction to next stop in central part of valley to southeast. Ash-flow sheets in western flank of these hills have been deformed into a broad, north-plunging syncline. Local compression is associated with the right-lateral Walker Lane fault system, one active strand of which follows axis of Warm Springs Valley. **3.5**

29.0 Turn right at stop sign, off Ironwood Rd. onto Amy Rd. **0.4**

29.4 Turn left off Amy Rd. onto Wilcox Ranch Rd. **1.8**

31.2 Turn left off Wilcox Rd. onto Twin Springs Rd. **0.3**

31.5 Turn left off Twin Springs Rd. onto Crossover Rd. **1.1**

32.6 Turn right off Crossover Rd. onto Wild Horse Rd. **1.0**

33.6 **STOP 1-2 (Deino). Zonation in Nine Hill Tuff and correlation with Bates Mountain Tuff.** Stop at end of road. Both the rhyolitic and overlying rhyodacitic parts of the Nine Hill Tuff were deposited here. (Fig. R4) above a local, unnamed, welded biotite–plagioclase–sanidine ash-flow tuff that forms the first ledge at base of hill. The Nine Hill consists of 60 m of high-silica rhyolite (75–76% SiO_2, volatile-free) overlain without a cooling break by 30 m of low-silica rhyolite–rhyodacite (70–72% SiO_2). The transition between the two compositions occurs within a vertical interval of only 10 cm. The change in silica is accompanied by changes in many other chemical and textural aspects (Deino, 1985), including a readily observable upward increase in the proportion of pumice and phenocrysts (from 3 to 12%). Upper and lower magma types are locally mingled in the transition zone. Here and elsewhere, the lower rhyolite part is virtually unzoned in major and trace elements, whereas the overlying more mafic tuff, presumably derived from hotter magma deeper in the pre-eruption chamber, has strong vertical gradients in many minor and trace elements (compare the Hildreth, 1981, general model of zonation in ash-flow deposits).

Similarities in age, paleomagnetic direction, lithology, and trace-element content suggest that the lower, high-silica part of the Nine Hill Tuff may correlate with unit D of the Bates Mountain Tuff (Grommé et al., 1972). Both units are widespread on either side of the Carson Sink and are thin, densely welded, phenocryst-poor, sanidine-dominant rhyolite tuff. Both have normal magnetic polarity and typical latest Oligocene–earliest Miocene natural remanent-magnetization directions—for the Nine Hill, D = 335.1°, I = 57.5°, a_{95} = 3.0 and for unit D, D = 341.1°, I = 57.7°, a_{95} = 5.0. But most remarkable is similarity in trace-element content, especially Nb and Zr (Fig. R5). The devitrified lower rhyolite part of the Nine Hill (47 analyses) in western Nevada averages 399 ± 3 (standard error of mean) ppm Zr and 29.9 ± 0.3 ppm Nb compared to 406 ± 4 ppm Zr and 30.5 ± 0.3 ppm Nb in devitrified unit D (9 analyses). These similarities are even more striking considering concentrations in more than 20 other tuffs in western Nevada which rarely exceed 270 ppm Zr and 24 ppm Nb (Fig. R5).

Turn around and go back to Wild Horse Rd., then left onto Crossover Rd., right onto Twin Springs Rd., right onto Wilcox Ranch Rd., right onto Amy Rd., left onto Ironwood Rd., and right (northeast) onto NV-445. Exit Warm Springs Valley via Mullens Pass between Virginia Mountains on north and eastern block of Pah Rah Range on south. Andesitic and dacitic intrusions as old as 20 Ma are exposed in the pass area, suggesting a possible source for

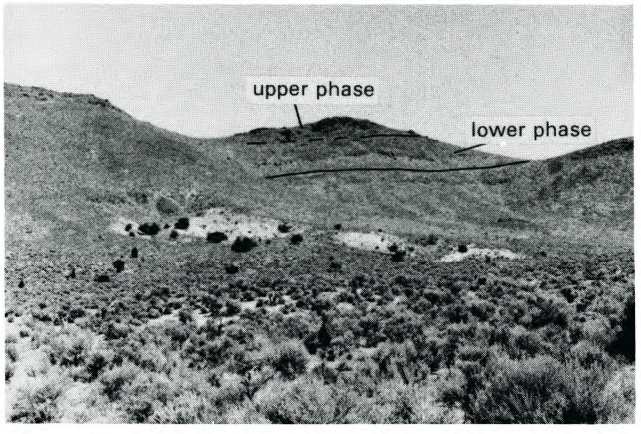

FIGURE R4—Exposure of Nine Hill Tuff at Stop 1-2.

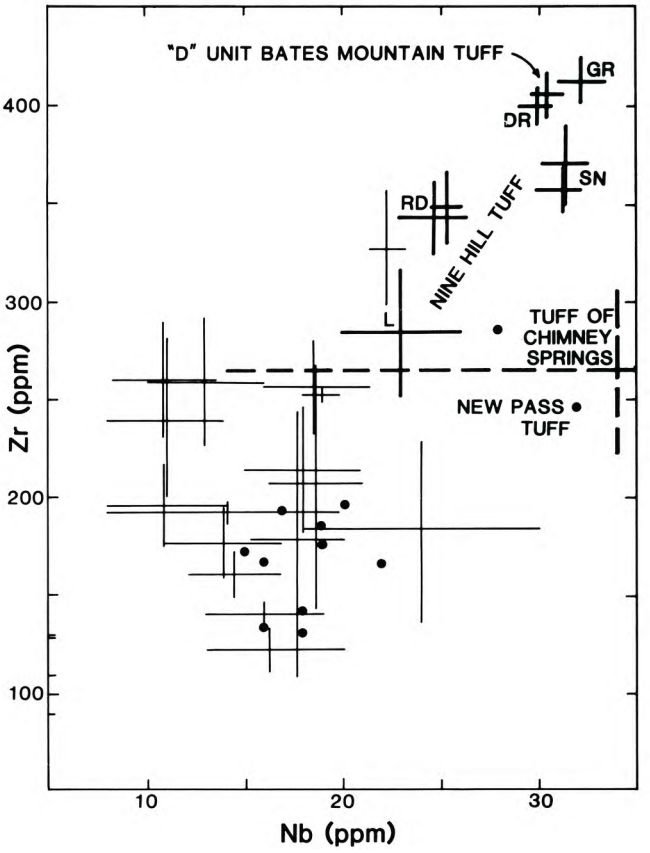

FIGURE R5—Nb–Zr concentrations in whole-rock samples of Cenozoic tuffs from west-central Nevada and the Sierra Nevada (SN; Deino, 1985). One to two analyses shown by filled circle. Error bars (3σ standard error of mean) on more than two analyses per unit. Nine Hill and one Bates Mountain Tuff analyses shown in heavier lines and tuff of Chimney Springs in heavy dashed line. Four analyses from the Yerington district are of Zr only. Labels on Nine Hill data are as follows: L, lithic tuff; RD, rhyodacitic tuff; DR, devitrified rhyolitic tuff; GR, glassy rhyolitic tuff.

contemporaneous volcanic rocks. Younger middle Miocene ash-flow tuffs are exposed north of Highway in the Pass. **22.3**

55.9 Turn right (southeast) off NV-445 onto NV-446 at Pyramid Lake (a fresh-water remnant of Pleistocene Lake Lahontan). **0.8**

56.7 Turn right onto dirt road and continue to sparsely shaded area on Mullen Creek. **0.7**

57.4 **LUNCH.** Go back to NV-446 and turn right (southeast), continuing on pavement. Note high-water terraces and tufa deposits associated with Lake Lahontan. **12.8**

70.2 Turn right onto NV-447. **14.9**

85.1 Turn left (east) at Wadsworth T-intersection, cross under I-80, continue east into Fernley, turn onto US-50, drive through Fallon (located in southern part of Carson Sink), continue east on US-50 past Salt Wells, Sand Springs Pass, and Middle Gate; stay on new US-50 past intersection with old highway. **88.4**

173.5 **STOP 1-3 (McKee). Thick intracaldera tuff in west side of the Desatoya Mountains** (Fig. R6). Stop on side of highway. The steep slopes and cliffs are composed of about 1000 m of crystal-rich welded tuff informally called the tuff of Desatoya Peak. This intracaldera unit consists of at least two ash-flow sequences separated in places by a lenticular sequence of tuffaceous sedimentary rocks, air-fall tuffs, volcanic breccias, and lava flows. These intervening rocks can be as much as 100 m thick and can be traced for about 15 km along strike before they pinch out. The outflow facies of the tuff of Desatoya Peak occurs in the northern part of the range (next stop). The tuff of Desatoya Peak is pink to brown, densely welded, crystal-rich, lithic, low-silica rhyolite (SiO_2 = 71 wt%) tuff. Phenocrysts of quartz, plagioclase, sanidine, and biotite lie in a eutaxitic groundmass of devitrified glass shards. K–Ar ages of biotite and sanidine are about 25 Ma.

Continue northeast on US-50. **21.3**

194.8 **STOP 1-4 (McKee). Outflow tuff sheets at north end of Desatoya Mountains.** Pull off highway. One or more of these cooling units belong to the tuff of Desatoya Peak and have their source to the south in the central and southern Desatoya Mountains where a caldera collapsed during and after their eruption. Other ash-flow sheets are distal parts of unnamed units from unknown sources. Some are recognized farther north and east of the Desatoya Mountains. The top unit is the New Pass Tuff (next stop).

Continue northeast on US-50. New Pass Range lies north of highway. **6.7**

201.5 **STOP 1-5 (McKee). New Pass Tuff.** Pull off highway into turnout. This ash-flow sheet is a useful, widespread stratigraphic marker in northern Desatoya Mountains, New Pass Range, central part of the Shoshone Mountains to the east, and probably extends west into the Clan Alpine Mountains and perhaps even farther west. It possibly correlates with tuff of Chimney Spring seen at Stop 1-1 because of similar petrographic properties and K–Ar age (22.0 ± 0.9 Ma).

Continue east on highway through New Pass into Smith Creek Valley, through a low part of the Shoshone Range and into the Reese River Valley. **27.0**

228.5 Turn left (north) off US-50 onto NV-305 toward Battle Mountain. **33.8**

262.3 **STOP 1-6 (McKee). Bates Mountain Tuff** (Fig. R7). Turn around at entrance to Reese River Narrows and park on west side of highway. Four cooling units are present here. The lowest lies on an eroded surface of Paleozoic strata or on older Tertiary sedimentary rocks or ash-flow tuffs. The Bates Mountain Tuff is one of the most widespread ash-flow tuffs in the central Great Basin. The most widely distributed cooling unit (unit D) has been mapped in a generally west-northwest belt across about 220 km in central Nevada (Fig. R3) and it may extend nearly twice this distance if Nine Hill Tuff (Stops 1-1 and 1-2) in western Nevada is correlative. The other cooling units (A, B, C—oldest to youngest) are thicker, less widespread, but of about the same volume as unit D.

The Bates Mountain Tuff is a sequence of rhyolitic (about 73–75% SiO_2) crystal-poor, welded ash-flow cooling units. Welded tuff is generally pink-to-red and contains about 10% or less of phenocrysts. Sanidine is most abundant, followed by plagioclase, quartz, and biotite. In most places, the cooling units are densely welded throughout and only locally do thin, partially welded or nonwelded zones of tuff occur at the base or top of the unit. Unit D has a zone near the base, which is charac-

FIGURE R6—View toward east of thick intracaldera tuff in west side of Desatoya Mountains, Stop 1-3.

FIGURE R7—Sequence of cooling units in Bates Mountain Tuff in Reese River Narrows, Stop 1-6.

terized by abundant gas cavities that give the rock the appearance of Swiss cheese (Fig. R8). This unusual lithology is very persistent and serves as a marker in mapping and correlation. Each cooling unit has a distinctive or unique natural remanent-magnetization direction which can be used for correlation, or noncorrelation, of the unit (Grommé et al., 1972). K–Ar ages (all ±0.7 Ma) from different localities are as follows:

D unit	22.8 Ma	(Sargent and McKee, 1969)
	23.1	(Grommé et al., 1972)
	23.3	(McKee and Stewart, 1971)
B or C unit	23.7	(Sargent and McKee, 1969)
	23.9	(McKee and Stewart, 1971)
	24.1	(McKee and Silberman, 1970)
A unit	24.7	(McKee and Silberman, 1970)

Proceed back (south) on NV-305. **33.8**

296.1 Turn left (east) off NV-305 onto US-50. **0.8**

296.9 Arrive in Austin, stop overnight. Austin, for years the seat of Lander County (recently moved to Battle Mountain), is in the center of the Reese River mining district. Silver ore was discovered in the canyon below Austin in 1862 and by the end of 1863 a town of 6000 inhabitants with accompanying banks, stores, saloons, and churches had been built. The first mill was built during that year, and within a few years 28 additional mills with a total of more than 400 stamps were in operation.

Production records are incomplete and inaccurate, but the best estimates indicate that about $25 million of ore was produced between 1863 and 1903, the peak year being 1868. Most of the value was in silver, but small amounts of gold, copper, lead, antimony, and zinc also were recovered. Ore occurs in narrow quartz veins that fill fractures in granitic rock of the Jurassic Austin pluton.

Day 2

Mainly rhyolitic ash-flow tuff sheets will be examined today. An early Oligocene caldera which contains spectacular landslide blocks will also be examined. During the afternoon we will drive past the well-known mining camps of Round Mountain, Tonopah, and Goldfield.

Mileage

0.0 Leave Austin, proceeding eastward on US-50 through Toiyabe Range. **3.0**

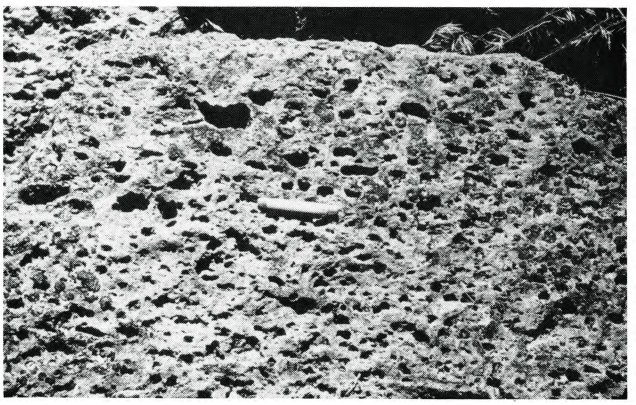

FIGURE R8—Densely welded tuff of unit D, Bates Mountain Tuff, showing characteristic gas cavities ("Swiss cheese"). 10 cm pocket knife for scale.

3.0 **STOP 2-1 (McKee). Bates Mountain Tuff deposited on erosion surface carved into Jurassic Austin granitic pluton.** Stop off highway at Austin Summit. In this eastward view, one and locally two cooling units are present, both thin and densely welded throughout. **9.0**

12.0 Turn right (south) onto NV-376. **0.3**

12.3 Turn left (east) onto dirt road. Drive southeast across Big Smoky Valley toward Petes Summit in Toquima Range. **8.0**

20.3 Turn right (south) on obscure dirt track. **2.2**

22.5 Turn right at crossroad. **2.0**

24.5 Take left-hand fork. **1.2**

25.7 Continue straight at crossroad. **2.0**

27.7 Continue straight to mouth of Clipper Gap Canyon. **0.4**

28.1 Turn left off road, up fan on dirt track. **0.2**

28.3 **STOP 2-2 (McKee and Grommé). Section of dacite to rhyolite, upper Oligocene to lower Miocene tuff sheets,** comprising at the base the tuff of Hoodoo Canyon, then three cooling units of Bates Mountain Tuff, and the overlying tuff of Clipper Gap (Figs. R9, R10).

Tuff of Hoodoo Canyon, a crystal-rich dacite tuff (Table R1) containing phenocrysts of plagioclase, biotite, pyroxene, and hornblende has a K–Ar age of 30.6 ± 1.0 Ma. It is representative of the voluminous Monotony compositional type, other units of which are exposed farther east in the Great Basin and will be seen the next three days. Nearby, the Hoodoo Canyon has been stripped by erosion from the underlying Ordovician argillaceous rocks and the Bates Mountain Tuff lies directly on Ordovician rocks.

The Bates Mountain Tuff is represented here by cooling units B, C, and D. Unit C is a compound cooling unit with a partial cooling break about midway through it. The four (in places five) cliffs are densely welded zones in the ash-flow sheets and belong to the various cooling units documented in Fig. R9 and Table R1.

New paleomagnetic data (Grommé, Hagstrum, and Gans, unpubl.) show that the tuff of Clipper Gap extends eastward to within 8 km of the Nevada–Utah state line northeast of Ely.

Proceed off fan to dirt road. **0.2**

28.5 Turn right (north) onto road out of canyon. **0.4**

28.9 Take right-hand fork. **2.0**

30.9 Continue straight through crossroad. **1.2**

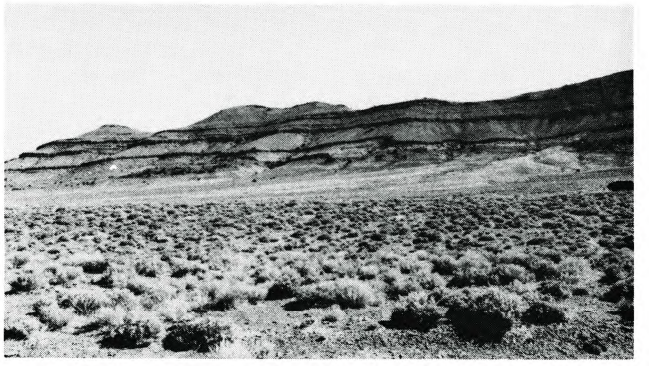

FIGURE R9—Sequence of tuff sheets at Clipper Gap, Stop 2-2.

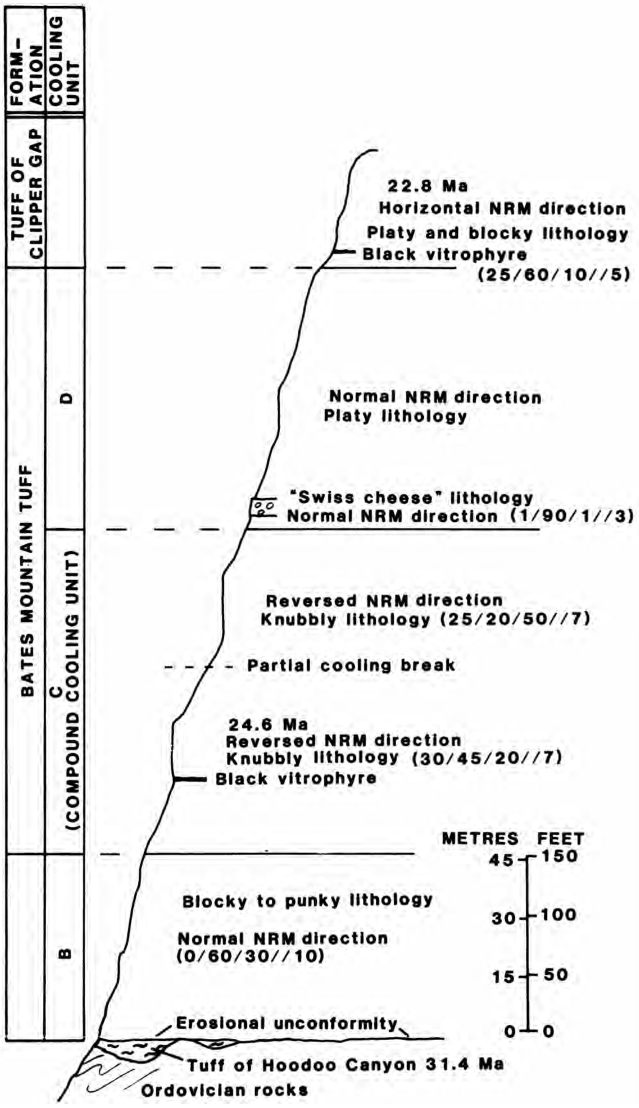

FIGURE R10-Data and stratigraphic nomenclature of units at Clipper Gap Canyon, Stop 2-2 (after McKee, 1976).

32.1 Fork comes in on left, continue straight. **2.0**

34.1 Turn left at crossroad. **1.9**

36.0 Turn left (northwest) onto Petes Summit Road. **8.4**

44.4 Turn left (south) onto NV-376. The Toiyabe Range to west contains granitic rocks of Middle Jurassic (155 Ma by K–Ar) and Late Cretaceous (75 Ma by K–Ar) age that intrude dark chert and shale of the Valmy Formation of Ordovician age. About 8.5 mi south of the turn onto NV-376, the range consists of a thick section (about 1000 m) of weakly metamorphosed quartzite, siltstone, and limestone of latest Precambrian, Cambrian, and Ordovician age. These rocks are folded in broad folds and most of the structure visible from the road is a west-dipping limb of one of the folds. The highest peak, Bunker Hill (elevation 11,474 ft), is a thrust plate of Ordovician limestone. Details of the geology are on the geologic map of the Austin quadrangle (McKee, 1976).

The visible part of the Toquima Range across Big Smoky Valley to east consists mostly of Oligocene and Miocene ash-flow sheets (including the Bates Mountain Tuff) that are nearly flat lying, and that form the tableland at the top of the range. These Tertiary rocks rest on Jurassic granitic rock and on lower and middle Paleozoic strata. Wildcat Peak, the highest feature in this part of the range (10,507 ft), is Pennsylvanian limestone and conglomerate lying unconformably on Ordovician chert and shale. Details of the geology are in McKee (1976). **21.1**

65.5 Turn left (southeast) onto dirt road toward Northumberland Canyon in the Toquima Range. **11.7**

77.2 **STOP 2-3. (McKee). General view of north edge of Northumberland caldera** (Fig. R11). Stop at mouth of Northumberland Canyon. In canyon directly north of road are chaotic landslide blocks of *Paleozoic strata* (Fig. R12) resting on welded Northumberland Tuff that erupted from a source south of the road. These landslide blocks are tectonic debris that slid into a caldera that had formed after eruption of part of the ash-flow sheet. Walk across

TABLE R1-Chemical analyses (in weight %) of Tertiary ash-flow tuffs from northern part of Toquima Range (McKee, 1976).

		Bates Mountain Tuff				
			Unit C			
	Tuff of Hoodoo Canyon	Unit B	lower cliff	upper cliff	Unit C	Tuff of Clipper Gap
SiO_2	65.1	71.0	73.6	75.0	73.3	75.3
$A1_2O_3$	16.2	12.9	12.9	13.2	13.0	12.4
Fe_2O_3	1.3	1.4	0.85	0.76	1.6	1.2
FeO	1.8	0.60	0.32	0.40	0.52	0.40
MgO	1.2	0.23	0.16	0.19	0.08	0.36
CaO	3.0	0.50	0.50	0.91	0.31	0.75
Na_2O	3.4	2.9	3.0	3.3	4.2	3.3
K_2O	5.1	5.8	4.8	4.8	5.2	4.7
H_2O+	2.2	0.53	0.21	0.70	0.49	0.72
H_2O-	0.55	3.5	2.8	0.40	0.71	0.68
TiO_2	0.47	0.16	0.11	0.10	0.19	0.12
P_2O_5	0.10	-	-	0.06	0.04	0.03
MnO	0.05	0.20	0.06	0.06	0.05	-
	100	100	100	100	100	100

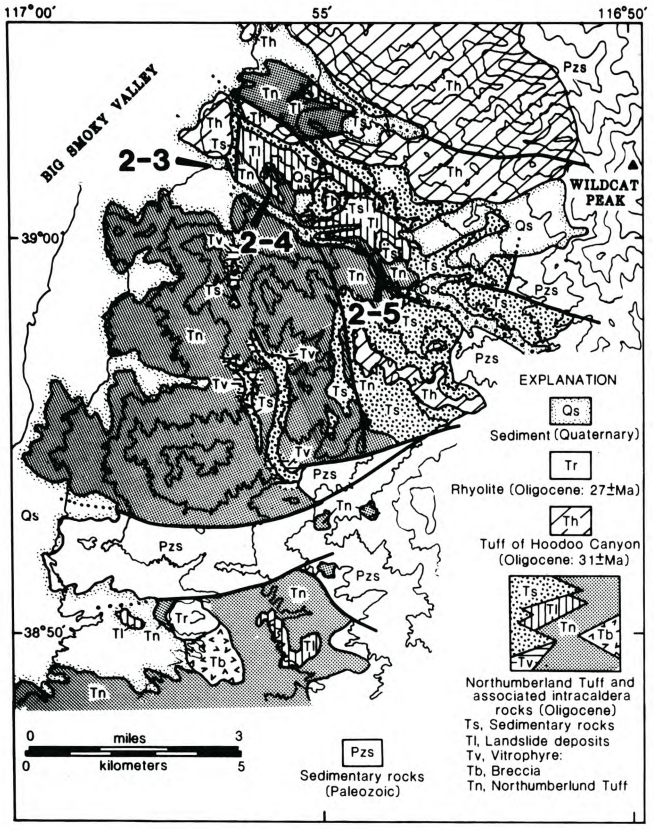

FIGURE R 11—Geologic map of the eastern part of Northumberland caldera in the Toquima Range (after McKee, 1974, and Kleinhampl and Ziony, 1985) around Stops 2-3 to 2-5.

stream bed north of road and examine welded tuff of Hoodoo Canyon which spread over the northern part of the caldera after it had been nearly filled with landslide blocks, water-laid sedimentary rocks, and post-collapse volcanic rocks. The tuff of Hoodoo Canyon has a K–Ar age of 31.4 Ma at this location, which is the younger limit for the time of existence of the Northumberland volcanic center. Note that the Hoodoo contains abundant biotite and plagioclase which is characteristic of the Monotony compositional type. In contrast, the rhyolitic (Table R1) Northumberland Tuff, erupted about 32 Ma, contains very little of either mineral and is rich in quartz and sanidine; it can be collected south of the road.

Continue up Northumberland Canyon, into altered and limonite-stained part of Northumberland Tuff beneath a large landslide block of Ordovician Vinini Formation. **0.9**

78.1 **STOP 2-4 (McKee). Altered landslide and tuff deposits.** Climb up north side of canyon, across altered zone and one of landslide blocks. Note alteration of tuff, and bleached and altered basal chert of the Ordovician Vinini Formation.

Continue up Northumberland Canyon, noting altered tuff and chaotic blocks along the south side of canyon. **1.9**

80.0 **STOP 2-5 (McKee). Intracaldera and postcaldera deposits. LUNCH.** Climb low ridge on north side of road. Cross altered tuff and landslide blocks of Paleozoic rock. Overlying these deposits are postcaldera conglomerate, sandstone, and thin rhyolite flows.

Continue up canyon. **0.7**

80.7 Spring and remains of foundation of an old mill. Rocks on low ridge north and east of mill site are sediments that accumulated in caldera moat.

Turn around and proceed back out of canyon toward west. **15.2**

95.9 Turn left (south) back onto NV-376. **20.0**

115.9 Mount Jefferson, 25 km to the east across Smoky Valley, is composed entirely of intracaldera ashflow tuff of the Mount Jefferson caldera, which is the best preserved of three nested collapse calderas that comprise the Toquima caldera complex formed during late Oligocene time from about 27.2 to 23.6 Ma (Boden, 1986). The Mount Jefferson caldera collapsed about 26.5 Ma with the eruption of the largely intracaldera tuff of Mount Jefferson. Two intracaldera members are recognized. These show an upward increase in phenocryst percent and a change from high-silica rhyolite to rhyodacitic compositions. Large landslide blocks and zones of landslide breccia are common, particularly in the lower part of the intracaldera pile. Postcollapse igneous activity and resurgence were modest, and the present elevation of the intracaldera block is largely the result of basin and range faulting.

Continue south on NV-376. **14.1**

130.0 The Round Mountain gold mine (Tingley and Berger, 1985) is located several kilometers to the east. Gold, with an average grade of less than 0.05 oz/ton, occurs as fracture fillings and disseminations, respectively, in densely and partly welded outflow sheet tuffs of the Toquima caldera complex. Hydrothermal activity and mineralization coincided closely with the period of activity of the caldera complex

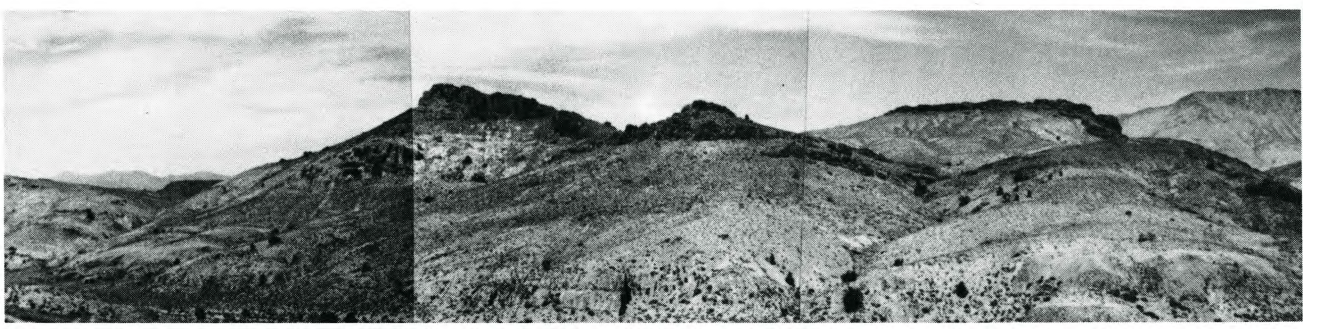

FIGURE R12—Landslide blocks of Paleozoic rocks as much as 2 km^2 in area (dark outcrops on skyline) resting on Northumberland Tuff near the caldera edge. Tuff is altered beneath blocks. From McKee (1976).

(Shawe et al., 1986). Gold is mined using open-pit methods and extracted using standard heap-leaching technology. **14.0**

144.0 The Manhattan gold district is situated about 10 km to the east. Although the district is located on the southern margin of the 25 Ma Manhattan caldera, in contrast to Round Mountain hydrothermal activity and mineralization took place appreciably later than caldera activity, at about 16 Ma (Shawe et al., 1986). **16.7**

160.7 The Big Ten Peak caldera, one of the larger collapse calderas of central Nevada, is centered about 30 km to the east. The Big Ten center was active at about the same time as the Toquima caldera complex (Boden, 1986; Shawe et al., 1987). Although outflow sheets are well developed on all sides of the caldera, much of the erupted rhyolitic pyroclastic material apparently ponded within the depression that formed concurrent with eruption. The Big Ten Peak caldera is noteworthy for the number and size of the landslide blocks within the intracaldera tuff prism. These blocks are chiefly of Paleozoic rock, and one of them is more than 1.5 km in length. **15.7**

176.4 Turn right (west) onto US-6 toward Tonopah. **5.0**

181.4 Arrive in Tonopah, a famous bonanza mining camp of the western United States. A recent comprehensive discussion of the geology of this classic district and surrounding areas has been given by Bonham and Garside (1979). Epithermal veins of the adularia–sericite type, containing silver sulfides and sulfosalts, are situated near the northern margin of a probable collapse caldera (Fraction caldera of Sargent and Roggensack, 1984) that formed during eruption of lower Miocene Fraction Tuff, which in turn overlies intermediate lavas of the Mizpah Formation. Veins are overlain and cut by pyroclastic rocks and associated domes of the Oddie and Brougher Rhyolites which form many hills at and near Tonopah (Fig. R13). Radiometric dating of preore and postore volcanic rocks and gangue minerals (Silberman et al., 1979) shows that mineralization took place within several million years of caldera formation.

Turn south onto US-95. **1.2**

182.6 Nye–Esmeralda County line. On right is large composite dome of Brougher Rhyolite (Fig. R13). **1.5**

184.1 Turn left on old US-95. **1.9**

186.0 The Divide district can be seen on hill to east. Hydrothermal activity and mineralization at Divide, which is several million years younger than that at Tonopah, is spatially, and apparently genetically, related to domes of Oddie Rhyolite. **1.1**

187.1 Hasbrouck Mountain to the west (Fig. R14) contains a very well-exposed fossil hot-spring-type gold–silver system of the Divide district and is situated near the southern part of the ring-fracture system of the caldera that formed on eruption of the Fraction Tuff. **2.2**

189.3 Dome of Brougher Rhyolite to west. Rejoin US-95. **10.9**

200.2 The orange outcrop of welded ash-flow tuff to the east is farthest northern exposure known of the upper Miocene Spearhead Member of the Stonewall Flat Tuff. To the southwest, isolated exposures of the Spearhead dip gently to the north. **8.5**

208.7 Goldfield, Nevada. Goldfield is a classic epithermal acid-sulfate type gold district. Nearly all production was from workings located within a small area centered less than 1 mi northeast of town. Mineralization took place about 20 Ma, and was largely controlled by shallow-dipping structures along the southwestern part of the ring-fracture system of a small caldera that formed in Oligocene time (Ashley, 1974, 1979). **0.3**

209.0 The Spearhead Member overlain by the Malpais Basalt is continuously exposed in the cliff to the southwest. **0.6**

209.6 Goldfield summmit. **0.2**

209.8 Stonewall Mountain can be seen ahead in the distance. **0.6**

210.4 The Spearhead Member of the Stonewall Flat Tuff is well exposed in the cliff to the west, where a complete vertical progression of unwelded, glassy ash-flow tuff grades upward into densely welded vitrophyre, which in turn grades upward into densely welded, primarily devitrified tuff. **4.0**

214.4 A thin (±1 m) outcrop of the lower, shard-rich phase of the Civet Cat Canyon Member of the Stonewall Flat Tuff is exposed about 200 m east of the highway. **7.8**

222.2 The main part of the Cuprite district is located east of the highway. The district includes a large area of spectacular, but barren, alunite- and kaolinite-

FIGURE R13—View toward northwest of large dome of Brougher Rhyolite located directly south of Tonopah. The dome lies along the northwestern part of the ring-fracture system of the Fraction caldera that formed on eruption of the Fraction Tuff (Sargent and Roggensack, 1984).

FIGURE R14—View toward northeast of Hasbrouck Mountain, a classic hot-spring-type Au–Ag system situated along the southern part of the ring-fracture system of the Fraction caldera (see Fig. R13).

bearing silica-rich, high-level, acid-leached volcanic rock that has been utilized by remote-sensing proponents in attempts to demonstrate the utility of their technology for mineral exploration (e.g., Abrams et al., 1977; Borngasser and Taranik, 1985). The district lies a short distance outside of the inferred location of the buried topographic rim of the Stonewall Mountain caldera (Noble et al., 1984). Alunite from acid-leached rock has a K–Ar age of 6.0 ± 0.3 Ma, which is within the limits of analytical uncertainty of the age of the outflow sheets of the Stonewall Mountain volcanic center (Nobel et al., 1988). The alteration at Cuprite is therefore interpreted as the result of late-stage hydrothermal activity of the Stonewall Mountain caldera cycle. **0.3**

222.5 Lida (Cottontail) Junction. To the east and southeast is the resurgent dome of the late Miocene (about 6.3 Ma) Stonewall Mountain volcanic center (Foley, 1978; Noble et al., 1984; Weiss and Noble, 1989), the youngest center of the southwestern Nevada volcanic field, and one of the four centers in the southern Great Basin from which peralkaline silicic magmas were erupted. The Spearhead Member of the Stonewall Flat Tuff has a known extent of more than 115 km from northwest of Goldfield to the Beatty–Bullfrog Hills to the south, and provides a lower limit on the time of movement on the Bare Mountain–Original Bullfrog detachment fault (Weiss et al., 1988). **2.0**

224.5 **STOP 2-6 (Noble). Stonewall Mountain volcanic center.** Stop, turn vehicles around, and park on east side of highway. This late Miocene volcanic center to the northeast is composed of a complex assemblage of resurgently uplifted intracaldera welded tuff of the Civet Cat Canyon Member cut by cogenetic intrusive rock. The present elevation of the intracaldera rocks reflects a combination of central resurgence and uplift along range-bounding normal faults. The buried topographic rim of the caldera that formed on eruption of the Spearhead Member is situated 4–5 km to the northeast of this stop, with proximity to the vent areas shown by the presence of lithic blocks of lava 0.5–2 m in diameter and abundant large blocks of nonvesiculated juvenile magmatic material within the most proximal parts of the outflow sheet (Weiss and Noble, 1989). We will walk to, and climb, the low ridge to the east (Fig. R15); the total round-trip hike will be about 1.5 mi (2.5 km).

The ridge consists largely of partly to densely welded and primarily devitrified and vapor-phase crystallized ash-flow tuff of the Spearhead Member. The several ledges represent subunits within the Spearhead. The uppermost part of the member is nonwelded, glassy, and contains blocks of glassy pumice that may exceed 0.5 m in diameter.

The uppermost part of the ridge is composed of ash-flow tuffs of the Civet Cat Canyon Member of the Stonewall Flat Tuff, which is separated from the underlying Spearhead Member by a complete cooling break. Although only several meters thick at this locality, the Civet Cat Canyon Member includes both shard-rich and phenocryst-poor tuff characteristic of the lower part of the unit and more phenocryst-rich tuff containing both white, phenocryst-poor and dark, phenocryst-rich pumice blocks characteristic of the uppermost part of the compositionally zoned unit. The porous, glassy lowermost part of the Civet Cat can be recognized by its distinctive orangish-yellow color; devitrified tuff is purplish gray to gray.

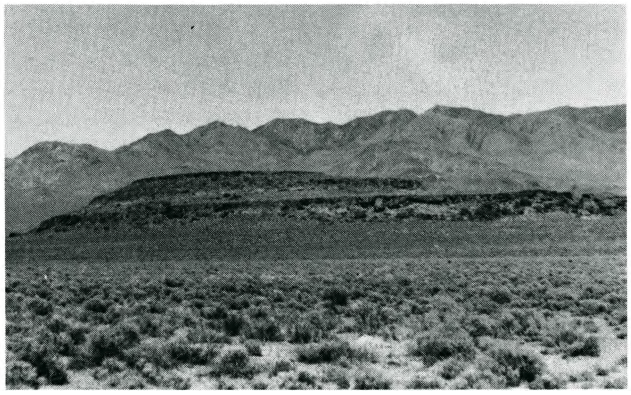

FIGURE R 15—View toward east of outcrop of outflow ash-flow tuff sheets of the Stonewall Flat Tuff. Lower cliffs are composed of the Spearhead Member; the upper cliff, which makes up less than 5% of thickness of tuff exposed, is the Civet Cat, Canyon Member. Stonewall Mountain in background.

Return to the vehicles and return to Tonopah.

Day 3

Stops today deal with very large volume Oligocene ash-flow deposits and a large source caldera containing thick intracaldera tuffs and landslide masses shed off the caldera wall. Two of the deposits are of the Monotony compositional type.

Mileage

0.0 Leave Tonopah heading east on US-6; mileage starts at crest of low pass east of town. **5.0**

5.0 Continue east past intersection with NV-376. **1.5**

6.5 Small oil refinery to south beyond airport processes crude from the Railroad Valley field which we will drive through later today. It is the only producing field in Nevada. **25.3**

31.8 Kawich Range in distance to southeast is location of Kawich caldera, apparently the source of tuff of White Blotch Spring; on the basis of composition, natural remanent-magnetization direction, and age the upper member of this unit correlates (Deino and Best, 1988) with the granite-weathering tuff and the Paharanagat Lakes Tuff to be seen later during the trip. **6.2**

38.0 To the northwest (Fig. R16), prominent ledges include two cooling units of the Isom compositional type from unknown sources. They overlie ash-flow deposits derived from the Big Ten Peak caldera located in the higher part of the Monitor Range farther to the north. **10.7**

48.7 The southern end of the aptly named Pancake Range lies across the valley to the northeast. **1.3**

50.0 Warm Springs roadhouse (abandoned) and intersection with NV-375. Continue heading straight (northeast) on US-6. **15.0**

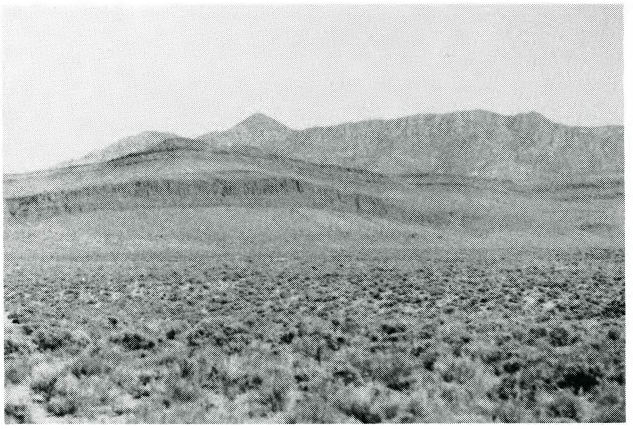

FIGURE R16—View of Georges Canyon Rim (low foothills) containing prominent ledges of ash-flow tuff of the Isom compositional type. Thick intracaldera tuff of Big Ten Peak emplaced about 25 Ma within its caldera forms high mountain in background.

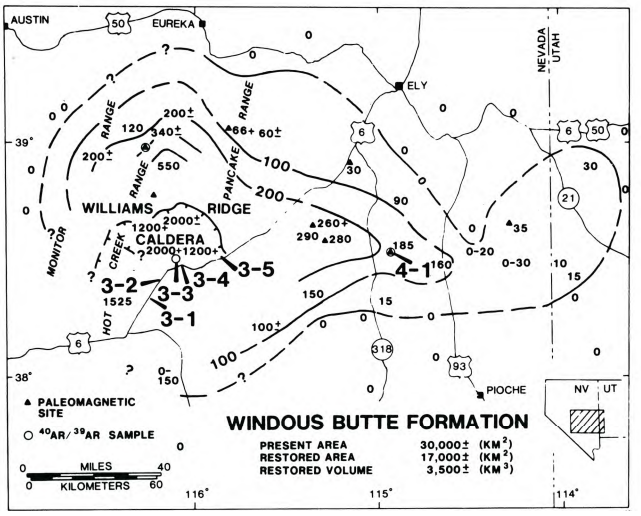

FIGURE R17—Distribution and thickness (in meters) of the Windous Butte Formation whose eruption caused collapse of the Williams Ridge caldera, which was subsequently filled with the tuff of Williams Ridge and Morey Peak, here considered to be part of Windous Butte Formation. Caldera margin mainly from Sargent and Roggensack (1984). Data on Windous Butte tuff from many published sources and unpublished field work of M. G. Best. Triangles indicate paleomagnetic sample locales of Grommé et al. (1972) and C. S. Grommé and J. T. Hagstrum (unpubl. data). Bold numbers are stops on this field trip. Zero thickness is based on absence of Windous between older and younger rocks. Area derived from planimetry, restored area based on an assumed east–west crustal extension of 50%, and volume derived by integration of areas inside isopachs.

65.0 **STOP 3-1 (Best and Deino). Caldera complex and associated ash-flow deposits in and near the Pancake Range.** Pull off highway into rest stop south of Blue Jay Maintenance Station. We are close to the western margin of a large cluster of calderas that formed during the Oligocene and early Miocene as four very large, regionally extensive ash flows were erupted together with many smaller volume extrusions (see overview paper Fig. 7, Table 2, and associated references). The exact locations of these depressions, particularly in the southern part, and their nature and evolution are poorly understood.

Prior to the major caldera-forming activity, rhyolite, dacite, and andesite lavas as old as about 38 Ma were extruded to form local discontinuous piles upon an erosion surface cut into Paleozoic rocks. At 31.37 ± 0.03 Ma (Deino, unpubl. data) at least 3000 km^3 of crystal-rich, low-silica rhyolite magma was broadcast, apparently mainly eastward (Fig. R17), and forms the Windous Butte Formation. This eruption was responsible for at least the initial collapse of the Williams Ridge caldera. The thick (at least 2 km) compositionally similar tuff of Williams Ridge and Morey Peak partially filled this depression 31.33 ± 0.03 Ma (Deino, unpubl. data). Intracaldera landslide breccias, minor local tuffaceous sedimentary rocks, a variety of lavas aggregating no more than a few hundred cubic kilometers, and probably several hundred cubic kilometers of crystal-rich low-silica rhyolite tuff filled the caldera. The tuff comprises several local, informal stratigraphic units roughly 31–30 Ma, which probably represent eruptions from the same magma system.

Following a brief hiatus, another voluminous (3000+ km^3) ash-flow eruption occurred 27.31 ± 0.03 Ma (Deino, unpubl. data) that formed the Monotony Tuff (Ekren et al., 1971) and an obscure caldera located mostly to the southeast of this stop (Fig. R18). The Monotony is a crystal-rich dacite and the type example of the Monotony compositional type.

Mostly rhyolite tuff sheets overlie the Monotony Tuff in this area. Cooling units of the Shingle Pass Tuff were formed from ash flows derived from an as yet poorly delineated source in the southern Quinn Canyon Range southeast of this stop (Fig. R19). Recent age determinations by Deino (unpubl.) on two units at Shingle Pass (Stop 4-2) are 26.68 ± 0.03 and 26.00 ± 0.03 Ma. The overlying large-volume tuff of Lunar Cuesta erupted about 25 Ma to form a caldera located to the northeast in the Pancake Range (Ekren et al., 1974). The youngest regional sheet is a crystal-rich, high-silica rhyolite erupted 22.65 ± 0.009 Ma (Deino and Best, 1988) associated with the Kawich caldera. In the Pancake Range this sheet is called the granite-weathering tuff.

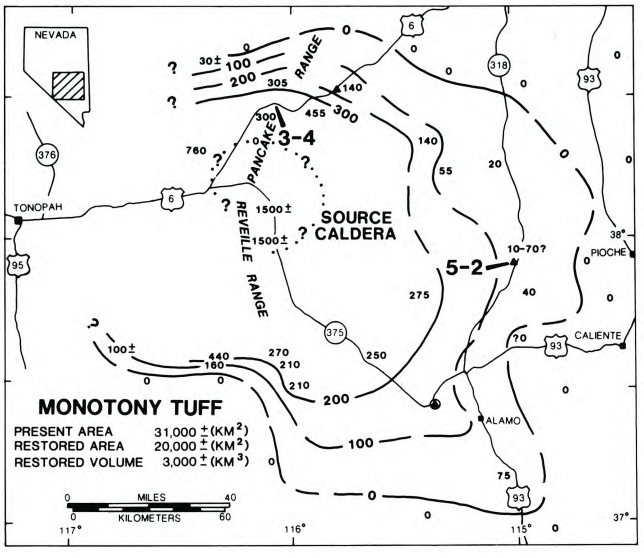

FIGURE R18—Distribution and thickness (in meters) of the Monotony Tuff. An obscure source caldera (dotted) may include a part of the Reveille Range. See caption of Fig. R17 for additional information.

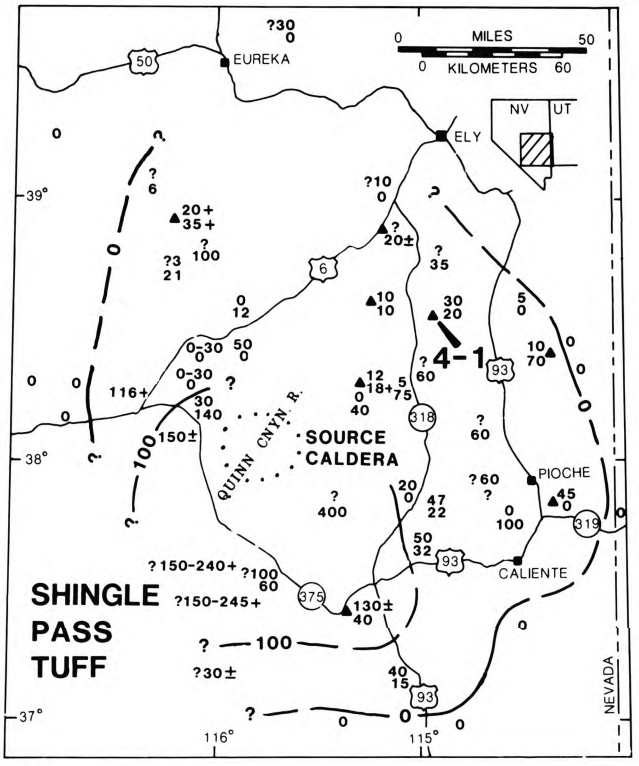

PRESENT AREA OF FORMATION	40,000± (KM^2)
RESTORED AREA	30,000± (KM^2)
RESTORED VOLUME OF UPPER MEMBER	1,100± (KM^3)
LOWER MEMBER	700± (KM^3)

FIGURE R19—Distribution, thickness (in meters), and probable source caldera (dotted outline from Sargent and Roggensack, 1984) of the two members of the Shingle Pass Tuff. Locales in southwestern part of map on Bombing and Gunnery Range have not been examined, but published maps indicate as many as six cooling units of Shingle Pass Tuff. Single thickness values indicate total for whole formation. Queries before a number indicate uncertain correlation and queries above or below a number indicate uncertain presence of upper or lower member, respectively. See caption of Fig. R14 for additional information.

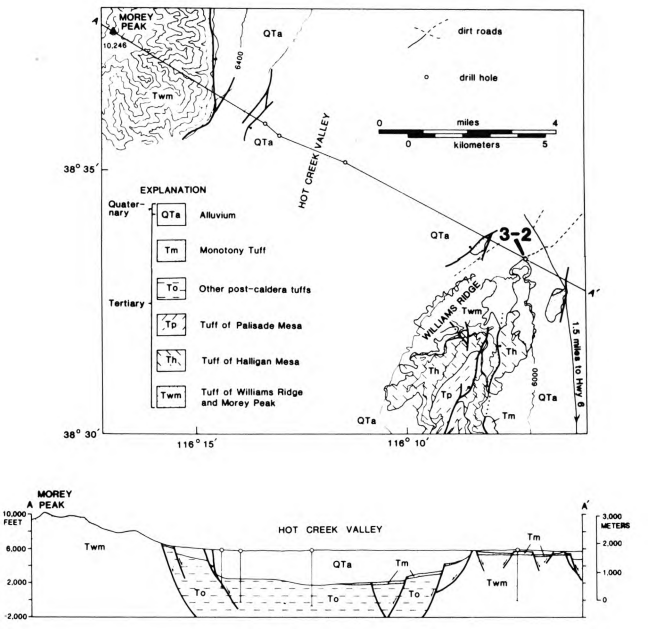

FIGURE R21—Simplified geologic map and cross section of a part of the Hot Creek Valley area (after Ekren et al., 1973; John, 1987) showing great thickness of tuff within the Williams Ridge caldera. Contour interval 400 ft.

Across the valley to the north in the Hot Creek Range, the entire eastern escarpment, about 1 km high beneath Morey Peak, is underlain by tuff of Williams Ridge and Morey Peak (Figs. R20, R21). This Basin and Range horst block may have partially resurged during evolution of the caldera (John, 1987) to expose the thick section of intracaldera tuff that is otherwise mostly observed in deep drill holes, as at Stop 3-3.

To the northeast, the dominant part of Palisade Mesa (Fig. R22; see also Snyder et al., 1972) consists of about 250 m of tuff of Halligan Mesa and younger tuff of Palisade Mesa. These appear to have been locally derived from within the Williams Ridge caldera soon after its collapse and will be examined at the next stop. Overlying these deposits, in ascending order, are the Monotony Tuff, the tuff of Lunar Cuesta, and, in the small peak, the granite-weathering tuff.

Due east of this stop, a >250 m thick section of Shingle Pass Tuff (absent just to the north) and younger, locally derived sheets are banked disconformably against the older tuffs of Halligan Mesa and Palisade Mesa; Ekren et al. (1974) interpreted this to be a segment of the topographic wall of the unnamed caldera associated with eruption of the Monotony Tuff.

Continue northeast on highway. **4.4**

69.4 **STOP 3-2 (Noble). Tuffs of Halligan Mesa and Palisade Mesa.** Pull off highway. These two deposits (Fig. R23) show features typical of simple

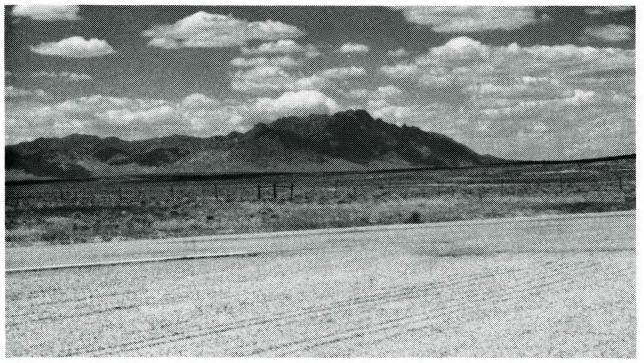

FIGURE R20—View northward from Bluejay Maintenance Station (Stop 3-1) on US-6 of Morey Peak, elevation 10,246 ft.

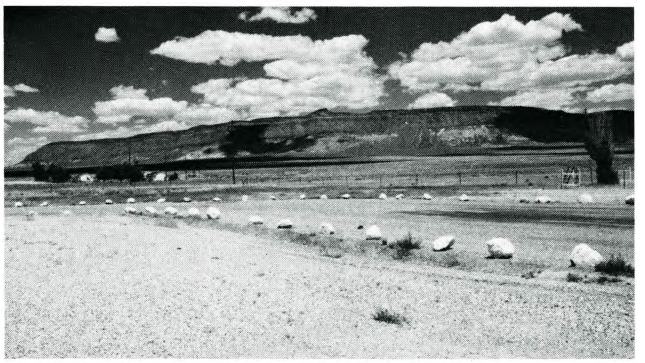

FIGURE R22—View northeastward from Bluejay Maintenance Station (Stop 3-1) on US-6 of Palisade Mesa.

FIGURE R23—Palisade Mesa at Stop 3-2. Lowest part of slope is upper, pale-gray to brown part of tuff of Halligan Mesa. Entire tuff of Palisade Mesa, from black basal vitrophyre up through devitrified zone, is exposed beneath Monotony Tuff (on skyline).

cooling units of crystal-rich ash-flow tuff in the Great Basin. Within a few meters above base is a prominently exposed, densely welded black vitrophyre that can be several meters thick. Overlying this, usually in sharp contact, is devitrified tuff in which degree of welding decreases and vapor-phase precipitation increases upward; the reddish-brown color of this devitrified zone gives way upward to lighter hues of red, brown, or gray. Columnar jointing in the tuff of Palisade Mesa at this stop is unusually well developed; anastomosing, subhorizontal parting surfaces bounding coherent columnar joint systems might indicate subtle cooling breaks or reflect effects of joint nucleation in the cooling deposit.

Both tuffs have 23–47% phenocrysts of which 20–45% is quartz, 18–42% sanidine, 22–46% plagioclase, 1–10% biotite, and 0–3% hornblende.

Continue northeast on highway. **6.6**

76.9 Turn left (north) onto gravel road and proceed toward Moores Station. **5.8**

81.8 Turn sharp left onto dirt road (easy to miss!) which doubles back to south a short distance before heading southwest. **0.6**

82.4 **Stop at end of road near collar of drill hole. STOP 3-3 (Noble and Best). Thick intracaldera tuff of Williams Ridge and Morey Peak.** A 1700 m drill hole here penetrated only this tuff (Fig. R21). An outcrop is just a short distance to south. It has 48–55% phenocrysts of which 22–27% is quartz, 2–25% sanidine, 48–54% plagioclase, 5–10% biotite, 2–6% hornblende, and a trace of two pyroxenes (Ekren et al., 1973).

Turn around and return to gravel road. **0.6**

83.0 Turn right (south) and return to highway. **5.8**

88.8 Turn left (northeast) onto highway. **1.0**

89.8 **STOP 3-4. (Noble and Best). Monotony Tuff** (Fig. R18). Pull off highway. The tuff here is a simple cooling unit 300 m thick. Elsewhere, the formation consists of as many as three cooling units. The Monotony is the youngest (27.31 ± 0.03 Ma) and the type unit of the crystal-rich dacite tuff sheets of the Monotony compositional type. It has 30–55% phenocrysts of which 10–32% is quartz, 5–12% sanidine, 46–63% plagioclase, 10–20% biotite, trace–4% hornblende, and as much as 5% augite (Snyder et al., 1972). Here it contains cognate clasts as much as 25 cm in diameter. Some are flattened, presumably because they were vesicular upon entrainment in the ash flow and were compacted after deposition. Others, however, are not flattened and could represent samples of nonvesiculated magma from the pre-eruption chamber.

Continue northeast on highway. **1.5**

91.3 Lunar Crater turnoff to south; continue straight. To east is the Lunar Crater basalt field developed since 6 Ma along a north-northeast-striking fissure system (Scott and Trask, 1971). It consists of numerous lava flows of alkaline basalt, some 70 cinder cones, and at least two maars—one of which, Lunar Crater, is a spectacular structure easily reached about 6 mi south of this intersection. Nearly every lava flow and ejecta deposit contains megacrysts and Ti–Al-rich xenoliths of gabbro and clinopyroxenite, but only three vents have erupted Cr-rich spinel peridotite of mantle origin (Menzies et al., 1987). Late Cenozoic (<6 Ma) basaltic volcanism is concentrated along the margins of the Great Basin and its only expression within the interior is here in the Lunar Crater field (Best and Hamblin, 1978; Fitton et al., 1988). **9.3**

100.6 Turn left (northeast) onto dirt road and proceed to radio relay station. **1.9**

102.5 **STOP 3-5 (Best and Noble). Landslide mass of Devonian limestone near margin of Williams Ridge caldera.** Stop at relay station. Shattered and altered limestone rests on altered tuff of Williams Ridge and Morey Peak (Figs. R24, R25) within 3 km of the caldera margin. When the landslide was emplaced the tuff must have been hot and still permeated with vapor to promote the alteration.

Turn around and head back down dirt road. **1.3**

103.8 Turn right (north) onto another dirt road. **4.4**

108.2 **STOP 3-6 (Best and Christiansen). Wah Wah Springs Formation.** Turn around and stop. Within the thick sequence of tuffs filling and overlapping the Williams Ridge caldera is the distal western

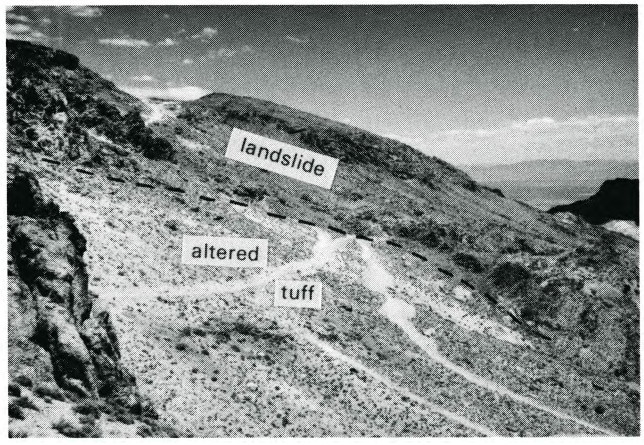

FIGURE R24—View at Stop 3-5 of shattered and altered landslide mass of Devonian limestone resting on altered intracaldera tuff of Williams Ridge and Morey Peak. See Fig. R25 for geologic map.

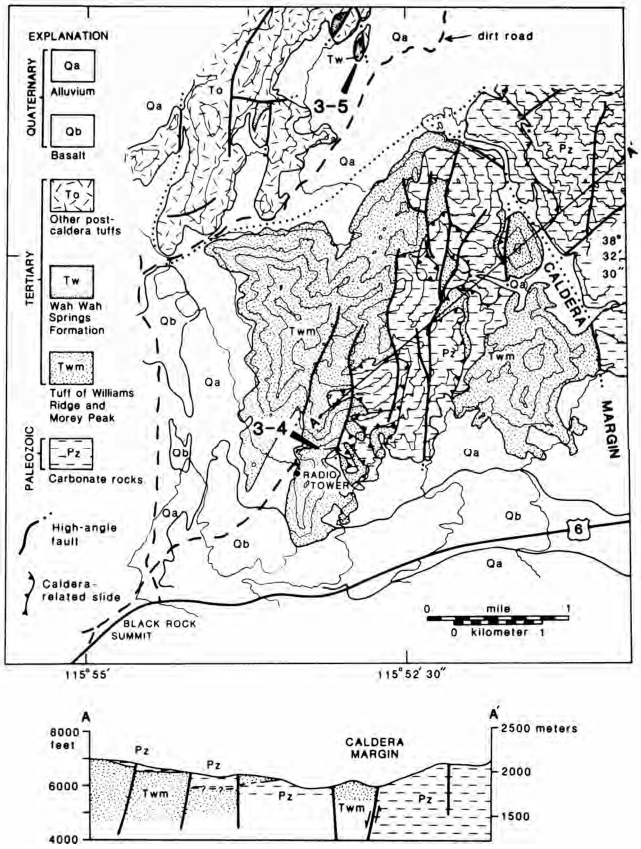

FIGURE R25—Geologic map and cross section of a segment of the eastern margin of the Williams Ridge caldera (simplified from Quinlivan et al. , 1974). Contour interval 200 ft. Bold numbers are stops on this field trip. See also Fig. R24.

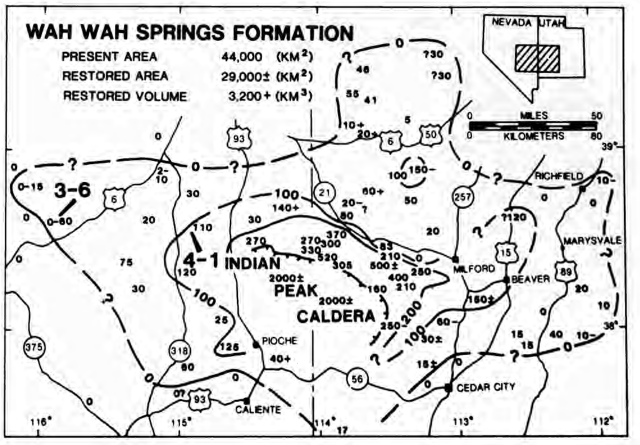

FIGURE R26—Distribution and thickness (in meters) of the Wah Wah Springs Formation whose eruption 29.5 Ma created the Indian Peak caldera. Line with tick marks is topographic margin; caldera is concealed on southwest within younger White Rock caldera (not shown).

margin of the very large outflow tuff member of the Wah Wah Springs Formation whose eruption 29.5 Ma produced the Indian Peak caldera that straddles the Nevada–Utah state line. (Fig. R26). Although to be seen again at Stops 4-2 and 5-3, its typical expression—black basal vitrophyre and overlying reddish-brown devitrified tuff—is best seen here.

The Wah Wah Springs is similar to other "twins" of the crystal-rich dacite Monotony compositional type except it is more calcic so that hornblende dominates over biotite, quartz is less abundant, and sanidine is absent. No other regionally extensive tuff in the Great Basin shares these particular compositional features. The mode is 40% total phenocrysts, of which 6% is quartz, 63% plagioclase, 10% biotite, 19% hornblende, and 2% augite; practically no variation in this mode is observed throughout the length and thickness of the outflow sheet and only slightly more quartz occurs in the intracaldera tuff.

Head back (south) toward highway. **4.4**

112.6 Turn right (southwest) at dirt crossroad. **0.6**

113.2 Turn left (east) onto US-6. **7.0**

120.2 Two cooling units of Monotony Tuff crop out along highway to southeast. **10.4**

130.6 Railroad Valley oil field produces from Oligocene tuff and the late Eocene and early Oligocene Sheep Pass Formation, a local clastic deposit in eastern Nevada. **7.5**

138.1 Ragged Ridge to east forms the north end of the Grant Range. The ridge is underlain by a steeply tilted (50° NE) section of Oligocene and early Miocene tuff sheets including in ascending order the Stone Cabin, Windous Butte, and Wah Wah Springs Formations and the Shingle Pass Tuff. Overlying this section is a thick (as much as 3 km) sequence of clastic sedimentary rocks, tuffs, and gravity-slide masses of the Miocene and Pliocene(?) Horse Camp Formation (Moores et al., 1968). The intensive post-volcanic deformation and sedimentation manifest here contrast sharply with the flat-lying rocks of the Pancake Range to west. **5.8**

143.9 Community of Currant. Continue northeast on US-6. **23.6**

167.5 On right (southeast) is Windous Butte, formation namesake. To south of butte, cuts into white Currant Tuff mark the Currant Creek hydrothermal magnesite deposits. Overlying tuff of Windous Butte Formation is unaltered. **5.1**

172.6 Intersection with NV-318; continue straight on US-6. **23.9**

196.5 Arrive in Ely. Stop overnight. Besides being the seat of White Pine County, Ely once supported Kennecott's large open-pit copper mine just to west. But since operations were shut down more than a decade ago, the only present activity in the region is in small gold mines some 80 km to the northwest.

Day 4

On this day only three stops are made. At the first two, we examine one of the most famous volcanic sections in the Great Basin—a sequence of seven regionally extensive, Oligocene to early Miocene ash-flow sheets from four different sources to the west, southwest, and south at Shingle Pass. The third stop is an overview of, and introduction to, the huge Indian Peak caldera complex.

Mileage

0.0 Leave Ely heading south on US-6. Mileage begins at intersection with US-50 in older part of downtown. **23.9**

23.9 Turn left (south) onto NV-318 and proceed down White River Valley. **11.8**

35.7 Downtown Lund. Continue south. **24.7**

60.4 Turn left onto gravel road, at cattleguard with white painted ends, and proceed eastward toward Shingle Pass in Egan Range. **5.0**

65.4 **STOP 4-1 (Grommé). Shingle Pass fault and Windous Butte Formation** (Fig. R27). Stop along road at washed out stone bridge. Some structural features here are of particular interest because they seem to indicate major extension broadly concurrent with volcanism. This northeast-trending valley follows the Shingle Pass fault across which the Paleozoic section has been dropped down to the northwest about 4 km. Some of this movement appears to have occurred not long before the volcanic rocks were deposited because a huge block of Paleozoic rock, believed by Kellogg (1960) to have slid off the fault scarp, rests on late Eocene and early Oligocene Sheep Pass Formation a mile north of this stop and is in turn overlain by the volcanic section. Tilted tuff sheets in this section indicate continued movement on the probably listric Shingle Pass fault after the youngest tuff was deposited 22.65 ± 0.03 Ma. These steep dips are unusual for the Egan Range and may suggest an eastward continuation of the area of considerable Tertiary extension seen yesterday east of Currant at Ragged Ridge in northern Grant Range.

Exposed in the wash and up ridge to north of here is the Windous Butte Formation (Cook, 1965), the lowest regional tuff sheet in this Shingle Pass section. Although comprising a single cooling unit with uniform paleomagnetic direction, the lower 20 m or so of the tuff has relatively small sparse phenocrysts whereas the overlying 150 m is much more porphyritic. The contact between these two welded tuffs can be seen next to a clump of willows on the northwest side of the wash.

Continue up dirt road. **0.5**

65.9 **STOP 4-2 (Best and Grommé). Well-known Shingle Pass section** (Fig. R28, Table R2). Turn around and stop at Shingle Spring southwest of corral. An extended hike progresses up through a 465 m section of seven regional tuff sheets deposited about 31–23 Ma and derived from central, southern, and eastern Nevada sources. Hike up gully across the road northwest of the corral almost to the saddle, turn right (east) and then descend down hill and up section.

The upper crystal-rich part of Windous Butte Formation is exposed on either side of gully. Near top of southeast side of the gully it is overlain by a few meters of black crystal-rich vitrophyre which is compositionally *unlike* the Windous Butte or the overlying Cottonwood Wash Tuff. This vitrophyre

TABLE R2—Stratigraphic sequence near Shingle Pass in southern Egan Range, Nevada. *Proportions of phenocrysts in whole rock; †plus trace of olivine and allanite.

Stratigraphic unit	Thickness (m)	Age (Ma)	Composition* (Q/S/P/B/H/Px/tot)
Pahranagat Lakes Tuff	20	22.65	8/5/4/1/tr/tr/18
Bauers Tuff Mbr., Condor Canyon Fm.	10	22.78	0/5/8/1/0/tr/14
Conglomerate	10 ±		clasts of Wah Wah Springs tuff
Shingle Pass Tuff			
Upper unit	40	26.00	tr/2/3/1/0/0/6
Lower unit	35	26.68	1/7/5/0/tr/1/14†
Wah Wah Springs Fm.	60	29.5	2/0/25/5/7/tr/40
Cottonwood Wash Tuff	120	30.6	5/0/24/6/5/tr/40
Windous Butte Fm.	165	31.37	
Upper part			10/6/18/4/3/tr/41
Lower part			
Conglomerate	400		clasts of Paleozoic rock

Dacitic lava flow

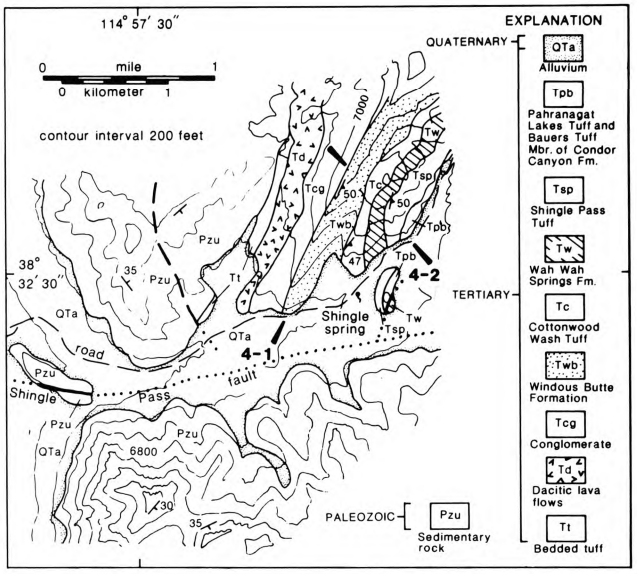

FIGURE R27—Geologic map of the area around Shingle Spring southwest of Shingle Pass in the southern Egan Range (compare Kellogg, 1960). Bold numbers are stops on this field trip. Pzu unit includes rocks as old as Cambrian south of the Shingle Pass fault, but as young as Pennsylvanian north of it. Shingle Pass lies 3 km northeast of end of road near northeast corner of map.

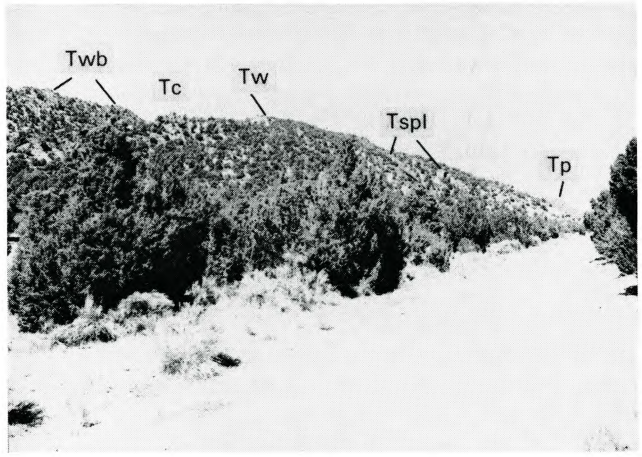

FIGURE R28—View looking northeast from Shingle Spring, Stop 4-2, at Tertiary section of ash-flow tuffs. See Table R2 for additional details. Twb, Windous Butte Formation exposed on southeast-facing slope; Tc, Cottonwood Wash Tuff; Tw, outflow-tuff member of Wah Wah Springs Formation; Tspl, lower unit in Shingle Pass Tuff; Tp, Pahranagat Lakes Tuff of Williams (1967).

closely resembles the Wah Wah Springs Formation, but improbably complicated faulting would be required to insert it into this lower stratigraphic position.

The Cottonwood Wash Tuff is the oldest of three very large, crystal-rich dacite ash-flow sheets of the Needles Range Group erupted from the Indian Peak caldera complex to the east (Fig. R29). A major part of the volume of the Monotony compositional type is represented in just these three deposits. The Cottonwood Wash has an average K–Ar age of 30.6 Ma (Best and Grant, 1987) and an estimated volume, corrected for crustal extension, of 1500 km^3. This volume does not include an unknown amount in a source depression or fault-bounded caldera buried beneath an area of alluvium. Like other dacite tuffs of the Group, most of the phenocrysts (about 25% of rock) are plagioclase with lesser amounts of biotite, hornblende, quartz, Fe–Ti oxides, and augite; however, the Cottonwood Wash is characterized by uncommonly large books of biotite and a lesser amount of hornblende, which is inconspicuous in hand sample.

The overlying outflow tuff member of the Wah Wah Springs Formation emplaced 29.5 Ma (Best and Grant, 1987), also seen at Stop 3-6, can be distinguished from the older Cottonwood Wash Tuff by prominent hornblende phenocrysts.

Above the Wah Wah Springs are two cooling units of the widespread Shingle Pass Tuff—a key stratigraphic marker in the Tertiary volcanic sequence of the central Great Basin (Fig. R19). Cook (1965) defined the Shingle Pass Ignimbrite (since called Shingle Pass Tuff on all U.S. Geological Survey maps) as a thin unit overlying dacitic tuffs in the Needles Range Group with a type section near Shingle Pass. He noted that it contains sparse (7–25%) phenocrysts, about half of which are sanidine, a third plagioclase, and the remainder quartz and mafic minerals. We have found that the few

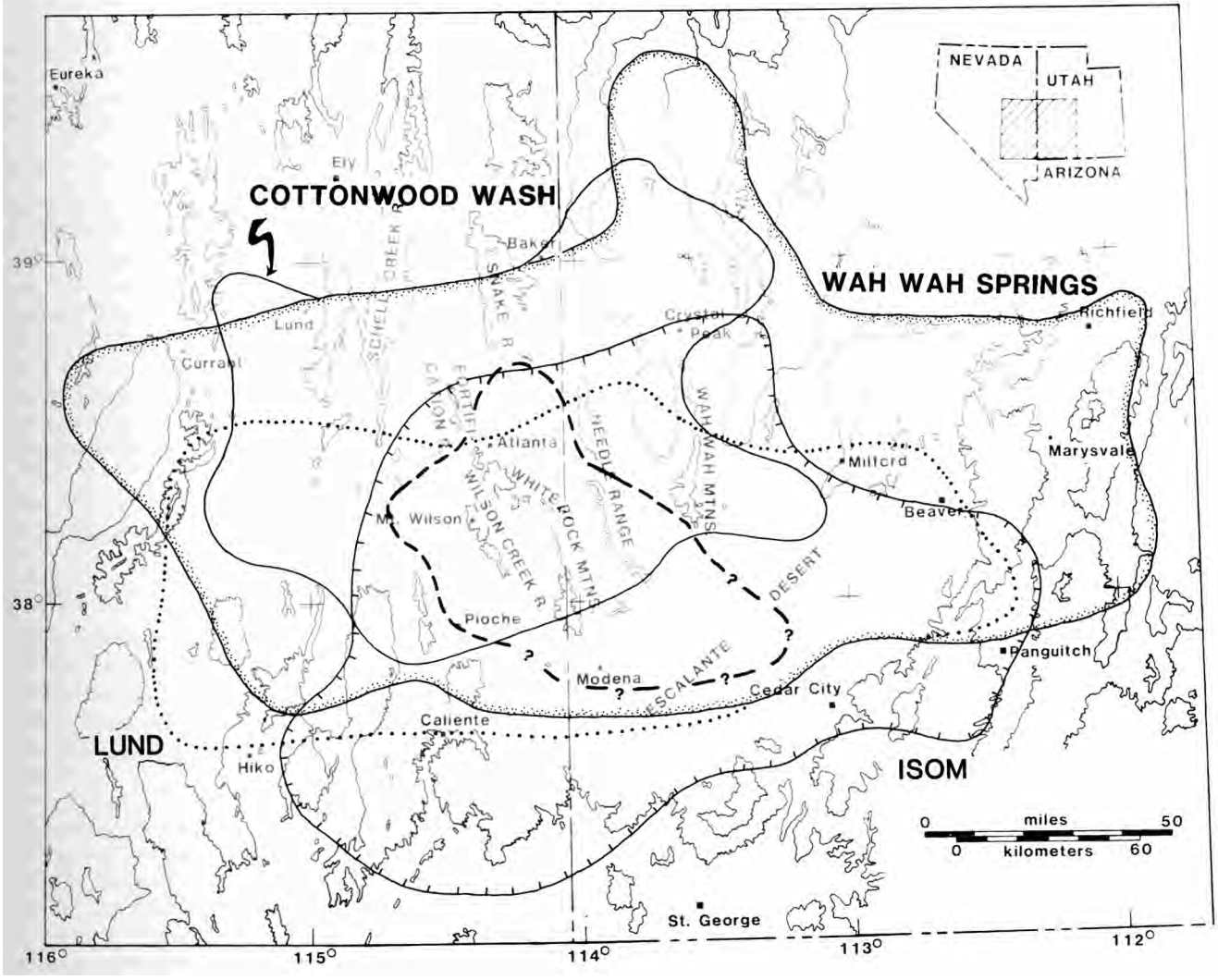

FIGURE R29—Indian Peak caldera complex (heavy line) astride the Utah–Nevada state line was produced by eruption of tuffs making up the Needles Range Group and Isom Formation (Fig. R30). Mapping at a scale of 1:24,000 in ranges near the center of the distribution of the 30.6 Ma Cottonwood Wash Tuff has disclosed no fault-bounded, or caldera, source; thus, it may be concealed beneath a broad alluvial area north of Atlanta or within the younger Indian Peak caldera. The southwestern part of this caldera, which collapsed 29.5 Ma during eruption of the Wah Wah Springs Formation, was engulfed 27.9 Ma into the White Rock caldera as tuff of the Lund Formation was erupted. About 27 Ma the small Mt. Wilson caldera formed within the White Rock caldera as the Ripgut Formation was erupted. Trachydacite tuffs of the Isom Formation were then erupted before 26.7 Ma from another concealed source near Modena.

percent of mafic phenocrysts, commonly seen in hand sample as rusty spots surrounding a black grain, constitute an unusual mineral assemblage for Oligocene tuffs in the Great Basin. Included are Fe-rich olivine, clino- and orthopyroxene, amphibole, and allanite (or chevkinite).

Cook (1965, figs. 5, 7) clearly showed three younger tuffs, but did not name them. We have found that the tuff directly overlying his Shingle Pass unit has a similar total phenocryst content, but contains about equal amounts of plagioclase and sanidine plus lesser biotite as the only mafic silicate. This unit is co-extensive with the underlying sheet in the Great Basin and so was probably derived from the same source in the Quinn Canyon Range (Fig. R19). Hence, we recognize upper and lower cooling units in the Shingle Pass Tuff.

The two youngest tuffs in the Shingle Pass section are separated from older units by a poorly exposed and possibly nonpersistent sandstone–conglomerate deposit which includes clasts as much as 0.5 m in diameter of Wah Wah Springs Formation. Overlying this clastic deposit is the Bauers Tuff Member of the Condor Canyon Formation (Williams, 1967) which is virtually identical in composition with the upper Shingle Pass Tuff. Here, at the distal northwest margin of the Bauers sheet (seen again at Stop 6-4), it has minute phenocrysts and lacks pumice lumps—both of which are more prominent nearer its source where it constitutes a veritable Shingle Pass twin.

The youngest sheet is the Pahranagat Lakes Tuff of Williams (1967), which will be seen again at Stop 6-4. It is a rhyolite tuff containing abundant white pumice lapilli and 20–35% total phenocrysts of (in order of diminishing amount) quartz, sanidine, plagioclase, biotite, and trace amounts of amphibole and Fe–Ti oxides. It probably correlates with the granite-weathering tuff, and with the upper tuff of White Blotch Spring (Deino and Best, 1988).

Drive back down valley to west. **5.6**

71.5 Turn left (south) onto NV-318. **29.3**

100.8 Turn left (east) onto gravel road to Bristol Wells. **2.7**

103.5 Take left fork to east. **18.0**

121.5 Turn left (northeast). Bristol silver mining district, now inactive, is to east. **3.6**

125.1 The Wilson Creek Range across Lake Valley to the east lies within the late Oligocene Indian Peak caldera complex—a cluster of overlapping sources of several tuffs, including the crystal-rich dacite Cottonwood Wash Tuff and Wah Wah Springs and Lund Formations (Figs. R29, R30). The next stop on the peak affords a better perspective of this complex; the more than 2 km of tuff beneath Mt. Wilson is only the top of an intracaldera section possibly 5 km and conceivably as much as 7 km thick.

Continue east, taking right fork. **2.8**

127.9 Turn right (south) onto US-93 toward Pioche. **5.5**

133.4 Straight ahead 8–10 km, the Pioche Hills consists of intensely faulted lower Cambrian quartzite, shale, and limestone that lie near the southwest margin of the Indian Peak caldera complex (Fig. R29; Best et al., 1989). Several now inactive mines west of the highway comprised the Pioche–Bristol mining district (Gemmill, 1968; Tschanz and Pampeyan, 1970) that produced in excess of $100 million in zinc, lead, silver, manganese, and gold since 1869. Because some igneous rocks associated with ore deposition have Cretaceous isotopic ages, it may only be fortuitous that the margin of the Indian Peak caldera complex passes through the district; a modern study of it in the context of Oligocene magmatism and caldera formation would be rewarding. **5.0**

AGE (Ma)	STRATIGRAPHIC UNIT: DACITE TUFF	STRATIGRAPHIC UNIT: RHYOLITE TUFF	DIMENSIONS OF TUFF: PRESENT AREA	DIMENSIONS OF TUFF: RESTORED AREA	DIMENSIONS OF TUFF: RESTORED VOLUME	SOURCE OF TUFF
27±	ISOM * FORMATION		28,000	20,000	1,300	SOUTHERN ESCALANTE DESERT
		RIPGUT FORMATION			400+	MT. WILSON CALDERA
27.9	LUND FORMATION		27,000	18,000	1,500+ 2,200	WHITE ROCK CALDERA
		RYAN SPRING FORMATION			300+	WITHIN OLDER INDIAN PEAK CALDERA
29.5	WAH WAH SPRINGS FORMATION		50,000	600+ 30,000	1,200± 2,000	INDIAN PEAK CALDERA
30.6	COTTONWOOD WASH TUFF		21,000	16,000	1,500±	SOUTH OF SNAKE RANGE
32±		ESCALANTE DESERT FORMATION			400+	PINE VALLEY CALDERA

* ISOM FORMATION IS TRACHYDACITE IN IUGS CLASSIFICATION

FIGURE R30—Stratigraphic relations and dimensional aspects of ash flows erupted from the Indian Peak magma locus. Ash-flow units in Escalante Desert Formation (not seen on this field trip) were derived from an obscure caldera source in Utah, almost entirely engulfed in younger Indian Peak caldera.

138.4 Turn left (east) onto gravel road; a sign here indicates the Caselton and Prince mines are reached in other direction (west). **3.8**

142.2 Take right fork to east. **8.4**

150.6 Take left fork to northwest. **12.5**

163.1 Switch-backs are in a 2 km thick intracaldera section of tuff and breccia (of Paleozoic carbonate rock) of the Ripgut Formation filling the Mt. Wilson caldera. To west and below road at this mileage is a 40 m thick cliff of black vitrophyre in the formation. **1.5**

164.6 Take right fork. **0.7**

165.3 **STOP 4-3 (Best and Christiansen). Panoramic view of Indian Peak caldera complex.** Turn around and stop at VORTAC station on top of Mt. Wilson. For orientation (Fig. R29): Wheeler Peak—second highest point in Nevada (elevation 13,061 ft)—is the prominent peak 60 km due north in the southern Snake Range and Indian Peak (9790 ft) lies 40 km east in the Needle Range in Utah. Figs. R31 to R35 detail an east to north perspective of the complex. To the south, mapping is incomplete.

The Indian Peak caldera complex was created from about 32 to 27 Ma as some 10^4 km^3 of recur-

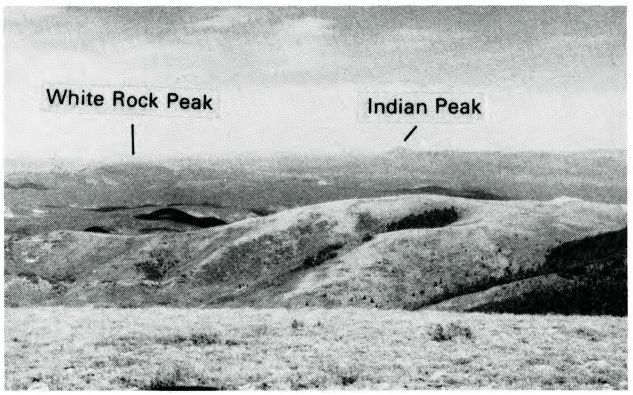

FIGURE R31—Panorama looking east from the top of Mt. Wilson, Stop 4-3, across Indian Peak caldera complex (Fig. R29). See Figs. R32 and R33 for geologic cross sections.

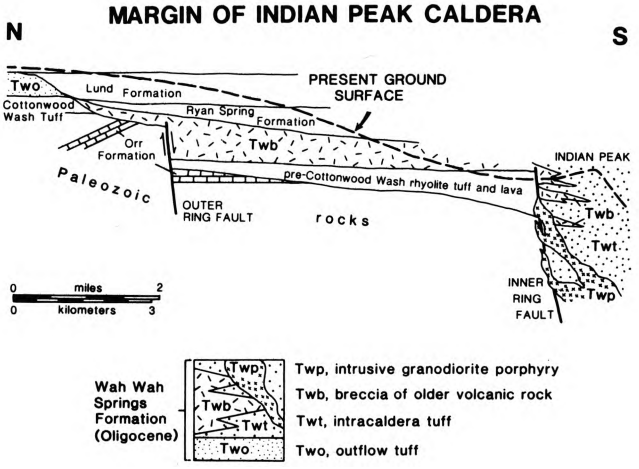

FIGURE R32—Idealized north–south cross section along crest of Needle Range in Utah, showing northeast margin of Indian Peak caldera restored to its pre-resurgence configuration (Best and Grant, 1987). Extensive faulting, probably in part associated with resurgence after collapse, is omitted.

rently erupted rhyolite and more voluminous and crystal-rich dacite magma was explosively discharged from a locus of activity astride the Nevada–Utah state line (Fig. R30). Two-pyroxene–plagioclase trachydacite ash flows were erupted at the close of activity. Pyroxene andesite lavas were extruded mostly during the early and late lifetime of the magma locus; their aggregate volume is probably only about 1% of the volume of ash-flow deposits. Rhyolite lavas compositionally similar to the rhyolite tuffs form an even more trivial volume in the complex.

Rhyolite tuffs (and minor local lava flows) are compositionally similar in containing modest amounts of mostly plagioclase and biotite phenocrysts, but some mineralogical and bulk chemical zonation is evident in compound cooling units, which are confined within older calderas. The more crystal-rich dacite tuffs which are compositionally similar to one another are an order of magnitude larger in volume; modal and bulk compositional variations within each of these Monotony compositional types are very small.

Mt. Wilson lies entirely within two and probably three calderas. Because the southwestern margin of the oldest Indian Peak caldera has caved into the White Rock caldera, its existence beneath Mt. Wilson is somewhat speculative. In the foothills of the Wilson Creek Range to the west and northwest of this stop is exposed a section possibly 3 km thick of intracaldera tuff of the Lund Formation in the White Rock caldera. The topographic margin of the youngest caldera, the Mt. Wilson, lies about 4 km to the north of this stop; this margin is defined by southward thinning masses of landslide breccias that interfinger with Ripgut tuff banked against a paleoescarpment cut into intracaldera tuff and breccia of the Lund Formation. Possibly 5 km of intracaldera tuff and landslide breccia associated with the superposed White Rock and Mt. Wilson calderas

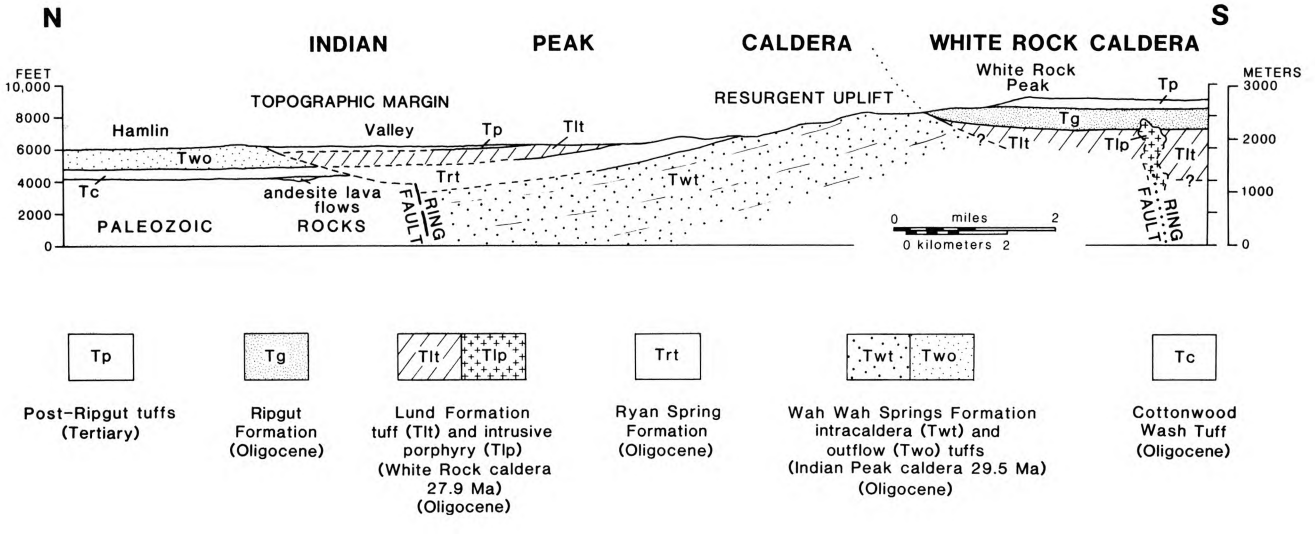

FIGURE R33—Generalized cross section from Hamlin Valley southward into the White Rock Mountains in Nevada just east of Stop 4-3, showing northern margins of the Indian Peak caldera and younger White Rock caldera (Best et al., 1989).

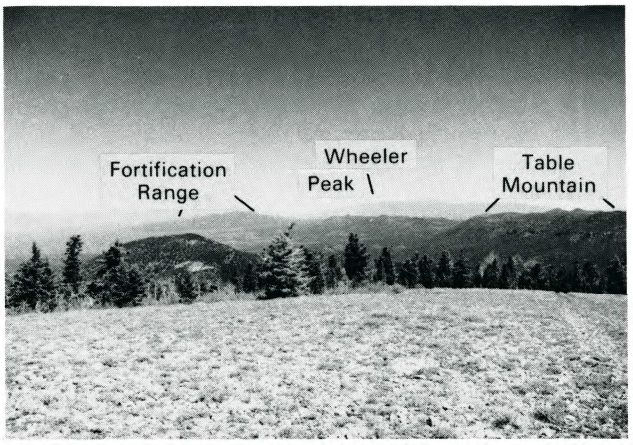

FIGURE R34—Panorama from Stop 4-3 on Mt. Wilson looking north. Table Mountain in foreground lies within caldera complex and is capped by several hundred meters of lower Miocene rhyolite tuffs and lava flows and latitic lava flows (Willis et al., 1987). Fortification Range (Loucks et al., 1989) lies just beyond northern margin of caldera complex. Low hills between Table Mountain and Fortification Range are capped by Isom Formation underlain by northward-thinning Ripgut Formation resting on intracaldera deposits of the White Rock caldera. Snow-capped Wheeler Peak in far distance.

underlie Mt. Wilson; this thickness could be as much as 7 km if the Indian Peak caldera also extends this far southwest.

Table Mountain north of Mt. Wilson is capped by as much as several hundred meters of a quasi-bimodal assemblage of olivine–pyroxene latite lava flows and high-silica, locally topaz-bearing, rhyolite tuffs and lava flows. This early Miocene sequence comprising the Blawn Formation (Willis et al., 1987; Best et al., 1987) was erupted from many local vents in and around the caldera complex and forms part of an east-northeast zone extending from central Utah into southern Nevada.

Drive down off mountain southwestward toward Pioche. **26.9**

192.2 Turn left (south) onto US-93; drive past Pioche. **28.7**

220.9 Arrive in Caliente; stop overnight.

Day 5

Four stops this day highlight the internal structure and stratigraphy of the Indian Peak caldera complex.

Mileage

0.0 Leave Caliente heading north on US-93. Mileage is counted from Union Pacific train station. **55.2**

55.2 Turn right (east) onto gravel road just south of Pony Springs rest stop. Sign says Atlanta 21 or 25 miles (traveler's choice!). Wilson Creek Range to east is entirely within caldera complex; Fortification Range to northeast is outside of it. **8.6**

63.8 Turn right (south) onto dirt road. **2.7**

66.5 **STOP 5-1 (Best). Intracaldera tuff and breccia of the Lund Formation in White Rock caldera.** Turn around and stop. Hike about 1 km to east of road to saddle. In these low hills, the northward dipping pile of apparently unfaulted intracaldera rocks (Fig. R36) has a thickness of possibly 3 km; a 2 km thick pile of intracaldera tuff of the Ripgut Formation overlies it in the Mt. Wilson caldera to the south.

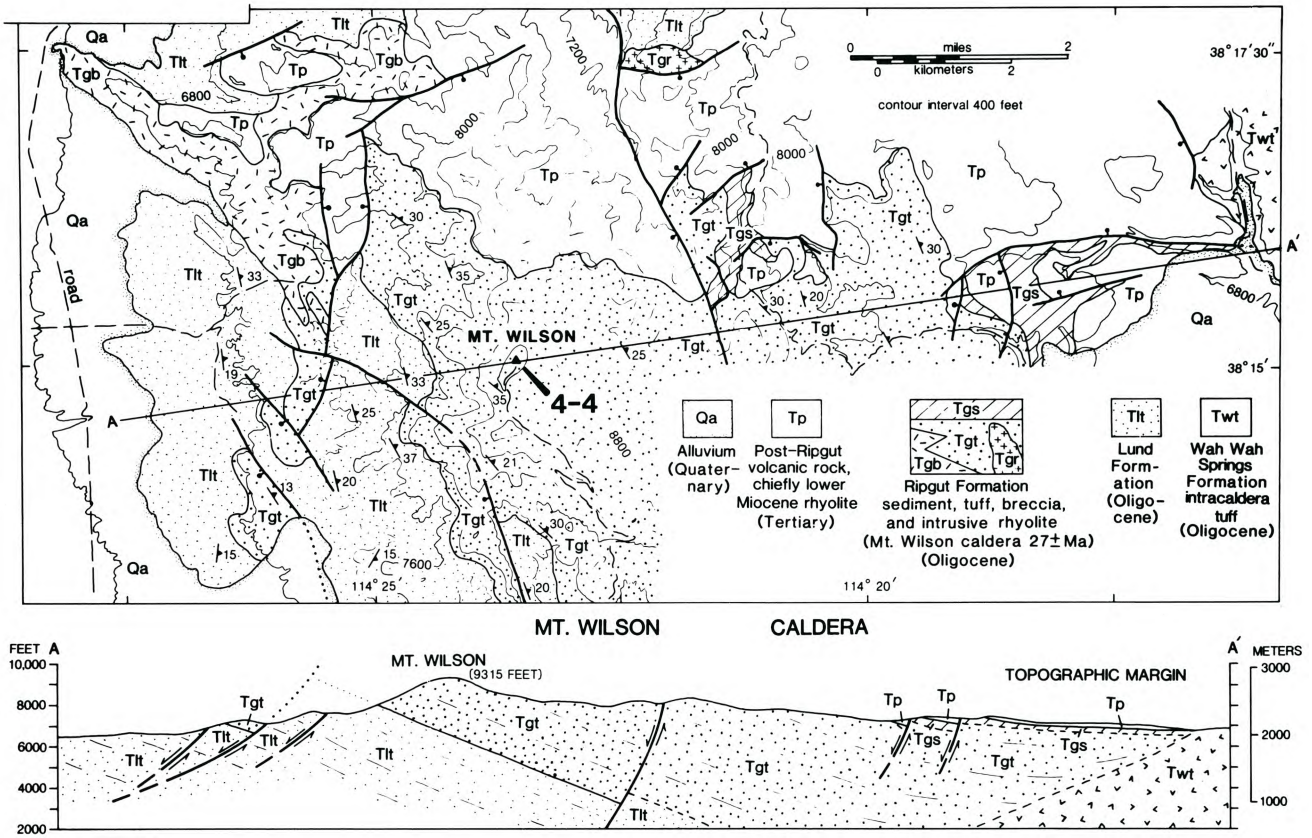

FIGURE R35—Geologic map of the area around Mt. Wilson and east–west cross section through it showing north and northeast margins of Mt. Wilson caldera that was the source of the Ripgut Formation (Willis et al., 1987). The northern topographic margin is marked by landslide breccias banked against the older intracaldera tuffs and breccias of the Lund Formation which accumulated in the White Rock caldera.

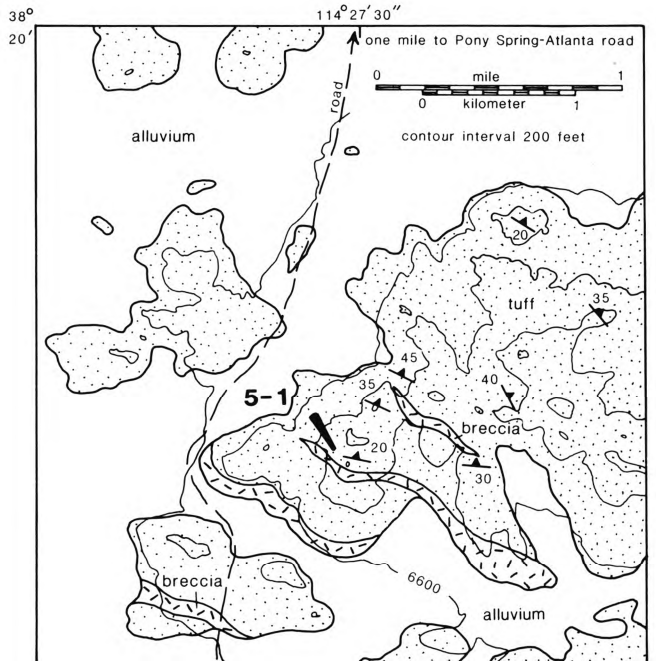

FIGURE R36—Geologic map of the area around Stop 5-1 within the White Rock caldera on the west flank of the Wilson Creek Range, showing thick intracaldera tuff and intercalated lenses of landslide breccia of the Lund Formation that accumulated during caldera collapse 27.9 Ma (Willis et al., 1987). Breccia consists of clasts of bleached Paleozoic carbonate rock and locally pink granite of unknown age.

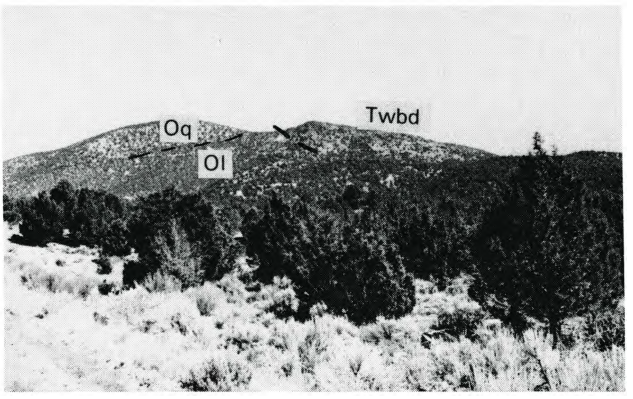

FIGURE R37—View looking northeast from Stop 5-2 of topographic margin of Indian Peak caldera southeast of Atlanta, showing landslide mass of silicified and brecciated dolomite formed during caldera collapse (Twbd) perched on top of autochthonous Ordovician limestone (Ol) and quartzite (Oq) . Compare with Fig. R38.

Tuff of the Lund Formation is a crystal-rich dacite of the Monotony compositional type, containing, in order of decreasing abundance, phenocrysts of plagioclase, quartz, biotite, hornblende, Fe–Ti oxides, sanidine, and titanite (sphene). Intercalated lenses of breccia several meters thick and 1 km or more in strike length are expressed only as hill slopes strewn with fragments of bleached Paleozoic carbonate rock no more than a few centimeters in diameter. One lens not far to the south has clasts of pink granitic rock. No exposures have been found to disclose the matrix surrounding the clasts. These breccia bodies must have been emplaced as landslides during continuous deposition of tuff because an envelope of black vitrophyre surrounds the breccia, indicating underlying as well as overlying hot ejecta quenched against it. These landslides must have traveled at least 10 km to this place of deposition as that is the shortest distance to pre-volcanic rock along the margin of the White Rock caldera.

Drive back (north) to main gravel road. **2.7**

69.2 Turn right (east) onto gravel road. To east is Table Mountain underlain by quasi-bimodal early Miocene volcanic sequence. **10.6**

79.8 **STOP 5-2 (Best). Overview of Atlanta mining district along topographic margin of Indian Peak caldera.** Pull off road. Reddish-black silicified and brecciated Ordovician and Silurian dolomite on the south flank of the hill to the northeast (Figs. R37, R38) is an allochthonous slice of rock that slid about 1 km into the Indian Peak caldera during eruption of Wah Wah Springs ejecta, and now rests on older Ordovician limestones forming the topographic escarpment of the depression. In some outcrops, argillized tuff of the Wah Wah Springs Formation forms a matrix around fragments of dolomite; in others, "veins" of tuff several centimeters in width lie in fractured dolomite. Locally between the allochthon and autochthon are exposures several meters in width of altered tuff.

The topographic margin of the caldera extends easterly for several kilometers beyond the hill. To this side, however, it makes a 90° turn to the north along the west flank of the hill. Breccia masses on either side of the road about 2 km north from this stop (one on the west is near the headframe of the inactive Hulse mine) consist of shattered Ordovician quartzite and minor dolomite apparently resting on tuff of the Ryan Spring Formation. This intracaldera rhyolite tuff, which can be seen on either side of the road at this stop, was erupted after the Wah Wah Springs and indicates recurrent subsidence of the Indian Peak caldera near the site of earlier collapse.

The topographic margin of the younger White Rock caldera converges from the south in this vicinity with the Indian Peak caldera.

The next stop will be at the Atlanta open-pit gold mine located on the northeast side of the hill and in a re-entrant jog into the topographic margin of the caldera complex. From there, the margin swings westerly for several kilometers (Fig. R29).

Continue north. **2.0**

81.8 **STOP 5-3 (Best). Atlanta mine.** Turn right (east) into area of waste dump from Atlanta open-pit mine and stop. **OBTAIN PERMISSION TO ENTER ONTO MINE PROPERTY.**

CAUTION: OVERSTEEP WALL OF PIT JUST TO SOUTH IS UNSTABLE. STAY WELL BACK FROM EDGE.

Silicified and brecciated, reddish-black Paleozoic dolomite on the east wall of the pit and argillized, varicolored tuff on the west (Fig. R39) clearly delineate the topographic margin of the caldera. Commercial gold–silver and trivial manganese–uranium deposits in the district are clearly related in space and time with the Indian Peak caldera complex. Tuffs of the Wah Wah Springs and Ryan Spring Formations in the pit are altered and mineralized

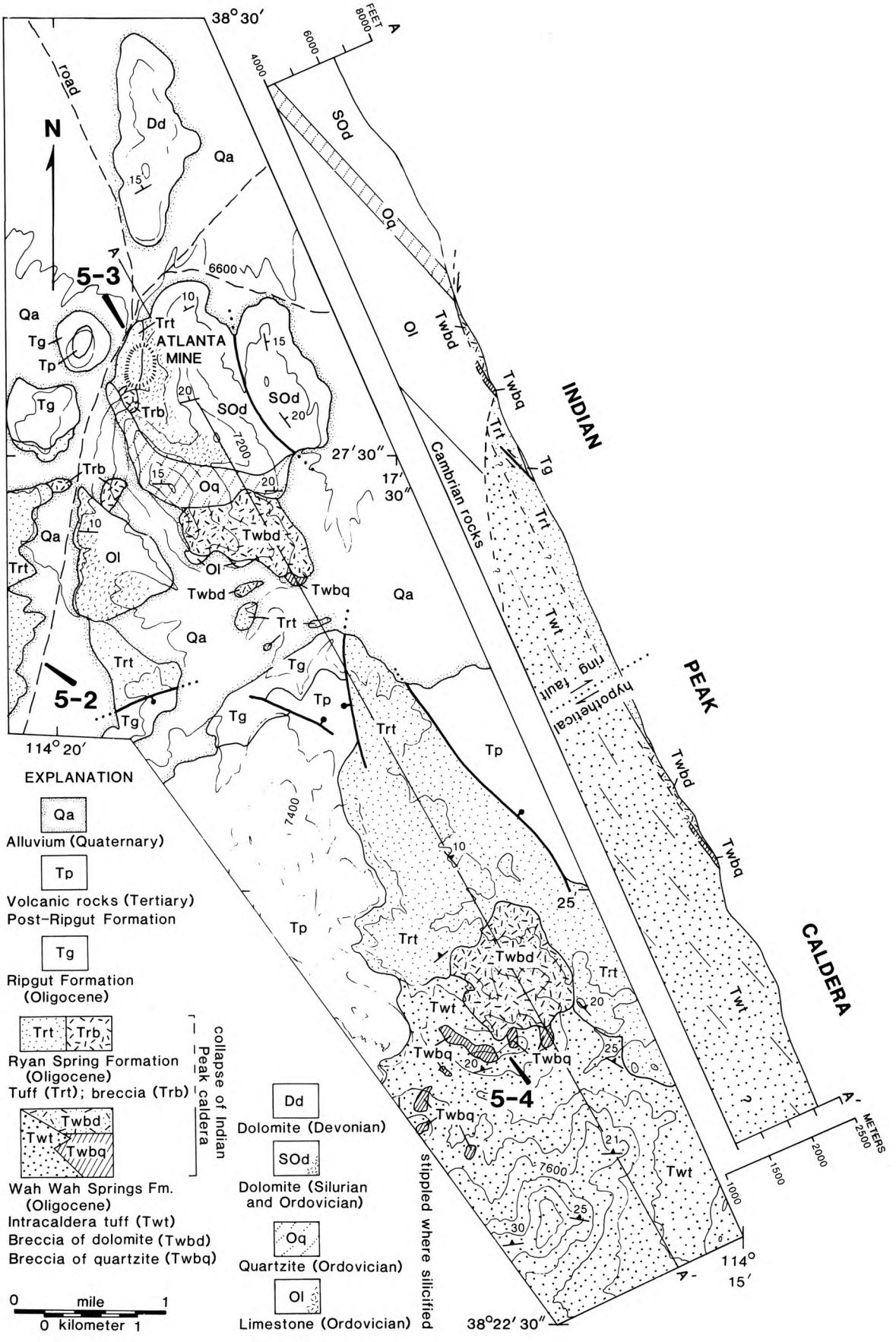

FIGURE R38—Geologic map and cross section of the margin of the Indian Peak caldera (Willis et al., 1987) near Atlanta and Stops 5-2 to 5-4. Contour interval 200 ft.

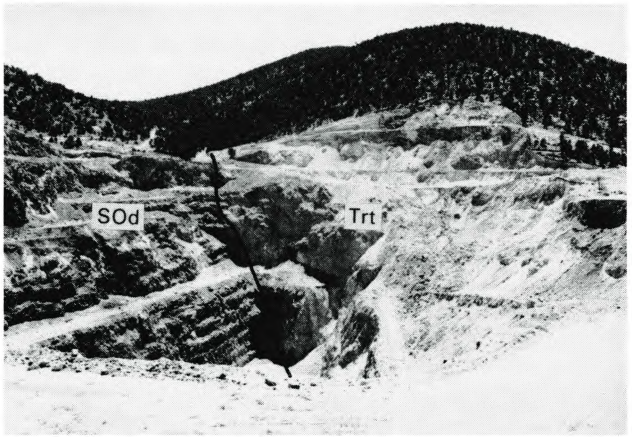

FIGURE R39—Southward view at Stop 5-3 into Atlanta open-pit mine located along a re-entrant in the topographic wall of Indian Peak caldera. Contact passes through center of pit between brecciated and silicified reddish-black Silurian and Ordovician dolomite (SOd) on east and altered, varicolored intracaldera tuff of Ryan Spring Formation (Trt) on west.

along with dolomite. Younger tuff of the Ripgut Formation exposed just west of the pit is somewhat altered whereas the overlying tuff of the Isom Formation emplaced about 27 Ma is fresh. Recurrent shallow crustal magmatism in the area, together with the re-entrant configuration of the caldera margin and possibly the nature of the Paleozoic sequence, all may have conspired to focus the exploitable mineralization. In Silver Park, 2.5 km west-southwest of Atlanta, dominantly silver mineralization reflects more distant hydrothermal activity.

Time permitting, tuff of the Isom Formation capping the small hill west of the pit will be examined. This densely welded trachydacite that contains phenocrysts of plagioclase and sparse clino- and orthopyroxene is the type unit of the Isom compositional type (Christiansen et al., 1988).

Proceed north on road. **0.6**

82.4 Take right fork. **0.4**

82.8 Take right fork again. **3.3**

86.1 Turn right (south) onto dirt road. This intersection is near the topographic wall of Indian Peak caldera. Paleozoic rocks underlie hills to north. To south in foothills of Table Mountain are large slide blocks of white Ordovician quartzite overlying a thick section of intracaldera tuff of the Wah Wah Springs Formation. **4.4**

90.5 **STOP 5-4 (Best). Slide blocks of quartzite and dolomite on tuff in Indian Peak caldera** (Fig. R38). Turn around and stop on either side of cabin. At cabin is a pumice- and lithic-rich tuff unit in the Ryan Spring Formation that overlies intracaldera tuff of the Wah Wah Springs Formation. Walk west along road until it crosses creek; then leave road and head north uphill. In saddle at top are exposures of the intracaldera tuff of the Wah Wah Springs Formation. Ridge to west is capped by slide mass of Ordovician quartzite and overlying dolomite. Although pervasively fractured, this is a stratigraphically coherent section that was more than 100 m thick and 3 km wide when emplaced onto the intracaldera Wah Wah Springs tuff in the caldera. Note additional remnants of white quartzite, on the south side of the canyon, resting on tuff that is approximately 2 km thick in this area.

This part of the Ordovician section is in place on the topographic rim of the caldera at least 4 km to the north. Projection of the stratal attitude of this section over the caldera indicates about 2 km of downward displacement, at least some of which could have occurred during eruption of tuffs of the Ryan Spring Formation.

Drive north toward Atlanta. **2.3**

92.8 Exposures of early Miocene latite and rhyolite lava flows to west. **2.1**

94.9 Turn left (west) onto gravel road. **25.6**

120.5 Turn left (south) onto US-93. **55.1**

175.6 Arrive in Caliente. Stop overnight.

Day 6

The last day of the field trip examines sheets of rhyolitic tuff erupted during waning Miocene ash-flow activity and the bimodal basalt—rhyolite association that characterizes the late Cenozoic (since about 17 Ma) of the eastern Great Basin.

Four of the regionally extensive early Miocene tuff sheets to be seen this morning were apparently derived from the Caliente cauldron complex whose northern margin lies near town (Fig. R40). Williams (1967), Noble et al. (1968), and Noble and McKee (1972) concluded on the basis of the distribution and thickness of tuff deposits and included clasts and associated thick accumulations of contemporaneous lava flows that the "Caliente depression," an area of subdued, low topography east of town, was probably the source area.

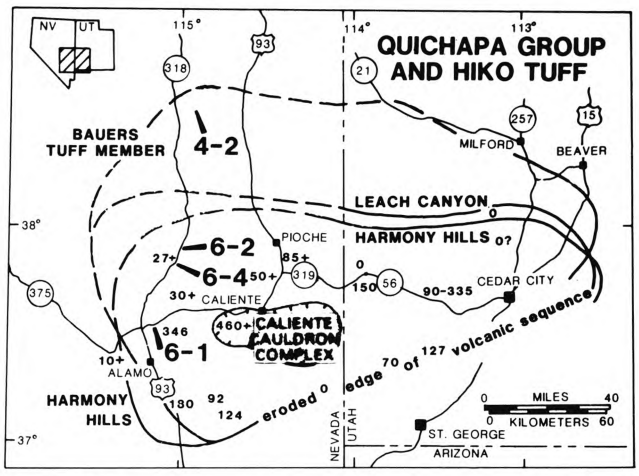

STRATIGRAPHIC UNITS	AGE (MA)	MINIMUM AREA (KM^2) PRESENT	RESTORED	MINIMUM VOLUME (KM^3) RESTORED
HIKO RACER CANYON	18.6	16,000	10,000	1,000
HARMONY HILLS	21±	21,000	13,000	700
BAUERS	22.7	34,000	23,000	1,000
LEACH CANYON	24±	22,000	15,000	1,800

FIGURE R40—Distribution of tuffs (heavy lines are zero isopachs) seen at Stops 6-1 and 6-4 that apparently were derived from the Caliente cauldron complex. Zero isopach not drawn for Hiko Tuff; numbers indicate its thickness (in meters) and that of the Racer Canyon Tuff, a compositionally similar unit of similar age but different natural remanent-magnetization direction, that occurs east of the complex. The age of the Hiko Tuff is from unpublished work of W. Taylor. All but the Hiko belong to the Quichapa Group of Williams (1967). The Bauers and the Swett Tuff Members comprise the Condor Canyon Formation; the Swett is much thinner than the Bauers and is not shown here. Unit thicknesses southeast of the cauldron complex partly from unpublished mapping by R. E. Anderson.

Ekren (*in* Ekren et al. , 1977) mapped a thick (460 + m) pile of Hiko Tuff west of town which he considered to be an intracaldera filling. This inference, together with the distribution of Paleozoic basement rock and gravity and aeromagnetic data, led Ekren et al. (1977) to postulate the existence of the larger, elongate Caliente cauldron complex. Current mapping at a scale of 1:24,000 by P. D. Rowley and R. E. Anderson of the U.S. Geological Survey is refining the earlier reconnaissance work and is delineating individual calderas within the complex (Rowley and Siders, 1988).

Mileage

0.0 Leave Caliente heading west on US-93. Mileage is counted from train station. The highway just west of Caliente passes exposures of bedded sandstones and siltstones that accumulated in the depression after deposition of the Hiko Tuff at 18.6 Ma, which is exposed in roadcuts farther west to Oak Springs Summit. The ledge-forming cooling unit overlying the sediments is the 14.1 Ma Kane Wash Tuff. Numerous northerly striking faults have cut and tilted the entire section. **18.1**

18.1 Continue straight (west) past Delamar turnoff to left, passing through a "forest" of Joshua trees, smaller cholla, and many other varieties of cacti. To northwest is the North Pahroc Range containing a sequence of 16 Miocene tuff sheets; to southwest is the South Pahroc Range, the upper half of which is a 346 m thick section of Hiko Tuff. **12.6**

30.7 Bulbous-weathering Hiko Tuff. **10.6**

41.3 **STOP 6-1 (Noble). Hiko and Kane Wash Tuffs.** Pull off highway. The crystal-rich, rhyolitic Hiko Tuff commonly weathers much like granite into bulbous forms (Fig. R41). It consists of about 40% phenocrysts of plagioclase and lesser quartz, sanidine, and biotite plus trace amounts of hornblende and sphene. Here it is overlain by the thin, rather densely welded Kane Wash Tuff, characterized by chatoyant sanidine.

Continue west on highway. **2.8**

44.1 Turn right (north) onto NV-318. **0.6**

44.7 Take right (north) fork toward Hiko up White River Valley. **25.2**

69.9 Entering White River Narrows at top of volcanic section, which will be examined from base upwards. **5.0**

74.9 Turn sharp left (west) onto unmarked and inconspicuous gravel road. **0.2**

FIGURE R41—Bulbous outcrops of Hiko Tuff near Stop 6-1.

75.1 **STOP 6-2 (Best and Christiansen). Petroglyph Cliff Ignimbrite.** Turn around and stop at water tanks. Walk a short distance up road to examine lower units in this famous White River Narrows section (Table R3, Fig. R42).

TABLE R3—Stratigraphic sequence from top of section at south end of White River Narrows to bottom of section to north at White Rock Spring along State Highway 318 (old 38) in Lincoln County, Nevada (compare Cook, 1965, fig. 29). Data partly from Williams (1967) and Wanda Taylor (written comm. 1987). *Proportions of phenocrysts in whole rock; †titanite (sphene).

Stratigraphic unit	Thickness (m)	Age (Ma)	Composition* (Q/S/P/B/H/Px/tot)
Basaltic-andesite lava flows	0-150	21-18	
Hiko Tuff	27 +	18.6	8/7/18/5/1/0/40,t†
Harmony Hills Tuff	0-6	21.0	3/0/31/8/4/3/50
Pahranagat Lakes Tuff	15	22.65	8/5/4/1/tr/tr/18
Condor Canyon Fm.			
Bauers Tuff Mbr.	26	22.78	0/5/8/1/0/tr/14
Swett Tuff Mbr.	10		0/0/8/2/0/0/10
Leach Canyon Fm.	104		5/3/6/1/tr/0/16,t†
Trachydacite tuff	5		0/0/5/0/0/tr/5
Hornblende-andesite lava flow	0-150		
Shingle Pass Tuff, Upper unit	20	26.00	tr/2/3/1/0/0/6
Tuff of Hancock Summit	12 +		10/11/7/1/0/0/29
Trachydacite tuff	20		0/0/10/0/0/1/11
Monotony Tuff(?), Upper unit	20-60		
Petroglyph Cliff Ignimbrite	20 ±		0/0/10/0/0/2/12
Monotony Tuff, Lower unit	50 ±	27.31	6/3/20/5/2/2/38
Lund Fm.	22 ±	27.9	6/tr/27/3/4/0/40,t†
Wah Wah Springs Fm.	30 ±	29.5	2/0/25/5/7/tr/40
Paleozoic rocks			

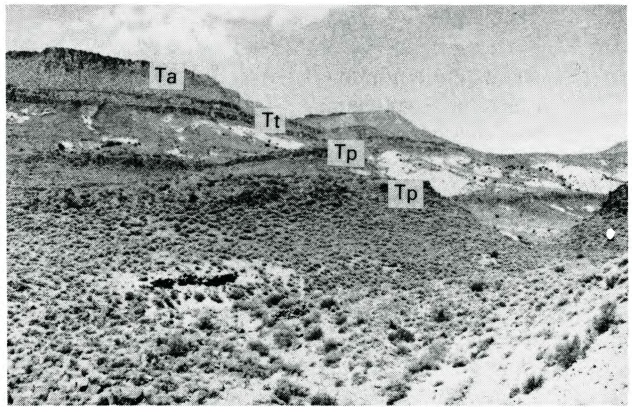

FIGURE R42—Looking northwest at Stop 6-2, toward White Rock Spring concealed behind nearest hill. This hill, capped by Petroglyph Cliff Ignimbrite (Tp), is a down-dropped fault block relative to same unit in prominent higher hill in middle distance. Directly underlying the Petroglyph Cliff is loosely welded Monotony Tuff. A small exposure of the sphene-bearing tuff of the Lund Formation occurs on the northeast side of the wash west of the fault. Overlying the Petroglyph Cliff is a loosely welded tuff containing abundant lithic clasts that might be a second unit of the Monotony, followed by a thin, densely welded cooling unit of trachydacite tuff (Tt) of the Isom compositional type that contains phenocrysts of plagioclase and pyroxene. Top of section is capped by a resistant hornblende andesite lava flow (Ta).

Above poor exposures of weakly welded Lund and Monotony dacite tuff deposits is the Petroglyph Cliff Ignimbrite, named and briefly described by Cook (1965). It is unusual in the Great Basin because of the high concentration of lapilli- and block-size fragments (Fig. R43) and could legitimately be called a welded tuff breccia. The clasts, as well as the matrix, contain the same phenocryst assemblage of plagioclase plus two pyroxenes; for that reason, together with their apparent plastic deformation, these clasts were probably bits of magma, vesicular as well as non-vesicular, ejected with the ash. This small volume deposit is found only here and in two ranges to the east and must have been vented in the immediate vicinity because clast size diminishes eastward and southward.

The Petroglyph Cliff is another of several latest Oligocene and early Miocene (27–23 Ma) deposits in the Great Basin of the Isom compositional type that contain modest amounts of phenocrysts of plagioclase, two pyroxenes, and Fe–Ti oxides. Another directly underlies the andesite lava flow above White Rock Spring at this stop.

Drive back toward highway. **0.2**

75.3 Turn right (south) onto NV-318. Volcanic units in range front to west dip gently south so that the thick andesite lava flow capping hill above Stop 6-2 drops down to valley level. **3.2**

78.5 **STOP 6-3 (Best and Grommé). Differential compaction in tuff sheets.** Pull off highway. This stop permits a southward view of the middle part of the sequence of tuff sheets shown in Table R3. To the west is the subject of a famous photograph and diagram by Cook (1965, fig. 29; Fig. R44 in this road log) where the Leach Canyon Formation and younger tuff deposits thin or pinch out northward over the stubby toe of the thick hornblende andesite lava flow. Cook concluded that, due to the differential and diminishing compaction of each successively deposited tuff, the topographic relief over the lava flow diminished as each younger ash flow swept across. Assuming the top of each flow was initially horizontal, he calculated about 50% compaction; i.e., the gas-inflated flows were at least twice as thick as the welded tuff. The compaction involved loss of gas between, as well as within, the pyroclasts.

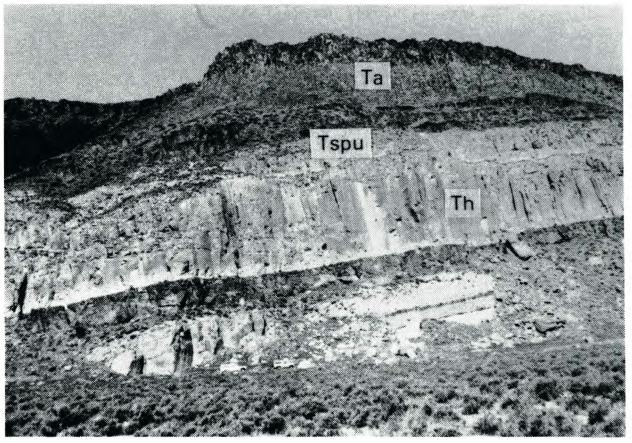

FIGURE R44—Looking west from Stop 6-3 at Petroglyph Cliff (just to left of vehicles). Petroglyphs are in probable Monotony Tuff. Above the Monotony is a dark-colored Isom compositional type unit which at Stop 6-2 lies just below a hornblende-andesite lava flow. Here, a crystal-rich rhyolite tuff, the tuff of Hancock Summit (Th), and the overlying upper unit of the Shingle Pass Tuff (Tspu) intervene between the Isom-type sheet and the andesite (Ta). To the right of the vehicles, the probable Monotony is thinner and underlain by a 1 m thick tuff that is probably the Petroglyph Cliff Ignimbrite; the latter is underlain by a local lahar and that by a second possible unit of the Monotony Tuff.

Continue heading south on highway (Fig. R45). **1.3**

79.8 **STOP 6-4 (Best). Lower Miocene rhyolite tuff sheets derived from Caliente cauldron complex** (Table R3, Figs. R40, R46). Pull off highway. Units contain modest amounts of phenocrysts (Leach Canyon Formation and Swett and Bauers Tuff Members of the Condor Canyon Formation) as well as abundant phenocrysts (Pahranagat Lakes and Hiko Tuffs). Although the Pahranagat Lakes Tuff was tentatively included by Williams (1967) in the Quichapa Group derived from the Caliente cauldron complex, it and the probably correlative upper tuff of White Blotch Spring and the granite-weathering tuff had their source in the Kawich caldera east of Tonopah.

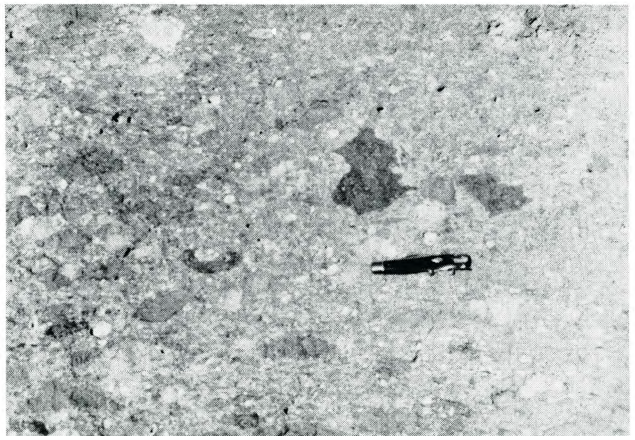

FIGURE R43—Petroglyph Cliff Ignimbrite has unusually abundant lapilli and blocks, most or all of which could be cognate on the basis of a modal composition similar to matrix, namely plagioclase and two pyroxenes. 10 cm pocket knife for scale.

FIGURE R45—Volcanic sequence looking south near Stop 6-3, at north end of White River Narrows. Units listed in Table R2 visible to right (west) of the highway are (ascending): tuff of Hancock Summit (coarse columnar joints at base of section); upper unit of Shingle Pass Tuff and overlying local, thin trachydacite tuff (in slope); Leach Canyon Formation (prominent cliff extending into Narrows to south); Condor Canyon Formation (ledgy slope above cliff).

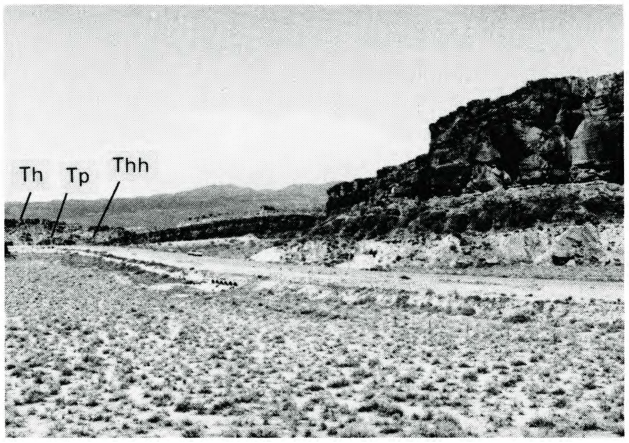

FIGURE R46—Volcanic sequence at Stop 6-4, at south end of the White River Narrows. Units listed in Table R2 visible to right (west) of the highway are: Leach Canyon Formation (light color, in roadcut); Condor Canyon Formation (Swett Tuff Member is mostly a black vitrophyre capped by about 4 m of orange tuff forming a slope; overlying Bauers Tuff Member is the prominent cliff); Pahranagat Lakes Tuff (Tp); Harmony Hills Tuff (Thh); Hiko Tuff (Th).

The Harmony Hills Tuff, only a thin nonpersistent deposit here at its western edge, is an unusually crystal-rich andesitic tuff derived about 21 Ma from the Caliente source area (Ekren et al., 1977). It is one of the youngest units in the Monotony compositional type.

Continue heading south on highway. **25.6**

105.4 Veer left, continuing on NV-318. **0.6**

106.0 Turn right (west) onto US-93 toward Alamo and Las Vegas. **4.9**

110.9 Community of Ash Springs. **4.0**

114.9 Rough-weathering unit dipping to the east on the west side of valley is Hiko Tuff. To the southeast, at about 10:00, the two lowermost units of the Kane Wash Tuff overlie a thick section of the Hiko Tuff. The lowermost unit (member O of Novak, 1984; see also Table R4) is brown and relatively thin. The second unit (member W) consists of a less resistant nonwelded white lower part that grades upward into a more resistant, partly to densely welded cap. **3.1**

118.0 Town of Alamo. **2.9**

TABLE R4—Nomenclature of ash-flow sheets of the Kane Springs Wash volcanic center. The status of unnamed units recognized by Cook (1965) between his units Tvk_1 and Tvk_2 and between units V_1 and V_2 of Novak (1984) is unclear. A thin cooling unit, here informally termed Member Y, with a very thin zone of porous glassy tuff, is present between Member W and Member V_1 in the Meadow Valley Mountains and in the Delamar Range (Noble, 1968). Unit V_3 of Novak is a cooling unit distinct from V_2.

Cook (1965)	Novak (1984)	This paper
Not recognized	Member V_3	Member V_3
Ignimbrite 4 of younger units	V_2	V_2
Three unnamed ignimbrites	Not recognized	Status unclear
Ignimbrite Tvk_3	V_1	V_1
Ignimbrites Tvk_2 and Tvk_{2x}	W	W
Unnamed sillar		Status unclear
Ignimbrite Tvk_1	O	O

120.9 Turn left (east) onto gravel road. Sign indicates "Buckhorn Ranch Road" in opposite (west) direction. **1.4**

122.3 **STOP 6-5 (Noble). Kane Wash Tuff.** Turn around and stop. The Kane Wash Tuff was recognized as a petrographically distinct unit by Cook (1965). The Kane Wash consists of at least six ash-flow sheets, all of rhyolitic composition, which have been given informal member status within the formation (Table R4). The lower three ash-flow sheets are subalkaline, whereas the upper three are of peralkaline character, as shown by the presence of groundmass sodic amphibole and/or pyroxene of devitrification and vapor-phase origin.

At this locality, the lower two units (members O and W) of the Kane Wash Tuff and the Hiko Tuff, which can be seen several hundred meters to the east, are exposed in an east-dipping, tilted fault block. The lowermost ash-flow sheet of the Kane Wash Tuff is exposed on the north side of the dirt road. After looking at it walk to the south for about 100 m to see the lower glassy portion of the overlying ash-flow sheet. In both units, note the abundance of sanidine and the low contents of biotite and phenocrysts of other mafic minerals.

Drive west to highway. **1.4**

123.7 Turn left (south) onto US-93. **4.3**

128.0 Cliffs of Kane Wash Tuff can be seen to the east and south. **6.0**

134.0 The type section of the Kane Wash Tuff can be seen at about 11:00. **2.9**

136.9 Middle Miocene basalt flows exposed east of highway overlie Kane Wash Tuff. **15.8**

152.7 Turn left on well-graded dirt road. After several miles road proceeds northeast up Kane Springs Wash. **14.0**

166.7 Cattleguard. **0.2**

166.9 Turn left (north) on ungraded dirt road. **0.2**

167.1 Cross cattleguard. **0.1**

167.2 Ford wash. Turn right and proceed to northeast on ungraded dirt road. The outflow sheets of the Kane Wash Tuff are well exposed on the southeast side of Kane Springs Wash in the cliffs that form the northeast flank of the Meadow Valley Mountains. The Kane Wash Tuff here overlies the Hiko Tuff and the underlying Harmony Hills Tuff and older ash-flow sheets, which in turn overlie Paleozoic carbonate strata. The light-colored lower part of member W, here largely altered to zeolite and/or smectite, is readily visible. This member is overlain by a thin cooling unit of subalkaline ash-flow tuff, here termed W_2, that is lithologically very similar to the upper part of member W. Two cooling units of peralkaline character (members V_1 and V_2 of Novak, 1984; see also Novak and Mahood, 1986) form the upper part of the section. The uppermost outflow sheet (V_3) is of small volume and is preserved only locally outside the caldera. Note the marked layering in member V_2, reflecting the presence of many distinct ash flows and/or sequences of ash flows. **5.8**

173.0 Old cattle corral. The cliffs behind the corral are composed of Hiko Tuff. **0.6**

173.6 Cross wash. Buried southern margin of the Kane

Springs Wash caldera is located near here (Fig. R47). Some, and probably all, of the ash-flow sheets of the Kane Wash Tuff had their origin in the Kane Springs Wash caldera (Noble, 1968). Although Novak (1984) has suggested that the earlier subalkaline units were erupted from a source area northwest of the Kane Springs Wash caldera, the local presence of swarms of lithic fragments including blocks greater than 0.5 m in diameter in the lower part of unit W at the margin of the caldera suggests that all the ash-flow sheets of the Kane Wash Tuff were erupted from the same vent area. Basaltic lava flows erupted about 13–11 Ma (Best et al., 1980; Novak, 1984) cap the older sequence of felsic rocks in the volcanic center and their erosional debris floods the terrain. **2.4**

176.0 **STOP 6-6 (Noble). Strongly rheomorphic ash-flow tuff of member V_2** (Fig. R47). The upper three members of the Kane Wash Tuff, of peralkaline composition and exhibiting marked vertical compositional zonations, as well as precursor and following trachyte and syenite, were erupted within a short period of geological time, probably less than 0.1 Ma. Subsidence apparently took place along the same ring-fracture system during this period, and member V_2 is found both outside and, locally, within the caldera. Here, member V_2 has experienced post-depositional flowage that produced well-expressed layering. Eruption of member V_3 was followed immediately by the eruption of a large lava dome complex composed of syenite and trachyte on the floor of the caldera, followed by rhyolite and intermediate lavas. **4.0**

180.0 **STOP 6-7 (Noble and Christiansen). Topaz rhyolite dome** (Fig. R47). The last event clearly attributable to the Kane Springs Wash volcanic center was the eruption of a large lava dome of topaz rhyolite along the northwestern part of the ring-fracture system at 13.4 ± 0.3 Ma. The close spatial and temporal association of both peralkaline and peraluminous silicic compositions is remarkable, and possibly unique in the Great Basin.

The Kane Springs Wash center typifies the bimodal basalt–rhyolite association that developed through much of the Great Basin after the early Miocene. More specifically, the evolution of silicic magmas from subalkaline rhyolitic to peralkaline rhyolitic and trachytic compositions, and the short period of time during which caps of highly evolved magma evolved in the magma chamber, are similar to relations at the late Miocene Black Mountain volcanic center to the west (Noble and Christiansen, 1974; Noble et al., 1984; Weiss et al., 1989).

Turn around and retrace route to US-93 and proceed south (left) to Las Vegas.

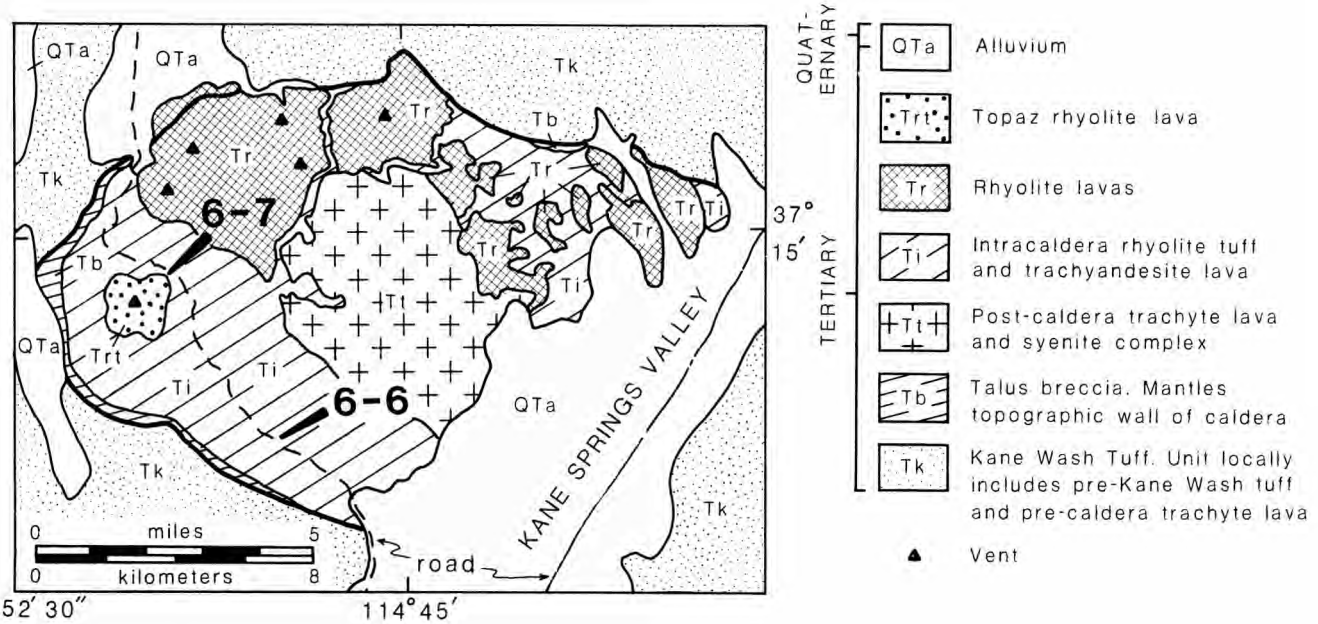

FIGURE R47—Geologic map of Kane Springs Wash caldera (after Noble, 1968; Novak and Mahood, 1986).

References

Abrams, M. J., Ashley, R. P., Rowan, L. C., Goetze, A. F. H., and Kahle, A. B., 1977, Mapping of hydrothermal alteration in the Cuprite mining district, Nevada, using aircraft scanner images for the spectral region 0.46 to 2.32 micrometers: Geology, 5: 713–718.

Anderson, R. E., and Ekren, E. B., 1968, Widespread Miocene igneous rocks of intermediate composition, southern Nye County, Nevada: Geological Society of America, Memoir 110: 57–63.

Armstrong, R. L., 1975, Cenozoic igneous history of the Cordillera north of 42° N. (abs.): Geological Society of America, Abstracts with Programs, 7(7): 981.

Armstrong, R. L., 1979, Cenozoic igneous history of the U.S. Cordillera from 42° to 49° N. latitude: Geological Society of America, Memoir 152: 265–282.

Armstrong, R. L., Ekren, E. B., McKee, E. H., and Noble, D. C., 1969, Space–time relations of Cenozoic silicic volcanism in the Great Basin of the western United States: American Journal of Science, 267: 478–490.

Ashley, R. P., 1974, Goldfield mining district; *in* Guidebook to the geology of four Tertiary volcanic centers in central Nevada: Nevada Bureau of Mines and Geology, Report 19: 49–66.

Ashley, R. P., 1979, Relation between volcanism and ore deposition at Goldfield, Nevada; *in* Ridge, J. D. (ed.), Papers on mineral deposits of western North America: Nevada Bureau of Mines and Geology, Report 33: 77–86.

Atwater, T., 1970, Implications of plate tectonics for the Cenozoic tectonic evolution of western North America: Geological Society of America, Bulletin, 81: 3513–3536.

Best, M. G., 1988a, Early Miocene change in direction of least principal stress, southwestern U.S.: Conflicting inferences from dikes and metamorphic core–detachment fault terranes: Tectonics, 7: 249–259.

Best, M. G., 1988b, Easterly trending Oligocene to early Miocene (30–20 Ma) paleotopography and other geologic features, southeastern Great Basin (abs.): Geological Society of America, Abstracts with Programs, 20(3): 143.

Best, M. G., and Grant, S. K., 1987, Stratigraphy of the volcanic Oligocene Needles Range Group in southwestern Utah and eastern Nevada: U.S. Geological Survey, Professional Paper 1433-A: 1–28.

Best, M. G., and Hamblin, W. K., 1978, Origin of the northern Basin and Range province: Implications from the geology of its eastern boundary: Geological Society of America, Memoir 152: 313–340.

Best, M. G., Christiansen, E. H., and Blank, H. R., Jr., 1989, Oligocene calc-alkaline rocks of the Indian Peak volcanic field, Nevada and Utah: Geological Society of America, Bulletin, 101 (in press).

Best, M. G., McKee, E. H., and Damon, P. E., 1980, Space–time–composition patterns of late Cenozoic volcanism, southwestern Utah and adjoining areas: American Journal of Science, 280: 1035–1050.

Best, M. G., Toth, M. I., Kowallis, B. J., Willis, J. B., and Best, V., 1989, Geologic map of Northern White Rock Mountains–Hamlin Valley area, Beaver County, Utah and Lincoln County, Nevada: U.S. Geological Survey, Miscellaneous Investigations Series Map I-1881.

Best, M. G., Mehnert, H. H., Keith, J. D., and Naeser, C. W., 1987, Miocene magmatism and tectonism in and near the southern Wah Wah Mountains, southwestern Utah: U.S. Geological Survey, Professional Paper 1433-B: 29–47.

Boden, D. R., 1986, Eruptive history and structural development of the Toquima caldera complex, central Nevada: Geological Society of America, Bulletin, 97: 61–74.

Bonham, H. F., Jr., and Garside, L. J., 1979, Geology of the Tonopah, Lone Mountain, Klondike, and Northern Mud Lake Quadrangles, Nevada: Nevada Bureau of Mines and Geology, Bulletin 92: 142 pp.

Borngasser, M. X., and Taranik, J. V., 1985, Evaluation of SPOT simulator data for the detection of alteration in Goldfield/Cuprite, Nevada: Photogrammetric Engineering and Remote Sensing, 51: 1109.

Burke, D. B., and McKee, E. H., 1979, Mid-Cenozoic volcano-tectonic troughs in central Nevada: Geological Society of America, Bulletin, 90: 181–184.

Bushman, A. V., 1973, Pre-Needles Range silicic volcanism, Tunnel Spring Tuff (Oligocene) west-central Utah: Brigham Young University Geology Studies, 20: 159–190.

Byers, F. M., Jr., Orkild, P. P., Carr, W. J., and Quinlivan, W. D., 1968, Timber Mountain Tuff, southern Nevada, and its relation to cauldron subsidence; *in* Nevada Test Site: Geological Society of America, Memoir 110: 87–97.

Byers, F. M., Jr., Carr, W. J., Christiansen, R. L., Lipman, P. W., Orkild, P. P., and Quinlivan, W. D., 1976, Geologic map of the Timber Mountain caldera area, Nye County, Nevada: U.S. Geological Survey, Miscellaneous Geological Investigations Map I-891, scale 1:48,000.

Carr, W. J., Byers, F. M., Jr., and Orkild, P. P., 1986, Stratigraphic and volcano-tectonic relations of Crater Flat Tuff and some other older volcanic units, Nye County, Nevada: U.S. Geological Survey, Professional Paper 1323: 28 pp.

Chadwick, R. A., 1985, Overview of Cenozoic volcanism in the west-central United States; *in* Flores, R. M., and Kaplan, S. S. (eds.), Cenozoic Paleogeography of west-central United States: Society of Economic Paleontologists and Mineralogists, pp. 359–382.

Christiansen, E. H., Best, M. G., and Hoover, J. D., 1988, Petrology of a trachytic tuff from a calc-alkaline volcanic center: the Oligocene Isom tuff, Indian Peak volcanic field, Utah and Nevada: American Geophysical Union (EOS) Transactions, 69.

Christiansen, E. H., Sheridan, M. F., and Burt, D. M., 1986, The geology and geochemistry of Cenozoic topaz rhyolites from the western United States: Geological Society of America, Special Paper 205: 82 pp.

Christiansen, R. L., 1979, Cooling units and composite sheets in relation to caldera structure; *in* Chapin, C. E., and Elston, W. E. (eds.), Ash-flow tuffs: Geological Society of America, Special Paper 180: 29–42.

Christiansen, R. L., and Lipman, P. W., 1972, Cenozoic volcanism and plate tectonic evolution of the western United States. II. Late Cenozoic: Royal Society of London, Philosophical Transactions (A), 271: 249–284.

Christiansen, R. L., Lipman, P. W., Carr, W. J., Byers, F. M., Jr., Orkild, P. P., and Sargent, K. A., 1977, Timber Mountain–Oasis Valley caldera complex of southern Nevada: Geological Society of America, Bulletin, 88: 943–959.

Cook, E. F., 1965, Stratigraphy of Tertiary volcanic rocks in eastern Nevada: Nevada Bureau of Mines, Report 11: 61 pp.

Cox, A. V., 1971, Remanent magnetization and susceptibility of late Cenozoic rocks from New Zealand: New Zealand Journal of Geology and Geophysics, 14: 192–207.

Cross, T. A., and Pilger, R. H., Jr., 1978, Constraints on absolute motion and plate interaction inferred from Cenozoic igneous activity in the western United States: American Journal of Science, 278: 865–902.

Dalrymple, G. B., and Duffield, W. A., 1988, High precision $^{40}Ar/^{39}Ar$ dating of Oligocene rhyolites from the Mogollon–Datil volcanic field using a continuous laser system: Geophysical Research Letters, 15: 463–466.

Deino, A. L., 1985, Stratigraphy, chemistry, K–Ar dating, and paleomagnetism of the Nine Hill Tuff, California–Nevada: Part I: Unpublished Ph.D. dissertation, University of California, Berkeley, 338 pp.

Deino, A. L., and Best, M. G., 1988, Use of high precision single-crystal $^{40}Ar/^{39}Ar$ ages and TRM data in correlation of an ash-flow deposit in the Great Basin (abs.): Geological Society of America, Abstracts with Programs, 20(7): 397.

Ekren, E. B., and Byers, F. M., Jr., 1976, Ash-flow fissure vent in west-central Nevada: Geology, 4: 247–251.

Ekren, E. B., Rogers, C. L., and Dixon, G. L., 1973, Geologic and Bouguer gravity map of the Reveille quadrangle, Nye County, Nevada: U.S. Geological Survey, Miscellaneous Investigations Map I-806.

Ekren, E. B., Anderson, R. E., Rogers, C. L., and Noble, D. C., 1971, Geology of the northern Nellis Air Force Base Bombing and Gunnery Range, Nye County, Nevada: U.S. Geological Survey, Professional Paper 651: 91 pp.

Ekren, E. B., Hinrichs, E. N., Quinlivan, W. D., and Hoover, D. L., 1973, Geologic map of the Moores Station quadrangle, Nye County, Nevada: U.S. Geological Survey, Miscellaneous Geologic Investigations Map I-756.

Ekren, E. B., Orkild, P. P., Sargent, K. A., and Dixon, G. L., 1977, Geologic map of Tertiary rocks, Lincoln County, Nevada: U.S. Geological Survey, Miscellaneous Investigations Series Map I-1041.

Ekren, E. B., Quinlivan, W. D., Snyder, R. P., and Kleinhampl, F. J., 1974, Stratigraphy, structure, and geologic history of the Lunar Lake caldera of northern Nye County, Nevada: U.S. Geological Survey, Journal of Research, 2: 599–608.

Ekren, E. B., Rogers, C. L., Anderson, R. E., and Orkild, P. P., 1968, Age of Basin and Range normal faults in Nevada Test Site and Nellis Air Force Range, Nevada; *in* Eckel, E. B. (ed.), Nevada Test Site: Geological Society of America, Memoir 110: 247–250.

Ekren, E. B., Byers, F. M., Jr., Hardyman, R. F., Marvin, R. F., and Silberman, M. L., 1980, Stratigraphy, preliminary petrology, and some structural features of Tertiary volcanic rocks in the Gabbs Valley and Gillis Ranges, Mineral County, Nevada: U.S. Geological Survey, Bulletin 1464: 54 pp.

Elston, W. E., 1984, Subduction of young oceanic lithosphere and extensional orogeny in southwestern North America during mid-Tertiary time: Tectonics, 3: 229–250.

Engebretson, D. C., Cox, A., and Gordon, R. G., 1985, Relative motions between oceanic and continental plates in the Pacific Basin: Geological Society of America, Special Paper 206: 59 pp.

Ewart, A., 1982, The mineralogy and petrology of Tertiary–Recent orogenic volcanic rocks: with special reference to the andesite-basaltic compositional range; *in* Thorpe, R. S. (ed.), Andesites: orogenic andesites and related rocks: John Wiley & Sons, New York, pp. 25–98.

Farmer, G. L., and De Paolo, D., 1983, Origin of Mesozoic and Tertiary granite in the western United States and implications for pre-Mesozoic crustal structure. 1. Nd and Sr isotopic studies in the geocline of the northern Great Basin: Journal of Geophysical Research, 88: 3379–3401.

Fitton, J. G., James, D., Kempton, P. D., Ormerod, D. S., and Leeman, W. P., 1988, The role of lithospheric mantle in the generation of late Cenozoic basic magmas in the southwestern United States: Journal of Petrology, Special Issue on the Lithosphere, pp. 331–349.

Foley, D., 1978, The geology of the Stonewall Mountain volcanic center, Nye County, Nevada: Unpublished Ph.D. dissertation, Ohio State University, Columbus, 139 pp.

Gans, P. B., Mahood, G., and Schermer, E. (submitted), Synextensional magmatism in the Basin and Range province: A case study from the eastern Great Basin: Geological Society of America, Special Paper series.

Garside, L. J., Bonham, H. F., Jr., Ashley, R. P., Silberman, M. L., and McKee, E. H., 1981, Radiometric ages of volcanic and plutonic rocks and hydrothermal mineralization in Nevada—Determinations run under the USGS–NBMG Cooperative Program: Isochron/West, no. 30: 11 pp.

Gemmill, P., 1968, The geology of the ore deposits of the Pioche District, Nevada; *in* Ridge, J. D. (ed.), Ore deposits of the United States, 1933–1967: American Institute of Mining, Metallurgy and Petroleum Engineering, the Graton–Sales Volume, pp. 1128–1147.

Gill, J. B., 1981, Orogenic andesites and plate tectonics: Springer-Verlag, New York, 385 pp.

Glazner, A. F., and Bartley, J. M., 1984, Timing and tectonic setting of Tertiary low-angle normal faulting and associated magmatism in the southwestern United States: Tectonics, 3: 385–396.

Gose, W. A., 1970, Paleomagnetic studies of Miocene ignimbrites from Nevada: Royal Astronomical Society, Geophysical Journal, 20: 241–252.

Grommé, C. S., McKee, E. H., and Blake, M. C., Jr., 1972, Paleomagnetic correlations and potassium–argon dating of middle Tertiary ash-flow sheets in the eastern Great Basin. Nevada and Utah: Geological Society of America, Bulletin, 83: 1619–1638.

Grunder, A. L., Gans, P. B., and Schermer, E. R., 1987, Time–composition trends of volcanic rocks associated with mid-Tertiary extension in east-central Nevada and adjacent Utah (abs.): Geological Society of America, Abstracts with Programs, 19(6): 384.

Heggeness, J. O., 1982, The geology of Ragged Top caldera: Unpublished M.S. thesis, University of Nevada, Reno, 107 pp.

Hildreth, W., 1981, Gradients in silicic magma chambers: Implications for lithospheric magmatism: Journal of Geophysical Research, 86: 10153–10192.

Hildreth, W., and Mahood, G., 1985, Correlation of ash-flow tuffs: Geological Society of America, Bulletin, 96: 968–974.

Hintze, L. F., 1975, Geologic highway map of Utah: Brigham Young University Geology Studies, Special Publication 3.

John, D. A., 1987, Geologic map of parts of the Morey and Fandango wilderness study areas, Nye County, Nevada: U.S. Geological Survey, Miscellaneous Field Studies Map MF-1847.

Kellogg, H. E., 1960, Geology of the southern Egan Range, Nevada; *in* Boethcher, J. W., and Sloan, W. W. (eds.), Guidebook to the Geology of east central Nevada: Intermountain Association of Petroleum Geologists, pp. 189–197.

Kleinhampl, F. J., and Ziony, J. I., 1985, Geology of northern Nye County, Nevada: Nevada Bureau of Mines and Geology, Bulletin 99A: 172 pp.

Lanphere, M. A., 1988, High resolution $^{40}Ar/^{39}Ar$ chronology of Oligocene volcanic rocks, San Juan Mountains, Colorado: Geochimica et Cosmochimica Acta, 52: 1425–1434.

Le Bas, M. J., Le Maitre, R. W., Streckeisen, A., and Zenettin, B., 1986, A chemical classification of volcanic rocks based on the total alkali–silica diagram: Journal of Petrology, 27: 745–750.

Lindsey, D. A., 1982, Tertiary volcanic rocks and uranium in the Thomas Range and northern Drum Mountains, Juab County, Utah: U.S. Geological Survey, Professional Paper 1221: 71 pp.

Lipman, P. W., 1975, Evolution of the Platoro caldera complex and related volcanic rocks, southeastern San Juan Mountains, Colorado: U.S. Geological Survey, Professional Paper 852: 128 pp.

Lipman, P. W., 1976, Caldera-collapse breccias in the western San Juan Mountains, Colorado: Geological Society of America, Bulletin, 87: 1397–1410.

Lipman, P. W., 1980, Cenozoic volcanism in the western United States: Implications for continental tectonics; *in* Continental Tectonics: National Academy of Sciences, pp. 161–174.

Lipman, P. W., 1984, The roots of ash-flow calderas in western North America: windows into the tops of granitic batholiths: Journal of Geophysical Research, 89: 8801–8841.

Lipman, P. W., 1987, Tectonic controls of Cenozoic magmatism in the southern Rocky Mountains (abs.): Geological Society of America, Abstracts with Programs, 19(5): 315.

Lipman, P. W., Prostka, H. J., and Christiansen, R. L., 1972, Cenozoic volcanism and plate-tectonic evolution of the western United States, I, early and middle Cenozoic: Royal Society of London, Philosophical Transactions (A), 271: 217–248.

Loucks, M. D., Tingey, D. G., Best, M. G., Christiansen, E. H., and Hintze, L. F., 1989, Geologic map of Fortification Range, Lincoln and White Pine Counties, Nevada: U.S. Geological Survey, Miscellaneous Investigations Series Map I-1866.

Mackin, J. H., 1960, Structural significance of Tertiary volcanic rocks in southwestern Utah: American Journal of Science, 258: 81–131.

Marsh, B. D., 1981, On the crystallinity, probability of occurrence, and rheology of lava and magma: Contributions to Mineralogy and Petrology, 78: 85–98.

McKee, E. H., 1970, Fish Creek Mountains Tuff and volcanic center, Lander County, Nevada: U.S. Geological Survey, Professional Paper 681: 17 pp.

McKee, E. H., 1971, Tertiary igneous chronology of the Great Basin of the western United States: implications for tectonic models: Geological Society of America, Bulletin, 82: 3497–3502.

McKee, E. H., 1974, Northumberland caldera and Northumberland Tuff; *in* Guidebook to the geology of four Tertiary volcanic centers in central Nevada: Nevada Bureau of Mines and Geology, Report 19: 35–41.

McKee, E. H., 1976, Geology of the northern part of the Toquima Range, Lander, Eureka, and Nye Counties, Nevada: U.S. Geological Survey, Professional Paper 931: 49 pp.

McKee, E. H., 1988, Paleogene landscape of the Great Basin (abs.): Geological Society of America, Abstracts with Programs, 20(3): 214.

McKee, E. H., and Conrad, J. E., 1987, Geologic map of the Desatoya Mountains Wilderness area, Churchill and Lander Counties, Nevada: U.S. Geological Survey, Miscellaneous Field Studies Map MF-1944.

McKee, E. H., and Noble, D. C., 1974, Timing of late Cenozoic crustal extension in the western United States (abs.): Geological Society of America, Abstracts with Programs, 6: 218.

McKee, E. H., and Noble, D. C., 1986, Tectonic and magmatic development of the Great Basin of western United States during late Cenozoic time: Modern Geology, 10: 39–49.

McKee, E. H., and Silberman, M. L., 1970, Geochronology of Tertiary igneous rocks in central Nevada: Geological Society of America, Bulletin, 81: 2317–2327.

McKee, E. H., and Silberman, M. L., 1975, Cenozoic igneous history of the southern Cordillera south of 42° N (abs.): Geological Society of America, Abstracts with Programs, 7(7): 1196–1197.

McKee, E. H., and Stewart, J. H., 1971, Stratigraphy and potassium–argon ages of some middle Tertiary tuffs from Lander and Churchill Counties, central Nevada: U.S. Geological Survey, Bulletin 1311-B: 28 pp.

McKee, E. H., Noble, D. C., and Silberman, M. L., 1970, Middle Miocene hiatus in volcanic activity in the Great Basin area of the western United States: Earth and Planetary Science Letters, 8: 93–96.

McKee, E. H., Noble, D. C., Hedge, C. E., and Bonham, H. F., 1972, Strontium isotopic composition of some lower Miocene rhyolitic tuffs and lavas from the northwestern Great Basin: U.S. Geological Survey, Professional Paper 800-D: 99–102.

Menzies, M. A., Arculus, R. J., Best, M. G., Bergman, S. C., Ehrenberg, S. N., Irving, A. J., Roden, M. F., and Schulze, D. J., 1987, A record of subduction processes and within-plate volcanism in lithospheric xenoliths of the southwestern USA: *in* Nixon, P. H. (ed.), Mantle xenoliths: John Wiley & Sons, New York, pp. 59–74.

Moores, E. M., Scott, R. B., and Lumsden, W. W., 1968, Tertiary tectonics of the White Pine–Grant Range region, east-central Nevada, and

some regional implications: Geological Society of America, Bulletin, 79: 1703–1726.

Morton, J. L., Silberman, M. L., Bonham, H. F., Jr., Garside, L. J., and Noble, D. C., 1977, K–Ar ages of volcanic rocks, plutonic rocks, and ore deposits in Nevada and eastern California: Isochron/West, no. 20: 19–29.

Naeser, C. W., and McKee, E. H., 1970, Fission-track and potassium–argon ages of Tertiary ash-flow tuffs, north-central Nevada: Geological Society of America, Bulletin, 81: 3375–3383.

Nilsen, T. H., and McKee, E. H., 1979, Paleogene paleogeography of the western United States; *in* Armentrout, C. M., Cole, M. R., and TerBest, H. (eds.), Cenozoic paleogeography of the western United States, Pacific Coast Paleogeography Symposium III: Society of Economic Paleontologists and Mineralogists, Pacific Section, pp. 257–276.

Noble, D. C., 1968, Kane Springs Wash volcanic center, Lincoln County, Nevada; *in* Eckel, E. B. (ed.), Nevada Test Site: Geological Society of America, Memoir 110: 109–116.

Noble, D. C., 1972, Some observations on the Cenozoic volcanic-tectonic evolution of the Great Basin, western United States: Earth and Planetary Science Letters, 17: 142–150.

Noble, D. C., 1988, Cenozoic volcanic rocks of the northwestern Great Basin: An overview; *in* Buffa, R., Cuffney, R., and Seedorff, E. (eds.), Hot-Spring gold deposits of northwestern Nevada and southeastern Oregon: Geological Society of Nevada, Special Publication no. 7: 31–42.

Noble, D. C., and Christiansen, R. L., 1974, Black Mountain volcanic center; *in* Guidebook to the geology of four Tertiary volcanic centers in central Nevada: Nevada Bureau of Mines and Geology, Report 19: 22–34.

Noble, D. C., and McKee, E. H., 1972, Description and K–Ar ages of volcanic units of the Caliente volcanic field, Lincoln County, Nevada, and Washington County, Utah: Isochron/West, no. 5: 17–24.

Noble, D. C., and Parker, D. L., 1975, Peralkaline silicic volcanic rocks of the western United States: Bulletin Volcanologique, 38: 803–827.

Noble, D. C., McKee, E. H., and Weiss, S. I., 1988, Nature and timing of pyroclastic and hydrothermal activity and mineralization at the Stonewall Mountain volcanic center, southwestern Nevada: Isochron/West, no. 51: 25–28.

Noble, D. C., McKee, E. H., Hedge, C. E., and Blank, H. R., Jr., 1968, Reconnaissance of the Caliente depression, Lincoln County, Nevada (abs.): Geological Society of America, Special Paper 115: 435–436.

Noble, D. C., McKee, E. H., Smith, J. G., and Korringa, M. K., 1970, Stratigraphy and geochronology of Miocene volcanic rocks in northwestern Nevada: U.S. Geological Survey, Professional Paper 700-D: 23–32.

Noble, D. C., Korringa, M. K., Church, S. E., Bowman, H. R., Silberman, M. L., and Heropoulos, C. E., 1976, Elemental and isotopic geochemistry of nonhydrated quartz latite glasses from the Eureka Valley Tuff, east-central California: Geological Society of America, Bulletin, 87: 754–762.

Noble, D. C., Sargent, K. A., Mehnert, H. H., Ekren, E. B., and Byers, F. M., Jr., 1968, Silent Canyon volcanic center, Nye County, Nevada; *in* Eckel, E. B. (ed.), Nevada Test Site: Geological Society of America, Memoir 110: 65–77.

Noble, D. C., Slemmons, D. B., Korringa, M. K., Dickinson, W. R., Al-Rawi, Y., and McKee, E. H., 1974, Eureka Valley Tuff of east-central California and adjacent Nevada: Geology, 2: 139–143.

Noble, D. C., Vogel, T. A., Weiss, S. I., Erwin, J. W., McKee, E. H., and Younker, L. W., 1984, Stratigraphic relations and source areas of ash-flow sheets of the Black Mountain and Stonewall Mountain volcanic centers, Nevada: Journal of Geophysical Research, 89: 8593–8602.

Novak, S. W., 1984, Eruptive history of the rhyolitic Kane Springs Wash volcanic center: Journal of Geophysical Research, 89: 8603–8615.

Novak, S. W., and Mahood, G. A., 1986, Rise and fall of a basalt–trachyte–rhyolite magma system at the Kane Springs Wash caldera, Nevada: Contributions to Mineralogy and Petrology, 94: 352–373.

Orkild, P. P., Byers, F. M., Jr., Hoover, D. L., and Sargent, K. A., 1968, Subsurface geology of Silent Canyon caldera, Nevada Test Site, Nevada; *in* Eckel, E. B. (ed.), Nevada Test Site: Geological Society of America, Memoir 110: 77–86.

Proffett, J. M., Jr., 1977, Cenozoic geology of the Yerington district, Nevada, and implications for the nature and origin of Basin and Range faulting: Geological Society of America, Bulletin, 88: 247–266.

Quinlivan, W. D., Rogers, C. L., and Dodge, H. W., Jr., 1974, Geologic map of the Portuguese Mountain quadrangle, Nye County, Nevada: U.S. Geological Survey, Miscellaneous Investigations Series Map I-804.

Ratté, J. C., Marvin, R. F., and Naeser, C. W., 1984, Calderas and ash-flow tuffs of the Mogollon Mountains, southwestern New Mexico: Journal of Geophysical Research, 89: 8713–8732.

Robinson, P. T., 1972, Petrology of potassic Silver Peak volcanic center, western Nevada: Geological Society of America, Bulletin, 83: 1693–1708.

Robinson, P. T., and Stewart, J. H., 1984, Uppermost Oligocene and lowermost Miocene ash-flow tuffs of western Nevada: U.S. Geological Survey, Bulletin 1557: 53 pp.

Rosenbaum, J. G., 1986, Paleomagnetic directional dispersion produced by plastic deformation in a thick Miocene welded tuff, southern Nevada: Implications for welding temperatures: Journal of Geophysical Research, 91: 12817–12834.

Rowley, P. D., and Siders, M. A., 1988, Miocene calderas of the Caliente caldera complex, Nevada–Utah: American Geophysical Union (EOS), Transactions, 69(44): 1508.

Rowley, P. D., Anderson, J. J., Williams, P. L., and Fleck, R. J., 1978, Age of structural differentiation between the Colorado Plateaus and Basin and Range provinces in southwestern Utah: Reply: Geology, 6: 572–575.

Rytuba, J. J., and McKee, E. H., 1984, Perakaline ash-flow tuffs and calderas of the McDermitt volcanic field, southeast Oregon and north-central Nevada: Journal of Geophysical Research, 89: 8616–8628.

Sargent, K. A., and McKee, E. H., 1969, The Bates Mountain Tuff in northern Nye County, Nevada: U.S. Geological Survey, Bulletin 1294-E: 12 pp.

Sargent, K. A., and Roggensack, K., 1984, Map showing outcrops of pre-Quaternary ash-flow tuffs and volcaniclastic rocks, Basin and Range province, Nevada: U.S. Geological Survey, Water-Resources Investigations Report 83-4119-E.

Scholz, C. H., Barazangi, M., and Sbar, M. L., 1971, Late Cenozoic evolution of the Great Basin, western United States, as an ensialic basin: Geological Society of America, Bulletin, 82: 2979–2990.

Scott, D. H., and Trask, N. J., 1971, Geology of the Lunar crater volcanic field, Nye County, Nevada: U.S. Geological Survey, Professional Paper 599-I: 22 pp.

Shawe, D. R., Naeser, C. W., Marvin, R. F., and Mehnert, H. H., 1987, New radiometric ages of igneous and mineralized rocks, southern Toquima Range, Nye County, Nevada: Isochron/West, no. 50: 3–7.

Shawe, D. R., Marvin, R. F., Andriessen, P. A. M., Mehnert, H. H., and Merritt, V. M., 1986, Ages of igneous and hydrothermal events in the Round Mountain and Manhattan gold districts, Nye County, Nevada: Economic Geology, 81: 388–407.

Silberman, M. L., Bonham, H. F., Jr., Garside, L. J., and Ashley, R. P., 1979, Timing of hydrothermal alteration–mineralization and igneous activity in the Tonopah mining district and vicinity, Nye and Esmeralda Counties, Nevada; *in* Ridge, J. D. (ed.), Papers on mineral deposits of western North America: Nevada Bureau of Mines and Geology, Report 33: 119–126.

Slemmons, D. B., 1966, Cenozoic volcanism of the central Sierra Nevada; *in* Bailey, E. H. (ed.), Geology of northern California: California Division of Mines and Geology, Bulletin 190: 199–214.

Smith, R. L., 1960, Zones and zonal variations in welded ash-flows: U.S. Geological Survey, Professional Paper 354-F: 11 pp.

Smith, R. L., 1979, Ash-flow magmatism; *in* Chapin, C. E., and Elston, W. E. (eds.), Ash-flow tuffs: Geological Society of America, Special Paper 180: 5–27.

Smith, R. L., and Bailey, R. A., 1968, Resurgent cauldrons; *in* Coats, R. R., Hay, R. L., and Anderson, C. A. (eds.), Studies in volcanology: Geological Society of America, Memoir 116: 613–662.

Snyder, R. P., Ekren, E. B., and Dixon, G. L., 1972, Geologic map of the Lunar Crater quadrangle, Nye County, Nevada: U.S. Geological Survey, Miscellaneous Geologic Investigations Map I-700.

Speed, R. C., and McKee, E. H., 1975, Age and origin of the Darrough felsite, southern Toiyabe Range, Nevada: U.S. Geological Survey, Journal of Research, 4(1): 75–81.

Steven, T. A., and Lipman, P. W., 1976, Calderas of the San Juan volcanic field, southwestern Colorado: U.S. Geological Survey, Professional Paper 958: 35 pp.

Steven, T. A., Rowley, P. D., and Cunningham, C. G., 1984, Calderas of the Marysvale volcanic field, west central Utah: Journal of Geophysical Research, 89: 8751–8764.

Stewart, J. H., 1983, Cenozoic structure and tectonics of the northern Basin and Range province, California, Nevada, and Utah: Geothermal Resources Council, Special Report 13: 25–40.

Stewart, J. H., and Carlson, J. E., 1976, Cenozoic rocks of Nevada: Nevada Bureau of Mines and Geology, Map 52.

Stewart, J. H., and McKee, E. H., 1977, Geology and mineral deposits of Lander County, Nevada: Part I, Geology: Nevada Bureau of Mines and Geology, Bulletin 88: 59 pp.

Sullivan, K. R., 1987, Isotopic ages of igneous intrusions in southeastern

Utah: Relation to space–time–composition patterns of Cenozoic igneous activity in Nevada, Utah, and Colorado (abs.): Geological Society of America, Abstracts with Programs, 19: 337.

Swanson, E. R., and McDowell, F. W., 1984, Calderas of the Sierra Madre Occidental volcanic field, western Mexico: Journal of Geophysical Research, 89: 8787–8800.

Taylor, W. J., Bartley, J. M., and Axen, G. J., 1987, Style and magnitude of Tertiary extension, Dry Lake Valley area, Nevada (abs.): Geological Society of America, Abstracts with Programs, 19(7): 865.

Tingey, D. G., 1986, Miocene mica peridotite dike swarm, Wasatch Plateau, Utah (abs.): Geological Society of America, Abstracts with Programs, 18(5): 418.

Tingley, J. V., and Berger, B. R., 1985, Lode gold deposits of Round Mountain, Nevada: Nevada Bureau of Mines and Geology, Bulletin 100: 62 pp.

Tschanz, C. M., and Pampeyan, E. H., 1970, Geology and mineral deposits of Lincoln County, Nevada: Nevada Bureau of Mines and Geology, Bulletin 73: 187.

Turrin, B. D., Bergquist, J. R., Turner, R. L., Plouff, D., Ponader, C. W., and Scott, D. R., 1988, Mineral Resources of the High Rock Canyon Wilderness Study Area, Washoe County, Nevada: U.S. Geological Survey, Bulletin 1707-D: 14 pp.

Vogel, T. A., Noble, D. C., and Younker, L. W., 1989, Evolution of the compositional layering in the Black Mountain magmatic system, SW Nevada: Journal of Geophysical Resarch, in press.

Vogel, T. A., Ryerson, R. A., Noble, D. C., and Younker, L. W., 1987, Limits to magma mixing based on chemistry and mineralogy of pumice fragments from a chemically zoned ash-flow sheet: Journal of Geology, 95: 659–670.

Weiss, S. I., and Noble, D. C., 1989, Internal stratigraphy of the Civet Cat Canyon Member of the Stonewall Flat Tuff: Facies relations and near-vent geology, Stonewall Mountain volcanic center, southern Nevada: Journal of Geophysical Research, in press.

Weiss, S. I., Noble, D. C., and McKee, E. H., 1988, Volcanic and tectonic significance of the presence of late Miocene Stonewall Flat Tuff in the vicinity of Beatty, Nevada (abs.): Geological Society of America, Abstracts with Programs, 20: A399.

Weiss, S. I., Noble, D. C., and McKee, E. H., 1989, Paleomagnetic evidence for an extremely short period of time between eruption of the Pahute Mesa and Trail Ridge Members of the Thirsty Canyon Tuff, southern Nevada: Journal of Geophysical Research, in press.

Wernicke, B. P., Christiansen, R. L., England, P. C., and Sonder, L. J., 1987, Tectonomagmatic evolution of Cenozoic extension in the North America Cordillera; *in* Coward, M. P., Dewey, J. F., and Hancock, P. L. (eds.), Continental Extensional Tectonics: Geological Society (London), Special Publication no. 28: 203–221.

Williams, P. L., 1960, A stained slice method for rapid determination of the phenocryst composition of volcanic rocks: American Journal of Science, 258: 148–152.

Williams, P. L., 1967, Stratigraphy and petrography of the Quichapa Group, southwestern Utah and southeastern Nevada: Unpublished Ph.D. thesis, University of Washington, Seattle, 139 pp.

Willis, J. B., Best, M. G., Kowallis, B. J., and Best, V. C., 1987, Preliminary geologic map of northern Wilson Creek Range, Lincoln County, Nevada: U.S. Geological Survey, Miscellaneous Field Studies Map MF-1971.

Witkind, I. J., and Marvin, R. F., 1988, Significance of new potassium–argon ages from the Goldens Ranch and Moroni Formations, Sanpete–Sevier Valley area, central Utah: Geological Society of America, Bulletin, in press.

Wust, S. L., 1986, Regional correlation of extension directions in Cordilleran metamorphic core complexes: Geology, 14: 828–830.

Zartman, R. E., 1974, Lead isotope provinces in the Cordillera of the western United States and their genetic significance: Economic Geology, 69: 792–805.

EXCURSION 4A:
Silicic volcanic rocks in the Snake River Plain—Yellowstone Plateau province

Bill Bonnichsen[1], Robert L. Christiansen[2], Lisa A. Morgan[3], Falma J. Moye[4], William R. Hackett[4], William P. Leeman[5], Norio Honjo[6], Margaret D. Jenks[1], and Martha M. Godchaux[7]

[1]*Idaho Geological Survey, University of Idaho, Moscow, Idaho 83843;* [2]*U.S. Geological Survey, MS 910, 345 Middlefield Road, Menlo Park, California 94025;* [3]*U.S. Geological Survey, MS 964, Box 25046, Federal Center, Denver, Colorado 80225-0046;* [4]*Department of Geology, Idaho State University, Pocatello, Idaho 83209;* [5]*National Science Foundation, Earth Science Division, Washington, D.C. 20550;* [6]*Keith-Wiess Geological Laboratories, Rice University, Houston, Texas 77251;* [7]*Department of Geology, Mount Holyoke College, South Hadley, Massachusetts 01075*

Introduction and overview

Bill Bonnichsen and Martha M. Godchaux

The Snake River Plain volcanic province (including the Yellowstone Plateau) extends from southwest to northeast across southern Idaho and adjoining parts of Oregon, Nevada, and Wyoming (Fig. 1). During the past 14 m.y. this elongate zone has been the site of extensive, bimodal, basalt—rhyolite volcanism. Although many exceptions exist, the general location of active volcanism has progressed from southwest to northeast along this zone and, at any particular

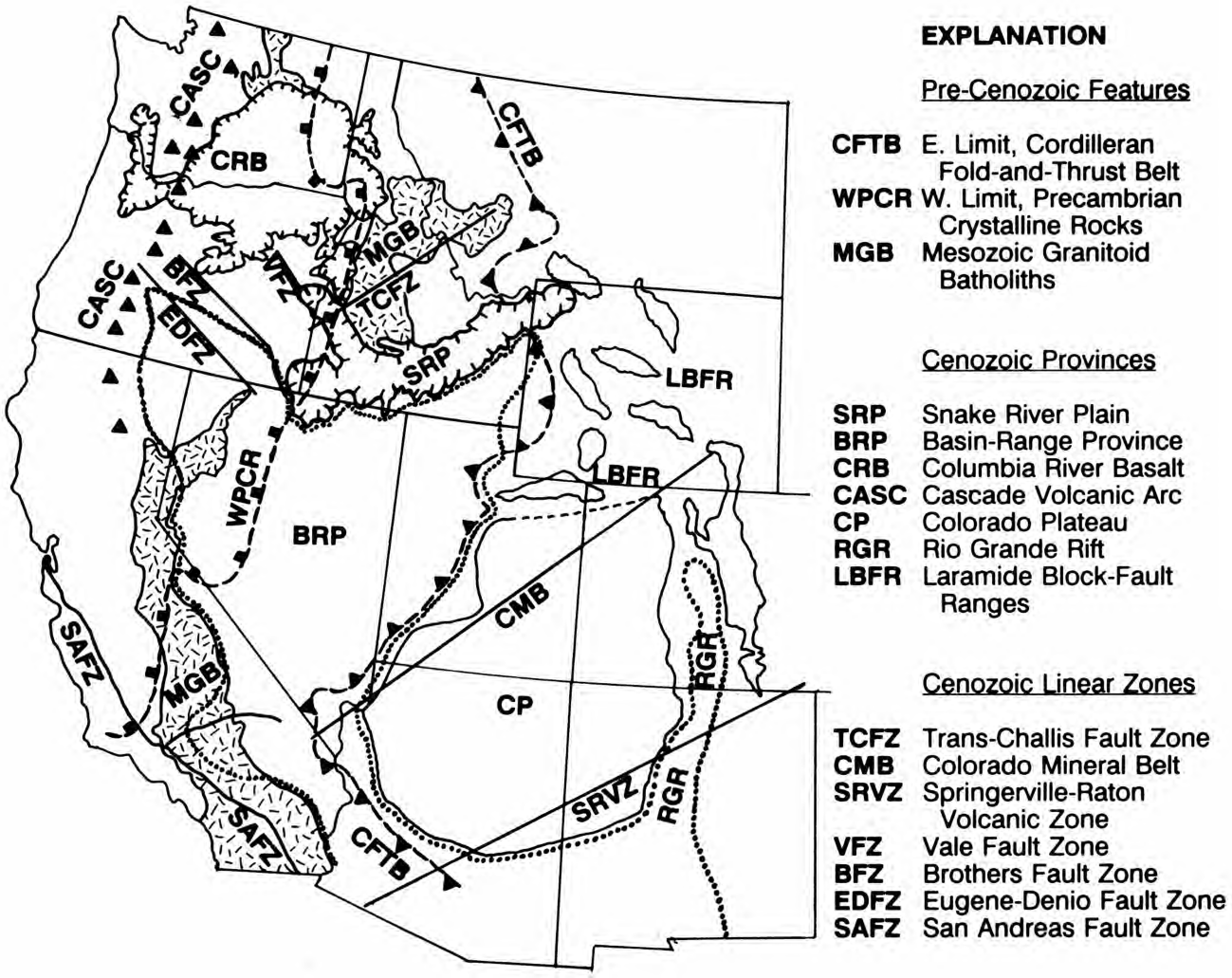

FIGURE 1—Location of the Snake River Plain—Yellowstone Plateau volcanic province in relation to certain other tectonic features, provinces, and linear zones of the western United States.

place or time, the type of volcanism has changed from silicic ignimbrites to rhyolite lava flows to basalt lava flows. The major time-transgressive component of the volcanism was the silicic activity that swept from west to east. The silicic volcanism appears to have started in the region near the junction of Idaho, Oregon, and Nevada (the Owyhee—Humboldt eruptive center; Bonnichsen and Kauffman, 1987), and perhaps at the other sites to the north in the vicinity of the Idaho—Oregon state line. After this activity had ceased, widespread basaltic eruptions occurred and, even later in the history of the evolving Snake River Plain, sporadic, small-volume silicic volcanic eruptions and additional basaltic eruptions took place.

The Snake River Plain volcanic province should be distinguished from the physiographic Snake River Plain. The volcanic province lies on either side of a nearly straight southwest—northeast-trending axis about 700 km long that trends from the Owyhee—Humboldt eruptive center near the Idaho—Oregon—Nevada junction to Yellowstone National Park in northwestern Wyoming (Fig. 1). Both topographically subdued plains and plateau areas, and uplifted mountainous areas, are contained within the volcanic province. The physiographic Snake River Plain, on the other hand, includes the plains-and-plateau topographic zone stretching southwestward from eastern Idaho, then following the western Snake River Plain graben northwestward to the vicinity of the Idaho—Oregon state line, forming an arcuate zone partly within the volcanic province and partly to the north of the volcanic province. Thus, in eastern Idaho the physiographic Snake River Plain coincides with the volcanic province, but in southwestern Idaho the physiographic Snake River Plain diverges northwestward from the axis of the volcanic province (Fig. 1).

Fig. 1 shows the position of the Snake River Plain—Yellowstone Plateau volcanic province in relation to other selected geologic elements (broad tectonic provinces and linear features) of the western United States. These elements can be divided into pre-Cenozoic, mainly early-rifting or compressional ones, and Cenozoic, mainly extensional ones.

Three generalized features of the pre-Cenozoic geology of the western U.S., all of which can be traced northward into Canada and southward into Mexico, are shown. The approximate eastern limit of the Cordilleran fold-and-thrust belt (Goodwin and Thompson, 1988) generally indicates the position and shape of the stable, non-disrupted, cratonic basement of North America. The position where this cratonic margin crosses the Snake River Plain volcanic province coincides with the boundary between the topographically high Yellowstone Plateau and the topographically low Snake River Plain. The western limit of all Precambrian crystalline rocks (Burchfiel, 1979), including blocks detached from the stable craton during late Precambrian rifting, coincides roughly with the western end of the Snake River Plain volcanic province. A collage of basement blocks, accreted terranes, and plutonic and volcanic rocks of various ages and types make up North America west of the fold-and-thrust belt. The principal outcrop areas of Mesozoic granitoid batholiths (Goodwin and Thompson, 1988) constitute a nearly continuous belt which may have been parallel to the late Mesozoic continental margin when emplaced. The central portion of this belt was displaced westward by late Cenozoic Basin and Range extension. Wernicke et al. (1988) estimate that this extension doubled the width of the northern Basin and Range province (100 km of extension) before 15 Ma ago, and nearly quadrupled the width of the southern Basin and Range province after 15 Ma ago (247 ± 56 km of movement of the Sierra Nevada batholith directed N73W ± 12° relative to the Colorado Plateau).

Cenozoic features of two types, major tectonic provinces and linear zones, are shown in Fig. 1. The tectonic provinces include (in order of time of inception): (1) the Colorado Plateau and the Laramide block-fault ranges of Wyoming and Colorado, (2) the Rio Grande rift and the Basin and Range province (Eaton, 1980), (3) the Cascade volcanic arc, and (4) the basalt-covered Columbia River Plateau (Swanson et al., 1975).

Among the many linear features that occur in the western U. S. , those near the Snake River Plain volcanic province were included in Fig. 1, along with a few others that are well known. These linear zones are faults or volcanic zones, or both, and they include a prominent northeast-trending group and an equally prominent northwest-trending group. Where fault displacements have been established, the northeast-trending fault zones show normal and left-lateral motion, whereas the northwest-trending fault zones show normal and right-lateral motion. Northeast-trending linear zones, from north to south, are: (1) the Trans-Challis fault zone (Kiilsgaard et al. , 1986), (2) the main Snake River Plain volcanic province trend, (3) the Colorado mineral belt (Lipman, 1980), and the Springerville—Raton volcanic zone (Lipman, 1980). Northwest-trending zones, from north to south, are: (1) the Vale fault zone and its continuation along the southwest side of the western Snake River Plain graben (Robyn and Hoover, 1982), (2) the Brothers and EugeneDenio fault zones (Robyn and Hoover, 1982), and (3) the San Andreas fault zone.

The Snake River Plain is, in effect, a boundary zone between differing sequences of geologic provinces that would be encountered on east—west traverses across the western U. S. at latitudes to the north and south (Fig. 1). Probably the most notable difference between a traverse along the southern edge of the Snake River Plain and one along the northern edge is the presence of the wide, tectonically extended Basin and Range province to the south. This type of tectonically stretched terrane is not nearly so extensive to the north. The Snake River Plain volcanic province developed during and after the period of most active extension in the northern Basin and Range province and forms much of the northern margin of that large tectonic and physiographic province. Accordingly, the Snake River Plain volcanic province probably represents a boundary zone that developed at the earth's surface and in the upper, brittle portion of the crust as the Basin and Range province was extended in an east—west direction. During approximately the last 14 million years, this southwest-to-northeast-trending tectonic boundary zone has been the site of numerous large rhyolitic and basaltic eruptions which accompanied the increasing fragmentation of the crust and upper mantle. These observations are consistent with an interpretation that numerous batches of basaltic magma formed in the upper mantle and rose into the crust. This influx of basaltic magmas triggered the melting of large volumes of crustal material to form the rhyolitic magmas that erupted; subsequent basaltic eruptions occurred as the crust became more dense (Bonnichsen, 1982b; Leeman, 1982a).

This seven-day field trip to the Snake River Plain—Yellowstone Plateau volcanic province will start in the Yellowstone Park area for days 1, 2, and 3. From there we will

move to the eastern Snake River Plain for day 4. Examination of the south side of the central part of the Plain will occupy days 5 and 6. During day 7, we will cross to the north side of the central part of the Plain, and then proceed across the Mount Bennett Hills and westward through the Camas Prairie to the western part of the Snake River Plain. The individual stops for the last four days of the trip are shown in Fig. 2, and the stops for days 1, 2, and 3 are plotted in Fig. 3. Our route will take us to the youngest units of the province first. As the trip progresses, the units we visit will be increasingly older, more deeply dissected, and to a certain degree more enigmatic, particularly during the last day when we examine the especially high-temperature units in the central part of the Plain. Thus, we will be progressing back in time, reversing the evolutionary development of the volcanic province, as we proceed westward on our trip.

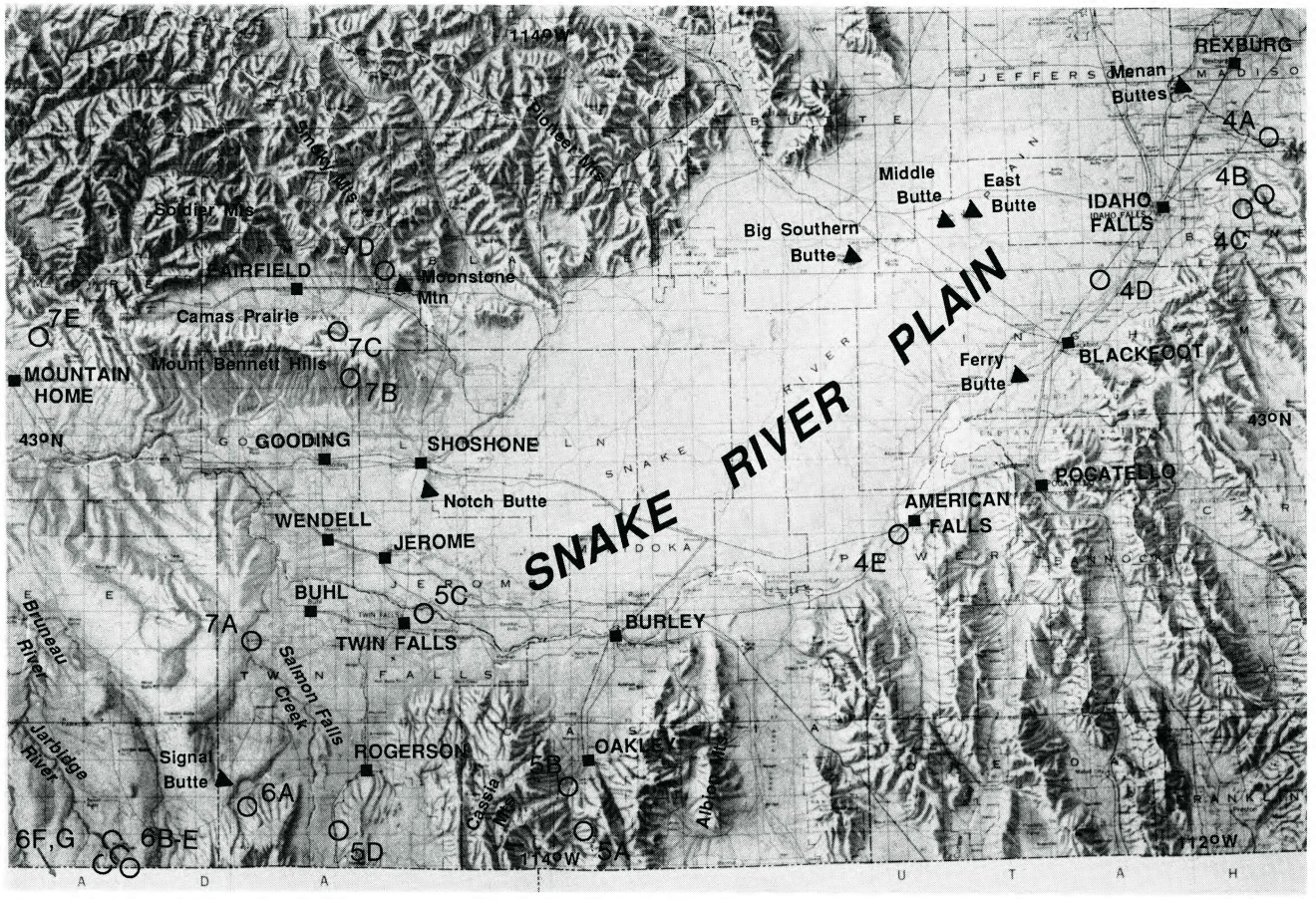

FIGURE 2—Locations of the stops for days 4, 5, 6, and 7 plotted on a shaded relief map of southern Idaho.

Days 1, 2, and 3: The Yellowstone Plateau volcanic field

Robert L. Christiansen

The Yellowstone Plateau, at the center of one of the Earth's largest volcanic fields, spans the Continental Divide between the Northern and Middle Rocky Mountains at an average elevation of about 2400 m. The eruptions of the Yellowstone Plateau volcanic field, entirely postdating 2.5 Ma, were exceedingly voluminous but are only the surficial expressions of the emplacement of a batholithic volume of rhyolitic magma to high crustal levels (Christiansen, 1979). Although the latest eruptions occurred about 70,000 years ago, an immense hydrothermal system and a variety of geophysical characteristics indicate the continued presence of an active shallow magma chamber (Smith and Christiansen, 1980; Smith and Braile, 1984).

Brief introduction to regional geology

The Yellowstone Plateau and its surrounding region preserve major rock units of Archean, Proterozoic, Paleozoic, Mesozoic, early Tertiary, and late Cenozoic ages. Although

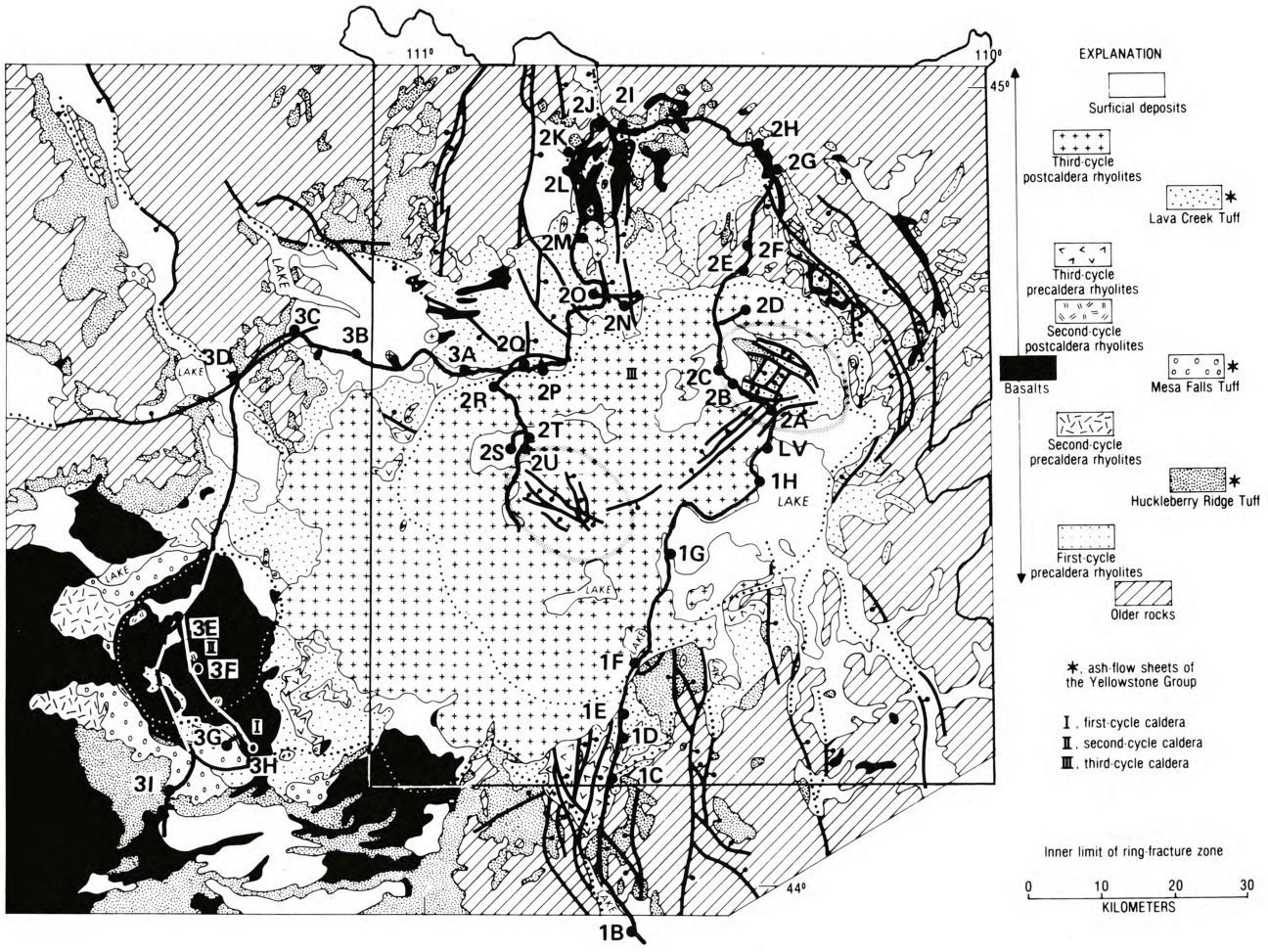

FIGURE 3—Generalized geologic map of Yellowstone National Park and vicinity, showing the stops for days 1, 2, and 3.

the field trip for which this guidebook was prepared emphasizes late Cenozoic volcanism and tectonism, a brief account of the broader aspects of the regional geology will enhance the trip.

Precambrian rocks of the region are mainly crystalline metamorphics. A major Archean regional metamorphism of about 2.6 Ga is recorded widely, but considerably older rocks are recognized as well (Ruppel, 1972; Reed and Zartman, 1973; Love and Keefer, 1975; James and Hedge, 1979). Proterozoic basaltic dikes are widespread. Paleozoic and Mesozoic sedimentary rocks were mainly deposited in shallow marine basins and adjacent coastal lowlands on a subsiding cratonic platform (Love, 1956; Ruppel, 1972; Love and Keefer, 1975). The shallow-marine older Paleozoic section comprises a Middle Cambrian clastic sequence overlain predominantly by carbonates of Upper Cambrian through Mississippian (Lower Carboniferous) age. Younger Paleozoic rocks include both clastic and carbonate lithologies. Triassic and Jurassic strata, including thick red beds, are mostly continental but also include marine strata. A shale-rich Lower Cretaceous marine sequence, deposited in deepening basins, is overlain by sandstone and shale deposited in shallower seas as the basins filled with sediments eroded from rising orogenic highlands farther west.

The Laramide orogeny disturbed the former cratonic foreland in latest Cretaceous to earliest Eocene time, forming large, northwest-trending, thrust-bounded anticlinal uplifts and deep adjacent basins that accumulated orogenic sedi ments (Love, 1956; Ruppel, 1972; Love et al. , 1973; Love and Keefer, 1975). This contractional deformation ended before the beginning of widespread andesitic volcanism of the Eocene Absaroka Volcanic Supergroup, mainly about 52-43 Ma (Smedes and Prostka, 1972). Central-vent Absaroka stratovolcanoes are represented by near-vent volcanic breccias and lavas, grading to more distal breccias and enveloped by alluvial-facies andesitic sedimentary strata. Shallow subvolcanic intrusions cut Paleozoic and Mesozoic rocks. Absaroka volcanism was succeeded in the Yellowstone region by widespread mid-Tertiary erosion.

Since the middle Miocene, the region has been broken by extensional normal faults, tectonically part of the basin—range system (Love et al. , 1973; Smith, 1978). South of the Yellowstone Plateau, these faults trend mainly northward; north of the plateau, they trend northwest to westward. Their displacements form fault-block ranges and basins that break across many Laramide structures, especially south of the plateau, but to the northwest these faults reactivate some of them. Regional late Cenozoic volcanism is characterized by abundant basalt or by bimodal rhyolite and basalt (Christiansen and McKee, 1978). The Yellowstone Plateau volcanic field is the active segment of a mainly rhyolitic system, associated with basalts and basin—range extension, that has propagated northeastward at about 4 cm/year since the middle Miocene. The track of this propagating volcanism is expressed physiographically as the subsided and basalt-covered floor of the eastern Snake River Plain.

Pleistocene glaciations produced major ice caps on the plateau as well as alpine glaciers in the surrounding mountains (Pierce, 1979; Richmond, 1986). Most prominently recorded are two late Pleistocene ice advances: the latest Pleistocene Pinedale glaciation and the next older major regional glaciation, the Bull Lake.

The Yellowstone Plateau volcanic field

The Yellowstone Plateau volcanic field records three cycles of voluminous rhyolitic activity (Christiansen and Blank, 1972; Christiansen, 1979, 1982, 1984). Each cycle began with eruptions of both basaltic and rhyolitic lavas, the rhyolites venting mainly from developing ring-fracture systems. The climax of each cycle was marked by extremely rapid and voluminous eruptions 300 to 2500 km^3 of rhyolitic magma in a few hours or days—as ash flows from the ring-fracture system and by collapse of the source area to form a large caldera. Postcollapse volcanism in each caldera has tended to fill it with rhyolitic lavas. Throughout each cycle, basaltic lavas continued to erupt around the margins but not within the major active rhyolitic source areas. The ash flows erupted at the climax of each cycle form three largely welded cooling units that make up the Yellowstone Group: the Huckleberry Ridge Tuff of 2.0 Ma, the Mesa Falls Tuff of 1.3 Ma, and the Lava Creek Tuff of 0.6 Ma. The caldera that formed during the climactic first-cycle Huckleberry Ridge eruption, largest of the three, spanned from Island Park (west of Yellowstone National Park), past the northern Teton Range and Jackson Hole on the south, to the center of the Yellowstone Plateau. The second-cycle Henrys Fork caldera is the smallest of the three; both it and the surface outcrop of the Mesa Falls Tuff are restricted to the Island Park area. The third-cycle Yellowstone caldera, related to the 1000 km^3 Lava Creek Tuff eruption, is 70 x 40 km across in the central part of the Yellowstone Plateau. Voluminous rhyolitic lavas (several individual flows exceeding 50 km^3) fill the central part of the caldera and overflow its western rim. Basalts encircle the Yellowstone Plateau; some of them erupted through the older rhyolitic centers of Island Park.

The Yellowstone caldera region hosts the largest hydrothermal system in the world, highlighted by numerous geysers (White et al., 1975). It accounts for an average heat flow from the caldera area that is 40 times greater than the global average (Fournier et al., 1976).

Day 1

This day of the trip will be led by Robert Christiansen. We will examine the tectonic setting of the Yellowstone Plateau, the interior structure of a large rhyolitic lava flow, the caldera-forming Lava Creek Tuff, part of the Yellowstone caldera, and the West Thumb Geyser Basin at the shore of Yellowstone Lake. Along the route of travel we will pass through the scenic basin–range valley of Jackson Hole, climb onto the Yellowstone Plateau from the south, and pass into the enormous Yellowstone caldera, within which we will remain for much of the next two days.

Mileage

0.0 Junction of Jackson airport road with main highway. View east to the Gros Ventre Range and a young fault scarp extending south from the Paleozoic bedrock of Blacktail Butte. To the west and north is an open view of the Teton Range and outwash fill of Pinedale age in the valley of Jackson Hole. **4.5**

4.5 Turn left at road junction to Moose Village and cross Snake River at Moose Visitor Center. **0.8**

5.3 Entrance Station, Grand Teton National Park. Beyond, the road climbs from a lower outwash terrace of Pinedale age to a higher terrace and passes several older eroded moraines. **2.6**

7.9 Taggart Lake trailhead on left. **0.7**

8.6 Roadside turnout on right. The view east (right) is to the Gros Ventre Range and Mt. Leidy Highlands, including the large Gros Ventre landslide of 1911. The view west (left) is to the Teton Range and a moraine of Pinedale age at its base. **1.5**

10.1 **STOP 1A. View of Teton Range faultline scarp,** scoured by late Pinedale glacial valleys. Turn left and park in Glacier Gulch turnout. The glaciated core of the Teton Range exposes Precambrian granitic gneisses and other metamorphic rocks. The Wall, a west-dipping cap of lower Paleozoic sedimentary rocks, is visible on the skyline. In the distance to the north, across Jackson Hole, are the distant west-tilted fault blocks of Huckleberry Ridge, Wildcat Ridge, and others, some of them capped by welded Huckleberry Ridge Tuff (2 Ma). A moraine of Bull Lake age is across the road on the right.

Continue north on the road through Jackson Hole. **1.8**

11.9 Pass south end of Jenny Lake loop road on left. The Pinedale-age Jenny Lake moraine is ahead on the left. Ahead, the road skirts the Jenny Lake moraine on the left on Pinedale outwash, passing through older moraines just beyond. **6.4**

18.3 Mt. Moran turnout on left. Stratified Eocene volcanic rocks in the area of Togwotee Pass and the southern Absaroka Range are visible in the distance ahead (northeast). Beyond, the road passes through the Jackson Lake end-moraine complex of Pinedale age. **5.1**

23.4 Cross Jackson Lake Dam. (As the dam is under repair, it may be necessary to detour to the right.) **1.1**

24.5 Roadside turnout on right. Signal Mountain, on the right, is a till-mantled and densely vegetated west-tilted fault block of 2 Ma Huckleberry Ridge Tuff overlying 4 Ma Conant Creek Tuff, each making a prominent bluff. To the north (left) are other west-tilted fault blocks, Pilgrim Mountain (also capped by Conant Creek and Huckleberry Ridge Tuffs) and Wildcat Ridge. The hills just ahead are underlain by Upper Cretaceous marine sedimentary rocks. **0.4**

24.9 Turn left at Jackson Lake Junction. Ahead, the road passes across the aggraded floor of Jackson Hole, through moraines of the moraine complex on the east side of Jackson Lake, and past the resort areas of Jackson Lake Lodge, Colter Bay Village, and Leeks Marina. **11.3**

36.2 **STOP 1B. View of Teton Range and Jackson Lake.** Pull into roadside turnout on left and park at edge of Jackson Lake. The west-tilted Teton Range, with its high-standing Precambrian core to the south, becomes lower and exposes north-dipping Paleozoic and Mesozoic sedimentary rocks on the north. This relation and the high structural relief of the

Tetons are composite features of the northwest-trending Laramide Gros Ventre–Teton uplift and the late Cenozoic north-trending, west-tilted normal-fault block of the modern Tetons. Upper Cretaceous sandstone and shale, nearly buried beneath Pinedale till across the road, are exposed in the bluff just below the turnout.

Continue on the road along the east side of Jackson Lake. **2.2**

38.4 Junction with road to Lizard Creek Campground on left. Beyond, the highway climbs a hill of poorly exposed Huckleberry Ridge Tuff mantled thickly by Pinedale till. **4.0**

42.4 Steamboat Mountain, ahead to the left, is a fault block within the graben of Jackson Hole with prominent outcrops of Huckleberry Ridge Tuff. In the distance to the north is the Pitchstone Plateau, a large rhyolitic lava flow erupted within the Yellowstone caldera. **3.0**

45.4 Cross Snake River at Flagg Ranch. To the west (left), the north end of the Teton Range plunges beneath the Yellowstone Plateau. On Huckleberry Ridge, to the right, the type section of the Huckleberry Ridge Tuff is in the cliff at the head of a prominent landslide scar, overlying Upper Cretaceous marine shale. Ahead on the skyline is the Pitchstone Plateau. Beyond here, the road enters the Snake River caldera segment, a portion of the partly buried first-cycle caldera related to eruption of the Huckleberry Ridge Tuff. A small outcrop of Lava Creek Tuff is exposed below the bridge at its south abutment. **2.7**

48.1 South Entrance to Yellowstone National Park. **1.2**

49.3 **STOP 1C. Internal structure in rhyolite lava flow.** Cross Crawfish Creek and park on right at trail to Moose Falls; walk down the short trail (about 40 m). Crawfish Creek falls across a bluff formed by a rhyolitic lava flow of the post-Huckleberry Ridge, pre-Lava Creek Lewis Canyon Rhyolite, about 0.9 Ma, that lies within the Snake River caldera segment. Flow layering in this spherulitic vitrophyre fans upward, indicating flowage to the east.

Return to the vehicles and continue up the road, which climbs onto the Lewis Canyon Rhyolite, mainly covered by Pinedale till; rhyolite crops out in only a few low roadcuts along the way. **2.9**

52.2 Roadside turnout along guardrail on right at approach to Lewis Canyon. Good exposures of rhyolite in the canyon. **0.5**

52.7 **STOP 1D. View of Lewis River Canyon and Lava Creek Tuff.** Park at roadside turnout along guardrail on right. Lavas of the Lewis Canyon Rhyolite are well exposed in the canyon. Huckleberry Ridge is prominent to the south and Mt. Hancock to the southeast. Both are gently west-tilted normal-fault blocks on which the Huckleberry Ridge Tuff caps a section of Paleozoic and Mesozoic sedimentary rocks. Huckleberry Ridge terminates abruptly northward along the course of the Snake River, where it is cut off by the south wall of the Snake River caldera segment, related to the eruption of members A and C of the Huckleberry Ridge Tuff. The caldera margin swings northward across the river and along the west side of the Red Mountains, seen to the east. The Red Mountains caldera segment was filled and partly buried by the youngest part of the Huckleberry Ridge Tuff (member C), which is thickened greatly within it. The Lewis Canyon Rhyolite, although about 1 m.y. younger than the Snake River caldera segment, largely filled the caldera and was later mantled by Lava Creek Tuff, which erupted to form the Yellowstone caldera farther north. The basal contact of the Lava Creek is exposed in the roadcut across the road from here. In the roadcut, glassy flow breccia at the top of the rhyolite flow is overlain by bedded fallout ash of the Lava Creek and, in turn, by welded ash-flow tuff. The basal ash flow is glassy but is overlain by a spherulitic zone about 1.5 m thick, typically bluish-gray in color and highly resistant to erosion; above is a devitrified zone of densely welded tuff.

Continue along the Park road following the rim of Lewis Canyon. Lewis Canyon Rhyolite remains prominent in the canyon; Lava Creek Tuff is exposed intermittently in the roadcuts, varying in thickness with the surface of the underlying rhyolite flows. As the level of the riverbed rises upstream, the contact between the units drops lower into the canyon. **2.0**

54.7 **STOP 1E. Lava Creek Tuff.** Park at guardrail with small turnout on curve and walk along outside of guardrail about 50 m upstream. Here the canyon of the Lewis River is cut entirely into member B of the Lava Creek Tuff. As the Yellowstone caldera is approached, the tuff becomes progressively thicker and has more and larger phenocrysts. Both underfoot and upstream from here, the tuff is devitrified and densely welded, with moderately well-developed columnar jointing.

Beyond, the road continues through good exposures of Lava Creek Tuff. **1.9**

56.6 Small roadside turnout on left at base of talus. The bluff above is the margin of the Pitchstone Plateau flow, a large rhyolitic lava flow that erupted in the southwestern part of the Yellowstone caldera and buries its rim. **1.4**

58.0 **STOP 1F. The Yellowstone caldera and Lewis Falls.** Park where there are roadside turnouts on both sides, just before the road crosses the Lewis River bridge. Near here the road crosses into the Yellowstone caldera. The Red Mountains to the east terminate abruptly northward at the caldera margin, which becomes progressively lower as it approaches the Lewis River along a dip slope of Lava Creek Tuff. There is no clear topographic expression of the caldera west of the river, where the Pitchstone Plateau flow buries the rim. The Aster Creek flow, an older rhyolitic lava flow erupted within the caldera to the east, partly fills it but was entirely contained within the wall. The Aster Creek flow is exposed as a vitrophyre in roadcuts on the low ridge north (left) of the road and holds up Lewis Falls.

From here the road crosses the Lewis River and passes other roadcuts in the Aster Creek flow. **1.3**

59.3 Lewis Lake Campground on left; just beyond is Lewis Lake, contained by large rhyolitic lava flows on all sides. Across the lake to the west is the edge of the Pitchstone Plateau, formed by a single very

large flow; the Aster Creek flow on the east is largely hidden from view by trees. **3.1**

62.4 Trailhead for Shoshone Lake on left. Beginning here, the road climbs onto another large rhyolitic lava flow, the Dry Creek flow, the source for which was at West Thumb of Yellowstone Lake. Outcrops, however, are sparse as most of the surface is covered by Pinedale till. **2.9**

65.3 Cross the Continental Divide. Waters south of here drain to the Pacific Ocean via the Snake and Columbia Rivers; waters to the north drain to the Atlantic Ocean via the Yellowstone, Missouri, and Mississippi Rivers. In a larger sense, the Yellowstone Plateau as a whole is the Continental Divide, but the actual location of the drainage divide is irregular across the plateau. **4.0**

69.3 At Y-junction, take right fork toward Lake. (Left fork goes to Old Faithful.) **0.2**

69.5 **STOP 1G. West Thumb Geyser Basin.** Turn right on road to West Thumb Geyser Basin; park in the large parking area and walk down to the boardwalk. Take the boardwalk loop through the basin from the parking lot to the lakeshore and back. Hot springs and geysers in the West Thumb Basin are perhaps more variable in temperature and discharge than in any other major thermal area of Yellowstone. Activity in the basin is sometimes quite vigorous, with new springs and increased geyser activity, while at other times it is cooler, supports abundant algae, and has only weak thermal discharge, possibly reflecting the influence of lake water on recharge to the basin. The recharge–discharge plumbing may be self-sealed by silica deposition at times and broken by fractures at other times to allow ingress of cold lake water.

Like most geyser basins of the Yellowstone Plateau, West Thumb is controlled by the ring-fracture zone of the Yellowstone caldera. It is localized where the zone is intersected by a line of young intracaldera rhyolitic vents, extending north-northwest across the caldera between aligned tectonic fault zones to the north and south to form the Central Plateau. The lake basin of West Thumb is a deep subcircular extension of Yellowstone Lake, the main basin of which is 10 km east. West Thumb probably had its origin as a relatively small caldera within the much larger Yellowstone caldera during a pyroclastic event that was part of the mainly lava-producing post-collapse volcanism of the past 150,000 years. The north, east, and south margins of the West Thumb caldera have been largely buried by younger rhyolite flows. To the east, beyond Yellowstone Lake, are the Absaroka Mountains. To the southeast is Flat Mountain, the truncated north face of which is part of the south margin of the Yellowstone caldera.

Return to the road and turn right. After passing the West Thumb Geyser Basin, the road continues to skirt extensive siliceous-sinter deposits and isolated hot springs near the lakeshore. **2.2**

71.7 Cross Little Thumb Creek. Along the lakeshore, the road provides good views to Flat Mountain and the Red Mountains at the south margin of the Yellowstone caldera. **1.1**

72.8 Roadside turnout on right; beyond, the road climbs onto the Dry Creek flow. Just past are poor outcrops of the tuff of Bluff Point, the product of the pyroclastic eruption that produced the West Thumb caldera. **0.4**

73.2 Roadcut on left is a good exposure of the tuff of Bluff Point. The basal contact, overlying the Dry Creek flow, is in the gully at the far end of the roadcut. Beyond here, there are few outcrops along the road other than lacustrine and glaciolacustrine terraces related to stands of Yellowstone Lake during retreat of the ice cap, some of which have been deformed by later uplift of the caldera. **3.5**

76.7 Roadside turnout on right. The sand bar offshore forms a lagoon along the shore. As the road continues for several miles beyond here on terraces above the lake, old bars rise in places between the road and the present lake, with meadows filling former lagoons. **1.6**

78.3 Pumice Point parking area on right. Good view across West Thumb to Flat Mountain and the Red Mountains at the south caldera wall. Some of the lacustrine sediments contain pumice from the rhyolitic lava flows that enclose the lake. **6.5**

84.8 **STOP 1H. View across the main basin of Yellowstone Lake.** Park in roadside turnout on right. To the northeast is Stonetop Mountain, in the southern part of the Sour Creek resurgent dome in the eastern part of the Yellowstone caldera, with a prominent area of hydrothermal alteration (Sulphur Hills) on its south side. Beyond the south (right) flank of Stonetop Mountain is Pelican Cone, a peak of Eocene andesites of the Absaroka Volcanic Supergroup outside the east margin of the caldera. The margin continues south along the west front of the Absaroka Mountains to Lake Butte, seen over Stevenson Island, then follows the east shore of Yellowstone Lake as far to the right as the area of view. The plateau rising to the higher part of the Absaroka Mountains is underlain mainly by the Lava Creek Tuff. Beyond the south part of the lake, the Two Ocean Plateau is a gently west-tilted fault block—the easternmost basin–range fault block south of the Yellowstone Plateau.

Continue on the Park road along the west side of Yellowstone Lake and across Bridge Bay. **3.8**

88.6 Junction with road to Lake Village on right. Turn right to Lake, where we will have lodging and meals for the night.

Day 2

This day of the trip will be led by Robert Christiansen. We will examine both the eastern and western segments of the Yellowstone caldera, a variety of active hydrothermal areas, the Grand Canyon of the Yellowstone, the Lava Creek Tuff, rhyolitic lavas both within and outside of the caldera, a rhyolite—basalt mixed-lava complex, and precaldera features (including basalts of the Yellowstone Plateau volcanic field and older, mainly intermediate rocks of the Absaroka Volcanic Supergroup). The route of travel is entirely within Yellowstone National Park, through the eastern caldera segment, out across its northeastern wall, around the northern part of the Park, re-entering the caldera in its western segment, and ending at Old Faithful.

Mileage

0.0 Return from Lake Village to main Park road junction and turn right. **1.6**

1.6 Road junction to East Entrance and Fishing Bridge on right. Continue straight ahead along west side of Yellowstone River, which drains Yellowstone Lake northward. Poor outcrops of rhyolite vitrophyre in roadcuts on left are top of West Thumb flow. **1.4**

3.0 Large outcrop of West Thumb flow on left. **1.4**

4.4 **STOP 2A. Contemporary uplift and related faults within Yellowstone caldera.** Park in parking area on right for LeHardy Rapids; walk down boardwalk to the river. The roadcut across the road exposes only Pinedale till, but the Yellowstone River cuts down into an upthrown fault block of Lava Creek Tuff. The erosionally resistant near-basal spherulitic zone forms the rapids. The Lava Creek Tuff here is uplifted within the Yellowstone caldera on the flank of the Sour Creek resurgent dome. Outcrops across the river are Lava Creek Tuff overlain by Pinedale till. The fault that brings the spherulitic zone up to the level of exposure here can be seen across the canyon; it and other northeast-trending faults that cut the Sour Creek dome are parts of the Elephant Back fault zone, a complex graben along an axis of active uplift and subsidence within the Yellowstone caldera. Vertical deformation rates as high as 2 cm/year have been measured over the past 55 years (Pelton and Smith, 1982; Dzurisin and Yamashita, 1987).

Below LeHardy Rapids the road follows a straight segment of the Yellowstone River controlled by a northwest-trending fault that locally breaks the Sour Creek dome. **2.9**

7.3 **STOP 2B. Mud Volcano Hydrothermal Area.** Turn in to Mud Volcano parking area on left and park. Walk the well-maintained trail clockwise from the south end of the parking lot. This is an excellent example of a small, vapor-dominated hydrothermal system. The thermal discharge is gas-rich, and the enclosing rocks and surficial deposits are intensely altered. The acidic thermal waters probably reflect shallow condensation from a large subsurface reservoir in which liquid water is subordinate to steam in fractures and pore spaces; steam is the pressure-controlling phase (White et al., 1971). Gases including H_2S rise with the steam and dissolve in the condensate to produce the acid waters. Temporal changes in activity in this basin appear to correlate with local seismicity.

Only Pinedale glacial deposits are exposed in the Mud Volcano area, except for a single outcrop of Lava Creek Tuff at Dragon's Mouth Spring. From above Mud Geyser at the south end of the loop trail, a good view to the east shows the west flank of the Sour Creek dome broken by a graben of the Elephant Back fault zone.

Return to the Park road and turn left. **0.2**

7.5 Roadside turnout on right for Sulphur cauldron. A research drill hole near here by the USGS in 1967 provided the data upon which the concept of vapor-dominated hydrothermal systems was based (White et al., 1971). **0.3**

7.8 Roadside turnout on right at entrance to Hayden Valley. This large, open valley is floored by glacial and lacustrine sediments with only local exposures of the underlying rhyolitic lavas. The valley is rimmed on the west by rhyolite flows from the Central Plateau and on the east by the Sour Creek resurgent dome. **4.2**

12.0 **STOP 2C. View of northeast part of Yellowstone caldera.** Park where there are large turnouts on both sides of road. Across the river to the east, the north end of Sour Creek dome descends into Hayden Valley. To the north is the Washburn Range, the northeast wall of Yellowstone caldera. In front of it are two early postcaldera rhyolitic lava flows, the Canyon flow and the overlying Dunraven Road flow, locally surmounted by a hydrothermally localized and altered kame mound. Northwest of the road is the edge of Hayden Valley flow, a rhyolitic lava from the Central Plateau. To the west is the crest of the Central Plateau, underlain by several large rhyolite flows. To the southwest, Crater Hills is another outcrop of hydrothermally localized and altered Pleistocene kame deposits.

Continue northward on the Park road. Beyond Alum Creek the road leaves Hayden Valley but continues along the Yellowstone River. **1.0**

13.0 Good outcrops of Hayden Valley flow on left; poorer outcrops of the perlitic margin of the flow are visible across the river. The flow was emplaced into a shallow lake on saturated bottom sediments, resulting in a highly perlitized margin and numerous clastic dikes. These are rarely well exposed but some can be seen in the banks across the river. **1.6**

14.6 Roadside turnout on right. Large roadcut on the left exposes the perlitic Hayden Valley flow resting on lacustrine sediments, some of which were squeezed up into the base of the flow at the north (right) end of the cut. **0.2**

14.8 Turn right at junction with Artist Point Road and cross the Yellowstone River. **1.0**

15.8 Roadcuts on both sides expose hydrothermally altered postcaldera lacustrine and alluvial sedimentary rocks that predate cutting of the Grand Canyon of the Yellowstone. Locally interbedded in these sediments are old sinter deposits, now recrystallized to chalcedony. **0.6**

16.4 **STOP 2D. Grand Canyon of the Yellowstone.** Parking area at end of road for Artist Point; park in the lot and walk down short trail (about 100 m) to the constructed overlook. The deeper part of the Grand Canyon is carved into the intensely altered Canyon flow. Upstream, the flow is relatively unaltered, and Lower Falls drops 94 m across a resistant ridge of steeply dipping flow layers. Downstream about 2 km the flow is again relatively unaltered. In the highly altered and colorful part of the canyon between, hydrothermal activity remains vigorous near river level although it is hard to see from the canyon rim unless the day is cold and humid. Alteration along the deep, narrow part of the Grand Canyon is controlled by the buried ring-fracture zone of Yellowstone caldera and by crossing fractures. Precanyon sedimentary rocks at the rim of the canyon on both sides are bleached white by surficial acid-sulfate alteration; rhyolite deeper in the canyon is

pervasively pyritized and oxidized to the yellowish colors that give this region its name. Across the canyon is an abandoned channel segment at about half the present depth of the canyon. That channel was filled by sediments behind an ice dam of Bull Lake age downstream and was probably kept free of ice, at least during stagnation of the ice sheet, by local thermal activity. On the skyline to the west, above Lower Falls, is the Solfatara Plateau flow at the north end of the Central Plateau.

Return to main road; turn right. **3.8**

20.2 Canyon Junction. Continue straight ahead toward Mt. Washburn and Tower Junction. Along road beyond the junction, most roadcuts expose glacial sediments (mainly till), only locally showing poor outcrops of underlying Canyon flow. **2.1**

22.3 Roadside turnout on right. The steep, open grass- and sage-covered slope on left is the wall of Yellowstone caldera, exposing rocks of Eocene Absaroka Volcanic Supergroup; the lower, forested area on right is the glaciated surface of Canyon flow within the caldera. From this point, the road climbs up onto caldera wall. **0.4**

22.7 Roadcut exposes Dunraven Road flow where it onlaps caldera wall. Although it is locally the youngest of the early caldera-filling rhyolite flows, it is indistinguishable in K–Ar age from either the caldera-forming Lava Creek Tuff or the earlier intracaldera Canyon flow. Both Canyon flow and Dunraven Road flow, unlike most rhyolites of the Yellowstone Plateau, are characterized by abundant phenocrysts of plagioclase but virtually lack sanidine. **0.8**

23.5 **STOP 2E. Overview of Yellowstone caldera from its north wall, the Washburn Range.** Park at Washburn Hot Springs overlook on right. In foreground is tree-covered surface of Canyon flow, abutting the caldera wall from within. The Grand Canyon of the Yellowstone cuts it in middle distance. Beyond is the low rise of Sour Creek dome, broken by a northwest-trending graben. To the east are the Mirror Plateau and Absaroka Mountains. Far to the southeast are the Red Mountains and, visible on a clear day, the Teton Range. The caldera rim can be followed from the Washburn Range, across the Grand Canyon, to the ridge with a prominent crescentic grassy area, and beyond to the ridge on far side of Broad Creek. The Canyon flow and Sour Creek dome block the view of the wall beyond, but it continues along far shore of Yellowstone Lake and in front of the Red Mountains. The southwest skyline is the Central Plateau, and farther to the west is Madison Plateau, 55 km away but still within western margin of the caldera.

Andesitic debris-flow breccia or conglomerate in the adjacent roadcut is cut by a 4 m thick silicic andesite dike of the Eocene Washburn volcanic center. Till-mantled outcrops of andesitic breccia and a few lava flows continue up the road toward Dunraven Pass. **1.5**

25.0 Dunraven Pass. The road here leaves Yellowstone caldera and traverses the north half of Washburn volcano, a major center of the Eocene Absaroka volcanic field; the south half is downdropped within the Yellowstone caldera. Along the road past here, note the coarse maximum sizes and angularity of blocks (a few of them prismatically jointed and probably hot when emplaced), very poor sorting, and weak stratification as well as the presence of a few lava flows. These features are indicative of proximity to the source of the breccias; in addition, there are numerous intrusive bodies between Washburn Hot Springs and the summit of Mount Washburn, although few of them are exposed along the road. **0.5**

25.5 Large unmarked turnout on left at a sharp right curve. Roadcut on right exposes andesite of the Washburn center, both as coarse volcanic breccias and as lavas. On the steep slopes of Mount Washburn ahead, northward primary dips of the volcanic breccias are evident. **2.4**

27.9 **STOP 2F. Andesites of the Washburn Range.** Park in pullout on left and walk down the slope and over to a prominent outcrop about 50 m from road. Both here and in the roadcut are exposures of andesitic debris-flow breccias of the Washburn volcanic center, still representing a relatively near-vent facies with northward primary dips. To the north and west along skyline is the rest of the Washburn Range, representing reworked volcanic rocks of Washburn and other contemporary volcanoes, distant from their sources. Between is the valley of Tower Creek. The densely forested, plateau-like surface above the inner gorges along the creek and its tributaries is underlain by Lava Creek Tuff, which entered the head of the valley from a low area on rim of Yellowstone caldera, out of sight to southwest. In distance to the north are the Beartooth Mountains, in which Archean rocks are exposed in the core of a Laramide uplift.

Return to the Park road and continue on northward. **2.0**

29.9 Chittenden Road (trailhead) to Mount Washburn on right. Note beyond here that, on average, block sizes in the andesitic breccias decrease and sorting and bedding improve with distance from the Mount Washburn volcanic center. **0.8**

30.7 Roadside turnout on right. View east to Specimen Ridge and Mirror Plateau (alluvial facies of Absaroka volcanic field) and northeast and north to Northern Absaroka and Beartooth Mountains. The tree-covered plateau above the canyons of Yellowstone River and its tributaries is underlain by Lava Creek Tuff that flowed outward from the caldera along the course of the river. The summit of Mount Washburn is visible 5 km to south. Most of the open grassy slopes near the road are underlain by Pinedale till, deposited both by the Yellowstone Plateau ice cap (with mainly Absaroka volcanic clasts) and, especially farther down the road, by large valley glacier of Lamar River from the east (with prominent Precambrian and Paleozoic clasts). **0.9**

31.6 Low morainal ridge crosses road, marking a stand of Lamar Valley glacier. Note that below here, Precambrian till boulders are relatively common. **3.8**

35.4 Good outcrop and roadcuts of Lava Creek Tuff on left. (There is a very small turnout on right at end of roadcuts.) The upper part of the cliff is devitrified densely welded tuff 8–10 m thick. Below is about

3 m of very hard and resistant gray spherulitic tuff, underlain by 5–6 m of densely welded vitrophyre and 1.5–2 m of nonwelded to partly welded glassy ash-flow tuff. Local lenses of sand and gravel plastered into fractures and ledges mark a previous course of Antelope Creek. At the base is about 1 m of bedded fallout ash. **0.6**

36.0 **STOP 2G. Tower Falls and The Narrows of the Grand Canyon of the Yellowstone.** Park in Tower Falls parking area on right and walk about 120 m down paved trail to fenced overlook of Tower Falls. (Dirt trail beyond goes about 500 m farther to base of falls.) Tower Falls drop over stratified Eocene andesitic breccias representing an alluvial facies distant from its source volcanoes. The "towers" are characteristic weathering features of the volcanic breccias, probably initially held up by large boulders. The Absaroka rocks are locally altered around small warm springs or steam vents. A complex erosional history is recorded along this stretch of the Yellowstone River. Before about 2.5 Ma, the drainage was along a broad open valley in which were ponded thick basaltic lavas and, subsequently, Huckleberry Ridge Tuff. The basalts, preserved locally, include the large overhanging cliff to the northwest above the canyon; within the valley of Yellowstone River, Huckleberry Ridge Tuff was largely stripped by erosion. That broad valley was subsequently incised by a narrower mountain valley that filled with gravels and interlayered basalt flows (basalt and gravel of The Narrows), now well exposed on opposite canyon wall; interlayered ash beds are dated at 1.2 Ma. These rocks have been pervasively altered by subsurface hot waters to give prominent yellowish color of the cliffs. The valley was later recut east of the present cliff of yellowish gravels and basalts and then filled again by Pinedale till; its edge can be discerned as a boulder line between the bare and vegetated slopes. Till covers the slope beyond. Thus, the deep canyon of The Narrows downstream from here has been cut entirely in post-Pinedale time—less than about 12,000 years.

Return to vehicles and continue along the main Park road. **0.4**

36.4 Overhanging Cliff on left is pre-Huckleberry Ridge basalt resting on gravels deposited in an old broad valley. Note prominent two-tiered columnar jointing. **0.2**

36.6 Roadside turnout on right above The Narrows, cut into Absaroka volcanic rocks and basalt and gravel of The Narrows. **0.2**

36.8 **STOP 2H. View of the lower Grand Canyon and Calcite Springs.** Park at Calcite Springs overlook on right and walk up stairs and along walkway. From this overlook the full depth of the young bedrock gorge in well-stratified Absaroka andesitic breccias can be seen. Downstream, these rocks are altered around Calcite Springs, but the typical erosional pinnacles are seen prominently from lower part of trail. Across the gorge, gravel and basaltic lavas of The Narrows are seen to fill the old valley against a west wall near the present gorge. In distance to north is the Beartooth block with its core of Precambrian granitic gneiss.

Return to vehicles and continue along main Park road. **1.0**

37.8 Old travertine deposits buried by Pinedale till exposed in roadcuts on right. **0.6**

38.4 Tower Junction; Roosevelt Lodge to left. The open glaciated valley is largely mantled by Pinedale till and marked by scattered but prominent boulders of Precambrian granitic gneiss from the Beartooth block. Subdued hills expose basaltic lavas of both pre-Huckleberry Ridge and post-Huckleberry Ridge but pre-Lava Creek ages. Forested uplands to left are underlain by alluvial facies of Absaroka Volcanic Supergroup. **1.4**

39.8 Road to Petrified Tree on left. The main road continues through alluvial-facies Absaroka volcanic rocks. **1.1**

40.9 Roadside turnout on right. Precambrian granitic gneiss crops out on Garnet Hill to north. Just beyond here is Floating Island Lake on left. Frost-riven outcrops of a partially welded ash-flow tuff in the Eocene Absaroka Volcanic Supergroup are prominent across lake. **1.2**

42.1 Dirt road to trailhead for Black Canyon of Yellowstone on right. Just past, low outcrops and roadcuts on both sides of road expose a shoshonitic lava flow beneath the Eocene welded tuff. Cliffs ahead, above road on left, are alluvial-facies Absaroka volcanics with abundant fossil leaves and other plant materials. Also in view from open area ahead are outcrops of pre-Huckleberry Ridge basalt across Yellowstone River to north. **1.9**

44.0 The road passes through good outcrops of alluvial-facies Absaroka volcanics on both sides, then enters an ice-marginal channel cut during retreat of the Pinedale glacier; the road follows the channel for several hundred meters before crossing it. **1.2**

45.2 Poor outcrops of a basaltic lava flow in Eocene Absaroka Volcanic Supergroup at head of another ice-marginal channel. Roadcuts beyond are cut mainly in alluvial-facies Absaroka volcanic rocks. **1.5**

46.7 Past Phantom Lake, in roadcuts on left, Huckleberry Ridge Tuff overlies Absaroka volcanic rocks unconformably on a baked contact. Beyond, near junction with Blacktail Plateau Road on left, are outcrops of post-Lava Creek basalt on both sides of road. **0.9**

47.6 Low spot on road (turnout on left) where it crosses trace of Gardiner fault, a Laramide reverse fault. On ridge ahead, exposed mainly on right, Mississippian (Lower Carboniferous) Madison Limestone is a sliver within the fault zone, mantled by Pinedale till. **0.7**

48.3 Summit along roadway, turnout on right, and junction with small service road on left. View of Blacktail Deer Plateau to west, with Washburn Range in distance to south (left). The plateau was extensively glaciated and is underlain by Huckleberry Ridge Tuff on eroded Absaroka volcanic rocks with a few outliers of Lava Creek Tuff. Some post-Lava Creek basalt flows are also present. Bedrock exposures occur only in small tree-lined gullies on grass- and

sage-covered, till-mantled plateau. **2.1**

50.4 Blacktail Lakes on right, at foot of Mt. Everts. This part of Mt. Everts is underlain by Upper Cretaceous marine shale and sandstone. **1.3**

51.7 Roadside turnout for Wraith Falls trail on left. Mt. Everts, to right, is the edge of an old valley that contained the spread of Lava Creek Tuff from south. A columnar-jointed basal zone of the Lava Creek is exposed in old drainage on the right. On the ridge of Wraith Falls, just to left, and on timbered ridge to west, thick sections of Lava Creek Tuff fill the old valley, overlying older basalts. The old drainage of Blacktail Deer Creek at this locality has since been captured by Lava Creek, flowing at the foot of the timbered ridge to the west. Now this valley is virtually undrained between here and Blacktail Lakes. The canyon incised by the captured drainage has guided the younger post-Lava Creek basalt flows down modern Lava Creek. **0.9**

52.6 Parking area for Undine Falls overlook on right. At Undine Falls, the drainage of Lava Creek is held up by a stack of pre-Lava Creek Tuff basalt flows, the Undine Falls Basalt, well exposed in cliffs across the creek from here. A rubbly exposure of Lava Creek Tuff overlies these basalts on the shoulder of Mt. Everts. Before Undine Falls Basalt and Lava Creek Tuff filled the valley south of Mt. Everts, the Huckleberry Ridge Tuff had spread across an older, broad valley to Mt. Everts and remains preserved as the rimrock on the south face of Mt. Everts above the Upper Cretaceous marine section.

In roadcuts just past here are exposures of post-Lava Creek basalts that partly filled the reincised valley of Lava Creek. These basalts lie on a surface cut down through Lava Creek Tuff into older Undine Falls Basalt. **0.5**

53.1 **STOP 2I. Huckleberry Ridge and Lava Creek Tuffs on Mt. Everts.** Park at roadside turnout on right just past stone wall. The roadcut and the cliff above it expose three flows of post-Lava Creek Tuff basalt emplaced into valley of Lava Creek before it was incised to its present depth. At top of cliff, the basalt laps against a rubbly outcrop of densely welded Lava Creek Tuff. Across canyon of Lava Creek to north, Mt. Everts is underlain mainly by Upper Cretaceous shale and sandstone but is capped by a prominent cliff of Huckleberry Ridge Tuff. The exposure of Huckleberry Ridge on the point at far left of cliff (seen readily from here with binoculars) exposes a basal vitrophyre of the ash-flow tuff, resting on bedded white fallout ash, which in turn overlies reddened gravels. The gravels contain mainly Absaroka volcanic lithologies and virtually lack Precambrian and Paleozoic rocks, indicating a source in Washburn Range to south. What appears to be a sag in the rimrock cliff is a paleovalley that had been cut through Huckleberry Ridge Tuff by a tributary of Lava Creek that drained southward from Mt. Everts and was later filled by Lava Creek Tuff, which sagged by differential compaction within the paleochannel. The Lava Creek Tuff also onlaps the east end of the cliff of Huckleberry Ridge Tuff just across canyon from here. About 15 km west down the road is Sepulcher Mountain, underlain by Absaroka volcanic rocks. The large travertine terraces of Mammoth Hot Springs can also be glimpsed from here.

Along road below, roadcuts and cliffs on left expose Lava Creek Tuff overlying Undine Falls Basalt. **1.7**

54.8 Cross Gardner River on high bridge. The river here is cut into sedimentary rocks of both Early and Late Cretaceous ages. The active Mammoth Hot Springs terraces are only part of the total travertine deposit related to Mammoth Hot Springs and its predecessors; such deposits extend from the rimrock on Terrace Mountain on skyline to below village of Mammoth Hot Springs ahead on right. The surrounding slopes are mainly covered by Pinedale till and landslides. **1.5**

56.3 Enter Mammoth Hot Springs; follow main road (with centerline). **0.3**

56.6 Main intersection in Mammoth Hot Springs; turn left. Drive across old travertine terrace with steaming sinkholes on left. **0.3**

56.9 Parking area on right. Liberty Cap is the prominent travertine cone near road on right; Opal Terrace is a prominent small travertine terrace on left. Ahead on right are Jupiter Terrace, Minerva Terrace, and the Main Terrace. The road ahead is on glacial and landslide deposits containing Pleistocene travertine boulders and older rocks. **1.5**

58.4 **STOP 2J. Overview of Mammoth Hot Springs region.** Park in large turnout on right. In foreground to north is the active part of the Main Terrace of Mammoth Hot Springs. Beyond to northwest is Sepulcher Mountain, underlain by Eocene rocks of Absaroka Volcanic Supergroup. In distance to north, beyond valley of Yellowstone River, is the Northern Absaroka Mountains (or Snowy Range), with Eocene volcanics overlying Precambrian and Paleozoic rocks of the Beartooth block. Across valley of Gardner River to east, Mt. Everts exposes Lower and Upper Cretaceous marine shales and sandstones locally intruded by Eocene andesitic sills and rimmed on south side by a cliff of Huckleberry Ridge Tuff that fills an old broad valley. With binoculars, note white band of fallout ash at base of this cliff at its left end. To right of present valley of Lava Creek, which is tributary to Gardner River, are cliffs of Lava Creek Tuff, making a plateau surface at a lower elevation than the eroded surface of Huckleberry Ridge Tuff on Mt. Everts. The Lava Creek Tuff filled a mountain valley that was cut through Huckleberry Ridge Tuff and was then capped by post-Lava Creek basalt. Also note cliffs of Undine Falls Basalt beneath Lava Creek Tuff in valley of Lava Creek. On skyline beyond is western part of Washburn Range, underlain by alluvial facies of Absaroka volcanic rocks. Farther right and prominent to south, Bunsen Peak is an Eocene dacitic stock that intrudes Lower Cretaceous sedimentary rocks. The roadcut immediately across from here exposes Jurassic shale and limestone, also present in subsurface beneath adjacent terraces of Mammoth Hot Springs.

Continue ahead on the Park road. **0.2**

58.6 Parking area and entrance to Mammoth Terrace Drive (one-way loop road) on right. Roadcuts on left are Jurassic sedimentary rocks. The main road beyond continues through till, landscape deposits, and some older travertine. **1.3**

59.9 Here the road crosses from the glaciated surface onto a postglacial landslide, with usually a break in the road surface. The slide crudely preserves the stratigraphy of the steep slopes above; the road traverses first through Cretaceous sedimentary rocks, then through blocks of Huckleberry Ridge Tuff, and finally through blocks from the Pleistocene travertine that caps Terrace Mountain to west. **0.4**

60.3 Silver Gate. A small loop road branches to right. The landslide here, called The Hoodoos, consists almost entirely of blocks of travertine from Terrace Mountain, seen ahead and to right. **0.8**

61.1 Golden Gate; parking area on left. Glen Creek cuts a small gorge through cliffs of Huckleberry Ridge Tuff between Terrace Mountain on north and the Eocene dacitic stock of Bunsen Peak on south, forming Rustic Falls, a small but lovely waterfall at head of gorge. The cliffs on both sides provide excellent exposures, though slightly altered, of the two most voluminous members of Huckleberry Ridge Tuff, members A and B, the contact between them lying at a partial welding break immediately opposite parking area. (**Caution:** traffic is often heavy here, visibility is restricted, and rocks fall frequently from unstable cliffs above road.) The gently west-dipping ash-flow tuff is phenocryst-poor near the contact, and multiple flow units in lower part of member B are marked by thin crystal-rich layers. Prominent cavities in the outcrops are weathered lithophysae. Upsection, toward Rustic Falls, truncated degassing pipes mark the top of a lithic-rich flow unit. At top of roadcut section is a zone of vapor-phase crystallization.

Looking downstream, past yellowish dacite porphyry cliffs of Bunsen Peak, the Huckleberry Ridge Tuff on Mt. Everts is seen to preserve the same stratigraphic units as here but at a lower elevation. Thus, a fault in the Mammoth area probably separates these blocks. **0.3**

61.4 Parking area on left for Bunsen Peak Road (dirt). The main road here enters Swan Lake Flat, an open glaciated valley. **0.9**

62.3 **STOP 2K. Overview of Swan Lake Flat and the Gallatin Range.** Park in large parking area on right at Swan Lake (a sign denotes "Geologic Exhibit"). This terrain is the product of extensional normal faulting of basin–range style. The Gallatin Range is an uplift block between normal-fault zones; like the Teton Range, it exposes a section from Precambrian through lower Tertiary on the flank of a northwest-trending Laramide anticlinal uplift bounded by thrust faults. On the south (left), the peaks from Mt. Holmes to Antler Peak are mainly Precambrian metamorphic and lower Paleozoic sedimentary rocks intruded by thick Eocene andesitic sills and laccoliths. Quadrant Mountain, due west, exposes Pennsylvanian (Upper Carboniferous) quartzitic sandstone. Electric Peak, at north end of range, exposes Upper Cretaceous marine sedimentary rocks intruded by a complex of Eocene sills. Sepulcher Mountain, at north end of Swan Lake Flat, is underlain by Eocene Absaroka volcanic rocks, and on Terrace Mountain to its right, Huckleberry Ridge Tuff is capped by Pleistocene travertine. Bunsen Peak to northeast is an Eocene stock that rises island-like through surfaces of gently west-dipping Huckleberry Ridge Tuff and Lava Creek Tuff that, along with younger basalt, form the densely forested, gently north-sloping plateau to the south and lie beneath valley fill of Swan Lake Flat.

Tectonically, the Gallatin Range is a slightly asymmetrical horst with a westward tilt and a master fault along its east side, facing Gardners Hole, which is out of sight behind the ridge west of here. That ridge exposes poorly both Eocene volcanic rocks and Huckleberry Ridge Tuff, forming a small west-dipping fault block between Gardners Hole and Swan Lake Flat. Huckleberry Ridge Tuff also dips west beneath Terrace Mountain and around Bunsen Peak, thus completing a set of three west-tilted normal-fault blocks, each of lesser displacement eastward.

This entire landscape was buried and sculpted by the Pinedale ice cap, fed both from the Yellowstone Plateau to the south and from glaciers that emerged from the Gallatin Range on the west. As a consequence, much of the valley and the low ridges within it are subdued and deeply mantled by till.

Continue southward along the Park highway. **2.3**

64.6 Turn left on short road along Gardner River to Sheepeater Cliffs Picnic Area. **0.2**

64.8 **STOP 2L. Mixed rhyolite and basalt lavas of Gardner River.** Park at Sheepeater Cliffs Picnic Area. (Primitive toilet available.) On the north side of picnic area and downstream along river are bluffs of columnar basalt of post-Lava Creek Tuff age. What at first appears to be talus at base of the bluff here is actually a pile of toppled columns, still nearly intact. Downstream and stratigraphically between the basalt and underlying Lava Creek Tuff is the mixed-lava complex.

Walk downstream along an unmaintained fishermen's trail about 250 m (6–8 minutes). After skirting talus at base of another basaltic cliff, the trail crosses a low bluff of weathered spherulitic and lithophysal rhyolite at west margin of the complex, which forms a series of cataracts along river. The mixed lavas are exposed in cliffy streambanks and as small outcrops and rubble along the trail just past this bluff. Both predominantly rhyolitic and predominantly basaltic lithologies are characterized by abundant inclusions of other compositions and by a range of phenocrysts and xenocrysts appropriate for both basaltic and rhyolitic compositions. Very irregular jointing probably relates to uneven cooling of the mixed lavas.

Return to vehicles, rejoin main road, and turn left. **0.5**

65.3 Cross Gardner River at junction with Obsidian Creek from south. From here, the road is along valley of Obsidian Creek, mainly following normal faults of small displacement in a forested plateau of Lava Creek Tuff. **1.7**

67.0 Parking area on right for Willow Park, an open meadow and willow bog in valley of Obsidian Creek. Along road beyond here are sparse, poor exposures of Lava Creek Tuff in low roadcuts, but most of the surface is mantled by Pinedale till. **2.6**

69.6 **STOP 2M. Obsidian Cliff.** Park at turnout on right for Obsidian Cliff exhibit. Rubbly talus on right along road approaching and along parking area is from Lava Creek Tuff on steep slopes above. Across road is Obsidian Cliff, the west margin of a 180 ka rhyolitic lava flow, the vent for which is about 1 km east. It is one of a series of both rhyolitic and basaltic vents along a corridor between Mammoth Hot Springs and Norris Geyser Basin. At this point, the flow filled a preexisting valley and chilled against the old valley wall, which has since been exhumed by Obsidian Creek. Note pronounced columnar jointing at the snout of the flow and prominent flow layering exposed by the cliff. The layering is generally subhorizontal near the base but becomes locally steep and contorted upward near top of flow.

Walk across road, to base of Obsidian Cliff on other side of Obsidian Creek. The talus exposes large blocks of spherulitic and lithophysal obsidian, with excellent examples of small-scale fluidal structures and of the types of crystallization typical of glassy rhyolite flows. Note that the flow totally lacks phenocrysts; the rhyolitic magma probably was maintained above its liquidus temperature by closely associated basaltic magma. The best obsidian, used widely for arrowheads and other artifacts by the stone-age residents of North America, is not found at this roadside locality but elsewhere along margins of this flow. **Note:** Do not collect from this locality, or others in the National Park, without prior permission from National Park Service.

Continue southward, following the Park road along valley of Obsidian Creek, where Lava Creek Tuff is largely mantled by Pinedale till. A variety of hydrothermal features, mainly small, is to be seen along the way. **3.5**

73.1 Roadside turnouts on both sides for Roaring Mountain on left. This highly acid-altered active fumarolic area steams profusely, as seen in cool or humid weather, but no longer has a loud, high-pressure discharge as it did in the late 19th century when it was named. The altered rock is Lava Creek Tuff; the contact between its two members is exposed along the line of bouldery outcrops midway up the bluff. **2.4**

75.5 Roadside turnout on right; Frying Pan Springs on both sides of road. From here south toward Norris Junction, hydrothermal alteration becomes more intense and pervasive. White outcrops along road are not sinter deposits but mainly Lava Creek Tuff bleached by acid-sulfate alteration. **1.0**

76.5 Large parking area off road to right, somewhat inconspicuous upon approach. View south to Norris Geyser Basin and to post-Lava Creek rhyolitic flows and domes along irregular skyline. The major flow south of the geyser basin is Gibbon River flow. Gibbon Hill is the prominent dome directly south; farther west (right) is a smaller dome, Paintpot Hill. The ridge beyond it to right is a normal-fault block underlain by Lava Creek Tuff. **1.6**

78.1 Norris Junction. Four-way stop sign; turn left toward Canyon Village. **1.6**

79.7 Turn right onto Virginia Cascade one-way loop road. The road ascends a dip-slope of Lava Creek Tuff, largely mantled by Pinedale till. **1.0**

80.7 **STOP 2N. Exposure of Lava Creek Tuff.** Park in pullout on left side of one-way road. Ahead is Virginia Cascade, descending across densely welded tuff of lower member (member A) of Lava Creek Tuff, which forms the cliffs of canyon wall below road. Walk back westward along road about 100 m to good outcrops of Lava Creek Tuff at a slight bend in road. Note that the outcrops of member A below road are phenocryst-rich and have several distinctive zones of lithophysae and closely spaced joints. The contact between members A and B is covered in slumped debris at base of roadcut, but the basal lithology of member B is poor in phenocrysts. Above, a second flow unit is more phenocryst-rich and has abundant lithic inclusions at its base. At the top of the exposure, phenocrysts are abundant.

Across the canyon, the densely forested slope is formed by Lava Creek Tuff, but on higher skyline farther west the Gibbon River flow spans the rim of Yellowstone caldera south of Norris Geyser Basin. In far distance to west is another west-tilted fault block of Lava Creek Tuff.

Beyond here the road continues along steep valley wall in member A of Lava Creek Tuff, past Virginia Cascade, and then opens into Virginia Meadows. **1.0**

81.7 End of one-way loop road; turn left onto main Park road. **0.5**

82.2 Roadway summit with distant view west to south end of Gallatin Range. Beyond here, the road descends a dip-slope of Lava Creek Tuff along the Virginia Cascades fault block, then crosses Gibbon River. **3.0**

85.2 Norris Junction. Continue straight ahead. **0.5**

85.7 **STOP 2O. Norris Geyser Basin.** Park in the parking area for Norris Geyser Basin. Norris Basin has the hottest shallow reservoir of any thermal area in Yellowstone National Park. It is characterized by mixed waters, including a dominant component of neutral or slightly alkaline chloride-rich water that deposits siliceous sinter profusely, but also by a component of acid-sulfate water that produces intense surficial alteration of the Lava Creek Tuff that encloses most of the basin. Porcelain Basin, the northern part of Norris, is characterized by numerous geysers, at least some of which are almost always in eruption; it can be viewed easily from the platform on north side of Norris Museum, about 150 m from the parking lot. The southern part of Norris, the "Back Basin," hosts several large, active features, including Steamboat Geyser with irregular and infrequent but powerful eruptions that reach more than 100 m. Echinus Geyser in the Back Basin has quite predictable eruptions; its slightly acidic waters produce a spiney texture around its pool and sometimes eject centimeter-sized fragments of pyrite and marcasite.

Return to Norris Junction and turn right. Beyond,

the road passes through low roadcuts of gently west-dipping Lava Creek Tuff south of Norris Geyser Basin. **2.0**

87.7 Elk Park, a broad, open meadow along Gibbon River. The meadow is underlain by lacustrine deposits on a downdropped fault block below tree-covered area to west. To right is Mt. Holmes at south end of Gallatin Range; to left along skyline are Gibbon Hill and the Gibbon River flow. **1.1**

88.8 Roadside turnout on right alongside Gibbon River Rapids. The good exposure in roadcut to left is west-dipping Lava Creek Tuff of member A; member B is poorly exposed in tree-covered area above road. This fault block is upthrown relative to Elk Park and dips west toward Gibbon Meadows; the rapids reflect downcutting of the river into the fault block. **0.9**

89.7 Roadside turnout on right. Gibbon Meadows, like Elk Park, is a sediment-filled, downdropped, west-tilted fault block; it faces the faultline scarp on tree-covered slopes to west and northwest; the Sylvan Springs thermal area across the meadows from here issues near the base of that scarp. From here, the dip-slope of the Gibbon River Rapids block can be seen to northeast and the summit of Mt. Holmes beyond. To south, Gibbon Hill (left) and Paint Pot Hill (right) are rhyolitic domes near south end of the Norris–Mammoth corridor, and the Gibbon River flow forms skyline. Active thermal areas at south end of Gibbon Meadows include the Geyser Springs Group, Gibbon Hill Geyser, and Artist Paint Pots. **0.7**

90.4 Roadside turnout on right at head of Gibbon River Canyon, confined by an uplifted fault block of Lava Creek Tuff on the west and by Gibbon River flow, emplaced onto downdropped block to east. The fault and related fractures along this canyon control numerous hydrothermal features. The fault is radial to Yellowstone caldera, the rim of which is about 3 km south. **2.4**

92.8 Sharp turn to right. Here Gibbon River leaves the trace of the north–south fault and turns westward along outer scarp of Yellowstone caldera. In this area, a slumped block of the caldera rim lies between outer scarp and inner wall of the caldera, and the river follows the base of the outer scarp. **0.2**

93.0 Cross Gibbon River. Beyond, the road passes below cliffs of member A of the Lava Creek Tuff on outer caldera scarp and through roadcuts and stream cuts in the slumped caldera block. Along this fault the densely welded pumice has been stretched into a marked down-dip lineation, and the welded tuff is pocked by numerous small pull-apart fractures lined with vapor-phase minerals, mainly sanidine, trydimite, and cristobalite. The Lava Creek Tuff matrix is notably oxidized and reddened. These features indicate that the fault formed while the still-hot tuff was welding and crystallizing. **1.1**

94.1 Broad curve to left. From here, the river turns southward, away from outer caldera scarp and across slumped block of caldera rim. Farther west the slumped block continues as Secret Valley, not visible from here. **0.5**

94.6 **STOP 2P. View of Gibbon Falls.** Pull left into parking area for Gibbon Falls and park. Just south of here, Gibbon River crosses from the slumped caldera block into main caldera basin. The falls represent headward retreat along Gibbon River from inner caldera scarp and are held up by vertically jointed, devitrified, and densely welded Lava Creek Tuff. Ahead, the forested surface of Nez Perce Creek flow, a large intracaldera rhyolitic lava flow of about 150 ka, forms skyline. Back to north, the outer caldera rim is visible.

Continue southward along the Park highway. **0.4**

95.0 Just past broad turn to west is a large turnout on left for Gibbon Falls Picnic Area. The road now is within inner caldera scarp along front of Secret Valley slumped block. Roadcuts beyond here are in member A of Lava Creek Tuff, and the broad forested plateau across Gibbon River to south is the Nez Perce Creek flow. Ahead down the road and through the trees are glimpses of the caldera wall farther west. **2.8**

97.8 **STOP 2Q. Outcrops of Lava Creek Tuff, member A.** Park on right at Tuff Cliffs Picnic Area. Primitive toilet facilities available. The cliff behind picnic area, about 150 m through the trees, is a recently formed exposure that resulted from partial failure of the steep slope during Hebgen Lake earthquake of 1959. The fresh exposures show relatively phenocryst-poor but pumice-rich lower part of member A in a series of thin flow units, many of them marked by conspicuous double grading (normal grading of lithic inclusions, reverse grading of pumice) and sorted partings between some of the units. Large talus blocks at base of cliff show phenocryst-rich upper part of member A from top of cliff. In these boulders, note conspicuous concentration of phenocrysts in the groundmass relative to those in the welded pumices, indicating elutriation of fine-ash matrix from the near-vent area.

The road beyond this stop continues at base of caldera scarp. Just west, the Secret Valley slumped-rim block ends and joins main outer caldera wall. **1.0**

98.9 Terrace Spring on right. Terrace Spring is one of relatively few travertine-depositing springs within Yellowstone caldera. The cliffs ahead and to right are Lava Creek Tuff on the caldera wall at Purple Mountain. Across river to south is gently west-sloping surface of the 150 ka Nez Perce Creek flow, whose source was on the Central Plateau to east; to southwest are cliffs at margin of younger West Yellowstone flow (about 110 ka) from a source to southwest on Madison Plateau. **0.6**

99.4 Madison Junction; continue straight ahead toward Old Faithful. Past parking area for Madison Museum, the road crosses Gibbon River; National Park Mountain on right is a flow margin of West Yellowstone flow. **0.6**

100.0 Turn right onto one-way Firehole Canyon Drive. Ahead, this road follows the Firehole River upstream through a canyon cut along eastern margin of West Yellowstone flow. The road is near the surface of Nez Perce Creek flow, glaciated before emplacement of West Yellowstone flow upon it. The

West Yellowstone flow was emplaced while a stagnating or retreating glacier remained in the area east of it, and features of its flow margin, including peculiar large reentrants and a perlitic carapace, reflect its emplacement against the ice. **0.4**

100.4 Roadside turnout on left. Across Firehole River is the front of West Yellowstone flow, here a scarp 250 m high. Flow layering is conspicuous, generally subhorizontal near the base but steeply inward-dipping higher on flow margins. It is marked by bands of spherulites and lithophysal crystallization. Beyond here, roadcuts on left are in Nez Perce Creek flow. **0.4**

100.8 **STOP 2R. Outcrop of flow breccia of Nez Perce Creek flow.** Park in roadside turnout on left, just past a large roadcut. This excellent exposure of the top of the Nez Perce Creek flow illustrates some aspects of the origin of rhyolitic flow breccias. Typical flow breccia is exposed in the natural outcrop behind vehicles. In the roadcut, however, the breccia is characterized by rounded blocks, many of them perlitized by hydration at high temperature, perhaps indicating that water was backed up locally by the flow during emplacement and that the breccia was partly reworked. The flow breccia is interleaved with steep individual flow layers of fluidal-textured rhyolite, locally themselves brecciated and rewelded. Thus, the breccia formed by breakup and talus-like collapse of the cooler carapace of the flow as the hotter interior continued to flow and to intrude its brecciated cap, brecciating and rewelding in turn within an intermediate zone between zones of brittle fracture and plastic flow.

Continue on the one-way Firehole Canyon Drive. **0.2**

101.0 Parking area on left for Firehole Falls. The falls are held up by a ledge of vertically flow-layered Nez Perce Creek flow. Roadcuts just beyond are excellent exposures of steeply inclined flow layers in the upper part of the flow, locally brecciated between and along flow layers. **1.2**

102.2 Firehole Cascades, at head of Firehole Canyon, on right. At stop sign, turn right onto main Park road. Ahead, roadcuts and riverbanks provide excellent exposures of Nez Perce Creek flow; higher on bluffs west of the river is the margin of West Yellowstone flow. **2.0**

104.2 Roadside turnout on right. Here the valley of the Firehole River has opened out above the two flows that bound the canyon below. Southward, the valley opens further into a basin floored by sediments that accumulated behind the constriction. **1.3**

105.5 Turn right on Fountain Flats Drive. Fountain Flats is the north end of Lower Geyser Basin. **0.1**

105.6 Cross Nez Perce Creek; Nez Perce Creek Picnic Area on right. The road crosses an old sinter plain indicating a former extent of hydrothermal activity in Lower Geyser Basin. Along the crest of Madison Plateau ahead and to right is the West Yellowstone flow. The conspicuous hill that rises above the skyline of the plateau is Twin Buttes, a hydrothermally localized and cemented englacial kame deposit that encloses a cluster of hydrothermal-explosion craters. The skyline to far left (east) is Elephant Back flow and its Firehole Lake lobe, from the Central Plateau. **0.6**

106.2 Roadside turnout on right. Low, irregular, tree-covered hills on left are ejecta from Pocket Basin, a Pinedale hydrothermal-explosion crater; ahead the road crosses onto the ejecta blanket. **0.5**

106.7 **STOP 2S. Pocket Basin hydrothermal-explosion crater.** Pull into parking area on right just before bridge over Firehole River. Ojo Caliente Spring, a superheated sinter-depositing spring that has rare geyser eruptions, is just south of parking area. From here, walk across the road on a trail above north bank of Firehole River through ejecta blanket from Pocket Basin. Note that blocks in the ejecta consist entirely of cemented sedimentary rocks from shallow levels beneath valley floor; no component from deeper bedrock levels is present. A variety of hot springs, mudpots, and fumaroles is scattered around the crater, which is breached by the river. If time permits, walk across the crater to far rim, about 50 m north of river, to some fine mud volcanoes.

Return to vehicles and back along the same road toward Nez Perce Creek. **1.1**

107.8 Turn right at junction with main Park road. **0.9**

108.7 **STOP 2T. View of Lower Geyser Basin.** Park at roadside turnout on right in the open valley of Lower Geyser Basin. Lower Geyser Basin is a wide valley enclosed by Madison Plateau on west (right) and Central Plateau on east (left) and southeast. Small hills to left are Porcupine Hills, a group of hydrothermally cemented englacial kame deposits, formed by hydrothermal melting of stagnant ice, that still have weak fumarolic and hot-spring activity. The similar but larger Twin Buttes rise to skyline about 6 km southwest. In front of Twin Buttes is a low, tree-covered ejecta blanket of Pocket Basin hydrothermal-explosion crater. At south end of open valley is the Fountain Group of geysers and hot springs, including some perpetually spouting vents.

Continue southward on the Park road. **1.5**

110.2 **STOP 2U. Hydrothermal features of the Fountain Group.** Turn in right to parking area for Fountain Paint Pot Trail and park. Follow boardwalk trail counterclockwise from north end of parking lot. A greater variety of hydrothermal discharge features can be seen conveniently from this area than perhaps any other in Yellowstone. The Fountain Group of geysers and perpetual spouters on the apron to north was seen from the road approaching the area. In addition, there are large nonerupting pools (including Silex Spring), fumaroles, and mudpots, the largest of which is Fountain Paint Pot. These features vary in character seasonally and become transitional in types, clearly relating to varying amounts of available water in the higher part of the area on a small hill of glacial deposits.

From summit of hill within boardwalk area, the view north across the geysers shows the West Yellowstone flow to northwest overlying Nez Perce Creek flow at Firehole Canyon to north. Visible beyond are the rim of Yellowstone caldera and Mt. Holmes at south end of Gallatin Range. To northeast are hydrothermal kames of Porcupine Hills. To south, the gentle northwest flank of the uplifted Mallard

Lake dome in the center of western segment of Yellowstone caldera, broken by normal faults, closes the basin and is onlapped from east by Elephant Back flow of about 150 ka from Central Plateau.

Return to vehicles and continue south on main Park road. **2.1**

112.3 Parking area for Midway Geyser Basin on right. Here are Grand Prismatic Spring, the largest in Yellowstone National Park, and Excelsior Geyser Crater, which discharges a large flow of hot water into Firehole River. On left, just beyond parking area, is an outcrop of Biscuit Basin flow, erupted into a caldera lake soon after formation of Yellowstone caldera. The flow consists of perlitic vitrophyre with well-developed flow foliation. Unlike those of most Yellowstone rhyolites, the feldspar phenocrysts are mainly plagioclase. **1.6**

113.9 Here the valley of Firehole River narrows again between flows from Madison Plateau to west (right) and the flank of Mallard Lake dome on the east (left), which rose within the caldera during a late magmatic insurgence at about 150 ka that began the voluminous latest episode of filling of the caldera by large rhyolitic lava flows. **4.0**

117.9 Traffic interchange; merge to right and cross over main Park road toward Old Faithful. **0.7**

118.6 Turn left on road to Old Faithful Inn. **0.4**

119.0 Parking area for accommodations and meals at Old Faithful Inn. Upper Geyser Basin is enclosed by flows from Madison Plateau on the west and by Mallard Lake dome on the east. From open area near Old Faithful, one of the grabens that breaks across the uplifted Mallard Lake dome is visible on skyline to east.

Upper Geyser Basin has the largest concentration of geysers on Earth; more geysers occur in this one area than are known altogether in the rest of the world. Many of the geysers are large and periodic, like Old Faithful and Grand Geyser; others are smaller or more irregular in their eruptive behavior. Many are distinguished by exquisitely detailed depositional features of their siliceous sinters. An evening walk through the basin on several well-maintained trails is generally a highly rewarding experience.

Day 3

This day of the trip will be led by Robert Christiansen. We will examine mainly older parts of the Yellowstone Plateau volcanic field, concentrating on the 2 Ma Huckleberry Ridge and 1.3 Ma Mesa Falls Tuffs, caldera structure related to their origins, and basalts peripheral to the active rhyolitic focus of the volcanic field. The route of travel out through the western part of Yellowstone caldera into the structural basin of West Yellowstone, over the southern par of the Madison Range, through Island Park—the source are of both Mesa Falls Tuff and part of Huckleberry Ridge Tuff—and onto the eastern Snake River Plain.

Mileage

0.0 Leave Old Faithful Inn and head back toward main Park road. **0.4**

0.4 Stop sign; turn right onto divided road. **0.7**

1.1 Merge right onto main Park road at interchange, heading toward Madison Junction. **15.8**

16.9 Turn left at Madison Junction. **0.1**

17.0 Road to Madison Campground on left. The road to west follows the canyon of Madison River. Cliffs to right are the wall of Yellowstone caldera, exposing pre-Lava Creek lavas of Mount Jackson Rhyolite capped by Lava Creek Tuff. **1.0**

18.0 Roadside turnout on left alongside Madison River. Cliffs across river to left are the steep margin of West Yellowstone flow within the caldera. **2.2**

20.2 **STOP 3A. View of breached caldera wall.** Park at roadside turnout on left. Across Madison River the margin of the postcaldera West Yellowstone flow rises 300 m above valley floor and is banked against caldera wall to west. More colorful cliffs ahead on left, at about 10:00, expose a lava flow of the precaldera Mount Jackson Rhyolite that forms caldera wall, breached by Madison River near this place. To right of road, high cliffs expose thick flows of Mount Jackson Rhyolite.

Return to Park road and continue down canyon of Madison River. **0.7**

20.9 Cliffs directly ahead from this straight stretch of road expose Lava Creek Tuff overlying Mount Jackson Rhyolite, which is also exposed to right. **2.8**

23.7 Lava Creek Tuff crops out on tree-covered ridge across river to right. Downstream, across the river, the lower grass- and sage-covered ridge is the right-lateral moraine of the Pinedale glacier that emerged from the canyon. **1.6**

25.3 Just past a large turnout on right, road passes through terminal moraine of the Pinedale glacier. Beyond here the road traverses a surface of outwash and glacial-flood deposits dominated by sand-sized obsidian fragments from caldera-filling rhyolite flows. **1.3**

26.6 Roadside turnout on right. Roadcut on left is a bedrock ridge surrounded by obsidian-sand plain consisting mainly of Lava Creek Tuff but cut at west end by a basaltic dike and partly overlain by a flow fed from the dike. Along the road ahead, the Madison Range may occasionally be glimpsed in distance. **1.5**

28.1 Outcrop of basalt on left rises above obsidian-sand plain. **2.4**

30.5 Leave Yellowstone National Park through West Entrance gate. **0.3**

30.8 Enter town of West Yellowstone, Montana. **0.1**

30.9 Turn right at intersection, following U.S. Highways 191, 287, and 20. **0.2**

31.1 Turn left at intersection onto US-20 where it turns off from on US-191 and 287 (which continue straight ahead). **0.7**

31.8 **STOP 3B. View of Madison Valley near West Yellowstone.** Road leaves West Yellowstone on US-20; park on street to left. Ahead the highway crosses Pinedale outwash fan and obsidian-sand plain, an aggradational surface that slopes very gently westward nearly to foot of Madison Range. To south, the margin of West Yellowstone flow forms Madison Plateau on skyline. To southwest are Henrys Lake Mountains, a southern extension of Madison Range separated from main part of the range by eastern part of the east–west Centennial fault through Targhee Pass, seen nearly due west. The Huckleberry

Ridge Tuff dips southeast and south off Henrys Lake Mountains, disappearing beneath West Yellowstone flow at Reas Pass to south.

Continue west on US-20 across obsidian-sand plain, crossing South Fork of Madison River. **6.5**

38.3 **STOP 3C. View of Yellowstone Plateau and Madison Range.** Denny Creek Road (dirt) on right; pull into turnout on left, just before junction. The subdued ridge on right is a moraine of Bull Lake age from the ice sheet that, before emplacement of West Yellowstone flow, extended eastward from the Yellowstone Plateau to foothills of Madison Range just northwest of here. To east is a good view back toward the Yellowstone Plateau, showing north-dipping Lava Creek Tuff sloping radially away from the caldera rim, which is breached by canyon of Madison River. Higher points near the canyon are outcrops of the pre-Lava Creek Mount Jackson Rhyolite; farther to right is Madison Plateau, burying west rim of caldera. To west, the high point on skyline is Lionhead Peak, underlain by Paleozoic limestones dipping south. Huckleberry Ridge Tuff dips southeast and east off Madison Range, defining it as an east-tilted block, and forms the densely tree-covered ridge to northwest and west. The Huckleberry Ridge dips toward Targhee Pass, near left end of Madison Range as seen from here, where it is offset by eastern extension of Centennial fault. The low, tree-covered platform to south of highway here is flat-lying Lava Creek Tuff, which onlaps the dipping Huckleberry Ridge Tuff. Far to the north, across valley of West Yellowstone, is a part of Madison Range north of Hebgen Lake, uplifted along Hebgen and Red Canyon faults, which broke during the magnitude 7.5 earthquake of August 17, 1959.

Continue west on US-20. **0.6**

38.9 Small dirt road angles off to right at east end of some large roadcuts. At this end of the cuts, flat-lying Lava Creek Tuff is poorly exposed but lies with a depositional contact on east-dipping Huckleberry Ridge Tuff (member B), which forms the prominent exposures farther into the roadcuts. **0.9**

39.8 Good exposure on right of Huckleberry Ridge Tuff at contact between members A and B. The same horizon is exposed high on the ridge ahead (south), offset across the east–west Centennial fault through Targhee Pass. **0.3**

40.1 Targhee Pass; turnouts on both sides. Huckleberry Ridge tuff is poorly exposed in the pass, which separates Henrys Lake Mountains to south from main Madison Range to north. The same horizon as is present near the pass, and is exposed in roadcuts just to east, is offset to skyline on south by Centennial fault. **2.1**

42.2 Targhee Creek Trail (dirt road) to right. On left near here are small exposures of Mississippian (Lower Carboniferous) limestone of Madison Group, but most of the roadcut and the opposite bank of gully expose thick outwash gravel. **0.8**

43.0 Tall gateway across dirt road on left at bend in highway. The east–west extension of Centennial fault through Targhee Pass emerges from behind ridge with exposures of Madison Limestone and passes along base of ridge to left. A Madison outcrop occurs within the tree-covered area high on ridge behind gate. **0.7**

43.7 About 50 m above road on the south (left), a large outcrop of Huckleberry Ridge Tuff on upthrown side of the east–west fault produces blocky talus. The highway here passes very nearly along trace of fault through Targhee Pass. **0.7**

44.4 Junction with ID-87 on right. Continue straight ahead on US-20. **0.3**

44.7 **STOP 3D. Centennial Mountains and Centennial fault.** Park in large turnout on right. (Valley View Truck Stop is 0.1 mi farther.) To west, the east–west Centennial Range faces north toward Centennial Valley. The range is a south-tilted normal-fault block with a core of Precambrian metamorphic rocks overlain by Paleozoic and Mesozoic sedimentary rocks. Sawtell Peak at east end, with a prominent aviation radar dome, is underlain by Eocene andesitic breccias, onlapped by a densely forested south-facing dip-slope of Huckleberry Ridge Tuff. The faultline scarp at the north base of the range has prominent Holocene displacement across glaciated canyons north of Sawtell Peak, continuous with the scarp in foreground that blocks the drainage to form Henrys Lake and that passes to right of here. To the east, this fault continues across Targhee Pass between main Madison Range on north and Henrys Lake Mountains on south. Far to the north, beyond Madison Range and Raynolds Pass, are high peaks of east-tilted Gravelly Range.

Continue westward on US-20. **0.9**

45.6 Road to Henrys Lake State Park on right. Ahead, the road is on upper Pleistocene outwash gravels on upthrown side of Centennial fault. Huckleberry Ridge Tuff not only forms prominent dip-slope on Centennial Range to west but also occurs along crest of Henrys Lake Mountains to east, dipping southeast and south. The low, tree-covered bench on both sides of valley ahead is untilted Lava Creek Tuff; its source, the Yellowstone caldera, is overlapped by rhyolitic lavas of Madison Plateau to southeast. **6.7**

52.3 Island Park Village on left; Sawtell Peak Road on right. The highway here rises onto a platform of Lava Creek Tuff above alluviated surface over which it has passed. Although exposures are poor here, the Lava Creek Tuff is well exposed in a roadcut about 0.3 mi beyond. **1.5**

53.8 Cross Henrys Fork of Snake River; Mack's Inn Resort across river on left. **1.0**

54.8 Roadcuts of Lava Creek Tuff on both sides of highway for next 1.5 mi. **5.8**

60.6 Road to Box Canyon on right. Timbered ridge seen in glimpses through the trees beyond to right is Thurmon Ridge, the north rim of Henrys Fork caldera. Beyond to southwest is Bishop Mountain on west rim of the caldera. **4.2**

64.8 Beyond village of Last Chance, roadcuts expose basalts that floor Henrys Fork caldera. **1.3**

66.1 **STOP 3E. View of Henrys Fork and Big Bend Ridge calderas.** Turn left onto Mesa Falls Scenic Drive and park alongside road; walk back across main highway (**carefully!**) to rail fence. From here, the rim that encloses the entire Island Park basin

on south, west, and north is visible. Far to the north, the crest of Madison Range is also visible. Slightly to left is Centennial Range, with Sawtell Peak at its eastern end. In middle distance between here and Centennial Range is Thurmon Ridge, the north wall of Henrys Fork caldera, source of the 1.3 Ma Mesa Falls Tuff. Mesa Falls Tuff on Thurmon Ridge onlaps pre-Mesa Falls, post-Huckleberry Ridge rhyolite flows on Bishop Mountain to west. Moonshine Mountain, the half-timbered hill in front of Bishop Mountain, is a downdropped block of Bishop Mountain flow (a biotite-bearing rhyolite, rare in this volcanic field). Left of Bishop Mountain is Big Bend Ridge, consisting mainly of Huckleberry Ridge Tuff but overlain locally by a thin Mesa Falls Tuff and enclosing the Big Bend Ridge segment of the first-cycle caldera, source of member B of Huckleberry Ridge Tuff. The summit on that ridge (High Point) and the conical hill that rises from floor of Island Park in front of Big Bend Ridge (Little Butte) are vents for younger basaltic and related lavas with affinities to those of the Snake River Plain farther west. The flat floor of Island Park basin is covered by less K-, Ti-, and P-rich olivine tholeiites that erupted from vents within the calderas after cessation of rhyolitic volcanism.

Continue south on Mesa Falls Scenic Drive on loess-covered basalt. **4.5**

70.6 Turn left onto Hatchery Butte road (unpaved). **0.4**

71.0 **STOP 3F. Outcrop of Island Park Rhyolite.** Park along roadside adjacent to rhyolite outcrops on left. This rhyolite is top of Osborne Butte dome, one of a group of post-Mesa Falls, 1.2 Ma rhyolitic lavas (the Island Park Rhyolite), that lies in a northwest-trending belt across Henrys Fork caldera. Note abundant large phenocrysts, especially the very large sanidines. If the day is clear, the Teton Range can be seen to the south. The tree-covered rise in middle distance to left of Tetons is a low shield at source vent for some of the post-caldera basalts of Island Park basin.

Turn around on the wide road or the adjacent open area. Watch out for logging trucks. (If necessary, drive ahead 0.6 mi to a small side road on right to facilitate turning around.) Return to paved road. **0.4**

71.4 At paved road, turn left. **7.9**

79.3 Road to Warm River Springs and Pole Bridge Campground on left. **0.9**

80.2 Turn right on Road 295 (otherwise unmarked), dirt or lightly oiled. **0.1**

80.3 The road descends toward canyon of Henrys Fork through basaltic lavas that floor Island Park basin. **0.1**

80.4 Beneath the basalt is poorly exposed, welded, platy-weathering, phenocryst-poor, gray Lava Creek Tuff, a distal facies that spread across the older caldera basin. Float of this lithology follows along roadcuts for about 0.3 mi. **0.3**

80.7 Poor exposure of pinkish vapor-phase zone of uppermost part of Mesa Falls Tuff with abundant large phenocrysts, especially of sanidine. **0.4**

81.1 **STOP 3G. Mesa Falls Tuff and basalts at Upper Mesa Falls.** Park at end of road. Walk down to brink of falls along any of several steep, rough, unmaintained trails. Here Henrys Fork of the Snake River plunges over a cliff of devitrified, densely welded Mesa Falls Tuff ponded within the first-cycle Big Bend Ridge caldera segment but outside rim of buried Henrys Fork caldera, source of Mesa Falls Tuff. This tuff is stratigraphically below the vapor-phase zone exposed poorly along the road down to here; cliffs across river are composed entirely of Mesa Falls Tuff. An earlier level of canyon-cutting is preserved as a terrace on this side, capped by basalts that can be seen by walking along canyon rim downstream about 100 m. If time permits, one can scramble down a steep trail near the base of the basalt cliffs to a spectacular view of Mesa Falls Tuff from below the falls.

Return along same dirt road back to canyon rim. **0.8**

81.9 Paved Mesa Falls Scenic Drive; turn right. **0.7**

82.6 Grandview Campground and Lower Mesa Falls Overlook; turn right. **0.1**

82.7 **STOP 3H. View of Lower Mesa Falls and Snake River Butte.** Park in parking lot for overlook. Walk back about 60 m to the overlook by a stone wall. Lower Mesa Falls, below here, and upper Mesa Falls, barely visible upstream, both expose Mesa Falls Tuff ponded to at least 100 m thickness in the Big Bend Ridge caldera segment. The entire height of the opposite canyon wall is in Mesa Falls Tuff; on this side, basalt both rims the canyon and forms a terrace above present river level. Both basaltic sequences erupted from vents within the second-cycle Henrys Fork caldera to north. Snake River Butte, a pre-Huckleberry Ridge rhyolitic lava flow, is on skyline to south-southwest, truncated at the rim of the first-cycle Big Bend Ridge caldera segment, which contained the major body of Mesa Falls Tuff, as seen from here. Far to the northwest, the peaks of Centennial Range may be seen.

Return to main paved road and turn left; backtrack along Mesa Falls Scenic Road, following same route taken to here. **13.9**

96.6 Turn left at junction with US-20. **2.3**

98.9 Along this open stretch of road, the Madison Plateau is seen to east (left) and the Teton Range to south-southeast. **2.7**

101.6 Riverside Campground on left. Beyond, the road climbs above level of basalt flows on floor of Island Park basin to a low platform of Lava Creek Tuff, poorly exposed in a few small roadcuts. **2.0**

103.6 The road is cut through the edge of a small basaltic cinder cone. From here south, the rest of Island Park basin is floored by basalt. **4.2**

107.8 The highway bends to left, past an unmarked road with a stop sign on left. From here, the highway ascends gently past outcrops of thick, densely welded Mesa Falls Tuff ponded within Big Bend Ridge caldera segment. **1.4**

109.2 Summit of highway at crest of Big Bend Ridge. The Mesa Falls Tuff was ponded north of here, and only a thin nonwelded to partially welded vapor-phase zone flowed farther southward over the old caldera rim. **0.2**

109.4 Anderson Mill Canyon Road on left. Along high-

way just beyond on right is a turnout; roadcuts on left and just ahead are thin, partially welded Mesa Falls Tuff. **0.6**

110.0 Thin Mesa Falls Tuff, including coarse basal fallout ash, is exposed just above road level in cuts on left. **0.4**

110.4 Roadcut on right exposes more densely welded Mesa Falls Tuff that fills an old valley incised into sloping flank of Big Bend Ridge. **0.7**

111.1 Leave Targhee National forest. Downslope along the road, densely welded Huckleberry Ridge Tuff occurs in gully to left, and discontinuous veneers of thin, partially welded to nonwelded Mesa Falls Tuff adhere to some slopes on both sides. **1.8**

112.9 Large outcrop on right of vapor-phase zone in Mesa Falls Tuff with thick basal fallout ash overlying densely welded Huckleberry Ridge Tuff. In gully to left, the Huckleberry Ridge Tuff forms broad, low-amplitude wave forms produced by slumping during welding on outward slope of Big Bend Ridge. **0.4**

113.3 Turn right on a narrow dirt road past a small log store about 50 m in from highway. Beyond is private property, and permission should be obtained if not previously arranged. Continue through gate past small fenced enclosure on right. **0.2**

113.5 **STOP 3I. Excellent exposure of basal bedded ash and distal ash flows of Mesa Falls Tuff.** Park in sand and gravel pit cut into Mesa Falls Tuff. Several well-exposed ash-flow tuffs are nonwelded to slightly welded, glassy to vapor-phase crystallized, and form a cooling unit about 4–5 m thick. The underlying bedded ash, about 15 km from the ring-fracture zone of Henrys Fork caldera, is about 5.5 m thick, resting on loess-covered Huckleberry Ridge Tuff. The lower 60 cm or so (typically obscured by pumiceous scree) is a coarse-crystal concentrate; the upper 5 m consists mainly of coarse pumiceous ash and small lapilli. Most of the deposit is fallout, with planar mantle bedding, but a few layers have well-developed cross-laminations, especially in upper 1.5 m at south end of pit, and may be pyroclastic-surge deposits. A thin (up to 25 cm) ash-flow tuff is locally interstratified in the upper 1 m of bedded ash. The natural surface above the pit is mantled by about 2 m of upper Pleistocene loess.

Return to US-20; turn right. **0.7**

114.2 Cross Henrys Fork at base of Big Bend Ridge and cross onto eastern Snake River Plain. Here, coarse gravels mantle basalts that typically floor the plain. **0.8**

115.0 Large turnout on left at Three Tetons Historical Marker. Excellent view of west side of Teton Range, descending northward to plunge beneath Yellowstone Plateau. The prominent northward and westward dip-slopes at north end of the range are underlain by Huckleberry Ridge Tuff and the older 4.3 Ma Conant Creek Tuff. To northeast is Snake River Butte, a pre-Huckleberry Ridge rhyolite flow broken by the caldera scarp at east end of Big Bend Ridge, which continues westward and slopes gently toward eastern Snake River Plain. In far distance to west-southwest is Juniper Buttes, a rhyolite–basalt center that rises above surrounding basaltic lavas of the plain. To south-southeast, the Big Hole Mountains are separated from Teton Range by fault-block basin of Pierres Hole. **2.1**

117.1 Ashton, Idaho. Flashing yellow light at main intersection of town, at the junction with ID-47 on left.

Day 4: Heise volcanic field

Lisa A. Morgan and Bill Bonnichsen

Neogene rhyolitic volcanism of the eastern Snake River Plain

A stratigraphic sequence and regional correlations have been established for three voluminous and extensive ignimbrites of the eastern Snake River Plain, ranging in age from 4.3 to 6.6 Ma. This stratigraphic package of densely welded ignimbrite sheets, together with associated volcanic rocks and sediments, forms the Heise volcanic field (Morgan et al., 1984; Hackett and Morgan, 1988) which is analogous in its development to the adjacent Quaternary Yellowstone Plateau volcanic field to the northeast (Christiansen and Blank, 1972; Christiansen, 1984).

Thirty years of local studies on Tertiary rhyolites around the eastern Snake River Plain have produced the complex " previous nomenclature" that is outlined in Table 1. Regional correlation of major ignimbrites from the Heise volcanic field has recently been accomplished with the aid of paleomagnetic remanent directions; radiometric ages; geo-

TABLE 1—Stratigraphic nomenclature for the three major ignimbrites of the Heise volcanic field. References: [1]Scholten et al. (1955); [2]Stearns and Isotoff (1956); [3]Carr and Trimble (1963); [4]Albee et al. (1975); [5]Prostka and Embree (1978); [6]Skipp et al. (1979); [7]McBroome (1981); [8]McBroome et al. (1981); [9] Morgan et al. (1984); [10]Morgan (1988a). Previous correlation of the tuff of Elkhorn Spring with the tuff of Blue Creek (McBroome et al., 1981; Morgan et al., 1984) is now known to be erroneous. See Fig. 4 for locations of inferred source calderas.

Previous nomenclature		Current nomenclature
Northern margin	**Southern margin**	
tuff of Spencer[6]	tuff of Heise[4, 5, 8] tuff of Heise C[4]	tuff of Kilgore[9]
tuff of Blue Creek[6, 7, 8]	tuff of Elkhorn Spring[9] Walcott Tuff [2, 3, 10]	tuff of Blue Creek[9]
tuff of Edie School[6] tuff of Edie Ranch[7, 8] School Rhyolite[1]	tuff of Spring Creek[5,8]	tuff of Blacktail[9]

chemistry; stratigraphic position; the compositions, sizes and relative abundances of phenocrysts; and macroscopic lithology. These correlations (e.g. , Morgan et al., 1984; Morgan 1988a) lead to the simpler terminology that is given under "present nomenclature" in Table 1. Formal stratigraphic names will soon be introduced (Morgan, 1988b, and unpubl. data), but we use the established terminology of Morgan et al. (1984) throughout this guide.

Deposits of the Heise volcanic field cover more than 35,000 km^2 in southeastern Idaho. Exposures are mostly limited to mountains along the margins of the eastern Snake River Plain, but correlative rhyolitic units have also been identified in subsurface boreholes drilled through Quaternary basalt on the plain (Doherty et al. , 1979). The three widespread ignimbrites of the Heise volcanic field are the 6.6 Ma tuff of Blacktail, the 6.0 Ma tuff of Blue Creek, and the 4.3 Ma tuff of Kilgore. In many places, these major ignimbrite sheets are found together as a stratigraphic package with local intercalated rhyolite lava flows, smaller-volume ignimbrites, pyroclastic-fall deposits, basaltic lava flows and tephra, and sediments. Although facies variations occur, all three of the major ignimbrites are composed of densely welded, crystal-poor, high-silica, peraluminous rhyolite.

The three widespread ignimbrites of the Heise volcanic field are inferred to have erupted from major calderas that are now largely buried beneath Quaternary basalts of the eastern Snake River Plain (Fig. 4). The earliest major eruption of the Heise volcanic field produced the immense, plain-wide Blacktail caldera, which was the source of the tuff of Blacktail and within which the later calderas were either nested or largely overlapped. The second major event, perhaps a phase of the initial event, produced the smaller, nested, Blue Creek caldera from which the tuff of Blue Creek erupted. A third major eruption produced the immense, plainwide, Kilgore caldera, the source of the tuff of Kilgore (Morgan, 1988a). Important evidence of these inferred source calderas is found along both margins of the eastern Snake River Plain, in the Poplar—Heise area on the southern margin (Stops 4A—C), and in the Howe Point, Lidy Hot Springs, and Spencer—Kilgore areas on the northern margin.

The dimensions of Neogene calderas beneath the eastern Snake River Plain are not accurately known because of burial by Quaternary basalts and because most rhyolite exposures occur along the margins of the plain. However, careful study of lateral variations in ignimbrite geometry and lithology allows inference of the directions and approximate distances to the source calderas. Facies changes within each ignimbrite as well as analyses of flow directions, volcanic and tectonic structures, and geophysical anomalies have all been used to infer the locations of the source calderas that are shown in Fig. 4. The estimated volumes of the Neogene Heise ignimbrites are comparable with those of the Quaternary Yellowstone ignimbrites (Fig. 5). It is probable that the buried Heise calderas have dimensions comparable to those of the better exposed Yellowstone Plateau volcanic field.

Road log

This day of the trip will be led by Lisa Morgan. We will examine: (A) the rhyolitic welded ignimbrite and lava-flow units exposed at Heise escarpment; (B) the Huckleberry

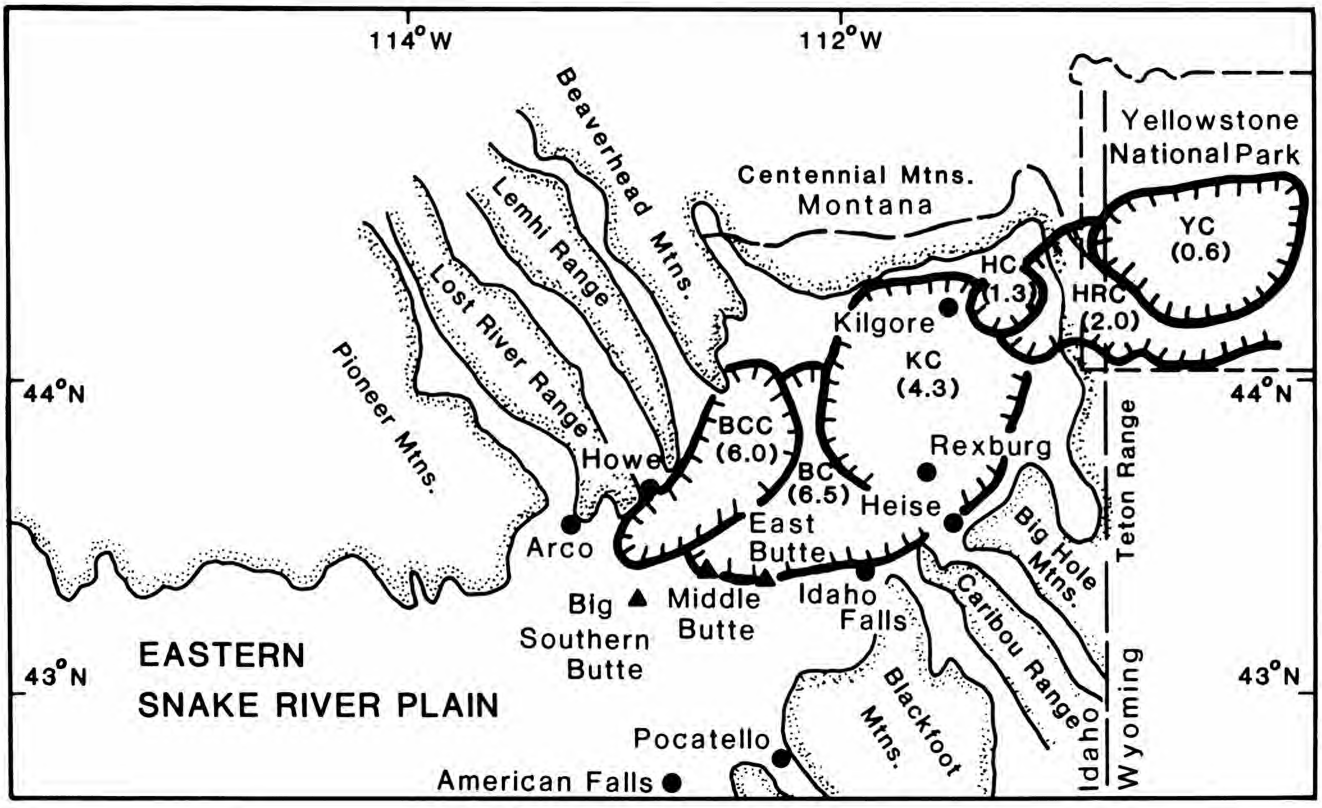

FIGURE 4—Inferred calderas of the Heise volcanic field (adapted from Morgan et al. , 1984) and the Yellowstone Plateau volcanic field (Christiansen, 1984). Ages of calderas (Ma; shown in parentheses) are based on age dates of major ignimbrites. Heise calderas are as follows: BC, Blacktail caldera; BCC, Blue Creek caldera; KC, Kilgore caldera. Calderas of Yellowstone—Island Park region are: HRC, Huckleberry Ridge caldera; HC, Henry's Fork caldera; YC, Yellowstone caldera.

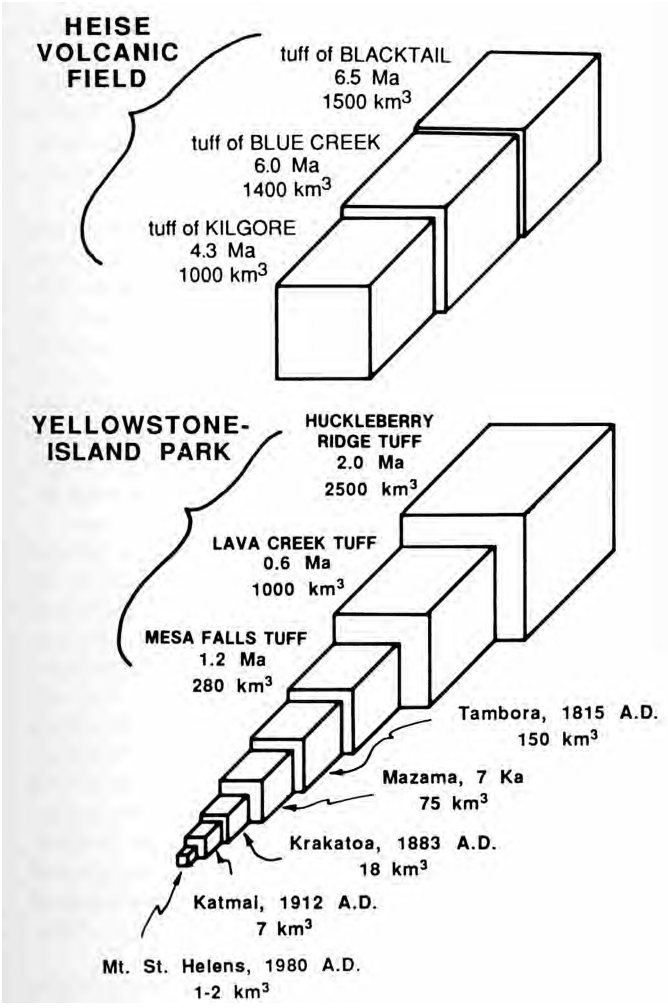

FIGURE 5—Estimated volumes of the Quaternary Yellowstone Group ignimbrite units and the Neogene Heise volcanic units, with selected Holocene and historical eruption volumes shown for comparison. Modified from Smith and Braile (1984).

Ridge Tuff, the tuff of Kilgore, and the unconsolidated pyroclastic-fall and surge deposits of the tuff of Wolverine Creek in the Meadow Creek Dugway area; (C) the Huckleberry Ridge Tuff, the tuff of Wolverine Creek, and the tuff of Blacktail exposed at the Blacktail recreation area east of Idaho Falls; (D) the Hells Half-Acre basalt flow between Idaho Falls and Blackfoot; and (E) the Walcott Tuff near American Falls. Today's route essentially follows the southeastern margin of the eastern Snake River Plain between Rexburg and Burley. Various basalt volcanoes and rhyolite domes can be seen in the interior of the Plain, and older rocks that have been deformed within the Overthrust Belt and uplifted along Basin and Range structures will be visible in the mountain ranges southeast of the Plain.

Mileage

00.0 Drive south-southwest from the southwest part of Rexburg, starting where the old Yellowstone Highway (old US-20 and US-191) turns from a west heading to a south-southwest heading, near the Best Western Motel. **1.1**

01.1 Pass, on the west (right), the turnoff to the south Rexburg entrance of bypass US-20, located about 0.4 mi to the west. **0.9**

02.0 Turn left onto Archer Road (marked as route to Heise) and head south. After leaving Rexburg, and for several miles along this road, North and South Menan Buttes are clearly visible to the east. These buttes are basaltic tuff rings that formed when basaltic magma intersected shallow ground water and erupted explosively during the Pleistocene (Hackett and Morgan, 1988). Archer Road eventually turns toward the east and then to the south again. **10.1**

12.1 Turn toward the east (left) at the intersection of 10,000 S and 600 E, leaving the main road. **1.1**

13.2 Turn south (right) at the intersection of 10,000 S and Snake River Road; follow Snake River Road. **3.6**

16.8 Continue east (straight) at the intersection of Heise Road and 5,050 E; follow Heise Road. **1.0**

17.8 **STOP 4A. Heise escarpment: Elutriation pipes near base of tuff of Elkhorn Spring; base-surge deposits near base of tuff of Wolverine Creek; ash-cloud deposits lying on quenched ash flow in capping sequence of tuff of Blacktail.** Park near the Heise pizza parlor and follow the trail that goes up escarpment on north side of road. When leaving, retrace route back to west. The Heise cliffs expose a thick section of Heise volcanics in the uplifted block of Grand Valley fault (Figs. 6, 7). The Heise cliffs are one of the main areas in which the stratigraphy of the Heise volcanic field has been established. The great thickness and coarseness of tuff of Kilgore and tuff of Blacktail, together with the large number of intercalated rhyolite lava flows, indicate that the Heise cliffs section is located near the overlapping margins of Kilgore and Blacktail calderas (Fig. 4). It was originally thought that all three major ignimbrites of Heise volcanic field were present in the Heise cliffs (Morgan et al., 1984), but more recent paleomagnetic and geochemical data (Morgan, 1988a) show that tuff of Blue Creek is not present.

The cliffs are capped by a thick section of 4.3 Ma tuff of Kilgore (Figs. 6, 7). Three lines of evidence suggest that part of tuff of Kilgore was erupted from a source near Heise: (1) the average thickness of tuff of Kilgore on Heise cliffs is about 30 m, (2) flow units in the ignimbrite contain coarse crystals and large lithic and pumice clasts, and (3) flow-direction indicators (Morgan, 1988a) suggest a source in the Poplar–Heise area.

The next prominent cliff-forming unit below tuff of Kilgore is tuff of Elkhorn Spring (Figs. 6, 7). This unit was previously correlated with the widely distributed 6.0 Ma tuff of Blue Creek (Morgan et al., 1984), but is now recognized as a local, smaller-volume unit. The tuff of Elkhorn Spring is best exposed in Heise cliffs where it is at least 60 m thick. Features of interest include the pink, nonwelded base containing numerous elutriation (degassing) pipes; the dark-brown to black, laminated basal vitrophyre containing small (<1 cm), light-colored pumice clasts; and the lower devitrified and vapor-phase zones containing post-emplacement extensional fractures lined with vapor-phase minerals.

Below tuff of Elkhorn Spring, the tuff of Wol-

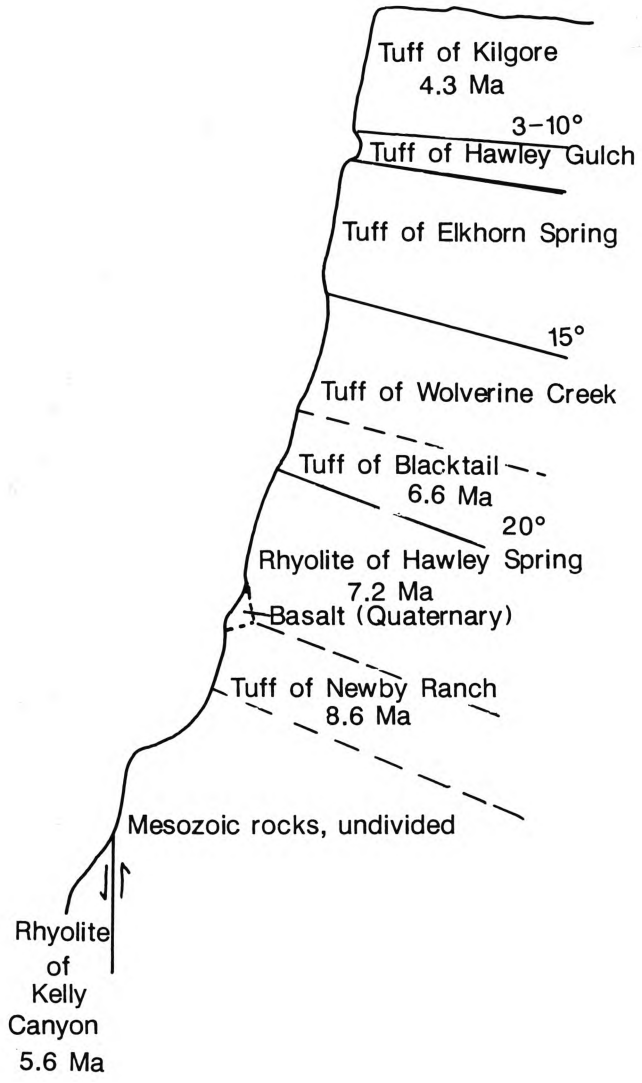

FIGURE 6—Schematic profile showing general stratigraphic relations seen in cliffs above Heise Hot Springs. The ignimbrite units gradually increase in dip with increasing age.

verine Creek forms a smaller set of softly rounded, gray cliffs containing many bird holes (Figs. 6, 7). The tuff of Wolverine Creek is a local, nonwelded, obsidian-shard-bearing, massive ignimbrite. We will examine the basal units containing alternating coarse- and fine-grained base-surge bed sets and coarse pumice units.

The 6.6 Ma tuff of Blacktail is located below tuff of Wolverine Creek and ranges in thickness from less than 8 m to more than 20 m in the Heise cliffs (Figs. 6, 7). Several cooling units are present. Of particular interest are two red vitrophyres capping the ignimbrite. The lower dark-red vitrophyre has a phenocryst content of about 7% and represents the quenched top of the ash-flow sheet, whereas the overlying pink vitrophyre has a phenocryst content of less than 2% and most likely represents the deposit from an ash cloud.

The 7.2 Ma rhyolite of Hawley Springs (Morgan et al., 1984) forms prominent steep cliffs below tuff of Blacktail (Figs. 6, 7) and has an undulating surface typical of many rhyolitic lava flows. This lava caps a sequence of white, laminated tuffaceous deposits which in turn overlie a thin basalt. This volcanic section is separated by a segment of the Grand Valley fault from the Permian Park City Formation which forms small hills adjacent to the road next to Heise Hot Springs. Other volcanic units exposed along Heise cliffs include, from younger to older, the local tuffs of Hawley Gulch, Dora Springs, and Newby Ranch (8.6 ± 0.5 Ma) and the rhyolite of Kelly Canyon (5.7 ± 0.1 Ma) (Morgan et al., 1984). **1.0**

18.8 Same intersection as mileage 16.8. Turn south (left) and cross Snake River. **1.2**

20.0 Turn south (left) at intersection of 100 N and 4,950 E. **2.0**

22.0 Turn west (right) on US-26. **1.5**

23.5 Turn south on road that leads to Ririe Dam recre-

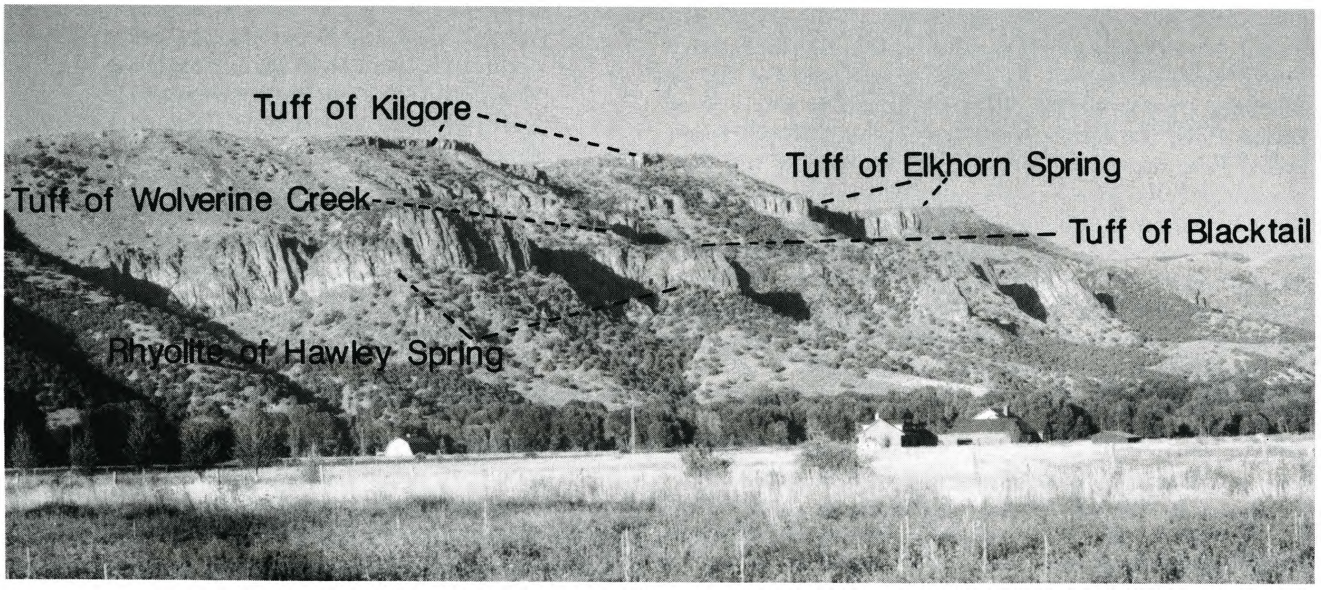

FIGURE 7—Escarpment above Heise Hot Springs showing the major, cliff-forming, volcanic units. At this locality the tuff of Blacktail is relatively thin (<8 m) and its thickness fluctuates in response to undulations in upper surface of the rhyolite of Hawley Springs lava flow, which it caps. The escarpment is approximately 400 m (1300 ft) high and the Snake River is at its base.

ation site at intersection of 14,500 E and Meadow Creek Road. **2.3**

25.8 Pass entrance to Ririe Dam. **3.9**

29.7 **STOP 4B. Meadow Creek Dugway: Variation in thickness of tuff of Kilgore over irregular paleotopography; differences in cooling zonation in tuff of Kilgore as thickness varies.** Park in lot near intersection of Meadow Creek and Mud Springs Roads. Walk to the two areas described below, and eventually meet vehicles at bottom of Meadow Creek Dugway grade (mileage 30.5). Walk northwest on Huckleberry Ridge Tuff along rim of the cliff for about 0.3 mi. Proceed down a small ravine through an excellent section of the 4.3 Ma tuff of Kilgore. Here tuff of Kilgore is an outflow-facies ignimbrite that is about 11 m thick (Fig. 8); it contains at least three cooling breaks that are marked by internal variations in degree of welding. Subtle zonations of mineralogy and trace-element concentrations occur within the ignimbrite and are further evidence that it was emplaced as several pyroclastic flows in rapid succession. The tuff of Kilgore rests on a thin (10 cm), well-sorted ash which overlies a thin (50 cm), orange, lithic-rich, nonwelded ignimbrite which, in turn, is separated from the underlying tuff of Wolverine Creek by a thin (1 cm) paleosol (Fig. 8).

Walk back toward road junction, then continue down road into Meadow Creek valley. The 2.1 Ma Huckleberry Ridge Tuff forms the rim of the cliff (Fig. 9) and is separated from the underlying 4.3 Ma tuff of Kilgore by a 40 cm thick paleosol. Continuous exposures of tuff of Kilgore show great thickness variation from less than 3 m to more than 13 m over a distance of 2 km, as a result of emplacement over irregular topography. The tuff of Kilgore contains multiple pyroclastic-flow units with locally derived lithics, lithic-concentration zones, and fines-depleted, crystal- and lithic-rich, ground-layer deposits. Beneath tuff of Kilgore are a coarse fluvial gravel, tuffaceous sediments, and tuff of Wolverine Creek. Farther down the road, across Mud Spring Creek, is an outflow-facies exposure of tuff of Blacktail. **0.8**

30.5 Bottom of grade at Meadow Creek Dugway. Large vehicles can turn around about 0.5 mi farther along this road. Return to US-26. **7.0**

37.5 Turn west (left) on US-26 (same intersection as mileage 23.5). **1.6**

39.1 Pass junction with road to Ririe. **1.3**

40.4 Turn south (left) on country road where business US-26 joins the main branch of the highway. **7.0**

47.4 Turn east (left) at junction with Lincoln Road. **2.2**

49.6 **STOP 4C. Blacktail recreation area: Ground-layer deposit at contact of members A and B of Huckleberry Ridge Tuff; contrasts in bedforms between ash-cloud surge deposits at top of tuff of Wolverine Creek and water-lain lacustrine deposits below Huckleberry Ridge Tuff; base-surge xenoliths from base of tuff of Wolverine Creek incorporated higher in that unit; crystal- and obsidian-shard-enriched elutriation pipes in upper part of tuff of Wolverine Creek; view into Blacktail caldera.** This stop includes two localities within continuous exposures of rhyolitic ignimbrites

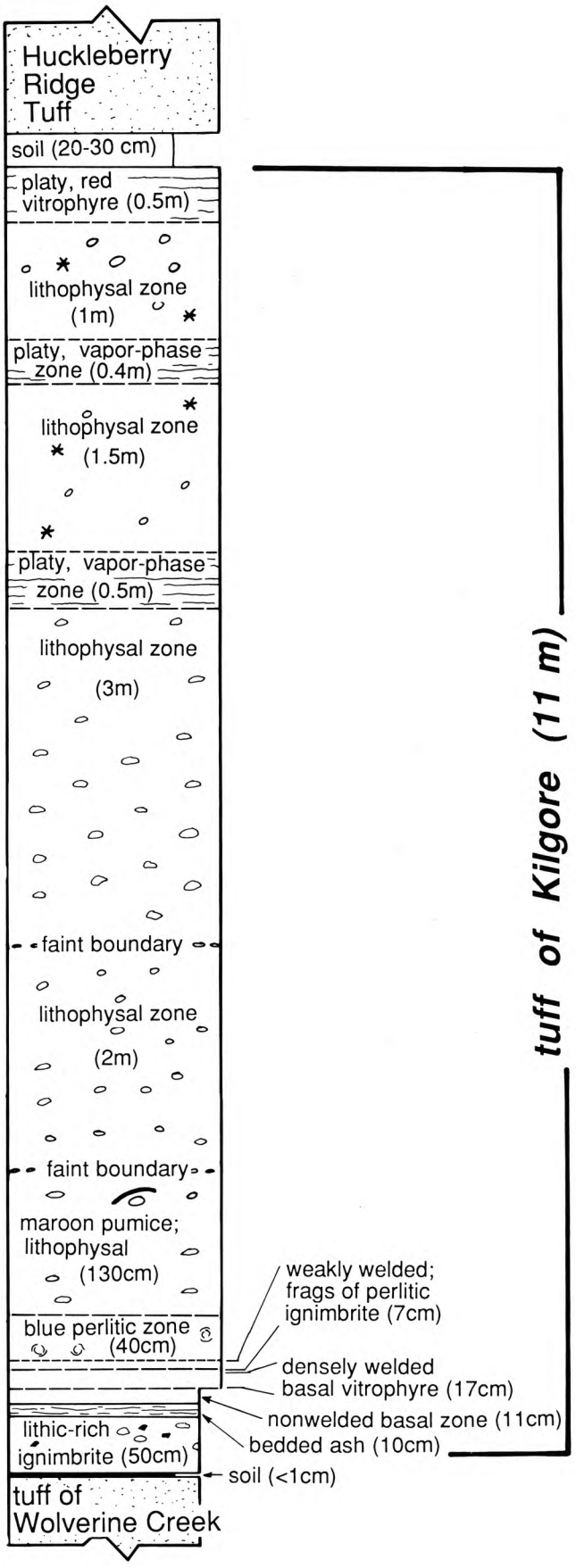

FIGURE 8—Schematic section of tuff of Kilgore exposed in a small ravine at Stop 4B, Meadow Creek Dugway. From Hackett and Morgan (1988).

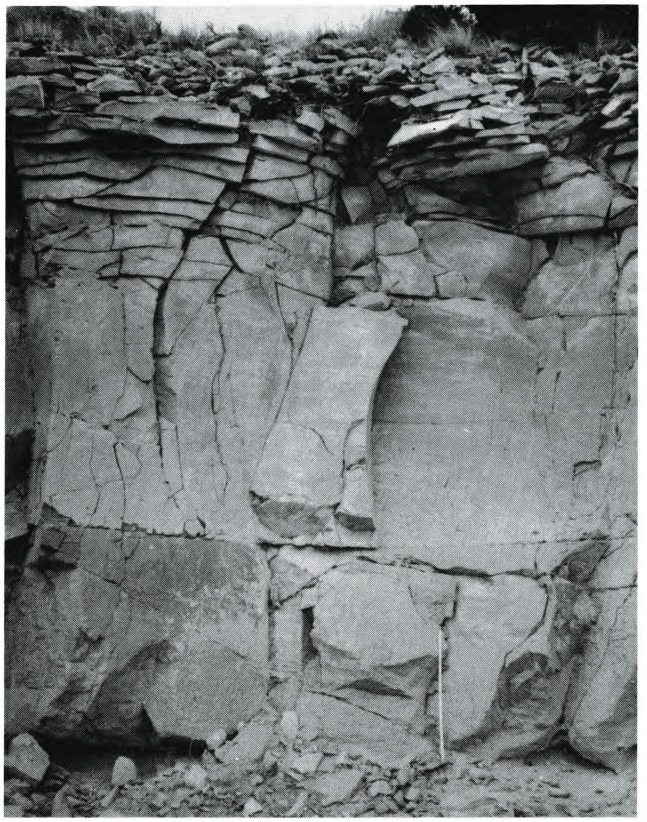

FIGURE 9—Huckleberry Ridge Tuff (2.1 Ma) at Stop 4B, Meadow Creek Dugway. The conspicuous parting and color change above the meter stick is the contact between members A and B. Photo W. R. Hackett.

near inferred structural margin of Blacktail caldera, source of the 6.6 Ma tuff of Blacktail. The first locality is a roadcut exposing gray and tan rhyolitic ignimbrites along left (north) side of paved road, where the road begins its steep descent to the reservoir. The second locality is tuff of Blacktail exposed by boat ramp, which is reached by walking or driving down paved road to Ririe Reservoir.

The Stop 4C roadcut is an excellent vantage point for an overview of the Heise volcanic units in this region. Exposed in valley to east (Fig. 10) is a stratigraphic section along the rim of Blacktail caldera (Morgan, 1988a). At boat ramp is the type locality of tuff of Blacktail, the 6.6 Ma ignimbrite of Heise volcanic field (Morgan et al., unpubl. data; see details below).

At the Stop 4C roadcut, two members of the 2.1 Ma Huckleberry Ridge Tuff (Christiansen and Blank, 1972; Christiansen, 1984) form the top of the exposure and cap the hill. The lower member A is nonwelded and poorly sorted, and it grades from tan at the base to pink at the top. Member A is separated from the overlying member B by a fines-depleted, lithic- and pumice-rich ground layer that ranges from 1 to 12 cm in thickness. Member B contains a pumice concentration zone about 18 cm from its base, and the upper part is pink, platy and crystal-poor. The Huckleberry Ridge Tuff rests conformably on a sequence of intercalated, fine-grained, planar-bedded, lacustrine ash units, and bedded, pumice-fall deposits (Fig. 11). These deposits in turn rest unconformably on tuff of Wolverine Creek, a local, nonwelded, obsidian-rich ignimbrite.

At this locality the tuff of Wolverine Creek contains crystal- and obsidian-rich, fines-depleted elutriation pipes (Fig. 12), together with pods of laminated, obsidian-rich ignimbrite that have abrupt terminations and soft-sediment-deformation features (Fig. 13). The laminated pods may be xenoliths of an earlier pyroclastic flow that remained coherent when picked up and incorporated in later emplacement units of tuff of Wolverine Creek.

Drive or walk downhill to boat ramp, where an excellent section of tuff of Blacktail is exposed (Fig. 10). At boat ramp the tuff is relatively thin (about 8–11 m) and undeformed. It is an outflow-facies ignimbrite that is composed of a basal vitrophyre (exposed only when water level is low), a devitrified, densely welded interior, a massive vapor-phase zone, a lithophysal zone, and a cap of black, densely welded vitrophyre. A 50 cm thick, red vitric ash overlies the black vitrophyre.

A few hundred meters northeast of boat ramp the tuff of Blacktail becomes greatly thickened (>150 m), is silicified and crystal-rich, and has tight flowage folds. This thick tuff represents the ponded intracaldera facies (Fig. 10). Lower in the valley is a mesa of canyon-filling Quaternary basalts. The ridge behind the mesa is capped by Huckleberry Ridge Tuff, underlain successively by the 4.3 Ma tuff of Kilgore, the tuff of Wolverine Creek, and the tuff of Blacktail. **1.0**

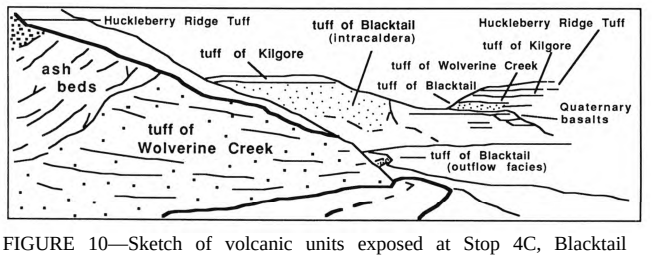

FIGURE 10—Sketch of volcanic units exposed at Stop 4C, Blacktail recreation area. View is toward the east, with Ririe Reservoir at lower right.

FIGURE 11—Water-deposited (lacustrine) tuffs (top), cross-stratified surge deposits (middle), and tuff of Wolverine Creek (lower left) exposed at Stop 4C, Blacktail recreation area. About 5 m of section is shown. Photo W. R. Hackett.

FIGURE 12—Fluid-escape structures (elutriation pipes) in upper part of tuff of Wolverine Creek, Stop 4C, Blacktail recreation area. Pencil near top of frame for scale. Photo W. R. Hackett.

FIGURE 13—Cross-stratified surge deposits (top) overlying tuff of Wolverine Creek (lower part of frame) at Stop 4C. Pods of laminated ignimbrite and flamelike fluid-escape structures are present within tuff of Wolverine Creek. Lens cap for scale. Photo W. R. Hackett.

50.6 Parking lot by Ririe Reservoir; retrace route. **3.3**

53.9 Same junction as mileage 47.4. Pass by Johnson Road and continue west on Lincoln Road toward Idaho Falls. **10.6**

64.5 Turn southwest (left) onto US-26 (Yellowstone Highway). **1.9**

66.4 Turn northwest (right) in downtown Idaho Falls onto Broadway Avenue in order to get to I-15. **1.1**

67.5 Join I-15 at exit 118 and drive southwest toward Blackfoot and Pocatello. As you travel southwest, East Butte, Middle Butte, and Big Southern Butte can be seen to the west near center of Snake River Plain. Big Southern Butte (on left) and East Butte (on right) are Pleistocene rhyolitic domes that have intruded through basaltic rocks of the eastern Snake River Plain, and Middle Butte is an elevated block of basalt flows. Big Southern Butte is the largest; it stands 760 m above the Plain and is 6.5 km across at its base. It has been dated at 0.3 Ma (Spear and King, 1982). **15.9**

83.4 **Stop 4D. Hells Half Acre rest stop: Ropy flow surfaces typical of pahoehoe lava; pressure ridges; squeeze-ups; collapse depressions.** Follow the short, self-guided nature tour available at this locality. The Hells Half Acre lava field is an area of fresh basalt covering about 400 km^2 (Karlo, 1977a, b; Kuntz and Dalrymple, 1979; Kuntz et al., 1979). The radiocarbon age of the lava field is 5200 ± 150 years B.P. (Kuntz et al., 1986). These flows originated from a vent area to the northwest. Near-vent volcanic products include basaltic pyroclastic rocks and lava-lake deposits. The volcanic field went through a number of eruptive phases and comprises eight lava flows. However, there is no indication of a significant time interval between the phases (Karlo, 1977a, b). Typically, the flows are of pahoehoe lava, with an appearance similar to this locality. **8.3**

91.7 Cross Snake River. **5.7**

97.4 Pass exit 89. From the overpass and farther south, Ferry Butte, a basalt shield, is visible to southwest. **16.3**

113.7 Take exit 72 onto I-86 and drive west toward Twin Falls. **4.3**

118.0 Pass the FMC and Simplot phosphate plants on south (left) side of highway. These are two of the processing plants for southeast Idaho phosphate. The major products are phosphate fertilizer and elemental phosphorus. **18.2**

136.2 Take exit 40, then turn west (right) on ID-39 toward American Falls. **1.7**

137.9 Turn north (right) onto ID-39 toward American Falls dam. **1.0**

138.9 American Falls dam. **0.6**

139.5 Turn left onto Lamb Weston Road and immediately turn left again onto Fish Hatchery Road. **0.3**

139.8 Turn left onto Idaho Power Road and descend into Snake River Gorge below dam. **0.3**

140.1 **STOP 4E. Walcott Tuff: Symmetrical zonation of cooling zones.** Follow the stairs and trail downstream to inspect type locality of Walcott Tuff (Fig. 14). When finished, drive back to American Falls. At this locality the entire thickness of Walcott Tuff is exposed below the basalt member of Little Creek

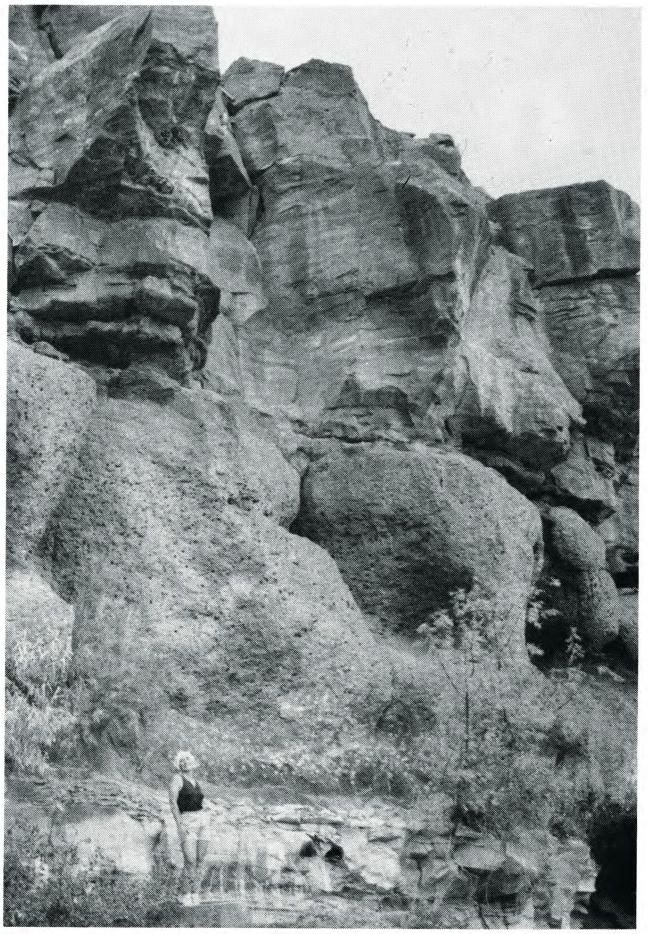

FIGURE 14—Walcott Tuff at Stop 4E, the unit's type locality in Snake River Gorge below American Falls dam. The overlying unit is the basalt member of Little Creek Formation (Carr and Trimble, 1963).

Formation (Carr and Trimble, 1963). The Walcott Tuff consists of two members, an upper member of black, glassy welded tuff and a lower member of white, bedded ash. The upper member of Walcott Tuff is an impressive, densely welded ignimbrite in terms of its cooling zonation symmetry. At this locality it is approximately 6–7 m thick. The ignimbrite is bounded near its base and at its top by slightly welded vitric ash that grades into densely welded vitrophyre. The vitrophyre grades into perlitic zones which in turn grade into a massive spherulitic interior. The 6.0 Ma Walcott Tuff has been correlated with the tuff of Blue Creek exposed extensively on the northern margin of the Plain, on the basis of paleomagnetic remanence directions, trace-element chemistry, and age dates (Morgan, 1988a, b). Its source is the Blue Creek caldera (Fig. 4) whose margin is best exposed at the southern tip of the Lemhi Range, across the Plain. **2.2**

142.3 Same junction as mileage 137.9; turn west (right) onto ID-37 (business I-86) toward Twin Falls. **2.9**

145.2 Join I-86 at exit 36, continue westward. **7.8**

153.0 Pass Massacre Rocks State Park (exit 20). **29.3**

182.3 Join I-84 and continue west toward Burley and Twin Falls. **13.0**

195.3 Take exit 208, then turn south (left) onto Overland Avenue toward Burley. **2.3**

197.6 Corner of Main and Overland in downtown Burley, where ID-27, US-30, and I-84 intersect.

Day 5: Silicic volcanics around the Cassia Mountains

William R. Hackett, Falma J. Moye, and Bill Bonnichsen

Geology of the Cassia Mountains and vicinity

The Cassia Mountains, at the southern side of the central Snake River Plain, consist largely of welded ash-flow-tuff units, probably erupted from several localities in the south-central Snake River Plain. Some of these sources may be a proposed caldera at the south end of the Oakley graben (Fig. 15), the area around Twin Falls, and the area that lies northwest and west of the range. Little detailed information is available on the geology of silicic units in the Cassia Mountains; it will be interesting in the next few years to see the pattern of silicic volcanism emerge as more research is conducted. Locally exposed in the interior of the Cassia Mountains are Paleozoic rocks that had been deformed and eroded into a hilly or mountainous terrain before the ash-flow units that cover most of the hills were erupted. The Cassia Mountains are bounded on the east by the graben-like Oakley Valley and on the west by the Rogerson—Jackpot graben. Both of these downdropped valleys contain an abundance of Snake River Plain-type silicic volcanic rocks.

Road log

This day of the trip will be led by Falma Moye, Bill Hackett (Stops 5A and 5B), and Bill Bonnichsen (Stops 5C and 5D). We will examine: (A) friable airfall tuff and welded ignimbrite in the Goose Creek area, (B) a rheomorphically deformed welded tuff in the Trapper Creek area, (C) the Shoshone Falls rhyolite lava flow, and (D) low- and high-temperature pyroclastic flows in the Rogerson—Jackpot graben. Today's route is partly along the southern margin of the central Snake River Plain, where several basalt shields can be seen, and partly within two valleys (probably graben) that extend southward away from the central Snake River Plain, and in which thick accumulations of rhyolitic volcanic products were deposited as the Plain evolved. Also, good

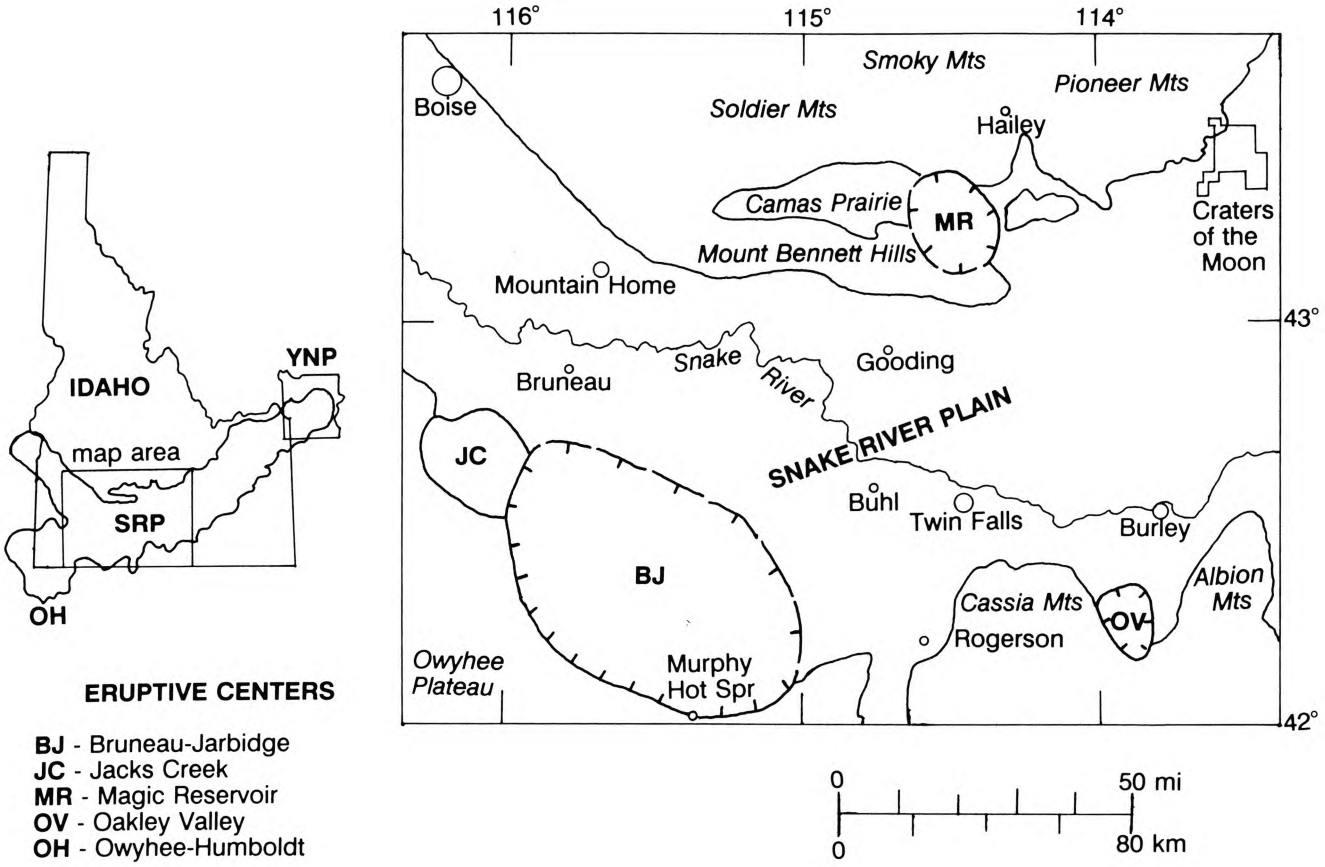

FIGURE 15—Locations of silicic eruptive centers and a possible caldera in the central Snake River Plain (SRP). Inset map shows overall extent of the Snake River Plain—Yellowstone Plateau volcanic province and location of Yellowstone National Park (YNP).

views will be available of the Basin and Range mountain ranges south of the plain, and of thick accumulations of welded-tuff sheets that extend southward onto some of these mountain ranges.

Mileage

00.0 Proceed south on ID-27 from junction of ID-27, US-30, and I-84 in downtown Burley (intersection of Main and Overland). As you drive south from Burley, the mountain range to the east (left) is the Albion Range. It is cored by Precambrian crystalline rocks and represents the westernmost Precambrian exposures in Idaho, south of the Snake River Plain. The mountains to the west (right) are the Cassia Mountains, or South Hills; they are underlain by Paleozoic rocks that have been nearly covered by a thick accumulation of welded pyroclastic flows which were erupted from silicic centers in the central Snake River Plain. **21.9**

21.9 Turn west (right) on Main Street in Oakley, Idaho. **0.5**

22.4 Turn south (left) on road to Oakley dam at sign to Oakley Hot Springs. **2.1**

24.5 Pass by road that turns west (right) to Oakley dam. **0.3**

24.8 Bear left at fork in road. As you proceed south along this road, note the excellent view to west (right) of the capping ash-flow sheet in Cassia Mountains. **6.2**

31.0 Pass road on east (left) that goes to Middle Mountain, and start down grade. **1.3**

32.3 Pass outcrop of Miocene lacustrine beds containing abundant rhyolitic ash. **1.3**

33.6 Pass Day Canyon Road that branches to right, stay left. The tuff of Day Canyon is a welded rhyolitic ignimbrite exposed at the intersection and on road to west (right). It is a single cooling unit enclosed within a thick section of bedded ash. **1.2**

34.8 Goose Creek is located to (west) right. Note thick bedded-ash deposits across valley. These beds contain both primary air-fall deposits and reworked tephra. **0.9**

35.7 **STOP 5A. Goose Creek section: Pyroclastic fall and surge deposits; welded ignimbrites; rheomorphic folding.** Climb hill on east (left) side of road. When leaving, turn around and drive northward on road. The Goose Creek reference section (Figs. 16, 17, and 18) illustrates the diverse assemblage of silicic pyroclastic fall, flow, and surge deposits that are exposed in this area. Although we have established a general stratigraphic framework for the deposits, our volcanic-facies analysis, radiometric dating, and structural studies are still in progress. Thus, our use of stratigraphic names is preliminary and informal.

The lower parts of most stratigraphic sections are dominated by fine, white, vitric tuffs. Decimeter-thick bedsets of planar-bedded, well-sorted ash, often containing accretionary lapilli, are probably distal plinian-fall deposits from unknown vents on the central (and western?) Snake River Plain. In many places, these fine tuffs have been briefly reworked

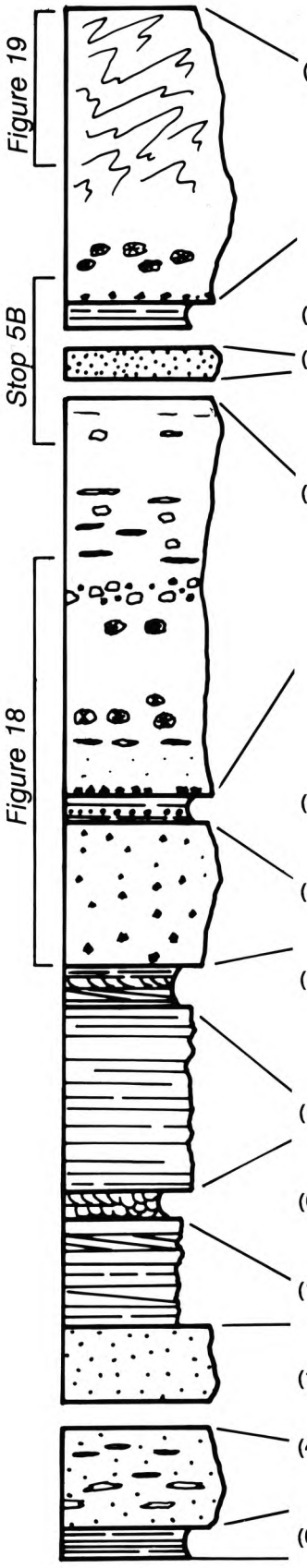

(30 m) ***TUFF OF GOOSE CREEK, Member B:***
Sharp, planar contact with underlying airfall has crystal-rich ground layer and rip-up clasts. Basal 0.5 m is gray, moderately welded crystal-vitric tuff with obsidian lithics to 4 mm. This grades upward into 0.7 m vitrophyre. Upper 28 m are densely welded, devitrified platy rhyolite with rheomorphic flow features; spherulites and lithophysal cavities are present in lower part.

(0.3 m) planar-bedded, vitric rhyolite airfall tuff

(1 m) covered

(0.5 m) buff-colored, unwelded rhyolite ignimbrite

(2 m) covered

(12 m) ***TUFF OF GOOSE CREEK, Member A:***
Sharp contact of ignimbrite with underlying airfall has scour features and ground layer. Basal 3.5 m grades up from 2 m of tan, unwelded ignimbrite to 1.5 m of dense vitrophyre. Upper 8.5 m have several spherulitic and lithophysal zones. An upper perlitic vitrophyre is locally present.

(0.3 m) thin-bedded, white to buff, planar stratified rhyolite airfall tuff with accretionary lapilli

(3.5 m) tan, unwelded rhyolite ignimbrite, containing normally-graded obsidian lithics (5 mm at base to 2 mm at top). Irregular basal contact is scoured into underlying surge.

(0.5 m) surge deposit: medium gray, coarse ash/fine lapilli tuff with planar- and low-angle cross-stratification, and lithic fragments up to 7mm.

(6 m) white to pale gray, planar-bedded, crystal-vitric rhyolite airfall tuff

(0.3 m) medium gray, poorly sorted, festoon cross-stratified, coarse ash to fine lapilli tuff: lapilli are similar to overlying airfall. Interpreted as surge deposit or reworked airfall tuff.

(1.5 m) light gray, planar- and low-angle cross-stratified, crystal-vitric rhyolite airfall tuff with cm-thick accretionary lapilli beds

(1 m) tan, unwelded crystal-vitric ash

(15 m) covered

(4 m) ***TUFF OF DAY CANYON:***
Basal 10 cm is moderately welded and grades upward into densely welded rhyolite ignimbrite.

(0.1 m) vitric rhyolite airfall tuff

(true base not exposed)

FIGURE 16—Goose Creek reference section, showing approximately 80 m of rhyolite tephra deposits exposed in Goose Creek valley: sec. 31, T21S, R22E, Blue Hill 1:24,000 quadrangle, Idaho. Thicknesses of units are not drawn to scale.

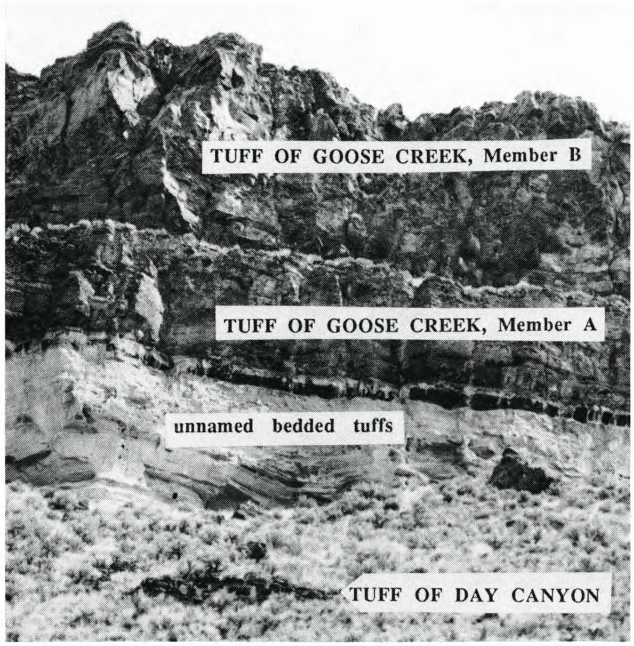

FIGURE 17—Goose Creek reference section.

by wind and water, as shown by the common presence of low-angle cross-strata and dunes. Isolated bedsets of coarser, less well-sorted, cross-stratified lapilli tuff are more difficult to interpret; they are either reworked tephra or primary surge deposits. When such units are interfingered with the bases of ignimbrites or have petrographic features similar to overlying ignimbrites, they are interpreted as ground-surge deposits.

FIGURE 18—Member A, tuff of Goose Creek, and underlying tephra deposits. The stratigraphic position of this photograph is given in Fig. 16. Meter stick for scale.

Welded rhyolitic ignimbrites are the most conspicuous and extensive deposits of the region, forming resistant cliffs that jut from scree slopes developed on bedded tuffs. Unwelded ignimbrites also occur, but are generally thinner and less laterally continuous. Phenocrysts of feldspar and pyroxene typically comprise 5–20% of the ignimbrites, and dense rhyolite lithic fragments up to 1 cm are common. Most units have well-developed basal vitrophyres, and strongly devitrified, massive to platy, internal zones with abundant spherulites and lithophysal cavities. Although the great thicknesses, dense welding, and large, abundant lithic fragments of the ignimbrites suggest nearby (perhaps several miles to tens of miles) source vents, the ash-fall deposits beneath the ignimbrites are both fine-grained and thin, suggesting that the Goose Creek area lay south of the dispersal axes for associated plinian-fall units.

Three welded ignimbrites are regionally important stratigraphic units (Fig. 16). The tuff of Day Canyon, the lowest unit exposed at this stop, is a densely welded, single-emplacement unit that is correlated with the ignimbrite noted at mileage 33.6. The massive, cliff-forming units at the top of the section are the tuff of Goose Creek, which is subdivided into two members. Member A is a regionally extensive, compound cooling unit that is correlative with ignimbrites in the Cassia Mountains to the west. It typically contains rheomorphic folds and platy jointing (mileage 48.4 and Stop 5B), and varies in thickness as a result of emplacement onto irregular topography. Member B has been dated at 8.5 Ma (sample 794A; Armstrong et al., 1975). **11.2**

46.9 Turn west (left) at Oakley dam turnoff, same location as at mileage 24.5. **0.7**

47.6 Cross bridge and turn left at junction. **0.5**

48.1 Take right fork and begin to climb hill. **0.3**

48.4 Note roadcut on right with spectacular exposure of rheomorphic folds in ignimbrite which is equivalent to the upper massive unit at Stop 5A. The folds are best seen when looking eastward (in direction opposite to your travel). We may stop if time allows. **0.3**

48.7 More exposures of rheomorphic folds in welded tuff. **0.7**

49.4 Rheomorphic folds in roadcut. **0.5**

49.9 Note view to northeast of Oakley Valley. The high peaks to the northwest are part of the Albion Range core complex. The low hills in the valley floor are underlain by ignimbrite. **0.3**

50.2 **STOP 5B. Rheomorphic folds in welded tuff; overview of stratigraphy.** Walk approximately 0.1 mi west along road to sharp curve, examining exposures along the way. Vehicles can turn around at the curve and pick up passengers there. At this stop we will examine the interval between members A and B of the tuff of Goose Creek, and rheomorphic features developed in both units. The stop also provides an overlook for discussion of regional stratigraphic relations.

The upper part of member A typically has platy jointing near the top, grading downward into a lithophysal zone, as can be seen below road. At this locality, the upper part of member A is unusually broken and folded; flow features are highlighted by red oxidized layers in the vitrophyre. The interval between members A and B is 3 m of tan, unwelded ignimbrite. Member B consists of a basal ground-surge deposit that is overlain by a thick, densely welded tuff with platy jointing and rheomorphic features throughout (Fig. 19).

From this vantage point we can look south along Goose Creek and west along Trapper Creek to see the regional extent of the units. The tuff of Goose Creek forms the conspicuous capping unit, and older ignimbrites are exposed in the bottom of Trapper Creek to west. Regional correlation of these units with extensive ignimbrites in Cassia Mountains to west has not yet been completed. The scree slopes between densely welded ignimbrites are developed on bedded air-fall tuffs from unknown sources. **0.1**

50.3 Turn around at curve and backtrack toward Oakley dam. **3.4**

53.7 Back at Oakley dam turnoff (mileage point 46.9), turn north (left) toward Oakley and Burley. **2.6**

56.3 Turn north (left) onto ID-27 in Oakley. For the first few miles north of Oakley, note escarpment located about 3 km to east. The welded-tuff sheets there are cut by several faults. This escarpment may be part of the eastern margin of a caldera (Fig. 15) from which the welded-tuff units noted at Stops 5A and 5B were erupted. If that escarpment is part of a caldera wall, then we are driving within the caldera, and the escarpment along northeast side of Cassia Mountains, visible about 10 km to east, might be the western wall. **7.7**

64.0 Pass The Knolls at this bend in highway. These hills are underlain by a northeastward-dipping rhyolite sheet (welded tuff?). This isolated exposure may be another point along the margin of a nearly buried caldera. Between here and Burley, three shield volcanoes can be seen to west and north in Snake River Plain. **14.2**

78.2 Cross intersection of ID-27, US-30 and I-84 in downtown Burley (same location as mileage 00.0), and continue north across Snake River on Overland Avenue. **2.1**

80.3 Cross over I-84, then turn right to go west on I-84 at exit 208 toward Twin Falls. **16.3**

96.6 Pass Hazelton Butte, a basalt shield volcano to south (left). **7.0**

103.6 Pass Skeleton Butte, a basalt shield volcano on north (right). **2.8**

106.4 Leave I-84 at exit 182, then turn south on ID-50 to head for Twin Falls. **1.1**

107.5 Cross Snake River canyon on Hansen Bridge. Slightly more than 100 m of basalt flows are exposed here. **0.4**

107.9 Turn west (right) onto Addison Avenue. **5.0**

112.9 Turn north (right) at intersection E 3000, N 3900, toward Shoshone Falls. **1.9**

114.8 Start down grade into Snake River canyon. The upper layers in canyon walls are basalt flows, and lower material is Shoshone Falls rhyolite. **1.1**

115.9 **STOP 5C. Rhyolite Lava Flow at Shoshone Falls Park: Massive interior of rhyolite lava flow; Shoshone Falls; Bonneville flood erosion.** Park in the main parking lot by the waterfall viewpoint. The Shoshone Falls rhyolite lava flow is exposed by Shoshone Falls (65 m high) and in adjacent canyon walls (Fig. 20). Note its massive interior, the sheeted and folded rocks at the top of the massive section, and the large lenses of breccia (Fig. 21) at the top of the flow. Particularly impressive is the large amount of breccia visible in northern wall of canyon, across river. Similar breccias are common at tops of many Snake River Plain rhyolite lava flows. However, this occurrence is especially thick and laterally extensive, and it shows little evidence that it was fused by heat from underlying lava, as is the case in many rhyolite lava flows. This flow may have run into standing water in ancient Lake Idaho (Jenks and Bonnichsen, 1987, and in press) when it was erupted about 6 Ma (Armstrong et al., 1975). Street and DeTar (1987) report that the Shoshone Falls rhyolite flow may be nearly 200 m thick near here, so only about the upper half is exposed at this point. Drilling indicates this flow lies above tuffaceous and oolitic sediments of prob-

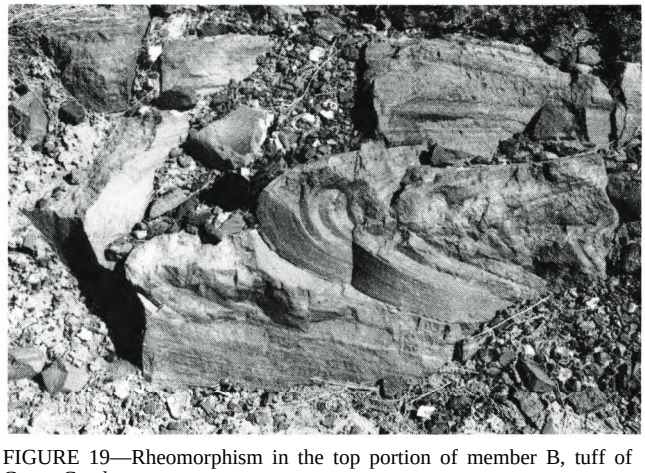

FIGURE 19—Rheomorphism in the top portion of member B, tuff of Goose Creek.

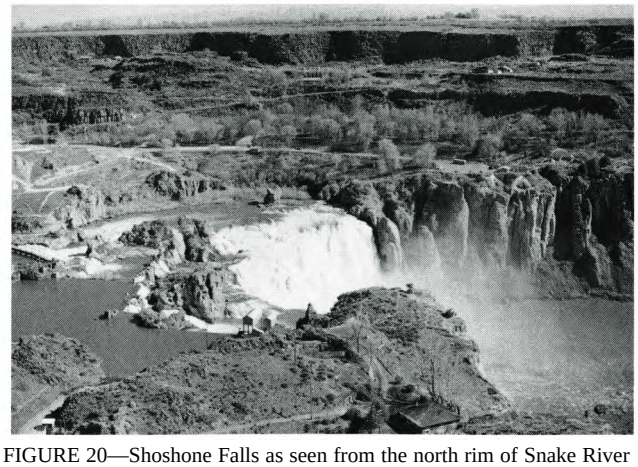

FIGURE 20—Shoshone Falls as seen from the north rim of Snake River canyon (Stop 5C). The waterfall plunges over the massive interior part of the Shoshone Falls rhyolite lava flow. Basalt flows form the upper canyon walls.

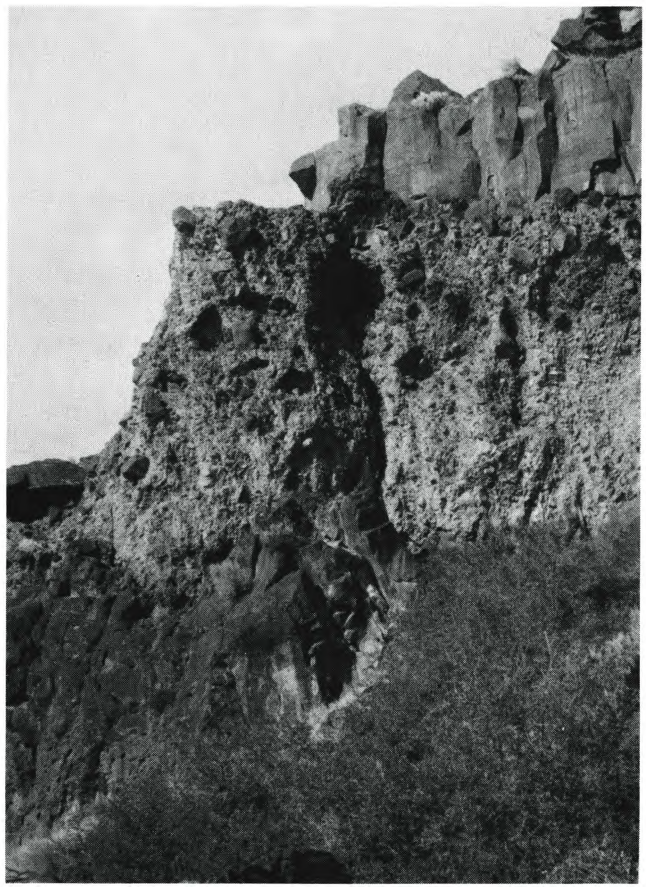

FIGURE 21-Breccia layer at top of Shoshone Falls rhyolite lava flow at Stop 5C.

able lacustrine origin, and these in turn lie on welded pyroclastic rocks similar to those exposed in Cassia Mountains a few kilometers to south. The chemical composition of Shoshone Falls rhyolite is listed in Table 2 and is typical of many rhyolite lava flows in the Snake River Plain volcanic province. The basalt flows that overlie the rhyolite have channels which were cut during the Bonneville flood. **3.0**

118.9 Back at same location as at mileage 112.9. Turn west (right) toward Twin Falls on Addison Avenue. **3.1**

122.0 Continue traveling west at junction with US-93 at intersection of Addison Avenue, Blue Lakes Boulevard, and Shoshone Street in Twin Falls. **5.9**

127.9 Turn south (left) on US-93 toward Jackpot. **14.5**

142.4 Pass through Hollister. As you drive south on US-93, the Cassia Mountains are visible to east (left). These hills are mainly composed of welded-tuff sheets that erupted from the region around Twin Falls, and possibly from the west. Locally, Paleozoic rocks are exposed beneath the welded-tuff units. Several basalt shield volcanoes are visible along this part of the route. **0.8**

143.2 Pass over top of a basalt shield at highway check station. **9.0**

152.2 Pass the south turnoff to Rogerson. As you travel south on US-93 from Rogerson to Jackpot, more welded-tuff units are visible on either side of the graben in which highway is located. The escarpment to east, 3–5 km away, is a continuation of Cassia Mountains. The Browns Bench escarpment, which was uplifted along a major fault, is visible 10–12 km to west, and contains many welded-tuff sheets. These sheets were erupted from the Snake River Plain region and probably include some from Bruneau–Jarbidge eruptive center several kilometers farther west. **12.0**

164.2 **STOP 5D. Low- and high-temperature pyroclastic flows: Contrast between L and H types of pyroclastic flows; fused top of air-fall ash; flow marks; flattened pumice clasts.** Stop along west (right) side of US-93 in large parking area across from long exposure of welded and bedded tuff. Examine exposures along highway and along old railroad grade west of highway. The upper part of this exposure is a vitrophyre layer 2–3 m thick (Fig. 22). This welded tuff was mapped by Earl Cook (Alief, 1962) as unit Tv2 (ignimbrite 2). The vitrophyre overlies 2 or 3 m of friable, layered, air-fall ash. The top of this ash layer was fused by heat from the overlying ignimbrite. The ash contains pumice-rich layers and lies on a tan, nearly structureless, nonwelded ash-flow tuff (Fig. 22) that resembles silt (was mistakenly interpreted as such in Bonnichsen et al., 1988).

Careful examination of the upper vitrophyre layer

TABLE 2-Chemical analyses of selected silicic and intermediate volcanic rocks from the Snake River Plain and vicinity. These rocks were analyzed by a combination of methods in several laboratories, and have been normalized to sums of 100%. Total iron is expressed as Fe_2O_3. Sample information: 1. Average of two analyses, Street and DeTar (1987). 2. Sample 1-459, Bonnichsen et al. (1988). 3. Sample X-37, Bonnichsen et al. (1988). 4. Sample 1-463, Bonnichsen and Citron (1982). 5. Sample 1-529, Bonnichsen et al. (1988). 6. Sample 1-15, Bonnichsen et al. (1988). 7. Sample L80-78, Honjo (1986). 8. Average of 12 analyses, Bonnichsen et al. (1988).

Unit	1. Shoshone Falls rhyolite	2. Cougar Point Tuff XV	3. Cougar Point Tuff XIII	4. Cougar Point Tuff XI	5. Dorsey Creek Rhyolite	6. Balanced Rock, upper unit	7. City of Rocks Tuff	8. Square Mountain ferrolatite
SiO_2	70.05	73.65	75.27	75.07	72.14	69.50	69.93	60.16
$A1_2O_3$	13.59	12.83	12.30	12.31	12.77	13.59	13.42	14.69
TiO_2	0.69	0.42	0.28	0.31	0.52	0.77	0.79	1.81
Fe_2O_3	4.67	3.06	2.40	2.38	4.24	4.78	4.63	9.29
MnO	0.07	0.05	0.04	0.02	0.07	0.07	0.07	0.13
CaO	1.90	1.40	0.81	0.84	1.64	2.28	2.34	5.10
MgO	0.69	0.50	0.23	0.12	0.39	0.83	0.84	1.93
K_2O	4.82	5.17	6.10	5.91	5.37	4.95	4.77	3.17
Na_2O	3.35	2.89	2.52	3.00	2.77	3.05	3.03	3.32
P_2O_5	0.17	0.06	0.04	0.03	0.09	0.16	0.17	0.40

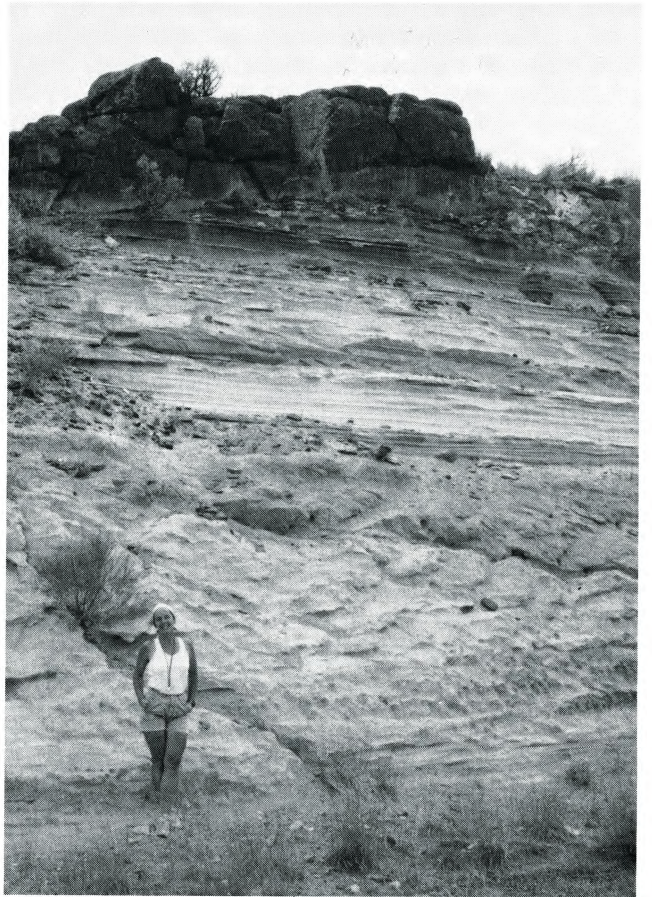

FIGURE 22—Silicic pyroclastic units at Stop 5D, showing the welded, glassy, type-H ignimbrite layer (top), overlying a laminated, ash-fall tuff layer, in turn lying on a massive, non-welded, type-L ignimbrite at base of exposure.

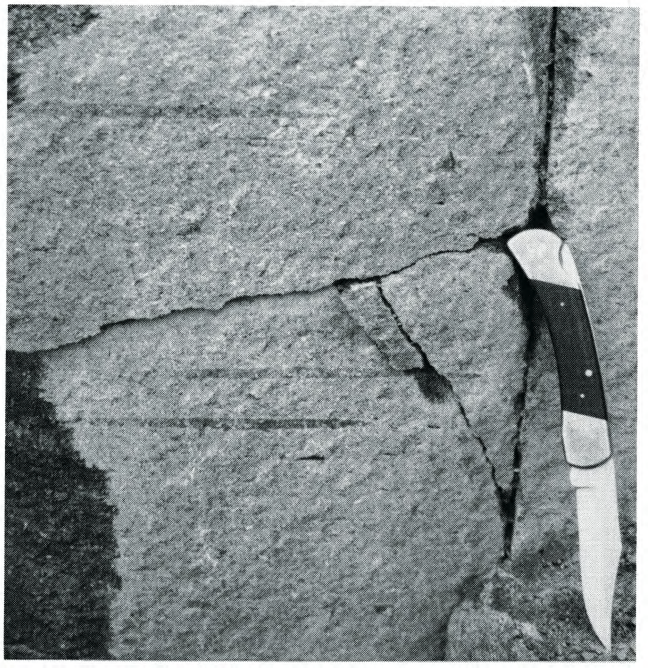

FIGURE 24—Flattened pumice clasts within the upper, glassy ignimbrite layer at Stop 5D.

reveals that it contains elongate vesicles and flow marks (Fig. 23), lensoidal inclusions (Fig. 24) that probably started as pumice clasts, and spherulites. The densely welded nature of this thin vitrophyre layer, the greatly flattened pumice inclusions and flow marks it contains, and the fusing of the underlying ash attest to the high temperature of the ignimbrite when it was emplaced. Its preservation as glass with only scattered spherulites indicates rapid cooling once it was in place, as would be expected for a layer this thin.

FIGURE 23—Elongate, flattened vesicles at Stop 5D, exposed on a subhorizontal surface in the glassy, type-H ignimbrite.

Subparallel streaks or flow marks (Fig. 23) and elongate vesicles are common in many of the high-temperature, welded-tuff units in the Snake River Plain volcanic province. These streaks vary considerably in appearance and size. They probably were gas cavities that became extremely stretched during flowage in the final stage of emplacement. The parallelism of the flow marks and stretched vesicles presumably reflects the direction the hot ash was flowing when it became capable of containing and preserving vesicles. These flow marks would be termed *primary* structures in the sense of Chapin and Lowell (1979) because they were formed during flowage away from the erupting source, rather than being *secondary* structures that formed later, during rheomorphism of the sheet. The flow marks and stretched vesicles in the upper vitrophyre layer of this exposure are subparallel to a N80W–S80E direction, suggesting that the ignimbrite source was to the west or northwest. Bonnichsen and Citron (1982) systematically measured flow marks within several other Cougar Point Tuff units and demonstrated their regional consistency within individual welded-tuff units (Fig. 25).

High-temperature (type H) welded-tuff sheets, as defined in this guide (Table 3), refer to those flows which became a layer of molten silicate liquid after eruption and during the final stage of emplacement, permitting the development, deformation, and preservation of gas bubbles. Medium-temperature (type M) welded-tuff sheets, on the other hand, lack liquid-state flowage features, such as elongate vesicles or flow marks, because their emplacement temper-

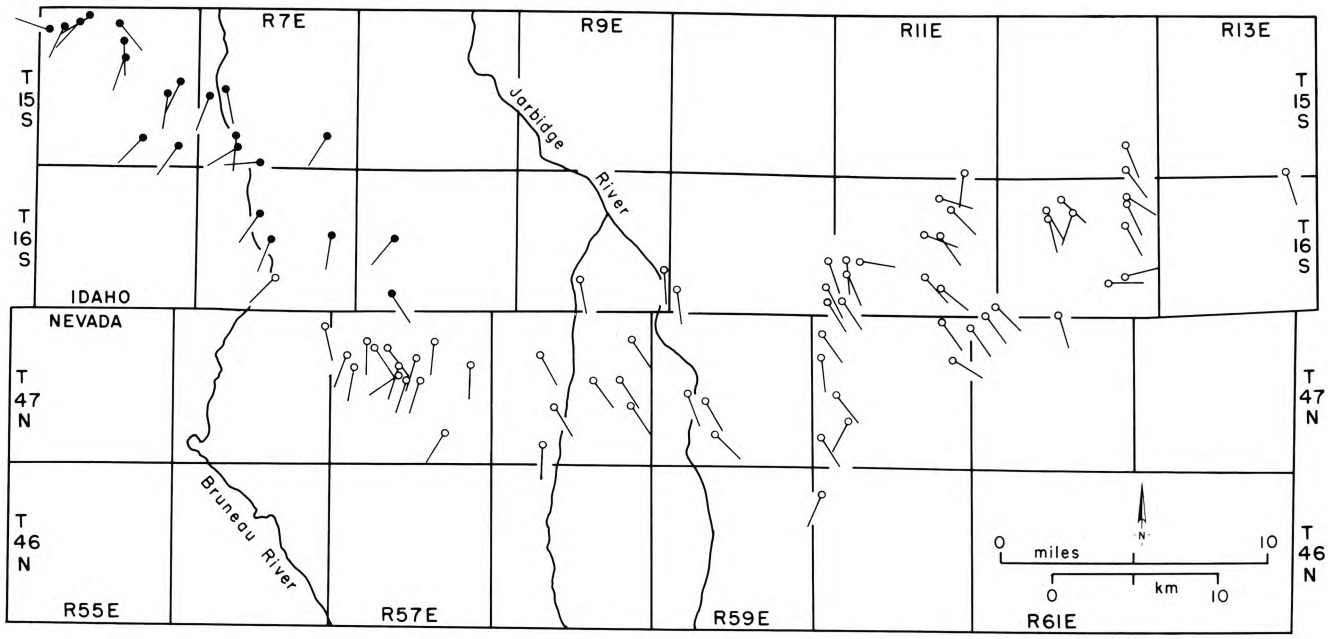

FIGURE 25—Regional distribution of flow azimuths, as measured from flow marks and elongate vesicles in Cougar Point Tuff units XV (solid symbols) and XIII (open symbols). The tails on the symbols indicate the inferred directions of flow away from the Bruneau–Jarbidge eruptive center. From Bonnichsen and Citron (1982).

TABLE 3—Ash-flow tuff types based on emplacement temperatures.

Low temperature (Type L) Up to 650°C	Medium temperature (Type M) 550–850°C	High temperature (Type H) 750–1050°C	Very high temperature (Type V) 950–1200+°C
Ash-flow tuff sheets are not welded and show only modest amounts of compaction.	Welded and densely compacted but lacking liquid-state flowage features.	Thoroughly welded and compacted, with restricted-size liquid-state flowage features.	The entire ash-flow tuff sheet may have undergone en-masse liquid-state flowage.
After emplacement, the ash-flow tuff does not revert to a silicate liquid. ←		→	After emplacement, the ash-flow tuff reverts to a mass of silicate liquid that can flow.

atures were too low for the ash to coalesce to a mass of silicate liquid. This distinction between high- and medium-temperature welded-tuff sheets, based on the presence or absence of features suggesting coalescence to a viscous liquid similar to that in a rhyolite lava flow before primary forward motion ceased, is similar to the presence or absence of Chapin and Lowell's (1979) primary welding, which occurs before primary forward motion ceases. Low-temperature (type L) pyroclastic flows were so cool that they did not weld significantly. Although precise temperature ranges have not been established, the transition between the H and M types is probably in the 750–850°C range, and the transition between the M and L types may be in the 550–650°C range. In this exposure, the upper vitrophyre, with its flow marks and dense welding, would be a type-H ignimbrite by the classification given in Table 3, whereas the lower, nonwelded pyroclastic flow would be a type-L ignimbrite. Perhaps the Walcott Tuff, which was viewed at Stop 4E, is a good example of a type-M ash flow, and the upper rhyolite sheet at Balanced Rock, to be viewed at Stop 7A, is an example of a type-V ignimbrite. **5.8**

170.0 Idaho–Nevada state line, about 1 mi north of Jackpot.

Day 6: The Bruneau—Jarbidge eruptive center

Bill Bonnichsen and Margaret D. Jenks

Bruneau—Jarbidge eruptive center

The Bruneau—Jarbidge eruptive center is a 95 x 55 km structural basin within the southwestern part of the Snake River Plain (Fig. 15). During the late Miocene, a sequence of 11 or more welded, ash-flow-tuff cooling units (the Cougar Point Tuff), 12 or more large rhyolite lava flows, and a series of olivine tholeiite basalt flows from more than 40 shield volcanoes were erupted from, and filled in, this basin. The Bruneau—Jarbidge eruptive center does not now have the physiographic form of a caldera, but it may contain one or more buried calderas. Most of the subsidence of its interior occurred between 11 and 10 Ma, during or just after

the eruption of the Cougar Point Tuff (Bonnichsen, 1982a).

Along its southern margin, the boundary zone of the eruptive center is outlined by a combination of down-to-thenorth faults of small displacement, a moat zone a few kilometers across filled with sediments and basalt, and the lateral transition from older, welded ash-flow tuffs on the south to younger rhyolite lava flows on the north. The eastern and northern margins of the eruptive center are buried beneath younger geologic units, primarily basalt flows. The boundaries of the eruptive center have been partially defined on the basis of aeromagnetic anomalies (Bonnichsen, 1982a).

The Cougar Point Tuff

The Cougar Point Tuff is a sequence of densely welded, rhyolitic ash-flow-tuff cooling units that erupted from the Bruneau—Jarbidge eruptive center during late Miocene time. The Cougar Point Tuff is best exposed in canyons of the Bruneau River and the East and West Forks of the Jarbidge River near the Idaho—Nevada state line. At the Black Rock escarpment reference section (Bonnichsen and Citron, 1982) in Bruneau Canyon, eight units are exposed and have an aggregate thickness of 400-475 m. At Cougar Point in the East Fork of Jarbidge Canyon, about 8 km south of Stop 6B , six of the units are exposed with a thickness of about 250 m. The Cougar Point Tuff units that are present in the East and West Forks of Jarbidge River canyon are indicated in Table 4.

By the end of the Cougar Point Tuff volcanism, the eruptive center had developed into a large structural and physiographic basin, which was filled by later volcanic and sedimentary deposits. The exposed part of the Cougar Point Tuff consists of outflow-facies rocks that extend beyond the margins of the eruptive center. The emplacement of each unit was a distinct volcanic event, and the units are separated by sedimentary layers. Four or more reversals of the earth's magnetic field occurred during the deposition of the Cougar Point Tuff (Bonnichsen, 1982a).

In general, each of the Cougar Point Tuff units is similar to the others in appearance and welding characteristics. Commonly, the units were formed by multiple ash emplacements, but are simple cooling units. In a vertical section through a unit, the typical zones from base to top consist of: (1) a basal layer of thinly bedded air-fall ash; (2) an overlying, basal vitrophyre layer; (3) a massive, relatively thick, devitrified central zone in which most early structures have been obliterated by matrix crystallization; and (4) an upper zone with abundant flow marks and folds.

The various Cougar Point Tuff units are similar in composition and in their temperature and mode of eruption. Quartz, sanidine, plagioclase, augite, pigeonite, fayalite, and Fe—Ti oxides are the principal phenocryst minerals. Hornblende and biotite are essentially absent, suggesting that the magmas were relatively hot and dry. Magma-temperature estimates based on the compositions of coexisting pyroxenes, feldspars, and Fe—Ti oxides suggest eruption temperatures for the Cougar Point Tuff units in the 8001000°C range (Table 5; and Honjo et al. , 1987, and in prep.). Applying the emplacement-temperature classification noted in Table 3, most of the Cougar Point Tuff units would be in the type-H category.

Chemical analyses of samples taken many kilometers apart reveal that each unit has a relatively narrow compositional range. Representative analyses from three units (XI, XIII, and XV) are shown in Table 2. Overall, the Cougar Point Tuff becomes increasingly femic upwards, but local reversals in the trend exist. A K—Ar age of 11.3 Ma was reported for one of the lower Cougar Point Tuff units. Initial strontium-isotope ratios indicate a predominantly, if not exclusively, crustal origin for the Cougar Point Tuff (Bonnichsen and Citron, 1982). This is the case for many other rhyolitic units in the Snake River Plain volcanic province.

TABLE 4—Stratigraphy of volcanic units exposed in and near the East and West Forks of the Jarbidge River canyon. Units are listed in order of increasing age. Magnetic polarity data from Bonnichsen (1982a). References for discussion of units and their area are: 1, Bonnichsen (1982b); 2, Bonnichsen and Citron (1982); 3, Bonnichsen and Jenks (in press); 4, Bonnichsen and Kauffman (1987); 5, Bonnichsen et al. (1988); 6, Coats (1964); 7, Hart and Aronson (1983).

Unit	Age (Ma)	Magnetic polarity	References
basalt of Big Flat	—	—	3
upper sediments	—	—	3
Diamond A basalt	—	—	3
lower sediments	—	—	3
Dorsey Creek Rhyolite	8.0, 8.22	normal	1, 3, 4, 5, 7
Columbet Creek basalt	—	reverse	3
Cougar Point Tuff: unit XV	—	normal	2, 5
unit XIII	—	normal	2
unit XII	—	normal	2
unit XI	—	reverse	2
unit X	—	—	2
unit IX	—	normal	2
unit VII	11.3	reverse	2
unit V	—	normal	2
Jenny Creek tuff	—	—	6
Jarbidge Rhyolite	17.2	—	6

Rhyolite lava flows

Of the 12 or so rhyolite lava flows that occur in the Bruneau—Jarbidge eruptive center, the only one that is exposed in the East or West Forks of the Jarbidge River canyon is the Dorsey Creek Rhyolite. It is described in more detail at Stop 6D and will be the only one visited during this day of the trip.

The rhyolite lava flows in the Snake River Plain volcanic province show variations in their thicknesses and in the types of internal structures that occur in their interiors and margins. A generalized longitudinal section from the vent area to the margin of an idealized flow is shown in Fig. 26. Rhyolite lava-flow interiors generally have three zones: a thick central zone of massive devitrified rhyolite, which overlies a complex basal zone and is capped by a structurally complicated upper zone. The basal zones consist of either massive vitrophyre layers or of breccia layers, or of a combination of both materials. Air-fall ash layers are uncommon below the rhyolite lava flows. The upper zones generally contain both glassy and devitrified portions and consist of massive, sheeted, folded, flow-layered, and brecciated rhyolite. All of the zones, but especially the upper ones, contain gas cavities of widely varying dimensions and abundance.

Flow margins typically consist of bulbous lobes of massive or sheeted rhyolite overlying basal breccia layers and separated by chaotic-appearing zones of steeply jointed or flow-layered rhyolite. The thicknesses of the interior portions of the flows typically are 50 m or more, and range up to 250 m. The flows are thinner near their margins, but seldom thin to less than 25 m (Bonnichsen, 1982b; Bonnichsen and Kauffman, 1987).

TABLE 5—Eruption temperatures of selected silicic volcanic units from the central Snake River Plain as determined by pyroxene geothermometry. [1]Temperatures in degrees Celsius from Honjo et al. (in prep.), calculated by method of Lindsley (1983). [2]Temperatures in degrees Celsius from Honjo et al. (in prep.), calculated by method of Davidson and Lindsley (1985). [3]SiO_2 with H_2O-free rock analysis normalized to 100%.

Unit	Sample	Temp.[1]	Temp.[2]	SiO_2[3]
Units associated with the Bruneau–Jarbidge eruptive center				
Cougar Point Tuff:				
Unit XV	1-783	910	900	72.7
Unit XIII	X-37	—	750	75.3
Unit XII	X-20	980	970	73.1
Unit XI	1-794	850	860	76.4
Unit XI	X-174	900	880	75.5
Unit VII	I-841	935	930	72.9
Rhyolite lava flows:				
Sheep Creek Rhyolite	I-1208	980	950	70.2
Crows Nest area rhyolite	I-1265	950	990	71.1
Bruneau Jasper Rhyolite	1-1052	900	910	74.7
Units associated with the Magic Reservoir eruptive center				
Idavada ignimbrites:				
Picabo-B Tuff	L80-30	1000	950	72.0
Gwin Springs Tuff	L80-64	1000	990	72.2
City of Rocks Tuff	L80-78	1000	970	69.9
Rhyolite lava flow:				
Magic Reservoir quartz latite	—	1030	990	69.2

Road log

This day of the trip will be led by Bill Bonnichsen. We will examine: (A) an example of primary flowage in a high-temperature ash-flow-tuff unit, (B) a panoramic view of the boundary zone between the Snake River Plain and the Basin and Range province, (C) Unit XV of the Cougar Point Tuff and the margin of the Bruneau—Jarbidge eruptive center, (D) the margin and interior of the Dorsey Creek Rhyolite lava flow, (E) a lithophysal zone in unit XIII of the Cougar Point Tuff, (F) the basal portion of unit XI of the Cougar Point Tuff, and (G) the Jarbidge Rhyolite. The route will follow the southern margin of the Snake River Plain and of the Bruneau—Jarbidge eruptive center. Basalt shields and other basalt volcanoes can be seen at the margin and in the interior of the Plain. Also visible is the transition from the plateau type of terrain that characterizes the Snake River Plain to the block-faulted mountain ranges in the Basin and Range province to the south. During the latter part of the day, we will drive along the bottom of Jarbidge Canyon, where the welded-tuff units are well exposed. Finally, we will visit the historic gold-mining town of Jarbidge, where the Jarbidge Rhyolite is exposed.

Mileage

00.0 Proceed north toward Rogerson on US-93 from the Idaho–Nevada state line, about 1 mi north of Jackpot. **17.8**

17.8 Turn left (west) at the service station at the south side of Rogerson and proceed through town. **0.1**

17.9 In town, turn left (west) on paved road toward Murphy Hot Springs and Jarbidge. Between Rogerson and Salmon dam several basalt shield volcanoes can be seen to the north. While driving the first few miles west from Rogerson, Salmon Butte is located straight ahead; it is the youngest basalt volcano in this part of the Snake River Plain, and probably is Pleistocene in age. It is situated near the intersection of the large fault along base of Browns Bench escarpment and the southern margin of the Snake River Plain. **7.7**

25.6 Cross Salmon dam. Here, basalt flows from Salmon Butte (the basalt with plagioclase glomerophenocrysts) partially filled a canyon that had been cut in older basalt and rhyolite units. Scattered rhyolite exposures, where the pre-Salmon Butte basalt canyon wall has been exhumed, are visible at west side of canyon. **5.9**

31.5 At this hill the road crosses a small basalt volcano. Inward-dipping basalt dikes separate dissimilar sections of sediments and basaltic tuff in the roadcut.

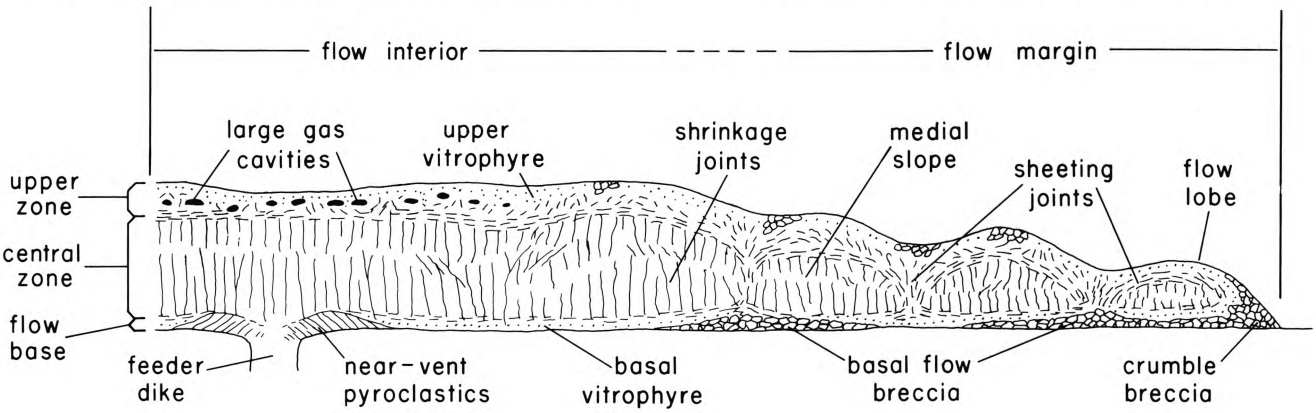

FIGURE 26—Schematic longitudinal section of an idealized southwestern Idaho rhyolite lava flow, showing internal zones and typical physical features. The vertical scale and the size of some features have been exaggerated. From Bonnichsen (1982b).

These dikes extend southeastward about 300 m. These features form a small crater that was partially filled by crossbedded, basaltic, glassy cinders and ash, and by sediments deposited during and after the final stage of the eruption. Ahead, on right (north of road) as you leave the small crater, is Cedar Creek Reservoir. Northwest of it is Cedar Butte, one of the more prominent basalt shield volcanoes in this part of the Snake River Plain.

Along this stretch of the drive, a topographic break is visible 2–4 km to the south. Beyond this break, where the land slopes more steeply to the north, are welded Cougar Point Tuff units that were erupted from the Snake River Plain. On this side of the break the rock units are more nearly horizontal rhyolite and basalt lava flows that fill the subsided zone from which the ash flows erupted. **3.4**

34.9 Cross Cedar Creek. Exposures of the upper part of a rhyolite lava flow are visible near here. **0.4**

35.3 Start up grade west of Cedar Creek where basalt flows and fine-grained sediments are exposed. After reaching top of grade the road travels on Bud Lewis Hill basalt flow for several kilometers. This flow was erupted from the Hill 5991 (elevation) volcano, which shows less than 15 m of relief and is located to south (visible from near Stop 6A). **4.7**

40.0 **STOP 6A. Primary flowage in welded-tuff sheet near House Creek Ranch: Stretched vesicles; flow marks; axiolites; boundary between vitrophyre and devitrified rhyolite.** Park at turnoff on left (southeast) side of road (opposite large pit excavated in sediments) and walk northeast about 250 m to a quarry located on southeast side of road. This thin, welded-tuff sheet contains numerous well-developed flow marks (Fig. 27); relatively large stretched vesicles; various small-scale flowage features; and very elongate axiolites (Fig. 28) concentrated along the boundary between the basal vitrophyre and the overlying devitrified zone. The flow marks, stretched vesicles, and axiolites have an average azimuth of N5W. These elongate features are similar to those noted at Stop 5D, but are much more abundant. Their presence suggests that this unit belongs in the type-H welded-tuff category, as indicated in Table 3. As at Stop 5D, these elongation features probably indicate the direction of final flowage and are considered to be primary structures in the sense of Chapin and Lowell (1979). A basalt dike–vent, discussed at mileage 40.2, is visible about 500 m west of the stop. **0.2**

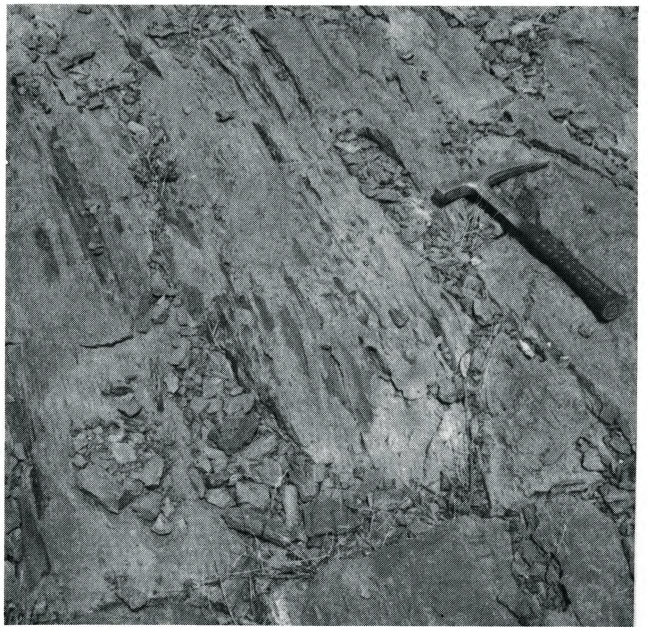

FIGURE 27—Flow marks developed on a subhorizontal surface in the type-H ignimbrite at Stop 6A.

FIGURE 28—Axiolites developed in the boundary zone between basal vitrophyre and devitrified interior of the type-H ignimbrite at Stop 6A. Note the star-shaped (in cross section), elongate cavities in the axiolites.

40.2 Pass two parts of a basalt dike cutting white bedded ash on north side of road. This dike fed the small basalt volcano, Hill 5822 (elevation), located 100–200 m north of the road, from which an unnamed basalt flow erupted. This feeder dike has been traced along the earth's surface for more than 1 km. The Hill 5822 vent is only about 15 m high, but the basalt flow from it extends nearly 1 km northward. This dike–vent is one of several similar tiny volcanoes located in this area. They are within the boundary zone between the downdropped Snake River Plain to the north and the highland area to the south, and may be associated with major, buried, plain-margin faults. **1.4**

41.6 Cross House Creek and pass ranch entrance. **0.8**

42.4 Pass junction with Roseworth–Castleford road on north (right). The hill about 3 km north of this junction is Signal Butte, another basalt shield. About here the road enters the Bruneau–Jarbidge eruptive center. The eastern marginal zone of the eruptive center (Bonnichsen, 1982a) passes through Signal Butte and Marshall Butte, another prominent basalt shield located farther north. From here on westward to the Murphy Hot Springs area, we will be driving within the eruptive center, but near its southeastern margin (Fig. 15). **2.1**

44.5 Another basalt dike cuts sediments and silicic ash beds on north (right) side of road. This dike fed a small volcano about 200 m to north, which erupted basalt lava that flowed northward. **4.1**

48.6 At this point, and extending westward for 1 km (0.7 mi), a section of sediments is exposed along the grade down to Mud Flat Draw. Here, gravel caps a section of sandy and silty material which, in turn, lies on bedded tuff. This gravel, which extends northward for many miles, probably was eroded during the uplift of Elk Mountain, 10–15 km to the south. Similar, generally post-rhyolite and pre- and post-basalt, sequences of sediments occur at other places along the southern margin of the Snake River Plain. West of the grade, several additional exposures of bedded, white, silicic ash are visible beside road. **3.5**

52.1 The Three Creek Rhyolite lava flow is exposed here, forming rim on west side of Three Creek valley. The flow at this exposure is nearly as thin as any rhyolite lava flow within the Snake River Plain. It is markedly flow-layered, contains numerous spherulites, has breccia at its base, and lies on approximately a foot of air-fall ash. This flow has an estimated minimum volume of 10 km^3 (Bonnichsen, 1982b) and underlies an area measuring 17 km from southeast to northwest in the southeastern part of the eruptive center (Citron, 1976). **7.2**

59.3 The road goes over a rise on north flank of Horse Hill. Horse Hill is a basalt shield volcano from which part of the basalt of Big Flat (Bonnichsen and Jenks, in press) was erupted and flowed northward. Its top, complete with a loess-filled crater, is located about 0.8 km to the south. We will see the basalt of Big Flat again at Stop 6B, where it forms the eastern rim of Jarbidge Canyon. **4.1**

63.4 Hill 5981 (elevation), about 0.8 km southeast of road, was another source of the basalt of Big Flat. The Jarbidge Mountains appear ahead and slightly to left along road from Horse Hill to Jarbidge Canyon. The Matterhorn, at an elevation of 3305 m, is the highest peak. These mountains are composed primarily of Jarbidge Rhyolite (Schrader, 1923; Coats, 1964, 1987) and were uplifted along the northeast-trending fault set which merges into faults that bound the east side of Browns Bench escarpment, which we viewed previously. **0.6**

64.0 **STOP 6B. Panoramic view from rim of Jarbidge Canyon: Snake River Plain to Basin and Range province transition; canyon-rim basalt.** Stop at the rim of Jarbidge Canyon in order to get an overview of geographic and geologic features near here. From the top of Murphy Hot Springs grade at rim of Jarbidge Canyon some interesting topographic features are visible (Fig. 29). In a clockwise order, beginning to south-southwest, are: A glacial cirque (called the crater by some of the locals) on the north end of Jarbidge Mountain (south-southwest); Bear Paw Mountain (west-southwest); Wilkins Island, the tableland between the East and West Forks of Jarbidge Canyon (southwest to west); the Black Rock hill basalt shield volcano (west-northwest, in the distance); the Diamond A Desert which is the tableland between Bruneau Canyon on the west and Jarbidge Canyon on the east (west to northwest); the Poison Butte basalt shield volcano (northwest); the Inside Desert which is the tableland laying east of Jarbidge Canyon (north); several other basalt shield volcanoes including Middle Butte, Juniper Butte, Pence Butte, and Horse Hill (north and northeast); Hill 5981, one of the basalt of Big Flat sources (east-northeast); Elk Mountain (east-southeast); Cougar Point on the East Fork of Jarbidge Canyon (south-southeast); and Biroth Ridge, which is capped by the Cougar Point Tuff, beyond Cougar Point (south-southeast).

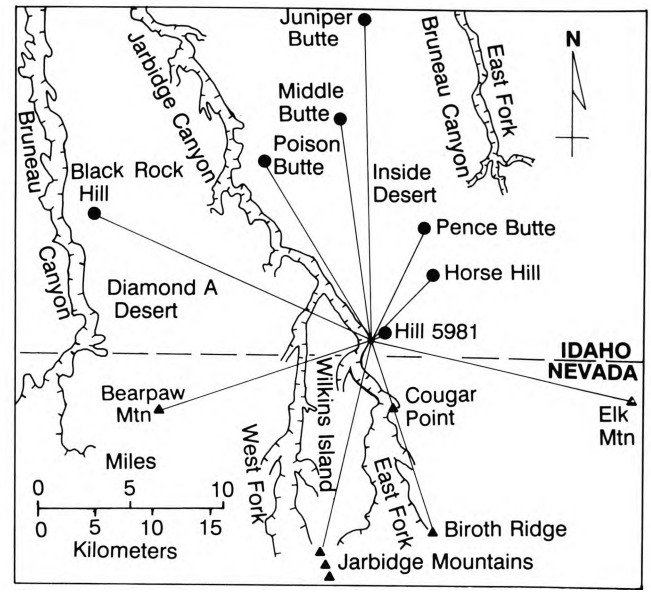

FIGURE 29—Star diagram showing the directions and locations of various features visible from Stop 6B.

The rim basalt on the east side of the canyon is basalt of Big Flat which was erupted from Horse Hill, Hill 5981, and perhaps other sources to the east. In the west canyon wall, across from this location, is a thick accumulation of sediments overlying Cougar Point Tuff. These sediments were deposited in the moat zone of the Bruneau–Jarbidge eruptive center; they thin both to south and to north. They vary from largely gravel in the upper part to a mixture of silt and volcanic ash in the lower part. These sediments are exposed along the Murphy Hot Springs grade. As we drive down the grade, prominent rock ledges across the canyon that dip gently northward are some of the Cougar Point Tuff units. **1.4**

65.4 **STOP 6C. Top of Cougar Point Tuff unit XV and eruptive-center margin: Small spherulites; accretionary lapilli; margin of Dorsey Creek Rhyolite.** Get out of vehicles at this location and walk the last kilometer down the grade to examine Cougar Point Tuff unit XV. Rejoin vehicles at bottom of grade near Murphy Hot Springs store. The exposures of unit XV in Jarbidge Canyon are the thin distal facies of the ash flow. Here, the unit is almost entirely glass, with small spherulites (Fig. 30) as the only sign of devitrification, indicating that the unit cooled rapidly after emplacement. At the very top of unit XV, an upward transition from quite hard, strongly welded ash to weakly fused ash that easily can be crushed by hand is exposed over a vertical distance of about 0.5 m. Near bottom of the canyon the next oldest welded-tuff unit (unit

FIGURE 30—Small spherulites enclosed within vitrophyre of Cougar Point Tuff unit XV, where the unit is only a few meters thick at Stop 6C, near Murphy Hot Springs.

XIII) is also visible. It is much thicker and almost completely devitrified. Along road on west side of canyon, the entire thickness of unit XV is visible (Fig. 31), including a section of air-fall ash below the ignimbrite that contains a 3 cm thick accretionary lapilli layer. From this west-side locality is an excellent view of the blunt edge of the Dorsey Creek Rhyolite lava flow.

In Bruneau Canyon, about 24 km west of this stop, unit XV ranges from 30 to nearly 100 m in thickness, where it is proximal to its buried source.

FIGURE 31—Cougar Point Tuff unit XV where its entire thickness is exposed on the west side of Jarbidge Canyon at Stop 6C. Note the thin layer of accretionary lapilli within the section of air-fall tuff beneath the welded tuff.

In that area the basal zone contains abundant, greatly flattened pumice fragments, but such fragments have not been observed in the more distal areas such as here in Jarbidge Canyon. The phenocryst minerals found in unit XV are plagioclase, sanidine, quartz, augite, pigeonite (proximal areas), fayalite (distal areas), and Fe–Ti oxides (Bonnichsen and Citron, 1982). Plagioclase is considerably more abundant than either quartz or sanidine. Phenocrysts are much more abundant in proximal portions of this unit than they are in distal parts. An analysis of one sample from unit XV is included in Table 2. This unit is one of the more femic of Cougar Point Tuff units. Unit XV is characterized by normal paleomagnetic polarity (Table 4) and had an eruption temperature of approximately 900°C (Table 5).

At this location the Cougar Point Tuff is overridden by the end of the Dorsey Creek Rhyolite. This relationship, along with the significant thickness of moat-zone sediments and the hot spring, are all related to the margin of the Bruneau–Jarbidge eruptive center (Fig. 32). Bonnichsen (1982a) proposed that the hot spring marks the location of a covered, post-Cougar Point Tuff and pre-Dorsey Creek Rhyolite fault within the boundary zone of the eruptive center. **0.7**

66.1 Murphy Hot Springs store. If time permits, cross Jarbidge River and climb about 0.4 km up grade on west side in order to see additional features in unit XV. **2.0**

68.1 **STOP 6D. Dorsey Creek Rhyolite lava flow: Basal breccia; sheeting joints; flow lobes; internal structures.** Here, the base of Dorsey Creek Rhyolite is well exposed. Examine this locality, then walk 0.3 mi northwest in order to examine internal features in the flow along the way. Park vehicles in large lot where East and West Forks of Jarbidge River join. The base of the Dorsey Creek Rhyolite lava flow consists of a breccia of glassy blocks in a matrix of ashy material (Fig. 33). Baked soil or silt is present beneath the flow, but no air-fall ash

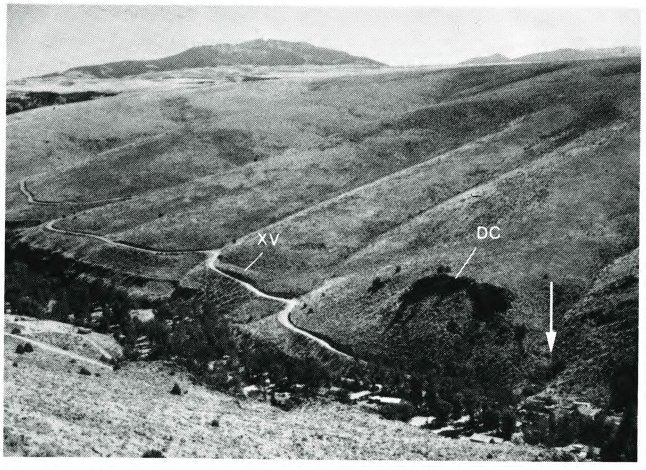

FIGURE 32—View from east rim of Jarbidge Canyon in Murphy Hot Springs area (Stop 6C). The southern end of Dorsey Creek Rhyolite (DC) is the prominent rock outcrop on right. Small exposures of the upper Cougar Point Tuff unit (XV) occur upstream. A deep-seated fault is inferred to occur at the margin of the Bruneau–Jarbidge eruptive center beneath the end of the Dorsey Creek Rhyolite, where the hot spring is located (below arrow).

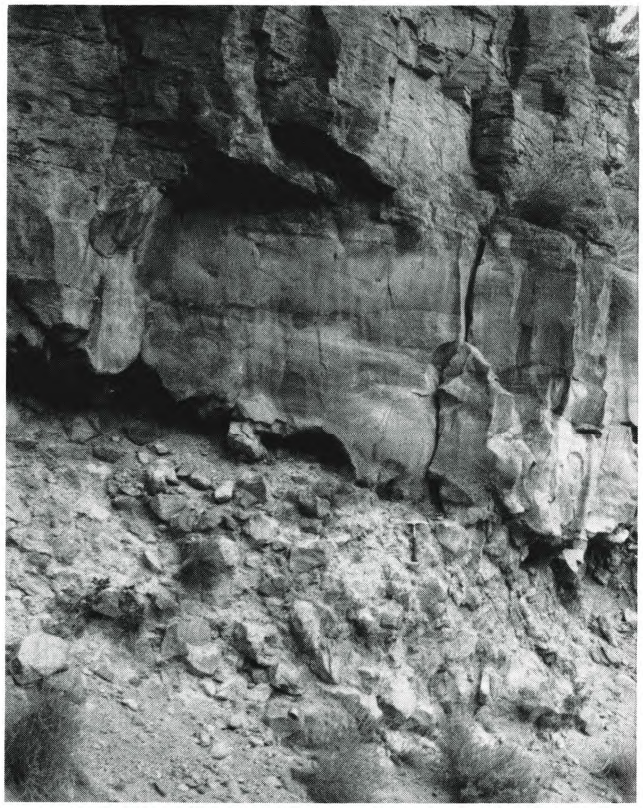

FIGURE 33—The base of Dorsey Creek Rhyolite lava flow at Stop 6D, near confluence of East and West Forks of Jarbidge River. The flow base consists of a breccia layer about 2 m thick, overlain by vitrophyre and then devitrified rhyolite.

can be seen. Well-developed sheeting joints and other features in the central zone of the flow are well exposed near the confluence of the East and West Forks, and the flow thins markedly southward toward its margin (Figs. 32, 34). Farther north in Jarbidge Canyon the flow becomes very massive (Fig. 35) and at places exceeds 200 m in thickness.

The Dorsey Creek Rhyolite is well exposed in Jarbidge Canyon, from Murphy Hot Springs to near confluence of Bruneau and Jarbidge Rivers, 40 km to northwest. This flow contains at least 75 km^3 of rhyolite and is one of the largest in southwestern Idaho (Bonnichsen, 1982b). The Dorsey Creek is one of the youngest rhyolite lava flows in Bruneau–Jarbidge eruptive center, with an age of between 8.0 and 8.22 Ma (Hart and Aronson, 1983).

The composition of a Dorsey Creek Rhyolite sample is given in Table 2. This analysis is from the more femic southern part of the flow. Generally, this flow contains phenocrysts of quartz, plagioclase, augite, pigeonite, and Fe–Ti oxides (Bonnichsen, 1982b). Its initial Sr-isotope ratio, which is 0.712, suggests that the unit was derived by fusion of crustal materials (Bonnichsen and Citron, 1982). **0.3**

68.4 Large parking lot at confluence of East and West Forks of Jarbidge River. When leaving, turn south (right) and follow road up the West Fork toward town of Jarbidge. **1.0**

69.4 Pass south end of Dorsey Creek Rhyolite flow (Fig. 34). Between this point and the mouth of Buck Creek, a thick section of sediments occurs in canyon walls beneath the rim basalt. This is part of the sediment-filled moat zone along margin of the eruptive center. **1.9**

FIGURE 34—Looking southwest, up West Fork of Jarbidge River canyon, from canyon rim above Stop 6D at confluence of East and West Forks of the river. In the foreground are exposures of Dorsey Creek Rhyolite. In distance, exposed in canyon walls, are sediments that fill the moat zone of Bruneau—Jarbidge eruptive center. The sediments are capped by basalt of Diamond A Desert.

71.3 Pass a small exposure of unit XV that is visible west of the stream. **0.4**

71.7 **STOP 6E. Cougar Point Tuff unit XIII at Buck Creek: View of Cougar Point Tuff units; lithophysal zone in unit XIII.** Park near road junction and walk up hill to rock knob located west of Jarbidge River and south of Buck Creek. Unit XIII is one of the most widespread of the Cougar Point Tuff units. At this locality we are near the center of its zone of distribution along the southern margin of Bruneau–Jarbidge eruptive center, where the unit is thickest. The unit contains a zone, about 2 m thick, of lithophysal rock (Fig. 36), located about two-thirds of the way up from base of the unit. This lithophysal zone has been traced for most of the distance that the unit follows along the eruptive-center margin, about 50 km, and probably represents a boundary between major emplacements of the unit. Unit XIII is one of the most salic of the

FIGURE 35—Massive interior of Dorsey Creek Rhyolite lava flow in Jarbidge Canyon near mouth of Columbet Creek, about 3 km northwest of Stop 6D.

FIGURE 36—Lithophysal zone within Cougar Point Tuff unit XIII at Stop 6E, near mouth of Buck Creek.

Cougar Point Tuff units; a typical chemical analysis is given in Table 2. It contains phenocrysts of quartz, sanidine, plagioclase, augite, pigeonite, fayalite, Fe–Ti oxides, tiny zircons, and very sparse hematized biotite flakes (Bonnichsen and Citron, 1982, and unpubl. data). Unit XIII is characterized by normal paleomagnetic polarity (Table 4).

From this location looking southward, several welded-tuff sheets that constitute the Cougar Point Tuff are visible (Fig. 37). Note that these units dip shallowly toward the eruptive-center boundary, located just to north beneath moat-zone sediments, whereas they are more nearly horizontal south of here. **0.8**

72.5 Cross Idaho–Nevada state line. **0.6**

73.1 **STOP 6F. Cougar Point Tuff unit XI in Jarbidge Canyon: Basal vitrophyre; lithophysal zone near boundary between successive emplacements.** Park alongside road and climb slope (Warning: the talus here is very loose!) on east (left) side of canyon up to base of cliff. Unit XI is one of the most widespread and voluminous of the Cougar Point Tuff units. In both Jarbidge and Bruneau Canyons it approaches 100 m in thickness. At this locality it can be seen to consist of several emplacements. Most notable is the thick, massive, lower emplacement, overlain by a layer of porous lithophysal rhyolite (Fig. 38). The basal vitrophyre is well exposed at this locality. It contains several large spherulites, but otherwise is a typical basal vitrophyre zone for a Cougar Point Tuff unit. An analysis is included in Table 2. The phenocryst minerals in unit XI include quartz, plagioclase, sanidine, pigeonite, augite, and Fe–Ti oxides (Bonnichsen and Citron, 1982). Unit XI is characterized by reversed paleomagnetic polarity (Table 4) and had eruption temperatures estimated in the 850–900°C range (Table 5). **4.1**

77.2 Pass Deer Creek grade road. This grade provides good access to Cougar Point Tuff units VII, IX, XI, XII, and XIII. **1.8**

79.0 Cross Jack Creek. **1.4**

80.4 Pass road to Mahoney Ranger Station. **0.3**

80.7 **STOP 6G. Jarbidge Rhyolite: Alteration; quartz phenocrysts.** Park alongside road and inspect Jarbidge Rhyolite exposure to east. The Jarbidge Rhyolite is 15–17 Ma and hosts the quartz–adularia veins that contain gold which has been mined episodically in the Jarbidge area since the early part of this century (Schrader, 1923; Coats, 1964, 1987). Although the Jarbidge Rhyolite has not been studied in much detail, it is apparent that it is part of a large

FIGURE 37—View south (upstream) from Stop 6E, of the West Fork of Jarbidge River canyon and the upper Cougar Point Tuff units. Units XI (bottom), XII, and XIII are visible; they are capped by basalt at canyon rim.

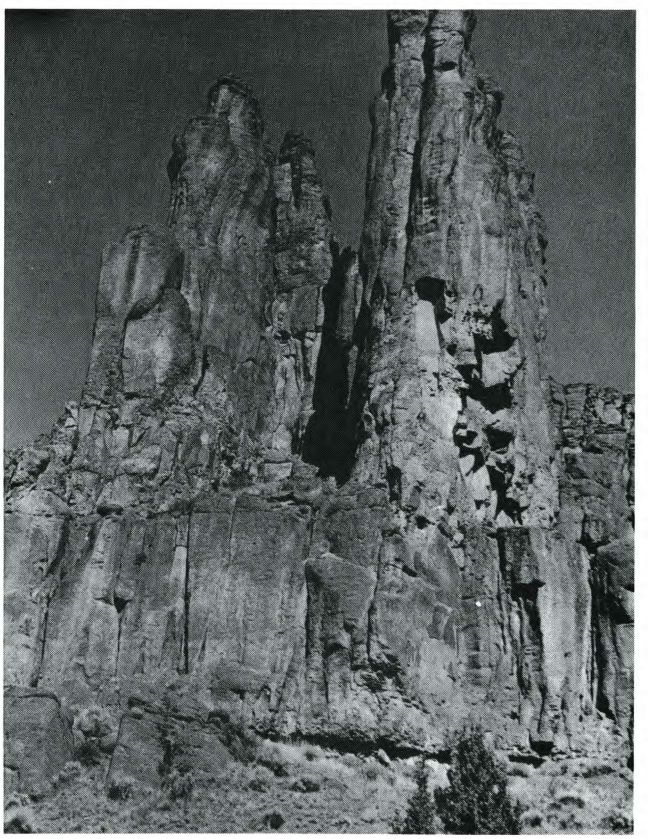

FIGURE 38—Erosional pillars in central zone of Cougar Point Tuff unit XI at Stop 6F in West Fork Jarbidge River canyon. The horizontal break about one-third of the way up from the cliff base is a boundary between successive ash emplacements. A lithophysal zone is just below this break. The basal vitrophyre is exposed in the alcove at base of cliff.

field of pre-Snake River Plain rhyolitic rocks exposed along the south side of the Snake River Plain to as far east as the Nevada–Utah state line (Stewart and Carlson, 1978; Coats, 1987). Its appearance is very different from that of any of the Cougar Point Tuff units. **0.8**

81.5 Road crosses West Fork of Jarbidge River in downtown Jarbidge. Turn around in Jarbidge and retrace route to Rogerson. **63.6**

145.1 Back at mileage 17.9 in Rogerson. Turn north (left). **0.8**

145.9 Turn north (left) on US-93 toward Twin Falls. **23.5**

169.4 Turn east (right) on US-30 and US-93 toward Twin Falls. **5.9**

175.3 Intersection of Blue Lakes Boulevard, Shoshone Street, and Addison Avenue in Twin Falls, where US-93 turns north.

Day 7: Balanced Rock and Mount Bennett Hills

William P. Leeman, Norio Honjo, and Bill Bonnichsen

Balanced Rock area

The central Snake River Plain contains extensive areas underlain by rhyolitic rocks, both lava flows and pyroclastic units. These are widely distributed northeast of the Bruneau-Jarbidge eruptive center and south of the Snake River, between Bruneau and Buhl (Figs. 2, 15). These rocks have received virtually no attention from geologists, except for general mapping that shows their overall exposure areas. Some of these exposures are in Salmon Falls Creek canyon in the western part of Twin Falls County, and two of the units can conveniently be visited there in the Balanced Rock area.

Mount Bennett Hills and Camas Prairie

The Mount Bennett Hills and the Camas Prairie constitute a structurally complex area situated just north of the central Snake River Plain, adjacent to where the western Plain diverges from the main Snake River Plain (Figs. 2, 15). The Mount Bennett Hills is an east—west-oriented complex horst which dips shallowly southward and extensively exposes several Snake River Plain rhyolite units. The Camas Prairie, located farther north, is an east—west-oriented graben. In this region, especially in the Mount Bennett Hills, northwesterly, east—west, and northeasterly trending fault systems are well developed, and generally postdate the volcanism.

The Neogene volcanic rocks in the Mount Bennett Hills and Camas Prairie overlie a basement composed of Paleozoic sedimentary rocks that are cut by Cretaceous and Tertiary granitic plutons, and erosional remnants of Eocene Challis volcanic rocks and associated sediments. The Neogene deposits include an early (about 9-10 Ma) sequence of rhyolitic ash-flow tuffs (Idavada Volcanics) erupted from sources in the Snake River Plain, south of the Mount Bennett Hills, and a later (younger than 6 Ma) lava-flow-dominated rhyolitic sequence erupted from the Magic Reservoir eruptive center in the eastern part of Camas Prairie. The rocks of the earlier sequence are exposed in upfaulted highlands along the margin of the Snake River Plain, and generally dip south, toward its center. Similar ash-flow tuffs progress in age from 13-14 Ma near the Idaho—Oregon—Nevada junction (Owyhee—Humboldt eruptive center, Fig. 15) to 0.6 Ma at Yellowstone; they record the voluminous, early, time-transgressive phase of Snake River Plain volcanism that swept from west to east (Armstrong et al. , 1975). The later silicic volcanism in the Mount Bennett Hills—Camas Prairie area (the lava-flow-dominated products of the Magic Reservoir eruptive center) is thus anomalously young for their geographic position in the general age-distribution pattern of rhyolitic ash-flow tuffs along the Snake River Plain—Yellowstone Plateau province.

Magic Reservoir eruptive center

Rhyolitic lavas and tuffs, basaltic lavas, and hybrid lavas younger than 6 Ma were erupted in the Magic Reservoir area. This volcanic rock suite is considered to be essentially bimodal, as the intermediate-composition magmas are thought to represent mixed silicic and mafic magmas (Honjo and Leeman, 1987). The volcanic section in the Magic Reservoir area (Schmidt, 1961; Malde et al. , 1963; Smith, 1966; Struhsacher et al. , 1982; Leeman, 1982b; Bonnichsen et al. , 1988) contains: (A) the Idavada Volcanics, which consist of welded-tuff units and minor intercalated basaltic lavas (10-19 Ma); (B) quartz latite lavas, hybrid ferrolatite lavas, and high-silica rhyolite tuffs and young domes (6-3 Ma) associated with the development of the Magic Reservoir eruptive center; and (C) young basaltic lavas that are similar in composition to other Snake River Plain basalts.

The Magic Reservoir eruptive center occupies a large portion of the eastern part of the Camas Prairie and part of the eastern Mount Bennett Hills (Fig. 15). It is elliptical in outline, measuring about 22 km from east to west and 29 km from north to south (Leeman, 1982b; Bonnichsen et al., 1988), and appears to have formed by the collapse of the earth's surface after the eruption of a large volume of silicic lava, principally the rhyolite of Magic Reservoir. It has been suggested to be a caldera (Leeman, 1982b), but it is unlikely that it is a typical caldera, since the main eruptive products are lava flows. Its boundary coincides with the locations of several young rhyolite domes, several large basaltic shields, and the large hot spring at Hot Springs Landing. The boundary on the north-northeast is a major fault with the down-thrown side to the south-southwest. Cretaceous granitic rocks are exposed in the upthrown block to the northeast and correlative ferrolatite lavas are offset by at least 120 m across this fault. The inferred western edge of the eruptive center

coincides with the easternmost exposures of Idavada Volcanics and older rocks. Elsewhere, the boundary is not well defined due to the cover of younger deposits. The interior of the Magic Reservoir eruptive center subsided and was filled by the rhyolite of Magic Reservoir and younger basalt flows and sedimentary deposits. The central portion of the eruptive center (in the easternmost Mount Bennett Hills) was subsequently uplifted along a major east—west-trending fault with downward displacement to the north. This fault, which offsets the ferrolatite lavas by a few hundred meters, forms the southern boundary of the Camas Prairie.

As a function of decreasing age, the rhyolites associated with the Magic Reservoir eruptive center become more siliceous, their phenocryst assemblages become more hydrous, and their calculated mineral-equilibrium temperatures decrease from above 1000°C (Magic Reservoir quartz latite) to 700°C (young domes) (Honjo et al. , 1987, and in prep.). These trends are consistent with progressive fractionation of the magmas. Early Pliocene or late Miocene ash-flow tuffs and related pyroclastic deposits were erupted from vents within the Magic Reservoir eruptive center, but the volume of these materials is small in comparison with the rhyolites at Yellowstone or at other eruptive centers within the Snake River Plain.

Road log

This day of the trip will be led by Bill Bonnichsen (Stops 7A and 7E) and Bill Leeman and Norio Honjo (Stops 7B, 7C, and 7D). We will examine: (A) two rhyolitic sheets in the Balanced Rock area, (B) the McHan Basalt and the City of Rocks Tuff, (C) a panoramic overview of the Camas Prairie and surrounding areas, (D) the Square Mountain ferrolatite near the margin of the Magic Reservoir eruptive center, and (E) the rhyolites of Rattlesnake Springs and of Frenchman Springs along the margin of the western Snake River Plain graben. As we follow today's route, which first traverses the central Snake River Plain, we will see a variety of basaltic phenomena. Later, the trip traverses the Mount Bennett Hills and the Camas Prairie, where the silicic volcanic units beneath the basaltic units are well exposed, and finally we will drive into and follow along the western Snake River Plain graben, where additional basaltic features can be seen.

Mileage

00.0 Proceed west on Addison Avenue (US-93) from the intersection of Blue Lakes Boulevard (US-93), Addison Avenue, and Shoshone Street in Twin Falls. This street merges with US-30, so as you proceed west from Twin Falls you will be following both 30 and 93. **5.9**

5.9 Pass junction with US-93, which goes south. Continue westward on US-30. **1.5**

7.4 Enter the town of Filer. **8.3**

15.7 Enter the town of Buhl, pass Clear Lakes Road to the north and Main Street to the northwest; leave US-30 and continue traveling westward. **1.0**

16.7 Pass Castleford Road to the south at southwestern corner of Buhl; continue traveling westward. **4.0**

20.7 Turn south at intersection just past Deep Creek. **3.0**

23.7 Turn west at intersection. **1.7**

25.4 Pass Sunset Butte, a basalt shield volcano north of the road. This probably is one of the sources of the Lucerne School Basalt (Malde and Powers, 1972) that extends as far as Snake River canyon, about 15 km to the north. **2.3**

27.7 Turn south at intersection. **1.0**

28.7 Turn west at intersection. **0.6**

29.3 Pass first outcrops of rhyolite as road goes down the grade into Salmon Falls Creek canyon. **0.8**

30.1 Cross Salmon Falls Creek. **0.5**

30.6 **STOP 7A. Balanced Rock Area rhyolite sheets: Balanced Rock; interior features of a rhyolite lava flow; a probable Type-V pyroclastic flow.** Leave vehicles here and walk back along road to mileage 29.3, examining the rhyolite exposures along the way. After completing this stop, return to southeast corner of Buhl (mileage 15.7) by same route that was followed to Balanced Rock. Two rhyolite sheets are exposed in the Balanced Rock area. Balanced Rock (Fig. 39) is within the upper flow, and the cliffs along the canyon bottom are within the lower unit. The grade on the west side of Salmon Falls Creek affords an excellent cross section through the internal zones of these flows. Two parallel, northwest-trending faults have somewhat uplifted the zone immediately northeast of the road relative to rocks exposed southwest of the road, so at first it may be confusing as to which portion of the rocks northeast of the road corresponds to rocks southwest of the road.

The lower rhyolite sheet is clearly a lava flow, and the traverse along the lower portion of the grade provides an excellent view of internal features in the upper zone of a typical rhyolite lava flow. Especially abundant in the upper part of this flow are breccias (Fig. 40), zones of alteration, local pyrite, spherulites, and other complex relations. The upper rhyolite sheet at Balanced Rock may be a pyroclastic unit (rather than a rhyolite lava flow as was previously suggested by Bonnichsen, 1982b; Bonnichsen and Kauffman, 1987; Bonnichsen et al., 1988). The very base of the upper sheet, as exposed on the west side of Salmon Falls Creek, shows a partially welded zone a few centimeters thick, lying on probable ash-fall tuff (Fig. 40). Immediately above

FIGURE 39—Balanced Rock, near Salmon Falls Creek canyon. This amazing feature has been eroded from the central zone of the upper rhyolite sheet at Stop 7A.

FIGURE 40—The boundary between the lower and upper rhyolite sheets at Stop 7A, in Salmon Falls Creek canyon. At the bottom of the photograph is the breccia at the top of the lower unit. It is overlain by tuffaceous sediments and ash-fall tuff which, in turn, are overlain by the basal vitrophyre of the upper unit. The lowermost few centimeters of this basal vitrophyre is only partially welded, suggesting that the upper unit is of pyroclastic origin, perhaps a type-V welded tuff.

this thin, partially welded zone the basal vitrophyre of the upper sheet is completely welded, contains flow bands, folds, and similar features indicating that it was entirely molten and flowed into its present position. If it is a welded pyroclastic flow, rather than a lava flow, it probably is the very high temperature type (Type V, Table 3).

Phenocryst minerals observed in these flows include plagioclase, augite, hypersthene, and Fe–Ti oxides. An analysis of the upper flow is included in Table 2. It is about as femic as any rhyolite unit in the Snake River Plain volcanic province. **14.9**

45.5 Same location as mileage 15.7, turn north on Clear Lakes road at southeastern corner of Buhl. **3.4**

48.9 Start down grade into Snake River canyon. **0.6**

49.5 Note well-exposed outcrops of partially disintegrated basalt for last 0.4 mi of the grade. This was mapped as Banbury Basalt by Malde and Powers (1972). The weathered, partially disintegrated condition, which we have called "water-affected," probably is the result of these flows running into a large lake, Lake Idaho (Jenks and Bonnichsen, 1987, and in press), that occupied this region during the Pliocene. **1.7**

51.2 Cross Snake River. Note basalt outcrop north of river and on left side of highway. This is an additional outcrop of water-affected Banbury Basalt. **0.5**

51.7 Note large trout farms along here for next 0.8 mi. These fish tanks utilize the large, cold-water springs that emerge from north wall of canyon as part of discharge from Snake River Plain aquifer. **1.2**

52.9 From here to top of grade notice the older, water-affected Banbury Basalt with its weathered appearance, overlain at canyon rim by fresh-looking Thousand Springs Basalt (Malde and Powers, 1972) that has a pillowed base. **0.3**

53.2 Top of Clear Lakes grade at north side of Snake River canyon. Proceed north 0.6 mi, then east 0.3 mi, then north again. Going north, pass from Thousand Springs Basalt into Sand Springs Basalt, then into Wendell Grade Basalt near pressure ridges located about 0.5 mi south of mileage 60.6. These basalt flows are Pleistocene in age and were erupted from various basalt shields located many kilometers to east. **7.4**

60.6 Turn east toward Wendell at intersection with Hagerman–Wendell road. **3.4**

64.0 Cross I-84. **1.1**

65.1 Turn north at center of Wendell on ID-46, toward Gooding. For much of the distance between Wendell and Gooding you will be traveling across the Wendell Grade Basalt which was erupted from Notch Butte, located about 24 km to the east, near town of Shoshone. This is one of the youngest basalt flows in the central part of the Snake River Plain. *Note well-developed pressure ridges on its surface.* **9.3**

74.4 Note Gooding Butte, a basalt shield volcano, to west. This was the source of Malad Member of Thousand Springs Basalt (Malde and Powers, 1972). **0.9**

75.3 Cross US-20-26, the Shoshone–Bliss road, and enter town of Gooding. **1.9**

77.2 Cross Big Wood River at north side of Gooding. **7.7**

84.9 Pass road on right that goes east to Turkey Lake. Note basaltic volcano, Turkey Head Butte, located about 1.6 km east of highway. **3.6**

88.5 Pass road on left that goes west to the Little City of Rocks. About 1 km west of the highway is the Little City of Rocks which contains hoodoos similar to those in more extensive City of Rocks farther west. The hoodoos are within the massive central zone of City of Rocks Tuff. **1.6**

90.1 **STOP 7B. City of Rocks Tuff: Basal vitrophyre; folds in devitrified zone.** Turn northeast (right) and proceed into Thorn Creek canyon. The round-trip distance from ID-46 to Stop 7B, about 3.5 mi, is not included within cumulative mileage of the road log. Stop 7B is near the abandoned farm buildings where there are excellent cliff exposures of City of Rocks Tuff. Here we climb through the section and see McHan Basalt and overlying City of Rocks Tuff. Driving up this canyon you can see a thin layer of ferrolatite capping east side of canyon above City of Rocks Tuff, while a thin ledge of McHan Basalt underlies City of Rocks Tuff on west side of canyon. The McHan Basalt, an olivine tholeiite, is typical

of basalt flows in this area, although it is more plagioclase-rich than typical olivine tholeiites of the Mount Bennett Hills region. The McHan Basalt has a K–Ar age of 9.44 ± 0.11 Ma and City of Rocks Tuff has a K–Ar age of 9.15 ± 0.13 Ma (Honjo et al., 1986).

The City of Rocks Tuff at this locality has a well-exposed basal vitrophyre which is overlain by devitrified rhyolite that locally shows tight folds with subhorizontal axial planes. This unit was emplaced upon faulted topography that had developed earlier on the older silicic units (the Idavada Volcanics) in the Mount Bennett Hills. The City of Rocks Tuff is a quartz latite (Table 2) that is distinctively crystal-rich, with phenocrysts of plagioclase, minor quartz, augite, hypersthene, Fe–Ti oxides, and traces of zircon and apatite in a glassy to devitrified groundmass. Its mineralogical and chemical composition is very similar to that of the upper rhyolite unit visited at Stop 7A in the Balanced Rock area. The compositions of the pyroxenes in this unit indicate probable eruption temperatures of 970–1000°C (Table 5). This unit thins and ultimately feathers out a short distance to the north. **2.9**

93.0 Pass graded road that goes west (left) to City of Rocks, which is a scenic locality with spectacular hoodoos eroded from City of Rocks Tuff. The rounded hills west of the road consist of gravels of the Hash Springs Formation, overlain by the Pliocene Burnt Willow Basalt (Smith, 1966). The cliff-forming ash-flow tuff exposed on both sides of highway is City of Rocks Tuff. **1.2**

94.2 Pass road leading to Thorn Creek Reservoir, to the east. From here we can look north a short distance and see the lower tuff of Gwin Springs Formation (Smith, 1966), one of the older ash-flow tuff units in the region, and the Schooler Basalt. The Schooler Basalt vented nearby and flowed southward onto the Snake River Plain. **0.9**

95.1 Pass Camas–Gooding County line. **4.4**

99.5 **STOP 7C. Overview of Camas Prairie at Johnson Hill: Camas Prairie graben, mountain ranges to north, escarpment bounding Mount Bennett Hills.** Pull into large parking area part way down Johnson Hill. Looking northward from here, Camas Prairie, an east–west-oriented graben, lies in near distance. Camas Prairie is about 15 km across and about 75 km in length. Across the Prairie, the mountains to northwest are the Soldier Mountains, those to north are the Smoky Mountains, and those to northeast are the Pioneer Mountains (Fig. 15). The escarpment that stretches east and west of this locality, along south side of Camas Prairie, is the result of a series of down-to-the-north normal faults that bound the north side of Mount Bennett Hills, cutting off the volcanic units we have just seen. Much of the floor of Camas Prairie before you is covered by a Pleistocene-age basalt unit, the Macon Basalt, that postdates formation of the graben. In the east part of Camas Prairie is the Magic Reservoir eruptive center, a slightly elliptical volcanic collapse structure, that has been discussed in some detail by Leeman (1982b) and by Bonnichsen et al. (1988). Some of the features which define the boundary of the Magic Reservoir eruptive center will be pointed out from Stop 7D, located at Square Mountain visible across the graben about 20 km northeast of here.

The view from this locality certainly suggests that Camas Prairie is a large graben. There has been some debate as to the origin and age of the structure. Cluer and Cluer (1986) proposed that the graben may be a pull-apart structure that formed in response to downwarping, to the south, of the Snake River Plain. They cite the presence in the Mount Bennett Hills of post-Challis (younger than Eocene) alluvial gravels containing clasts derived from granitic, sedimentary, and Challis volcanic terranes, and propose that these deposits were part of an extensive outwash fan derived from sources north of Camas Prairie. If these deposits originally were continuous across the valley, then they provide a maximum, post-Eocene, time constraint for the faulting. It can also be demonstrated, however, that several of the Idavada ash-flow tuffs thinned against preexisting topography during their northward transport (ca 10–9 Ma; Honjo et al., 1986) from eruptive centers in the Snake River Plain; hence, the Mount Bennett Hills must have had positive topographic relief 9 m.y. ago. In addition, because only one or two thin remnants of the Idavada ash-flow tuffs can be found north of Camas Prairie, the Mount Bennett Hills must have been a significant barrier to northward distribution of these ignimbrites. The occurrence of significant structural offsets in the ferrolatite lavas indicates that many of the northwest- and east–west-trending faults bounding the graben have been active since approximately 5.7 Ma. In fact, much of the relief on the north side of the eastern Mount Bennett Hills must have formed since that time. Furthermore, small scarps in Macon Basalt indicate that at least minor faulting has occurred since 0.9 m.y. ago. The evidence thus suggests that formation of Camas Prairie is not simply related to subsidence associated with initial volcanism in the Snake River Plain, but that the Prairie has continued to develop over the interval of time since then. **2.5**

102.0 The road crosses a small-displacement fault scarp in Macon Basalt. **4.7**

106.7 At intersection with US-20, turn east toward Sun Valley. **8.9**

115.6 Camas County–Blaine County line. Turn left here on graded road to north. **1.9**

117.5 Turn right (north) at intersection with Camp Creek road. From here to Stop 7D we drive through exposures of Square Mountain Ferrolatite lavas. Note the abundance of sheeting joints that typically are complexly folded. **2.9**

120.4 **STOP 7D. Square Mountain Ferrolatite: Inclusions in ferrolatite; overall nature of ferrolatite flows; view of Moonstone Mountain and Magic Reservoir eruptive center.** Leave vehicles at roadcut in foliated biotite granodiorite. We cross the creek at this point, climb 500 ft to top of Square Mountain, and walk to its southeast corner where large crustal xenoliths are abundant in Square

Mountain ferrolatite. Total walking time will be about one hour. After returning to vehicles, we drive back to US-20 along the same route.

The thicknesses and distribution of the ferrolatite lavas were apparently controlled by preexisting topography. They probably flowed from vents in this area, but actual vent locations are not known with certainty. Note well-developed sets of sheeting joints in portions (flow-channel margins?) of the ferrolatite flows. Some areas are cut by as many as three sets of subvertical joints (shear joints?), whereas adjacent areas (flow-channel interiors?) exhibit moderately developed columnar joints.

On the east side of Square Mountain and north of Moonstone Mountain, the local concentrations within lavas of large gneissic xenoliths of crustal materials are thought to be proximal to vents because it is unlikely that the xenoliths could have been transported far. Similar lavas occur in hills east of Magic Reservoir, in foothills on north and northeast sides of the eastern Mount Bennett Hills (where small crustal xenoliths have also been found), along southwestern margin of the Magic Reservoir eruptive center, and in a large area north of Moonstone Mountain. All of the ferrolatite lavas are remarkably similar in spite of their wide distribution, and evidence for ferrolatite vents has not been recognized in any part of the Magic Reservoir eruptive center, except near Square Mountain.

This excursion will take us through a poorly exposed section of granitic rocks, to the unconformable ferrolatite cap on the west side of Square Mountain. We will walk to one of the better xenolith localities where gneissic blocks in excess of 1 m in diameter can be observed; locally such blocks comprise more than 20% of the outcrop (Fig. 41). Many xenoliths were extensively fused and injected with veins of ferrolatitic magma. It is interesting to note that all xenoliths are felsic; amphibolites and other mafic lithologies seem to be absent. Representative xenolith samples from this location that were analyzed isotopically (Leeman et al., 1985), were found to have Sm–Nd and Pb–Pb model ages of about 2.8 Ga. Thus, these xenoliths infer the presence of Precambrian basement beneath this portion of the Snake River Plain province.

FIGURE 41—Gneissic inclusions in Square Mountain ferrolatite at Stop 7D, southeast corner of Square Mountain.

Stratigraphic and field relations in the eastern Mount Bennett Hills indicate that the ferrolatite lavas are approximately 5.7 Ma. The ferrolatites (or "tholeiitic andesites") (see Table 2 for average composition) are rich in phenocrysts, including plagioclase, augite, pigeonite, minor hypersthene and magnetite, and sparse ilmenite. They also contain markedly embayed xenocrysts, up to 3 mm in diameter, of anorthoclase (commonly sieve-textured) and quartz, and relicts of Nb-rich ilmenite. The groundmass contains sodic plagioclase, pyroxenes and Fe–Ti oxides. Detailed microprobe analyses of these minerals and the bulk compositions of the ferrolatite lavas suggest that the magmas were mixtures of subequal proportions of the rhyolite of Magic Reservoir and olivine tholeiite basalt (Honjo and Leeman, 1987).

Looking southeastward from the xenolith locality, Moonstone Mountain can be seen at a distance of about 4 km. Moonstone Mountain is a silicic dome with K–Ar age dates of 3.88 ± 0.06 and 3.02 ± 0.05 Ma (Honjo et al., 1986). It lies on the north margin of the Magic Reservoir eruptive center and is the largest of several rhyolitic domes that were injected in the vicinity of the northeastern margin of this structure between 3 and 4 Ma. The view southward from Square Mountain is into the interior of the Magic Reservoir eruptive center, where rhyolite of Magic Reservoir (4.2–5.8 Ma) is widely distributed and is overlain at various localities by Square Mountain ferrolatite and Macon Basalt. **4.8**

125.2 At intersection with US-20, turn west (right) toward Fairfield. **8.9**

134.1 Pass junction with ID-46 and continue west toward Fairfield. **4.0**

138.1 Pass town of Fairfield. **41.2**

179.3 Pass Hill City. **12.8**

192.1 Cross Cat Creek Summit. **8.4**

200.5 Pass road to Anderson Ranch dam. **5.5**

206.0 Pass road to Prairie. **3.7**

209.7 Pass Tollgate Cafe. **0.5**

210.2 Pass Immigrant Road on left. **1.0**

211.2 **STOP 7E. Rattlesnake Springs rhyolite sheet: Difficulty of distinguishing rhyolite lava flows from Type-V pyroclastic flows; view of western Snake River Plain.** Stop 0.1 mi before (north of) powerline that crosses highway. Go through gate on west (right) and follow dirt road along powerline to exposures at top of ridge west of highway. After going through gate in fence near crest of ridge, go up slope to north (right) to examine top of rhyolite of Frenchman Springs and the section through overlying rhyolite of Rattlesnake Springs.

The rhyolite of Rattlesnake Springs which caps this ridge is one of about 10 silicic volcanic units that Wood and Gardner (1984) have mapped in the western part of the Mount Bennett Hills. They have

divided these units into two groups, the earlier being rhyolite units of the Bennett Mountains, and the latter rhyolite units of the Danskin Mountains. One of the earlier units of the Bennett Mountain group has been dated at 11.0 ± 0.6 Ma, but none of the younger Danskin Mountain group have been dated. Structurally, the Danskin Mountain group laps onto older units of the Bennett Mountain group, probably indicating subsidence of the western Snake River Plain along major faults between times of emplacement of the two groups.

The rhyolites of Frenchman Springs and of Rattlesnake Springs are the two oldest of the group of silicic units of the Danskin Mountains. They pinch out eastward against the older group of units about 3 km east of this locality. As can be seen in the landscape here, there is a suggestion of listric faulting along the northeastern margin of the western Snake River Plain graben, with rotation of blocks away from the graben, presumably along curved fault planes that dip more and more shallowly toward the center of the graben. This is the only place along the margin of the Snake River Plain where such listric-fault activity is indicated.

The rhyolite of Rattlesnake Springs at this stop has a nicely developed basal vitrophyre, containing many folds and layers of devitrified material (Fig. 42). No basal air-fall ash is present beneath the flow; instead it lies on a layer of baked, red-colored sediment, probably an old soil horizon. Locally, a minor amount of basal breccia is present at the bottom of the basal vitrophyre layer, but there is no suggestion of a thin zone of partially welded material at the bottom of the basal vitrophyre like that observed at Stop 7A (upper sheet in Balanced Rock area). From these observations one might conclude that the rhyolite of Rattlesnake Springs is probably a rhyolite lava flow rather than a welded pyroclastic flow. Although not enough field work has been conducted in this region to determine whether this is really the case, it seems probable. Comparison of many of the features in this unit with those of the upper rhyolite sheet in the Balanced Rock area of Stop 7A clearly points out the difficulty of distinguishing rhyolite lava flows from the Type-V welded pyroclastic flows, unless careful field work is done at appropriate localities within a unit.

The view from this stop includes the central portion of the Snake River Plain as you look south, and the western Snake River Plain as you look southwest and westward. Across the western part of the Plain is the Owyhee Range, composed largely of Tertiary volcanic rocks predating the Snake River Plain. To the west, at a distance of about 10 km, is Lockman Butte, one of several Pleistocene-age basaltic volcanoes near Mountain Home. Back to the east is the extensive mass of rhyolitic rocks that forms the western part of Mount Bennett Hills. This area contains the thickest exposed section of silicic rocks within the Snake River Plain volcanic province. About 1000 m (Wood and Gardner, 1984) of rhyolite is exposed in this area. **10.3**

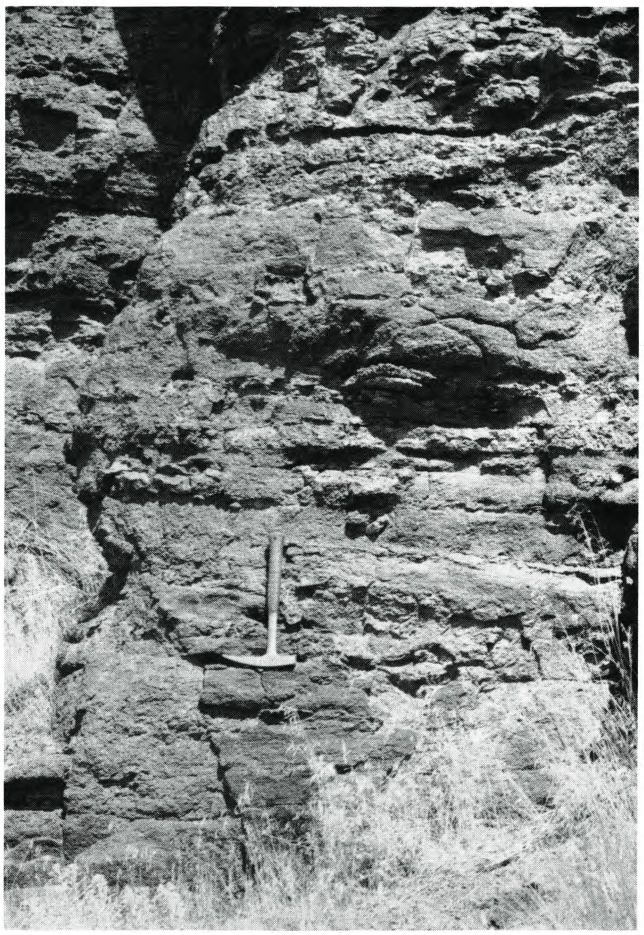

FIGURE 42—Basal vitrophyre zone of Rattlesnake Springs rhyolite unit at Stop 7E, showing well-developed interlayering of glassy and devitrified rhyolite.

221.5 Join I-84 at exit 95, turn northwest (right) and proceed toward Boise. **41.5**

263.0 Intersection of I-84 and Vista Avenue in Boise, exit 53, for Boise Airport.

References

Albee, H. F., Prostka, H. J., Jobin, D. A., and Love, J. D., 1975, Field trip guide to the Idaho–Wyoming thrust fault zone: Geological Society of America, Rocky Mountain Section, Guidebook 28, Field Trip 4: 22 pp.

Alief, M. H., 1962, Variation in SiO_2, Al_2O_3, Fe_2O_3, CaO, MgO, Na_2O, K_2O, and H_2O in some ignimbrites in southern Twin Falls County, Idaho: Unpublished M.S. thesis, University of Idaho, Moscow, 60 pp.

Armstrong, R. L., Leeman, W. P., and Malde, H. E., 1975, K–Ar dating, Quaternary and Neogene volcanic rocks of the Snake River Plain, Idaho: American Journal of Science, 275: 225–251.

Bonnichsen, B., 1982a, The Bruneau–Jarbidge eruptive center, southwestern Idaho; *in* Bonnichsen, B., and Breckenridge, R. M., (eds.), Cenozoic geology of Idaho: Idaho Bureau of Mines and Geology, Bulletin 26: 237–254.

Bonnichsen, B., 1982b, Rhyolite lava flows in the Bruneau–Jarbidge eruptive center, southwestern Idaho; *in* Bonnichsen, B., and Breckenridge, R. M. (eds.), Cenozoic geology of Idaho: Idaho Bureau of Mines and Geology, Bulletin 26: 283–320.

Bonnichsen, B., and Citron, G. P., 1982, The Cougar Point Tuff, southwestern Idaho and vicinity; *in* Bonnichsen, B., and Breckenridge, R.

M. (eds.), Cenozoic geology of Idaho: Idaho Bureau of Mines and Geology, Bulletin 26: 255–281.

Bonnichsen, B., and Jenks, M. D. (in press), Geologic map of the Jarbidge River Wilderness Study Area, Owyhee County, Idaho: U.S. Geological Survey, Miscellaneous Field Investigations Map, scale 1:50,000.

Bonnichsen, B., and Kauffman, D. F., 1987, Physical features of rhyolite lava flows in the Snake River Plain volcanic province, southwestern Idaho; *in* Fink, J. H. (ed.), The emplacement of silicic domes and lava flows: Geological Society of America, Special Paper 212: 119–145.

Bonnichsen, B., Leeman, W. P., Jenks, M. D., and Honjo, N., 1988, Geologic field trip guide to the central and western Snake River Plain, Idaho, emphasizing the silicic volcanic rocks; *in* Link, P. K., and Hackett, W. R. (eds.), Guidebook to the geology of central and southern Idaho: Idaho Geological Survey, Bulletin 27: 247–281.

Burchfiel, B. C., 1979, Geologic history of the central western United States: Nevada Bureau of Mines and Geology, Report 33: 1–11.

Carr, W. J., and Trimble, D. E., 1963, Geology of the American Falls quadrangle, Idaho: U.S. Geological Survey, Bulletin 1121-G: 44 pp.

Chapin, C. E., and Lowell, G. R., 1979, Primary and secondary flow structures in ash-flow tuffs of the Gribbles Run paleovalley, central Colorado; *in* Chapin, C. E., and Elston, W. E. (eds.), Ash-flow tuffs: Geological Society of America, Special Paper 180: 137–154.

Christiansen, R. L., 1979, Cooling units and composite sheets in relation to caldera structure; *in* Chapin, C. E., and Elston, W. E. (eds.), Ash-flow tuffs: Geological Society of America, Special Paper 180: 29–42.

Christiansen, R. L., 1982, Late Cenozoic volcanism of the Island Park area, eastern Idaho; *in* Bonnichsen, B., and Breckenridge, R. M. (eds.), Cenozoic geology of Idaho: Idaho Bureau of Mines and Geology, Bulletin 26: 345–368.

Christiansen, R. L., 1984, Yellowstone magmatic evolution: Its bearing on understanding large-volume explosive volcanism; *in* Explosive volcanism: Inception, evolution, and hazards: National Academy of Sciences, Washington, D.C., pp. 84–95.

Christiansen, R. L., and Blank, H. R., Jr., 1972, Volcanic stratigraphy of the Quaternary rhyolite plateau in Yellowstone National Park: U.S. Geological Survey, Professional Paper 729-B: 18 pp.

Christiansen, R. L., and McKee, E. H., 1978, Late Cenozoic volcanic and tectonic evolution of the Great Basin and Columbia Intermontane regions; *in* Smith, R. B., and Eaton, G. P. (eds.), Cenozoic tectonics and regional geophysics of the western Cordillera: Geological Society of America, Memoir 152: 283–311.

Citron, G. P., 1976, Idavada ash-flows in the Three Creek area, southwestern Idaho, and their regional significance: Unpublished M.S. thesis, Cornell University, Ithaca, New York, 83 pp.

Cluer, J. K., and Cluer, B. L., 1986, The late Cenozoic Camas Prairie rift, south-central Idaho: Contributions to Geology, University of Wyoming, Laramie, 24(1): 91–101.

Coats, R. R., 1964, Geology of the Jarbidge quadrangle, Nevada–Idaho: U.S. Geological Survey, Bulletin 1141-M: 24 pp.

Coats, R. R., 1987, Geology of Elko County, Nevada: Nevada Bureau of Mines and Geology, Bulletin 101: 112 pp.

Davidson, P. M., and Lindsley, D. H., 1985, Thermodynamic analysis of quadrilateral pyroxenes. Part II: Model calibration from experiments and applications to geothermometry: Contributions to Mineralogy and Petrology, 91: 390–404.

Doherty, D. J., McBroome, L. A., and Kuntz, M. A., 1979, Preliminary geologic interpretation and lithologic log of the exploratory text well (INEL-1), Idaho National Engineering Laboratory, eastern Snake River Plain, Idaho: U.S. Geological Survey, Open-File Report 79-1248: 10 pp.

Dzurisin, D., and Yamashita, K. M., 1987, Vertical surface displacements at Yellowstone caldera, Wyoming, 1976–1986: Journal of Geophysical Research, 92: 13,753–13,766.

Eaton, G. P., 1980, Geophysical and geological characteristics of the crust of the Basin and Range province; *in* Continental tectonics: National Academy of Science, Washington, D.C., pp. 96–113.

Fournier, R. O., White, D. E., and Truesdell, A. H., 1976, Convective heat flow in Yellowstone National Park; *in* Proceedings, Second United Nations Symposium on the Development and Use of Geothermal Resources, San Francisco, Calif., 1975: U.S. Government Printing Office, 1: 731–739.

Goodwin, E. B., and Thompson, G. A., 1988, The seismically reflective crust beneath highly extended terranes: evidence for its origin in extension: Geological Society of America, Bulletin, 100: 1616–1626.

Hackett, W. R., and Morgan, L. A., 1988, Explosive basaltic and rhyolitic volcanism of the eastern Snake River Plain, Idaho; *in* Link, P. K., and Hackett, W. R. (eds.), Guidebook to the geology of central and southern Idaho: Idaho Geological Survey, Bulletin 27: 283–301.

Hart, W. K., and Aronson, J. L., 1983, K–Ar ages of rhyolite from the western Snake River Plain area, Oregon, Idaho, and Nevada: Isochron/West, no. 36: 17–19.

Honjo, N., 1986, Petrology and geochemistry of the Magic Reservoir eruptive center, Snake River Plain, Idaho: Unpublished M.S. thesis, Rice University, Houston, Texas, 511 pp.

Honjo, N., and Leeman, W. P., 1987, Origin of hybrid ferrolatite lavas from Magic Reservoir eruptive center, Snake River Plain, Idaho: Contributions to Mineralogy and Petrology, 96: 163–177.

Honjo, N., Bonnichsen, B., and Leeman, W. P., 1987, High-temperature rhyolites from western-central Snake River Plain: Comparative geothermometers (abs.): Geological Society of America, Abstracts with Programs, 19(7): 706–707.

Honjo, N., Bonnichsen, B., Leeman, W. P., and Stormer, J. C., Jr. (in prep.), High-temperature rhyolites from the central and western Snake River Plain, Idaho.

Honjo, N., McElwee, K. R., Duncan, R. A., and Leeman, W. P., 1986, K–Ar ages of volcanic rocks from the Magic Reservoir eruptive center, Snake River Plain: Isochron/West, no. 46: 15–19.

James, H. L., and Hedge, C. E., 1979, Age of basement rocks of southwest Montana: Geological Society of America, Bulletin, 91: 11–15.

Jenks, M. D., and Bonnichsen, B., 1987, Lake Idaho: New perspectives through basalt stratigraphy (abs): American Association of Petroleum Geologists, Bulletin, 71: 1008.

Jenks, M. D., and Bonnichsen, B. (in press), Subaqueous basalt eruptions into Pliocene Lake Idaho, Snake River Plain, Idaho; *in* Chamberlain, V. E., Breckenridge, R. M., and Bonnichsen, B. (eds.), Guidebook to the geology of northern and western Idaho, and vicinity: Idaho Geological Survey, Bulletin 28.

Karlo, J. F., 1977a, The geology and Bouguer gravity of the Hell's Half Acre and their relation to volcano-tectonic processes within the Snake River Plain rift zone, Idaho: Unpublished Ph.D. dissertation, State University of New York, Buffalo, 152 pp.

Karlo, J. F., 1977b, Geology of the Hell's Half Acre lava field; *in* Greeley, R., and King, J. S. (eds.), Volcanism of the eastern Snake River Plain, Idaho: A comparative planetary geology guidebook: National Aeronautics and Space Administration, NASA CR-154621: 121–131.

Kiilsgaard, T. H., Fisher, F. S., and Bennett, E. H., 1986, The Trans-Challis fault system and associated precious metal deposits, Idaho: Economic Geology, 81: 721–724.

Kuntz, M. A., and Dalrymple, G. B., 1979, Geology, geochronology and potential volcanic hazards in the Lava Ridge–Hells Half Acre area, eastern Snake River Plain, Idaho: U.S. Geological Survey, Open-File Report 79-1657: 72 pp.

Kuntz, M. A., Spiker, E. C., Rubin, M., Champion, D. E., and Lefebvre, R. H., 1986, Radiocarbon studies of latest Pleistocene and Holocene lava flows of the Snake River Plain, Idaho: Data, lessons, interpretations: Quaternary Research, 25: 163–176.

Kuntz, M. A., Scott, W. E., Skipp, B., Hait, M. H., Jr., Embree, G. F., Hoggan, R. D., and Williams, E. J., 1979, Geologic map of the Lava Ridge–Hells Half Acre area, eastern Snake River Plain, Idaho: U.S. Geological Survey, Open-File Report 79-669, scale 1:62,500.

Leeman, W. P., 1982a, Development of the Snake River Plain–Yellowstone Plateau province, Idaho and Wyoming: An overview and petrologic model; *in* Bonnichsen, B., and Breckenridge, R. M. (eds)., Cenozoic geology of Idaho: Idaho Bureau of Mines and Geology, Bulletin 26: 155–177.

Leeman, W. P., 1982b, Geology of the Magic Reservoir area, Snake River Plain, Idaho; *in* Bonnichsen, B., and Breckenridge, R. M. (eds.), Cenozoic geology of Idaho: Idaho Bureau of Mines and Geology, Bulletin 26: 369–376.

Leeman, W. P., Menzies, M. A., Matty, D. J., and Embree, G. F., 1985, Strontium, neodymium, and lead isotopic compositions of deep crustal xenoliths from the Snake River Plain: Evidence for Archean basement: Earth and Planetary Science Letters, 75: 354–368.

Lipman, P. W., 1980, Cenozoic volcanism in the western United States: implications for continental tectonics; *in* Continental tectonics: National Academy of Science, Washington, D.C., pp. 161–174.

Lindsley, D. H., 1983, Pyroxene thermometry: American Mineralogist, 68: 477–493.

Love, J. D., 1956, Summary of geologic history of Teton County, Wyoming, during late Cretaceous, Tertiary, and Quaternary times: Wyoming Geological Association, Guidebook, 11th Annual Field Conference, pp. 140–150.

Love, J. D., and Keefer, W. R., 1975, Geology of sedimentary rocks in southern Yellowstone National Park, Wyoming: U.S. Geological Survey, Professional Paper 729-D, 60 pp.

Love, J. D., Reed, J. C., Jr., Christiansen, R. L., and Stacy, J. R., 1973,

Geologic block diagram and tectonic history of the Teton region, Wyoming–Idaho: U.S. Geological Survey, Miscellaneous Geologic Investigations Map I-730.

Malde, H. E., and Powers, H. A., 1972, Geologic map of the Glenns Ferry–Hagerman area, west-central Snake River Plain, Idaho: U.S. Geological Survey, Miscellaneous Geologic Investigations Map I-696, scale 1:48,000.

Malde, H. E., Powers, H. A., and Marshall, C. E., 1963, Reconnaissance geologic map of west-central Snake River Plain, Idaho: U.S. Geological Survey, Miscellaneous Geologic Investigations Map I-373, scale 1:125,000.

McBroome, L. A., 1981, Stratigraphy and origin of Neogene ash-flow tuffs on the north-central margin of the eastern Snake River Plain, Idaho: Unpublished M.S. thesis, University of Colorado, Boulder, 74 pp.

McBroome, L. A., Doherty, D. J., and Embree, G. F., 1981, Correlation of major Pliocene and Miocene rhyolites, eastern Snake River Plain, Idaho: Montana Geological Society, Guidebook, Southwest Montana Field Conference, pp. 323–330.

Morgan, L. A., 1988a, Explosive rhyolitic volcanism on the eastern Snake River Plain, Idaho: Unpublished Ph.D. dissertation, University of Hawaii, Manoa, 191 pp.

Morgan, L. A., 1988b, Paleomagnetic correlations of major ignimbrites on the eastern Snake River Plain (abs.): Geological Society of America, Abstracts with Programs, 20(6): 433.

Morgan, L. A., Doherty, D. J., and Leeman, W. P., 1984, Ignimbrites of the eastern Snake River Plain: evidence for major caldera-forming eruptions: Journal of Geophysical Research, 89: 8665–8678.

Pelton, J. R., and Smith, R. B., 1982, Contemporary vertical surface displacement in Yellowstone National Park: Journal of Geophysical Research, 87: 2745–2761.

Pierce, K. L., 1979, History and dynamics of glaciation in the northern Yellowstone National Park area: U.S. Geological Survey, Professional Paper 729-F: 90 pp.

Prostka, H. J., and Embree, G. F., 1978, Geology and geothermal resources of the Rexburg area, eastern Idaho: U.S. Geological Survey, Open-File Report 78-1009: 15 pp., 2 plates.

Reed, J. C., Jr., and Zartman, R. E., 1978, Geochronology of Precambrian rocks of the Teton Range, Wyoming: Geological Society of America, Bulletin, 84: 561–582.

Richmond, G. M., 1986, Stratigraphy and chronology of glaciation in Yellowstone National Park; *in* Richmond, G. M., and Fullerton, D. S. (eds.), Quaternary glaciations in the northern hemisphere: London, Pergamon Press, in press.

Robyn, T. L., and Hoover, J. D., 1982, Late Cenozoic deformation and volcanism in the Blue Mountains of central Oregon: Microplate interactions?: Geology, 10: 572–576.

Ruppel, E. T., 1972, Geology of pre-Tertiary rocks in the northern part of Yellowstone National Park: U.S. Geological Survey, Professional Paper 729-A: 66 pp.

Schmidt, D. L., 1961, Quaternary geology of the Bellevue area in Blaine and Camas Counties, Idaho: Unpublished Ph.D. dissertation, University of Washington, Seattle, 125 pp.

Scholton, R., Keenmon, K. A., and Kupsch, W. O., 1955, Geology of the Lima region, southwestern Montana and adjacent Idaho: Geological Society of America, Bulletin, 66: 345–404.

Schrader, F. C., 1923, The Jarbidge mining district, Nevada, with a note on the Charleston district: U.S. Geological Survey, Bulletin 741: 86 pp.

Skipp, B. A., Prostka, H. J., and Schleicher, D. L., 1979, Preliminary geologic map of the Edie Ranch quadrangle, Clark County, Idaho, and Beaverhead County, Montana: U.S. Geological Survey, Open-File Report 79-845, 1 sheet.

Smedes, H. W., and Prostka, H. J., 1972, Stratigraphic framework of the Absoroka Volcanic Supergroup in Yellowstone National Park region: U.S. Geological Survey, Professional Paper 729-C: 33 pp.

Smith, C. L., 1966, Geology of eastern Mount Bennett Hills, Camas, Gooding, and Lincoln Counties, Idaho: Unpublished Ph.D. dissertation, University of Idaho, Moscow, 129 pp.

Smith, R. B., 1978, Seismicity, crustal structure, and intraplate tectonics of the interior of the western Cordillera; *in* Smith, R. B., and Eaton, G. P. (eds.), Cenozoic tectonics and regional geophysics of the western Cordillera: Geological Society of America, Memoir 152: 111–144.

Smith, R. B., and Braile, L. W., 1984, Crustal structure and evolution of an explosive silicic volcanic system at Yellowstone National Park; *in* Explosive volcanism: Inception, evolution, and hazards: National Academy of Sciences, Washington, D.C., pp. 96–109.

Smith, R. B., and Christiansen, R. L., 1980, Yellowstone Park as a window on the Earth's interior: Scientific American, 242(2): 84–95.

Spear, D. B., and King, J. S., 1982, The geology of Big Southern Butte, Idaho; *in* Bonnichsen, B., and Breckenridge, R. M. (eds.), Cenozoic geology of Idaho: Idaho Bureau of Mines and Geology, Bulletin 26: 395–403.

Stearns, H. T., and Isotoff, A., 1956, Stratigraphic sequence in the Eagle Rock volcanic area near American Falls, Idaho: Geological Society of America, Bulletin, 67: 19–34.

Street, L. V., and DeTar, R. E., 1987, Geothermal resource analysis in Twin Falls County, Idaho; *in* Geothermal investigations in Idaho: Idaho Department of Water Resources, Water Information Bulletin No. 30, Part 15, 46 pp. plus appendices.

Stewart, J. H., and Carlson, J. E., 1978, Geologic map of Nevada: U.S. Geological Survey, scale 1:500,000.

Struhsacker, D. W., and Jewell, P. W., Zeisloft, J., and Evans, S. H., Jr., 1982, The geology and geothermal setting of the Magic Reservoir area, Blaine and Camas Counties, Idaho; *in* Bonnichsen, B., and Breckenridge, R. M. (eds.), Cenozoic geology of Idaho: Idaho Bureau of Mines and Geology Bulletin 26: 377–393.

Swanson, D. A., Wright, T. L., and Helz, R. T., 1975, Linear vent systems and estimated rates of magma production and eruption for the Yakima basalt on the Columbia Plateau: American Journal of Science, 275: 877–905.

Wernicke, B., Axen, G. J., and Snow, J. K., 1988, Basin and Range extensional tectonics at the latitude of Las Vegas, Nevada: Geological Society of America, Bulletin, 100: 1738–1757.

White, D. E., Muffler, L. J. P., and Truesdell, A. H., 1971, Vapor-dominated hydrothermal systems compared with hot-water systems: Economic Geology, 66: 75–97.

White, D. E., Fournier, R. O., Muffler, L. J. P., and Truesdell, A. H., 1975, Physical results of research drilling in thermal areas of Yellowstone National Park, Wyoming: U.S. Geological Survey, Professional Paper 892: 70 pp.

Wood, S. H., and Gardner, J. N., 1984, Silicic volcanic rocks of the Miocene Idavada Group, Bennett Mountain, southwestern Idaho: Final contract report to the Los Alamos National Laboratory from Boise State University, 55 pp.

EXCURSION 12B:
South Cascades arc volcanism, California and southern Oregon

L. J. P. Muffler[1], C. R. Bacon[1], R. L. Christiansen[1], M. A. Clynne[1], J. M. Donnelly-Nolan[1], C. D. Miller[2], D. R. Sherrod[1], and J. G. Smith[1]

[1]*U.S. Geological Survey, Menlo Park, California 94025;* [2]*U.S. Geological Survey, Cascades Volcano Observatory, Vancouver, Washington 98661*

Introduction

The Cascade Range is a late Tertiary and Quaternary volcanic arc that extends north from northeastern California through Oregon and Washington into British Columbia. The volcanic arc lies above an easterly dipping active subduction zone along which the Juan de Fuca, Gorda, and Explorer plates are thrust beneath the North American plate (Riddihough, 1984). In addition to the major composite volcanoes that have erupted andesites, dacites, and even rhyolites, there are many smaller, commonly monogenetic vents that erupted primarily calc-alkaline basalt and basaltic andesite throughout the history of the arc (McBirney, 1978; Luedke and Smith, 1981, 1982; Smith and Luedke, 1984; Guffanti and Weaver, 1988). The volcanic arc is active, with certain historic eruptions at Lassen Peak (1914-17) and Mount St. Helens (mid-1800's; 1980-86), and possible historic eruptions at Mt. Shasta (1786), Mt. Baker (mid-1800's), Mt. Hood (mid-1800's) , Mt. Rainier (mid-1800's) and Cinder Cone (east of Lassen Peak; 1851?).

This field guide is designed as a six-day introduction to the volcanic geology of the Cascade Range in northern California and southern Oregon (Fig. 1). Emphasis is placed on four major Quaternary volcanic centers of the High Cascades:

The Lassen volcanic system: An andesitic stratovolcano with a large, young silicic domefield on its northeast flank.

Medicine Lake volcano: A largely basaltic shield complex in an extensional environment just east of the main axis of the High Cascades.

Crater Lake (Mount Mazama): Site of a catastrophic pyroclastic eruption of a zoned magma chamber about 6800 years ago.

Mount Shasta: A classic subduction-zone stratocone.

The guide also treats regional Quaternary basaltic and andesitic volcanism of the High Cascades and includes a leg through the Western Cascade Range, the mildly deformed and deeply eroded mid-Tertiary analog of the younger High Cascades.

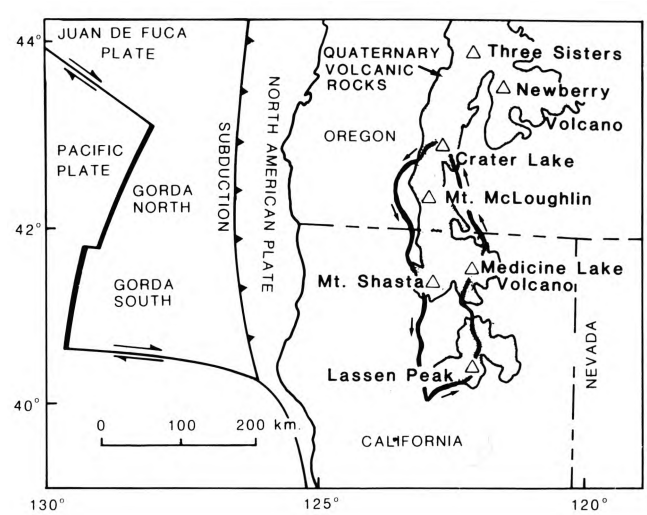

FIGURE 1—Map of the southern Cascade Range showing Quaternary volcanic rocks (pattern) and field-trip route.

Most of the basic geologic mapping, petrology, geochemistry, and isotopic dating upon which this guide is based have been developed in the last 10 years as part of the Geothermal Research Program of the U.S. Geological Survey. In turn, these modern investigations rest on the foundations provided by Howel Williams (1932a, 1932b, 1942) and Charles A. Anderson (1933a, 1933b, 1940, 1941) in their pioneering investigations of volcanism in the southern Cascade Range.

Acknowledgments

We acknowledge with gratitude the able assistance of Anne E. Gartner in preparation of the illustrations, as well as helpful technical reviews by Marianne Guffanti and Donald W. Peterson.

Lassen Volcanic National Park and vicinity

Michael A. Clynne and L. J. Patrick Muffler

Summary

This leg of the field trip provides an overview of Quaternary volcanic rocks in and around Lassen Volcanic National Park, with a stop at each major stratigraphic unit of the Lassen volcanic center. Additional stops focus on the 1915 eruption of Lassen Peak, the Lassen geothermal system, regional tectonism, and mafic volcanism.

On a regional scale, Quaternary volcanism in the southernmost Cascade Range is predominantly basaltic to andesitic and consists of hundreds of coalescing volcanoes of

small to medium volume (10^{-3} to 10^2 km^3) and relatively short lifetimes (10^0 to 10^3 yrs). Superimposed on this regional mafic volcanism are a few long-lived, much larger volcanic centers that have erupted products ranging from basaltic andesite to rhyolite.

Each of the larger centers consists of an andesitic composite cone and flanking silicic domes and flows. Four such centers younger than about 3 Ma have been recognized in the Lassen area (Fig. 2). Each was built in three stages:

Stage I: Cone-building basaltic andesite and andesite lava flows and pyroclastic rocks.

Stage II: Thick, cone-building lava flows of andesite and silicic andesite.

Stage III: Silicic domes and flows flanking the main cone.

The silicic magma chamber of Stage **III** provides a heat source for a hydrothermal system that develops within the core of the main cone. Alteration of permeable rocks of the cone facilitates glacial and fluvial erosion of the central part of the volcano. The result is selective preservation of a resistant rim of Stage-II lavas and flanking silicic rocks around a central depression. The three older volcanic centers in the Lassen area, the Dittmar, Maidu, and Yana volcanic centers, have reached this stage, and their hydrothermal systems are extinct. The fourth and youngest center, here called the Lassen volcanic center (LVC), hosts active silicic volcanism and a well-developed active hydrothermal system.

Stages I and **II** of LVC produced the Brokeoff volcano (BV), an 80 km^3 andesitic stratocone (Fig. 3). The bulk of BV consists of Stage-I deposits (olivine—augite and hypersthene—augite andesite lava flows and stratified pyroclastic deposits) that erupted from a central vent at 600-470 ka. Stage I culminated in eruption of a small volume of hornblende—pyroxene dacite lava. During Stage **II,** which lasted about 70,000 yrs, thick flows of porphyritic augite—hypersthene silicic andesite, generally lacking interbedded pyroclastic material, were erupted. Stage **III** was initiated by eruption of at least 50 km^3 of rhyolitic magma (Rockland airfall and ash flows) at about 400 ka. This eruption is thought to have produced a caldera that is now filled by a silicic domefield. This domefield consists of three groups of rocks totaling about 30-50 km^3:

Group 1: Hornblende—biotite rhyodacite lavas related to the Rockland magma (e.g., Raker Peak).

Group 2: Six domes and flows of 2-pyroxene—hornblende dacite lavas erupted at 250-200 ka (e.g., Bumpass Mtn.; Ski Heil Peak; Mt. Helen).

Group 3: Hornblende—biotite dacite and rhyodacite erupted as domes, lava flows, and pyroclastic flows in at least 10 episodes, mostly during the past 100 ka (e.g., Lassen Peak; Chaos Crags).

Throughout Stage **III,** large flows of hybrid andesite totaling 10 km^3 and consisting of thoroughly mixed mafic and silicic magma were erupted peripherally to the silicic domefield, primarily on the Central Plateau.

Porphyritic andesite and dacite with high $A1_2O_3$, low TiO2, and medium K_2O contents and FeO/MgO ratios of 1.5-2.0 are the most abundant rock types in LVC. Sparsely porphyritic rhyolite pumice (Rockland) is the single most voluminous unit. Basaltic andesite, rhyodacite, and hybrid andesite are subordinate in abundance. Rocks of LVC resemble other calc-alkaline volcanic rocks emplaced on continental margins overlying sialic crust. Major-element Harker-variation diagrams of LVC show smooth trends from 53 to 75% SiO_2 (Clynne, 1984). The general compositional evolution is from mafic to silicic with time, although the evolution is not strictly sequential (Fig. 4). Petrographic characteristics and geochemical systematics indicate a complex origin for mafic and intermediate LVC magmas, involving mixing and crystal fractionation of heterogeneous mantle-derived parental melts. Partial melting of young mafic crust may play a role in the origin of the more silicic magmas. Hybrids and ubiquitous quenched mafic inclusions provide abundant evidence for the interaction of mafic and silicic magma. The long span of activity at LVC and the presence of a large hydrothermal system imply an evolving magma chamber.

LVC differs from most other Cascade volcanoes by having a larger volume of silicic rocks, perhaps due to moderate east—west extension, which favors retention of mafic magma by mixing with more differentiated magma in the crust. The present magma system of LVC can be envisaged (Fig. 5) as an evolving body of magma 5-8 km in diameter in the middle crust (10-20 km depth) under the northwest part of LVC. The upper portion of the chamber contains crystal-rich rhyodacite, which has varied little in composition over at least the last 50 ka years. The system is probably zoned to more mafic compositions at depth. Basalt from depth provides heat and material input to maintain the system in its partially molten state.

Despite the volcanologic and petrologic evidence of a magma system, teleseismic and seismic-refraction studies (Berge and Monfort, 1986; Berge and Stauber, 1987) have failed to detect a magma chamber beneath LVC. A 25 km, oval, 50 mGal negative gravity anomaly is centered on the silicic domefield and the Central Plateau (hybrid andesites) of LVC. This gravity low is probably the expression of low-density volcanic rocks near the surface and Quaternary plutonic rocks at depth. North-northwest-trending normal faults in the Lassen region reflect the impingement of Basin and Range tectonics on the Cascade arc (Guffanti and Weaver, 1988).

Ages of Pleistocene rocks in the Lassen region are based on K—Ar dates by G. B. Dalrymple and A. L. Cook, ^{14}C and U—Th dates by D. A. Trimble and S. W. Robinson, and paleomagnetic determinations by D. E. Champion.

Field guide

Mileage

0.0 At Red Bluff turn east from Interstate 5 onto California Highways 36 and 99. **2.1**

2.1 Turn left on CA-36 toward Susanville and Lassen Volcanic National Park. **1.7**

3.8 Roadcuts in Quaternary terrace gravels related to the Sacramento River. **1.1**

4.9 Contact of terrace gravels overlying Tuscan Formation (3.3–2 Ma). The Tuscan Fm. forms a widespread apron west of the southernmost Cascade Range, and consists predominantly of volcanic mudflows (lahars) derived primarily from the Yana and Dittmar volcanic centers. Volcanic sedimentary deposits of fluvial origin are locally significant. Silicic ash-flow and air-fall tuffs, basaltic to andesitic lava flows, and intrusions also occur. The Tuscan Fm. originally covered about 5000 km^2 to a maximum thickness of 500 m and had a volume of 1200 km^3 (Lydon, 1968). Weathering and erosion of de-

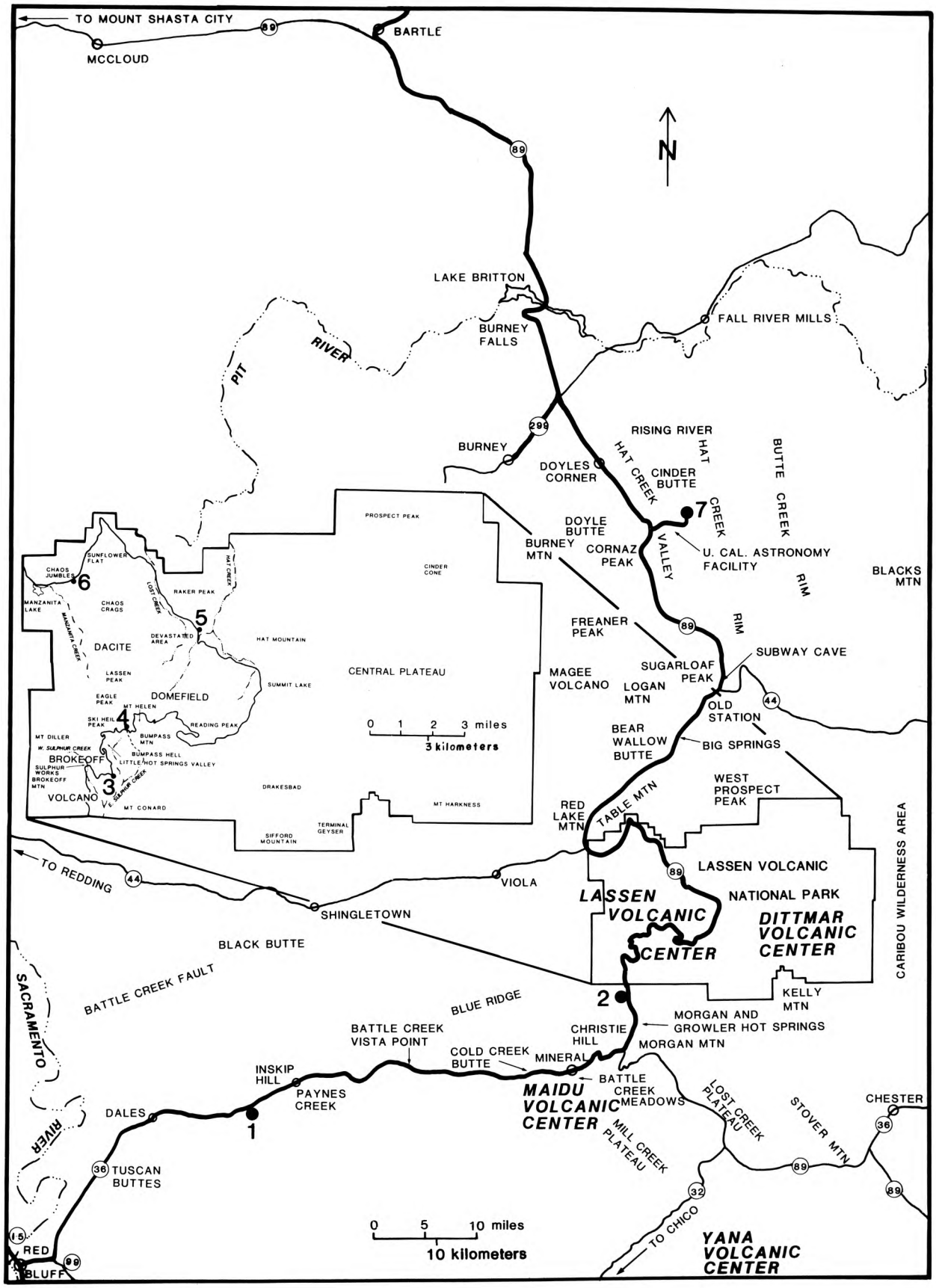

FIGURE 2—Map of the Lassen region showing field-trip route.

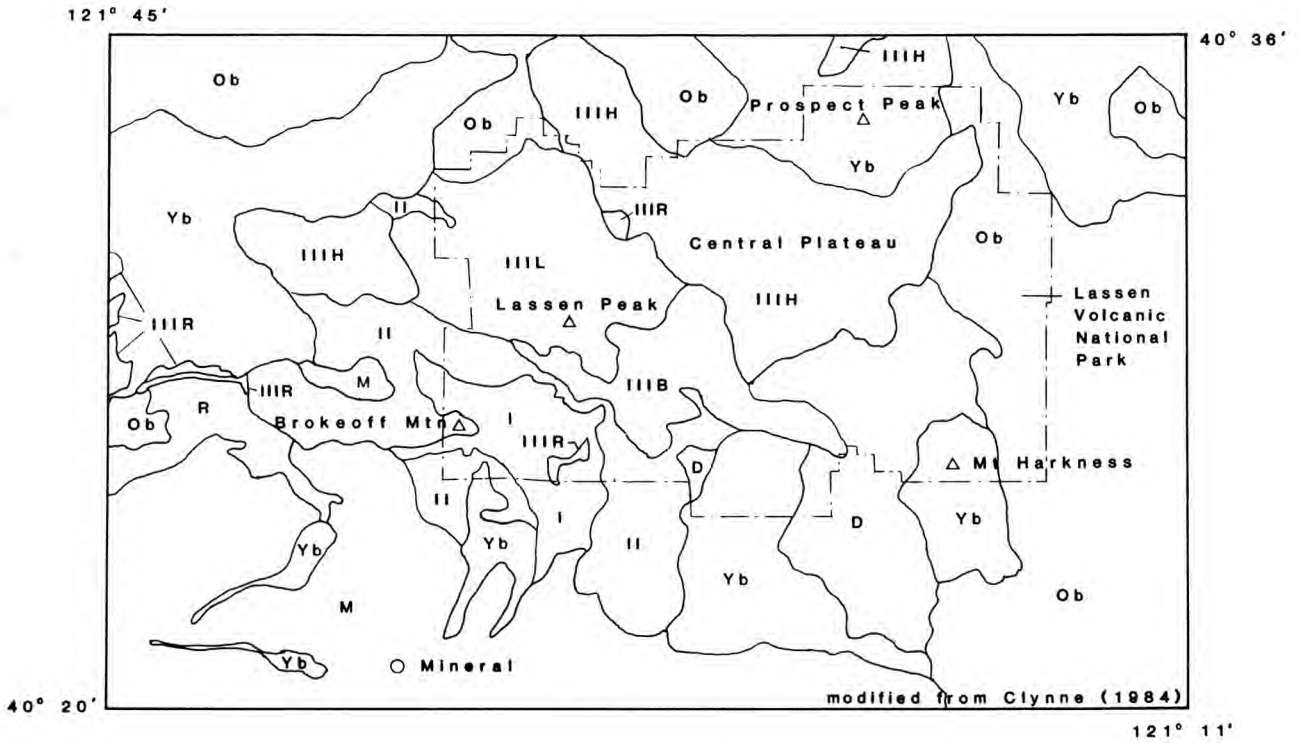

Scale 1:250,000

0 5 10 Miles

0 10 Kilometers

VOLCANIC CENTERS

REGIONAL VOLCANISM

LASSEN VOLCANIC CENTER

STAGE III

IIIT — Hybrid andesites; shields and cones; augite andesite and olivine andesite; 0.30-0 Ma

IIIL — Dacite domefield; domes, flows and pyroclastic flows; hornblende-biotite dacite and rhyodacite, mostly 0.1-0 Ma

IIIB — Dacite domefield; domes and flows; 2-pyroxene-hornblende dacite, .25-.20 Ma

IIIR — Rockland Tephra & associated debris flows, domes and flows; hypersthene-hornblende rhyolite and hornblende-biotite rhyolite approximately .40 Ma

STAGE II

II — Brokeoff Volcano; flows; augite-hypersthene andesites; .47-.40 Ma

STAGE I

I — Brokeoff Volcano; flows and stratified pyroclastic deposits; olivine-augite andesite and 2-pyroxene andesite, .60-.47 Ma; flows; 2-pyroxene-hornblende dacite; .47 Ma

MAIDU VOLCANIC CENTER

M — Composite cone; mafic andesite to andesite; dacite domefield; rhyolite flows; 0.8-2.0 Ma

DITTMAR VOLCANIC CENTER

D — Composite cone; mafic andesite to dacite and peripheral silicic rocks; approximately 1.4-2.0+ Ma

Yb — Younger basalts to andesites; shield volcanoes & cinder cones

Ob — Older basalts to andesites; shield volcanoes & cinder cones

FIGURE 3—Generalized geologic map of Lassen Volcanic National Park and vicinity.

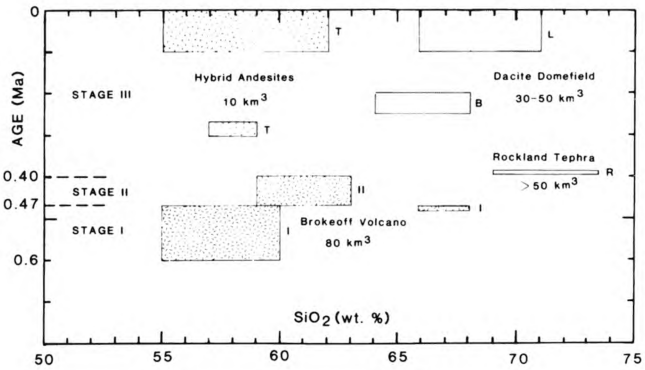

FIGURE 4—Time–composition diagram for rocks of the Lassen Volcanic Center. Symbols as in Fig. 3. Some units in Stage III with poorly constrained ages may fall outside the indicated fields. Volume estimates are approximate.

bris-flow matrix produces a characteristic "stony plain." **5.2**

10.1 In the distance ahead is the scarp of the east-trending Battle Creek fault. This fault cuts rocks as young as 1 Ma, but lavas slightly younger than 400 ka drape the scarp without offset. **3.2**

13.3 The settlement of Dales and the intersection with county road A16 to the left; continue straight on CA-36. For the next mile there are views at 12:00 of the west side of Brokeoff volcano (BV) and of parts of the Maidu volcanic center (MVC). **5.7**

19.0 Roadcuts for the next 3 mi alternate between Tuscan Fm. and lava flows from Inskip Hill, a late Pleistocene shield volcano located trenchward of the Cascade arc. Inskip Hill is composed of calc-alkaline basalt that is depleted in incompatible elements relative to the majority of basalts found in the Lassen area. **0.8**

19.8 **STOP 1. Debris avalanche in the uppermost part of the Tuscan Fm.** Pull off on broad turnout on right side of road; the debris avalanche is exposed in the roadcut directly opposite the turnout. **Beware of high-speed logging trucks when crossing the highway.** The deposit is probably about 2 Ma, has lost its original hummocky topography, and consists of megablocks of various volcanic rock types in a matrix of crushed material (Fig. 6). The three most abundant rock types (dark-gray ash-flow tuff with black pumice and sporadic fragments of obsidian; light-gray ash-flow tuff; andesite rich in large green clinopyroxene) can be traced to their source in the Dittmar volcanic center, approximately 48 km east.

Notable features of this debris flow are the heterogeneity of the matrix composition, the invasion of matrix material into fractures and joint surfaces of lava blocks, the jigsaw fit of some blocks, and features indicating laminar flow of matrix material beneath the megablocks at the base of the deposit.

In the roadcut 150 m west, the megabreccia is underlain by an ash-flow tuff of lithology identical to the ash-flow tuff blocks in the megabreccia. Between the ash-flow tuff and the megabreccia is a discontinuous, poorly sorted, channel-filling alluvial deposit.

The roadcut 150 m east exposes thin basalt flows from Inskip Hill, 2.7 km north-northeast. **11.3**

31.1 Battle Creek Vista Point. View of the Tuscan Fm. overlain by the Blue Ridge Rhyolite (1.2 Ma), a single 15 km^3 flow from the Maidu volcanic center (MVC). Similar huge flows form Lost Creek Plateau, Mill Creek Plateau, and Stover Mtn. on the southeast flank of MVC. **0.4**

31.5 White deposits of Rockland ash flow (0.4 Ma) with orange soil are exposed in low roadcuts for the next 2.5 mi. **5.2**

36.7 Roadcuts of andesitic flows and pyroclastic rocks from the MVC. **2.2**

38.9 Quarry in the cinder cone of Cold Creek Butte, an upper Pleistocene olivine–augite calc-alkaline basalt. Flows from this vent dammed Battle Creek to create Battle Creek Meadows. **1.1**

40.0 Bare rubble to right is a basalt flow from Cold Creek Butte. **0.1**

40.1 Cross the South Fork of Battle Creek into Battle Creek Meadows, the center of the hydrothermally altered and deeply eroded core of the andesitic stratocone of MVC; andesites of the stratocone are exposed on the cliffs north of the creek. The stratocone of MVC was active from about 2 to 1.5 Ma. The petrologic evolution of MVC is similar to that of the younger LVC. **1.7**

41.8 Mineral Lodge. To the east, CA-36 climbs over the

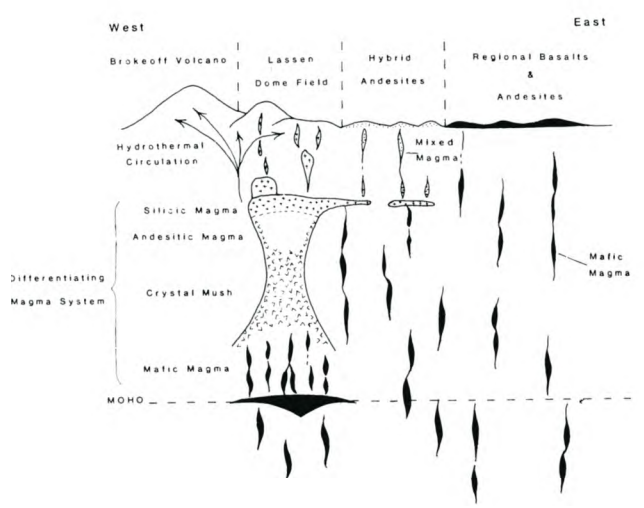

FIGURE 5—Model of Lassen volcanic center.

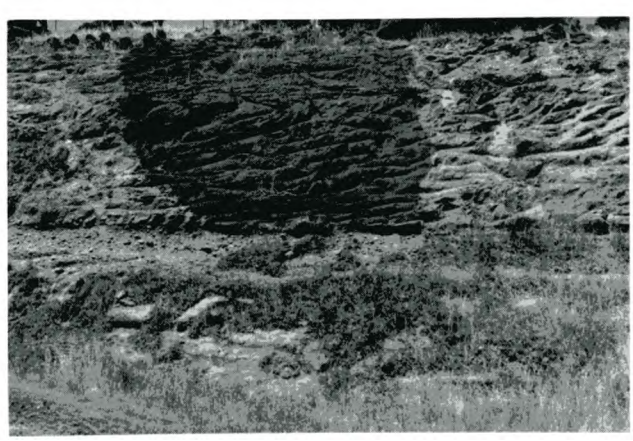

FIGURE 6—Roadcut exposing debris flow in the Tuscan Formation (Stop 1).

resistant rim of the andesitic stratocone of the MVC. The intensity of hydrothermal alteration diminishes abruptly. **2.4**

44.2 White roadcuts for the next 2 mi are in altered dacites of Christie Hill, one of many dacite domes emplaced at 1.1 Ma as part of Stage III of MVC. **2.1**

46.3 Turn left onto CA-89. To the right for the next 1.4 mi is the dacite dome of Morgan Mtn., another of the Stage-III dacite domes of MVC. The valley to the left between Christie Hill and Morgan Mtn. is filled by a 300 ka olivine basaltic andesite flow from a vent high on the flank of Brokeoff volcano (BV). This flow represents a return to regional mafic volcanism after the extinction of BV at 400 ka. **2.3**

48.6 Exposure in roadcut to left of glacial till of middle Tioga age (approximately 25–18 ka). Glacial deposits in LVNP and vicinity are thought to represent at least five periods of glaciation, which have been tenuously correlated to Sierra Nevadan glacial stratigraphy by Crandell (1972) and Kane (1982). **1.6**

50.2 **STOP 2. Bluff Falls Quarry.** Park on right, walk 100 m north, cross the highway carefully, and climb up the slope just north of the small stream. The quarry exposes nearly the entire thickness of a typical silicic andesite lava flow from Stage II of BV. The base of the flow (not exposed here) consists of thin, reddened, scoriaceous flow breccia, which is overlain by a massively jointed, faintly flow-banded, glass-rich zone (Fig. 7). This zone grades upward into a thick zone of thin platy jointing. In the flow interior, platy jointing is nearly horizontal to slightly wavy, but at flow edges it can be ramped upward or highly contorted. On the glaciated flanks of BV, the orientation of the platy jointing can be used to map flow edges and flow direction. The platy interior of the flow grades upward into a zone with columnar joints superimposed on the platy jointing. The upper surface of the flow is glassy and vesicular.

This flow is a porphyritic, 60% SiO_2 rock containing abundant plagioclase, hypersthene, and augite phenocrysts in a cryptocrystalline groundmass. Sparse olivine xenocrysts are derived from disaggregation of abundant glomeroporphyritic clots that have gabbroic composition and texture and consist of the same minerals as the phenocrysts plus olivine. Patchy recrystallization of the plagioclase, vague exsolution lamallae in the pyroxenes, and solid-state replacement of olivine by orthopyroxene suggest that the clots represent cumulate material removed from an andesite magma similar to the andesite of Bluff Falls Quarry and incorporated into its present host. These clots are abundant in all Stage-II lava flows. **1.6**

51.8 Entrance station for Lassen Volcanic National Park. Just beyond is the Lassen Chalet, with a restaurant, rest rooms, and Park information. The entrance station and the buildings beyond are located on a large landslide that 3310 years ago moved 7 km down Mill Creek from the cliff at the base of Brokeoff Mtn.

Note that **collecting or disturbing rock, mineral, or other natural specimens in Lassen Volcanic National Park is prohibited except by special permit. 1.0**

52.8 Sulphur Works, the most accessible of the thermal areas in LVNP. A short boardwalk guides visitors safely through an area of drowned fumaroles, boiling pools, and steaming ground. **1.4**

54.2 **STOP 3. Diamond Peak in the center of Brokeoff volcano (BV).** Most of the BV rocks that can be seen from this viewpoint (Fig. 8) are at least incipiently altered, and most areas in the core of the cone are strongly to totally altered. Flows and breccias on Diamond Peak dip steeply eastward, indicating that the Stage-I summit vent of BV was nearby to the west. To the south, in the glacial valley of Mill Creek, the base of BV is exposed where it overlies rocks of MVC. Mill Canyon and the flanks of Brokeoff Mtn. expose nearly the entire BV stratigraphy. Thick flank flows of olivine–augite and hypersthene–augite andesite can be correlated across Mill Canyon with no offset by faulting. The triangle-shaped peak of Brokeoff Mtn. to the west is resistant to erosion by virtue of a thick flow of dacite that ended Stage I. To the east, Little Hot Springs Valley displays numerous thermal features. Cliffs

FIGURE 7—Features of a silicic andesite lava exposed in the Bluff Falls Quarry (Stop 2).

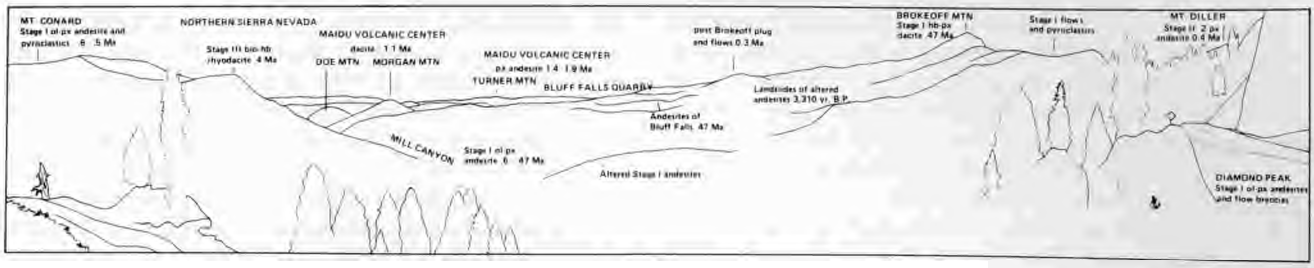

FIGURE 8—Panorama of Brokeoff volcano from Diamond Peak (Stop 3).

on the east side of the valley expose thin lava flows of Stage I intercalated with hydrothermally altered flow breccias and pyroclastic deposits. The cliffs are capped by Stage-II flows. To the southeast, Stage-I flows and breccias form most of Mt. Conard. The cliff forming the prominent shoulder above Mill Canyon is a single Stage-II lava flow overlain by a thick rhyodacite lava flow of Stage III, Group 1. Both flows followed the course of a canyon cut in Stage-I rocks of BV. The rhyodacite flow is about 400 ka and illustrates the amount of erosion in the core of BV since that time.

Williams (1932a) attributed the amphitheater in the central area of BV to a caldera-forming pyroclastic eruption. Our detailed mapping, however, has failed to reveal caldera-bounding faults. On the contrary, although the cone is deeply eroded, the stratigraphy is coherent. The Rockland tephra, originally thought to be older than BV, has been shown to be younger than the cone and contains BV rocks as lithic fragments; its source appears to have been the north flank of the BV. Thus, the central depression of BV was probably caused by fluvial erosion greatly enhanced by hydrothermal alteration and glaciation. Valley walls of altered rock oversteepened by glacial erosion were further destabilized by rapid fluvial downcutting. During interglacial times, landslides were a significant mass-wasting process. A large proportion of the terrain below Brokeoff Mtn. and Mt. Diller consists of landslide deposits, and the valley of Sulphur Creek below Sulphur Works is filled by reworked landslide material. **2.6**

56.8 White, kaolinite-rich altered Stage-I andesite of BV at sharp bend in road. **0.6**

57.4 Just before the south end of Emerald Lake the road crosses the contact between the uppermost preserved rocks of BV and the 250 ka pyroxene–hornblende dacite dome of Ski Heil Peak (Group 2 of Stage III). Straight ahead, Eagle Peak is a 57 ka rhyodacite dome (part of Group 3) that was preceded by a flow (the cliffs ringing the mountain), air-fall pumice (that mantles Ski Heil Peak), and a pyroclastic flow. **0.4**

57.8 **STOP 4. Four-kilometer round-trip walk to Bumpass Hell.** First, walk out to the south end of the parking lot for excellent views of all three stages of the LVC. The parking lot is built on the contact between Stage-II BV flows and Stage-III dacites of Group 2. Note the glacial striations and glacial boulders; the prominent 2 m boulder is pyroxene dacite from Bumpass Mtn.

The gentle, level trail to Bumpass Hell winds along the contact between Stage II and Stage III of LVC. The massive dacite of Bumpass dome (Group 2 of Stage III) is marked by well-preserved glacial striae. All the dacite domes of the Group 2 have suffered extensive glacial erosion. Although their shape has not been greatly modified, no trace of an outer glassy or pumiceous carapace or talus mantle is preserved. The middle part of the trail has been blasted from the massively jointed devitrified interior of the dome. At the viewpoint where the trail turns east, 0.85 km from the parking lot, Stage-II andesite is exposed. The upper flow surface of the andesite was eroded before deposition of the overlying dacite breccia.

The Lassen geothermal system (Fig. 9) consists of a central vapor-dominated reservoir at a temperature of 235°C underlain by a reservoir of hot water (Muffler et al., 1982; Ingebritsen and Sorey, 1985). The focus and major thermal upflow is at Bumpass Hell, which is located at the vent for Bumpass Mtn., along the contact between BV and the Stage-III silicic domefield. Natural discharge from the deep hot-water part of the Lassen geothermal system occurs only at Morgan Hot Springs and Growler Hot Spring, both located in the canyon of Mill Creek nearly 1000 m below Bumpass Hell. These springs, which discharge near-neutral chloride water and deposit silica, occur at the contact between BV rocks and rocks of the underlying MVC. Part of the deep hot water also flows laterally to the southeast, where it is encountered in well Walker "O" No. 1 at Terminal Geyser.

Bumpass Hell (Muffler et al., 1983) contains numerous superheated fumaroles, one of which had a temperature in the summer of 1988 of 161.4°C (C. J. Janik, oral comm.). Approximately 75 major fumaroles, acid-sulfate hot springs, and mudpots, plus a myriad of smaller features, occur in an area of approximately 0.13 km^2 that is intensely altered to an aggregate of opal and kaolinite. Much of the surface of the active part of Bumpass Hell is covered

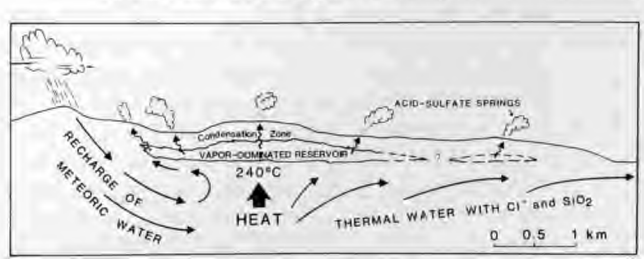

FIGURE 9—Schematic cross section of the Lassen geothermal system (from Muffler et al., 1982).

with orange and yellow sulfates. Pyrite is common in many of the hot springs as linings of the vents and discharge channels, as scum floating on the surface of pools, and as dispersions in gray or black mudpots.

The acid-sulfate water from Bumpass Hell is typical of hot springs related to a vapor-dominated reservoir in having low pH, high sulfate, and no significant Cl. Most other thermal areas in LVNP have thermal features and chemistry similar to Bumpass Hell and are also manifestations of the vapor-dominated reservoir. Some springs near Sulphur Works, in Little Hot Springs Valley, and at Drakesbad are relatively rich in HCO_3^- and deposit travertine. These springs are interpreted to be surface discharge from the zone of steam condensate that overlies the vapor-dominated reservoir (Muffler et al., 1982). **1.3**

59.1 The large parking lot marks the start of a good trail that gains 600 m in elevation as it switchbacks for 4 km to the summit of Lassen Peak, a dacite dome complex that we think was emplaced between 29,000 and 18,000 years ago. At the summit one can see the 1915–17 eruption craters and deposits and on a clear day have good views of the Sierra Nevada, Sacramento Valley, Coast Ranges, Klamath Mountains, Mount Shasta, and the Medicine Lake Highlands. **0.2**

59.3 Summit of road at 8512 ft. To the right is the Mt. Helen dome, rich in mafic blobs, and on the left is the Kings Creek flow, a 30 ka hornblende–biotite rhyodacite flow. This flow and associated pyroclastic flows issued from a vent now covered by Lassen Peak. Much of the pumiceous glassy carapace and structure of the flow is preserved because it has not been heavily glaciated. Directly ahead, the next roadcut exposes thick breccia at the base of the flow. To the right beyond Mt. Helen are the 230 ka pyroxene–hornblende dacite dome and flow complex of Bumpass Mtn. and a short stubby pyroxene–hornblende dacite flow from Mt. Helen. **0.7**

60.0 View of Reading Peak, a deeply glaciated, 212 ka pyroxene–hornblende dacite dome complex of Group 2. To the right and behind Reading Peak are Mt. Harkness (a late Pleistocene basaltic andesite shield), Kelly Mtn. (a remnant of the Dittmar volcanic center), and Sifford Mtn. (another late Pleistocene basaltic andesite shield). **2.5**

62.5 Excellent view of Lassen Peak at 12:00, Mt. Helen at 10:30, and Bumpass Mtn. at 9:30. The shoulder to the left of Bumpass Mtn. is Stage-II andesite of BV. Farther to the left is Mt. Conard, composed of Stage-I andesites. **2.0**

64.5 Cross Kings Creek. To the left is the dacite dome of Reading Peak. To the right is the large dacite flow which vented at Bumpass Mtn. **0.8**

65.3 The skyline to the right, visible through the trees for the next 2.7 mi, is in the Caribou Wilderness Area, an intensely glaciated area of many small late Pleistocene basalt and andesite vents. **1.3**

66.6 Elevation 7000 ft. For the next 3/4 mi, volcanic vents of the Central Plateau are visible to the right through the trees. Rocks of the Central Plateau are all hybrid andesites. The youngest is Cinder Cone, which definitely erupted 450 years ago and may have erupted in 1851. At 12:00 is Hat Mtn., dated at approximately 25 ka. Exposed along the road is monolithologic till derived from Reading Peak. **1.5**

68.1 Summit Lake. For the next 3 mi, the road passes through till with sporadic outcrops of Stage-III rhyodacite. **3.3**

71.4 **STOP 5. Devastated Area parking lot.** New field studies by Christiansen and Clynne (1986 and unpublished mapping) and a reanalysis of previous work provide a geologic map at 1:24,000 and a revised scenario of the May 1915 eruptions of Lassen Peak. After a year of intermittent steam blasts and formation of a summit crater 350 m in diameter, in mid-May of 1915 lava welled into the crater to form a small dome of black glassy dacite. The dome grew for five or six days and on the night of May 19–20 was disrupted by a single explosion. No juvenile material was ejected by this explosion, but fragments of the still hot dome fell on the snow-covered upper flanks of Lassen Peak, generating an avalanche that flowed 5 km down a 0.8 km wide path. Fragmentation of the avalanching lava blocks melted enough snow to generate a large debris flow that went 15 km further down Lost Creek. Also on the night of May 19–20, dacite lava erupted from the vent opened by the dome-disrupting explosion, spilled over the low west and northwest crater rims, and flowed approximately 300 m down the steep slopes.

After two quiet days, an explosive subplinian eruption on the afternoon of May 22 produced a new crater and erupted compositionally layered (banded) dacite–andesite pumice and unlayered dacite to rhyodacite pumice. Fallback onto the still partly snow-covered east slope of Lassen Peak generated a pyroclastic flow that incorporated snow. Melting of this snow transformed the pyroclastic flow into a highly fluid debris flow which continued down Lost Creek. Continued eruption of pumice deposited a fallout lobe to the east and produced several smaller viscous debris flows on the slopes of Lassen Peak.

In the May 1915 eruptions, four types of volcanic rock were produced from Lassen Peak: (1) a black lava dome (64–65% SiO_2) formed between May 14 and 19 and a dacitic lava flow (64–65% SiO_2) emplaced on May 19, (2) dark bands in banded pumice (60–61% SiO_2), (3) light bands in banded pumice (64–69% SiO_2) and unlayered light pumice erupted on May 22, and (4) quenched inclusions of andesitic magma (57–60% SiO_2) that occur in the lavas and light pumice.

The black lava dome and flow and the light pumice contain large plagioclase, biotite, hornblende, and quartz phenocrysts in a glassy groundmass with plagioclase, clinopyroxene, hypersthene, and oxide microphenocrysts. Two populations of each phenocryst type are present: one that is unresorbed, and one that is strongly resorbed. Olivine phenocrysts (Fo_{84}, 2400 ppm Ni) are present in all the rock types.

The dark pumice bands have small olivine phenocrysts in a dark glassy groundmass with tiny pyroxene and plagioclase microlites. All degrees and scales of mixing between the light and dark bands can be found.

Quenched inclusions up to 50 cm across comprise as much as 5% of the black lavas and light pumice bands. The gray to black inclusions have phenocrysts of olivine in a microvesicular network of acicular plagioclase, clinopyroxene, and hypersthene microphenocrysts, with abundant interstitial light- to dark-brown glass. The dark pumice bands and the quenched inclusions also contain resorbed felsic phenocrysts.

All the 1915 rock types are mixtures. End members are hornblende–biotite rhyodacite (70% SiO_2) and olivine basalt or basaltic andesite (52–54% SiO_2). The quenched andesitic inclusions contain about 35% silicic components. The black lavas were formed by disaggregation of quenched inclusions in rhyodacite and contain about 30–40% mafic components. Dark bands in banded pumice are similar in composition to quenched andesitic inclusions, and light bands are similar in composition to black lava.

Leaving the Devastated Area parking lot, the cliff ahead and to the right is the rhyolite of Raker Peak. This rhyolite belongs to Group 1 of Stage III and has a composition identical to the most silicic Rockland tephra. The glaciated front face of the dome may have been a caldera-bounding fault related to eruption of the Rockland magma. Note the internal flow structure of the dome revealed by truncation. For the next 1.8 mi, the road crosses 1915 mudflows, then a Tioga moraine, and then drops down onto the mudflows again. **2.5**

73.9 Lost Creek. 1915 debris flows overlie pyroclastic flows from the 1000 years old Chaos Crags eruptions; excellent exposures of both can be seen in quarries 1.5 km upstream.

For the next 2 mi, the road passes through Tioga till that contains boulders of dacite from Lassen Peak. **2.1**

76.0 To the left are the Sunflower Flat domes, a group of seven 35 ka hornblende–biotite rhyodacite domes preceded by eruption of air-fall pumice and a pyroclastic flow (the flat over which the road passes). Mature forest obscures the relatively youthful morphology. **0.6**

76.6 Two-pyroxene andesite of Table Mtn. on the right came from a vent at 10:30. **1.4**

78.0 Talus on left is from one of the Sunflower Flat dacite domes; the road is once again on pyroclastic flow of Sunflower Flat. **0.8**

78.8 Edge of Chaos Jumbles. **0.6**

79.4 **STOP 6. Chaos Crags, Chaos Jumbles, and quenched mafic inclusions.** Detailed geologic mapping (R. L. Christiansen and M. A. Clynne, unpublished) has added significant new detail to the general stratigraphy of the Chaos Crags given by Crandell et al. (1974). The initial event of the Chaos Crags eruptive sequence 1000 years ago was the eruption of pumice and lithic debris and the formation of a tuff cone (Table 1). Eruption of two pyroclastic flows, A and B, quickly followed; these were confined to the valleys of Lost and Manzanita Creeks, where they flowed to a distance of 5 km. Dome 0 grew in the vent of the pyroclastic eruptions and then was partly destroyed by a large pyroclastic eruption that emplaced the widespread pyroclastic flow C. At 3 km from the vent, pyroclastic flow C became confined to the drainages of Lost Creek and Manzanita Creek, where it flowed to a distance of

TABLE 1—Summary of events in the formation of Chaos Crags. Unpublished data of R. L. Christiansen and M. A. Clynne, with ^{14}C and tree-ring correlation ages from the USGS Menlo Park Radiocarbon Laboratory.

Three cold rockfall avalanches from dome 2 formed Chaos Jumbles, ^{14}C age 275 ± 25 years (weighted average of three samples), tree-ring correlation age 1619 ± 63 A.D.

Hiatus of approximately 700 years

Hot dome-collapse pyroclastic flow from dome 4
Emplacement of dome 4
Emplacement of dome 3b
Warm dome-collapse avalanche from 3a
Emplacement of dome 3a
Hot dome-collapse pyroclastic flow from dome 2
Emplacement of dome 2

Hiatus??

Emplacement of dome 1
Explosive disruption of dome 0 by eruption of pyroclastic flow C, accompanied by a coignimbrite fall deposit and formation of a tuff cone, ^{14}C age 1062 ± 14 years (weighted average of seven samples), tree-ring correlation age 984 ± 15 A.D.

Hiatus of approximately 75 years

Emplacement of dome 0
Eruption of two column-collapse pyroclastic flows, A and B, ^{14}C age 1124 ± 15 years (weighted average of seven samples), tree-ring correlation age 911 ± 27 A.D.
Initial vent opening, air-fall pumice and lithic deposit and formation of a tuff cone

18 km and 28 km, respectively. A coignimbrite fall deposited a lobe of pumice that can be traced for 40 km northeast. Near the vent, the coignimbrite fall deposit contains blocks of dome-0 lava up to 1 m across.

A series of domes was then emplaced in numerical order of Table 1. Dome 3 of Crandell et al. (1974) is now recognized as two domes: 3a and 3b. Domes 2, 3a, and 4 had hot collapse events that produced short pyroclastic flows. Approximately 300 years ago, the Chaos Jumbles were formed when dome 2 partially collapsed in three cold rockfall avalanches.

All the Chaos Crags units are porphyritic hornblende–biotite dacites or rhyodacites containing 66–70% SiO_2. Dense rocks contain about 40% crystals of plagioclase, biotite, hornblende, quartz, and xenocrystic olivine. The total volume of the Chaos Crags deposits is on the order of 2 km^3.

Quenched inclusions ("blobs") of mafic magma occur in all the rocks but are especially abundant in the later domes. The quenched inclusions consist of a microvesicular network of acicular plagioclase, pyroxene, and hornblende microphenocrysts, with abundant interstitial glass. Euhedral grains of oxide are a conspicuous accessory. The inclusions have a variety of textures from aphyric (with a relatively coarse-grained groundmass) to porphyritic (with a relatively fine-grained groundmass). The phenocrysts in the porphyritic variety are resorbed felsic crystals derived from mixing with the silicic host magma at the time of inclusion formation. Where both aphyric and porphyritic types occur in the same inclusion, the finer-grained porphyritic material concentrically surrounds the coarser-grained aphyric material. Some quenched inclusions also contain olivine, calcic plagioclase, and clinopyroxene phenocrysts inherited from their basaltic parent.

The Chaos Jumbles consist of three separate rockfall avalanches covering 6.8 km^2 that can be distinguished on the basis of flow margins and grain characteristics. The deposits consist of a monolithologic breccia of Chaos Crags dacite blocks in a matrix of pulverized dacite. The deposits have steep distal and lateral margins 3–5 m in height. The first rockfall avalanche was the largest and traveled 4.5 km with 650 m vertical drop from the breakaway scar on dome 2 of Chaos Crags. The other avalanches were successively smaller and shorter, but thicker. The avalanche paths were controlled by existing topography. The initial direction of each avalanche was west-northwest, toward Table Mtn. The first avalanche deposit rode up onto Table Mtn., where it is found up to 100 m above the valley floor, before being deflected to the west. Groovelike linear features are interpreted by Eppler et al. (1987) to be strike–slip faults caused by compression during flow as the deposit was deflected by Table Mtn. Regularly spaced surface ridges are oriented perpendicular to the direction of flow. The avalanches apparently were emplaced as a high-yield-strength material capable of deforming and shearing rather than a plug of nondeforming material being carried on a deforming basal layer (Eppler et al., 1987). **1.6**

81.1 To the left across Manzanita Lake can be seen Loomis Peak and Eagle Peak, both Stage-III rhyodacite domes. The oldest of the three Chaos Jumbles rockfall avalanches crossed and dammed Manzanita Creek. Radiocarbon ages of wood samples collected by D. A. Trimble from trees submerged in the lake that formed behind the dam confirm the conclusion of Crandell et al. (1974) that all three avalanches occurred in quick succession about 300 years ago. **0.7**

81.8 Turn right on CA-89 and CA-44. Roadcuts are in pyroclastic flow from Eagle Peak, dated at 57 ka. **1.3**

83.1 Eskimo Summit. Cinder cones to the left belong to the Red Lake Mtn. center, source of basaltic andesite flows to the west and north. For the next 6 mi, the road lies on these calc-alkaline flows. **4.6**

87.7 Flat to the right displays boulders of the 1915 mudflow lying on 1000 years old pyroclastic flow from Chaos Crags. **1.0**

88.7 To left is the flow front of a young but undated pyroxene andesite from Bearwallow Butte. **0.9**

89.6 The flat plateau at 12:00 is the Hat Creek Rim, uplifted along a normal fault bounding the Hat Creek Valley on the east. The rounded shield volcano on the skyline is Blacks Mtn., an olivine andesite. Good views to the south of Lassen Peak and Chaos Crags. **2.1**

91.7 Big Springs, source of much of the water in Hat Creek, discharge along a prominent fault that uplifted lower Pleistocene diktytaxitic basalt, exposed in roadcuts for the next 0.7 mi. **0.7**

92.4 Old Station Post Office, on glacial outwash. **1.5**

93.9 Parking area for the trail to the vents of the Hat Creek Basalt, a diktytaxitic low-K olivine tholeiite (LKOT) flow of probable late Pleistocene age that extends north for 20 mi. **1.6**

95.5 Highway 44 turns right to Susanville. Continue straight on Highway 89. **0.3**

95.8 Turnoff right to Subway Cave, a lava tube in the Hat Creek Basalt. For the next 3.6 mi, the road is on the Hat Creek Basalt. The prominent bare flows on the left are 2-pyroxene andesite from Sugarloaf Peak. **3.7**

99.5 Cross Hat Creek at Bridge Picnic Area, passing onto lower Pleistocene olivine–plagioclase basalt. **3.3**

102.8 Wilcox Road. Roadcuts for 1.5 mi are Hat Creek Basalt, followed by roadcuts in Pleistocene andesites from vents to the west. **4.3**

107.1 Turn right off Highway 89 onto Doty Road at Fireside Village. **1.5**

108.6 Turn right at small white sign for the University of California Radio Astronomy Facility. **1.9**

110.5 Road to right to University of California Radio Astronomy Facility. Continue straight. At 1:30 is a young fault scarp along the Hat Creek fault, across which the Hat Creek Basalt was uplifted 30 m. **0.5**

111.0 End of paved road. Turn left on cindered road up fault scarp. **0.3**

111.3 **STOP 7. The Cascade Crest (Fig. 10), the Hat Creek fault, and basalt magma types.** Walk care-

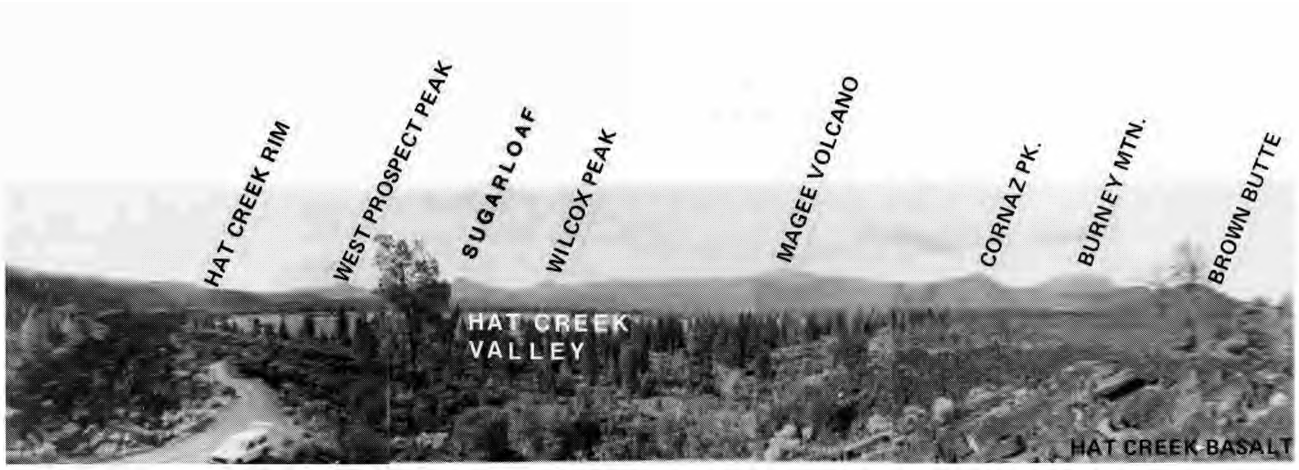

FIGURE 10—Panorama from the Hat Creek fault scarp (Stop 7).

fully 30 m to the north on the tilted flow surface of the Hat Creek Basalt.

To the south is the retreated fault scarp of the Hat Creek Rim and the younger, lower scarp that cuts the Hat Creek Basalt. Rocks exposed on the retreated fault scarp are calc-alkaline basalts and andesites in general similar to the volcanic rocks west of Hat Creek Valley. Previous workers (e.g., Anderson, 1940) have interpreted the younger scarp as a lava-slump scarp produced by the withdrawal of lava from a temporarily dammed part of the Hat Creek Basalt. Our recent geologic mapping, however, shows that the scarp in the Hat Creek Basalt is a true fault scarp. Gravels overlying the Hat Creek Basalt are displaced up to 20 m by the scarp. Furthermore, 0.8 km north of this stop, a strand of the fault cuts through the Hat Creek Basalt into the underlying basaltic andesite from Cinder Butte. Finally, scarps cutting the Hat Creek Basalt exist only along preexisting older fault scarps along the east side of the valley; there are no scarps in the Hat Creek Basalt where it lies against nonfaulted volcanic rocks on the west side of the valley.

Near the central parts of individual strands of the Hat Creek fault, the scarps cutting the Hat Creek Basalt are single and vertical, reaching a maximum height of 30 m. Near the end of individual strands, however, the scarps decrease in height and pass into monoclinal folds where the recent movement on the fault has been taken up by adjustment along columnar cooling joints in the basalt flow.

The existence of such a prominent, young fault with no associated modern seismicity suggests that movement on the Hat Creek fault is episodic over periods of perhaps hundreds or thousands of years.

Two types of mafic lavas occur in the area surrounding the Lassen volcanic center. The first is similar to low-K olivine tholeiite (LKOT) found throughout the northwest part of the Great Basin (called HAOT by Hart et al., 1984). LKOT are highly fluid magmas erupted from fissures and producing valley-filling lava flows. The rocks are typically aphyric or contain sparse olivine or plagioclase phenocrysts in a holocrystalline, often diktytaxitic groundmass composed of plagioclase, augite, olivine, and magnetite. LKOT are abundant in the Pliocene and Pleistocene record but rare within the presently active axis of the Cascades, where they are exposed primarily in fault scarps. A wave of LKOT volcanism may have progressed west across the Cascade axis 1–2 million years ago in conjunction with impingement of Basin and Range tectonism on the Lassen portion of the Cascade arc (Guffanti and Weaver, 1988).

LKOT from the northwest Great Basin form a homogeneous geochemical group showing little variability (Hart et al., 1984), and LKOT from the Lassen area are chemically equivalent to the average LKOT from the Great Basin. The bulk of these rocks are primitive (Mg# >65; >100 ppm Ni). Distinctive features of LKOT are low SiO_2 (48–50%), low alkalis, low large-ion lithospheric (LIL) elements, and flat rare-earth-element (REE) patterns.

The second magma type is similar to orogenic lavas from continental and mature island arcs and here is designated calc-alkaline basalt and associated andesite (CABA). CABA forms shield volcanoes and lava flows with associated cinder cones. CABA basalts have 49–53% SiO_2, 4–11% MgO, FeO/MgO 0.7–1.7, 0.5–1.8% TiO_2, and 0.2–1.5% K_2O. Modeling suggests that CABA andesites can be derived from basalts by crystal fractionation of observed phenocryst phases, but magma mixing and assimilation also probably occur. Based on abundances and ratios of incompatible trace elements, three groups of CABA can be recognized within a continuum. A **normal** group of medium K_2O basalts and andesites forms the main trend. A **depleted** group contains lower abundances of TiO_2, K_2O, and incompatible trace elements, except for Sr in which it is often greatly enriched. An **enriched** group contains higher amounts of incompatible trace elements and titanium-group elements, characteristics normally associated with alkalic rocks.

Preliminary interpretation of isotopic and trace-element systematics of LKOT and CABA suggests that the most primitive samples of the two basalt types could be primary and that they cannot be related by any closed system or assimilation process (T. D. Bullen and M. A. Clynne, unpublished data). We are left with the alternative that the mantle source

region and conditions of generation of basaltic magmas are heterogeneous in the Lassen region.

Return down cindered road and paved road to the west. **2.7**

114.0 Turn right at T junction. **0.9**

114.9 Turn right on CA-89. Road is still on Hat Creek Basalt. Lower Pleistocene andesites exposed on slopes to west. **4.2**

119.1 Doyles Corner. The most northerly outcrops of the Hat Creek Basalt occur in this meadow. Rising River, 1.6 km to the right, is fed by an immense group of cold springs discharging ground water derived from the Lassen highlands 45 km south. The low fault scarp 0.5 km straight ahead exposes a Pleistocene diktytaxitic LKOT. **4.9**

124.0 Flashing red stop light at junction with CA-299. Continue straight. **5.8**

129.8 Turnoff left to Burney Falls. Continue straight. **1.7**

131.5 South end of bridge across Lake Britton in the valley of the Pit River. Roadcuts both north and south of the bridge expose Pliocene diatomite interlayered with diktytaxitic LKOT. **1.1**

132.6 Roadcut on right exposes pillow lava interbedded with lacustrine sedimentary rocks, diatomite, and air-fall tuffs. **8.5**

141.1 Road to right to Dana and MacArthur. Continue straight. **11.4**

152.5 Cross railroad. **1.2**

153.7 Turn right on Harris Spring Road toward Medicine Lake. **0.1**

153.8 Stop sign at railroad tracks. **4.3**

158.1 Intersection with paved road to right.

Medicine Lake volcano, California

Julie M. Donnelly-Nolan

Summary

Medicine Lake volcano is a Pleistocene and Holocene shield volcano covering about 2500 km^2 with a volume of about 600 km'. It slower flanks are dominated by mafic lavas, especially basalt, which is commonly primitive high-alumina basalt. Higher on the volcano, andesitic lavas dominate, and some high-silica lavas are present, notably the late Holocene rhyolites and dacites of Glass Mountain and Little Glass Mountain, and the Medicine dacite flow. Well-preserved Holocene flows of a variety of compositions from basalt to rhyolite will be seen on this field trip, as well as evidence of tectonic activity in the form of open ground cracks and major normal faults.

The classic geologic reference for Medicine Lake is Anderson (1941), which contains excellent descriptions and the best published geologic mapping of the volcano. Numerous other papers have been written about the volcano, particularly petrologic studies by Mertzman (1977a, 1977b), Grove and Baker (1984), Grove and Donnelly-Nolan (1986), and Grove et al. (1988). These papers and Donnelly-Nolan (1988) include references to earlier work.

A previous field guide contains more logistical information and some different stops (Donnelly-Nolan, 1987). Some of the stops written up here (Fig. 11) have been taken directly from that guide, although additional information has been added.

Field guide

Mileage

0.0 Junction of paved roads 4.3 mi north of Highway 89 and Bartle. Turn right and drive northeast across Pliocene high-alumina basalt known regionally as the Warner Basalt (Anderson, 1941). Note thickness of red soil, much thicker than on any Medicine Lake lavas. **9.1**

9.1 The road drops over an east-facing fault scarp onto post-glacial basalt erupted from the south flank of Medicine Lake volcano. The road crosses the lava tube that begins at Giant Crater and can be traced at least 23 km, making it one of the longest known lava tubes (Greeley and Baer, 1971). **8.8**

17.9 Sign for Jot Dean ice cave and parking area. The cave is in Giant Crater lava erupted at Double Hole Crater. Note the deflation that occurred here after the flow formed a "high-water mark" and the lava flowed away to the south. **0.7**

18.6 Turn left onto good graveled road that heads west toward Grasshopper Flat. Half a mile after the turnoff, pass the large spatter vent of Double Hole Crater on your left. Continue west another 1.7 mi to shallow quarry on left. **2.2**

20.8 **STOP 1. Giant Crater event.** Turn into quarry on left and park on mafic air-fall from Chimney Crater, one of many vents that erupted basaltic lava during the Giant Crater event about 10.6 ka (D. E. Champion, unpublished ^{14}C data) (Fig. 12). Walk southwest up hill on near-vent agglutinate that has apparently been intruded and uplifted by compositionally identical basaltic lava (52.7% SiO_2) that can be seen in the east wall of Chimney Crater, located about 400 m west of the vehicles. This viscous lava is the earliest and most silicic lava erupted during the Giant Crater event, which may have continued for as much as a few tens of years on the basis of paleomagnetic data (D. E. Champion, unpublished data). Successively more mafic lava was

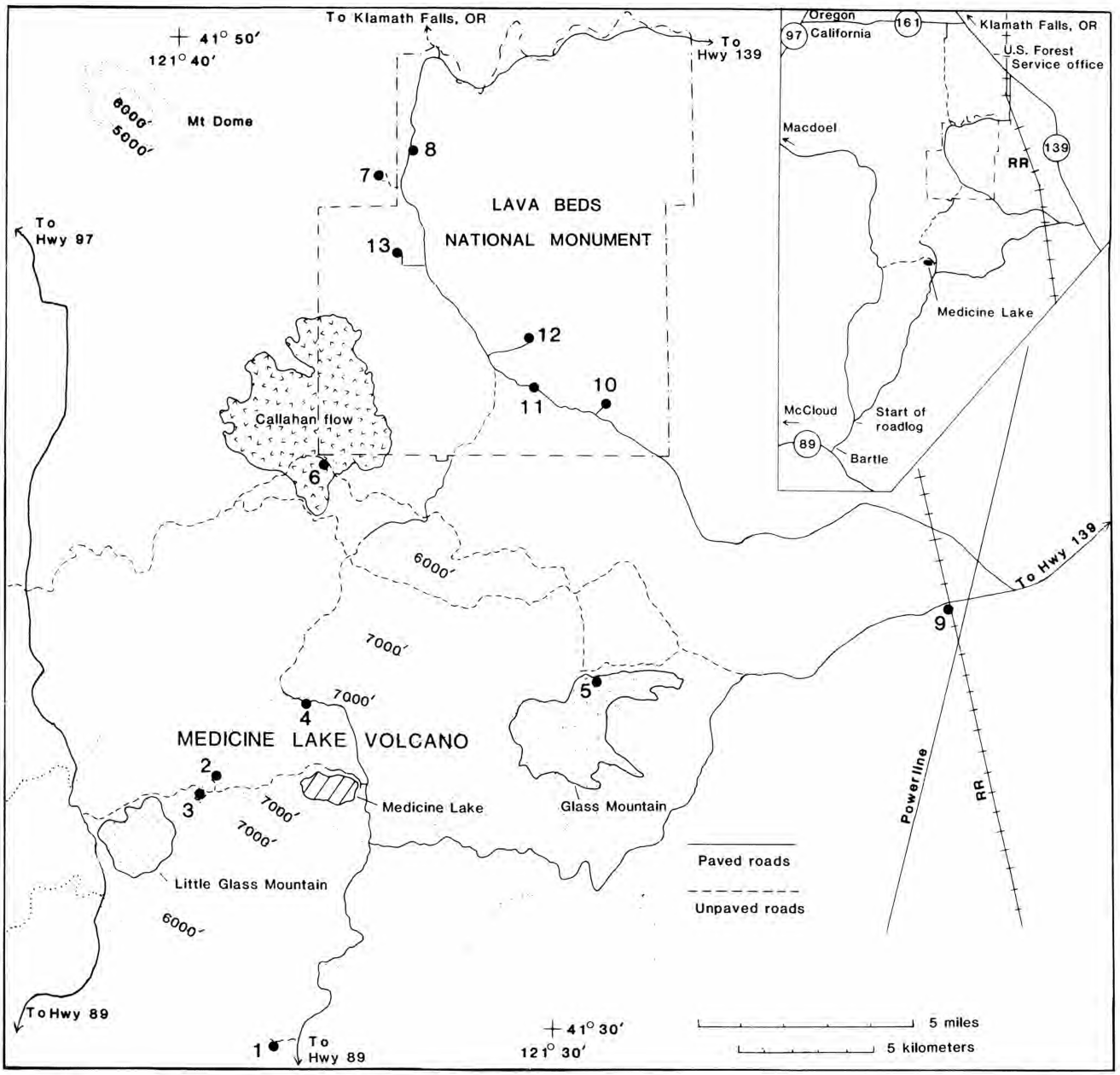

FIGURE 11—Location map of Medicine Lake volcano showing major roads and features, and field-trip stops

produced from a number of vents including Chimney Crater, Giant Crater, Double Hole Crater, and several other unnamed vents aligned N 55° E, N 5° E, and N 20° W. Chimney Crater and vents to the north and south aligned N 5° E produced contaminated basaltic lava containing quartz, sodic plagioclase, and iron-rich orthopyroxene xenocrysts (see groups I and II in Fig. 13). Melted silicic inclusions several centimeters across have been found at Chimney Crater. Numerous silicic inclusions that have "popped" can be found in the Chimney Crater agglutinate. Look in the mafic spatter between the crater and the vehicles for round void spaces up to several centimeters across that have a rind of dark-gray rhyolitic-looking glass. Mafic cumulate inclusions can also be found in the agglutinate. Chimney Crater also erupted more mafic, more fluid lava (group III in Fig. 13) that overflowed to the west and traveled by lava tube in the direction of Giant Crater to the west-southwest. It is unclear whether there is any connection between the Chimney tube and Giant Crater. Subsequently, lavas of group IV erupted in large volumes, perhaps exceeding 2 km^3 from Giant Crater and Double Hole Crater. Much of the lava transport to the south was by lava tubes formed during this part of the event. The south end of the flow consists mostly of group-V lava, basalt with about 0.12% K_2O that was produced from the most primitive composition by fractional crystallization of olivine. Group-V lava was transported by tube from Giant Crater, although little of the approximately 1.5 km^3 of this material is found near the vent. Most of the group-VI lava, the most primitive composition containing only 0.07% K_2O, was transported away from the vents by lava tube. Volume of this diktytaxitic group-VI basalt is less than

FIGURE 12—Aerial view of Giant Crater, Chimney Crater, and other vents of the Giant Crater system (Stop 1).

0.5 km^3. We will not see any of the group-IV, -V, or -VI lava on this trip, but much older lava of nearly identical composition can be seen at Stop 9 of the Lava Beds segment of the field trip. Total volume of the Giant Crater event is estimated at 5 km^3, one of the largest units known at Medicine Lake volcano and five times larger than the largest known silicic eruption, Glass Mountain (Donnelly-Nolan, 1988).

Retrace route and return to paved road. **2.3**

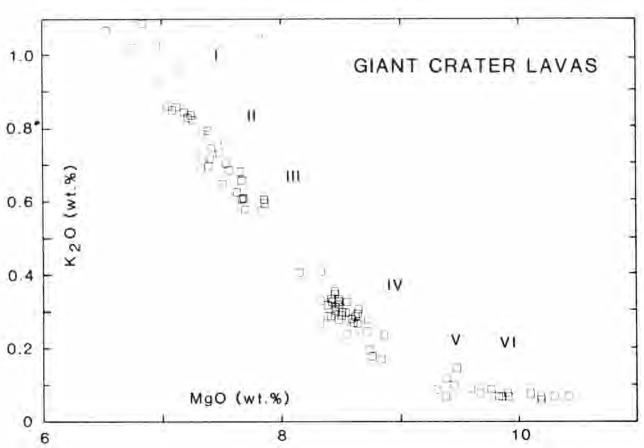

FIGURE 13—Plot of K_2O vs. MgO for Giant Crater lavas (Donnelly-Nolan and T. L. Grove, unpublished data) (Stop 1). Groups I–VI are labeled.

23.1 Turn left on paved road and drive north toward Medicine Lake. **6.3**

29.4 Junction of paved roads. Continue straight ahead to the north. Road crosses the poorly defined south rim of the Medicine Lake caldera. **1.6**

31.0 Turn left on paved road toward Medicine Lake. **0.4**

31.4 At stop sign at T-junction, turn right and follow paved road around north side of Medicine Lake past end of pavement at entrance to Medicine campground. Continue straight at guard station. **1.7**

33.1 Dead-end road to Schonchin Spring on right; continue straight. **0.6**

33.7 Keep right at a Y-junction of equally poor roads. **1.6**

35.3 Turn right onto a nearly hidden narrow dirt track marked by a green arrow. Follow it north, then northwest to first wide spot on left where several vehicles can be parked. **0.3**

35.6 **STOP 2. Cracks.** Cross the road and walk about N 30° E through area of fallen trees. You will begin to see large cracks in the ground. Continue walking northeast about 100 m to the largest crack near the edge of unlogged forest. This crack is as deep as 10 m and about as wide (Fig. 14). There is evidence of collapse that occurred about 1985. Note that the ragged edges of the cracks can be fit back together in an east–west sense. This set of cracks developed in andesite over a buried rhyolite dike (Fink and

FIGURE 14—Ground crack that opened during Little Glass Mountain eruptions (Stop 2). Jon Fink for scale. Snow is several feet deep.

Pollard, 1983) during emplacement of the late Holocene Little Glass Mountain and several domes of identical composition on trend farther to the northeast. The walls of the cracks expose the interior of a fountain-fed andesite flow. You can readily see the agglutinated texture and angular lithic fragments typical of this type of flow. The andesite was erupted from the glaciated cinder cone just south of the parking spot. Return to vehicles and retrace route to road junction. **0.3**

35.9 Turn right and drive west to base of Little Mt. Hoffman. **0.2**

36.1 Junction of dirt roads. Proceed straight ahead on left-hand road. **0.7**

36.8 **STOP 3. Little Mt. Hoffman lookout.** Take middle of the three branches of the road as you approach the summit of Little Mt. Hoffman. Located on the west rim of the caldera, this is one of the best viewpoints on the volcano. Spread out below you to the west is the late Holocene rhyolite of Little Glass Mountain. Mt. Shasta dominates the western skyline. Sixteen kilometers east is the dome of Glass Mountain (see Stop 5), on the east side of the caldera. To the south on a clear day you can see Lassen Peak, and to the north, Mt. McLoughlin and sometimes even Mt. Scott on the east rim of Crater Lake caldera. To the north on the lower flank of Medicine Lake volcano is the area where flooding took place following emplacement of andesite tuff (Donnelly-Nolan and Nolan, 1986, and Stop 7 description). The age of Little Mt. Hoffman is unknown, but I think that it was overtopped by glacial ice during the late Pleistocene. Little Mt. Hoffman cinders contain 51.7% SiO_2.

Little Glass Mountain has been the subject of several recent papers (Mertzman and Williams, 1981; Fink, 1983; Grove and Donnelly-Nolan, 1986). This flow and the time- and composition-equivalent domes to the northeast contain a suite of inclusions varying from granite to hornblende gabbro cumulate to basaltic and andesitic magmatic blobs.

Retrace route east past turnoff to Stop 2. **3.0**

39.8 View of Medicine Lake to right at Guard station. Continue straight. **1.1**

40.9 Pavement resumes. Continue straight. **0.6**

41.5 Turn left away from Medicine Lake. **0.3**

41.8 Turn left onto main paved road from south. Road narrows to north. Follow it around the late Holocene Medicine dacite flow, which lies just north of Medicine Lake on the northwest floor of the caldera, and drive west up the south-facing north rim of the caldera. **3.1**

44.9 **STOP 4. North rim of caldera.** Pause at the wide turnout on the left, half-way up the brush-covered slope. This is a brief photo stop for a view of the Medicine dacite flow and Medicine Lake to the south. The lake sits in a bed of glacial clay that prevents the water from draining away into the permeable volcanic rocks. The caldera does not appear to be the result of ash-flow eruptions. The suggestion of Anderson (1941) that it resulted from voluminous eruption of andesite lavas around the rim of the caldera appears to be the best explanation, although previous eruptions early in the history of the volcano may have initiated the summit depression. The andesite of the north rim is very similar to the andesite at Stop 2; both are late Pleistocene in age and both have been glaciated. The muted topography of the caldera is partly a result of glaciation, which has stripped the tops of lava flows and rounded off cinder cones. This rim andesite has been glaciated, and an outcrop displaying good glacial polish and striations can be seen on the left just after the vehicle completes the climb up the rim and turns to the north.

Continue driving north. **0.5**

45.4 Pavement ends just beyond intersection. Continue straight (north) on very rough road. **3.9**

49.3 Intersection of major graveled roads. Turn right on Cougar Butte Road. Continue east on this main graveled road to first major road on right. **6.3**

55.6 Turn right and proceed south. Good dirt road becomes narrow track in pumice. Pumice cover thickens markedly as you approach Glass Mountain. When you arrive in the pumice mining area, drive toward the front of the big rhyolite flow that sparkles ahead of you. Turn left on the major haul road, then right onto a small road around the front of the rhyolite lobe rising steeply above you. Park at the edge of the flow where a big pile of obsidian obstructs a bulldozer track that goes up onto the flow. **2.1**

57.7 **STOP 5. Glass Mountain** (Fig. 15). Walk up the bulldozer cut and examine the rhyolite. Pieces range from black aphyric obsidian to pumiceous, lighter-

FIGURE 15—Aerial view of part of Glass Mountain flow. Location of Stop 5 is shown where youngest rhyolite lobe comes down across earlier dacite lobe. Dome formed by last-erupted rhyolite is in middle distance.

colored samples; some samples have interesting textures that show evidence of breakage, oxidation, and flowage while still hot. This rhyolite forms the youngest lobe of Glass Mountain. It contains about 74% SiO_2; USGS rock-chemistry standard RGM-1 was collected from this lobe. The bulk of the flow is rhyolite ranging from 73 to 74% SiO_2, some of which contains basaltic andesite magmatic inclusions, although this youngest lobe contains none. Below you on the east is the earliest part of the flow, consisting of dacite of about 67% SiO_2, which contains abundant magmatic inclusions of basaltic andesite. This flow was studied by Anderson (1933b), who pointed out that the rhyolite and dacite are intimately mingled in places, but do not appear to mix into gradational types. My observations suggest that this is not strictly true, and I have collected a few transitional samples. Eichelberger (1975) first explained all the mafic inclusions as lithic fragments but later recognized that they had been injected into the host dacite and rhyolite as liquid blobs (Eichelberger, 1981). Two mixing events are suggested: first a basaltic component was mixed into rhyolite magma and homogenization to dacite took place; secondly, basaltic andesite magma was injected into the dacite, forming blobs that chilled against the host silicic magma. Glass Mountain lava erupted from a dike trending N 30° W, along which are at least 13 vents, two or three for the main flow, one forming a small dome to the south, and 10 forming domes to the north. The dome to the south and the six northernmost domes contain a varied suite of inclusions in addition to the typical basaltic andesite blobs. Some magmatic inclusions contain abundant olivine and are basaltic. Hornblende gabbro cumulates are present, as are granitic fragments. The range of inclusion types is similar to that found in the slightly older Little Glass Mountain flow. The age of these late Holocene flows is uncertain, but is estimated to be about 1000 years. Heiken (1978) reviewed the ^{14}C and stratigraphic evidence.

Return to vehicles and retrace the route north from the pumice mining area to the T-intersection with Cougar Butte Road. **2.0**

59.7 Turn left onto Cougar Butte Road. **0.3**

60.0 Turn right at first good road. This road proceeds approximately northwest down the north flank of the volcano. **5.5**

65.5 Cross paved Medicine Lake–Lava Beds road onto narrow dirt road that was an old railroad grade when logs were carried away by train rather than by truck. Drive west about 3 mi onto late Holocene basaltic andesite flow shown on Anderson's 1941 map as the Callahan flow. Where you initially intersect the flow, its silica content is 52.2%. Just beyond is Cinder Butte, the principal vent (54–55% SiO_2). Silicic inclusions that were partly melted can be found among the cinders that make up the cone. Proceed past the cone to a small quarry in the flow. **3.2**

68.7 **STOP 6. Callahan flow.** Quarrying has exposed the center of a small flow lobe that has been sampled here more than once for paleomagnetism and chemistry. SiO_2 content of the lava here is 54.1%. The paleomagnetic direction (D. E. Champion, unpublished data) is in good agreement with a ^{14}C date of 1110 ± 60 years (Donnelly-Nolan and Champion, 1987) from a dead tree in the edge of the flow. The flow fronts on the north and east edges of the flow are steep and high, indicating viscous lava, and the silica content at these localities is 57–58%. As many as five sub-flows of different compositions have been recognized (J. M. Donnelly-Nolan, T. L. Grove, and R. J. Kinzler, unpublished data, and Kinzler, 1985), such that the earliest lava is most silicic and the latest is more mafic by nearly 6% SiO_2, suggesting a stratified magma reservoir.

Retrace route east to paved road. **3.1**

71.8 Turn left onto paved road. **1.7**

73.5 Pavement ends as you enter Lava Beds National Monument. Note sign for Mammoth Crater as you enter the monument. This pit crater appears to have been the source for several major lava tubes that distributed basalt throughout the monument and beyond. Several additional vents to the north are part of the same event, which produced about 5 km^3 of basaltic lava in a very short time span (D. E. Champion, unpublished paleomagnetic data) in the late Pleistocene. **2.6**

76.1 Turn left on main paved road through Lava Beds National Monument. **2.9**

79.0 Scenic overlook to right. Good view as you drive northwest of north-trending fault blocks tilted to the west. Mt. McLoughlin is visible in the distance. **3.1**

82.1 Turn left on a paved road that quickly becomes dirt. **0.5**

82.6 Keep right at Y-junction onto less frequently used road. **0.1**

82.7 Keep left at Y-junction at large juniper trees. **0.1**

82.8 **STOP 7. Andesite tuff.** Walk down into shallow gully on left and examine the brownish-red ash-flow tuff that forms low outcrops on both sides. SiO_2 content of single pumice lumps is about 63%. Estimated thickness here, prior to some quarrying, was less than 2 m, perhaps less than 1 m. The base of the tuff is exposed at the north end of the gully. This small patch of partially welded andesite tuff is one of many on the north and west sides of Medicine Lake volcano. It is also present in a few small patches on the east side. The spatial distribution of the tuff indicates that it was erupted at or near the center of the volcano. The largest pumice and lithic fragments are found in the one large outcrop in the caldera, suggesting a source within the caldera. The tuff is younger than one of the andesite flows on the northwest rim of Medicine Lake volcano (the andesite in the cracks at Stop 2), but that andesite flow is not broken by any caldera-forming faults, implying that eruption of the tuff was not responsible for creating the caldera. The complete absence of the tuff anywhere on the caldera rim, together with indications of hydrothermal alteration at the caldera outcrop, indicate that the tuff erupted through an ice cap on the volcano and deposited in the caldera on the only exposed ground surface, where a fumarole had melted the ice. Coarse gravels and anastomosing dry channels cut in the tuff on the

northwest flank of the volcano indicate that meltwater from the interaction of the ash flow and the ice formed a catastrophic flood (Donnelly-Nolan and Nolan, 1986). The tuff has not been dated directly, but the indirect argument about the presence of an ice cap, together with evidence from younger lava flows, some of which have been glaciated, point to a late Pleistocene age predating the latest glaciation. Anderson (1941) recognized the andesite tuff, but incorrectly interpreted its common exposure in the bottoms of gullies to indicate that it was one of the volcano's oldest units. Stratigraphically, the tuff is of major importance as the volcano's only marker bed.

Retrace route to paved road. **0.7**

83.5 Turn left on paved road. **0.8**

84.3 **STOP 8. Devils Homestead overlook.** Stop at overlook along the Gillem fault and view the basalt of Devils Homestead below you. The basalt was erupted from spatter vents at Fleener Chimneys farther south along the fault. To the south is a panoramic view of Lava Beds National Monument and the Medicine Lake shield, the north flank dotted with cinder cones (Fig. 16). To the north, Gillem fault continues and forms the west margin of Tule Lake basin. Medicine Lake volcano lies astride the south end of the Klamath graben in a strongly extensional tectonic environment east of the main axis of the Cascades.

Continue north on paved road that turns east near the north edge of the monument. **2.6**

86.9 Turn left (north) on Hill Road and follow it to the north boundary of the monument where the road is graveled for about 7 mi. Gillem fault scarp is on left; Tule Lake (in places reclaimed for farmland) on right. **9.0**

95.9 Headquarters of Klamath Basin National Wildlife Refuges on left after pavement resumes. Continue straight north. **3.9**

99.8 Turn left on Highway 161 (State Line Road) and almost immediately turn right on Malone Road and continue driving north (you are now in Oregon). **1.9**

101.7 Turn left on Oregon Highway 39. **2.2**

103.9 Prominent flagpole with American flag at center of Merrill.

FIGURE 16—View of Medicine Lake shield from northeast

Lava Beds National Monument

Julie M. Donnelly-Nolan

Samples may not be collected in Lava Beds National Monument. Note also that rattlesnakes may be present. The trip route is shown in Fig. 11.

Field guide

Mileage

0.0 Prominent flagpole with American flag at center of Merrill, Oregon. Drive southeast on Oregon Highway 39. **2.6**

2.6 Bear 30° right on OR-39 toward Tule Lake. **2.4**

5.0 State line. Continue straight on the highway, which becomes California Highway 139. **3.7**

8.7 Flashing yellow light at town of Tulelake. **1.5**

10.2 Modoc County Line. Excellent views to the right of Gillem Bluff, Medicine Lake Highland, and Mt. Shasta in the far distance. **5.8**

16.0 On the right are eroded palagonite tuff rings formed by eruption of basalt into ancient Tule Lake, a basin that has been present for at least 3 Ma and fresh for most of its history despite its lack of a surface

outlet (D. P. Adam, unpublished results from 1100 ft drill core). On the left is what little remains of the largest of the World War II Japanese-American relocation camps. **14.3**

30.3 Highway crosses over a railroad at Perez Overhead. Good view to the right of Medicine Lake Highland; the prominent gray area is the Glass Mountain flow, and the white patches are pumice quarries. **2.8**

33.1 Turn right on County Highway 97. **2.6**

35.7 To right is National Forest Road 10 to Lava Beds National Monument. Continue straight. **1.5**

37.2 **STOP 9. Tionesta high-alumina basalt.** Park at graveled area to the left of road just past railroad tracks. Walk back east across the railroad tracks, then north along a jeep track to a conspicuous pine tree, and then a short distance west to the railroad. Examine diktytaxitic, tholeiitic high-alumina basalt (SiO_2 47.7%, Al_2O_3 18.3%, K_2O 0.07%, TiO_2 0.70%) in walls of railroad cut. Samples from this unit have been studied by Nockolds and Allen (1953), Yoder and Tilley (1962), Hart (1971), and Philpotts et al. (1971), as well as by Anderson (1941), all of whom documented the primitive nature of the lava. Basalts similar to this one can be found all around the lower flanks of Medicine Lake volcano as well as predating the volcano. They have erupted throughout the history of the volcano into post-glacial time (e.g., basalt of Giant Crater) and represent the parental material for the derivative lavas of Medicine Lake volcano by a variety of processes including assimilation, mixing, and fractional crystallization (Grove and Baker, 1984; Donnelly-Nolan, 1988). This basalt was called Warner Basalt by Anderson (1941), but it is much younger than most basalt of the Modoc Plateau that is generally described under this loosely used name. Its surface has been muted by a covering of glacial outwash gravel and late Holocene white pumice from Glass Mountain. The basalt probably erupted from now-buried vents on the east flank of Medicine Lake volcano.

Walk approximately 50 m directly toward a conspicuous snag in line with Lyons Peak (just to left of Glass Mountain) to north–south tensional cracks related to regional extensional tectonics. Follow cracks south to paved road.

Retrace route east along paved road. **1.5**

38.7 Turn left on National Forest Road 10 toward Lava Beds National Monument. **9.9**

48.6 Enter Lava Beds National Monument. **2.1**

50.7 Turn right toward Valentine Cave. **0.2**

50.9 **STOP 10. Valentine Cave.** In the words of Aaron Waters (see Donnelly-Nolan et al., 1981, p. 143), who studied and mapped the monument caves for the Park Service:

"Valentine is an interesting, clean and varied cave. Here one can see a lava-tube system which is almost undamaged by post-lava collapse. The cave shows most of the features to be found in lava tubes: among them pahoehoe floors, lava pools, and lava cascades; well developed lavacicles and dripstone on ceilings and walls; extraordinarily interesting lava benches, one of which marks a high-level stand of viscous lava that attempted to crust outward from the walls; and still another kind of bench made by penetration and 'bulldozing' away of collapse blocks and rubble as molten lava under hydraulic pressure forced its way through the tube. Large pillars around which the lava stream divided and reunited are present in the upper part of the cave. The central part of the cave shows interesting lava falls and cascades through which the lava stream was transferred from a higher level to a lower level. Downstream from this area of breakdowns, the Valentine tube subdivides into distributaries which are gradually phased out downstream by filling with lava."

The basalt of Valentine Cave has an SiO_2 content of 52.8%, unusually high for a unit with such well-developed lava tubes. The spatter vents for this flow lie about 5.5 km to the southwest outside the monument. The flow overlies unconsolidated glacial-outwash sediments. This is one of three units in the monument that host the nearly 300 lava-tube caves, most of which occur along the half-dozen tube systems of the basalt of Mammoth Crater (e.g., Skull Cave, Mushpot Cave).

Return to main road. **0.2**

51.1 Turn right at T-junction with main road. **1.7**

52.8 **STOP 11. Visitors Center and Mushpot Cave.** This brief stop will allow you to look at the displays in the Visitors Center and buy books and postcards if you wish, as well as visit the restrooms. Mushpot Cave is located in the center of the parking lot and is lighted.

Return to main paved road and turn left. **1.4**

54.2 Road to left to Mammoth Crater; continue straight. **0.4**

54.6 Turn right onto Lyons Road. **1.1**

55.7 **STOP 12. Skull Cave.** This enormous lava tube transported lava from Modoc Crater, one of the vents of the Mammoth Crater event, around the south and east sides of the preexisting andesite of Schonchin Butte (large cinder cone with lookout, just to the north) to the northeast part of the monument and the edge of Tule Lake. At least three lava tubes are stacked on top of each other at this locality. As many as five levels have been found in at least one cave in the basalt of Mammoth Crater. Note that the law of superposition fails here because the inner lava is youngest and is commonly underneath older lava.

Return to the main monument road. **1.1**

56.8 Turn right at T-junction with main road. **3.5**

60.3 Turn left to Fleener Chimneys on paved road that becomes gravel almost immediately. **0.8**

61.1 **STOP 13. Fleener Chimneys.** Climb on and around Holocene spatter vents for Devils Homestead basalt flow. Note that near-vent lava is pahoehoe, not aa. SiO_2 content is 50.9%. The vents are located on the Gillem fault. Vents for basalt at Medicine Lake volcano are typically spatter cones such as these or lava ponds. Cinder cones are rare as vents if silica content is below 52%.

Drive vehicles back to paved road. **0.8**

61.9 Turn left at T-junction with main road. Drive north about 2 mi where the road turns northwest and crosses the aa basalt flow known as the Devils Homestead, the downstream equivalent of Fleener Chimneys lava. Ahead of you is the fault scarp called Gillem

Bluff. The road turns north up the face of the fault. **2.9**

64.8 Devils Homestead Overlook. Continue north on paved road that turns east near the north edge of the monument. **2.6**

67.4 Turn left (north) on Hill Road and follow it to the north boundary of the monument where the road is graveled for about 7 mi. Gillem fault scarp is on left; Tule Lake (in places reclaimed for farmland) on right. **9.0**

76.4 Headquarters of Klamath Basin National Wildlife Refuges on left after pavement resumes. Continue straight north. **3.9**

80.3 Turn left on Highway 161 (State Line Road) and almost immediately turn right on Malone Road and continue driving north (you are now in Oregon). **1.9**

82.2 Turn left on Oregon Highway 39. **2.2**

84.4 Prominent flagpole with American flag at center of Merrill.

Klamath Basin

David R. Sherrod

Summary

The Klamath Basin is a composite graben that forms the westernmost structural trough of the Basin-and-Range physiographic province in Oregon and California. The south part of the basin includes Tule Lake and Lower Klamath Lake; the north part contains Upper Klamath Lake and Agency Lake. Bedrock in the Klamath Basin is chiefly late Miocene and Pliocene basalt lava flows and late Miocene to Holocene fluvial and lacustrine sedimentary rocks. Some Quaternary basalt was erupted along the south edge of the basin near Tule Lake, California.

Lower Klamath Lake, now drained and reclaimed as farmland, occupies a simple graben that coincides with a gravity depression of 20 mGal relief relative to adjacent lowlands. To account for this gravity anomaly, the sedimentary fill may be as thick as 2 km (Sammel and Peterson, 1976).

Klamath Falls is built on a sequence of northeast-tilted fault blocks that separate the alluviated north and south parts of the Klamath Basin. Homes and businesses in Klamath Falls use thermal water for space heating, tapping approximately 600 wells that produce water at 15°-95°C from depths of 20-550 m (Peterson and McIntyre, 1970; Sammel and Peterson, 1976). The water is heated by deep circulation along range-bounding faults.

Field guide

Mileage

0.0 Mileage begins at city center, off-ramp of U.S. Highway 97 (Fig. 17). **US-97 in the Klamath Basin is a narrow, high-speed highway with heavy truck traffic. Use caution, particularly in attempting to pull off at any point. 2.3**

2.3 Oregon Institute of Technology (OIT) at 2:00. Both OIT and the adjacent hospital utilize warm geothermal waters for space heating and cooling. **0.8**

3.1 Upper Klamath Lake on left. Diatomite quarry on right. Quarry operations and roadcuts along highway near here expose basalt that invades late Miocene or Pliocene diatomite and sandstone. **2.8**

5.9 Excellent views at 11:00 of north Klamath Basin and Upper Klamath Lake. Upper Klamath Lake is the largest lake in Oregon, covering about 24,000–28,000 hectares (60,000–70,000 acres). The lake, which averages 2–3 m depth, floods a graben that extends nearly to Crater Lake. The east escarpment of the graben has 450 m of structural and topographic relief in the Klamath Falls area. Although topographic relief diminishes toward the north, the structural relief probably persists. Gravity data indicate that 0.4–1.2 km of sedimentary rocks may fill the basin north of Modoc Point (Veen, 1982). **2.1**

8.0 Truck stop at Shady Pine Road. Quarry exposes the footwall of a normal graben-bounding fault cutting Pliocene(?) basalts. **1.2**

9.2 Roadcuts to right for 0.3 mi expose Pliocene basaltic-andesite lava flows and breccia. A 2–5 m thick bed of dark-gray to orangish-brown epiclastic and pyroclastic mafic strata, which locally separates lava flows, is deformed and cut by massive intrusions and brecciated lava. Near the north end of these exposures, the clastic interval contains an angular unconformity, with underlying beds dipping as steeply as 70–80° E. The tilting is probably the result of deformation along an extensional fault; the abundance of near-vent material in the clastic rocks suggests that volcanism and deformation were synchronous. **0.3**

9.5 Algoma Road. At 12:00 is a good view of fault escarpments created by differential displacement along splays of the range-bounding fault system. Basalt at top of escarpment on right has been dated by K–Ar at about 2 Ma.

Many prominent peaks of the Cascade Range from Mt. McLoughlin north to the Crater Lake area can be seen to the west and northwest (Fig. 18). Mt. McLoughlin is a shield volcano built of olivine- and clinopyroxene-phyric basaltic andesite lavas that surround a vent complex of basaltic andesite cinders and palagonitized lapilli (Maynard, 1974). The precipitous north slopes of the volcano result from late

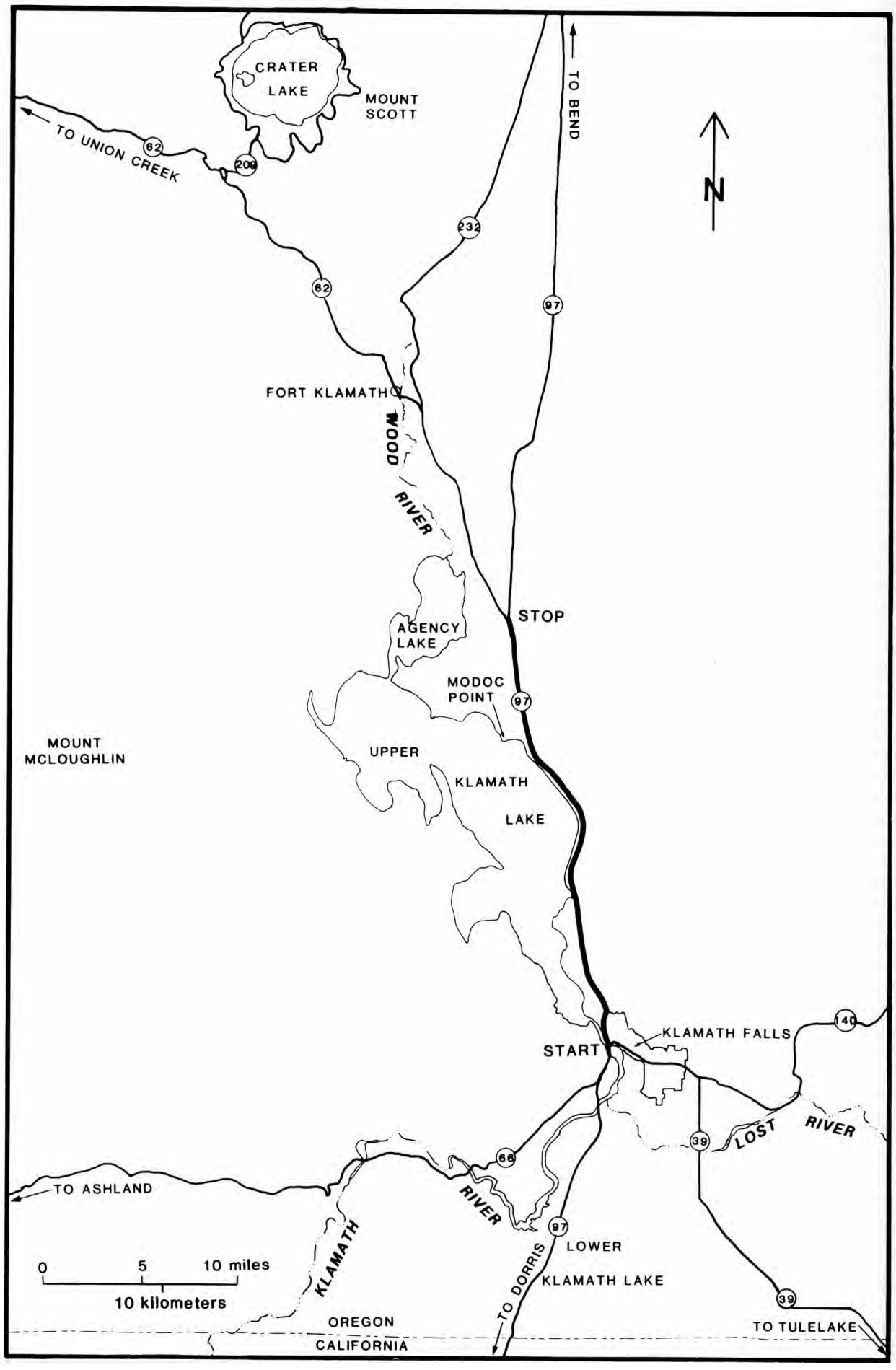

FIGURE 17—Route map for Klamath Basin.

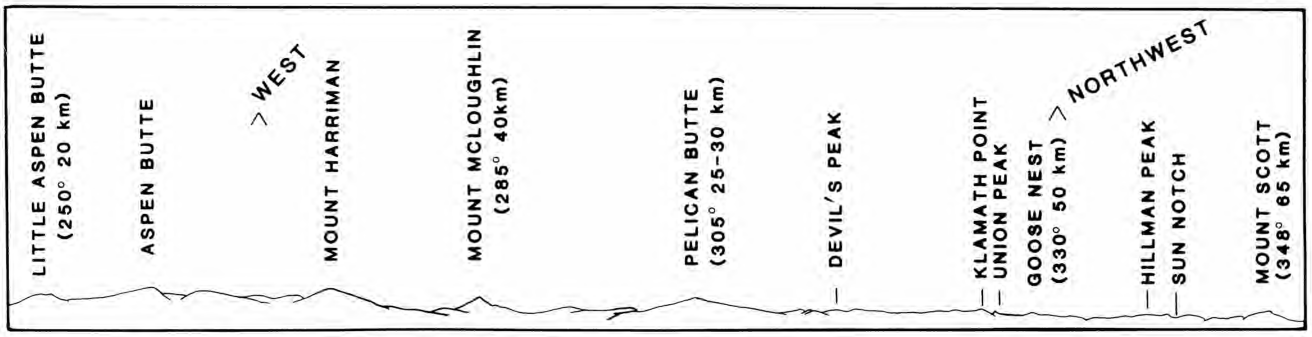

FIGURE 18—Skyline panorama of Cascade Range looking west and northwest across Upper Klamath Basin. Distance (in km) and azimuth (in degrees) from junction of U.S. Highway 97 and Algoma Road (mile 9.5 in guidebook). Crater Lake is in the mountains between Hillman Peak and Mt. Scott.

Pleistocene glaciations. Mt. McLoughlin is probably younger than 100 ka, based on its erosional state compared to other dated volcanoes in the Cascade Range. **2.7**

12.2 Hagelstein Park. A U.S. Forest Service road 30 m north of the park proceeds up the escarpment described above. One of the best views of the Klamath Basin and adjacent Cascade Range is obtained by driving some way up this road and taking a short walk to the escarpment edge. **5.1**

17.3 Junction to left with Modoc Point Road. Continue north on US-97. **6.1**

23.4 Pull into left lane, stop at stop sign, and turn left on OR-62 toward Crater Lake National Park.

Mount Mazama and Crater Lake caldera, Oregon

Charles R. Bacon

Summary

Crater Lake partially fills the caldera within Mt. Mazama at Crater Lake National Park, southern Oregon (Fig. 19). Mt. Mazama is an andesitic stratovolcano cluster that collapsed 6845 ± 50 years BP during a catastrophic, compositionally zoned, pyroclastic eruption of about 50 km^3 of magma. Prior to its climactic eruption, Mt. Mazama was one of the major Quaternary volcanoes of the Cascade Range. Mazama's eruptive history has been delineated by recent mapping of its caldera walls and flanks. Products of the climactic eruption partially fill surrounding valleys and mantle the slopes and caldera rim.

The first detailed account of the geology of the Park was USGS Professional Paper 3, by Diller and Patton (1902). Howel Williams showed in his classic monograph (1942) that the caldera formed by collapse and suggested that the compositional zonation reflected sequential tapping of a layered magma chamber. Other authors have reported on the zoned ignimbrite, most recently Bacon and Druitt (1988). The climactic eruption took place in two stages: single-vent and ring-vent phases; the ring-vent phase coincided with caldera collapse (Bacon, 1983). The single-vent phase produced the widespread air fall (climactic pumice fall) from a Plinian eruption column, followed by the Wineglass Welded Tuff, an ignimbrite deposited by ash flows that formed when the column collapsed. Deposits of the ring-vent phase range from pumiceous ignimbrite in the valleys around Mazama to coignimbrite lithic breccia (lag breccia) near the caldera rim (Druitt and Bacon, 1986).

After construction of the stratovolcano complex of Mt. Mazama and prior to the climactic eruption, several rhyodacitic lava flows were emplaced. These lavas apparently were derived from the climactic chamber during various stages of its growth. The andesite and dacite lavas of Mt. Mazama are well exposed in the caldera walls and along the Rim Drive. Mt. Mazama is built upon basaltic to andesitic High Cascade lava flows and, on its east and south sides, on an extensive field of rhyodacite lava flows. Basaltic andesite and lesser amounts of andesite and basalt were erupted from monogenetic vents and small shield volcanoes throughout the Quaternary, and these are visible on the flanks of Mt. Mazama and beyond.

This guide, revised after Bacon (1987), serves for a long one-day excursion through the Crater Lake National Park, concentrating on features near the caldera-rim drive. Ages of Pleistocene rocks quoted in the guide are based on unpublished K—Ar dates by M. A. Lanphere and, in part, on paleomagnetic determinations by D. E. Champion.

Field guide

Mileage

0.0 Junction of U.S. Highway 97 and Oregon Highway 62, just past the Rapids Cafe. **7.6**

7.6 Small quarry to right as OR-62 curves left. Near-vent spatter and scoria, along with a feeder dike, are all cut by a normal fault. **6.6**

14.2 Cattle Crossing Cafe in Fort Klamath. **2.1**

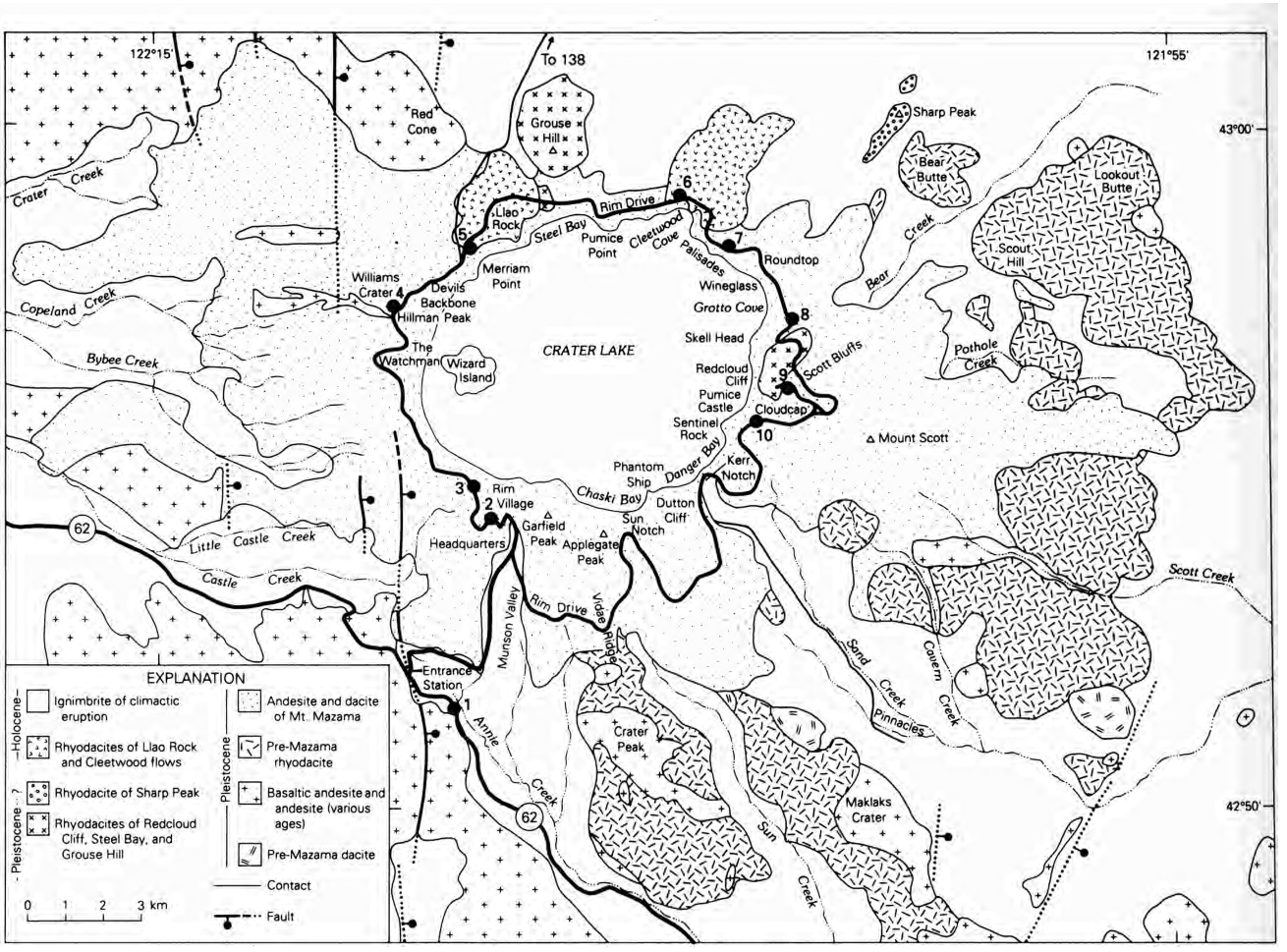

FIGURE 19—Generalized geologic map of Mount Mazama with field-trip route and stops indicated.

16.3 To the right for the next mile is an excellent view of the peaks on the Cascade crest and the rim of Crater Lake caldera. From west to east, summits to the north are the andesitic cinder cone of Crater Peak, Garfield and Applegate Peaks and Dutton Cliff on the south rim, and Mt. Scott just east of the caldera. **4.1**

20.4 Boundary of Crater Lake National Park. **Note that collecting or disturbing rock or other natural specimens in Crater Lake National Park is prohibited except by special permit.**

The road climbs the gentle slope of the ring-vent-phase ignimbrite where the conifer forest begins. Between here and Stop 1 note cuts in the top of the ignimbrite; precipitous canyon walls of Annie Creek are cut into columnar-jointed ignimbrite. High Cascade basaltic andesite and andesite are west of the road; high bluffs to east are pre-Mazama rhyodacite. **8.6**

29.0 **STOP 1. Godfrey Glen; turnout (note stone wall with sign) with view of Annie Creek Canyon.** Excellent exposure of valley-filling medial-facies pumiceous ignimbrite of ring-vent phase of climactic eruption (Figs. 20 and 21; Bacon, 1983, figs. 6c, 6d, 7, and 9; Druitt and Bacon, 1986; Bacon and Druitt, 1988). Lower half of section is silicic ignimbrite dominated by rhyodacite pumice clasts with 70.4% SiO_2 (all SiO_2 values are recalculated volatile-free). Most of upper half is mixed ignim-

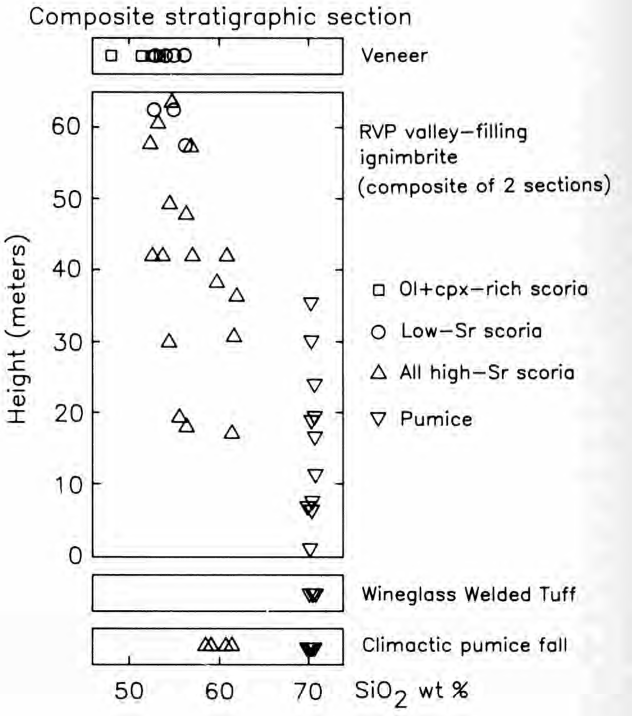

FIGURE 20—Variations in proportions of silicic pumice, olivine-free scoria, and olivine-bearing scoria through a composite section of valley-ponded medial ignimbrite at Stop 1. More than 50 clasts counted at each level. After Druitt and Bacon (1986, fig. 12).

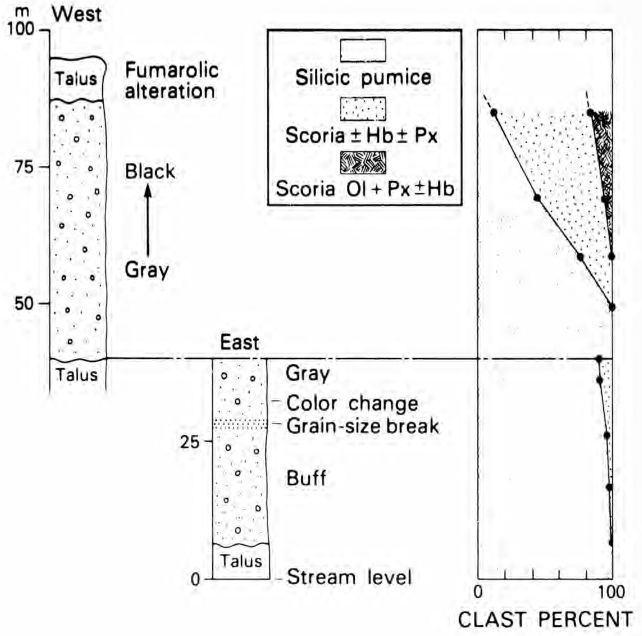

FIGURE 21—Composite stratigraphic section of climactic ejecta. Scoriae have been divided into high-Sr and low-Sr types derived from at least two distinct andesitic parental magmas. Olivine- and clinopyroxene-rich scoriae crystallized from basaltic magma or were contaminated with gabbro. Climactic pumice fall can be examined at Stop 6, Wineglass Welded Tuff at Stop 7, and veneer at Stop 5. After Bacon and Druitt (1988, fig. 6).

brite containing 20 to 80% silicic pumice, the rest being andesitic to basaltic scoria of 61 to 48% SiO_2. The uppermost approximately 9 m are mafic ignimbrite with <20% silicic pumice. Scoriae in valley-filling ignimbrite generally are hornblende- and plagioclase-phyric; olivine- and clinopyroxene-rich clasts occur near the top of the section. Most scoriae apparently are cumulates. The color change from buff below to gray above reflects increasing emplacement temperature of the matrix of the deposit upward, as much as its composition. Note the bleached zone of fumarolic alteration beneath the uppermost 1 m of fine ash. Erosion-resistant pinnacles and coarse columnar joints (near Duwee Falls on tributary on opposite side of Annie Creek) result from vapor-phase induration (partial welding and columnar jointing of ignimbrite downstream along Annie Creek apparently results from greater glass content of ignimbrite matrix farther from source). Entire section was deposited without significant breaks, as no sharp grain-size breaks are evident. Note, however, rusty-stained lithic-rich horizon near lower part of deposit. Good exposures of mixed ignimbrite are accessible just beyond the north end of the long turnout. Garfield and Applegate Peaks on the caldera rim are visible on the skyline to the north. Lithic breccia high on the slopes of these peaks and in the adjacent valleys forms the proximal facies of the same eruptive unit exposed here at Annie Creek. **0.7**

29.7 View to left of Arant Point, a sub-volcanic intrusion of olivine andesite cut by a normal fault. **0.4**

30.1 Turn right from OR-62 onto road to Crater Lake. **0.2**

30.3 Entrance station to Crater Lake National Park. **3.8**

34.1 To right is road to east rim of Crater Lake. Continue straight. Information, literature, and restrooms are available at Park Headquarters on left between 8 a.m. and 5 p.m. First cut on right beyond the headquarters exposes coarse lithic breccia of proximal facies of ring-vent-phase pyroclastic-flow deposits of the climactic eruption (Bacon, 1983; Druitt and Bacon, 1986, fig. 3). Roadcut is in a bedform near the east side of Munson Valley. Similar material underlies floor of Munson Valley in this vicinity. Lag breccia also occurs on summits of all nearby peaks, both in the lee of, or upslope from, obstacles and locally on the upper slopes of Mt. Mazama (Fig. 22). Longitudinal and transverse bedforms are common in the lag breccia. **1.3**

35.4 **STOP 2. Dacitic fragmental deposits.** Pull off into turnout on south (left) side immediately after hairpin turn from northeast to southwest. Long straight cut exposes two subunits of approximately 40 ka dacitic fragmental rocks (Bacon, 1983: 77–79). Eastern subunit is monolithologic debris-flow or avalanche deposit that apparently records collapse of dome(s) southwest of Mazama's summit. Similar material is present in the tree-covered swale high on Garfield Peak to the east. Western subunit is the younger and contains the same dacite, altered dacite, and dense, prismatically jointed dacite and pumiceous dacite blocks believed to represent the final pulse of magma responsible for destruction of the dome(s) (Bacon, 1985, fig. 7). The western subunit is thought to be a lithic pyroclastic-flow deposit. The dacite contains chilled inclusions of andesite magma (Bacon, 1986, figs. 7, 8, table 3). **1.4**

36.8 **STOP 3. Rim Village and view of caldera.** At the intersection of Rim Drive (left) and road to Rim Village (right), turn right for parking. Morning light is good for viewing north and west caldera walls (Fig. 23), afternoon for east walls (Stop 10; Fig. 24). Between 400 and about 40 ka, the locus of andesitic volcanism moved approximately 10 km

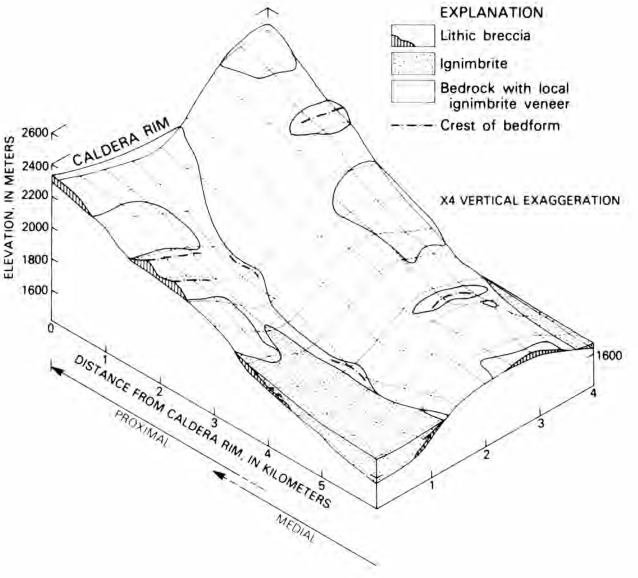

FIGURE 22—Schematic sketch of areal distributions of lithic breccia and ignimbrite and their relationships to surface topography. After Druitt and Bacon (1986, fig. 2).

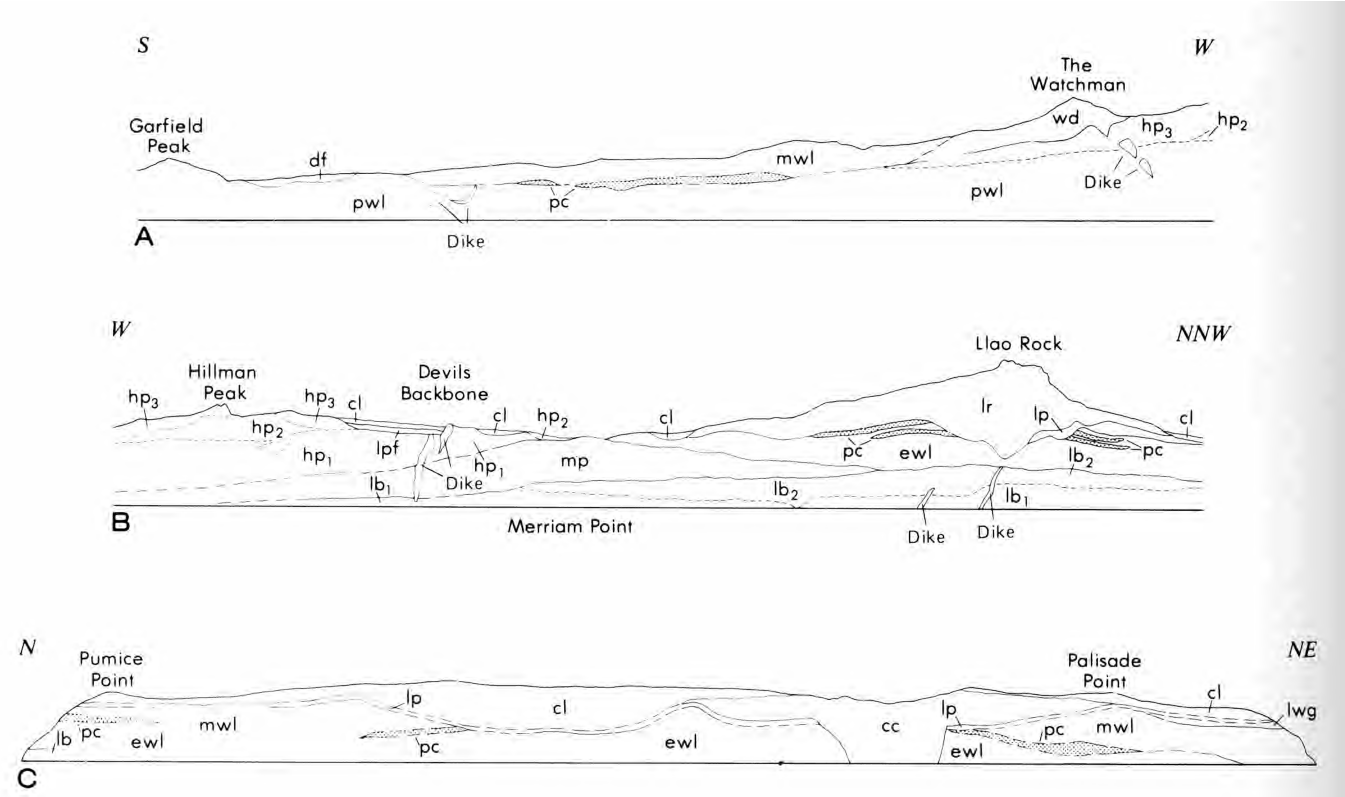

FIGURE 23—Geologic sketch maps of caldera walls; bases from photographic panoramas and not to scale. Thicknesses of most dikes exaggerated. Modified after Bacon (1983, fig. 4).

A, Southwest wall: hp = intrusions, lavas, and fall deposits of Hillman Peak; pc = dacitic ignimbrite; pwl = pre-Wisconsinan lava flows; wd = The Watchman and related dacite flows and dike; mwl = middle Wisconsinan lava flows; df = dacitic fragmental deposits of Stop 2.

B, Northwest wall: lb = lava sheets of Llao Bay; mp = lava flows and domes and fragmental deposits of Merriam Point; ewl = early Wisconsinan lava flows; pc = dacitic tephra, lower unit and deposit in C provisionally correlated with tephra of Pumice Castle; 1pf= dacitic lithic pyroclastic-flow deposits correlated with those of Stop 2; 1p = Llao Rock pumice fall; lr = Llao Rock rhyodacite flow; cl = undivided deposits of climactic eruption. Most climactic deposits are not visible from this angle.

C, North wall: lwg = late Wisconsinan till; cc = Cleetwood rhyodacite flow. Note backflow at Cleetwood Cove (Stop 6). Cleetwood pumice fall is included in unit 1p from Cleetwood Cove to east.

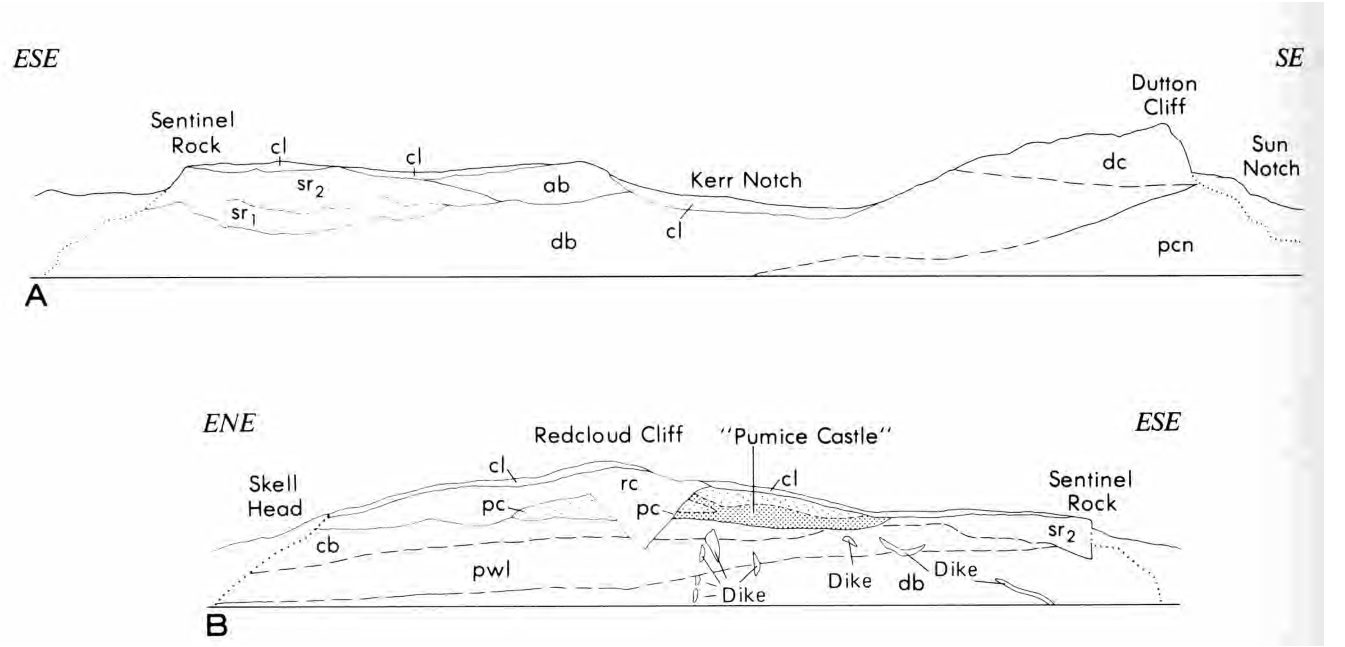

FIGURE 24—Geologic sketch maps of caldera walls; bases from photographic panoramas and not to scale. Modified after Bacon (1983, fig. 3).

A, Southwest wall: pcn = lavas and fragmental deposits of Phantom Cone; db = lavas of Danger Bay; ab = lavas of Anderson Bluffs; dc = lavas of Dutton Cliff; sr = intracanyon lavas of Sentinel Rock. Kerr Notch is beheaded glacial valley.

B, East wall: cb = lava sheets of Cloudcap Bay; pc = dacite tephra (heavy stippling) and lava (light stippling) of Pumice Castle; rc = Redcloud Cliff rhyodacite flow. Deposits of climactic eruption not shown where less than a few meters thick.

from east to west during construction of Mt. Mazama. Imposing cliff on north caldera wall is Llao Rock, the vent-filling rhyodacite flow and associated pumice-fall deposit dated at 7015 ± 45 years BP by radiocarbon (Bacon, 1983). This compositionally zoned silicic eruption (72–70% SiO_2) preceded the climactic eruption by about 100 to 200 years (Bacon, 1983, p. 105). The walls below Llao Rock consist of andesite and dacite flows and minor dacite tephra. As many as five eroded surfaces are present. Lava at lake level here has been dated at about 190 ka. Sheet-like thin flows here, and elsewhere in the walls, consist of agglutinated spatter topped by rubble. Such fountain-fed lavas grade from bomb beds and agglutinate near source, through streaky lava flows with thick rubbly tops, to distal homogeneous lava with relatively thinner rubble zones.

Eye-shaped cliff at rim east of Llao Rock marks the rhyodacite of Steel Bay (71.6% SiO_2), believed to be one of the earliest products of the climactic magma chamber, emplaced about 30 ka. The ages of this flow and its cousins, Grouse Hill and Redcloud Cliff, are constrained to within the interval of about 20–30 ka by field relations and measurements of paleomagnetic secular variation (D. E. Champion, unpubl. data, 1985). East of Llao Rock are Pumice Point, approximately in line with symmetrical, flat-topped cone of Timber Crater north of caldera, and Cleetwood Cove, immediately right of tour boat dock (boats are light blue). Cliffs at rim of Cleetwood Cove (Stop 6) are in rhyodacitic Cleetwood Flow, identical in composition (volatile-free) to climactic pumice and still hot when caldera collapsed. The dark lava descending to water level is the "backflow," which oozed into the caldera during collapse (Bacon, 1983: 100–101, fig. 11). West of Llao Rock are Devils Backbone dike, Hillman Peak, and The Watchman. Gray vegetated slope just below rim south of Devils Backbone marks lithic pyroclastic-flow deposit correlated with that of Stop 2. Hillman Peak consists of pyroxene andesite, overlain by hornblende andesite (forms gray scree slopes on near-vent fall deposits), overlain by pyroxene andesite with prominent augite and blocky plagioclase. All are about 70 ka. The Watchman flow is about 50 ka. The dike feeding the dacite flow that forms The Watchman can be seen on the caldera wall below the saddle between The Watchman and Hillman Peak. In the southwest wall are lavas older than Hillman Peak, an eroded surface overlain by dacitic ignimbrite that weathers orange, and andesite flows as young as about 50 ka (Bacon, 1985, figs. 6, 7). Wizard Island is the tip of a thick pile of postcaldera andesite that apparently was erupted when the lake level was about 90 m lower.

Return to intersection and turn right (northwest) on Rim Drive. **2.1**

38.9 Long, unpaved turnout on left side of road across from large cut in andesite lava. Younger flow shows glassy brecciated base grading into subtle columns, then upward into platy joints that parallel flow base. Platy zone grades up into coarsely blocky-jointed interior. Original rubbly top has been removed by glaciation. In some flows a second set of platy joints forms steeply dipping sheets high in the flow where this set dominates. Plagioclase phenocrysts in this flow have a distinctive seriate texture. Older flow is more typical of Mazama andesites with plagioclase, augite (green), hypersthene (brown), and titanomagnetite phenocrysts, common glomerocrystic clots, and sparse magmatic inclusions. Olivine (yellow) is a common minor constitutent of many Mazama andesites. **0.4**

39.3 Cut on northeast of road exposes crudely bedded lag breccia lying on glaciated surface of dacite lava similar to The Watchman flow (Druitt and Bacon, 1986, fig. 6). Fumarolic alteration shows that the breccia was deposited hot. Note platy jointing in The Watchman flow between here and Stop 7. **0.5**

39.8 The Watchman flow. Paved turnout on left where Rim Drive heads north across The Watchman dacite flow gives good view to south to Mt. McLoughlin (61 km) and Mt. Shasta (200 km). Union Peak is the eroded core of a cinder cone atop a basaltic-andesite shield in the middle distance. In the road-cut, a remnant of the pumiceous blocky carapace of the dacite flow can be examined and seen to grade down through glassy dacite into devitrified rock. This lava has 67.5% SiO_2 and contains rare andesitic magmatic inclusions. Its porphyritic texture and 2-pyroxene, plagioclase, and Fe–Ti oxide phenocrysts are typical of Mazama dacites. **1.4**

41.2 **STOP 4. View to north, and Williams Crater.** Large turnout on northwest side of road gives view of Red Cone (north) and Bald Crater (north-northwest) basaltic andesite cinder cones, and part of the south face of Llao Rock. In the middle distance, left to right, are Mt. Bailey, Diamond Peak (beyond Diamond Lake), and Mt. Thielsen. Three Sisters volcanoes may be seen in the far distance on clear days. To reach Williams Crater (formerly Forgotten Crater, Bacon, 1983: 80–82) walk south along Rim Drive. In the first cut note lag breccia bleached by fumarolic alteration lying on basaltic lapilli from Williams Crater, which in turn rest on andesite breccia of the youngest unit of the Hillman Peak Center. The andesite lava has distinctive blocky plagioclase phenocrysts, hypersthene, and prominent augite. Just past this cut turn west and walk about 400 m to Williams Crater, noting the small dacite dome immediately south of where you left the road. This dome is the easternmost lava of the Williams Crater complex which consists of a basalt flow, cinder cone, and three more flows of commingled andesite and dacite with basalt inclusions. Before reaching Williams Crater, note the arcuate bedform of lag breccia banked against it. Most clasts here are variably altered andesite from conduit or vent walls. Systematic variation in clast lithology around the caldera is evidence for multiple vents during this part of the eruption. Note rounding of these clasts due to thermally induced spalling of corners. Some clasts are highly altered, friable andesite; others are partially fused granitoids. Matrix here contains hornblende andesite pumice. At some localities, juvenile material is zoned from rhyodacite pumice at the base to mafic scoria upward.

Williams Crater contains basaltic bombs cored with angular fragments of commingled andesite–dacite lava, themselves bearing inclusions of the basalt. Walk to the south side of the cinder cone and visit the 10 m cliff in commingled lava to see a variety of proportions of andesite and dacite. A basaltic(?) dike evidently intersected the margin of a silicic magma reservoir, venting first basalt, but forcing convective mixing in the reservoir. The basalt is contaminated with ubiquitous gabbroic fragments up to a few millimeters across, variably disaggregated, which are responsible for a more mafic composition of the lava than that of the original basaltic andesite(?) liquid. This contaminated basalt thoroughly mixed with dacite to form hybrid andesite which then mingled with the dacite. Blobs of basalt occur in both andesite and dacite, and may have been incorporated in dacite before the mixing that produced the andesite. Fragments of the commingled magma were thrown out in the basaltic eruption. Finally, viscous commingled lava oozed from vents on a trend radial to the present caldera. All of these events took place rapidly because paleomagnetic results obtained by D. E. Champion show the same direction of thermo-remanent magnetization for all units of Williams Crater. The dacite is chemically most similar to that of the fragmental deposits in Munson Valley (Stop 2); tephra from Williams Crater lies on the deposit south of Devils Backbone noted at Stop 3. **1.2**

42.4 Below second of two big paved turnouts on right side of road is a glacially striated outcrop of hornblende andesite of Hillman Peak (middle unit). Similar rock crops out about 30 m west of the road. Nearby are mafic blocks in the final veneer deposit of the climactic eruption. These are plagioclase–pyroxene cumulates with variable amounts of olivine or poikilitic hornblende. The veneer locally mantles lag breccia, which to the west occurs in bedforms with clasts to 5 m (Druitt and Bacon, 1986, fig. 10). Llao Rock can be seen well from this point. The bedded climactic pumice fall present near its summit was eroded from its flanks by ring-vent-phase pyroclastic flows. The dark streak truncating air-fall beds on Llao Rock is scoria-bearing ignimbrite veneer. **0.3**

42.7 Turn right at junction of East Rim Drive and North Entrance Road. At caldera rim, lag breccia grades down into pumiceous ignimbrite which grades down into a small outcrop of the Wineglass Welded Tuff (Stop 7) that lies on bedded fall deposits. **0.3**

43.0 **STOP 5. Llao Rock obsidian and proximal ignimbrite.** Park in very large turnout on left side of road past big cut in obsidian on right. Ignimbrite veneer lies on lag breccia at north end of cut. About 20 cm of pink vitric ash, the ash-cloud deposit or layer 3 of Sparks et al. (1973), caps the veneer. The climactic pumice fall and most of the original blocky pumiceous carapace of the Llao Rock flow have been removed by the pyroclastic flows. Pumiceous rhyodacite grades down into obsidian, which becomes lithophysal and spherulitic deeper into the flow south along the cut. Note abundant andesitic magmatic inclusions (Bacon, 1986, figs. 5, 6, table 2). **1.4**

44.4 For the next half mile there are glimpses northeast of Grouse Hill (70–71% SiO_2), previously thought to be Holocene (Bacon, 1983, 1985) and now believed to be Pleistocene (ca. 20–30 ka). Grouse Hill is chemically and mineralogically similar to the rhyodacites of Steel Bay and Redcloud Cliff (Bacon and Druitt, 1988). **0.5**

44.9 Cut in the rhyodacite of Steel Bay (hill 7352′ of Bacon, 1983, 1985, fig. 8). Rock contains plagioclase, hornblende, augite, hypersthene, titanomagnetite, and ilmenite phenocrysts, plus rare andesitic inclusions. Cuts between here and Stop 6 are in andesite erupted about 50 ka. **1.1**

46.0 Pumice Point. Long paved turnout on right provides access to Pumice Point. Walk about 300 m east along abandoned and overgrown road to rim at Pumice Point. Visible on the steep slope below are the following deposits, from base to top: (1) Faintly orange air-fall pumice erupted from a vent near the east wall of the caldera at Pumice Castle (Stop 10) and resting on glaciated andesite; (2) a glaciated andesite lava flow dated at about 50 ka and filling an erosional depression in the pumice of (1); (3) a few feet of light-gray Llao Rock pumice fall forming a gentle slope above the lava; (4) climactic pumice fall, pinkish, in well-defined beds with nonwelded pyroclastic-flow interbeds, supporting the steep slope; (5) orange, incipiently welded Wineglass Welded Tuff grading upward into (6) lag breccia; (7) ignimbrite veneer; (8) ash-cloud deposit, as at Stop 5; (9) crystal and lithic ash, presumably re-ejected from the caldera by phreatic explosions following collapse; and (10) a few feet of wind-reworked material forming a small dune at the caldera rim. Near the base of (4) is 1 m thick, reddish, incipiently welded bed of climactic air-fall pumice that contains rare hornblende andesite scoria and partially fused granitoid blocks. **1.2**

47.2 Parking lot to left for trail to lake and tour boats. Lake tour takes 2 hours, with optional stop at Wizard Island. Highly recommended for a second day. Inquire at Park Headquarters or Crater Lake Lodge for current schedule and fee. Allow 20 minutes to descend and 30 minutes to hike out of caldera. Trail has good exposures of partly welded Wineglass Welded Tuff, and cuts showing climactic air fall, lithic-rich Cleetwood air-fall, and Llao Rock air fall lying on till. Lava flow below till is silicic andesite dated at about 100 ka. Underlying material may be an avalanche deposit of related blocks that preceded emplacement of the lava flow. **0.3**

47.5 **STOP 6. Cleetwood Cove.** Park at paved turnout on right across road from brick-red pumice. Below are cliffs in Cleetwood rhyodacite flow and tongue of lava (backflow) that oozed down caldera wall during ring-vent phase of climactic eruption (Bacon, 1983, fig. 11). Cliffs east of cove show internal flow structure of lava. Roadcut exposes climactic pumice fall lying on Cleetwood flow. Near their mutual contact these units are highly oxidized. Nowhere but on top of this lava flow is the pumice

fall oxidized and sintered. The pumice, which was hot enough when it landed to support steep slopes, fell as a hot blanket on the cooling lava flow, trapping and heating air. This trapped air, and possibly also degassing of the lava, resulted in the oxidation. Fumarolic alteration cuts the air-fall pumice and overlying lag breccia showing that the entire climactic eruption took place before the Cleetwood flow cooled completely (Bacon, 1983, fig. 8). About 180 m north of the road is the first of a series of small rift valleys transverse to the direction of flow, formed as the brittle upper surface of the flow broke up while its fluid interior flowed north (presumably in response to seismicity associated with caldera collapse) and south into the caldera. Faults bounding the valleys cut climactic pumice fall and thin Wineglass Welded Tuff (Stop 7). Lithic breccia is banked against the walls of these valleys showing that caldera collapse began before the ring-vent phase ended (Bacon, 1983, fig. 12). **1.5**

49.0 **STOP 7. Wineglass Welded Tuff, Palisade flow, and view of caldera walls.** Park at the west end of the paved turnout on right and walk to the caldera rim. You are standing on the Wineglass Welded Tuff, the top of which has been scoured away by the ring-vent-phase pyroclastic flows. Note how the Wineglass thins to the west of here as it rises to higher elevation and is thickest in the topographic depression between here and the prominent cliff to the east (Roundtop); the Wineglass is not present on the summit of Roundtop and other high points. The Wineglass consists of up to four flow units of rhyodacitic ignimbrite that form a single cooling unit. It was deposited by heat-conserving, valley-hugging ash flows that emanated from the collapsed eruption column of the single-vent phase (Bacon, 1983: 92–93, fig. 9). Here the top of the ignimbrite shows gash fractures parallel to the caldera rim, indicating that, where sufficiently thick, the tuff slumped toward the caldera while still hot and plastic. This is compelling evidence for the rapidity of events during the climactic eruption. The large pumice slope on the wall south of the flat bench that forms Skell Head south-southeast of here shows a fine section of air falls of the Llao Rock, Cleetwood, and climactic eruptions overlain by the Wineglass Welded Tuff capped by lag breccia (Druitt and Bacon, 1986, fig. 5). There, the Wineglass shows four distinct flow units, the top one being a vitrophyre. The lag breccia appears crudely bedded into five units. The lower two contain rhyodacite pumice, the next two hornblende andesite pumice, and the top one mafic scoria, showing that the breccia mimics the stratigraphic order of the zoned valley-filling ignimbrite.

The craggy top of the Palisade flow (dacite) that forms the cliffs just to the west of Stop 7 has been glaciated, and the flow occupies an old glacial valley carved against the older silicic andesite of Roundtop to the east. This is also a good place to see features on the east and south caldera walls. The cliff-forming flows below the rim north from Skell Head are inclusion-bearing silicic andesites, the younger of which is the subject of Stop 8. The Redcloud Cliff rhyodacite flow (70–71% SiO_2) forms the prominent cliff on the east wall just south of Skell Head, filling its vent crater and spilling to the north over earlier dacite (Fig. 24). It is compositionally similar to the rhyodacites of Grouse Hill and Steel Bay, and is late Pleistocene in age (ca. 20–30 ka). Immediately south and stratigraphically below Redcloud Cliff are Pumice Castle and related dacite flows described at Stop 10. Andesites below the dacites fall into at least two groups between about 220 and 340 ka. Between Pumice Castle and Kerr Notch (the lower of two beheaded glacial valleys) is Sentinel Rock (best seen from the west in afternoon light) where thick intracanyon low-silica dacite flows (about 300 ka) lie on glaciated older andesite (about 340 ka). Between Kerr and Sun Notches is Dutton Cliff. The oldest rocks exposed on the caldera wall, about 400 ka, are at water level below Dutton Cliff; they make up Phantom Cone (Williams, 1942). Stripes on the wall with moderate initial dips highlight pervasively altered rubbly tops of agglutinated andesite flows; their dense interiors, having been less permeable, show little effect of hydrothermal alteration from this distance. Phantom Ship is the small island and is partly composed of dikes related to the adjacent Phantom Cone. From Dutton Cliff to water level beneath Sun Notch three sets of andesite flows are exposed. The top is fresh olivine-bearing pyroxene andesite, the middle altered andesite, and the lowest altered andesite with abundant magmatic inclusions. Applegate Peak and Garfield Peak form the summits of the south wall, west of Sun Notch. All are pyroxene andesite and low-silica dacite flows except the top two flows of Garfield Peak, which are hornblende andesite (about 220 ka). The altered flows near water level below the big talus slopes between Applegate and Garfield Peaks comprise Chaski slide, a block of caldera wall that failed to slide completely into the caldera, presumably during the main collapse event. West of Garfield Peak is the head of Munson Valley, site of Crater Lake Lodge and Rim Village, which are built on the dacitic debris-flow and lithic pyroclastic-flow deposits of Stop 2. **1.0**

50.0 Wineglass. Small unpaved turnout on right where Rim Drive meets the caldera rim after traversing the andesite flow of Roundtop provides limited access to Wineglass. Wineglass refers to the shape of a scree chute below here. Excellent exposures of the Wineglass Welded Tuff lying on climactic pumice fall can be seen from the southeast side of the valley. The uppermost 1 m of the fall deposit is oxidized because emplacement of the Wineglass on warm pumice trapped and heated air. Lag breccia lies on the Wineglass. This is the locality where hot fiamme oozed over the surface of an open fracture (a larger version of those seen from above at Stop 7) before the tuff completely cooled; the block on the caldera side of the fracture has since fallen away revealing tongues of devitrified glass hanging over the inclined fracture surface. Because the caldera must have been present at the time of fracturing,

caldera collapse took place shortly after emplacement of the Wineglass, i.e. during the ring-vent phase of the climactic eruption (Bacon, 1983: 102). Beneath the scree below, climactic pumice fall lies on Cleetwood air-fall pumice, which rests on Llao Rock pumice. The 7015 ± 45 yrs BP radiocarbon age of the Llao Rock eruption was determined on charcoal at the base of the Llao Rock pumice here. Below the air-fall units is till containing glassy andesite derived from the flow underneath. This lava flow displays spectacular radiating columnar joints that grade into shattered glassy blocks upward into the till. The flow evidently encountered ice. Similar features can be seen in many other less obvious examples of chilled lava around the caldera. **1.0**

51.1 **STOP 8. Inclusions in andesite.** Park in small picnic area on right. Walk 100 m back through the woods and then along shoulder of Rim Drive to a cut in lava on the southwest side of the road. Observe abundant magmatic inclusions of andesite (60% SiO_2) in silicic andesite (62% SiO_2). The host is the younger of two compositionally identical flows that are about 70 ka (Bacon, 1985, fig. 6; 1986, figs. 9–15, table 4). Inclusions larger than about 12 cm have exceptionally porous (diktytaxitic) cores with denser rinds a few centimeters thick. Because of a relatively small initial thermal contrast between porphyritic host and nearly aphyric inclusion magmas, incomplete undercooled crystallization of inclusions resulted in a large fraction of vapor-saturated residual liquid (75% SiO_2). Most of this liquid was expelled from cores of inclusions, by then rigid crystal meshes, by gas filter-pressing owing to differential vapor pressure between host lava and cores of large inclusions. Consequently, cores are more mafic (56% SiO_2) than the original inclusion bulk composition. Although the rind texture is not common, andesitic inclusions are abundant in many silicic andesite and dacite flows of Mt. Mazama, particularly in the relatively old rocks of Mt. Scott and the east and south caldera walls. The cut at this stop is high in the holocrystalline interior of the flow; the upper glassy zone of the flows is preserved locally near their distal ends, where glass-lined segregation vesicles can be seen in inclusions. Inclusions are most abundant near the tops of flows, apparently because tops of flows were erupted later and advanced more rapidly than the underlying lava. Inclusions may have been incorporated into the host from a deeper level in the magma reservoir by forced convection during flow of magma up the eruption conduit.

Returning to vehicles, on the right side 25 m beyond the last andesite lava is an exposure of climactic pumice fall lying on Cleetwood pumice separated by about 2 cm of fine ash which marks the beginning of the climactic eruption.

Between picnic area and Mt. Scott Trail, roadcuts expose rhyodacite of Redcloud Cliff for about 1.5 mi, then dacite of Cloudcap and Scott Bluffs. **2.6**

53.6 Parking area on left for Mt. Scott Trail and view of Mt. Scott, which consists of the oldest dated lavas of Mt. Mazama, about 420 ka. This cone is made up of sheets of agglutinated low-silica dacite. Andesitic inclusions are abundant. Glaciation has exposed the core of the volcano. Hydrothermal alteration variably affects these rocks, and these features can be seen readily on the trail to the summit. The summit ridge is capped by climactic pumice fall and lag breccia. **0.2**

53.8 Turn right on Cloudcap Road. Cuts are in dacites as on Rim Drive below. **0.8**

54.6 **STOP 9. Rhyodacite lava and pumice, welded dacite air-fall pumice, and view of northeast flank of Mt. Mazama.** Pull off on paved shoulder to right. Cut on left exposes five air-fall pumice deposits and a steeply dipping rib of lava. From east to west, in stratigraphic order, the units are: (1) buff to orange dacite pumice with blocky plagioclase and pyroxene, similar to the tephra of Pumice Castle; (2) white hornblende rhyodacite pumice with abundant coarse lithic blocks, the proximal air-fall for the Redcloud Cliff vent; (3) rhyodacite lava grading from pumiceous blocks up through obsidian into lithophysal and spherulitic rhyodacite, believed to be a glaciated "bathtub ring" of lava left after most of an oversteepened dome slid north to form the Redcloud Cliff flow; (4) Llao Rock and (5) Cleetwood air-fall pumice poorly exposed beneath scree; (6) climactic pumice fall supporting a small cliff; and (7) lag breccia of the ring-vent phase of the climactic eruption. Walk around the west end of this exposure and up through the trees over the lava to a brick-red 2 m cliff east of the cut. This is welded air-fall pumice similar to that of Pumice Castle. From here one can see many features. In the distance are Mt. Thielsen and tree-covered lateral moraines extending to the east; the Gibraltar-like west-facing scarp of Walker Mtn., 50 km northeast near the town of Chemult (approximate limit of ring-vent-phase ignimbrite); the toad-back silhouette of Newberry volcano, 110 km northeast; and the shield-like form of Yamsay Mtn., 55 km east. In the middle distance are the late Pleistocene andesitic shield and cone of Timber Crater to the north and ignimbrite-floored flats of Klamath Marsh to the east. Closer features are the higher domes of the Sharp Peak group of at least 12 small rhyodacite domes thought to have been erupted from the climactic chamber (Bacon, 1985, fig. 8; Bacon and Druitt, 1988); several pre-Mazama rhyodacite domes surmounting thick flows (Bear Butte, Lookout Butte, Scout Hill, approximately 400 to 700 ka; climactic lag breccia occurs on the summit of Lookout Butte); cliffs to the north in the silicic andesite flow of Stop 8; cliffs in the Redcloud Cliff flow; and the dacite flows of Scott Bluffs. **0.3**

54.9 Cloudcap overlook. Return to Rim Drive, bearing to right at Y junction. **1.1**

56.0 Stop sign at Rim Drive. Next cuts are in dacite similar to flows of Scott Bluffs and nearby cuts on Rim Drive and Cloudcap Road. **1.1**

57.1 **STOP 10. Pumice Castle overlook.** Large paved turnout where Rim Drive bends left. Best view is from a few feet west of the stone wall. The view of the northeast wall of the caldera includes the Cleetwood flow, Palisade flow, Roundtop flow, and Wineglass. Redcloud Cliff dominates the east wall

in the foreground. Cliff at rim south of Redcloud Cliff is in Pleistocene dacite flow lying on tephra of Pumice Castle. The latter consists of dacite pumice that is nonwelded at the south end of the exposure but becomes progressively more densely welded to the north. Ages of lava flows above and below the tephra of Pumice Castle suggest that this dacite erupted about 70 ka. Just south of Redcloud Cliff this deposit includes several vitrophyric layers and a stubby lava flow. The top of the air-fall pumice has been "fused" by the overlying lava flow. Pumice Castle is the prominent brick-red–orange set of towers with resistant welded layers. Below the pumice are sheets of basaltic andesite (about 220 ka) lying on altered andesite lavas (as old as 340 ka) and debris-avalanche deposits. Numerous dikes cut the pre-Pumice Castle rocks. In the trees just below the caldera rim immediately east of the turnout is an exposure of partly welded Wineglass Welded Tuff, the southeasternmost such outcrop at the rim. Confinement of the Wineglass to depressions from just south of Llao Rock clockwise to here indicates the vent for the single-vent phase of the climactic eruption was northeast of the summit(s) of Mt. Mazama. Large lithic blocks in the climactic pumice fall above Pumice Castle are consistent with proximity to the vent, which may have been located between here and Cleetwood Cove. Here, as elsewhere, lag breccia lies on the Wineglass. Thick lag breccia also mantles air-fall pumice above Redcloud Cliff and the dacite flow above Pumice Castle. The next two turnouts provide good views of the south caldera walls. **2.5**

59.6 Road on left to Pinnacles, which has spectacular exposures of rather atypical ring-vent-phase ignimbrite. Note lag breccia on right. Cuts south of here are in silicic andesite and low-silica dacite flows. **1.9**

61.5 View to south of Klamath graben, upper Klamath Lake (48 km), and Medicine Lake volcano (160 km), the broad shield-like form beyond upper Klamath Lake. Snow-capped Mt. Shasta (175 km) also may be visible. **1.0**

62.5 Turnout on left with view northwest to Applegate Peak. Silicic andesite and low-silica dacite flows grade from agglutinated lava upward into bomb beds in each "flow" at the caldera rim, and south down the flank into streaky lava flows with rubbly tops. Lavas in cuts here on Rim Drive are strongly flow-banded olivine-bearing silicic andesites of Dutton Cliff (ca. 210 ka) except the last cut before Sun Notch, which exposes altered, older andesite (≈320 ka). **1.0**

63.5 Parking area for trail to Sun Notch. A 400 m walk to the caldera rim yields a fine view of Phantom Ship and Dutton Cliff. A gully about 30 m up the road from the east end of the parking area exposes lag breccia resting on Llao Rock pumice fall. The breccia contains included blocks of climactic air-fall pumice and friable altered andesite. **1.4**

64.9 Vidae Falls on right. Visible from Rim Drive south of here are gray cliffs of distant canyon walls to southeast in pre-Mazama rhyodacite flows. **0.6**

65.5 Crater Peak trailhead. Columnar base and platy interior of silicic andesite flow well exposed in cut where Rim Drive leaves valley of Sun Creek and crosses Vidae Ridge immediately east of trailhead. **1.5**

67.0 Roadcuts on right expose moraine on east wall of Munson Valley. **0.9**

67.9 Stop sign across from Park Headquarters. Turn left (south). **4.0**

71.9 Intersection with OR-62. Turn right toward Medford. Just west of intersection, the road rises along and over scarp of east-facing normal fault cutting three Pleistocene olivine andesite flows. **6.0**

77.9 Columnar-jointed medial Mazama ignimbrite can be seen on right in the canyon of Castle Creek for 0.9 mi west from this point. **7.5**

85.4 Long (0.3 mi) cut on right exposes nonwelded distal silicic Mazama ignimbrite. At the far (west) end, a flow-unit contact is visible at the reversely graded base of the flow unit that makes up most of the vertical exposure; the tops of both flow units consist of coarse pumice blocks. Flow-unit breaks are rare in the ignimbrite. **2.5**

87.9 Junction of Highways 62 and 230.

Western Cascades, southern Oregon and northern California

James G. Smith

Summary

This section of the field trip passes through the volcanic rocks of the Western Cascade Range (Fig. 25). This sequence of gently deformed and slightly metamorphosed volcanogenic rocks and associated sedimentary rocks is a more deeply eroded mid-Tertiary analogue of the younger rocks of the High Cascades.

In southern Oregon and northern California, the volcanic rocks of the Western Cascade Range were deposited 35 to 15 Ma and form a simple homocline dipping east to northeast. Folds are lacking, and the sequence is cut by only a few faults. The present outcrop belt marks the approximate location of the mid-Tertiary arc. However, volcanic edifices of the High Cascades unconformably cover the eastern part of the arc, and the exact location of the axis of the Western Cascade Range is uncertain. In southern Oregon and northern California, there is a hiatus between the Western Cascade rocks (35 to 15 Ma) and the High Cascade rocks (<7 Ma).

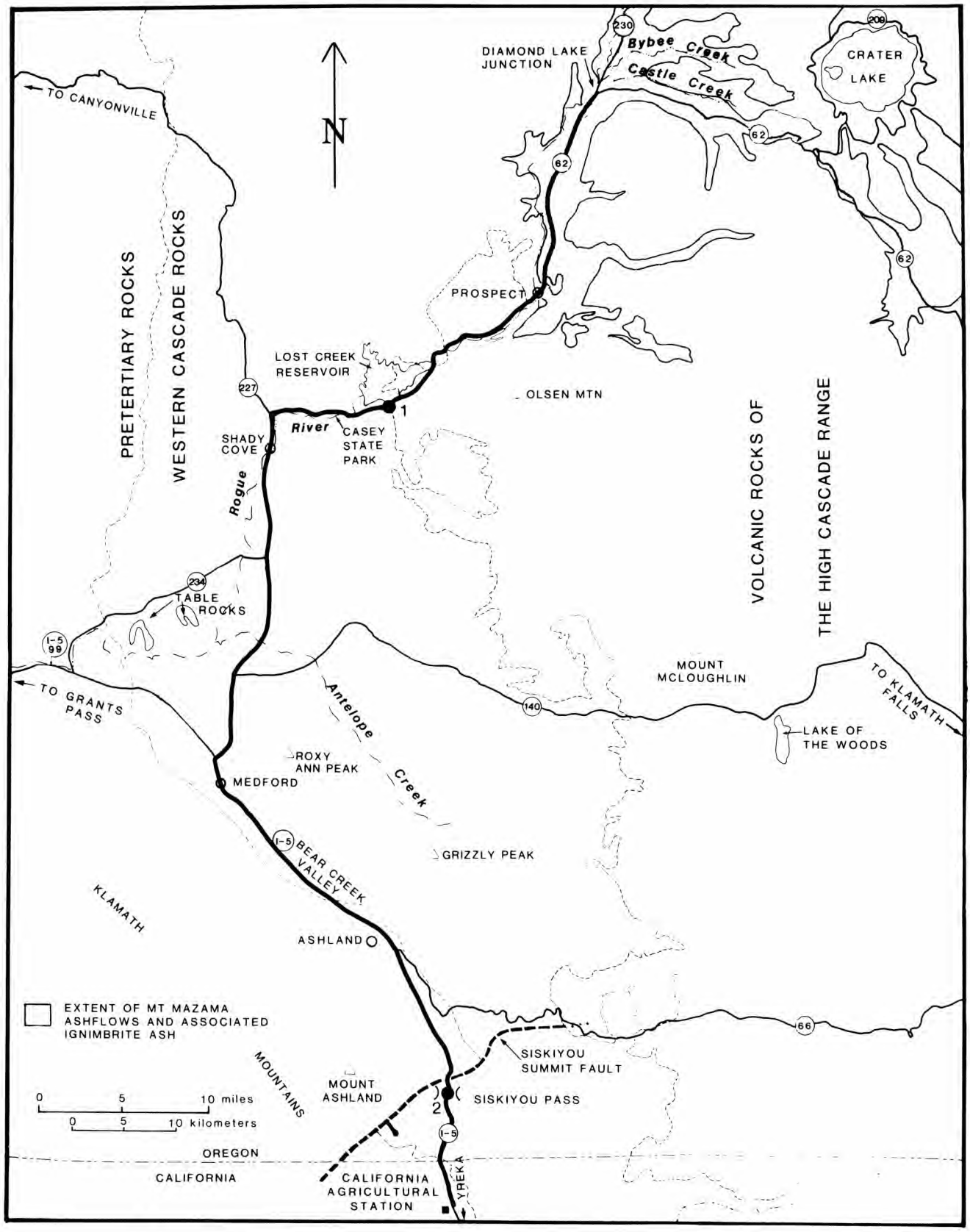

FIGURE 25—Route map for Western Cascade Range of southern Oregon and northern California

Only a few geochemically oriented studies have been done in the volcanic rocks of the Western Cascade Range in southern Oregon and northern California. They suggest that there is neither a difference in chemistry between the Western and High Cascade sequences nor a systematic change in composition with time.

The Western Cascade sequence contains only a narrow range of lithologies, is stratigraphically complex, and is poorly exposed. The lack of lithologic diversity and the stratigraphic complexity result from the way in which volcanic and volcaniclastic rocks were formed, deposited, and reworked in this subaerial arc environment. Hundreds of small overlapping and intertonguing volcanogenic and sedimentary units make up the range. Individual lithostratigraphic units are discontinuous and commonly interbedded in an intricate fashion. Widespread marker units are lacking throughout much of the sequence. Lithologic correlation, even of similar stratigraphic sequences, is unreliable without corroborating radiometric ages or detailed mapping. These factors have discouraged studies, and geologic knowledge of the Western Cascade Range lags behind that of the High Cascades.

Field guide

Mileage

0.0 Diamond Lake Junction (intersection of Oregon Highways 62 and 230). Proceed south on OR-62. From Bybee Creek (1.5 km north of Diamond Lake Junction) to the head of the Cascade Gorge (32 km south), the canyon of the Rogue River contains a succession of thin flows of primitive, low-K tholeiitic basalt that apparently issued from vents in the drainage of Castle Creek. These basalt flows transformed the 200 m deep, V-shaped ancestral valley of the Rogue River into a nearly flat valley floor 1.6 to 4.5 km wide that slopes about 12 m/km. Overlying the intracanyon basalt is up to 10 m of Mazama ash-flow tuff. The ash flows sped down the major drainages off the west and south flanks of Mt. Mazama, made a 90° turn at the Rogue River, and continued south for many more kilometers. Locally, ash flows ran up the west side of the Rogue Valley as much as 30 m. **1.0**

1.0 Rogue River Gorge viewpoint. Good view of intracanyon basalt and Mazama ignimbrite. **1.5**

2.5 Natural Bridge Campground. Rogue River flows through a lava tube in intracanyon basalt. **9.5**

12.0 Prospect Ranger Station on left. **1.9**

13.9 For the next several miles, Olsen Mtn., a Pliocene shield volcano with a prominent parasol drainage pattern, is visible at 10:00 to 12:00. The hills to the right (northwest) are underlain by interstratified basalt and andesite flows, ash-flow tuff, tuff breccia, lapilli tuff, and volcanic sediment of the Western Cascade Range. In this area, the rocks are between 25 and 15 Ma. Between here and Medford, Highway 62 proceeds generally down-section through this north-northwest-striking, northeast-dipping homoclinal sequence of volcanic rocks and volcanic sedimentary rocks, which here total more than 5.5 km. **4.5**

18.4 Gorge Restaurant on left. Leave Pleistocene intracanyon basalt and start descent into Rogue River Canyon. Roadcuts on the right for the next 1.5 mi expose typical olivine basalt flows of the Western Cascade Range. The flows are approximately 20 Ma and fill a broad paleovalley cut into volcanic sediment and ash-flow tuff. These are exceptionally good exposures in which to observe flows and flow-contact features; elsewhere in the Western Cascade Range, distinguishing flows from sills is a common problem. **0.3**

18.7 Large roadcut at wide shoulder on right. Paleovalley in Western Cascade basalt is filled by lower Pleistocene intracanyon flow of fresh pahoehoe basalt with local palagonitic hyaloclastite channel fill at its base. **1.3**

20.0 North end of bridge over Lost Creek Reservoir in the valley of the Rogue River. For the next 0.6 mi, roadcuts expose intracanyon Pleistocene basalt flows. Just beyond a curve, the highway ascends to the top of these intracanyon flows and continues across them for a mile. To the left (south) is the eroded edge of the Olsen Mtn. shield volcano, of Pliocene age. To the right (north) across the reservoir are good views of the east-northeast-dipping volcanic rocks of the Western Cascade Range. **1.3**

21.3 To right is entrance to camping area at Stewart State Park. **0.3**

21.6 On left (south), roadcut of mafic hyaloclastite from Olsen Mtn. **0.6**

22.2 Entrance to day-use area, Stewart State Park. **0.5**

22.7 Roadcut on left through massive nonvesicular olivine-bearing basalt or basaltic andesite of Olsen Mtn., part of a 1 km wide flow that moved north down a radial valley eroded into the shield and continued on to the valley of the Pliocene Rogue River. **0.9**

23.6 For the next 0.7 mi the road cuts through another series of intracanyon olivine-bearing basalt or basaltic andesite flows from Olsen Mtn. Columnar joints spaced 10 to 20 cm apart are typical of the lower part of these flows. **0.6**

24.2 Roadcuts expose columnar-jointed, black, glassy, 2-pyroxene, olivine-bearing andesite of Table Rocks (late Miocene age; 7 Ma). These distinctive flows are the oldest flows assigned to the volcanic rocks of the High Cascades in southern Oregon and northern California. Flat-topped erosional remnants crop out along the Rogue River's valley walls for 30 mi from 1 mi east of Prospect to the Table Rocks 10 mi north of Medford. Near Prospect the flows are 100 m thick, decreasing only slightly downstream to Table Rocks where they are still 75 m thick. Their volume was at least 6.3 km^3. Insignificant weathering of flow tops suggests that all the flows erupted within a short period. **0.5**

24.7 View at 2:00 of Lost Creek Dam and part of Lost Creek Reservoir. **0.1**

24.8 **STOP 1. Basalt flows of the Western Cascade Range.** Make a sharp horseshoe bend to the right onto a nearly hidden, unmarked, dirt road. Exposures are in roadcuts on both sides of highway. **Even though the shoulder is wide, be extremely cautious about traffic, particularly log trucks.** Roadcuts expose 28–25 Ma basalt flows. Closely spaced jointing, recrystallization (indicated by dull, mottled groundmass textures), and zeolites in vesicles

and fractures are typical features of mafic and intermediate flows of the Western Cascade Range. Incised and channelized flows, irregular flow contacts, and cross-cutting dikes suggest a nearby source. Both abutments of Lost Creek dam are in this series of flows. **0.7**

25.5 Contact between basalt flows and altered ash-flow tuff of the Western Cascade Range. [Similar ash-flow tuffs can be viewed safely on the north side of Lost Creek Reservoir along Takelma Drive, to the right just beyond the bridge over the Rogue River, 0.8 mi ahead.] **1.0**

26.5 Casey State Park on left. For the next 7 mi, Highway 62 passes through poorly exposed interbedded andesite and basaltic andesite flows, tuff breccia, lapilli tuff, and small intrusives. **1.4**

27.9 Pasture land on both sides of the road in this area is probably underlain by reworked Mazama ash. **1.7**

29.6 Entrance to Rogue Elk County Park on left. On the right is a deposit of reworked Mazama ash that marks the farthest known extent of Mt. Mazama ash, 72 km along the Rogue River from the Rim of Crater Lake. **3.3**

32.9 Junction with OR-227 to Canyonville. [Those wishing to see a well-exposed section of Western Cascade tuff breccia, lapilli tuff, and finer-grained volcaniclastic beds typical of the alluvial facies of Smedes and Prostka (1972), will find it along OR-227 and in the adjacent creek bed. The Western Cascade Range contains many thick sections like this one. Massive to poorly sorted, matrix-supported tuff breccia and lapilli tuff form beds 0.5 to 3 m thick, with planar tops and bottoms. Both ash-flow tuff and debris-flow deposits are present. Locally, diagenesis, weathering, and poor exposure limit the ability to distinguish between these two different types of deposits. Continental volcanic sandstone and siltstone sequences are interbedded with tuff breccia and lapilli tuff. Sandstone and siltstone beds range from a few centimeters to a few decimeters thick, with sharp planar contacts. Locally broad, shallow channels with low-angle bed forms are present. This sequence is interpreted as having been deposited on aggrading volcanic dispersal aprons at some distance from volcanic vents. Volcanically induced high-energy depositional packages (e.g., debris-flow deposits; ash-flow tuff) alternate with lower-energy, fluvial, traction-current and overbank deposits.]

Continue on OR-62, which turns left and heads south for the next 15 mi into the Medford Valley. The highway is parallel to the strike of the volcanic rocks of the Western Cascade Range, and this part of the trip crosses very little section. In many places rocks are poorly exposed and highly weathered. **0.2**

33.1 Roadcut in hypersthene andesite of the Western Cascade Range. **2.2**

35.3 Leave Shady Cove and cross Rogue River. Small quarry on left cuts through small mafic intrusion in the Western Cascade rocks. **2.6**

37.9 To the right are gently dipping slopes of Western Cascade lavas and sedimentary rocks. **2.3**

40.2 Hamell Road. The marshy pasture land to the left (east) is typical of low areas underlain by partly welded recrystallized ash-flow tuff of the Western Cascade Range. **1.6**

41.8 Junction with OR-234 to Sams Valley, Gold Hill, and Grants Pass. Mt. McLoughlin is visible from time to time for the next several miles at about 9:30. **5.1**

46.9 Cross Antelope Creek. Road ascends onto a mid-Pleistocene fan terrace. A sequence of six stepped geomorphic surfaces was recognized by Parsons and Herriman (1976) in the Medford area. This surface, the Roxy Ann surface, is the next-to-oldest and is 30–45 m above the present flood plain of the Rogue River. **2.5**

49.4 Junction with OR-140 to Lake of the Woods and Klamath Falls. Mesas at 3:00 are capped by 7 Ma andesite flows of Table Rock. **2.4**

51.8 Central Point junction. Low hills at 10:30 are underlain by small Tertiary intrusives that were emplaced into upper Eocene continental sediment derived from the Klamath Mtns. to the west (right). **3.2**

55.0 Turn left onto Interstate 5 south. For the next 15 mi I-5 ascends Bear Creek Valley. To the right (west) are the Klamath Mtns., underlain by several tectono-stratigraphic terranes composed of complexly faulted and highly deformed late Paleozoic, Triassic, and Jurassic metamorphic and intrusive rocks. More than 1200 m of Upper Cretaceous unmetamorphosed, dominantly marine sandstone, siltstone, and conglomerate (the Hornbrook Fm.) was deposited unconformably as an overlap assemblage across the older terranes. A sequence of upper Eocene and lower Oligocene(?) fluvial conglomerate and sandstone derived from Mesozoic and Paleozoic rocks in the Klamath Mtns. unconformably overlies the Hornbrook Fm. This Tertiary sequence is as thick as 2150 m, but thins abruptly to the south. Both the Hornbrook Fm. and the Tertiary rocks dip gently east and extend an unknown distance under the volcanic rocks of the Western Cascade Range. Volcaniclastic sediment and tuff coming from the nascent High Cascade volcanic arc are interbedded in the youngest part of the continental sequence. For a detailed description of the Hornbrook Fm. and lower Tertiary rocks between Medford and Yreka see the field-trip guide of Nilsen et al. (1984).

The rounded tree-covered hill in the middle distance at 9:00 is Roxy Ann Peak. The change in slope at the shoulders of the peak marks the approximate contact between upper Eocene continental sandstone and conglomerate and the unconformably overlying volcanic rocks of the Western Cascade Range. A K–Ar date on the lowermost flows on Roxy Ann Peak gave an age of 30.8 ± 2 Ma. **4.0**

59.0 On left (east), turbidites of the Hornbrook Fm. are exposed in roadcut, with upper Eocene fluvial sandstone in the upper part of the hill. **1.2**

60.2 Upper Eocene and lower Oligocene(?) continental sandstone and conglomerate make up the lower half of the mountainside rising to the left. The prominent cliff part way up the slope is a conglomerate lens. Basaltic andesite flows and interlayered tuff breccia

of the Western Cascade Range dated at 25–30 Ma crop out along the upper half of the slope. **1.5**

61.7 On left are roadcuts exposing upper Eocene fluvial conglomerate. **1.4**

63.1 Just beyond the rest area, the highway crosses the contact between upper Eocene rocks and the Hornbrook Fm. **4.0**

67.1 Weigh station. The smooth slopes to the left (northeast) behind the weigh station are the front of a large landslide. Most of the section visible from here is basaltic andesite and andesite flows and associated tuff breccia of the Western Cascade Range. The section is nearly 3.6 km thick. Rocks at the base of the section are about 30 Ma, and rocks at the top of Grizzly Peak (at 10:00) are about 25 Ma for an accumulation rate of 400 m/m.y. The flows and tuff breccia accumulated on coalescing dispersal aprons around volcanic centers. The lateral continuity of beds and uniformity of attitude suggest that the accumulation area was some distance from the source volcanoes. **4.1**

71.2 Second Ashland exit at OR-66. **1.2**

72.4 At 10:00 in the middle of the valley is a small Tertiary plug intruded along the contact of the Hornbrook Fm. and the upper Eocene sedimentary rocks. **2.4**

74.8 Roadcut on right exposes sandstone and pebble conglomerate of the Hornbrook Fm. **0.6**

75.4 Contact between Hornbrook Fm. and small Tertiary intrusion. Both the intrusion and the Hornbrook Fm. are hydrothermally altered near the contact.

For the next 4.5 mi, roadcuts are in the Mt. Ashland pluton (Late Jurassic age) and screens of metamorphic rock of Paleozoic or Mesozoic age; intrusion of the Mt. Ashland pluton hornfelsed the regionally metamorphosed schist and gneiss. The unconformity with the overlying Hornbrook Fm. dips steeply to the east (left). **0.6**

76.0 Exposures of Mt. Ashland pluton. **1.0**

77.0 Exposures of roof pendants of metasedimentary biotite schist and quartz–biotite gneiss. **2.3**

79.3 Roadcuts expose the Mt. Ashland pluton (capped by a grus layer) and the overlying Hornbrook Fm. **0.6**

79.9 Offramp to Mt. Ashland. Highway crosses the poorly exposed Siskiyou Summit fault, a north-northeast-trending normal scissors fault down to the southeast. West of I-5, the fault juxtaposes Hornbrook Fm. and Oligocene volcaniclastic sediments against the Mt. Ashland pluton. East of I-5, the fault puts Hornbrook Fm. and upper Eocene and lower Oligocene(?) continental sedimentary rocks against Oligocene volcanic rocks of the Western Cascade Range. The Siskiyou Summit fault is one of a series of widely spaced faults radial to Condrey Mtn., 25 km southwest, and is thought to have formed as a result of some 7 km of vertical doming centered on Condrey Mtn. between about 14 and 5 Ma (Mortimer and Coleman, 1984). Displacement on the Siskiyou Summit fault southwest of I-5 may be as much as 5.5 km, but only 8 km east of I-5 no offset is detectable. **1.1**

81.0 **STOP 2. Recrystallized volcaniclastic sediments and ash-flow tuffs of the Western Cascade Range.** Truck brake-check area at summit of Siskiyou Pass. Pull off on right. Volcaniclastic sediments are more prevalent in the north part of the roadcut. Note: (1) broad, shallow channels, and (2) the wide variety of rock types, including roundstone conglomerate channel fill, fine overbank sand, lacustrine silt, and poorly sorted volcanic diamicton (interpreted as mudflows). The green color on fresh surfaces is typical of unweathered Western Cascade volcaniclastic rocks. The recrystallization assemblage includes zeolites (primarily heulandite with some clinoptilolite), chlorite (probably an iron-rich variety), calcite, and chalcedony (Bestland, 1985). A gray, white-weathering, partly welded ash-flow tuff is exposed, starting about one-third of the way through the cut. The ash-flow tuff fills a shallow channel which is best seen in the roadcut on the east side of the highway **(do not attempt to cross this dangerous interstate highway!)**. Although the rock appears fresh, Bestland (1985) described very fine-grained clinoptilolite replacing the vitric matrix. At the south end of the roadcut, ash-flow tuffs 2–3 m thick are separated by volcaniclastic sandstone, conglomerate, and siltstone. **0.8**

81.8 The dark cliffs above the highway to the left are a 30 Ma intracanyon basalt flow. **0.5**

82.3 Yellow and buff volcaniclastic sandstone and siltstone are exposed in cuts on both sides of road. **0.4**

82.7 Light-colored outcrops on left are pumice lapilli ash-flow tuff dated at 29.9 ± 1.5 Ma by K–Ar. The section is repeated farther along in the roadcut by a small fault. A basaltic dike also intrudes the section here. **2.8**

85.5 California state line. On right, the roadcut exposes thin-bedded, rhythmically interbedded, basin-plain turbidites of the Hornbrook Fm. **1.6**

87.1 Prominent rim to the left (east) is formed by a Tertiary basaltic sill intruded into the Hornbrook Fm. **0.7**

87.8 Railroad overcrossing. The large rounded hill at 11:30 is Black Mtn., a large andesitic intrusion with many landslides on its sides, emplaced along the contact between the Hornbrook Fm. and the volcanic rocks of the Western Cascade Range. The railroad grade to the left is cut into Hornbrook Fm. Higher up the hill, volcanic rocks of the Western Cascade Range lie directly on the Hornbrook Fm. without any intervening upper Eocene sedimentary rocks. The cliff in the Western Cascade rocks exposes an ash-flow tuff. **3.5**

91.3 Agricultural inspection station.

Mount Shasta and vicinity

Robert L. Christiansen and C. Dan Miller

Summary

Mt. Shasta is the largest stratovolcano of the Cascade chain. At nearly 500 km^3, it is comparable in volume to such stratocones as Fuji-san and Cotopaxi. The peak rises to an elevation of 4317 m, more than 3200 m above its base, and dominates the landscape of northern California.

The route of this trip (Fig. 26) approaches Mt. Shasta from the north through Shasta Valley, largely floored with the debris of an enormous volcanic-sector avalanche that virtually destroyed an ancestral Mt. Shasta about 350 ka (Crandell et al. , 1984; Crandell, in press). Only a small remnant of this older volcanic edifice remains, but the volume of the Shasta Valley debris avalanche is about 45 km^3.

The bulk of Mt. Shasta is a composite feature built over the stump of the destroyed older volcano; it comprises four major cones built around discrete eruptive centers (Fig. 27; Christiansen and Miller, 1976; Christiansen et al. , 1977). Each of these cones appears to have grown mainly in a short episode, perhaps only a few hundred or a few thousand years (Christiansen, 1982, 1985), that produced numerous lavas from a central vent. Virtually all the lavas of the major cone-building episodes are 2-pyroxene silicic andesites. Following each of these episodes, the cones underwent significant erosion and less frequent eruptions from the central vent and, in most instances, from flank vents as well. The latest eruptions within the central craters produced dacitic domes and pyroclastic flows; flank eruptions typically produced either cinder cones and flows of basalt to basaltic andesite or domes and pyroclastic flows of dacite to rhyodacite. Pyroclastic flows are particularly conspicuous on the west flank of Shastina, the prominent cone on Mt. Shasta's west side (Miller, 1978).

The Mt. Shasta magmatic system has evolved more or less continuously since at least 590 ka. The Sargents Ridge cone, oldest of the four cones that formed the present volcano after major sector collapse, is younger than about 250 ka, but has experienced two major glaciations. The next younger, the Misery Hill cone, is younger than about 130 ka and has been sculpted in one major glaciation. The twc younger cones are Holocene: Shastina, west of the cluster of other central vents, was formed mainly between 9.7 and 9.4 ka; the Hotlum cone may overlap Shastina in age bui appears to be mainly younger. Mt. Shasta has continued tc erupt at least once every 600-800 years since 10 ka (Miller, 1980). Its most recent eruption probably was in 1786 (Finch. 1930).

Field guide

Mileage

0.0 Agricultural Inspection Station on Highway I-5 South. **1.6**

1.6 Offramp to Henley–Hornbrook. The low hills along the road are underlain by Upper Cretaceous Hornbrook Fm. At 11:00 is Black Mtn., a resistant knob of intrusive andesite of the Western Cascades. Sharper ridges to the right and in the distance are pre-Tertiary metamorphic rocks of the Klamath Mtns., mainly representing oceanic crust and marine metasedimentary and metavolcanic rocks of Paleozoic and early Mesozoic age. **1.5**

3.1 Large roadcut in sandstone of the Hornbrook Fm. The basal contact lies in the next gully to west. **0.5**

3.6 Large roadcut in greenstone of the Klamath Mtns. sequence. Most roadcuts beyond here for about the next 10 mi expose similar greenstone and some interstratified chert. **1.3**

4.9 Cross Klamath River. The river flows west to the ocean through a deep canyon. Large roadcuts along the road for the next several miles are all in metamorphic rocks of the Klamath Mtns. **6.2**

11.1 **STOP 1. View across the volcanic debris avalanche of Shasta Valley to Mt. Shasta.** Exit right at offramp for vista point. The conspicuously hummocky topography of Shasta Valley is the expression of a volcanic debris avalanche deposit that is exposed south to Black Butte, the prominent steep-sided dome at the west foot of Mt. Shasta, 50 km away. The deposit resulted from an enormous sector collapse of an ancestral Mt. Shasta. The flat valley floor between the hummocky megablocks is a matrix facies of debris flows (lahars) that resulted from dewatering of the avalanche. These debris flows were forced through the narrow valley of the Shasta River just west of here (right) and ponded in the wider valley upstream to an average thickness of 75 m (Crandell, in press). Downstream (farther north), the debris flows must have entered the Klamath River. A few of the larger hills surrounded by the hummocky debris avalanche are eroded remnants of Tertiary Western Cascades volcanic rocks that once extended across Shasta Valley.

On the skyline to the east (left) are three young basaltic andesite shields of the High Cascades built on eroded volcanic rocks of the Western Cascades (left to right): The Goosenest (late Pleistocene), Herd Peak (Pliocene), and The Whaleback (late Pleistocene). Outcrops northeast across the highway are intrusive andesites of the Western Cascades.

The higher terrane to the west and southwest is entirely underlain by metamorphic rocks of the Klamath Mtns.; prominent at the south end of the view is Mt. Eddy, underlain by the Trinity ophiolitic complex of early Paleozoic age.

Return to I-5 South. **0.9**

12.0 Cross Shasta River. **5.4**

17.4 Offramp to CA-3 to Ft. Jones and Weaverville; continue on I-5 South. Note that the Shasta Valley volcanic debris avalanche did not enter the valley of Yreka, separated from the main Shasta Valley by a low bedrock ridge to the left. Hills on both sides are underlain by metasedimentary rocks of Ordovician and Silurian age. **7.3**

24.7 Exit right at offramp for Gazelle; at stop sign, turn left across I-5. **0.3**

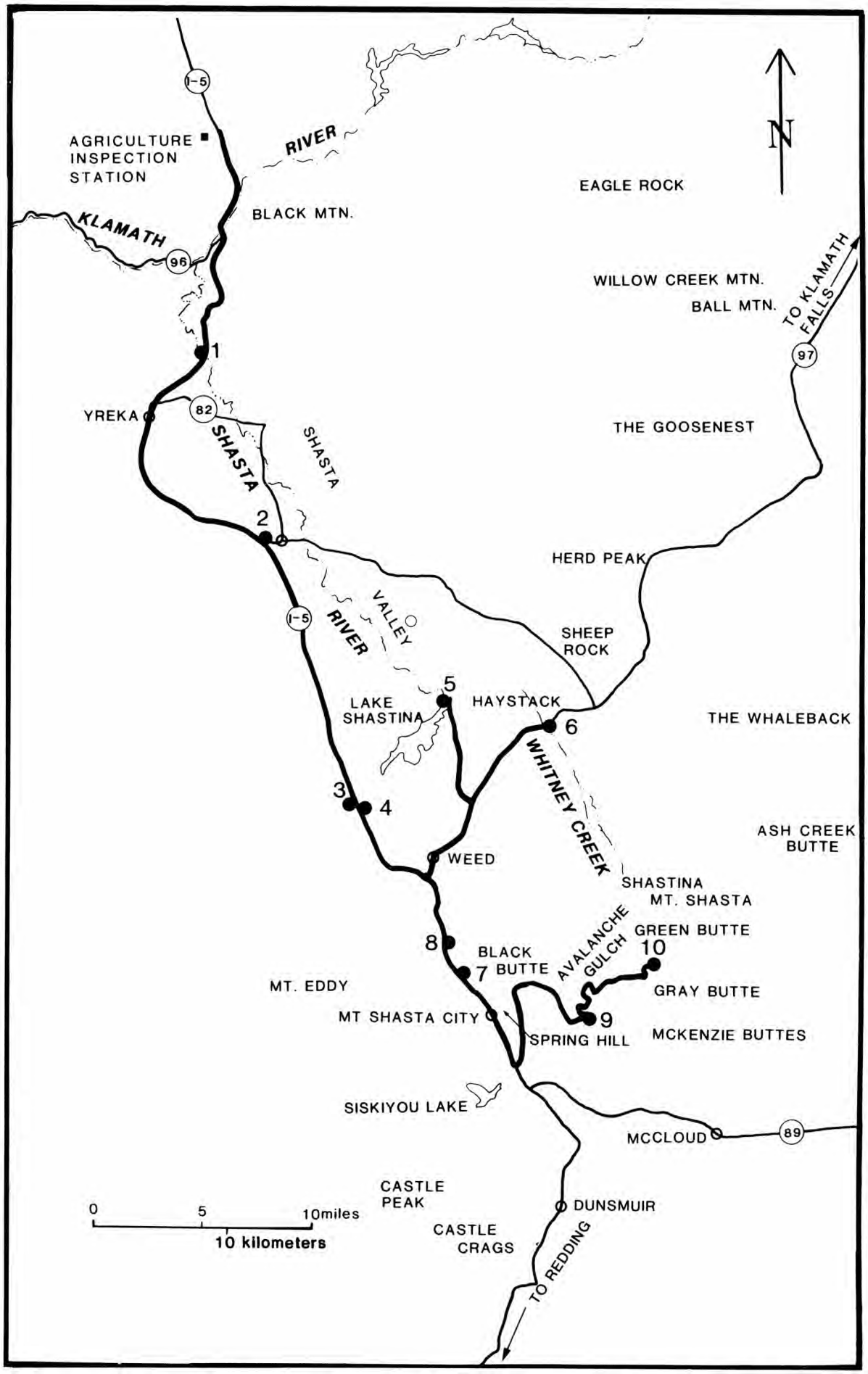

FIGURE 26—Route map for Mount Shasta and vicinity.

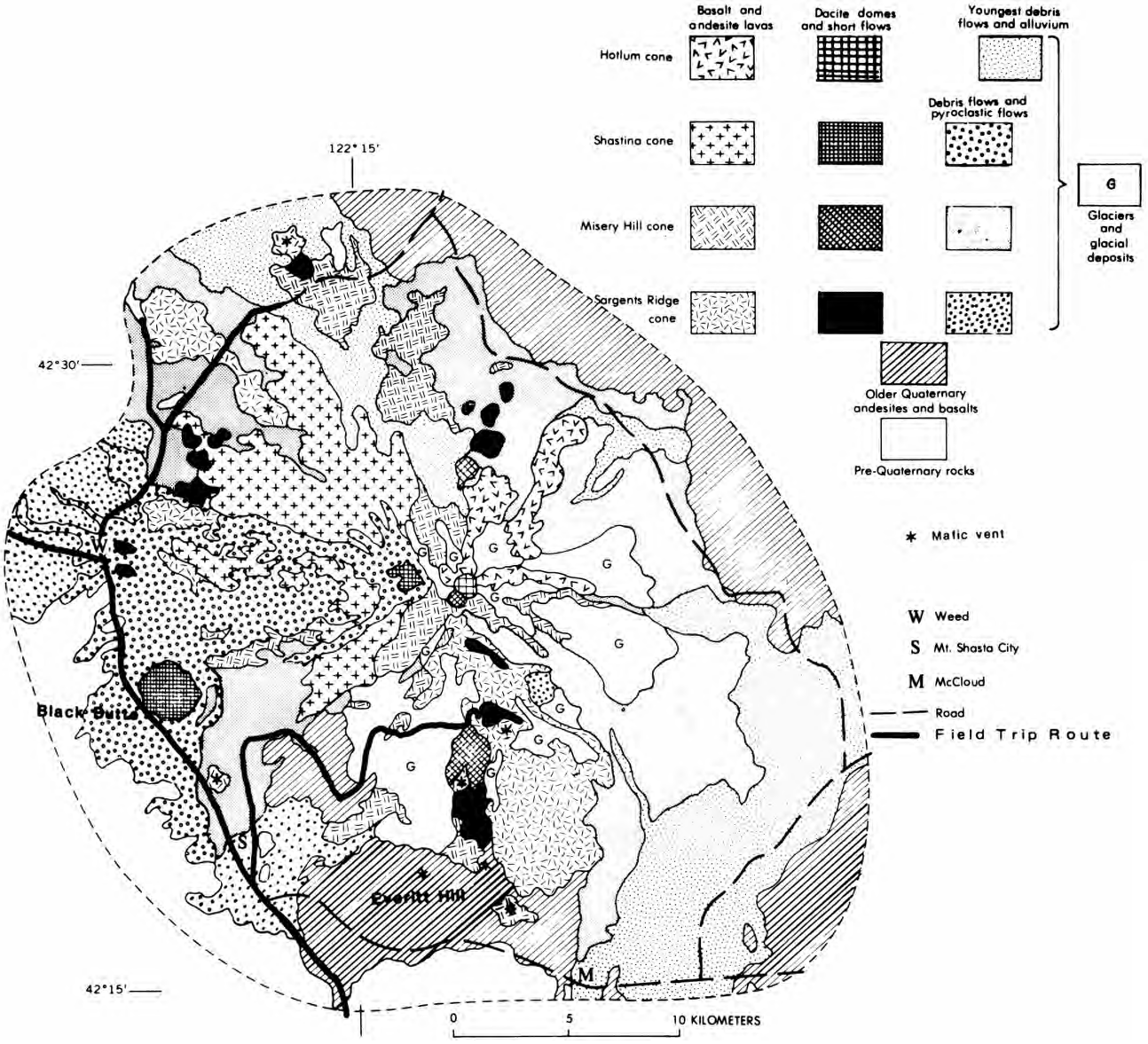

FIGURE 27—Geologic map of Mount Shasta.

25.0 **STOP 2. View across the Shasta Valley volcanic debris avalanche to Mt. Shasta.** Park along the wide roadside while still high on the overpass ramp but just past the bridge over I-5. Low, rounded hills across the road to northeast are megablocks of the avalanche deposit; the flat surface in the immediate foreground is underlain by debris flows of the matrix facies. The steep-sided dome of Black Butte is prominent at the west foot of Mt. Shasta. On the skyline to the east is a group of late Pliocene to early Holocene basaltic andesite shield volcanoes along the main Cascades axis, including (left to right) Eagle Rock, Willow Creek Mtn., Ball Mtn., The Goosenest, Herd Peak, The Whaleback, and Ash Creek Butte. The Goosenest has a prominent agglutinate cone at its central vent, probably typical of many of these shields but not always well preserved on the older ones; Ash Creek Butte is carved by prominent glacial cirques that removed much of a similar agglutinate cone.

Low hills to the north and across the highway to the southwest are phyllites of Ordovician age.

Continue ahead. **0.4**

25.4 Gas station and restaurant at Grenada. Turn around and return across overpass to the west side of I-5. **0.5**

25.9 Turn left onto onramp to I-5 South. **1.5**

27.4 Cross railway overpass. I-5 near here traverses the flat surface of matrix-facies debris flows of the Shasta Valley debris avalanche. **2.1**

29.5 From here south for several miles, I-5 passes through hills that are megablocks in the volcanic debris avalanche; the flat surface between the hills is underlain by debris flows of the matrix facies. **3.3**

32.8 Offramp to Louie Road on right; continue on I-5 South. Beyond here, I-5 climbs through megablocks of the Shasta Valley debris avalanche **1.0**

33.8 To the right is the first of two large closed depressions in the surface of the debris avalanche. **3.8**

37.6 I-5 leaves the megablock terrain and crosses a flat-

surfaced terrace developed on debris flows of the debris-avalanche matrix facies. The surface on this terrace is marked by prominent stone polygons and other patterned-ground features, produced by periglacial processes during the late Pleistocene glaciations. **0.7**

38.3 **STOP 3. Rest stop.** Exit right at offramp to rest stop, toilet facilities, and vista point. Return to vehicles and continue along frontage road. **0.4**

38.7 Turn right on road to Weed Airport. At intersection, turn left and continue along the road under the highway. **0.4**

39.1 **STOP 4. Matrix facies of the Shasta Valley debris avalanche.** Park at turnout on right, opposite junction with road to Weed Airport. Walk a few meters south to cross a barbed-wire fence and descend to low cuts along the railroad. The variety of volcanic rock types in the deposits is representative of the ancestral Mt. Shasta, which consisted mainly of silicic andesites and subordinate dacites. A few basaltic andesites are also present. Note the rounding of the fragments and the indurated fine-grained matrix. The deposit dates from about 350 ka and has a fairly well-developed soil, mainly expressed as a deep zone of oxidation. From the banks above the railroad cuts is a good view south to Mt. Shasta and to Black Butte, a dacitic dome complex at its west foot.

Turn around and return by the same roads to the frontage road for I-5 South. **0.6**

39.7 Re-enter I-5 South. The highway continues along the patterned-ground surface on a matrix-facies terrace of the Shasta Valley debris avalanche. **2.3**

42.0 Offramp to Stewart Springs Road and Edgewood; continue on I-5 South. I-5 South climbs through large ridges that are megablocks in the Shasta Valley volcanic debris avalanche—virtually intact fragments of the ancestral edifice of Mt. Shasta. The roadcuts provide excellent exposures of these megablocks, which consist predominantly of unconsolidated volcanic diamictons that are locally disturbed and cut by numerous small faults but remain in upright, subhorizontal attitudes and have largely coherent stratigraphy. **2.7**

44.7 Exit right at offramp to north Weed and US-97; at stop sign, turn left through underpass beneath I-5, then right at the next stop sign, following signs to Weed and Klamath Falls. **0.9**

45.6 Stop at intersection with flashing red light and then turn left onto US-97; just beyond, cross railroad on overpass. **0.7**

46.3 First of several roadcuts on both sides in megablocks of Shasta Valley debris avalanche. **1.2**

47.5 Apple Valley Road. Roadcut on right and a sand and gravel pit farther to right expose ash-cloud deposit from pyroclastic flows erupted at the summit of Shastina. Beyond here, the road drops onto a surface underlain by older pyroclastic flows of early Holocene age. Hills to left are megablocks in the debris avalanche that underlies the pyroclastic flows. Hills to right are andesitic lava flows from the Shastina central vent; they overlie the pyroclastic flows. Also to right are several older dacitic domes. **2.5**

50.0 Turn left onto road to Lake Shastina and Big Springs. The road crosses pyroclastic flows from Mt. Shasta dated at about 9.7 ka; note a poorly developed soil—about 70 cm of yellowish oxidation. In the distance to the left, beyond the debris-avalanche megablocks, are ridges of the Klamath Mtns. underlain by metamorphic and plutonic rocks. On the skyline to right are basaltic andesite shields along the main Cascades axis. **2.5**

52.5 Irregular ridge on right and ahead is an andesite flow from the oldest part of modern Mt. Shasta, the Sargents Ridge cone. It is deeply weathered, overlies megablocks of the Shasta Valley landslide, and is overlain by early Holocene pyroclastic flows from Mt. Shasta. **0.3**

52.8 Entrance to golf resort and restaurant on left; continue on main road. **0.6**

53.4 Roadcut through a megablock of the Shasta Valley debris avalanche. The younger Sargents Ridge andesitic lava flow overlaps this megablock on the right. The flat surface along which most of the road passes overlies an early Holocene pyroclastic flow. **0.7**

54.1 Entrance to Lake Shastina resort development on left; continue on main road. **0.9**

55.0 The road descends from the pyroclastic-flow surface onto the debris-flow fan of Whitney Creek, on which debris flows continue to be deposited this far from Mt. Shasta during years of heavy snowmelt and high runoff. On the left, the road passes a megablock of the Shasta Valley volcanic debris avalanche. **0.2**

55.2 **STOP 5. Megablock of the Shasta Valley volcanic debris avalanche and view of Mt. Shasta.** At a gate that closes off a paved road on the left, turn around and park. Cross the gate on foot and walk up the paved road straight ahead. About 200 m up the road, just past the crest of a hill, turn right onto a dirt road blocked by a cable and walk about another 250 m across the dam of Lake Shastina to a quarry on the other side. This quarry provides an excellent exposure into one of the megablocks of the Shasta Valley volcanic debris avalanche. The materials of the block are principally unconsolidated pyroclastic flows, volcanic debris flows, and sediments, including several successive buried soils. Numerous normal faults of varied orientations and displacements cut the block, but the section remains subhorizontal and upright, and its stratigraphy remains coherent.

To the southeast is Mt. Shasta. The summit and north and northeast flanks are the young Hotlum cone. Shastina is in front and to right but is not clearly outlined from this perspective. The small ridge between these cones is part of the breached crater rim of the Misery Hill cone. Below Mt. Shasta in a line toward us are andesitic lava flows erupted from the summit vent of Shastina. One lava flow from the older Sargents Ridge cone emerges from beneath the visible edifice of Mt. Shasta in a line toward Lake Shastina, abutting megablocks of the Shasta Valley debris avalanche. Black Butte, to the south, is a young dacitic flank dome of the Shastina cone; between it and Shastina, but closer to us, are several older dacitic flank domes that are overlapped by Shastina lavas.

Along the skyline to the east (right to left, north from Mt. Shasta) are The Whaleback, Sheep Rock (eroded andesitic breccias of the older Western Cascades), Herd Peak, and The Goosenest. The sparsely tree-covered area of Shasta Valley beyond the grassy surface of the Whitney Creek debris-flow fan is underlain by basalt of 300 ka that overlaps and helps to date the Shasta Valley debris avalanche.

Return to vehicle and retrace route south to US-97. **5.2**

60.4 Turn left onto US-97. After the turn, the hill on the left is a megablock in the Shasta Valley debris avalanche. To the right, the early Holocene pyroclastic-flow surface is overlain by the snout of a lava flow from the central vent of Shastina. **0.6**

61.0 Roadcut on right exposes an early Holocene pyroclastic flow from Mt. Shasta that forms the surface in this area and shows a weak soil profile, mainly expressed as about 70 cm of yellowish oxidation. Near here, this pyroclastic flow is dated at 9.7 ka. **0.3**

61.3 Turnout just past low crest. About 4.5 km away at 2:00 is Cinder Cone, an old basaltic flank vent just beyond an even older flow (with the prominent railroad cut). To the left is a good view down Shasta Valley of the debris avalanche. **1.5**

62.8 Area to the left of highway displays outcrops of an andesitic lava flow from the Sargents Ridge cone. The lava postdates the Shasta Valley debris avalanche but underlies early Holocene pyroclastic flows. **1.6**

64.4 Turnoff on right, opposite the end of a dirt road with stop sign on left. A few meters south (right) of the road is the steep flow-front scarp, about 20 m high, of the Lava Park flow, an andesitic block lava that erupted from a flank vent of Shastina at about 9.5 ka. This is the only Shastina andesite not erupted from the central crater. Although not a stop on the regular field trip, a climb from here to the top of this flow provides a view superior to that of Stop 6. (If this climb is made, however, be cautious of **poison oak,** which grows on the scarp and in the gully at its base and can cause a severe skin rash). **0.3**

64.7 Dirt road on right; continue on highway. View at 10:00 of Haystack, an old dacitic flank dome of Mt. Shasta, and a composite cinder cone farther left. The large shield volcano ahead on the skyline is The Whaleback. **0.9**

65.6 **STOP 6. View of the younger cones of Mt. Shasta.** Park at large turnout on right by green fence just before bridge across Whitney Creek. Walk through the gate (marked by a red post) near the bridge and proceed a short distance upstream along the bank of Whitney Creek. The creek is fed from daily meltwater runoff from the Whitney glacier and is often dry in the morning but runs later in the day; runoff may vary from a trickle to a torrent. Note the debris-flow levees along both banks. To the south, the Hotlum and Shastina cones of Mt. Shasta are prominent, with a remnant of the breached crater rim of the Misery Hill cone between them at the head of the Whitney glacier; the edge of the summit dome of Misery Hill is also visible to the left of the rim.

Low hills to the east are lava flows of the Misery Hill cone that emerge from beneath the younger Hotlum cone on the north side of the compound stratovolcano. The top of Haystack, an older dacitic flank dome, is just visible beyond them to the northeast. The Lava Park flow, an early Holocene block lava from a flank vent of Shastina, is prominent to the southwest (right).

Turn vehicles around and return on US-97 toward Weed. **5.2**

70.8 Lake Shastina Road on right; continue on US-97. **4.5**

75.3 Stop at flashing red light. Turn left onto Weed Blvd. Pass through Weed and under I-5. **0.5**

75.8 Turn left onto onramp to I-5 South. Hill to the left of the highway is an old dacitic flank dome of Mt. Shasta. **1.3**

77.1 Offramp to South Weed Blvd.; continue on I-5 South. The valley bottom here is a constructional surface of pyroclastic flows from the summit vent of Shastina. Ahead on the right is a large megablock of the Shasta Valley volcanic debris avalanche—the nearest to the ancestral cone that is still exposed. Roadcut ahead is in Shastina pyroclastic flows. On the left ahead is Black Butte, a dacitic flank dome of Shastina and its youngest eruptive product. At least four and perhaps five emplacement units of the dome are expressed geomorphically. **2.0**

79.1 Offramp to Summit Dr. and Truck Village Dr.; continue on I-5 South. Hummocky terrain is the surface of hot-avalanche deposits and pyroclastic flows from Black Butte. **2.3**

81.4 Exit right on offramp to Abrams Lake Road. At stop sign, turn left across highway. **0.4**

81.8 Turn left onto onramp to I-5 North. **1.2**

83.0 **STOP 7. Black Butte hornblende dacite.** Park at large turnout on right, 0.1 mi beyond sign for Black Butte summit. Talus from the Black Butte dome comes down to the roadside and offers opportunities to examine the lithology of this hornblende dacite. The fresh lithology from the interior of the dome is gray with dark hornblende phenocrysts, generally with hollow centers and plagioclase cores; a pink lithology with oxyhornblende represents the surficial carapace of the dome. **0.8**

83.8 Exit right on offramp for Truck Village Dr. At stop sign, turn right and pass Truck Village on right. **0.3**

84.1 At T-intersection, turn left. **0.3**

84.4 Roadcut in a large, internally shattered block of dacite in a hot-avalanche deposit from the emplacement of the Black Butte dome.

Continue ahead on main paved road. **0.7**

85.1 **STOP 8. Shastina and Black Butte pyroclastic flows.** Turn around and park in open area past end of pavement. Walk west down into railroad cut. The major exposures are flows from the Shastina summit vent, distinguished by dacite blocks that contain phenocrysts of hornblende, hypersthene, and augite. A pyroclastic flow from Black Butte, recognized by large cored hornblende phenocrysts but lacking pyroxene, overlies the Shastina flow in pockets, especially at the south end of the cut. Black Butte rises prominently to the south; several em-

placement units are recognizable topographically. To the east, Shastina rises conspicuously on the west side of Mt. Shasta, with a fan of pyroclastic flows mantling its west flank.

Return along paved road toward Truck Village. **1.0**

86.1 At intersection, turn right and continue beneath I-5. **0.2**

86.3 Turn left onto onramp to I-5 South and return to the highway. **1.9**

88.2 Offramp to Abrams Lake Road; continue on I-5 South, which passes through hummocky topography of Black Butte hot-avalanche deposits and pyroclastic flows. **0.5**

88.7 Sand-and-gravel pit on right, where pyroclastic flows of Black Butte are quarried for aggregate. **0.6**

89.3 Exit right on offramp to Mt. Shasta City. On the left is Spring Hill, an old andesitic lava cone on the west flank of Mt. Shasta. **0.9**

90.2 Mt. Shasta City Park on right; continue ahead on main road. **0.4**

90.6 Cross railroad tracks, a spur from the main line to the right. **0.2**

90.8 Bear right at Y-intersection. **0.3**

91.1 Traffic light at major intersection in Mt. Shasta City. Turn left onto East Alma St. Proceed through the intersection with the flashing yellow light and follow the road with the double yellow line as it curves around a school and baseball field. **0.6**

91.7 Stop at flashing red light; turn left onto Everitt Memorial Highway. **0.4**

92.1 Cross railroad tracks. Beyond, the road climbs gradually on a fan of upper Pleistocene pyroclastic flows from Mt. Shasta, which postdate the building of the Misery Hill cone. **1.0**

93.1 Gentle curves in road. On left ahead is Black Butte. High peak on the west skyline is Mt. Eddy, which exposes the Trinity ophiolitic complex. **0.7**

93.8 Road on left to Black Butte Trail; continue on highway, which continues to climb the surface of upper Pleistocene pyroclastic flows. **1.7**

95.5 Road on left to McBride Springs Campground, at which a spring issues from the base of an andesitic lava flow from Shastina where it lies on the older pyroclastic flows. Continue on Everitt Memorial Highway. **0.2**

95.7 Wide turnout on right at orange sign "Elevation 4790 feet, 4 miles." Shastina on the left. Ahead, post-Misery Hill pyroclastic flows onlap steep tree-covered bluffs that rise to the left of the road, a remnant of ancestral Mt. Shasta. **0.6**

96.3 Road crosses gully onto a steeper slope. Roadcuts on the left ahead expose 590 ka andesitic lava flows, overlain by colluvial and pyroclastic deposits of varied thickness and weathered to a deep, brightly colored soil. The lavas are part of the only remnant of ancestral Mt. Shasta that existed before the 350 ka sector collapse. **2.4**

98.7 Orange sign "7 miles, elevation 5600 feet." At a sharp curve left and a small side road to the right, about 25 m past the sign, is good exposure of porphyritic andesite of ancestral Mt. Shasta. The prominent curved platy jointing is common in many Cascades andesitic lavas. **1.0**

99.7 Orange sign "Elevation 5900 feet, 8 miles." On left just beyond the sharp curve ahead is a good example of the deep weathering profile developed on the lavas and surficial deposits of ancestral Mt. Shasta. **0.5**

100.2 Turnoff on right for John Everitt Vista Point. To the right and behind is a view south to Castle Crags and Castle Peak, erosional features of a Jurassic granitic pluton. To the southwest are Siskiyou Lake and Mt. Shasta City at the foot of debris-flow and pyroclastic-flow fans from Mt. Shasta. To the west is the ophiolite complex on Mt. Eddy. To the northwest is the top of Black Butte. **0.3**

100.5 **STOP 9. View of the older cones of Mt. Shasta.** Park at turnout on right. On the left is the early Holocene cone of Shastina, overlapping lavas from the apparent summit cone, the Misery Hill cone. The true summit, on the Hotlum cone, is blocked from view by Misery Hill, a dacite dome that rises within the crater of the cone named for it. To the right of Misery Hill is a prominent ledge, Red Banks, formed by agglutinated fallout pumice erupted from the summit crater of the Misery Hill cone at about 9.7 ka. The prominent glaciated valley leading directly toward here from Red Banks is Avalanche Gulch. Just to the right of Red Banks is Sargents Ridge, which exposes lavas that dip north, back under the Misery Hill cone, and define the north flank of the Sargents Ridge cone; south dips on the skyline define the opposite flank of the Sargents Ridge cone.

A north–south line of flank vents marks the skyline to the east, on the south flank of the Sargents Ridge cone. The highest prominent vent feature is Gray Butte, a glaciated dacite dome; next below is an andesitic cinder cone; next are two more dacite domes (upper and lower McKenzie Buttes, with ski runs cut into the vegetation of the upper); less conspicuous at the foot of the mountain at the south end of the line is the top of Signal Butte, an andesitic lava cone. Farther right, to the south from here, is Everitt Hill, a 450 ka basaltic andesite shield volcano.

The roadcut on the left side of the road exposes the deep soil developed on ancestral Mt. Shasta and part of an andesitic lava flow. Spoil from the cut lies at the roadside in the turnout, providing relatively fresh samples of the andesitic lava. Note the abundant corroded plagioclase and moderately abundant hypersthene phenocrysts. **0.2**

100.7 Sign "Elevation 6260 feet, 9 miles." **0.6**

101.3 Red Fir Flat at the top of the remnant of ancestral Mt. Shasta. **0.1**

101.4 On left is the south end of the loop road to Sand Flat and Horse Camp; continue on paved road. **0.4**

101.8 Orange sign "Elevation 6650 feet, 10 miles." Large roadcut on the left cuts through the first of three morainal ridges, the right-lateral moraines of the youngest major Pleistocene glacier of Avalanche Gulch. **0.2**

102.0 On left is the north end of the loop road to Sand Flat and Horse Camp; continue on paved road. **0.3**

102.3 On left is large exposure of the right-lateral moraine of Avalanche Gulch. Ahead is Mt. Shasta and the

glaciated valley of Avalanche Gulch, with Sargents Ridge on the right. To the right is Gray Butte, a glaciated dacitic dome at the head of the north–south vent alignment on the south flank of the Sargents Ridge cone. In the far distance to the south, Lassen Peak can be seen on a clear day. **0.4**

102.7 Sign "Elevation 6860, 11 Miles." Just beyond on left is Bunny Flat Trailhead. **0.2**

102.9 Roadcut on left in glaciated andesite flow of Misery Hill cone. Similar roadcuts ahead expose Misery Hill andesite flows, overlying till of the latest major glaciation, and pockets of the 9.7 ka pumice of Red Banks. Along the road beyond, note the widespread sandy mantle that covers all other units; this material is colluvially reworked lithic ash from Holocene vulcanian eruptions at the summit of the Hotlum cone. **1.1**

104.0 Low roadcuts on left in glacial deposits overlying Misery Hill andesitic lava. **0.4**

104.4 Panther Meadows, a thick accumulation of colluvial sand-sized lithic ash from vulcanian eruptions of the Hotlum cone. **0.4**

104.8 Sign "Elevation 7550 feet, 13 miles." **0.5**

105.3 **STOP 10. Sargents Ridge and Misery Hill cones.** Park in large parking area at Ski Bowl Trailhead. The view from the parking area or, better, from the old ski lodge just above, shows clearly the eroded edifice of the Sargents Ridge cone, with quaquaversal dips from a center just east of the sharp pinnacles of Sargents Ridge. Two glaciations have carved major valleys and left narrow arêtes between them, including the prominent ridge just east of here. Behind Sargents Ridge rises the massive bulk of the Misery Hill cone, also glaciated but in only one glaciation and thus less deeply eroded. The arête to the east exposes the interior of a silicic andesite flow of the Sargents Ridge cone with sparse but conspicuously large hornblende phenocrysts. The prominent butte on the west side of the glaciated Ski Bowl valley is Green Butte (although it is predominantly gray and reddish), a glaciated pile of basaltic andesite agglutinates and spatter-fed lavas that had a component of highly magnesian basaltic magma; at an elevation of more than 2800 m, this may be the highest mafic vent in the Cascades (Anderson, 1974). Below the Ski Bowl, on the east side of the valley, is the glaciated dacite dome of Gray Butte (with a microwave antenna on one of its summits). The floor of the Ski Bowl valley is mantled by the irregular surface of a rock-glacier deposit of early Holocene age. Mantling it is a mixed colluvium of lithic ash from younger vulcanian eruptions near the summit.

To the southwest and west can be seen several ranges of the Klamath Mtns., underlain by metamorphic and plutonic rocks of Paleozoic and Mesozoic age. To the south is the Jurassic granitic pluton of Castle Crags. The higher range to the southwest is the Trinity Alps. To the west, partly hidden from view, is Mt. Eddy. Draining south from Mt. Shasta is the Sacramento River, which has carved a deep canyon through the Klamath Mtns. Everitt Hill, a shield volcano of about 450 ka on the south flank of Shasta, fed long flows of basaltic andesite down the canyon before it had reached its present depth.

Time permitting, some short walks can be taken from here. Particularly interesting are the outcrops of agglutinates and spatter-fed lavas of Green Butte, a round-trip walk of 30–45 minutes.

Return to Mt. Shasta City by Everitt Memorial Highway. **13.6**

118.9 Flashing red light just past Mt. Shasta High School; turn right and follow the road with the double yellow line as it curves around a baseball field and school. Proceed one block past the intersection with the flashing yellow light. **0.5**

119.4 Traffic light at intersection; turn left from East Alma St. onto Mt. Shasta Blvd. **0.2**

119.6 Traffic light at intersection; turn right from Mt. Shasta Blvd. onto West Lake St. toward I-5.

The following section contains only a brief outline of features seen along 1-5 South from Mt. Shasta City to Redding. It is intended only as a sketch of some features of interest, lists no stops, and is not an authoritative guide to the geology of this part of the eastern Klamath Mtns.

Mileage

0.0 Traffic light at intersection of Mt. Shasta Blvd. and West Lake St. in Mt. Shasta City. Proceed west on West Lake St. **0.1**

0.1 Cross railroad tracks. **0.4**

0.5 Cross I-5 on overpass, then curve right onto onramp to I-5 South. **1.9**

2.4 Offramp for CA-89; continue on I-5 South. Roadcuts for next 1.5 mi provide poor exposures of some volcanic debris flows from Mt. Shasta that date from the time of the Sargents Ridge cone. **1.5**

3.9 Weigh station on right. **1.1**

5.0 Offramp for Mott Road and Dunsmuir Ave.; continue on I-5 South. **0.5**

5.5 In a roadcut on left, across the other lanes of the freeway, basaltic andesite lava from the 450 ka Everitt Hill shield south of Mt. Shasta is exposed beneath volcanic debris flows from the Sargents Ridge cone. **1.6**

7.1 Offramp for Dunsmuir Ave. and Siskiyou Ave.; here the highway crosses from a constructional surface of debris flows and underlying basaltic andesite lava flow onto eroded metamorphic rocks of the eastern Klamath Mtns. For about the next 25 mi through the canyon of the Sacramento River, roadcuts along the highway expose mainly serpentinized ultramafic rocks and greenstone of lower Paleozoic age with well-developed reddish soils. **1.4**

8.5 Cross the Sacramento River. **2.8**

11.3 Offramp for Crag View Dr. and Railroad Road; view on right to Castle Crags, a spectacularly exposed Jurassic granitic pluton. **3.2**

14.5 Offramp for Castella and Castle Crags State Park. **0.2**

14.7 View back toward the right up Castle Creek to Castle Crags. **4.1**

18.8 Flume Creek Road; continue on I-5 South. **0.8**

19.6 Roadcuts on both sides expose a columnar lava flow of basaltic andesite from Everitt Hill, the 450 ka shield volcano at the south foot of Mt. Shasta. This lava appears to have flowed down the canyon of

the Sacramento River for at least 30 km, although it has not yet been studied in detail. **1.1**

20.7 Offramp for Sims Road; continue on I-5 South. **1.5**

22.2 For the next half mile, roadcuts on both sides expose the columnar lava flow of basaltic andesite from Everitt Hill overlying old gravels deposited by the Sacramento River. **Note that this section of I-5 was being re-routed in the summer of 1988;** the log follows the old highway and thus will give only a general idea of the geology along the new route. **0.4**

22.6 Shotgun Creek Road and Shotgun Cafe to right; continue on I-5 South. **0.5**

23.1 Columnar lava flow of basaltic andesite from Everitt Hill overlies gravels at top of high roadcuts on both sides of the highway. **2.4**

25.5 Columnar basaltic-andesite flow overlies gravel in roadcut on right. **2.2**

27.7 Pollard Flat Cafe and store on left. Most outcrops in roadcuts below here are fine-grained and thin-bedded low-grade metasedimentary rocks of the Mississippian (Lower Carboniferous) Bragdon Fm. **1.1**

28.8 Columnar basaltic-andesite flow overlies gravel in roadcuts on both sides. **0.4**

29.2 La Moine Road on right; continue on I-5 South. **2.6**

31.8 Red soil of Tertiary age developed in the Bragdon Fm. and colluvium is particularly conspicuous near here. **0.4**

32.2 Dog Creek Road on right and Delta Road on left; continue on I-5 South. **0.4**

32.6 Cross Dog Creek; in roadcuts beyond are more exposures of columnar basaltic andesite lava flow. **5.2**

37.8 Beginning of bridge across Lake Shasta. **6.6**

44.4 Offramp for O'Brien and Shasta Caverns Roads; continue on I-5 South. **1.2**

45.6 View east (left) across Shasta Lake to prominent outcrops along a ridge of the Permian McCloud Limestone, which bears a well-preserved Tethyan fauna. **2.2**

47.8 Beginning of bridge across Shasta Lake. View back northeast up the McCloud River Arm to prominent outcrops of McCloud Limestone; view east up the Pitt River Arm to the Magee volcano, a glaciated basaltic-andesite composite cone along the Cascades crest. **1.8**

49.6 Conspicuous outcrop of McCloud Limestone ahead, about 1 km to the east. **0.8**

50.4 Offramp for Fawndale Road and Wonderland Blvd.; continue on I-5 South past sign "Elevation 1000 feet." **1.5**

51.9 Pass from deeply weathered and eroded metamorphic rocks of the eastern Klamath Mtns. onto a surface of Pliocene and Quaternary gravels in the north part of the Sacramento Valley. **2.4**

54.3 Offramp for Central Valley and Shasta Dam; continue on I-5 South. Red soil in Upper Cretaceous sedimentary rocks poorly exposed near the highway. **1.2**

55.5 Offramp for Pine Grove Ave.; continue on I-5 South. Upper Cretaceous sedimentary rocks poorly exposed for about 2 mi along the highway. **2.4**

57.9 Offramp for Redding and Market St. Beyond here, the low roadcuts expose only eroded gravels of the northern Sacramento Valley.

References

Anderson, A. T., Jr., 1974, Evidence for a picritic volatile-rich magma beneath Mt. Shasta, California: Journal of Petrology, 15: 243–267.

Anderson, C. A., 1933a, The Tuscan formation of northern California, with a discussion concerning the origin of volcanic breccias: University of California, Department of Geological Sciences Bulletin, 23(7): 215–276.

Anderson, C. A., 1933b, Volcanic history of Glass Mountain, northern California: American Journal of Science, 26: 485–506.

Anderson, C. A., 1940, Hat Creek lava flow: American Journal of Science, 38: 277–492.

Anderson, C. A., 1941, Volcanoes of the Medicine Lake Highland, California: University of California Publications, Bulletin of the Department of Geological Sciences, 25(7): 347–422.

Bacon, C. R., 1983, Eruptive history of Mount Mazama and Crater Lake caldera, Cascade Range, U.S.A.: Journal of Volcanology and Geothermal Research, 18: 57–118.

Bacon, C. R., 1985, Implications of silicic vent patterns for the presence of large crustal magma chambers: Journal of Geophysical Research, 90: 11,243–11,252.

Bacon, C. R., 1986, Magmatic inclusions in silicic and intermediate volcanic rocks: Journal of Geophysical Research, 91: 6091–6112.

Bacon, C. R., 1987, Mount Mazama and Crater Lake caldera, Oregon: Geological Society of America, Centennial Field Guide—Cordilleran Section, 1: 301–306.

Bacon, C. R., and Druitt, T. H., 1988, Compositional evolution of the zoned calc-alkaline magma chamber of Mount Mazama, Crater Lake, Oregon: Contributions to Mineralogy and Petrology, 98: 224–256.

Berge, P. A., and Monfort, M. E., 1986, Teleseismic residual study of the Lassen Volcanic National Park region in California: U.S. Geological Survey, Open-File Report 86-252, 71 pp.

Berge, P. A., and Stauber, D. A., 1987, Seismic refraction study of upper crustal structure in the Lassen Peak area, northern California: Journal of Geophysical Research, 92(B10): 10,571–10,579.

Bestland, E. A., 1985, Stratigraphy and sedimentology of the Oligocene Colestin Formation, Siskiyou Pass area, southern Oregon: Unpublished M.S. thesis, University of Oregon, Eugene, 150 pp.

Christiansen, R. L., 1982, Volcanic hazard potential in the California Cascades: California Division of Mines and Geology, Special Publication 63: 41–59.

Christiansen, R. L., 1985, The Mount Shasta magmatic system; *in* Guffanti, M., and Muffler, L. J. P. (eds.), Proceedings of the Workshop on Geothermal Resources of the Cascade Range: U.S. Geological Survey, Open-File Report 85-521: 31–33.

Christiansen, R. L., and Clynne, M. A., 1986, The climactic eruptions of Lassen Peak, California, in May, 1915 (abs.): Eos, 67: 1247.

Christiansen, R. L., and Miller, C. D., 1976, Volcanic evolution of Mount Shasta, California (abs.): Geological Society of America, Abstracts with Programs, 8(3): 360–361.

Christiansen, R. L., Kleinhampl, F. J., Blakely, R. J., Tuchek, E. T., Johnson, F. L., and Conyac, M. D., 1977, Resource appraisal of the Mt. Shasta wilderness study area, Siskiyou County, California: U.S. Geological Survey, Open-File Report 77-250: 53 pp.

Clynne, M. A., 1984, Stratigraphy and major-element geochemistry of the Lassen Volcanic Center, California: U.S. Geological Survey, Open-File Report 84-224: 168 pp.

Crandell, D. R., 1972, Glaciation near Lassen Peak, northern California: U.S. Geological Survey, Professional Paper 800-C: 179–188.

Crandell, D. R. (in press), Gigantic debris avalanche of Pleistocene age from ancestral Mount Shasta volcano, California, and debris-avalanche hazard zonation: U.S. Geological Survey, Bulletin.

Crandell, D. R., Mullineaux, D. R., Sigafoos, R. S., and Rubin, M., 1974, Chaos Crags eruptions and rockfall–avalanches, Lassen Volcanic National Park, California: U.S. Geological Survey, Journal of Research, 2(1): 49–59.

Crandell, D. R., Miller, C. D., Glicken, H. X., Christiansen, R. L., and Newhall, C. G., 1984, Catastrophic debris avalanche from ancestral Mount Shasta volcano, California: Geology, 12: 143–146.

Diller, J. S., and Patton, H. B., 1902, The geology and petrography of Crater Lake National Park: U.S. Geological Survey, Professional Paper 3: 167 pp.

Donnelly-Nolan, J. M., 1987, Medicine Lake Volcano and Lava Beds National Monument, California: Geological Society of America, Centennial Field Guide—Cordilleran Section, pp. 289–294.

Donnelly-Nolan, J. M., 1988, A magmatic model of Medicine Lake volcano, California: Journal of Geophysical Research, 93(B5): 4412–4420.

Donnelly-Nolan, J. M., and Champion, D. E., 1987, Geologic map of Lava Beds National Monument, northern California: U.S. Geological Survey, Miscellaneous Investigations Series Map I-1804, scale 1:24,000.

Donnelly-Nolan, J. M., and Nolan, K. M., 1986, Catastrophic flooding and eruption of ash-flow tuff at Medicine Lake volcano, California: Geology, 14: 875–878.

Donnelly-Nolan, J. M., Ciancanelli, E. V., Eichelberger, J. C., Fink, J. H., and Heiken, G., 1981, Roadlog for field trip to Medicine Lake Highland; *in* Johnston, D. A., and Donnelly-Nolan, J. M. (eds.), Guides to some volcanic terranes in Washington, Idaho, Oregon, and northern California: U.S. Geological Survey, Circular 838: 141–149.

Druitt, T. H., and Bacon, C. R., 1986, Lithic breccia and ignimbrite erupted during the collapse of Crater Lake caldera, Oregon: Journal of Volcanology and Geothermal Research, 29: 1–32.

Eichelberger, J. C., 1975, Origin of andesite and dacite: Evidence of mixing at Glass Mountain in California and at other circum-Pacific volcanoes: Geological Society of America, Bulletin, 86: 1381–1391.

Eichelberger, J. C., 1981, Mechanism of magma mixing at Glass Mountain, Medicine Lake Highland Volcano, California; *in* Johnston, D. A., and Donnelly-Nolan, J. M. (eds.), Guides to some volcanic terranes in Washington, Idaho, Oregon, and northern California: U.S. Geological Survey, Circular 838: 183–189.

Eppler, D. B., Fink, J., and Fletcher, R., 1987, Rheological properties and kinematics of emplacement of the Chaos Jumbles rockfall avalanche, Lassen Volcanic National Park, California: Journal of Geophysical Research, 92(B5): 3623–3633.

Finch, R. H., 1930, Activity of a California volcano in 1786: Volcano Letter, no. 308: 3.

Fink, J. H., 1983, Structure and emplacement of a rhyolitic obsidian flow: Little Glass Mountain, Medicine Lake Highland, northern California: Geological Society of America, Bulletin, 94: 362–380.

Fink, J. H., and Pollard, D. D., 1983, Structural evidence for dikes beneath silicic domes, Medicine Lake Highland, California: Geology, 11: 458–461.

Greeley, R., and Baer, R., 1971, Hambone, California and its magnificent lava tubes—Preliminary report (abs.): Geological Society of America, Abstracts with Programs, 3(2): 128.

Grove, T. L., and Baker, M. B., 1984, Phase equilibrium controls on the tholeiitic versus calc-alkaline differentiation trends: Journal of Geophysical Research, 89: 3253–3274.

Grove, T. L., and Donnelly-Nolan, J. M., 1986, The evolution of silicic lavas at Medicine Lake Volcano, California: Implications for the origin of compositional gaps in calc-alkaline series lavas: Contributions to Mineralogy and Petrology, 92: 284–302.

Grove, T. L., Kinzler, R. J., Baker, M. B., Donnelly-Nolan, J. M., and Lesher, C. E., 1988, Assimilation of granite by basaltic magma at Burnt Lava flow, Medicine Lake volcano, northern California: Decoupling of heat and mass transfer: Contributions to Mineralogy and Petrology, 99: 320–343.

Guffanti, M., and Weaver, C. S., 1988, Distribution of late Cenozoic volcanic vents in the Cascade Range: volcanic arc segmentation and regional tectonic considerations: Journal of Geophysical Research, 93(B6): 6513–6529.

Hart, S. R., 1971, K, Rb, Cs, Sr and Ba contents and Sr isotope ratios of ocean floor basalts: Philosophical Transactions of the Royal Society of London (A), 268: 573–587.

Hart, W. K., Aronson, J. L., and Mertzman, S. A., 1984, Areal distribution and age of low-K, high-alumina olivine tholeiite magmatism in the northwestern Great Basin: Geological Society of America, Bulletin, 95: 186–195.

Heiken, G., 1978, Plinian-type eruptions in the Medicine Lake Highland, California, and the nature of the underlying magma: Journal of Volcanology and Geothermal Research, 4: 375–402.

Ingebritsen, S. E., and Sorey, M. L., 1985, A quantitative analysis of the Lassen hydrothermal system, north central California: Water Resources Research, 21(6): 853–868.

Kane, P. S., 1982, Pleistocene glaciation, Lassen Volcanic National Park, California: Geology, 35(5): 95–105.

Kinzler, R. J., 1985, A field, petrologic, and geochemical study of the Callahan lava flow, a basaltic andesite from Medicine Lake shield volcano, California: Unpublished M.S. thesis, Massachusetts Institute of Technology, 100 pp.

Luedke, R. G., and Smith, R. L., 1981, Map showing distribution, composition, and age of late Cenozoic volcanic centers in California and Nevada, scale 1:1,000,000: U.S. Geological Survey, Miscellaneous Investigations Series, Map I-1091-C.

Luedke, R. G., and Smith, R. L., 1982, Map showing distribution, composition, and age of late Cenozoic volcanic centers in Oregon and Washington, scale 1:1,000,000: U.S. Geological Survey, Miscellaneous Investigations Series, Map I-1091-D.

Lydon, P. A., 1968, Geology and lahars of the Tuscan Formation, northern California: Geological Society of America, Memoir 116: 441–475.

Maynard, L. C., 1974, Geology of Mount McLoughlin: Unpublished M.S. thesis, University of Oregon, Eugene, 139 pp.

McBirney, A. R., 1978, Volcanic evolution of the Cascade Range: Annual Review of Earth and Planetary Sciences, 6: 437–456.

Mertzman, S. A., Jr., 1977a, The petrology and geochemistry of the Medicine Lake Volcano, California: Contributions to Mineralogy and Petrology, 62: 221–247.

Mertzman, S. A., Jr., 1977b, Recent volcanism at Schonchin and Cinder Buttes, northern California: Contributions to Mineralogy and Petrology, 61: 231–243.

Mertzman, S. A., Jr., and Williams, R. J., 1981, Genesis of Recent silicic magmatism in the Medicine Lake Highland, California: Evidence from cognate inclusions found at Little Glass Mountain: Geochimica et Cosmochimica Acta, 45: 1463–1478.

Miller, C. D., 1978, Holocene pyroclastic-flow deposits from Shastina and Black Butte, west of Mount Shasta, California: U.S. Geological Survey, Journal of Research, 6(3): 611–624.

Miller, C. D., 1980, Potential hazards from future eruptions in the vicinity of Mount Shasta volcano, northern California: U.S. Geological Survey, Bulletin 1503: 43 pp.

Mortimer, N., and Coleman, R. G., 1984, A Neogene structural dome in the Klamath Mountains, California and Oregon; *in* Nilsen, T. H. (ed.), Geology of the Upper Cretaceous Hornbrook Formation, Oregon and California: The Pacific Section of the Society of Economic Paleontologists and Mineralogists, Los Angeles, Calif., Book 42: 179–186.

Muffler, L. J. P., Jordan, R., and Cook, A. L., 1983, Thermal features and topography of Bumpass Hell and Devils Kitchen, Lassen Volcanic National Park, California: U.S. Geological Survey, Miscellaneous Field Studies Map 1484, 1:2,000.

Muffler, L. J. P., Nehring, N. L., Truesdell, A. H., Janik, C. J., Clynne, M. A., and Thompson, J. M., 1982, The Lassen geothermal system: Proceedings of the Pacific Geothermal Conference, Auckland, New Zealand, pp. 349–356 (also available as U.S. Geological Survey Open-File Report 82-926).

Nilsen, T. H., Elliott, M. A., Purdom, W. B., 1984, Description of field trip stops and roadlog, Upper Cretaceous Hornbrook Formation, southern Oregon and northern California; *in* Nilsen, T. H. (ed.), Geology of the Upper Cretaceous Hornbrook Formation, Oregon and California: The Pacific Section of the Society of Economic Paleontologists and Mineralogists, Los Angeles, Calif., Book 42: 9–41.

Nockolds, S. R., and Allen, R., 1953, The geochemistry of some igneous rock series: Geochimica et Cosmochimica Acta, 4: 105–142.

Parsons, R. B., and Herriman, R. C., 1976, Geomorphic surfaces and soil development in the upper Rogue River Valley, Oregon: Journal of the Soil Science of America, 40: 933–938.

Peterson, N. V., and McIntyre, J. R., 1970, The reconnaissance geology and mineral resources of eastern Klamath County and western Lake County, Oregon: Oregon Department of Geology and Mineral Industries, Bulletin 66: 70 pp.

Philpotts, J. A., Martin, W., and Schnetzler, C. C., 1971, Geochemical aspects of some Japanese lavas: Earth and Planetary Science Letters, 12: 89–96.

Riddihough, R. P., 1984, Recent movements of the Juan de Fuca plate system: Journal of Geophysical Research, 89: 6980–6994.

Sammel, E. A., and Peterson, D. L., 1976, Hydrologic reconnaissance of the geothermal area near Klamath Falls, Oregon, with a section on preliminary interpretation of geophysical data: U.S. Geological Survey, Water-Resources Investigations 76-127: 129 pp.

Smedes, H. W., and Prostka, H. J., 1972, Stratigraphic framework of the

Absaroka Supergroup in the Yellowstone National Park region: U.S. Geological Survey, Professional Paper 727-C, 33 pp.

Smith, R. L., and Luedke, R. G., 1984, Potentially active volcanic lineaments and loci in western conterminous United States; *in* Explosive Volcanism: Inception, Evolution, and Hazards: National Academy Press, Washington, D.C., pp. 47–66.

Sparks, R. S. J., Self, S., and Walker, G. P. L., 1973, Products of ignimbrite eruptions: Geology, 1: 115–118.

Veen, C. A., 1982, Gravity anomalies and their structural implications for the southern Oregon Cascade Mountains and adjoining Basin and Range province: Unpublished M.S. thesis, Oregon State University, Corvallis, 86 pp.

Williams, H., 1932a, Geology of the Lassen Volcanic National Park, California: University of California, Department of Geological Sciences Bulletin, 21(8): 195–385.

Williams, H., 1932b, Mount Shasta, a Cascade volcano: Journal of Geology, 40(5): 417–429.

Williams, H., 1942, The geology of Crater Lake National Park, Oregon: Carnegie Institution of Washington, Publication 540: 162 pp.

Yoder, H. S., Jr., and Tilley, C. E., 1962, Origin of basalt magmas: An experimental study of natural and synthetic rocks systems: Journal of Petrology, 3(3): 342–532.

EXCURSION 13B:
Long Valley caldera and Mono-lnyo Craters volcanic chain, eastern California

Roy A. Bailey[1], C. Dan Miller[2], and Kerry Sieh[3]
[1]U.S. Geological Survey, Menlo Park, California 94025; [2]U.S. Geological Survey, Cascades Volcano Observatory, Vancouver, Washington 98661;
[3]Divison of Geological & Planetary Science, California Institute of Technology, Pasadena, California 91125

Geologic summary

Setting

Long Valley caldera (Fig. 1) is located at the western edge of the Basin and Range province straddling the eastern frontal fault escarpment of the Sierra Nevada, in which it forms a reentrant or offset commonly referred to as the "Mammoth embayment." The floor of the caldera ranges in elevation from 2000 m in its eastern half, where it is dominated by Lake Crowley and sage and grass-covered Long Valley, to 2600 m in its western half which is hillier and heavily forested. The caldera walls rise steeply to elevations of 3000-3500 m on all sides except the east and southeast where the floor rises only 150 m before merging with the Volcanic Tableland at 2300 m elevation. The MonoInyo Craters volcanic chain extends from the western part of Long Valley caldera northward from Mammoth Mountain to Mono Lake, a distance of 50 km. Although commonly described as subparallel to the Sierran front, the chain trends nearly due north at a noticeable angle to the northwest-trending Sierran faults (Figs. 1, 2). The prevolcanic basement in the area is mainly Mesozoic granitic rocks of the Sierra Nevada batholith plus Paleozoic metasedimentary rocks and Mesozoic metavolcanic rocks of the Mt. Morrison and Ritter Range roof pendants. The late Tertiary terrain upon which Long Valley volcanism was initiated was a maturely eroded upland drained by westward-flowing streams.

Volcanism

Volcanism associated with Long Valley caldera (Bailey et al. , 1976; Bailey, 1989) began with widespread eruption of trachybasaltic–trachyandesitic lavas between 3.6 and 2.2 Ma. Erosional remnants of these precaldera lavas are scattered discontinuously over a 4000 km^2 area around the caldera (Fig. 2), a distribution that suggests an extensive mantle source region for these initial mafic eruptions. Slightly younger rhyodacite domes and flows associated with these mafic lavas erupted near the north and northwest rims of the present caldera between 3.2 and 2.6 Ma. They probably represent the onset of deep-crustal magmatic accumulation and differentiation that eventually culminated in formation of the large, shallow Long Valley magma chamber from which subsequent more silicic eruptions originated. The first eruptions from this silicic chamber were on the northeast rim of the present caldera at Glass Mountain, where 1000 m of high-silica rhyolite domes, flows, and tuffs accumulated between 2. 1 and 0.8 Ma (Metz and Mahood, 1985).

Catastrophic rupturing of the roof of the silicic magma chamber at 0.73 Ma expelled at least 600 km^3 of rhyolite magma as plinian ash falls and incandescent ash flows. This partial emptying of the chamber caused collapse of its roof to form the 2-3 km deep oval depression of Long Valley caldera. The resulting ash-flow deposits, the Bishop Tuff (Gilbert, 1938; Hildreth, 1979), inundated 1500 km^2 around the caldera and accumulated locally to thicknesses approaching 200 m on the Volcanic Tableland and to lesser thicknesses in upper Owens Valley, Adobe Valley, and Mono Basin. A large volume of Bishop Tuff also ponded within the caldera as it collapsed; although the tuff is not exposed at the surface within the caldera, drill holes have confirmed that as much as 1500 m of Bishop Tuff is buried beneath younger volcanic and sedimentary caldera fill. During this climactic eruption, associated plinian ash clouds drifted thousands of kilometers downwind and deposited an ash layer (informally termed the Bishop ash) as far east as Kansas and Nebraska (Izett, 1982), as well as in southern California (Merriam and Bischoff, 1975); it is found in deep-sea cores from the East Pacific Ocean (Sarna-Wojcicki et al., 1987).

After collapse of the roof of the magma chamber, rhyolitic volcanism continued on the caldera floor. Pyroclastic eruptions followed by extrusion of thin, hot, fluid rhyolite flows produced a 100-500 m thick sequence of intracaldera tephra and lavas informally designated as the early rhyolite. They are typically aphyric to sparsely porphyritic, containing less than 5% crystals of plagioclase, hypersthene, biotite, and Fe–Ti oxides. They contrast strikingly with the preceding crystal-rich Bishop Tuff, suggesting a marked change in magmatic conditions after caldera collapse. Simultaneous renewal of magma pressure accompanying this early rhyolite episode uplifted, arched, and faulted the early rhyolite flows and tephra, forming a resurgent dome with a northwest-trending medial graben (Figs. 2, 5). The resurgent dome formed within 100,000 yrs after caldera collapse, between 730 and 650 ka as constrained by K–Ar ages of the contemporaneous early rhyolite flows (Bailey et al., 1976; Mankinen et al. , 1986).

After a quiescent interlude of about 100,000 yrs, crystal-rich rhyolite again began erupting within the caldera, mainly in the moat—probably from ring fractures peripheral to the resurgent dome. This coarsely porphyritic rhyolite, informally designated as the moat rhyolite, typically contains up to 20% phenocrysts of plagioclase, quartz, sandidine, biotite, hornblende, and Fe–Ti oxides. It forms thick, steep-sided domes and flows suggesting higher viscosity and lower temperature than the early rhyolite, and it probably signaled the onset of cooling and crystallization of the magma chamber. The moat rhyolite erupted at about 200,000 yr intervals at 500, 300, and 100 ka in clockwise succession around the resurgent dome, in the northern, southeastern, and western sectors of the moat, respectively. The 100 ka western moat rhyolites appear to be the youngest extrusions so far derived from the Long Valley magma chamber. However, recent

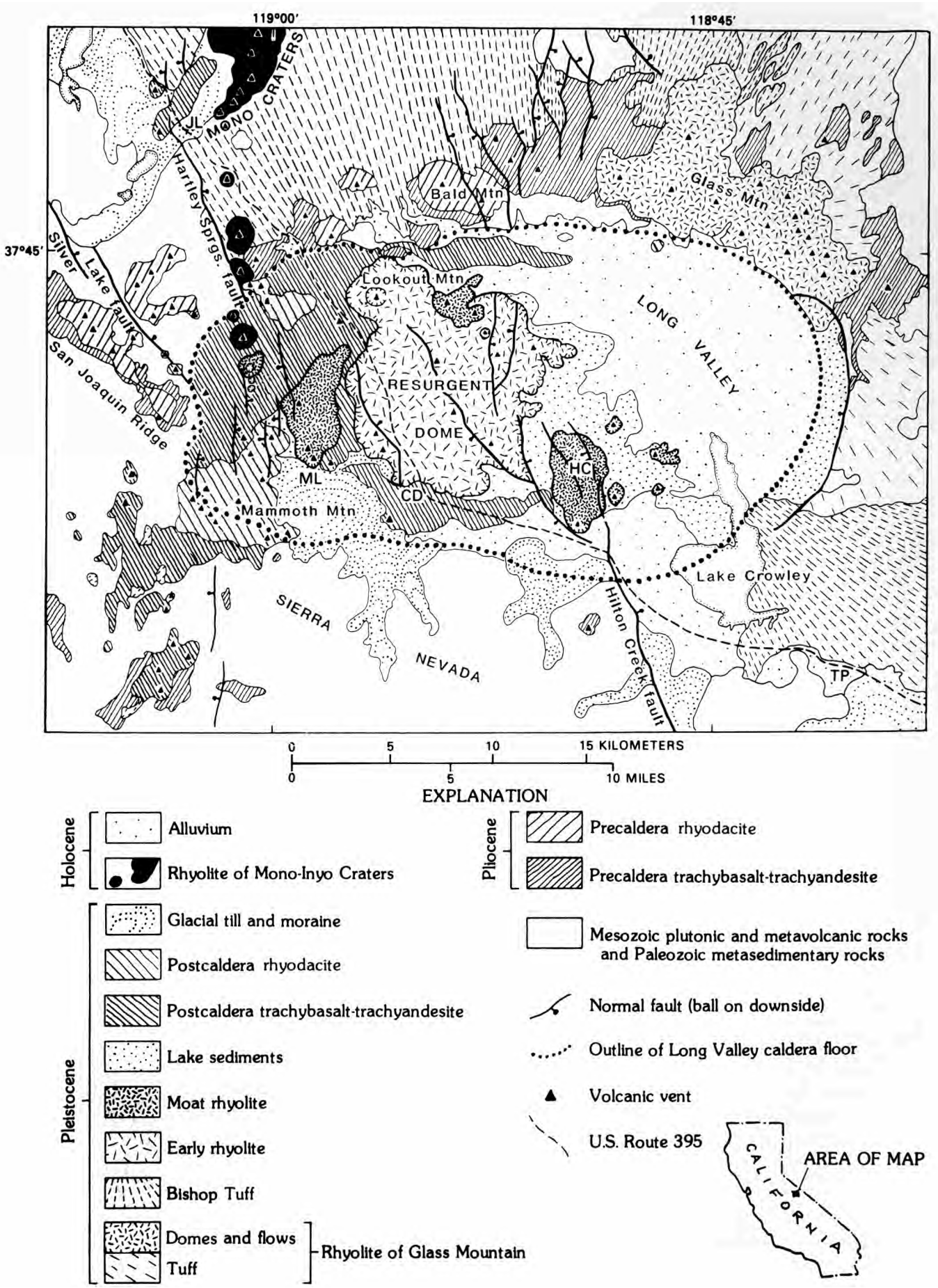

FIGURE 2—Geologic map of Long Valley caldera. JL, June Lake; ML, Mammoth Lakes; CD, Casa Diablo; HC, Hot Creek; TP, Toms Place (modified from Bailey, 1987).

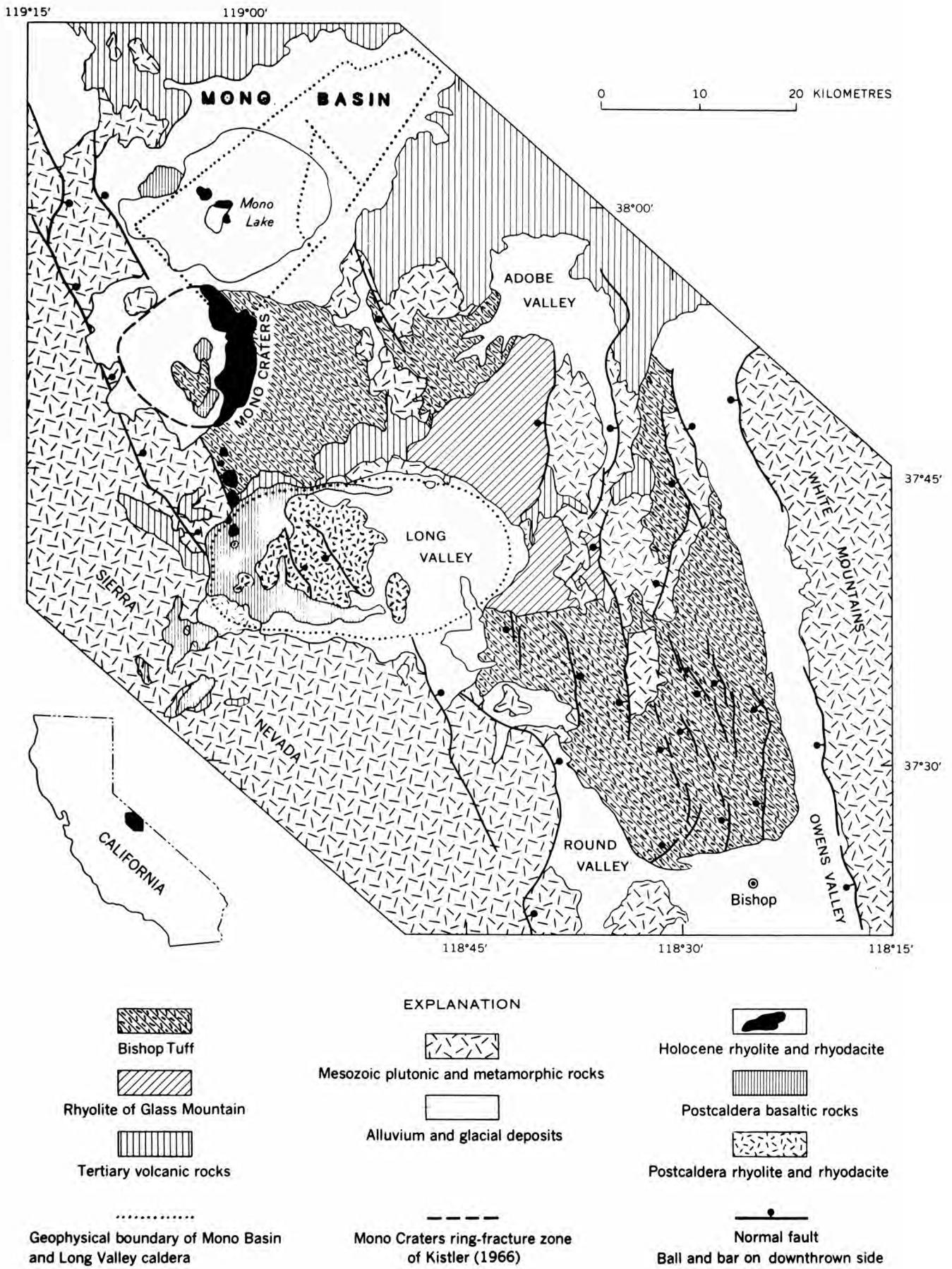

FIGURE 1—Generalized geologic map of the Long Valley—Mono Basin area, eastern California (from Bailey et al., 1976). Geophysical boundaries of Mono Basin and Long Valley caldera from Pakiser (1961) and Pakiser et al. (1960).

seismological and geodetic studies suggest that a body of partially molten magma still underlies the resurgent dome and is a potential source for future eruptions (see below: Recent seismicity and ground deformation).

This 3.6 Ma to 100 ka mafic-to-silicic sequence of volcanism centered on Long Valley caldera is overlapped spatially and temporally by the Mono-Inyo Craters volcanic chain, a younger mafic-to-silicic sequence localized along a 50 km north-trending fissure system extending from Mammoth Mountain on the southwestern caldera rim through the western caldera moat to Mono Lake. This younger sequence began between 300 and 200 ka with the eruption of trachybasaltic–trachyandesitic lavas in and near the west moat, where they accumulated to at least 250 m thickness and poured around the resurgent dome sending lava tongues eastward into both the north and south moat (Fig. 2). Younger mafic lavas vented successively farther north near June Lake (40-20 ka) and at Black Point on Mono Lake (13,300 yrs B .P.), suggesting localization along a northward-propagating fissure system. During these mafic eruptions, rhyodacite domes and flows erupted sporadically in the western part of the caldera as well as farther north in and near Mono Lake. The greatest accumulations of rhyodacite are on the northwest and southwest caldera margins where the fissure system apparently intersected caldera ring fractures. On the southwest caldera rim, between 200 and 50 ka, repeated extrusion of rhyodacite domes and flows built the imposing cumulovolcano of Mammoth Mountain.

Rhyolites began erupting along the Mono-Inyo fissure system about 35 ka—first at the Mono Craters chain, northwest of the caldera, and more recently at the Inyo Craters chain, which spans the northwest caldera rim and extends into the west moat. The Mono Craters form a 17 km long, arcuate chain of 30 or more coalesced rhyolite domes, flows, and craters ranging in age from about 35 ka to 600 yrs B.P. (Wood, 1977b; Sieh and Bursik, 1986). They are composed of high-silica rhyolite and consist predominantly of aphyric to sparsely porphyritic obsidian, pumiceous glass, and tephra (Kelleher and Cameron, 1989). The most recent of these eruptions occurred at the northern end of the chain from a 6 km long line of vents that ejected about 1 km^3 of magma as plinian and subplinian pyroclastic falls and pyroclastic flows and surges followed by vent-filling domes and flows (Sieh and Bursik, 1986).

The Inyo Craters chain forms a 12 km long, discontinuous line of mainly low-silica rhyolite domes, flows, and craters ranging in age from about 6000 to 500 yrs B.P. The youngest Inyo eruptions (650-550 yrs B .P.) began explosively (Figs. 10-12) and culminated with extrusion of Obsidian, Glass Creek, and Deadman Creek domes (Fig. 9) which apparently were fed by a shallow, 8 km long rhyolite dike (Miller, 1985). The two southernmost of these youngest domes consist of two distinctly different rhyolites—a light-colored, coarsely porphyritic, pumiceous rhyolite and a more silicic, sparsely porphyritic rhyolite—which are locally commingled in spectacular "marbled-cake" fashion. Petrologic and geochemical studies (Sampson and Cameron, 1987) indicate that the two types probably came from separate magma chambers and commingled within the conduits during eruption. The youngest Inyo eruptions succeeded the youngest Mono eruption by only a few years (Sieh and Bursick, 1986), so that the northern and southern ends of the MonoInyo chain were active almost simultaneously about 600 yrs B.P.

Phreatic eruptions both preceded and succeeded these youngest magmatic eruptions along the Inyo chain. Shortly before the Inyo tephra eruptions, phreatic explosions broke out on the north face of Mammoth Mountain, forming six small craters subparallel to the caldera wall. Shortly after the tephra eruptions, several phreatic eruptions occurred in the west moat near Deer Mountain, a 115 ka dome of moat rhyolite, forming several large craters, two of which contain the Inyo Craters Lakes. The latter eruptions, according to radiocarbon dating and dendrochronological evidence (Wood, 1977a), occurred between 1340 and 1460 A.D. The most recent eruptive activity in the region, however, occurred in Mono Lake between 1720 and 1850 A.D. , with the emergence of Paoha Island during intrusion of a rhyolite cryptodome (Stine, 1984). There is also a report of an apparent sulfurous steam eruption in Mono Lake during an earthquake in 1890 (Holden, 1892: 18), but the original source of the report (The Homer Mining Index, 1890) was of notoriously questionable reliability and neither the earthquake nor the eruption could be corroborated.

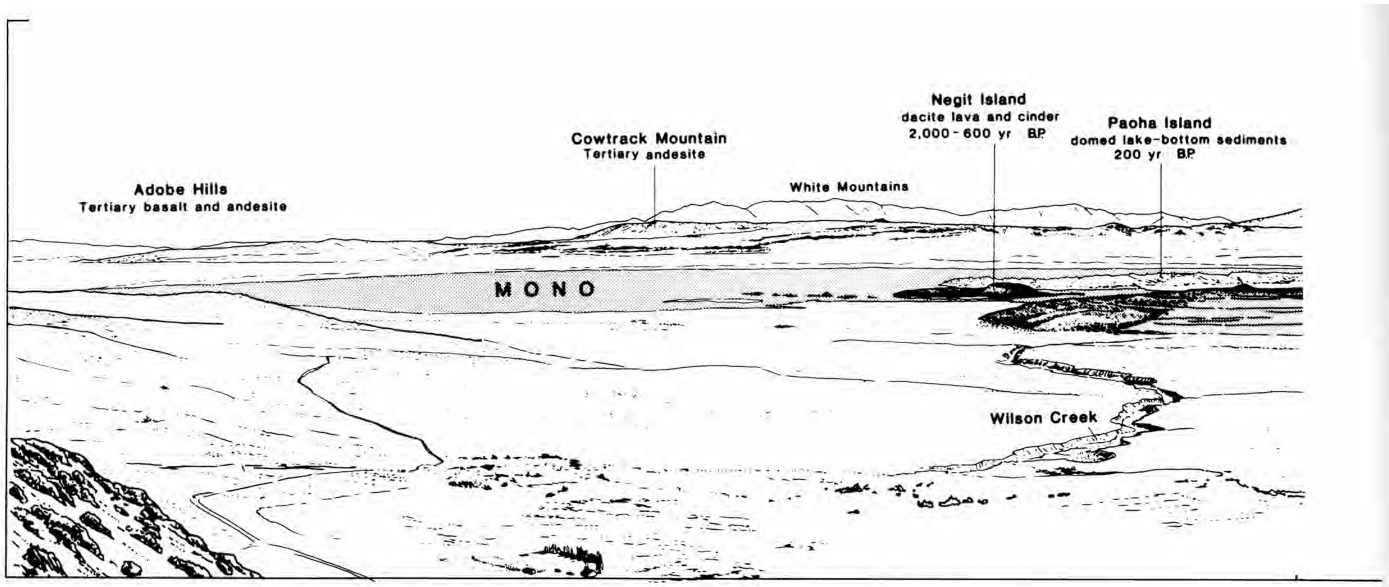

FIGURE 3—Panorama of Mono Basin from Conway Summit overlook (Stop 1). View

Structure

The caldera ring fracture is not exposed, but its general location is suggested by the distribution of the moat rhyolite vents which are within the annular caldera moat and peripheral to the resurgent dome. The dominant structural trend in the Long Valley region is northwest, subparallel to the Sierran frontal fault zone which parallels the elongation of the Sierran plutons and the associated roof pendants. Within the caldera, this northwest trend is reflected by the medial graben on the resurgent dome and by the alignment of the vents of the early and moat rhyolites.

Two major Sierran frontal faults transect the caldera, the Hilton Creek fault on the southeast and the Hartley Springs fault on the northwest (Fig. 2). These faults, which show major pre- and postcaldera displacement outside the caldera, terminate as major escarpments at the caldera margin and continue within only as minor discontinuous splinters. This marked difference in intracaldera and extracaldera displacement suggests that the subcauldron magma chamber tended to hydraulically dampen or absorb intracaldera fault movements and that only recently has the chamber roof thickened sufficiently as a result of cooling and crystallization to behave rigidly and to transmit tectonic stresses through the cauldron block (Bailey et al., 1976). An alternative, or possibly additional, explanation for the lack of significant structural relief on intracaldera tectonic faults is that regional extension within the caldera has been accommodated volumetrically by repeated injection of magma into the chamber or into fissures and faults (Bursik and Sieh, 1989).

Recent seismicity and ground deformation

Based on the 200,000 yr eruption periodicity of the moat rhyolite and on the age of the youngest 100 ka west moat domes, future eruptions from the residual Long Valley magma chamber would seem only a remote possibility, not to be expected for another 100,000 yrs. However, an unusual succession of earthquake swarms, including a sequence of magnitude-6 earthquakes in May 1980 and another of magnitude-5 earthquakes in January 1983, accompanied by 50 cm uplift of the resurgent dome, suggests that new magma has been injected into the chamber and possibly into the south moat ring-fracture zone (Savage and Clark, 1982; Savage and Cockerham, 1984). Although the intensity of seismicity and the rate of uplift and horizontal distention across the resurgent dome have decreased since 1984, circumstantial structural and geophysical evidence indicates the persistence of a residual magma chamber beneath the caldera as well as the potential for future eruptions (Hill et al., 1985; Rundle and Hill, 1988). Statistically, however, the more likely site for future eruptions in the region is along the Mono-Inyo Craters volcanic chain where eruptions have occurred most recently about 450, 700, 1200, and 1345-1469 A.D. (Miller, 1985; Sieh and Bursik, 1986; Sieh, unpubl. data). The potential hazards associated with possible future eruptions in the area have been outlined by Miller et al. (1982).

Day 1: Reno, Nevada, to Mammoth Lakes, California, via US-395

About 13 mi south of Bridgeport, California (0.9 mi past Conway Summit sign), turn RIGHT off US-395 into Scenic Viewpoint.

STOP 1. Conway Summit overlook: Mono Basin. From this vantage point (Fig. 3; see also Fig. 19), the entire Mono Basin and most of its important geologic features can be seen. Mono Lake, in the center of the basin, is the saline remnant of a much larger Pleistocene fresh-water lake known as Lake Russell, named for Israel C. Russell, who first mapped the area in 1881 (Russell, 1889). The surface elevation of Mono Lake is presently at about 1941 m, and it has been declining at a rate of about 1 m per year as a result of diversion of most of its fresh-water inflow to the city of Los Angeles. The shore of Lake Russell once lapped against the foot of the granite slope immediately below the overlook, and its former highest strandline at 2188 m (Putnam, 1950) can be seen along the steep slope west of Mono Lake. Lake Russell overflowed a low pass to the southeast and by a circuitous route through Adobe Valley drained into Owens Valley, 80 km to the south and just east of the White Mountains on the distant southeast skyline. The buff-colored flat-topped mound on the near shore of Mono Lake is Black Point, a terraced, sublacustrine, basaltic cinder and pala-

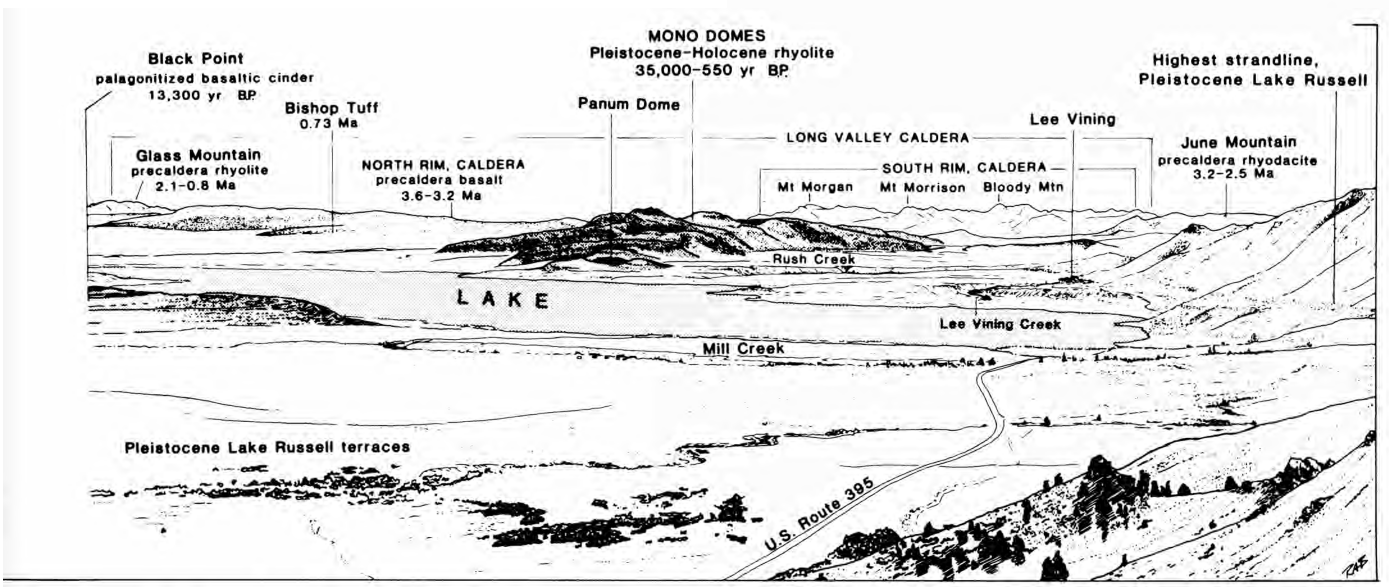

is to southeast with high points along the rim of Long Valley caldera on the skyline.

gonite cone that formed 13,300 yrs B.P. (Christensen and Gilbert, 1964; Lajoie, 1968). The dark hat-shaped island, Negit, and the several small islets to the east are dacitic and rhyolitic lava domes and flows that range in age from about 2000 to about 220 yrs B.P. (Stine, 1984). The largest, light-colored island, Paoha, consists mainly of lake-bottom sediments apparently uplifted by intrusion of a rhyolite cryptodome (Lajoie, 1968) between 1720 and 1850 A.D. (Stine, 1984). Beyond the south shore of the lake lie the Mono Craters, a 17 km long arcuate chain of rhyolite domes and flows ranging in age from 35,000 to 600 yrs B.P. (Wood, 1977b; Sieh and Bursik, 1986). The peaks on the distant skyline beyond the Mono Craters (Mt. Morgan, Mt. Morrison, and Bloody Mountain) mark the south wall of Long Valley caldera, which extends from Glass Mountain westward to Mammoth Mountain, barely visible on the skyline beyond June Mountain. The steep escarpment immediately west of Mono Lake marks the Lee Vining fault, one of the main faults bounding the east front of the Sierra Nevada. It formed over the past 3 m.y. and has at least 2000 m of structural relief (Gilbert et al., 1968). It has been active in the Holocene and displaces moraines of the Tioga glaciation about 20 m at the mouth of Lundy Canyon, 5 km south of the viewpoint. In contrast, displacement on the range-front faults farther south and west of the Mono Craters appears to have diminished in the past few ten-thousand years as the Craters have become active. This relation suggests that locally along that segment of the Sierran front, dike intrusion beneath the Craters has replaced normal faulting as the principal mechanism for accommodating extension (Bursik and Sieh, 1989).

Continue south on US-395 to Mammoth Lakes via June Lake Loop.

Day 2: Long Valley caldera circuit (Fig. 4)
(Begins and ends in Mammoth Lakes)

From Mammoth Lakes go west on CA-203 to Mammoth Mountain Ski Lodge. Take gondola to Mammoth Mountain summit (3372 m) and walk about 200 m southeast along crest.

STOP 2. Summit of Mammoth Mountain: Long Valley caldera overview. The view northeast from the summit of Mammoth Mountain (Fig. 5) encompasses the entire expanse of Long Valley caldera, from the west rim on the left to the east rim beyond Lake Crowley, and from the south rim at Laurel Mountain on the right to the north rim at Bald Mountain. The steep hummocky terrain in the immediate foreground below is composed of rhyodacite lavas of Mammoth Mountain, which was built on the southwest caldera rim between 200 and 50 ka. The summit dome, underfoot, is the youngest extrusion on the mountain (52 ka) and consists of coarsely porphyritic, hornblende–biotite rhyodacite typical of other postcaldera rhyodacites in the caldera. Extending beyond the foot of Mammoth Mountain to the left and right are the west and south caldera moat, respectively,

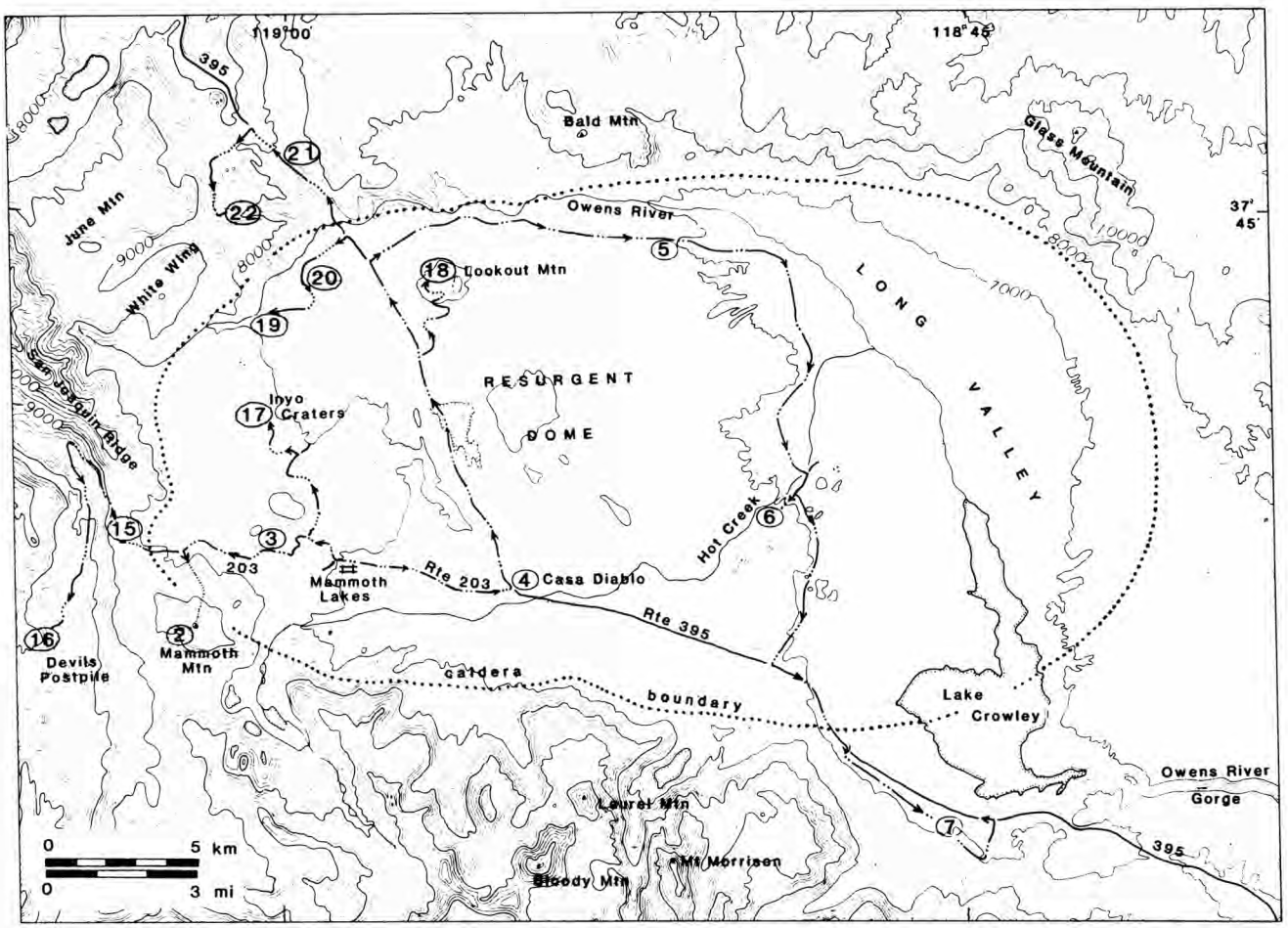

FIGURE 4—Map of Long Valley caldera showing routes and stops of Days 2, 4, and 5. (Number of dots along route indicates day: two dots is Day 2, etc.).

underlain mainly by 200–60 ka postcaldera trachybasalt and trachyandesite flows that partially encircle the resurgent dome (Fig. 2), which is underlain by 730–650 ka aphyric to sparsely porphyritic flows and tuffs of the *early rhyolite*. At three sites around the resurgent dome are clusters of porphyritic hornblende–biotite rhyolite domes and flows of the *moat rhyolite* sequence; they include North dome on the north flank (520 ka), Hot Creek flow on the southeast (288 ka), and Mammoth Knolls on the west (106–97 ka). In the distant center is Glass Mountain, a 2.1–0.8 Ma precaldera high-silica rhyolite complex which has been truncated on the southwest by caldera collapse. The White Mountains, on the distant skyline, bound the eastern side of the Owens Valley rift and rise to 4373 m (nearly 300 m higher than the local Sierran peaks); they are underlain by Mesozoic plutons and Paleozoic roof-pendant rocks. On the left, extending from the west moat northward to Mono Lake are the rhyolite domes and flows of the Inyo and Mono Craters, the culminating effusions of the Mono-Inyo Craters volcanic chain.

Return to gondola and ski lodge at base of mountain. Retrace CA-203 east toward Mammoth Lakes, going 9.4 mi to Earthquake Fault; turn LEFT into visitors parking area.

STOP 3. Earthquake Fault. Earthquake Fault is a vertical fissure 2–3 m wide, as much as 20 m deep, and about 0.7 km long, crossing the surface of an eroded and pumice-mantled glassy rhyodacite flow. Sunlight does not reach the bottom of the cleft most of the year, and snow and ice usually persist at its bottom through summer. The fissure merges to the north with a fault that can be traced for an additional 2.5 km across the crest of Southwest dome where it shows as much as 10 m west-downward displacement. The fault is one of several that define a north-trending en-echelon graben subparallel to the Inyo Craters chain in the west moat. At Earthquake Fault, the "fault" shows little or no vertical displacement; irregularities in the joint faces on either side of the cleft can be perfectly matched and show mainly horizontal pull-apart movement with slight right-lateral offset. Earthquake Fault and the related en-echelon system were first mapped by seismologists Benioff and Gutenberg (1939), and for several years they and their Caltech colleagues periodically measured the distance between stainless steel pins set in the walls of the cleft in an effort to measure strain in the region. Measurements made through the mid-1940's showed widening of 1 mm or so; however, after a 20 yr hiatus, a measurement in 1967 revealed that the cleft had closed sufficiently to prevent insertion of the steel caliper-bar between the pins, and the measurements were discontinued (Francis E. Lerner, written comm. 1982). During the 1980–1983 Mammoth Lakes earthquake swarms, the ladders to the bottom of the cleft were damaged and later removed as a safety precaution. During the same swarms, a number of collapse pits as much as 5 m in diameter and equally as deep formed along the northern extension of the fault. Similar but smaller pits also formed along other faults in the Inyo en-echelon system farther north.

Continue east on CA-203 through Mammoth Lakes to the T-junction beyond US-395; turn LEFT at the junction and LEFT again just beyond the Mammoth–Pacific Geothermal Power Plant; go to the sharp bend at the top of the hill and park on the right.

STOP 4. Casa Diablo: Geothermal activity; 1980–1983 seismic epicenter. Casa Diablo Hot Springs is on the south edge of the resurgent dome on a major northwest-trending fault within the medial graben. The rock exposed in the hillsides to the north is sparsely porphyritic, biotite-bearing early rhyolite that issued from a vent on the crest of the resurgent dome about 6 km to the north. Postcaldera trachybasalts, ranging in age from 129 to 62 ka, have flooded the south moat and lapped against the rhyolite of the resurgent dome. Across the south moat rises the steep south wall of the caldera dominated by Mount Morrison, Laurel Mountain, and Bloody Mountain which are underlain mainly by Paleozoic metasedimentary rocks locally intruded by Cretaceous granite. At Casa Diablo, a 1605 m exploratory geothermal drill hole passed through 460 m of the early rhyolite, 914 m of Bishop Tuff, and penetrated Paleozoic metasedimentary basement rock at 1377 m. The depth to basement at Casa Diablo indicates a total subsidence of about 2100 m in the south moat. Within the upper part of Bishop Tuff, a 50 m thick layer of granite breccia was encountered; the similarity of the granite to that exposed on the south wall of the caldera suggests that it is a megabreccia slide block that avalanched off the wall during the later stages of caldera collapse.

During the seismic swarms of 1980–83, when the resurgent dome rose 50 cm, the south moat from Casa Diablo to Convict Creek, a distance of 8 km, was the principal locus of intracaldera seismicity. Modeling of the seismicity and associated ground deformation (Savage and Clark, 1982; Savage and Cockerham, 1984; Rundle and Whitcomb, 1984, 1986) led to the conclusion that new magma had not only welled into the chamber beneath the resurgent dome but also possibly had intruded the south moat ring-fracture zone to depths as shallow as 3 km, thereby raising serious concern about the imminence of an eruption. During that episode a previously dormant fumarole at Casa Diablo was vigorously reactivated, and two new hot springs broke out along the southern edge of the resurgent dome. Currently, a scientific drill hole targeted to a depth of 5–7 km is being drilled on the resurgent dome by Sandia National Laboratory (Rundle et al., 1986) to explore the cause of the recent uplift and thermal activity.

Hot springs, fumaroles, and areas of active hydrothermal alteration are particularly prevalent in the south and southeast caldera moat and adjacent flanks of the resurgent dome, mainly localized along faults. The heat source for these features has been presumed to be the residual magma chamber beneath the resurgent dome, but drill holes show that hot waters are confined to relatively shallow aquifers (<700 m) and that except in the west moat temperatures decline or do not increase substantially to maximum drilled depths of 2000 m. Possible explanations for this puzzling thermal distribution are that cold ground-water flow through the deeper caldera fill masks the deep thermal source or that the principal heat source is not beneath the resurgent dome but is a younger magma body related to the Inyo Craters chain in the west moat (Blackwell, 1985; Sorey, 1985). Maximum temperatures measured in drill holes in the caldera are about 220°C, but chemical geothermometry indicates deep reservoir temperatures near 240°C. Efforts to utilize this geothermal resource include development of two 7 megawatt binary electrical power plants at Casa Diablo Hot Springs, breeding of trout at a California State fish hatchery in nearby warm-spring waters, and use of thermal waters in a public swimming pool at Whitmore Hot Springs.

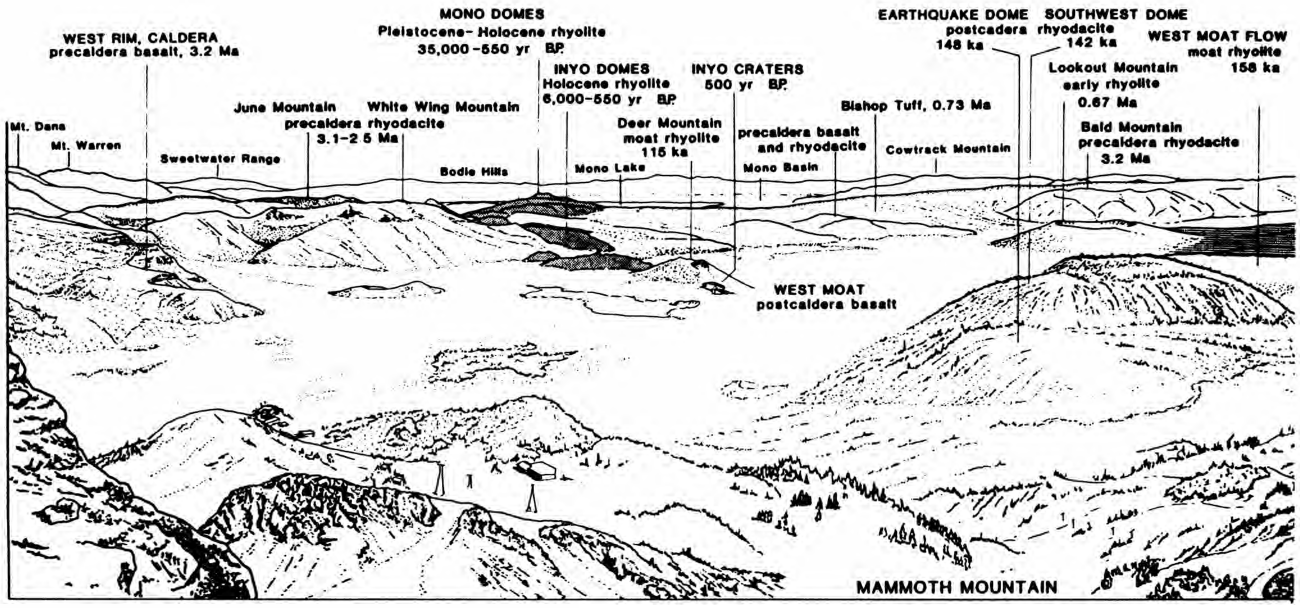

FIGURE 5—Panorama of Lone Valley caldera from the summit of Mammoth

Return to US-395; turn RIGHT and go north about 13 mi to Owens River Road. Turn RIGHT (east) and follow Owens River Road 6.7 mi to a large gravel pit on right; park in the pit and walk to its south rim.

STOP 5. Owens River Road gravel pit: north moat viewpoint. This pit, in Pleistocene periglacial gravels, is in the middle of the north moat of the caldera. The steep escarpment to the north is the northern caldera wall, underlain by Mesozoic plutonic and Paleozoic metasedimentary rocks and capped with 3.5–2.2 Ma precaldera trachybasalts and trachyandesites. On the rim to the northwest is Bald Mountain, composed of 3.4 Ma precaldera rhyodacite domes and flows. On the far western skyline is the crest of the Sierra Nevada and somewhat closer and lower the western caldera rim. On the northeast rim is Glass Mountain, a 2.1–0.8 Ma precaldera rhyolite complex, the southwestern half of which is downfaulted and buried within the caldera. The low, flat surface south of Glass Mountain is the southeast caldera rim and beyond is the Volcanic Tableland, underlain by the Bishop Tuff. The high Sierran peaks on the southern skyline mark the south rim of the caldera. The low forested hills in the south foreground are the resurgent dome, underlain by 730–650 ka tuffs and aphyric rhyolite flows of the *early rhyolite*. In the near southwest, the high knob rising above the surface of the resurgent dome is a 520 ka lava dome of the *moat rhyolite,* composed of coarsely porphyritic hornblende–biotite rhyolite. On the sage-covered lower slopes of the resurgent dome, lake terraces and strand lines of Pleistocene Long Valley Lake may be seen. On the north side of Owens River Road, the moat is floored by a 15 km long, 108 ka, postcaldera trachybasalt flow that erupted from a vent in the west moat. The dark-brownish crags marking the southern edge of this flow can be traced from the gap at Big Springs just north of Lookout Mountain on the west to near the base of Glass Mountain on the east. The flow, which shows no evidence of having flowed into water, indicates that the caldera lake was confined to the eastern moat and may have been completely drained by this time. Just beyond the toe of the trachybasalt flow, at the very base of Glass Mountain, is a small conical hill—a small, undated, postcaldera rhyodacite dome that appears to have erupted subaqueously in Pleistocene Long Valley Lake in early postcaldera time.

Continue on Owens River Road east and south to the T-junction just beyond the small bridge across Hot Creek (7.4 mi); turn RIGHT at junction and bear RIGHT at next junction (0.5 mi); continue 1 mi to Hot Creek Recreational Area parking lot on the right.

STOP 6. Hot Creek Gorge: southeast moat rhyolite; hot-spring activity. Hot Creek is the lower reach of Mammoth Creek where several vigorous hot springs issue from its bottom forming this popular bathing area. Hot Creek Gorge has been incised into a 288 ka moat rhyolite lava flow that erupted from a vent on the south shore of Pleistocene Long Valley Lake, which at that time was about 4 km to the south at an elevation of 2195 m. The flow coursed northward into the lake, becoming entirely subaqueous in the vicinity of the present gorge. The initially hot glassy rhyolite was pervasively hydrated by interaction with the lake water and later was partly hydrothermally altered by local hot-spring activity. Outcrops of partly altered, perlitized flow breccia are exposed along the paved trail leading to the bottom of the gorge.

The Hot Creek flow is a sparsely porphyritic, sanidine–augite-bearing rhyolite of the moat sequence. Its chemistry and mineralogy differ from that of older, more coarsely porphyritic hornblende–biotite rhyolites in the north and southeast moat, and its chemical fractionation pattern (relative to older flows) is similar to that of Bishop Tuff. These petrographic and chemical changes at about 300 ka possibly reflect thermal rejuvenation of the Long Valley magma chamber brought about by a new influx of mafic magma into the roots of the magmatic system, as shortly thereafter trachybasalts began erupting in the west moat (Bailey, 1984a). Renewed uplift of the resurgent dome probably accompanied this magmatic rejuvenation, as at this time a sudden influx of coarse detritus derived from the resurgent dome built extensive flanking deltas into the caldera lake. These deltaic sediments are intensely silicified and permeated with fossil hot springs and fumaroles, suggesting that increased wide-

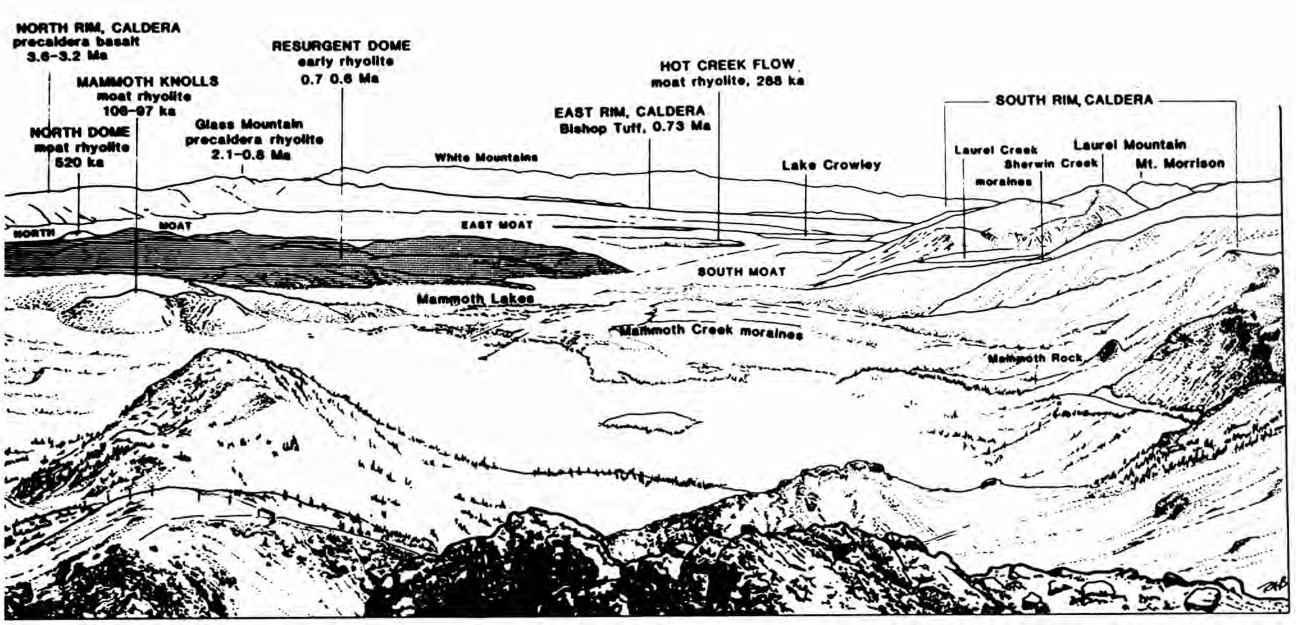

Mountain (Stop 2). View is to northeast, with Mono Basin just visible to north.

spread hydrothermal activity also accompanied this magmatic and structural activity.

Thermal springs issue from the stream banks all along Hot Creek Gorge, but the largest and hottest springs are localized on two north-trending faults that bound a shallow, 1 km wide graben transecting the Hot Creek flow and gorge (Fig. 2). The numerous smaller, cooler springs along the creek between the two faults are produced by lateral flow of hot water from the faults through the basal breccia of the rhyolite flow where mixing with cold meteoric water occurs. The several boiling pools in the gorge (93°C at this elevation) commonly change in vigor and configuration in response to local earthquakes and are also significantly affected by seasonal rise and fall of the water level in the creek. The white deposits lining the pools are calcium carbonate (travertine). Numerous older travertine deposits surround extinct hot springs at higher levels along the gorge.

Return east along Hot Creek Road and turn RIGHT (south) at first junction (1 mi); continue 2.5 mi to US-395; turn LEFT (east) onto US-395 and continue 1.7 mi to Crowley Lake exit; turn RIGHT onto Crowley Lake Drive and continue 3.5 mi to Crowley Lake Community Center on left; park well clear of the adjacent fire station and walk between buildings to about 50 m behind them.

STOP 7. Crowley Lake overlook: Pleistocene Long Valley Lake; Hilton Creek fault. During early postsubsidence time, Long Valley caldera was filled by a large lake known as Pleistocene Long Valley Lake (Mayo, 1934), and its terraces and strandlines are well preserved along the eastern caldera wall where they are traceable from the base of Glass Mountain to Lake Crowley. From this viewpoint in early morning or late afternoon low-angle light, the terraces are particularly evident along the caldera wall beyond Lake Crowley. Terrace remnants also are preserved locally on the flanks of the resurgent dome. Uplift of the resurgent dome gradually raised the lake level above the low southeastern caldera rim (east of Lake Crowley), where it overflowed and cut the Owens River Gorge. Gradual downcutting accompanied by intermittent tectonic lowering of the southeast rim along the Sierran front eventually drained the lake. Although these terraces have not been dated directly, geologic relations and dated intracaldera volcanic units suggest that the higher terraces are the oldest and the lower ones the youngest and that the lake was extant between about 600 and 100–50 ka. Scattered on many of the lake terraces are glacial erratics of granitic rocks that could have come only from plutons exposed in the High Sierra west of the caldera, and which must have been carried across the lake by icebergs from glaciers on the western shore. Similar erratics are lodged on the terraces of the resurgent dome which was an island in the lake at that time. (Lake Crowley is a modern, man-made reservoir impounded by a dam built in 1941 by Los Angeles Department of Water and Power; it is not a remnant of Pleistocene Long Valley Lake.)

Along the eastern caldera wall, successively higher terraces show progressively greater downwarp to the south (Christensen, 1966)—a consequence of repeated faulting along the eastern Sierran front producing reverse drag on the downthrown side. This relation has been argued as evidence for listric faulting along the front.

The view in the opposite direction, to the west of the viewpoint, is of the Hilton Creek fault escarpment. At its base, south (left) of McGee Creek Canyon, can be seen the light-colored jagged trace of the slickensided fault surface cutting Paleozoic Hilton Creek Marble. The topographic relief on the fault is nearly 1200 m and probably more than half of it postdates formation of Long Valley caldera. It has been active in the Holocene, as moraines of the Tioga glaciation at the canyon mouth are displaced about 15 m down to the east, and minor ground breakage occurred during the 1980 magnitude-6 earthquake swarm.

Continue east on Crowley Lake Drive 0.9 mi; turn LEFT and go 0.9 mi to US-395; turn LEFT (west) and return to Mammoth Lakes.

Day 3: Bishop Tuff circuit (Fig. 6) (Begins and ends in Mammoth Lakes)

Take US-395 south to Toms Place and continue 1 mi to the wide turnout on the right, opposite a 20 m high roadcut on the left.

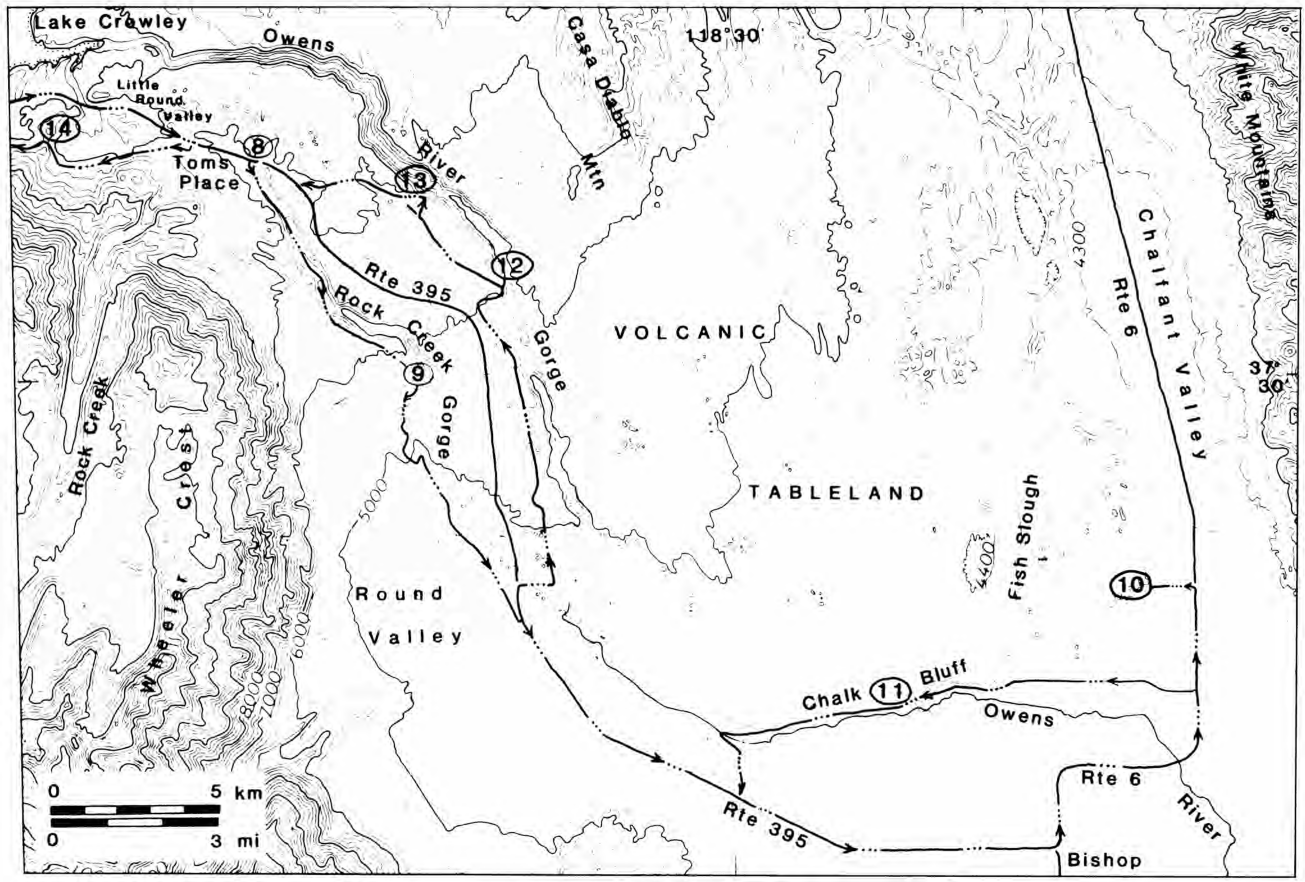

FIGURE 6—Map of Volcanic Tableland showing route and stops of Day 3.

STOP 8. Big Pumice Cut: Bishop Tuff–Sherwin Till contact. In this roadcut on the north side of US-395, the basal, bedded pumice fall and overlying non-welded ash flows of the 0.73 Ma Bishop Tuff rest on the weathered Sherwin Till (Sharp, 1968). The contrasting modes of emplacement of the pumice-fall and ash-flow members of the Bishop Tuff are well displayed here—the eastward-dipping airborne pumice fall mantling the initial sloping surface of the deeply weathered till, and the overlying fluidized ash flows banking against the slope, with their nearly horizontal pumice swarms converging with the dipping pumice-fall beds. Vertically cutting the tuff and till are several north-trending clastic dikes that are subparallel to major Sierran frontal faults in the area. In the till, some of these dikes cut cleanly through large boulders weathered to incoherent gruss. The source for the clastic dike fillings is a Pleistocene glacio-fluvial deposit that overlies the tuff at the top of the roadcut; note how the dikes become finer-grained downward, with only the upper parts containing pebbles and cobbles.

Carefully U-turn back onto US-395 and return 0.1 mi to Rock Creek Canyon Road; turn LEFT and go 5.5 mi to a turnout on right overlooking Round Valley.

STOP 9A. Round Valley viewpoint: Deformation of Bishop Tuff; fumarolic mounds. From this viewpoint the surface of the Bishop Tuff slopes about 5° southward into Round Valley, a prominent depression bounded on the west by the Wheeler Crest fault which forms one of the more imposing scarps along the eastern Sierran front. Although 5° does not seem a particularly steep slope, when considered within the context that initial dips on the Bishop Tuff elsewhere (and on ash-flow tuffs in general) seldom exceed 1 or 2°, it is evident that the Bishop Tuff in Round Valley has been structurally downwarped at least 600 m against the Sierran front. As a consequence of this structural oversteepening of the tuff surface, 20 m or more of the uppermost unconsolidated part of the tuff has been removed by erosion, accentuating the relief on the many fumarolic mounds (Sheridan, 1970) that rise above the stripped surface. These fumarolic mounds, which are widely distributed on the Volcanic Tableland, are arranged locally in crude dendritic patterns that mimic the approximate courses of pre-eruption stream valleys, suggesting that their main source of volatiles was streams overrun by Bishop ash flows.

Continue 0.3 mi and park at junction with Swall Meadow Road. Walk 100 m east to rim of Rock Creek Gorge.

STOP 9B. Lower Rock Creek Gorge overlook: Zonation in the Bishop Tuff. Down-canyon on the east wall of the gorge, the internal zonation of the Bishop Tuff is well displayed. Here, the tuff laps around a granitic high on the Sierran frontal fault scarp and thickens southward toward Round Valley. Exposed from the base upward are: (1) the lower nonwelded zone (in contact with the granite), (2) lower vitrophyre (dark-gray layer dipping down-canyon), (3) central devitrified zone (brown zone gradually thickening down-canyon), and (4) upper buff vapor-phase zone. The upper, vitric, nonwelded zone has been removed by erosion.

Continue south 7.7 mi to junction with US-395; turn RIGHT (southeast) onto US-395 and continue 9.5 mi to

junction with US-6; turn LEFT (north) on US-6 and continue 8.5 mi to Rudolf Road; turn LEFT and go 0.8 mi to Insulating Aggregates Co. pumice quarry (inactive).

STOP 10. Bishop Pumice Quarry: Bishop Tuff, basal pumice fall and distal ash flows. Exposed in this quarry are 4 m of basal pumice fall and 4–6 m of distal ash flows of the Bishop Tuff. The pumice fall is roughly divisible into: (1) a lower third composed of moderately well-bedded ash and fine pumice lapilli; (2) a middle third that is lighter-colored, less well bedded and sorted, and coarser, with pumice lapilli up to 2 cm in diameter; and (3) an upper third that is darker-colored, more distinctly bedded, with numerous fine-to-coarse alternations containing pumice lapilli up to 4 cm in diameter. Discontinuous dark manganiferous(?) streaks are present in the upper third of the deposit. The lack of distinct discontinuities in the lower two-thirds suggests continuous deposition over a relatively short time, with activity becoming more variable or intermittent in the upper third. The tendency for lithic clasts as well as pumice lapilli to increase upward in size suggests generally increasing eruption intensity. Very subtle low-angle crossbedding together with the poor sorting in the lower part suggest deposition from very dense, laterally drifting, eruption clouds. The overlying ash flows are generally massive and poorly sorted, but the basal few centimeters consist almost entirely of fine ash, which locally also shows faint low-angle crossbedding suggestive of pyroclastic surge. The lowermost 2 m of the ash flows contain many discontinuous swarms of relatively coarse pumice lapilli and blocks, indicating complex multiflow deposition near this distal part of the formation.

Interbedded within the pumice-fall sequence at the north end of the quarry is a 1–2 m thick, unsorted, tongue-shaped deposit with an irregular upper surface; it is buff-colored and consists of unusually coarse pumice blocks and lapilli in an ashy matrix; it resembles a pyroclastic flow, but is more likely a mudflow, possibly formed by choking of local streams with tephra during the plinian episode.

At one or two localities in the quarry, low-angle reverse faults with as much as 1 m displacement can be seen. The fault planes incline eastward with decreasing dip and become bedding-plane faults that are difficult to trace laterally. In this structural setting, near the western boundary fault of the White Mountains and on the eastern edge of the Volcanic Tableland, which is broken by numerous normal faults, reverse faults seem anomalous. Possibly they are related to local compressional wedging or bending within downfaulted blocks in an otherwise extensional region.

Return to US-6, turn RIGHT (south) and go 2.5 mi to Jean Blanc Road; turn RIGHT (west) and go 3.3 mi to Fish Slough; just beyond Fish Slough crossing, bear LEFT (southwest) onto Chalk Bluff Road; go 1 mi to where the road rises over prominent white outcrops along the base of Chalk Bluff; park beyond the rise in meadow on left and walk back to the roadcut.

STOP 11. Chalk Bluff: Glass Mountain fluvio-lacustrine sediments and ash. Chalk Bluff is the southern edge of the Volcanic Tableland, which is underlain principally by Bishop Tuff. The cliffs at the top of the bluff are partly welded Bishop ash flows. The basal pumice fall is obscured here by talus and slope wash, but is exposed locally in gullies along the bluff. The tuffaceous sediments exposed in this roadcut and adjacent outcrops underlie the Bishop Tuff. They include massive unsorted tuffaceous deposits—possibly thin ash flows or mudflows; evenbedded and crossbedded ashy silts and sands, commonly showing soft-sediment deformation—probably lake beds; and two primary ash-fall beds, informally designated as the Glass Mountain-G and Glass Mountain-D ash beds (Izett, 1981; Sarna-Wojcicki et al., 1984), which have been dated 1.0 and 0.9 Ma, respectively. Except for the uppermost 1–2 m below the Bishop Tuff, the entire section is reversely magnetized and is believed to be within the Matuyama Reversed Polarity Chron (J. C. Liddicoat, as quoted *in* Sarna-Wojcicki et al., 1984). The chemistry, mineralogy, and age of the ash beds and the prevalence of small obsidian clasts throughout the section suggest that most of the materials were derived from precaldera rhyolite eruptions at Glass Mountain on the northeast rim of the caldera.

Continue west on Chalk Bluff Road 4.5 mi to Pleasant Valley Dam Road; turn sharp LEFT (southeast) and go 1.7 mi to US-395; turn RIGHT (west) and go 5.8 mi to Gorge Road; turn RIGHT (east) and go 0.7 mi to T-junction; turn LEFT (north) and go 6.0 mi; at Y bear RIGHT and go 0.2 mi to locked gate. Park on left and walk down powerhouse road to bottom of canyon and return (0.8 mi roundtrip).

STOP 12. Owens River Gorge: Section of Bishop Tuff; rosette jointing. The Los Angeles Department of Water and Power (LADWP) upper powerhouse road descends the west wall of Owens River Gorge and affords spectacular closeup views of a 150 m thick section of Bishop Tuff on the east wall. At the same time, the road permits close-hand examination of roadcuts and outcrops that show the vertical changes in density and texture of the entire tuff section.

On the east wall of the gorge, the Bishop Tuff displays a remarkable variety of columnar jointing. In the upper half of the cliff the joint columns are remarkably well-formed five- to six-sided columns 1–3 m in diameter. Locally these columns curve and converge downward toward common foci, forming joint rosettes. These rosettes are the loci of large fossil fumaroles. At the top of the gorge directly above many of these joint rosettes are fumarolic mounds like those seen on the Bishop Tuff surface near Round Valley. The distribution of these mounds close to the present gorge suggests that the volatiles responsible for their formation were derived in part from the ancestral Owens River, which was overrun and vaporized by Bishop ash flows.

In the lower half of the gorge, in dark-gray, densely welded tuff, the joint columns are much larger, 10–20 m in diameter, and are relatively crudely formed as a consequence of slower cooling around more widely spaced cooling centers. Locally, some of these large joint columns have secondary horizontal joint columns developed perpendicular to their primary surface. Between the upper and lower tiers of joint columns is a broadly undulating, ill-defined parting that marks the contact between two sub-cooling units of the Bishop Tuff. This parting and another like it at the top of the gorge near the gate represent brief hiatuses in deposition of the tuff and show that the tuff consists of multiple cooling units (Sheridan, 1967). However, the partings probably do not represent intervals of more than a few days or weeks (Hildreth, 1979) or at most 2–3 yrs (Snow and Yund, 1988). The prominent crystal-rich parting near the gate is the contact between the Tableland and Gorges cooling units (Hildreth, 1979); the Tableland (upper) unit contains two

pyroxenes and has Fe–Ti-oxide temperatures of 737–763°C, whereas the Gorges (lower) unit lacks pyroxenes and has lower oxide temperatures of 725–736°C.

Exposures along the left (west) side of the powerhouse road display almost the entire range of lithologic variation in the Bishop Tuff. Near the upper gate the rock is light-gray to pinkish or purplish, porous, poorly to moderately welded, vapor-phase tuff. Downward, the tuff grades through brown to dark gray, becomes progressively less porous and more densely welded, and displays conspicuous eutaxitic texture. In the most densely welded, darker-gray facies, eutaxitic texture is almost entirely obscured by devitrification. At the first major left bend in the road, however, eutaxitic texture becomes more prominent over a 5 m interval where scattered obsidian fiamme occur, suggesting a minor eruptive/cooling interval. The tuff below this level is monotonously dark gray, densely welded, and devitrified to the bottom of the gorge. The basal contact is not exposed in the gorge, but the powerhouse foundation was excavated in dense eutaxitic vitrophyre, indicating that the base is not far below.

Return from the upper gate to Gorge Road (0.2 mi); turn sharp RIGHT (north) and go 1.8 mi to Y-junction; bear RIGHT following new pavement 0.3 mi; turn LEFT onto narrow dirt road and go 0.1 mi; park near rock-ring fireplace and walk to edge of gorge.

STOP 13. Upper Owens River Gorge overlook: Gorge stratigraphy and structure. Owens River Gorge is incised into the surface of the Volcanic Tableland and here crosses a north-trending fault zone that has been intermittently active for the past 3–4 m.y. The bottom of the gorge is cut in Triassic Wheeler Crest Quartz Monzonite, which is overlain by a 20 m thick sequence of 3.2 Ma precaldera trachybasalt flows that erupted from a vent about 1 km north of the gorge. Locally overlying the trachybasalt are a few meters of outwash gravel of the Shewin glaciation. The upper 60 m of the gorge exposes partly welded ash flows of Bishop Tuff. Down-gorge, the tuff thickens to a maximum of about 200 m, gradually becoming more densely welded and intensely jointed. Up-gorge, the tuff thins over the quartz monzonite high formed by the north-trending fault zone, multiple strands of which can be seen on the opposite canyon wall. Increasingly greater offset down-to-the-east in successively older units—the Bishop Tuff, trachybasalt, and quartz monzonite—demonstrates the growth nature of the fault zone.

Continue 0.2 mi along dirt road to aqueduct surge tank and junction with unpaved U.S. Forest Service road; continue straight ahead following unpaved road 2.5 mi to US-395; turn RIGHT and go 2.1 mi to Toms Place exit; turn LEFT then immediately RIGHT on Crowley Lake Drive past Toms Place and continue 3.0 mi to road curve in saddle on ridge beyond Little Round Valley; park on right shoulder beyond saddle.

STOP 14. Little Round Valley: Bishop Tuff–glacier contact; fumarolic pipes. Exposures in and around Little Round Valley suggest that active glaciers existed in the Sierra Nevada when the 0.73 Ma Bishop Tuff erupted. The north side of Little Round Valley is a steep, semicircular scarp that exposes three cooling units of Bishop Tuff. On the basis of mineralogy and Fe–Ti-oxide temperatures, the lower and middle units belong to the Gorges unit and the upper to the Tableland unit (Hildreth, 1979: 47). The lower and middle units are unusual in that they contain numerous indurated, pipe-like, fossil fumaroles, which locally stand out in relief around the northern edge of the valley and are particularly evident in outcrops and roadcuts along US-395, as well as in this saddle. Within Little Round Valley are but a few low outcrops and roadcuts of Bishop Tuff which are poorly to nonwelded, strongly oxidized, and unusually rich in lithic clasts that are commonly concentrated in irregular clots or entrained in steep pipes or chimneys. The tentative interpretation of the morphology of the valley and the distribution of the lithic-rich chimneys and fumarolic pipes is that at the time of eruption of the Bishop Tuff, Little Round Valley was occupied by a small, steep-fronted, lobate glacier that flowed from the south out of Rock Creek valley. The northern terminus of the glacier probably coincided with the present steep, arcuate, northern margin of Little Round Valley. During eruption of the Bishop Tuff, ash flows banked against the toe of the glacier and probably also mantled the surface of the terminal lobe. Interaction between the hot tuff and the glacial ice along the steep, lobate contact generated abundant steam, which streamed through the adjacent poorly consolidated tuff forming myriads of fumaroles now preserved as indurated pipe- and rib-like forms. Gradual melting of the glacial ice-lobe caused settling of the tuff embanked against the toe of the glacier, and the tuff became oxidized and intermixed with glacial debris melting out of the ice; the resulting heterogeneous deposit now thinly mantles the valley floor. Glacial till occurs locally along the steep slopes above and south of Little Round Valley, but no large terminal moraine is evident, though it could be buried beneath the Bishop Tuff ringing the valley. Complete melting of the ice-lobe formed a crescent-shaped lake in Little Round Valley. It eventually overflowed northward across the surface of the Bishop Tuff and cut a small, steep-sided gorge leading to the head of the Owens River Gorge, which is now drowned by Lake Crowley. If the glaciation represented by this glacier was separate from the Sherwin glaciation, how significant or widespread it was is not known.

Continue north on Crowley Lake Drive to US-395; turn LEFT and return to Mammoth Lakes.

Day 4: Devils Postpile—Inyo Craters (Fig. 4) (Begins and ends in Mammoth Lakes)

Follow CA-203 west from Mammoth Lakes to Minaret Summit (6.4 mi). Turn RIGHT into Minaret Vista parking area.

STOP 15. Minaret Vista: Sierran Cretaceous basement and Tertiary volcanic rocks. The view west from Minaret Vista overlooks the deep, glaciated canyon of the Middle Fork of the San Joaquin River and the Ritter Range beyond, the most prominent peaks of which, viewed from south to north, are the jagged Minarets, massive Mt. Ritter, and Banner Peak. The rocks of the Ritter Range include coarse metavolcanic breccias, welded tuffs, and associated granitic plutons that are part of a deeply dissected Cretaceous caldera probably comparable in size to Long Valley caldera but formed in a Cretaceous island arc rather than a Plio-Pleistocene continental setting (Fiske and Tobisch, 1978; Tobisch et al., 1986).

San Joaquin Canyon is an ancient drainage that predates uplift of the Sierra Nevada. The river was initially estab-

lished on the gradually rising western slope of the Sierra Nevada in Tertiary time, possibly as early as 25 Ma (Huber, 1981). It formerly drained a large area east of the present Sierran crest, but at about 3 Ma, during initiation of Sierran frontal faulting, the upper reaches were beheaded by faulting and dammed by eruption of basaltic lavas. Blockage of this drainage formed ephemeral lakes, as many of the canyon-filling lavas are thick pillow complexes. These Tertiary lavas and associated overlying rhyodacite domes and breccias are part of the 3.6–2.2 Ma precaldera sequence that heralded the more silicic eruptions from the Long Valley magma chamber. They are exposed along San Joaquin Ridge, which extends north from Minaret Vista and forms the present drainage divide. Two Teats and San Joaquin Mountain, the two most prominent peaks along the divide, are dissected remnants of large rhyodacite domes and their surrounding pyroclastic cones.

During early Pleistocene time the Middle Fork was re-excavated by repeated glaciations and acquired its present broad, U-shaped form. Intracanyon remnants of the Bishop Tuff indicate that the valley was temporarily filled by the caldera-forming eruptions but has been re-excavated by more recent glaciations.

Continue west on CA-203 to Devils Postpile National Monument (about 6 mi). Park at the Visitors Center and follow the footpath 0.3 mi to the Postpile.

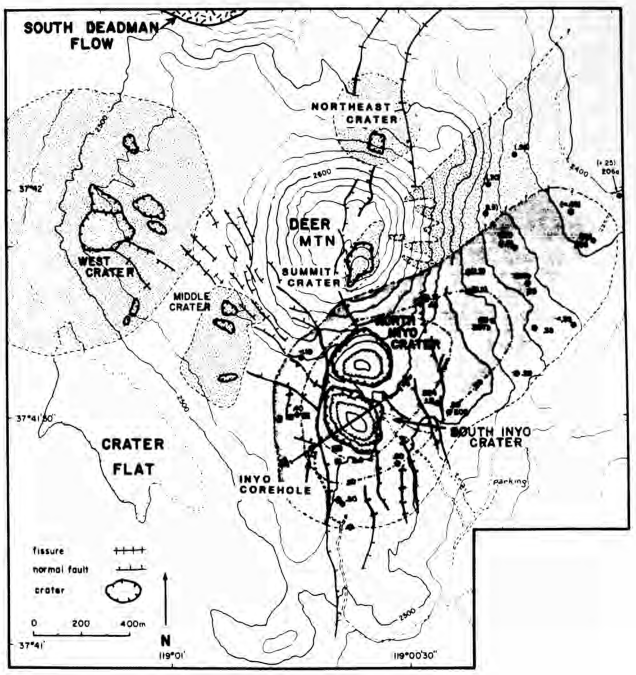

FIGURE 7—Geologic map of Inyo Craters (Stop 17) showing faults, fissures, and distribution of phreatic deposits from north and south craters (dark-shaded) and summit, middle, and west craters (light-shaded) (from Mastin, 1988). Line A-A' is section line of Fig. 8.

STOP 16. Devils Postpile National Monument: Basalt joint columns. Devils Postpile National Monument is renowned for its spectacular display of columnar-jointed basalt, which rivals the displays at Fingal's Cave in Scotland and Giant's Causeway in Ireland, but is more limited in extent.

The Middle Fork of the San Joaquin River in the vicinity of Devils Postpile is excavated mainly in Cretaceous porphyritic granite. In late postcaldera time the deeply glaciated valley was partially filled by the trachybasaltic lavas of the Devils Postpile. Although not precisely dated, the Postpile flow and several other related flows probably erupted 200–100 ka, about the same time that similar flows were erupting in the west moat of Long Valley caldera. Local geologic relations suggest that formation of the Postpile columns was the consequence of ponding of the lava behind a recessional moraine. The Postpile flow has since been eroded by subsequent glaciations, as is shown by the finely polished and striated outcrops along the trail at the top of the Postpile.

Leave Devils Postpile National Monument, returning on CA-203 about 10 mi toward Mammoth Lakes; 0.7 mi past Earthquake Fault turn LEFT (north) on Mammoth Scenic Loop and go 2.5 mi to Inyo Craters turnoff (signed); turn LEFT (west) and follow unpaved road 1.1 mi to Inyo Craters parking area; park and follow trail 0.3 mi west to the craters.

STOP 17. Inyo Craters: Phreatic explosion craters and deposits. The Inyo Craters (Fig. 7) are three northerly aligned, phreatic explosion craters (Rinehart and Huber, 1965) on the south flank and summit of Deer Mountain, a 115 ka porphyritic rhyolite dome in the west moat of the caldera. The two southernmost craters (informally designated as north crater and south crater) are about 200 m in diameter, about 60 m deep, and contain small lakes; the crater on the summit of Deer Mountain (informally referred to as summit crater) is smaller, irregular in outline, breached on its south side, and dry. The lake in south crater is yellowish green, suggesting the presence of suspended sulfur, but the water is cold (11°C) and other evidence of thermal influx is lacking. The lake in north crater is colored brown with organic matter. Despite apparent differences in morphology and vegetation, all three craters formed at nearly the same time, probably within hours or days. They erupted in succession from north to south, as the light-colored deposits from summit crater underlie the darker ones of north crater, which in turn underlie the darkest ones of south crater—relations that are well exposed in the northeast wall of north crater and on the east flank of Deer Mountain (Mastin, 1988). The light-colored debris around summit crater is composed primarily of pulverized hornblende–biotite rhyolite of Deer Mountain dome, whereas the darker debris around north and south craters consists largely of fragmented trachyandesite derived from flows like those exposed in the walls of south crater. In the north wall of south crater, exposed in succession above the trachyandesite flows, are: (1) trachyandesitic cinder from nearby vents to the northeast and southeast (10 m), (2) pumiceous rhyolite tephra from the Inyo domes magmatic eruptions centered a few kilometers to the north (1 m), and (3) coarse, crudely bedded phreatic explosion deposits mainly from south crater (13 m). The latter, which extend as far as 1 km from the crater (Fig. 7), consist mainly of trachybasalt–trachyandesite blocks in a grayish-brown, compact to semi-indurated, fine-grained matrix; blocks and boulders of granite and metamorphic rocks, probably derived from subsurface glacial till or possibly Sierran basement, also are included in the debris. A battered log incorporated in the deposit of south crater yielded a radiocarbon age of 710 ±60 yrs B.P., which together with dendrochronological data gave a calendar age of between 1340 and 1460 A.D. for the phreatic eruptions (Wood, 1977a).

The terrain around the craters is broken by many north-trending faults and fissures (Fig. 7), which show up to 20 m displacement individually and define a graben 0.6 km

wide and 2.5 km long. The graben probably formed as a consequence of uplift and distension above a rising dike (Mastin and Pollard, 1988), which probably generated the phreatic explosion craters. To test this hypothesis, Sandia National Laboratories (Eichelberger et al., 1988) slant-drilled an 865 m scientific corehole (Fig. 8) eastward at an angle of 68° from a site on the top of the fault scarp just west of south crater. It passed through a 320 m sequence of postcaldera trachyandesite and trachybasalt flows, about 50 m of gravel, 360 m of tuffs and flows of the early rhyolite, 63 m of glacial till, and terminated in 30 m of Paleozoic quartzite presumed to be Sierran basement rock. At a depth of about 600–650 m, within the early rhyolite section and directly beneath the center of south crater, the hole penetrated an apparent vent breccia consisting primarily of pulverized early rhyolite and postcaldera trachybasalt. Included within the breccia were small pumiceous fragments of a distinctive high-silica rhyolite, apparently juvenile and considered to be the magma that generated the phreatic explosions (Eichelberger et al., 1988). Presumably a dike or conduit of this magma rising from depth encountered water-saturated tuffs of the early rhyolite, causing explosive flashing of the water to steam, which in turn reamed a vent through the overlying postcaldera trachybasalt sequence, producing the Inyo explosion craters and surrounding phreatic deposits. Surprisingly, little or no juvenile rhyolite magma reached the surface during the eruptions.

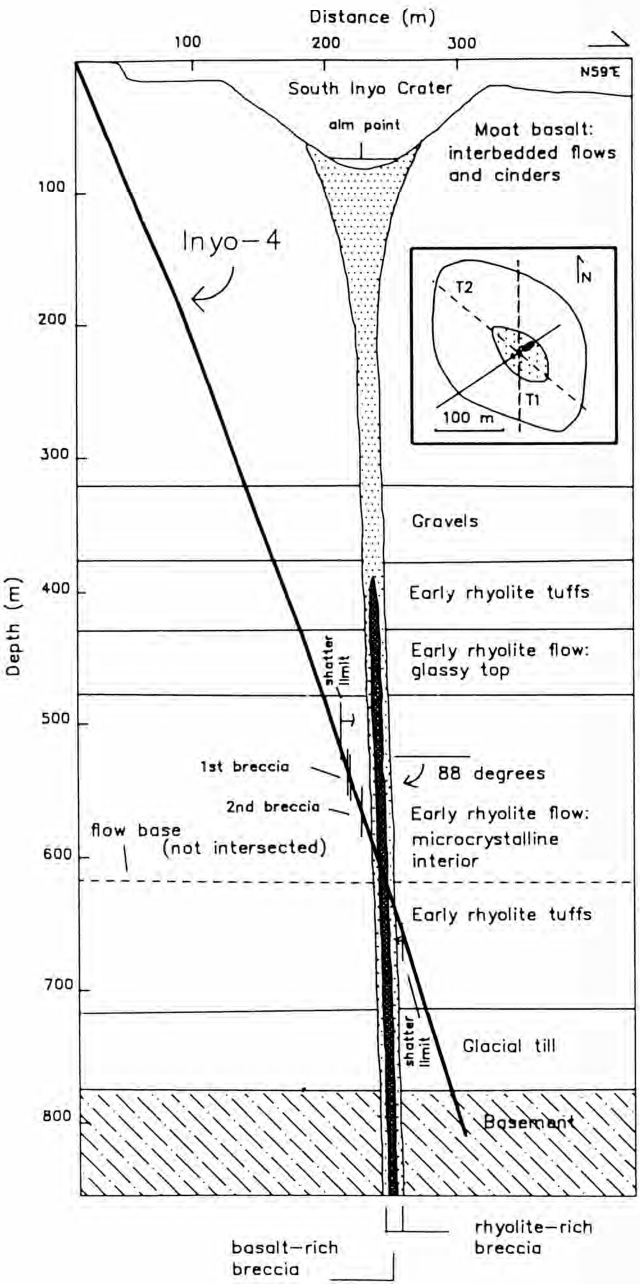

FIGURE 8—Path of Inyo Craters corehole with generalized stratigraphy and interpreted breccia structure of phreatic vent. Inset shows path of corehole (solid line) in plan view with outline of crater rim and lake; heavy bars on corehole path in inset show location of breccia zones at depth. T1 and T2 are main north—south and subsidiary northwest—southeast trends of faults and fissures in area. From Eichelberger et al. (1988).

Return to parking area and retrace route to Mammoth Lakes via Mammoth Scenic Loop and CA-203.

Day 5: Inyo domes circuit (Fig. 4) (Begins and ends in Mammoth Lakes)

Follow US-395 north from CA-203 junction 5.2 mi to Mammoth Scenic Loop (on left); turn RIGHT (east) and follow gravel road 3.1 mi to summit of Lookout Mountain.

STOP 18. Lookout Mountain: Overview of Inyo domes and western caldera moat. Lookout Mountain is a small rhyolite stratovolcano with a summit crater 2 km in diameter, which forms the tree-covered depression immediately west of the viewpoint. The volcano is in the northwest moat on the northern edge of the resurgent dome, and, although not part of the resurgent dome, it is constructed of interstratified 0.69 Ma flows and tuffs of the early rhyolite. The aphyric obsidian underfoot is typical of the early rhyolite.

To the west (Fig. 9) can be seen the west moat of the caldera, underlain mainly by 150–60 ka postcaldera trachybasalts and trachyandesites, and the west and northwest wall of the caldera, underlain by Sierran granitic and metamorphic rocks and capped by Pliocene precaldera volcanic rocks. In the middle distance are the barren, craggy, Holocene rhyolite dome-flows of the Inyo Craters chain, including from north to south: Wilson Butte, Obsidian Dome, Glass Creek Dome, and Deadman Creek Dome. Wilson Butte is the oldest of the four (1350 yrs B.P.) and is chemically and petrographically similar to high-silica rhyolites of Mono Craters, visible on skyline to north. Obsidian, Glass Creek, and Deadman Creek domes are younger and all about the same age (650–550 yrs B.P.). Obsidian Dome is composed mainly of sparsely porphyritic low-silica rhyolite, and Glass Creek and Deadman Creek domes are composed of commingled sparsely and coarsely porphyritic low-silica rhyolites. Activity at these three younger vents occurred within a very short interval, progressed from initial phreatic explosions through pyroclastic eruptions, and concluded with passive lava extrusion, the latter occurring only after pyroclastic activity had ceased at all three vents. Pyroclastic eruptions began at the Deadman Creek vent and shifted to the Obsidian Dome vent and then to the Glass Creek vent. The minimum calendar age of the tephras, based on crossdating of tree rings of Jeffrey pines growing on the deposits, is 1369, 1433, and 1469 A.D., respectively (David Yamaguchi *in* Miller, 1985). The distribution of the tephras was mainly to the northeast and southwest (Figs. 10–12). North–south alignment of the Inyo phreatic and magmatic vents and their association with subparallel grabens and fissures suggest that the eruptions were fed by an 8 km long dike (Miller, 1985) that tapped and commingled rhyolite

magmas from at least two sources (Bailey et al., 1976; Sampson and Cameron, 1987). This feeder dike transected the caldera margin as Obsidian Dome erupted outside the caldera, Glass Creek Dome erupted on the caldera rim and flowed down the northwest wall, and Deadman Creek Dome erupted well within the caldera.

Return to US-395; turn RIGHT (north) and go 2.8 mi to Deadman Creek Road; turn LEFT (west) and go 2.5 mi to South Deadman Creek Campground; park off road to left of campground entrance and walk to the bluff east of, and overlooking, the campground.

STOP 19. Deadman Creek Campground: Deadman Creek pyroclastic-flow sequence. From the eastern bluff of Deadman Creek, the craggy edge of Deadman Creek Dome can be seen through the trees just to the west. It is the southernmost of the Inyo domes and the vent for most of the deposits at this and the next stop. The lava dome represents the final, relatively passive, vent-filling stage of the Deadman Creek eruptions.

In the embankment of Deadman Creek is exposed a pyroclastic-flow sequence more than 10 m thick (Fig. 13). It consists of multiple flow units interbedded with surge deposits. They extend several kilometers to the west of the dome and 6 km to the northeast, beyond US-395, covering a 15 km^2 area (Miller, 1985). The main flow unit has a pink oxidized center which contains charcoal branches and twigs and shows reverse grading of pumice lapilli and blocks and normal grading of lithic clasts. Radiocarbon ages of the flow units range from 510 ± 100 to 770 ± 120 yrs B.P.; stumps of Jeffrey pine on the deposit have as many as 615 annual rings.

At this near-vent location, the pyroclastic flow is overlain by a series of thin pyroclastic-flow and -surge deposits that vary in thickness from 1 to 2.5 m and form dunes, hillocks, and levees on the modern ground surface. This upper sequence of deposits contains occasional bits of charcoal and shows considerable variation in bedding, grading, and sorting that records near-vent variations in eruptive mode and intensity. Such variations are not seen in pyroclastic-flow deposits more distant from the vent (e.g., at Stop 20, about 2 km to the east).

Return east on Deadman Creek Road and go 1.0 mi; park on right shoulder at top of hill.

STOP 20. Deadman Creek Road: Deadman Creek pyroclastic sequence. The roadcut on north side of road exposes about 3 m of pyroclastic deposits that overlie a 100 ka dark rhyodacite flow (postcaldera) exposed downhill along the road. The pyroclastic sequence includes tephra deposits erupted from at least three separate vents over the last 1700 yrs. At the bottom of the section (Fig. 14) is 25 cm of a pyroclastic flow, with its base not exposed. The deposit contains charcoal twigs and limbs and shows no evidence of soil oxidation or erosion of its flat upper surface. Its source vent is unknown, but its radiocarbon age is 1660 $\pm$ 140 yrs B.P. (Miller, 1985).

Overlying the pyroclastic flow is a 1–1.5 cm thick, fine, grayish-white rhyolite ash that probably is correlative with a 600 yrs B.P. gray, glassy-ash sequence in the northern Mono Craters (Sieh and Bursik, 1986). Overlying this ash is 55 cm of bedded lapilli fall composed of varying mixtures of juvenile pumice, obsidian, and lithic clasts that erupted from the Deadman Creek vent. At this locality, this unit is east of the axis of the northeast-trending Deadman Creek tephra lobe (Fig. 10), which is more than 2 m thick near its vent, more than 20 km long, and covers more than 80 km^2.

Above the Deadman Creek tephra deposit is a 2 m thick pyroclastic flow, probably correlative with the main pyroclastic flow exposed in the embankment at Deadman Creek Campground (Stop 19). Although much thinner, it retains its pink oxidized interior and contains charcoal fragments, but it shows none of the vertical or lateral variability evident near the campground.

Return to US-395 (1.6 mi); turn LEFT (north) and go 0.9 mi to Deadman Summit; park on right shoulder.

STOP 21. Deadman Summit: Inyo tephra deposits. This 2.2 m high roadcut is about 1.5 km northeast of Obsidian Dome, visible through the trees to the southwest. Like Stop 20, this roadcut exposes pyroclastic units that erupted from at least three separate vents during the last 1200 yrs. At the base of the section (Fig. 15) is a pyroclastic flow more than 25 cm thick, with its base not exposed. The unit contains small charcoal fragments and shows no evidence of soil oxidation or erosion of its flat upper surface. The source vent for this unit is uncertain but it is likely Wilson Butte, about 1.5 km to the northwest. The age of this unit is unknown, but it predates the overlying 600 yrs B.P. grayish-white ash from the northern Mono Craters, which here is 3 cm thick, slightly thicker than at the previous stop and closer to its source.

Overlying the grayish-white ash is a 1.7 m thick sequence of lapilli-fall beds that erupted from the Obsidian Dome vent. This sequence lies on the axis of a tephra lobe that can be traced 25 km northeast and covers an area of more than 140 km^2 (Fig. 11). Individual tephra layers vary in thickness from a few to 25 cm and consist of varying mixtures of juvenile pumice, obsidian, accessory lithic fragments, and occasional accidental fragments. No radiocarbon age has been obtained from this Obsidian Dome sequence, but it overlies the Deadman Creek tephra and pyroclastic flow sequences exposed at Stops 19 and 20. Jeffrey pines growing on the Obsidian Dome sequence have as many as 525 annual rings; the sequence thus appears to be between 615 and 525 yrs old (Miller, 1985).

Continue 0.4 mi north on US-395; turn LEFT onto Glass Creek Road and go 2.4 mi to Glass Creek. Park amongst the large Jeffrey pines at the south edge of Obsidian Dome and walk up the bulldozer road to the surface of the dome.

STOP 22-A. Glass Creek: Obsidian Dome margin and squeeze-up. The steep, south-facing talus escarpment composed of obsidian blocks is the southern edge of Obsidian Dome (Fig. 16), which vented 1 km to the north. The morphology of the dome edge is virtually unmodified since it formed about 600 yrs ago. The road up the escarpment leads to a commercial pumice prospect and provides access to a scientific corehole drilled through the distal end of the dome-flow. The corehole revealed details of the internal lithology and structure not evident from surface exposures (Eichelberger et al., 1985; Manley and Fink, 1987; Fink and Manley, 1987) and, together with data from another corehole through the conduit of the dome, has provided a better understanding of the role of volatiles during lava extrusion (Taylor et al., 1983; Eichelberger et al., 1986; Westrich et al., 1988).

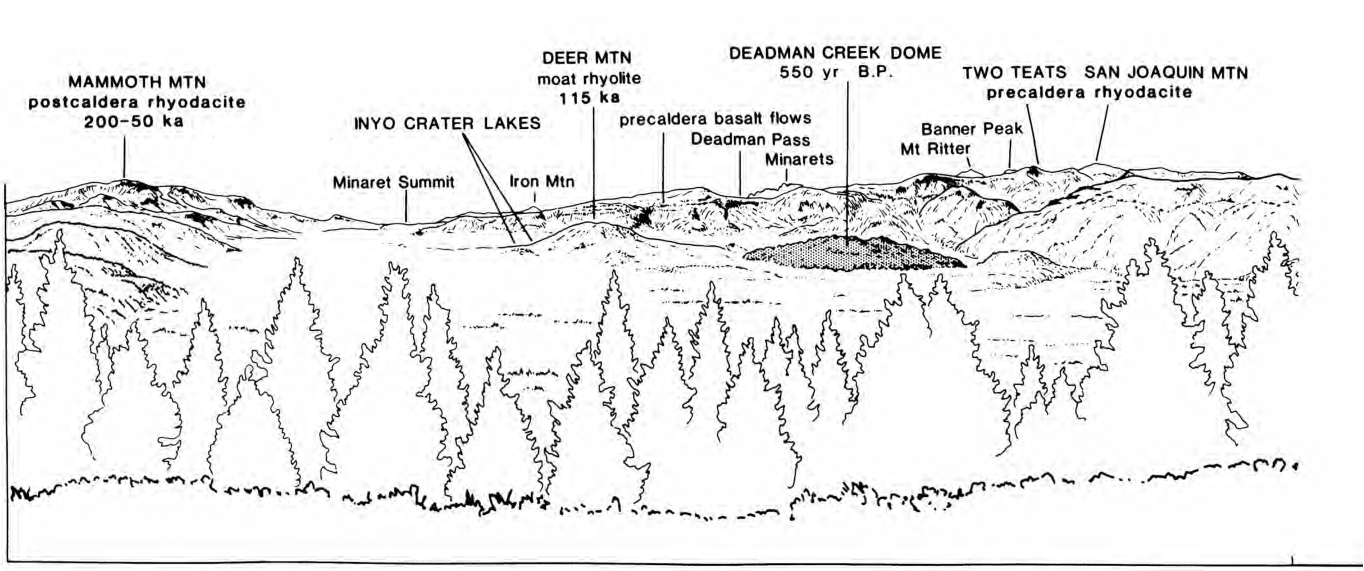

FIGURE 9—Panorama of west moat of Long Valley caldera from west summit of Lookout

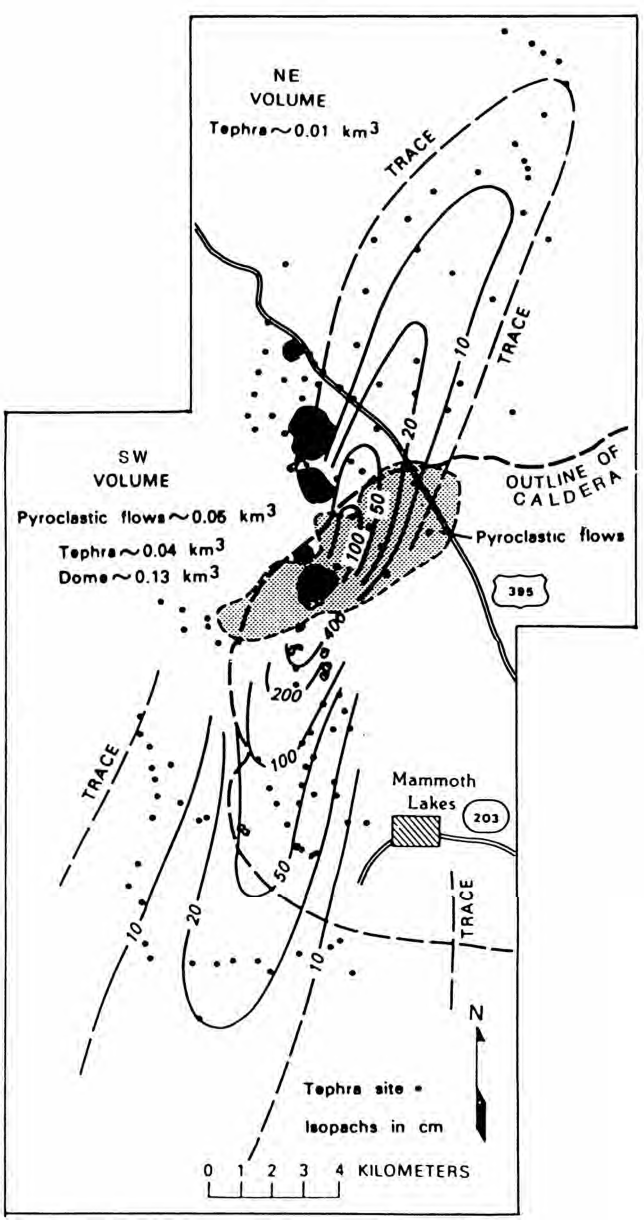

FIGURE 10—Isopach map of tephra deposits from Deadman Creek vent, Inyo volcanic chain. Northeast and southwest tephra lobes correspond to first and second eruptive pulses, respectively (from Miller, 1985).

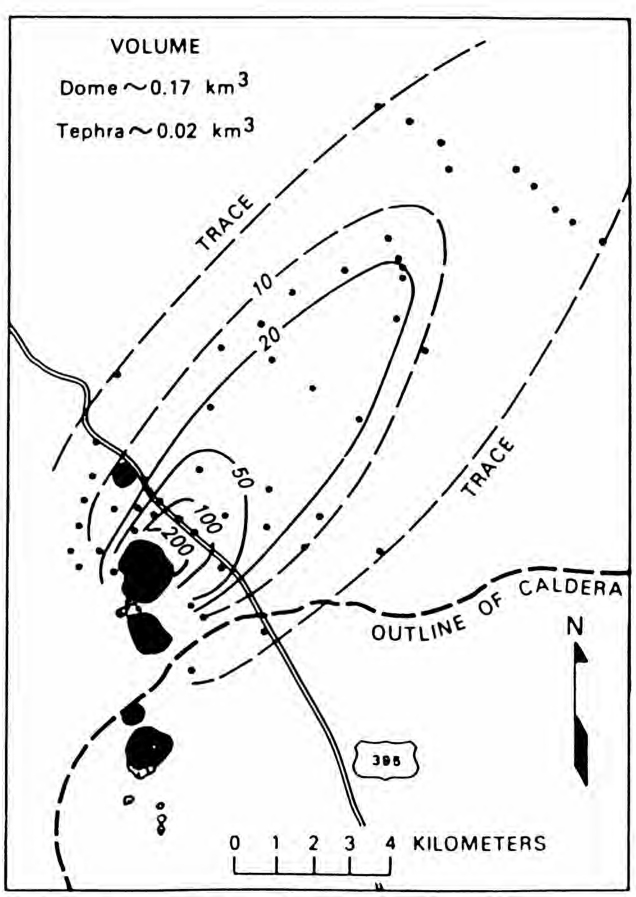

FIGURE 11—Isopach map of tephra deposits from Obsidian Dome vent, Inyo volcanic chain (from Miller, 1985).

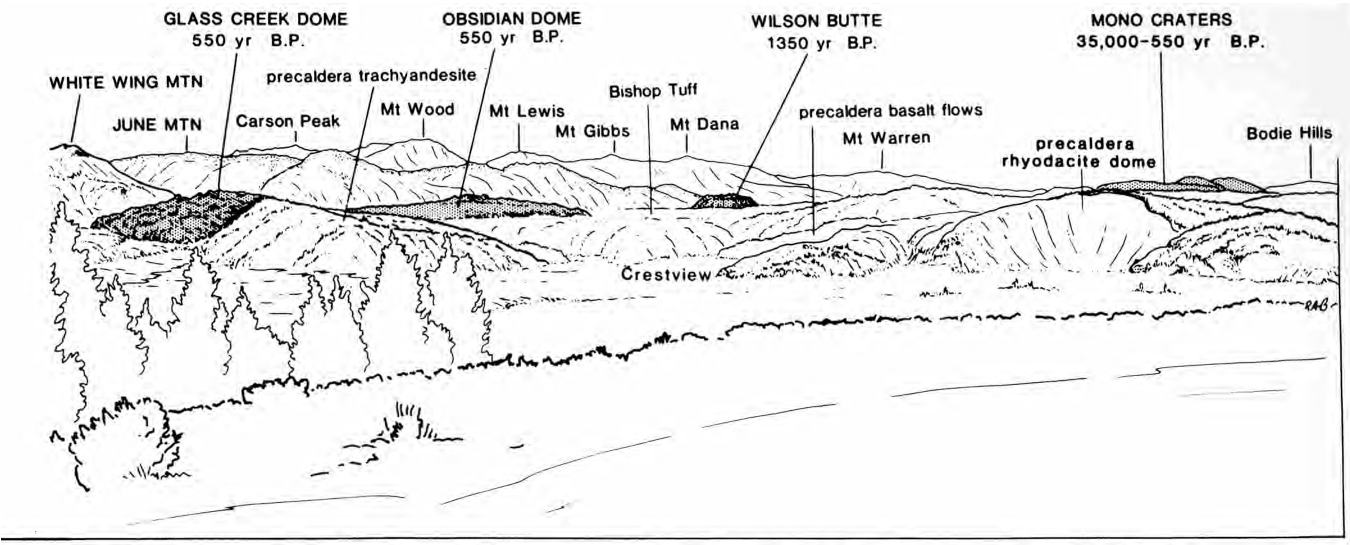

Mountain (Stop 18), showing north–south alignment of domes (shaded) in Inyo volcanic chain.

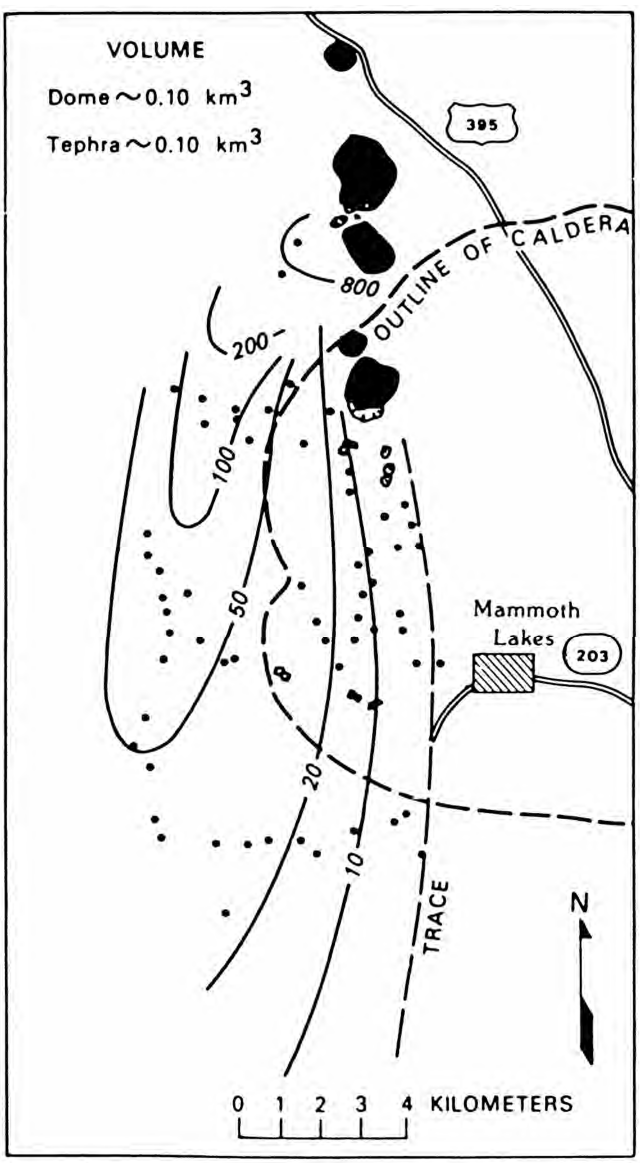

FIGURE 12—Isopach map of tephra deposits from Glass Creek vent, Inyo volcanic chain (from Miller, 1985).

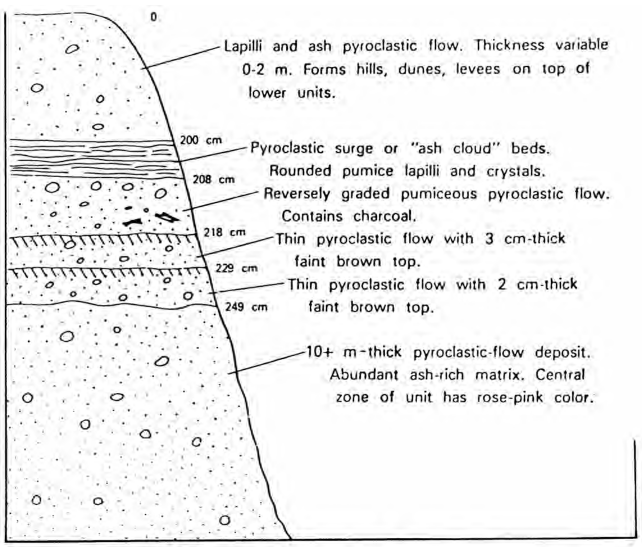

FIGURE 13—Sketch of stratigraphic section of Inyo pyroclastic-flow and -surge deposits exposed along entrance road to south Deadman Creek Campground (Stop 19) (from Miller, 1984).

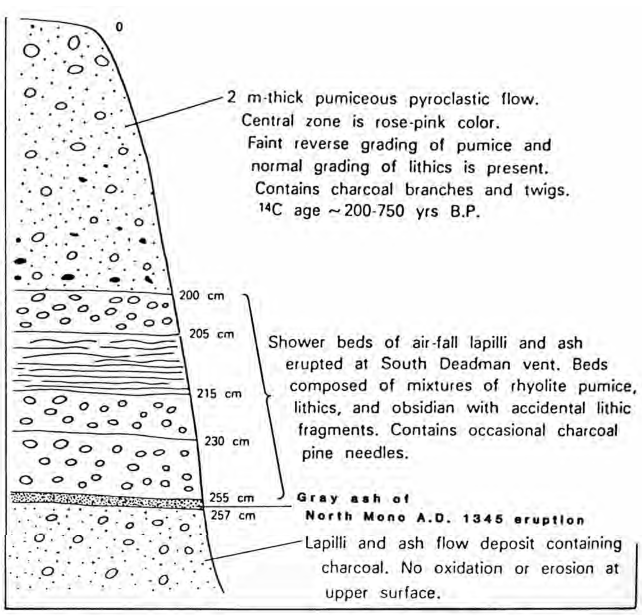

FIGURE 14—Sketch of stratigraphic section in excavation along Deadman Creek Road (Stop 20) (from Miller, 1984).

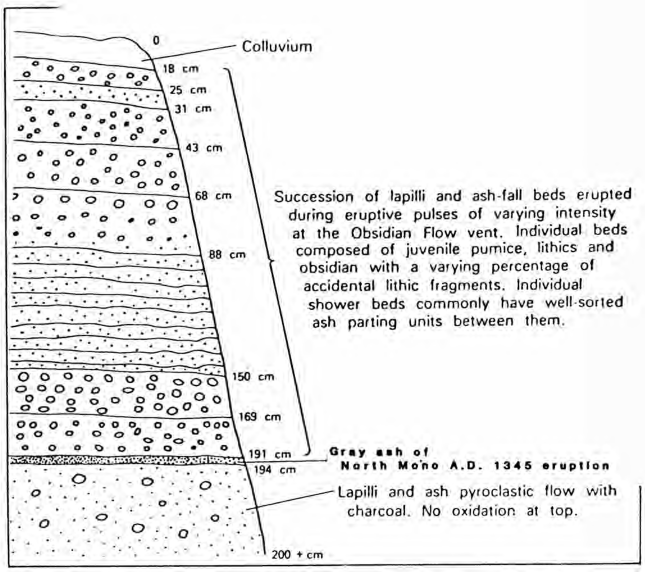

FIGURE 15—Sketch of stratigraphic section in excavation at Deadman Summit (Stop 21) (from Miller, 1984).

Near the drill site on the flow surface is an unusual feature commonly referred to as a squeeze-up, or crease structure, composed of very coarsely vesicular obsidian. The feature is roughly circular in plan, about 100 m in diameter, slightly depressed below the general level of the flow surface, and bisected by a central "crease," about which flow foliation and lineation symmetrically fan outward. The crease in such structures is usually oriented perpendicular to the flow margin, subparallel to the direction of flow. It appears to form as a result of lateral or tangential spreading of the flow carapace, allowing more fluid, gas-rich lava from the flow interior to well up to the surface (Anderson and Fink, 1987). Such features most commonly form where flows move onto gentler slopes and where forward movement slows and lateral spreading increases.

Return to base of dome and walk to north brink of gulch cut by Glass Creek; descend to creek and walk east (left) 50 m to steep undercut south bank that exposes pyroclastic-flow deposits.

STOP 22-B. Glass Creek pyroclastic sequence. Exposed along Glass Creek are poorly sorted pumiceous flowage deposits, at least one of which is incipiently welded. These deposits have an aggregate thickness of 25 m near the source vent and can be traced for several kilometers down-valley. Although they resemble deposits of pumiceous pyroclastic flows, these strata probably were generated from thick, near-vent accumulations of Glass Creek tephra deposits that avalanched down the steep slopes west of the vent (Miller, 1985). Along the creek bottom are numerous pumiceous bread-crust bombs that have been eroded from the deposits.

Walk upstream (west) about 500 m along the fishermen's trail on north bank to road crossing the creek and follow road south (left) 200 m to base of Glass Creek Dome.

STOP 22-C. Glass Creek Dome: Commingled rhyolite lava. Directly south of Glass Creek is the steep, talus- and block-mantled, north margin of Glass Creek Dome. The dome is composed of two distinctive rhyolites (Bailey, 1984b; Sampson, 1987): (1) sparsely porphyritic rhyolite, typically consisting of black obsidian or vitrophyre and occurring mainly on the dome margins, and (2) light-gray, pumiceous, coarsely porphyritic, hornblende–biotite rhyolite, occurring mainly in the center. Between the margin and center is an intervening zone where the two lava types have commingled, producing fascinating "marbled cake" structures (Fig. 17) that illustrate the contrast in viscosity between the relatively fluid obsidian and the more viscous porphyritic rhyolite. Petrologic and chemical studies (Sampson and Cameron, 1987) indicate that the two contrasting rhyolites originated and evolved in separate chambers, possibly confirming a suggestion (Bailey et al., 1976) that the sparsely and coarsely porphyritic types came from the Mono Craters and Long Valley magma chambers, respectively, and that they commingled along an interconnecting fissure just prior to eruption.

Return across Glass Creek to road on north side; walk 200 m west (left) to crest of knoll on south side of road.

STOP 22-D. Glass Creek: Cratered dome. Against the nearby Sierran frontal fault scarp (Hartley Springs fault) is a small rhyolite dome about 300 m in diameter, with a crater in its summit. It is informally referred to as "Cratered dome." This dome is chemically and petrographically similar to Obsidian Dome and probably was extruded at about the same time, as it appears to intrude and bake (oxidize) the phreatic and pyroclastic deposits on its flanks. The summit crater (Fig. 18) is about 100 m in diameter, 30–35 m deep, and has a discontinuous inner bench about 10–15 m below the rim. This bench suggests that the crater formed by collapse rather than explosion, because crags on the bench match those on the rim, suggesting that they are subsided remnants of radial ribs that initially occupied the summit of the dome. Such small collapse craters also are found on several domes in the Mono Craters chain to the north where relationships are more obvious. Typically, no explosion debris mantles the benches and rims of such craters, affirming their nonexplosive origin. Possibly they form by slow degassing and thermal contraction of the conduit or by actual magma withdrawal.

Return to Mammoth Lakes, via Glass Creek Road and US-395 south.

Day 6: Mono Craters circuit (Fig. 19) (Begins and ends in Mammoth Lakes

Go north on US-395 about 14 mi from CA-203 junction to Pumice Mine Road; turn RIGHT and go 0.4 mi to gravel road: turn LEFT and go 1.7 mi; park adjacent to road and walk northwest to crater rim.

STOP 23. Devils Punch Bowl, north crater. The dome northwest of the road is part of the Mono Craters, an arcuate chain of high-silica rhyolite domes, flows, and craters (Fig. 20) that erupted between about 35,000 and 600 yrs B.P. (Wood, 1977b; Lajoie and Robinson, 1982; Sieh and Bursik, 1986). The arcuate form of the chain, which includes more than 30 vents, is the result of eruption along a structural zone of weakness (Fig. 1) that coincides with the mylonitized margin of a subcircular Cretaceous pluton centered on Aeolian Buttes (Kistler, 1966). Chemically, the Mono Craters lavas are remarkably homogeneous, but they do show subtle differences in trace elements and accessory minerals, suggesting that they did not erupt from a single chamber (Kelleher and Cameron, 1989). The older extrusions (35,000–

FIGURE 16—Vertical airphoto of Obsidian Dome and Glass Creek Dome, Inyo volcanic chain. A, B, C, D correspond to Stops 22-A, -B, -C, -D.

3000 yrs B.P.) tend to be moderately to sparsely porphyritic, whereas the younger ones (2000–600 yrs B.P.) are virtually aphyric, suggesting that the latter erupted at higher temperature or from shallower depth, or both (Bailey, 1982). The appearance of aphyric lavas also coincides with an apparent increase in volumetric eruption rate (Wood, 1977b).

The dome northwest of the road is a body of porphyritic rhyolite that erupted more than 1200 yrs ago; obsidian hydration-rind dating of a similar nearby dome suggests that the dome is late to middle Holocene in age (Wood, 1977b;

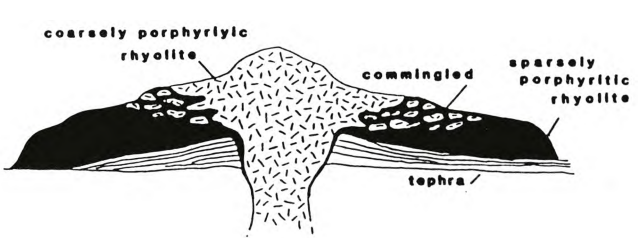

FIGURE 17—Schematic cross section of Glass Creek Dome showing distribution of marginal sparsely porphyritic rhyolite, central coarsely porphyritic rhyolite, and commingled zone, Inyo volcanic chain (Stop 22-C).

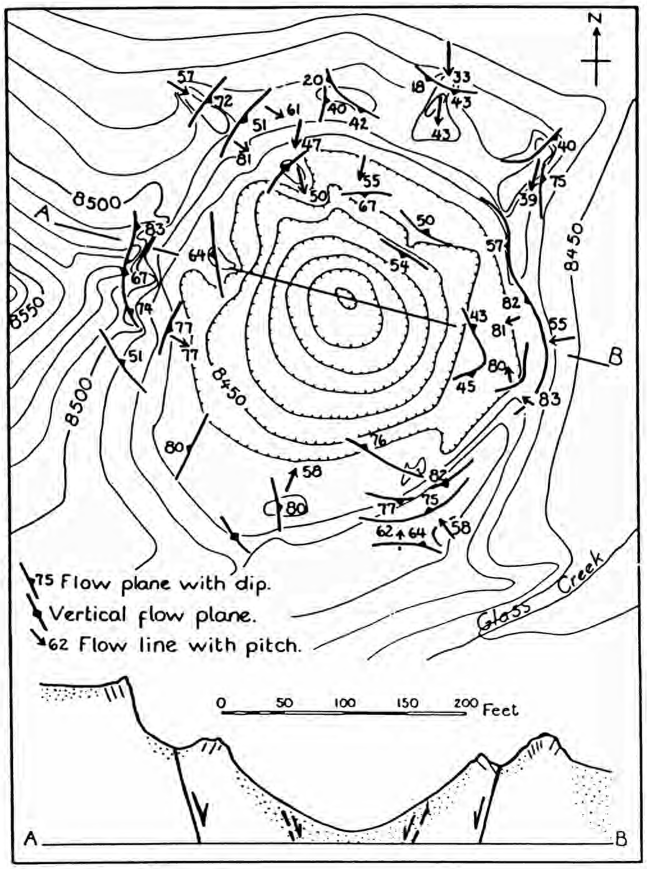

FIGURE 18—Map and cross section of Cratered dome, Inyo volcanic chain (Stop 22-D) (modified from Mayo et al., 1936).

Sieh and Bursik, unpubl. data). The dome sits between the ridges of tephra that probably were created during the same eruption that created the dome.

In the cleft between the dome and the tephra ridge is an excavation, open for inspection, which reveals pyroclastic-flow and -fall deposits associated with two subsequent eruptive episodes. Yellowish-brown ash and lapilli from the 600 yrs B.P. eruption of the Inyo chain are exposed in the upper few tens of centimeters of the excavation. Underlying these Inyo pyroclastic-fall beds is a thin gray ash derived from eruptions at the north end of the Mono chain. Discussion of this ash, which erupted about 1345 A.D., just prior to the Inyo eruption, will be deferred until later in the day when the near-source equivalent and associated dome are seen. Beneath the gray North Mono ash deposits are pyroclastic-flow and -fall deposits associated with the South Mono eruption of 700 A.D. The fall deposits near the bottom of the pit were erupted from sources now buried beneath and just north of South Coulee (Fig. 20). The blocky bed above the fall beds consists of juvenile and accessory debris produced during the creation of the large crater a few hundred meters northwest of the excavation.

Return to road and drive northeast 0.7 mi; turn RIGHT onto another gravel road and go east about 1.5 mi; turn LEFT (north) onto a wider gravel road and go 0.3 mi to a gravel road that forms a Y with the main gravel road.

In this region, about 4 km east of the Mono Craters, aphyric pyroclastic falls and surges blanket the ground surface. These beds are stratigraphically beneath the 700 A.D. beds of the South Mono eruption and are constrained by radiocarbon dating to have been erupted between 345 and 535 A.D. Their source has not been identified yet, but it must lie within the southern half of the Mono Craters.

Bear LEFT at the Y and continue north about 1.8 mi along the edge of the forest.

Off to the left, across the sandy plain, the prominent, barren flow is South Coulee. The volume of this aphyric rhyolite flow is about 0.5 km^3; it flowed from the crest of the chain down both the eastern and western flanks. Radiocarbon dating constrains its emplacement to about 700 A.D. The pumiceous surface of the flow has been mined for several decades by the U.S. Pumice Company of Lee Vining and is used to face buildings and as ornamental stone in landscaping.

At the next Y-junction bear LEFT and go about 0.5 mi to another Y-junction; bear LEFT again and go west and then south for about 0.5 mi.

The small swale crossed by the road a few tens of meters east of the end of South Coulee is a channel that has been beheaded by a young, north-trending fault along the eastern flank of the chain. The fault is a west-dipping normal fault that may have slipped during the South Mono eruption in response to the evacuation of magma through vents now beneath and immediately north of South Coulee.

Continue south on the pumice mine road 0.15 mi to the borrow pit and park.

STOP 24. South Coulee borrow pit: South Mono pyroclastic sequence. This old, man-made cut exposes three pyroclastic-flow deposits of the 700 A.D. South Mono eruption. The cut is not deep enough to expose most of the fall beds of this eruptive episode, but near the top of the cut, gray glassy fall beds are exposed. The source for these beds is beneath and/or just north of South Coulee. Some observers have suggested that these represent a phreatoplinian phase of the eruption. The dark, thin, fall bed rich in accessory clasts between the lower flow beds is from the eruption that formed the crater at Stop 23.

Retrace route north along gravel road about 0.6 mi; turn LEFT and go north about 1.8 mi; turn LEFT again and continue 1.5 mi to intersection with CA-120 (paved).

To the left (west) is the east flank of the northern half of the Mono Craters chain. The most recent eruption in this vicinity took place about 1345 A.D. and is called the North Mono eruption (Sieh and Bursik, 1986). The volume of magma erupted during this episode was about 1 km^3. The barren, rocky flow to the left and through the trees is North Coulee; its volume represents about half that of the entire eruptive episode.

Turn LEFT onto CA-120 and go 2.2 mi until just out of the sparse forest.

This stretch of CA-120 rests on thick pyroclastic flows of the North Mono eruption. These flows emanated at the crest of the chain from vents that are now buried by North Coulee.

Turn sharply RIGHT (east) onto a gravel road and go 0.7 mi to a borrow pit in the sparse forest.

STOP 25. Stratigraphy of the North Mono eruption. Much of the stratigraphy of the three most recent major eruptions of the Mono Craters is visible in this borrow pit. In the upper few meters of the south wall are pyroclastic-fall, -flow, and -surge beds of the North Mono eruption. These beds rest on a bioturbated, buried ground surface that

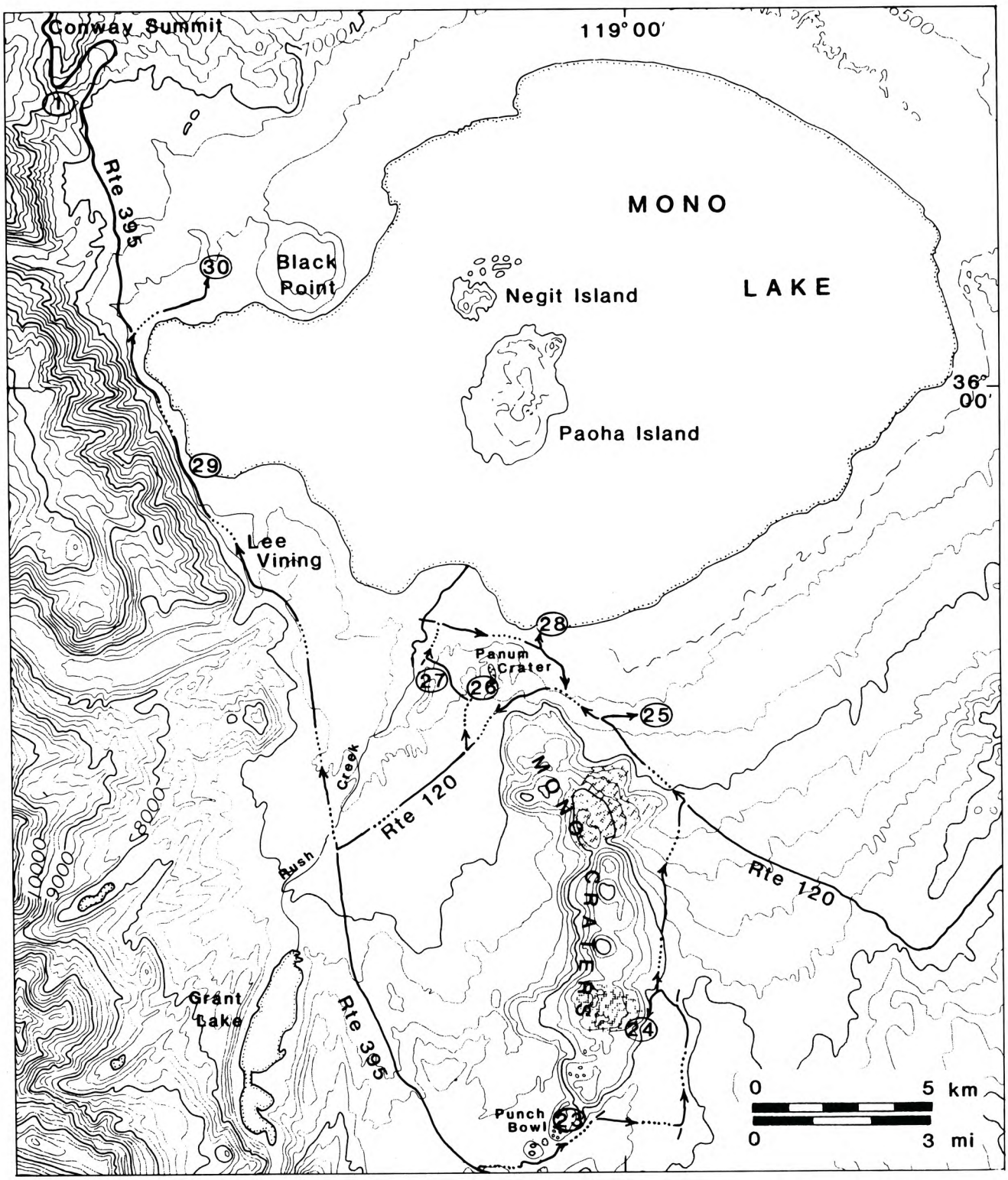

FIGURE 19—Map of Mono Craters and Mono Lake showing routes and stops of Days 1 and 6.

formed between 700 and 1345 A.D. on fall beds of the South Mono sequence about 1 m thick. The volumes of the two eruptions are similar, but the South Mono sequence at this site, being more distant from its sources, is thinner.

Beneath the floor of the pit is a series of fall and surge beds that were deposited during an eruptive episode between 385 and 595 A.D. The sources of these beds are uncertain, but they probably underlie Pumice Pit dome and Northwest Coulee, a few kilometers to the west (Fig. 20). Recall that deposits east of the southern part of the chain also were erupted during this period.

Isopachs of the first bed of the North Mono sequence (bed 1) show that it was erupted from a linear vent now buried by North Coulee (Fig. 21). This locality is marked by the dot next to "222" in the figure. The isopach map of the second bed (bed 2) reveals that it erupted from a source farther north, now buried by Upper Dome (Fig. 22). This locality is marked by the dot next to "96" in the figure.

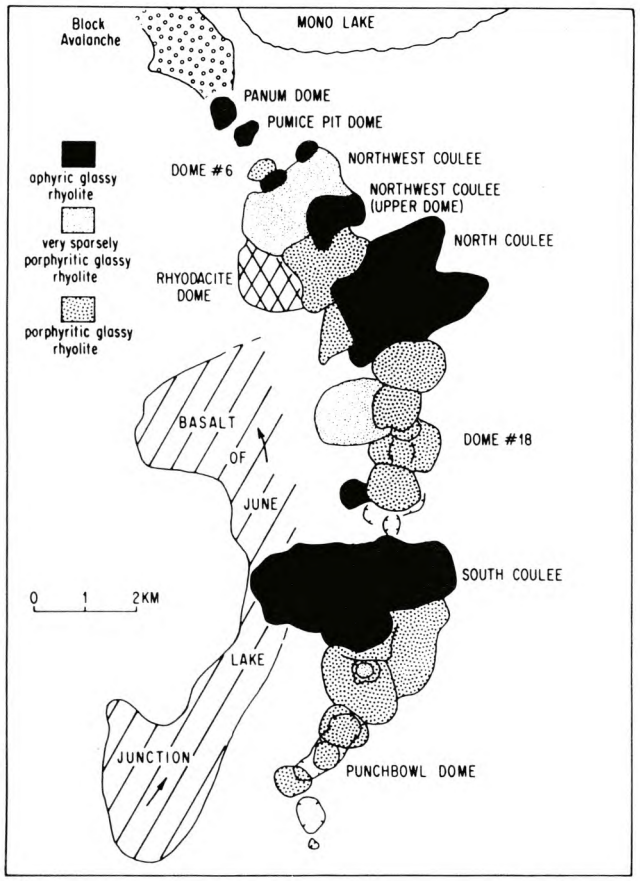

FIGURE 20—Geologic map of Mono Craters chain showing distribution of aphyric, sparsely porphyritic, and porphyritic rhyolites (from Sieh, 1984, modified from Wood, 1977b).

The next several fall beds emanated from sources now beneath North Coulee and Upper Dome. Bed 7, a pyroclastic-fall bed noted for its high percentage of accidental and accessory clasts, erupted from a source very near, if not under Upper Dome (Fig. 23). This locality is marked by the dot next to "130" in the figure. Above Bed 7 is a distinctive white pyroclastic-surge bed. Above the surge bed is a thick sequence of planar-bedded, gray, glassy fall beds, very similar to those that cap the South Mono eruption sequence at Stop 24, near South Coulee.

Return to CA-120 and turn RIGHT (west).

The barren flow about 1 km to the left is Upper Dome, which was extruded during the 1345 A.D. North Mono eruption. The sparsely forested flow northwest of Upper Dome is Northwest Coulee, probably erupted between 385 and 595 A.D.

Go 0.9 mi northwest on CA-120.

The small barren dome a few hundred meters to the left is Cratered Dome. It is another dome associated with the 1345 A.D. North Mono eruption.

Continue another 0.9 mi west on CA-120.

The road traverses the southern flank of a crater, within which is a small, circular, pumiceous, aphyric rhyolite dome called Pumice Pit dome. It may have been extruded between 385 and 595 A.D. It is thickly mantled by surge, fall, and

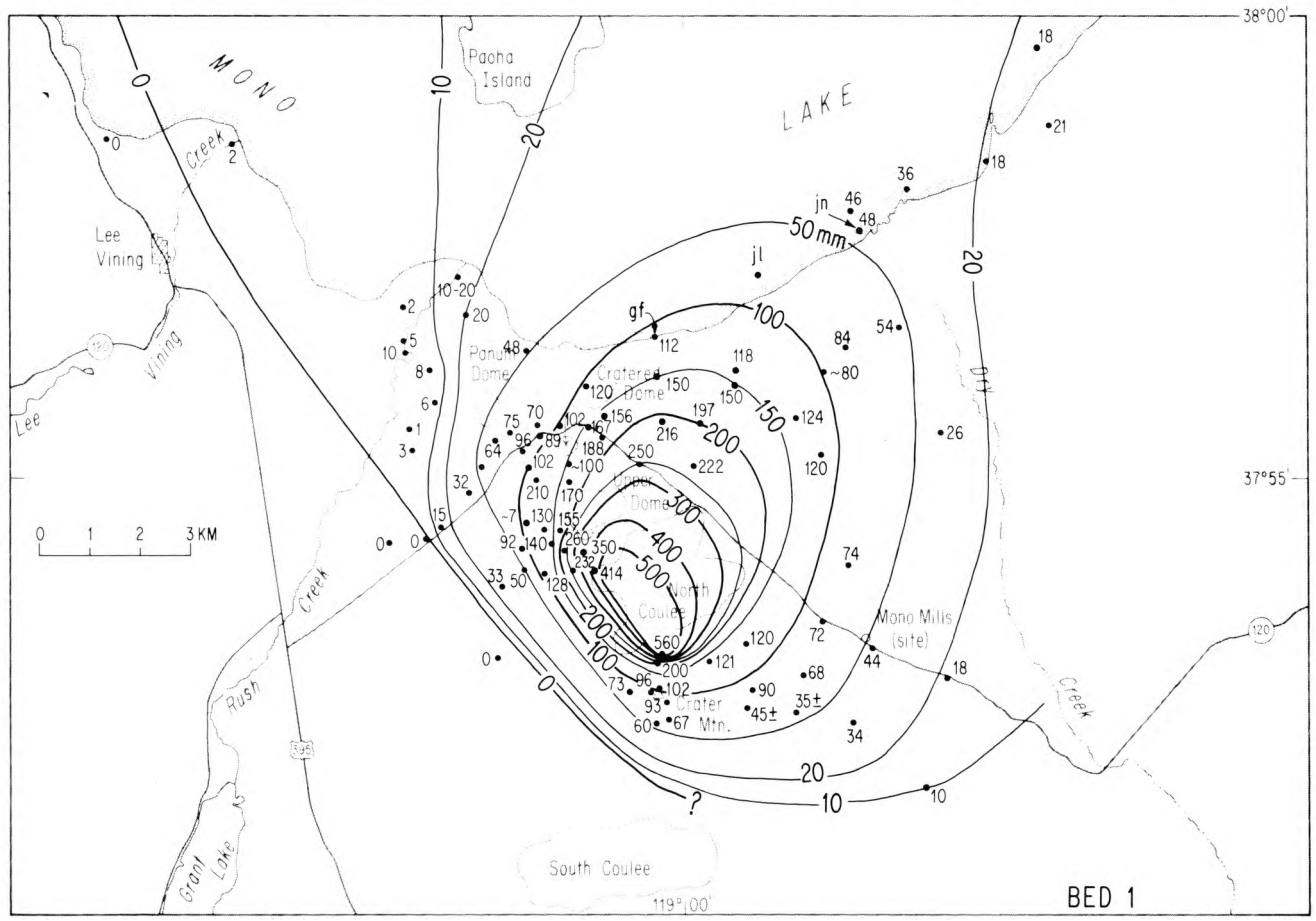

FIGURE 21—Proximal isopach map of bed 1, North Mono eruption, shows that low-level winds blew northeast during eruption. Shape of 500 mm isopach shows that bed-1 tephra issued from a northwest-trending linear vent or line of vents now buried beneath North Coulee. From Sieh and Bursik (1986).

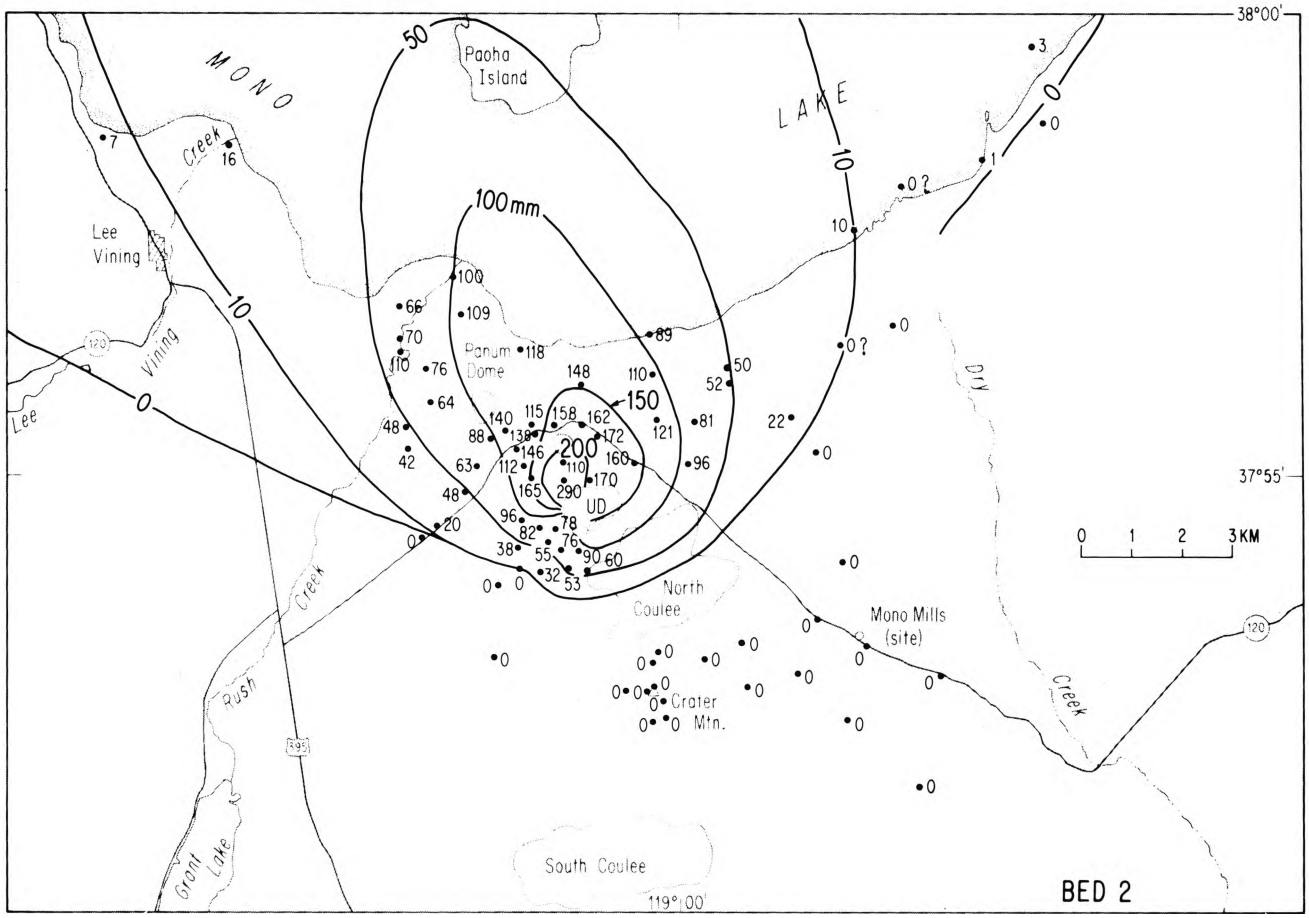

FIGURE 22—Near-vent isopach map of bed 2, North Mono eruption, shows that tephra was blown north-northwest from vent now buried beneath Upper Dome (UD) (from Sieh and Bursik, 1986).

flow beds of the North Mono sequence, particularly those that emanated from Panum Crater, whose tephra ring and dome are immediately to the northwest (Fig. 24).

Continue another 0.9 mi southwest on CA-120 to the first northbound gravel road *beyond* the one marked "Panum Crater" and turn RIGHT (north) toward Panum Crater.

This road traverses a field of volcanic dunes (Fig. 24), the crests of which have amplitudes of about 1 m and wave lengths of about 5–10 m. The dunes are roughly concentric about a point just south of Panum Crater and are composed principally of subrounded lapilli and blocks of white, silvery, attenuated pumice. The deposit represents the bedload of a highly inflated eruption cloud that emanated from Panum Crater before deposition of the tephra ring and dome.

Continue 0.8 mi to the Panum Crater parking area and follow the trail to the summit of the dome.

STOP 26. Panum Crater. Panum Crater (Figs. 20, 24) is the northernmost and youngest vent of the North Mono eruption (Sieh and Bursick, 1986). The stratigraphic sequence of deposits emplaced during this youngest activity (Fig. 25) includes (in ascending order): (1) a vent-clearing breccia, (2) four pyroclastic-flow and -surge deposits varying considerably in character, (3) a tephra-ring deposit, and (4) a composite, crater-filling dome. The sequence suggests two episodes of explosive activity from the same vent, each followed by dome extrusion. The initial vent-clearing eruption produced an early tephra ring and crater, from which early pyroclastic-flow and -surge deposits were erupted. An early dome rising into this crater apparently collapsed or exploded laterally, breaching the northwest side of the tephra ring and sending a block avalanche or coarse pyroclastic flow northwestward into Mono Lake (Wood, 1977b; Sieh and Bursik, 1986). This outburst possibly caused momentary decompression in the conduit and more pyroclastic flows followed. Subsequent, less energetic, pyroclastic-fall eruptions partially healed the breach in the northwest side of the tephra ring, and finally the current composite dome was extruded. Panum Dome consists of three subunits (Fig. 26) extruded in succession in the east and southwest, the south, and finally the north. Both the eastern and southwestern subunits have a thin mantle of tephra on them, suggesting that they are the shouldered-aside remnants of the early dome that exploded and produced the northwest breach in the crater rim and the block avalanche to the northwest. Extrusion of the southern and northern parts of Panum Dome concluded the North Mono eruption episode. Reconstruction of the 1345 A.D. North Mono vents suggests that they developed above a rising rhyolite dike that broke to the surface in northward succession (Fig. 27).

From the Panum parking area follow 4-wheel-drive road north 1.0 mi; park on the left overlooking gully on the left.

STOP 27. Panum block-avalanche deposit. The surface to the right of the road northwest of Panum Crater is underlain by the Panum block-avalanche deposit of Wood (1977b). Many car-sized blocks may be seen littering its surface, and subdued longitudinal flow ridges are evident

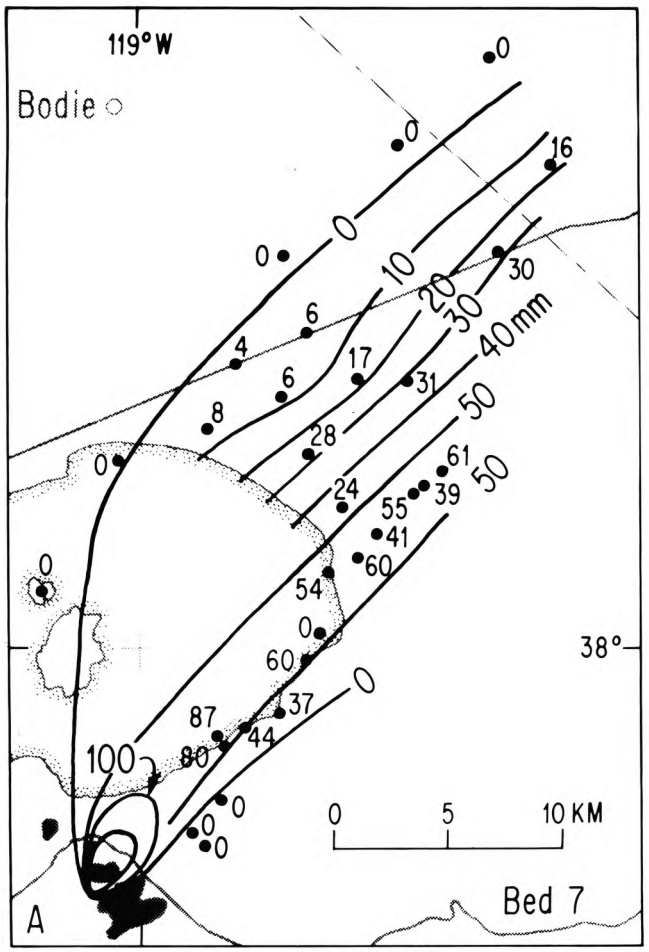

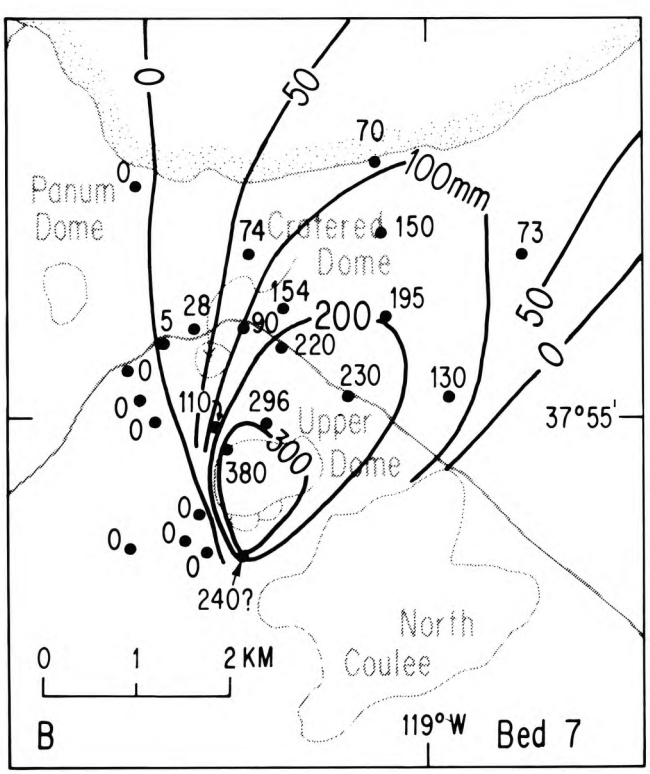

FIGURE 23—Isopach maps of bed 7, North Mono eruption. **A,** Distal data show remarkable asymmetry and elongation of isopachs. **B,** Near-vent data show vent was near or under Upper Dome. From Sieh and Bursik (1986).

from the air (Fig. 24). The deposit is confined between opposing west- and northeast-facing linear declivities that may be either sector-graben fault scarps or erosional scarps produced during emplacement of the coarse, high-energy flow by scouring of the soft substrate, which consists mainly of lake sediments and pyroclastic deposits.

In the gully to the left of the road, the internal structure of the block-avalanche deposit is well exposed. It is about 7 m thick here, but probably several tens of meters thick near its source and thins to 1 m at its distal end near the shore of Mono Lake. The deposit is a fines-depleted, clast-supported breccia consisting of partially agglutinated lapilli and blocks (Sieh and Bursik, 1986). About 90% of the clasts are angular fragments of dense to weakly pumiceous gray glass, on the surface of which are numerous white, powdery, impact marks, indicating that they were rigid during emplacement. About 10% of the clasts are oblate blocks of black to light-gray pumiceous glass with pronounced lumpy, bread-crusted surfaces, into which are impressed and agglutinated many of the smaller angular clasts. Paleomagnetic studies (Salyards, 1986) indicate that the deposit was emplaced at a temperature above 600°C. The association of contrasting rigid and viscid clasts in the deposit, together with their high-temperature emplacement, suggest an origin by collapse of a partially molten dome, most likely the early dome in Panum Crater.

Continue north and west along the 4-wheel-drive road 0.9 mi to junction with gravel road; turn RIGHT and go 0.6 mi to Rush Creek crossing; turn RIGHT (east) and go 1.9 mi; turn LEFT to Mono Lake State Nature Preserve parking area. Follow the self-guided trail to the shore and back to the parking area.

STOP 28. Mono Lake State Nature Preserve: Tufa towers. The delicate, castellated, white towers along the shore of Mono Lake are calcareous sublacustrine spring deposits formed where fresh-water springs percolate through lake-bottom sediments and flow up through the saline water. Calcium in the fresh water combines with carbonate of the saline lake water, resulting in precipitation, possibly catalyzed by algae, of calcite or aragonite. The towers formed entirely underwater and are being exposed as the lake level declines. Numerous signs along the well-marked trail through the tufa towers and along the lake shore describe the many fascinating and unique features of the Mono Lake habitat, including its brine shrimp, brine flies, bird life, and Indian and early settlement history.

From tufa towers parking area go south (up-hill) 0.9 mi to CA-120; turn RIGHT (west) and go 4.8 mi to US-395; turn RIGHT (north) and go 7.0 mi (through Lee Vining) to Mono Lake Marina; turn RIGHT into parking area and walk to lakeshore.

STOP 29. Mono Lake Marina: Rafted pumice blocks. The western and northern shores of Mono Lake are strewn with thousands of large (up to 2 m), subangular to subround blocks of biotite-bearing rhyolite pumice, which apparently formed during a sublacustrine eruption. The buoyant blocks probably floated to the surface of the dense, saline lake water and drifted ashore, where they lodged and later became coated with calcareous tufa. The blocks are concentrated at and below the 1948 m strandline and are absent above, indicating that the lake was at that level at the time of eruption (Stine, 1984). In lower Lee Vining Creek, pine

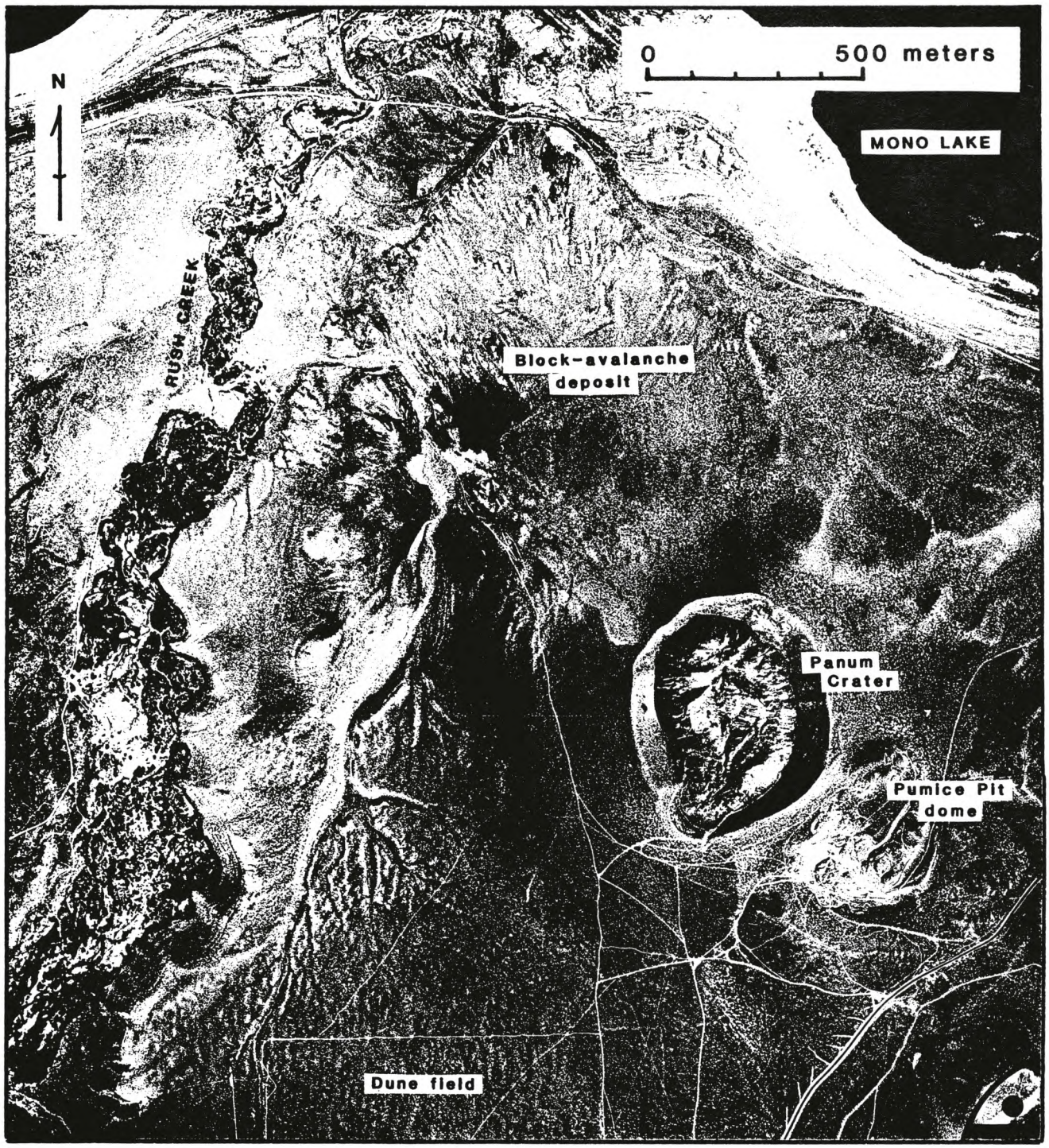

FIGURE 24—Vertical airnhoto of Panum Crater and associated pyroclastic deposits.

cones sandwiched between one of these blocks and overlying river gravel gave a radiocarbon age of 1495 ± 45 yrs B.P., providing a minimum age for the eruption. Excavations here at the marina show the blocks to lie well above a 1990 yrs B.P. Mono Craters ash bed; thus, the eruption probably occurred between about 250 and 450 A.D. The site of the eruption is not known with certainty, but extrusions of similar pumiceous rhyolite occur on two of the islets northeast of Negit Island and also on Paoha Island. These, or possibly other vents still submerged, are likely sources, as the greatest concentration of blocks is along the nearby northern lakeshore.

Continue north on US-395 2.5 mi to Danberg Park Road (just beyond Mono Inn); turn RIGHT (east) and go 2.0 mi to prominent roadcut in lake sediments and black ash on right, beyond Mill Creek crossing.

STOP 30. Mill Creek: Basaltic ash layer of Black Point. The 2 m thick basaltic ash layer exposed in the roadcut on the right, on the upper east side of Mill Creek, is in the uppermost part of the Wilson Creek Formation of Lajoie (1968, 1969), which consists predominantly of fine clayey silts and sands and intercalated rhyolite ash beds and deltaic gravels. The formation constitutes most of the exposed sed-

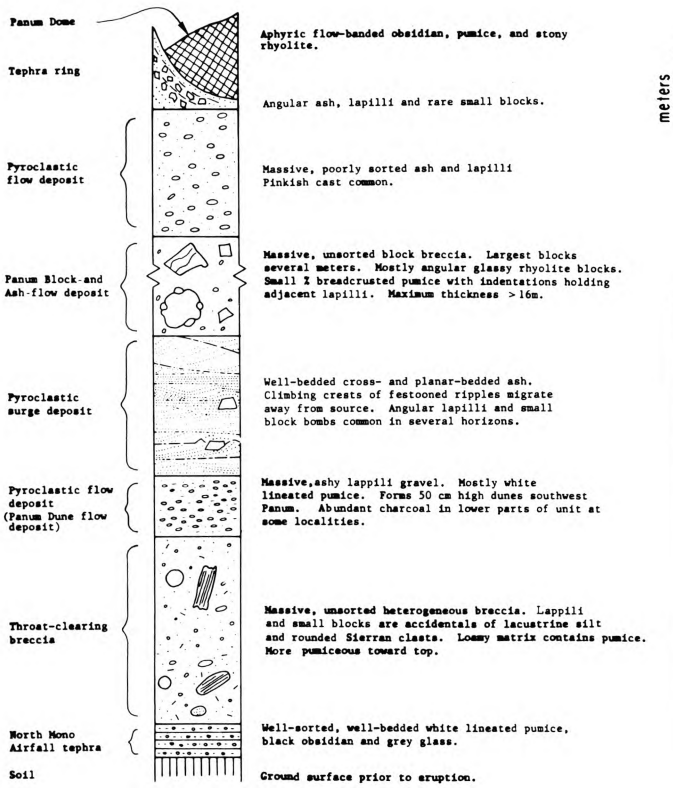

FIGURE 25—Generalized columnar section of North Mono eruption deposits in vicinity of Panum Crater (from Sieh and Bursik, 1986).

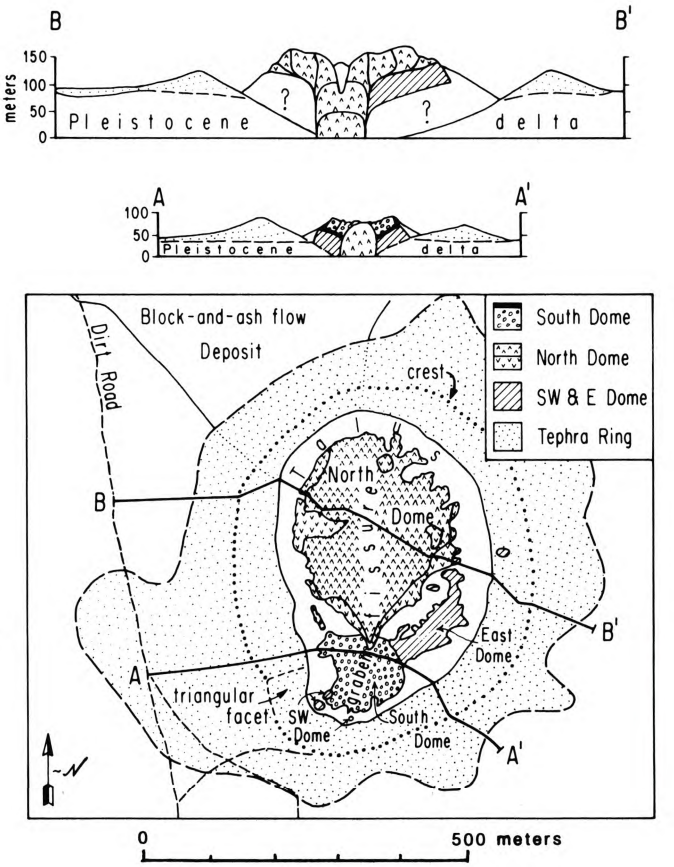

FIGURE 26—Generalized map and cross sections of Panum Dome (Stop 26) (from Sieh and Bursik, 1986).

iments around Mono Lake. On the basis of radiocarbon dating of ostracodes and calcareous tufa and estimated sedimentation rates (Lajoie and Robinson, 1982), it ranges in age from 36,000 to 11,000 yrs B.P. and was approximately coeval with the latest Pleistocene glaciations and with the early eruptions of the Mono Craters.

The basaltic ash layer exposed here was derived from eruptions at Black Point about 13,300 ± 500 yrs B.P. (Lajoie, 1968). The ash was deposited in at least 110 m of water, and the abundant climbing ripple marks indicate emplacement by south- to southwest-directed turbid bottom currents, probably flowing from glaciated Lundy Canyon to the west. The penecontemporaneous deformation probably formed as the water-saturated sediments slumped downslope to the south, triggered either by slope instability or possibly by earthquakes associated with the Black Point eruptions (Lajoie, 1968).

Return to US-395; turn RIGHT (south) and return to Mammoth Lakes.

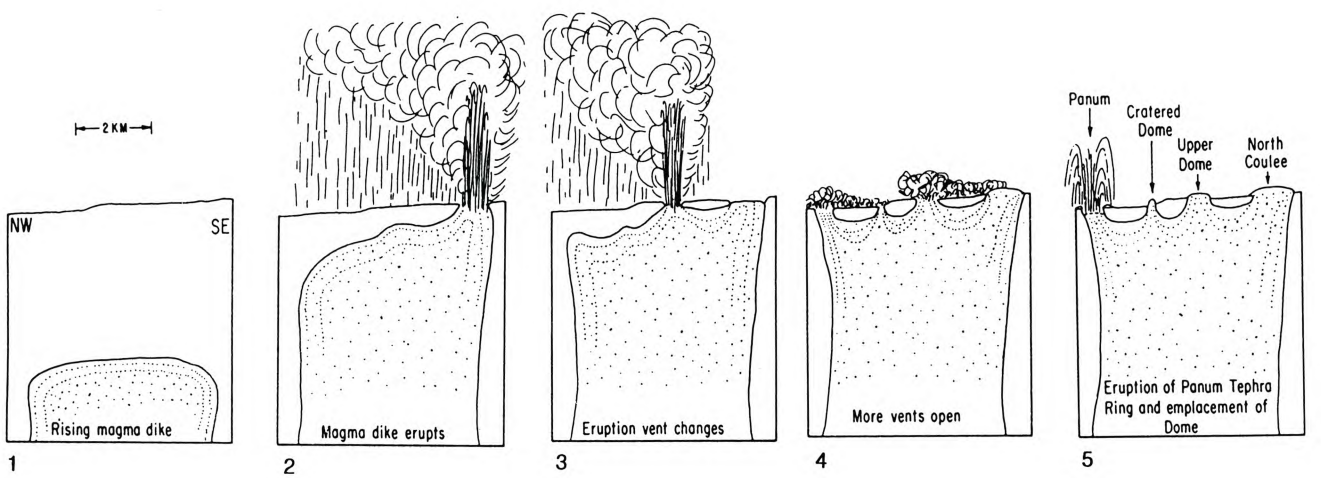

FIGURE 27—Hypothetical development of North Mono eruption episode above a rising rhyolite dike (from Sieh, 1984).

References

Alpha, T. R., Bailey, R. A., Lajoie, K. R., and Clarke, M. M., 1983, Physiographic diagrams of Long Valley, Mono and Inyo Counties, California: U.S. Geological Survey, Miscellaneous Field Studies Map 1659, 2 sheets.

Anderson, S. W., and Fink, J. H., 1987, Modelling crease structures on silicic lava flows: American Geophysical Union, Transactions, 68(44): 1545.

Bailey, R. A., 1982, Other potential eruption centers in California: Long Valley–Mono Lake, Coso, and Clear Lake volcanic fields: California Division of Mines and Geology, Special Publications 63: 17–28.

Bailey, R. A., 1984a, Chemical evolution and current state of the Long Valley magma chamber; *in* Hill, D. P., Bailey, R. A., and Ryall, A. S. (eds.), Proceedings of Workshop XIX: Active tectonic and magmatic processes beneath Long Valley caldera, eastern California: U.S. Geological Survey, Open-File Report 84-939: 24–40.

Bailey, R. A., 1984b, Introduction to the Late Cenozoic volcanism and tectonism of the Long Valley–Mono Basin area, eastern California; *in* Lentz, J., Jr. (ed.), Guidebook for western geological excursions: Department of Geological Sciences, MacKay School of Mines, University of Nevada (Reno), 2: 56–67.

Bailey, R. A., 1987, Long Valley caldera, eastern California: Geological Society of America, Centennial Field Guide—Cordilleran Section, pp. 163–168.

Bailey, R. A., 1989, Geologic map of Long Valley caldera, Mono–Inyo Craters volcanic chain, and vicinity, eastern California: U.S. Geological Survey, Miscellaneous Investigation Series Map I-1933, scale 1:62,500.

Bailey, R. A., Dalrymple, G. B., and Lanphere, M. A., 1976, Volcanism, structure, and geochronology of Long Valley caldera, Mono County, California: Journal of Geophysical Research, 81(5): 725–744.

Benioff, H., and Gutenberg, B., 1939, The Mammoth "Earthquake Fault" and related features in Mono County, California: Seismological Society of America, Bulletin, 29: 333–340.

Blackwell, D. D., 1985, A transient model for the geothermal system of Long Valley caldera, California: Journal of Geophysical Research, 90(B13): 11229–11241.

Bursik, M. I., and Sieh, K. E., 1989, Range-front faulting and volcanism in the Mono Basin, eastern California: Journal of Geophysical Research (in press).

Christensen, M. N., 1966, Late Cenozoic crustal movements in the Sierra Nevada of California: Geological Society of America, Bulletin, 77: 163–182.

Christensen, M. N., and Gilbert, C. M., 1964, Basaltic cone suggests origin of some guyots: Science, 143(3603): 240–242.

Eichelberger, J. C., Lysne, P. C., Miller, C. D., and Younker, L. W., 1985, Research drilling at Inyo domes, 1984 results: American Geophysical Union, Transactions, 66(17): 186–187.

Eichelberger, J. C., Carrigan, C. R., Westrich, H. R., and Price, R. H., 1986, Nonexplosive silicic volcanism: Nature, 323: 598–602.

Eichelberger, J. C., Vogel, T. A., Younker, L. W., Miller, C. D., Heiken, G. H., and Wohletz, K. H., 1988, Structure and stratigraphy beneath South Inyo Crater, Long Valley caldera, California: Journal of Geophysical Research, 93(B11): 13208–13220.

Fink, J. H., and Manley, C. R., 1987, Origin of pumiceous and glassy textures in rhyolite domes and flows: Geological Society of America, Special Paper 212: 77–88.

Fiske, R. S., and Tobische, O. T., 1978, Paleogeographic significance of volcanic rocks of the Ritter Range pendant, central Sierra Nevada; *in* Howell, D. G., and McDougall, K. A. (eds.), Mesozoic Paleogeography of the Western United States: Society of Economic Paleontologists and Mineralogists, Pacific Section, Los Angeles, California, pp. 209–222.

Gilbert, C. M., 1938, Welded tuff in eastern California: Geological Society of America, Bulletin, 49: 1829–1862.

Gilbert, C. M., Christiansen, M. N., Al Rawi, Y., and Lajoie, K. R., 1968, Structural and volcanic history of Mono Basin, California-Nevada: Geological Society of America, Memoir 116: 275–329.

Hildreth, W., 1979, The Bishop Tuff: Evidence for the origin of compositional zoning in silicic magma chambers; *in* Chapin, C. E., and Elston, W. E. (eds.), Ash-flow tuffs: Geological Society of America, Special Paper 180: 43–75.

Hill, D. P., Bailey, R. A., and Ryall, A. S., 1985, Active tectonic and magmatic processes beneath Long Valley caldera, eastern California: An overview: Journal of Geophysical Research, 90(B13): 11111–11120.

Holden, E. S., 1892, Earthquakes in California in 1890 and 1891: U.S. Geological Survey, Bulletin 95: 31 pp.

Huber, N. K., 1981, Amount and timing of Late Cenozoic uplift and tilt of the central Sierra Nevada, California—evidence from the upper San Joaquin River Basin: U.S. Geological Survey, Professional Paper 1197: 28 pp.

Izett, G. A., 1981, Volcanic ash beds: Recorders of upper Cenozoic silicic pyroclastic volcanism in western United States: Journal of Geophysical Research, 86(B11): 10200–10222.

Izett, G. A., 1982, The Bishop ash bed and some older compositionally similar ash beds in California, Nevada and Utah: U.S. Geological Survey, Open-File Report 82-582: 47 pp.

Kelleher, P. C., and Cameron, K. L., 1989, The geochemistry of the Mono Craters–Mono Lake islands complex, eastern California: Journal of Geophysical Research (in press).

Kistler, R. W., 1966, Structure and metamorphism in the Mono Craters quadrangle, Sierra Nevada, California: U.S. Geological Survey, Bulletin 1221-E: 53 pp.

Lajoie, K. R., 1968, Late Quaternary stratigraphy and geologic history of Mono Basin, eastern California: Unpublished Ph.D. dissertation, University of California, Berkeley, California, 271 pp.

Lajoie, K. R., 1969, Late Quaternary stratigraphy and geologic history of Mono Basin, eastern California: Dissertation Abstracts (B), 30(3): 1202.

Lajoie, K. R., and Robinson, S. W., 1982, Late Quaternary glacio-fluvial chronology, Mono Basin, California (abs.): Geological Society of America, Abstracts with Programs, 14(4): 179.

Mankinen, E. A., Grommé, C. S., Dalrymple, G. B., Lanphere, M. A., and Bailey, R. A., 1986, Paleomagnetism and K–Ar ages of volcanic rocks from Long Valley caldera, California: Journal of Geophysical Research, 91(B1): 633–652.

Manley, C. R., and Fink, J. H., 1987, Internal structure of rhyolite flows as revealed by research drilling: Geology, 15: 549–552.

Mastin, L. G., 1988, Phreatic eruption processes at Inyo Craters, Long Valley caldera, California: Unpublished Ph.D. dissertation, Stanford University, Stanford, California, 50 pp.

Mastin, L. G., and Pollard, D. D., 1988, Surface deformation and shallow dike-intrusion processes at Inyo Craters, Long Valley caldera, California: Journal of Geophysical Research, 93(B11): 13221–13235.

Mayo, E. B., 1934, The Pleistocene Long Valley Lake in eastern California: Science, 80: 95–96.

Mayo, E. B., Conant, L. C., and Chelikowski, J. R., 1936, Southern extension of the Mono Craters, California: American Journal of Science, 32: 81–97.

Merriam, R., and Bischoff, J. L., 1975, Bishop Ash: A widespread volcanic ash extended to southern California: Journal of Sedimentary Petrology, 45: 207–211.

Metz, J. M., and Mahood, G. A., 1985, Precursors to the Bishop Tuff eruption: Glass Mountain, Long Valley, California: Journal of Geophysical Research, 90(B13): 11121–11126.

Miller, C. D., 1984, Chronology and stratigraphy of recent eruptions at the Inyo volcanic chain; *in* Stine, S., Wood, S., Sieh, K., and Miller, C. D. (eds.), Holocene paleoclimatology and tephrachronology east and west of the central Sierran crest: Friends of the Pleistocene, Pacific Cell, Field Trip, October 12–14, 1984, Guidebook: pp. 88–96.

Miller, C. D., 1985, Holocene eruptions at the Inyo volcanic chain, California: Implications for possible eruptions in Long Valley: Geology, 13: 14–17.

Miller, C. D., Mullineaux, D. R., Crandell, D. R., and Bailey, R. A., 1982, Potential hazards from future volcanic eruptions in the Long Valley–Mono Lake area, east-central California and Nevada—a preliminary assessment: U.S. Geological Survey, Circular 877: 10 pp.

Pakiser, L. C., 1961, Gravity, volcanism, and crustal deformation in Long Valley, California: U.S. Geological Survey, Professional Paper 424-B: B250–B253.

Pakiser, L. C., Press, F. C., and Kane, M. F., 1960, Geophysical study of Mono Basin, California: Geological Society of America, Bulletin, 71: 415–448.

Putnam, W. C., 1950, Moraine and shoreline relationships at Mono Lake, California: Geological Society of America, Bulletin, 61: 115–122.

Rinehart, C. D., and Huber, N. C., 1965, The Inyo Crater Lakes—a blast in the past: California Division of Mines and Geology, Mineral Information Service, 18(9): 169–172.

Rundle, J. B., and Hill, D. P., 1988, The geophysics of a restless caldera—Long Valley, California: Annual Review of Earth and Planetary Sciences, 16: 251–271.

Rundle, J. B., and Whitcomb, J. H., 1984, A model for deformation in

Long Valley, California, 1980–1983: Journal of Geophysical Research, 89(B11): 9371–9380.

Rundle, J. B., and Whitcomb, J. H., 1986, Modeling gravity and trilateration data in Long Valley, California, 1983–1984: Journal of Geophysical Research, 91(B12): 12,675–12,682.

Rundle, J. B., Carrigan, C. R., Hardee, H. C., and Luth, W. C., 1986, Deep drilling in the magmatic environment, Long Valley caldera: American Geophysical Union, Transactions, 67(21): 790–791.

Russell, I. C., 1889, Quaternary History of the Mono Valley, California: U.S. Geological Survey, Eighth Annual Report, pp. 263–394.

Salyards, S. L., 1986, Thermal and depositional constraints on a block-and-ash-flow deposit from Panum Crater, Mono County, California, from paleomagnetic analysis (abs.): Geological Society of America, Abstracts with Programs, 18(2): 180.

Sampson, D. E., 1987, Structures and textures of the lavas of the Inyo chain, eastern California: Implications for feeder-dike and conduit geometries; *in* Fink, J. H. (ed.), The emplacement of silicic domes and lava flows: Geological Society of America, Special Paper 212: 89–101.

Sampson, D. E., and Cameron, K. L., 1987, The geochemistry of the Inyo volcanic chain: Multiple magma systems in the Long Valley region, eastern California: Journal of Geophysical Research, v. 92, n. B10, p. 10403–10421.

Sarna-Wojcicki, A. M., Bowman, H. R., Meyer, C. E., Russell, P. C., Woodward, M. J., McCoy, G., Rowe, J. J., Jr., Baedecker, P. A., Asaro, F., and Michael, H., 1984, Chemical analyses, correlations, and ages of Upper Pliocene and Pleistocene ash layers of east-central and southern California: U.S. Geological Survey, Professional Paper 1293: 40 pp.

Sarna-Wojcicki, A. M., Morrison, S. D., Meyer, C. E., and Hillhouse, J. W., 1987, Correlation of upper Cenozoic tephra layers between sediments of western United States and the East Pacific Ocean, and comparison with biostratigraphic and magnetostratigraphic age data: Geological Society of America, Bulletin, 98: 207–233.

Savage, J. C., and Clark, M. M., 1982, Magmatic resurgence in Long Valley caldera, California: Possible cause of the 1980 Mammoth Lakes earthquakes: Science, 217: 531–533.

Savage, J. C., and Cockerham, R. S., 1984, Earthquake swarm in Long Valley caldera, California, January 1983: Evidence for dike injection: Journal of Geophysical Research, 89(B10): 8315–8324.

Sharp, R. P., 1968, Sherwin Till–Bishop Tuff geological relationships, Sierra Nevada, California: Geological Society of America, Bulletin, 79: 351–364.

Sheridan, M. F., 1967, Double cooling-unit nature of the Bishop Tuff in Owens River Gorge, California (abs.): Geological Society of America, Special Paper, 115: 351.

Sheridan, M. F., 1970, Fumarolic mounds and ridges of the Bishop Tuff, California: Geological Society of America, Bulletin, 81: 851–868.

Sieh, K., 1984, Most recent eruptions of the Mono Craters, eastern central California; *in* Stine, S., Wood, S., Sieh, K., Miller, C. D. (eds.), Holocene paleoclimatology and tephrachronology east and west of the central Sierran crest: Friends of the Pleistocene, Pacific Cell, Field Trip, October 12–14, 1984, Guidebook, pp. 53–74.

Sieh, K., and Bursik, M., 1986, Most recent eruption of the Mono Craters, eastern central California: Journal of Geophysical Research, 91(B12): 12539–12571.

Snow, E., and Yund, R. A., 1988, Origin of cryptoperthites in the Bishop Tuff and their bearing in its thermal history: Journal of Geophysical Research, 93(B8): 8975–8984.

Sorey, M. L., 1985, Evolution and the present state of the hydrothermal system in Long Valley caldera: Journal of Geophysical Research, 90(B13): 11219–11228.

Stine, S., 1984, Late Holocene lake level fluctuations and island volcanism at Mono Lake, California; *in* Stine, S., Wood, S., Sieh, K., Miller, C. D., (eds.), Holocene paleoclimatology and tephrachronology east and west of the central Sierran crest: Friends of the Pleistocene, Pacific Cell, Field Trip, October 12–14, 1984, Guidebook, pp. 21–49.

Taylor, B. E., Eichelberger, J. C., and Westrich, H. R., 1983, Hydrogen isotopic evidence of rhyolitic magma degassing during shallow intrusion and eruptions: Nature, 306(5943): 541–545.

Tobisch, O. T., Saleeby, J. B., and Fiske, R. S., 1986, Structural history of continental volcanic arc rocks, eastern Sierra Nevada, California: A case for extensional tectonics: Tectonics, 5(1): 65–94.

Westrich, H. R., Stochman, H. W., and Eichelberger, J. C., 1988, Degassing of rhyolitic magma during ascent and emplacement: Journal of Geophysical Research, 93(B6): 6503–6511.

Wood, S. H., 1977a, Distribution, correlation, and radiocarbon dating of late Holocene tephra, Mono and Inyo Craters, eastern California: Geological Society of America, Bulletin, 88: 89–95.

Wood, S. H., 1977b, Chronology of late Pleistocene and Holocene volcanics, Long Valley and Mono Basin geothermal areas, eastern California: U.S. Geological Survey, Geothermal Research Program, Final Technical Report (reprinted as U.S. Geological Survey, Open-File Report 83-747: 76 pp., 1983).

EXCURSION 14B:
Cordilleran volcanism, plutonism, and magma generation at various crustal levels, Montana and Idaho

Compiled by Donald W. Hyndman
Department of Geology, University of Montana, Missoula, Montana 59812

Introduction

This six-day field trip examines emplacement of Late Cretaceous to Eocene felsic magmas at various crustal levels, from deep continental crust to the earth's surface. The trip is in three parts, each approximately two days long.

1. Idaho batholith: deep plutonic, with no preserved volcanic rocks that are known to be related.
2. Boulder batholith—Elkhorn Mountains Volcanics: shallow plutons with some preserved volcanic rocks erupted from them.
3. Challis Volcanics: broad volcanic field erupted from calderas, with some exposure of magma-chamber plutons.

Idaho batholith: This major granitoid batholithic complex is one of several in a generally north—south trend along the axis of the North American Cordillera. These complexes follow the 0.705 $^{87}Sr/^{86}Sr$ initial-ratio boundary which marks the western edge of old continental North America against younger crust of oceanic affinity to the west. In this area, at least, the more mafic rocks, across a major mylonitic suture zone to the west, are accreted microcontinental terranes, volcanic arcs, and scraps of oceanic crust.

The Idaho batholith is dominantly granodiorite with a prominent belt of quartz diorite to tonalite along its western border. It has been intruded by abundant mafic to intermediate synplutonic mafic dikes which mixed with the batholith and which probably contributed much of the heat needed to melt the continental crust to form the batholith magmas. The batholithic complex represents the deep levels of exposure of a volcanic arc, surrounded by a broad area of sedimentary rocks regionally metamorphosed at about the

Boulder batholith—Elkhorn Mountains Volcanics: This major latest Cretaceous granite to granodiorite batholith was emplaced into miogeoclinal sedimentary rocks just behind the outer edge of the Cordilleran overthrust belt. It appears to overlap in time with emplacement of at least some of the felsic main-phase units of the Idaho batholith.

The Boulder batholith was emplaced at very shallow levels beneath a broad area of Elkhorn Mountains Volcanics erupted from the same magma chamber(s). Smaller, more mafic plutons were emplaced in the early stages around its borders. The volcanic rocks are of similar composition, dominantly felsic to intermediate, with some basaltic units. Emplacement at such shallow levels requires that the rising magmas must have been nearly dry. Major ash-flow tuffs of the Elkhorn Mountains Volcanics erupted through epicontinental calderas, a few of which have been identified in and around the batholith.

Challis Volcanics: This large volcanic pile was erupted behind the Cordilleran overthrust belt in Eocene time after crystallization of the Idaho batholith. These arc(?) magmas were erupted onto miogeoclinal sedimentary rocks; their shallow magma-chamber plutons were emplaced into the eastern half of the earlier, much deeper Idaho batholith and onto its flanking sedimentary rocks.

The Challis Volcanics are dominantly felsic ash-flow tuffs in the upper part, with dominantly mafic to intermediate volcanic rocks in the lower part. Much of the volcanic pile was erupted from major calderas or cauldrons, many of which have been mapped. At least one major magma-chamber pluton, the Casto pluton, is exposed.

Plutonism at deep crustal levels: The Idaho batholith, Montana and Idaho

Donald W. Hyndman[1] and David A. Foster[2]

[1]Department of Geology, University of Montana, Missoula, Montana 59812; [2]Department of Geological Sciences, State University of New York, Albany, New York 12222

Idaho batholith environment

General aspects and regional tectonics

The Idaho batholith was emplaced into the Precambrian continental crust of North America, just east of a major collisional suture zone bounding a microcontinent to the southwest (Fig. 1). Beginning about 120 Ma, the Seven Devils/Wallowa terrane arrived in western Idaho, colliding with the Precambrian rifted margin of old North America, and completing docking with plugging by quartz dioritic plutons about 85 to 82 Ma (Snee et al. , 1987). The boundary is marked by a major mylonitic suture zone, the western Idaho suture zone, that trends northward in western Idaho near the western edge of the Idaho batholith, curves westward near the town of Orofino at latitude 46°30'N, and disappears under the Miocene Columbia River basalts. At

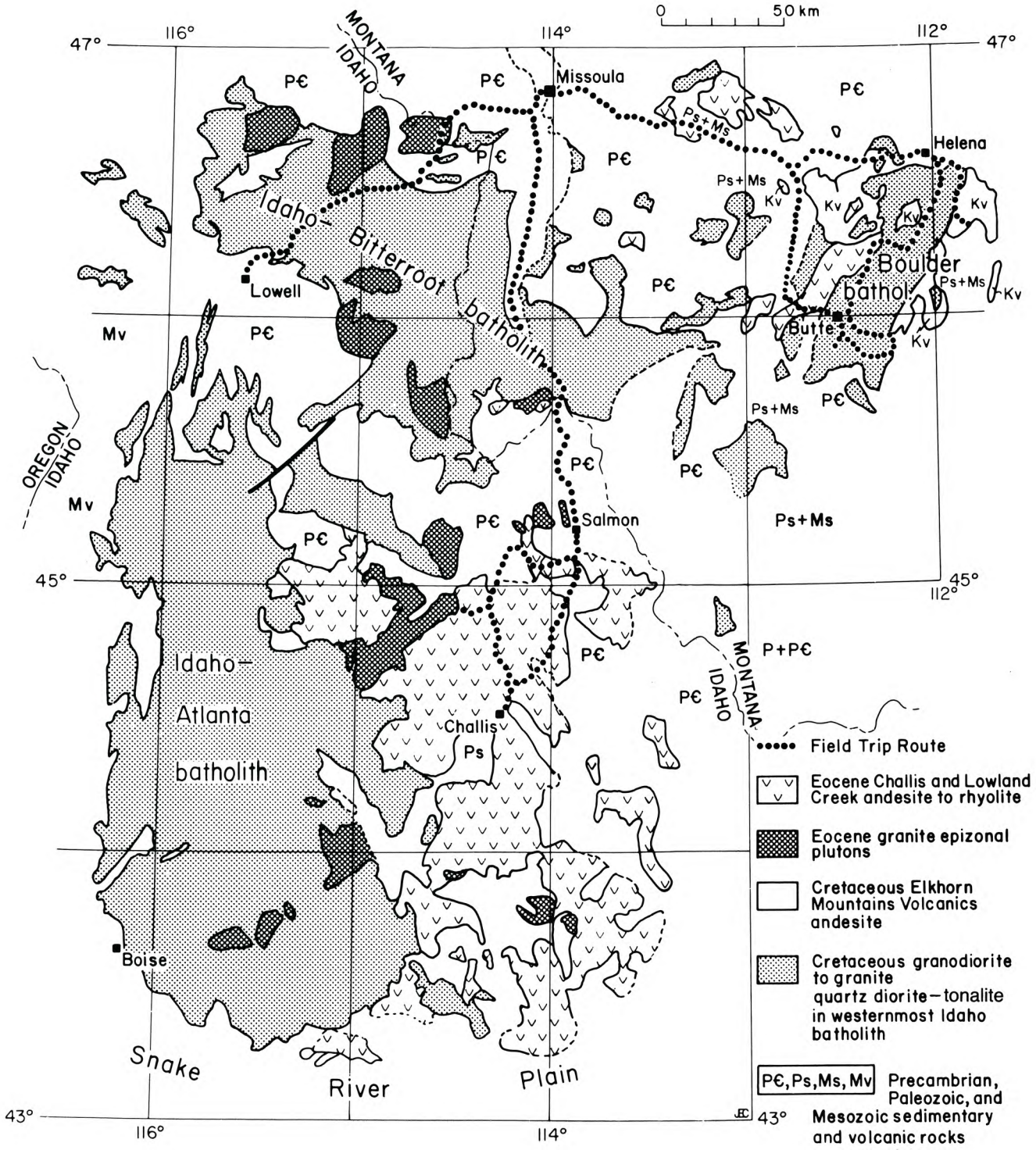

FIGURE 1—Geological map of the Idaho batholith region. Route of the field trip is shown as a heavy dotted line.

the curve in the suture zone, the microcontinent was being underthrust northeastward at a 50° plunge under North America. At least 80 km of transport are documented in deformed mafic dikes in the mylonite zone (Strayer et al. , 1987). The suture closely follows the boundary between generally mafic rocks of oceanic affinity on the west and generally felsic rocks of continental affinity on the east, and between $^{87}Sr/^{86}Sr$ initial ratios of less than 0.704 on the west and greater than 0.706 on the east (Armstrong et al., 1977; Fleck and Criss, 1985).

Proterozoic semipelitic to quartzose and impure calcareous sedimentary rocks of the Belt Supergroup underlying most of northwestern Montana and northern Idaho were subjected to regional Precambrian burial metamorphism to the greenschist facies. Metamorphism reached lower grades higher in the stratigraphic section. During Mesozoic time, rocks adjacent to the northern Idaho batholith were deformed and regionally/dynamothermally metamorphosed to grades reaching as high as the sillimanite zones (cf. , Hyndman et al. , 1988), an effect that extends as much as 70 km from the batholith contact (Fig. 2). In contrast to the massive, spotted fabric of the Precambrian burial metamorphism, the

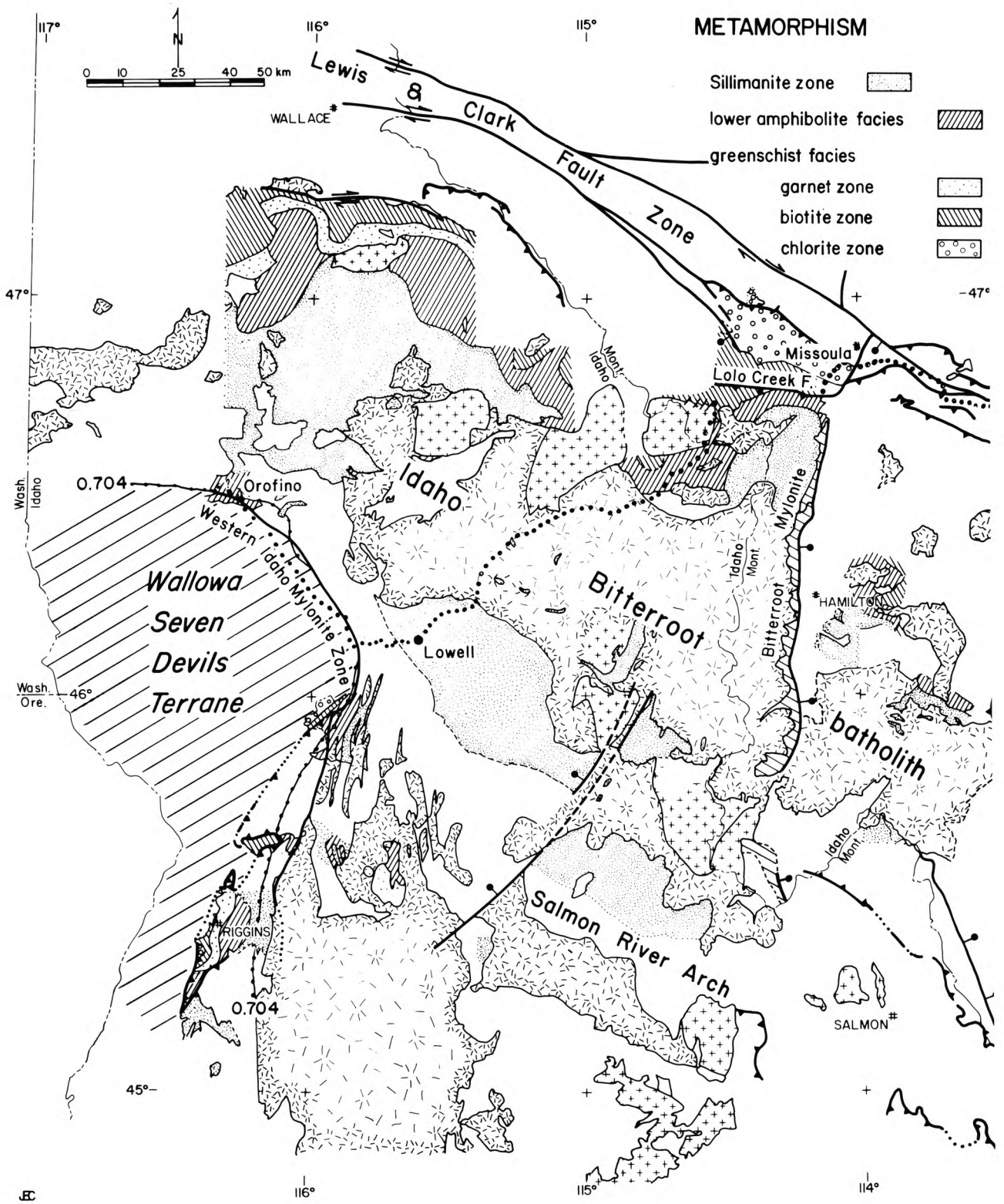

FIGURE 2—Metamorphic map of the Idaho batholith region. Route of the field trip is shown as a dotted line.

Mesozoic regional metamorphism formed well-foliated schists and gneisses. Metamorphic grades increase progressively, in most areas, toward the batholith. However, locally the isograds are cut at low angles by the batholith contact, demonstrating that intrusion postdated regional metamorphism. Mineral assemblages that include quartz, muscovite, biotite, staurolite, sillimanite, and kyanite suggest that rocks north and northwest of the batholith were formed at depths greater than 24 km, somewhat less to the southeast (Rice, 1987). Melting formed anatectic migmatites at the highest metamorphic grades, suggesting that this regional metamorphism accompanied crustal melting to form the Idaho batholith.

Main-phase units of the northern Idaho batholith, or Idaho-Bitterroot batholith, are granite to granodiorite emplaced in latest Cretaceous time between about 65 and 80 or possibly

85 Ma (Fig. 3). The timing, immediately after collision along the western Idaho suture zone, and the proximity of the batholith to that zone, suggest that subduction to form the batholith lay west or southwest of the western Idaho suture zone. The 14,000 km^2 Idaho-Bitterroot batholith was apparently emplaced into a broad synclinorium trending southeastward in the Proterozoic Belt Supergroup. The rocks are felsic, medium-grained, and massive or nearly so. Much of the deep line of section along the Lochsa River, the section followed by the field trip, is relatively homogeneous mineralogically and chemically (Hyndman, 1984), but elsewhere the batholith shows considerable variation within the range of granite and granodiorite (Toth, 1987; Reid, 1987).

The western border zone, about 20% of the width of the Idaho batholith, consists of somewhat older intrusions of biotite—homblende quartz diorite to tonalite. The rocks are massive to foliated on steep surfaces trending approximately parallel to the western Idaho suture zone. These lie on the oceanic, southwest side of the Sr-isotope boundary.

Sheets and other bodies of tonalitic and quartz diorite orthogneiss occur elsewhere in the deeper and border zones of the batholith (cf. , Taubeneck, 1971; Chase, 1973; Wiswall and Hyndman, 1986; Hyndman and Foster, 1988). These mafic-rich rocks may mark the deepest levels of the Idaho batholith, as also inferred for the Sierra Nevada batholith (Ross, 1985).

Large, voluminous swarms of synplutonic basaltic andesite to andesite dikes and small areas of gabbroic complex cut the batholith (Hyndman and Foster, 1988). In one 10 km wide section along the Lochsa River valley, we measured 20% dikes, by volume. Mafic synplutonic dikes are also widespread in the tonalite/quartz diotite of the western border zone of the batholith.

Intrusive relations indicate that the mafic dikes in the Idaho-Bitterroot batholith were emplaced in the same time period as the main-phase granites. Evidence for such a synplutonic nature includes the following (Hyndman and Foster, 1988):

1. Mafic dikes cut the host granite as tabular, sharply bounded bodies; some are stretched, thinned, segmented, or dismembered, or are folded in undeformed granite.
2. Many of the mafic dikes show foliation, lineation, and mylonitic texture imposed by post-emplacement movement of the granite. Some are foliated oblique to the walls of the dike (Fig. 4A).
3. Mafic dikes grade into rounded blobs or mafic schlieren in the granite (Fig. 4B).
4. Mafic dikes are cut by tabular or ptygmatic dikes of the host granite, are metamorphosed by heat from the host granite, or contain late alkali feldspar megacrysts like those in the granite.
5. Granite within 1 m or so of some of the dikes is contaminated and more mafic than normal Idaho batholith granite.
6. Granite and andesite in composite dikes show small-scale intermingling; elsewhere, rounded blobs of basalt have thin rims of leucogranite.
7. The complete range of chemical composition of the syn-

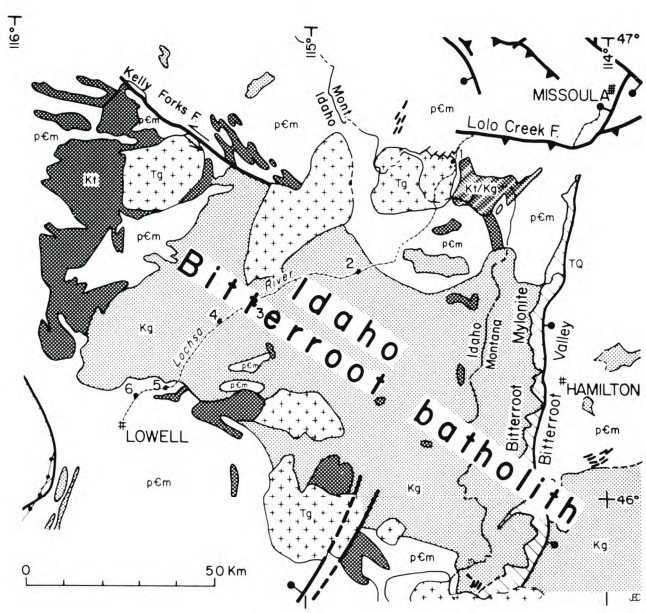

FIGURE 3—Intrusive map of the northern Idaho batholith. —
sheet-like intrusions of border zones
—main-phase batholith: composition, texture, foliation.

FIGURE 4—A, Basaltic dike with a strong foliation and lineation has intruded granite that remained massive. The basalt appears to have chilled in, and been deformed by, the granite before it crystallized completely. US-12, milepost 124.95. **B,** An andesitic dike intermediate in composition and texture between fine-grained basaltic inclusions and coarser-grained intruded granite. Basaltic magma appears to have chilled against, and mixed with, intruded granite magma to form andesite. US-12, milepost 124.75.

plutonic dikes (Table 1), from basaltic andesite to dacite, lies along a linear major-element trend which includes the composition of the enclosing granite to granodiorite. A magma-mixing interpretation of this trend is supported by megascopic and abundant microscopic disequilibrium textures in intermediate rock types.

Given the nature of their interaction with the enclosing granite, synplutonic mafic magmas appear to have been injected at early, intermediate, and late stages in the evolution of the granite. Because voluminous, high-temperature, mafic magmas apparently were emplaced throughout crystallization of the granite of the Idaho-Bitterroot batholith, they must have added considerable heat. As suggested by Hyndman and Foster (1988), the mafic magmas, rising above the subduction zone, probably provided the additional heat required to melt the lower continental crust to form the granitoid magmas of the Idaho batholith.

Pegmatites and minor aplites occur in several environments. A few early, concordant muscovite-biotite-quartz-feldspar pegmatites pinch and swell and show 1 to 3 mm biotite selvages in pelitic to quartzofeldspathic country rocks. These probably formed by anatexis during regional metamorphism. Most of the pegmatitic dikes were emplaced by injection (Chase and Johnson, 1977), during or after regional metamorphism, many probably associated with emplacement of the main-phase units of the batholith.

Many tabular, post-metamorphic muscovite-quartz-feldspar pegmatites 5 to 25 cm thick have been injected into planar fractures. Another group of tabular pegmatites or aplites, 1 cm to 2 m thick, dips 5 to 25° west, northwest, or north, regardless of the dip or degree of deformation of the enclosing rock. These subhorizontal pegmatitic sheets are emplaced only into granodiorites and granites of the western 16 km of the Lochsa River valley section (west of milepost 120; see road log), and extend only 1.3 km into the country rocks (Hyndman, 1983). The surfaces of the pegmatite dikes are marked by slickenside striae plunging downdip to the northwest, indicating post-emplacement slip and probably shear-surface control of emplacement.

Several stages of deformation are recognized in the Idaho batholith environment (cf. , Hietanen, 1961; Chase, 1973; Reid et al., 1973; Nold, 1974; Hyndman et al., 1988). Tight isoclinal folds with strong axial-plane schistosity were formed in deformation D1, but they are difficult to find. A few large folds verging away from the batholith have been described. The major amphibolite-facies regional metamorphism surrounding the batholith, and described above, produced the axial-plane schistosity of D1 folds. Open to nearly isoclinal folds that deform the dominant schistosity, and develop a new weak to locally strong axial-plane schistosity with muscovite and biotite, formed during D2 deformation. These folds tend to have nearly vertical plunges near the batholith

TABLE 1-Chemistries of representative quartz diorites and synplutonic mafic dikes in the Idaho-Bitterroot batholith. Major-element analyses by x-ray spectrometry, Washington State University.

	Western border zone quartz diorites and tonalites			Synplutonic mafic dikes in Idaho batholith			Idaho batholith
	quartz diorite 180	quartz diorite 292	quartz diorite 322	fine-grained basaltic andesite 135.9A	fine-grained foliated andesite 139.3C	very fine-grained black andesite 116.0	granodiorite average
	(from Hietanen, 1962)			(Hyndman and Foster, 1988)			(Hyndman, 1984)
SiO_2	57.30	59.16	60.35	54.19	58.08	61.32	71.23
TiO_2	0.74	0.85	0.75	2.28	0.98	1.23	0.20
$A1_2O_3$	17.64	18.15	18.22	15.21	17.29	16.85	15.74
Fe_2O_3	1.88	1.57	1.27	4.53	3.56	3.34	0.65
FeO	4.29	4.08	3.62	5.19	4.08	3.82	0.73
MnO	0.11	0.10	0.08	0.14	0.11	0.08	0.025
MgO	4.26	3.13	2.84	6.46	4.60	2.56	0.39
CaO	7.11	6.47	5.95	6.36	6.87	4.88	1.93
Na_2O	3.72	3.71	4.10	3.19	2.64	2.91	4.44
K_2O	1.38	1.47	1.28	1.57	1.94	2.69	3.69
H_2O (LOI)	1.16	0.79	1.09				0.49
CO_2	0.21	0.03	0.02				
P_2O_5	0.21	0.032	0.27	0.54	0.19	0.33	0.06
Zr (ppm)				106	17	90	131.5
Nb				42	13	19	13.1
Y				23	17	17	12.3
Rb				56	56	96	83.1
Sr				681	536	616	896.9
Ba				645	535	944	1520.9
Rare-earth elements							
La (ppm)				38.0	18.6	39.8	25
Ce				79.1	35.7	77.7	52
Pr				9.0	6.3	8.6	
Nd				37.2	16.9	32.6	
Sm				7.4	3.5	5.6	
Eu				2.27	1.14	1.64	
Gd				6.3	3.3	4.38	
Dy				4.6	2.9	3.1	
Ho				0.82	0.56	0.6	
Er				3.31	1.64	1.7	
Yb				1.77	1.54	1.4	
Lu				0.24	0.22	0.19	

contacts, perhaps as a result of rise of the batholith magmas during D3. Upright and relatively open concentric and flexural slip folds of the earlier metamorphic schistosity formed during D3 deformation, probably during the final stages of forceful emplacement of the batholith. No new axial-plane schistosity formed.

Therefore, a model for formation of the northern Idaho batholith is as follows: The Seven Devils/Wallowa terrane of eastern Oregon and western Idaho docked in Late Cretaceous time near the present western edge of the Idaho batholith, a boundary marked by a major mylonite zone and the Sr-isotope initial-ratio boundary. Subduction on a separate zone southwest of the terrane between about 120 to 80 Ma and 80 to 65 Ma gave rise to the mafic western border and the felsic main-phase magmas, respectively, of the Idaho batholith. Partial melting formed basaltic andesite magmas in the mantle wedge above the subducted oceanic plate, and those high-temperature magmas rose into the overlying crust. Outboard of old continental North America, they crystallized to form tonalite and quartz diorite plutons. Where the mafic magmas rose into the old granitoid continental crust, they heated the crust, caused regional metamorphism, and ultimately caused secondary melting to form the granodiorite and granite magmas of the Idaho batholith. The synplutonic mafic dikes now preserved in the Idaho batholith formed by continued rise of the same mafic magmas.

Field trip

General aspects

The Idaho batholith field trip traverses a well-exposed cross section of the northern Idaho batholith, briefly examines the broad aspects of this deep-seated granitoid batholith and its regionally metamorphosed country rocks, and considers the role of synplutonic mafic magmas from the mantle in providing heat for melting of continental crustal rocks to form the more felsic main-phase units of the batholith.

Day 1—Examination of the broad aspects of this deep-seated granitoid batholith and its regionally metamorphosed country rocks, including:

1. the low- to high-grade regional metamorphic rocks of the eastern border zone,
2. the sheet-like intrusions of the contact zones of the granitoid rocks,
3. the main-phase granodiorite to granite of the batholith,
4. the high- to medium-grade regional metamorphic rocks and sheet-like intrusions of the western border zone,
5. injection migmatites of the border-zone rocks,
6. some of the structures which relate to emplacement of the batholith.

Day 2—Examination of the more mafic, early to synplutonic quartz diorite to tonalite to basaltic andesite intrusions which are thought to originate in the mantle, and consideration of their role in providing heat for melting of continental crustal rocks to form the more felsic, main-phase units of the batholith. Major features to be examined include:

1. early western border-zone tonalites,
2. fine-grained synplutonic dikes of basaltic andesite to andesite which cut the batholith and make up about 20% of the batholith volume in this area,
3. small granitoid dikes which cut the dikes of basaltic andesite,
4. complex mixing relationships between the basaltic andesite magmas and the granitoid magmas of the batholith,
5. subhorizontal granitoid to pegmatite sheets which cut the batholith.

Field-trip guide

Mileposts (m.p.) refer to small green signs at edge of road.

Day 1: Missoula, Montana, to Lowell, Idaho, via US-12. Day 2: Lowell, Idaho, to Missoula, Montana, via US-12.

Stops are designated Day 1 or Day 2, but read in a single direction from east to west for those who may later want to combine Day 1 and Day 2 into a single trip.

Head southwest on US-93 from Missoula, Montana.

Mileage

0.0 (m.p. 90.1) Bridge across Bitterroot River at south edge of Missoula. **1.7**

1.7 (m.p. 88.4 to 87.4) Roadcuts in red to pale-brownish to pale-greenish, well-layered mudstones of Proterozoic Missoula Group of the Belt Supergroup. These rocks show ripple marks and mudcracks indicative of deposition in shallow water, either a tidal flat or river floodplain. Similar, poorly exposed rocks continue almost to Lolo. **5.0**

6.7 (m.p. 83.4 on US-93 = m.p. 32.6 on US-12) Junction US-93 and US-12 at Lolo. Travel west on US-12 which follows the Lolo Creek fault, a steep reverse fault with the south side up. Wallace Formation (underlies Missoula Gr.) sedimentary rocks of the biotite zone of the greenschist facies are on the north or downthrown side; Ravalli Group quartzite (underlies Wallace Formation) in the amphibolite facies is on the upthrown side. Prichard Formation semipelitic metasedimentary rocks of the lower Belt Supergroup, underlying the Ravalli Group farther south, are in the sillimanite zones bordering the northern Idaho batholith. Along US-12, for 25 mi west of Lolo (to Lolo Hot Springs at m.p. 7.3), pale-gray to white, poorly bedded quartzite of the Ravalli Formation alternates with dark, rusty-weathering, thin-bedded dolomitic siltstone of the Wallace Formation. **6.6**

13.3 (m.p. 26.0 to 25.1) Mt. Lolo (elevation 2780 m), visible on the skyline to the south (left), is in sillimanite zone Prichard Formation metasediments (see Wehrenberg, 1972). The northeast corner of the Idaho batholith is 15 km farther south. **4.0**

17.3 (m.p. 22.0) Pale-gray quartzite of the Ravalli Group in roadcut. **3.9**

21.2 (m.p. 18.1 to 8.1) Roadcuts are mostly in thinly layered Wallace Formation sedimentary rocks with variable degrees of rusty weathering. **10.6**

31.8 (m.p. 7.5) **STOP 1-1. Epizonal Lolo batholith.** Large exposure of the Eocene Lolo batholith at Lolo Hot Springs, just inside contact of the batholith. It is a shallow, hypersolvus, A-type granite with miarolitic cavities. **7.2**

39.0 (Montana m.p. 0.0 = Idaho m.p. 174.35) Lolo Pass on Montana–Idaho state line (Idaho mileposts follow). **3.8**

42.8 (m.p. 170.8) Small metamorphosed gabbroic layered intrusion studied by Jens (1974). The black, ultramafic layers of diopside and hornblende alter-

nate with gray, mafic layers of foliated amphibolite. The intrusion is faulted and cut by many discordant pegmatites but its age, although premetamorphic, is uncertain. **1.1**

43.9 (m.p. 169.75; just northeast of bridge across Crooked Fork Creek) **STOP 1-2. Brushy Fork stock.** Exposure of quartz diorite or granodiorite of the Brushy Fork stock (Nold, 1974), cutting metamorphosed Belt quartzite. It is a medium-grained biotite–quartz diorite or tonalite with about 20% biotite. The foliation is about 113°/71°NE. The granitoid rock is cut by a discordant muscovite granite pegmatite/aplite dike. A 1 m long xenolith of muscovite–biotite quartzite has foliation and layering concordant to the foliation in the granitoid intrusion. Crosswarps of the schistosity are at about 90°. **4.0**

47.9 (m.p. 165.8) Calc-silicate paragneiss, probably metamorphosed Wallace Formation of Belt Supergroup, has reached the amphibolite facies. Layering at 074°/45°N is cut by a concordant muscovite–biotite quartzofeldspathic alaskite dike about 15 cm thick and a discordant dike 45 cm thick. A vertical granite dike 3 or 4 m thick has reacted with diopside to form black hornblende. Several fine-grained mafic dikes about 60 cm to 1 m thick dip gently northeast. These are internally foliated and contain small biotite porphyroblasts. **1.7**

49.6 (m.p. ~164.05) **STOP 1-3. Metamorphosed Wallace Formation.** A rock slide made up of large blocks of well-layered metamorphosed Wallace Formation with actinolite–diopside–plagioclase layers and biotite–quartzite layers. The largest block above the road shows a well-developed dilational pegmatite with thin aplite and pegmatite borders. Smaller blocks just below road and slightly east show a rippled-looking surface: are these preserved ripple marks or the intersection of a spaced cleavage with the layering and schistosity? **4.6**

54.2 (m.p. 159.5; 0.1 mi. northeast of Papoose Creek) Nearly vertical dark-gray synplutonic mafic dikes cut granite and metasedimentary rocks of the Idaho batholith border zone. The dikes trend nearly parallel to the roadcut. The dikes are metamorphosed and now consist of biotite–plagioclase rock. Strong foliation and slight lamination in the dikes are essentially parallel to the dike walls. Granite and pegmatite dikes up to 1.2 m thick cut the mafic dikes. **3.0**

57.2 (m.p. 156.45) Small pullout just east of curve on south side of road. **STOP 1-4. Early megacryst-rich Idaho batholith.** Megacryst-rich biotite granodiorite, apparently an early, complexly deformed phase of the Idaho batholith, shows complex veining by granitic dikes; the most photogenic exposures are in blocks below road and slightly east of highway pullout. K-feldspar megacrysts average about 2.5 × 4 cm and have white plagioclase rims. They are subhedral and make up 5 to 10% of the rock, though locally they make up 15 to 20 cm zones with up to 35% megacrysts. The groundmass contains no K-feldspar. Consider alternative origins for the K-feldspar megacrysts.

(a) Early formed phenocrysts? Consider magma/rock composition on an An–Ab–Or ternary diagram (not in the K-feldspar-first field). Why is there no K-feldspar in the groundmass? (no apparent peritectic relationship to eliminate K-feldspar).

(b) Late-magmatic grains (such a crystallization order would be plausible from experimental T-X_{H_2O} diagrams of Whitney, 1975), large because of higher water content of magma in late stages? Consider why they are subhedral and some have concentrically enclosed inclusions of other minerals in the rock. Replacement of preexisting groundmass? We believe this to be the correct explanation.

(c) Post-magmatic porphyroblasts. Note that one or two straddle granodiorite/country rock contacts. If they are isochemical metamorphic porphyroblasts, why is only the K-feldspar so coarse? Why the concentric inclusions? If they are metasomatic porphyroblasts, why are the K-feldspar porphyroblasts essentially confined to the granodiorite and not present in the country rocks?

Foliation oriented 140°/74°SW is marked by K-feldspar megacrysts, plagioclase, and biotite. Irregular criss-crossing veins of biotite–quartz–feldspar pegmatite and alaskite are 1 to 10 cm thick. Dikes of layered medium-grained granite are up to 1 m thick and locally as much as 3 and 6 m thick. The subtly graded layers have variable mafic content and grain size with "tops" up. **7.6**

64.8 (m.p. 148.9) **STOP 2-5. Quartz diorite orthogneiss.** Unit continues from 144.55 to 156.5. A big roadcut in dark-gray, biotite-rich quartz diorite orthogneiss is cut by many criss-crossing pegmatite and alaskite dikes 1 to 60 cm wide. Plagioclase making up about 40% of the rock occurs as 4 to 7 mm subhedral white grains. Scattered translucent megacrysts of K-feldspar have white rims of plagioclase 1 or 2 mm thick. Quartz diorite orthogneiss cuts layered paragneiss (metamorphosed Belt?). One planar, subhorizontal fine-grained mafic dike 30 to 60 cm thick cuts the other rocks. **7.0**

71.8 (m.p. 141.9) Main-phase biotite granite with 1–2% K-feldspar megacrysts. A few faint schlieren are at N55°W/37°NE. Very fine-grained, dark-gray mafic dikes 15 to 30 cm thick cut the granite. The mafic dike at southwest end of outcrop (near 141.85) shows foliation oblique to its borders. **0.1**

71.9 (m.p. 141.85) **STOP 1-5. Main-phase Idaho batholith.** Essentially massive-megacryst-bearing, main-phase granite. Faint 2 to 5 cm schlieren are at N40°W/45°NE. Very irregular 15 to 60 cm mafic dikes cut the granite on curved fractures. One mafic dike contains a 2 × 5 cm xenolith of medium-grained granite. **2.6**

74.5 (m.p. 139.2) **STOP 2-4. Idaho batholith showing complex interaction with mafic dike magmas.** Granodiorite complex exposed back to 139.1 shows complex interactions between magmas. Medium-grained biotite granodiorite is inhomogeneous, has more felsic zones, more mafic zones, and granitic pegmatites. Zones rich in pink K-feldspar appear to be associated with crosscutting joints and are probably alteration zones imposed in Tertiary time. The granodiorite is cut by a mafic dike and contains angular mafic xenoliths resembling the dike. The granodiorite is in curving, irregular contact with a

finer-grained, more mafic phase which is cut by pod-shaped masses and dikes of granite. The more mafic phase contains angular xenoliths of fine-grained mafic dike material that are, in turn, cut by fine-grained, light-gray felsic dikelets 1 to 6 mm thick. The granodiorite has more mafic areas, swirled more mafic granodiorite, and granitic patches (some rounded and some swirled with granodiorite). Another sheet of mafic rock, less than 1 m thick and 5 m long, is cut by pegmatites higher in the outcrop. Masses of mafic rock and granitic areas become larger and more defined; most of the mafic xenoliths are cut by ptygmatic veins of granite.

Below the road, at the stream edge (behind the "anglers" sign), a large, light-colored block of rock about 2 m across shows nearly white, medium-grained granite cutting 15 cm layers of mesotype medium-grained biotite granodiorite that is foliated oblique to the granite. The granite is also weakly foliated subparallel to layers in the granodiorite. Both granite and granodiorite are cut by planar joints about 80° to the foliation, which show pink, medium-grained K-feldspar alteration zones about 2 cm wide. This alteration was probably associated with Tertiary intrusions nearby. Oblique diffuse shears about 30° to the layers, combined with the foliation, resemble mylonitic S–C surfaces. **4.9**

79.4 (m.p. 134.3) Good, somewhat weedy pullout on south side of road. **STOP 2-3. Synplutonic mafic dikes in Idaho batholith.** A sample of quartz monzodiorite at 134.15 has been dated at 66 Ma—U–Pb zircon lower intercept of 66 Ma (Schuster and Bickford, 1985). Three dikes in the roadcut show synplutonic mafic-dike relationships. The dike at the southwest end of the roadcut is thin, poorly exposed, and mylonitic. The thick (3.2 m) dike in the center of the cut is fine-grained, gray basaltic andesite to andesite with some areas containing 1 to 2 mm mafic spots. The dike is very inhomogeneous, consisting of many rounded inclusions or blobs of andesite with thin rims of felsic material and a matrix of andesite. It contains one 5 cm rounded inclusion of granite.

The mafic dike on the northeast end of the roadcut curves and steepens upward into a thick sheet or sill which shows clear synplutonic relationships with the host granite. It is somewhat finer-grained, having been chilled against the intruded granite. Numerous granitic dikes and ptygmatic granitic pods injected into the thick mafic sheet are contorted and pinch and swell. Some seem to surround pillows of andesite. Below the mafic sheet, the granitic rock is contaminated to a very inhomogeneous granodiorite to quartz diorite to granodiorite with many felsic and mafic inclusions. The more mafic granitoid rocks from high on the outcrop can be sampled in the loose material in the borrow pit. A loose block halfway down to the river and 5 or 6 m downstream from the thickest dike shows fine-grained, dark-gray dike rock laced with medium-gray, more felsic dikelets. Several other blocks nearby show the same. **5.7**

85.1 (m.p. 128.55 to 128.7) Synplutonic gabbroic/peridotite complex. The brownish-weathering peridotite or hornblende pyroxenite in the central part of the long exposure may be a differentiated magma chamber of the "mafic dike magma"(?). Also present is hornblende-rich (~50%) metagabbro.

To the southwest is a hornblende diorite to biotite granodiorite injection zone, probably a zone of mixing between mafic and felsic magmas. The mafic mineral content is highly variable and the lighter-colored phases contain darker inclusions. Sharply bounded xenoliths of more mafic diorite are enclosed. Farther southwest these rocks are cut by granodiorite to granite. **0.1**

85.2 (m.p. 128.45) State of Idaho Highway Maintenance Shop. **3.5**

88.7 (m.p. 125.0) Pullout on south side of road. **STOP 2-2. Synplutonic mafic dikes, magma mingling.** Walk through 125.0–124.9 and consider the total percentage of "mafic" dike material. There are numerous dikes and many dike–granite relationships. The mafic dikes show sharp to moderately sharp, irregular to planar contacts to granitoid rock. Some dikes are foliated and veined at a large angle to contacts; 3 mm mafic "phenocrysts" are now altered. The granodiorite is inhomogeneous. Some dikes are lineated, have streaks of granitoid material, and contain numerous small mafic spots (pseudomorphs of small mafic phenocrysts). Angular xenoliths of metaandesite contain 1–2 mm mafic spots in granodiorite. Some dikes show intermingling of andesite and granite. Granitoid areas in some dikes are more contaminated by the mafic dike magma. One dacite dike shows veins, streaks, spots, megacrysts, inclusions of felsic material, and a xenolith of a mafic dike. One area of small dikes grades out into schlieren. Note that boulders near river at 124.95 show mafic dikes grading into pillows and schlieren.

About 400 m downstream from m.p. 125 (23 m downstream from Noseeum Creek flowing under the road in a huge pipe), and below the road, is a loose block showing medium-grained granite in contact with fine-grained, dark-gray, elongate inclusions of mafic dike material, which are surrounded by a "mixed" zone of intermediate composition and grain size. **2.6**

91.3 (m.p. 122.4; near big pine tree on outside bend of road) Pulloff on south side of road at 122.5. **STOP 2-1A. Comingling mafic and felsic magmas.** This large area of mafic dike rock is marginally exposed, but shows much interaction with the granite. Upslope ~8 m are some good exposures of comingled mafic and felsic magmas. The granite contains a few 2 to 10 cm subrounded xenoliths of mafic dike rock. Many good, clean exposures are in loose blocks on mid-slope between road and river—especially 30 m upstream to 40 m downstream from the big pine tree. **3.8**

95.1 (m.p. 118.6) Mafic dikes with xenocrysts(?). Massive, intermediate-composition mafic dikes have very small gabbroic xenoliths, now altered white. One dike has chilled margins. The mafic dikes cut biotite granite with some K-feldspar megacrysts. Country rock to the west, across a steeply dipping fault, is a foliated migmatitic calc-silicate gneiss containing

much diopside. Alaskite dikes 1 to 8 cm thick criss-cross the outcrop of gneiss, the most prominent set dipping 15°NW. **2.6**

97.7 (m.p. 116.0) Massive main-phase granite. A large, irregular xenolith of contorted biotite-rich gneiss is enclosed in the granite which also shows faint but distinct schlieren. A few gently dipping pegmatite dikes, 2 to 45 cm thick, cut the granite and are discordant to the mafic schlieren. A steeply dipping, dark-gray, fine-grained andesite dike, 8 to 12 cm thick, cuts the granite. Another basaltic dike appears as a large angular "patch" with a chilled border on one side and sheared on the other side. A pod of fine-grained rhyolite (Eocene?) about 2 m thick dips 10 to 20°NE and has a wavy contact with the granite. **3.5**

101.2 (m.p. 112.5) **STOP 1-6. Gneiss cut by layered granite sheet.** Biotite quartzofeldspathic gneiss and veined gneiss with foliation oriented 107°/78°NE is cut by a subhorizontal, layered granite sheet. The layered granite sheet is graded with mafic grains concentrated toward the base of each 2 to 30 cm thick layer. This layered granite sheet from m.p. 112.4 to 112.75 is about 1 to 3 m thick and cuts main-phase granite. It may represent movement on a subhorizontal shear in the late stages of crystallization of the granite (a late magmatic "mylonite" zone). The layered granite sheet is cut at m.p. 112.65 by a gently dipping, 2 to 5 cm thick muscovite–quartz–feldspar pegmatite. A fine-grained, greenish-white rhyolitic dike about 5 m thick cuts both the layered granite sheet and the thin later pegmatite at m.p. 112.70. **1.2**

102.4 (m.p. 111.3) Main-phase granite of the Idaho batholith contains about 10% megacrysts of K-feldspar; most of the megacrysts are about 1 × 2 or 3 cm. The rock is rather inhomogeneous in places; some gneissic schlieren contain steeply plunging folds. **0.8**

103.2 (m.p. 110.5) Intrusion breccia at contact of granodiorite cutting biotite-rich country rock with somewhat contorted, near-vertical foliation. The folds plunge very steeply. A gently southwest-dipping pegmatite dike about 2 m thick cuts the intrusion breccia. Just to the east is massive fine- to medium-grained granodiorite containing many wavy, streaky xenoliths and schlieren. Several pegmatite dikes 5 to 75 cm thick dip gently northwest. **1.2**

104.4 (m.p. 109.3) Calc-silicate gneiss (Wallace Formation?) in metamorphosed Belt Group with steep foliation is cut by subconcordant, irregular veins of streaky hornblende granodiorite and a few 8 cm thick veins of aplite. **4.5**

108.9 (m.p. 104.75) **STOP 2.1. Early megacryst-rich tonalitic unit.** The best exposures are in blocks between road and river. This megacryst-rich biotite granodiorite is a tonalitic rock with K-feldspar megacrysts. K-feldspar megacrysts also exist in some granitic dikes that cut the megacryst granodiorite. This unit cuts and locally contains xenoliths of biotite–quartz schist that may be metamorphosed Belt. Megacrysts and biotite define a steep foliation; small folds in the schist plunge 63° → 125°. Foliation of megacrysts is crenulated on a decimeter scale. The rock becomes strongly sheared and even mylonitic on some limbs; the megacrysts become augen in the sheared areas. Undeformed discordant granitic dikes up to 40 cm thick cut the megacryst granodiorite parallel to the axial planes of the crenulations. A few mafic dikes show mutually cross-cutting relationships with megacryst granodiorite and approximately parallel the most attenuated or sheared limbs of crenulations of granodiorite. The mafic dikes are themselves foliated.

The sequence of events appears to be: (1) intrusion and foliation of the megacryst granodiorite; (2) intrusion of mafic dikes, probably overlapping with crenulation of the megacryst granodiorite; and (3) intrusion of granitic dikes parallel to the crenulations. If the biotite–quartz schist is metamorphosed Belt, the megacryst granodiorite cannot be pre-Belt basement and is presumed to be early phase Idaho batholith. **1.4**

110.3 (m.p. 103.4) Eocene dikes containing euhedral phenocrysts of quartz. **0.2**

110.5 (m.p. 103.15) Foliated biotite-tonalitic orthogneiss shows mafic schlieren, xenoliths, and diffusely bounded pegmatitic phases. **1.1**

111.6 (m.p. 102.1) High-grade migmatite. A medium-grained, laminated, biotite–quartz–feldspar gneiss with foliation at 116°/76°NE is cut by a concordant biotite–quartz–feldspar pegmatite 2 m or more thick, and by a steeply dipping, dark-gray, fine-grained 60 cm andesite dike with 30% plagioclase phenocrysts. **5.2**

116.8 (m.p. 96.85, near bridge across Lochsa River at Lowell) A medium-grained kyanite–biotite quartzofeldspathic gneiss is foliated at 145°/52°SW. The schistosity is crenulated on the scale of the 1 to 3 mm grains. Metasedimentary rocks in this region west of the contact of the Idaho-Bitterroot batholith have been described by Greenwood and Morrison (1973) and Reid et al. (1979). Farther west, the flood basalts of the Columbia River Plateau have filled the ancestral valley of the Clearwater River and are, in places, exposed near the road. Still farther northwest, toward Orofino, long roadcuts on the south side of the Clearwater River expose diorites and tonalites of the Late Cretaceous Kamiah plutonic complex.

References

Armstrong, R. L., Taubeneck, W. H., and Hales, P. O., 1977, Rb–Sr and K–Ar geochronometry of Mesozoic granitic rocks and their Sr isotopic composition, Oregon, Washington, and Idaho: Geological Society of America, Bulletin, 88: 397–441.

Chase, R. L., 1973, Petrology of the northeast border zone of the Idaho batholith, Bitterroot Range, Montana: Montana Bureau of Mines and Geology, Memoir 43: 28 pp.

Chase, R. L., and Johnson, B. R., 1977, Border-zone relationships of the northern Idaho batholith: Northwest Geology, 6-1: 38–50.

Fleck, R. J., and Criss, R. E., 1985, Strontium and oxygen isotope variations in Mesozoic and Tertiary plutons of central Idaho: Contributions to Mineralogy and Petrology, 90: 291–308.

Greenwood, W. R., and Morrison, D. A., 1973, Reconnaissance geology of the Selway–Bitterroot Wilderness Area: Idaho Bureau of Mines and Geology, Pamphlet 154: 30 pp.

Hietanen, A., 1961, Relationship between deformation, metamorphism, metasomatism, and intrusion along the northwest border zone of the Idaho batholith, Idaho: U.S. Geological Survey, Professional Paper 424-D: 161–164.

Hietanen, A., 1962, Metasomatic metamorphism in western Clearwater County, Idaho: U.S. Geological Survey, Professional Paper 344-A: 116 pp.
Hyndman, D. W., 1983, The Idaho batholith and associated plutons, Idaho and western Montana; *in* Roddick, J. A. (ed.), Circum-Pacific Batholiths: Geological Society of America, Memoir 159: 213–240.
Hyndman, D. W., 1984, A petrographic and chemical section through the northern Idaho batholith: Journal of Geology, 92: 83–102.
Hyndman, D. W., and Foster, D. A., 1988, The role of tonalites and mafic dikes in the generation of the Idaho batholith: Journal of Geology, 96: 31–46.
Hyndman, D. W., Alt, D., and Sears, J. W., 1988, Post-Archean metamorphic and tectonic evolution of western Montana and northern Idaho; *in* Ernst, W. G. (ed.), Metamorphism and Crustal Evolution of the western United States: Prentice Hall, Englewood Cliffs, N.J., pp. 332–361.
Jens, J. C., 1974, A layered ultramafic intrusion near Lolo Pass, Idaho: Northwest Geology, 3: 38–46.
Nold, J. L., 1974, Geology of the northeastern border zone of the Idaho batholith, Montana and Idaho: Northwest Geology, 3: 47–52.
Reid, R. R., 1987, Structural geology and petrology of a part of the Bitterroot lobe of the Idaho batholith; *in* Vallier, T. L., and Brooks, H. C. (eds.), Geology of the Blue Mountains Region of Oregon, Idaho, and Washington: The Idaho Batholith and Its Border Zone: U.S. Geological Survey, Professional Paper 1436: 37–58.
Reid, R. R., Morrison, D. A., and Greenwood, W. R., 1973, The Clearwater orogenic zone: A relic of Proterzoic orogeny in central and northern Idaho: Belt Symposium, University of Idaho, Moscow, pp. 10–56.
Reid, R. R., Bittner, E., Greenwood, W. R., Ludington, S., Lund, K., Motzer, W. E., and Toth, M., 1979, Geologic section and roadlog across the Idaho batholith: Idaho Bureau Mines and Geology, Information Circular 34: 20 pp.
Rice, J. M., 1987, Polymetamorphism in northern Idaho: a schistose scenario of Belt and batholith: Geological Society of America, Abstracts with Programs, 19(7): 818.
Ross, D. C., 1985, Mafic gneiss complex (batholith root?) in the southernmost Sierra Nevada, California: Geology, 13: 288–291.
Schuster, R. D., and Bickford, M. E., 1985, Chemical and isotopic evidence of the northeastern Idaho batholith: Journal of Geology, 93: 727–742.
Snee, L. W., Lund, K., and Davidson, G., 1987, Ages of metamorphism, deformation, and cooling of juxtaposed oceanic and continental rocks near Orofino, Idaho: Geological Society of America, Abstracts with Programs, 19(5): 335.
Strayer, L. M., IV, Hyndman, D. W., and Sears, J. W., 1987, Movement direction and displacement estimate in the western Idaho suture zone mylonite: Dworshak Dam/Orofino area, west central Idaho: Geological Society of America, Abstracts with Programs, 19(7): 857.
Taubeneck, W. H., 1971, Idaho batholith and its southern extension: Geological Society of America, Bulletin, 82: 1899–1928.
Toth, M. I., 1987, Petrology and origin of the Bitterroot Lobe of the Idaho batholith; *in* Vallier, T. L., and Brooks, H. C. (eds.), Geology of the Blue Mountains Region of Oregon, Idaho, and Washington: The Idaho Batholith and Its Border Zone: U.S. Geological Survey, Professional Paper 1436: 9–35.
Wehrenberg, J. P., 1972, Geology of the Lolo Peak area, northern Bitterroot Range, Montana: Northwest Geology, 1: 25–32.
Whitney, J. A., 1975, The effects of pressure, temperature, and X_{H_2O} on phase assemblages in four synthetic rock compositions: Journal of Geology, 83: 1–81.
Wiswall, G., and Hyndman, D. W., 1986, Emplacement of the main plutons of the Idaho batholith; *in* Vallier, T. L., and Brooks, H. D. (eds.), Geology of the Blue Mountains Region of Oregon, Idaho, and Washington: The Idaho Batholith and Its Border Zone: U.S. Geological Survey, Professional Paper 1436: 59–72.

Volcanism and plutonism at shallow crustal levels: The Elkhorn Mountains Volcanics and the Boulder batholith, southwesern Montana

Carolyn Rutland[1], Harry W. Smedes[2], Robert I. Tilling[3], and William R. Greenwood[4]
[1]*Science Application International, Las Vegas, Nevada 89109;* [2]*6340 Americana Dr., Apt. 304, Willowbrook, Illinois 60514;*
[3]*U.S. Geological Survey, Menlo Park, California 9402S;* [4]*U.S. Geological Survey, Reston, Virginia 22092*

Introduction

The Upper Cretaceous Elkhorn Mountains Volcanics (EMV) and Boulder batholith of southwestern Montana provide an example of a large-volume, epizonal, volcanic—plutonic complex whose deep level of erosion has exposed the co-genetic intrusive rocks while preserving sizeable portions of the volcanic field (Robinson et al. , 1968; Klepper et al. , 1971). Such a volcanic—plutonic association provides a unique opportunity for evaluation of many aspects of the evolution of a shallow-crustal magmatic system, such as geochemical relations of both the volcanic and plutonic rocks and the nature of intrusive—extrusive relationships at the present level of exposure. Studies of these have contributed to an improved understanding of the processes and mechanisms controlling the earliest and latest development of a large, complex magmatic system and its subsequent modification.

The many geologic, geophysical, and geochemical aspects of the EMV and the Boulder batholith are consistent with the accepted model of the general caldera cycle considered typical of eroded ash-flow fields, such as the San Juan field in southwestern Colorado (Steven and Lipman, 1976) and the Timber Mountain—Oasis Valley caldera complex in southern Nevada (Byers et al. , 1976), and its subjacent, cogenetic plutonic system (Lipman, 1979, 1984). During the early evolution of the magmatic system, volcanic activity was the surface manifestation of the igneous system, producing the variety of primary and reworked eruptive materials in the EMV, most importantly lava flows and ash-flow sheets. During this period, the sources of the ash flows and lava flows of the EMV may have comprised several superimposed calderas and vents, whose eruptive products overlapped. Although each eruptive episode would have tapped its own localized magma chamber, all were probably related to a larger, complex magmatic system whose final crystallization products were the plutons of the Boulder batholith. Indeed, the development of the cogenetic plutonic

rocks may be broadly traced within the same time frame. Thus, each cycle of volcanic activity reflects the upward movement of magma, climaxing with ash-flow eruption and the failure of the roof of a particular chamber or cupola, and then waning as the remaining material cooled. The final cooling and crystallization stages of the magmatic system resulted in the plutons of the Boulder batholith.

For many years, but principally from 1949 to 1970, the EMV and the Boulder batholith were the focus of field and laboratory research by members of the U.S. Geological Survey. The northeastern part of the EMV—Boulder batholith complex lies within the proposed Elkhorn Wilderness Study Area, whose economic potential was evaluated jointly by the U.S. Geological Survey and the U.S. Bureau of Mines (Greenwood et al. , 1978).

The following summary of the regional igneous relationships is from these references and our own unpublished work. Potassium—argon ages cited in this guidebook have been recalculated using the decay constants of Steiger and Jager (1977) now accepted in geochronology, and thus are slightly older than the published ages. Most of the field mapping of the EMV—Boulder batholith complex was done before 1972, and the classification and nomenclature used in nearly all the original sources we cite are slightly modified from Johannsen (1939), as shown in Fig. 1A. For continuity and consistency, we continue to use that scheme rather than the more recent and now commonly accepted classification and nomenclature of Streckeisen (1973, 1976) shown in Fig. 1B. For example, rather than renaming over 75% of the exposed batholith the " Butte granite/monzonite," we continue to refer to the Butte Quartz Monzonite by its formal stratigraphic name of the modified Johannsen (1939) classification.

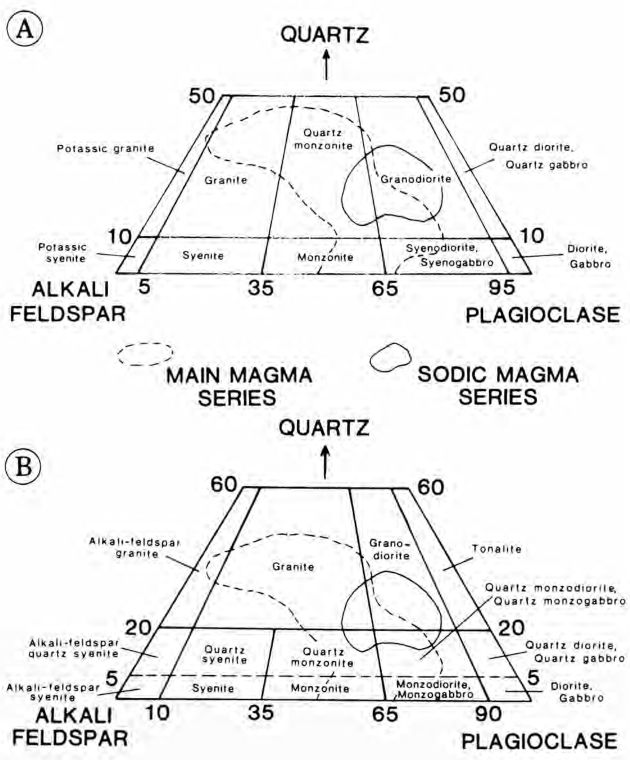

FIGURE 1-Classification and nomenclature of plutonic rocks: **A,** scheme used in this paper (modified from Johannsen, 1939); **B,** scheme of Streckeisen (1976). Fields of modes of rocks of the Boulder batholith from Tilling (1973, fig. 16).

Regional geologic setting

The EMV—Boulder batholith region is east of the Idaho batholith within th Helena salient of the frontal Cordilleran fold and thrust bet (Fig. 2). The region is dominated by Sevier-style thrusting on the north, whereas the southernmost part of the volcanics and older rocks are folded and, like the southern satellite plutons, faulted in structures related to Laramide-style deformation of the Rocky Mountain foreland (Schmidt and Hendrix, 1981). These two structural styles developed coevally from Late Cretaceous to late Paleocene time (about 80 to 60 Ma ago). Eruption of the EMV took place from about 81 to 76 Ma, partly overlapping emplacement of the Boulder batholith, which took place from approximately 80 to 70 Ma ago (Tilling et al. , 1968).

The Elkhorn Mountains Volcanics

General statement

The Elkhorn Mountains Volcanics (EMV) are most extensively preserved in the Elkhorn Mountains, located about 30 km southeast of Helena, Montana, and discontinuously cover much of the region ringed by the cities and towns of Deer Lodge, Helena, Townsend, Three Forks, Whitehall, and Butte (Fig. 2). They are the remnants of an extensive volcanic field estimated to have covered nearly 26,000 km^2, to have been at least 3.5 km and perhaps as much as 4.6 km thick (Smedes, 1966), and to have comprised one of the earth's largest ash-flow fields (Smith, 1960). The EMV were intruded by the Boulder batholith and make up much of its margins and remaining roof (Fig. 3).

Klepper et al. (1957) divided the volcanics into three informal volcanogenic members. We have retained that terminology here for convenience in referring to a specific part of the volcanic pile, although no correlations of lithostratigraphic or chronostratigraphic boundaries have been established from one mountain range to another. There is no formal stratigraphy for the EMV.

The lower member is locally as much as 1500 m thick; it consists predominantly of lava flows, autobrecciated lavas, mudflow breccia, water-laid volcaniclastic rocks, and sparse, thin sheets of andesitic ash-flow tuff. The middle member is as much as 2500 m thick in places. It consists of numerous sheets of rhyolitic welded tuff and interbedded andesitic and basaltic volcaniclastic rocks. The upper member ranges widely in thickness and is at least 600 m in places. It consists dominantly of reworked material of the middle and lower units, together with some juvenile ash. The deposits largely accumulated in fault-bounded depressions and in stream beds. In its northernmost exposures (Fig. 3), the upper member is comprised of a large field of basalt lava flows and flow breccia.

During and following deposition of the upper unit, faulting became more intense in places and parts of the volcanic pile foundered into shallow magma reservoirs which resulted in complex intrusive masses with related sills and dikes.

Agglomerate, other deposits of vent facies, and remnants of stratovolcanoes indicate that sources of the basaltic and andesitic deposits are widespread. Although deep erosion has obliterated all geomorphic expression (calderas), we have used characteristics and informal criteria of cauldrons (Lipman, 1984) to infer the probable sites of cauldrons (Fig. 3). Evidence includes stratigraphic characteristics, such as abrupt thickening of welded tuff toward a central location,

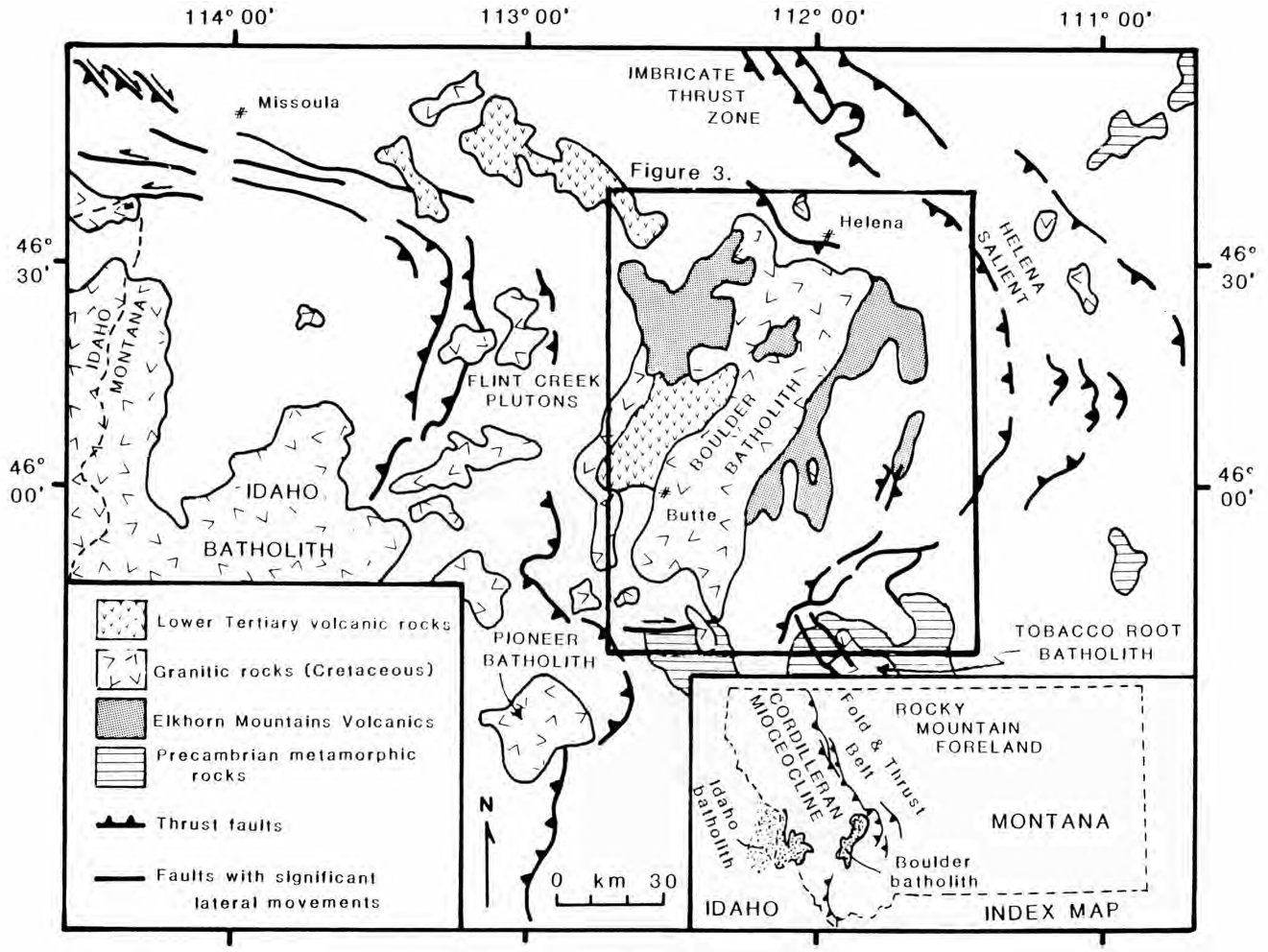

FIGURE 2—The tectonic setting of the EMV—Boulder batholith region (after Schmidt et al., 1979). Area of Fig. 3 shown by outline.

units interpreted as chaotic intracaldera fill, arcuate faults separating significantly different volcanic units, and ring dikes. We have emphasized in particular what we suspect to be roots of eroded cauldrons; we will examine one of these sites at Stop 1-2.

Geochemistry of the Elkhorn Mountains Volcanics

The geochemistry of the EMV is not well understood; difficulties in interpretation arise from alteration of original compositions by various post-eruption processes. From regional analyses, Tilling (1973, 1974a) described the EMV as differing in composition among the lower and middle members, as well as from many of the plutonic units. Table 1 gives representative analyses of some units of the EMV and the Boulder batholith.

A recent systematic study of the geochemistry of lava flows and ash-flow sheets in the southern Elkhorn Mountains (Rutland et al. , 1984; Rutland, 1985, 1986) shows this particular sequence to be characterized by relatively constant Th/Ta ratios and enrichment of Ce, Ta, Hf, Zr, Yb, and Th. The common parent magma of the EMV and the Boulder batholith was probably high-K calc-alkaline, as suggested by the relatively high Zr and Hf abundances in these rocks. These chemical signatures are consistent with the hypothesis that these volcanic rocks are related by evolution of a single magmatic source. The entire magma system may have been far more heterogeneous; it is not known how representative the sequence studied in detail by Rutland is of the entire EMV field. The whole EMV magmatic system probably consisted of several separately evolving, but perhaps physically linked, large magma bodies. As shown by Tilling (1974a), very few analyses of the EMV, regardless of strati-graphic position, fall within the compositional fields for Butte Quartz Monzonite and related silicic facies, which make up more than three-quarters of the batholith. Yet, many analyses of the ash flows of the middle member of the EMV plot within a more silicic and potassic extension of the field for these predominant plutonic rocks, suggesting that these voluminous silicic ash flows were probably derived from the same magma that mostly crystallized subsurface to form the Butte Quartz Monzonite" (Tilling, 1974a, fig. 2 and p. 1925).

The Boulder batholith

General statement

The Boulder batholith is a composite calc-alkalic intrusive body comprised of numerous coalesced epizonal plutons and isolated satellitic plutons that range from potassic ultramafic rocks and melagabbro, through granodiorite and quartz monzonite to granite and syenite. It is exposed over an area of about 5700 km^2 (Klepper et al. , 1974). The batholith is an elongate, north-northeast-trending body of about 100 by 50 km. The largest pluton, the Butte Quartz Monzonite,

TABLE 1-Representative chemical analyses of some units of the Elkhorn Mountains Volcanics and the Boulder batholith. With two exceptions, the letter symbols for the units are the same as in Fig. 3: *Ki,* intrusive rocks contemporaneous with the Elkhorn Mountains Volcanics; *m,* mafic rocks; *gd,* granodiorite; *bqm,* Butte Quartz Monzonite; *f,* felsic quartz monzonite; *a,* alaskite; *inc*, mafic inclusion in *bqm; rc,* Rader Creek pluton; *d,* Donald pluton; *c,* Climax Gulch pluton.

Unit	Elkhorn Mountains Volcanics (Kv)							Boulder batholith										
	Lower member			Middle member			Ki	Main magma series							Sodic magma series			
								m	gd	bqm		f	a	inc	rc	d	c	
Sample Number**	1	2	3	4	5	6	7	8	9	10	11	12	13	14	15	16	17	18
SiO_2	52.7-60.0	59.3-65.7	59.6	71.6	65.6-69.6	71.2	54.8	54.5	61.14	64.8	64.92	71.5	76.7	58.8	62.3	70.4	65.18	72.5
$A1_2O_3$	12.5-16.5	16.6-17.3	17.4	15.4	16.7-17.1	15.2	15.1	12.4	15.28	15.7	15.46	14.2	12.4	15.4	16.8	15.3	15.60	14.8
Fe_2O_3	} 10.2-6.8*	3.4-2.5	3.3	1.2	2.3-1.8	1.2	2.3	1.0	1.90	1.9	1.81	1.2	0.6	2.5	2.7	1.6	1.77	0.89
FeO		2.7-4.3	3.2	0.73	1.1-1.4	0.77	6.0	6.8	4.52	2.8	2.70	1.4	0.77	4.2	2.8	1.1	2.66	0.92
MgO	10.9-1.7	2.0-2.2	2.6	0.60	2.5-0.66	0.65	5.0	11.4	3.41	2.2	2.05	0.93	0.14	3.6	2.3	0.66	2.20	0.51
CaO	8.3-4.6	4.6-4.0	5.2	1.5	2.6-1.4	1.7	8.1	6.8	5.51	4.4	4.24	2.9	0.81	5.4	5.3	2.6	4.14	1.8
Na_2O	1.8-3.4	2.1-1.7	2.6	2.6	2.6-4.2	3.6	2.1	2.2	2.78	3.1	3.06	2.9	2.2	2.7	3.4	4.0	3.09	3.6
K_2O	3.0-4.1	4.3-3.9	3.4	5.2	5.4-4.5	5.0	0.64	3.2	3.34	3.9	3.94	4.2	5.8	5.6	2.6	3.4	3.75	3.7
TiO_2	0.79-1.1	0.78-0.85	0.72	0.4	0.84-0.75	0.46	0.90	0.59	0.82	0.60	0.53	0.26	0.13	0.69	0.51	0.26	0.54	0.29
P_2O_5	0.41-0.48	0.37-0.39	0.34	0.14	0.2-0.09	0.04	0.46	0.42	0.26	0.19	0.18	0.16	0.90	0.26	0.23	0.12	0.19	0.09
MnO	0.15-0.12	0.14-0.09	0.16	0.04	0.07-0.14	0.08	0.17	0.12	0.12	0.08	0.09	0.08	0.02	0.17	0.14	0.08	0.10	0.06
H_2O^+		1.3-1.5		}0.51	1.2-0.46		}2.8	}0.68	}0.65		0.59	}0.42	}0.42		0.71	}0.52	0.57	0.80
H_2O^-		0.5-0.1			0.1-0.12						0.12				0.22		0.13	0.07
CO_2		1.7-0.01		0.08	0.05-0.03		1.8	<0.05	0.09		0.06	0.06			<0.05	0.06	0.02	<0.05
BaO									0.08		0.09							
S									0.01		0.05							
Loss on ignition	1.6-2.05		1.5			0.31				0.57				0.36				

makes up over 75% of the exposed batholith. Estimates of thickness of the batholith range widely (Tilling, 1974b), from less than 5 km (Hamilton and Myers, 1974) to more than 15 km (Klepper et al. , 1974). Radiometric-age determinations for the batholith range from approximately 80 to 70 Ma; the Butte Quartz Monzonite was probably emplaced from 76 to 74 Ma ago (Tilling et al. , 1968). In general the younger plutonic rocks tend to be more felsic than the older ones, the leucocratic granodiorites and quartz monzonites being the youngest (Knopf, 1957, 1963; Tilling et al., 1968).

Two-magma-series model for the batholith

Tilling (1973) showed that most rocks of the Boulder batholith can be assigned to one of two magma series, the main (or potassic) series and the sodic series (Fig. 3). The main series, represented primarily by plutons in the northern and central parts of the batholith, is characterized by higher K_2 O and lower Na_2O at any given SiO_2 content than those of the sodic series. Plutons of the sodic series lie mostly in the southern part of the batholith. The distribution of Rb, Sr, Th, and U, and of Pb, O, and H isotopes also distinguishes the two groups (Tilling, 1973, 1977). In a trace-element study of the plutons in the southern part of the batholith, Lambe (1981) presented SiO_2 variation diagrams for Nb, Zr, Pb, Cu, and Ba that also exhibit different patterns for each magma series.

The differences between the two magma series cannot be ascribed simply to change in chemical and isotopic composition of magma with time, because the intrusive sequences of the two series overlap. For example, the granodiorite of Rader Creek is the earliest known member of the sodic series but is older than the Butte Quartz Monzonite of the main series. The Climax Gulch pluton (sodic series) is younger than the Butte Quartz Monzonite. All the members of the main series appear to have differentiated from a single parental magma, whereas the various plutons of the sodic series do not seem to be related by magmatic differentiation. Magmas that formed the sodic-series rocks are inferred to have been derived from two or more discrete sources of distinct Rb/Sr and Sr and Pb isotopic ratios, or from a single heterogeneous source characterized by intrinsic differences in Rb/Sr and Sr and Pb isotopic ratios from one part to another.

Collectively, interpretations of the isotopic data and chemical analyses support the results of mapping studies that indicate a cogenetic relationship between the EMV and the Boulder batholith (e.g., Klepper et al. , 1957; Robinson, 1963; Robinson et al., 1968; Smedes, 1966; Smedes et al. , 1988). Doe et al. (1968) concluded that the lead isotopic data for the batholith and the volcanics (represented by only two samples) are compatible with the inferred genetic relationship between them. Tilling (1973, 1974a) presented chemical and isotopic evidence comparing the EMV with the main and sodic series of the batholith and concluded that the volcanics resemble more closely the more mafic rocks of the plutonic main series and are distinctly different from any rocks of the sodic series" (Tilling, 1974a: 1925). The results of trace-element studies by Lambe (1981) are also consistent with a genetic relationship between the EMV and the plutonic main series. Hence the EMV only show chemical affinity with rocks of the main magma series, whereas they contain no known extrusive equivalents of the sodic magma series (Tilling, 1974a). These observations have been substantiated by a recent systematic study of the geochemistry of the EMV (Rutland et al. , 1984; Rutland, 1985, 1986).

We will make stops at representative plutons of each magma series (Fig. 3). Main series: Stop 1-3, early mafic plutons; Stops 2-1 and 2-2, the Butte Quartz Monzonite; Stops 2-4 and 2-5, late silicic facies. Sodic series: Stop 23, granodiorite of Rader Creek; Stop 2-5, Climax Gulch pluton.

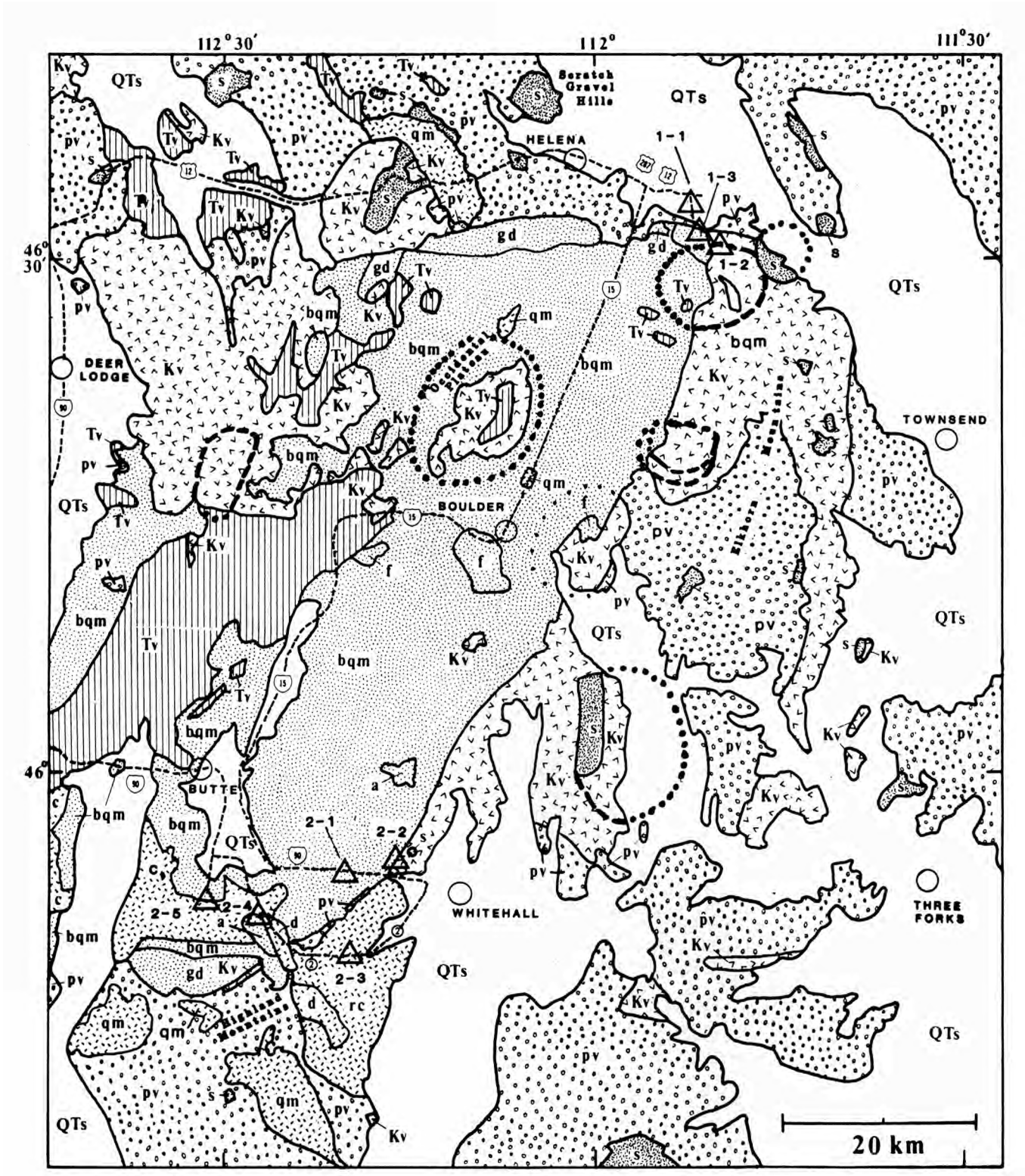

Shape and contact relations

Most plutons of the batholith and the satellitic stocks are steep-walled bodies. Exceptions include many of the aplite-alaskite—pegmatite bodies, which commonly are gently dipping sheets that cut other batholith rocks; the Moose Creek pluton, a moderately inclined irregular laccolith (Smedes et al. , 1980); and the granitic facies of the Climax Gulch pluton, which is overall sheet-like. The contact on the east margin of the batholith is remarkably straight; it consists chiefly of Butte Quartz Monzonite cutting the EMV and the granodiorite of Rader Creek. The straightness of this contact and of sheared rocks along it is interpreted as evidence for the emplacement of the eastern part of the Butte Quartz Monzonite along a preexisting fault zone of north-northeast trend, parts of which were obliterated by stoping during emplacement. About 30 km east of Butte, north of Interstate 90, the contact of the EMV and the batholith is a hybrid zone of rock so intensely sheared, recrystallized, and injected that the contact is blended (Stop 2-2). Near the northern end of the eastern margin, a downward-tapering screen

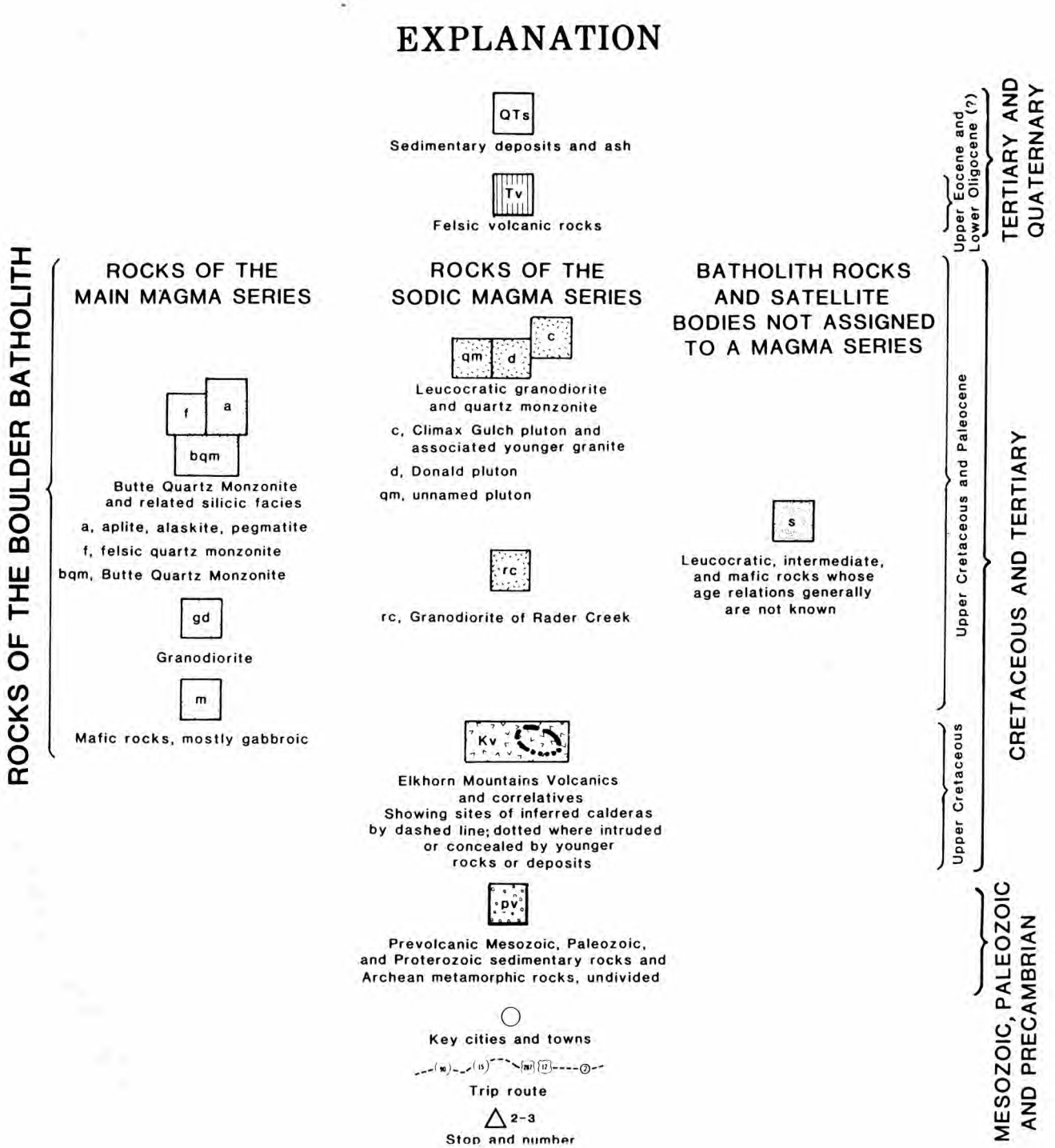

FIGURE 3—Generalized geologic map of the Boulder batholith region (after Smedes et al., 1988), showing plutons of the main and sodic magma series (after Tilling, 1973), inferred sites of possible eruptive sources (calderas) of the Elkhorn Mountains Volcanics (this work), and the route and stops of the field trip.

of sheared and thermally metamorphosed volcanic rocks separates the main batholith mass from a large dike-like lobe to the east. Near the southern end of the eastern margin, a narrow septum of sheared rocks, late Precambrian to Late Cretaceous in age, separates the Butte Quartz Monzonite from the older granodiorite of Rader Creek. North of the batholith, this fault offsets prevolcanic sedimentary rocks by at least 1000 m (west side up) and perhaps some left-lateral displacement.

Contact-metamorphosed Paleozoic and Mesozoic sedimentary strata wrap the north and south ends of the batholith and steepen toward the contact. At the north, the country rocks chiefly are in contact with granodiorite and early mafic rocks that predate the main mass of the batholith. The contact is highly irregular in detail, but overall the strike roughly parallels the south-dipping host rocks. However, at depth the batholith may steepen and dip northward, as suggested by the presence of satellitic stocks which probably are de-roofed cupolas of the main mass. The inferred gentle northward dip of the batholith is compatible with the formation

of a broad contact aureole, locally as much as 2.5 km wide, composed of hornfels and other contact-metamorphic rocks (Knopf, 1957; Rice, 1977). Metamorphic grade changes from pyroxene hornfels to albite—epidote hornfels facies with increasing distance from the batholith (Smedes, 1966).

At the south end of the batholith, the Paleozoic and Mesozoic country rock and primary foliation of the batholith strike about east—west and are vertical or steep. A zone of contact metamorphism, which is narrow compared with that at the north end, is consistent with the steep contact. Locally, forcible emplacement of the plutons is indicated by shearing, vertical stretching, and displacement of the country rock. The western wall of the batholith is buried beneath younger deposits, although many remnants of the roof are exposed in the western part of the batholith region. Those exposures reveal that roof generally dips gently westward.

Some late plutons of the batholith, including abundant bodies of aplite—alaskite—pegmatite, were emplaced along a north-northeast-trending zone along the central axis of the batholith. This zone also marks the locus of abundant late-stage veins (shown in detail by Becraft et al. , 1963, and Smedes, 1966), as well as dikes and plugs of post-batholith quartz latite and rhyolite. Discontinuous screens of pre-batholith volcanic and older rocks with complex fault relations lie near the western limit of the exposures of the batholith.

Collectively, the shapes of contact relations of the plutons indicate that faults of north-northeast trend played a prominent role before, during, and after batholith emplacement and post-batholith volcanism.

Internal structures

Most rocks of the Boulder batholith are massive and do not exhibit a strongly expressed fabric (Grout and Balk, 1934). However, the marginal parts of some plutons and, less commonly, their interiors show internal steep planar foliation, defined by parallel alignment of platy minerals and/or discoid inclusions, or gently dipping schlieren in roof zones. Locally, the plutonic rocks contain abundant mafic inclusions, composed of sharply outlined to diffuse aggregates of mafic minerals and plagioclase of the same composition as in the host rock.

In places, two or more distinct types of steep foliation are preserved in the same rock; these structures are well developed in plutons in the southwestern part of the batholith. An older foliation, consisting of aligned mafic minerals, mafic inclusions, and plagioclase, is interpreted to be caused by primary flow during pluton emplacement; a younger foliation, marked by aligned alkali-feldspar phenocrysts is interpreted to reflect late crystal growth along incipient joints that formed late in the cooling history, after the pluton had largely solidified. Joints that formed still later during the cooling of some main-series plutons, especially the Butte Quartz Monzonite, became the loci for injection of felsic rocks (principally aplite, alaskite, and pegmatite) and, very rarely, mafic rocks. In the granodiorite of Rader Creek, the emplacement of mafic bodies was in part joint controlled. Some later generations of fractures were occupied by metalliferous quartz veins and/or by thin dikes of diverse composition. We will examine some of these internal structures in the Butte Quartz Monzonite at Stops 2-1 and 2-5.

Description of stops and road log

We will spend two days examining the EMV—Boulder batholith complex, making stops at a possible cauldron rim, the intrusive contact between the Boulder batholith and the EMV, and a representative selection of the plutons of the main series and the sodic series.

Day 1

We will drive east from Helena on US-287/12. Road log begins at East Helena city limits. We plan to provide additional material including sketches and other geological information at some of the stops. These materials are not included in this article because of space limitations, but are available from the authors on request.

Mileage

0.0 Entering East Helena (city limit sign). **0.6**

0.6 Slag pile (on right) of East Helena smelter, one of five presently operating lead smelters in the world (1987). **0.7**

1.3 County Road 518 turnoff on right (south). Continue east on US-287/12. **1.8**

3.1 Turn right (south) onto gravel road. **0.6**

3.7 **STOP 1-1. Overview of geologic setting of the Elkhorn Mountains Volcanics.** The purpose of this stop is to point out some major geologic features related to the EMV and the Boulder batholith (Fig. 4). Location of traverse of Stop 1-2 can be seen from here. **3.2**

6.9 S-curve in road. Blocky outcrops to right and left are quartzite of the Pennsylvanian Quadrant Formation. **0.7**

7.6 BM 4684 (Louisville 7½′ quadrangle, NE¼ sec. 21, T9N, R2W). Brownish-weathered outcrop of syenogabbro on the left is part of the Kokoruda Ranch Complex of Smedes (1966). We will look at some of these rocks later at Stop 1-3. (This is the turnoff for Stop 1-3.) Continue south on gravel road. **1.1**

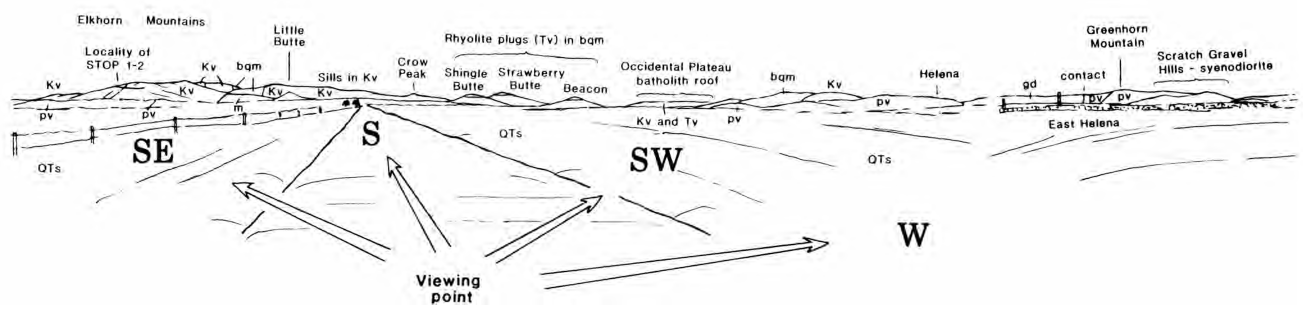

FIGURE 4—Views of major geologic features visible from Stop 1-1; arrows point to directions of view. Letter symbols in this and subsequent figures are same as those in Fig. 3.

8.7 Turn left (east) onto ranch road and drive through green metal gate. Permission for access to the property between the county road and the Helena National Forest Boundary ahead must be obtained from Bill and Ardis Kokoruda and Harley and Pat Ziesman, all of East Helena. **0.5**

9.2 Fork in road; take left fork. **0.8**

10.0 Helena National Forest Boundary. We drive on the Forest Service road approximately 2 mi en-route to Stop 1-2. We will pass the Chicago mine (11.4 mi), a breccia-pipe deposit developed at the contact between the lower and middle members of the Elkhorn Mountains Volcanics, which is marked by an intrusive andesite (Smedes, 1966: 106). More recent studies indicate that near the Chicago mine the lower and middle members are juxtaposed by a steep, down-to-the-south fault, interpreted to be the structural rim of a volcanic cauldron, and that the andesite is a steep dike intruded along that contact and interpreted to be a ring dike (Greenwood et al., 1978). The Chicago mine, the nearby Last Hope mine, and many unmapped prospect pits and shafts are developed at and near the contact of the dike with rocks of the middle member. The veins consist of quartz, carbonate minerals, pyrite, arsenopyrite, and small amounts of sphalerite and chalcopyrite. Gangue minerals are diopside, hedenbergite, garnet, tourmaline, epidote, and magnetite. The vein minerals fill fissures and partially replace the wall rocks. The mines were worked for gold but also produced small amounts of silver, lead, copper, and zinc. The upper parts of the veins are oxidized and yielded high-grade gold ore. The mineralogy and structural setting at the Chicago and Last Hope mines are similar to those of the Skyline mine, the site of another possible volcanic cauldron in the southern Elkhorn Mountains. **2.1**

12.1 **STOP 1-2. Examination of inferred structural rim of a volcanic cauldron. Lunch.** We will disembark from the vans, walk eastward on the road to the crest of the ridge, and make a traverse north along the ridge. The traverse will take us from the interior of an inferred cauldron and across its rim.

At this stop we will look at three rock types exposed in a continuous section of the lower, middle, and upper members of the EMV (Figs. 5, 6). The rocks to be traversed exhibit characteristics interpreted as the structural rim of a deeply eroded volcanic cauldron. Given the deep level of exposure of the EMV, the petrologic and structural relations from such locations are the best evidence of ancient calderas (Figs. 3, 5).

1-2a: The youngest rock type we will examine is the lower part of a densely welded tuff of the middle member of the EMV. The entire unit is about 425 m thick and is laminated at the top. The middle and lower parts, interpreted as intracaldera fill, are chaotically arranged blocks of laminated and unlaminated welded tuff, some 30 m in diameter.

1-2b: To the north, the andesite dike, about 130 m wide, intrudes the welded tuff. The south 15 m of the dike is of pépérite, formed by a mixing of magma and country rock, each retaining its identity even on a microscopic scale. Clastic dikes are also

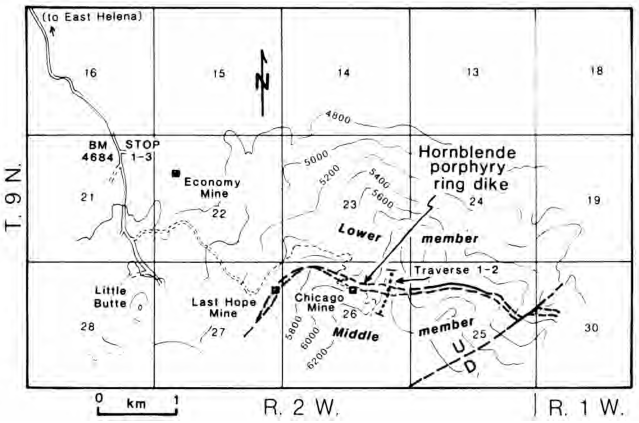

FIGURE 5—Sketch map showing rocks and contact relations of the Elkhorn Mountains Volcanics at Stop 1-2 (simplified from Smedes, 1962, pl. 1), interpreted to indicate the possible structural rim of a cauldron. Note location of Stop 1-3. Selected contours given in feet.

present. Pépérite and associated clastic dikes are common in the EMV, and are interpreted as caused by magma intruded into semiconsolidated moist sediment that is only shallowly buried. This implies that the dike was only slightly younger than the sediments. The pépérite contains about 50% clasts, some of which are as large as 1 m in diameter. We interpret this intrusion as a ring dike and hypothesize the following sequence of events: ash-flow eruption, caldera collapse, several episodes of thick infilling of intracaldera ash flow, separated by intermittent episodes of subsidence that caused chaotic jumbling and rheomorphism of welded-tuff blocks and formation of ponds into which sediment was deposited; injection of the ring dike along the caldera rim, locally mixing with the moist sediment

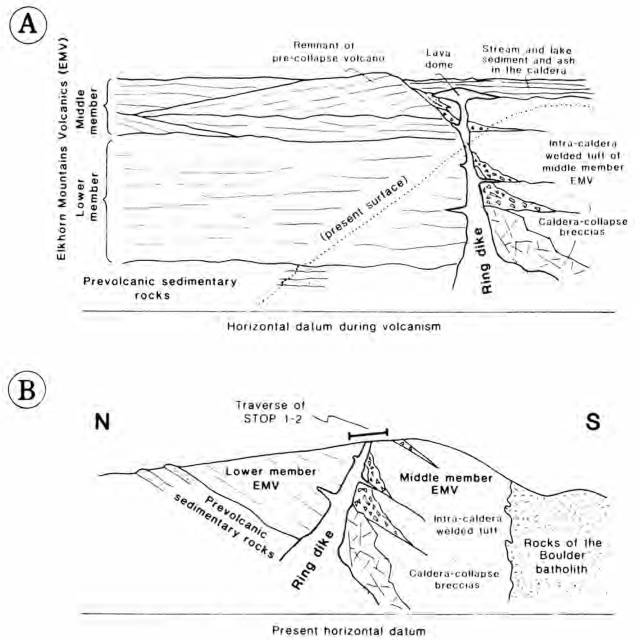

FIGURE 6—A, Hypothetical cross section of the volcanic pile before regional deformation and plutonism; dotted line indicates the approximate position of present surface. B, Present-day cross section reflecting post-eruption tilting (about 35°) of the strata, intrusion of batholith, and deep erosion. The traverse of Stop 1-2 spans only a small part of the EMV stratigraphic sequence.

to form pépérite, and probably extending to the surface to form lava domes and flows since removed by erosion (Fig. 6).

1-2c: The northern margin of the dike is in contact with a conglomerate in the lower member of the EMV. This rock unit is about 100 m thick; we will look only at its upper part. Throughout most of its thickness, this conglomerate contains well-rounded cobbles and boulders as large as 1 m in diameter. The majority of the clasts are of welded tuff and andesite porphyry, the latter similar to the dike described above. Return to vehicles and retrace route to county road. **4.2**

Turn right (north) on county road.

Turn right (east) on ranch road (BM 4684).

16.3 **STOP 1-3. Early mafic plutons of the Boulder batholith.** The purpose of this stop is to examine rocks representative of the earliest stage of intrusive activity of the Boulder batholith, in particular of the main series. These mafic rocks are mostly gabbro, syenogabbro, diorite, syenodiorite, and monzonite. These are now preserved in scattered places along the margin of the batholith, and include those of the Kokoruda Ranch Complex, exposed here.

These early mafic rocks have thermally metamorphosed the country rocks to produce hornfels and tactite zones over 100 m thick in many places. Thermally metamorphosed xenoliths abound locally, especially in the northern and western parts of the complex; some are as much as 200 m long. Many of the xenoliths clearly are of hornfelsed EMV; others are of unidentifiable hornfelsed shale, sandstone, or carbonate rocks. In some places, xenoliths of many rock types are close together, interpreted as indicating considerable churning of stoped blocks. Return to Helena for supper and overnight.

Day 2

We will drive south from Helena on 1-15. Road log begins at the east edge of Butte (Fig. 3).

Mileage

0.0 Junction of I-90 and I-15. Continue southward and thence eastward on I-90. From here to Stop 2-1, Butte Quartz Monzonite (BQM) and related silicic rocks are cut by dikes and sheets of aplite–alaskite–pegmatite and by narrow veinlets of pyrite–quartz–siderite that facilitate local zones of deep weathering to grus. Note size and amount of xenoliths and spheroidal weathering. **6.1**

6.1 Homestake pluton, which grades into or cuts the BQM, on left. **1.8**

7.9 Rest Area. Comfort Stop. Throughout the area east of the Continental Divide, but especially just beyond the Rest Area, look north (left) across the ravine to see spectacular exposures of vertical north–south sheeted joints in the BQM, which have produced sharp wedges and pinnacles. **1.4**

9.3 Railroad tunnel on left (north). **0.8**

10.1 **STOP 2-1. Joints, schlieren, inclusions, and pegmatites in the Butte Quartz Monzonite.** The purpose of this stop is to walk eastward along the shoulder on the south side of I-90 for about 300 m to examine joints, schlieren, numerous mafic-rich inclusions, and pegmatites in the BQM. Nearly horizontal sheeted joints in the BQM, slightly concave upward, plunge gently northwestward. Look for these near the top of the outcrop. The principal question to be addressed, and observations to be made, relate to the schlieren. They are of mafic-rich quartz monzonite and granodiorite. In places, they are injected by, and seem to be partly replaced by, pegmatite. These are interpreted as either remnants of a roof plate or as segregations produced during fracture and flowage in partly solidified magma near a flat roof.

The mafic-rich inclusions are sharply bounded, equidimensional, rounded, and generally fine-grained. Consider the origin of these inclusions. Are they xenoliths? restite? synmagmatic blobs? cognate inclusions?

The flat joints are either (1) related to the schlieren and associated pegmatites, or (2) due to stress-relief by decompression during erosion, i.e., related to the erosion surface. It is possible that, once formed by processes related to the schlieren, they subsequently controlled what the erosion surface would be. Such flat joints are seen at several places for a mile or more eastward along I-90, but are not common at all throughout the batholith.

Return to vehicles and continue eastward on I-90. In the next 2 mi, notice more of the nearly horizontal, gently arched, sheeted joints on the south side of the highway and closely spaced quartz–pyrite veinlets that produced rusty alteration and seem to control the development of grus, in contrast to the intervening pillars of unaltered rock. **0.7**

10.8 Rounded knob on skyline far to the north (at 11:00) is a "Christmas-tree" complex of alaskite (shown in Fig. 3). Very light-colored spires in low ground just this side of the alaskite complex are Spire Rocks, similar in composition and texture to the Homestake pluton. Rocks of this type are interpreted from field relations, petrography, and lead-isotope ratios as having crystallized from a residuum of the BQM magma that was intruded into incompletely crystallized BQM.

For the next 1.3 mi, there are excellent exposures of BQM to the left (north). **2.3**

13.1 Milepost 240. A poorly exposed thin septum of metavolcanic rocks separates the BQM from a small area of older granodiorite of Rader Creek that is buried on the east by Cenozoic deposits, but is well exposed to the south (right). **1.7**

14.8 Pipestone Exit 241. Turn off I-90 and go under the Interstate. Travel westward on gravel road on north side of I-90. Road is on poorly consolidated Cenozoic deposits (Fig. 3). Distant bedrock to the north is EMV, and to the south is granodiorite of Rader Creek. The isolated rocky hill near the junction of the gravel road and I-90 is silicified and pyritized andesite or microdiorite porphyry. This is an inlier of a large irregular sheet that is intrusive into and genetically part of the EMV. The silicified rock is light gray, brittle, and irregularly stained rusty brown due to oxidation of small pyrite crystals. The granodiorite of Rader Creek, exposed a short distance to the south, may underlie the an-

desite porphyry here at shallow depth and may be the cause of the silicification. **0.7**

15.5 Notice the overgrown old placer workings on benches along the south side of Big Pipestone Creek. **1.9**

17.4 **STOP 2-2. Contact of the Butte Quartz Monzonite and the Elkhorn Mountains Volcanics.** Cross Burlington Northern Railway tracks and park at turnoff just beyond tracks. We will be walking northward along the railroad tracks.

The purpose of this stop is to study the nature of the contact of the batholith (BQM) with pre-batholith rocks of the EMV (Fig. 7). Critical observations include that: (1) there is virtually no contamination or chilling of the BQM as the contact is approached; (2) the immediate contact zone is a hybrid zone of rock so intensely recrystallized and impregnated with magmatic materials that it is not possible to place the contact within narrow limits; and (3) the extent and nature of deformation of the volcanic rocks diminishes away from the contact.

The traverse starts in BQM, which is rather coarse-grained and nonporphyritic. This is a good place to collect fresh samples of BQM, although heavily sooted over by passing trains. In the first cuts, the railroad tracks are nearly parallel to the contact so that for 200 m they only go a few tens of meters normal to the contact (Fig. 7). The actual contact is just north of the signal light about 150 m from the starting point. Note the weak preferred orientation of mafic minerals in the BQM roughly parallel to the contact.

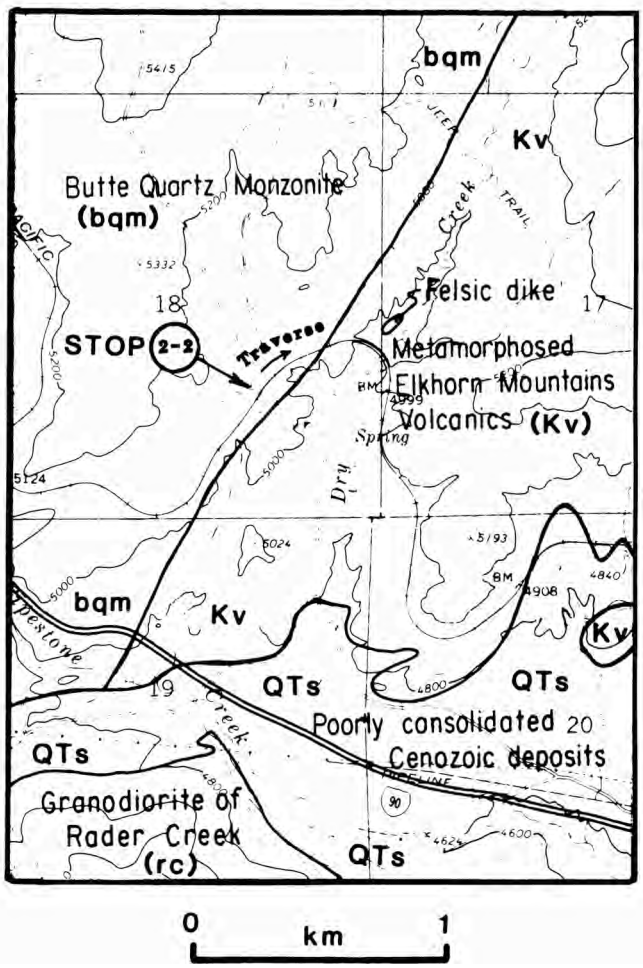

FIGURE 7—Sketch map of contact of Butte Quartz Monzonite and the Elkhorn Mountains Volcanics in the Dry Creek area, Stop 2-2; traverse follows along railroad tracks, beginning where they cross the road ($SE^1/_4$ sec. 18).

Little contamination is apparent in the batholith rocks, but the metavolcanics are intensely brecciated, impregnated, and irregularly laced with veinlets of highly variable granitic rock. Outward from the batholith, the replacement-breccia contact zone grades into an impregnated granofels zone consisting of biotitic, coarsely recrystallized volcanic rocks with many streaks and patches of granitic rock. Within the contact zone, only a few meters wide, it is not clear whether some rocks are contaminated BQM or metasomatically recrystallized EMV.

In the central part of the first deep cut, the volcanic rocks are highly sheared and are cut by granitic seams both along and across the shear planes. Near the far end of the cut, relict textures indicate that the metavolcanic rocks were pyroxene andesite or diorite porphyry. The pyroxene has been converted to amphibole, and much metamorphic biotite is scattered through the rock. At the very end of the cut, highly schistose volcanics are seen on the east wall. In places, individual sheared-out fragments can be seen.

Between the first and second cuts, about 200 m away, we will stop along the rock embankment to point out the batholith contact farther north and south (Fig. 8), and a large felsic dike in the ravine below.

In the second cut, which is about 300 m away from the contact, the original volcanic textures are better preserved, and there was virtually no impregnation by granitic emanations. Sheared breccias and intrusive or flow rocks with relict plagioclase phenocrysts are exposed. Note the younger fractures and veinlets normal to the foliation. These veinlets of quartz, pyrite, and a carbonate mineral are similar to the veins that have been prospected in the region. Oxidation of pyrite produced staining and bleaching adjacent to the veins.

The last cut we will study is near railroad sign "48." Principal features to see here are: (1) the effects of shearing, which are less intense although still conspicuous; (2) veinlets of retrograde epidote, albite, and chlorite, with local pods of calc-silicate minerals that follow several main joint sets and that probably formed just after the principal metamorphism; and (3) still younger veinlets of quartz–pyrite–carbonate. Near the far (south) end of the last cut, note welded tuff dipping steeply west that has slight to no shearing. This exposure indicates that there was considerable folding or tilting of the wall rocks in addition to shearing. Relict texture shows characteristic frayed appearance of the ends of collapsed pumice, and the draping of pumice over solid rock fragments, indicative of compaction and welding of an ash-flow tuff.

Return to Pipestone Exit of I-90. **2.4**

19.8 Go back under I-90 and stay left (NOT to camping area) on gravel road that goes east and then south

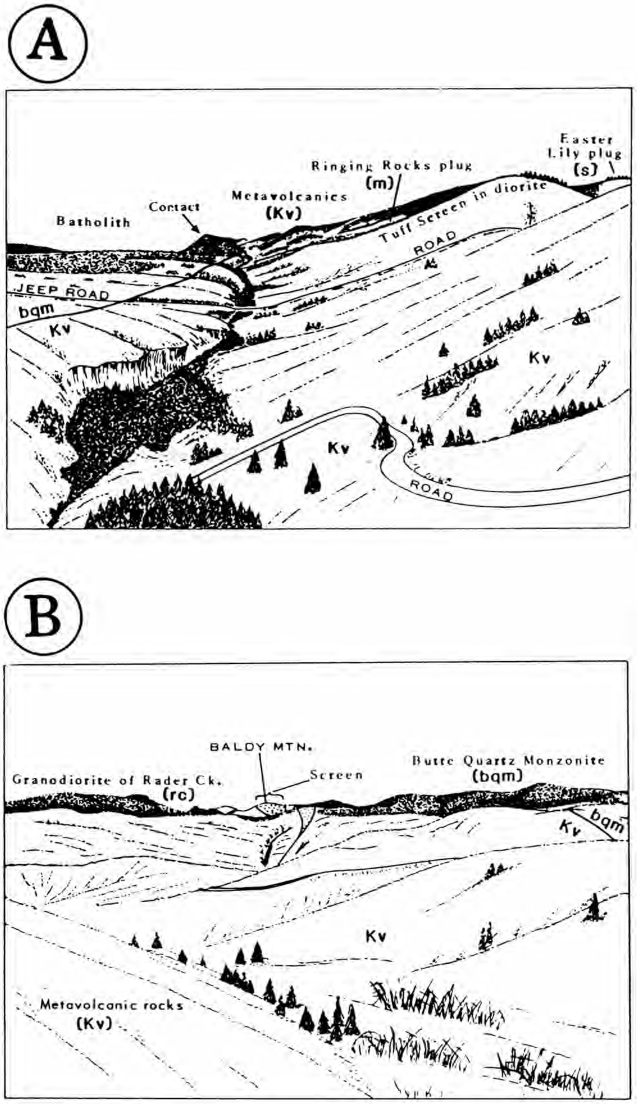

FIGURE 8—Vistas of the batholith contact from Stop 2-2. **A,** Looking northward along Dry Creek. **B,** Looking southwestward toward the Highland Mountains. Stippled area indicates a screen of contact-metamorphosed sedimentary and volcanic rocks separating the granodiorite of Rader Creek and Butte Quartz Monzonite (see Fig. 3).

to old Pipestone Hot Springs Spa. Low bluff in middle distance is of classic "Pipestone beds" (informal name), a source of Oligocene vertebrate fossils. **1.2**

21.0 Cutoff to spa. Turn right and drive by abandoned spa site. **1.0**

22.0 Outcrops on right are pinkish-gray, K-rich variant of the granodiorite of Rader Creek, which also occurs in hills beyond. Mountains to southeast (at about 11:00) are the Tobacco Root Range. Valley fill is Tertiary ash-rich lacustrine and fluvial beds. **1.4**

23.4 Ahead and to the left are exposures of the granodiorite of Rader Creek with Pipestone beds lapping onto them. **0.2**

23.6 Junction with MT-2. Turn right onto highway. **0.6**

24.2 Pipestone beds on right and on low slopes to the left, lapping onto the granodiorite of Rader Creek. Inliers of granodiorite of Rader Creek for next mile. **0.6**

24.8 Junction with MT-41. Continue on MT-2. **0.5**

25.3 Placer gravels on left. **1.9**

27.2 Granodiorite of Rader Creek. Epidote on joint surfaces gives outcrop a green cast. Fresh surfaces are bluish gray; weathered surfaces are reddish brown. Rock is equigranular and contains clots of mafic minerals and "ratty"-appearing biotite. Xenoliths and aplite dikes are sparse in this pluton. **1.1**

28.3 **STOP 2-3. Granodiorite of Rader Creek. Lunch.**

The purpose of this stop is to see the oldest and largest pluton of the sodic magma series. Walk eastward back to deep roadcut near the Highway Maintenance Station. Be careful of much loose overhanging rock in roadcut. Note late magmatic or deuteric veinlets with bleached zones characterized by epidote and chlorite along joints. Granodiorite of Rader Creek becomes gradually more felsic westward along this route. This is a good location for collecting samples of this pluton. **0.6**

28.9 Timbered rounded peak and sparsely timbered grassy knob to left (10:00) at about milepost 70 are mafic ("lamprophyric") plugs that cut the Rader Creek pluton. **1.2**

30.1 Junction with Toll Mountain Road. **1.1**

31.2 Forest boundary. Entering Deer Lodge National Forest. **0.2**

31.4 Roadcut on north is in rusty-colored brecciated granodiorite of the Rader Creek pluton cut by pegmatitic and felsic stringers, locally cemented by masses of tourmaline. **0.9**

32.3 Straight ahead are more white cliffs and castellated spires of the Donald pluton. To left in railroad cut is poorly exposed contact of the granodiorite of Rader Creek and the BQM. **0.4**

32.7 Road curves to right. At curve, small exposure of Donald pluton with BQM on three sides (W, N, E), just 20–30 m west of sign "Continental Divide 2 miles." BQM is porphyritic; phenocrysts stand out as nubs on weathered faces. Shortly beyond are more views of cliffs of the Donald pluton. Road cuts in and out of Donald pluton but lies mostly in BQM. **2.5**

35.2 Pipestone Pass on the Continental Divide. Rocks exposed are grussy leucogranodiorite of the Donald pluton. **0.5**

35.7 BQM in a hairpin turn. On northwest wall is a dark olive-colored, highly altered lamprophyric dike. **1.8**

37.5 Turn sharply left onto gravel road of Roosevelt Drive. **1.0**

38.5 Road goes under railroad trestle. **0.3**

38.8 **STOP 2-4. Large aplite–alaskite body.** The objective of this brief stop is to examine variations in textures and mineralogy of this aplite–alaskite–pegmatite body that intrudes the BQM. This body is representative of the youngest felsic facies of the BQM. Local hydrothermal alteration is present. Local miarolitic cavities enclose terminated quartz crystals and some muscovite, molybdenite, pyrite, and minor chalcopyrite. Iron-oxide staining (spots) is due to oxidation of sulfides. There are virtually no inclusions. **0.9**

39.7 Return to highway and continue westward toward Butte. **0.8**

40.5 Butte archery range. Look uphill to the north (right) to see layered alaskite sheets cutting BQM. **1.6**

42.1 Junction with Highway 375; continue on MT-2 (left). **3.1**

45.2 Junction with Highway 393—Basin Creek road. Turn left onto this road and drive south toward Red Mountain (Proterozoic rocks) in the Highland Mountains south of the batholith. Next 3 mi of road is over the surface of upper Cenozoic "granite wash." Several surfaces, some depositional and some erosional, are preserved on these deposits. Some surfaces bevel both the "granite wash" and BQM with no break in slope. At Newcomb siding, thin ash beds can be seen in these poorly consolidated deposits. **3.7**

48.9 Cross railroad grade (former Chicago, Milwaukee, St. Paul, and Pacific Railroad). **1.1**

50.0 Small outcrops on west side of road are quartz latite dikes cutting BQM. These dikes probably are related to the Eocene Lowland Creek Volcanics. From here south to Roosevelt Drive (Herman Gulch), we pass through a terrane of BQM cut by abundant steeply and gently dipping dikes of layered alaskite, pegmatite, and aplite, and still-younger metalliferous quartz veins and faults. **0.2**

50.2 Herman Gulch, junction of Basin Creek Road and Roosevelt Drive. Continue south. **0.3**

50.5 Roadcut. **STOP 2-5. Contact of Butte Quartz Monzonite and slightly younger quartz monzonite of the Climax Gulch pluton.** The objectives of this stop are: (1) to observe a layered alaskite dike; (2) to examine the petrology and structure of typical sparsely porphyritic BQM and the petrology, size, shape, and spatial frequency of inclusions; and (3) to walk from the BQM toward and across the contact with the highly porphyritic quartz monzonite of the Climax Gulch pluton, the youngest dated member of the sodic series.

1. The layered, inclined dike of alaskite is typical of thousands of dikes that cut the BQM at all exposed levels, mine workings, and deep drill holes. Some of these have complex geometry and change over a short distance from vertical to horizontal and back to vertical, or are even "overturned." There is no consistent pattern or symmetry of the arrangement and distribution of the different-textured layers that make up these bodies. Those of us who have examined countless numbers of these bodies conclude that the textural differences must have been produced in the manner described by Fournier (1968) as due to a continuous process in which the degree of saturation of the dike fluid with water played a decisive role. "Pressure quenching" due to release of increments of the gas phase during repeated opening of the fracture resulted in very fine-grained felsic aplite.

Where poorly exposed, the mapped extent of these dikes and sheets gives the false portrayal of a complex, steep-sided plug of much greater volume than is actually visible. Especially where these bodies dip subparallel with the surface, their outcrop form is complexly irregular.

2. The host rock for the alaskite dike is sparsely porphyritic BQM that is representative of the main volume of the BQM. In places, a very weak and subtle foliation defined by oriented mafic minerals can be discerned. This also is typical. The "woolsack" terrain produced by joint-controlled spheroidal weathering is widespread throughout this batholith and many others around the world.

3. The Climax Gulch pluton is quartz monzonite that is readily distinguished from the BQM in the field only by its very highly porphyritic texture and more pronounced foliation, marked by aligned K-feldspar phenocrysts. In many places there are two foliations, generally at high angles to one another. The older of these is of weakly aligned plagioclase and mafic minerals, whereas the younger is of more conspicuously aligned K-feldspar phenocrysts. Although in many places the contact of the Climax Gulch pluton with the BQM is sharp, here it is blended.

Return to vehicles. Travel north on Highway 393 (South Harrison Ave.), under I-90. Follow curve of Harrison Ave. half-left and continue on to traffic light at Utah St. **4.8**

55.3 Turn right onto Utah St. (Business I-90/15); continue up hill to Park Street; turn right. Continue east on Park Street; turn right. Continue east on Park Street to visitor center and observation point at Berkeley Pit. **1.6**

56.9 Visitor center. End of field guide. Information about the Berkeley pit and the Butte mines will be handed out on site. We will have supper in Butte and return to Missoula for overnight.

References

Becraft, G. E., Pinckney, D. M., and Rosenblum, S., 1963, Geology and mineral deposits of the Jefferson City quadrangle, Jefferson and Lewis and Clark Counties, Montana: U.S. Geological Survey, Professional Paper 428: 101 pp., map 1:48,000.

Byers, F. M., Jr., Carr, W. J., Orkild, P. P., Quinlivan, W. D., and Sargent, K. A., 1976, Volcanic suites and related cauldrons of Timber Mountain–Oasis Valley caldera complex, southern Nevada: U.S. Geological Survey, Professional Paper 979: 70 pp.

Doe, B. R., Tilling, R. I., Hedge, C. E., and Klepper, M. R., 1968, Lead and strontium isotope studies of the Boulder batholith, southwestern Montana: Economic Geology, 63: 884–906.

Fournier, R. B., 1968, Mechanisms of formation of alaskite, aplite, and pegmatite in a dike swarm, Yosemite National Park, California; *in* Coats, R. R., Hay, R. L., and Anderson, C. A. (eds.), Studies in Volcanology: Geological Society of America, Memoir 116: 249–274.

Greenwood, W. R., Ludington, S., Miller, W. R., and Hanna, W. F., 1978, Mineral resource assessment, with sections on geophysical exploration, geochemical exploration, uranium and thorium potential; *in* Chapter A, Mineral resources of the Elkhorn Wilderness Study Area: U.S. Geological Survey, Open-File Report 78-325: 7–82, map 1:48,000.

Grout, F. F., and Balk, R., 1934, Internal structures in the Boulder batholith: Geological Society of America, Bulletin, 45: 877–896.

Hamilton, W. B., and Myers, W. B., 1974, Nature of the Boulder batholith of Montana: Geological Society of America, Bulletin, 85: 365–378.

Johannsen, A., 1939, A descriptive petrography of the igneous rocks: University of Chicago Press, 318 pp.

Klepper M. R., Robinson, G. D., and Smedes, H. W., 1974, On the nature of the Boulder batholith of Montana: Geological Society of America, Bulletin, 85: 1563–1580.

Klepper, M. R., Weeks, R. A., and Ruppel, E. T., 1957, Geology of the southern Elkhorn Mountains, Montana: U.S. Geological Survey, Professional Paper 292: 82 pp., maps at 1:31,250.

Klepper, M. R., Ruppel, E. T., Freeman, V. L., and Weeks, R. A., 1971, Geology and mineral deposits, east flank of the Elkhorn Mountains, Broadwater County, Montana: U.S. Geological Survey, Professional Paper 665: 66 pp., map at 1:48,000.

Knopf, A., 1957, The Boulder batholith of Montana: American Journal of Science, 255: 81–103.
Knopf, A., 1963, Geology of the northern part of the Boulder batholith and adjacent area, Montana: U.S. Geological Survey, Miscellaneous Geological Investigation Map I-381, 1:48,000. Northern part revised on basis of unpublished maps of R. G. Schmidt, 1978, 1:48,000.
Lambe, R. N., 1981, Crystallization and petrogenesis of the southern portion of the Boulder batholith, Montana: Unpublished Ph.D. dissertation, University of California, Berkeley, 171 pp.
Lipman, P. W., 1979, Emplacement of high-level granitic batholiths: Evidence from the San Juan volcanic field of Colorado and the Boulder batholith of Montana: Geological Society of America, Abstracts with Programs, 11: 467.
Lipman, P. W., 1984, The roots of ash-flow calderas in western North America: Windows into the tops of granitic batholiths: Journal of Geophysical Research, 89: 8801–8841.
Rice, J. M., 1977, Contact metamorphism of impure dolomitic limestone in the Boulder aureole, Montana: Contributions to Mineralogy and Petrology, v. 59, pp. 237–259.
Robinson, G. D., 1963, Geology of the Three Forks quadrangle, Montana, with descriptions of igneous rocks by H. Frank Barnett: U.S. Geological Survey, Professional Paper 370: 143 pp.
Robinson, G. D., Klepper, M. R., and Obradovich, J. D., 1967, Overlapping plutonism, volcanism, and tectonism in the Boulder batholith region, western Montana: Geological Society of America, Memoir 116: 557–576.
Rutland, C., 1985, The geochemistry of the Elkhorn Mountains Volcanics and its relationship to the magma chamber of the Boulder batholith: Unpublished Ph.D. dissertation, Michigan State University, East Lansing, 96 pp.
Rutland C., 1986, Geochemistry of the Elkhorn Mountains Volcanics, southwestern Montana: Implications for the early evolution of a volcanic–plutonic complex: Geological Society of America, Rocky Mountain Section, Abstracts with Programs, 18(5): 408.
Rutland, C., Vogel, T. A., and Greenwood, W. R., 1984, Major-element chemical evolution of the Cretaceous Elkhorn Mountains Volcanics, southwestern Montana: Geological Society of America, Abstracts with Programs, 16(6): 641.
Schmidt, C. J., and Hendrix, T. E., 1981, Tectonic controls for thrust belt and Rocky Mountain foreland structures in the northern Tobacco Root Mountains–Jefferson Canyon area, southwestern Montana: Montana Geological Society, 1981 Field Conference Guidebook, pp. 167–180.
Schmidt, C. J., Smedes, H. W., Suttner, L. J., and Vitaliano, C. J., 1979, Near-surface batholiths, related volcanism, tectonism, sedimentation, and mineral deposition: Guidebook for Penrose conference—Granite II: Geological Society of America, Gregson, Montana, June 24–29, 111 pp.
Smedes, H. W., 1962, Preliminary geologic map of the northern Elkhorn Mountains, Jefferson and Broadwater counties, Montana: U.S. Geological Survey, Map MF-243.
Smedes, H. W., 1966, Geology and igneous petrology of the northern Elkhorn Mountains, Jefferson and Broadwater counties, Montana: U.S. Geological Survey, Professional Paper 510: 116 pp.
Smedes, H. W., 1988, Preliminary map of plutonic units of the Boulder batholith, southwestern Montana: U.S. Geological Survey, Open-File Report 88-283, map 1:200,000.
Smedes, H. W., Hammond, P., and Hanna, W., 1980, Geology and Mineral-resources evaluation of the Humbug Spires Primitive Area, Montana: U.S. Geological Survey, Open-File Report 80-836.
Smedes, H. W., Klepper, M. R., and Tilling, R. I., 1968, Boulder batholith: Description of geology and road log (Field Trip No. 3), Rocky Mountain Section Meeting: Geological Society of America, May 1968, Bozeman, Montana, 21 pp.
Smith, R. L., 1960, Ash flows: Geological Society of America, Bulletin, 71: 795–842.
Steiger, R. H., and Jager, E., 1977, Subcommission on geochronology—convention on the use of decay constants in geo- and cosmochronology: Earth and Planetary Science Letters, 36: 359–362.
Steven, T. A., and Lipman, P. W., 1976, Calderas of the San Juan volcanic field, southwestern Colorado: U.S. Geological Survey, Professional Paper 958: 35 pp.
Streckeisen, A., 1973, Plutonic rocks: Classification and nomenclature recommended by the IUGS Subcommission on the Systematics of Igneous Rocks: Geotimes, 18: 26–30.
Streckeisen, A., 1976, To each plutonic rock its proper name: Earth-Science Reviews, 12: 1–33.
Tilling, R. I., 1973, Boulder batholith, Montana: A product of two contemporaneous but chemically distinct magma series: Geological Society of America, Bulletin, 84: 3879–3900.
Tilling, R. I., 1974a, Composition and time relations of plutonic and associated volcanic rocks, Boulder batholith region, Montana: Geological Society of America, Bulletin, 85: 1925–1930.
Tilling, R. I., 1974b, Estimating the "thickness' of the Boulder batholith, Montana, from heat-flow and heat-productivity data: Geology, 2: 457–460.
Tilling, R. I., 1977, Interaction of meteoric waters with magmas of the Boulder batholith, Montana: Economic Geology, 72: 859–864.
Tilling, R. I., Klepper, M. R., and Obradovich, J. D., 1968, K–Ar ages and time span of emplacement of the Boulder batholith, Montana: American Journal of Science, 266: 671–689.

Eocene magmatism, Challis volcanic field, central Idaho

Richard F. Hardyman
U.S. Geological Survey, Reno, Nevada 89557

Introduction

The Challis Volcanics of Idaho constitute one part of an extensive belt of compositionally diverse volcanic and plutonic rocks of Eocene age that occur throughout the northwestern United States. The Challis volcanic field is the largest and perhaps most diverse of the volcanic fields in this Eocene magmatic province. Deep erosion of the Challis Volcanics in central Idaho since the end of the Eocene has dissected many of the source vents for the volcanic rocks and exposed subjacent cogenetic plutons.

This report provides an overview of magmatic events that resulted in deposition of rocks of the Eocene Challis volcanic field, central Idaho, and emplacement of the Casto pluton and other intrusive rocks associated with this extensive volcanic field. More detailed descriptions of the volcanic units and local stratigraphic and structural relationships in the central and northern part of the field are in McIntyre et al. (1982), Leonard and Marvin (1982), Ekren (1985), and Hardyman (1985). Preliminary descriptions and strati-graphic relations of Challis volcanic rocks in the southern part of the volcanic field, which consists of similar strati-graphic sequences in the same time frame but apparently different volumes of explosive products, are reported in Moye et al. (1988). Descriptions of the Eocene granitic rocks associated with the volcanic terrane are in Bennett and Knowles (1985).

Challis volcanic rocks

Stratigraphic and structural framework

Eocene volcanism in central Idaho began about 51 Ma ago, culminated in large-volume explosive eruptions between about 49 and 45 Ma, and was essentially over by about 40 Ma. The Challis volcanic field in central Idaho consists of a lower sequence of mafic and intermediate volcanics (51-49 Ma) and an upper sequence of felsic volcanics (49-45 Ma). These volcanic rocks are cut by mafic to felsic intrusions as young as 40 Ma and a major granitic pluton, the Casto pluton, was emplaced into the volcanic pile about 47-44 Ma.

The lower part of the volcanic sequence consists of thick accumulations of lavas, breccias, and dome-complex intrusive rocks of intermediate and mafic compositions. These rocks, which locally exceed 1000 m in thickness, were erupted from numerous small stratovolcanoes, shield volcanoes, and dome complexes. They were deposited on an erosional surface with more than 300 m of structural and topographic relief, carved on Precambrian and Paleozoic sedimentary rocks. The lower part of the Challis volcanic sequence may have resembled a regionally extensive lava plateau infilling around and over local pre-Tertiary fault-block promontories. Numerous vents of moderate relief dotted the plateau at the onset of explosive volcanism.

Large-volume silicic pyroclastic eruptions dominated magmatic activity in the Challis volcanic field for about 4 million years. These events began with eruptions of rhyodacite magma, evolved through eruptions of quartz latite and rhyolite, and terminated with eruption of alkali rhyolite magma. The older rhyodacitic volcanism initiated development of a huge cauldron complex nearly 110 by 65 km (60 by 35 mi) in dimensions, extending northwest from Challis, Idaho, to nearly the Salmon River, where the river flows west across Idaho. The younger quartz latite to alkali rhyolite pyroclastic eruptions formed smaller calderas superimposed " cookie-cutter" fashion on this cauldron terrane (Fig. 1).

Although intermediate to mafic magmatic activity had significantly waned by the onset of silicic pyroclastic volcanism, eruptions of mafic and intermediate magma continued well into the period of silicic volcanism throughout the region. Intermediate intrusions locally postdate the silicic volcanic rocks (Leonard and Marvin, 1982; McIntyre et al., 1982; Fisher et al., 1983).

Emplacement of the 47-44 Ma Casto granite into the cauldron-related pyroclastic rocks and subsequent erosion have separated the Challis volcanic field in this extensive cauldron region into two geographic subregions. Challis volcanic rocks and related calderas lying northwest of the Casto pluton are designated parts of the Thunder Mountain cauldron complex (Leonard and Marvin, 1982). Calderas and related rocks lying southeast of the pluton are part of the Van Horn Peak cauldron complex (Ekren, 1981). Although separated into two volcanotectonic subregions, it must be emphasized that the sequence of volcanic units and caldera development in both regions shows similar evolutionary trends. It seems more appropriate to consider both subregions as part of an extensive intermediate lava field on which developed a vast cauldron complex that began with subsidence of a Toba-sized depression (that for the most part encompassed both geographic subregions). Subsequent collapse of individual areas formed isolated to overlapping Valles-sized calderas. Following deep erosion, this terrane is now separated into two areas separated by exposures of the Casto pluton. For ease of discussion, the cauldron-related rocks and calderas will be treated as parts of either the Thunder Mountain or Van Horn Peak cauldron complex areas.

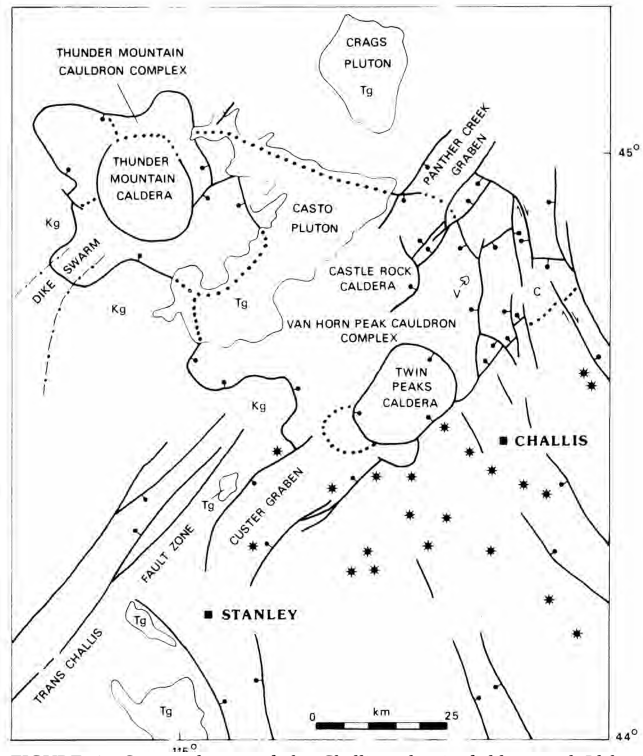

FIGURE 1—Structural map of the Challis volcanic field, central Idaho, showing major cauldron and caldera boundary faults, related grabens, intermediate-lava eruptive centers, and the Casto pluton. Modified from Hardyman (1985). Tg = Tertiary granite, Kg = Cretaceous rocks of Idaho batholith, V = Van Horn Peak fissure vent, C = Corral Creek cauldron segment, dotted line = boundary of inferred calderas; star symbol = intermediate lava eruptive centers.

Numerous high-angle, northwest- to northeast-striking, normal and strike—slip faults were in existence prior to volcanism (Hobbs et al., 1975; Hays et al., 1978; McIntyre and Hobbs, 1987). Many of these faults experienced renewed displacements during the period of Challis volcanism and some northeast-trending faults were conduits for intrusive rhyolites that cut pyroclastic rocks as young as 45 Ma in the upper part of the volcanic sequence. Movement on some of these northeast-trending faults, that are part of the trans-Challis fault system (Kiilsgaard and Lewis, 1985; Kiilsgaard et al., 1986), may be as young as Holocene (Kiilsgaard and Lewis, 1985).

Intermediate and mafic lavas

Lavas and local intrusive rocks of intermediate to mafic composition dominate the lower sequence of rocks of the Challis volcanic field throughout central Idaho. In the Thunder Mountain and Van Horn Peak cauldron complexes, these rocks are generally buried beneath cauldron-related ashflow-tuff sequences. South and southeast of the Van Horn Peak cauldron complex, however, outflow-tuff sheets from the cauldron complex have for the most part been removed by erosion and the intermediate to mafic lava pile is well exposed. In the vicinity of Challis, Idaho, and the region

extending to the southeast (southeast part of the Challis 1° x 2° quadrangle) numerous source vents for these rocks have been mapped (McIntyre et al., 1982; Fig. 1). In this region, the intermediate lava pile is as much as 1000 m thick. Farther to the south and southeast (Hailey and Idaho Falls 1° x 2° quadrangles) the intermediate lava pile (predominantly andesite flows and tuff breccias) is as much as 700 m thick (Moye et al., 1988). To the northwest, in the Thunder Mountain cauldron complex, the lower intermediate lavas are at least 500 m thick (Fisher et al., 1983).

Rocks making up the intermediate lava pile are divisible into two groups based on their appearance: light-colored rocks that are distinctly porphyritic, and dark-colored, crystal-poor "basaltlike" rocks. The conspicuously porphyritic rocks contain phenocrysts of plagioclase and various combinations of clinopyroxene, orthopyroxene, hornblende, biotite, and altered olivine. Chemical analyses of these porphyritic light-colored rocks show that they are best called dacite and rhyodacite (McIntyre et al., 1982). The dark "basaltlike" rocks include potassium-rich andesite, andesite, latite, and minor volumes of magnesium-rich basalt and potassium-rich basalt.

The dacite and rhyodacite were erupted from numerous small (about 8 km in diameter) stratovolcanoes and dome complexes. Intrusive breccias, or near-vent facies eruptive breccias, are common to many of these source vents.

Pyroclastic rocks of the Van Horn Peak cauldron complex

Corral Creek segment: The first significant explosive magmatic event of the Van Horn Peak cauldron complex was the eruption of lithic-rich dacite or rhyodacite tuff informally named the tuff of Corral Creek (Ekren, 1985). The eruption of this tuff caused caldera collapse of the Corral Creek segment of the Van Horn Peak cauldron complex (Fig. 2). Subsidence was controlled by preexisting northeast- and northwest-striking faults. Extrusion of this tuff was immediately followed by eruption of dacitic and latitic lavas that together with mudflow breccias rapidly infilled the collapsed block. The tuff of Corral Creek is about 200 m thick within the Corral Creek collapse segment. Overlying infilling lavas and breccias are as much as 900 m thick.

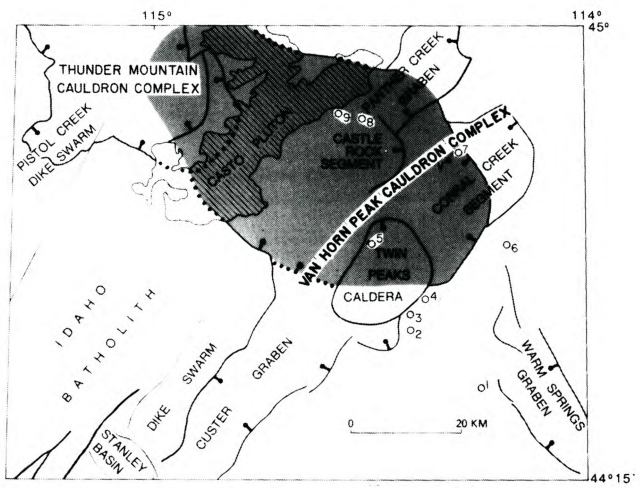

FIGURE 2—Map of the Van Horn Peak and Thunder Mountain cauldron complexes. Shaded area is inferred area of cauldron collapse that originated with the eruption of the tuff of Ellis Creek. From Ekren (1985). Numbered circles refer to field-trip stops.

Van Horn Peak cauldron: Major subsidence of the Van Horn Peak cauldron complex accompanied eruption of voluminous amounts of rhyodacitic and quartz latitic magma about 48.4 Ma ago. The products of these events, the tuff of Ellis Creek and overlying tuff of Eightmile Creek, were associated with collapse of an elliptical area about 70 km long and 40 km wide that included most of the area of the Van Horn Peak cauldron complex. This area is now occupied by the present exposure of the Casto pluton and much of the southeastern part of the Thunder Mountain cauldron complex (Fig. 2). Remnants of the outflow of these immense ash-flow-tuff eruptions are preserved as far as 25-35 km south and east of the cauldron-complex boundary. The tuff of Ellis Creek outflow sheet alone probably had an original volume of at least 400 km3. Locally, this outflow sheet is more than 300 m thick. The tuff of Ellis Creek is at least 1500 m thick where preserved within the cauldron complex, and intracauldron tuff of Eightmile Creek is 600-800 m thick (Ekren, 1985).

Collapse of the Toba-sized depression, formed as a result of the eruption of the tuff of Ellis Creek and tuff of Eightmile Creek, was closely followed by eruptions of a cauldron-filling sequence of densely welded quartz latitic to rhyodacitic ash-flow tuffs. These tuffs, the tuffs of Camas Creek—Black Mountain, are characterized by small (2 mm or less) phenocrysts. Plagioclase is the dominant phenocrystic mineral, altered pyroxene is the principal mafic mineral, biotite (ubiquitous) and hornblende are secondary, and quartz and alkali feldspar are generally sparse or absent.

Some of the Camas Creek—Black Mountain ash-flow tuffs were erupted from the Van Horn Peak welded-tuff vent (Ekren, 1981), located near the east-central margin of the Van Horn Peak cauldron complex (Fig. 2). Welded tuffs of the outer rim of this cone-shaped vent correlate with cooling units of the lower part of the Camas Creek—Black Mountain package. The tuff of Van Horn Peak, which forms the inner core of the vent, correlates with the youngest intracauldron units of the Van Horn Peak cauldron. The tuffs of Camas Creek—Black Mountain are at least 3000 m thick within the cauldron complex.

Ash-flow tuffs of the tuff of Pennal Gulch are interpreted to be outflow equivalents of the tuffs of Camas Creek—Black Mountain. Near Challis, Idaho, the Pennal Gulch unit includes interbedded subaerial and subaqueous tuffs and sediments. The Pennal Gulch unit is approximately 370 m thick.

Castle Rock segment: Eruption of crystal-rich quartz latite and rhyolite ash-flow tuff was the next significant magmatic event to occur in the Van Horn Peak cauldron complex. Venting of quartz latitic and rhyolitic magma caused the initial collapse of the Castle Rock half-moon or trapdoor caldera (Fig. 2). Two ash-flow-tuff cooling units, collectively called the quartz—biotite tuff, were deposited. This unit is at least 300 m thick within this cauldron segment. Thickness relations of the quartz—biotite tuff in the Panther Creek graben, compared to the Castle Rock cauldron segment, suggest that the Panther Creek graben had begun to subside before deposition of the quartz—biotite tuff.

Continued collapse of the Castle Rock cauldron segment accompanied eruption of the tuff of Castle Rock. This sequence of cauldron- and graben-filling tuff consists of five cooling units totaling 630 m in thickness. These tuffs are rhyolitic, crystal-rich ash-flow tuffs that closely resemble the tuff of Challis Creek that was erupted from the Twin Peaks caldera (see below), but differ in that they contain

sparse but ubiquitous biotite and are quite rich in small volcanic lithic fragments. The tuff of Challis Creek, in contrast, contains so little biotite that these grains are rarely observed in hand specimen or thin section, and lithic fragments are sparse.

Twin Peaks caldera: The Twin Peaks caldera formed about 45 Ma ago with the eruption of approximately 320 km^3 of alkali rhyolite ash-flow tuff, the tuff of Challis Creek. This Valles-size caldera (Fig. 1), with dimensions of 20 by 14 km, is the youngest recognized collapse structure of the Van Horn Peak cauldron complex (Hardyman, 1985). The tuff of Challis Creek is at least 1300 m thick within the caldera, and erosional remnants of this tuff are preserved as far as 40 km from the caldera. The tuff of Challis Creek within the caldera consists of two thick cooling units of alkali rhyolite ash-flow tuff that are distinct in that they contain abundant sanidine and quartz and little or no plagioclase or ferromagnesian minerals.

Northeast-trending faults of the trans-Challis fault system probably influenced the collapse of the Twin Peaks caldera. The fairly linear northern and southern margins of the caldera may have formed by collapse along preexisting northeast-trending faults in the pre-Tertiary basement and older Tertiary volcanic rocks (Hardyman, 1981).

Pyroclastic rocks of the Thunder Mountain cauldron complex

Initial collapse of the Thunder Mountain cauldron complex accompanied eruption of rhyodacitic to rhyolitic ash-flow tuffs about 47 Ma ago. These tuffs, the informal "dime and quarter" unit of Ekren (1985), are the Thunder Mountain cauldron complex analogue of the Camas Creek—Black Mountain tuffs in the Van Horn Peak cauldron complex. They are generally densely welded, crystal-poor tuffs characterized by well-flattened pumice lapilli the size of dimes and quarters. For the most part they are quartz-poor rocks containing predominantly plagioclase and clinopyroxene in excess of minor biotite and hornblende. The intracauldron thickness of the "dime and quarter" tuff unit, including intercalated thin tuffaceous sediments and latite lavas, exceeds 500 m.

A thick sequence of rhyolite tuffs and lavas referred to as the "buff rhyolite" occupies the northwest part of the Thunder Mountain cauldron. These are nearly aphyric (about 1% phenocrysts) rocks containing plagioclase, traces of biotite, and an altered prismatic mafic mineral. This unit may be as thick as 1000 m and could be associated with a separate caldera within the larger cauldron (Leonard, pers. comm. 1988). These rhyolites are inferred to be older than the Sunnyside rhyolite of the younger Thunder Mountain caldera (see below) (Leonard and Marvin, 1982).

Thunder Mountain caldera: Eruption of quartz latite and rhyolite ash-flow tuffs, the Sunnyside rhyolite of Leonard and Marvin (1982), about 45-46 Ma produced the Thunder Mountain caldera, the youngest collapse structure recognized in the Thunder Mountain cauldron complex. The Sunnyside rhyolite consists of a lower sequence of ash-flow tuffs and an upper ash-flow-tuff unit; locally these are separated by megabreccia up to 100 m thick (Ekren, 1985).

The lower Sunnyside consists of at least three compositionally zoned, crystal-rich ash-flow-tuff cooling units. Each cooling unit grades upward from a rhyolitic base rich in quartz and alkali feldspar to a quartz latite top rich in plagioclase and biotite and low in quartz and alkali feldspar (Ekren, 1985). In contrast, the upper Sunnyside tuff is a multiple-flow compound cooling unit that is rhyolitic from base to top. This unit contains alkali feldspar and quartz, essentially no plagioclase, and only sparse biotite. This tuff is the Thunder Mountain cauldron complex counterpart to the tuff of Challis Creek in the Van Horn Peak cauldron complex. The combined thickness of the Sunnyside rhyolite ash-flow tuffs is about 900 m within the Thunder Mountain caldera.

Post-cauldron intrusive rocks

Intracauldron pyroclastic rocks in both the Van Horn Peak and Thunder Mountain cauldron complexes are cut by intrusive rocks ranging in composition from basalt to rhyolite. The basaltic intrusive rocks are sparse and generally occur as dikes that locally may be feeders for minor lava flows intercalated with the pyroclastic rocks. These rocks typically contain plagioclase and pyroxene phenocrysts and only rarely olivine.

In the Van Horn Peak cauldron complex and adjacent Panther Creek and Custer grabens, the dominant post-ash-flow-tuff intrusive rocks are a gray dacite porphyry unit, intrusive rhyolites, and a distinct pink quartz porphyry that is most closely associated with the Casto pluton (see discussion below).

The gray dacite porphyry occurs in exposures of small pluton and stock-size dimensions that in aggregate approach the exposed dimensions of the Casto pluton. The gray porphyry is a gray to green porphyritic rock consisting of 3050% phenocrysts of plagioclase as large as 1 cm, and varying proportions of biotite, hornblende, and pyroxene. Locally, this unit contains scattered quartz phenocrysts and is everywhere somewhat hydrothermally altered. This unit intrudes the quartz—biotite tuff of the Van Horn Peak complex and all older tuffs. Locally, the gray porphyry is nearly concordant with the older intracauldron tuffs and some masses may form laccoliths.

Intrusive rhyolites are light-gray, tan, and pinkish-red, generally crystal-poor porphyritic rocks containing phenocrysts of sanidine and quartz in variable amounts, and locally plagioclase and biotite. These intrusive rocks typically form steeply discordant dikes and small stock-like intrusions and flow-dome complexes. Isotopic ages of rhyolite intrusions in the Van Horn Peak cauldron complex range from about 49 to 44 Ma. Rhyolite dikes cut the youngest tuff of Challis Creek within the Twin Peaks caldera and are locally hydro-thermally altered (Hardyman, 1985). Many rhyolite intrusions of the Van Horn Peak complex are elongate in a northeast—southwest trend, parallel to the trans-Challis fault system.

Post-cauldron-collapse intrusive rocks in the Thunder Mountain cauldron complex range in age from 47 to 37 Ma (Leonard and Marvin, 1982). These intrusive rocks include quartz diorite and granite porphyry stocks and aphyric to crystal-poor, porphyritic rhyolite and latite dikes, dike swarms, and small irregular intrusions. Similarly to the Van Horn Peak complex, post-cauldron-collapse intrusive rocks in the Thunder Mountain complex are also commonly hydrothermally altered.

Intrusive rocks of the Van Horn Peak and Thunder Mountain cauldron complexes are for the most part hypabyssal equivalents of Tertiary diorite—monzodiorite and granite epizonal plutonic rocks that intrude Cretaceous granitic rocks throughout the Atlanta lobe of the Idaho batholith (Bennett

and Knowles, 1985). These epizonal diorite—monzodiorite and granite plutons and hypabyssal dacite—rhyodacite and rhyolite intrusions undoubtedly are the intrusive equivalents of the pyroclastic sequences of the cauldron complexes. Some mafic and intermediate dikes in the cauldron complexes probably represent vestiges of the magmas producing the older intermediate lava piles in the Challis volcanic field, but these nonexplosive volcanic rocks have yet to be related to any major plutonic bodies (Bennett and Knowles, 1985).

Casto pluton and related felsic intrusions

General lithology

The Casto pluton was first mapped and described by Ross (1934), who noted that the principal rock type was a pink granite with associated subordinate hornblende granite and quartz monzonite and that the pluton intruded the lower part of the Challis volcanics. The pink granite is generally coarse-grained and has an average modal mineralogy of about 28% quartz, 48% microperthite, 13% oligoclase, 7% biotite, and 3% hornblende. Quartz content can range from as low as 10% to as much as 50%. The hornblende granite and quartz monzonite are medium-grained and somewhat porphyritic. Potassium—argon ages of the Casto pluton range from about 47 to 44 Ma (from Leonard and Marvin, 1982; Armstrong, 1975, recalculated).

The Casto pluton, as well as other Eocene plutons in central Idaho such as the Sawtooth and Crags plutons, contain miarolitic cavities indicative of shallow epizonal emplacement. The cavities often contain crystals of microcline, smoky quartz, beryl, topaz, and fluorite. The Tertiary pink granite tends to be similar chemically to the felsic Cretaceous plutonic rocks, but with a narrower range in silica content than in the Cretaceous granites. In addition, the Eocene granites such as the Casto pluton are more evolved and generally contain less aluminum, magnesium, and calcium and more potassium (Bennett and Knowles, 1985). Gamma-ray spectrometry measurements reported by Bennett and Knowles (1985) also show that the Tertiary granites have an average uranium, thorium, and potassium-40 content two to three times higher than granitic rocks of the Cretaceous Idaho batholith.

Oxygen and hydrogen isotopic studies by Taylor and Magaritz (1978) and Criss and Taylor (1983) in the Idaho batholith showed that large-scale meteoric-hydrothermal circulation systems were developed around epizonal Tertiary plutons. More recent isotopic studies of the Challis volcanic rocks of the Van Horn Peak and Thunder Mountain cauldron complexes (Fig. 3) have revealed that the largest meteoric-hydrothermal system ever documented around a single pluton is centered on the Casto pluton (Criss et al. , 1984).

A distinct pink felsic rock of similar modal mineralogy to the Casto pluton, but with a dominant porphyritic texture, forms dikes, small plugs, and irregular, generally northeast-southwest-elongated intrusive bodies that cut rocks of the Casto pluton and all pyroclastic rocks of the Thunder Mountain cauldron complex. This pink porphyry also intrudes most pyroclastic units of the Van Horn Peak cauldron complex, including the gray porphyry intrusive unit.

The pink porphyry, "pink granophyre" of Ross (1934), typically contains 20-35% phenocrysts (about 4 mm in diameter) of bipyramidal smoky quartz and alkali feldspar in subequal amounts, less abundant plagioclase, and sparse biotite in a micrographic to microgranular groundmass.

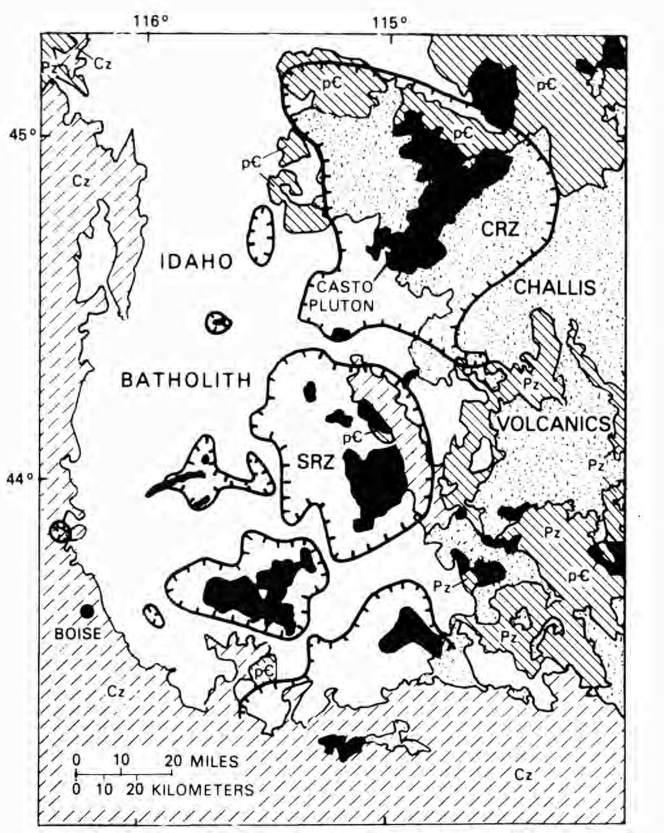

FIGURE 3—Map of southern Idaho batholith and adjacent Challis volcanic terrane showing boundaries (hachured lines) of large meteoric-hydrothermal alteration systems. The largest of these, the Casto ring zone (CRZ), is centered on the Casto pluton; the Sawtooth ring zone (SRZ) is centered on the Sawtooth pluton. Stipple pattern indicates Challis volcanic rocks; lined patterns indicate Precambrian (p€) and Paleozoic (Pz) or Cenozoic (Cz) rock units; solid pattern indicates Tertiary granites. From Criss et al. (1984).

Locally, pink porphyry intrusive masses are extremely coarse-grained, with partially resorbed quartz bipyramids up to 1 cm and alkali feldspar and plagioclase up to 3 cm in size. These coarsely porphyritic varieties have a graphic-textured groundmass. A single sanidine crystal from one of these coarse-grained pink porphyry dikes yielded a potassium—argon age of 44.4 ± 1.0 Ma (McIntyre et al., 1982).

Relation to Challis volcanic rocks

As recognized by Ross (1934) and pointed out by Cater et al. (1973), the Casto pluton intrudes its own ejecta. At present erosion levels, the pluton is in intrusive contact with only the thick lower rhyodacitic sequence of intracauldron tuffs of both the Van Horn Peak and Thunder Mountain cauldron areas. Whether the pluton intruded into the upper rhyolitic sequence of the intracauldron section, which undoubtedly once blanketed the entire cauldron terrain, is speculative.

Ash-flow tuffs within both the Thunder Mountain and Van Horn Peak cauldrons are tilted away from the Casto pluton along its northwest and southeast flanks, respectively. The pluton, therefore, occupies the core of a regional northeast-trending anticline flanked by the Thunder Mountain cauldron to the northwest and the Van Horn Peak cauldron to the southeast.

Dips of the older rhyodacitic Ellis and Camas Creek—Black Mountain tuffs on the southeast flank of the pluton

are as great as 75 to locally 90° in the vicinity of Meyers Cove. Dips of these units on the Thunder Mountain side of the pluton are locally as great, but generally somewhat less. Regional northwest tilt of the younger rhyolitic Sunnyside tuff on the Thunder Mountain side of the pluton is generally only about 15-25°. Likewise, regional southeast tilts of the unconformably younger tuff of Challis Creek on the Van Horn Peak cauldron side of the pluton are generally only 5-15°. It seems reasonable, therefore, that the Casto pluton may have started its ascent into the lower part of the Challis volcanic sequence prior to eruption of magma to produce the Sunnyside and Challis Creek rhyolitic tuffs and prior to collapse of the youngest calderas of the volcanic field.

Most of the cauldron-filling pyroclastic rocks of both the Van Horn Peak and Thunder Mountain cauldron complexes are to some degree hydrothermally altered. Tuffs in the lower rhyodacitic part of the sequence are ubiquitously altered to propylitic mineral assemblages. Near the Casto pluton, these rocks are so thermally affected that they are barely recognizable as ash-flow tuffs. It is to these altered pyroclastic rocks along with some outcrops of altered gray porphyry that Ross (1934) applied the name "Casto Volcanics," a name that subsequently has been abandoned.

Tuffs of the younger rhyolitic part of the intracauldron sequence, especially those farthest away from the Casto pluton, are the least hydrothermally altered. These tuffs, however, are locally strongly altered along major faults, and altered at higher temperatures and for a longer period of time (Criss et al. , 1984).

Discussion

The sequence of volcanic rocks of the Challis volcanic field of central Idaho consists of a thick section of intermediate and mafic lavas that formed an extensive lava plateau upon which a vast cauldron complex formed with transition from relatively passive lava eruptions to explosive volcanism. Ash-flow tuffs produced by the explosive phase of volcanism are now mostly preserved within the eroded cauldron complex where they exceed 6000 m in thickness.

The presence of the same ash-flow-tuff cooling units of the lower rhyodacitic part of the pyroclastic sequence in both the Thunder Mountain and Van Horn Peak cauldron areas indicates that these two cauldron complexes did not originate as two distinct and separate complexes that, once formed, were further separated by the emplacement of the Casto pluton. Instead, the two areas are part of the same vast cauldron complex that may have initiated as a large volcanotectonic depression in which subsequent individual calderas developed. By the time the youngest calderas developed with eruption of the rhyolite and alkali rhyolite Sunnyside and Challis Creek tuffs, respectively, at either end of the cauldron complex, the source substrate for these felsic magmas must have been of batholithic dimensions.

Individual cupolas of magma may have risen diapirically from a batholith-sized source substrate to sufficiently shallow levels of the crust to give rise to the Thunder Mountain and Twin Peaks calderas. Contemporaneously, a third bulge or cupola of magma rose to a level necessary to invade the lower and thickest part of the volcanic pile and cooled to form the Casto pluton. Whether the Casto magma ever vented to the surface is uncertain. If it did, its products have been removed by erosion. High fluorine content of Tertiary granites in central Idaho indicates that they formed from dry melts which were able to rise to shallow crustal levels before crystallizing (Bennett and Knowles, 1985). Perhaps the Casto magma was initially dry or devolatized by the time it rose to levels where it might have produced pyroclastic eruptions.

Field trip

Day 1

Mileage

0.0 **START.** Intersection of US-93 and main street of Challis, Idaho. Proceed south on US-93 out of Challis. **0.9**

0.9 Tree-covered mountain top at about 2:00 to the west-southwest is Blue Mountain, one of several eruptive/intrusive centers for rhyodacitic magma dated at 49.3 ± 1.4 Ma (Armstrong, 1975; recalculated). Treeless hills in the foreground are composed of younger andesite and latite intermediate lavas. The flat farmland to your left is Round Valley through which flows the Salmon River. **0.4**

1.3 Idaho Historical Society marker on your left explains that Round Valley was discovered in 1822 by an expedition of Hudson's Bay Company fur trappers led by Michel Bourdon. **1.0**

2.3 Junction of US-93 and ID-75; turn right on ID-75 toward Stanley and Sun Valley, Idaho. **0.8**

3.1 Cliff exposures on your right are of massive and locally autobrecciated porphyritic rhyodacite. **1.6**

4.7 **STOP 1. Outcrop of rhyodacite** forming small ridge adjacent to highway on your right (adjacent to turn-off for Birch Creek road to the west). Observe nearly horizontal columnar jointing in massive rhyodacite dike that intrudes rhyodacite autobreccia (also interpreted to be intrusive). Cliffs across the Salmon River to the east are also of this same rhyodacite. Be careful of highway traffic at this stop. Turn around and head back toward Challis. **2.4**

7.1 Junction of ID-75 and US-93. Turn left and proceed to Challis. The mountain range straight ahead on the east side of Round Valley is the Pahsimeroi Mountains which form the northern part of the Lost River Range of east-central Idaho. The dark-brown cliff-forming outcrops are composed of quartzite of indeterminate age (possibly late Proterozoic, Lower Cambrian, or Lower Ordovician). White-buff and brick-red rocks farther north are Challis volcanics, principally the subaqueous tuffs and sediments of the Pennal Gulch unit and the tuff of Challis Creek which forms the brick-red cap rocks.

The tuff of Challis Creek also forms erosional remnants on the crest of the Pahsimeroi Mountains. Thus, structurally, Round Valley is a graben (Warm Spring Creek graben) that is one of the northernmost of the Basin and Range grabens that extend north of the Snake River Plain into east-central Idaho. The 1983 Borah Peak earthquake epicenter is located approximately 78 km southeast of Round Valley along the west side of the Lost River Range in this same graben. **1.5**

8.6 Entering Challis, Idaho. Small hills just north of town at about 11:00 consist of reddish-brown cap rock of tuff of Challis Creek overlying light-colored tuffs and sediments of the Pennal Gulch unit; the same relationships are visible at about 2:00 across

Round Valley and on the east side of the Salmon River. The tuff of Challis Creek here is outflow from the Twin Peaks caldera located about 22 km northwest of Challis. The tuff of Challis Creek near town (dated at 45.0 ± 1.3 Ma, Armstrong, 1975; recalculated) forms gently to moderately east-dipping cuestas related to small block rotations on moderately west-dipping faults. **0.7**

9.3 Junction of US-93 and main street of Challis. Turn left and proceed west through town. **1.0**

10.3 Leave west end of Challis and proceed west on paved road up Garden Creek. **1.6**

11.9 Cross Garden Creek. Outcrops on your right along road are of rhyodacite intrusive/flow rock overlain in ridge beyond (north of road) by tuff of Challis Creek. Little, if any, of the Pennal Gulch unit is present in the exposures beneath the tuff of Challis Creek cap rock. This indicates that there was considerable erosional relief prior to the eruption of the tuff of Challis Creek from the Twin Peaks caldera. **1.8**

13.7 Klug Gulch. Exposures in hills on both sides of road are all of rhyodacite intrusive/flow rock. **0.7**

14.4 End of pavement, immediate fork in gravel road; take right fork. **0.6**

15.0 Mill site to the right is a fluorite-processing facility. Fluorite is mined underground and in local open pits from hydrothermal veins in the Bayhorse Dolomite (Upper Cambrian and/or Lower Ordovician) exposed in hill just to west above road. The Bayhorse Dolomite here is intruded and locally overlapped by the rhyodacite. Fluorite-mineralized veins occur along northwest-trending high-angle faults that display dextral movement. **1.2**

16.2 Mill Creek summit. Proceed west into Mill Creek drainage. **0.8**

17.0 Big Hill Creek. Exposures in roadcut to left just past creek crossing are of Bayhorse Dolomite. **0.2**

17.2 Craggy dark-brown outcrops at about 1:00 across valley are of massive rhyodacite. The mountain with trees to the north-northwest is Corkscrew Mtn. which is also composed of rhyodacite dated at about 50.4 ± 1.8 Ma. Note large ancient landslide (hummocky topography) extending from the flank of Corkscrew Mtn. into Mill Creek. **0.4**

17.6 Outcrops in hillslope across Mill Creek directly ahead are of Bayhorse Dolomite that here displays evidence of ground-water dissolution and cave development. **0.2**

17.8 Cross Mill Creek. **0.6**

18.4 Outcrops along road here and for the next 3 mi up Mill Creek are of Ramshorn Slate (Ordovician), a thin-bedded, characteristically laminated argillite, siltstone, and sandy siltstone that is stratigraphically above the Bayhorse Dolomite. Most of the Ramshorn Slate has a very well-developed slaty or axial-plane cleavage that cuts across open, wavy, and locally tight isoclinal folds defined by the bedding. **3.4**

21.8 Cross Mill Creek again. **0.8**

22.6 Junction of Mill Creek road and Pine Summit road; turn right and proceed north across Mill Creek on road to Pine Summit. **0.9**

23.5 Cattleguard and fence line at Pine Summit. Exposures on ridge along fence line to east are of rhyodacite, mostly mantled by land-slipped debris and colluvium. **0.5**

24.0 Fork in dirt road; stay to left to Mosquito Flat Reservoir. **0.6**

24.6 **STOP 1. Overview of Twin Peaks caldera.** **1.5**

26.1 Junction of Pine Summit road and Challis Creek road. Turn right. The road from last stop to here and to Challis Creek below crosses ancient landslide deposits which were responsible for damming Challis Creek to form Mosquito Flats, perhaps sometime in latest Pleistocene or early Holocene. **1.1**

27.2 Open rockslide area on road and lower triangular ridge spur area to north across Challis Creek consist of rhyodacite; the rest of the exposures on north side of Challis Creek are of densely welded ash-flow tuff, the tuff of Challis Creek, which here forms thick intracaldera fill of Twin Peaks caldera. **0.4**

27.6 Cross Challis Creek. **0.4**

28.0 **STOP 3. Tuff of Challis Creek.** Typical dark-brown, densely welded tuff of lower cooling unit for the most part and vitrophyre (perhaps from base of upper cooling unit). **0.4**

28.4 Cross Lodgepole Creek. **2.2**

30.6 **STOP 4. Ring-fracture intrusive.** Exposures at this stop are of coarse porphyritic, altered and sheared, plagioclase-bearing rock of intermediate composition. This unusual rock has not been found anywhere else in the Challis volcanic field. The exposure is along the ring-fracture fault of the Twin Peaks caldera and is interpreted to be a ring-fracture intrusive that has subsequently been altered and weakly mineralized. A strong magnetic high (about +450 nanoteslas) here is centered along the ring-fracture fault. Many plagioclase phenocrysts are fractured and often display a "coffin" shape suggesting they are elongate parallel to the *b* crystallographic axis rather than the *c* axis.

Exposures surrounding this outcrop consist of caldera-wall slump debris or "megabreccia" that consists of blocks of tuff of Challis Creek and intermediate lava in an altered clayey tuff and/or detrital matrix. Megabreccia debris is exposed in roadcuts along north side of road, down-drainage, for next 0.5 mi. This material is then overlain by rounded glacial outwash cobbles and boulders from Bear Creek, which drains from Twin Peaks.

Exposures across Challis Creek to south are of rhyodacite intrusive rock of Cork Screw Mtn., which are mantled and surrounded by ancient landslide deposits through which Challis Creek now cuts. **1.0**

31.6 View to northwest at about 8:00 is up Bear Creek toward Twin Peaks and center of Twin Peaks caldera. Greenish-gray rocky outcrop in small hill at about 9:00 is of older tuff of Camas Creek–Black Mountain which forms bedrock wall of the caldera in this vicinity. **0.1**

31.7 Cattleguard and Bear Creek. **0.7**

32.4 Stop sign; junction Challis Creek road and road to River of No Return Wilderness. Turn left. **0.6**

33.0 Small cuesta to right (north) is of ash-flow tuff of

the tuff of Camas Creek–Black Mountain. Outcrops making up tree-covered mountain just to north are of intracaldera tuff of Challis Creek. Proceed across White Valley Creek, up gravel bench, to Sleeping Deer Ranch gate. The southern margin of the Twin Peaks caldera passes through this immediate vicinity. **0.2**

33.2 Gate to Sleeping Deer Ranch; proceed through electrically operated gate. **0.6**

33.8 Electric gate on other side of Sleeping Deer Ranch; follow road west-northwest up Bear Creek. Bedrock along road is intracaldera tuff of Challis Creek. **2.5**

36.3 Cross Bear Creek. The road is traversing glacial moraine deposits. **0.8**

37.1 Junction of Twin Creek road and Sleeping Deer road; continue to right on Sleeping Deer road. **3.0**

40.1 Bedrock is tuff of Challis Creek. **0.4**

40.5 Twin Peaks cabin. Turn right a few yards beyond and proceed on Sleeping Deer Road. **0.5**

41.0 Custer and Lemhi County line and boundary of River of No Return Wilderness. **0.2**

41.2 **BRIEF PAUSE. Megabreccia containing house-size blocks** in hillslope to north across upper Warm Springs Creek. Road for next 0.5 mi traverses zeolitically altered ash-flow tuff and some megabreccia blocks. **0.9**

42.1 J. Fell Creek sign. **1.6**

43.7 Head of Spider Creek. Exposures on uphill side of road are of megabreccia deposit containing cobble- to house-size blocks of tuff of Challis Creek and extracaldera tuffs and lavas that formed original north wall of caldera. **0.2**

43.9 **STOP 5. Rhyolite dike** at 90° corner. Hike back along road and/or hillside to observe megabreccia deposit. Drivers proceed on road to van turn-around location 1.2 mi ahead at junction of Sleeping Deer road and Parker Mountain road. Drivers turn vehicles around and return to pick up participants. Retrace route to Sleeping Deer Ranch. **17.7**

61.6 Leave main (east) gate of Sleeping Deer Ranch. **0.7**

62.3 Junction of Sleeping Deer road and Challis Creek road; cattleguard; proceed straight ahead on Challis Creek road across cattleguard. Outcrops in hills on both sides (north and south) of Challis Creek just after sharp curve in road are of rhyodacite intrusive and flow rock. **0.5**

62.8 Pats Creek road to left (north). **0.6**

63.4 Beginning of pavement. Outcrops and scree slopes on north side of road are of aphyric latite lavas that are below tuff of Ellis Creek and locally intrude tuff of Ellis Creek. **1.0**

64.4 Curve in road above ranch houses; grayish-green rocks in hillside directly ahead are tuff of Ellis Creek and local sediments that are underlain by latite lavas. Some latite dikes cut across into tuff of Ellis Creek and are overlain by latite of post-Ellis Creek age. The Ellis Creek here is extracaldera ash-flow tuff and is about 90–120 m thick in these exposures. To north, in Van Horn Peak cauldron, intracauldron Ellis tuff is at least 1300 m thick. **1.9**

66.3 Cross Challis Creek. **5.1**

71.4 Junction of Challis Creek road and main street of Challis. Turn left and proceed to motels.

Day 2

Mileage

0.0 **START.** Junction of US-93 and main street of Challis; proceed north out of Challis on US-93. **2.1**

2.1 View to left (west) is up Challis Creek to Twin Peaks and intracaldera fill of Twin Peaks caldera. Outcrops straight ahead in cliffs on east side of Salmon River (to right) are of bedded tuffs of Pennal Gulch sequence, which are locally capped by erosional remnants of the outflow sheet of tuff of Challis Creek (brick-red caprock). Tree-covered dip-slope on horizon at about 9:00 (northwest) is Red Butte, which is composed of rhyolite lava related to ring-fracture intrusions along east margin of Twin Peaks caldera. **2.6**

4.7 Cross Challis Creek. **1.5**

6.2 McKnab Point. Outcrops are of aphyric basaltic-looking rock in cliff on left side of road; the Salmon River is to right of road. Chemically, this rock is an andesite. It overlies tuff of Ellis Creek, that can be seen in light greenish-gray hill in gulch in left foreground, and is overlain by tuffs of Pennal Gulch. Dull pinkish-red outcrops in hill to right are of pre-Tertiary quartzite. The exposures to left of highway for next 2–3 mi and on lower Morgan Creek road show Ellis tuff deposited on a pre-Tertiary erosional surface of considerable relief. **1.9**

8.1 Junction of US-93 and Morgan Creek road; turn left (west) onto Morgan Creek road. **0.3**

8.4 **STOP 6. Outflow facies of tuff of Ellis Creek.** Cattleguard; park vans in turnout to left. Exposures in roadcut on left are of outflow facies of tuff of Ellis Creek. Tuff is rhyodacitic and densely welded here. As we proceed up Morgan Creek, note the great amount of local erosional relief on the pre-Teritary quartzite over which Ellis tuff is deposited. **1.8**

10.2 Leave pavement. Exposures in this canyon are of Swauger Formation (middle Proterozoic) quartzite. **2.9**

13.1 Cattleguard; outcrops again are Ellis tuff lapping onto pre-Tertiary quartzite. **1.9**

15.0 Cattleguard; outcrops in canyon are intermediate lavas (lavas of Block Creek) which underlie Ellis tuff. **1.8**

16.8 Cattleguard; still in lavas of Block Creek (at Millick Gulch). **3.4**

20.2 **STOP 7. View of Van Horn Peak** to west up Van Horn Creek. Van Horn Peak is a welded tuff vent (Ekren, 1981) that consists of two distinct vent-filling tuffs that are correlative with the tuffs of Camas Creek and Black Mountain that form thick intracauldron fill above tuff of Ellis Creek in Van Horn Peak cauldron complex. The Van Horn Peak tuff vent lies just inside ring fracture formed during eruption of tuff of Ellis Creek. **1.8**

22.0 Cattleguard just north of Corral Creek; entering Salmon National Forest, leaving Challis National Forest. Poor exposures along road in this area are

of pre-Tertiary metasedimentary rocks overlain by morainal debris. **0.5**

22.5 Cattleguard; drop into Panther Creek drainage. **0.9**

23.4 Rocks exposed in roadcut on right are middle Proterozoic Yellowjacket Formation. **3.5**

26.9 Opal Creek and turnoff (to right) to Opal Lake. Bare hill slope to right is of glacial moraine deposits. **3.1**

30.0 Cross Panther Creek and take lefthand turn at immediate road intersection. Proceed west to Myers Cove. **0.9**

30.9 Rabbit Foot Summit; keep on main road to right. Light-colored outcrops along road for next 0.5 mi are tepee-shaped monoliths and varicolored hoodoo exposures of weakly welded, pumiceous, lithic-rich rhyolite tuff at least 100 m thick that correlates with tuff of Castle Rock. The tuff of Castle Rock is preserved in Panther Creek graben, which we are now in, and in Castle Rock trapdoor cauldron segment exposed about 13 km southwest of Rabbit Foot Summit. Collapse of this cauldron segment probably occurred with eruption of quartz–biotite tuff that underlies tuff of Castle Rock.

From Rabbit Foot Summit to Meyers Cove we traverse downsection through much of the pyroclastic section of Challis volcanic field, which here is in excess of 4500 m thick. The reason we are able to see so deep into the intracauldron fill of Van Horn Peak cauldron complex is due to preservation in northeast-trending Panther Creek graben and to moderate to steep regional east-southeast tilt of the section due to intrusion of Casto pluton into core of cauldron complex. From youngest to oldest, the volcanic units we traverse through are tuff of Castle Rock, quartz–biotite tuff, and tuffs of Camas Creek–Black Mountain. **3.6**

34.5 Cattleguard. **1.9**

36.4 Outcrop on right on curve and large outcrops just around bend are of quartz–biotite ash-flow tuff. **0.9**

37.3 Arrastra Creek to left; open scree slope on right ahead and large outcrop above are tuffs of Camas Creek–Black Mountain. **1.4**

38.7 Road to Rams Horn Resort on Rams Creek to right; continue left. **0.8**

39.5 Cattleguard; outcrops from here down drainage to Myers Cove are essentially all in tuffs of Camas Creek–Black Mountain. **2.8**

42.3 Myers Cove. Proceed on main road to right. **0.1**

42.4 **STOP 8.** Next campground area—stop and look at **tuffs of Camas Creek–Black Mountain. 0.5**

42.9 Birch Creek Outfitters gate on Camas Creek. **1.4**

44.3 Mill site and miner's quarters for old fluorite mine at Duck Creek. **1.2**

45.5 Through Birch Creek Outfitters site to Camas Creek trailhead.

STOP 9. Hike down Camas Creek to Casto pluton. Exposures in cliffy outcrops above trail near trailhead are tuffs of Camas Creek–Black Mountain. The first exposures along trail are Ellis tuff with vertical dips and containing just barely recognizable (darker than matrix) pumice and pebble-size lithic and cognate fragments. Farther along trail are talus fragments of white quartzite derived from large (up to house size) blocks of Precambrian quartzite included within the Ellis tuff. These blocks of basement rock probably slid off north rim of the cauldron complex as subsidence accompanied eruption of tuff of Ellis Creek. At the end of this hike, we will observe equigranular pink granite of Casto pluton and two varieties of pink porphyry, one with and one without quartz phenocrysts, that intrude the equigranular pink granite. The contact between Casto pluton and Ellis tuff is not exposed at the level of Camas Creek Trail, but is well constrained. (Hike time down Camas Creek Trail to Casto pluton and return is about 90 min., plus 30 min. for discussion).

Retrace route to Myers Cove and Rabbit Foot Summit. **16.4**

61.9 Junction Myers Cove road and Panther Creek road; turn right (south) and proceed up Panther Creek to Morgan Creek Summit and down Morgan Creek, retracing route back to US-93. **23.0**

84.9 Junction of Morgan Creek road and US-93. End of field trip. Turn left (north) on US-93 to Salmon, Idaho, and north back to Missoula, Montana (approximately 160 mi).

References

Armstrong, R. L., 1975, The geochronometry of Idaho: Isochron West, no. 14: 1–50.

Bennett, E. H., and Knowles, C. R., 1985, Tertiary plutons and related rocks in central Idaho; *in* McIntyre, D. H. (ed.), Symposium on the geology and mineral deposits of the Challis 1°×2° quadrangle, Idaho: U.S. Geological Survey, Bulletin 1658: 81–95.

Cater, F. W., Pinckney, D. M., Hamilton, W. B., Parker, R. L., Weldin, R. D., Close, T. J., and Zilka, N. T., 1973, Mineral resources of the Idaho Primitive Area and vicinity, Idaho, with a section on the Thunder Mountain district by B. F. Leonard, and a section on aeromagnetic interpretation by W. D. Davis: U.S. Geological Survey, Bulletin 1304: 431 pp.

Criss, R. E., Ekren, E. B., and Hardyman, R. F., 1984, Casto ring zone: A 4,500-km^2 fossil hydrothermal system in the Challis volcanic field, central Idaho: Geology, 12: 331–334.

Ekren, E. B., 1981, Van Horn Peak—a welded tuff vent in central Idaho: Montana Geological Society, Field Conference and Symposium Guidebook to Southwest Montana, pp. 311–315.

Ekren, E. B., 1985, Eocene cauldron-related volcanic events in the Challis quadrangle; *in* McIntyre, D. H. (ed.), Symposium on the geology and mineral deposits of the Challis 1°×2° quadrangle, Idaho: U.S. Geological Survey, Bulletin 1658: 45–58.

Fisher, F. S., McIntyre, D. H., and Johnson, K. M., 1983, Geologic map of the Challis 1°×2° quadrangle, Idaho: U.S. Geological Survey, Open-File Report 83-523: 41 pp., 2 oversized, sheets, scale 1:250,000.

Hardyman, R. F., 1981, Twin Peaks caldera of central Idaho: Montana Geological Society, Field Conference and Symposium Guidebook, southwest Montana, pp. 317–322.

Hardyman, R. F., 1985, The Twin Peaks caldera and associated ore deposits; *in* McIntyre, D. H. (ed.), Symposium on the geology and mineral deposits of the Challis 1°×2° quadrangle, Idaho: U.S. Geological Survey, Bulletin 1658: 97–105.

Hays, W. H., McIntyre, D. H., and Hobbs, S. W., 1978, Geologic map of the Lone Pine Peak quadrangle, Custer County, Idaho: U.S. Geological Survey, Open-File Report 78–1060.

Hobbs, S. W., Hays, W. H., and McIntyre, D. H., 1975, Geologic map of the Clayton quadrangle, Custer County, Idaho: U.S. Geological Survey, Open-File Report 78-1060.

Kiilsgaard, T. H., and Lewis, R. S., 1985, Plutonic rocks of Cretaceous age and faults in the Atlanta lobe of the Idaho batholith, Challis quadrangle; *in* McIntyre, D. H. (ed.), Symposium on the geology and mineral deposits of the Challis 1°×2° quadrangle, Idaho: U.S. Geological Survey, Bulletin 1658: 29–42.

Kiilsgaard, T. H., Fisher, F. S., and Bennett, E. H., 1986, The trans-Challis fault system and associated precious-metal deposits: Economic Geology, 81: 721–724.

Leonard, B. F., and Marvin, R. F., 1982, Temporal evolution of the Thunder Mountain caldera and related fractures, central Idaho; *in* Bonnichsen, W., and Breckenridge, R. M. (eds.), Cenozoic geology of Idaho: Idaho Bureau of Mines and Geology, Bulletin 26: 23–41.

McIntyre, D. H., and Hobbs, S. W., 1987, Geologic map of the Challis quadrangle, Custer and Lemhi Counties, Idaho: U.S. Geological Survey, Map GQ-1599, scale 1:62,500.

McIntyre, D. H., Ekren, E. B., and Hardyman, R. F., 1982, Stratigraphic and structural framework of the Challis Volcanics in the eastern half of the Challis $1° \times 2°$ quadrangle, Idaho; *in* Bonnichsen, W., and Breckenridge, R. M. (eds.), Cenozoic geology of Idaho: Idaho Bureau of Mines and Geology, Bulletin 26: 3–22.

Moye, F. J., Hackett, W. R., Blakley, J. D., and Snider, L. G., 1988, Regional geologic setting and volcanic stratigraphy of the Challis volcanic field, central Idaho; *in* Link, P. K., and Hackett, W. R. (eds.), Guidebook to the geology of central and southern Idaho: Idaho Geological Survey, Bulletin 27: 87–97.

Ross, C. P., 1934, Geology and ore deposits of the Casto quadrangle, Idaho: U.S. Geological Survey, Bulletin 854: 135 pp.

Selected conversion factors*

TO CONVERT	MULTIPLY BY	TO OBTAIN
Length		
inches, in	2.540	centimeters, cm
feet, ft	3.048 x 10^{-1}	meters, m
yards, yds	9.144 x 10^{-1}	m
statute miles, mi	1.609	kilometers, km
fathoms	1.829	m
angstroms, Å	1.0 x 10^{-8}	cm
Å	1.0 x 10-^{4}	micrometers, µm
Area		
in^2	6.452	cm^2
ft^2	9.29 x 10^{-2}	m^2
yds^2	8.361 x 10^{-1}	m^2
mi^l	2.590	km^2
acres	4.047 x 10^3	m^2
acres	4.047 x 10^{-1}	hectares, ha
Volume (wet and dry)		
in^3	1.639 x 10^1	cm^3
ft^3	2.832 x 10^{-2}	m^3
yds^3	7.646 x 10^{-1}	m^3
fluid ounces	2.957 x 10^{-2}	liters, 1 *or* L
quarts	9.463 x 10^{-1}	1
U.S. gallons, gal	3.785	1
US. gal	3.785 x 10^{-3}	m^3
acre-ft	1.234 x 10^3	m^3
barrels (oil), bbl	1.589 x 10^{-1}	m^3
Weight, mass		
ounces avoirdupois, avdp	2.8349 x 10_1	grams, gr
troy ounces, oz	3.1103 x 10^1	gr
pounds, lb	4.536 x 10^{-1}	kilograms, kg
long tons	1.016	metric tons, mt
short tons	9.078 x 10^{-1}	mt
oz mt^{-1}	3.43 x 10^1	parts per million, ppm
Velocity		
ft sec^{-1} (= ft/sec)	3.048 x 10^{-1}	m sec^{-1} (= m/sec)
mi hr^{-1}	1.6093	km hr^{-1}
mi hr^{-1}	4.470 x 10^{-1}	m sec^{-1}

TO CONVERT	MULTIPLY BY	TO OBTAIN
Pressure, stress		
lb in^{-2} (= lb/in^2), psi	7.03 x 10^{-2}	kg cm^{-2} (= kg/cm^2)
lb in^{-2}	6.804 x 10^{-2}	atmospheres, atm
lb in^{-2}	6.895 x 10^3	newtons (N)/m^2, N m^{-2}
atm	1.0333	kg cm^{-2}
atm	7.6 x 10^2	mm of Hg (at 0° C)
inches of Hg (at 0° C)	3.453 x 10^{-2}	kg cm^{-2}
bars, b	1.020	kg cm^{-2}
b	1.0 x 10^6	dynes cm^{-2}
b	9.869 x 10^{-1}	atm
b	1.0 x 10^{-1}	megapascals, MPa
Density		
lb in^{-3} (= lb/in^3)	2.768 x 10^1	gr cm^{-3} (= gr/cm^3)
Viscosity		
poises	1.0	gr cm^{-1} sec^{-1} *or* dynes cm^{-2}
Discharge		
U.S. gal min^{-1}, gpm	6.308 x 10^{-2}	l sec^{-1}
gpm	6.308 x 10^{-5}	m^3 sec^{-1}
ft^3 sec^{-1}	2.832 x 10^{-2}	m^3 sec^{-1}
Hydraulic conductivity		
U.S. gal day^{-1} ft^{-2}	4.720 x 10^{-7}	m sec^{-1}
Permeability		
darcies	9.870 x 10-13	m^2
Transmissivity		
U.S. gal day^{-1} ft^{-1}	1.438 x 10^{-7}	m^2 sec^{-1}
U. S. gal min^{-1} ft^{-1}	2.072 x 10^{-1}	1 sec^{-1} m^{-1}
Magnetic field intensity		
gausses	1.0 x 10^5	gammas
Energy, heat		
British thermal units, BTU	2.52 x 10^{-1}	calories, cal
BTU	1.0758 x 10^2	kilogram-meters, kgm
BTU lb^{-1}	5.56 x 10^{-1}	cal kg-1
Temperature		
°C + 273	1.0	°K (Kelvin)
°C + 17.78	1.8	°F (Fahrenheit)
°F - 32	5/9	°C (Celsius)

**Divide by* the factor number to reverse conversions.
Exponents: for example 4.047 x 10^3 (see acres) = 4,047; 9.29 x 10^{-2} (see ft^2) = 0.0929.

Editors: Charles E. Chapin, Jiri Zidek

Graphics: Monte M. Brown

Typeface: Display heads: Spartan
Text: Times

Presswork: Miehle Single Color Offset
Harris Single Color Offset

Binding: Smyth sewn with softbound cover

Paper: Cover on 17-pt. Kivar
Text on 70 lb white matte

Ink: Cover—PMS 320
Text—Black

Quantity: 2000

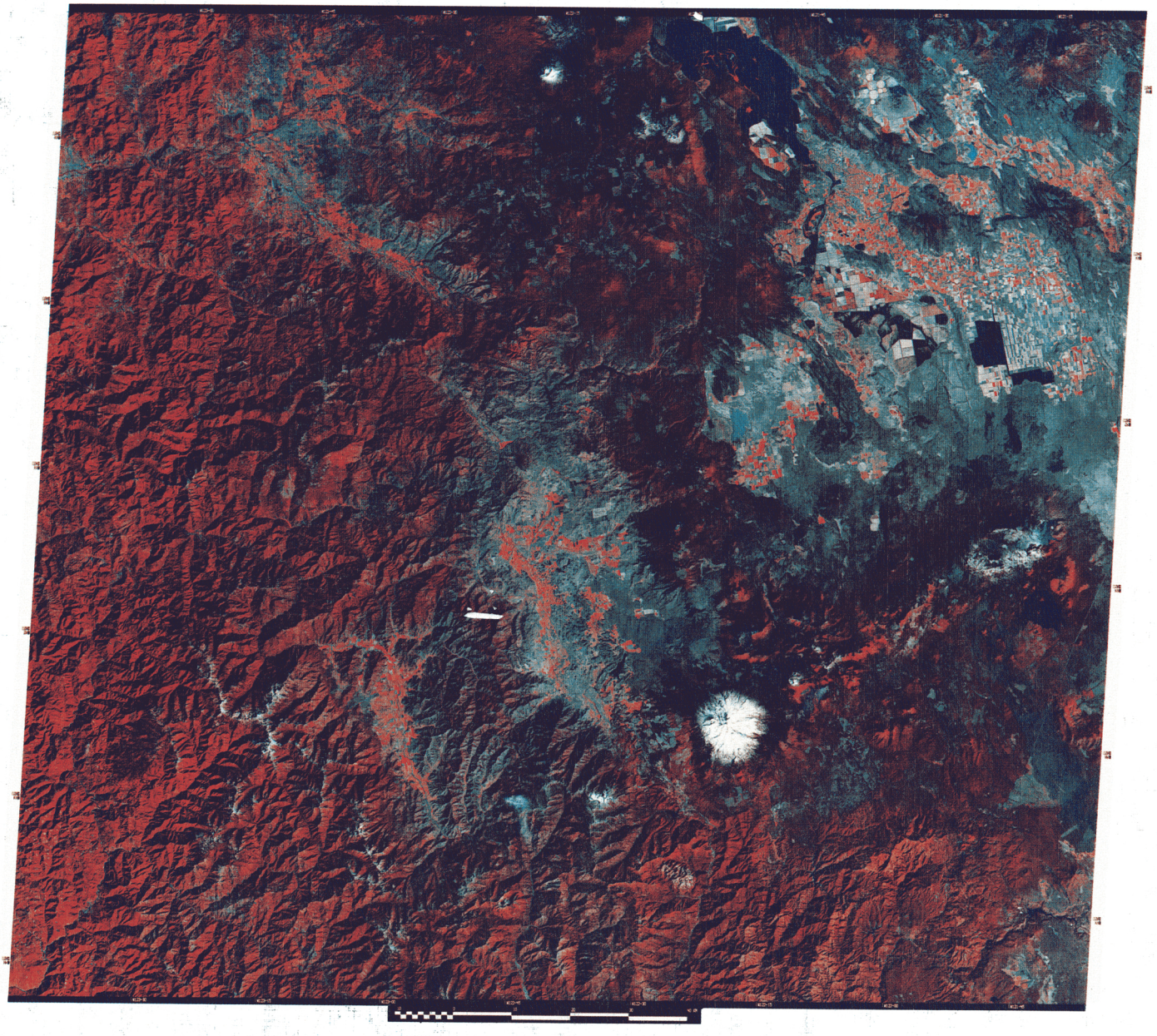

NEW MEXICO BUREAU OF MINES AND MINERAL RESOURCES